Imaging Anatomy

Text and Atlas Volume 1

Lungs, Mediastinum, and Heart

Farhood Saremi

Associate Editors
Damian Sanchez-Quintana
Hiro Kiyosue
Francesco F. Faletra
Meng Law
Dakshesh B. Patel
R. Shane Tubbs

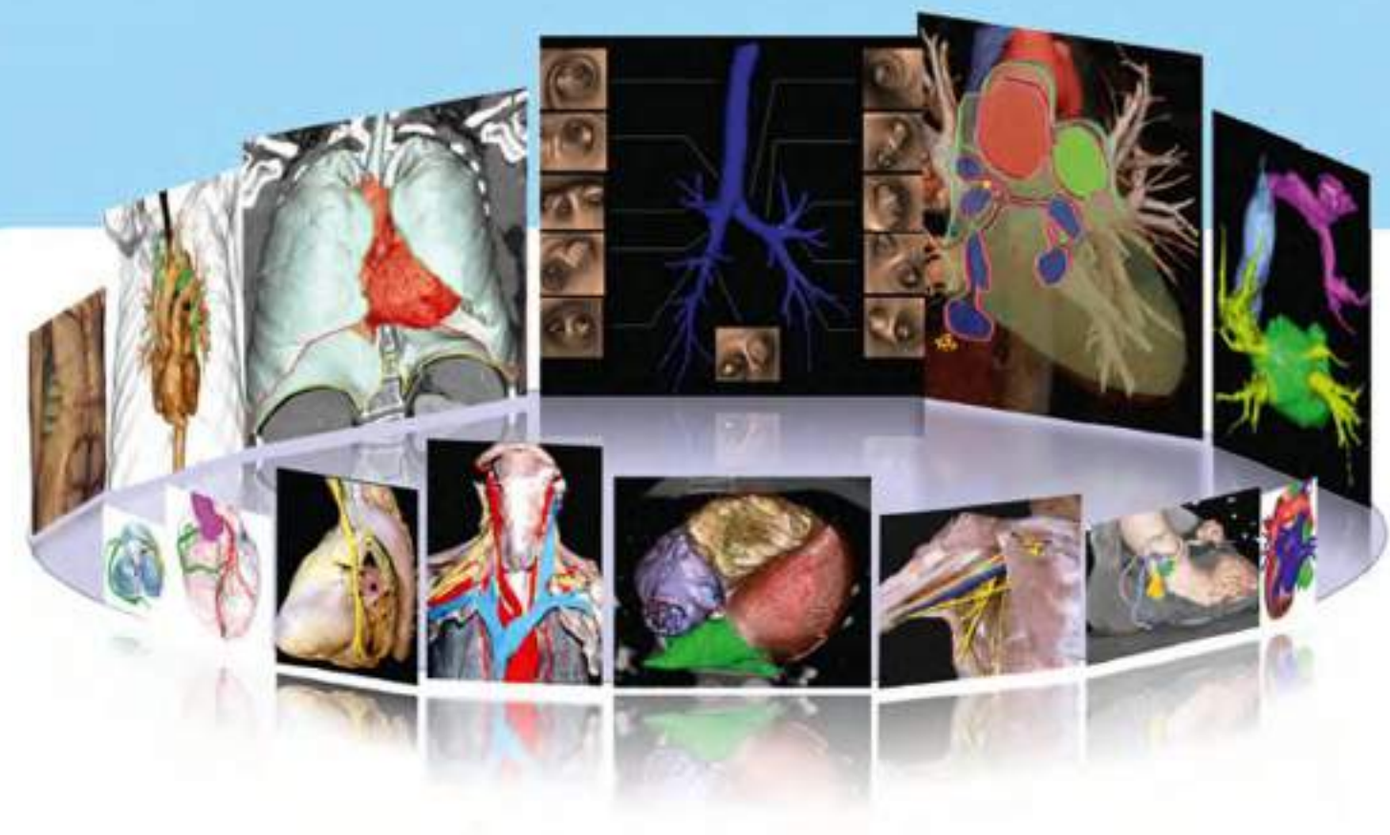

Thieme

Thieme

Imaging Anatomy

Text and Atlas Volume 1
Lungs, Mediastinum, and Heart

Farhood Saremi, MD
Professor of Radiology and Medicine
Department of Radiology
University of Southern California
Keck Medicine of USC
Los Angeles, California, USA

Associate Editors

Damián Sánchez-Quintana, MD, PhD
Professor of Human Anatomy
Faculty of Medicine
Department of Anatomy and Cell Biology
University of Extremadura
Badajoz, Spain

Hiro Kiyosue, MD
Associate Professor of Radiology
Department of Radiology
Oita University Hospital
Yufu City, Oita Prefecture, Japan

Francesco F. Faletra, MD
Professor of Cardiology
Division of Cardiology
Director of Cardiac Imaging Service
Fondazione Cardiocentro Ticino
Lugano, Switzerland

Meng Law, MD
Professor of Radiology, Neurology, and Neurological Surgery
University of Southern California
Biomedical Engineering
Viterbi School of Engineering
Director of Neuroradiology and the Neuroradiology Fellowship Program
Keck Medicine of USC
Los Angeles, California, USA

Dakshesh B. Patel, MD
Associate Professor of Clinical Radiology
Department of Radiology
University of Southern California
Keck Medicine of USC
Los Angeles, California, USA

R. Shane Tubbs, MD
Professor, Chief Scientific Officer, and Vice President
Seattle Science Foundation
Seattle, Washington, USA

616 illustrations

Thieme
New York • Stuttgart • Delhi • Rio de Janeiro

Library of Congress Cataloging-in-Publication Data
Names: Saremi, Farhood, editor.
Title: Imaging anatomy. Lungs, mediastinum, and heart / [edited by] Farhood Saremi ; associate editors, Damian Sanchez-Quintana, Hiro Kiyosue, Francesco F. Faletra, Meng Law, Dakshesh B. Patel, R. Shane Tubbs.
Other titles: Lungs, mediastinum, and heart
Description: New York : Thieme, [2021] | Includes bibliographical references and index. | Summary: "This atlas provides high-quality multiplanar and volumetric color-coded imaging techniques utilizing CT, MRI, or angiography, supplemented by cadaveric presentations and color drawings that best elucidate each specific anatomic region. Twenty-one chapters with concise text encompass thoracic wall, mediastinum, lung, vascular, and cardiac anatomy, providing readers with a virtual dissection experience. Many anatomical variants along with pathological examples are presented"– Provided by publisher.
Identifiers: LCCN 2021001915 (print) | LCCN 2021001916 (ebook) | ISBN 9781626239883 (hardcover) | ISBN 9781626239890 (ebook)
Subjects: MESH: Lung–anatomy & histology | Lung–diagnostic imaging | Mediastinum–anatomy & histology | Mediastinum–diagnostic imaging | Heart–anatomy & histology | Heart–diagnostic imaging | Diagnostic Imaging–methods | Atlas
Classification: LCC QM261 (print) | LCC QM261 (ebook) | NLM WF 17 | DDC 612.2/4–dc23
LC record available at https://lccn.loc.gov/2021001915
LC ebook record available at https://lccn.loc.gov/2021001916

Important note: Medicine is an ever-changing science undergoing continual development. Research and clinical experience are continually expanding our knowledge, in particular our knowledge of proper treatment and drug therapy. Insofar as this book mentions any dosage or application, readers may rest assured that the authors, editors, and publishers have made every effort to ensure that such references are in accordance with **the state of knowledge at the time of production of the book.**

Nevertheless, this does not involve, imply, or express any guarantee or responsibility on the part of the publishers in respect to any dosage instructions and forms of applications stated in the book. **Every user is requested to examine carefully** the manufacturers' leaflets accompanying each drug and to check, if necessary in consultation with a physician or specialist, whether the dosage schedules mentioned therein or the contraindications stated by the manufacturers differ from the statements made in the present book. Such examination is particularly important with drugs that are either rarely used or have been newly released on the market. Every dosage schedule or every form of application used is entirely at the user's own risk and responsibility. The authors and publishers request every user to report to the publishers any discrepancies or inaccuracies noticed. If errors in this work are found after publication, errata will be posted at www.thieme.com on the product description page.

Some of the product names, patents, and registered designs referred to in this book are in fact registered trademarks or proprietary names even though specific reference to this fact is not always made in the text. Therefore, the appear-ance of a name without designation as proprietary is not to be construed as a representation by the publisher that it is in the public domain.

© 2021 Thieme. All rights reserved.

Thieme Medical Publishers, Inc.
333 Seventh Avenue, 18th Floor
New York, NY 10001, USA
www.thieme.com
+1 800 782 3488, customerservice@thieme.com

Cover design: Thieme Publishing Group
Typesetting by DiTech Process Solutions, India

Cover design: Thieme Publishing Group
Typesetting by DiTech Process Solutions, India

Printed in the United States of America by King Printing Co., Inc. 5 4 3 2 1

ISBN 978-1-62623-988-3

Also available as an e-book:
eISBN 978-1-62623-989-0

This book, including all parts thereof, is legally protected by copyright. Any use, exploitation, or commercialization outside the narrow limits set by copyright legislation, without the publisher's consent, is illegal and liable to prosecution. This applies in particular to photostat reproduction, copying, mimeographing, preparation of microfilms, and electronic data processing and storage.

Contents

Preface xi
Farhood Saremi

Contributors xii

1. Thoracic Wall 1

Introduction 1

Embryology 1

Bony Thorax 1

Ribs 1
Sternum 5

Anatomical Variations of the Bones 11

Pectus Excavatum and Pectus Carinatum 14

Chest Wall Pathologies 14

Muscles of the Chest Wall 17

Muscles of the Anterior Chest Wall 17
Abdominal Wall Muscles 22
Muscles of the Posterior Chest Wall 23
Erector Spinae Muscles 29
Thoracolumbar Fascia 29
Intercostal Muscles 29
Muscles of the Thoracic Inlet 36
Subclavius Muscle 37

Arterial Supply to the Thoracic Wall 39

Thyrocervical Trunk 42
Internal Thoracic Artery 42
Thoracoacromial Artery 46
Lateral Thoracic Artery 46
Subscapular Artery 47

Intercostal Neurovascular Bundle 47

Veins of the Chest Wall 52

Thoracic Outlet Syndrome 52

Anatomy of the Thoracic Outlet 56

2. Tracheobronchial System 70

Introduction 70

Embryology 70

Tracheal Anatomy 70

Vascular and Nerve Supply 76

Carina and Bronchial Anatomy 77

Hilar Anatomy 79

Segmental Bronchial Anatomy 80
Characteristics of Small Airways 83
Bronchial Vascular Anatomy 84

Main Anatomical Variations and Malformation 87

Complementary Role of CT and Fiberoptic Bronchoscopy 92

Dynamic Airway Evaluation 92

Pathology 92

3. Mediastinum and Thymus 103

Introduction 103

Compartmentalized Anatomy 103

ITMIG Classification 103

Components 106

Ligaments 106

Thymus 110

Mediastinal Fat 115

Lymph Nodes 115

Lymphatic Vessels 121

Thoracic Duct 121

Nerves 124

Phrenic Nerves 124

Vagus Nerves ... 124
Sympathetic Chains ... 124
Superior Pulmonary Sulcus ... 128

4. Lungs ... 135

Introduction ... 135
Embryology ... 135
Anatomy ... 135
Lobes and Segmental Anatomy ... 135
Secondary Pulmonary Lobule and Pulmonary Acini ... 137
Interalveolar Air Drift ... 139
Pulmonary Function ... 139
Lung Ventilation ... 139
Lung Circulation ... 140
Pulmonary Artery Microcirculation ... 141
Bronchial Artery Circulation ... 142
Bronchopulmonary Arterial Collateral Flow ... 142
Ventilation to Perfusion Matching ... 142
Imaging of Lung Function ... 142
Radiological Diagnosis of Pulmonary Abnormalities ... 142

5. The Pleura ... 149

Introduction ... 149
Embryology ... 149
The Pleura ... 149
Boundaries and Pleural Recesses ... 155
Histology ... 155
Blood Supply ... 155
Innervation ... 155
Lymphatic Drainage ... 157
Incomplete and Accessory Fissures ... 157
Common Diseases of the Pleura ... 161
Pleural Effusion ... 161
Pneumothorax ... 161
Pleural Masses ... 161

6. Pulmonary Artery and Vein ... 170

Pulmonary Artery ... 170
Pulmonary Vein ... 170
Embryology ... 189
Pulmonary Arteries ... 189
Pulmonary Veins ... 191
Developmental Failure ... 191
Persistent Truncus Arteriosus ... 191
Aberrant Left Pulmonary Artery ... 191
Systemic Arterial Supply to the Lung ... 191
Pulmonary Arteriovenous Malformation ... 191
Anomalous Pulmonary Venous Return ... 193
Pulmonary Artery Diameters in Pathologies ... 193

7. Pulmonary and Systemic Veins ... 199

Introduction ... 199
Systemic Veins ... 199
Superior Vena Cava ... 199
Brachiocephalic Veins ... 202
Left Superior Intercostal Vein ... 202
Azygos System and Inferior Vena Cava ... 205
Embryology ... 205
Variants and Pathologies ... 205
Pulmonary Veins ... 209
Anatomy ... 209
Embryology ... 209
Ostial Pulmonary Vein ... 214
Structure of the Pulmonary Vein Ostia ... 215
Techniques for Catheter Ablation of Atrial Fibrillation ... 217
Pathology ... 217
Anomalies ... 219

8. Thoracic Aorta and Major Branches 224

Anatomy 224

Ascending Aorta 224

Branches from the Ascending Aorta 227

Aortic Arch 227

Branches from the Aortic Arch 230

Descending Thoracic Aorta 235

Branches from Descending Aorta 235

Embryological Development 239

Anatomical Variations and Anomalies 243

Right Aortic Arch 243
Double Aortic Arch 243
Aberrant Right Subclavian Artery 246
Patent Ductus Arteriosus 246
Left Vertebral Artery Originating from Aortic Arch 246
Coarctation of the Aorta 248
Pseudocoarctation of the Aorta 248

9. Lymphatics and Nerves of the Thorax 251

Introduction 251

Nerves 251

Innervation of Thoracic Wall 251
Vagus Nerves 252
Phrenic Nerves 254
Sympathetic Nerves 256
Motor Innervation of the Diaphragm 257
Pulmonary Innervation 257
Esophageal Innervation 257

Cardiac Innervation 258

Lymphatics 259

Lymphatic Drainage of the Thoracic Wall 259
Lymphatic Drainage of the Lungs 261
Thoracic Duct 261
Thymus Lymphatics 264
Esophageal Lymphatics 264
Mediastinum 264
Pericardial and Cardiac Lymphatics 267

10. Diaphragm 271

Introduction 271

Embryology 271

Anatomy 272

Central Tendon 272
Muscular Attachments 272
Variable Appearance of the Diaphragmatic Muscular Slips 272
Diaphragm Ligaments 279
Diaphragmatic Crus 279

Diaphragmatic Hiatuses 282

Vena Cava Hiatus 282
Esophageal Hiatus 282
Aortic Hiatus 282
Sternocostal Triangle (Larrey's Space, Morgagni's Foramen) 282
Lumbocostal Triangle (Bochdalek's Foramen) 282
Tiny Diaphragmatic Fenestrations 282

Diaphragmatic Hernias 282

Hiatal Hernia 282
Morgagni's Hernia 286
Bochdalek's Hernia 286

Innervation 287

Blood Supply 287

Arteries 287
Veins 288
Lymphatics 289

Physiology 289

Dysfunction of the Diaphragm 290

Phrenic Nerve Injury 290

Eventration 292

Other Pathologies 292

11. Breast Anatomy 296

Introduction 296

Embryology and Development 296

Breast Parenchyma 298

Ducts and Lobules 298

Nipple–Areolar Complex 305

Neuromuscular Anatomy and Chest Wall 307

Lymphatics and Axilla 308

Vascular Anatomy 311

Arterial System ... 311
Venous System ... 313

12. General Anatomy of the Heart ... 315

Introduction ... 315
Heart Borders in the Thorax ... 315
Anatomical Position of the Cardiac Structures ... 316
Anatomical Surfaces and Angles of the Heart ... 316
Right Atrium ... 325
Superior Right Atrium Landmarks ... 329
Anterolateral Right Atrium Landmarks ... 334
Inferior Right Atrium Landmarks ... 340
Medial Right Atrium Landmarks ... 345
Left Atrium ... 346
Components of the Left Atrium ... 349
Pulmonary Vein Ostia ... 350
Left Atrial Appendage ... 354
Important Periatrial Structures ... 354
Interatrial Septum ... 359
Patent Foramen Ovale ... 359
Atrial Septal Aneurysm ... 366
Right Ventricle ... 366
Right Ventricular Outflow Tract ... 374
Right Ventricle Size ... 375
Right Ventricle Function ... 377
Tricuspid Valve ... 378
Pulmonary Valve ... 382
Left Ventricle ... 382
Left Ventricular Outflow Tract ... 389
Mitral Valve ... 389
Aortic Valve ... 392
Membranous Septum ... 395
Left Ventricular Function ... 398
Ventricular Septum ... 401
Atrioventricular Conduction Axis ... 401

13. Atrioventricular Septal Region ... 407

Introduction ... 407
Anatomical Arrangement of the Base of the Ventricular Mass ... 407
The Cardiac Valvar Attachments ... 408
The Inaccurate Notion of a "Cardiac Skeleton" ... 410
The Inferior Pyramidal Space ... 412
The Membranous Septum ... 412
The Atrial Septum ... 412
The Atrioventricular Conduction Axis ... 416
The Right-Sided Paraseptal Areas ... 416
The Atrioventricular Valves and Papillary Muscles ... 420
The Arterial Roots ... 422
Conclusion ... 426
Acknowledgments ... 426

14. The Aortic Valve ... 430

Introduction ... 430
Anatomy ... 430
Ventriculoarterial Junction ... 430
Aortic Leaflets ... 430
Aortic Annulus ... 430
Interleaflet Triangles ... 434
Sinuses of Valsalva ... 434
Sinotubular Junction ... 434
Aortic Diseases ... 434
Lambl's Excrescences ... 436
Papillary Fibroelastoma ... 436
Bicuspid Aortic Valve ... 436
Aortic Stenosis ... 438
Aortic Leaflet Prolapse ... 441
Aortic Endocarditis ... 441
Dilation of the Aortic Root (Aortic Aneurysm) ... 443

15. Pulmonary Valve ... 446

Introduction ... 446
Embryology ... 446
Anatomy ... 446
Arterial Supply ... 450

Imaging Techniques ... 456

Pathologies ... 456

Pulmonary Valve Stenosis ... 456

Pulmonary Regurgitation ... 458
Congenital Heart Disease and the Pulmonary Root ... 459
Valve Replacement ... 459

16. The Mitral Valve ... 461

Introduction ... 461

Mitral Valve Apparatus ... 461

Mitral Annulus ... 461
Mitral Leaflets ... 463
Chordae Tendineae ... 463
Papillary Muscles ... 468

Anatomical Variant ... 470

Common Pathologies ... 470

Mitral Valve Regurgitation ... 470
Organic Mitral Insufficiency ... 470
Functional Mitral Regurgitation ... 474
Mitral Valve Stenosis ... 475

17. The Tricuspid Valve Apparatus ... 477

Introduction ... 477

Formation of the Tricuspid Valve ... 477

Normal Tricuspid Valve ... 478

Tricuspid Annulus ... 483

Imaging of the TV Apparatus Morphology ... 483

Tricuspid Annulus Measurements ... 486

Morphological Abnormalities of Tricuspid ... 487

Tricuspid Valve Dysfunction ... 487

18. Coronary Arteries and Myocardial Perfusion ... 489

Introduction ... 489

Epicardial Coronary Arteries ... 489

Embryology ... 489
Gross Anatomy ... 489
Segmental Classification ... 489
Common Variants ... 493

Participants of Intercoronary Connections ... 507

Interventricular Septum ... 507

Conotruncal Arterial Circulation ... 510

Arterial Supply of the Conduction System ... 511

Sinoatrial Nodal Artery ... 513
S-Shaped Posterior SAN Artery ... 513
Atrioventricular Nodal Artery ... 513

Atrial Branches ... 514

Kugel's Artery ... 514
Right Superior Descending (Septal) Artery ... 514

Coronary Microvasculature ... 515

Coronary Blood Flow and Myocardial Perfusion ... 515

CT Imaging after Coronary Bypass Graft ... 516

19. The Coronary Veins ... 520

Introduction ... 520

Development of the Cardiac Veins ... 520

Classification of the Coronary Veins ... 520

Smaller Cardiovascular System (Thebesian Vessels) ... 521

Thebesian Sinusoids of Special Structures ... 521
Conduction System ... 523
Papillary Muscles ... 523
Left Ventricle Venoluminal Thebesian Vessels ... 523

Atrial Venous System ... 524

Veins of the Left Atrial Wall ... 524
Veins of the Right Atrial Wall ... 526

Coronary Sinus Tributaries ... 530

Imaging Methods ... 530
Great Cardiac Vein ... 530
Inferior Interventricular Vein ... 531
Left Posterior (Posterolateral) and Left Marginal Veins ... 534
Small Cardiac Vein ... 534
Oblique Vein of the Left Atrium (Marshall) ... 534
Ventricular Septal Veins ... 536
Valves of Coronary Veins ... 536
Coronary Sinus Boundaries ... 536
Variation of the Coronary Vein Sizes ... 536

Coronary Veins and Congenital Heart Disease 536
Cardiac Resynchronization Therapy 537
Other Topics 545
Coronary Sinus Interatrial Muscle Connections 545
Relationship of Coronary Veins and the Mitral Annulus 545
Coronary Sinus Retrograde Cardioplegia Perfusion Delivery 550
Conclusion 550

20. The Pericardium 554
Introduction 554
Embryology 554
Pericardium 555
Pericardial Reflection 559
Transverse Sinus 559
Oblique Sinus 563
Imaging of the Pericardium 563
Percutaneous Approach to Pericardial Cavity 563
Common Pathologies 564
Extracardiac Fat 564

21. Appendix 571
Catheter, Support Devices and Drains on Plain X-rays 571

Index 579

Preface

In the preface of his anatomy text collection *de Humani Corporis Fabrica*, published in 1543, Andreas Vesalius wrote "… anatomy should rightly be regarded as the strong foundation of the whole art of medicine …", acknowledging the fundamental role the study of anatomy has in the practice of medicine. Furthermore, one of the major lasting successes of his influential anatomy series was the ability to reproduce many superb illustrations of human anatomy dissection which was made possible by technical developments during his time.

Likewise, recent advancement in imaging technology and the development of newer post-processing software has increased our ability to image and show anatomic detail of the human organs. At the same time, over past decade, the literature is filled with many precious anatomy articles and related topics. Unfortunately, there is an increasing gap between our fundamental core anatomy reference texts and our understanding and depiction of human anatomy using modern imaging and post-processing methods. The idea for this project arose from the necessity for a text to fill this gap and describe anatomy in the context of current advances in imaging technology and science.

CT and MR have been the traditional methods in performing noninvasive studies, and both have immensely contributed to our ability to deliver accurate diagnostic information. Current generation MR and CT as well as dedicated peripheral and intraluminal ultrasound provide the spatial and contrast resolutions required to demonstrate anatomic details with unprecedented accuracy.

When it comes to the assessment of details, there is no imaging modality that can compete with the speed, accuracy and spatial resolution of new CT scanners. Volume rendering and mutliplanar reformations facilitate understanding of the complex structures such as heart, vessels, and bones. With current scanners the entire anatomic span of the major organs can be covered in a few seconds with spatial resolution of less than 0.5 mm^3. In this series, this technology along with state of the postprocessing methods have been used to create volumetric color-coded images.

On the other hand, MRI provides high levels of contrast resolution that would be difficult to obtain with CT. High-field MRI provides superb resolution of brain anatomy. Taking advantage of a 7 Tesla MR scanner at our facility, high quality images were obtained to complete the chapters of the neuroanatomy volume (volume 4). Using MR tractography, it is possible to detail the anatomic course of the white tracts and with new post processing software it is further possible to map areas of the brain cortex and subfield regions of small structures such hippocampus. These technologies have ushered in a new era for investigation of brain anatomy and are being used for the planning of sophisticated brain surgeries and for localization of small regions of interest.

This imaging anatomy series is a reference atlas and text with a practical discussion of specific topics along with examples of anatomical variants. Divided into four major volumes, each takes the instructive format of a classic text but infused with a large number of images and illustrations to teach readers anatomy via state of the art cross-sectional and volumetric imaging. The volumes are divided into lung/mediastinum/heart, abdomen/pelvis, musculoskeletal, and head/neck/spine imaging. Peripheral vasculature and nerves have been included in musculoskeletal volume.

The length of each chapter and number of images vary in accordance with the complexity of the topic. In all instances, effort has been made to provide a concise yet comprehensive review of the topic. Each chapter contains an in-depth review of the anatomy and anatomical variants. Pertinent embryology, microanatomy, and a brief description of physiology are discussed in each chapter. Post-surgical anatomy and important gross and surgical pathology images are included.

The text is supported by high-quality cross-sectional images with correlative 3D and color-coded CT and MR views. Up to date references are used to support the text. Many new topics in radiology and surgery have been gathered from the recent 10-year literature. Surgical and clinical applications in each anatomy topic are presented by relevant images. In order to make each topic understandable, difficult anatomical concepts are supported by sketches as well as cross-sectional and topographic cadaveric views provided by internationally known anatomists. Superb cadaveric views are provided by Professors Sánchez-Quintana, Shane Tubbs, and the late Albert L. Rhoton Jr. High-resolution axial cadaveric cuts are provided by University of Auckland, New Zealand, thanks to efforts of Professor Ali Mirjalili.

As the author and chief editor of this textbook, I was fortunate to have assistance of other editors who have shared their experiences for specific parts of this compilation. Countless contributors from high-ranking academic institutions with extensive experience in imaging, surgery, human anatomy and embryology, have also provided substantial work and shared their expertise. Together over more than five years of constant work, we have created a comprehensive textbook and atlas on imaging and surgical anatomy that aims to serve a broad spectrum of the medical community including the medial students, radiologists, surgeons, clinicians and research scholars.

Finally, this collaborative effort would have remained unfinished without the unreserved assistance and expert guidance of the product development editors of Thieme Publishers, William Lamsback (Executive Editor), Brenda Bunch (Production Editor), Torsten Scheihagen (Managing Editor), Mary Wilson (Testing Specialist), and their team of professional medical illustrators.

Farhood Saremi
Los Angeles, California
December 2020

Contributors

Robert H. Anderson, BSc, MD, FRCPath
Professor of Anatomy and Embryology
Institute of Genetic Medicine
Newcastle University
Newcastle-upon-Tyne, United Kingdom

Gina Cavallo, MD
Department of Surgery
Morristown Medical Center
Morristown, New Jersey

Sumudu N. Dissanayake, MD
Cardiothoracic Imaging & Interventions, Body Division
Department of Radiology
Kaiser Permanente
Anaheim, California

Francesco F. Faletra, MD
Professor of Cardiology
Division of Cardiology
Director of Cardiac Imaging Service
Fondazione Cardiocentro Ticino
Lugano, Switzerland

Cameron Hassani, MD
Associate Clinical Professor
Divisions of Thoracic and Diagnostic Cardiovascular Imaging
Department of Radiological Sciences
Ronald Reagan UCLA Medical Center
Los Angeles, California

Norio Hongo, MD
Department of Radiology
Oita University Hospital
Yufu City, Oita Prefecture, Japan

Hiro Kiyosue, MD, PhD
Associate Professor of Radiology
Department of Radiology
Oita University Hospital
Yufu City, Oita Prefecture, Japan

Meng Law, MD
Professor of Radiology, Neurology, and Neurological Surgery
University of Southern California
Biomedical Engineering
Viterbi School of Engineering
Director of Neuroradiology and the Neuroradiology Fellowship Program
Keck Medicine of USC
Los Angeles, California, USA

Sandy C. Lee, MD
Assistant Professor of Radiology
Department of Radiology
University of Southern California
USC University Hospital
Los Angeles, California

Leah Lin, MD
Assistant Professor of Radiology
Department of Radiology
University of Southern California
USC University Hospital
Los Angeles, California

Miyuki Maruno, MD
Assistant Professor
Department of Radiology
Oita University Hospital
Yufu City, Oita Prefecture, Japan

Shumpei Mori, MD
Associate Professor of Cardiology
Division of Cardiovascular Medicine
Department of Internal Medicine
Kobe University Graduate School of Medicine
Kobe, Hyogo Prefecture, Japan

Horia Muresian, MD, PhD
Cardiovascular Surgery
University Hospital of Bucharest
Bucharest, Romania

Dakshesh B. Patel, MD
Associate Professor of Clinical Radiology
Department of Radiology
University of Southern California
Keck Medicine of USC
Los Angeles, California, USA

Ashley Prosper, MD
Assistant Clinical Professor
Divisions of Thoracic and Diagnostic Cardiovascular Imaging
Department of Radiological Sciences
Ronald Reagan UCLA Medical Center
Los Angeles, California

Damián Sánchez-Quintana, MD, PhD
Professor of Human Anatomy
Faculty of Medicine
Department of Anatomy and Cell Biology
University of Extremadura
Badajoz, Spain

Farhood Saremi, MD
Professor of Radiology and Medicine
Department of Radiology
University of Southern California
Keck Medicine of USC
Los Angeles, California, USA

Diane E. Spicer, BSc
Department of Pediatric Cardiology
University of Florida
Gainesville, Florida, USA
Johns Hopkins All Children's Heart Institute
St. Petersburg, Florida, USA

R. Shane Tubbs, MD
Professor, Chief Scientific Officer, and Vice President
Seattle Science Foundation
Seattle, Washington, USA

1 Thoracic Wall

Farhood Saremi and Damián Sánchez-Quintana

◆ Introduction

The thoracic (chest) wall is composed of the rib cage, inner and outer muscles, vessels, lymphatics, fascia, and skin. The rib cage is formed by the ribs, costal cartilages, sternum, and thoracic vertebrae. The thoracic inlet is the passage of the trachea, aortic arch arteries, major veins, and lymphatics. The outlet of the thorax is covered by the diaphragm. The thoracic wall protects the heart, major vessels, lungs, and part of the liver and spleen. It provides a flexible skeletal framework to promote respiratory movements, stabilize the actions of the diaphragm, shoulders, and arms.[1] The chest also provides attachments for the proper function of the neck, chest, and upper abdomen muscles. Chest wall dysfunction is associated with significant complications and rapid life-threatening consequences. Knowledge of the anatomy and function of the thoracic wall is essential in imaging interpretation of the chest pathologies. This chapter focuses on chest anatomy and function, with emphasis on common anatomical variants and pathologies.

◆ Embryology

The somitic mesoderm gives rise to the osseous parts of the ribs and vertebrae. The lateral plate mesoderm is where the sternum and appendicular (limb) skeleton develop whereas the cranial neural crest forms the branchial arch, craniofacial bones, and cartilage.[2]

Ossification of the mesoderm occurs in two forms. In the first form, ossification occurs directly within preexisting mesenchymal tissue. This type of ossification is called intramembranous which is common in flat bones (e.g., skull). In the second form, the mesenchymal progenitor cells differentiate into the chondrocytes that form hyaline cartilage and ossification occurs within hyaline cartilage. The second type is called endochondral ossification.

The rib primordium is identifiable in the fifth week of development (▶ Fig. 1.1). These primordial ribs are aligned ventrolaterally, next to the intervertebral disks, into the hypaxial muscle anlagen. The first seven to eight ribs increase in length, while the length of the last four ribs will be progressively shorter from cranial to caudal. By the seventh week, the first eight ribs bend toward the sternal anlagen. The primary rib ossification center is located near the angle of the ribs and mostly become cartilaginous during weeks 13 to 14 of development and later become ossified. At birth most ribs are ossified. Secondary rib ossification centers appear later at puberty. The ventral ends of the ribs remain cartilaginous, the so-called “costal cartilage.” Later in life partial calcification of the costal cartilages is a universal finding.

The sternal primordium is first identifiable at 6.5 weeks of development as three mesenchymal condensations; a single median center known as “presternal” and a pair of lateral centers known as “sternal bars.”

The presternal condensation forms the sternal manubrium in the seventh week which extends to the second rib in the eighth week. At the seventh week, the paired sternal bars move from the lateral to the inferior aspect of the manubrial primordium. By eight weeks, the sternal bars extend to the level of the seventh rib and begin to align with the manubrium and fuse with each other. The medial fusion of the sternal bars continues to the level of the fifth rib in the ninth week but remains bifid more caudally until fusion is complete in the 10th week to form the cartilaginous sternum. Sternal ossification centers appear from superior to inferior direction before birth except in the xiphoid process which appears during childhood (▶ Fig. 1.2). In the neonate, the manubrium contains one main ossification center. Ossification of the body of the sternum occurs shortly after birth. The number and position of ossification centers vary. By the end of the first year, most individuals have three to four center of ossifications in the sternal body separated from each other by cartilaginous bands (▶ Fig. 1.2). These bands are connected to the end of the costal cartilages. Union of the bands begins at about puberty and continues to the age of 25 craniocaudally (▶ Fig. 1.2, ▶ Fig. 1.3). The xiphoid process may remain ununited in some individuals.

All muscles develop from the somitic dermomyotomes. Muscles of the chest and abdominal wall are grouped into the hypaxial (ventral group) and epaxial (dorsal group) muscles based on their different innervations by the ventral and dorsal rami, respectively. At 5 weeks of development, separate epaxial and hypaxial myotomal compartments with separate dorsal and ventral spinal nerves will become identifiable (▶ Fig. 1.1).

The muscle cells of the ventral body wall develop from the hypaxial half of the dermomyotome and are innervated by the ventral branch of the spinal nerves. The differentiation of the single band of hypaxial muscle into separate layers will be apparent at the end of the sixth week. At this time the external oblique, internal oblique, transverse abdominal, and rectus abdominal muscles will differentiate. The intercostal and all abdominal wall muscles become identifiable as separate entities from the common myotomal band at 6 to 6.5 weeks of development. The epaxial myotomal compartment will form the paraspinal muscles.

◆ Bony Thorax

The thoracic skeleton is an osteocartilaginous framework that surrounds and protects the thoracic viscera and supports the mechanical function of ventilation. The bony thorax is formed by the sternum anteriorly and the thoracic vertebrae posteriorly, interconnected by the 12 paired ribs and their costal cartilages[3,4,5,6] (▶ Fig. 1.2, ▶ Fig. 1.3, ▶ Fig. 1.4).

Ribs

The upper seven ribs directly articulate to the sternum by costal cartilages. These first seven ribs are called true ribs. In contrast, the costal cartilages of the 8th, 9th, and 10th ribs connect to each other and with the 7th costal cartilage. These ribs are called false ribs. The 11th and 12th ribs are called floating because they have

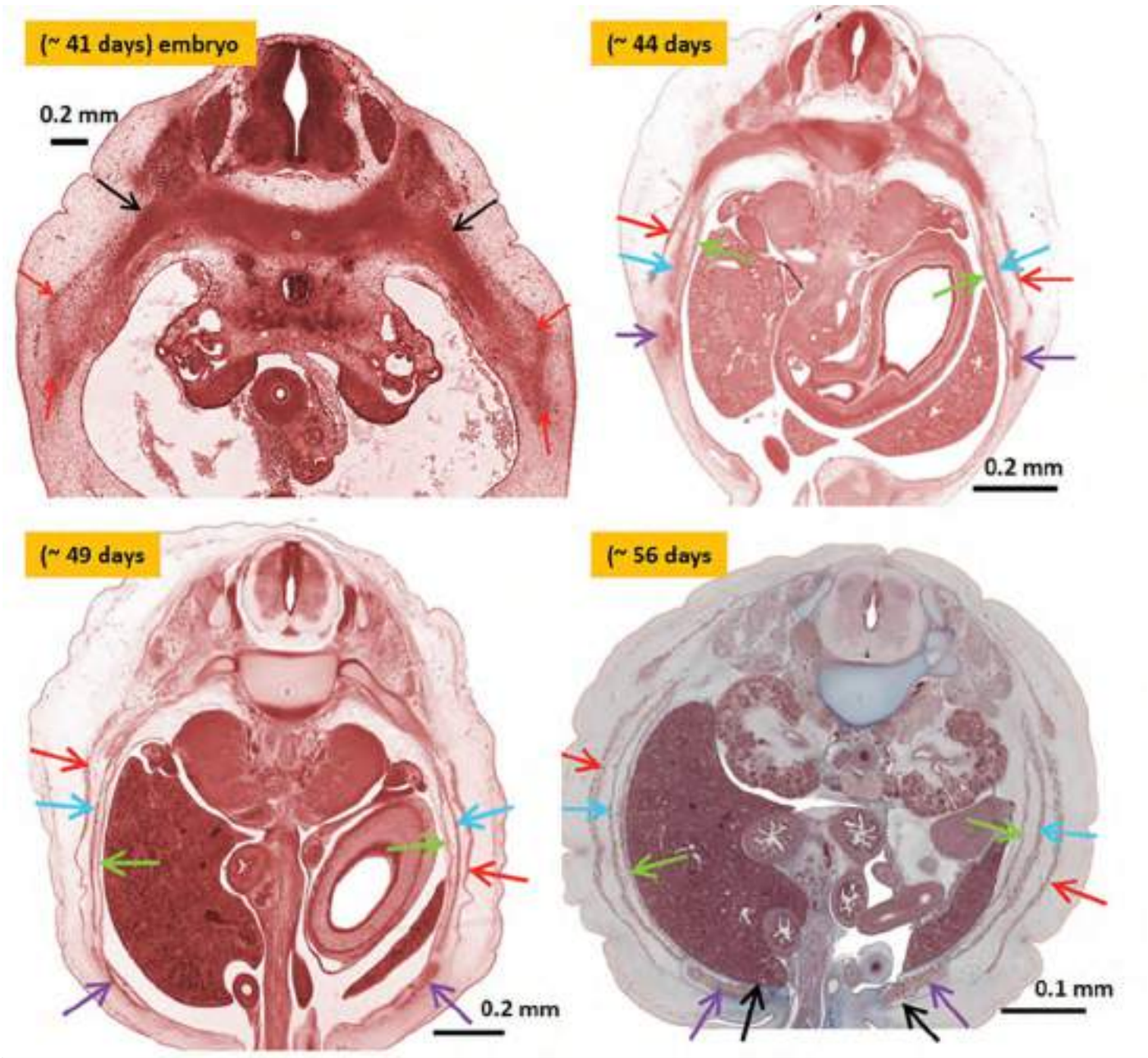

Fig. 1.1 Bones and hypaxial muscles of the ventral body wall. Carmine-stained (41–49 days) and azan-stained (56 days) histological sections of the embryo are shown. At 41 days, the muscular mass (*red arrows*) and the ribs (*black arrows*) can be distinguished. After 44 days, the abdominal wall muscles are distinguished: green, transverse abdominal; cyan, internal oblique; red, external oblique; purple, abdominal rectus muscle. The sheath of the rectus muscle is readily visible at 56 days section (*black arrow*). Used with permission from Mekonen et al 2015.[2]

no anterior attachment. Each rib consists of a head, a neck, a shaft, and a costal cartilage (▶ Fig. 1.5). The head and neck are close to the spine. At costovertebral junctions, the rib's head is articulated by two synovial demifacet joints to the posterolateral aspect of two vertebral bodies at the intervertebral disks (▶ Fig. 1.5). The inferior rib facet is joined with vertebral body at the same number. Exceptions are the first, 11th, and 12th ribs in which there is a single articular facet (▶ Fig. 1.6). The 10th rib is sometimes floating with a single costovertebral facet. The costovertebral junctions are covered with a capsule and reinforced by the radiate ligament (▶ Fig. 1.5).

The neck of the rib spans between the head and the tubercle. The neck of the rib, at its distal end where the rib tubercle is located, articulates with the transverse process of the numerically corresponding vertebra (▶ Fig. 1.5; ▶ Fig. 1.6). The costotransverse joint is a synovial joint covered with a capsule and

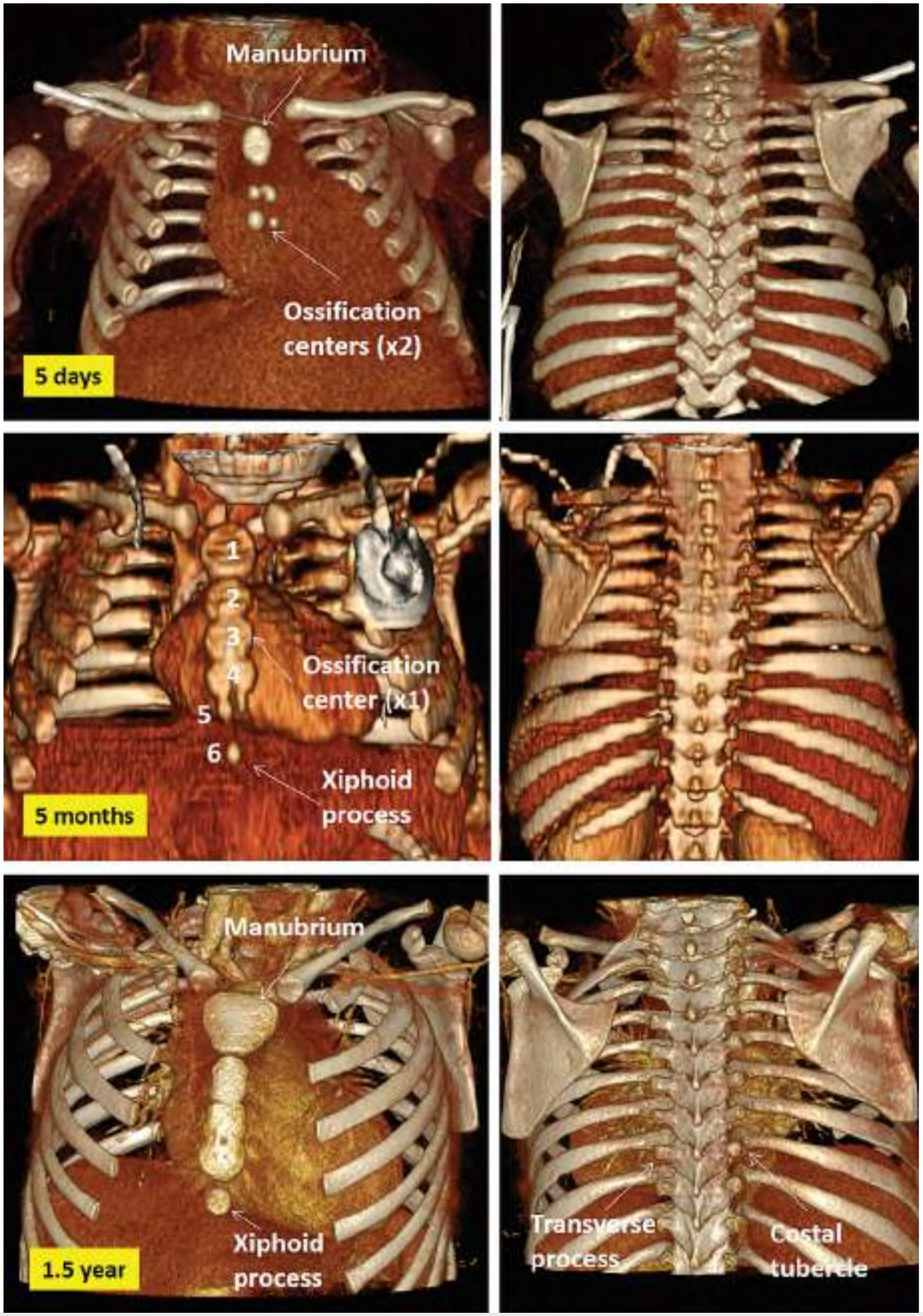

Fig. 1.2 Anterior and posterior views of the chest at three ages are shown. Note that the inferior thoracic aperture is relatively wide in early life. Sternal ossification centers appear from superior to inferior direction before birth except in the xiphoid process which appears during childhood. Ossification of the body of the sternum occurs shortly after birth. The manubrium contains one main ossification center. The number and position of ossification centers of the sternal body vary. In this case, at day 5 of life, two ossification centers exist at each level. Also, note that costotransverse joints are not well developed and spinous processes are not fused in midline. By the end of the first year, most individuals have three to four centers of ossification in the sternal body separated from each other by cartilaginous bands. These bands are connected to the end of the costal cartilages. Osseous union of the band begins at about puberty. The xiphoid process may ununited in some individuals. A sternal hole is seen in the 1.5-year-old patient.

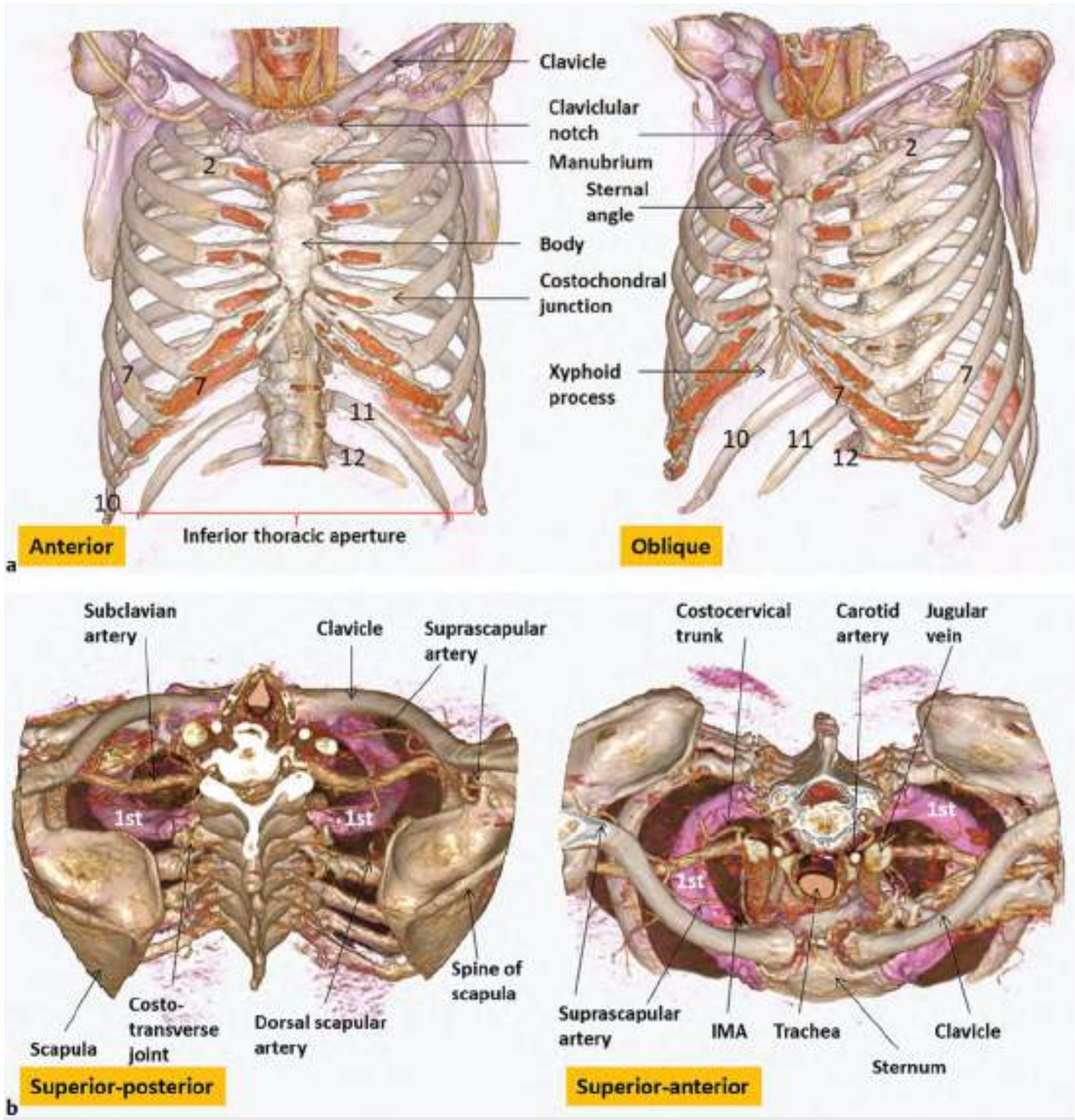

Fig. 1.3 **(a)** Volume-rendered computed tomography (CT) shows bony thorax in an adult. The thorax appears barrel-shaped. The costal cartilages are partially calcified. The xiphoid is ossified but remains unfused. The upper seven ribs directly articulate to the sternum by costal cartilages. The costal cartilages of the 8th, 9th, and 10th ribs connect with the 7th. The 11th and 12th ribs remain floating. **(b)** Superior views demonstrate the structures of the thoracic inlet. The first ribs are colored in red. IMA, internal mammary artery.

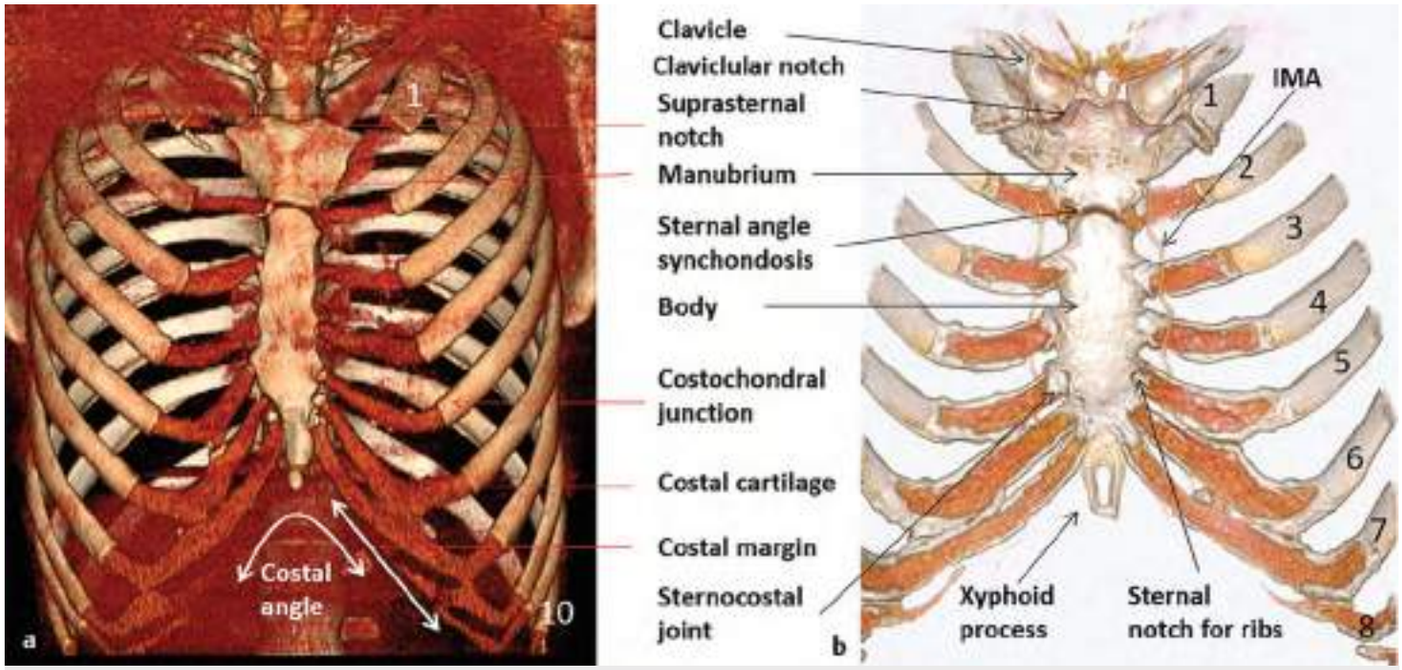

Fig. 1.4 Costal cartilages. **(a)** Noncalcified. **(b)** Partially calcified (tramline). The sternum consists of the manubrium, body, and xiphoid process.

strengthened by the costotransverse ligament complex (▶ Fig. 1.5). It is absent at the 10th,11th, and 12th ribs. The costotransverse ligament complex consists of the main costotransverse ligament, lateral costotransverse ligament, and superior costotransverse ligament (▶ Fig. 1.5). Other associated ligaments include ligament of the neck of the rib, ligament of tubercle of the rib, and an accessory ligament (▶ Fig. 1.5).

Secondary ossification centers appear for the head and tubercle of the rib at puberty. The 11th and 12th ribs have no necks or tubercles. The shaft of the rib starts distally to the costotransverse joint. The ribs curve and slope inferiorly such that their sternal ends and the costal cartilages are more caudal than their dorsal ends. The ribs are connected with each other by the intercostal muscles. Intercostal vessels and nerves run in the intercostal spaces. The first rib is an important rib that protects the thoracic inlet structures (▶ Fig. 1.3). The first rib is the shortest, broadest, and most curved of all ribs with no significant move during quiet respiration. From anterior to posterior the following muscles attach to the first rib; the subclavius, anterior scalene, first digitation of the serratus anterior, and middle scalene (▶ Fig. 1.7). The serratus anterior, serratus posterior superior, and posterior scalene muscles attach to the second rib. The longissimus and iliocostalis muscles attach to the posterior ribs. The iliocostalis muscles attach to the rib angle where rib starts to bend and the longissimus muscles attach between the tubercle and angle.

The rib cage morphology changes with age and sex. At birth, ribs are oriented horizontally but gradually become sloped. From birth through adolescence, the rib cage increases in size and ribs move inferiorly (▶ Fig. 1.2, ▶ Fig. 1.3). There is also a decrease in thoracic kyphosis. From young adulthood into elderly age, there will be increasing kyphosis and more horizontal course of the ribs relative to the spine.[7] Additional age-related increase size of the upper thorax is seen compared to the lower thorax. This transforms the pyramidal infant thorax into the barrel-shaped one of adults[8] (▶ Fig. 1.3).

Sternum

The sternum is a flat bone that connects the ribs anteriorly via chondral tissue. The sternum consists of three regions: the manubrium, body, and xiphoid process (▶ Fig. 1.4). In the adult, it measures approximately 15 to 20 cm in length. The superior margin of the manubrium connects to the clavicles via the right and left clavicular notches at each corner. The sternoclavicular joints are diarthrotic synovial joints with an articular fibrocartilage disc in between (similar to the temporomandibular joint) (▶ Fig. 1.8). Each joint is covered by the anterior and posterior sternoclavicular ligaments. The sternocleidomastoid muscles attach to the superior margin of the sternum. The notch between the attachments of the sternocleidomastoid muscles is called suprasternal notch (▶ Fig. 1.4). Above the suprasternal notch, the interclavicular ligament connects the two clavicular heads. Laterally, the manubrium is attached to the first rib. The costal cartilage of the

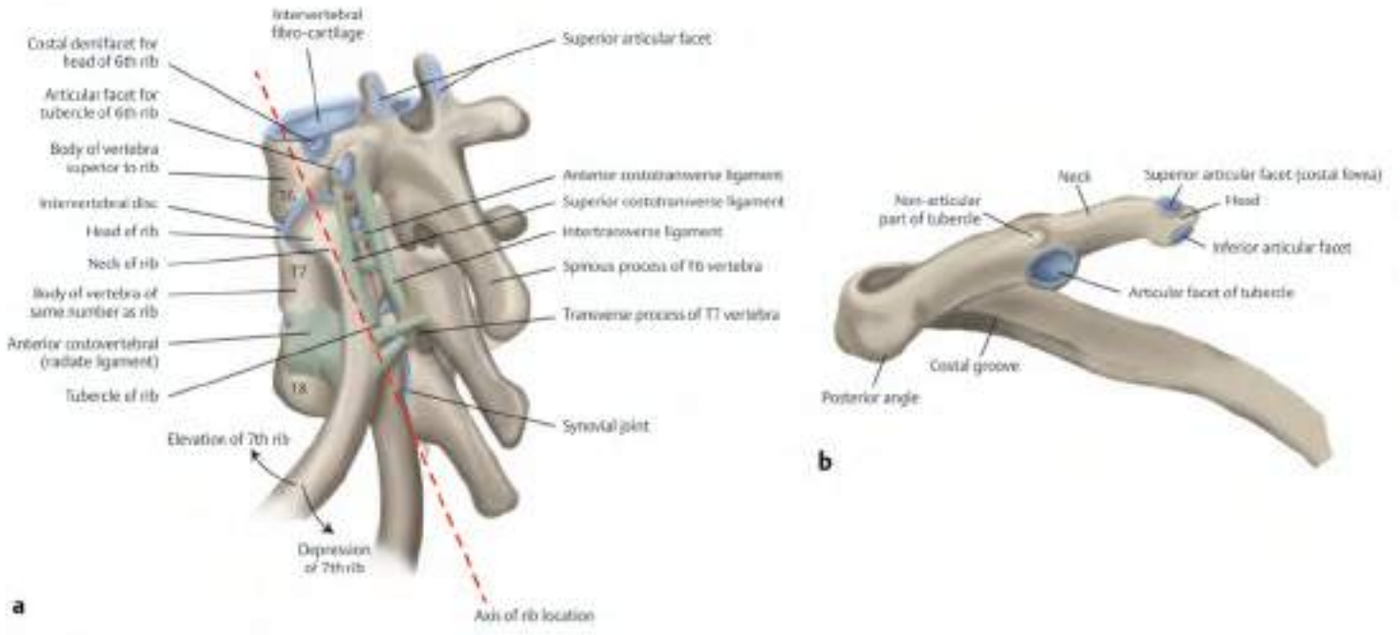

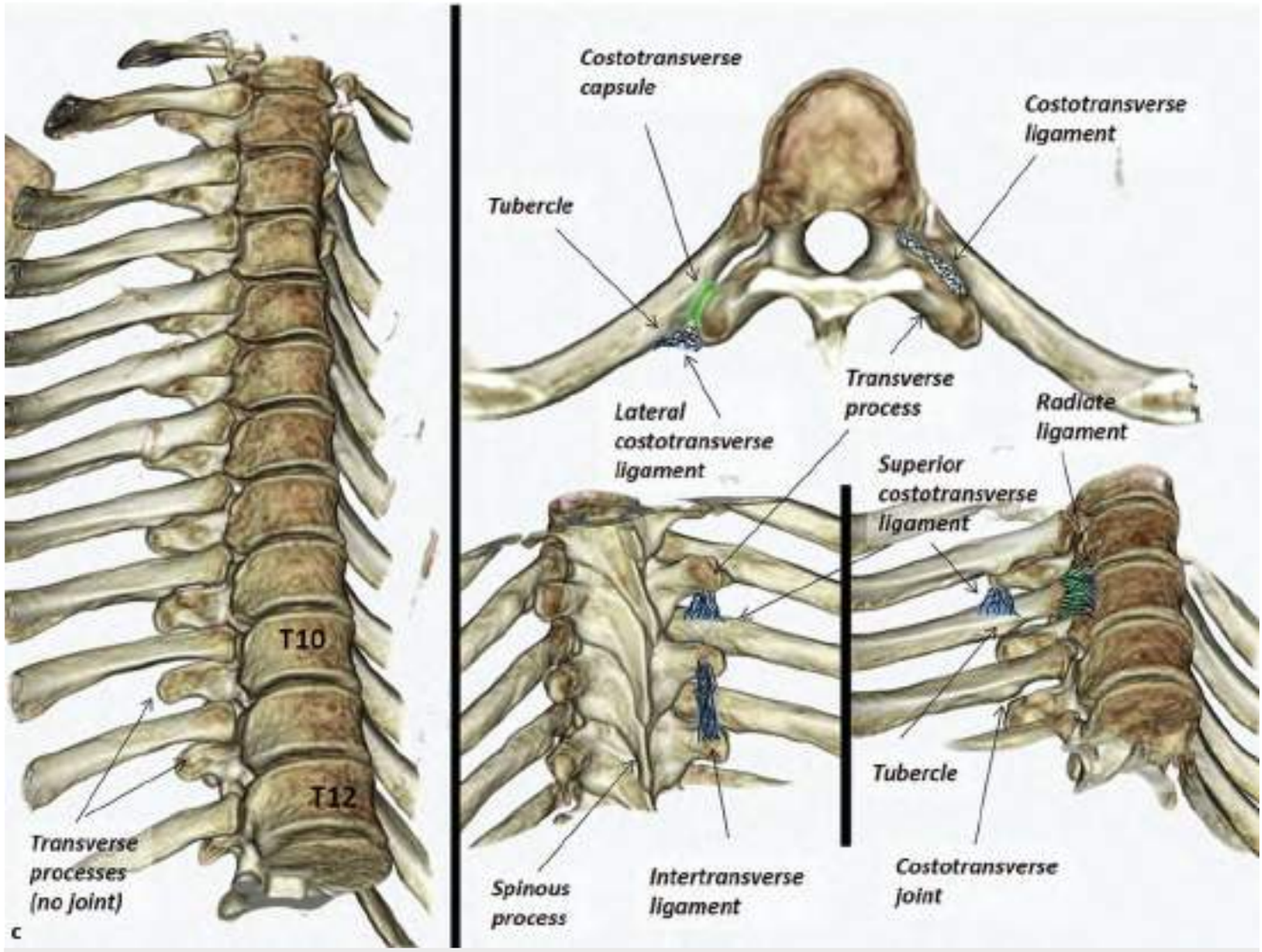

Fig. 1.5 (a–c) Components, articular surfaces, and ligaments of the ribs. The costovertebral junctions are reinforced by the radiate ligament. The costotransverse ligament complex consists of the main costotransverse ligament, lateral costotransverse ligament, and superior costotransverse ligament. It is absent at the 10th, 11th, and 12th rib.

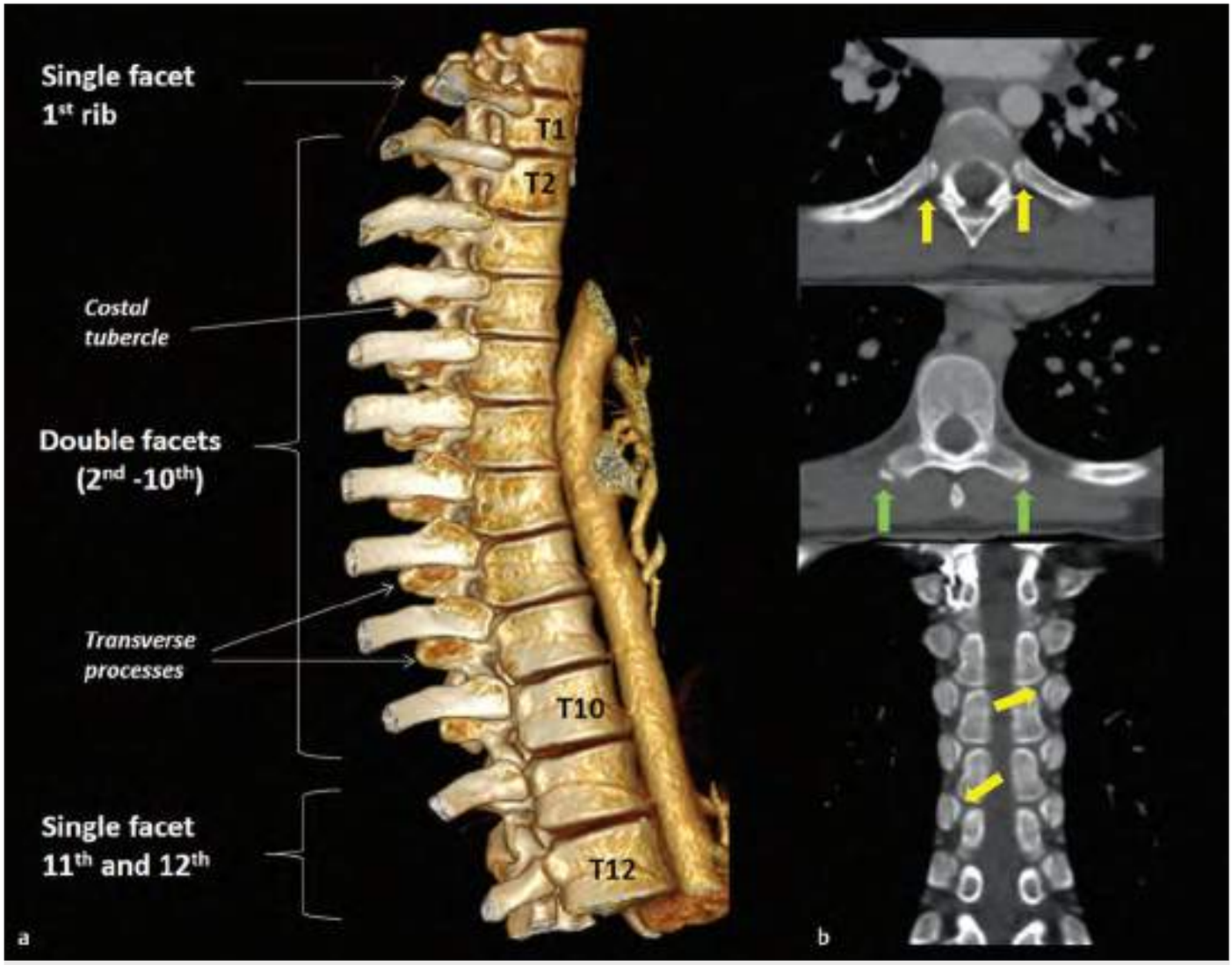

Fig. 1.6 **(a)** At the 2nd through the 10th costovertebral junctions, the rib's head is articulated by two synovial demi facet joints to the posterolateral aspect of two vertebral bodies at intervertebral disks. The inferior rib facet is joined with the vertebral body at the same number. Exceptions are the first, 11th, and 12th ribs and in some cases 10th rib in which there is a single articular facet. **(b)** Incomplete fusion of ossified secondary ossification centers of the medial ribs (*yellow arrows*) and thoracic transverse processes (*green arrow*).

second rib is attached to the junction of the manubrium and body of the sternum (▶ Fig. 1.4). The sternothyroid and sternohyoid muscles attach to the posterior manubrium (▶ Fig. 1.8).

The anterolateral aspect of the body sternum is attached to the pectoralis major muscle. The superior and inferior sternopericardial ligaments attach to the posterior wall of the manubrium and xiphoid process, respectively (▶ Fig. 1.9). On either side of the posterior sternum, the transversus thoracis muscles take origin.

There are six notches on each side of the sternal body which receive the cartilages of the second through seventh ribs. The superior margin of the body forms a bony ridge which is called the sternal angle of Louis (▶ Fig. 1.4). This anatomical landmark corresponds with T3/T4 posteriorly (▶ Fig. 1.10). The tracheal bifurcation is usually located below the sternal angle. The joint between the manubrium and the body at the sternal angle allows the sternal body to move anteriorly. The xiphoid process varies in shape and length in different individuals. The seventh costal cartilages also articulate with the anterior or anterolateral portion of the xiphoid process.

The female adult sternum is located lower compared to the male sternum.[8] Compared to female, the body of the male sternum is usually twice as long as the manubrium.[9]

The dominant blood supply to the sternum is provided by the internal mammary (thoracic) arteries that interconnect with the posterior intercostals, lateral thoracic, and transverse cervical arteries.

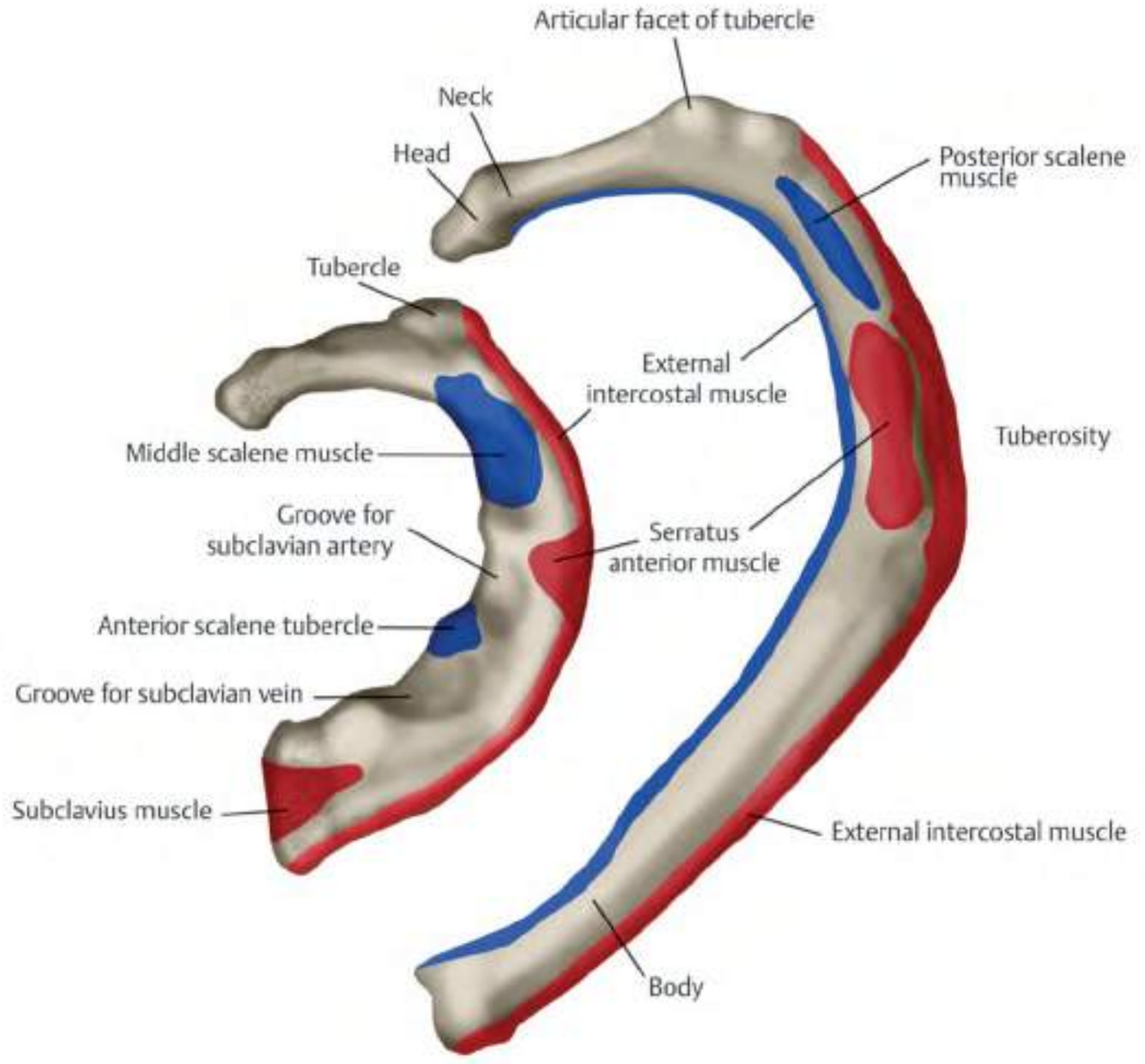

Fig. 1.7 Muscle attachments to the superior aspect of the first and second ribs.

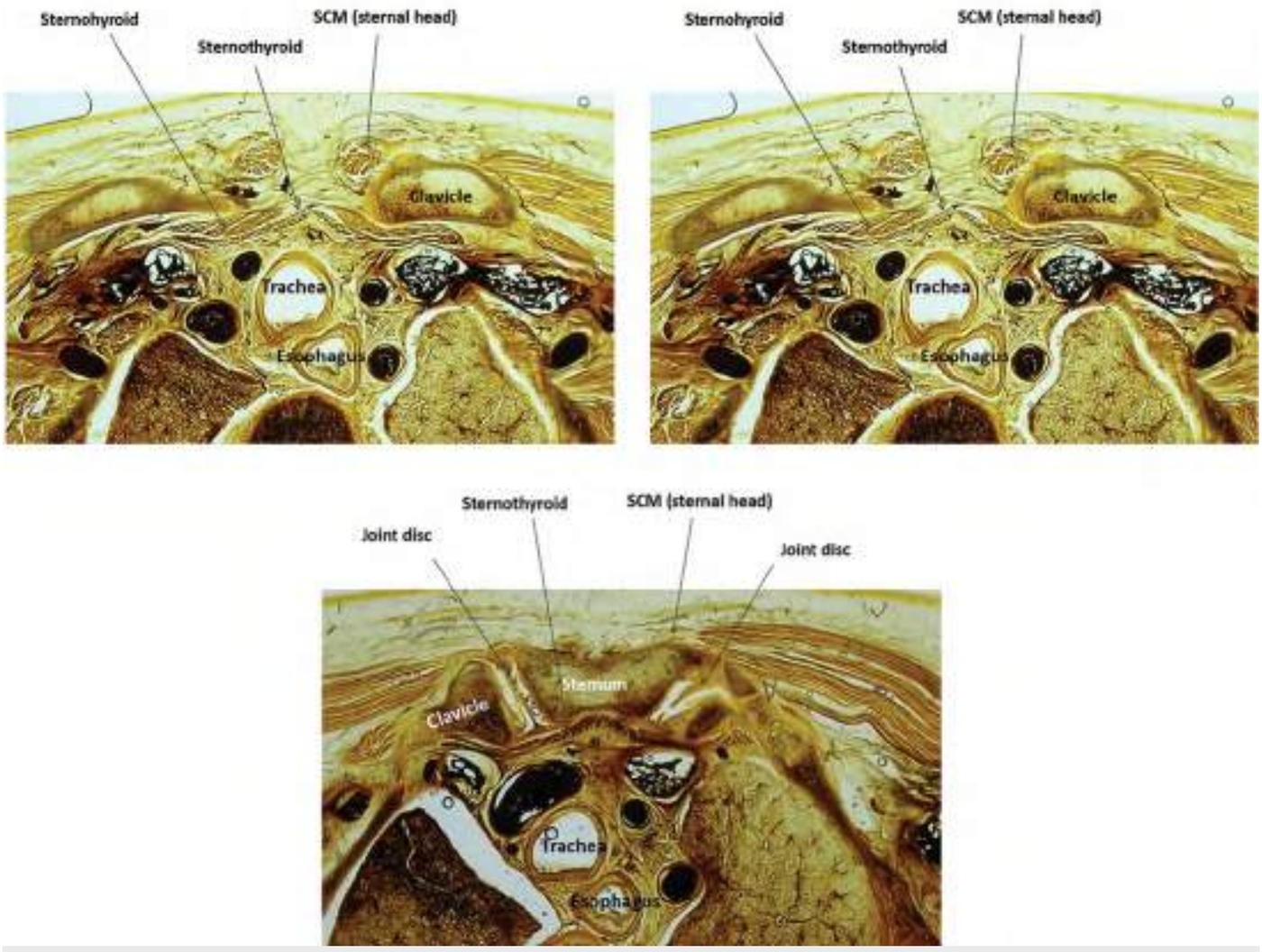

Fig. 1.8 Sternocleidomastoid (SCM), sternothyroid, and sternohyoid muscles attaching to the sternum. The sternal head of the SCM is tendinous and arises from the anterior surface of the manubrium. The sternothyroid and sternohyoid muscles attach to the posterior manubrium. The sternoclavicular joints of their respective disks are clearly shown.

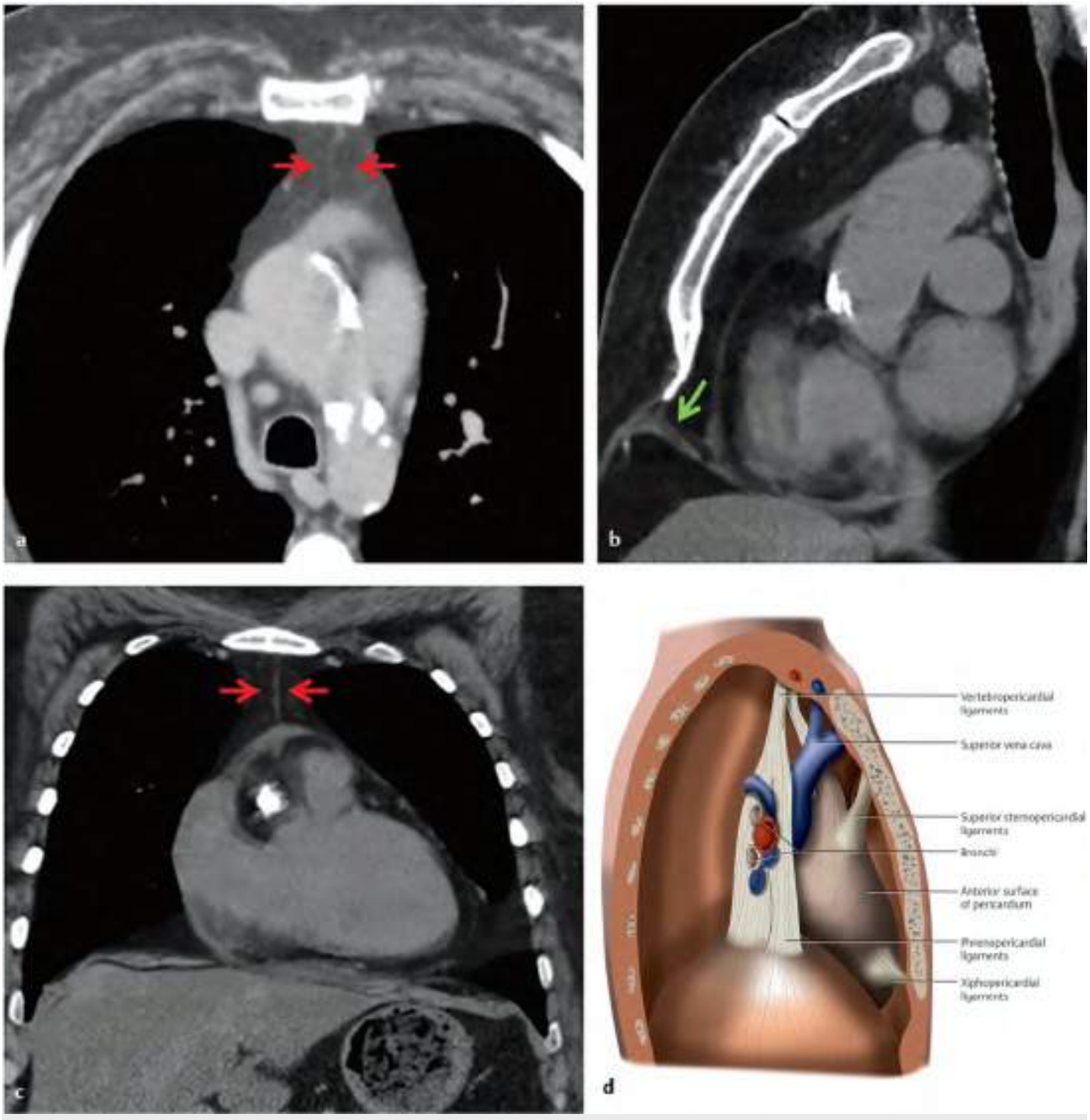

Fig. 1.9 (a–d) Sternopericardial ligaments. The superior (*red arrows*) and inferior (*green arrow*) sternopericardial ligaments attach to the posterior wall of the manubrium and xiphoid process, respectively.

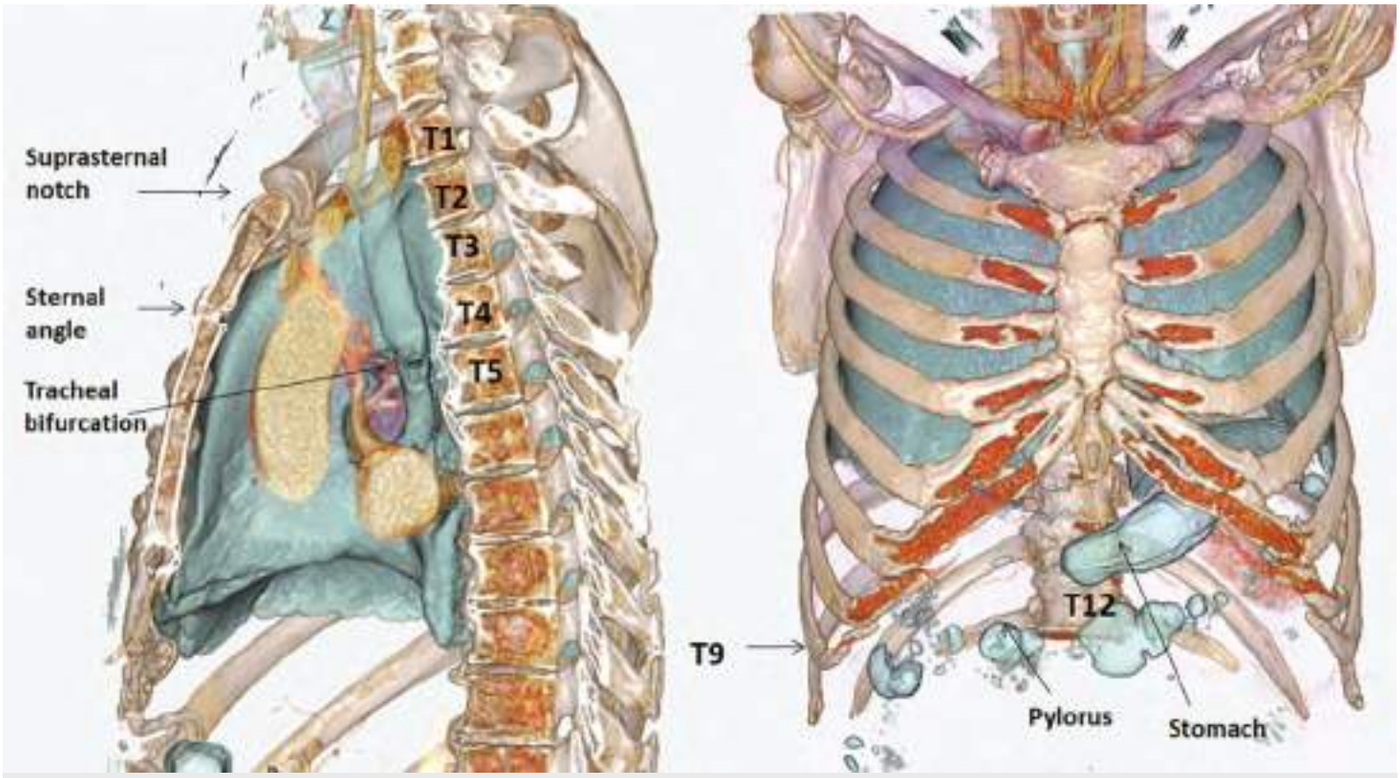

Fig. 1.10 The sternal angle of Louis corresponds with T3/T4 posteriorly. The tracheal bifurcation is usually located below the sternal angle at T4/T5. The inferolateral margin of the ninth rib is at the level of the first lumbar vertebra and the pylorus.

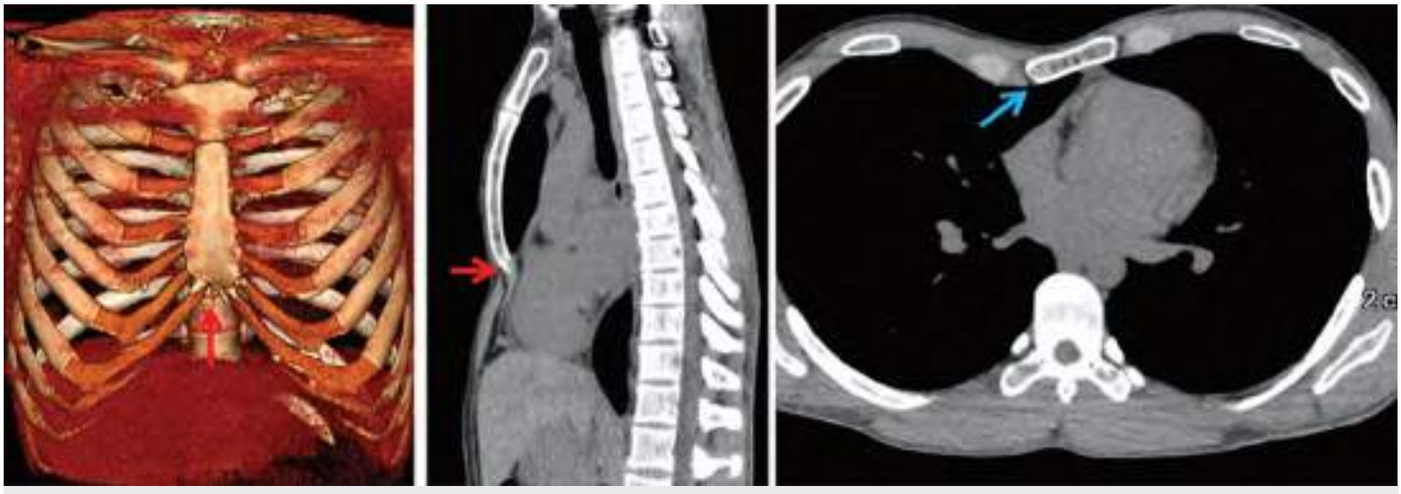

Fig. 1.11 Mild pectus excavatum (*red arrow*) and tilted sternum (*blue arrow*) are common chest variants.

◆ Anatomical Variations of the Bones

Minor variations of the anterior chest wall is common and can be seen in 30% of children and adults.[10] These variations include tilted sternum, prominent convexity of the anterior ribs and costal cartilages, mild pectus excavatum, and mild pectus carinatum (▶ Fig. 1.11).

There are various types of anomalies and deformities of the ribs. Common variants include developmental fusion of two or more ribs, articulation or bridge formation between two ribs, bifid rib (forked rib), and short rib. These morphological anomalies may have a sex predilection, and occur more frequently on the right side than on the left side.[3]

In a bifid rib, the distal end of the rib appears bifurcated (▶ Fig. 1.12**a**). The distal end may remain unfused or form a rounded hole or an elongated fissure.[11] The defect is filled with muscles which is supplied by a branch from the intercostal artery of the rib above it. The intercostal nerves may run on both sides of the rib defect. Bifid ribs are more common in males than females and occur most frequently in the third and fourth ribs. An intrathoracic rib is a rare type of bifid rib in which a supernumerary rib, arises from a rib or vertebral body[12] (▶ Fig. 1.12**b**; ▶ Fig. 1.13).

A cervical rib is a supernumerary or accessory rib arising from the seventh cervical vertebra on one or both sides. It may

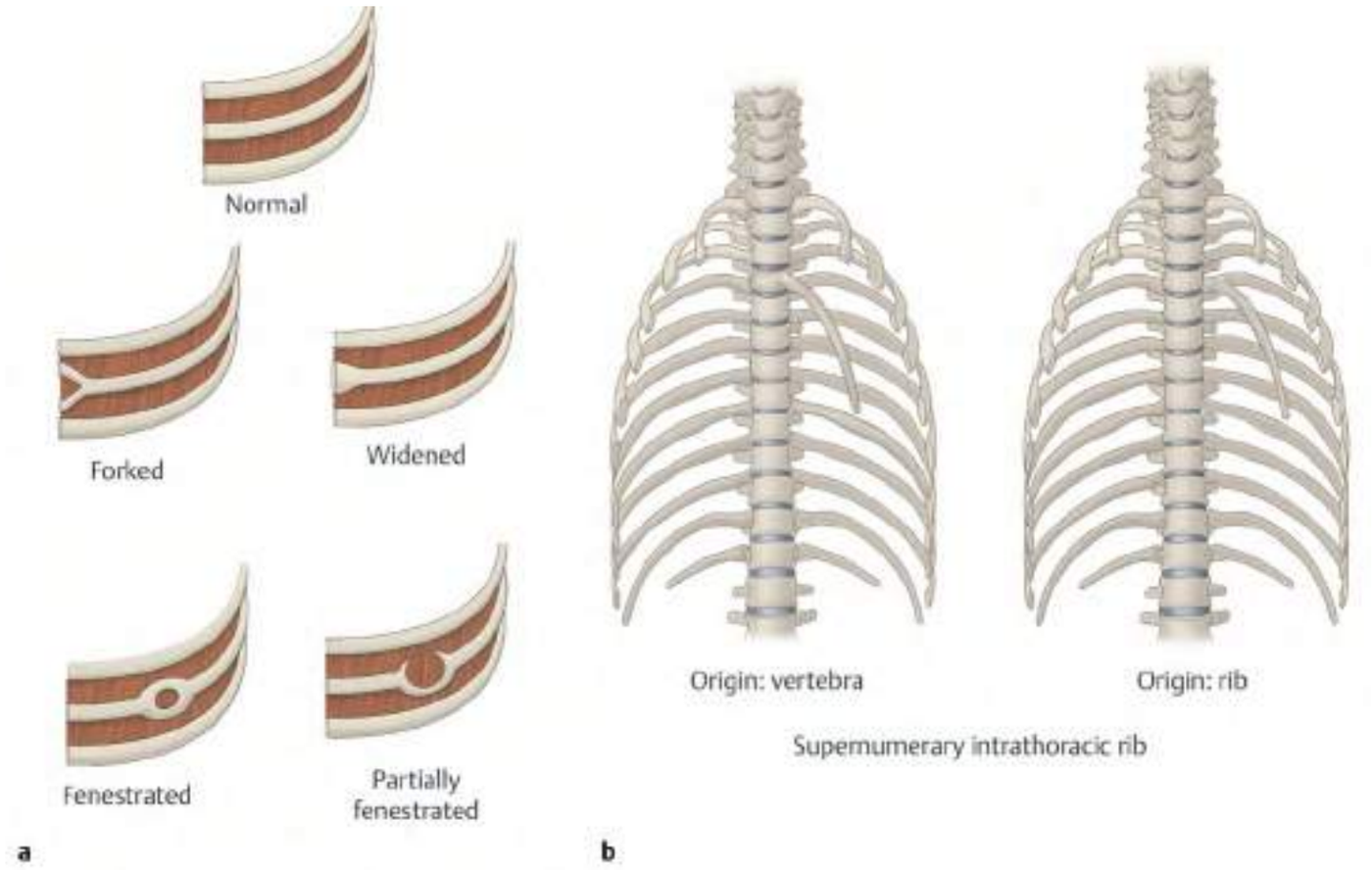

Fig. 1.12 **(a)** Developmental abnormalities of ribs. **(b)** Supernumerary intrathoracic rib. Used with permission from Song et al 2009[11] and Kamano et al 2006.[12]

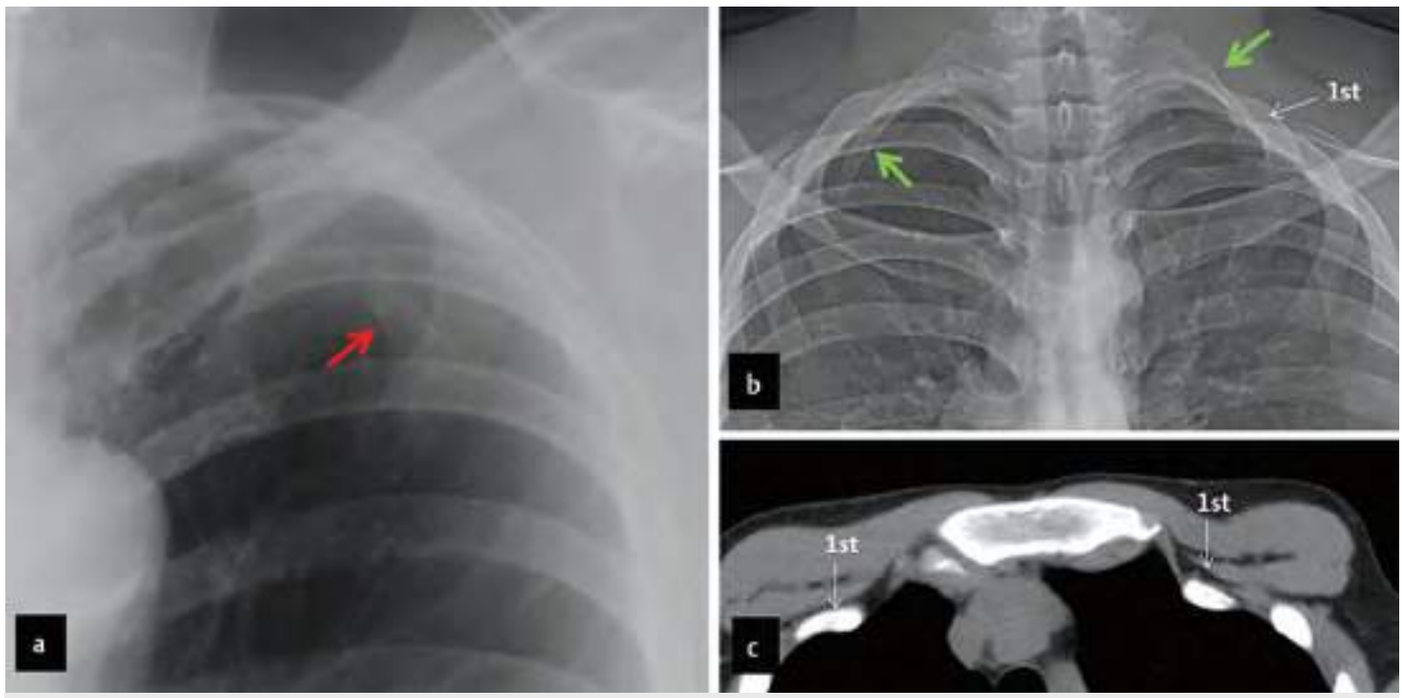

Fig. 1.13 Anatomical variants of the bony chest wall. **(a)** Supernumerary intrathoracic rib (*arrow*). **(b)** Bilateral cervical ribs (*arrows*). On the left side, it has formed a pseudoarticulation with the first rib. **(c)** Note short first ribs on CT of the same patient.

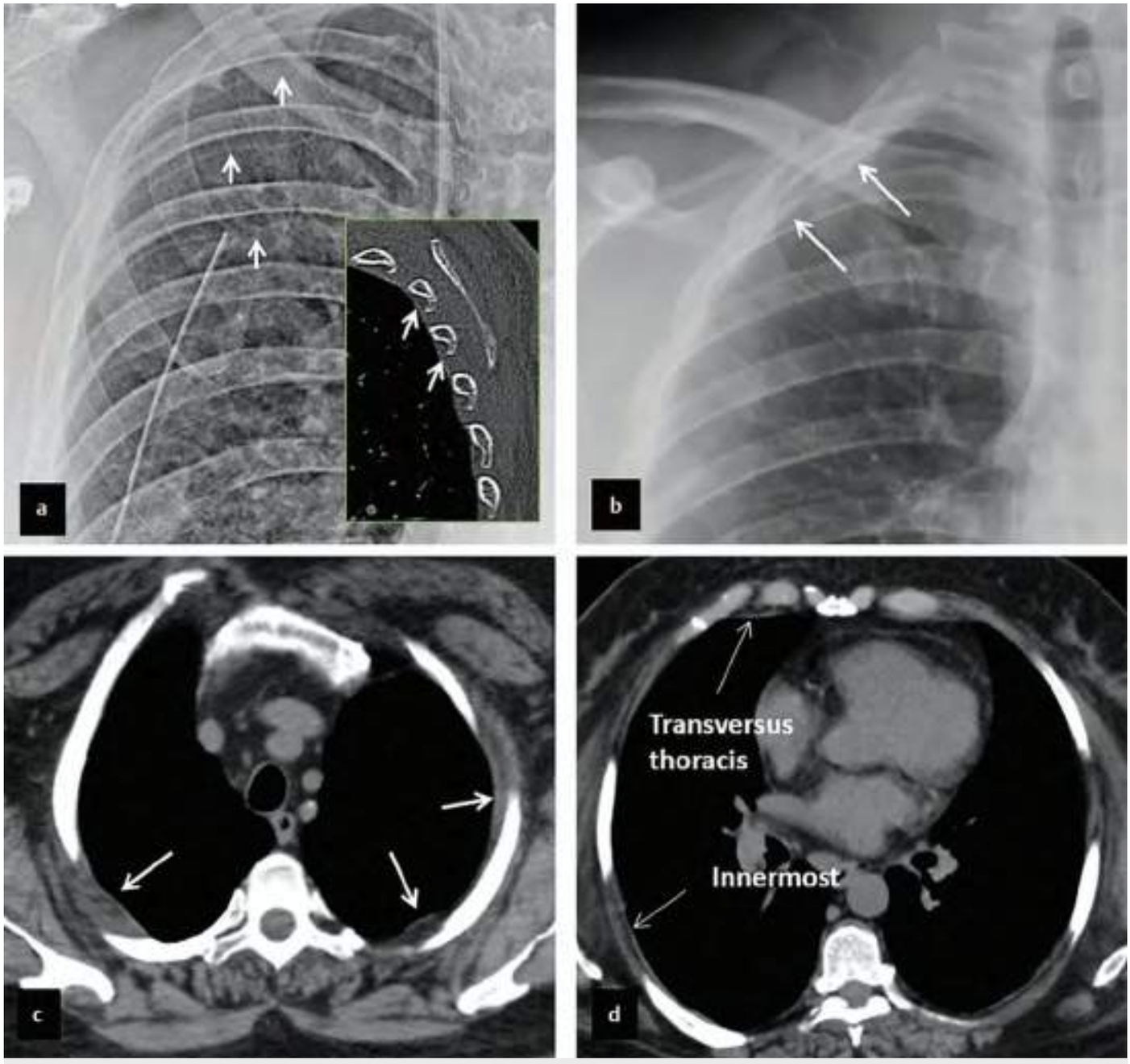

Fig. 1.14 **(a)** Bony edge of the costal groove is seen as a thin, sharp hairline along the inferior margin of the ribs (*arrows*). Soft companion shadows represent extrapleural fat and muscle. **(b)** Posteroanterior chest radiograph shows rib companion shadows projecting adjacent to the inferior and inferolateral margins of the ribs (*arrows*). **(c, d)** Companion shadow is shown on CT (*arrows*), representing the extrapleural fat and the innermost and subcostalis muscles.

articulate to the first rib or end freely. It is seen in less than 1% of the population and is more common in females with slight predominance on the left side[13] (▶ Fig. 1.13). They are most commonly an incidental finding or are associated with the Klippel–Feil anomaly. The cervical is commonly associated with sacralization of the L5 lumbar spine.[14] The cervical rib can cause thoracic outlet syndrome by compression of the brachial plexus or subclavian artery between the cervical rib posteriorly, the anterior scalene anteriorly, and the first rib inferiorly. A lumbar rib is another anatomical variant manifested as a rudimentary or extra rib arising in the lumbar region. It is seen in roughly 1% of the population.[15] A lumbar rib is shorter than the 12th thoracic rib and its course tends to be more horizontal. Both cervical and lumbar ribs manifest an exaggerated development of the transverse process.

Eleven pairs of ribs occur in 5 to 8% of normal individuals and in one-third of patients with trisomy 21 syndrome.[16]

On frontal chest radiographs, it is common to see a thin, smooth, soft tissue density parallel the lower margins of the first and second ribs and the axillary portions of the lower ribs (▶ Fig. 1.14). These companion shadows represent the fat and muscles located in the intercostal spaces and should not be mistaken with pleural thickening or pneumothorax. The bony edge of the costal groove is seen as a thin, sharp hairline along the inferior margin of the ribs on frontal chest X-rays and should not be confused with a pneumothorax (▶ Fig. 1.14**a**). Postoperative

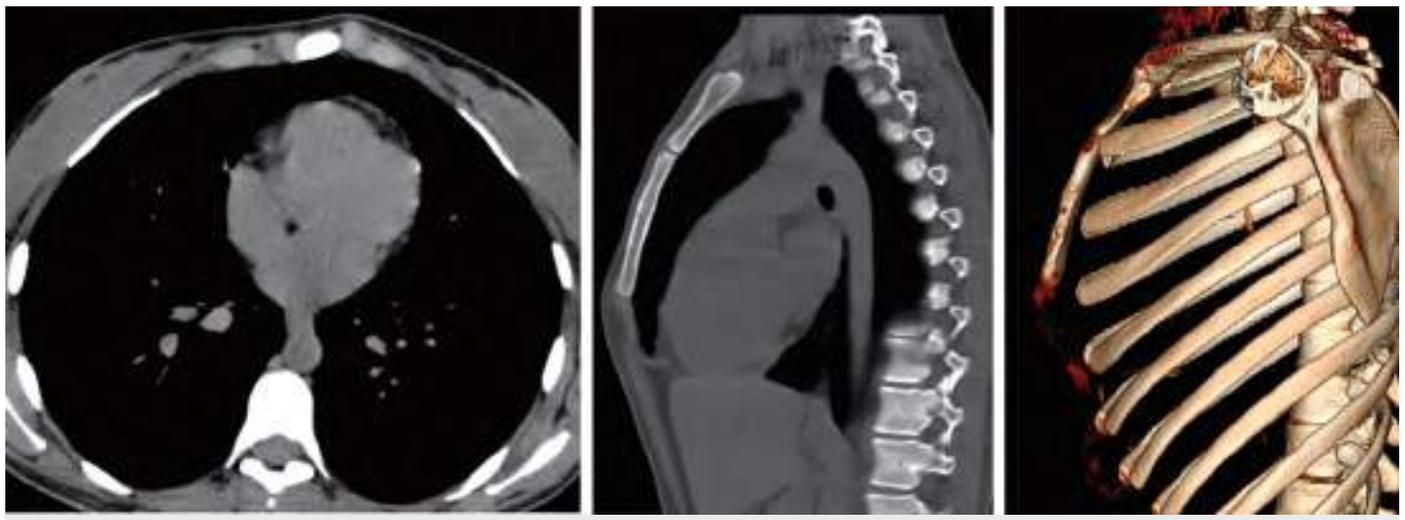

Fig. 1.15 A 15-years-old adolescent girl with pectus carinatum. In pectus carinatum, the lengths of costal cartilage are longer than usual.

changes of the chest wall such as sternal wires, partial rib resection, and partial fusion of the ribs are common imaging findings.

Anatomical variation of the sternum is also common. If the fusion of the sternal bars is incomplete, a vertical fissure or perforation may be present in the sternum. The sternal foramen is a common asymptomatic developmental defect (▶ Fig. 1.2). It is probably due to incomplete fusion of the third and fourth ossification centers. The awareness of this anomaly is important in acupuncture practice. Cleft (bifid) sternum is a rare congenital defect due to failed midline fusion of the sternum. The cleft may be complete and incomplete.[17] Association with pectus excavatum, craniofacial hemangiomas, diastasis of the abdominal rectus muscles, and omphalocele is common.[18]

Pectus Excavatum and Pectus Carinatum

Chest deformities are among the most common congenital anomalies. Pectus excavatum or funnel chest is the most common chest wall malformation occurring in approximately 1 out of every 500 live births (▶ Fig. 1.11). Pectus carinatum appears to be two to four times less frequent than pectus excavatum (▶ Fig. 1.15). The etiology is probably due to an imbalance growth of costal cartilage and ribs.[19] Both malformations can be present at birth but is usually recognized only during early childhood. Men are involved four times more often than women.[20]

It is usually seen as an isolated congenital abnormality. However, it is occasionally associated with cardiac abnormalities, such as Marfan's, Noonan's, and Turner's syndromes.[21] In pectus excavatum, there is a depression of the anterior chest wall as a result of dorsal deviation of the sternum and the third to seventh rib or costal cartilage.[21] There are characteristic findings on frontal chest radiography, including an indistinct border of the right side of the heart, left ward shift of the heart, and downward angulation of the anterior portions of the ribs. Computed tomography (CT) scan is the best technique to show the anomaly (▶ Fig. 1.16). Pulmonary or cardiac compression can result in restrictive lung disease and decreased right ventricle function (▶ Fig. 1.16).

Pectus carinatum presents by a protrusion of the sternum and ribs (▶ Fig. 1.16). In pectus carinatum, the lengths of costal cartilage are longer than usual so the ribs appear shorter.[19] The anomaly is usually asymptomatic and isolated but other diseases including scoliosis, Marfan's syndrome, Morquio syndrome, or Poland's anomaly may be found. Anomalously widened sternum with severe anterior angulation is rarely seen (▶ Fig. 1.17).

◆ Chest Wall Pathologies

Plain radiographs are often used to evaluate chest wall pathologies. Cross-sectional techniques such as CT, sonography, and magnetic resonance imaging (MRI) have been shown to be more useful in the evaluation of muscle and soft tissue (▶ Fig. 1.18).

Rib asymmetry is an associated finding with scoliosis. Ribs on one side may be shorter. Most people with mild scoliosis demonstrate no rib asymmetry.[22]

Chest wall pain after trauma can be due to a variety of factors, including osseous injuries such as fractures, injuries to the soft tissues such as muscle contusion or tears, and, less commonly, injury to the costal cartilage. Osseous injury involving the ribs and sternum is common. In a radiological assessment of the chest wall with CT scan attention to associated vascular and soft tissue injuries is of utmost importance. In fracture of the first and second ribs and the sternum attention to vascular injury is important. Fractures of the anterior ribs and even the sternum are common findings after vigorous cardiopulmonary resuscitation. Fracture of the left lower ribs may be associated with the spleen and left kidney injury and fractures of the rib necks can be a sign of spinal fracture.

The costal cartilage injury is best shown by MRI using fat-saturated T2-weighted imaging.[23,24] The most frequently injured

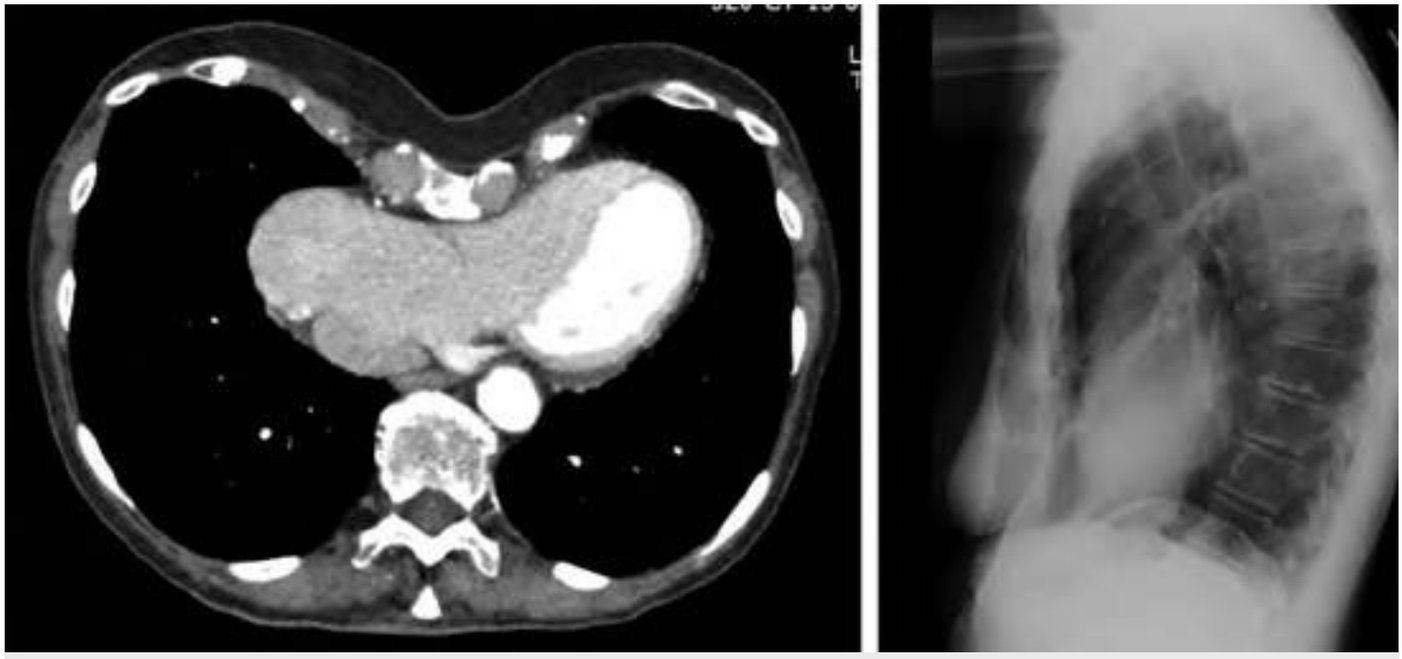

Fig. 1.16 Severe pectus excavatum. Note compression deformity of the heart between the sternum and thoracic spine.

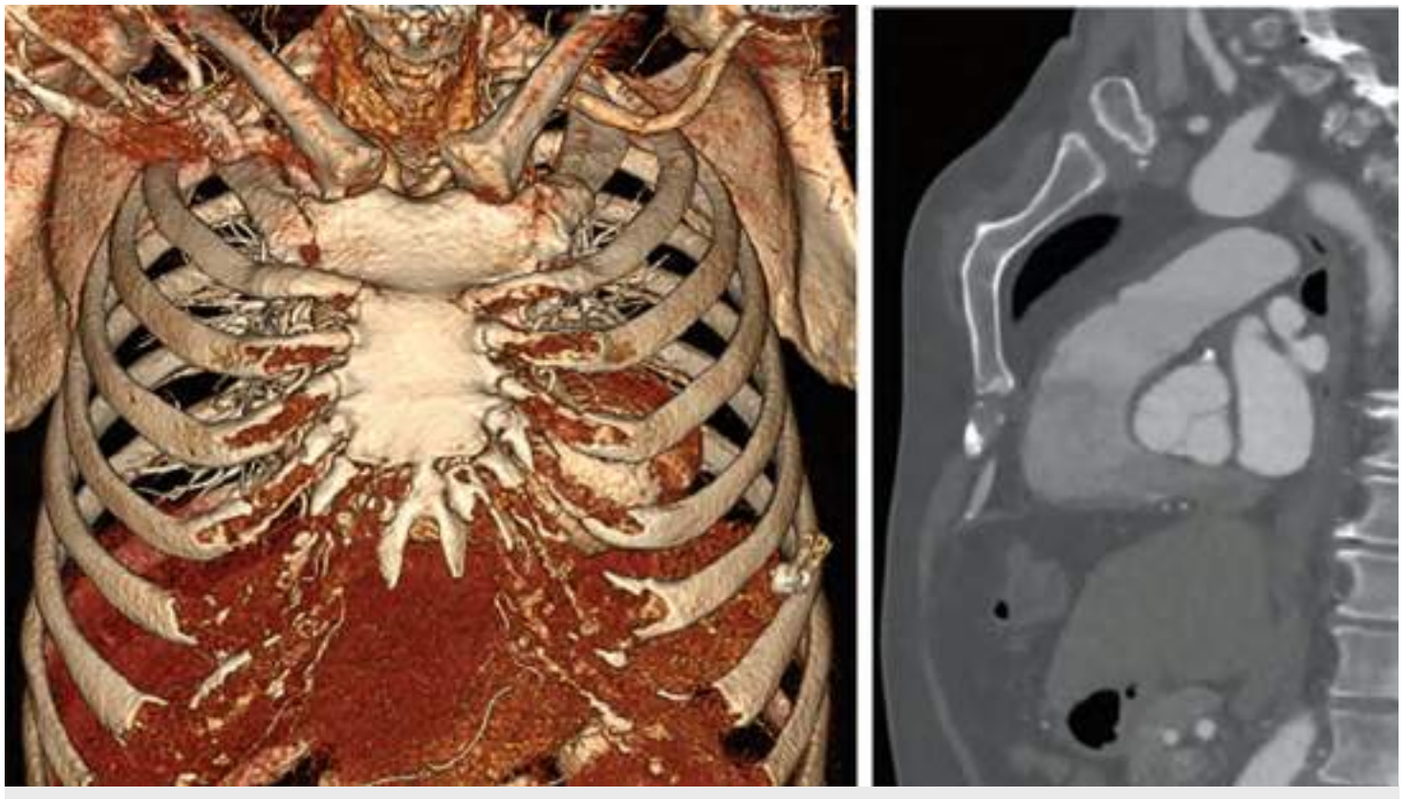

Fig. 1.17 Anomalously widened sternum with severe anterior angulation.

site is reported at the first rib involving sternochondral or costochondral junctions.[23] Injury of the xiphoid process after trauma, cardiopulmonary resuscitation, or surgical incision can cause exuberant bony proliferation at this anatomical level.

Ribs and sternum are common sites of involvement in inflammatory diseases, primary tumors, or metastatic malignancies (▶ Fig. 1.18). Reactive periosteal thickening of the rib and sternum is common after trauma, surgery, and adjacent infectious processes. Rib or sternal osteomyelitis is relatively rare. Osteitis of the sternomanubrial joint is uncommon and could be related to rheumatoid arthritis, psoriatic arthritis, or ankylosing spondylitis (▶ Fig. 1.18). Fibrous dysplasia is a benign condition due to the proliferation of fibrous tissues in the bones. It is the most common cause of a benign expansile lesion of the ribs.[25]

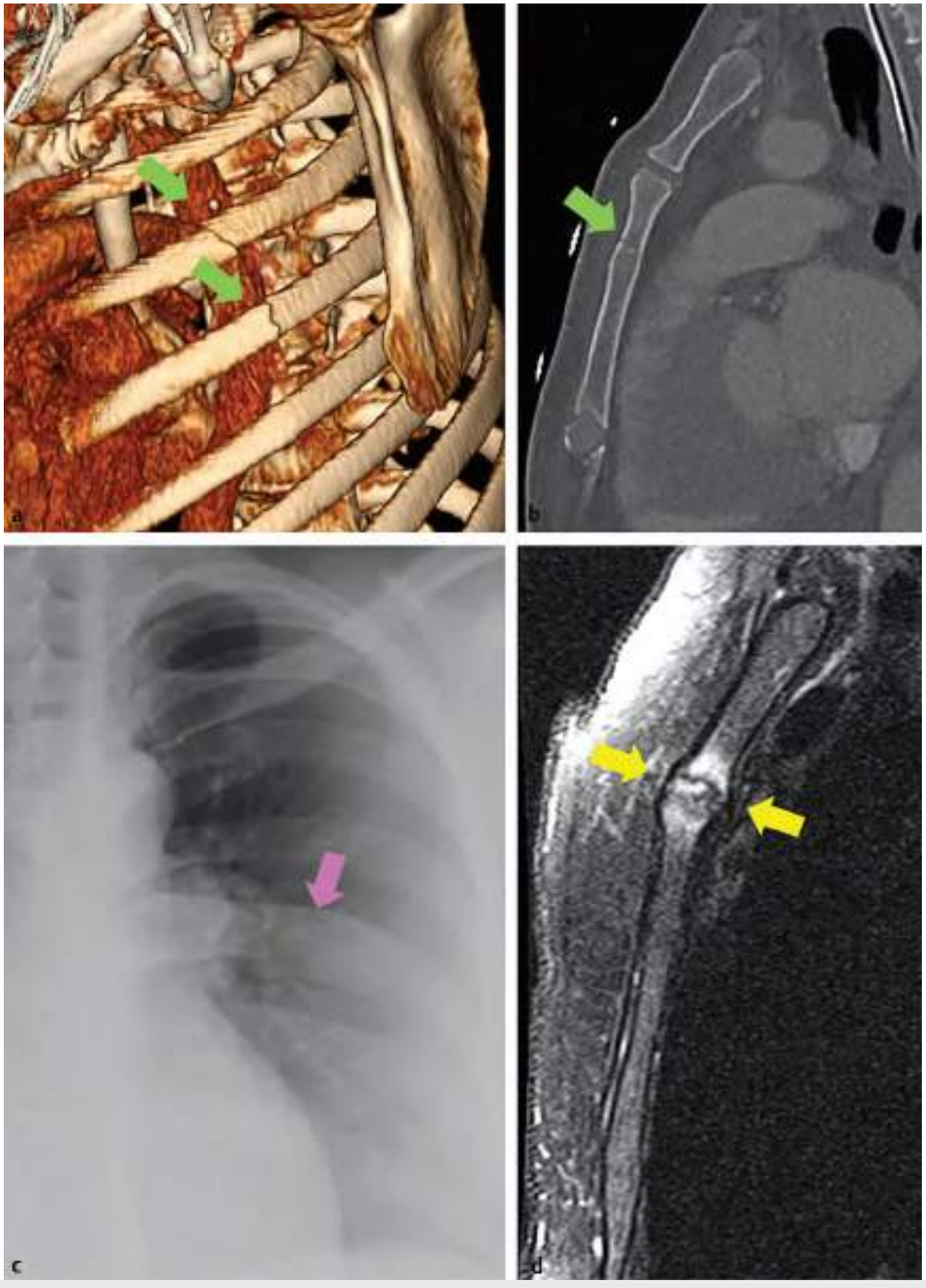

Fig. 1.18 (a, b) Postcardiopulmonary resuscitation of nondisplaced rib, and sternal fractures (*arrows*). **(c)** Fibrous dysplasia is common benign abnormality of the ribs. Widened ribs (*arrows*) with a ground-glass density of the involved bone. **(d)** Osteoarthritis of the manubriosternal synchondrosis is shown by MRI (*arrows*).

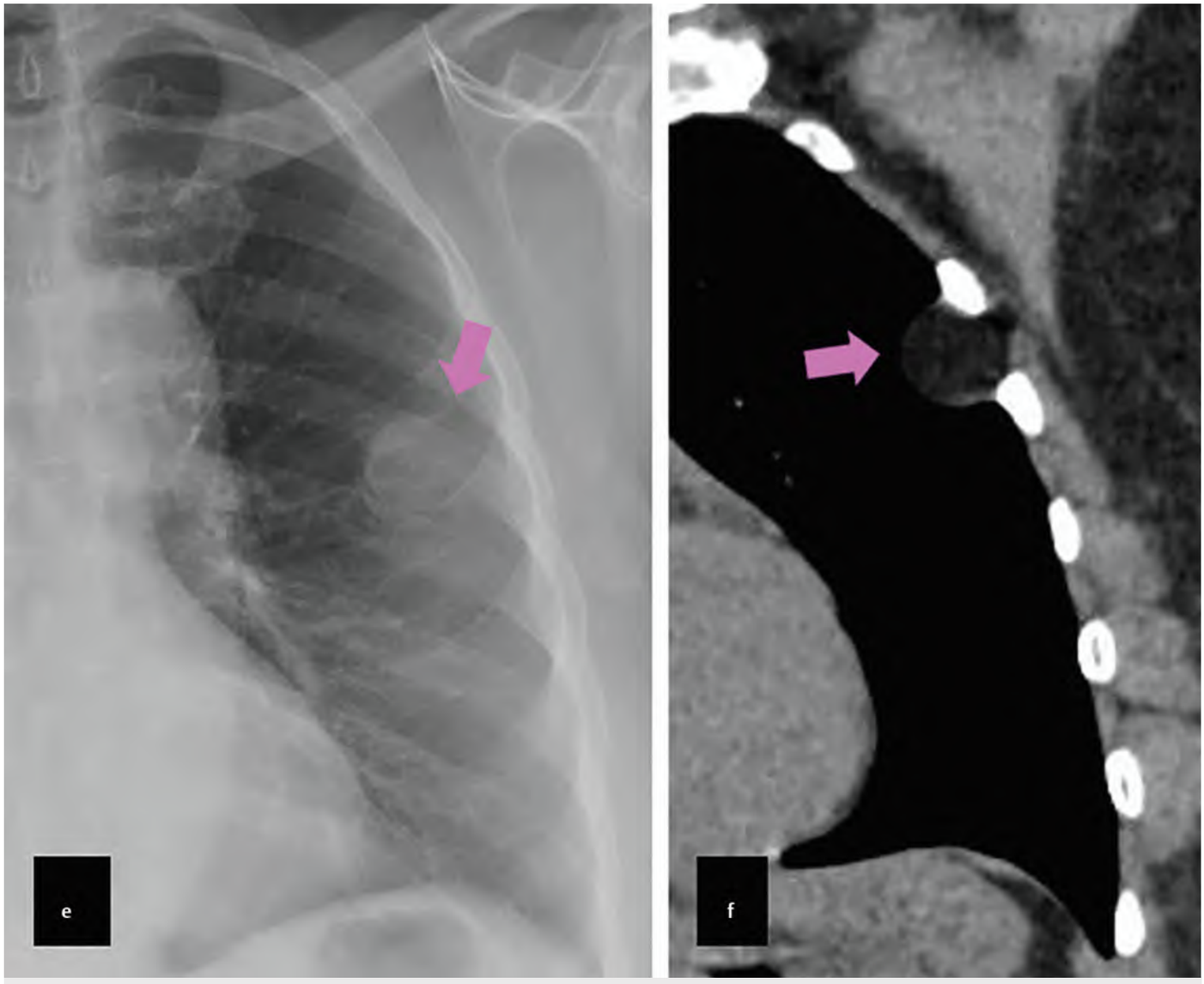

Fig. 1.18 (e, f) Left chest wall lipoma (*arrows*).

Imaging characteristics include, bone lucency with a "ground-glass" matrix, expansion, and remodeling. Lesions arising from chest soft tissue is also common (▶ Fig. 1.18).

◆ Muscles of the Chest Wall

Functionally, the muscles of the chest wall are divided into two main groups: inspiratory and expiratory.[26] The principal muscle of inspiration is the diaphragm. This structure is reviewed in detail in Chapter 10, Diaphragm. With assistance from the external intercostal muscles, the diaphragm contracts during inspiration to enlarge the thoracic cavity. Other inspiratory muscles include the sternocleidomastoid and scalene muscles. These muscles are secondary accessory muscles that expand the chest volume by elevating the sternum and upper ribs of the thorax.

Major expiratory muscles include the rectus abdominal, internal oblique, and external oblique muscles.[1] These muscles decrease lung volumes by constricting the rib cage in a downward motion and by compressing the abdominal compartment and raising internal pressure.

However, these muscles only come into play as expiratory muscles during exercise or forced breathing maneuvers. At resting state, expiration is a passive process brought about by the recoil of the lungs and rib cage at the end of inspiration. The internal intercostal muscles also help in expiratory action moving ribs downward and inward.

Muscles of the Anterior Chest Wall

Major muscles of the anterior and anterolateral chest wall include the pectoralis major, pectoralis minor, serratus anterior, rectus abdominal, and external oblique (▶ Fig. 1.19, ▶ Fig. 1.20). The sternalis muscle is an uncommon accessory muscle (please see ▶ Fig. 1.71, ▶ Fig. 1.72 at the end of the chapter).

Pectoralis Major

The pectoralis major is a fan-shaped muscle that covers the anterior superior portion of the chest and forms the anterior axillary fold. The pectoralis major has a complex morphology with two major segments. The proximal segment is subdivided into the

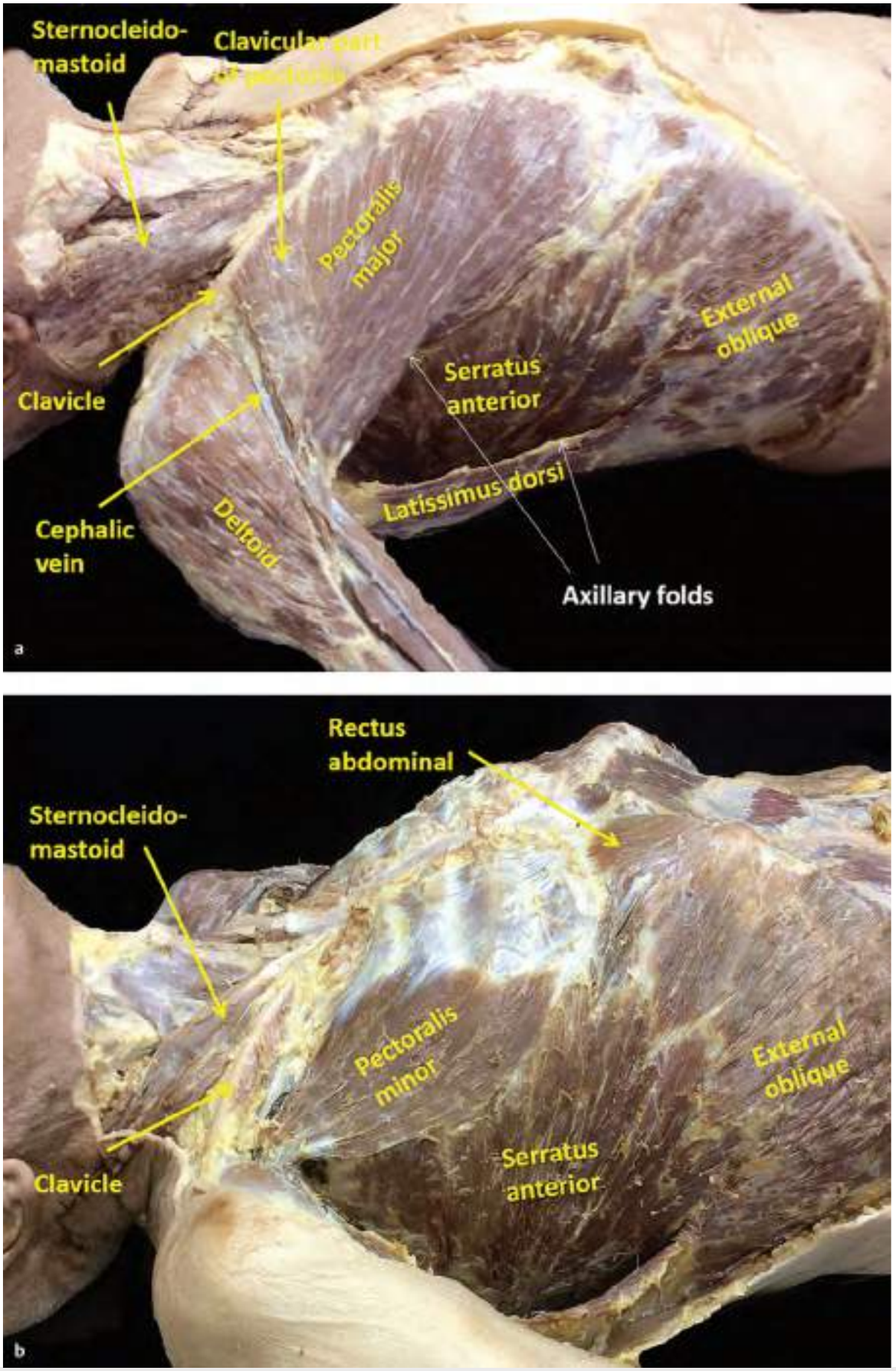

Fig. 1.19 Chest wall muscles. **(a)** Right lateral view. The latissimus dorsi and teres major muscles form the posterior axillary fold and the pectoralis major forms the anterior axillary fold. The pectoralis major overlies the pectoralis minor and extends between the sternum and the clavicle. **(b)** The pectoralis major is removed. The pectoralis minor originates from the third, fourth, and fifth ribs near the costal cartilages and attaches to the coracoid process of the scapula. The serratus anterior muscle arises from the lateral aspects of the first eighth to ninth ribs. The external oblique muscle originates from the inferior edge of the 6th through 12th ribs.

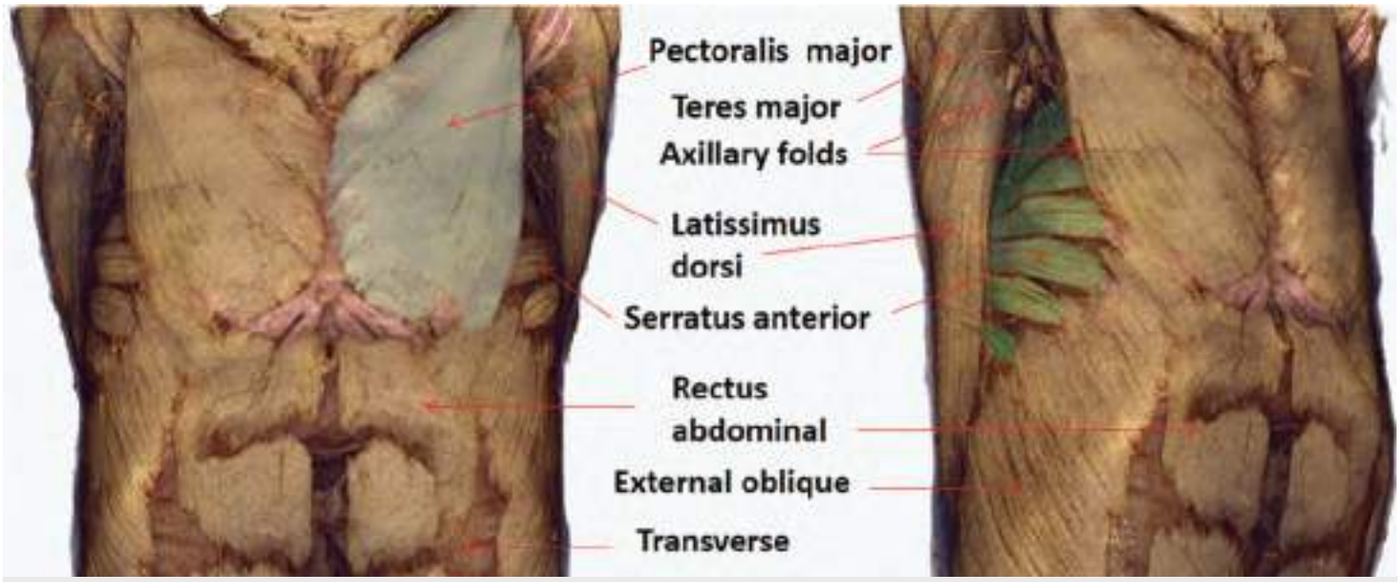

Fig. 1.20 Muscles of the anterior chest wall.

clavicular and manubrial parts, and the distal segment into the sternocostal, costal and abdominal parts[28,29] (▶ Fig. 1.19, ▶ Fig. 1.20, ▶ Fig. 1.21, ▶ Fig. 1.22). The clavicular part arises from the medial half of the clavicle and the manubrial part from the manubrium and the medial aspect of the first and second ribs (▶ Fig. 1.21**b**). The sternocostal part originates from the sternal body and medial aspect of the third to sixth ribs. The sternal origin of the muscle is from the lateral border of the sternum with an average width of 7 mm.[27] The middle part of sternum is not covered with muscle (▶ Fig. 1.20). The abdominal part is a separate layer that is located dorsal to the costal part, but occasionally originates from the aponeurosis of the external oblique abdominal muscle. The insertion tendon has a bilaminar U shape and attaches to the anterior surface of the humeral diaphysis, just lateral to the biceps brachii long head tendon (▶ Fig. 1.21, ▶ Fig. 1.22).[28,29] The clavicular and manubrial parts insert into the anterior limb of the U, the sternocostal part inserts into the inferior cup of the tendon, and the costal and abdominal parts insert into the posterior limb of the tendon.[28] This configuration of the pectoralis major muscle is analogous to the appearance of an unfolded handheld fan.[29]

Each part of muscle has a distinct vascular and nerve supply that runs in the epimysium on the posterior surface of the pectoralis major muscle.[30] The muscle is supplied by the thoracoacromial artery (a branch of the axillary artery) and the lateral thoracic artery (a branch of the subclavian artery). It also receives segmental blood supply from the internal mammary artery by way of intercostal perforators. The pectoral muscles are innervated by the lateral and medial pectoral nerves, branches of the brachial plexus. The two pectoral nerves are usually connected immediately distal to the thoracoacromial artery by the ansa pectoralis.[31] The lateral branch innervates the upper parts and the medial branch innervates the lower parts of the pectoralis major. These nerves may be injured after trauma, breast surgery, lymph node dissection, and pectoralis major muscle transfers. Nerve injury causes muscle atrophy.

The main function of the pectoralis major is to adduct, internally rotate, and flex the humerus.

Rupture of pectoralis major muscle is uncommon. The muscle is at greatest risk when the shoulder is in an abducted, extended, and externally rotated position with maximal muscle tension.[32] Poland's syndrome is a rare congenital anomaly characterized by the unilateral absence of the sternal portion of the pectoralis major muscle and sometimes ipsilateral symbrachydactyly (abnormally short and webbed fingers)[33] (▶ Fig. 1.23). It is more common in males and usually affects the right side. The pectoralis major muscle may be used either as a muscle or musculocutaneous flap for reconstructive chest wall surgery and subpectoral breast augmentation.[26]

Pectoralis Minor

The pectoralis minor is a thin triangular muscle lying deep to the pectoralis major. It originates from the third, fourth, and fifth ribs near the costal cartilages (▶ Fig. 1.19, ▶ Fig. 1.21, ▶ Fig. 1.22).

However, the location of the costal origins of the muscle is highly variable.[34] Muscle fibers of the pectoralis minor ascend laterally to attach to the superomedial border of the coracoid process of the scapula (▶ Fig. 1.21, ▶ Fig. 1.22).

The axillary vessels and brachial plexus lie posterior to the muscle. The medial pectoral nerve supplies the pectoralis minor muscle.[31] The function of the pectoralis minor is to tilt the scapula anteriorly. Insertional tendinopathy of pectoralis minor is a cause of shoulder pain in weightlifters.[35]

Pectoralis minimus is a small accessory muscle located under the pectoralis major muscle and medial to the pectoralis minor muscle. It originates from the first or second costal cartilages and inserts on the coracoid process.[36]

Sternalis Muscle

The sternalis (parasternalis) muscle is an uncommon muscle variant of the anterior thoracic wall.[37] It lies between the superficial fascia and the pectoral fascia and runs parallel to the sternum. The size of the muscle is variable and ranges from a few short fibers to a well-formed muscle (▶ Fig. 1.24). It is found

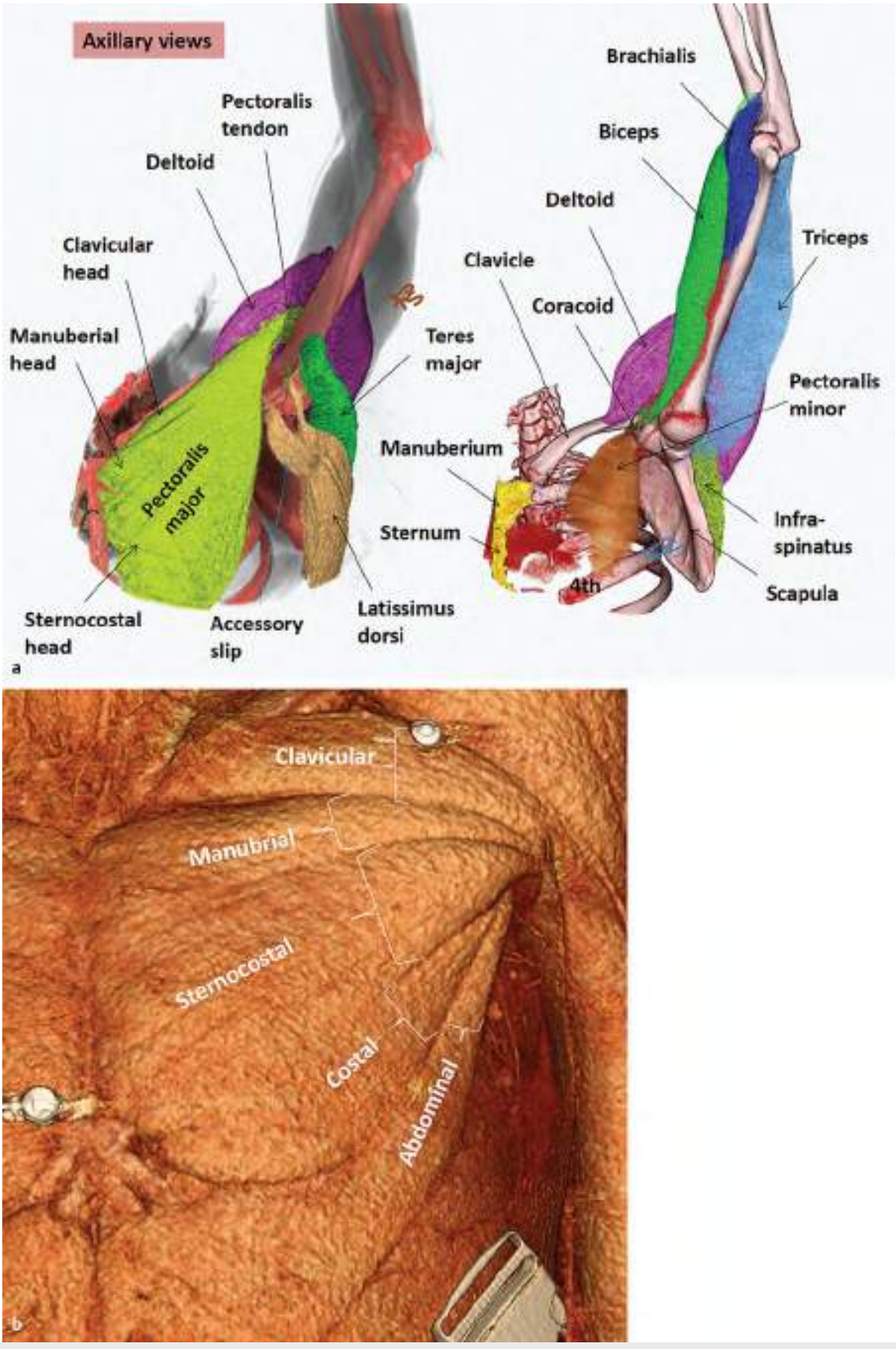

Fig. 1.21 **(a)** Volume-rendered color-coded CT images of the axillary region. The pectoralis major is a fan-shaped muscle that forms the anterior axillary fold. The muscle arises from the medial half of the clavicle and the medial aspect of sternum. The insertion tendon has a bilaminar U shape and attaches to the anterior surface of the humeral diaphysis, just lateral to the biceps brachii long head tendon. The latissimus dorsi and teres major muscles form the posterior axillary fold. The pectoralis minor is a thin triangular muscle lying deep to the pectoralis major. It originates from the upper ribs near the costal cartilages and inserts on the coracoid process of the scapula. **(b)** The pectoralis major has two major segments. The proximal segment is subdivided into the clavicular and manubrial parts, and the distal segment into the sternocostal, costal, and abdominal parts.

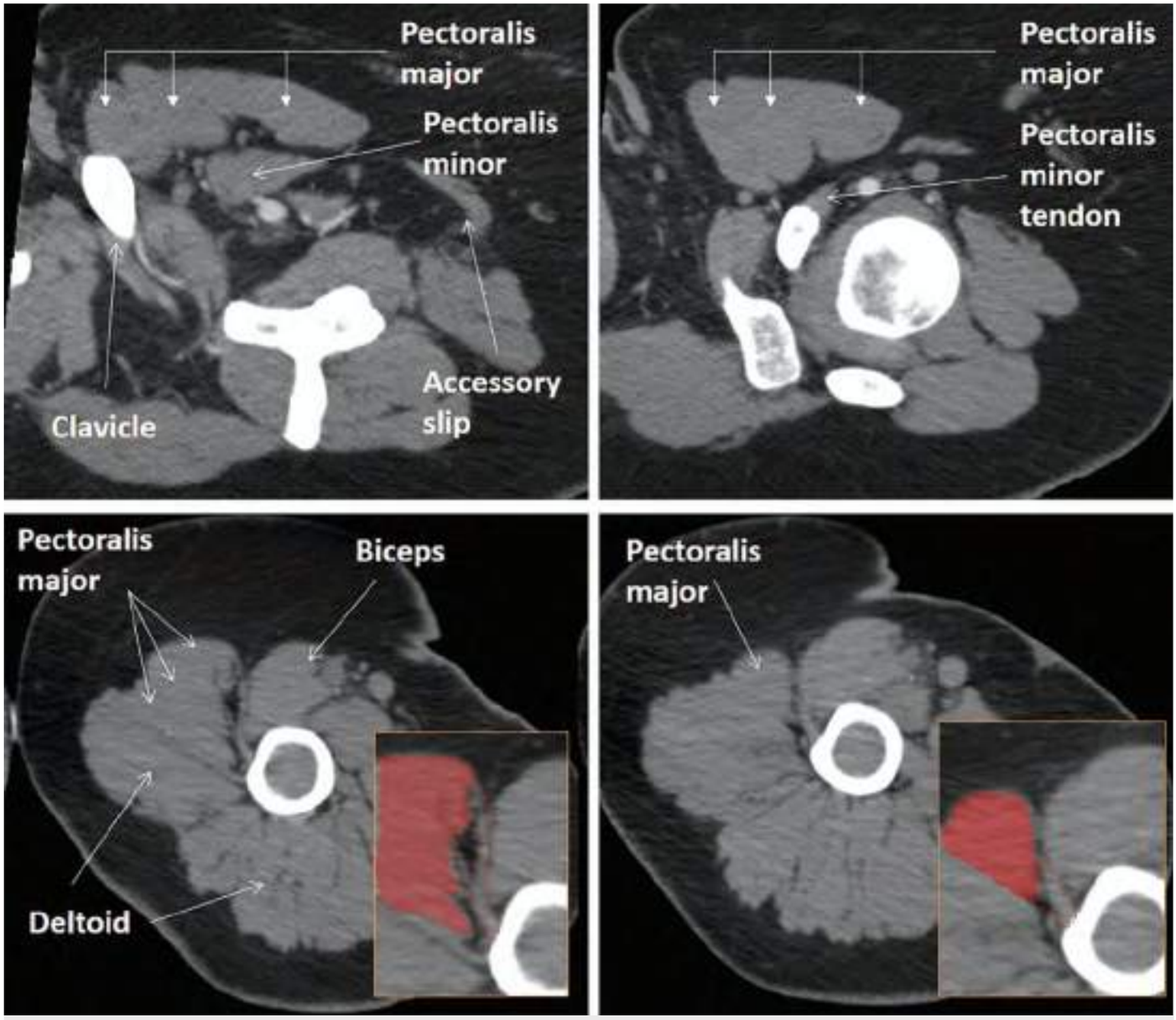

Fig. 1.22 Axial CT images at four levels from top to bottom showing pectoralis major muscle components and tendon insertion to humerus just lateral to the long head of biceps tendon. The v-shaped connection of the pectoralis tendons is shown in the inlay images (*dashed red lines*). The two layers are fused prior to tendon insertion on the humerus. The insertion point is not separable from the long tendon of the biceps in this example. Pectoralis muscle is colored in red. Also seen is the attachment of the pectoralis minor tendon to the coracoid process of the scapula.

unilaterally (4.5–6%) or bilaterally (1.7%).[38] The muscle arises from the upper sternum and the infraclavicular region. The insertion point is variable including the pectoral fascia, lower ribs, costal cartilages, rectus abdominal muscle sheath, or the abdominal external oblique muscle aponeurosis. Innervation of the sternalis muscle is provided by branches of pectoral nerves (55%) and/or intercostal nerves (43%).[38] The function of the sternalis muscle still remains unknown, but it may help to elevate the lower chest wall.[39] On CT or MR studies, it is seen as a vertically oriented parasternal flat and bandlike structure surrounded by fatty tissue (▶ Fig. 1.24). When unilateral, it should not be confused with pathologies in mammogram or CT studies of the chest.

Serratus Anterior

The serratus anterior muscle arises from the lateral aspects of the first eight to nine ribs. The upper half of the muscle fibers attach to the superior angle and medial border of the scapula. The lower fibers attach to the medial aspect of the inferior scapular angle (please see ▶ Fig. 1.71, ▶ Fig. 1.72 at the end of the chapter). The serratus anterior is frequently used to cover a lobar or mainstem bronchial stump.[40]

The serratus anterior muscle is supplied by the branches of the subscapular, thoracodorsal, and lateral thoracic arteries (Appendix image series). The thoracodorsal artery enters the muscle superior on its anterior surface and gives off multiple small branches before terminating in the latissimus dorsi muscle.[41]

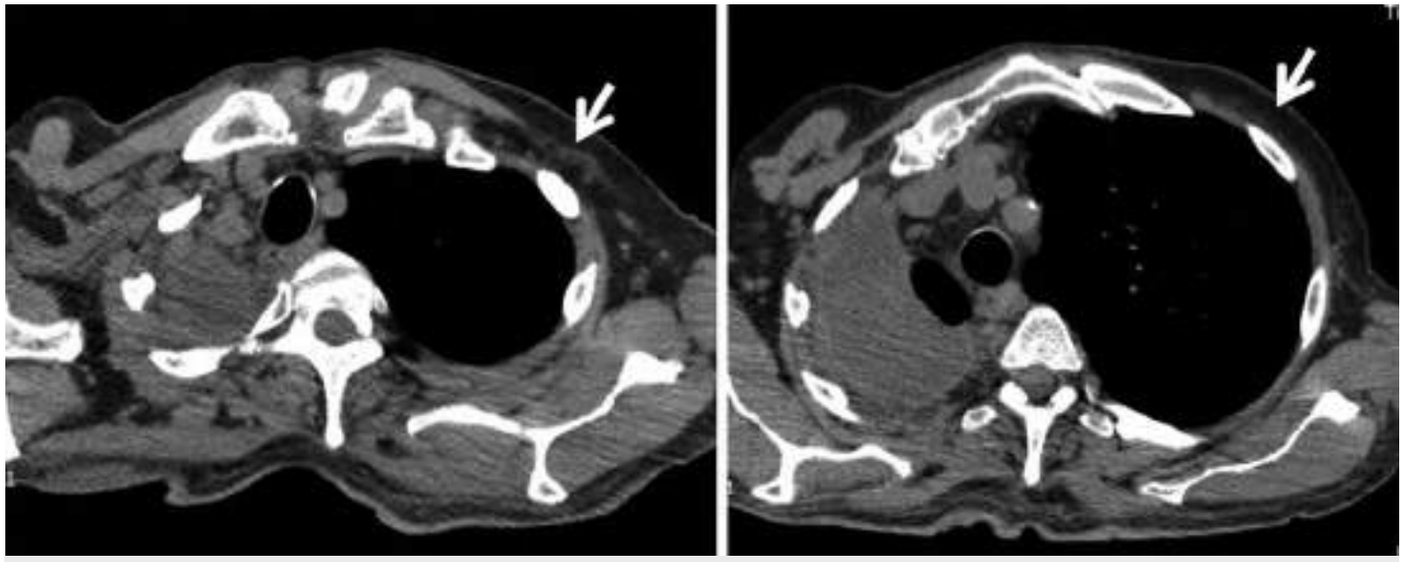

Fig. 1.23 A 63-year-old patient with Poland's syndrome. Absence of the lateral part of the left pectoralis muscles (*arrows*) is shown. Other muscles are unremarkable. Also shown is a loculated right pleural effusion.

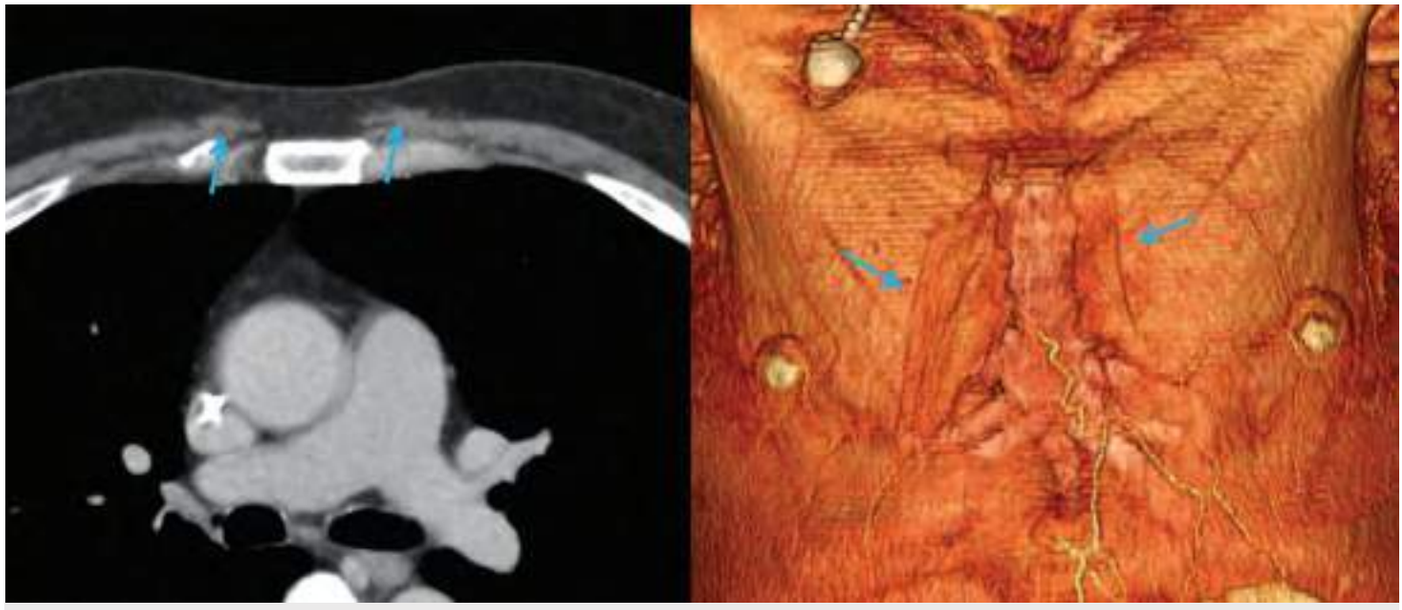

Fig. 1.24 Sternalis muscle. Axial and volume-rendered CT images show two bandlike vertically oriented parasternal tubular structures (*arrows*) anterior to the pectoralis major muscles.

Innervation of the serratus anterior muscle is via the long thoracic nerve of Bell, which originates at the anterior rami of the C5 to C7 (or C8) spinal nerves. It travels inferiorly along the outer surface of the serratus anterior muscle entering the axilla (▶ Fig. 1.25). The long thoracic nerve can be visualized using high-resolution sonography.[42] The nerve may be injured during axillary lymph node dissection or radical mastectomy. The serratus anterior is important in shoulder stabilization during arm elevation, ensuring fixation, and upward rotation of the scapula. The classical clinical picture of nerve injury is scapular winging and the inability to elevate the arm.[43] Serratus anterior muscle pain syndrome is one of the causes of chronic chest pain of noncardiac origin. It is characterized by taut bands (tense muscle fibers), commonly described as trigger points. The trigger point can be treated by ultrasound-guided injection of anesthetic agents.[44]

Elastofibroma is a relatively common pathology of the lateral chest that should not be mistaken with the serratus anterior muscle (▶ Fig. 1.26).

Abdominal Wall Muscles

Abdominal wall muscles cover part of the lower anterior and lateral chest wall. The rectus abdominal muscle originates from the xiphoid process and fifth to seventh costal cartilages and inserts on the pubic symphysis. Blood supply is provided by the superior and inferior deep epigastric arteries. The external oblique muscle originates from the inferior edge of the 6th through 12th ribs (▶ Fig. 1.27). The muscle fans out to insert on the iliac crest, linea alba, and pubic and inguinal ligaments. Innervation is from the inferior six intercostal nerves, and blood supply primarily derives

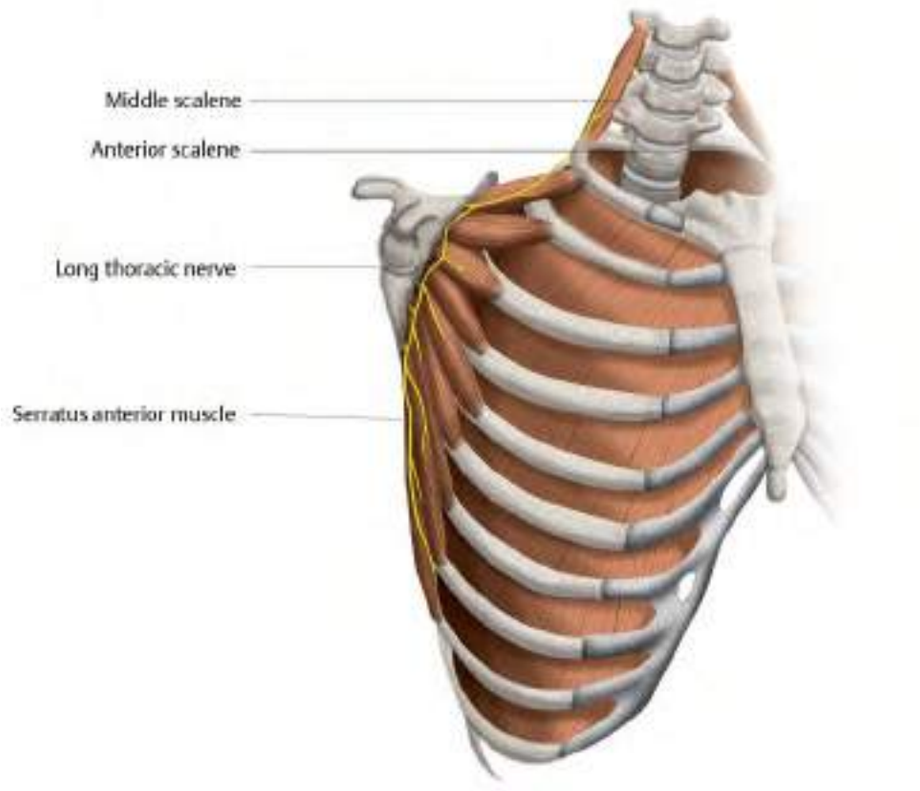

Fig. 1.25 Serratus anterior muscle and long thoracic nerve. Innervation of the serratus anterior muscle is via the long thoracic nerve, which originates at the anterior rami of the C5 to C7 spinal nerves. It travels inferiorly along the outer surface of the serratus anterior muscle entering the axilla. The long thoracic nerve can be visualized using high-resolution ultrasound of CT. The classical clinical picture of nerve injury is scapular winging and the inability to elevate the arm.

from branches of the lower six posterior intercostal arteries.[45] The caudal part of the muscle is supplied by branches of the deep circumflex iliac artery.[46]

The internal oblique muscle is located deep to the external oblique muscle. The very superior fibers insert into the inferior border of the last three to four ribs. The internal oblique muscle is vascularized by the ascending branch of the deep circumflex iliac artery, lower six posterior intercostal arteries, and lateral branches of the deep inferior epigastric artery.[47] The transverse abdominal muscle is the innermost muscle of the abdominal wall. It originates from the five lower ribs, thoracolumbar fascia, iliac crest, and the outer third of the inguinal. The muscle inserts medially into the rectus sheath though a broad aponeurosis.

Muscles of the Posterior Chest Wall

Muscles of the posterior chest wall include the latissimus dorsi, trapezius, serratus posterior superior, serratus posterior inferior, rhomboid, and erector spinae muscles.

Latissimus Dorsi

The latissimus dorsi is a large, flat, dorsolateral muscle on the trunk, which extends posterior to the arm. Medially, it is partly covered by the trapezius (▶ Fig. 1.28). The latissimus dorsi originates from the spinous processes of thoracic (T7–T12) vertebrae, inferior three or four ribs, inferior angle of scapula thoracolumbar fascia, and iliac crest. It wraps around the lateral chest wall to insert on the floor of intertubercular sulcus of the humerus (▶ Fig. 1.21). The latissimus dorsi and teres major muscles form the posterior axillary fold (▶ Fig. 1.19, ▶ Fig. 1.20, ▶ Fig. 1.21). Anterior and posterior muscle slips, found in 2% of cases, usually extend to pectoralis major or teres major[48] (▶ Fig. 1.21). Asymmetric muscle slip should not be confused with pathology (▶ Fig. 1.26).

The anterior and superior parts of the muscles along with the serratus anterior are supplied by the thoracodorsal artery, a branch of the subscapular circumflex artery. The posterior part is supplied by the intercostal perforators. Nerve supply is by the thoracodorsal nerve.[41] The latissimus dorsi is involved in extension, adduction against resistance, horizontal abduction, flexion from an extended position, and internal rotation of the shoulder joint. It also has a synergistic role in extension and lateral flexion of the lumbar spine. A tight latissimus dorsi may be one cause of chronic shoulder and back pain. The latissimus dorsi has been used for rotator cuff repair. It is the most frequently used muscle for the reconstruction of the lateral and anterior chest wall defects.

Rhomboid

The rhomboid minor and major muscles are posterior chest muscles that run obliquely between the medial margin of the scapula and spinal processes of T2 to T5 (▶ Fig. 1.28, ▶ Fig. 1.29). The

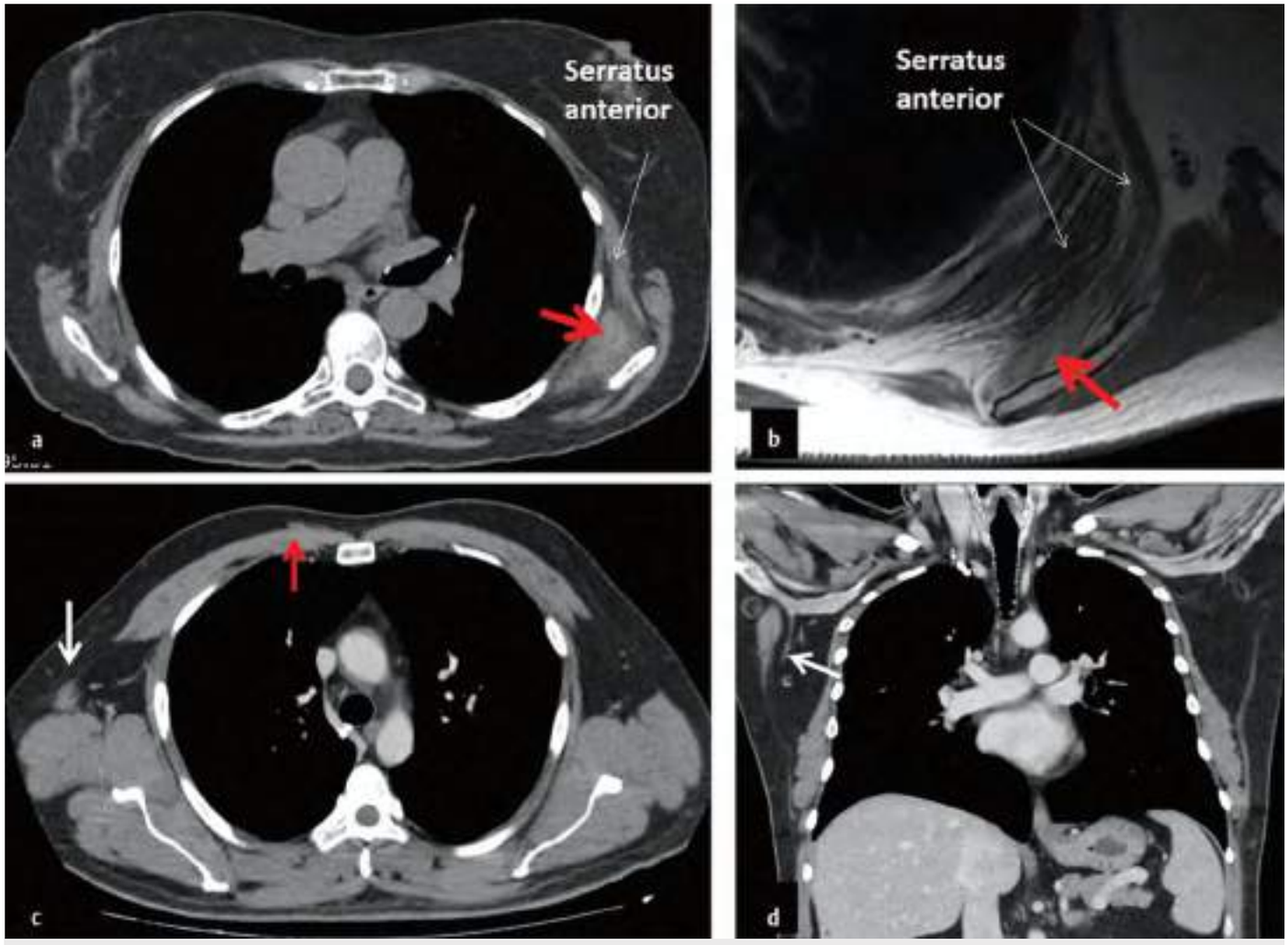

Fig. 1.26 Elastofibroma in two different patients. **(a)** CT scan. **(b)** MRI scan. Elastofibroma dorsi is a benign fibrous tumor in the infrascapular regions, deep to the serratus anterior and latissimus dorsi muscles (*arrows*). **(c, d)** Accessory muscle slip of the right latissimus dorsi (*white arrows*) extends to the pectoralis fascia in a patient with melanoma. This anatomical variant should not be confused with metastasis. Also, a small sternalis muscle on the right is seen (*red arrow*).

rhomboid minor is located superior to the rhomboid major and both are covered by the trapezius muscle (please see ▶ Fig. 1.71, ▶ Fig. 1.72 at the end of the chapter). Rhomboid muscles work along with the serratus anterior and pectoralis minor to maintain the scapula pressed against thoracic wall by retracting it toward the spine. The arterial supply is provided by the dorsal (descending) scapular artery. This artery also supplies the levator scapulae and trapezius muscles. The dorsal scapular artery is the deep branch of the transverse cervical artery (a branch of the thyrocervical trunk).

The rhomboids are innervated by rhomboid nerve which is the terminal branch of dorsal scapular nerve. The dorsal scapular nerve is single nerve that arises from the C5 spinal nerve and occasionally from the C3, C4, and C6 roots.[48,49] It penetrates the middle scalene muscle, and runs on the ventral side of the levator scapulae muscle and rhomboid muscles near the medial border of the scapula. Paralysis of the suprascapular nerve commonly occurs in avulsion injuries of the brachial plexus causing disturbance of the elbow flexion and shoulder elevation. Transfer of the spinal accessory nerve to the suprascapular nerve is performed most often to treat the problem.[50]

Trapezius

The trapezius is a large muscle that covers the posterior aspect of the occipital region of the skull, the neck, and the superior part of the thorax and attaches the upper limb to the skull and vertebrae (▶ Fig. 1.28). The trapezius muscle fibers are divided into superior, middle, and inferior fibers, each of which exhibits a different action. The superior fibers originate at the superior nuchal line and external occipital protuberance and reach the lateral portion of the clavicle. The middle fibers originate from the spinous processes of the seventh cervical to the third thoracic vertebrae and are inserted on the acromion. This part represents the strongest portion of the muscle that helps to retract the scapula. The inferior fibers arise in most thoracic spinous processes and are inserted along the spine of the scapula. The inferior part depresses the scapula and lowers the shoulder.

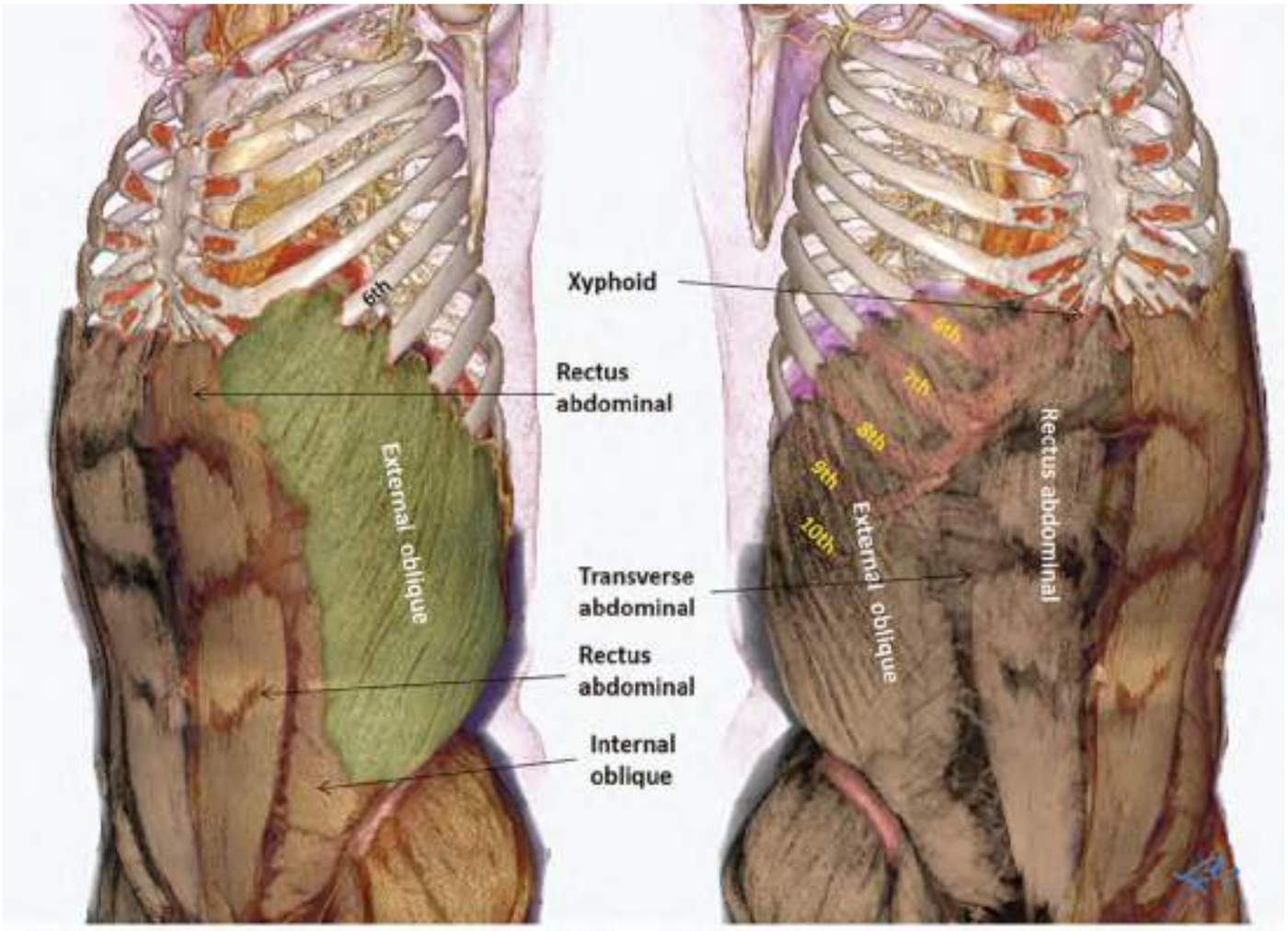

Fig. 1.27 Abdominal wall muscle attachments to lower anterior and lateral chest wall. The rectus abdominal muscle originates from the xiphoid process and fifth to seventh costal cartilages. The external oblique muscle originates from the inferior edge of the 6th through 12th ribs.

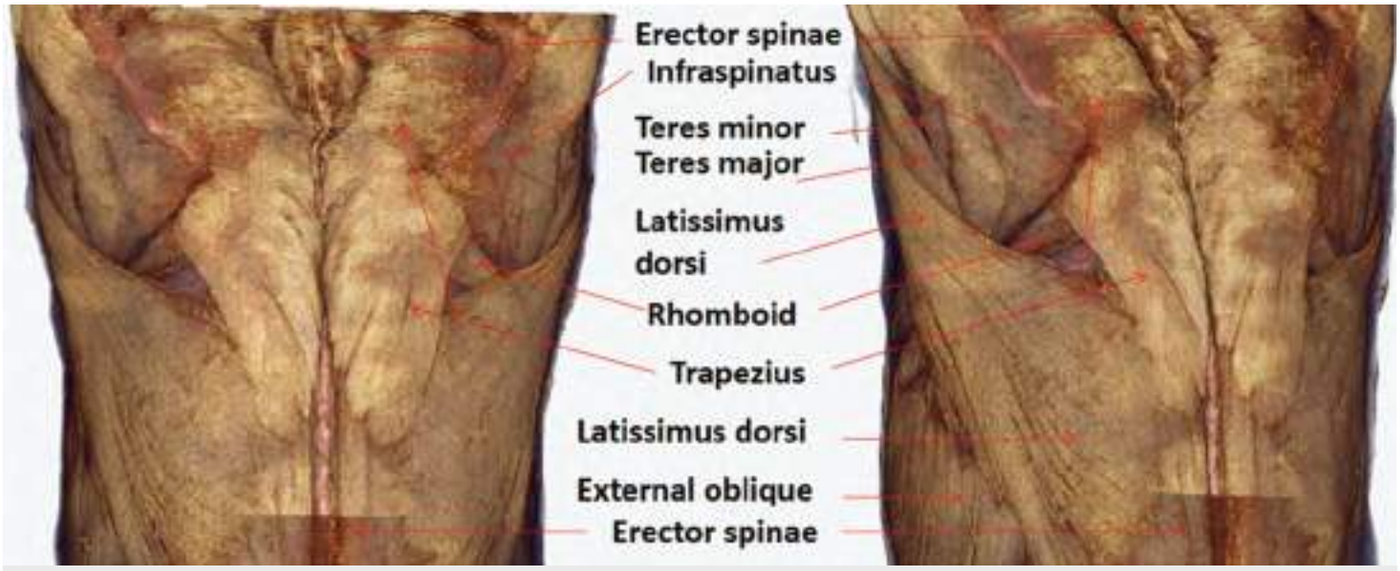

Fig. 1.28 Muscles of the posterior chest wall. Muscles that can be visible superficially include the latissimus dorsi, trapezius, rhomboid, and erector spinae muscles. The serratus posterior superior and serratus posterior inferior are also posterior muscles but deeply located. The latissimus dorsi is a large, flat, dorsolateral muscle that is partly covered by the trapezius.

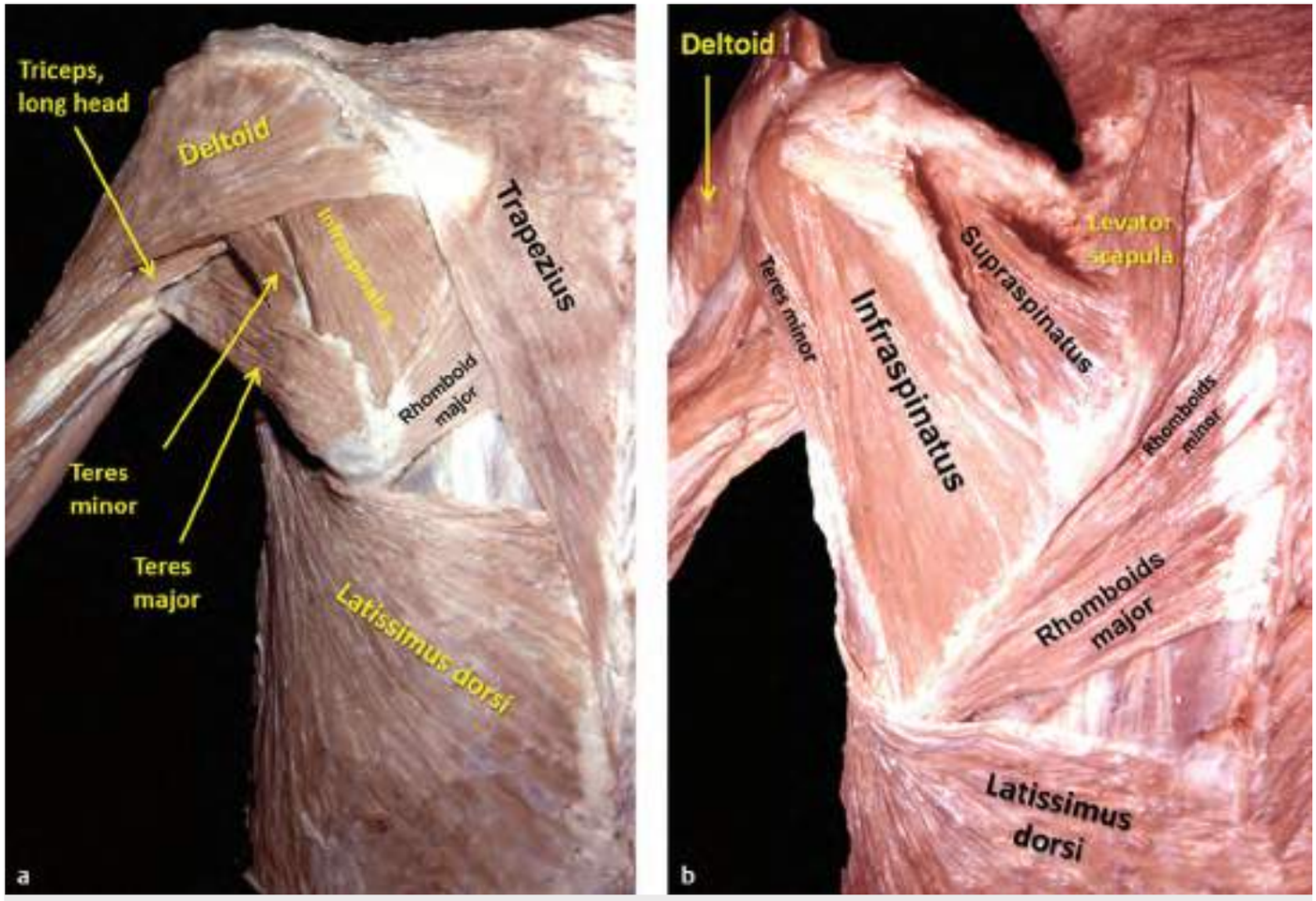

Fig. 1.29 Posterior chest wall muscles **(a)** before and **(b)** after removal of the trapezius muscle. The rhomboid minor and major muscles are shown running obliquely between the medial margin of the scapula and spinal processes of T2 to T5.

Its major blood supply is the transverse cervical artery, a branch of the thyrocervical trunk.

Its secondary blood supply includes occipital branches and intercostal perforators.

The accessory nerve (11th cranial nerve) provides motor supply to the superior and middle parts of the trapezius and also to the sternocleidomastoid muscles.[50,51] Damage of the accessory nerve results in trapezius muscle weakness, atrophy, and shoulder disability. The inferior portion of the muscle is innervated by the C3 and C4 cervical plexus. During modified radical neck dissection, the main identification point of the accessory nerve is in the posterior triangle, behind the posterior margin of the sternocleidomastoid muscle at Erb's point, where the greater auricular nerve crosses the accessory nerve.[52] The knowledge of anatomical variations of the accessory nerve is of clinical importance during neck dissection. Lee et al studied the anatomy of the accessory nerve at level IIb.[53] They found that the nerve passes anterior to the internal jugular vein in 40% and posterior to the vein in 57% of the cases.[53]

Myofascial pain syndrome is a common cause of chronic musculoskeletal pain. This syndrome presents clinically as referred pain, a limited range of joint motion, and a local twitch response following mechanical stimulation of certain muscular and fascial areas, also known as myofascial trigger points.[54] Myofascial trigger points are identified by palpation of a locally painful knot during clinical examination. Active trigger points frequently originate in the trapezius muscle.

Serratus Posterior Superior Muscle

The serratus posterior superior is a small deeply located muscle covering a small portion of the posterosuperior chest wall (▶ Fig. 1.30, ▶ Fig. 1.31). It covers the erector spinae muscles and is overlaid by the rhomboid muscles (please see ▶ Fig. 1.71, ▶ Fig. 1.72 at the end of the chapter). The muscle extends between the spinous processes of the C7 to T3 and the upper borders of the second through fifth posterior ribs. The serratus muscles are supplied by the intercostal arteries and innervated by the intercostal nerves. The serratus posterior superior elevates upper ribs to help deep inspiration.

Serratus Posterior Inferior Muscle

The serratus posterior inferior muscle is also a relatively small, comb-like muscle covering a small portion of the posterosuperior abdominal wall and the posteroinferior chest wall (please see ▶ Fig. 1.71, ▶ Fig. 1.72 at the end of the chapter). It covers the erector spinae muscles and overlaid by the latissimus dorsi

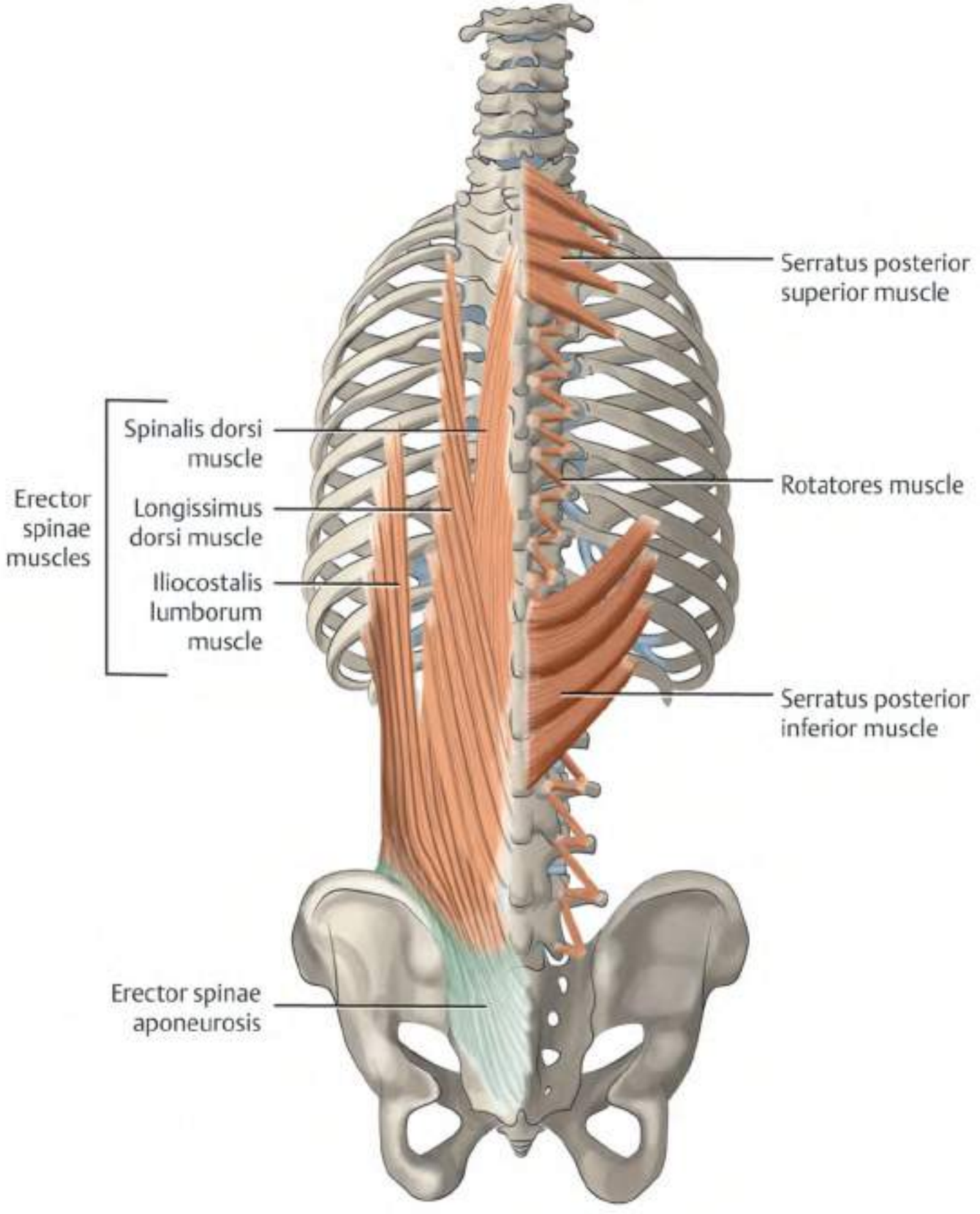

Fig. 1.30 Serratus posterior superior, serratus posterior inferior, erector spinae, and rotators muscles.

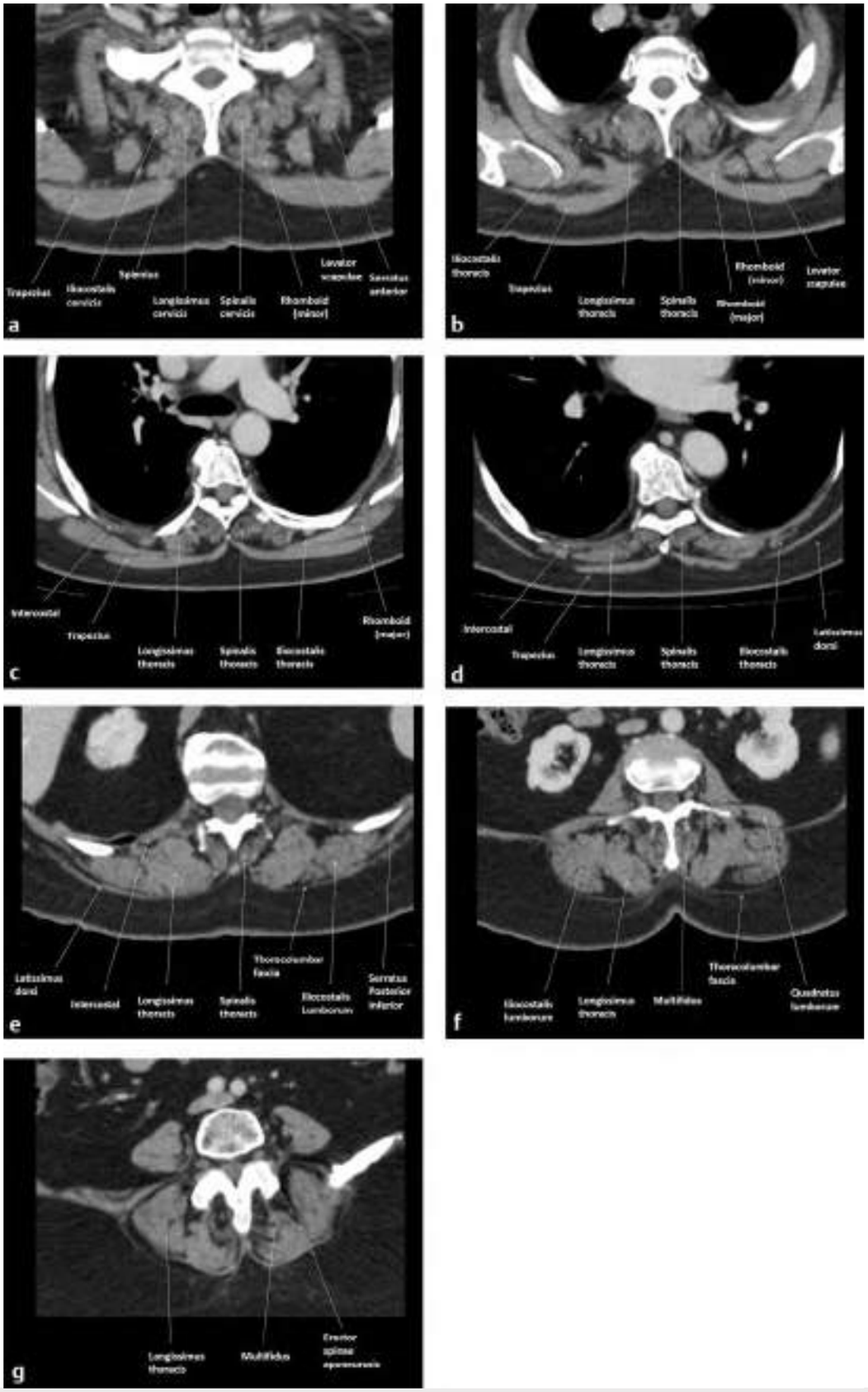

Fig. 1.31 (a–g) Erector spinal muscles. These muscles from lateral to medial include the iliocostalis, longissimus, and spinalis. Each muscle is also subdivided into three parts depending on the anatomical coverage.

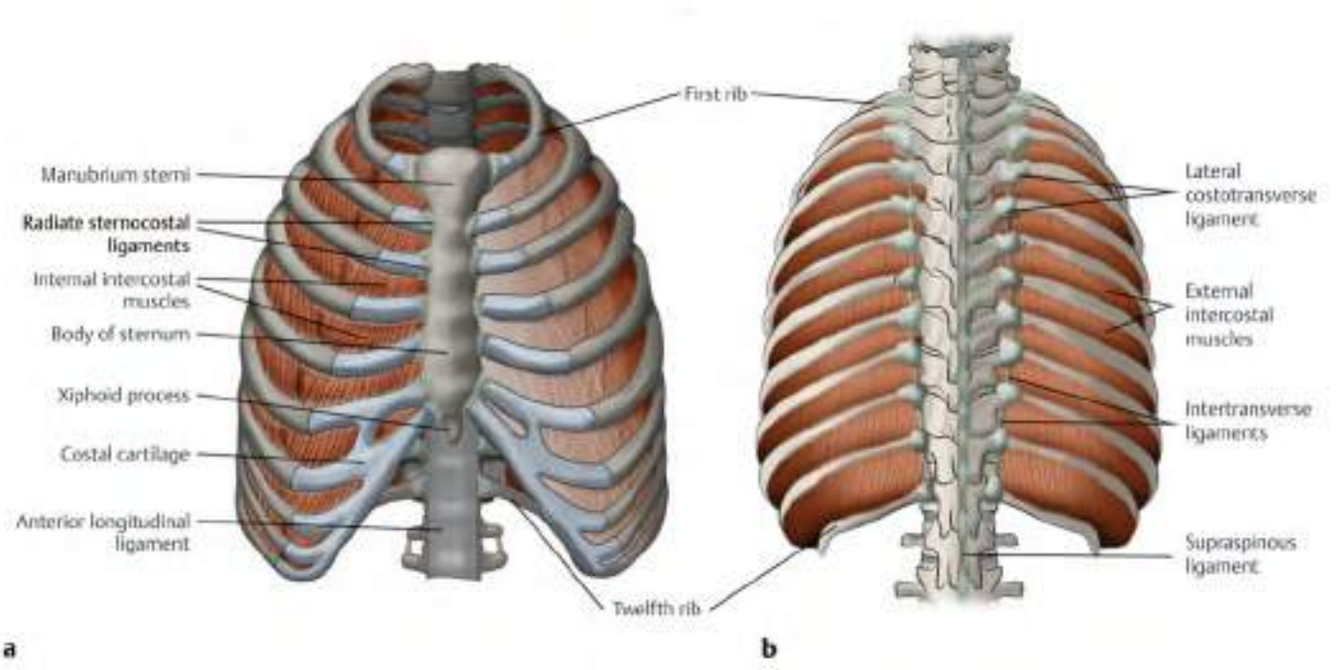

Fig. 1.32 Intercostal muscles: (**a**) anterior view, (**b**) posterior view. (Adapted with permission from Thieme Atlas of Anatomy, General Anatomy and Musculoskeletal System, Thieme 2005, Illustrations by Karl Wesker and Markus Voll.)

muscle. The serratus posterior inferior extends from the spinous processes of T11 to L2 to insert onto the lower border of the last four ribs lateral to the iliocostalis muscle insertions (▶ Fig. 1.30, ▶ Fig. 1.31). Medially, its aponeurosis blends with the thoracolumbar fascia. The serratus posterior inferior muscle contributes to forced expiration and extension/rotation of the trunk.

Erector Spinae Muscles

The erector spinae are a deep muscle group that runs parallel to the spine and covers the posterior medial walls of the chest and abdomen. It is divided into three columns by three muscles. These muscles from lateral to medial include the iliocostalis, longissimus, and spinalis (▶ Fig. 1.30, ▶ Fig. 1.31). Each muscle is also subdivided into three parts depending on the anatomical coverage. For example, the iliocostalis is partitioned into the lumborum, thoracis, and cervicis. The longissimus and spinalis are partitioned into the thoracis, cervicis, and capitis.

The iliocostalis attaches to the transverse process of C6–C4 at its cervical levels. At the thoracic level, it interconnects the posterior ribs lateral to the rib angles (please see ▶ Fig. 1.71, ▶ Fig. 1.72 at the end of the chapter). The longissimus is located between the other two muscles and becomes larger in the lower thoracic and lumbar regions. It mainly originates from the transverse processes and posteromedial ribs and interconnects them together. At its uppermost end, the longissimus connects to the mastoid process of the temporal bone. The spinalis muscle is the smaller one on the sides of the spinous processes and connects them together.

Thoracolumbar Fascia

The thoracolumbar fascia is a complex of several membranous layers that separates the paraspinal muscles from the muscles of the posterior abdominal wall, quadratus lumborum, and psoas major (please see ▶ Fig. 1.71, ▶ Fig. 1.72 at the end of the chapter). This complex structure wraps around the erector spinae muscles of the lower back and sacral region (▶ Fig. 1.31).

Intercostal Muscles

The intercostal muscles include the external, internal, and innermost muscles[5] (▶ Fig. 1.32, ▶ Fig. 1.33, ▶ Fig. 1.34). The external intercostal muscles form the outer layer of the intercostal muscles extending between the costochondral junction to the tubercle of the rib. They are thicker than the internal intercostal muscles. The internal intercostal muscles form the inner layer of the intercostal muscles extending between the sternocostal junction to the tubercle of the rib. The fibers of external intercostal are oriented obliquely from a more posterior point on the upper rib to a more anterior point on the lower rib. The fibers of internal intercostal are oriented obliquely in an opposite direction, from a relatively anterior point on the upper rib to a more posterior point on the lower rib[4] (▶ Fig. 1.32, ▶ Fig. 1.33, ▶ Fig. 1.34, ▶ Fig. 1.35).

In the parasternal region, the external intercostal muscle is replaced by the anterior intercostal membrane, a thin aponeurosis (▶ Fig. 1.35). The only muscle fibers in the parasternal region are those of the internal intercostals also known as parasternal intercostals (▶ Fig. 1.35, ▶ Fig. 1.36). In the paravertebral region, the internal intercostal muscle may be absent. Instead, the space is covered by the levatores costarum muscles and the posterior intercostal membrane (▶ Fig. 1.37). The 12 levatores costae are small muscles extending between the tip of the transverse process of the vertebra and the inferior rib on each side (▶ Fig. 1.30). In each intercostal space, thin but firm layers of fascia cover the outer surface of the external intercostal.

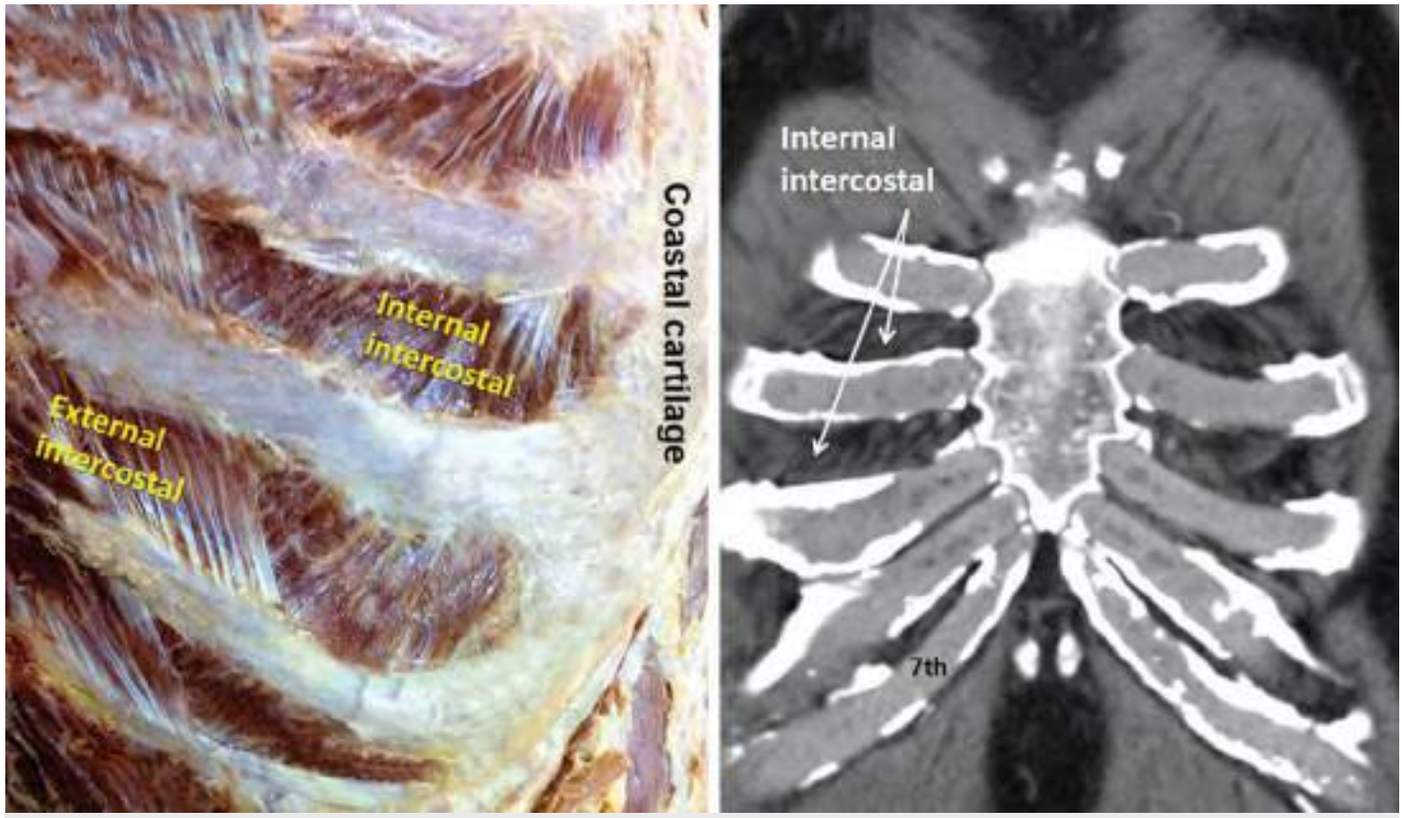

Fig. 1.33 Intercostal muscles in the parasternal region. The only intercostal muscle fibers in the parasternal region are those of the internal intercostals, the parasternal intercostals.

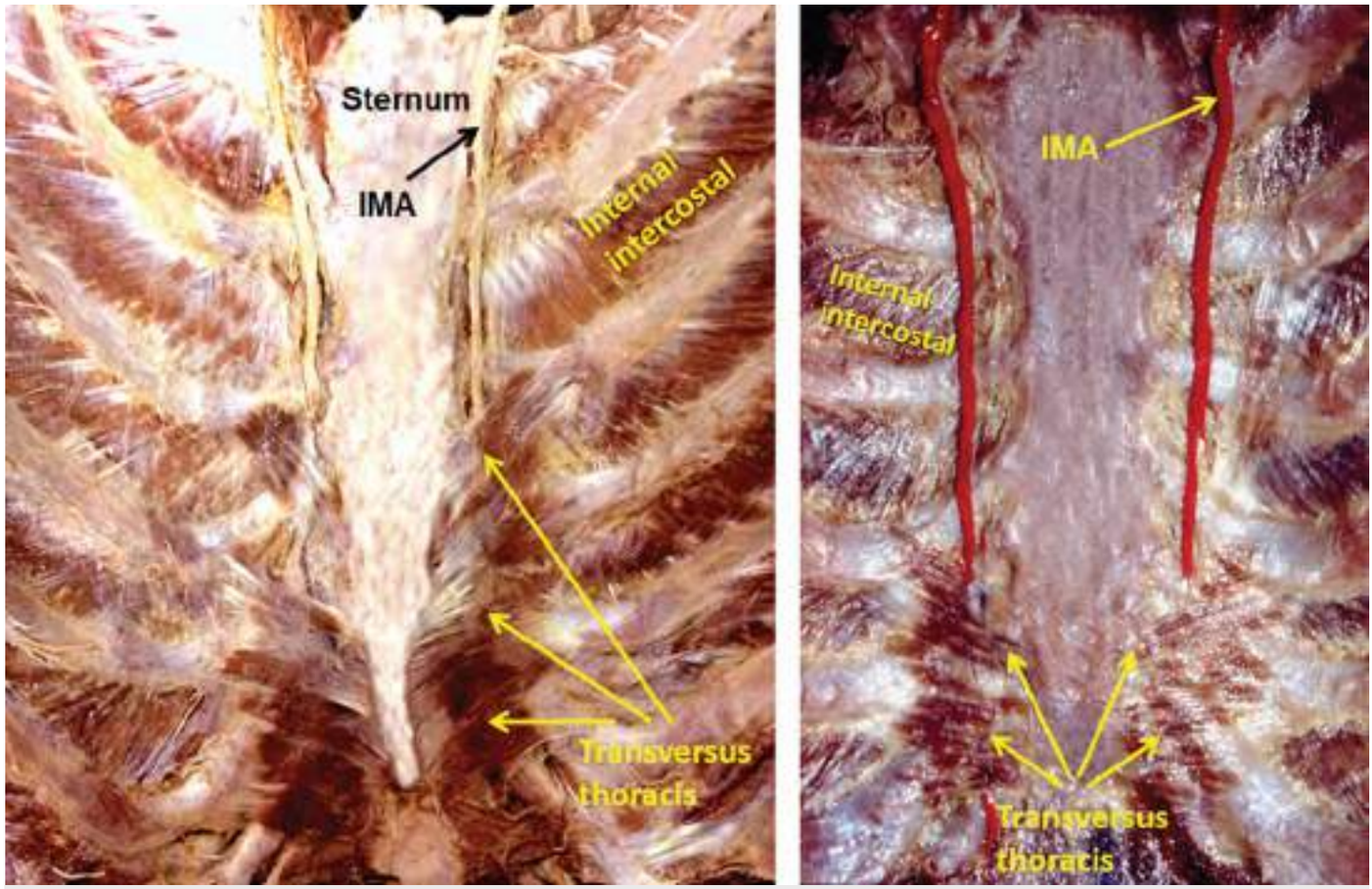

Fig. 1.34 Intercostal muscles in the parasternal region, retrosternal views showing the transversus thoracis muscles. The transversus thoracis runs obliquely between the posterior surface of the lower sternal body and the xiphoid process to insert on the second through sixth ribs/costal cartilages. IMA, internal mammary artery.

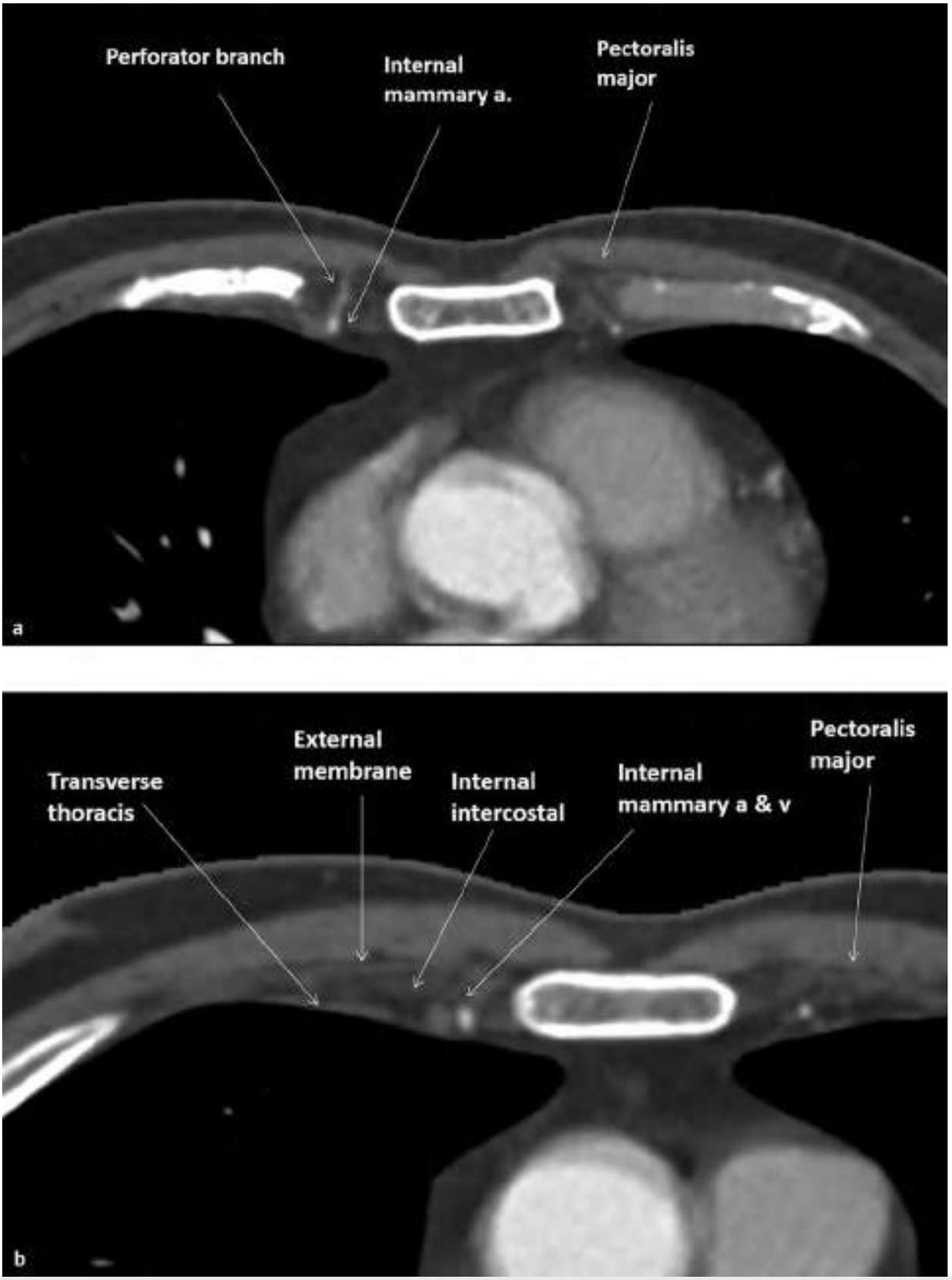

Fig. 1.35 (a, b) Axial CT images showing the intercostal muscles in the parasternal region. In the parasternal region, the external intercostal muscle is replaced by a thin aponeurosis known as the anterior intercostal external membrane. The only muscle fibers in the parasternal region are those of the internal intercostals. A, artery; V, vein.

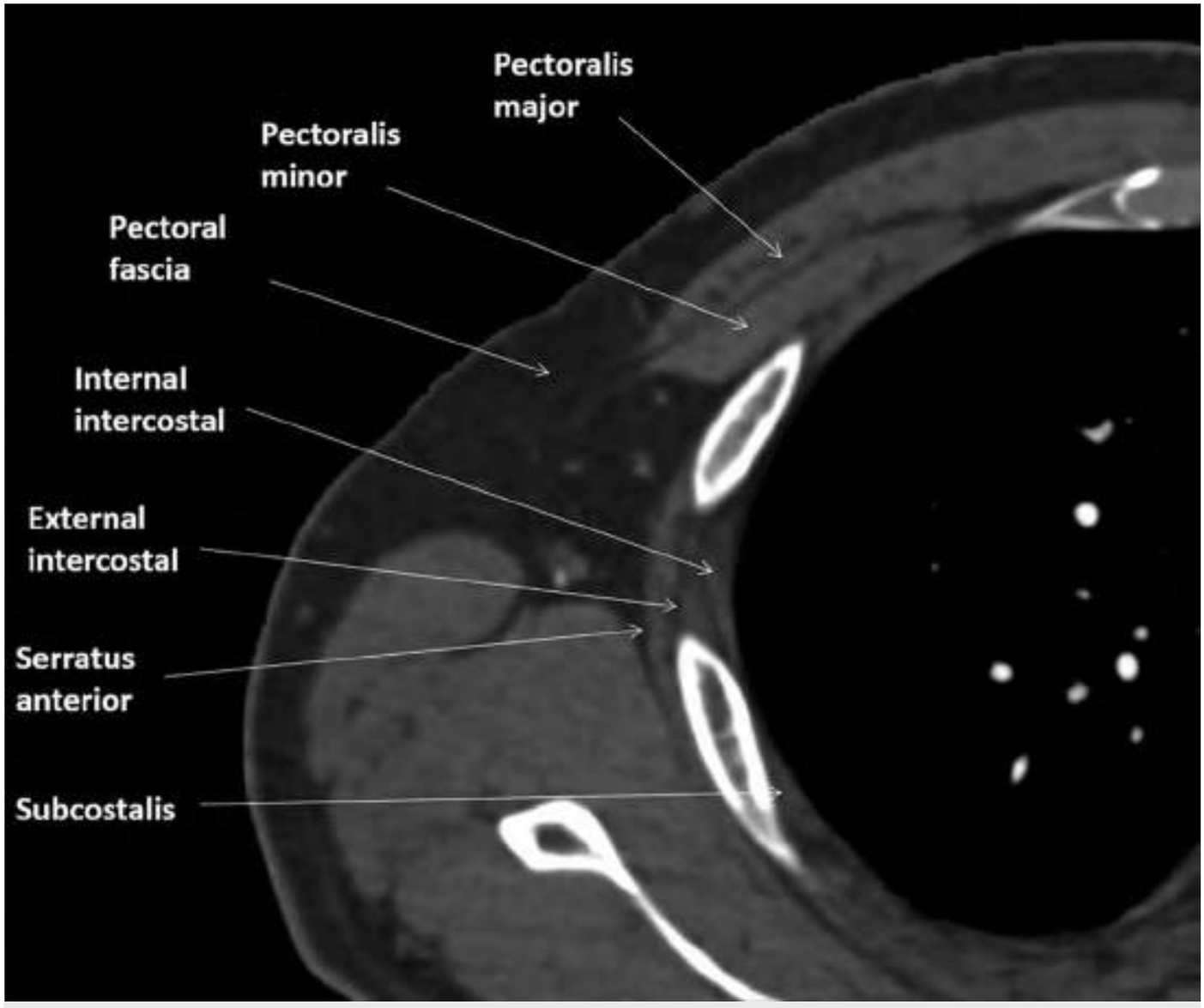

Fig. 1.36 Intercostal muscles in the lateral chest wall. Both internal and external muscles are well formed.

The innermost intercostal muscles are variable, incomplete, and deepest muscle layer. Depending on location, these muscles are divided into three groups: subcostalis, lateral innermost, and transversus thoracis. The subcostalis muscles are located posterolaterally and extend over two or three ribs (▶ Fig. 1.14, ▶ Fig. 1.37). They are better developed in the lower chest wall (please see ▶ Fig. 1.71, ▶ Fig. 1.72 at the end of the chapter). The lateral group fibers run parallel to the fibers of the internal intercostal muscles but separated from each other by intercostal nerves and vessels. The parasternal intercostal regions are covered on their inner surface by four to five thin muscle slips known as the transversus thoracis (triangularis sterni, or sternocostalis). The transversus thoracis originates from posterior surface of the lower sternal body and the xiphoid process. Its muscle fibers run laterally and superiorly (parallel to the anterior external intercostal fibers) to insert on the second through sixth ribs/costal cartilages (▶ Fig. 1.34). The most frequent lowest rib attachment is the sixth rib.[55] The highest muscle attachment may reach to the second rib to cover the internal thoracic artery. Variants including complete absence, asymmetry, presence of a slip attached from the second to fourth rib cartilages and continuation with the fibers of the transverse abdominal muscle have been described.

All the intercostal muscles are innervated by the intercostal nerves and supplied by the intercostals arteries. The main intercostal nerve runs between the pleura and the inferior aspect of the rib and gives off the external and internal branches to the corresponding intercostals muscles. The intercostal nerve also gives off branches to the transversus thoracis and several abdominal muscles.

The primary effect of the intercostal muscle contraction is to displace the ribs.[56] Ribs have limited motion at the vertebral end. The costovertebral and costotransverse joints together form a hinge. Therefore, the respiratory movements of the rib occur primarily through a rotation around the long axis of its neck. With each inspiration, the ribs are moved in the cranial direction, and the sternum will be displaced anteriorly. Consequently, both the lateral and anteroposterior diameters of the rib cage increase with inspiration. This implies that the muscles that elevate the ribs have an inspiratory effect on the rib cage, whereas the

Fig. 1.37 **(a)** Intercostal muscles in the paraspinal region. In the paravertebral region, the internal intercostal muscle may be absent. Instead, the space is covered by the levatores costarum muscles and the posterior intercostal membrane. (**b**)The innermost intercostal muscles are variable, incomplete, and the deepest muscle layer. The lateral group fibers run parallel to the fibers of the internal intercostal muscles but separated from each other intercostal nerves and vessels.

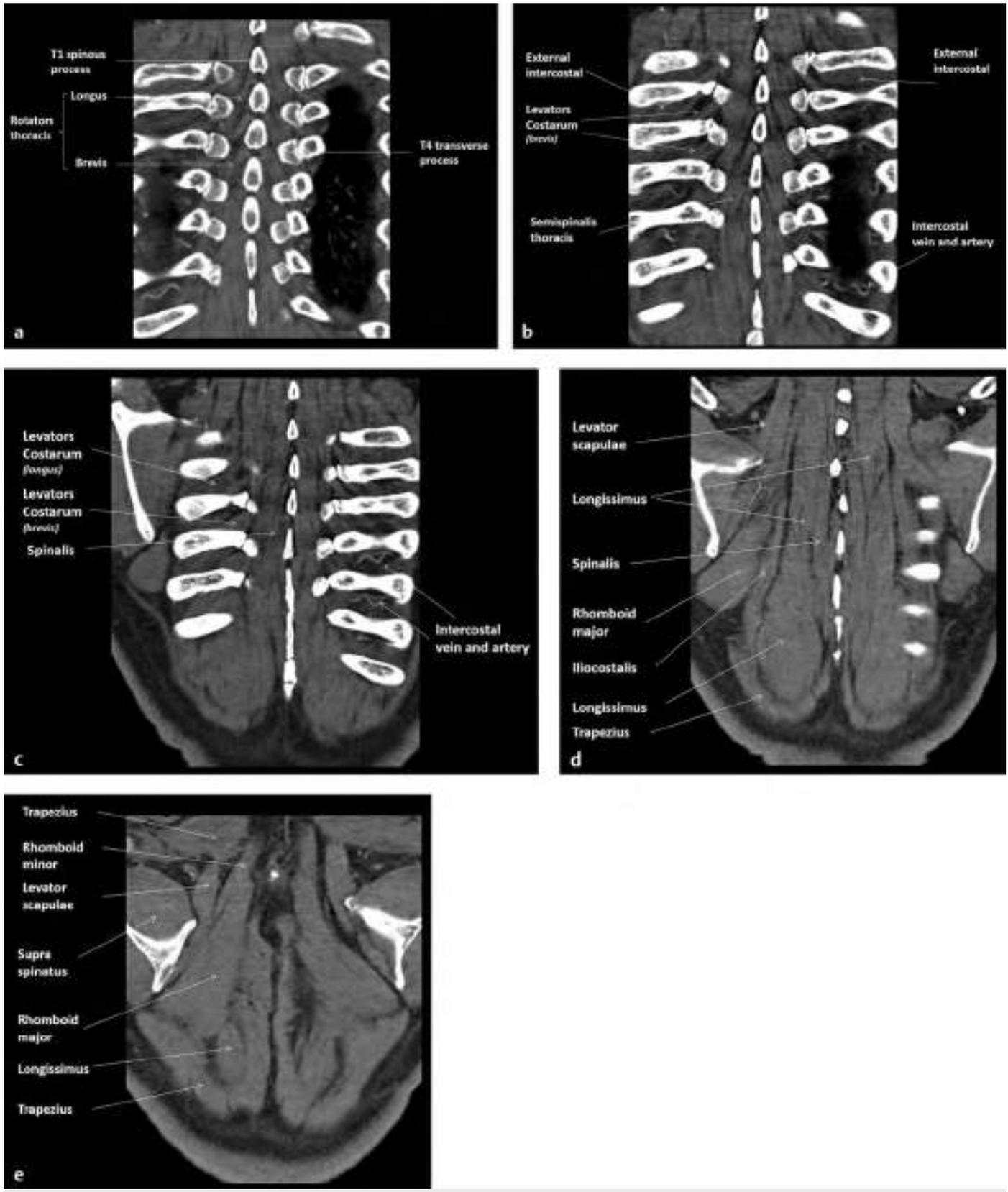

Fig. 1.38 (a–e) In the paravertebral region, the internal intercostal muscle may be absent. Instead, the space is covered by the levator costae and the posterior intercostal membrane. The levator costae are small muscles extending obliquely and parallel to the external intercostales between the tip of the transverse process of the vertebra and the inferior rib.

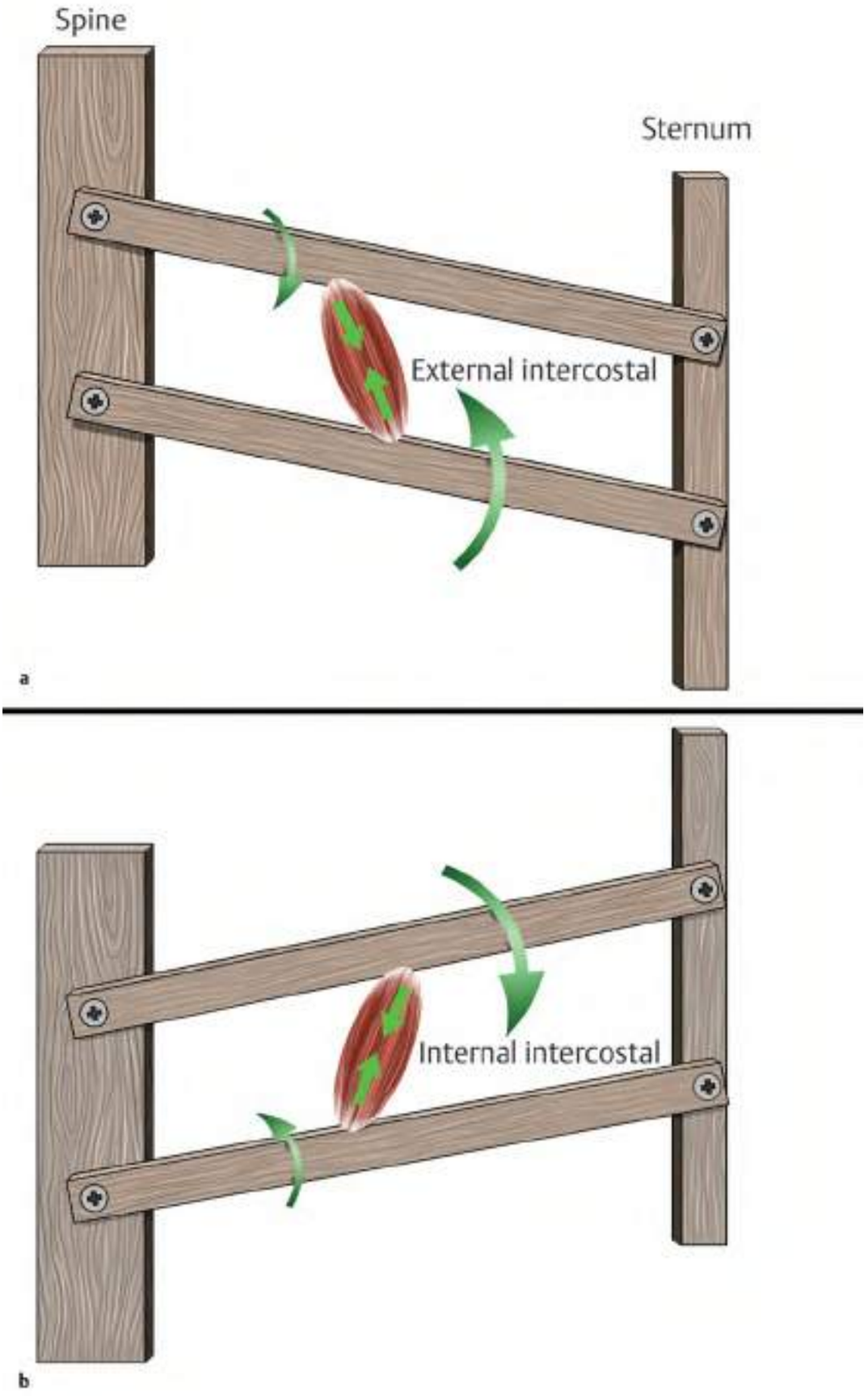

Fig. 1.39 (a, b) Diagram illustrating the action of the intercostal muscles as proposed by Hamberger. The primary effect of the intercostal muscle's contraction is to displace the ribs. At the spinal side, the costovertebral and costotransverse joints together form a hinge. Therefore, the muscles that elevate the ribs have an inspiratory effect on the rib cage (i.e., upper posterior external intercostal muscles), whereas the muscles that lower the ribs have an expiratory effect on the rib cage (i.e., lower internal interosseous intercostal and transversus thoracic muscles). The torques acting on the ribs during contraction of these muscles are represented by arrows. Used with permission from De Troyer et al 2005.[56]

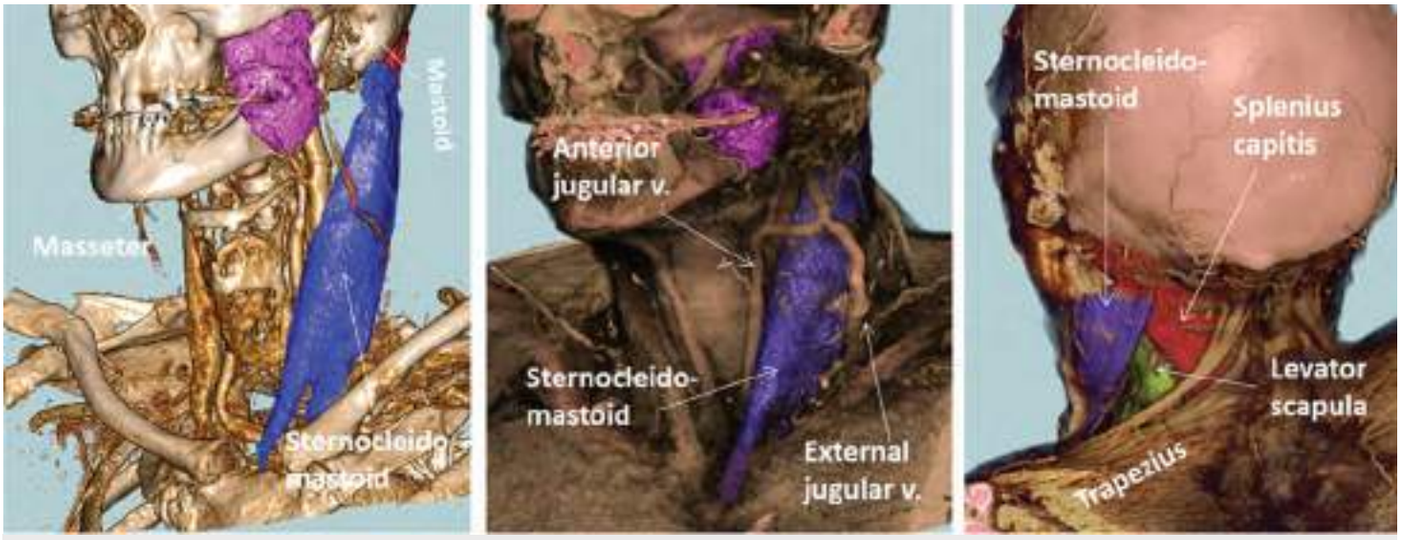

Fig. 1.40 The sternocleidomastoid muscle. The sternal head is tendinous and arises from the anterior surface of the manubrium and the clavicular head is muscular and arises from the medial third of the clavicle. The muscle inserts into the lateral surface of the mastoid process and divides the neck into the anterior and posterior triangles.

muscles that lower the ribs have an expiratory effect on the rib cage (▶ Fig. 1.38). The inspiratory effect of the intercostal muscle function is primarily related to the contraction of the upper posterior external intercostal muscles and to a lesser degree to the levatores costae and the parasternal intercostal muscles. The lower internal interosseous intercostal and transversus thoracis muscles have an expiratory mechanical advantage.[57] Spontaneous quiet expiration in supine humans is essentially a passive process.

Muscles of the Thoracic Inlet

Muscles that attach to the inlet of thorax include scalene, sternocleidomastoid, and sternohyoid muscles.

Sternocleidomastoid

The sternocleidomastoid muscle is a craniocervical muscle that divides the neck into the anterior and posterior triangles (Appendix image series). The sternal head is tendinous and arises from the anterior surface of the manubrium, whereas the clavicular head is muscular and arises from the superior surface of the medial third of the clavicle (▶ Fig. 1.8, ▶ Fig. 1.39). The muscle inserts into the lateral surface of the mastoid process and the lateral half of the superior nuchal line.[58] The sternocleidomastoid has a dual innervation, one from the accessory nerve and the second from the cervical plexus (C1–C3). The upper third of the sternocleidomastoid muscle is supplied by branches of the occipital artery and the middle third of the muscle is supplied by branches of the superior thyroid and/or external carotid arteries. The arterial blood supply of the lower third of the sternocleidomastoid muscle is provided by a branch of the suprascapular artery of the thyrocervical trunk.[59] Morphological variations of the sternocleidomastoid muscle are uncommon. Double bellies of the clavicular portion has been reported.[60]

The sternocleidomastoid muscle is responsible for the stabilization of head posture and the control of head movement.[60]

Scalene Muscles

The scalene muscles include the anterior scalene (scalenus anterior), middle scalene (scalenus medius), and posterior scalene (scalenus posterior)[61] (▶ Fig. 1.40, ▶ Fig. 1.41). Scalenus minimus (Sibson's muscle) is sometimes present behind the lower portion of the anterior scalene. This is innervated by the cervical spinal nerves (C3–C7).[61,62] The scalene muscles run from the transverse processes of the cervical vertebrae to the first and second ribs. Variations in the attachments and the size of the scalene muscles are common. The anterior and middle scalene muscles attach to the anterior and posterior tubercles of the cervical transverse processes, respectively. The anterior scalene origin varies between C3 and C7. The middle scalene muscle arises from C2 to C6 with attachments to C2 or C7 in 50 to 60%.[63] It is thicker and longer than the anterior scalene muscle. The posterior scalene muscle arises from posterior tubercles of transverse processes of C4 to C6 in 50% and from C5 and C6 in 50%.

The anterior scalene inserts on the tubercle on the anteromedial aspect of the first rib (▶ Fig. 1.7). It lies behind the sternocleidomastoid muscle. The middle scalene attaches to the upper surface of the lateral aspect of the first rib (▶ Fig. 1.7). The posterior scalene inserts to outer surface of the second rib behind the tubercle for the serratus anterior muscle (▶ Fig. 1.42).

The scalenus minimus may originate from the transverse process of the seventh or sixth cervical vertebrae and insert on the first rib behind the subclavian artery groove (▶ Fig. 1.43). Recognition of this muscle is important for the diagnosis of the thoracic outlet syndrome. It could be responsible for signs of compression of the brachial plexus. Scalenus minimus is present in 5 to 46% of individuals and 28% are bilateral.[61,62]

The scalene muscles are lateral flexors of the cervical spine. They also rotate the cervical spine. When both sides simultaneously contract, they contribute to flexion. The scalene muscles are also accessory muscles of respiration. If neck is hyperextended, these muscles help to raise the upper ribs in forced inspiration.

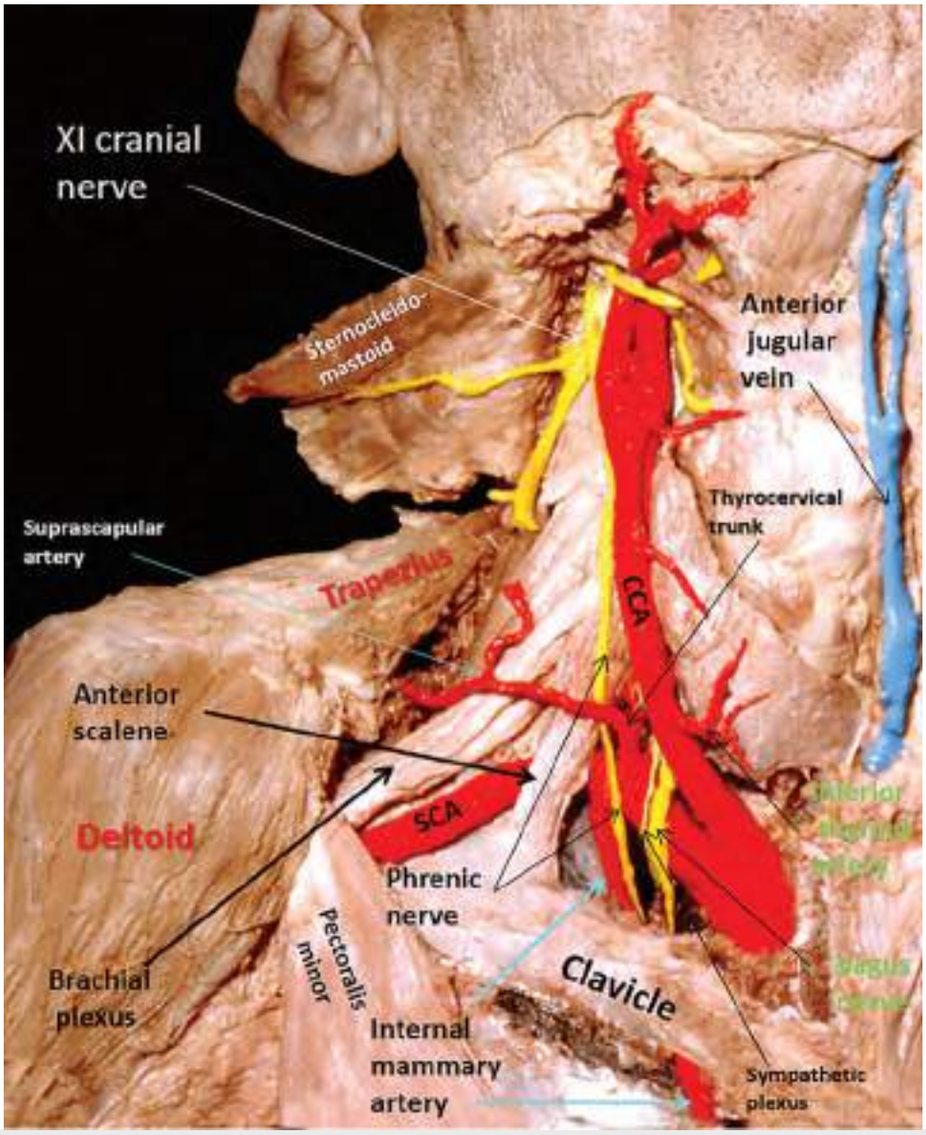

Fig. 1.41 Right lateral neck showing relationship of the neurovascular structures with the anterior scalene and pectoralis minor muscles. CCA, common carotid artery; SCA, subclavian artery.

Subclavius Muscle

The subclavius is a small elongated muscle running underneath the clavicle. It arises from the first costochondral junction, anterior to the costoclavicular ligament and inserts laterally into the inferior clavicular groove (▶ Fig. 1.44). It is supplied by the thoracoacromial artery and innervated by the C5 and C5 nerves. Anatomical variations are not uncommon. Duplicated subclavius and subclavius posticus are described. The subclavius posticus is a supernumerary muscle beneath the clavicle. It extends between the sternal end of the first rib and the superior border of the scapula. It may play a role in development of the thoracic outlet syndrome.[64] The subclavius posticus (also known as the sternoscapularis) passes anterior to the subclavian vein and the brachial plexus. This explains the possible occurrence of the thoracic outlet syndrome. It may compress the suprascapular nerve.[65]

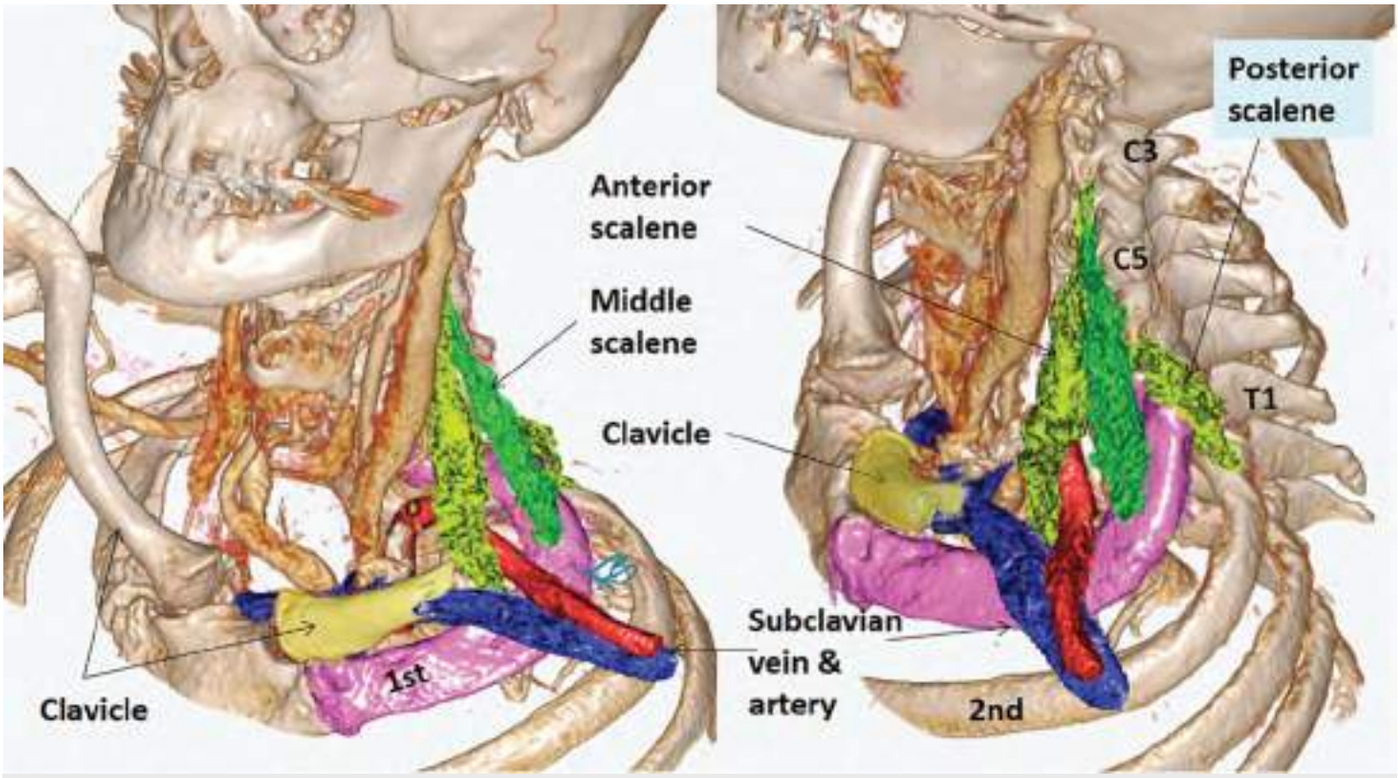

Fig. 1.42 Relationship of the scalene muscles with the vessels of the left thoracic inlet. The anterior scalene inserts on the tubercle on the anteromedial aspect of the first rib anterior to the subclavian artery. The middle scalene attaches to the upper surface of the lateral aspect of the first rib. The posterior scalene inserts to outer surface of the second rib behind the tubercle for the serratus anterior muscle.

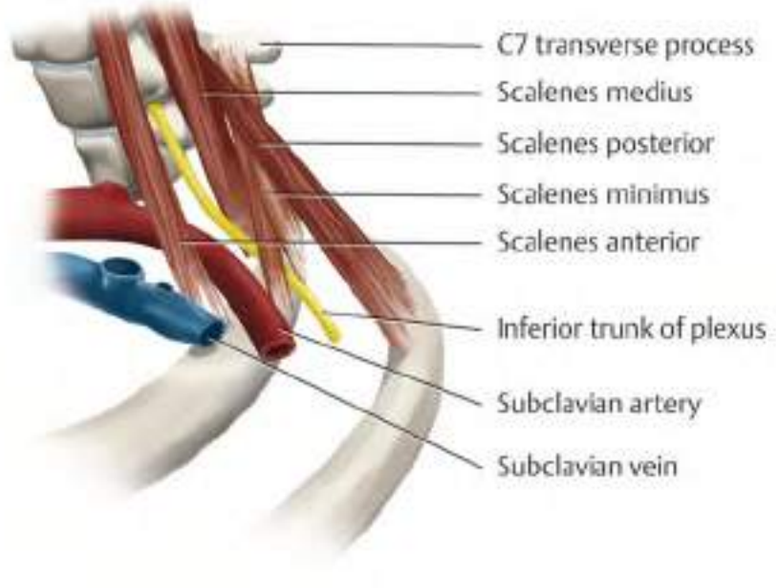

Fig. 1.43 Scalenus minimus. The scalenus minimus may originate from the transverse process of the seventh or sixth cervical vertebrae and insert on the first rib behind the subclavian artery groove. It may cause compression of the brachial plexus. Used with permission from Harry et al 1997.[61]

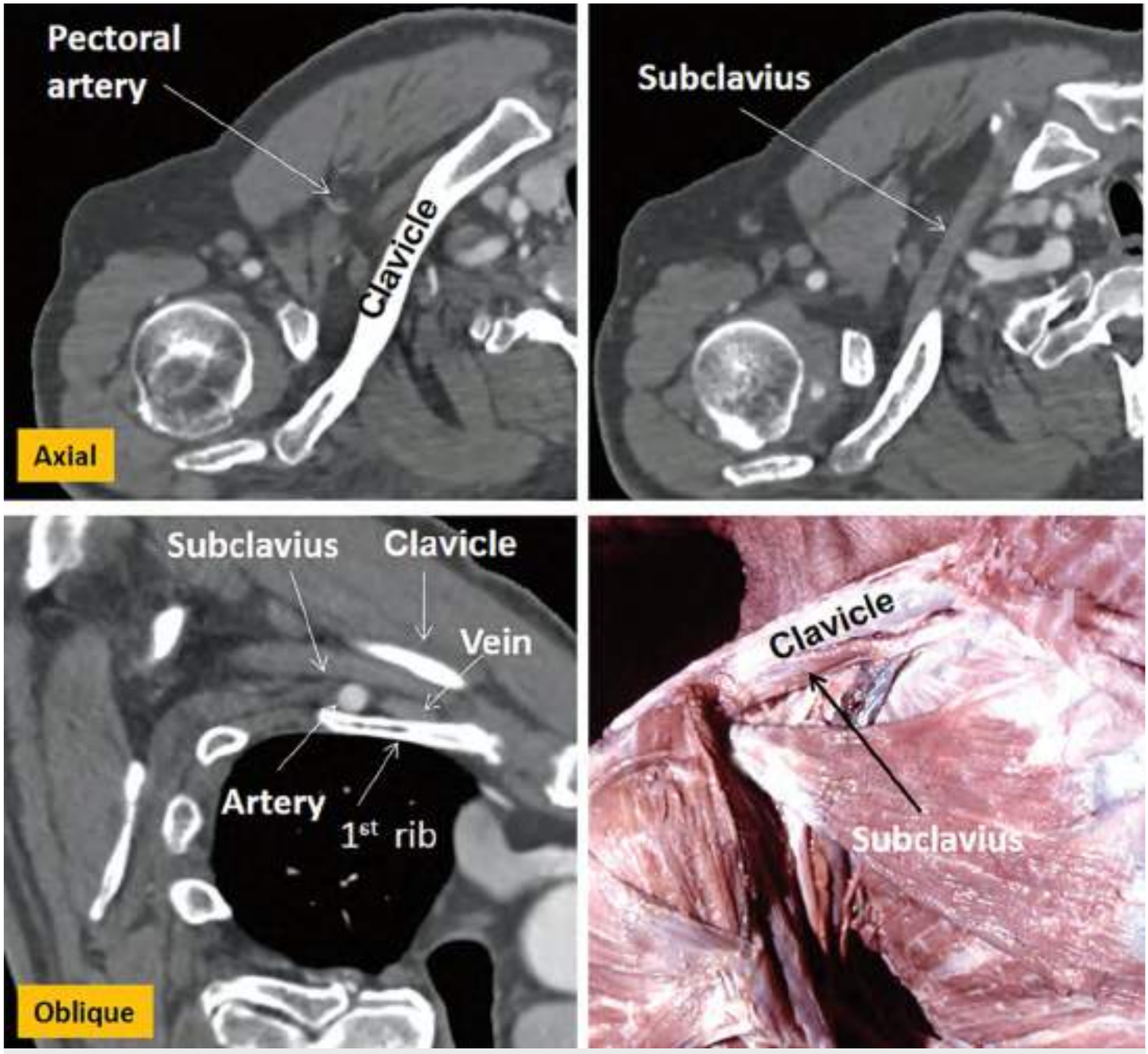

Fig. 1.44 Subclavius and costoclavicular space. The subclavius arises from the first costochondral junction and inserts laterally into the inferior clavicular groove. The subclavian vein passes between the subclavius and the first rib in the costoclavicular space.

◆ Arterial Supply to the Thoracic Wall

Most arterial branches to the chest wall are from the axillary and subclavian arteries (▶ Fig. 1.45, ▶ Fig. 1.46, ▶ Fig. 1.47, ▶ Fig. 1.48, ▶ Fig. 1.49, ▶ Fig. 1.50). Posterior intercostal arteries arise from the descending aorta.

The right subclavian artery arises from the innominate artery and the left subclavian artery originates directly from the aorta. Each subclavian artery is divided into three segments (▶ Fig. 1.45).

The first segment is short and extends to the medial border of the anterior scalene. The left subclavian artery is the last branch of the aortic arch. It is longer than the right subclavian, and in most cases, forms a groove in the mediastinal margin of the left upper lobe. In rare cases, the left subclavian invaginates deep to form a tunnel in the lung (▶ Fig. 1.46). Branches of the first segment include the vertebral, internal thoracic, and thyrocervical arteries (▶ Fig. 1.47).

The second segment is the part passing between the anterior and middle scalene muscles. At this level, the subclavian vein is located anterior to the scalenus anterior (▶ Fig. 1.46). The second segment gives origin to the costocervical trunk which splits into the deep cervical and superior intercostal arteries.

The third segment extends the outer margin of the first rib and from this point it becomes the axillary artery. The dorsal scapular artery arises from the third segment and supplies the levator scapula and rhomboid muscles. The dorsal scapular artery may arise from the transverse cervical artery.

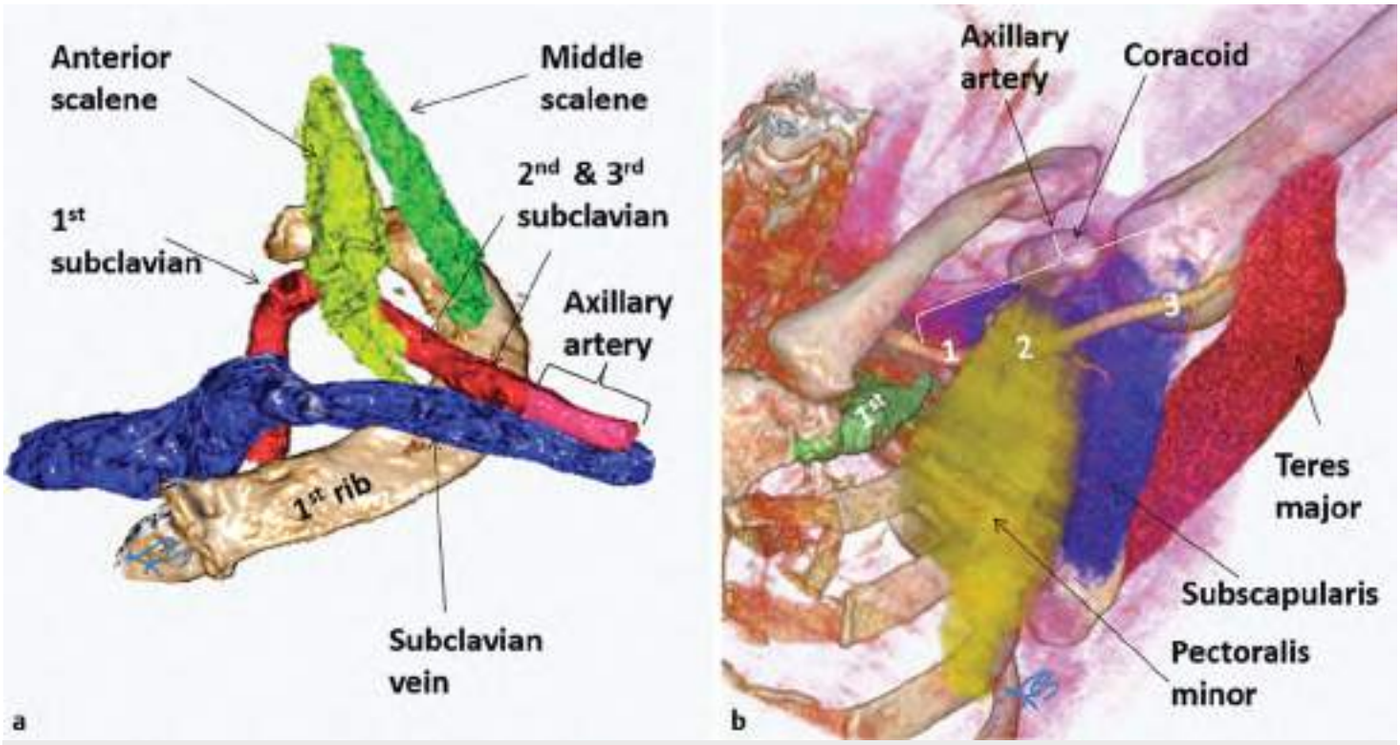

Fig. 1.45 Subclavian and axillary arteries. **(a)** Each subclavian artery is divided into three segments. The first segment extends to the medial border of the anterior scalene. The second segment passes between the anterior and middle scalene muscles. The third segment extends the outer margin of the first rib and from this point it becomes the axillary artery. **(b)** The axillary artery extends from the lateral border of the first rib to the margin of teres major muscle to become the brachial artery. The axillary artery is also divided into three segments based in reference to the pectoralis minor muscle margins with the second part passing behind this muscle.

Fig. 1.46 Left subclavian invagination into the medial margin of the left upper lobe (*arrow*).

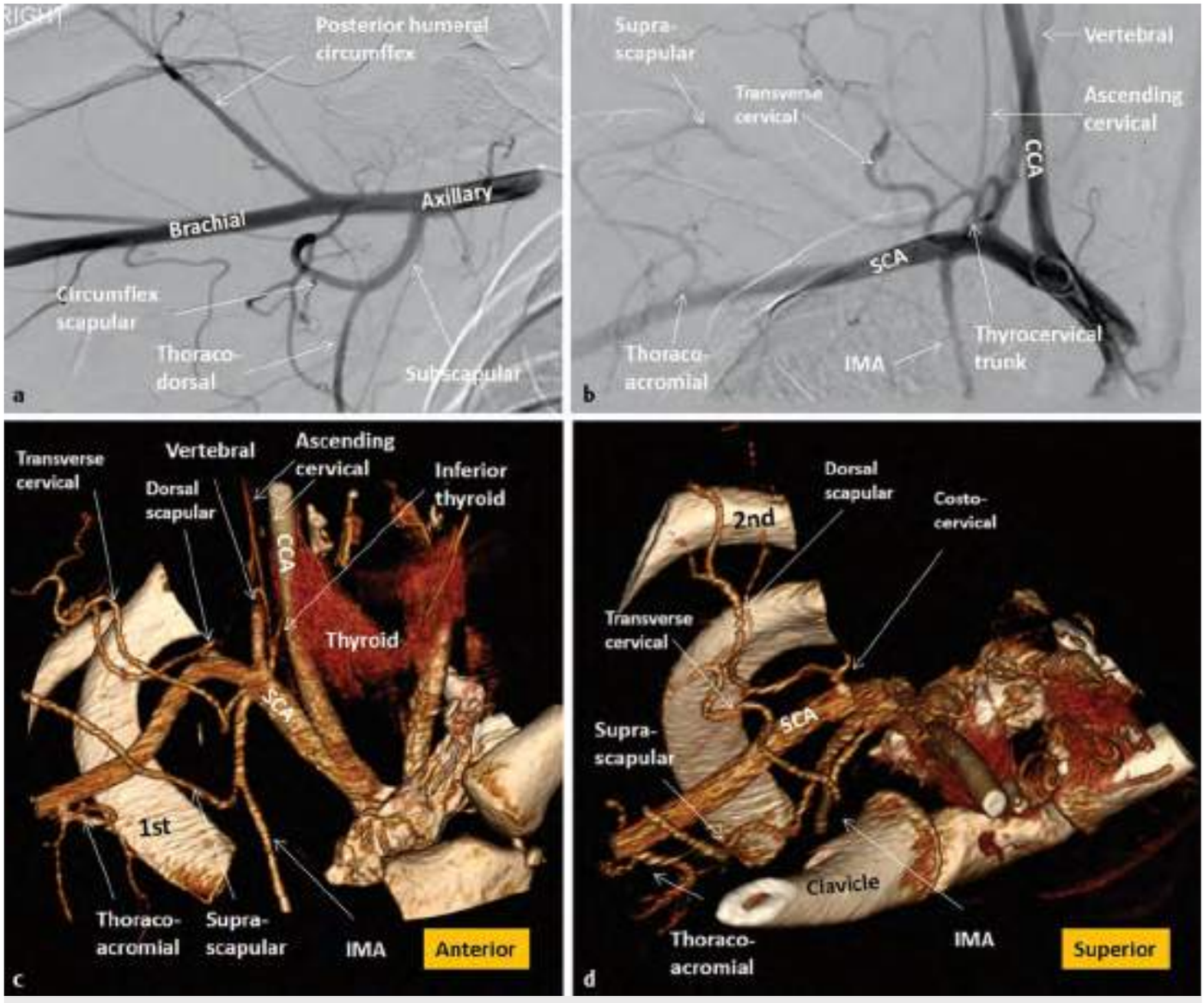

Fig. 1.47 **(a)** Right subclavian artery (SCA) and **(b)** right axillary artery angiograms showing normal anatomy. **(c, d)** Two views of CT angiogram showing branches of the right subclavian artery. CT images show that suprascapular artery arises from the IMA and dorsal scapular from the costocervical trunk. CCA, common carotid artery; IMA, internal mammary artery, SCA, subclavian artery.

The axillary artery extends from the lateral border of the first rib to the inferior margin of teres major muscle to become the brachial artery. The axillary artery is also divided into three segments based in reference to the pectoralis minor muscle margins with the second part passing behind this muscle (▶ Fig. 1.46). The first segment (one branch) gives origin to the superior (supreme) thoracic artery. The second segment branches (two branches) include the thoracoacromial and lateral thoracic arteries. The third segment branches (three branches) include the subscapular, anterior humeral circumflex, and posterior humeral circumflex arteries.

Variation in the order or number of branches from different segments of the axillary or subclavian artery is common[66] and typically involves the lateral thoracic, subscapular, and posterior humeral circumflex branches (66%).[67] The thoracoacromial artery consistently originates from the first or second part of the axillary artery. Early branching of the axillary artery into two brachial arteries is possible.[68] Rare cases of the ulnar arteries originating from the axillary artery are reported.[69] Passage of the subclavian artery anterior to the anterior scalene is also reported.[70]

The scapular circulatory anastomosis around the scapula provides collaterals between the first segment of the subclavian artery and the third segment of the axillary arteries in case the artery is occluded. These arteries include the transverse cervical, dorsal scapular, suprascapular, and subscapular arteries (▶ Fig. 1.49).

Enlargement of normal systemic arteries is encountered in patients with bronchiectasis, pulmonary tuberculosis, other pulmonary infections, pulmonary thromboembolism, or chronic obstructive pulmonary disease. These enlarged systemic arteries include the bronchial arteries, intercostal arteries, internal mammary arteries, inferior phrenic arteries, branches of the thyrocervical trunk, branches of the hepatic arteries, and branches of the abdominal aorta. These systemic arteries are considered to supply the lungs by means of anastomoses between bronchial and

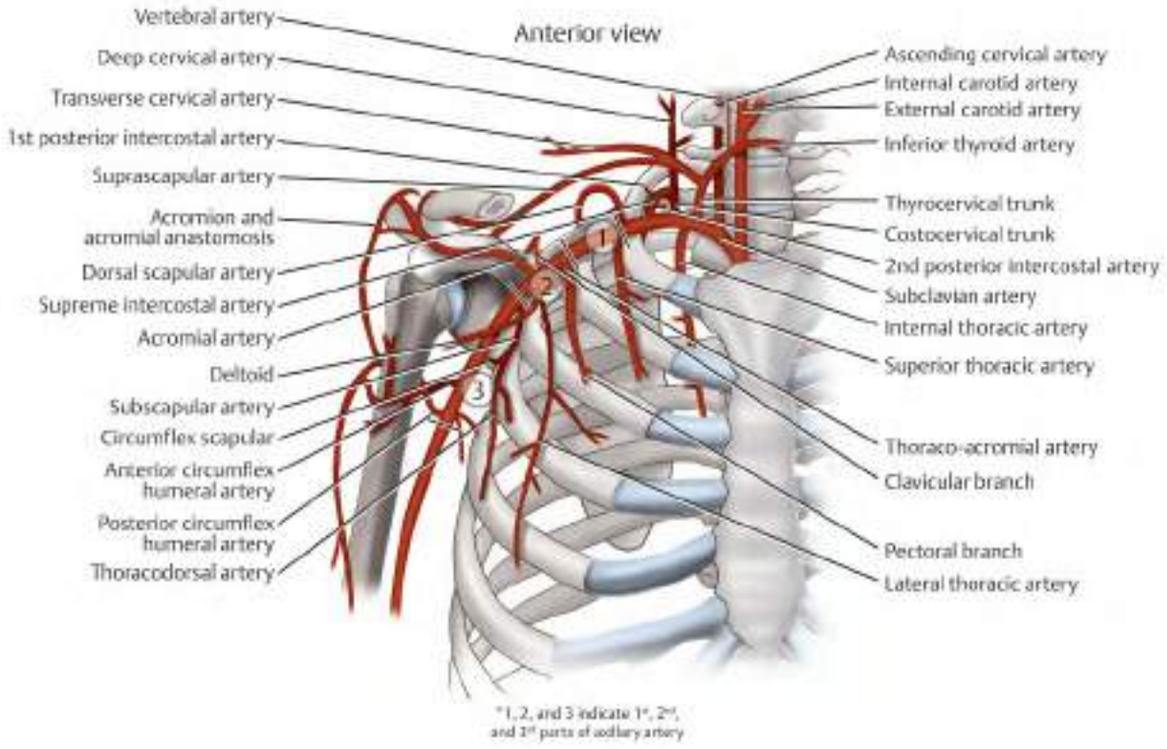

Fig. 1.48 Arterial branches of the subclavian artery and right axillary arteries.

pulmonary arteries within the lung parenchyma or through transpleural systemic–pulmonary artery anastomoses.

Thyrocervical Trunk

The thyrocervical trunk arises from the first segment of the subclavian artery immediately distal to the vertebral artery (▶ Fig. 1.41, ▶ Fig. 1.47, ▶ Fig. 1.48). Soon after takeoff, it branches into the inferior thyroid, suprascapular, ascending cervical, and transverse cervical arteries (▶ Fig. 1.51, ▶ Fig. 1.52). Anomalous origin of the vertebral artery from the thyrocervical trunk is rarely seen.[71]

The suprascapular artery runs laterally along the superior border of the scapula to enter the supraspinatus fossa to move between the scapular bone and the supraspinatus muscle (▶ Fig. 1.52). The artery then passes through the great scapular notch to the infraspinatus fossa, where it anastomoses with the scapular circumflex artery and the descending branch of the transverse cervical artery.

The transverse cervical artery runs laterally and parallel to the suprascapular artery. The dorsal scapular artery is a branch of the transverse cervical in 25% and together form the cervicodorsal trunk. It moves inferiorly, together with the dorsal scapular nerve, along the medial border of the scapula (▶ Fig. 1.51). The dorsal scapular artery anastomoses with the subscapular artery branches (▶ Fig. 1.49).

Internal Thoracic Artery

The internal thoracic (mammary) arteries originate from the ascending segment of the subclavian artery in 75% and from the arcuate segment of the subclavian artery in 20%[72] (▶ Fig. 1.41). Rarely, they arise from a common trunk with other arteries including the thyrocervical trunk, dorsal scapular artery, thyroid artery, or costocervical trunk[73] (▶ Fig. 1.47). The internal thoracic arteries terminate into the musculophrenic and superior epigastric arteries. The superior epigastric artery (*green arrows*) originates from the internal thoracic artery at the level of the sixth and seventh rib and descends to enter the rectus sheath, where it anastomoses with the deep inferior epigastric branch of the external iliac (▶ Fig. 1.53).

From their origin, the internal thoracic arteries cross the brachiocephalic vein and sternoclavicular joint and then run in the parasternal region behind the second to sixth costal cartilages, at a distance of about 1 cm from the sternal margin. From the third intercostal space the artery locates between the transversus thoracis muscle and the intercostal muscles where it gives off branches at each intercostal space.

The internal thoracic arteries give off sternal, perforating, anterior intercostal, and mediastinal branches.[74] The pericardiacophrenic artery originates from the internal thoracic arteries in 90%[75] (▶ Fig. 1.53). The sternal branches usually arise from a common trunk with intercostal artery or perforators. The sternal vessels are important because decreased blood supply to the sternum after internal thoracic artery dissections may lead to bone necrosis. However, it is reported that after sternotomy and bilateral grafting of internal thoracic arteries, the decrease in blood supply to the sternum is reversible in 1 month, thanks to the collateral vessels.[76,77] To protect the vascular supply to the sternum, it is suggested to ligate the sternal and intercostal branches as close to the internal thoracic artery as possible.

The length of arteries varies from 150 to 220 mm, with a mean of 180 to 185 mm.[78] In more than 90%, the artery bifurcates at its

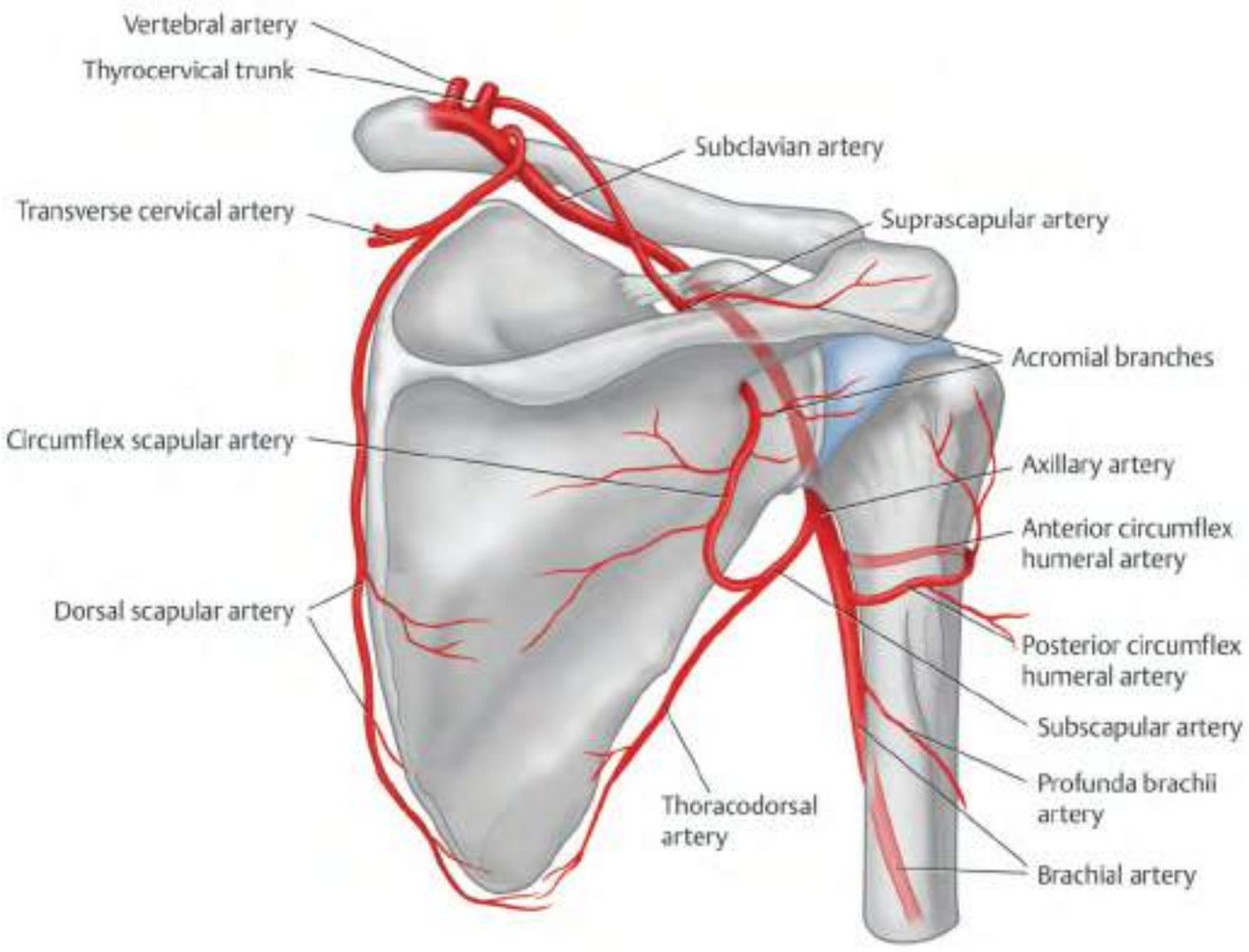

Fig. 1.49 Arterial branches of the scapula and circulatory anastomosis around the scapula.

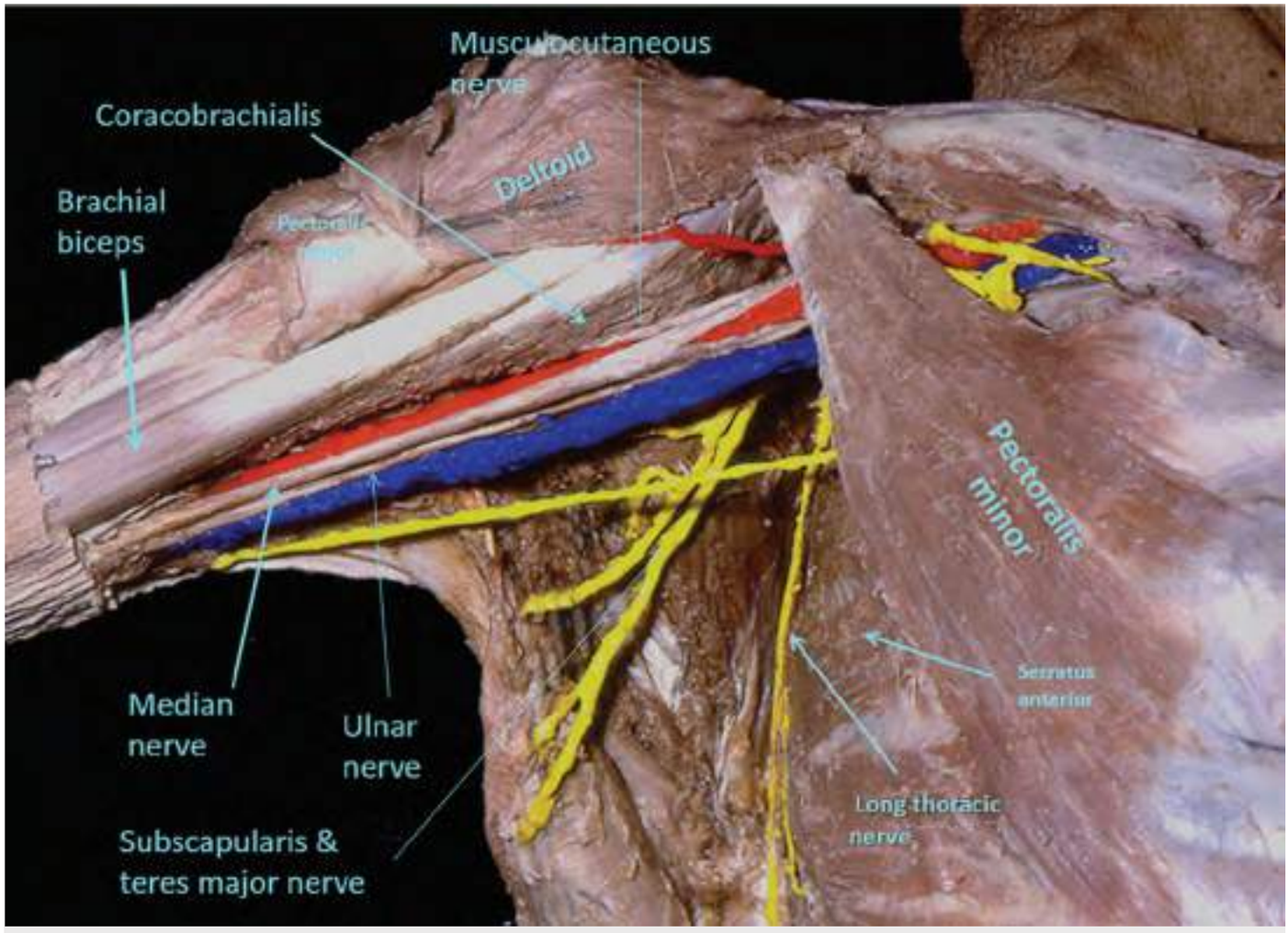

Fig. 1.50 Brachial neurovascular bundle. The long thoracic nerve is shown. It runs with the lateral thoracic vessels and supplies the serratus anterior muscle.

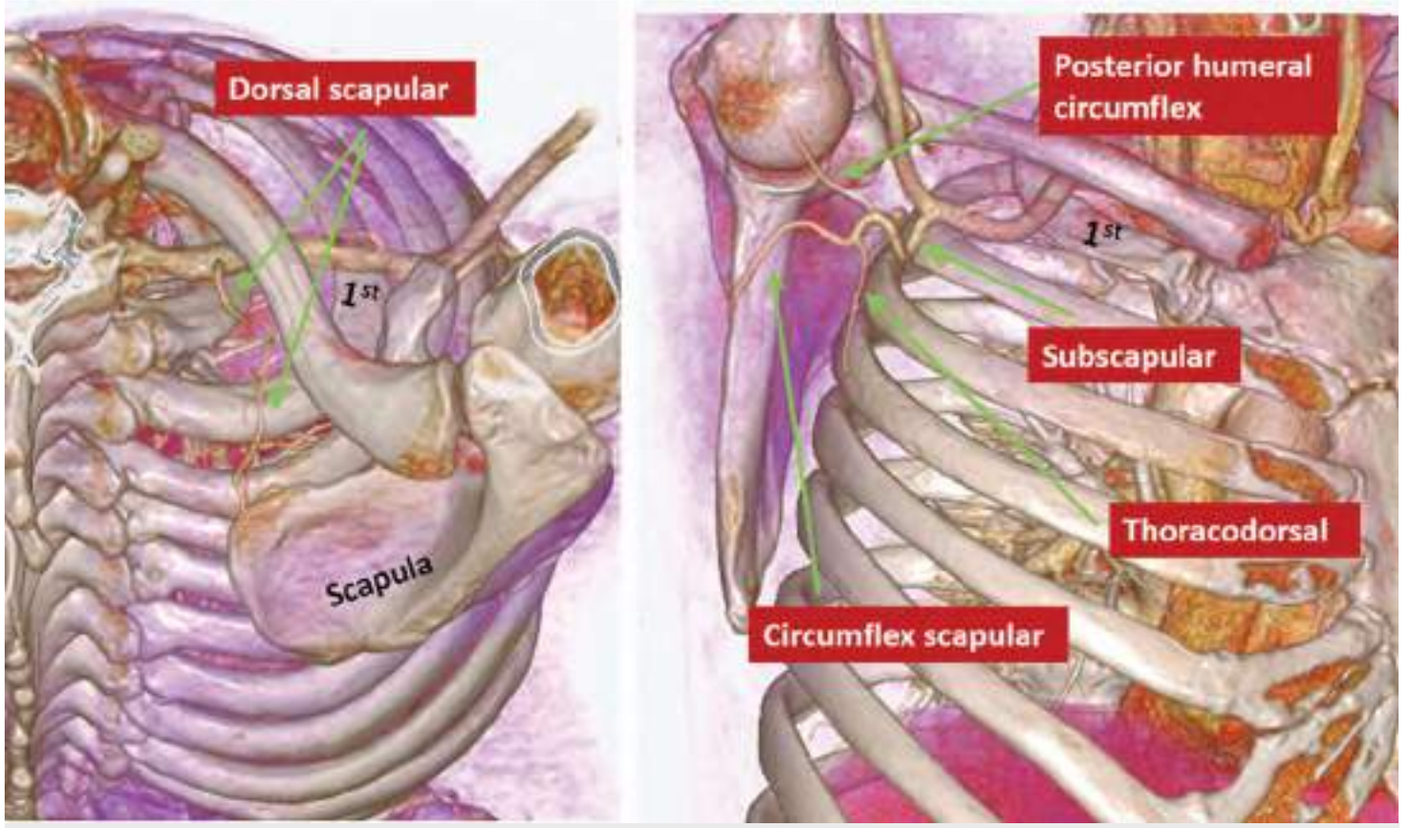

Fig. 1.51 Dorsal scapular and subscapular arteries. The dorsal scapular artery arises from the third segment and supplies the levator scapula and rhomboid muscles. The subscapular artery arises from the third segment of the axillary artery. Common origin with the posterior humeral circumflex artery is common and seen in 42%.

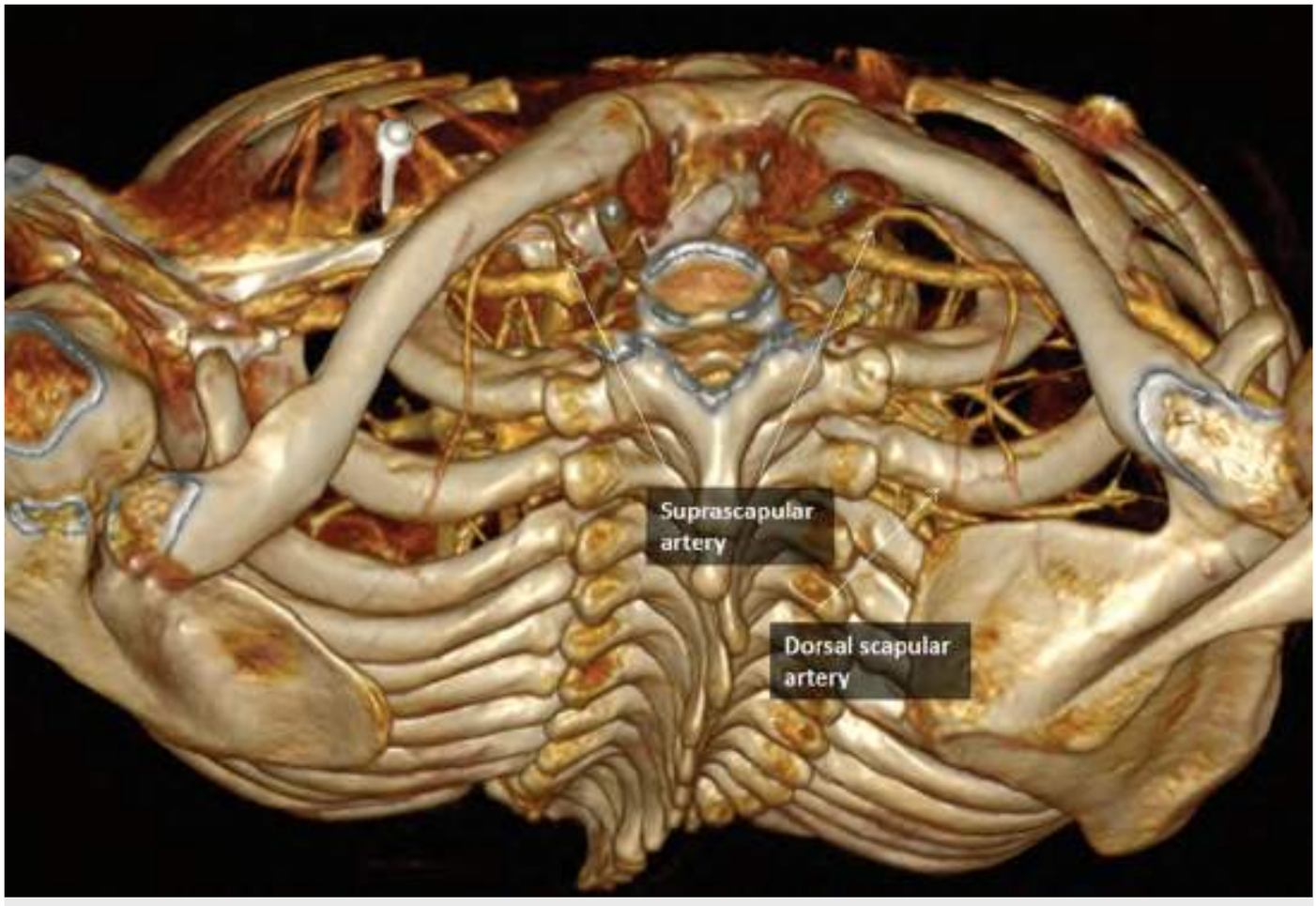

Fig. 1.52 Dorsal scapular and suprascapular arteries. The suprascapular artery is a branch of the thyrocervical trunk. The dorsal scapular artery is a branch of the transverse cervical artery. In this case, the dorsal scapular artery arises from the subscapular artery.

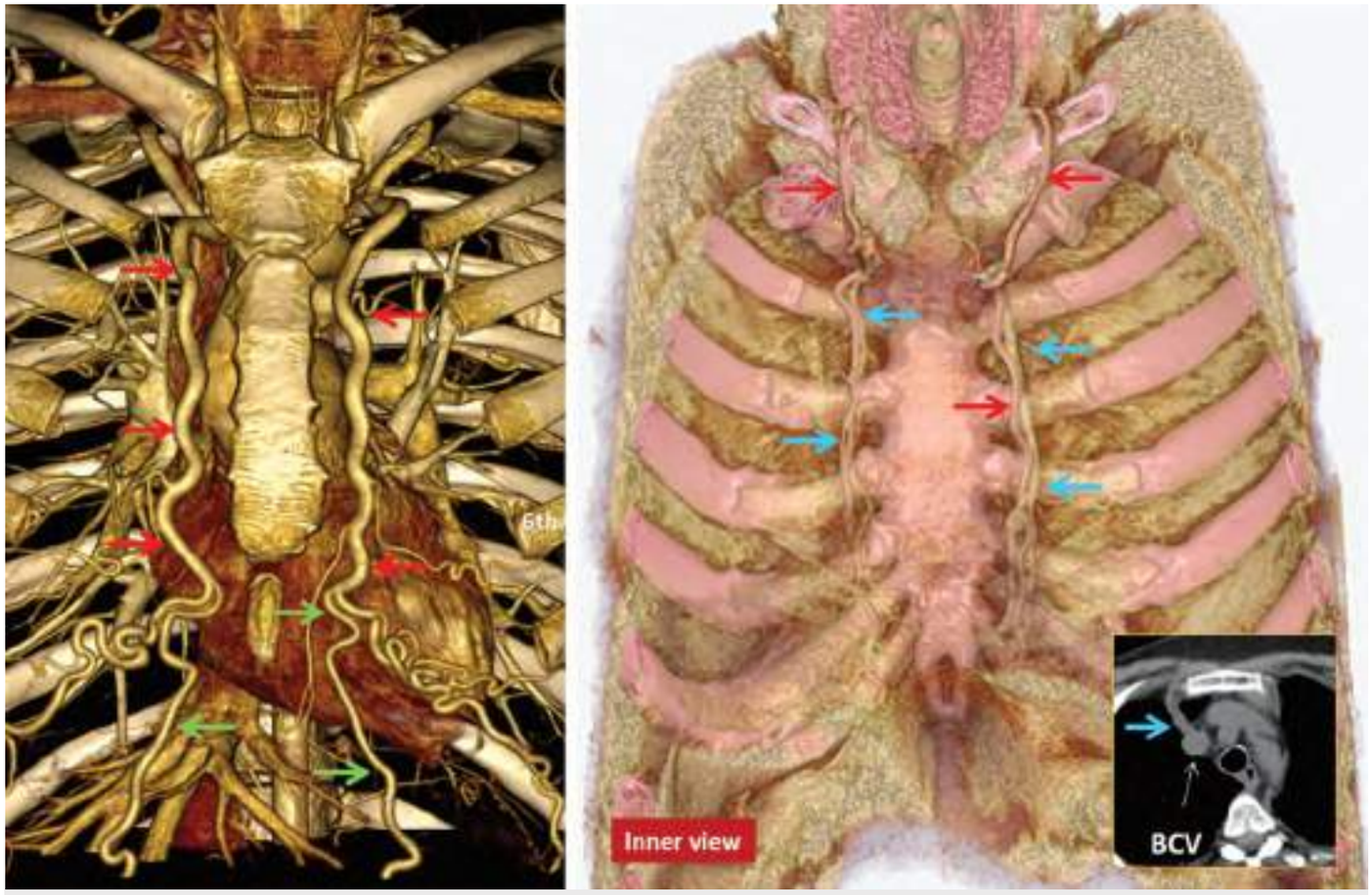

Fig. 1.53 Internal thoracic arteries and veins. The internal thoracic arteries (*red arrows*) run in the parasternal region behind the second to sixth costal cartilages and give off branches at each intercostal space. The superior epigastric artery (*green arrows*) originates from the internal thoracic artery at the level of the sixth and seventh rib and descends to enter the rectus sheath, where it anastomoses with the deep inferior epigastric branch of the external iliac. The internal thoracic veins (*blue arrows*) are single or double venae comitantes running in parallel to the internal thoracic artery and draining into the brachiocephalic vein (BCV).

terminal end into the superior epigastric and musculophrenic arteries. The most frequent termination point is the sixth intercostal space, but it may vary between the third and seventh ribs. In its course, the internal thoracic artery may show a medial concavity in 20%. Henriquez–Pino et al reported rectilinear course in 34%, medial concavity in 30%, lateral concavity in 29%, and tortuosity in 7%.[75] The presence of a third terminal, diaphragmatic branch in seen 7% of the cases. A lateral internal thoracic branch called "lateral costal branch" or "accessory" may be seen in 4% originating from the existing internal thoracic and anastomoses with the neighboring intercostal arteries. In 11% of the cases the internal thoracic artery is found hypoplastic or absent.[79]

The left internal thoracic artery is a common conduit for the coronary artery bypass surgery (CABG). It is found to be an artery with elastic properties that is resistant to atherosclerosis, although cases of diseased arteries have been reported in the literature.[80]

The internal thoracic veins are single or double venae comitantes running in parallel to the internal thoracic artery[81] (▶ Fig. 1.53). If double, they unite to form a single vein draining into the brachiocephalic vein. The tributaries of the internal thoracic veins correspond to the branches of the internal thoracic arteries. In 78% the internal thoracic veins connect each other by a venous arch at the level of the xiphisternal joint.

Thoracoacromial Artery

The thoracoacromial artery arises from the first or second segment of the axillary artery, proximal to the coracoid attachment of the pectoralis minor.[67] Major branches include the pectoral, acromial, clavicular, and deltoid. The pectoral branch runs between the pectoralis major and minor (please see ▶ Fig. 1.71, ▶ Fig. 1.72 at the end of the chapter). The deltoid branch moves laterally to run in the groove between the deltoid and pectoralis muscles along with the cephalic vein. Rarely, the radial artery may arise directly from the thoracoacromial artery.[82]

Lateral Thoracic Artery

The lateral thoracic artery originates from the axillary artery or one of its branches and travels along the lateral chest wall to supply the serratus anterior, pectoralis major, and subscapularis muscles (▶ Fig. 1.54). Branches are sent to the axilla and breast soft tissues. The lateral thoracic artery may originate from the

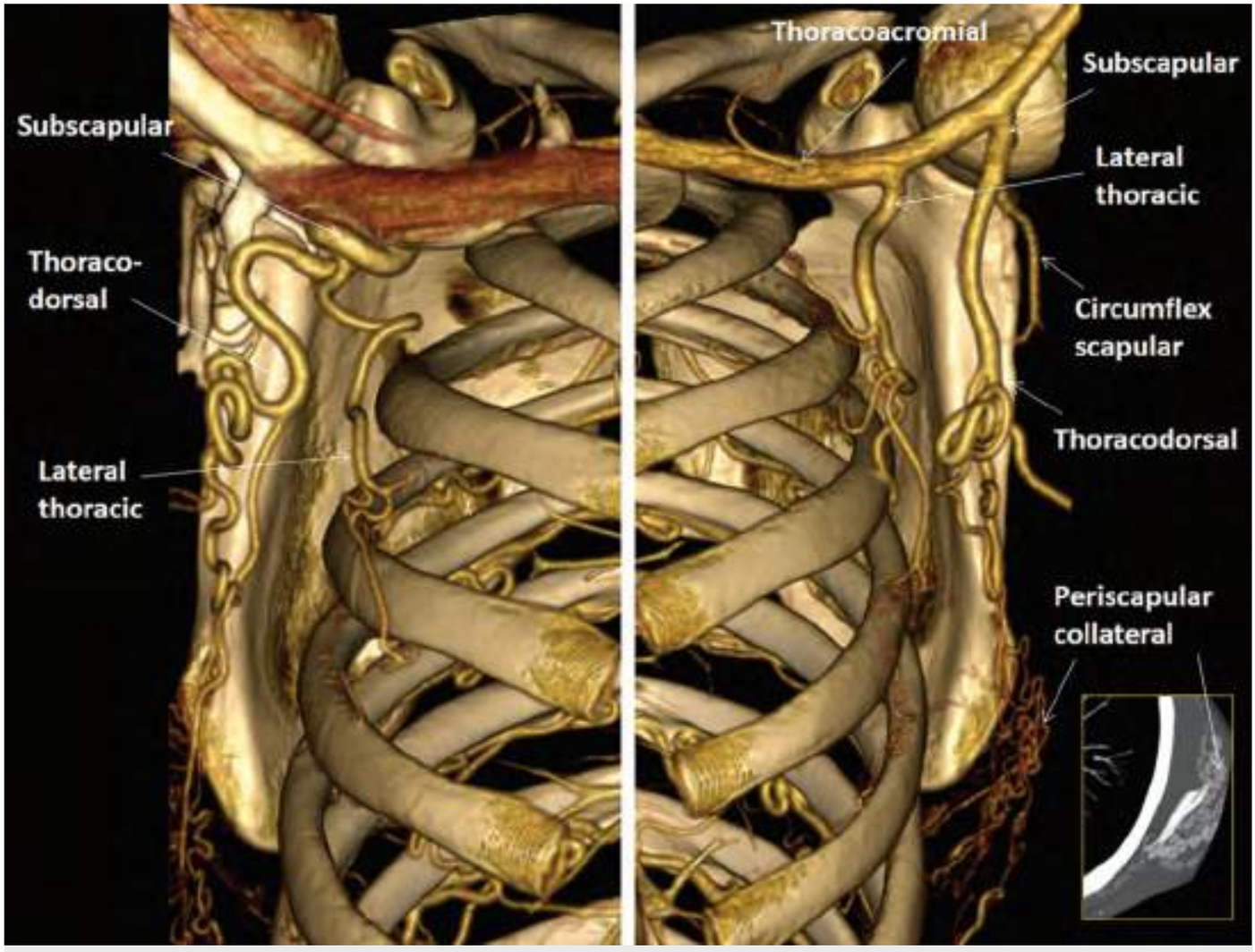

Fig. 1.54 Right lateral and left lateral CT angiograms in the same patient are shown. On the right side both the lateral thoracic artery and thoracodorsal arteries arise from a common trunk. This variant is seen in 5 to 7%. The subscapular artery divides into the circumflex scapular and thoracodorsal arteries. Note extensive periscapular collaterals in this patient with coarctation of the aorta.

axillary, thoracoacromial, thoracodorsal, suprascapular, or subscapular arteries.[83,84] The most common variant origin of the lateral thoracic artery is from the thoracoacromial artery (67%) and the second most common is the axillary artery (17%).[83] Origin of the thoracodorsal artery from the lateral thoracic artery is seen in 7% and the subscapular artery from the lateral thoracic artery in 5%[85] (▶ Fig. 1.54).

Subscapular Artery

The subscapular artery, the largest branch of the axillary artery, arises at the lower border of the subscapularis muscle and follows to the inferior angle of the scapula, where it anastomoses with the lateral thoracic, intercostal arteries, and descending branch of the dorsal scapular artery.[85] High origin of the subscapularis is seen in 35%. A common variant is common origin with the posterior humeral circumflex artery in 42%[67] (▶ Fig. 1.51). The artery divides into two major branches of the circumflex scapular and thoracodorsal arteries (▶ Fig. 1.54). The circumflex scapular branch enters the infraspinous fossa on the dorsal surface of the scapula. Duplicated circumflex scapular arteries are found in 4% of patients.[86] The thoracodorsal artery supplies branches to the latissimus dorsi and serratus anterior muscles. It travels inferiorly with the thoracodorsal nerve. In 10% it originates directly from the axillary artery.[67] This artery has an important place in reconstructive surgery. The thoracodorsal artery pedicle is used in several different flaps, primarily latissimus dorsi and serratus anterior flaps.

◆ Intercostal Neurovascular Bundle

The intercostal neurovascular bundle runs medial to the internal intercostal muscles and depending on the location may be covered internally by the innermost intercostals, subcostal muscles, or transverse thoracic muscles.[87] In the intercostal space, the intercostal vein is superior to the intercostal artery and intercostal nerve (▶ Fig. 1.55).

Three arteries (one large posterior, two small anterior arteries) supply each intercostal space. There are two anterior intercostal arteries in each intercostal space, one coursing above and one

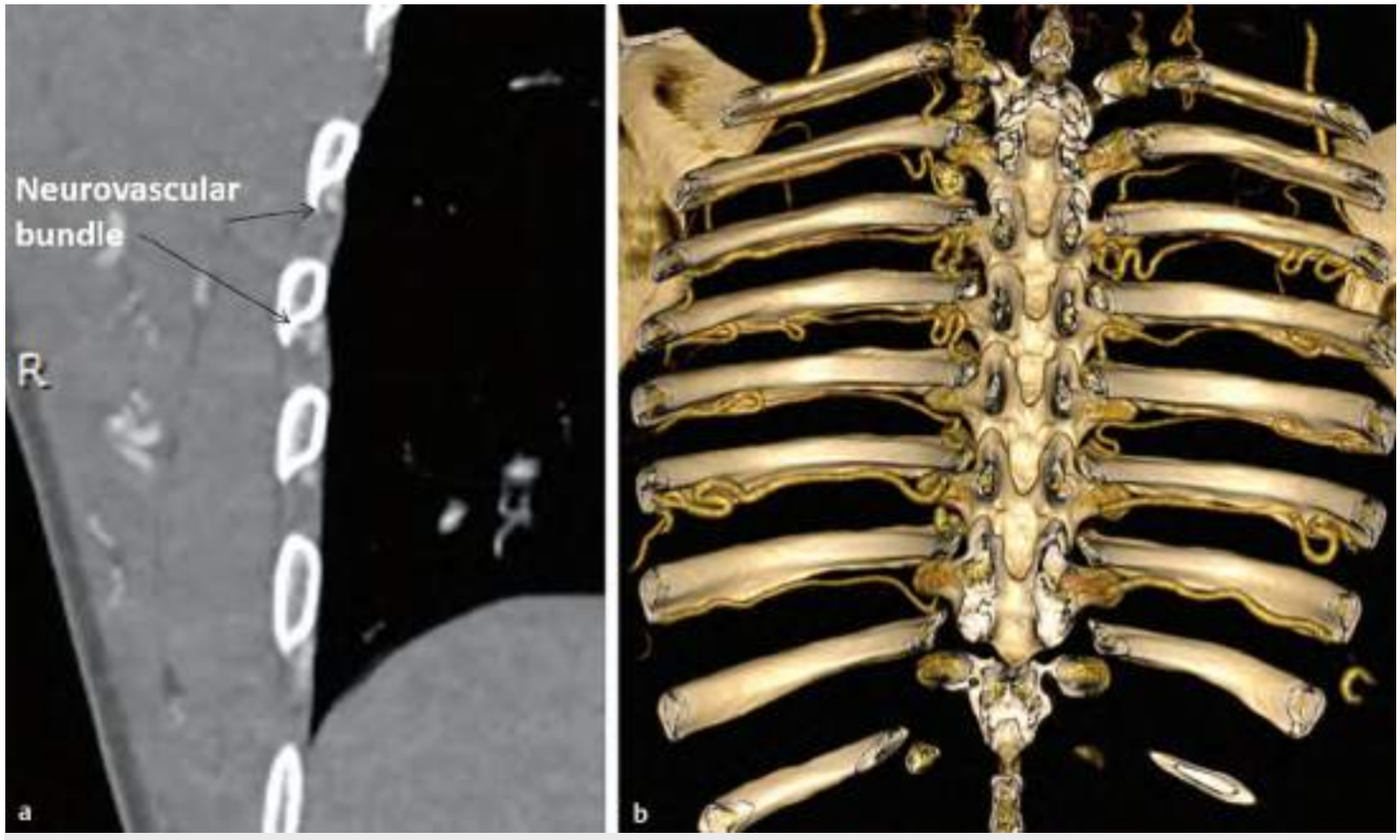

Fig. 1.55 Coronal CT image showing intercostal arteries in the lateral intercostal groove. **(a)** Right lateral chest wall. At this level, the neurovascular bundle is shielded by the superior rib. (**b**) Posterior chest wall in a volume-rendered view. Enlarged intercostal arteries in a patient with coarctation of the descending aorta. Variability in the position of the intercostal artery and their tortuosity especially in the posterior chest wall is common. Knowing these anatomical variants would be important in order to find the safest point for transthoracic procedures. At 3 cm lateral distance from the spine, 80% of intercostal arteries pass in the middle of the intercostal space. This location is risky for transthoracic approach. Farther laterally, the artery is usually shielded by the superior rib.

coursing below each rib (▶ Fig. 1.56). The arteries anastomose each other laterally. The right aortic intercostals are longer than the left because of the position of the aorta. They pass anterior to the vertebral bodies and posterior to the esophagus, thoracic duct, and azygos vein.

The first two posterior intercostal arteries originate from the superior intercostal artery, which is a branch of the costocervical trunk (▶ Fig. 1.57). The costocervical trunk is the second branch of the subclavian artery and divides into the deep cervical artery and the superior intercostal artery. The first and second intercostals anastomose with the third posterior intercostal artery arising from the descending aorta. The other nine intercostal arteries originate from the descending thoracic aorta (▶ Fig. 1.57).

The anterior intercostal arteries are much smaller. The upper six intercostal spaces are supplied by the internal mammary artery. The seventh, eighth, and ninth anterior intercostal spaces are supplied by the musculophrenic artery which is the terminal branch of the internal mammary artery and ends in the diaphragm (▶ Fig. 1.56). The first two anterior intercostal spaces may also be supplied by the supreme thoracic artery which is the first artery arising from the axillary artery or a branch of the thoracoacromial artery. The supreme thoracic artery branches may anastomose with the internal mammary artery.

The intercostal arteries provide multiple musculocutaneous perforators especially in the posterior chest and approximately 5 cm of the spinous processes of the vertebrae which supply the lateral and posterior portions of the intercostal spaces (▶ Fig. 1.58). The 4th through the 11th posterior intercostal arteries are the dominant direct cutaneous perforators.[88] The intercostal artery perforator flaps are commonly used for the reconstruction of defects over the chest wall. The posterolateral intercostal artery perforator may be large and traverse two or three levels of intercostal spaces.[89] Knowledge of the anatomical location of the perforator is important during percutaneous thoracic approaches to avoid injury. Posterior intercostal arteries also give rise to the bronchial, radiculomedullary, and paraspinal muscle branches.

Transthoracic percutaneous procedures (i.e., biopsy, drainage) are among common interventional procedures in radiology.[90] Variability in intercostal artery position and tortuosity especially in the posterior chest wall is potentially important clinical factor in order to find the safest point for transthoracic procedures. This variability is greater in older patients and in more cephalad rib spaces. Coarctation of the aorta may result in highly tortuous intercostal arteries, which provide collateral blood flow that circumvents the stenotic aortic segment (▶ Fig. 1.55). At 3 cm lateral distance from the spine, 17% of arteries are shielded by the superior rib, compared with 97% at 6 cm. Farther laterally, the artery travels closer to the inferior border of the rib above and reaches the intercostal groove[91] (▶ Fig. 1.55). This suggests that pleural

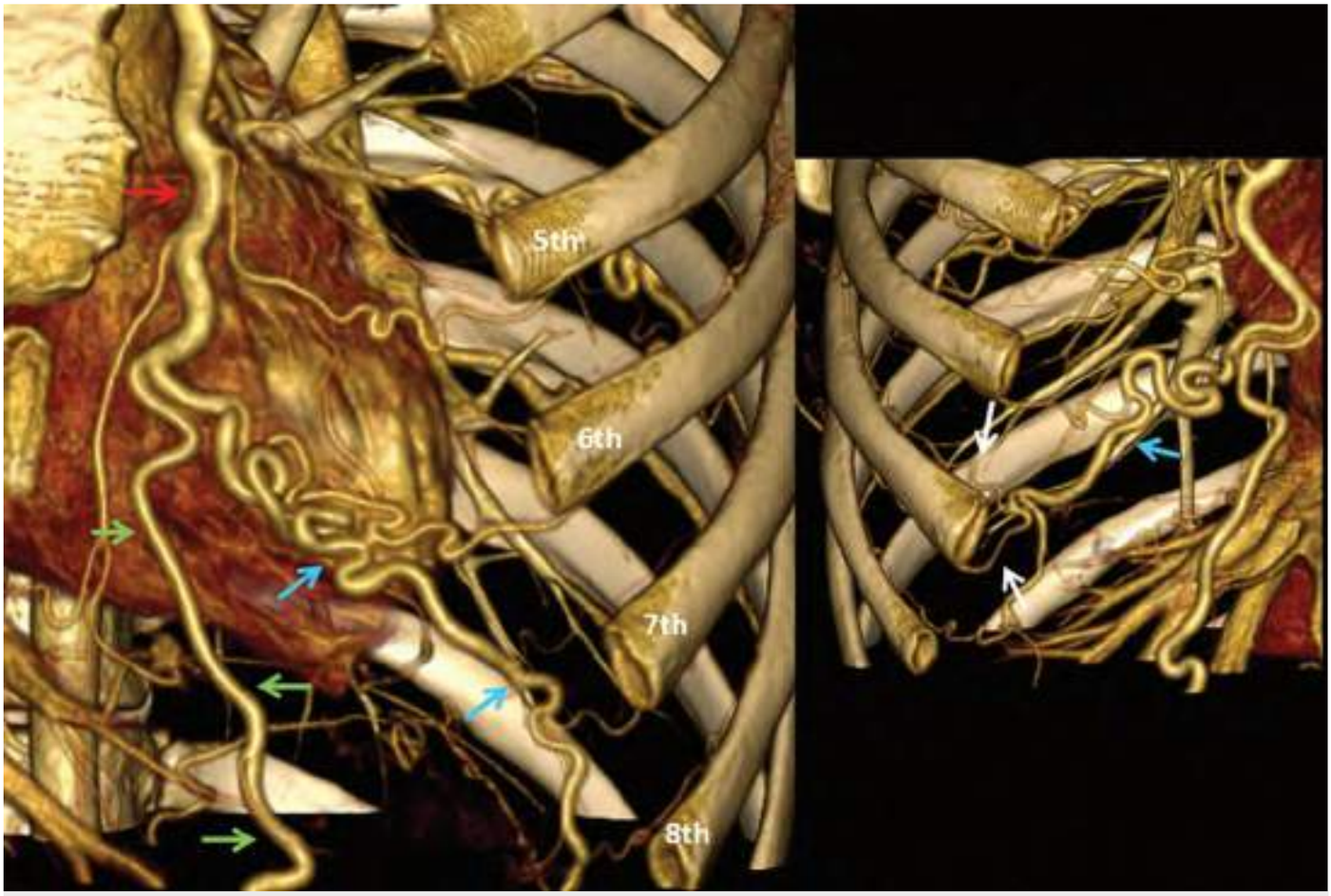

Fig. 1.56 Intercostal arteries arising from the musculophrenic artery (*blue arrows*). The seventh, eighth, and ninth anterior intercostal spaces are supplied by the musculophrenic artery. There are two anterior intercostal arteries, one above and one below each rib (*white arrows*). The superior epigastric artery (*green arrows*) is also shown arising from the distal end of the internal thoracic artery (*red arrow*).

interventions can be safely conducted more lateral than 6 cm from the spinous process to avoid the intercostal artery injury.[92]

The intercostal veins have a similar distribution to that of the intercostal arteries. The first intercostals vein on the right drains to the right brachiocephalic vein and the rest drain into the azygos vein. On the left all intercostal veins but those located in the upper three or four intercostal spaces drain into the hemiazygos and accessory hemiazygos veins. Upper left three or four drain into the supreme (highest) intercostal and the superior left intercostals vein with the former connecting the brachiocephalic vein near the

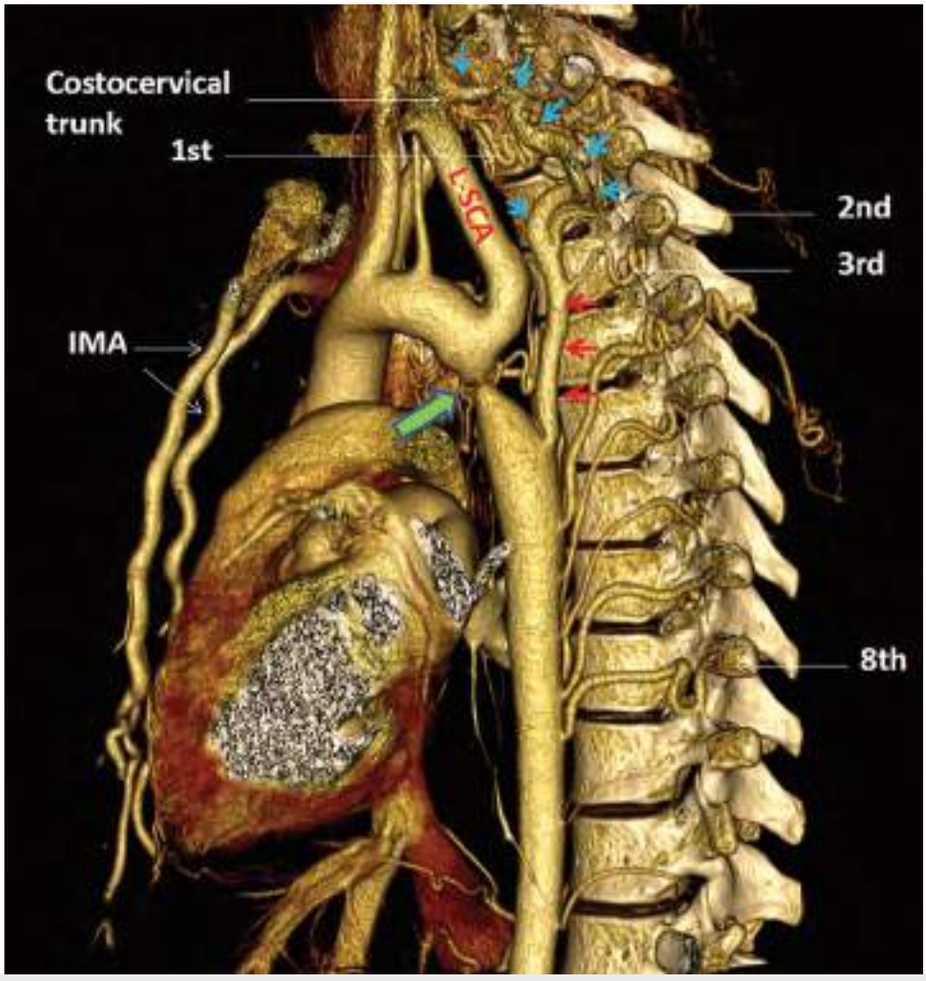

Fig. 1.57 Intercostal arteries in a patient with severe coarctation of the descending aorta (*green arrow*). The first two posterior intercostal arteries originate from the superior intercostal artery (*blue arrow*), which is a branch of the costocervical trunk. The costocervical trunk is the second branch of the subclavian artery and divides into the deep cervical artery and the superior intercostal artery. In this patient, the first and second intercostals anastomose with the third posterior intercostal artery (*red arrows*) arising from the descending aorta bypassing the coarctation. IMA, internal mammary artery; L-SCA, left subclavian artery.

vertebral vein and the later bridging between the left brachiocephalic vein and the accessory hemiazygos vein. The venous valves direct blood toward the azygos venous system. The anterior intercostal spaces drain anteriorly to the internal thoracic veins.

Thoracic spinal nerves exit the intervertebral foramina and immediately divide into ventral and dorsal rami. The dorsal ramus supplies the posterior thoracic wall muscles and bones and the ventral ramus forms intercostal nerves.

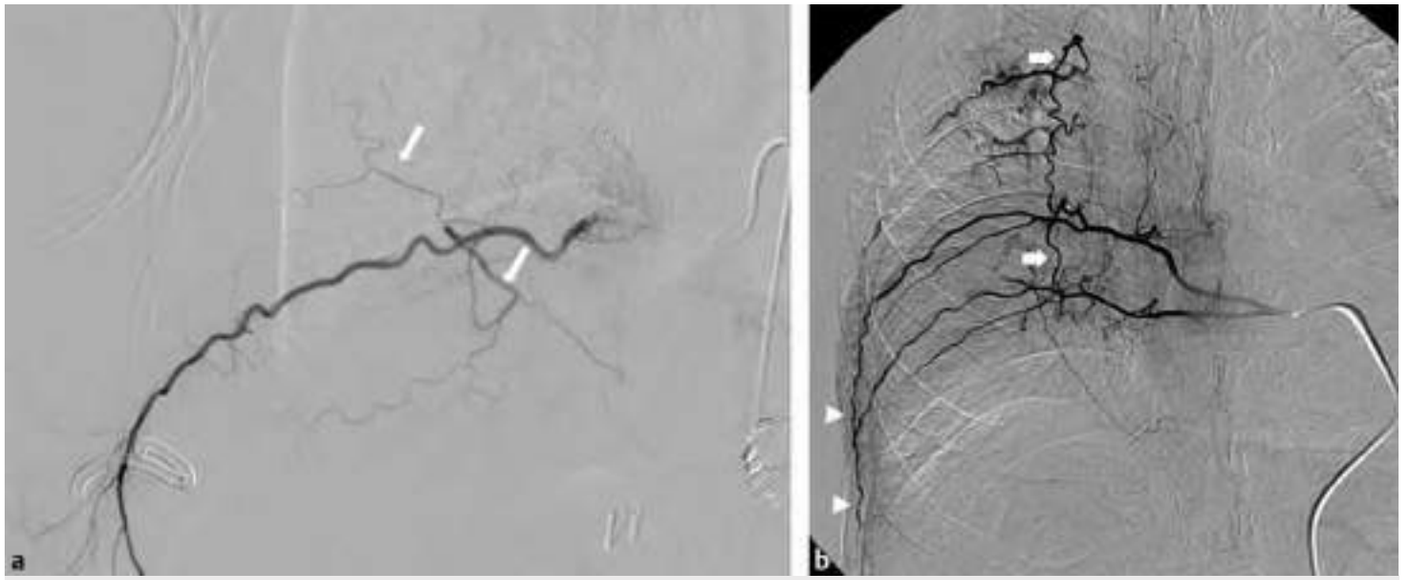

Fig. 1.58 (a, b) Selective angiography of the intercostal arteries showing intercostal artery perforators (*arrows*). **(b)**The lateral intercostal artery perforator (*arrows*) traverses three levels of intercostal spaces. The intercostal arteries provide multiple musculocutaneous perforators especially in the posterior chest and approximately 5 cm of the spinous processes of the vertebrae which supply the lateral and posterior portions of the intercostal spaces. Used with permission from Jeon et al 2015.[89]

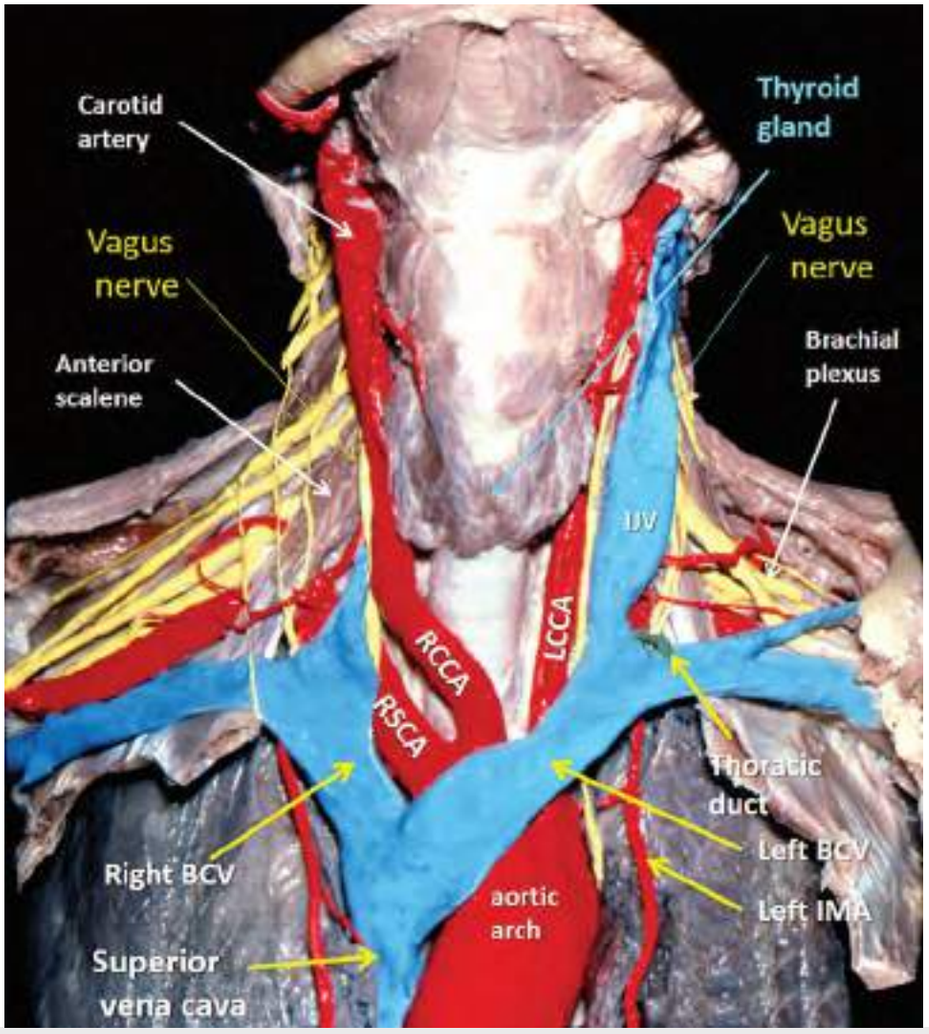

Fig. 1.59 Thoracic inlet vasculature. BCV, brachiocephalic vein; IMA, internal mammary artery; IJV, internal jugular vein; LCCA, left common carotid artery; LSCA, left subclavian artery; RCCA, right common carotid artery; RSCA, right subclavian artery.

◆ Veins of the Chest Wall

Veins of the chest wall accompany arteries and drain into the axillary, subclavian, and brachiocephalic arteries (▶ Fig. 1.59, ▶ Fig. 1.60, ▶ Fig. 1.61, ▶ Fig. 1.62).

The axillary vein is formed by the continuation and confluence of the basilic vein and the brachial veins near the lateral border of the pectoralis major muscle. It ends at the outer margin of the first rib. The cephalic vein joins the axillary vein near its termination. The axillary vein receives blood from the intercostal, thoracoacromial, lateral thoracic/thoracoepigastric, and subscapular veins. The anterior circumflex humeral vein usually empties into the lateral brachial vein and the posterior circumflex humeral vein into the axillary vein or subscapular vein. The subclavian vein is the continuation of the axillary vein and joins the internal jugular vein to form the innominate vein (▶ Fig. 1.59, ▶ Fig. 1.60). This junction is named the venous angle. Venous blood of the shoulder girdle flows via the pectoral and scapular veins into the subclavian vein. The subclavian vein also receives the external jugular vein, anterior jugular vein, and thoracic duct (on the left) and right lymphatic duct (on the right) (▶ Fig. 1.59). Venous bulging is common at the confluence with the thoracic duct. One to three valves are seen in almost all the axillary and subclavian veins. The axillary and the subclavian veins are main conduits for insertion of central venous catheters and pacemaker leads. Placement of these catheters or leads may be complicated by thrombosis of the related vein. Upper primary deep venous thrombosis in the upper extremity is rare, either due to effort thrombosis (Paget–Schroetter syndrome) or idiopathic.

◆ Thoracic Outlet Syndrome

Thoracic outlet syndrome is a poorly understood uncommon condition that can happen when the neurovascular bundle to the arm is compressed by one or more anatomical structures that make up the thoracic inlet (superior thoracic aperture). The neurovascular bundle is composed of the subclavian artery, subclavian vein, and brachial plexus[93,94] (▶ Fig. 1.63). The symptoms of thoracic outlet syndrome are most often caused by compression of the nerves of the brachial plexus in above 90% of cases. The remainder of cases is due to vascular compression. Typically, the compression is caused by the first rib and variations in the position of the anterior scalene muscle but can also be caused by a cervical rib or fibrotendinous bands. The cervical rib may fuse with the first rib, causing compression on the nerves and subclavian artery. The subclavius muscle, which attaches to the front of

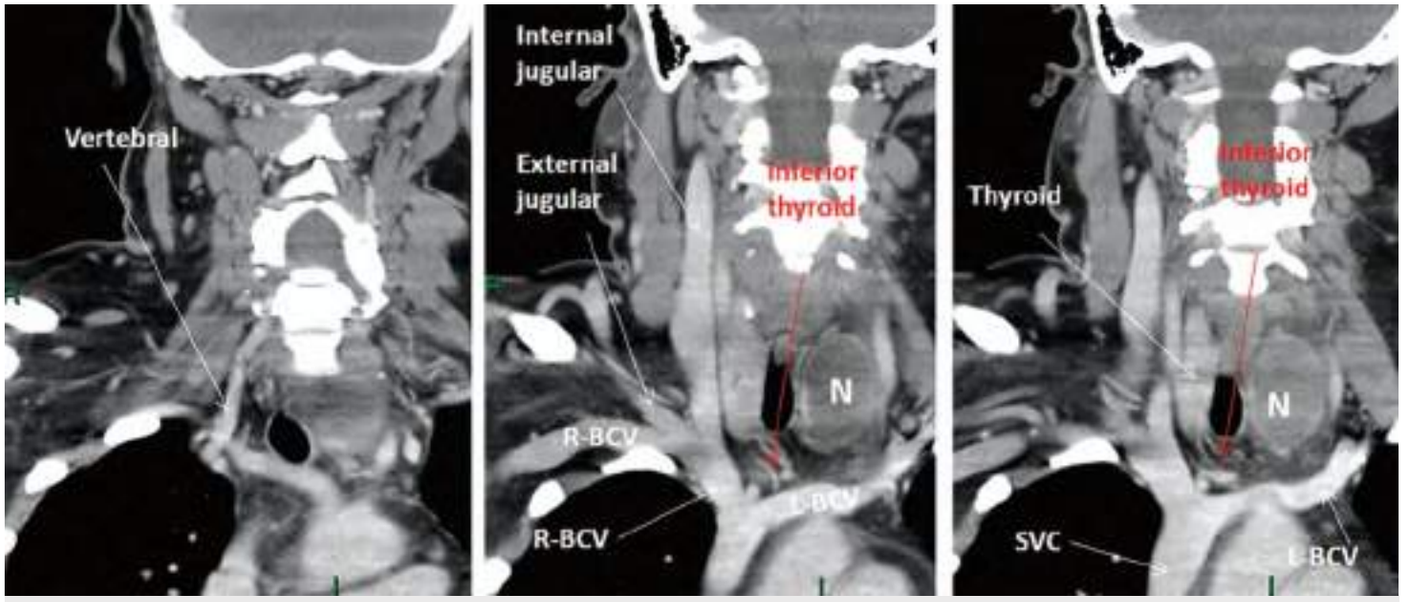

Fig. 1.60 CT contrast venography, from posterior to anterior, showing the confluence of the jugular and brachiocephalic veins. N, thyroid nodule; L, left; R, right; BCV, brachiocephalic vein; SVC, superior vena cava.

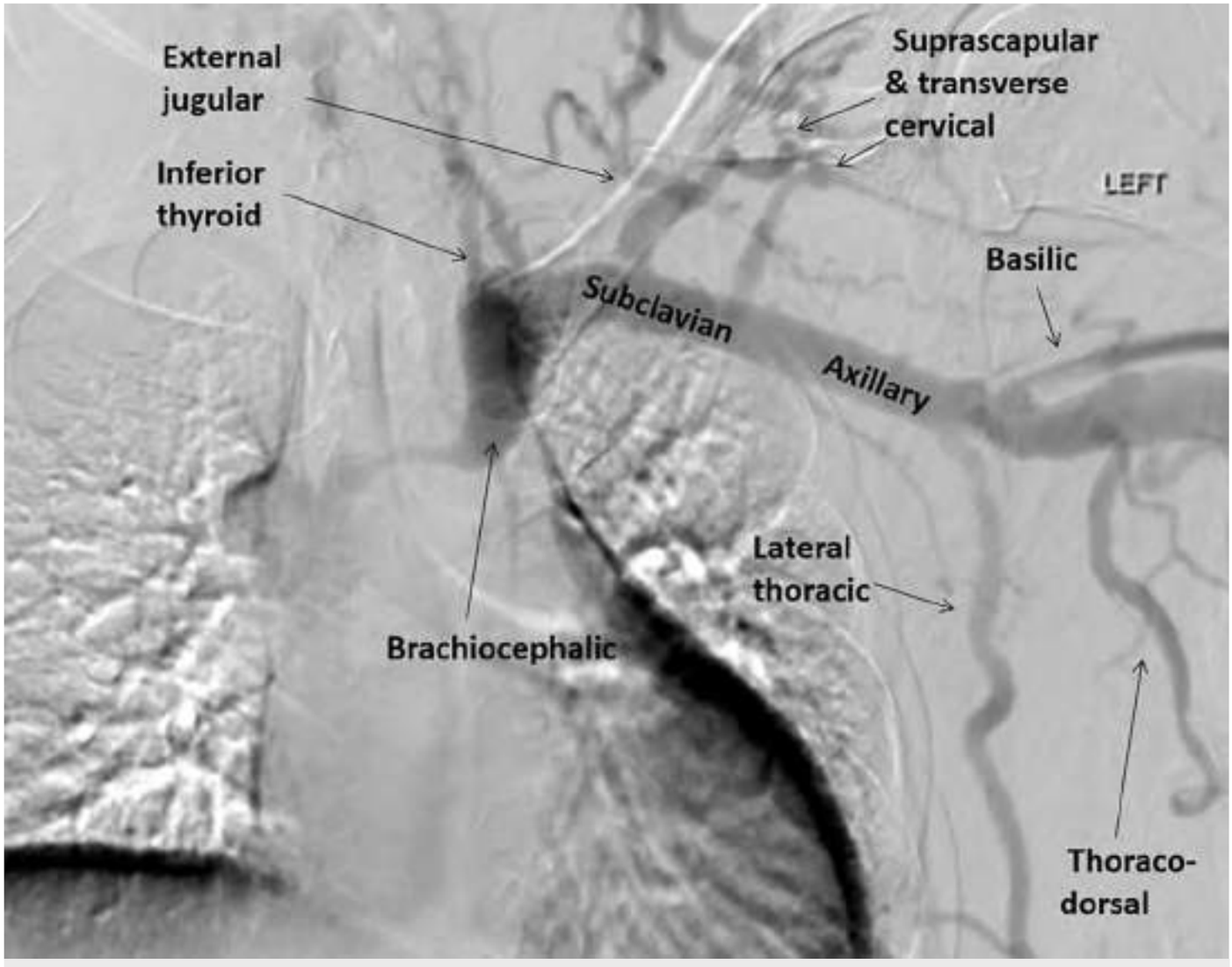

Fig. 1.61 Contrast venography showing tributaries of the axillary and subclavian veins.

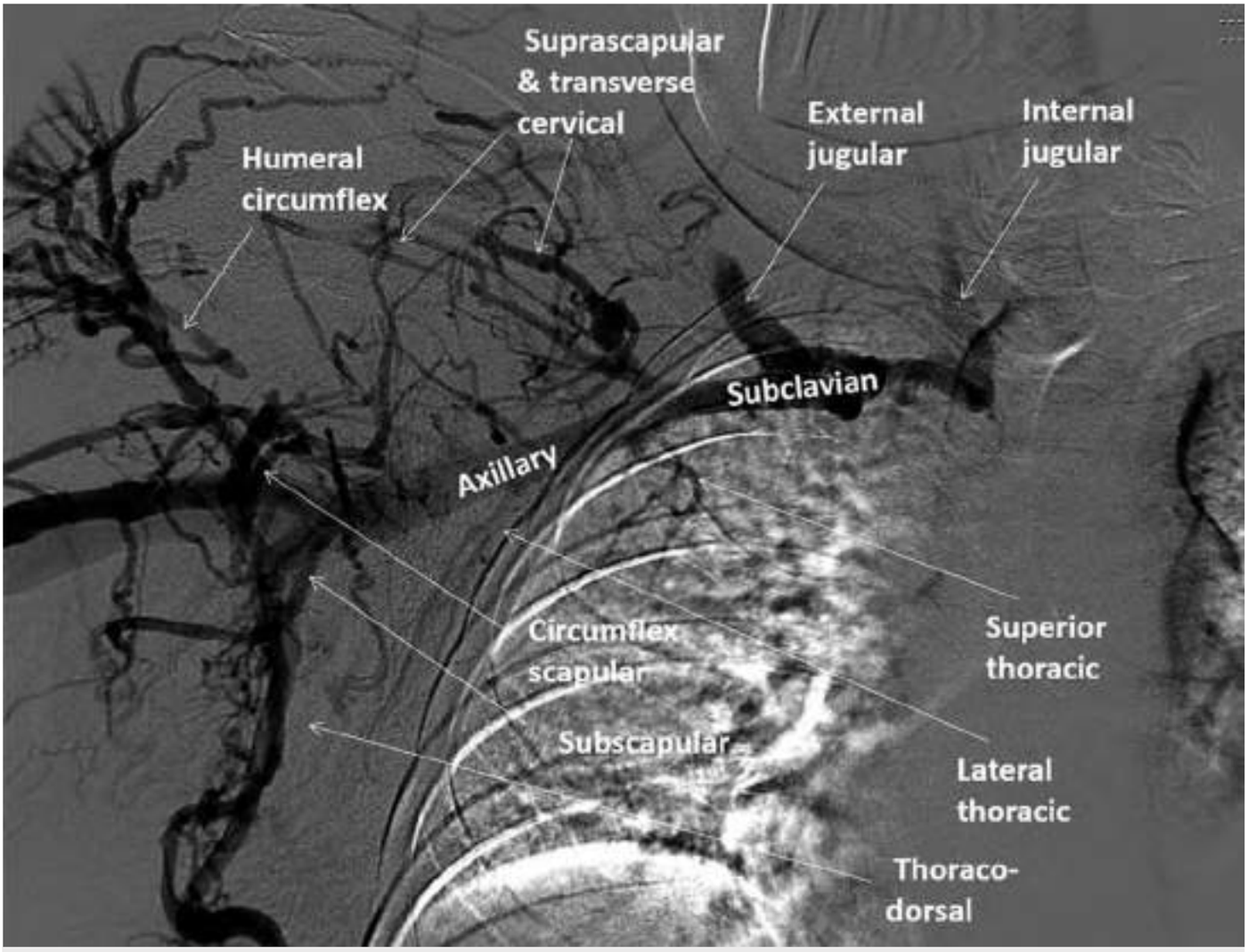

Fig. 1.62 Contrast venography showing tributaries of the right axillary and subclavian veins.

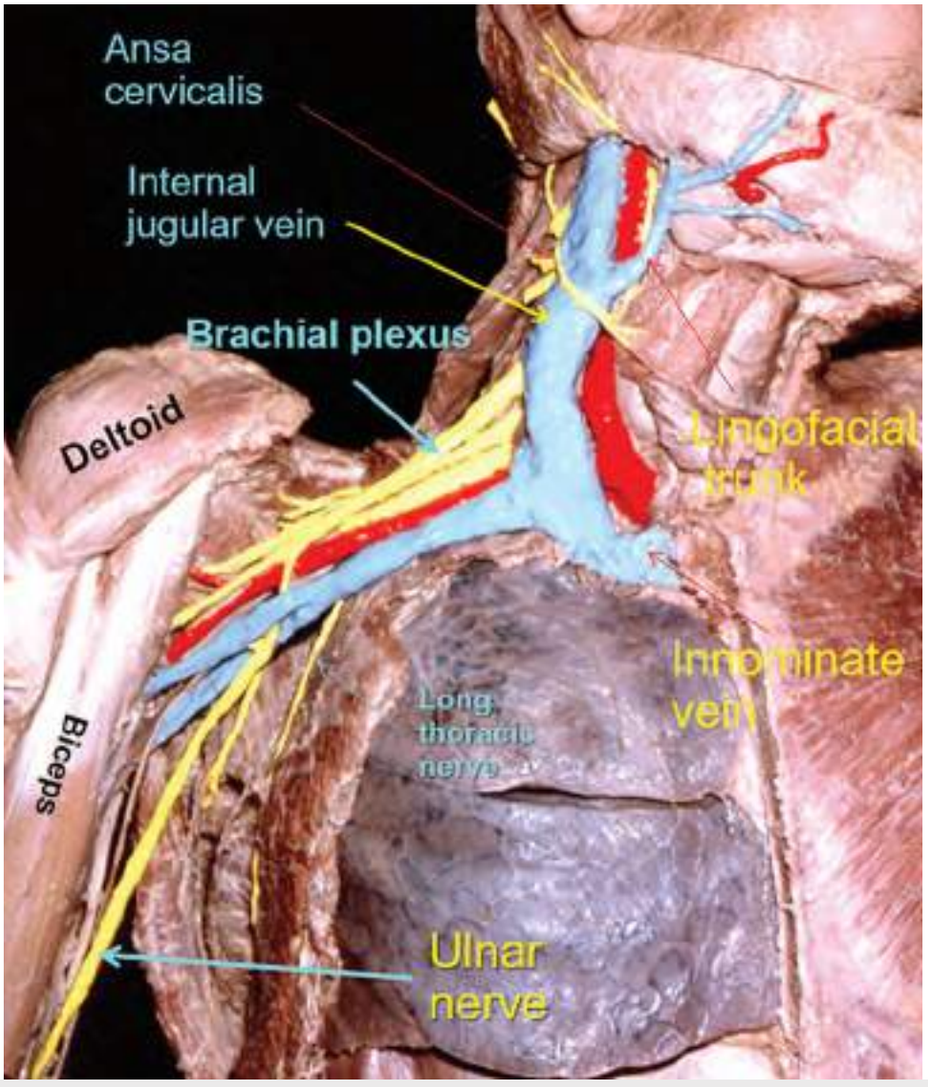

Fig. 1.63 Basic anatomy of the thoracic outlet neurovascular structures. The subclavian artery is located anterior to the brachial plexus and posterior to the subclavian vein. The ansa cervicalis is shown passing anterior to the internal jugular vein. This nerve loop arises from the cervical plexus. The long thoracic nerve is shown lateral to the serratus anterior muscle.

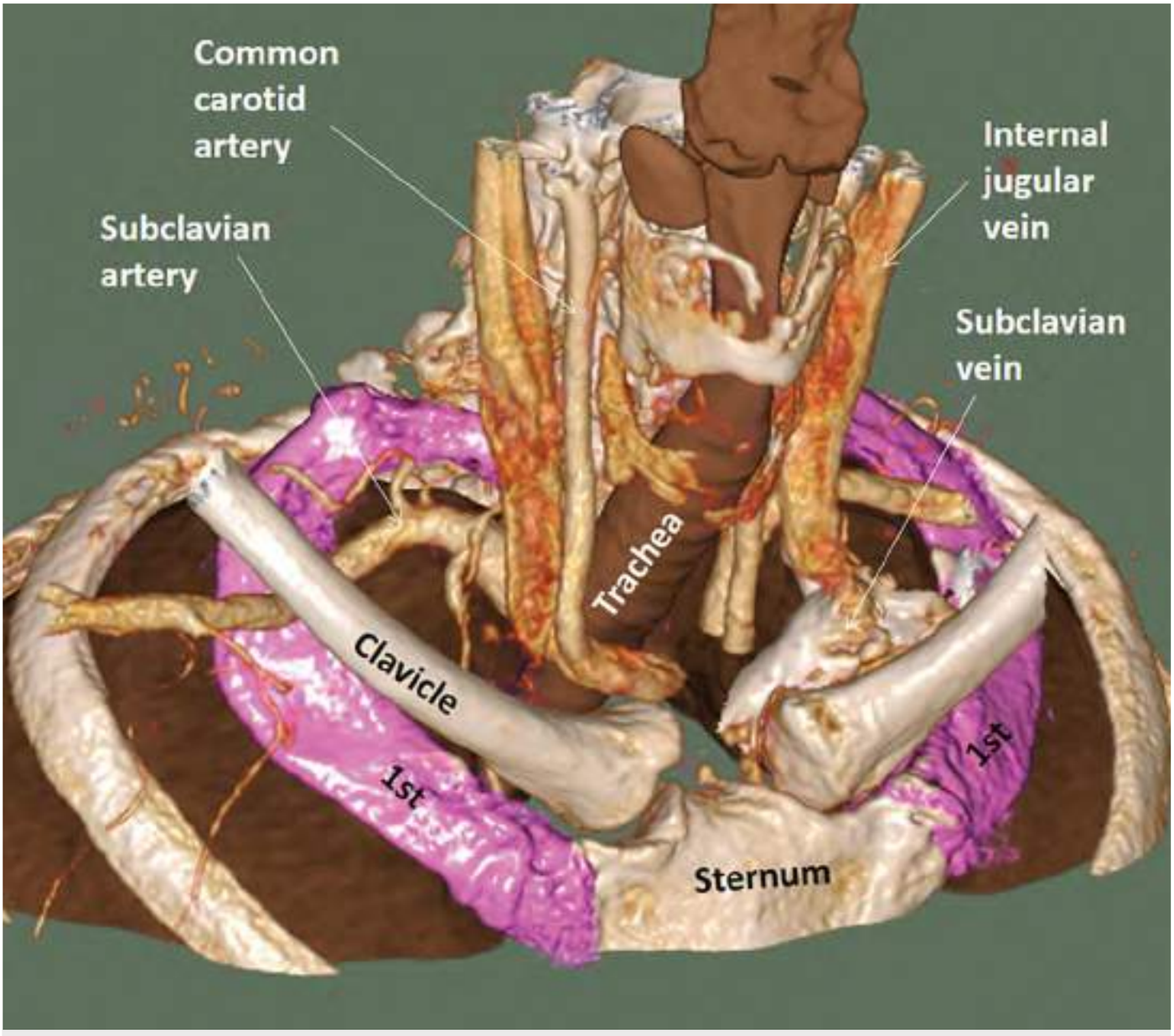

Fig. 1.64 Inlet of the thorax. The thoracic inlet is bounded by the T1 posteriorly, the first ribs laterally, and the superior border of the manubrium anteriorly. Thoracic outlet syndrome is compression of the brachial plexus, subclavian artery, or subclavian vein above the thoracic inlet.

the first rib, can also compress the subclavian vein. Patients with a history of trauma or injury to any structures in or around the thoracic outlet are at increased risk. Fractures of the clavicle and fist rib and secondary exuberant callus formation can also contribute to the development of thoracic outlet syndrome.

Anatomy of the Thoracic Outlet

The thoracic inlet is bounded by the T1 posteriorly, the first ribs laterally, and the superior border of the manubrium anteriorly (▶ Fig. 1.3, ▶ Fig. 1.64). It is important to know that compression of the neurovascular bundle causing thoracic outlet syndrome is above the thoracic inlet not at or below it.

Three anatomical regions are involved in thoracic outlet syndrome namely, the interscalene triangle, the costoclavicular space (cervicoaxillary canal), and the pectoralis minor or subcoracoid space[93] (▶ Fig. 1.65). The interscalene triangle is the most common location for the compression of the brachial plexus and the costoclavicular space is the most common location for the compression of the veins.

The interscalene triangle is formed between the anterior and middle scalene muscles with the first rib being the base of triangle. The structures passing through it include the roots and trunks of the brachial plexus and the third part of the subclavian artery (▶ Fig. 1.65). The subclavian arteries ascend into the neck before arching laterally to pass behind the anterior scalene muscle (▶ Fig. 1.66). The artery passes near the base of the triangle forming a groove on the superior border of the first rib. The inferior trunk of the brachial plexus formed by the union of the ventral rami of nerves C8 and T1 passes posterior to the anterior scalene muscle above the subclavian artery (▶ Fig. 1.65).

The costoclavicular space is formed between the medial side of the clavicle and the superior margin of the first rib (▶ Fig. 1.65, ▶ Fig. 1.66). The subclavius muscle forms the inner aspect of this

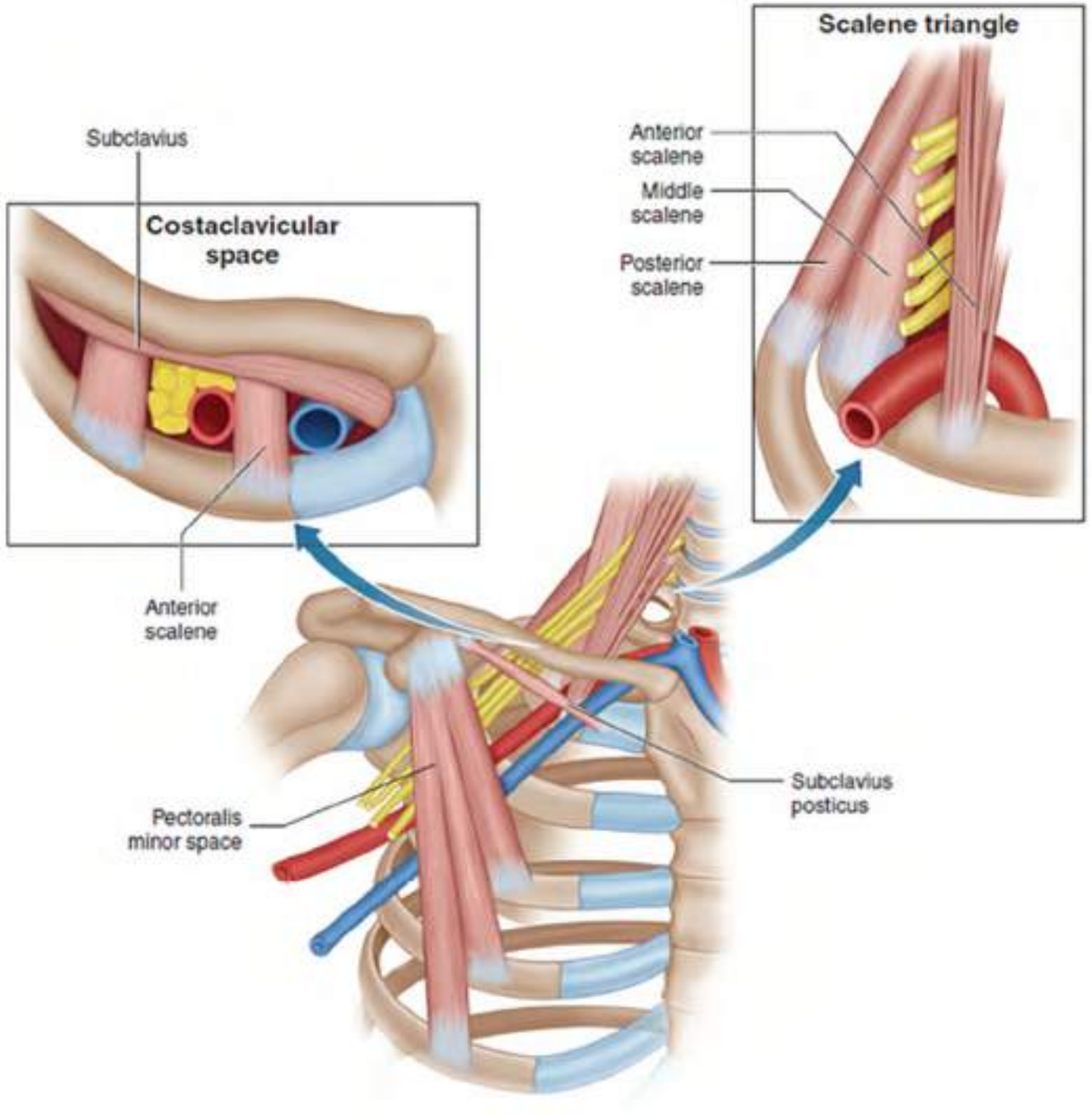

Fig. 1.65 The three potential spaces of compression of the thoracic outlet neurovascular bundle. The inferior trunk of the brachial plexus (C8 and T1) passes posterior to the scalene anterior muscle along with the subclavian artery. Compression of the subclavian artery and the brachial plexus is usually between the anterior and middle scalene muscles or secondary to a large cervical rib. The subclavian vein crosses the first rib anterior to the scalene anterior muscle and may be compressed at the costoclavicular space. The subclavius posticus is a supernumerary muscle between the sternal end of the first rib and the superior border of the scapula. It may play a role in development of the thoracic outlet syndrome. Used with permission from Klaassen et al 2014.[93]

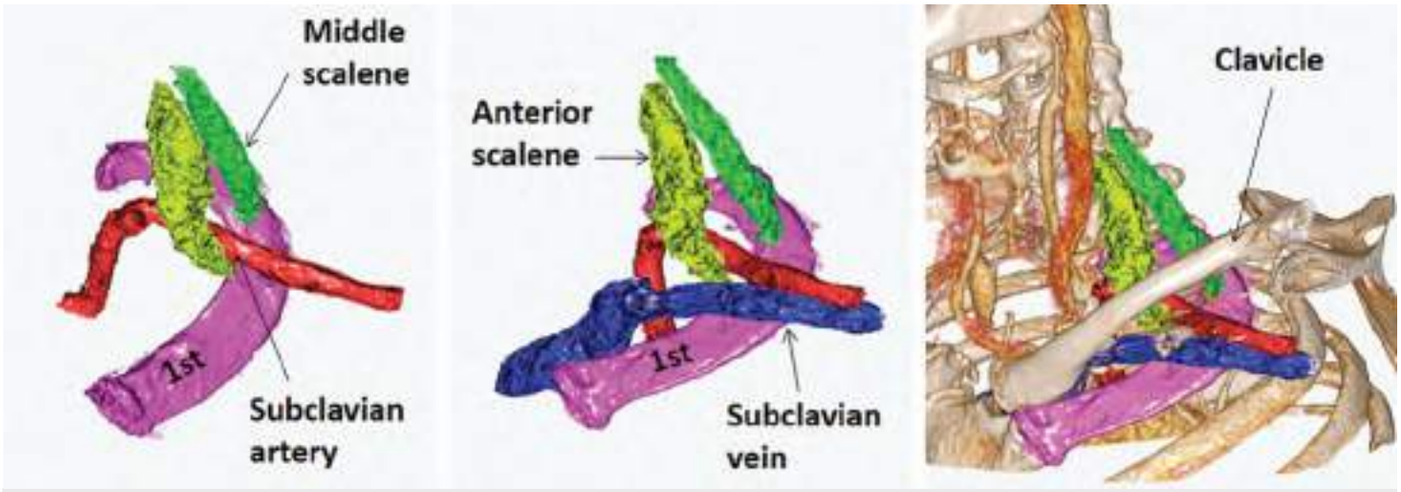

Fig. 1.66 Relationship of the left scalene muscles and clavicle with the subclavian artery and vein.

space and is limited anteriorly by the anterior scalene muscles. The subclavian vein is located medially in this space and can easily be compressed between the two bones when the arm is extended and abducted even in normal exercise.

Types of Thoracic Outlet Syndrome

There are three different types of thoracic outlet syndrome but it is not unusual to have more than one type. These three types include neurogenic, arterial, and venous. The neurogenic thoracic outlet syndrome is the most common type and the most difficult to diagnose.

Neurogenic Type

The brachial plexus is the network of nerves that arise from the C5 through T1 nerve roots and travel to the arm. In the study performed by Urschel and Razzuk compression of the lower plexus (ulnar nerve) was six times more common than the compression of the upper plexus (median nerve).[95] Compression of both nerves is also common.[95] The brachial plexus lies between the anterior scalene and middle scalene muscles in only 60% of instances. Variation of the plexus with respect to the anterior scalene muscle is common and increases the frequency of thoracic outlet syndrome. C5 or C6 may pass through or anterior to the anterior scalene muscle contributing to symptoms of upper plexus compression.[61,96] Brachial plexus nerves may pass through the scalene minimus and cause symptoms of compression.[61] Patients with wide first ribs vertebral end width of the first rib (> 15 mm at vertebral end and/or wider sternal end width of the first rib (> 20 mm) may develop thoracic outlet syndrome.[97]

Symptoms of neurogenic thoracic outlet syndrome include numbness and tingling down the arm especially with activities that involve overhead reaching, such as taking an item off a high shelf, or extending the arms, such as typing. Electrophysiological nerve conduction study is a common diagnostic procedure which allows detection of decreased action potential conductance caused by nerve compression. Neurogenic thoracic outlet syndrome is often initially treated with thoracic outlet-specific physical therapy and injection of botulinum toxin A (Botox) into the scalene muscles. Transaxillary first rib removal relieves neurovascular decompression of both upper and lower plexuses.

Arterial Type

The subclavian artery is usually compressed when a cervical rib is involved (▶ Fig. 1.67, ▶ Fig. 1.68). Two-thirds of patients with arterial compression have associated bone anomalies including cervical ribs, first rib anomalies, or fracture.[98] Less likely reason is the variations in the anatomical location of the anterior scalene muscle. There are many variations in the course of the subclavian artery and its relationship with the anterior scalene muscle. The artery may pass anterior to or through the muscle.[99] Abnormal anterior insertion of the anterior scalene muscle may also be a contributory factor in the compression of the subclavian vein at the costoclavicular angle. Absence of the anterior scalene muscle is a rare anomaly that may result in the neurovascular structures being compressed against the first rib in the costoclavicular space.[100] There are also variations in the course of the brachial plexus in relation to the anterior scalene muscle.

Arterial thoracic outlet syndrome can cause coolness, achiness, soreness of the arm, and pallor of the palms that worsen with overhead activity. Patients are at risk for developing arterial thrombosis and distal necrosis.[101] CT angiography is the best available technique for diagnosis. Image findings include arterial narrowing, thrombosis, occlusion, and poststenotic dilation. Patients with arterial complications often require surgical decompression of the rib and/or scalene muscles along with transarterial interventions (stent, thrombolysis).

Cervical ribs occur in less than 1% of the general population. The incidence is higher (10%) in patients with thoracic outlet syndrome. Symptomatic cervical ribs are large and frequently fused to the first rib by fibrous bands, cartilage, or bony pseudoarticulation[12] (▶ Fig. 1.67, ▶ Fig. 1.68). In addition to arterial compression, the inferior trunk of the brachial plexus takes an acute course that predisposes to compression and traumatic neuritis.[93] Arterial compression is more common.[97] Resection of both the cervical rib and first rib is suggested to prevent the need for a second operation.[97]

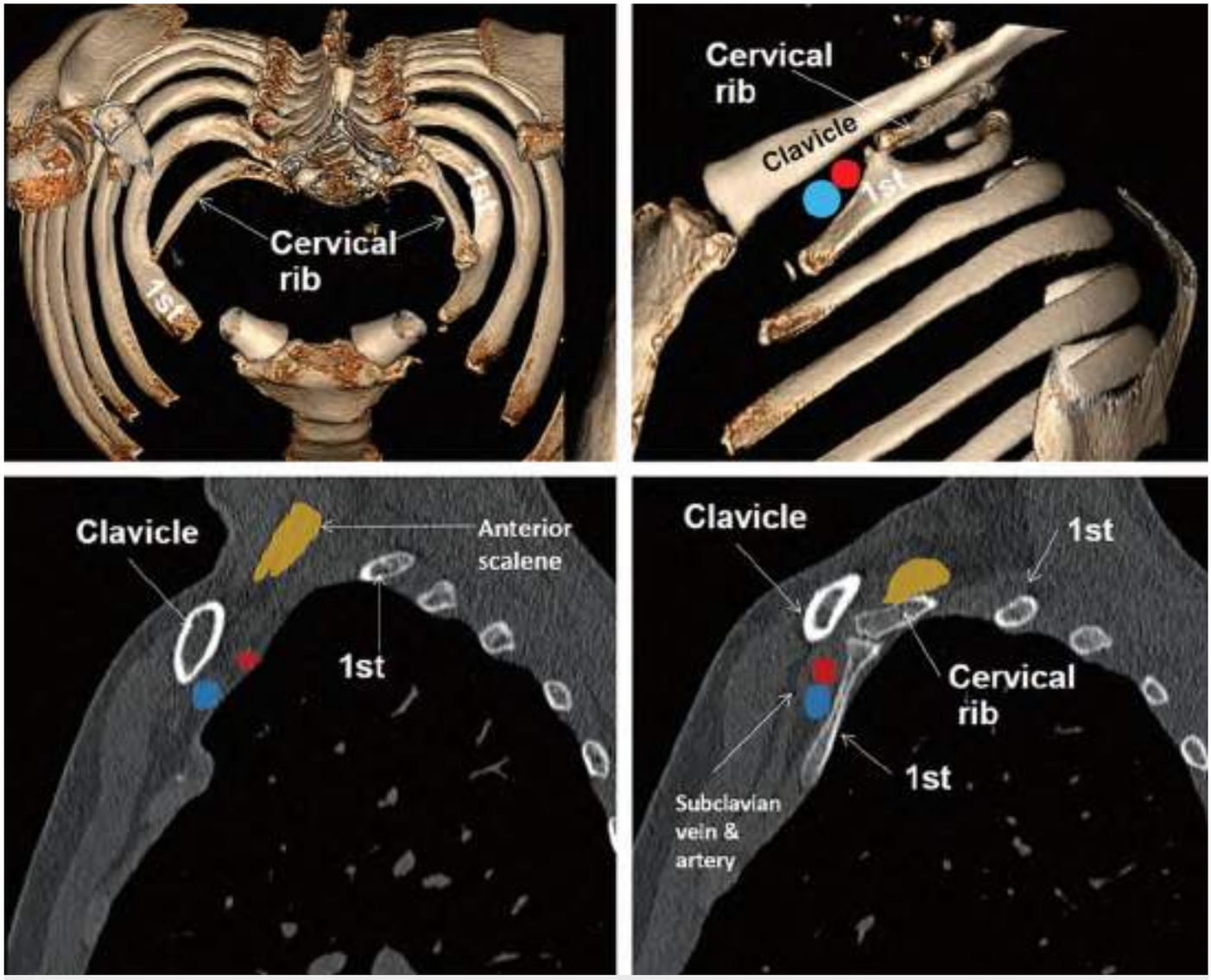

Fig. 1.67 Upper row demonstrates superior and left lateral views of the bony chest wall in a patient with bilateral cervical ribs. On the left, the cervical rib connects with a tubercle arising from the first rib. Lower row demonstrates sagittal CT images at the level of the left cervical rib. Color-coded structures show the relative position of the subclavian vessels and the anterior scalene with the cervical rib.

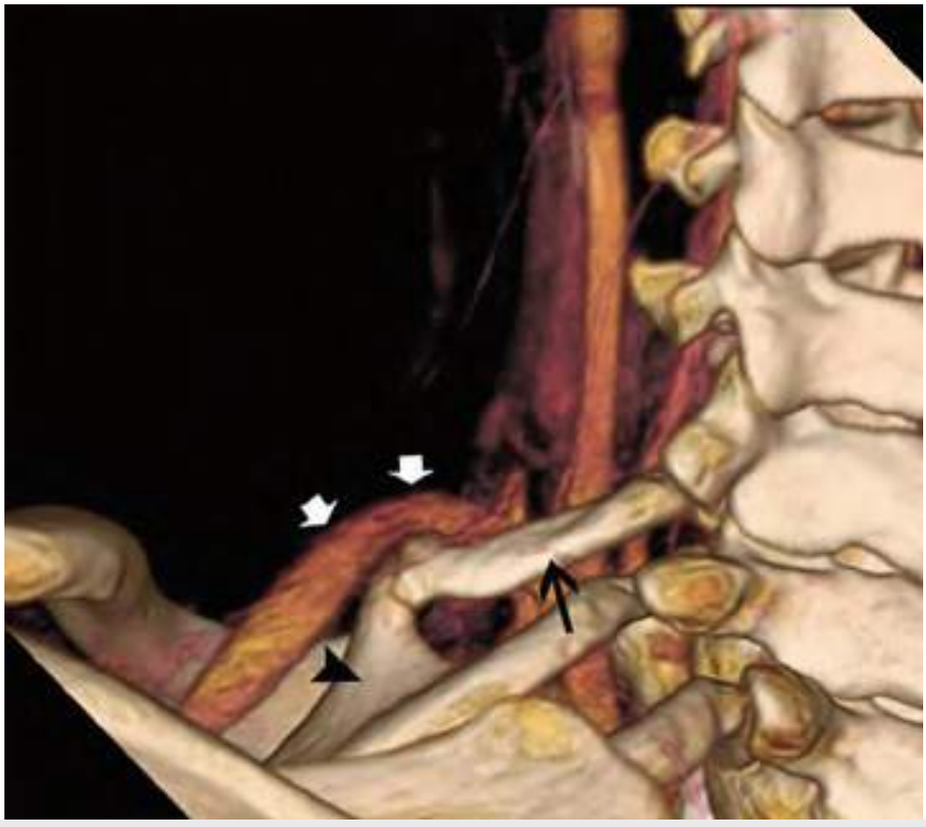

Fig. 1.68 CT angiogram demonstrates cervical rib (*black arrow*) connecting with a bony protuberance jutting from the first rib (*black arrowhead*). The left subclavian artery (*white arrow*) is seen passing over the bony protuberance (*black arrowhead*) of the first rib. Used with permission from Klaassen et al 2014.[93]

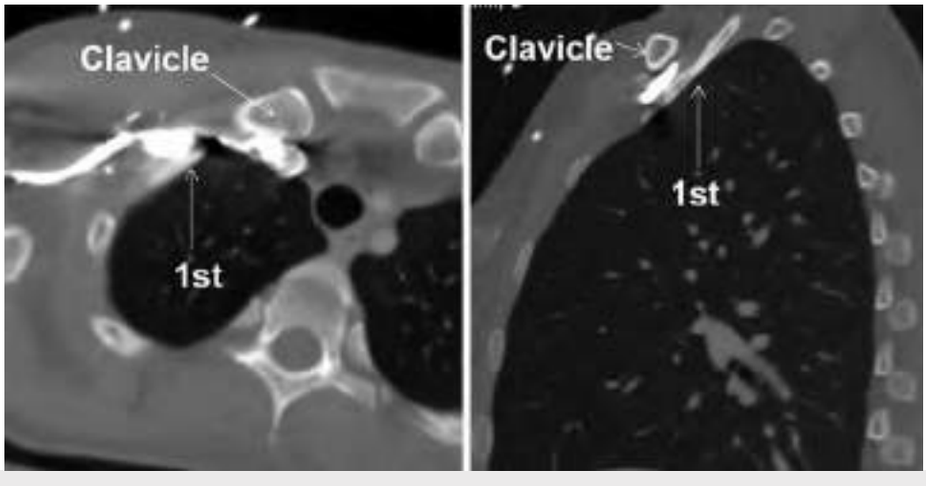

Fig. 1.69 Compression of the subclavian vein at the costoclavicular space between the first rib and the medial clavicle.

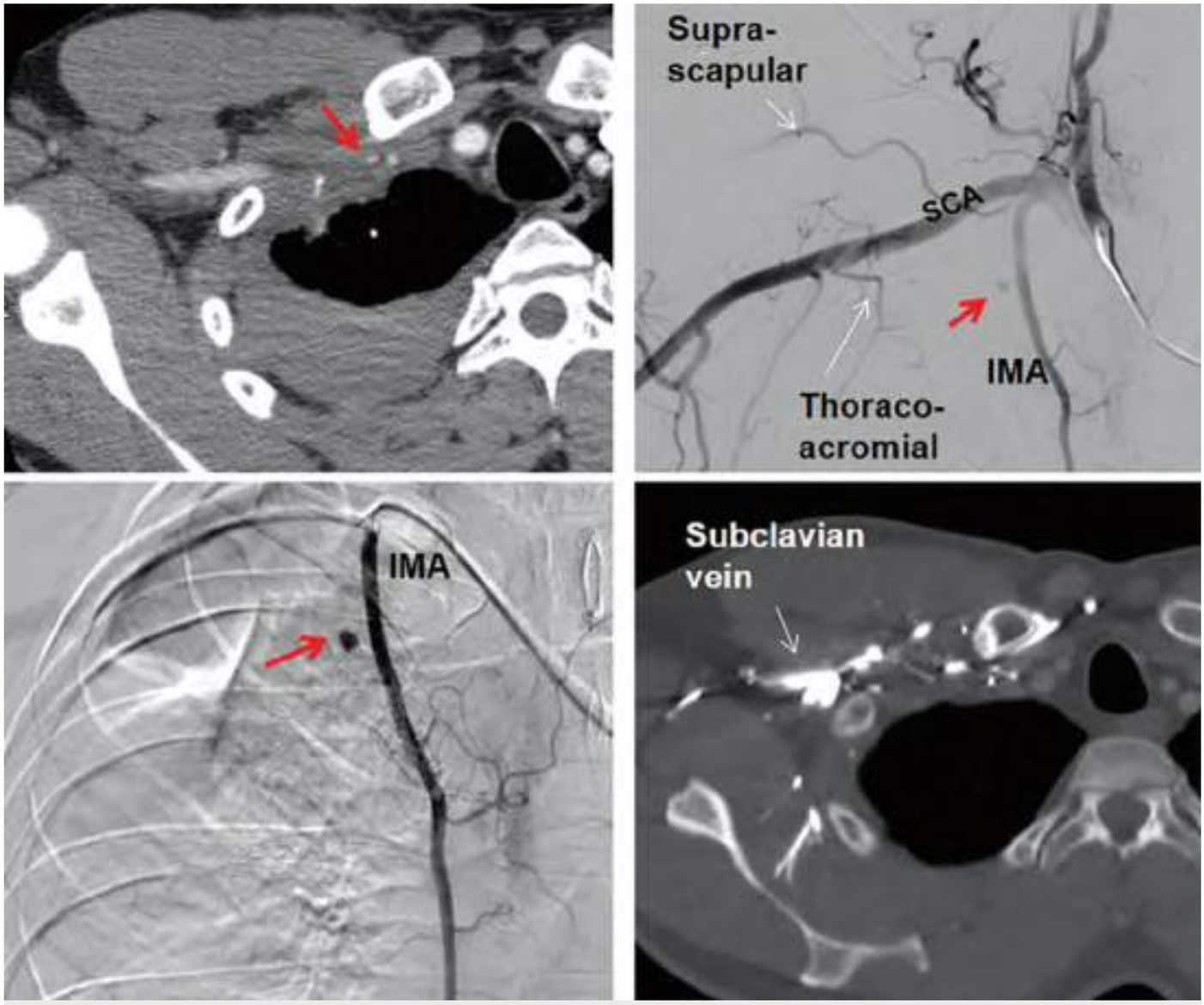

Fig. 1.70 Status post resection of the first rib and anterior scalenectomy for Paget–Schroetter. Patient developed severe hemothorax. CT and later angiography showed a small aneurysm (*red arrows*) from an intercostal branch of the internal mammary artery (IMA) at the site of rib resection which was successfully embolized. Follow-up CT showed persistent occlusion of the right subclavian vein. Note, the sternal and intercostal branches of the IMA on selective injection. SCA, subclavian artery.

Venous Type

Venous thoracic outlet syndrome occurs due to chronic and repeated extrinsic compression of the subclavian and axillary veins.[102] It is a disorder of the anterior part of the thoracic outlet region where the subclavian vein passes in the intersection of the clavicle and first rib (costoclavicular space) (▶ Fig. 1.69). A hypertrophied anterior scalene can compress the vein from behind. The subclavius muscle can further narrow the space at the costoclavicular junction. Deformity of the clavicle and first rib and soft tissue scar formation after trauma are additional contributing factors. Adams et al demonstrated that even in normal patients the subclavian vein can easily be compressed within the costoclavicular space with arm abduction.[103] This is a common image finding in CT angiography study of the chest which is usually performed with arms extended above the head (▶ Fig. 1.69).

Continuous compression, extrinsic fibrosis, and endothelial damage occur, which lead to deep vein thrombosis. Axillary–subclavian vein thrombosis is also known as Paget–Schroetter syndrome or effort thrombosis syndrome.[104,105] It is a relatively infrequent disorder that occurs predominantly in young, otherwise healthy people who participate in repetitive upper extremity activity. High-level athletes who compete in swimming, rowing, baseball (especially pitchers), and weightlifting are particularly vulnerable. About 40 to 80% of patients recall an activity that involves repetitive or prolonged hyperabduction or external rotation involving the upper extremities in the past 24 hours.

Most patients complain of heaviness and pain in the affected arm. Swelling of the shoulder and arm and skin discoloration are clinical findings. For venous thoracic outlet syndrome, common diagnostic tests used include CT venography or Doppler ultrasound studies. Treatment includes thrombolysis or venous stenting. Open surgical venous reconstruction is rarely necessary. Complications after surgery can be shown with CT or angiography (▶ Fig. 1.70)

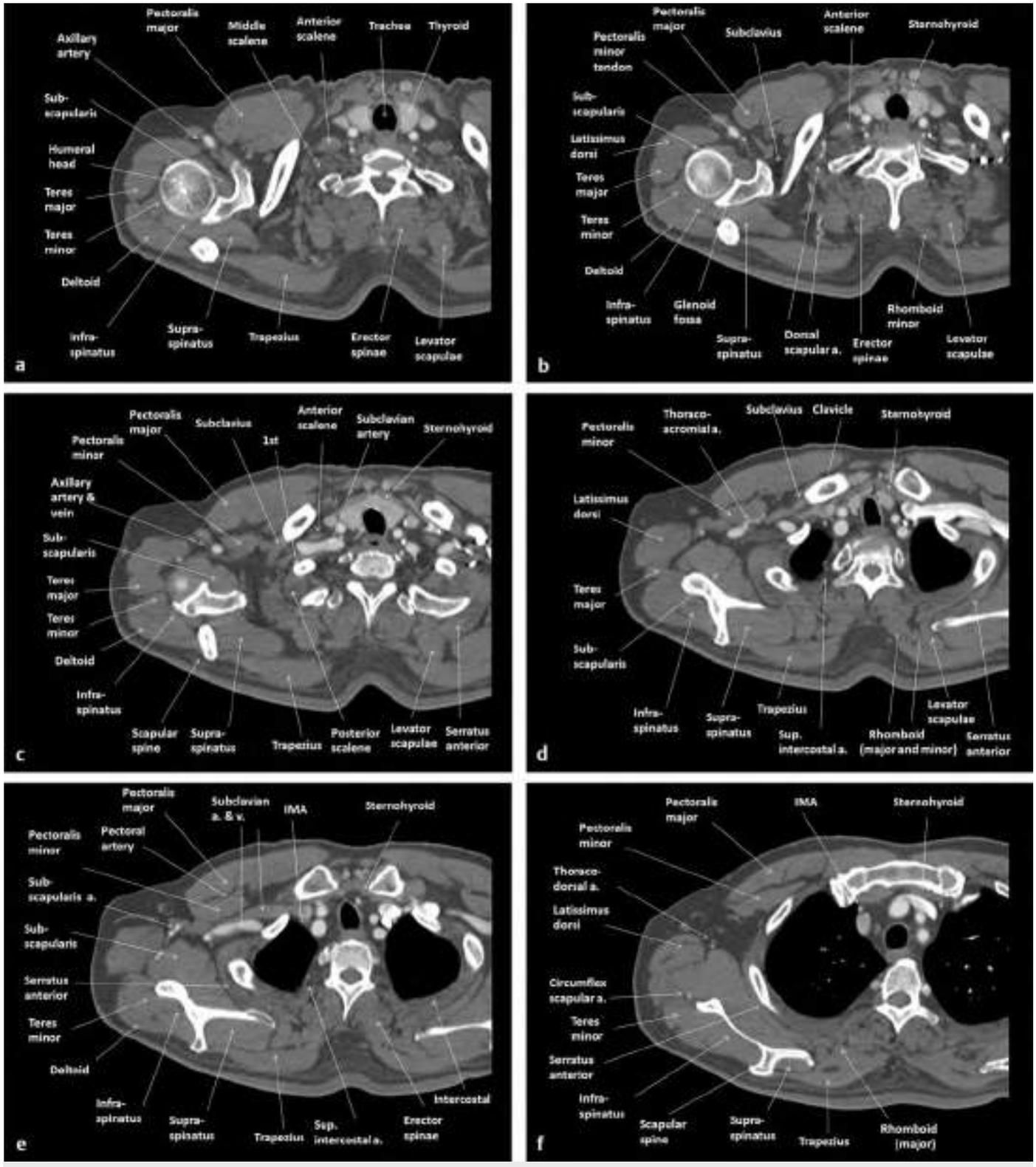

Fig. 1.71 (a–f) Axial CT from top to bottom showing structures of a normal chest wall.

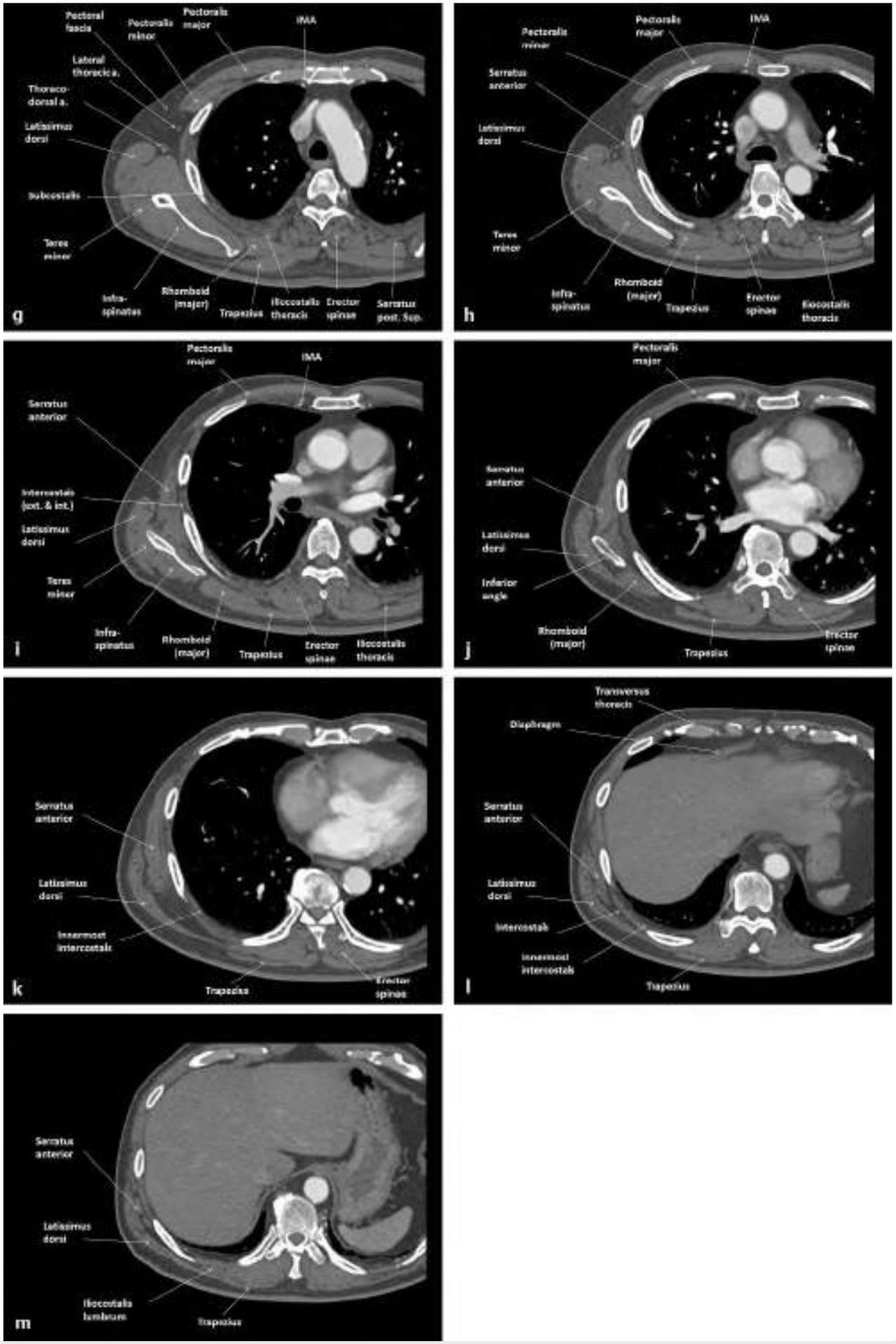

Fig. 1.71 (g–m) Axial CT from top to bottom showing structures of a normal chest wall.

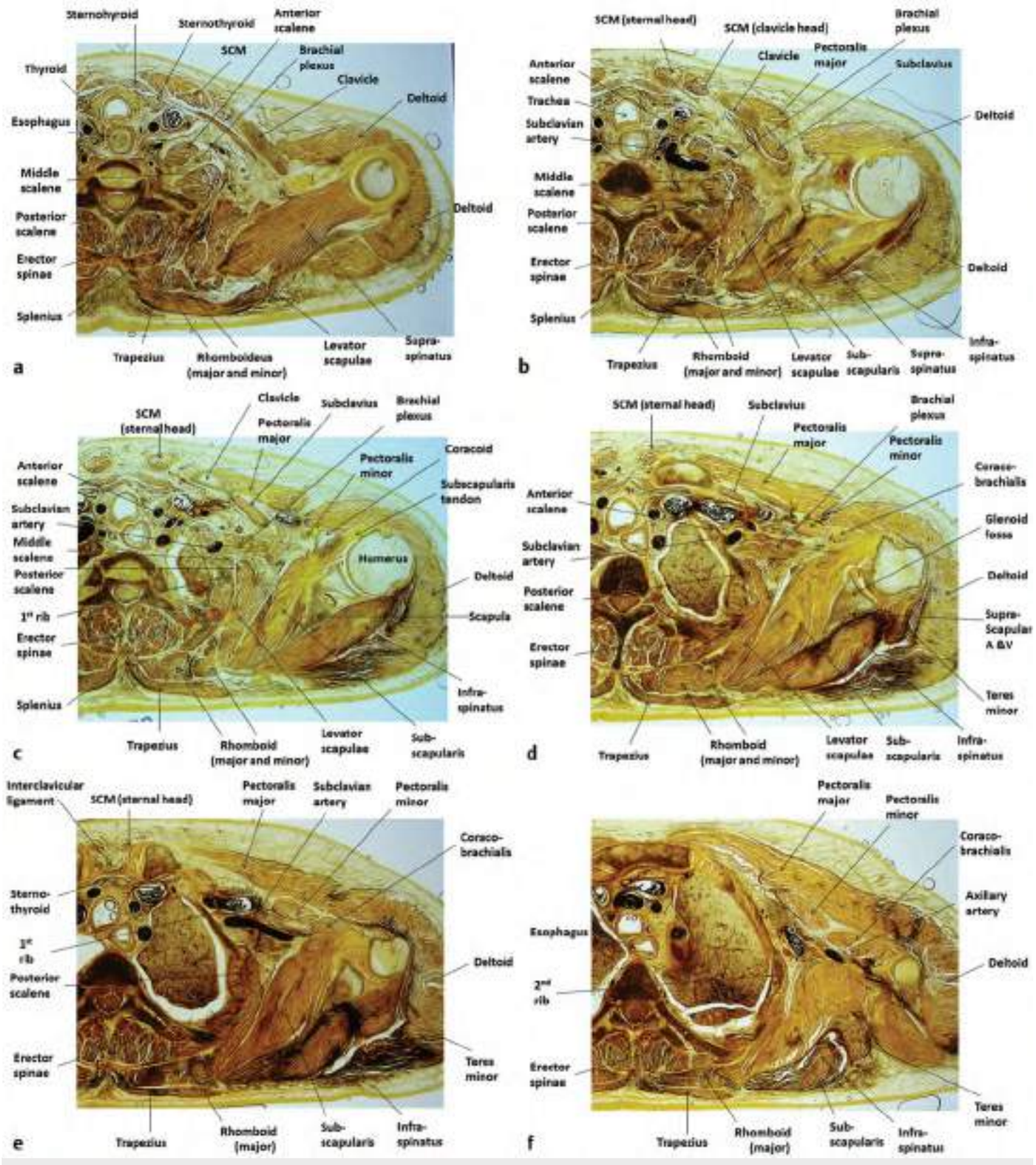

Fig. 1.72 **(a–f)** Axial cadaveric cuts showing muscles of the chest wall.

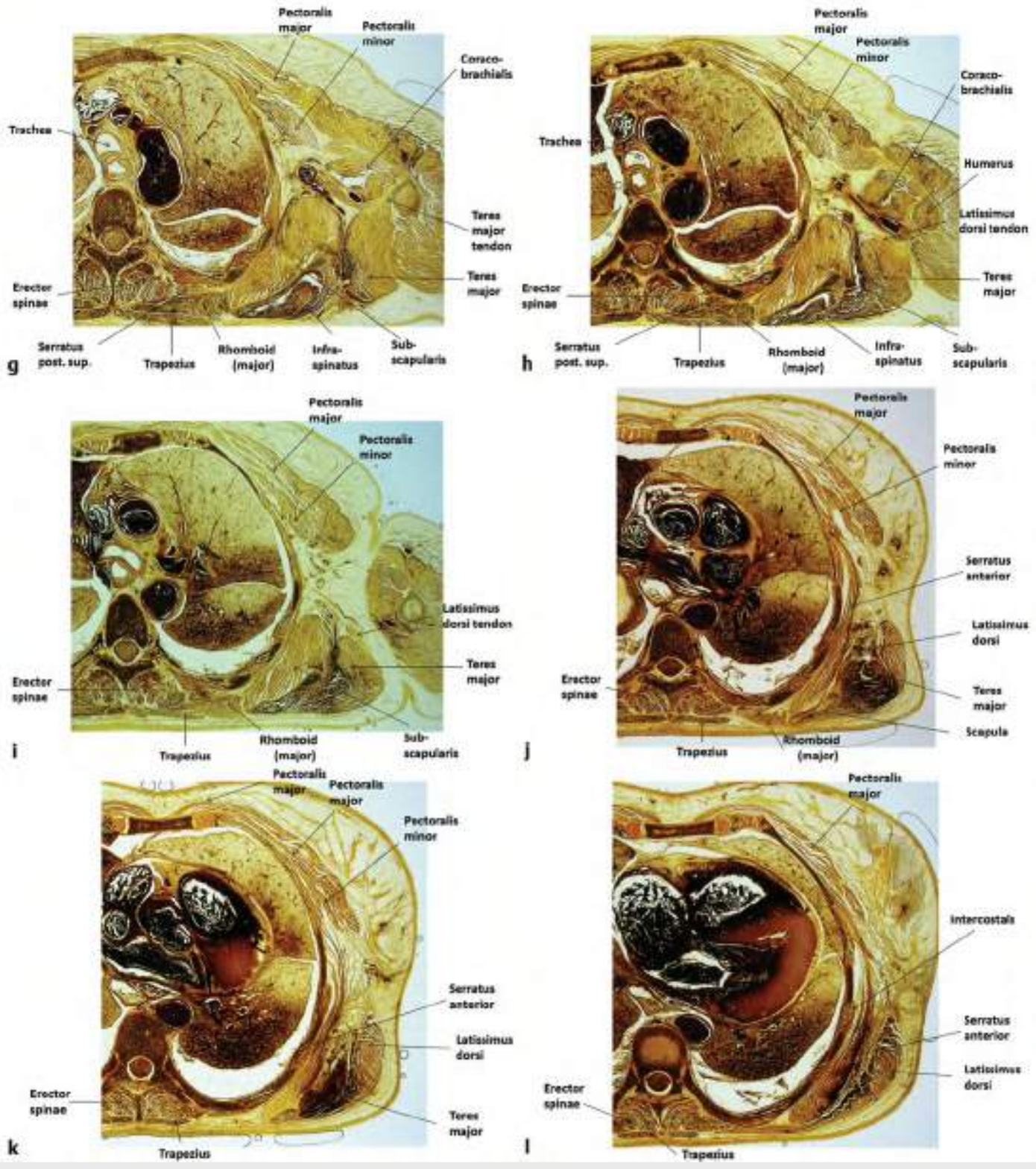

Fig. 1.72 (g–l) Axial cadaveric cuts showing muscles of the chest wall.

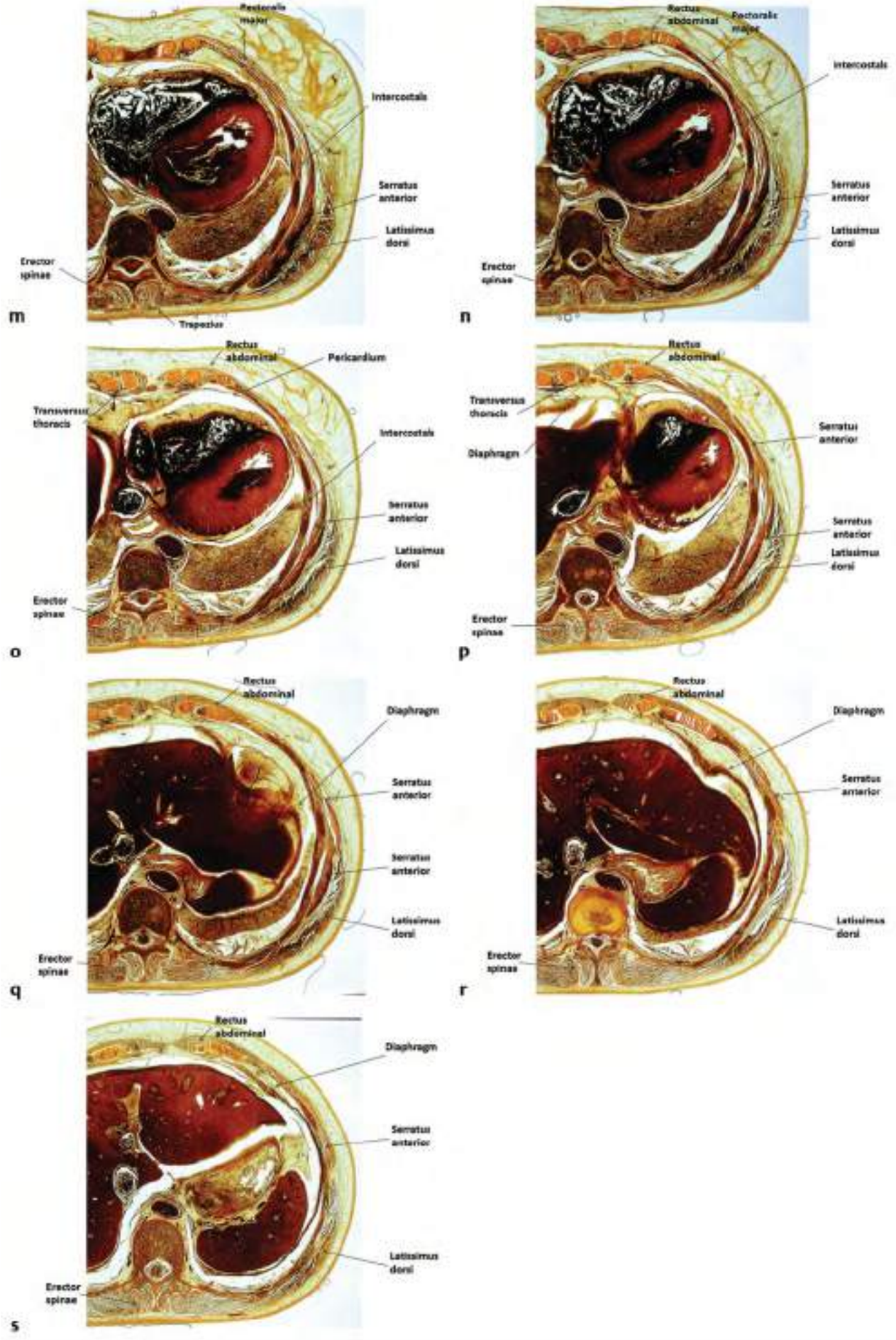

Fig. 1.72 (m–s) Axial cadaveric cuts showing muscles of the chest wall.

References

[1] Clemens MW, Evans KK, Mardini S, Arnold PG. Introduction to chest wall reconstruction: anatomy and physiology of the chest and indications for chest wall reconstruction. Semin Plast Surg.; 25(1):5–15

[2] Mekonen HK, Hikspoors JP, Mommen G, Köhler SE, Lamers WH. Development of the ventral body wall in the human embryo. J Anat.; 227(5):673–685

[3] Kurihara Y, Yakushiji YK, Matsumoto J, Ishikawa T, Hirata K. The ribs: anatomic and radiologic considerations. Radiographics.; 19(1):105–119, quiz 151–152

[4] Graeber GM, Nazim M. The anatomy of the ribs and the sternum and their relationship to chest wall structure and function. Thorac Surg Clin.; 17 (4):473–489, vi

[5] Naidu BV, Rajesh PB. Relevant surgical anatomy of the chest wall. Thorac Surg Clin.; 20(4):453–463

[6] Carrier G, Fréchette E, Ugalde P, Deslauriers J. Correlative anatomy for the sternum and ribs, costovertebral angle, chest wall muscles and intercostal spaces, thoracic outlet. Thorac Surg Clin.; 17(4):521–528

[7] Weaver AA, Schoell SL, Stitzel JD. Morphometric analysis of variation in the ribs with age and sex. J Anat.; 225(2):246–261

[8] Bastir M, García Martínez D, Recheis W, et al. Differential growth and development of the upper and lower human thorax. PLoS One.; 8(9):e75128

[9] Ramadan SU, Türkmen N, Dolgun NA, et al. Sex determination from measurements of the sternum and fourth rib using multislice computed tomography of the chest. Forensic Sci Int.; 197(1–3):120.e1–120.e5

[10] Donnelly LF, Frush DP, Foss JN, O'Hara SM, Bisset GS, III. Anterior chest wall: frequency of anatomic variations in children. Radiology.; 212(3):837–840

[11] Song WC, Kim SH, Park DK, Koh KS. Bifid rib: anatomical considerations in three cases. Yonsei Med J.; 50(2):300–303

[12] Kamano H, Ishihama T, Ishihama H, Kubota Y, Tanaka T, Satoh K. Bifid intrathoracic rib: a case report and classification of intrathoracic ribs. Intern Med.; 45(9):627–630

[13] Brewin J, Hill M, Ellis H. The prevalence of cervical ribs in a London population. Clin Anat.; 22(3):331–336

[14] Erken E, Ozer HT, Gulek B, Durgun B. The association between cervical rib and sacralization. Spine.; 27(15):1659–1664

[15] Aly I, Chapman JR, Oskouian RJ, Loukas M, Tubbs RS. Lumbar ribs: a comprehensive review. Childs Nerv Syst.

[16] Glass RB, Norton KI, Mitre SA, Kang E. Pediatric ribs: a spectrum of abnormalities. Radiographics.; 22(1):87–104

[17] Fokin AA. Cleft sternum and sternal foramen. Chest Surg Clin N Am.; 10 (2):261–276

[18] Tocchioni F, Ghionzoli M, Lo Piccolo R, et al. Sternal cleft and pectus excavatum: a combined approach for the correction of a complex anterior chest wall malformation in a teenager. Ann Thorac Surg.; 99(6):e131–e135

[19] Park CH, Kim TH, Haam SJ, Jeon I, Lee S. The etiology of pectus carinatum involves overgrowth of costal cartilage and undergrowth of ribs. J Pediatr Surg.; 49(8):1252–1258

[20] Dean C, Etienne D, Hindson D, Matusz P, Tubbs RS, Loukas M. Pectus excavatum (funnel chest): a historical and current prospective. Surg Radiol Anat.; 34(7):573–579

[21] Cobben JM, Oostra RJ, van Dijk FS. Pectus excavatum and carinatum. Eur J Med Genet.; 57(8):414–417

[22] Stokes IA, Dansereau J, Moreland MS. Rib cage asymmetry in idiopathic scoliosis. J Orthop Res.; 7(4):599–606

[23] Malghem J, Vande Berg B, Lecouvet F, Maldague B. Costal cartilage fractures as revealed on CT and sonography. AJR Am J Roentgenol.; 176(2):429–432

[24] Subhas N, Kline MJ, Moskal MJ, White LM, Recht MP. MRI evaluation of costal cartilage injuries. AJR Am J Roentgenol.; 191(1):129–132

[25] Grabias SL, Campbell CJ. Fibrous dysplasia. Orthop Clin North Am.; 8(4):771–783

[26] Miller JI, Jr. Muscles of the chest wall. Thorac Surg Clin.; 17(4):463–472

[27] Sanchez ER, Howland N, Kaltwasser K, Moliver CL. Anatomy of the sternal origin of the pectoralis major: implications for subpectoral augmentation. Aesthet Surg J.; 34(8):1179–1184

[28] Chomiak J, Dungl P. Reconstruction of elbow flexion in arthrogryposis multiplex congenita type I. Part I: surgical anatomy and vascular and nerve supply of the pectoralis major muscle as a basis for muscle transfer. J Child Orthop.; 2(5):357–364

[29] Chiavaras MM, Jacobson JA, Smith J, Dahm DL. Pectoralis major tears: anatomy, classification, and diagnosis with ultrasound and MR imaging. Skeletal Radiol.; 44(2):157–164

[30] David S, Balaguer T, Baque P, et al. The anatomy of the pectoral nerves and its significance in breast augmentation, axillary dissection and pectoral muscle flaps. J Plast Reconstr Aesthet Surg.; 65(9):1193–1198

[31] Porzionato A, Macchi V, Stecco C, Loukas M, Tubbs RS, De Caro R. Surgical anatomy of the pectoral nerves and the pectoral musculature. Clin Anat.; 25 (5):559–575

[32] Bak K, Cameron EA, Henderson IJP. Rupture of the pectoralis major: a meta-analysis of 112 cases. Knee Surg Sports Traumatol Arthrosc.; 8(2):113–119

[33] Yiyit N, Işıtmangil T, Saygın H. Eight patients with multiple bilateral thoracic anomalies: a new syndrome or bilateral Poland's syndrome? Ann Thorac Surg.; 97(5):1758–1763

[34] Sanchez ER, Sanchez R, Moliver C. Anatomic relationship of the pectoralis major and minor muscles: a cadaveric study. Aesthet Surg J.; 34(2):258–263

[35] Chadwick CJ. Tendinitis of the pectoralis major insertion with humeral lesions. A report of two cases. J Bone Joint Surg Br.; 71(5):816–818

[36] Turgut HB, Anil A, Peker T, Barut C. Insertion abnormality of bilateral pectoralis minimus. Surg Radiol Anat.; 22(1):55–57

[37] Snosek M, Tubbs RS, Loukas M. Sternalis muscle, what every anatomist and clinician should know. Clin Anat.; 27(6):866–884

[38] Young Lee B, Young Byun J, Hee Kim H, et al. The sternalis muscles: incidence and imaging findings on MDCT. J Thorac Imaging.; 21(3):179–183

[39] Raikos A, Paraskevas GK, Tzika M, et al. Sternalis muscle: an underestimated anterior chest wall anatomical variant. J Cardiothorac Surg.; 6:73

[40] Arnold PG, Pairolero PC, Waldorf JC. The serratus anterior muscle: intrathoracic and extrathoracic utilization. Plast Reconstr Surg.; 73(2):240–248

[41] Bartlett SP, May JW, Jr, Yaremchuk MJ. The latissimus dorsi muscle: a fresh cadaver study of the primary neurovascular pedicle. Plast Reconstr Surg.; 67 (5):631–636

[42] Lieba-Samal D, Morgenbesser J, Moritz T, et al. Visualization of the long thoracic nerve using high-resolution sonography. Ultraschall Med.; 36(3):264–269

[43] Elhassan B. Pectoralis major transfer for the management of scapula winging secondary to serratus anterior injury or paralysis. J Hand Surg Am.; 39 (2):353–361

[44] Vargas-Schaffer G, Nowakowsky M, Eghtesadi M, Cogan J. Ultrasound-guided trigger point injection for serratus anterior muscle pain syndrome: description of technique and case series. A A Case Rep.; 5(6):99–102

[45] Moschella F, Cordova A. A new extended external oblique musculocutaneous flap for reconstruction of large chest-wall defects. Plast Reconstr Surg.; 103 (5):1378–1385

[46] Schlenz I, Burggasser G, Kuzbari R, Eichberger H, Gruber H, Holle J. External oblique abdominal muscle: a new look on its blood supply and innervation. Anat Rec.; 255(4):388–395

[47] Yang D, Morris SF, Geddes CR, Tang M. Neurovascular territories of the external and internal oblique muscles. Plast Reconstr Surg.; 112(6):1591–1595

[48] Bhatt CR, Prajapati B, Patil DS, Patel VD, Singh BG, Mehta CD. Variation in the insertion of the latissimus dorsi & its clinical importance. J Orthop.; 10 (1):25–28

[49] Tubbs RS, Tyler-Kabara EC, Aikens AC, et al. Surgical anatomy of the dorsal scapular nerve. J Neurosurg.; 102(5):910–911

[50] Mirjalili SA, Muirhead JC, Stringer MD. Ultrasound visualization of the spinal accessory nerve in vivo. J Surg Res.; 175(1):e11–e16

[51] Soo KC, Strong EW, Spiro RH, Shah JP, Nori S, Green RF. Innervation of the trapezius muscle by the intra-operative measurement of motor action potentials. Head Neck.; 15(3):216–221

[52] Lanisnik B, Zargi M, Rodi Z. Identification of three anatomical patterns of the spinal accessory nerve in the neck by neurophysiological mapping. Radiol Oncol.; 48(4):387–392

[53] Lee SH, Lee JK, Jin SM, et al. Anatomical variations of the spinal accessory nerve and its relevance to level IIb lymph nodes. Otolaryngol Head Neck Surg.; 141(5):639–644

[54] Akamatsu FE, Ayres BR, Saleh SO, et al. Trigger points: an anatomical substratum. BioMed Res Int.; 2015:623287

[55] Jelev L, Hristov S, Ovtscharoff W. Variety of transversus thoracis muscle in relation to the internal thoracic artery: an autopsy study of 120 subjects. J Cardiothorac Surg.; 6:11

[56] De Troyer A, Kirkwood PA, Wilson TA. Respiratory action of the intercostal muscles. Physiol Rev.; 85(2):717–756

[57] De Troyer A, Ninane V, Gilmartin JJ, Lemerre C, Estenne M. Triangularis sterni muscle use in supine humans. J Appl Physiol (1985).; 62(3):919–925

[58] Saha A, Mandal S, Chakraborty S, Bandyopadhyay M. Morphological study of the attachment of sternocleidomastoid muscle. Singapore Med J.; 55(1):45–47

[59] Kierner AC, Aigner M, Zelenka I, Riedl G, Burian M. The blood supply of the sternocleidomastoid muscle and its clinical implications. Arch Surg.; 134 (2):144–147

[60] Mehta V, Arora J, Kumar A, et al. Bipartite clavicular attachment of the sternocleidomastoid muscle: a case report. Anat Cell Biol.; 45(1):66–69

[61] Harry WG, Bennett JD, Guha SC. Scalene muscles and the brachial plexus: anatomical variations and their clinical significance. Clin Anat.; 10(4):250–252

[62] Natsis K, Totlis T, Didagelos M, Tsakotos G, Vlassis K, Skandalakis P. Scalenus minimus muscle: overestimated or not? An anatomical study. Am Surg.; 79 (4):372–374

[63] Rusnak-Smith S, Moffat M, Rosen E. Anatomical variations of the scalene triangle: dissection of 10 cadavers. J Orthop Sports Phys Ther.; 31(2):70–80

[64] Smayra T, Nabhane L, Tabet G, Menassa-Moussa L, Hachem K, Haddad-Zebouni S. The subclavius posticus muscle: an unusual cause of thoracic outlet syndrome. Surg Radiol Anat.; 36(7):725–728

[65] Cogar AC, Johnsen PH, Potter HG, Wolfe SW. Subclavius posticus: an anomalous muscle in association with suprascapular nerve compression in an athlete. Hand (NY).; 10(1):76–79

[66] Durgun B, Yücel AH, Kizilkanat ED, Dere F. Multiple arterial variation of the human upper limb. Surg Radiol Anat.; 24(2):125–128

[67] Hattori Y, Doi K, Sakamoto S, Satbhai N. Anatomic variations in branching patterns of the axillary artery: a multidetector-row computed tomography angiography study. J Reconstr Microsurg.; 29(8):531–536

[68] Cavdar S, Zeybek A, Bayramiçli M. Rare variation of the axillary artery. Clin Anat.; 13(1):66–68

[69] Jacquemin G, Lemaire V, Medot M, Fissette J. Bilateral case of superficial ulnar artery originating from axillary artery. Surg Radiol Anat.; 23(2):139–143

[70] Uemura M, Takemura A, Suwa F. Bilateral subclavian arteries passing in front of the scalenus anterior muscles. Anat Sci Int.; 82(3):180–185

[71] Strub WM, Leach JL, Tomsick TA. Left vertebral artery origin from the thyrocervical trunk: a unique vascular variant. AJNR Am J Neuroradiol.; 27 (5):1155–1156

[72] Wiśniewski M, Krakowiak-Sarnowska E, Szpinda M, Sarnowski J. The internal thoracic artery in human foetuses. Folia Morphol (Warsz).; 63(1):19–23

[73] Paraskevas G, Natsis K, Tzika M, Ioannidis O, Kitsoulis P. Abnormal origin of internal thoracic artery from the thyrocervical trunk: surgical considerations. J Cardiothorac Surg.; 7:63

[74] Pietrasik K, Bakon L, Zdunek P, Wojda-Gradowska U, Dobosz P, Kolesnik A. Clinical anatomy of internal thoracic artery branches. Clin Anat.; 12(5):307–314

[75] Henriquez-Pino JA, Gomes WJ, Prates JC, Buffolo E. Surgical anatomy of the internal thoracic artery. Ann Thorac Surg.; 64(4):1041–1045

[76] Carrier M, Grégoire J, Tronc F, Cartier R, Leclerc Y, Pelletier LC. Effect of internal mammary artery dissection on sternal vascularization. Ann Thorac Surg.; 53(1):115–119

[77] Berdajs D, Zünd G, Turina MI, Genoni M. Blood supply of the sternum and its importance in internal thoracic artery harvesting. Ann Thorac Surg.; 81 (6):2155–2159

[78] Paliouras D, Rallis T, Gogakos A, et al. Surgical anatomy of the internal thoracic arteries and their branching pattern: a cadaveric study. Ann Transl Med.; 3(15):212

[79] Nizanowski C, Noczyński L, Suder E. Variability of the origin of ramifications of the subclavian artery in humans (studies on the Polish population). Folia Morphol (Warsz).; 41(3):281–294

[80] Marx R, Clahsen H, Schneider R, Sons H, Klein RM, Gülker H. Histomorphological studies of the distal internal thoracic artery which support its use for coronary artery bypass grafting. Atherosclerosis.; 159(1):43–48

[81] Loukas M, Tobola MS, Tubbs RS, et al. The clinical anatomy of the internal thoracic veins. Folia Morphol (Warsz).; 66(1):25–32

[82] Lee H, Moon YS, Park HS, Kim HT, Choi IJ. A radial artery originating from the thoracoacromial artery. Surg Radiol Anat.

[83] Loukas M, du Plessis M, Owens DG, et al. The lateral thoracic artery revisited. Surg Radiol Anat.; 36(6):543–549

[84] Paraskevas GK. High or low incidence of the lateral thoracic artery's origin from the thoracoacromial artery? Surg Radiol Anat.; 37(7):887–889

[85] Olinger A, Benninger B. Branching patterns of the lateral thoracic, subscapular, and posterior circumflex humeral arteries and their relationship to the posterior cord of the brachial plexus. Clin Anat.; 23(4):407–412

[86] Şentürk S, Efe D, Özkan A, Göncü RG, Zümrüt M. Multidetector computed tomography angiography to evaluate the subscapular arterial tree. Microsurgery.; 35(8):640–644

[87] Rendina EA, Ciccone AM. The intercostal space. Thorac Surg Clin.; 17(4):491–501

[88] Hamdi M, Spano A, Van Landuyt K, D'Herde K, Blondeel P, Monstrey S. The lateral intercostal artery perforators: anatomical study and clinical application in breast surgery. Plast Reconstr Surg.; 121(2):389–396

[89] Jeon EY, Cho YK, Yoon DY, Seo YL, Lim KJ, Yun EJ. Angiographic analysis of the lateral intercostal artery perforator of the posterior intercostal artery: anatomic variation and clinical significance. Diagn Interv Radiol.; 21(5):415–418

[90] Da Rocha RP, Vengjer A, Blanco A, de Carvalho PT, Mongon ML, Fernandes GJ. Size of the collateral intercostal artery in adults: anatomical considerations in relation to thoracocentesis and thoracoscopy. Surg Radiol Anat.; 24(1):23–26

[91] Choi S, Trieu J, Ridley L. Radiological review of intercostal artery: anatomical considerations when performing procedures via intercostal space. J Med Imaging Radiat Oncol.; 54(4):302–306

[92] Helm EJ, Rahman NM, Talakoub O, Fox DL, Gleeson FV. Course and variation of the intercostal artery by CT scan. Chest.; 143(3):634–639

[93] Klaassen Z, Sorenson E, Tubbs RS, et al. Thoracic outlet syndrome: a neurological and vascular disorder. Clin Anat.; 27(5):724–732

[94] Grunebach H, Arnold MW, Lum YW. Thoracic outlet syndrome. Vasc Med.; 20(5):493–495

[95] Urschel HC, Jr, Razzuk MA. Neurovascular compression in the thoracic outlet: changing management over 50 years. Ann Surg.; 228(4):609–617

[96] Natsis K, Totlis T, Tsikaras P, Anastasopoulos N, Skandalakis P, Koebke J. Variations of the course of the upper trunk of the brachial plexus and their clinical significance for the thoracic outlet syndrome: a study on 93 cadavers. Am Surg.; 72(2):188–192

[97] Chang KZ, Likes K, Davis K, Demos J, Freischlag JA. The significance of cervical ribs in thoracic outlet syndrome. J Vasc Surg.; 57(3):771–775

[98] Criado E, Berguer R, Greenfield L. The spectrum of arterial compression at the thoracic outlet. J Vasc Surg.; 52(2):406–411

[99] Konuşkan B, Bozkurt MC, Tağil SM, Ozçakar L. Cadaveric observation of an aberrant left subclavian artery: a possible cause of thoracic outlet syndrome. Clin Anat.; 18(3):215–216

[100] Collins RM, Bhana J, Patricios JS, et al. Thoracic outlet syndrome in a patient with absent scalenus anterior muscle. Clin J Sport Med.; 24(3):268–270

[101] Davidovic LB, Kostic DM, Jakovljevic NS, Kuzmanovic IL, Simic TM. Vascular thoracic outlet syndrome. World J Surg.; 27(5):545–550

[102] Moore R, Wei Lum Y. Venous thoracic outlet syndrome. Vasc Med.; 20 (2):182–189

[103] Adams JT, DeWeese JA, Mahoney EB, Rob CG. Intermittent subclavian vein obstruction without thrombosis. Surgery.; 68:147–165

[104] Illig KA, Doyle AJ. A comprehensive review of Paget-Schroetter syndrome. J Vasc Surg.; 51(6):1538–1547

[105] Thompson RW. Comprehensive management of subclavian vein effort thrombosis. Semin Intervent Radiol.; 29(1):44–51

2 Tracheobronchial System

Farhood Saremi and Hiro Kiyosue

◆ Introduction

Anatomical knowledge of the trachea, mainstem bronchi, segmental bronchi branch pattern, relationship with neighboring structures and anatomical variants are important for radiologists and pulmonologists to localize, diagnose, and treat lesions.

Advanced bronchial endoscopic techniques as well as the possibility of virtual bronchoscopy using high-resolution computed tomography (CT) images have opened new ways to study the bronchial system. Multislice CT scanners can cover the entire lung during a single breath hold to create high-quality volumetric data allowing generation of superb multiplanar and volume-rendered images including specific postprocessing techniques for airway imaging, such as virtual bronchography and virtual bronchoscopy. Dynamic CT acquisition allows evaluation of the bronchial wall integrity and function during different phases of the respiratory cycle.

In this chapter, the anatomy and anatomical variants of the tracheobronchial tree will be reviewed and relevant pathologies will be discussed. At the hilar level the relationship of the bronchi to the pulmonary arteries and veins will be reviewed.

◆ Embryology

Tracheobronchial and lung growth is subdivided into five distinct stages: embryonic, pseudoglandular, canalicular, saccular, and alveolar.[1,2,3,4] While there is some overlap of these stages, it is generally agreed that weeks 0 to 6 of gestation comprise the embryonic stage, weeks 6 to 16 the pseudoglandular stage, weeks 16 to 24 the canalicular stage, weeks 24 to term the saccular stage and the alveolar stage continues during the first 3 years of postnatal life. Development of the pulmonary circulation occurs in parallel with lung development. The respiratory portion of the gut will be separated from the esophageal portion by the tracheoesophageal septum which is formed from the lateral ingrowths of the surrounding mesoderm.

The rudiment of the respiratory tree develops as a median laryngotracheal diverticulum (lung bud) arising from the anterior wall of the foregut between third and fourth week of embryonic development.[1,2] Shortly thereafter, the right and left lung buds appear, the laryngotracheal tube forms, and the trachea separates from the esophagus. The thyroid cartilage develops from the ventral ends of the cartilages of the fourth branchial arch and the cricoid cartilage and cartilages of the trachea develop from the sixth branchial arch during the sixth week. The trachea increases rapidly in length from the fifth week onward. Three growing points on the right side and two on the left side corresponding to primary lobar bronchial buds soon appear.[2] During the embryonic and pseudoglandular stages each primary bronchial bud undergoes rapid and continuous stages of dichotomous arborization that, by birth, gives rise to 18 to 23 generations of bronchial divisions. Therefore, by week 17 (end of the pseudoglandular stage), all preacinar airways, as well as corresponding vessels are present and the acinar limits can be identified.[1] During this period, the airways are blind tubules lined by columnar or cuboidal epithelium, hence the term pseudoglandular. Terminal bronchiole, respiratory bronchioles, and alveoli develop mainly during the canalicular and saccular stages (24 weeks till birth). Differentiation of the cuboidal epithelium into type I and type II cells, initiation of air–blood barriers, and the start of surfactant production also occur in these stages and the lungs migrate inferiorly, so that by birth the bifurcation of the trachea reaches the level of T4. At birth, further maturation of the lung parenchyma and the surfactant system continues during the first few years of life. Infants born prematurely have underdeveloped lungs (pulmonary hypoplasia) and often require assistance to maintain adequate respiration. Lung growth is influenced by physical factors such as the amount of amniotic fluid, lung liquid volume and pressure, and fetal breathing movements.[5,6,7]

Any defect during embryonic development of the tracheobronchial tree can result in congenital malformations. Incomplete separation of the trachea from the foregut can cause various forms of tracheobronchial fistulas. Abnormalities of the bronchial branching pattern occur during embryonic and pseudoglandular stages. It is likely that defects causing supernumerary tracheal bronchi occur during the early embryonic stage (before week 6), at about 29 to 30 days, as the lobar bronchi start to differentiate, whereas displaced bronchi are more likely to occur during pseudoglandular stage (after week 6).[8,9,10]

◆ Tracheal Anatomy

The trachea is a cartilaginous and membranous tube located below the subglottic region. The subglottis or subglottic region is a short airway passage in the lower portion of the larynx that extends from a plane approximately 1 cm below the free margin of the true vocal cords to the lower border of the cricoid cartilage[11,12,13,14] (▶ Fig. 2.1, ▶ Fig. 2.2, ▶ Fig. 2.3). The trachea extends between the cricoid cartilage at C5–C6 level and the carina approximately at T4–T5 level[11,12,13,14] (▶ Fig. 2.4).

In the adult, the tracheal length ranges from 10 to 16 cm. The adult trachea is, on average, 15 cm long. It is longer in men than in women. The first half of the trachea is located above the thoracic inlet when the neck is extended but it becomes entirely intrathoracic in hyperflexion position. Surgeons leave the neck in a neutral position to decrease tension on trachea after segmental tracheal resection. Position of the neck is also important when assessing the position of endotracheal tubes (ETs) on chest radiograph. With flexion, the end of the ET can easily move from a midtracheal position to the carina or even lower into the orifice of the right main bronchus (▶ Fig. 2.5).

The trachea moves in midline from an anterior position at the neck to a posterior position at the carina. The trachea often can be deviated to the right at the level of the aortic arch, with a greater degree of displacement in the setting of advanced age or aortic dilation and tortuosity. Anatomical relationship of the

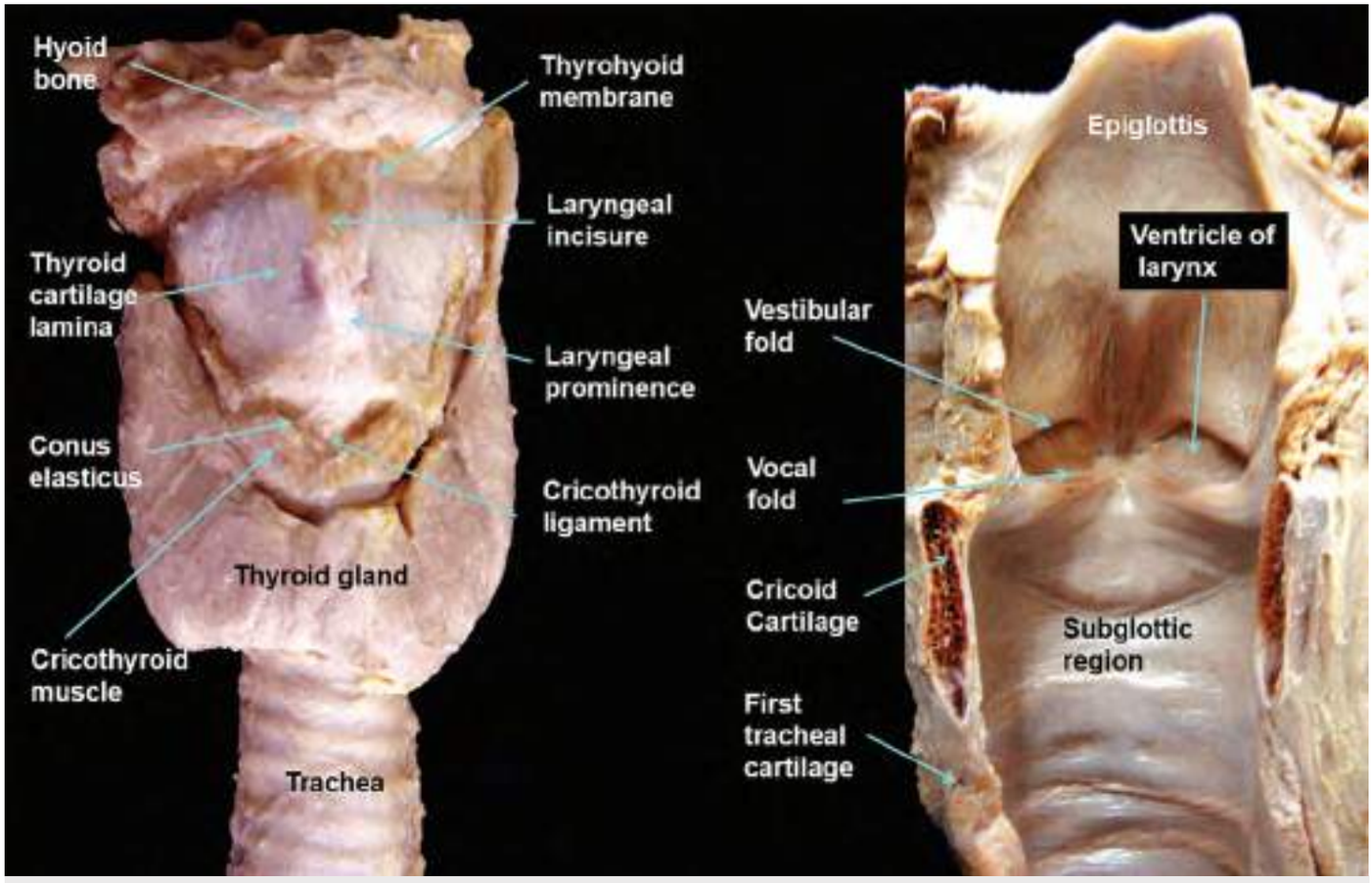

Fig. 2.1 Laryngotracheal junction and associated structures.

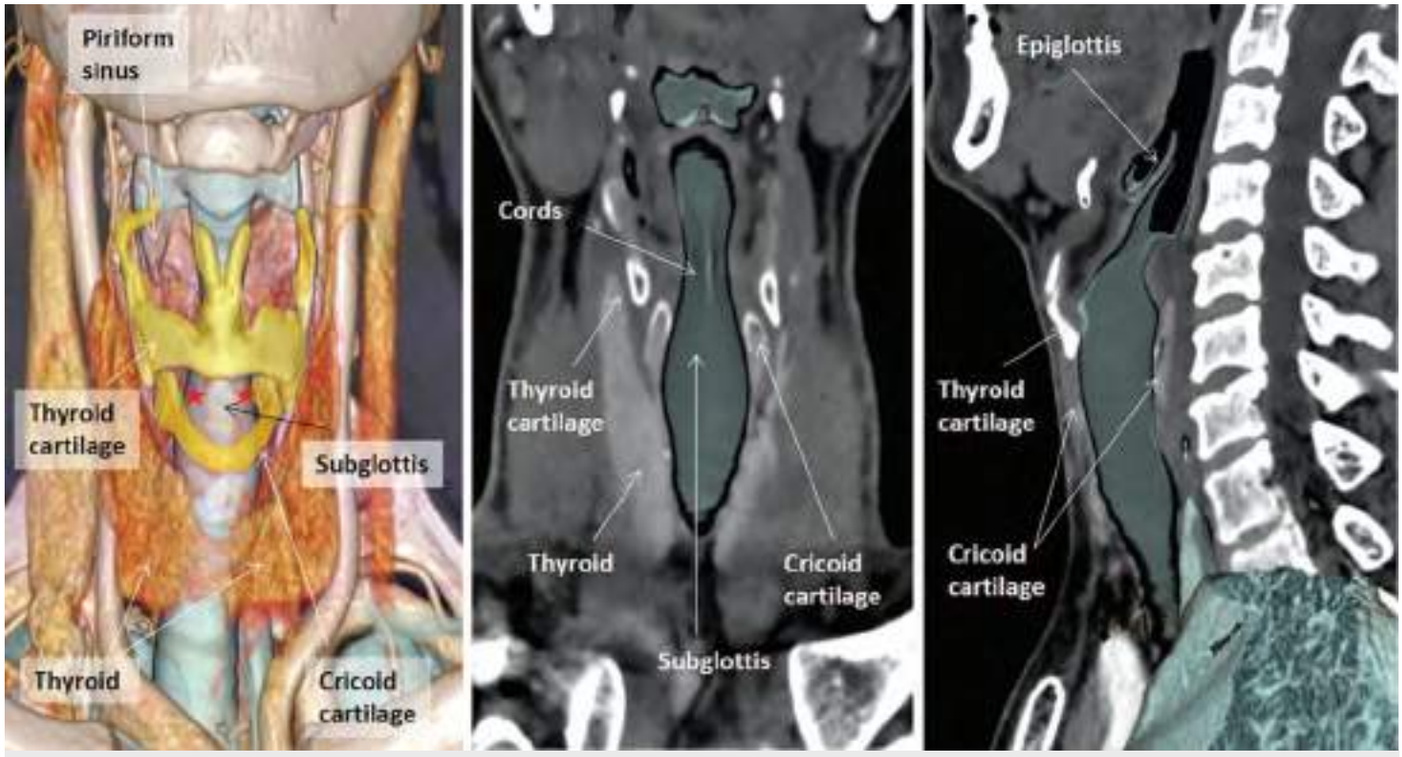

Fig. 2.2 Subglottic region and conus elasticus. Frontal volume-rendered CT, coronal, and sagittal views are shown. The subglottis is located in the lower portion of the larynx below the vocal cord and above the lower margin of the cricoid cartilage. The conus elasticus (*red stars*) is anterolateral aspect of the subglottis located on the sides of the cricothyroid ligament. The piriform sinuses are seen on either side of the laryngeal orifice.

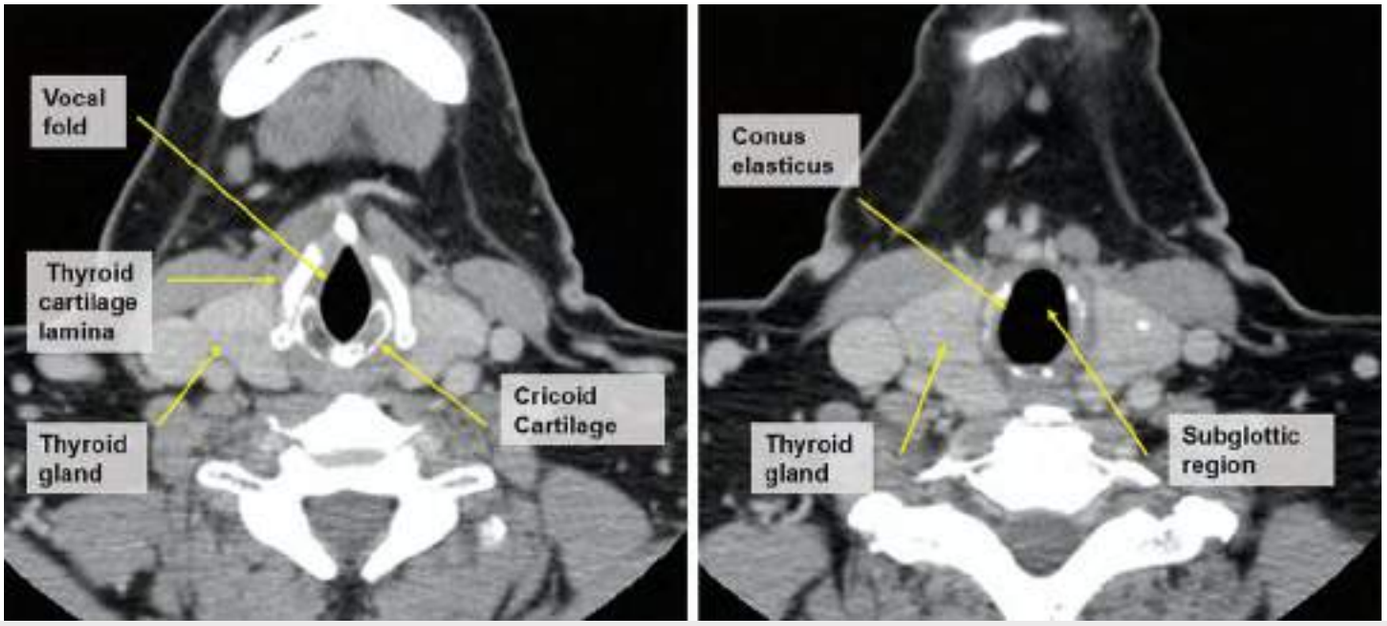

Fig. 2.3 Axial CT images at the level of the tracheal origin. In the neck, the thyroid covers the second or third tracheal rings of the trachea anteriorly. The trachea starts below the cricoid cartilage and subglottis. Vocal cords are seen just above the cricoid cartilage.

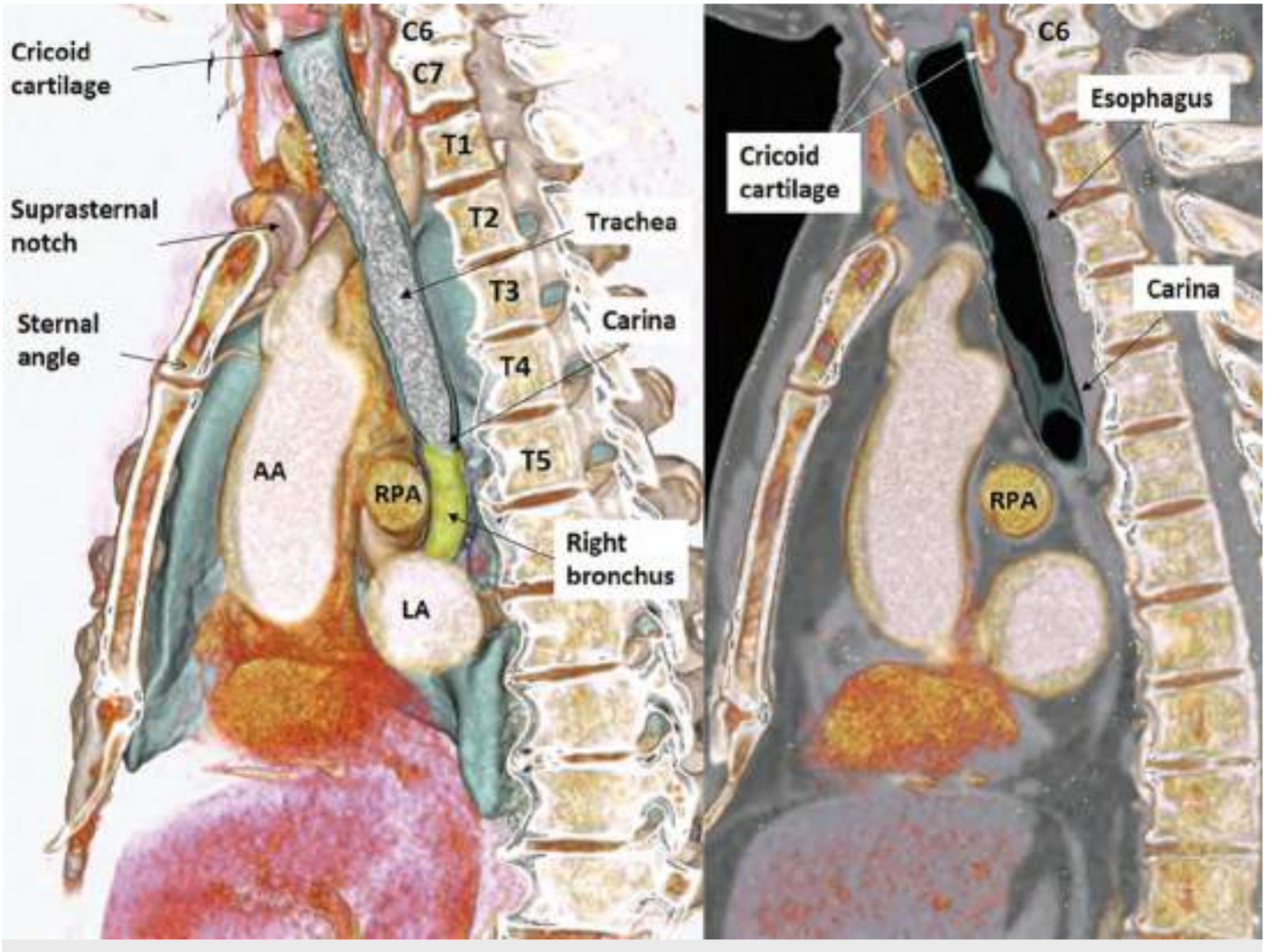

Fig. 2.4 Tracheal relationship. Midsagittal views of the thorax. The trachea starts from the cricoid cartilage at C5–C6 level. The tracheal bifurcation is located below the level of the sternal angle anteriorly and the T4 to T5 disc space posteriorly. Half of tracheal length is above the sternal notch. The right main bronchus continues along the long axis of the trachea and stays behind the right pulmonary artery (RPA). AA, ascending aorta; LA, left atrium.

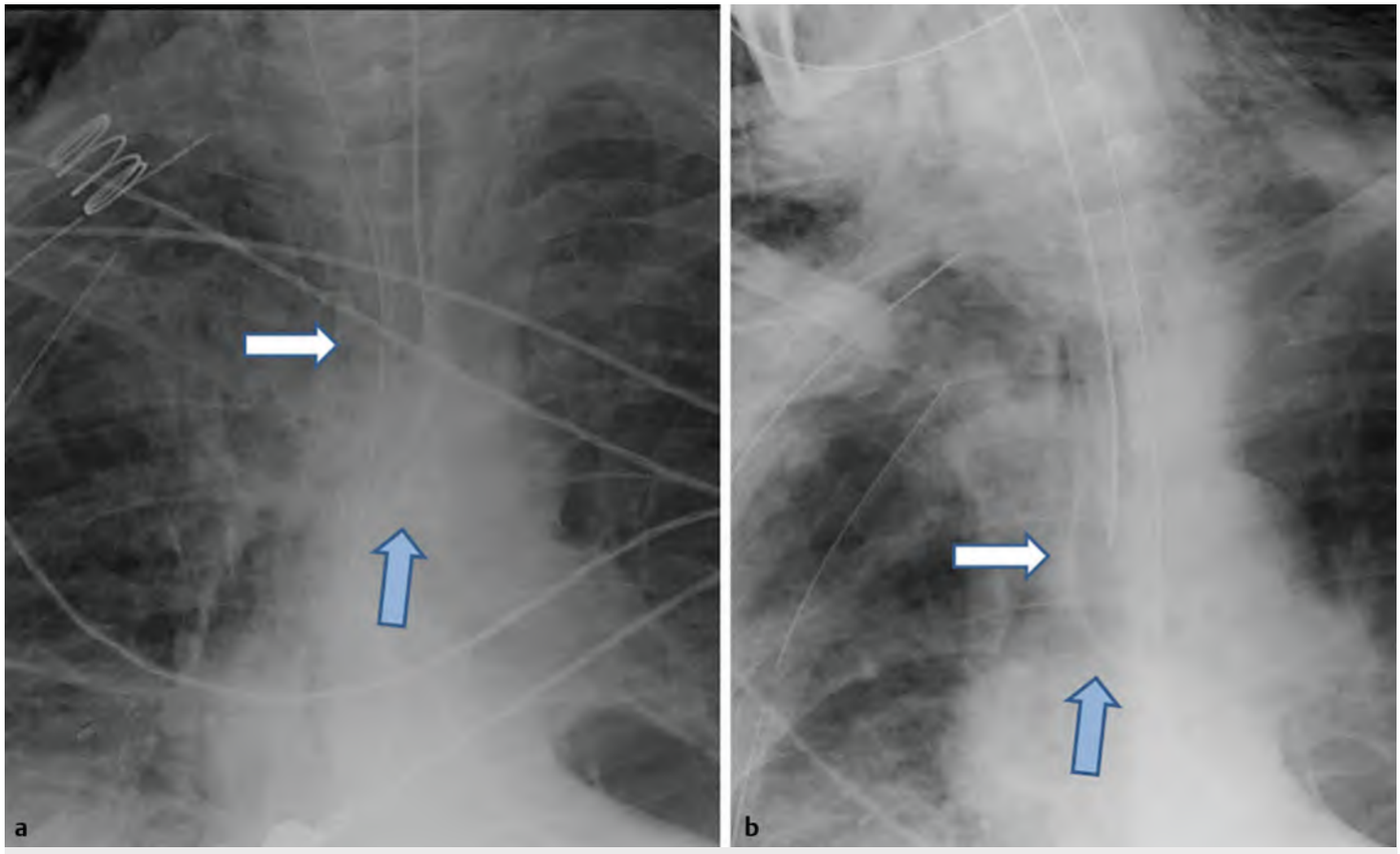

Fig. 2.5 Positional change of the endotracheal tube (ET) from neutral **(a)** and flexion **(b)** of the neck. The end of endotracheal tube (*white arrows*) can easily move from a midtracheal position in neutral neck position to the carina (*blue arrows*) or even lower into the orifice of the right main bronchus with neck flexion.

trachea to adjacent organs can best be assessed with CT. In the neck, the thyroid and thyroid isthmus cover the second or third tracheal rings of the trachea anteriorly and the esophagus moves behind the trachea. In the mediastinum, the innominate artery crosses over the midtrachea obliquely from its site of origin in the aortic arch and the right and left brachiocephalic veins are located anterior to the innominate artery (▶ Fig. 2.6, ▶ Fig. 2.7). The superior vena cava is anterior and to the right of the trachea. Posteriorly, the membranous trachea is in contact with the esophagus on the left and vertebral bodies on the right.

The trachea has an anterior and lateral U-shaped cartilaginous portion and a posterior membranous part lined by ciliated pseudostratified respiratory columnar epithelium. The membranous part consists of fibrous sheath with smooth trachealis muscle. The trachea is made of 16 to 22 cartilaginous rings connected each other by elastin tissue. Each ring is approximately 0.5 cm in length. With age, the cartilaginous portion becomes more rigid and calcified. In CT studies of the chest, calcification of the tracheobronchial tree is common finding in patients aged 40 years and older especially in women (▶ Fig. 2.8). Practical clinical significance of tracheal calcification remains unknown. It is more common in patients who have been on long-term anticoagulation medication, such as warfarin sodium. In general, senile calcification occurs commonly in structures made of hyaline cartilage (e.g., thyroid, cricoid, and part of the arytenoid cartilages, and tracheal rings), but it is rare in structures made of elastic fibrocartilages.[11]

The average diameter in a normal trachea is 22 mm in men and 19 mm in women.[15] The cricoid cartilage is the narrowest part of the trachea with an average diameter of 17 mm in men and 13 mm in women. In men, the coronal diameter ranges from 13 to 25 mm and the sagittal diameter ranges from 13 to 27 mm. In women, the average coronal diameter is 10 to 21 mm and the sagittal is 10 to 23 mm.[14,16] The tracheal lumen narrows slightly as it moves toward the carina. The cartilaginous tracheal wall is about 2 to 3 mm in thickness in both men and women, with a tracheal lumen that is often ovoid in shape.

The trachea is a dynamic and distensible organ that changes in diameter with respiration and variation in intrathoracic pressure (▶ Fig. 2.9). On inspiration, the cross-section appearance of the trachea is usually U-shaped especially in men and less commonly elliptical especially in women.[17] On expiration, posterior membrane flattens or bows anteriorly causing up to 30% decreased sagittal diameter in normal individuals. Chronic obstructive pulmonary disease (COPD) may lead to enlargement of the trachea (saber-sheath appearance) and in some cases softening of the tracheal rings (▶ Fig. 2.9). Saber-sheath trachea refers to diffuse coronal narrowing of the intrathoracic portion of the trachea with the concomitant widening of the sagittal diameter.

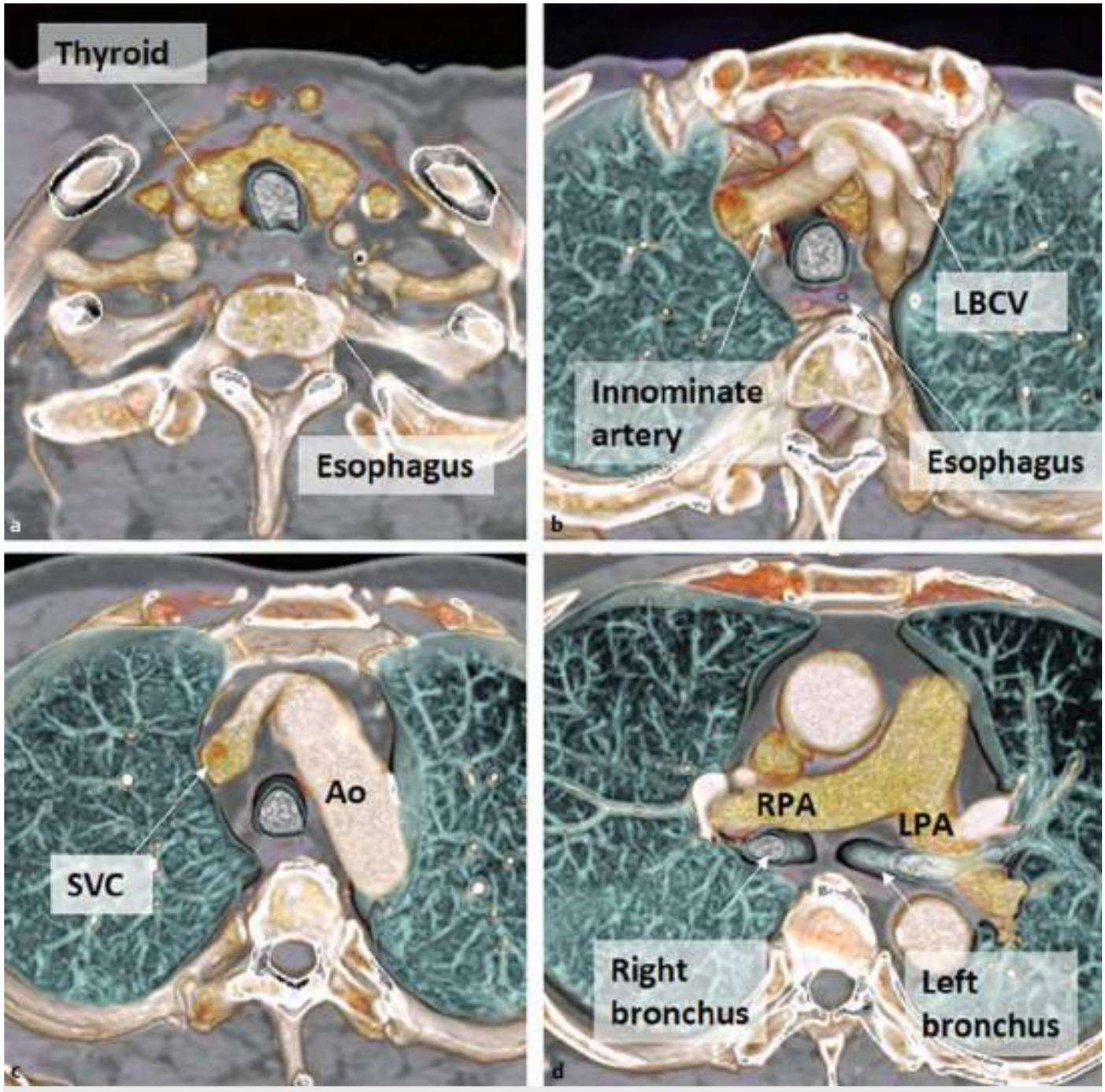

Fig. 2.6 Anatomical relationship of the trachea to adjacent organs. Axial views are shown. (**a**) In the neck, the thyroid and thyroid isthmus cover the second or third tracheal rings of the trachea anteriorly and the esophagus moves behind the trachea. (**b**) In the mediastinum, the innominate artery crosses over the midtrachea obliquely from its site of origin in the aortic arch and the right and left brachiocephalic veins (LBCV) are located anterior to the innominate artery. (**c**)The superior vena cava (SVC) is anterior and to the right of the trachea and the aortic arch (Ao) on the left. Posteriorly, the membranous trachea is in contact with the esophagus on the left and vertebral bodies on the right. (**d**)The right pulmonary artery (RPA) lies anterior and inferior to the carina. The right main bronchus passes posterior to the RPA. The left main bronchus passes posterior to the main pulmonary artery (MPA) and inferior to the left pulmonary artery (LPA).

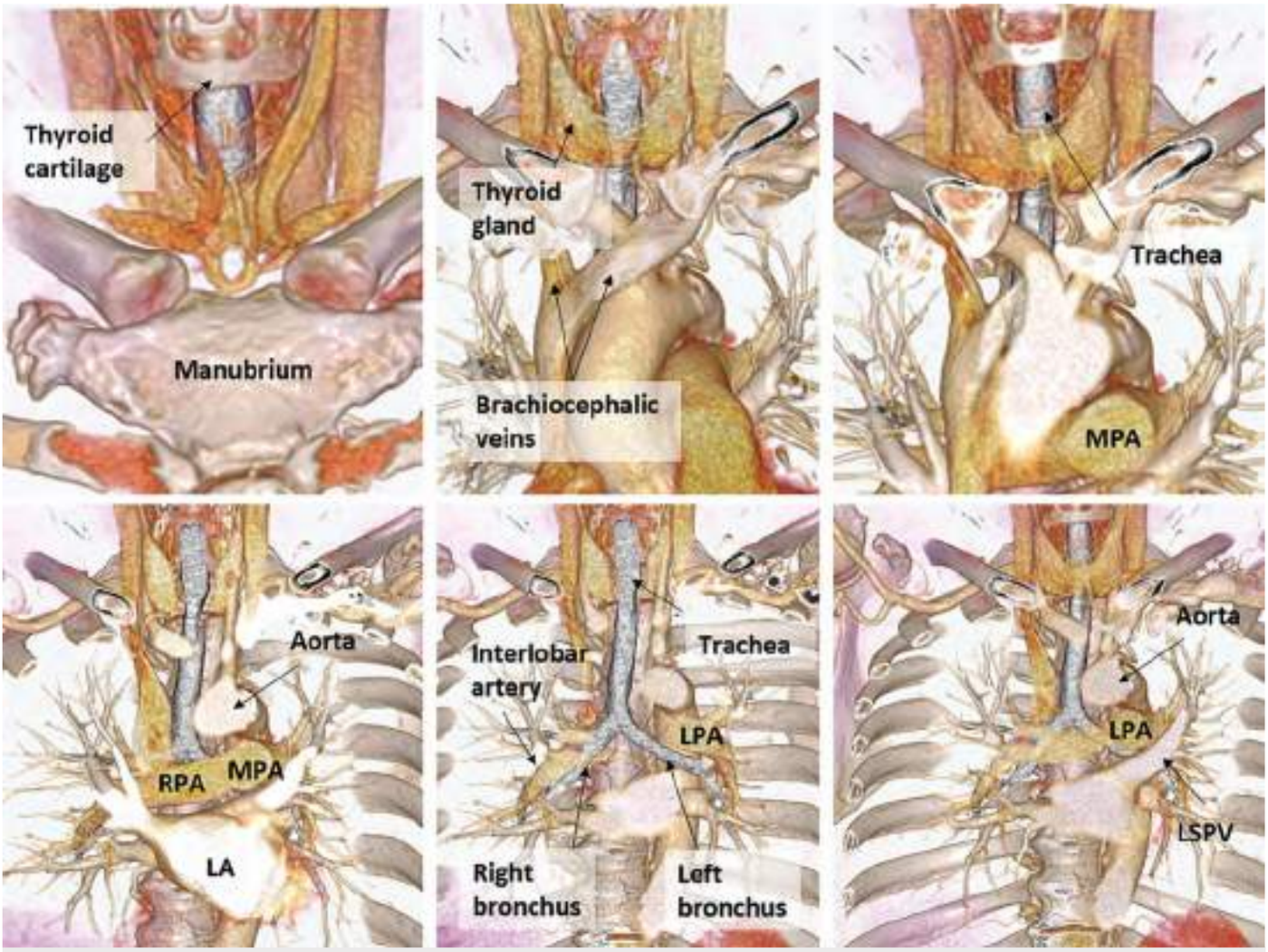

Fig. 2.7 Anatomical relationship of the trachea to adjacent organs. Coronal views are shown. In the neck, the thyroid and thyroid isthmus cover the second or third tracheal rings of the trachea anteriorly and the esophagus moves behind the trachea. The right pulmonary artery (RPA) lies anterior and inferior to the carina. The right main bronchus passes posterior to the RPA. The left main bronchus passes posterior to the main pulmonary artery (MPA) and inferior to the left pulmonary artery (LPA). LA, left atrium; LSPV, left superior pulmonary vein.

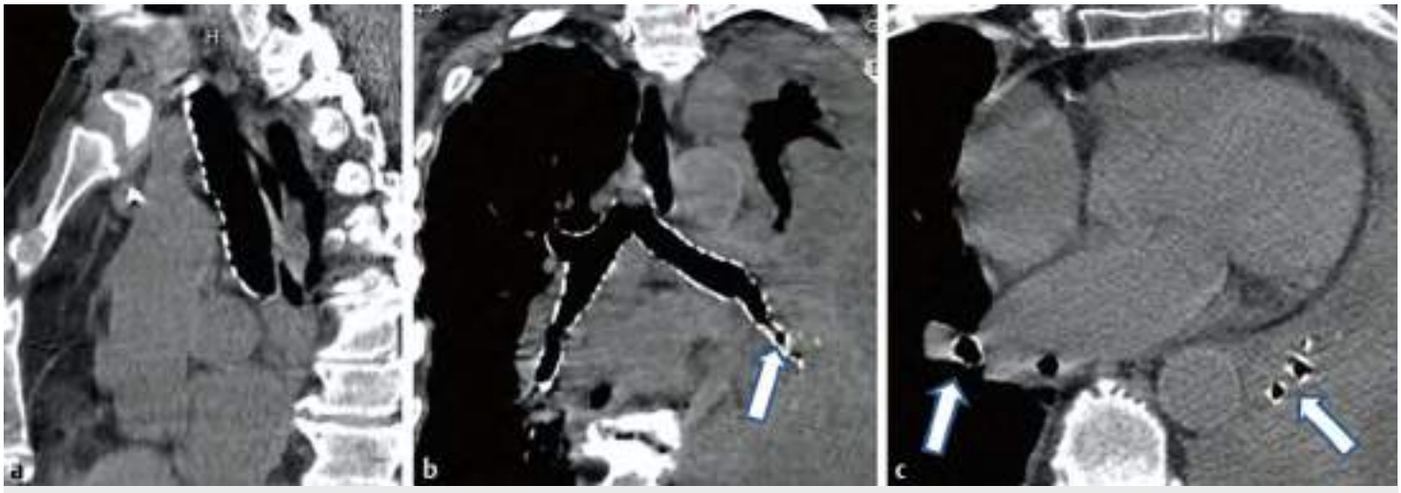

Fig. 2.8 Tracheobronchial senile calcification. Sagittal **(a)**, coronal **(b)**, and axial CT **(c)** images are shown. In general, senile calcification occurs commonly in structures made of hyaline cartilage such as tracheobronchial rings. The membranous trachea is spared. Calcification extends to the segmental bronchi (arrows) but usually not beyond it.

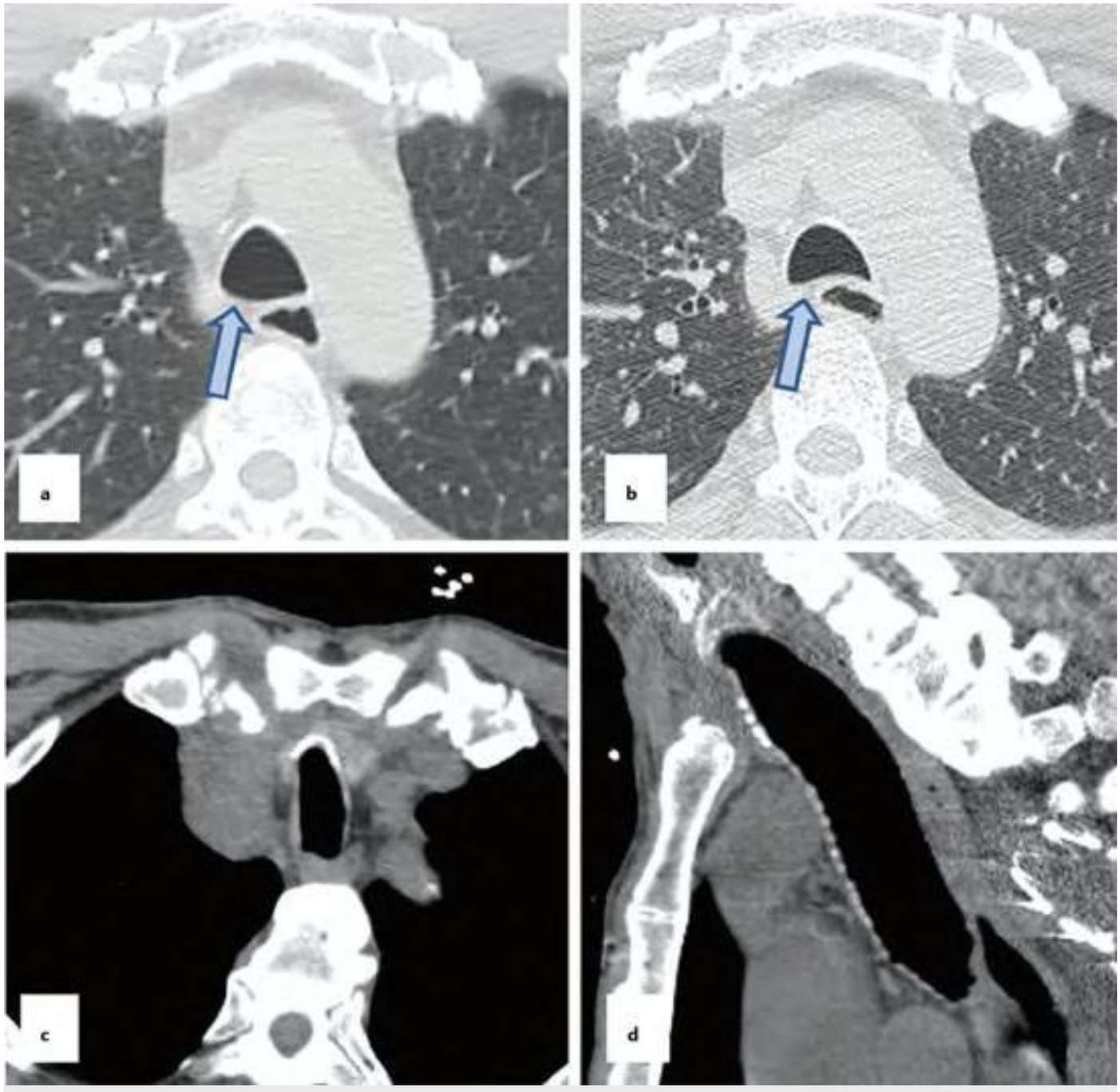

Fig. 2.9 Axial CT images in inspiration **(a)** and expiration **(b)** showing expiratory reduction of the tracheal lumen area (*blue arrows*) due to inward bulging of the membranous trachea. This phenomenon is called benign dynamic airway collapse. **(c)** Axial and **(d)** sagittal CT showing saber-sheath appearance of the trachea referring to diffuse coronal narrowing of the intrathoracic portion of the trachea with the concomitant widening of the sagittal diameter.

Vascular and Nerve Supply

Arterial supply to the proximal trachea is mainly provided by the tracheoesophageal branches of the inferior thyroid artery. The distal trachea on the other hand is supplied by the bronchial arteries.[11,12,13] Small branches arising from the subclavian, internal mammary, and innominate arteries also supply the trachea. The tracheoesophageal arteries divide into tracheal and esophageal branches near the tracheoesophageal groove (▶ Fig. 2.10). The tracheal arteries give rise to superior and inferior rami that connect with corresponding tracheal artery branches from the levels above and below. Between the cartilaginous rings, the tracheal arteries also penetrate into the submucosa and form an extensive submucosal capillary plexus. Whereas the tracheal cartilages receive their blood supply from tracheal branches, the membranous trachea is vascularized by esophageal arteries.

Venous drainage of the trachea is generally into the azygos/hemiazygos system. The lymphatic drainage of the trachea is through the low and high paratracheal nodal chains.

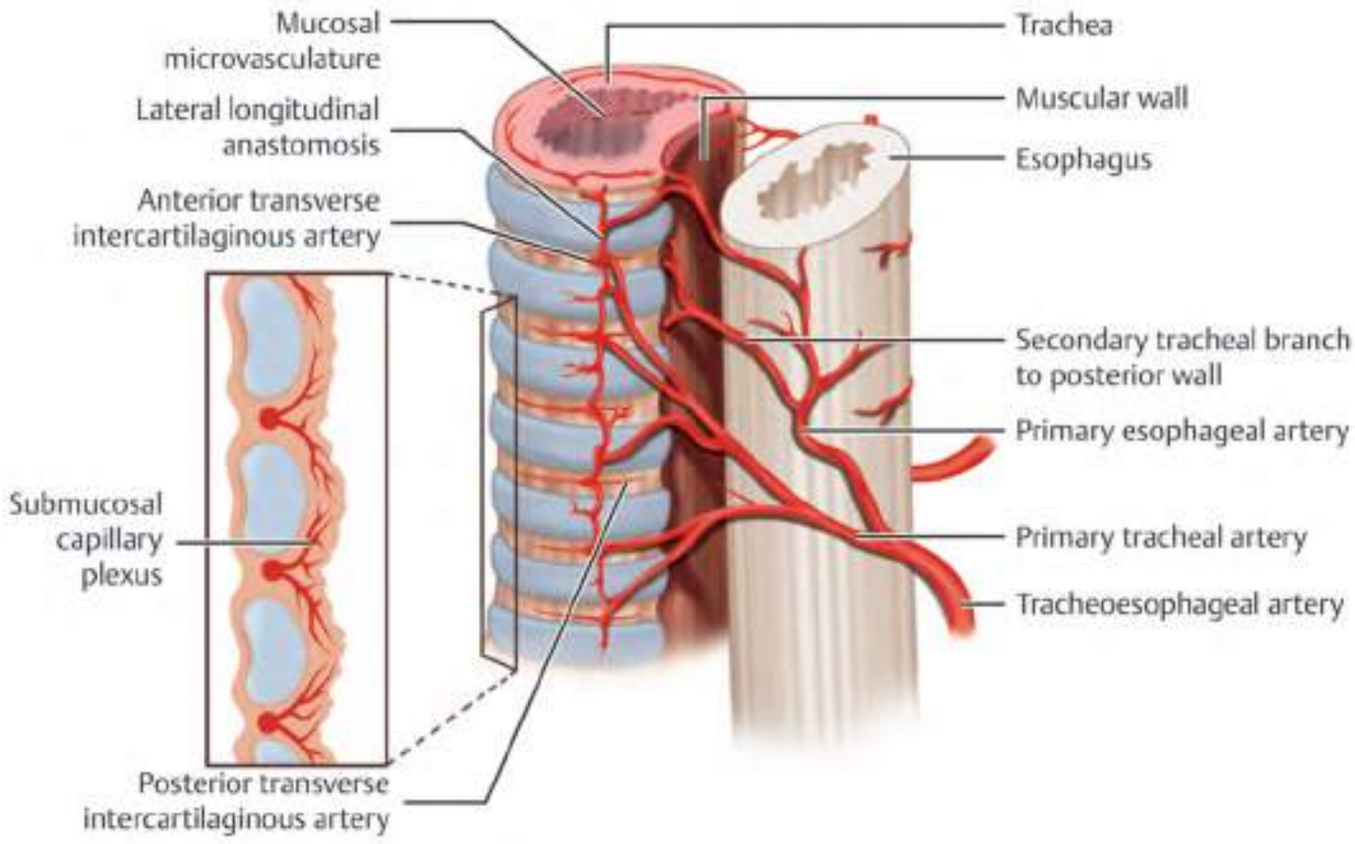

Fig. 2.10 Arterial blood supply of the trachea by tracheoesophageal artery. The tracheoesophageal arteries divide into tracheal and esophageal branches near the tracheoesophageal groove. The tracheal arteries give rise to superior and inferior rami that connect with corresponding tracheal artery branches from the levels above and below to supply the tracheal rings. The membranous trachea is supplied by the esophageal branches. Adapted from Thurnher et al 2007.[11]

The thoracic sympathetic chain and inferior ganglion of the vagus nerve are responsible for tracheobronchial muscle tone (bronchoconstriction or bronchodilation) and mucous production. Afferent vagal fibers control sneezing and cough reflex.

◆ Carina and Bronchial Anatomy

The trachea bifurcates at the carina into the right and left mainstem bronchi.[16] The tracheal bifurcation is located below the level of the sternal angle anteriorly and the T4 to T5 disc space posteriorly (▶ Fig. 2.4). The angle between the two main stem bronchi varies among individuals and is generally greater in children than in adults. The right mainstem bronchus lies in a more vertical orientation relative to the trachea, whereas the left mainstem bronchus lies in a more horizontal plane. The right pulmonary artery lies anterior and inferior to the carina. The main pulmonary artery is considerably anterior than the left main bronchus. The right main bronchus passes posterior to the right pulmonary artery. The left main bronchus passes posterior to the main pulmonary artery and inferior to the left pulmonary artery (▶ Fig. 2.6, ▶ Fig. 2.7). The left mainstem bronchus is longer than the right mainstem bronchus and it travels underneath the aortic arch to reach the posterior left hilum (▶ Fig. 2.7). This anatomical course makes surgical manipulation of the left main bronchus difficult.

The diameter of the right mainstem bronchus is an average of 17.5 mm in men and 14 mm in women.[18] The right mainstem bronchus continues as the bronchus intermedius after the takeoff of the right upper lobe bronchus. The average distance from the tracheal carina to the takeoff of the right upper lobe bronchus is 2 cm in men, whereas it is approximately 1.5 cm in women (▶ Fig. 2.11, ▶ Fig. 2.12). The right upper lobe bronchus arises several centimeters above the middle lobe bronchus, and the right superior bronchus (B6) arises just inferior to the orifice of the middle lobe bronchus, nearly opposite to it (▶ Fig. 2.11).

The anatomical distance from tracheal carina to the bifurcation of the left-sided bronchus is approximately 4 to 5 cm in length. It is a little shorter in women. The left main bronchus divides into the left upper and the left lower lobe bronchi (▶ Fig. 2.12). The common trunk of the left lower lobe is 1 cm longer than that of the right lower lobe (▶ Fig. 2.12).

The right main bronchus is about 1 mm larger than the left. The bronchus intermedius is approximately 1 mm less than the left main bronchus. The average diameter of the left main bronchus is 16.5 mm in men and 13 mm in women.[15] The average diameter of the right main bronchus is 17.5 mm in men and 14 mm in women. The average diameter of the bronchus intermedius is 15 mm in men and 12 mm in women. In both sexes, the mean diameter of the cricoid was shown to be the same as that of the left main bronchus.[15]

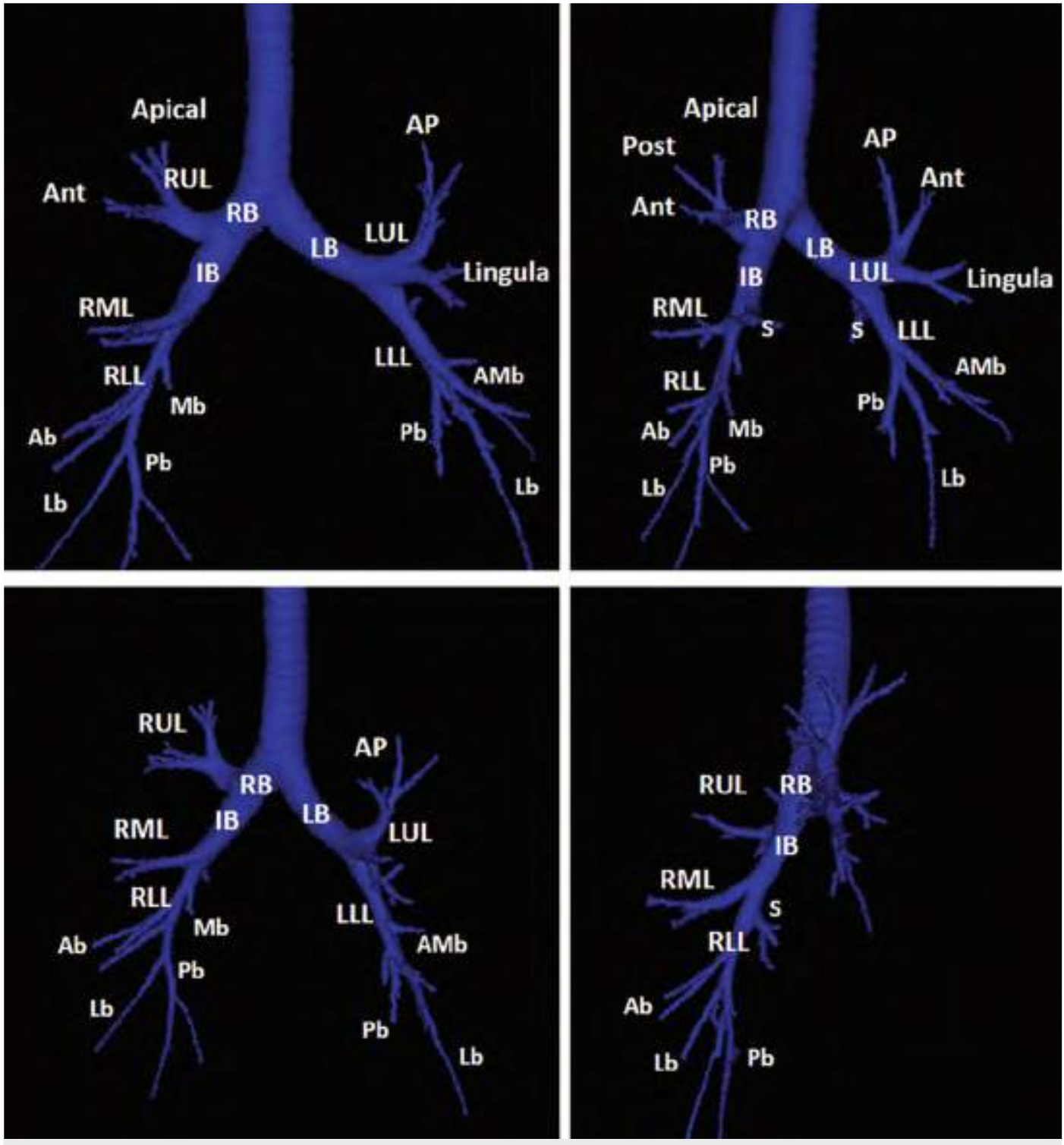

Fig. 2.11 The right mainstem bronchus (RB) lies in a more vertical orientation relative to the trachea, whereas the left mainstem bronchus (LB) lies in a more horizontal plane. The superior and inferior divisions (lingular bronchi) arise together from the left upper lobe (LUL) bronchus. The common trunk of the left lower lobe (LLL) is longer than that of the right lower lobe (RLL). The right upper lobe (RUL) bronchus arises, several centimeters above the right middle lobe (RML) bronchus. The intermediate bronchus (IB) is slightly narrower than the LB. The basal segments of the right lower lobes include the posterior (Pb), lateral (Lb), anterior (Ab), and medial (Mb) basal segments. The left lower lobe divides into a superior segment (S) and three basal segments namely the anteromedial basal (Amb), lateral basal (Lb), and posterior basal (Pb). AP, apicoposterior; S, superior segment.

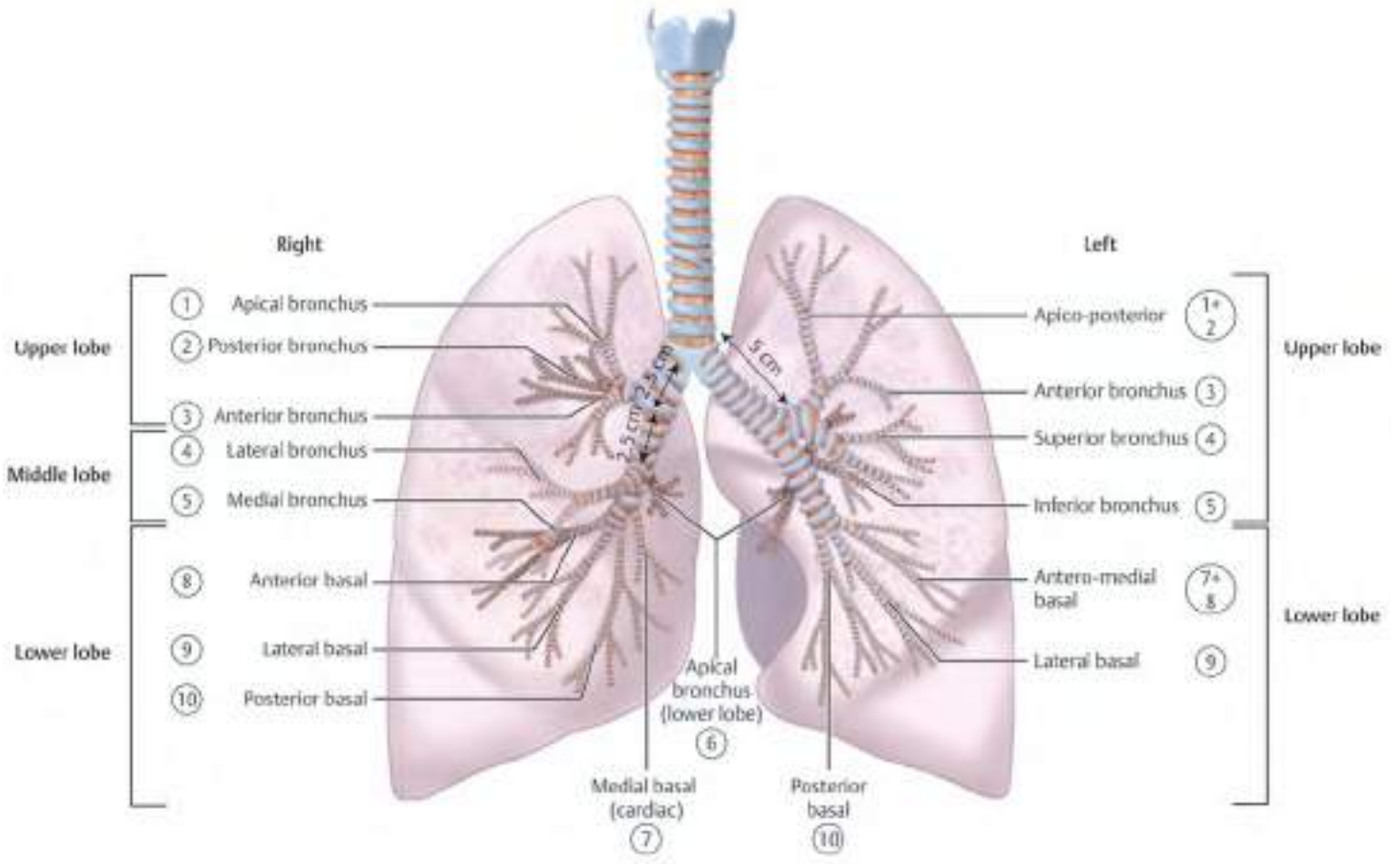

Fig. 2.12 Jackson–Huber classifications that describe and names the divisions in accordance with the anatomical space orientation. Right basal medial (B7) does not exist as seen in the right lower lobe. Instead, it is incorporated into the basal anteromedial (B8) branch. In the left upper lobe, apicoposterior is designated as B1 + 2. B4 and B5 refer to branches of the lingula and right middle lobe.

◆ Hilar Anatomy

The relationship of the bronchi to the pulmonary arteries differs between the lungs. The right upper lobe bronchus lies behind and beneath the right pulmonary artery, whereas the left main bronchus passes beneath the left pulmonary artery before it gives rise to the left upper bronchus.

The right upper lobe bronchus is called eparterial, since it arises above the superior margin of the right pulmonary artery. The right main bronchus is located below the azygos arc and posterior to the right pulmonary artery. The left upper lobe bronchus is said to be hyparterial, since it originates below the level of the left pulmonary artery (▶ Fig. 2.13, ▶ Fig. 2.14). As a matter of fact, in many cases, the left main bronchus is also hyparterial. There are two pulmonary veins in each hilum. The superior vein is located higher and anterior to the inferior vein. On the right side, both are located in the lower half of the hilum below the bronchus and pulmonary artery. On the left side, the left superior pulmonary vein is located anterior to the left bronchus and below the artery whereas the left inferior pulmonary vein is located below the left bronchus.

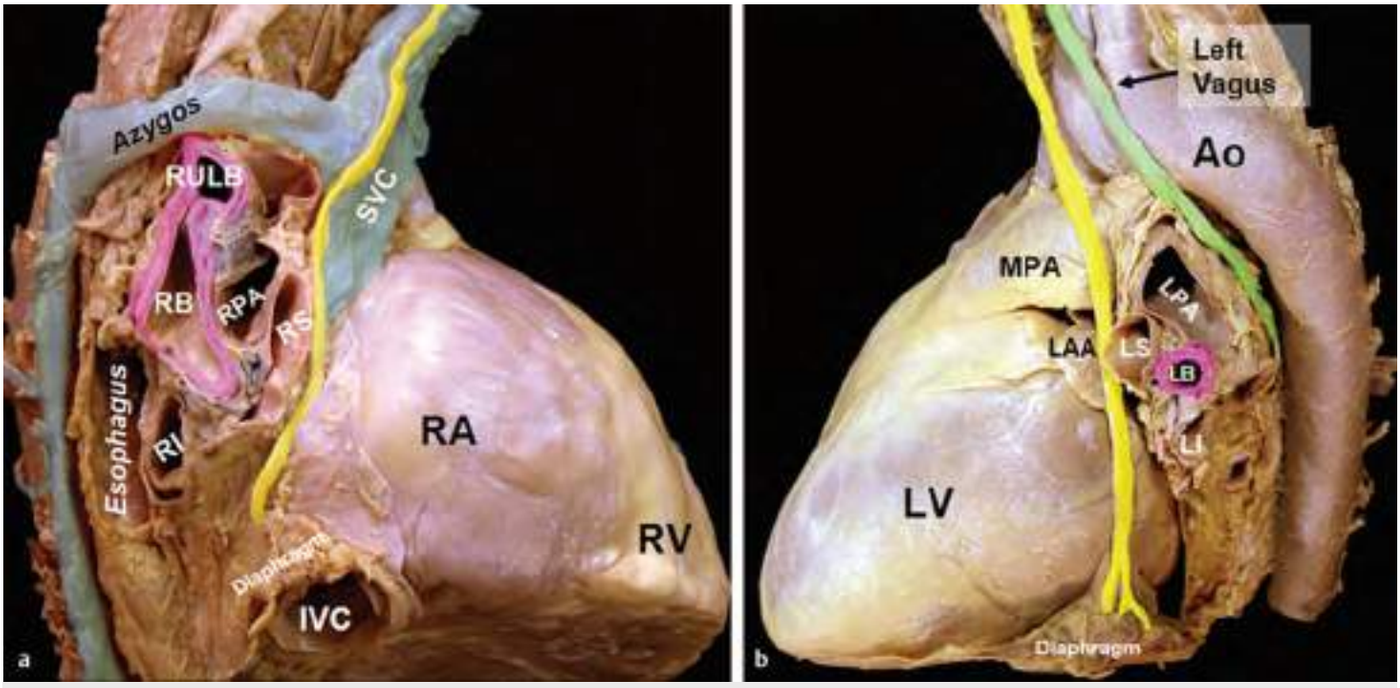

Fig. 2.13 Pulmonary hila. (**a**) Right hilar view. The right upper lobe bronchus (RULB) is called eparterial as it courses above the right pulmonary artery (RPA). (**b**) Left hilar view. The right bronchus (RB) is called hyparterial as it courses below the RPA. The right phrenic nerve (colored in yellow) is closely related to the superior cava vena (SVC), right superior pulmonary vein (RS), and the inferior vena cava (IVC). The left phrenic nerve moves anterior and lateral to the aortic arch (Ao), alongside the distal part of main pulmonary artery (MPA), left atrial appendage (LA), and the lateral wall of the left ventricle to penetrate the left part of the diaphragm. LB, left bronchus; LI, left inferior pulmonary vein; LPA, left pulmonary artery; LS, left superior pulmonary vein; LV, left ventricle; RA, right atrium; RB, right bronchus; RI, right inferior pulmonary vein; RPA, right pulmonary artery; RV, right ventricle.

◆ Segmental Bronchial Anatomy

Anatomical knowledge of the segmental bronchial branch patterns and their variants is very important for radiologists and pulmonologists in order to localize, diagnose, and even treat lesions.

Advanced endoscopic techniques as well as the possibility of virtual bronchoscopy using high-resolution CT images have opened new ways to study the bronchial system.[19,20,21] Multislice CT can cover the entire lung during a simple breath hold and create high-quality volumetric data allowing generation of superior multiplanar and volume-rendered images including specific techniques for airway imaging, such as virtual bronchography and virtual bronchoscopy[21] (▶ Fig. 2.15).

Three types of recognizable nomenclatures are used to classify the airway[22]. In radiology and thoracic surgery, Boyden's classification is commonly used to describe segmental bronchial anatomy.[23,24] The most commonly used by pulmonologists is the Jackson–Huber classification[25] (▶ Fig. 2.12). In these classifications, the segments and subsegments are classified in accordance with the anatomical space orientation (▶ Table 2.1). Segmental bronchi (B) are assigned a number from 1 to 10 (please see ▶ Fig. 2.29 at the end of the chapter). Another less popular system is the Yamashita Japanese classification.[26] The difference between these classifications is minimal. In endoscopists' classification, the anterior bronchi of the upper lobes are labeled B3 (B2 in Boyden's) and posterior bronchi of the upper lobes are labeled B2 (B3 in Boyden's).[2]

There are 10 segmental bronchi in the right lung and 8 to 10 in the left lung. The right bronchus divides into three lobar bronchi and the left main bronchus divides into two lobar bronchi (▶ Fig. 2.15). The first branch of the right bronchus is the right upper lobe bronchus arising 1 to 2.5 cm below the carina and courses laterally for a distance of 1 to 2 cm before trifurcating into the apical, anterior, and posterior segments. This is the only

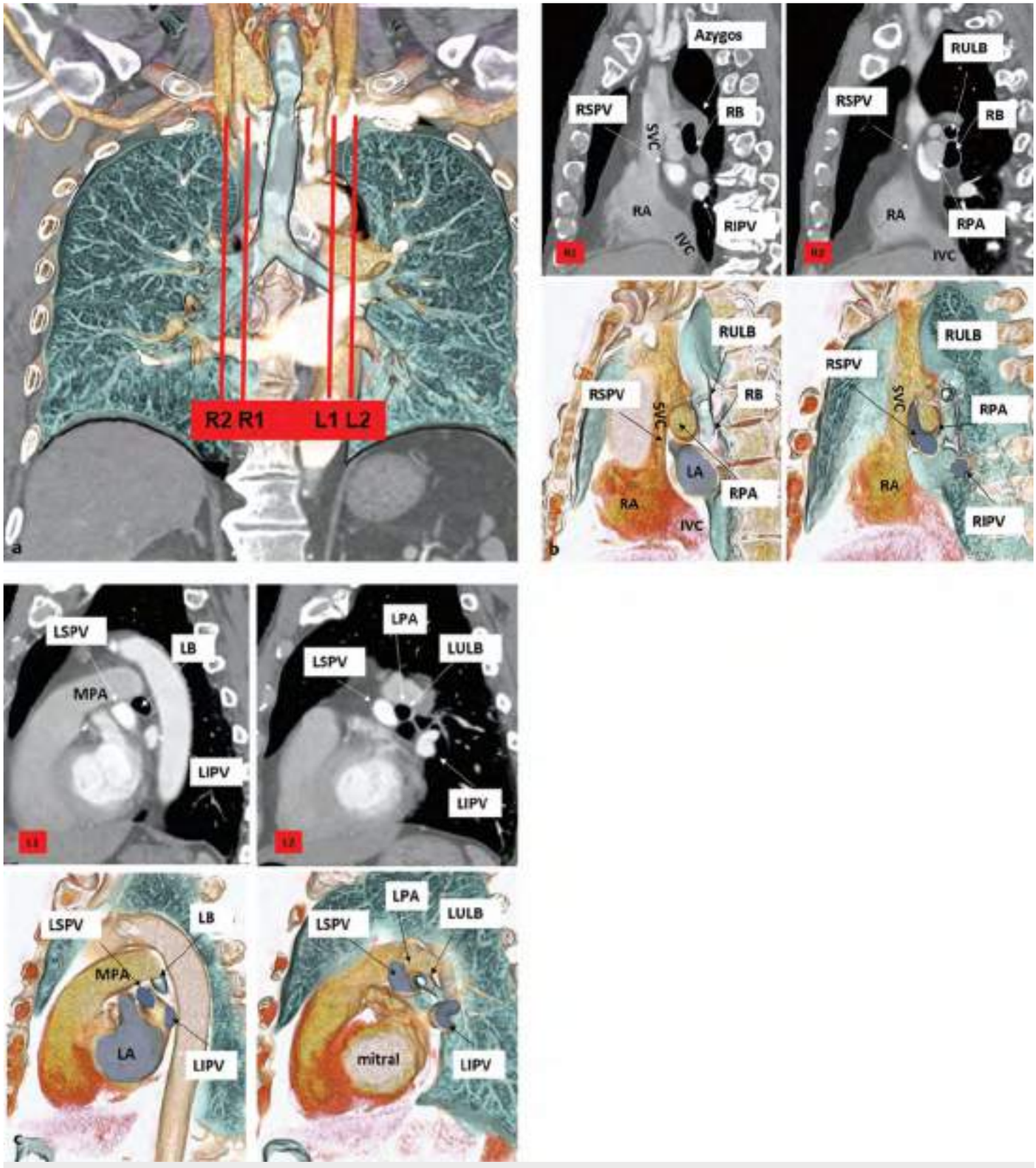

Fig. 2.14 (a–c) Hilar anatomy is shown on sagittal images. The right upper lobe bronchus (RULB) is called eparterial, since it arises above the superior margin of the right pulmonary artery (RPA). The right main bronchus (RB) is located below the azygos arc and posterior to the RPA. The left upper lobe bronchus (LULB) is said to be hyparterial, since it originates below the level the left pulmonary artery (LPA). As a matter of fact in many cases the left main bronchus is also hyparterial. There are two pulmonary veins (PVs) in each hilum. The superior vein is located higher and anterior to the inferior vein. On the right side both are located below in the lower half of the hilum inferior to the bronchus and pulmonary artery. On the left side, the left superior PV (LSPV) is located anterior to the left bronchus and below the artery whereas the left inferior PV (LIPV) is located below the left bronchus. IVC, inferior vena cava; L, left; LA, left atrium; MPA, main pulmonary artery; R, right; RA, right atrium; RIPV, right inferior pulmonary vein; RSPV, right superior pulmonary vein; SVC, superior vena cava.

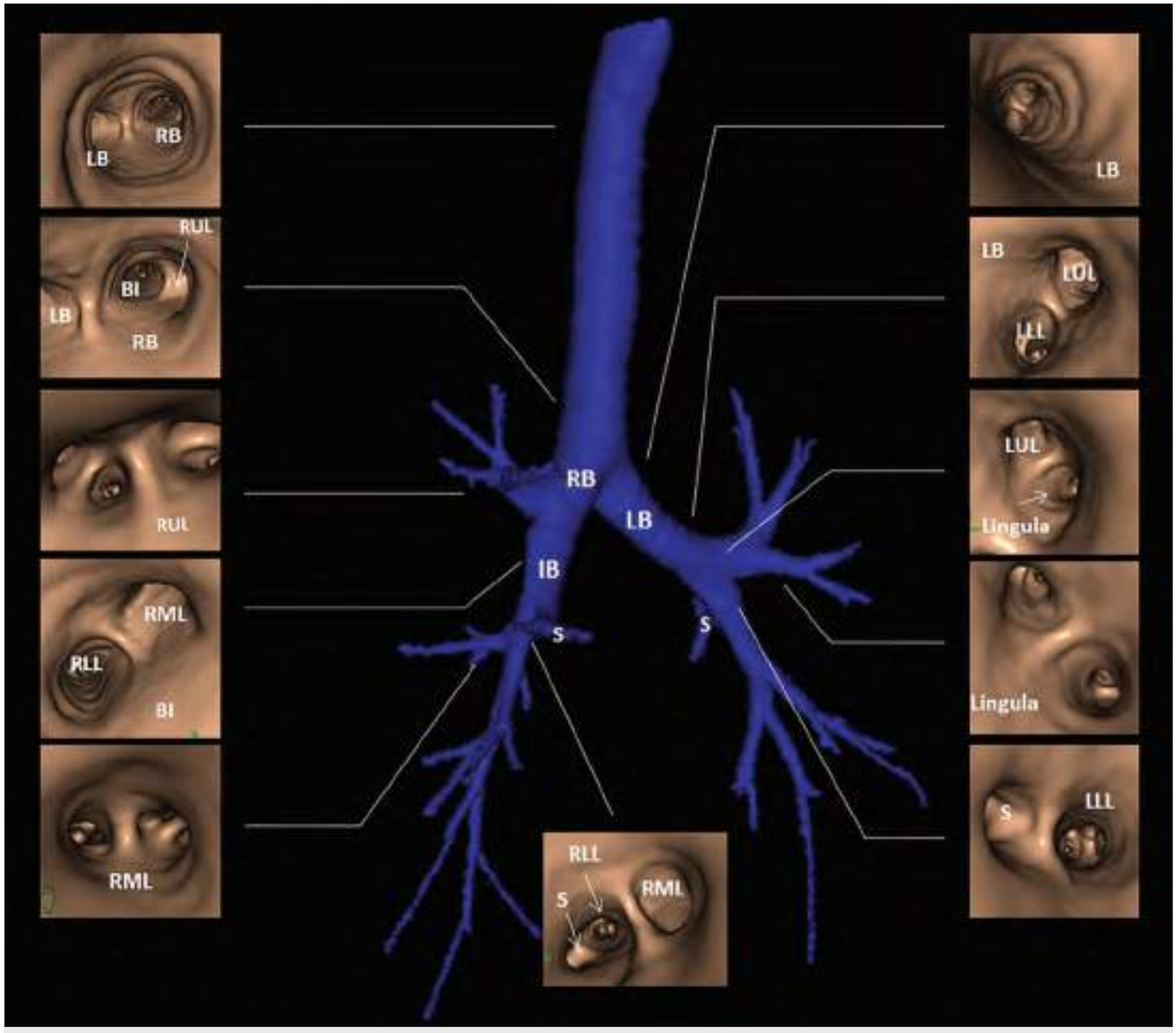

Fig. 2.15 Virtual bronchography and virtual bronchoscopy reconstructed from 1 mm CT images. The right mainstem bronchus (RB) lies in a more vertical orientation whereas the left mainstem bronchus (LB) lies in a more horizontal plane. LUL, left upper lobe bronchus; LLL, left lower lobe; RLL, right lower lobe; RUL, right upper lobe; RML, right middle lobe bronchus; IB, intermediate bronchus; S, superior segment.

bronchus in the tracheobronchial tree that has three orifices.[25] The orifice of the right upper lobe is a very important landmark to identify while performing fiberoptic bronchoscopy in order to distinguish the right from the left mainstem bronchus. The apical segment divides into the anterior and apical subsegments. The posterior segment moves posteriorly and divides into the anterior and lateral subsegments. The anterior segment divides into the anterior and lateral subsegments.

After the origin of the right upper bronchus, the right bronchus is called the intermediate bronchus (bronchus intermedius). It measures 2 to 2.5 cm in length and then splits into the middle lobe bronchus and the lower lobe bronchus. The intermediate bronchus can easily be identified in CT images. It runs posterior to the right pulmonary artery and inferior and medial to the right interlobar artery.

The right middle lobe and the superior (apical) segment of the right lower lobe arise approximately at same level. It has the shape of a letter D intraluminally. The right middle lobe emerges anterolaterally with a 1 to 2 cm length before it divides into the medial and lateral segments. These two segmental branches move in the X–Y plane and hard to differentiate on posteroanterior chest radiograph. The lateral segmental bronchus is visualized over a greater distance. The right lower lobe divides into one superior segment and four basal segments. The superior segment delimits the posterior end of the bronchus intermedius. It divides into the medial, superior, and lateral subsegments. The basal segments of the right lower lobes include the posterior, lateral, anterior, and medial subsegments (▶ Fig. 2.12).

The left main bronchus divides into the upper and lower lobar branches. The left upper lobe bronchus has a superior and an

Table 2.1 Segmental and subsegmental bronchus

Right		Left	
Segmental	**Subsegmental**	**Segmental**	**Subsegmental**
Upper lobe		Upper lobe	
B1, apical	B1a, apical	B1 + 2, apicoposterior	B1 + 2a, apical
	B1b, anterior		B1 + 2b, posterior
B2, posterior	B2a, posterior		B1 + 2c, lateral
	B2b, lateral		
B3, anterior	B3a, lateral	B3, anterior	B3a, lateral
	B3b, anterior		B3b, anterior
			B3c, superior
Middle lobe			
B4, lateral	B4a, superior	B4, superior lingula	B4a, lateral
	B4b, lateral		B4b, medial
B5, medial	B5a, superior	B5, inferior lingula	B5a, superior
	B5b, inferior		B5b, inferior
Lower lobe		**Lower lobe**	
B6, apical	B6a, superior	B6, apical	B6a, superior
	B6b, lateral		B6b, lateral
	B6c, medial		B6c, medial
B7, medial	B7a, posterior	B7, medial	
	B7b, anterior		
B8, anterior	B8a, lateral	B8, anterior	B8a, lateral
	B8b, basal		B8b, basal
B9, lateral	B9a, lateral	B9, lateral	B9a, lateral
	B9b, basal		B9b, basal
B10, posterior	B10a, posterior	B10, posterior	B10a, posterior
	B10b, lateral		B10b, lateral
	B10c, basal		B10c, basal

inferior (lingular) division (▶ Fig. 2.15). The superior division divides into the apicoposterior and anterior segments. The apicoposterior bronchus may be single or divide into the apical and the posterior segments. The anterior segment defines of the inferior border of the left upper lobe. The lingular branch extends 2 to 3 cm downward in an inferolateral direction before dividing into the superior and inferior segments. The left lower lobe divides into a superior segment and three basal segments namely the anteromedial basal, lateral basal, and posterior basal. The anterior basal and medial basal are collectively called anteromedial basal segment. Isolated medial basal segment may be present in one-third of the population.

Characteristics of Small Airways

In contrast to the main bronchi, the hyaline cartilage in the wall of the secondary (segmental) and tertiary (subsegmental) bronchi is patchy and these airways contain more smooth muscles and their mucosa is lined with pseudostratified ciliated columnar cells containing mucus-secreting glands (▶ Fig. 2.16). The tertiary bronchi subdivide into the bronchioles and at the level of the secondary lobules where the terminal bronchioles are located intramural cartilage is absent. The terminal bronchioles (final section of the conducting airway) are lined with simple cuboidal epithelium containing club cells but without goblet cells. The diameter of bronchioles is approximately 0.3 to 2 mm. The respiratory bronchioles are divisions of the terminal bronchioles and connect with the alveolar ducts and sacs that are responsible for gas exchange. Small airways of less than 2 mm in diameter are low resistance and normally contribute about 10% of the total resistance to flow.[26] Obstruction of these small tubes may remain asymptomatic because air can enter the air spaces beyond the occluded airways via collateral channels. Another important difference between large and small airways is that the total cross-sectional area of small airways can be several orders of magnitude greater than the total cross-sectional area of the large airways. Presence of a

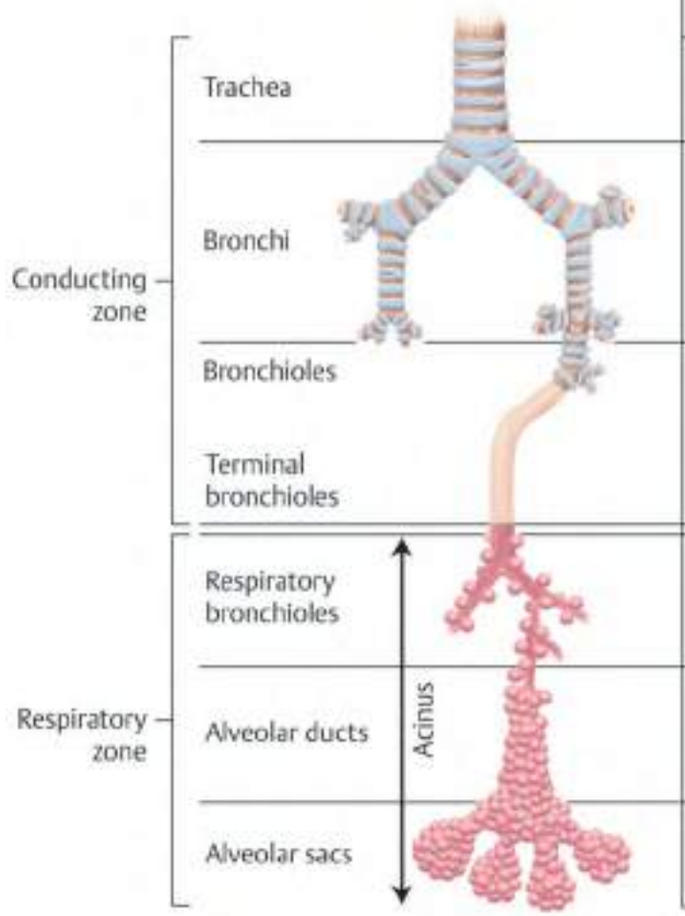

	Number	Cilia	Smooth muscle	Cartilage	Generation
Trachea	1	Yes	Yes	Yes	0
Bronchi	2 4 8	Yes	Yes	Patchy	1 2 3
Bronchioles Terminal bronchioles	–	Yes	Yes	No	4 ↓ 16
Respiratory bronchioles	–	Some	Some	No	17 18 19
Alveolar ducts	–	No	Some	No	20 21 22
Alveolar sacs	6×10^8	No	No	No	23

Fig. 2.16 Classification of the branching pattern of the bronchial tree.

surfactant with a low surface tension in small airway protects them from closing at low lung volumes.

Bronchial Vascular Anatomy

The bronchial circulation normally consumes less than 1% of the cardiac output. Almost 90% of vascular supply to the carina and main bronchi is provided by the bronchial arteries. Distally, they provide vascular supply to the lobar and segmental bronchi.[27,28,29,30] The bronchial arteries also provide systemic blood supply to the trachea, esophagus, visceral pleura, pulmonary veins, and thoracic lymph nodes.

There are usually three bronchial arteries, two on the left side and one on the right side (▶ Fig. 2.17). In rare occasion up to five bronchial arteries may be seen. The bronchial arteries arise from the medial aspect (or rarely lateral) of the descending thoracic aorta between the upper border of T5 and the lower border of T6 in 90% of cases or from intercostal arteries located 2 to 3 cm distal to the origin of the left subclavian artery.[31] The origin of the bronchial arteries can easily be localized with CT angiography. Angiographic landmark of the bronchial arteries' origin is 1 cm above or below the level of the left main bronchus as it crosses the descending thoracic aorta[28] (▶ Fig. 2.18).

The right bronchial artery occasionally originates directly from the aorta but in 60% originates as a common trunk with an intercostal artery. An accessory right bronchial artery is seen in 7% of cases.[31] Occasionally, the right bronchial artery has a conical triangular infundibulum at its origin that should not be mistaken with aneurysm.[30] Common trunk of the left and right bronchial arteries is also common and may be seen in 30% of cases (▶ Fig. 2.18**a**). Occasionally, the blood supply to the bronchial system is provided from unusual sites such as the inferior aortic arch, distal descending thoracic aorta, subclavian artery, internal mammary artery, and even a coronary artery[30,32] (▶ Fig. 2.19).

The bronchial veins anastomose with each other to form a dual venous plexus in the bronchial wall; the subepithelial plexus and the adventital plexus that are interconnected by short venous radicles. About 80% of the venous drainage from the bronchial arterial system empties into the pulmonary veins through the bronchopulmonary anastomoses although some of it may empty into the azygos and accessory hemiazygos system or the left superior intercostals vein. Since the bronchial veins communicates with the pulmonary venous system, systemic venous hypertension not only causes interstitial edema, but it may augment airway edema due to obstruction of bronchial veins. Bronchial lymphatic drain in to the subcarinal and low paratracheal nodes.

The bronchial microvasculature provides nutrient blood flow to the airway epithelium and is important for proper mucociliary

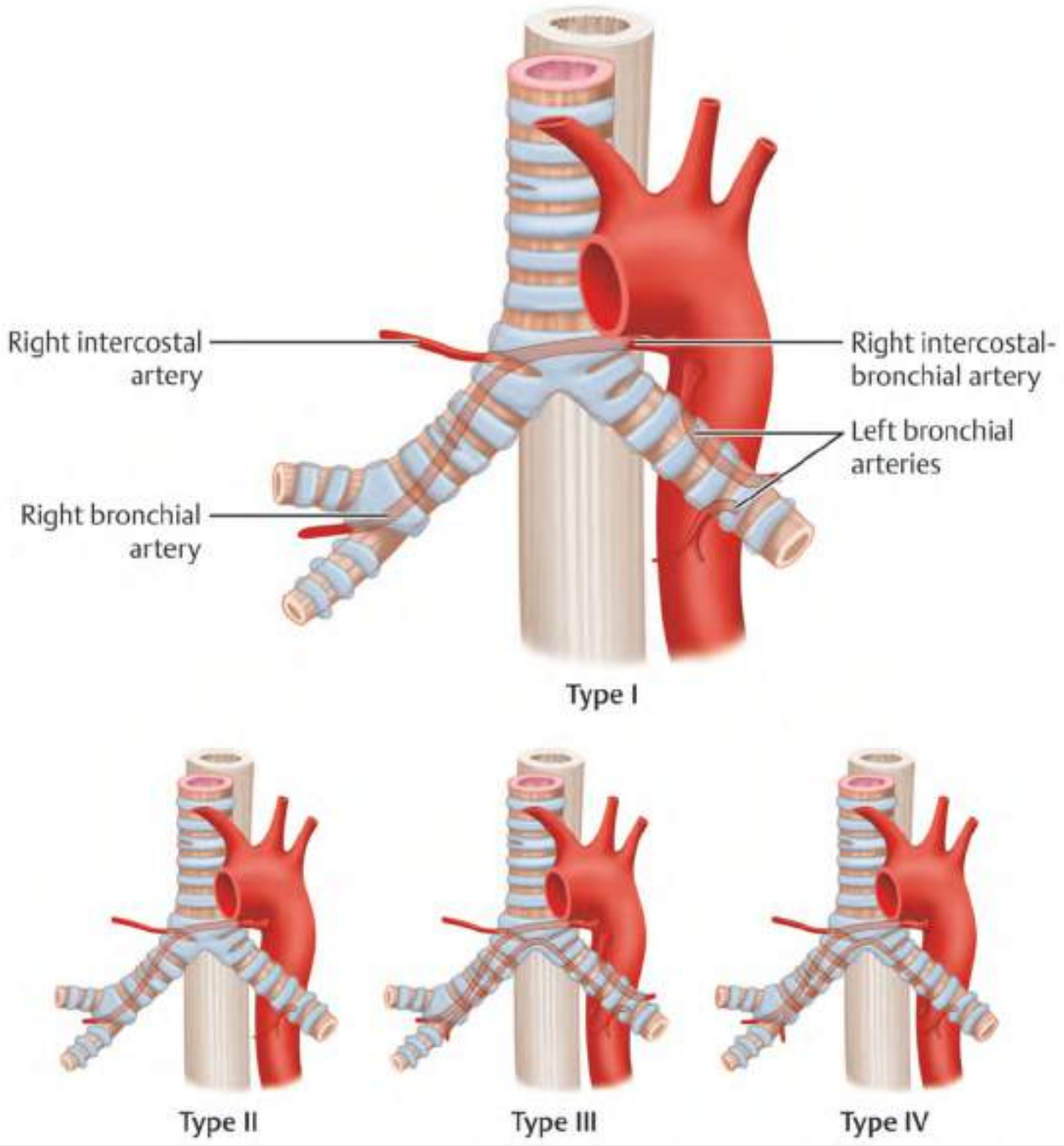

Fig. 2.17 Drawing shows the four most common variations in bronchial artery anatomy. Type 1 has one right bronchial artery and two left bronchial arteries (40%); type 2 has one right bronchial artery and one left bronchial artery (20%); and type 3 has two right bronchial arteries and two left bronchial arteries (20%). Adapted from Walker et al 2015.[29]

function. Normal bronchial circulation in important for healing of bronchial anastomosis and probably reduces the incidence of bronchial dehiscence (i.e., after lung transplantation).[33] After hypertrophy, such as occurs in chronic lung (i.e., cystic fibrosis) and heart (i.e., tetralogy of Fallot) diseases, the bronchial vasculature can contribute substantially to gas exchange.

Congestion of the bronchial vasculature may narrow the airway lumen in inflammatory airway diseases, and formation of new bronchial vessels (angiogenesis) is implicated in the pathology of a variety of chronic inflammatory, infectious, and ischemic pulmonary diseases.[34] Abnormal bronchial arteries are usually large (> 2 mm in diameter), undergo smooth muscle wall hypertrophy, and often have a tortuous mediastinal course. Enlargement of the bronchial arteries is a common finding in ischemic lung tissue in patients with systemic hypoxemia, alveolar hypoxia, chronic pulmonary infarction, and various inflammatory disorders such as

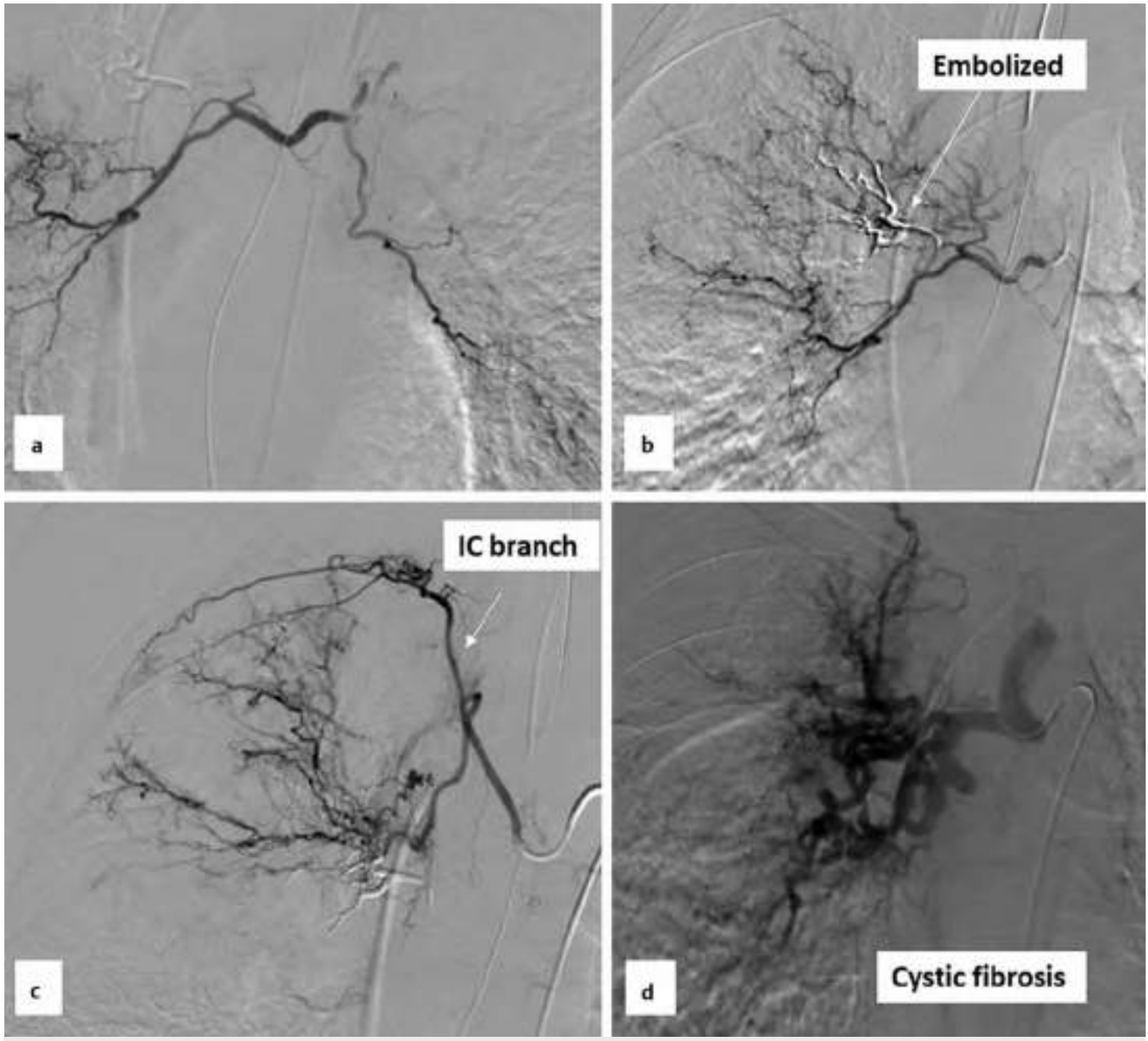

Fig. 2.18 Bronchial arteries shown by selective catheter angiogram. **(a)** Common right and left trunk. **(b)** Single right trunk in a patient with recurrent hemoptysis. Note mildly enlarged tortuous vessels. Some vessels were embolized to prevent hemoptysis. **(c)** Common right intercostobronchial trunk. IC, intercostal branch. **(d)** Very large right bronchial artery due to chronic bronchitis in a patient with cystic fibrosis.

tuberculosis and cystic fibrosis (▶ Fig. 2.18, ▶ Fig. 2.19). In chronic pulmonary tuberculosis, tortuosity, hypertrophy, and proliferation of the bronchial arteries supplying diseased lung can cause recurrent hemoptysis that in severe cases demands rapid percutaneous catheter embolization to prevent asphyxiation and death.

Occlusion of a pulmonary artery to one lung stimulates angiogenesis in the bronchial circulatory of that lung to prevent infarction.[34] In congenital absence of one pulmonary artery (atresia, tetralogy of Fallot), the bronchial blood flows as high as 25% of the cardiac output has been reported.[35] An example of enlarged left bronchial artery in patient with agenesis of pulmonary artery is shown (▶ Fig. 2.19).

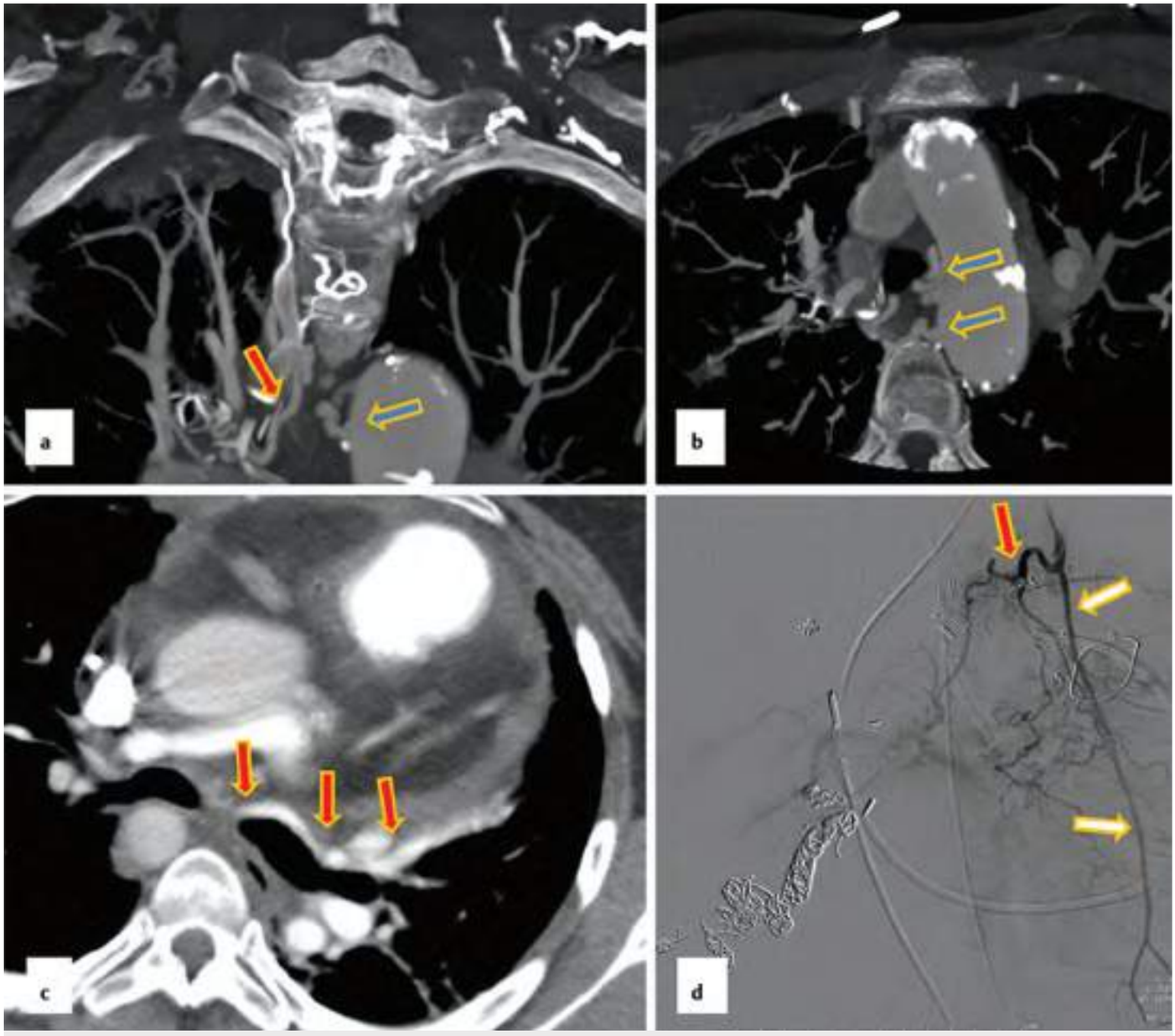

Fig. 2.19 **(a)** Coronal and **(b)** axial CT images showing enlarged bronchial arteries (*red arrow*) arising from medial margin of the aortic arch (*blue arrows*). **(c)** Axial CT and (**d**) angiogram in a patient with atresia of the pulmonary artery showing enlarged left bronchial (*red arrows*) artery. Ectopic origin of one of left bronchial artery (*red arrow*) from the internal mammary artery (*white arrows*) is seen.

◆ Main Anatomical Variations and Malformation

Variation in the distribution pattern and location of the segmental bronchial subdivisions is common (▶ Table 2.2). For example, the typical trifurcation of the right upper lobe bronchus is seen in only 30 to 50% of the population and in many cases it appears bifurcated. On the contrary, abnormal bronchi originating from the trachea or main bronchi are rare. Most tracheobronchial anomalies are isolated and discovered incidentally. However, incidence of the tracheobronchial anomalies is higher in congenital diseases.[36] For example, tracheal bronchus is seen more frequently in children with congenital heart disease. Most of tracheobronchial anomalies are either displaced or supernumerary bronchi. A supernumerary bronchus may be blind ending or connect to the lung parenchyma. Congenital absence may involve a lung, a lobe, or a segment.

As explained earlier in this chapter, in situs solitus the right upper lobe bronchus is in an eparterial position and the left upper lobe bronchus is in a hyparterial position (▶ Fig. 2.20). This relationship will be inverted in situs inversus. Other rare variants include right bronchial isomerism in asplenia syndrome and left bronchial isomerism in polysplenia syndrome[8] (▶ Fig. 2.21).

Table 2.2 Normal findings and most common bronchial variants in 30 healthy patients

Level	Right lung	Rate (%)	Left lung	Rate (%)
Right upper lobe or culmen	Trifurcation B1, B2, B3	30	Bifurcation into culmen and lingual	83
	Bifurcation B1 + 2, B3	26	Trifurcation B1 + 3, B2, B4 + 5	17
	Bifurcation B1 + 3, B2	16	Bifurcation B1 + 3, B2, B4 + 5	Rare
	Bifurcation B2 + 3, B1	6	Level of origin of B1 + 3a, B1 + 3b	Variable
	Bifurcation B2 + 1b, B3 + 1a	22	B1 + 3c	
Middle lobe or lingua	Bifurcation B4, B5	100	Lateral B4 and medial B5	25
	Horizontal type	77		
	Superoinferior type	23		
Lower lobe	Bifurcation B6a + b, B6c	> 60	Bifurcation B6a, B6b + c	45
	Superposition B6 + b, B6c	5	B* visible	26
	B* visible	56	Bifurcation B7 + 8, B9 + 10	76
	B7 => B7a + b	90	True B7 separated from B8	14
	Boyden's types I, II	73	Trifurcation B7 + 8, B9, B10	10
	Boyden's type III	17		
	B8 => B7a, B10 => B7b	10		
	Bifurcation B8, B9 + 10	68		
	Bifurcation B8 + 9, B10	13		
	Bifurcation B7 + 8, B9 + 10	3		
	Trifurcation B8, B9 + 10	10		
	Quadrification B7, B8, B9, B10	6		

Source: Adapted from Evans JA. Aberrant bronchi and cardiac vascular anomalies. Am J Med Genet 1990;35:46–54.

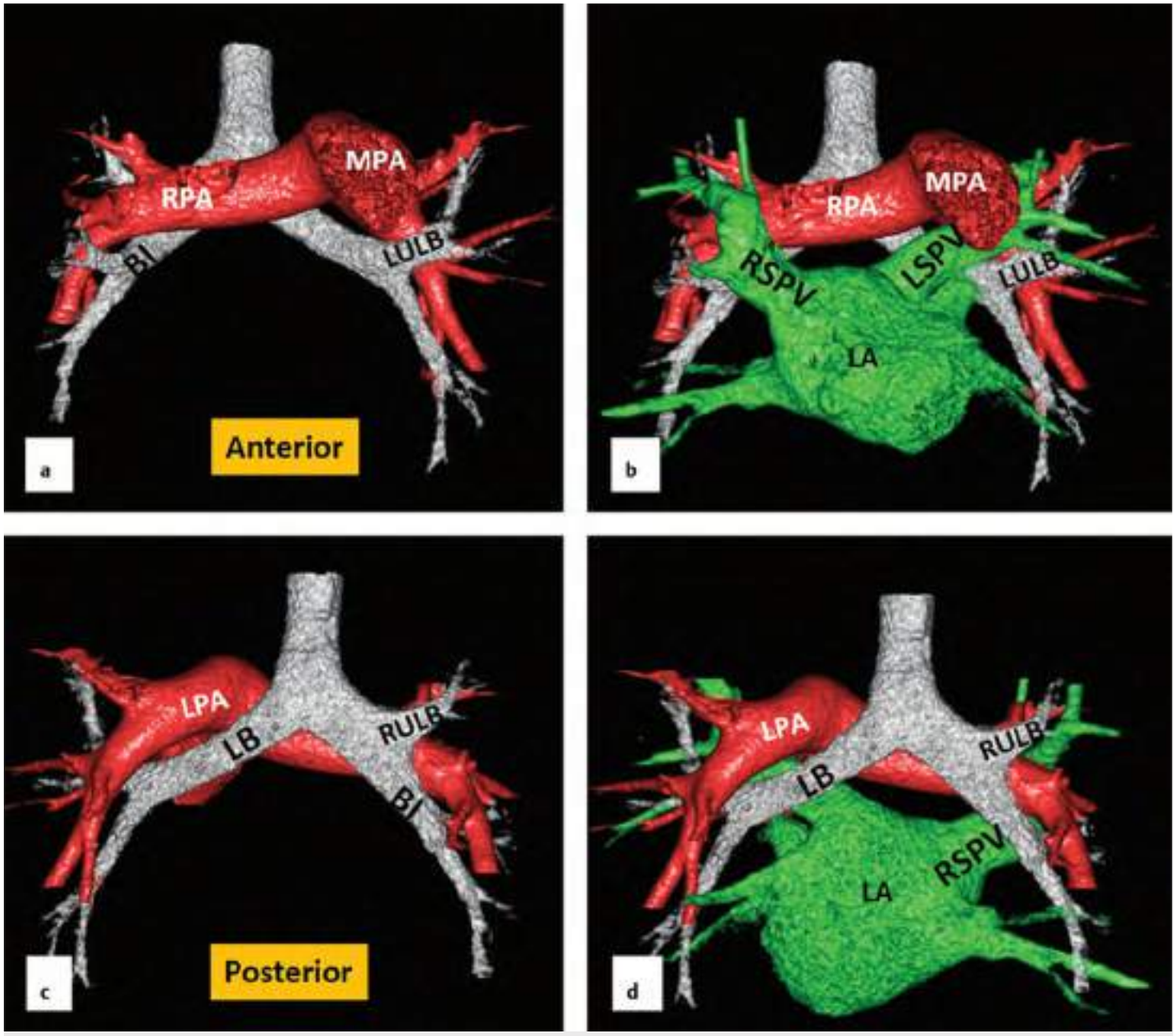

Fig. 2.20 Normal relationship of the right and left mainstem bronchi with pulmonary arteries and pulmonary veins. Anterior **(a,b)** and posterior **(c,d)** views are presented. The right upper lobe bronchus (RULB) is in an eparterial position and the left upper lobe bronchus (LULB) is in a hyparterial position. This relationship will be inverted in situs inversus. BI, bronchus intermedius; LA, left atrium; LB, left bronchus; LPA, left pulmonary artery; LSPV, left superior pulmonary vein; MPA, main pulmonary artery; RSPV, right superior pulmonary vein.

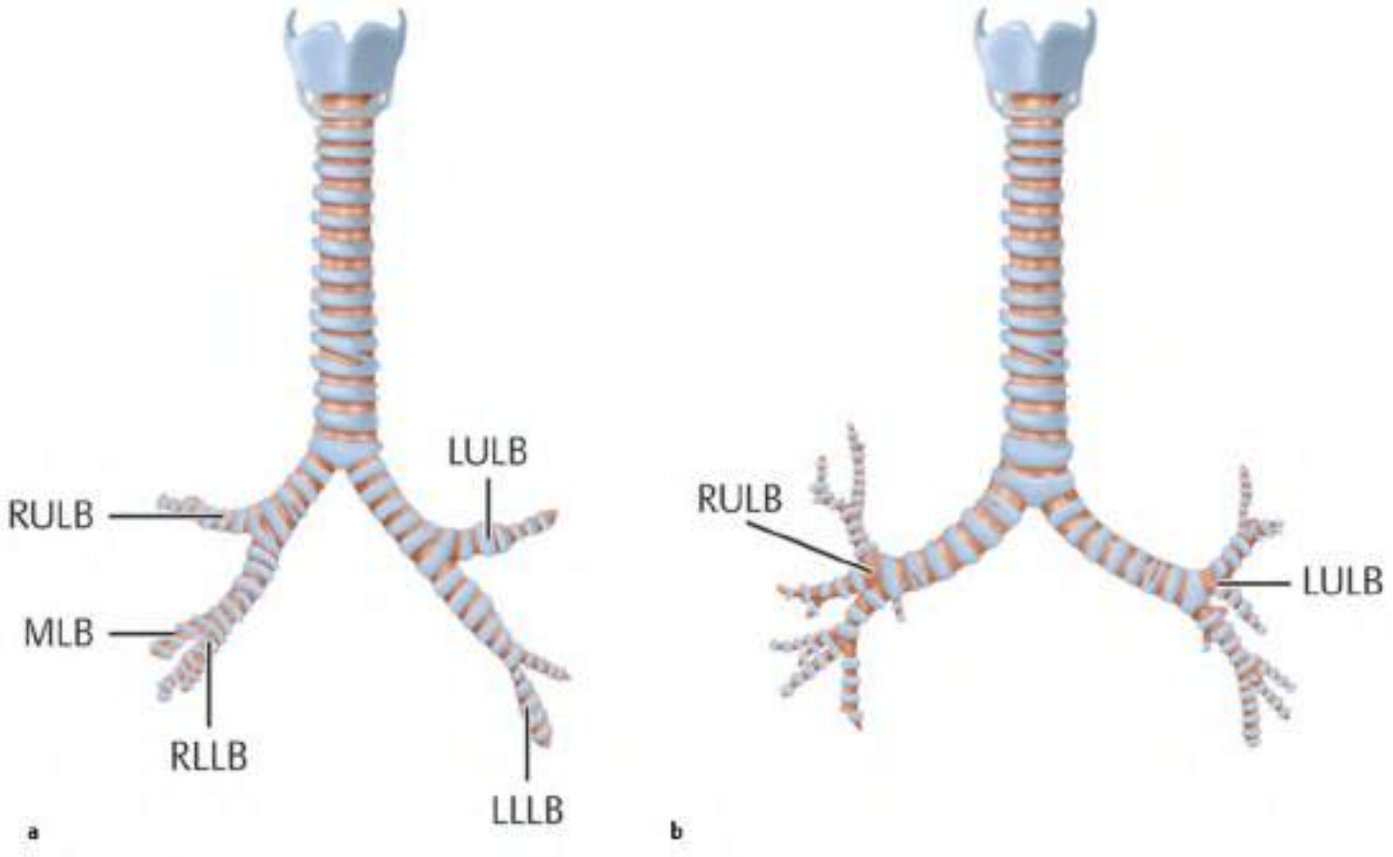

Fig. 2.21 **(a)** Right bronchial isomerism. **(b)** Left bronchial isomerism.

Blind-ended bronchi are called bronchial diverticula. This congenital finding should not be confused with acquired bronchial outpouching commonly seen in COPD. A common outpouching is seen at the thoracic inlet arising from the right side of trachea (▶ Fig. 2.22**a**). In 0.25 to 3% of general population, there is an abnormal takeoff of the right upper lobe bronchus from the right tracheal wall above the carina. This benign anomaly is called tracheal bronchus and appears to be more common in men (▶ Fig. 2.22**b**). Anomalous bronchi arising from the intermediate bronchus, left side of trachea, or left bronchus are also reported using different terminologies.[37] For example, those arising from the left bronchus are called left eparterial or prehyparterial bronchi (▶ Fig. 2.23).

Rarely the right upper lobe bronchus originates directly from the trachea. In high-riding right middle lobe bronchus, it arises at the level of the right upper lobe bronchus or together form a common trunk. In the later, its appearance is similar to that of normal left bronchus anatomy. However, the right upper lobe bronchus remains eparterial, a finding that differentiates it from left bronchial isomerism.

Superior displacement of superior subsegmental bronchus (B6a) of the superior segment of the lower lobe (B6a) is rarely

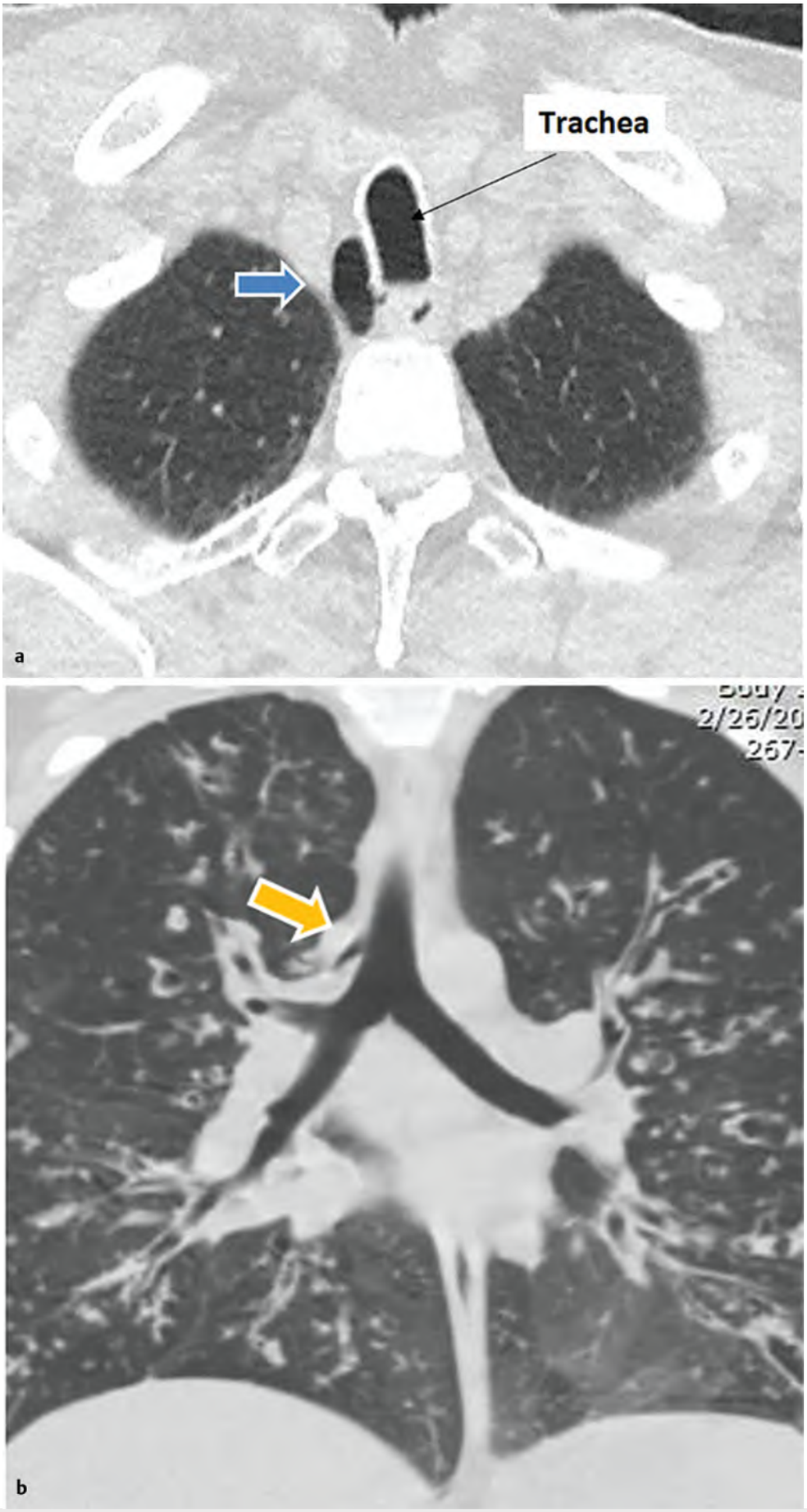

Fig. 2.22 **(a)** Axial CT shows a diverticular structure (*blue arrow*) arising from the right margin of the trachea at thoracic inlet. **(b)** Small tracheal bronchus (*yellow arrow*) arising from the right margin of the trachea above the right main bronchus. Note extensive bilateral bronchiectasis in this patient with cystic fibrosis.

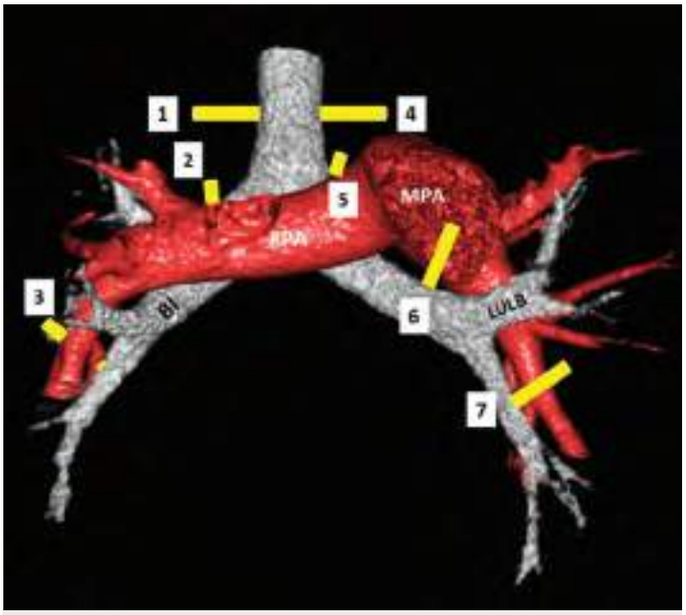

Fig. 2.23 Aberrant bronchi are shown: 1. Right tracheal bronchus; 2. preeparterial; 3. posteparterial; 4. left tracheal; 5. left eparterial; 6. prehyparterial; and 7. posthyparterial. BI, bronchus intermedius; LULB, left upper lobe bronchus; MPA, main pulmonary artery; RPA, right pulmonary artery.

seen arising from the main bronchus or the intermediate bronchus (suprasuperior bronchus). It should be differentiated from a very common variant called subsuperior bronchus (B*) which arises posteriorly below the level of the superior segment of the lower lobe.[9]

An accessory cardiac bronchus is a rare blind-end supernumerary bronchus (0.08%) arising from the medial wall of the right main bronchus or intermediate bronchus opposite to the origin of the right upper lobe bronchus. It is usually asymptomatic. Rarely, cardiac bronchus is seen on the left side (▶ Fig. 2.24**a**). Presence of bronchial mucosa and cartilage in histology distinguishes it from a diverticulum. Enhancing tissue mass due to vestigial or rudimentary lung parenchyma is seen in 35.7 to 50% of cardiac bronchus.[9] Another very rare bronchial anomaly is called bridging bronchus (▶ Fig. 2.24**b**). It is an aberrant bronchus from the left bronchus that crosses the midline to partially or totally supply the right lung.[8,15]

◆ Complementary Role of CT and Fiberoptic Bronchoscopy

Flexible fiberoptic bronchoscopy is a diagnostic and therapeutic procedure of great value in the clinical practice to visualize the airway and its pathological alterations.[38] Aside from diagnosis, bronchoscopy enables complementary procedures such as biopsies, stent and valve placement, or laser bronchial surgery. Technical advancement has increased the ability of the interventional pulmonologist to access more distal parts of the bronchial tree and implement new techniques. At the same time, rapid evolution of CT technology and postprocessing techniques such as virtual bronchoscopy have increased the accuracy of depicting normal and pathological details of the respiratory system[39] (▶ Fig. 2.15). Using CT images for guidance, bronchoscopic sampling of lesions located deeper within the lung has become easier. Using CT images, localization of the peribronchial lymph nodes for transbronchial needle aspiration and biopsy has improved. Nodal biopsy is primarily used to exclude malignant involvement of the mediastinal and hilar lymph nodes during lung cancer staging[40] (▶ Fig. 2.25). In addition to CT, availability of real-time endobronchial ultrasound has further increased the yield in transbronchial needle samplings.

Dynamic Airway Evaluation

On expiration, positive pleural pressure causes the posterior tracheal membrane to bulge into the tracheal lumen.[41,42] In healthy individuals, the degree of forward prolapse of the posterior tracheal wall is limited by the resistive tension of the posterior tracheal membrane and by smooth muscle contraction (▶ Fig. 2.9). Less than 50% tracheal luminal expiratory reduction has historically been considered physiological and called "benign dynamic airway collapse." Tracheomalacia, tracheobronchomalacia, and excessive dynamic airway collapse are three terminologies used to describe pathological tracheal narrowing in expiration. The first two describe luminal reduction from cartilage softening and the third refers to luminal reduction from exaggerated posterior tracheal membrane movement[43,44,45] (▶ Fig. 2.26).

Expiratory tracheal narrowing is a frequent occurrence that can cause symptoms of airway obstruction, such as dyspnea, wheeze, and exercise intolerance. The reference standard for diagnosis has traditionally been bronchoscopy; however, this method has significant limitations. Expiratory tracheal disorders can readily be detected by dynamic volume multidetector computed tomography (MDCT), a noninvasive method that will potentially enable detection and quantification of these conditions[46] (▶ Fig. 2.26).

◆ Pathology

Diseases of the airways can cause luminal narrowing (stenosis) or luminal widening (bronchiectasis). A late complication of many chronic inflammatory processes and infections of the airway is bronchial wall destruction and secondary bronchiectasis[47] (▶ Fig. 2.22**b**).

Short-segment luminal narrowing most commonly is caused by intrinsic or extrinsic neoplasms or by benign stricture usually following tracheostomy or endotracheal intubation. Focal stenosis is common after segmental resections or end–end anastomosis after lung transplantation (▶ Fig. 2.27). Treatment of benign stricture with transluminal stent placement is a common practice.

Primary tumors of the trachea and main bronchi are rare and usually malignant caused by squamous cell carcinoma and adenoid cystic carcinoma.[48] Right middle lobe syndrome is seen as recurrent infectious episodes due to postobstructive atelectasis from external compression of right middle lobe orifice by lymph nodes.

Narrowing of the airway beyond a length of 3 cm is considered long-segment narrowing. Many of the inflammatory, infiltrative, and infectious diseases of the airway cause long-segment narrowing. Tracheobronchomalacia is another cause of diffuse narrowing the trachea and main bronchi (▶ Fig. 2.26). In adults,

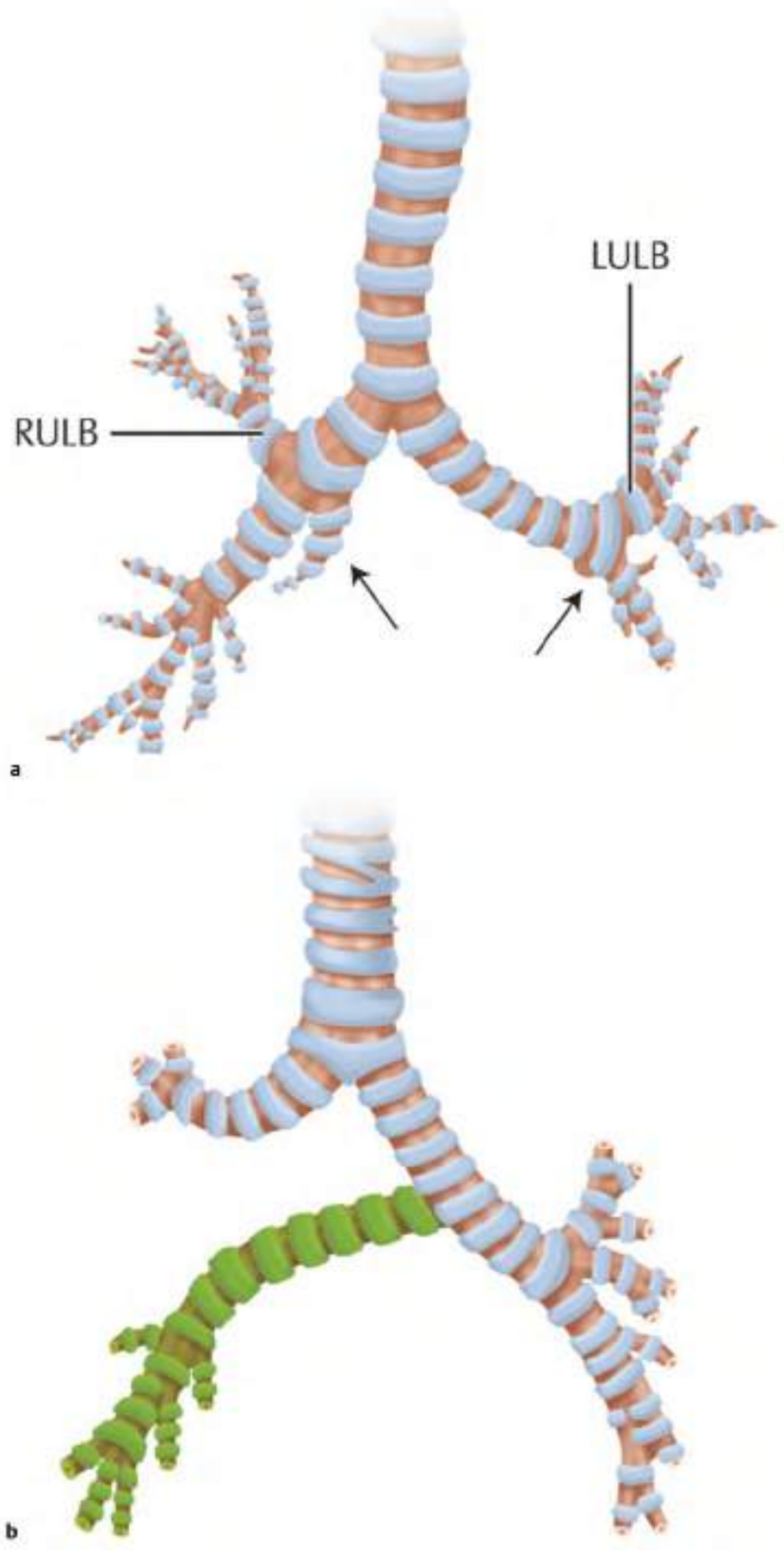

Fig. 2.24 **(a)** Bilateral cardiac bronchus (*arrows*). Cardiac bronchus is the only bronchus originating from the medial wall of either the right bronchus or the intermediate bronchus. LULB, left upper lobe bronchus; RULB, right upper lobe bronchus. **(b)** Bridging bronchus.

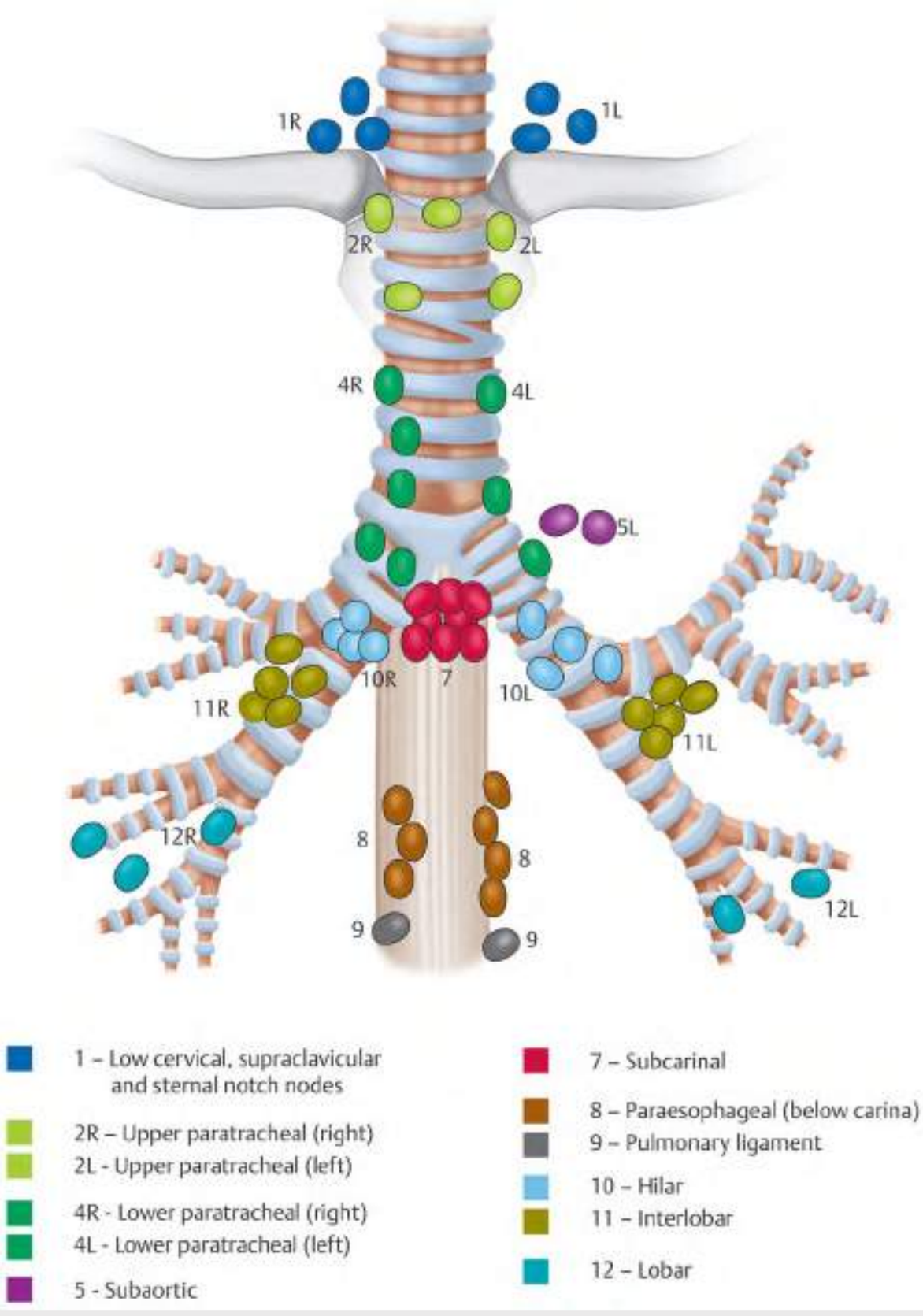

Fig. 2.25 Lymph nodes potentially amenable to sampling by endobronchial ultrasound (EBUS), transbronchial needle aspiration (TBNA), or EBUS-TBNA are indicated on the current lymph node map proposed by the International Association for the Study of Lung Cancer. The lymph node stations that are potentially amenable to TBNA correspond to stations 4, 5, 7, 10, and 11, but TBNA is most often used to sample subcarinal lymph nodes (station 7). Esophageal ultrasound may be used to sample stations 5, 7, 8, and 9. L, left; R, right. Adapted from Wang 1994.[39]

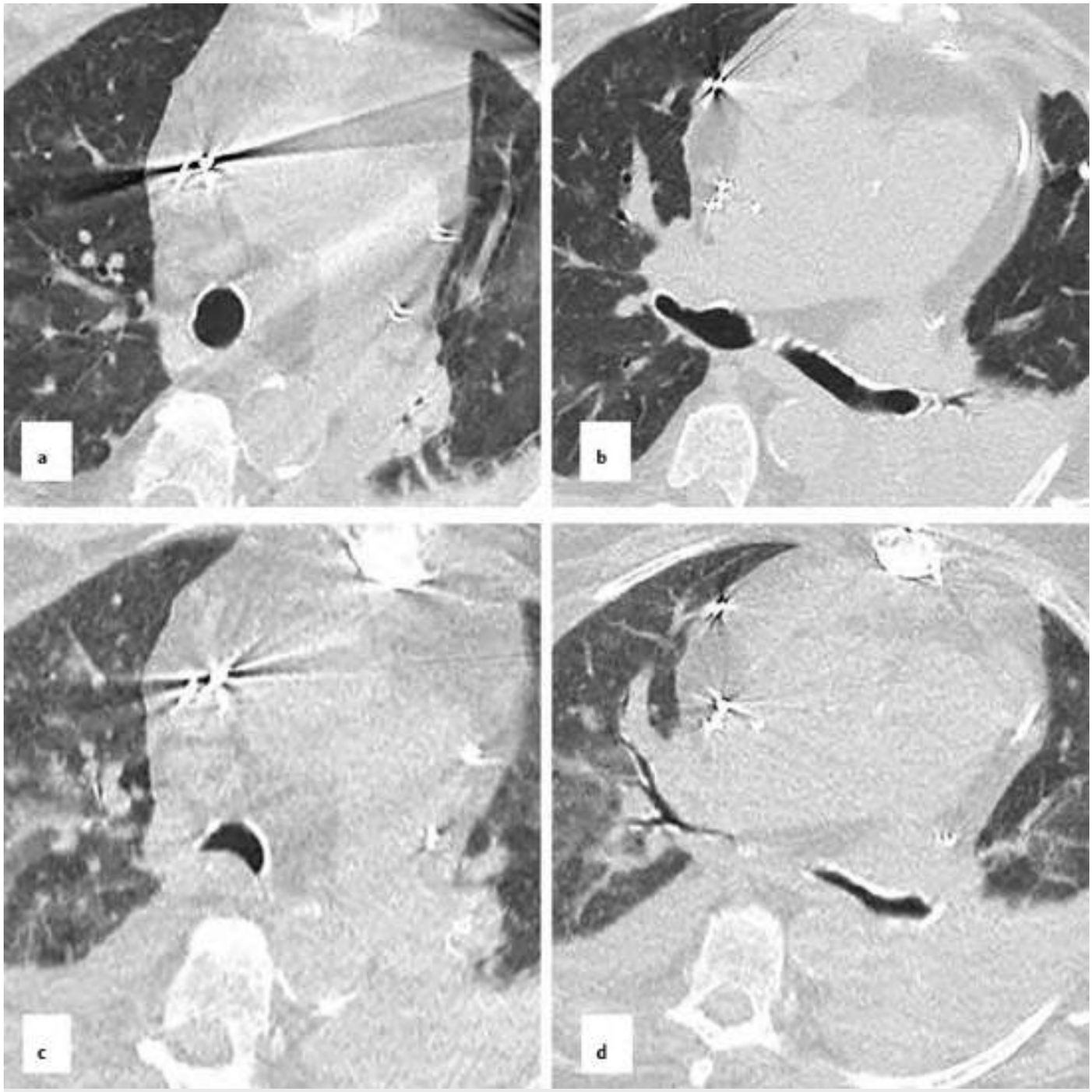

Fig. 2.26 Excessive dynamic airway collapse: **(a)** and **(b)** are inspiratory and **(c)** and **(d)** are expiratory CT images. If tracheal narrowing in expiration exceeds 50% as a result of posterior wall laxity, the condition is termed as excessive dynamic airway collapse. In contrast, in tracheomalacia, the tracheal cartilage is soft; therefore, it is the anterior and lateral walls that deform excessively on expiration, resulting in tracheal narrowing.

secondary tracheobronchomalacia is more common than the primary disease (i.e., relapsing polychondritis). Postintubation tracheal injury, surgical anastomosis, and trauma with damage to the cartilage are common causes of focal tracheobronchomalacia. Chronic irritation of the airway from smoking or air pollution and COPD result in tracheobronchial damage and diffuse type of tracheobronchomalacia (▶ Fig. 2.26). Saber-sheath trachea is a common finding in chronic obstructive lung disease and may be associated with mild tracheomalacia (▶ Fig. 2.9).

Bronchitis and bronchiolitis are the most common pathologies of the bronchial system. Common imaging manifestations of inflammation of the bronchi include wall thickening and mucous plugging. These findings are common in chronic airway diseases including COPD, cystic fibrosis, and asthma.[49] Pathological changes are related structural bronchial alterations due to subepithelial membrane thickness, mucous gland hypertrophy, and smooth muscle hypertrophy.[46] CT images show irregular inner surface with the presence of small outpouchings and diverticula (▶ Fig. 2.28). Damage to bronchial cartilage induces alternated narrowing and dilation of the airways in advanced disease, explaining why bronchiectasis may be seen on CT scans in COPD patients. See also ▶ Fig. 2.29.

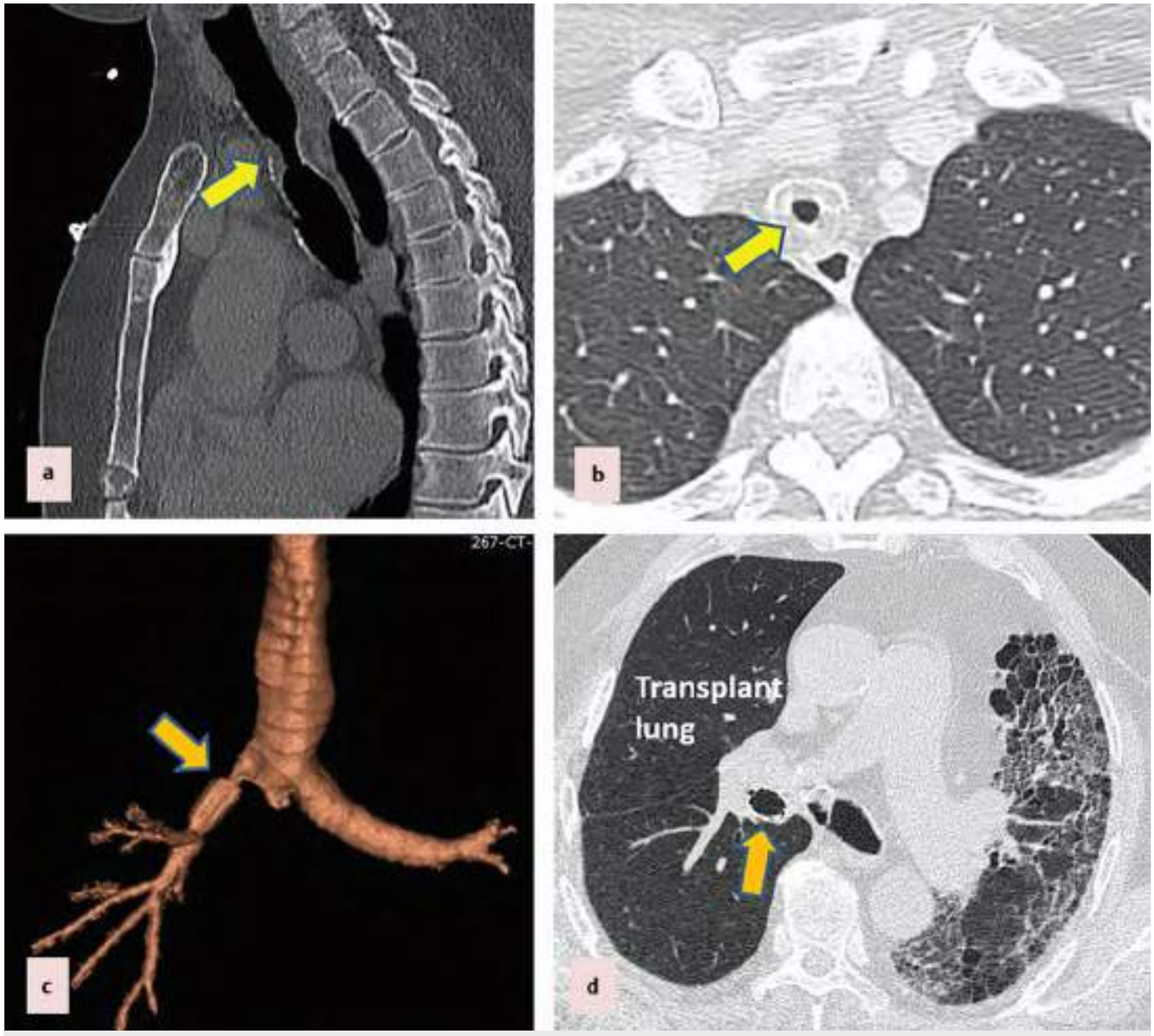

Fig. 2.27 **(a)** Sagittal CT and **(b)** axial CT showing focal circumferential tracheal stenosis after tracheostomy (*arrows*). **(c,d)** Status post right lung transplant with stenosis of the right main bronchus at the anastomosis repaired with bronchial stenting (*arrows*).

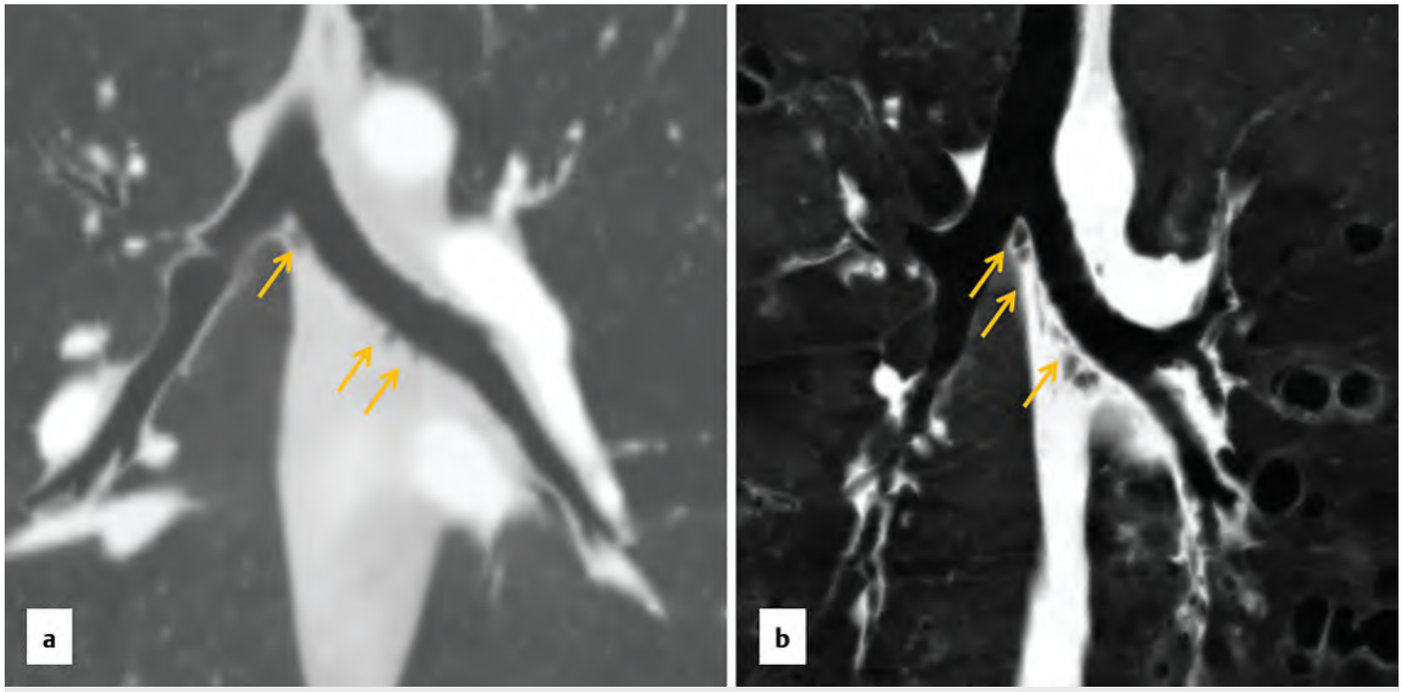

Fig. 2.28 **(a)** Patient with bronchitis. **(b)** Patient with cystic fibrosis. Coronal CT shows multiple small air containing outpouchings along the inferior margins of the main stem bronchi (*arrows*) representing dilated submucosal glands.

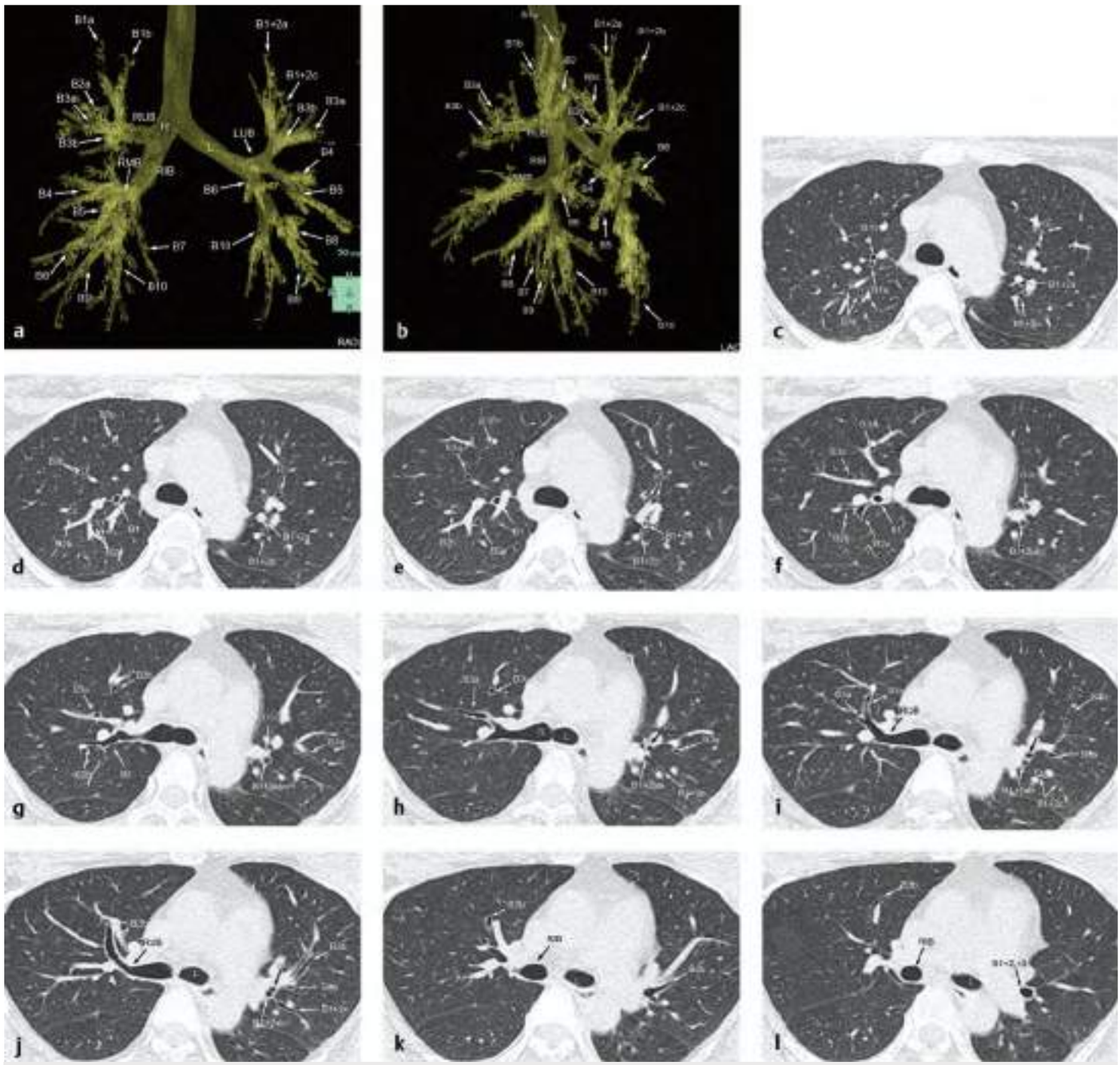

Fig. 2.29 Image series shows bronchial segmental anatomy based on Jackson–Huber classification. Axial and coronal images are presented.

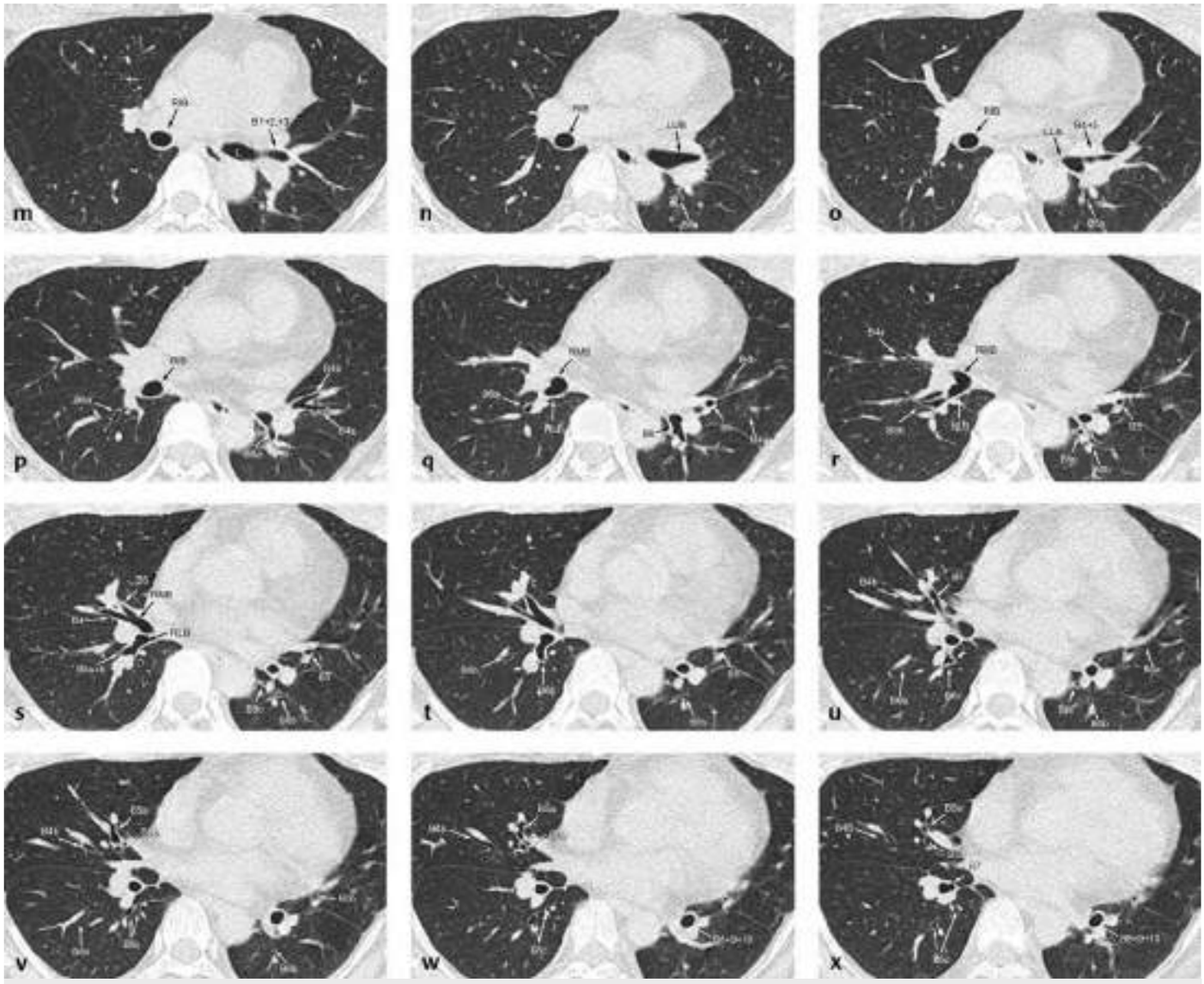

Fig. 2.29 (m–x)

(*Continued*)

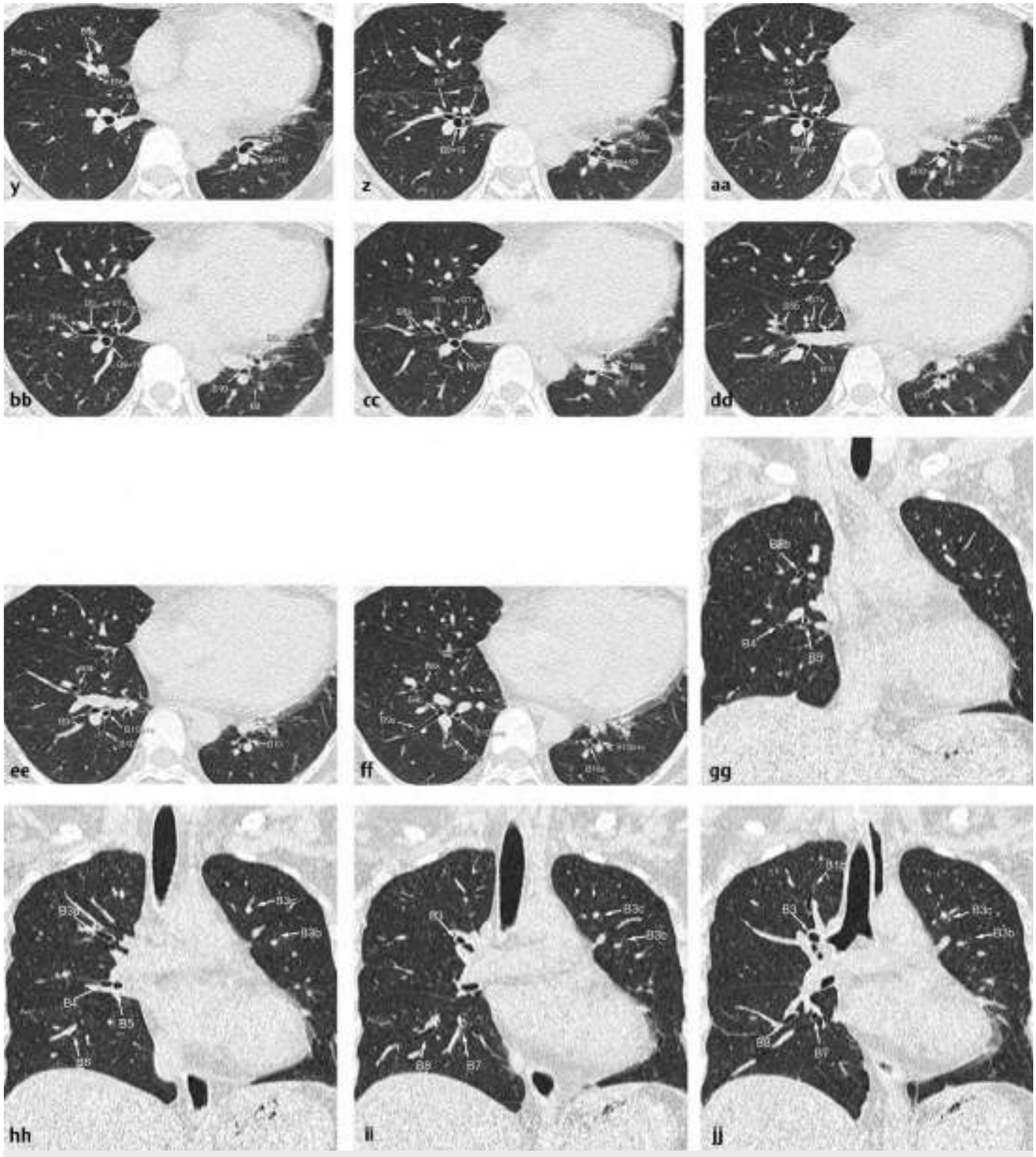

Fig. 2.29 (*Continued*) **(y–jj)**

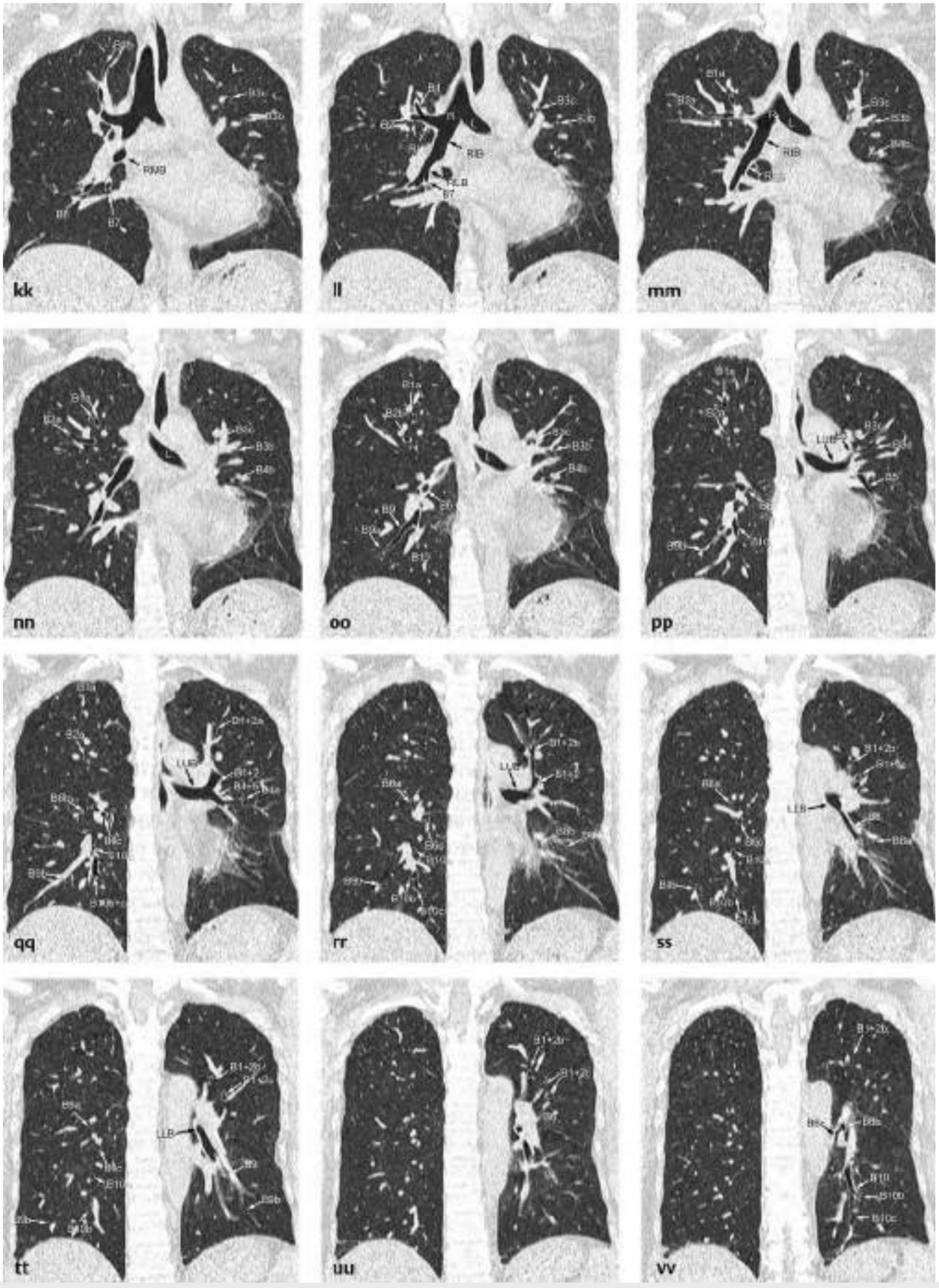

Fig. 2.29 (kk–vv)

References

[1] Boyden EA. Observations on the anatomy and development of the lungs. J Lancet.; 73(12):509–512

[2] Hutchins GM, Haupt HM, Moore GW. A proposed mechanism for the early development of the human tracheobronchial tree. Anat Rec.; 201(4):635–640

[3] Smith LJ, McKay KO, van Asperen PP, Selvadurai H, Fitzgerald DA. Normal development of the lung and premature birth. Paediatr Respir Rev.; 11 (3):135–142

[4] Wu CS, Chen CM, Chou HC. Pulmonary hypoplasia induced by oligohydramnios: findings from animal models and a population-based study. Pediatr Neonatol.

[5] Kasprian G, Balassy C, Brugger PC, Prayer D. MRI of normal and pathological fetal lung development. Eur J Radiol.; 57(2):261–270

[6] Ruano R, Joubin L, Aubry M-C, et al. A nomogram of fetal lung volumes estimated by 3-dimensional ultrasonography using the rotational technique (virtual organ computer-aided analysis). J Ultrasound Med.; 25(6):701–709

[7] Chassagnon G, Morel B, Carpentier E, Ducou Le Pointe H, Sirinelli D. Tracheobronchial branching abnormalities: lobe-based classification scheme. Radiographics.; 36(2):358–373

[8] Ghaye B, Szapiro D, Fanchamps JM, Dondelinger RF. Congenital bronchial abnormalities revisited. Radiographics.; 21(1):105–119

[9] Evans JA. Aberrant bronchi and cardiovascular anomalies. Am J Med Genet.; 35(1):46–54

[10] Drevet G, Conti M, Deslauriers J. Surgical anatomy of the tracheobronchial tree. J Thorac Dis.; 8 Suppl 2:S121–S129

[11] Thurnher D, Moukarbel RV, Novak CB, Gullane PJ. The glottis and subglottis: an otolaryngologist's perspective. Thorac Surg Clin.; 17(4):549–560

[12] Minnich DJ, Mathisen DJ. Anatomy of the trachea, carina, and bronchi. Thorac Surg Clin.; 17(4):571–585

[13] Boiselle PM. Imaging of the large airways. Clin Chest Med.; 29(1):181–193, vii

[14] Seymour AH. The relationship between the diameters of the adult cricoid ring and main tracheobronchial tree: a cadaver study to investigate the basis for double-lumen tube selection. J Cardiothorac Vasc Anesth.; 17(3):299–301

[15] Campos JH. Update on tracheobronchial anatomy and flexible fiberoptic bronchoscopy in thoracic anesthesia. Curr Opin Anaesthesiol.; 22(1):4–10

[16] Taybi H, Capitanio MA. Tracheobronchial calcification: an observation in three children after mitral valve replacement and warfarin sodium therapy. Radiology.; 176(3):728–730

[17] Hyde DM, Hamid Q, Irvin CG. Anatomy, pathology, and physiology of the tracheobronchial tree: emphasis on the distal airways. J Allergy Clin Immunol.; 124(6) Suppl:S72–S77

[18] Mehta S, Myat HM. The cross-sectional shape and circumference of the human trachea. Ann R Coll Surg Engl.; 66(5):356–358

[19] Thomas BP, Strother MK, Donnelly EF, Worrell JA. CT virtual endoscopy in the evaluation of large airway disease: review. AJR Am J Roentgenol.; 192(3) Suppl:S20–S30, quiz S31–S33

[20] Grenier PA, Beigelman-Aubry C, Fétita C, Prêteux F, Brauner MW, Lenoir S. New frontiers in CT imaging of airway disease. Eur Radiol.; 12(5):1022–1044

[21] Boyden EA. A critique of the international nomenclature on bronchopulmonary segments. Dis Chest.; 23(3):266–269

[22] Jackson CL, Huber JF. Correlated anatomy of the bronchial tree and lungs with a system of nomenclature. Dis Chest.; 9:319–326

[23] Yamashita H. Roentgenologic Anatomy of the Lung. 1st ed. Tokyo: Igaku-Shoin; 1978

[24] Beder S, Küpeli E, Karnak D, Kayacan O. Tracheobronchial variations in Turkish population. Clin Anat.; 21(6):531–538

[25] Macklem PT. The physiology of small airways. Am J Respir Crit Care Med.; 157 (5 Pt 2):S181–S183

[26] Marchand P, Gilroy JC, Wilson VH. An anatomical study of the bronchial vascular system and its variations in disease. Thorax.; 5(3):207–221

[27] Tanomkiat W, Tanisaro K. Radiographic relationship of the origin of the bronchial arteries to the left main bronchus. J Thorac Imaging.; 18(1):27–33

[28] Cauldwell EW, Siekert RG. The bronchial arteries; an anatomic study of 150 human cadavers. Surg Gynecol Obstet.; 86(4):395–412

[29] Walker CM, Rosado-de-Christenson ML, Martínez-Jiménez S, Kunin JR, Wible BC. Bronchial arteries: anatomy, function, hypertrophy, and anomalies. Radiographics.; 35(1):32–49

[30] Carles J, Clerc F, Dubrez J, Couraud L, Drouillard J, Videau J. The bronchial arteries: anatomic study and application to lung transplantation. Surg Radiol Anat.; 17(4):293–299

[31] Lee WH, Jung GS, Cho YD, Jung MH, Cha TJ. Anomalous bronchial artery originating from the right coronary artery in a patient with angina (2009: 4b). Eur Radiol.; 19(7):1822–1825

[32] Daly RC, McGregor CG. Routine immediate direct bronchial artery revascularization for single-lung transplantation. Ann Thorac Surg.; 57(6):1446–1452

[33] Charan NB, Baile EM, Paré PD. Bronchial vascular congestion and angiogenesis. Eur Respir J.; 10(5):1173–1180

[34] Williams MH, Jr, Towbin EJ. Magnitude and time of development of the collateral circulation to the lung after occlusion of the left pulmonary artery. Circ Res.; 3(4):422–424

[35] Ming Z, Lin Z. Evaluation of tracheal bronchus in Chinese children using multidetector CT. Pediatr Radiol.; 37(12):1230–1234

[36] Wooten C, Patel S, Cassidy L, et al. Variations of the tracheobronchial tree: anatomical and clinical significance. Clin Anat.; 27(8):1223–1233

[37] Starshak RJ, Sty JR, Woods G, Kreitzer FV. Bridging bronchus: a rare airway anomaly. Radiology.; 140(1):95–96

[38] Nair A, Godoy MC, Holden EL, et al. Multidetector CT and postprocessing in planning and assisting in minimally invasive bronchoscopic airway interventions. Radiographics.; 32(5):E201–E232

[39] Wang KP. Staging of bronchogenic carcinoma by bronchoscopy. Chest.; 106 (2):588–593

[40] Jokinen K, Palva T, Sutinen S, Nuutinen J. Acquired tracheobronchomalacia. Ann Clin Res.; 9(2):52–57

[41] Wagnetz U, Roberts HC, Chung T, Patsios D, Chapman KR, Paul NS. Dynamic airway evaluation with volume CT: initial experience. Can Assoc Radiol J.; 61 (2):90–97

[42] Lee KS, Sun MRM, Ernst A, Feller-Kopman D, Majid A, Boiselle PM. Comparison of dynamic expiratory CT with bronchoscopy for diagnosing airway malacia: a pilot evaluation. Chest.; 131(3):758–764

[43] Boiselle PM, O'Donnell CR, Bankier AA, et al. Tracheal collapsibility in healthy volunteers during forced expiration: assessment with multidetector CT. Radiology.; 252(1):255–262

[44] Baroni RH, Feller-Kopman D, Nishino M, et al. Tracheobronchomalacia: comparison between end-expiratory and dynamic expiratory CT for evaluation of central airway collapse. Radiology.; 235(2):635–641

[45] Leong P, Bardin PG, Lau KK. What's in a name? Expiratory tracheal narrowing in adults explained. Clin Radiol.; 68(12):1268–1275

[46] Brillet PY, Fetita CI, Saragaglia A, et al. Investigation of airways using MDCT for visual and quantitative assessment in COPD patients. Int J Chron Obstruct Pulmon Dis.; 3(1):97–107

[47] Javidan-Nejad C. MDCT of trachea and main bronchi. Thorac Surg Clin.; 20 (1):65–84

[48] Aysola RS, Hoffman EA, Gierada D, et al. Airway remodeling measured by multidetector CT is increased in severe asthma and correlates with pathology. Chest.; 134(6):1183–1191

[49] Jeffery PK. Remodeling in asthma and chronic obstructive lung disease. Am J Respir Crit Care Med.; 164(10 Pt 2):S28–S38

3 Mediastinum and Thymus

Cameron Hassani and Farhood Saremi

◆ Introduction

The mediastinum (Latin, *media* = middle and *stare* = to stand; i.e., that which stands in the middle) is a compartment within the thorax which contains all the thoracic organs, apart from the lungs and pleura. It is bounded superiorly by the thoracic inlet and inferiorly by the diaphragm. The sternum and ribs form the anterior-most margin of the mediastinum and the vertebral column forms the posterior margin. Laterally, it is bounded by the mediastinal pleura on both sides. The mediastinum is a complex area containing structures vital to life, both large and small, such as the heart, major vessels, trachea, esophagus, nerves, and lymph nodes. Fat also makes up a large component of the mediastinum. In this chapter, the anatomy of above structures will be reviewed. Azygous system, systemic veins, aorta, and pulmonary arteries are discussed in related chapters.

◆ Compartmentalized Anatomy

It is useful to divide the mediastinum into compartments for the purposes of forming a differential diagnosis when dealing with masses in the mediastinum. However, the mediastinum lacks true anatomical boundaries to serve as a basis for compartmentalized anatomy. As a result, several differing models have been developed in attempts to compartmentalize the mediastinum.[1,2] Each model is different from the next, and some are based on plain chest radiography. As may be expected, there is discordance between the different models.

Traditionally and historically, radiologists have mostly used systems which divided the mediastinum into anterior, middle, posterior, and sometimes superior mediastinal compartments, based on chest radiograph. More recently formalized systems based on cross-sectional computed tomography (CT) imaging and expert consensus have been proposed. Initially a four-compartment model (anterior, middle, posterior, and superior mediastinum) by the Japanese Association for Research of the Thymus (JART) and then a three-compartment model by the International Thymic Malignancy Interest Group (ITMIG) have been introduced.[3] It should be emphasized; these models and all the various historical models are based on expert opinion and preferences, as there are no real anatomical planes to separate the "anterior," "middle," and "posterior" mediastinum. These compartments exist to optimize the clinician's ability to identify and distinguish pathology based on location.[4,5] We will further discuss the ITMIG classification schema which will likely become the most widely accepted system.

◆ ITMIG Classification

The ITMIG adopted the following system for compartmentalization of the mediastinum (▶ Fig. 3.1, ▶ Fig. 3.2, ▶ Fig. 3.3). ITMIG divides the mediastinum into three compartments: (**a**) prevascular (anterior mediastinum), (**b**) visceral (middle mediastinum), and (**c**) paravertebral (posterior mediastinum) compartments (▶ Table 3.1).

The prevascular compartment (anterior mediastinum) is bounded by the thoracic inlet superiorly, the diaphragm

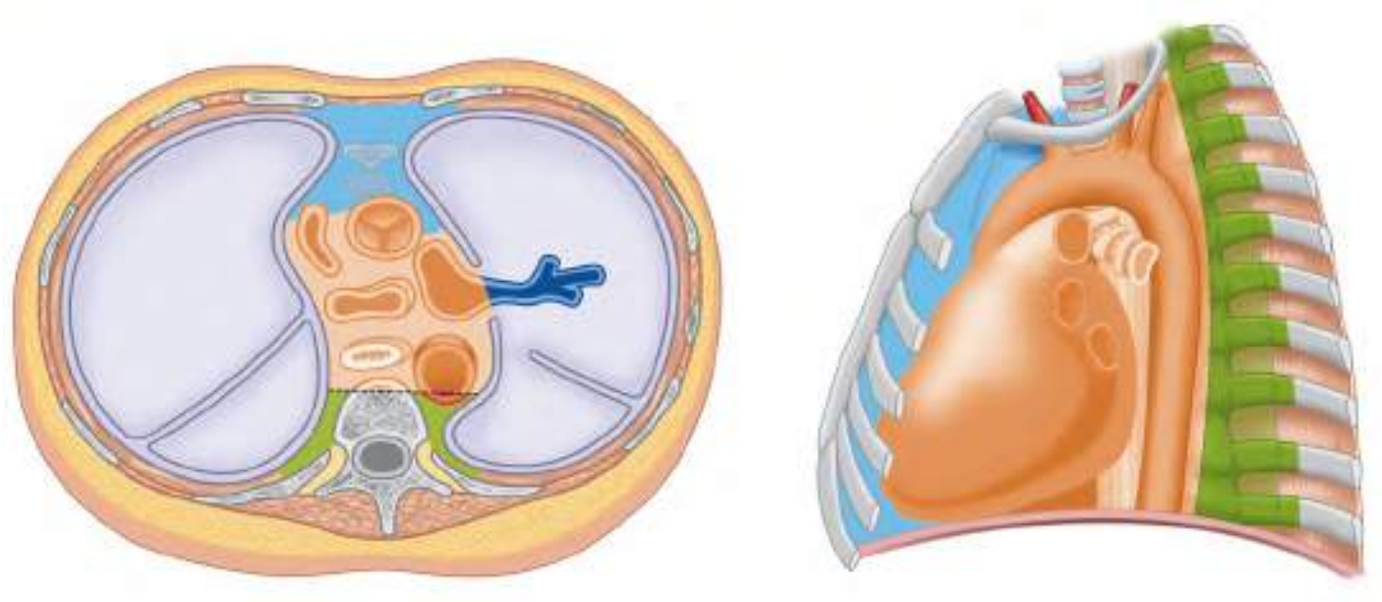

Fig. 3.1 Mediastinal compartments: blue—prevascular (anterior mediastinum), orange—visceral (middle mediastinum), and green—paravertebral (posterior mediastinum) compartments.

Table 3.1 Mediastinal compartment's (ITMIG) CT-based classification

Name	Boundaries	Contents
Prevascular (anterior) compartment	**Superior:** Thoracic inlet	Thymus, lymph nodes, brachiocephalic vein, and fat
	Inferior: Diaphragm	
	Anterior: Anterior aspect of pericardium	
	Lateral: Mediastinal pleura	
Visceral (middle) compartment	**Superior:** Thoracic inlet	Pericardium, heart, superior vena cava, ascending thoracic aorta, aortic arch, arch vessels, descending thoracic aorta, proximal (intrapericardial) pulmonary arteries, thoracic duct, trachea/carina, esophagus, lymph nodes, vagus nerves, and phrenic nerves
	Inferior: Diaphragm	
	Anterior: Anterior aspect of pericardium	
	Posterior: Visceral–paravertebral compartment boundary line	
	Lateral: Mediastinal pleura	
Paravertebral (posterior) compartment	**Superior:** Thoracic inlet	Thoracic spine and paravertebral soft tissues, fat, autonomic nervous plexus
	Inferior: Diaphragm	
	Anterior: Visceral–paravertebral compartment boundary line	
	Posterior: Vertical line along the posterior margin of the chest wall and the lateral margin of vertebral transverses processes	
	Lateral: Mediastinal pleura	

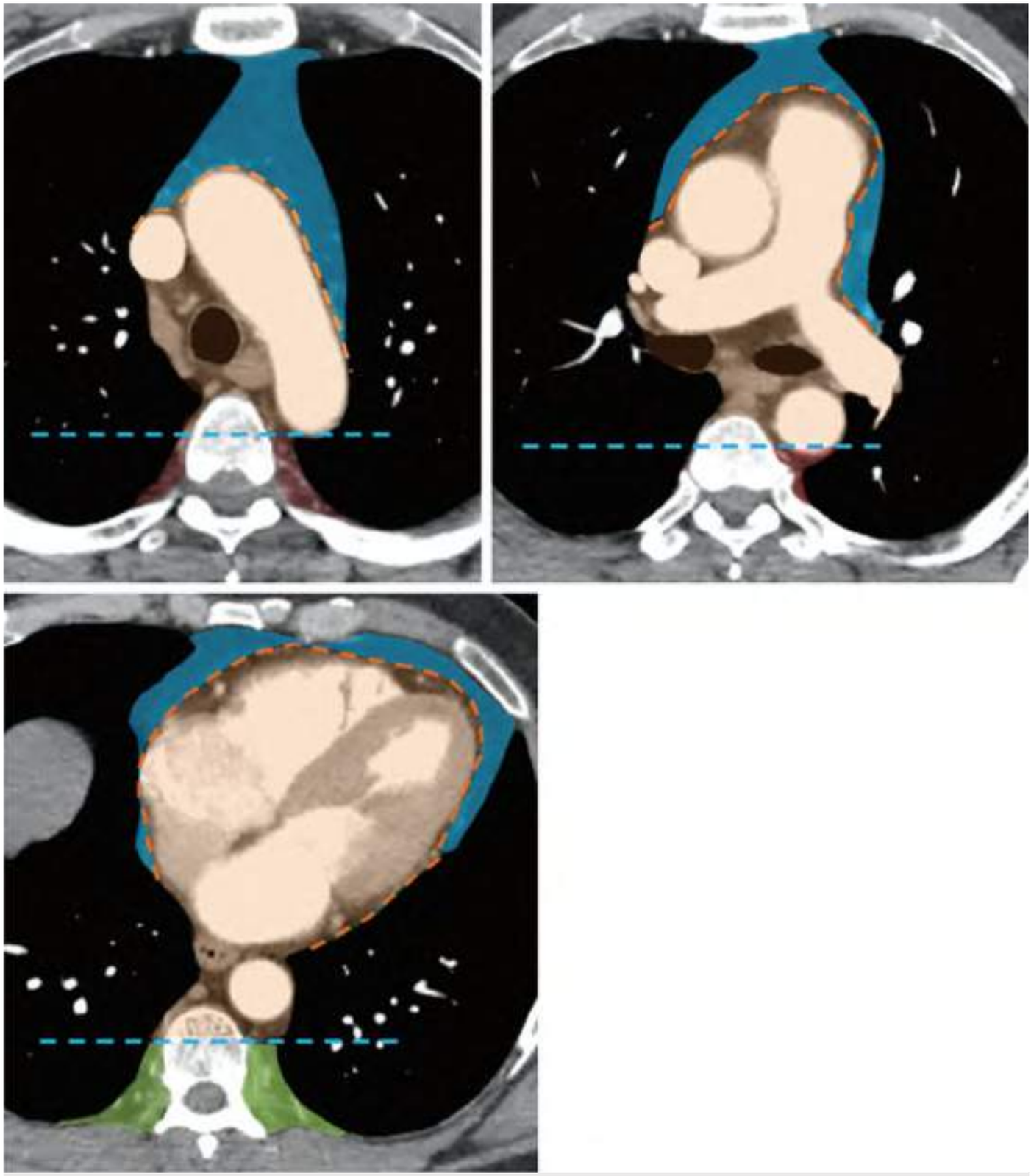

Fig. 3.2 Sequential axial images of the thorax demonstrating the boundaries and compartments of the ITMIG mediastinal classification system. Blue—prevascular (anterior mediastinum), orange—visceral (middle mediastinum), and green—paravertebral (posterior mediastinum) compartments. Visceral–paravertebral compartment boundary is shown by dashed blue line and the pericardium margin is shown by orange line.

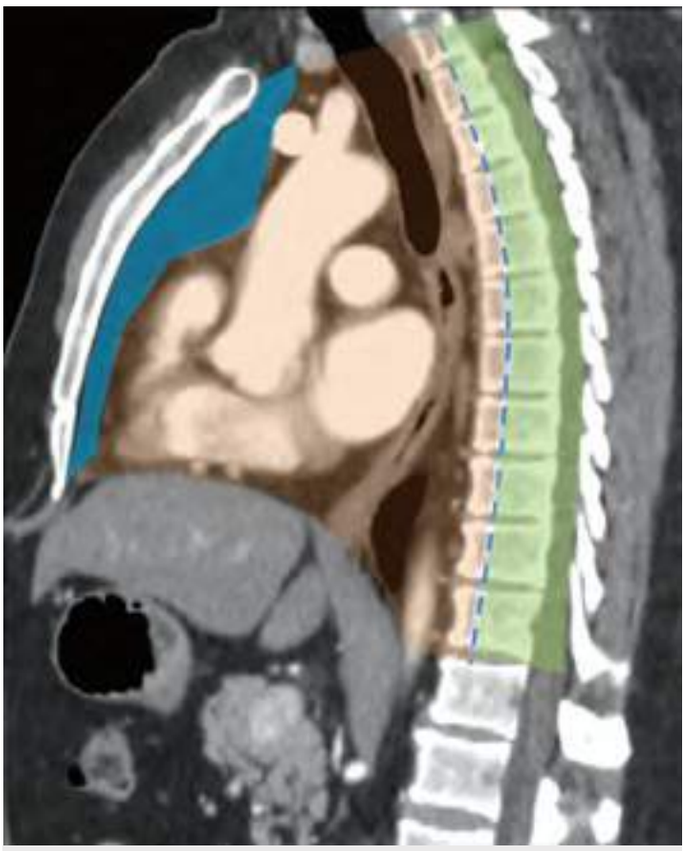

Fig. 3.3 Sagittal image of the thorax demonstrating the boundaries and compartments of the ITMIG mediastinal classification system.

inferiorly, the sternum anteriorly, the anterior aspect of the pericardium posteriorly, and the mediastinal pleura laterally. The major components of this compartment are the thymus, lymph nodes, left brachiocephalic vein, and fat. The prevascular compartment extends from the thoracic inlet to the diaphragm, always anterior to the heart and pericardium. Displacement of these structures posteriorly is a useful tool to localizing any mass of questionable origin to the prevascular compartment. Common pathologies include thymic lesions, teratoma, lymph node diseases, and hematoma. The prevascular compartment is a common location for collection of hematoma after trauma or surgery.

The visceral compartment (middle mediastinum) is bounded by the thoracic inlet superiorly, the diaphragm inferiorly, and the anterior pericardium anteriorly. The posterior margin is defined by a line connecting points on each vertebral body 1 cm posterior to the anterior cortex of the vertebral bodies, the so-called "visceral–paravertebral compartment boundary line." The major components of this compartment are the pericardium, heart, superior vena cava, ascending thoracic aorta, aortic arch, descending thoracic aorta, proximal (intrapericardial) pulmonary arteries, thoracic duct, trachea/carina, esophagus, nerves, and lymph nodes.[6,7]

The paravertebral compartment (posterior mediastinum) is bounded by the thoracic inlet superiorly, the diaphragm inferiorly, the visceral compartment anteriorly ("visceral–paravertebral compartment boundary line" which is defined in the preceding paragraph) and a vertical line along the posterior margin of the chest wall and the lateral margin of vertebral transverse processes posteriorly. The major structures of this compartment are the thoracic spine, paravertebral soft tissues/fat, and autonomic nervous plexus. Enlarged lymph nodes can be found anywhere in the mediastinum. Common focal pathologies include nerve/nerve sheath masses (i.e., neurofibroma, schwannoma) and tumors of the sympathetic chain such as paraganglionic cell neoplasms. Other uncommon pathologies extramedullary hematopoiesis (i.e., thalassemia), neurenteric cysts, and rarely meningoceles.

◆ Components

Ligaments

The contents of the mediastinum are suspended/anchored to the chest wall or connected one another via a series of ligaments. While many of them are quite small, several of these ligamentous connections are large enough to be appreciated by CT or magnetic resonance imaging (MRI).

Inferior Pulmonary Ligament

The inferior pulmonary ligament (IPL) is a double layer of pleura which becomes continuous with intervening connective tissue to form a contiguous ligament (▶ Fig. 3.4) (see Chapter 4, Pleura). Specifically, at the level of the pulmonary hilum both the anterior and posterior pleura come together and encase the hilum. Just below the pulmonary vein, artery, and bronchus the two pleura (along with intervening veins and lymphatics) fuse together to form the IPL.[8,9] The IPL, which takes a triangular shape at the hilar level, travels caudally along the mediastinal pleural surface to either terminate at the diaphragmatic pleura or end as a free edge. At axial CT, it is most commonly seen as a well-defined linear opacity extending horizontally from the paravertebral (posterior) mediastinal pleural surface.[10] It is best seen at the level of the diaphragm, where a slight widening of its base (in order to contact the diaphragm) makes it more apparent (▶ Fig. 3.5, ▶ Fig. 3.6).

While the IPL is an extraparenchymal structure, yet it can be surrounded by lung parenchyma especially in emphysematous lungs, giving it the appearance of intraparenchymal subsegmental atelectasis or scarring. The IPL has clinical significance for lung cancer staging, as lymphadenopathy in the IPL is considered a station 9 lymph node. IPL functions to anchor the lower lobe to both the mediastinum and the diaphragm. In patients with disruption of the IPL, there is a reported increased incidence of lung torsion, thought to be due to increased mobility of the lower lobe. IPL may be injured in trauma, and posttraumatic pneumatocele especially in children can be observed at this anatomical area.

Ligamentum Arteriosum

Ligamentum arteriosum (LA) is a small ligament which is a remnant of the fetal ductus arteriosus. The LA is seen as a calcified structure in nearly 50% of adults near the aortic arch passing into the aortic–pulmonary window.[11] A calcified LA is considered an insignificant normal finding; however, it is many times mistaken

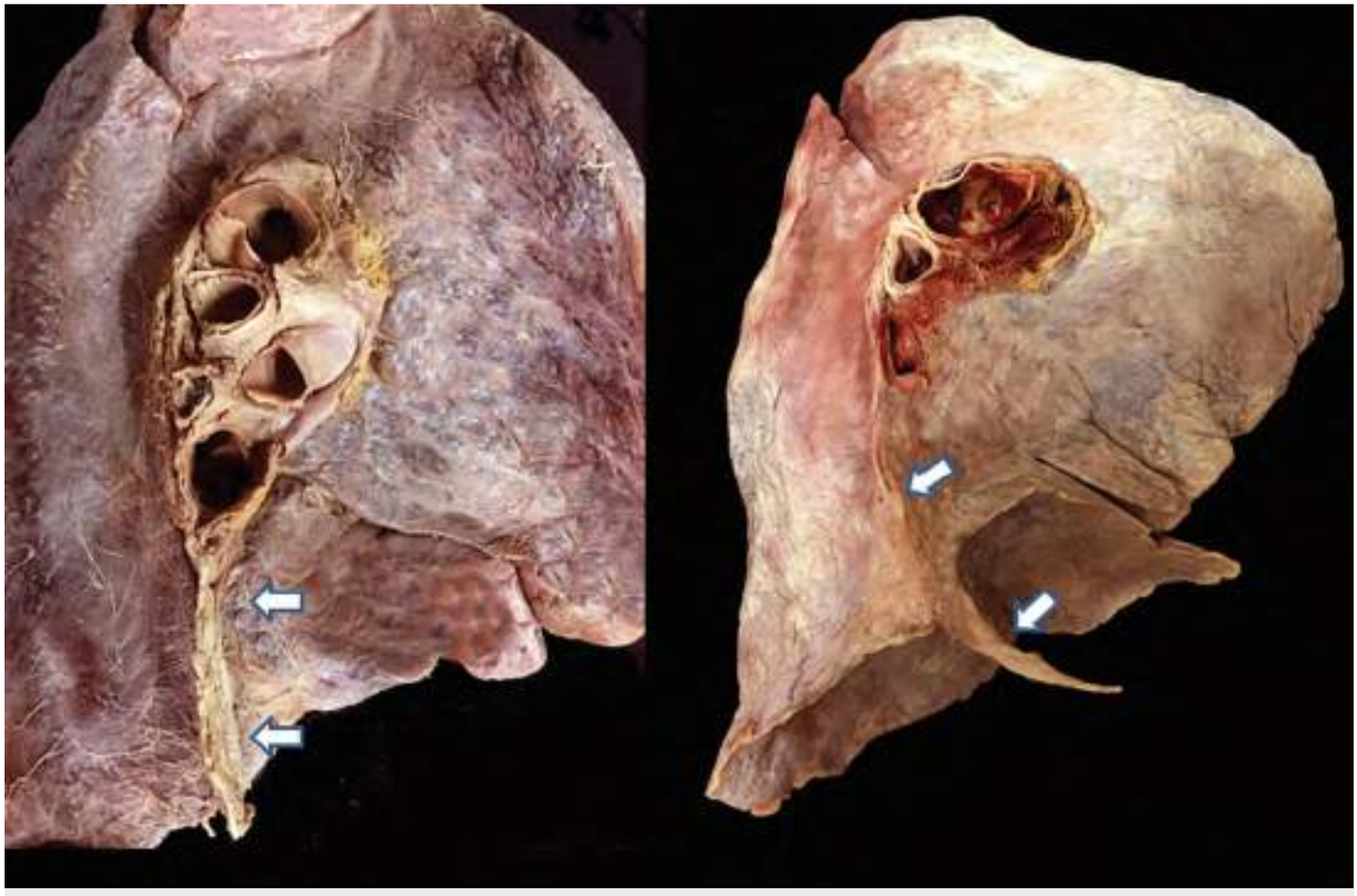

Fig. 3.4 Medial surface of the left lung demonstrating the inferior pulmonary ligament (*arrows*) in relation to the pulmonary hilum.

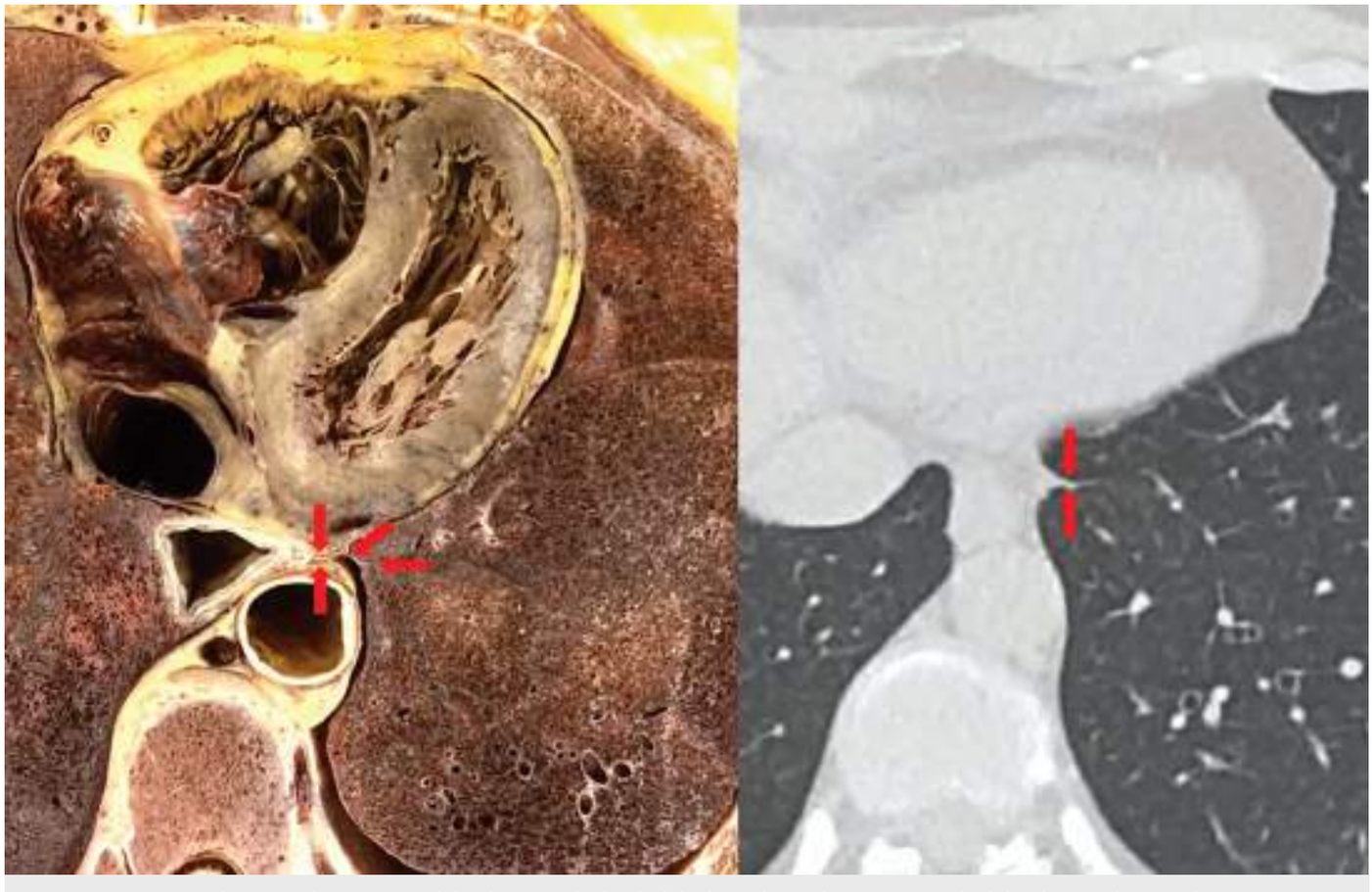

Fig. 3.5 Transverse cadaveric and CT images of the thorax at the level of the lower heart demonstrating the left inferior pulmonary ligament (*arrows*).

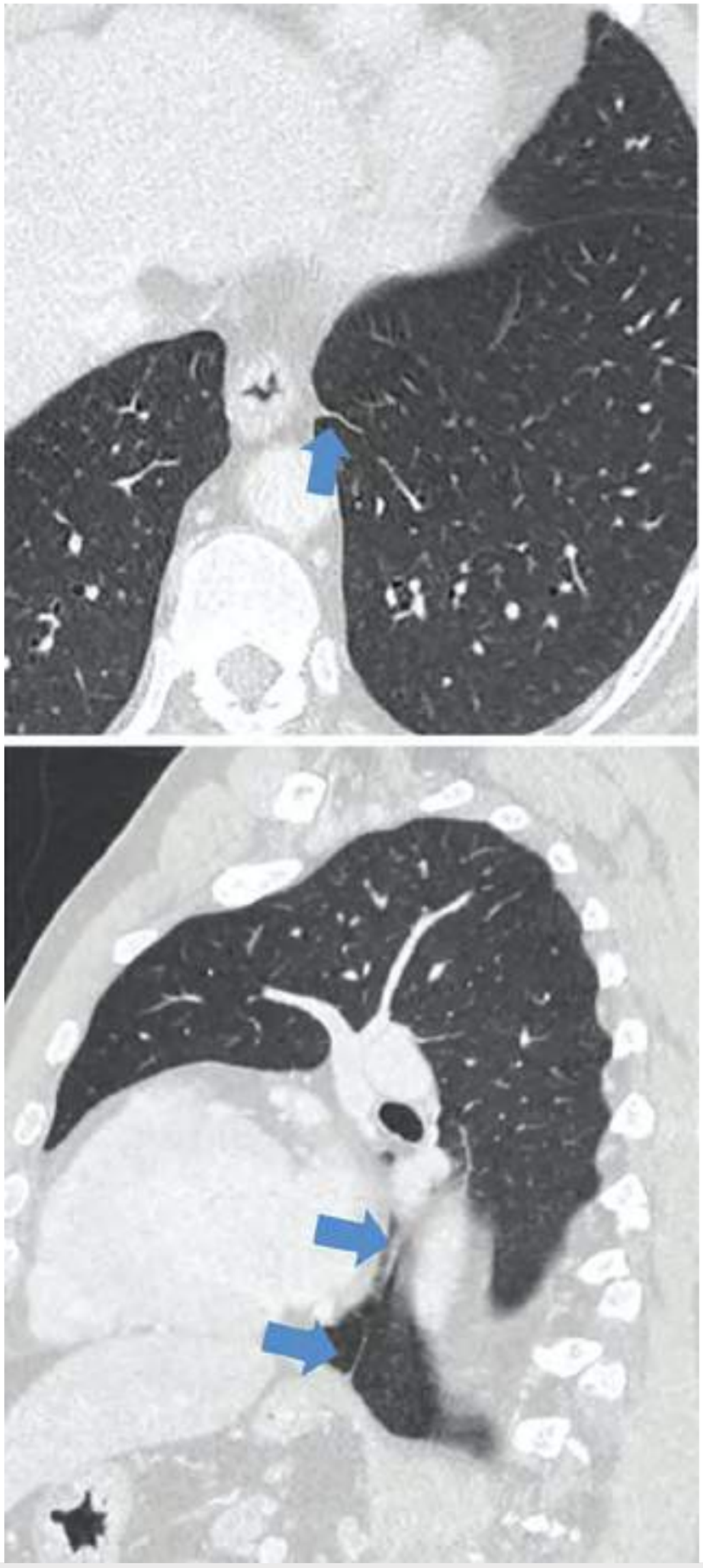

Fig. 3.6 Transverse and sagittal CT images of the thorax demonstrating the left inferior pulmonary ligament (*arrows*).

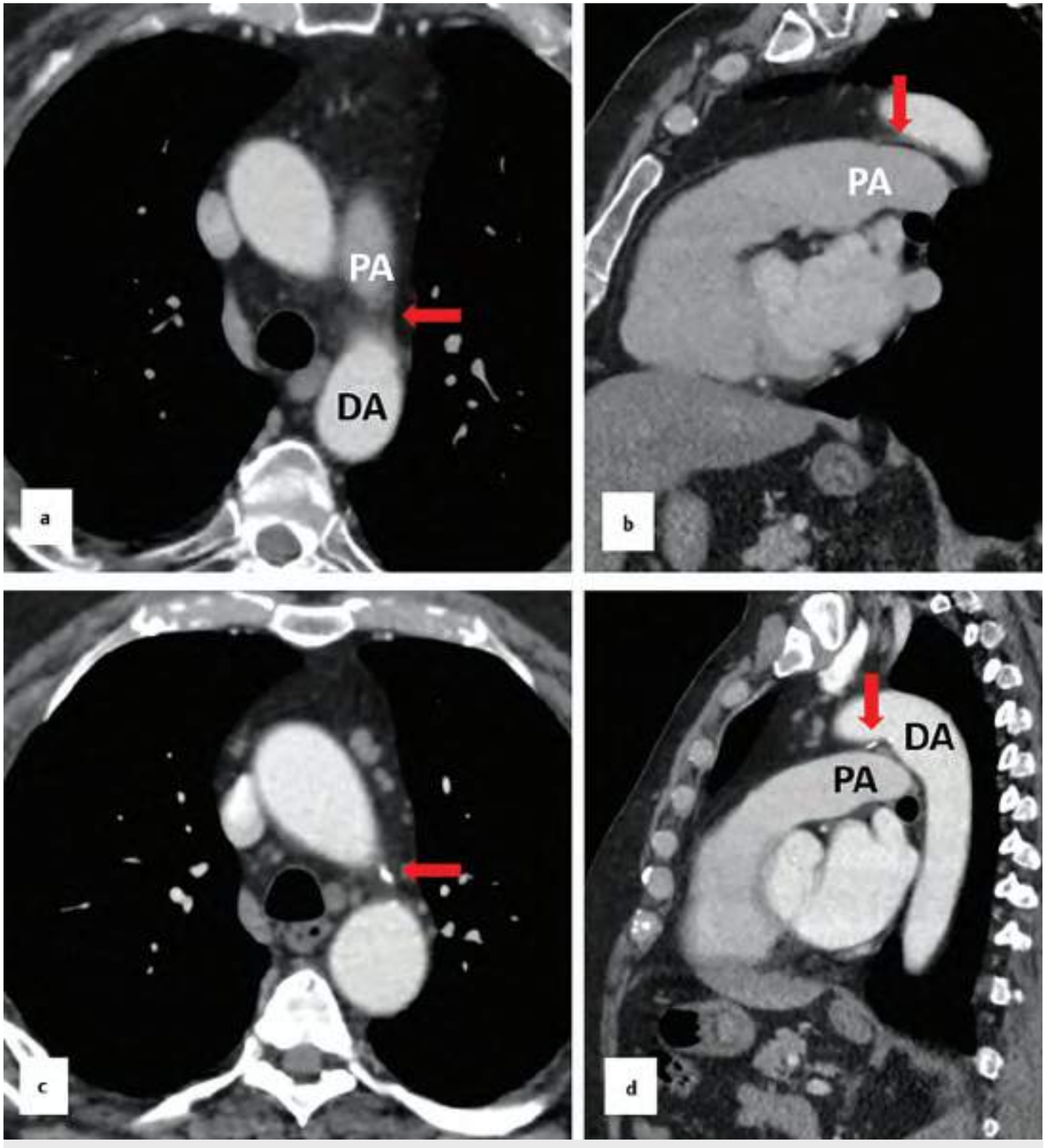

Fig. 3.7 **(a)** Transverse and **(b)** sagittal CT images of the thorax demonstrating a non-calcified ligamentum arteriosum (*arrows*) which can be very thin, small, and easily missed when not calcified. **(c)** Transverse, and **(d)** sagittal CT images of the thorax demonstrating a calcified ligamentum arteriosum (*arrows*). This ligament extends between the descending arch of the aorta (DA) and left pulmonary artery (PA).

for aortic atherosclerotic disease[12] (▶ Fig. 3.7). The calcification may be a single focus in the setting of a noncalcified tubular structure, a linear or curvilinear calcification, or large clumped calcifications. The LA is a notable piece of anatomy as it is theorized that a fixed tethering of the aorta by this ligament accounts for a large proportion of aortic injuries in the area of the LA. It should be remembered that the LA serves as an important landmark/border when distinguishing aortopulmonary (AP) window (station 5) lymph nodes from left paratracheal (station 4L) lymph nodes, the former being to the left of the LA.

Sternopericardial Ligaments

There are both superior and inferior sternopericardial ligaments (SPLs) which attach the fibrous pericardium to the posterior surface of the sternum. The superior SPL attaches the pericardium to the manubrium, while the inferior SPL attaches to the xiphoid process (▶ Fig. 3.8).

Pericardiophrenic or Phrenopericardial Ligament

The pericardiophrenic ligament (PPL) is a triangular structure which is formed by the combination of pleural reflection, right phrenic nerve, and pericardiophrenic bundle vessels. At CT, it has a very similar appearance to the IPL, however, the PPL has a characteristic position either lateral or anterior to the inferior vena cava (IVC) (▶ Fig. 3.9). Sometimes, the phrenic nerve and/or pericardiophrenic bundle can be seen as distinct structures entering the PC.

Thyrothymic Ligament

The thyrothymic ligament connects the thyroid to the upper parts of the thymus on either side of the neck and mediastinum (▶ Fig. 3.10). The inferior extents of these ligaments pass into the mediastinum as they connect to the thymus. They serve as an important anatomical landmark during neck dissection when searching for the parathyroid glands. In cases of mediastinal parathyroid adenoma, many times the adenoma is located along this ligament.

◆ Thymus

The thymus is relatively centrally located in the prevascular compartment of the mediastinum (▶ Fig. 3.10, ▶ Fig. 3.11). It resides between the sternum anteriorly and the pericardium, aortic arch, and left brachiocephalic vein posteriorly.[13,14] Laterally the thymus is bordered by the mediastinal pleural surfaces.

While this is the classic normal location of the thymus, it can also be located ectopically in the neck. This is in part the result of thymic development, in which the normal thymus descends from the third and possibly fourth pharyngeal pouches down the neck and into the mediastinum. Any arrest of this pathway will result in ectopic thymic tissue. In 20 to 25% of people, separate islands of residual thymic tissue can be found in the neck, mediastinum, and lung as a result of the thymic development process.

The thymus grows during fetal development, through birth into puberty where it achieves its largest relative size (▶ Fig. 3.12). After puberty, a process of involution begins and the thymus diminishes in size as age increases[15,16] (▶ Fig. 3.12). This normal involution is known to accelerate with exogenous steroid use. The thymus has a prime role in the peripheral immune system, and the age-related normal involution is thought to be related to weaker overall immune systems in the elderly. Why this occurs remains a mystery.[17]

The thymus is comprised of two distinct lobes which are connected centrally by loose connective tissue or an intermediate lobe (▶ Fig. 3.12, ▶ Fig. 3.13). A capsule made of collagenous fibers encases both of these lobes. Capsular septa separate the lobes into smaller cortical lobules, with the deeper medullary

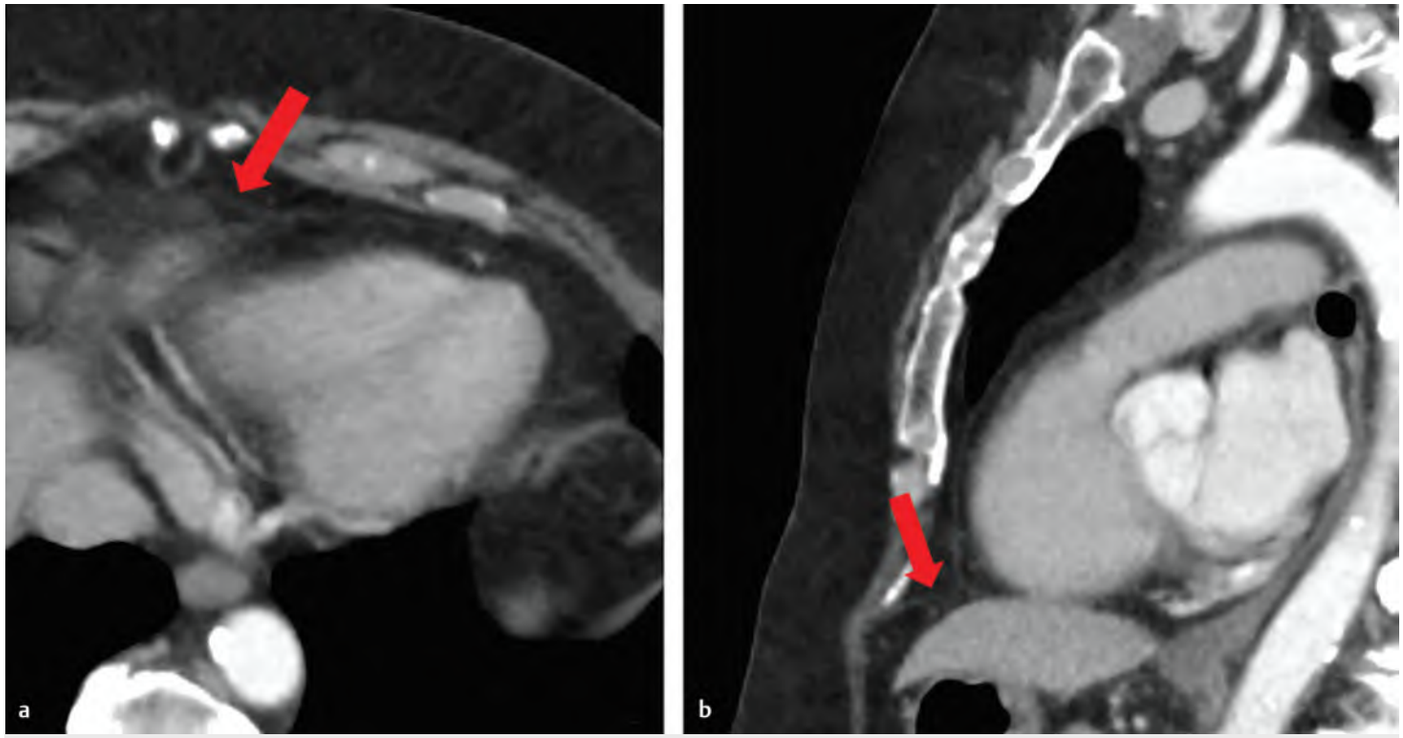

Fig. 3.8 Sternopericardial ligament: **(a)** axial and **(b)** sagittal CT. The sternopericardial ligament (*arrows*) attaches the fibrous pericardium to the posterior surface of the sternum, best seen on sagittal projection **(b)**.

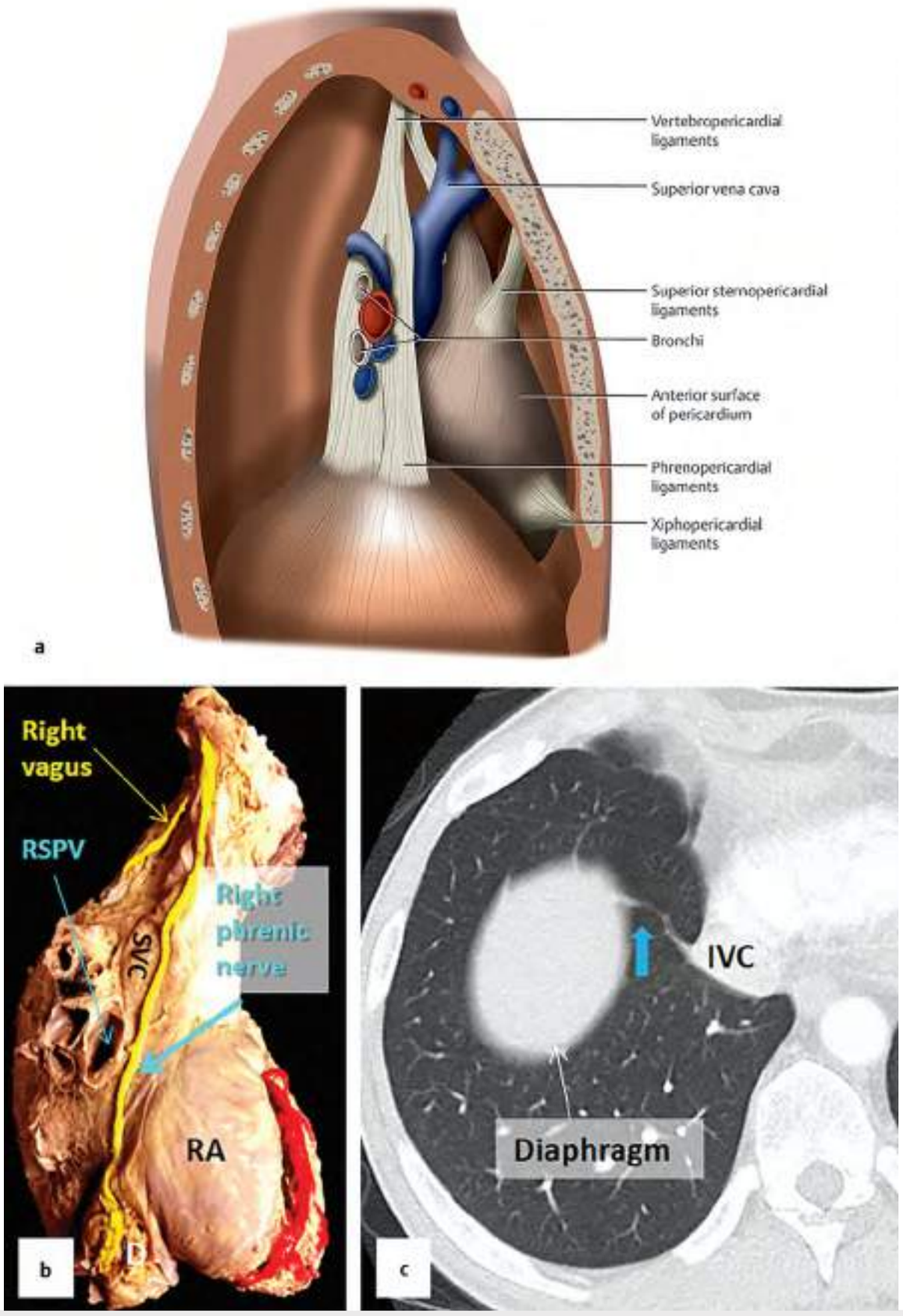

Fig. 3.9 **(a)** Pericardial ligaments. The pericardiophrenic ligament (PPL) is a triangular structure which is formed by the combination of pleural reflection, right phrenic nerve, and pericardiophrenic bundle vessels. **(b)** Anatomical course of the right phrenic artery is shown. **(c)** The PPL (*red arrows*) is a linear structure which is usually seen projecting at the level of the inferior vena cava (IVC) or anterior to the IVC (*blue arrow*) while the inferior pulmonary ligament is usually more posteriorly located (not shown). D, diaphragm; RA, right atrium; RSPV, right superior pulmonary vein; SVC, superior vena cava.

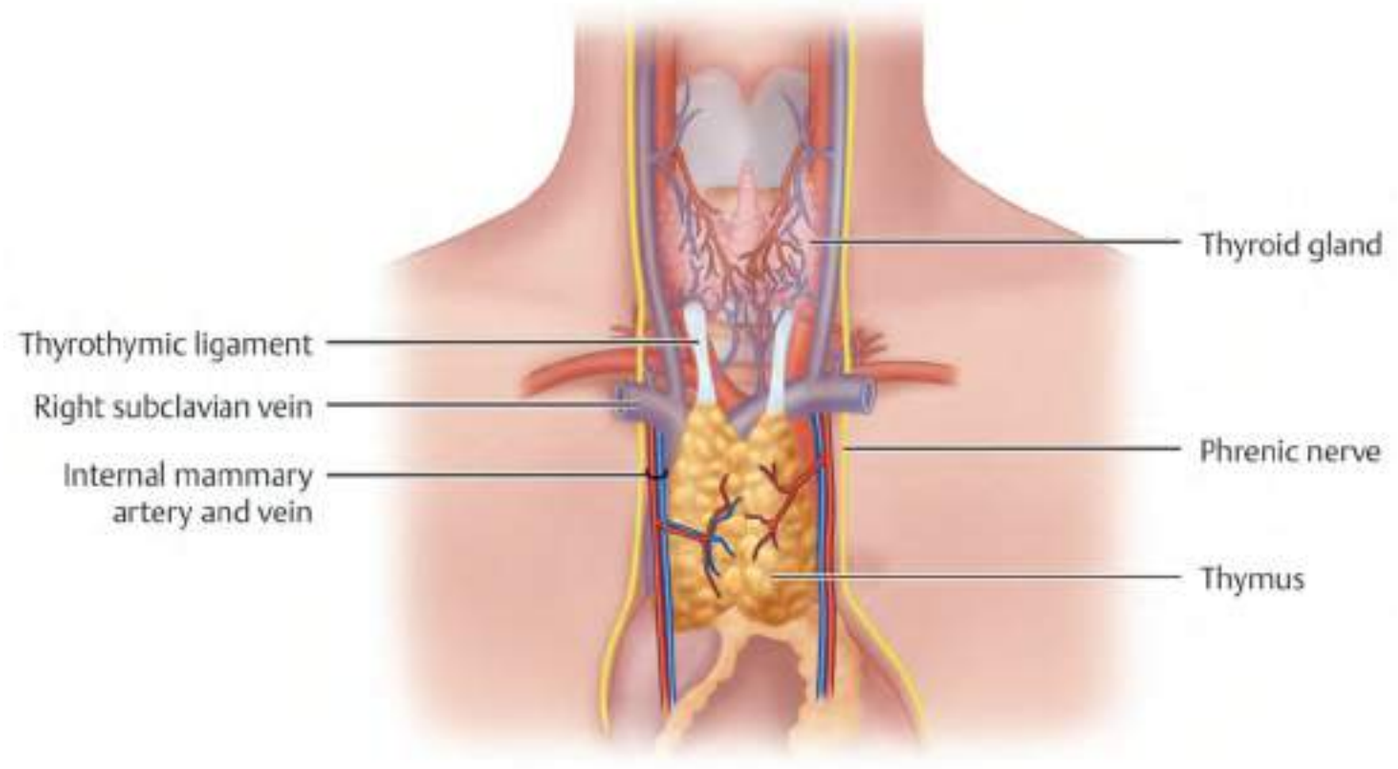

Fig. 3.10 Drawing of the normal thyroid, thymus, and the thyrothymic ligament. The thyrothymic ligament maintains connection between the two glands across the thoracic inlet.

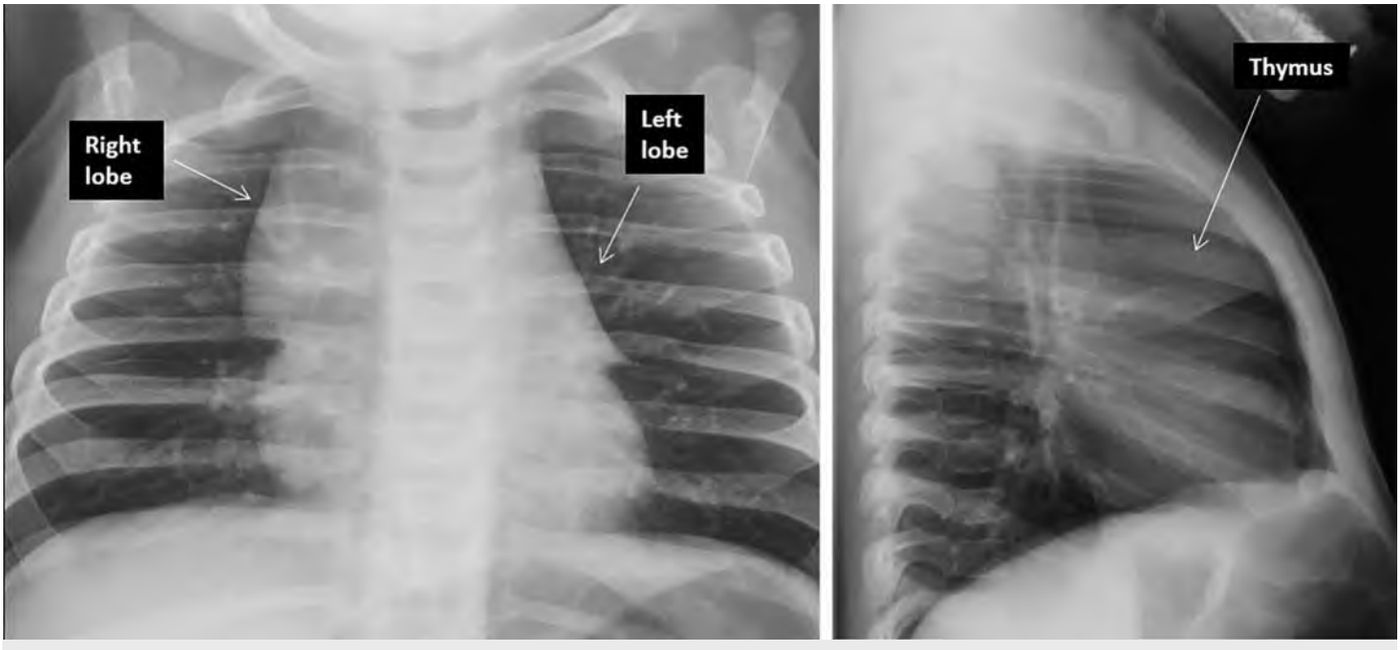

Fig. 3.11 Large thymus in a pediatric patient. Anteroposterior and lateral chest X-rays showing bilobed appearance of the thymus.

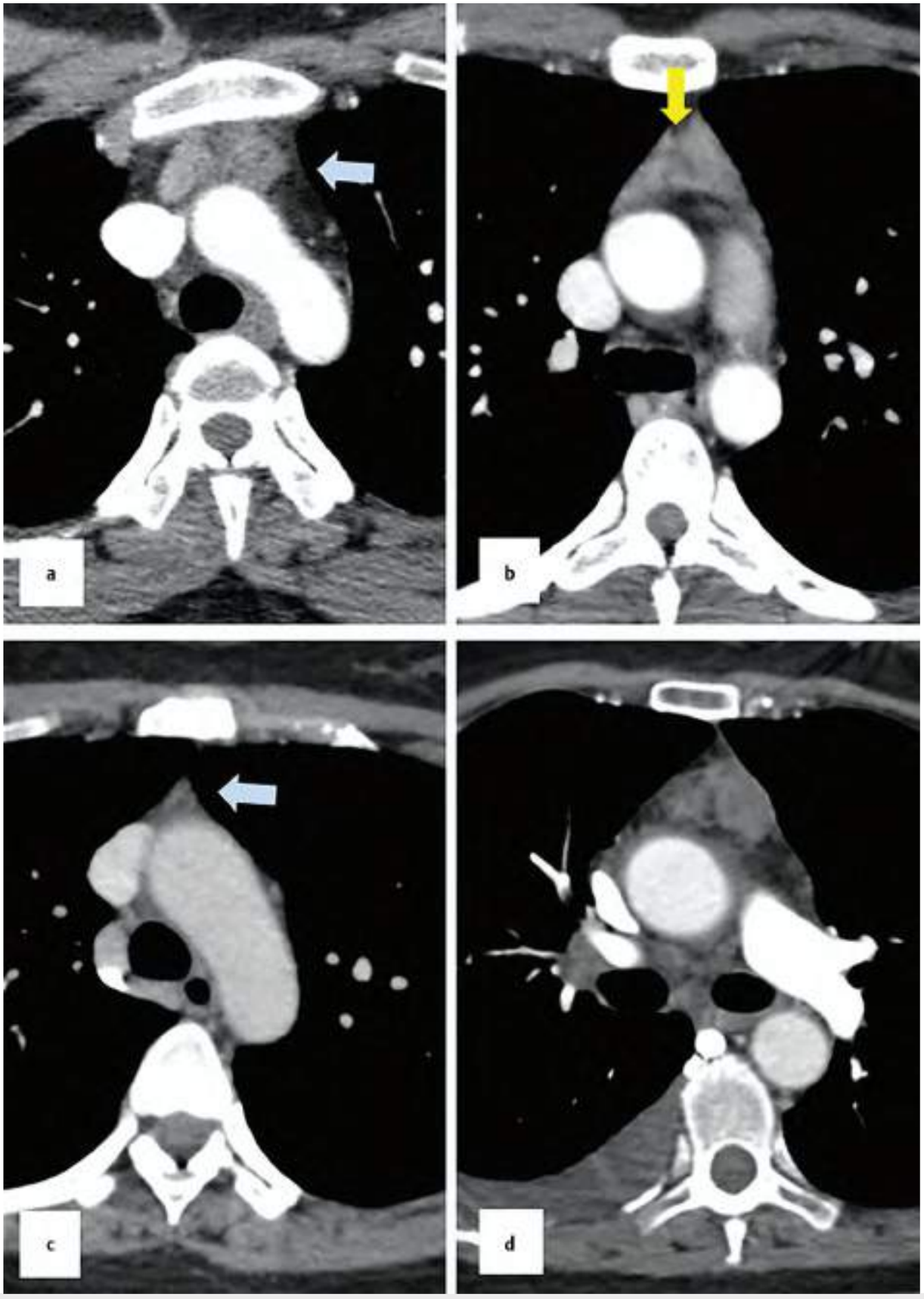

Fig. 3.12 Serial images of the thymus (*arrows*) demonstrate normal involution as age increases in a **(a)** 14-year-old, **(b)** an 18-year old, **(c)** a 24-year old patient. Note the normal bilobed appearance of the thymus in **(a)** and triangular shape which conforms to the mediastinum in **(b)**. Intercalated fat within the thymus increases with age. With close attention, the intermediate lobe of the thymus (*arrow* in **c**) can be seen as a distinct structure which maintains a connection between the left and right lobes. In certain patients, thymic rebound is also observed, for example **(d)** an adult female undergoing chemotherapy. Notice the thymus maintains a bilobed appearance in **(d)**.

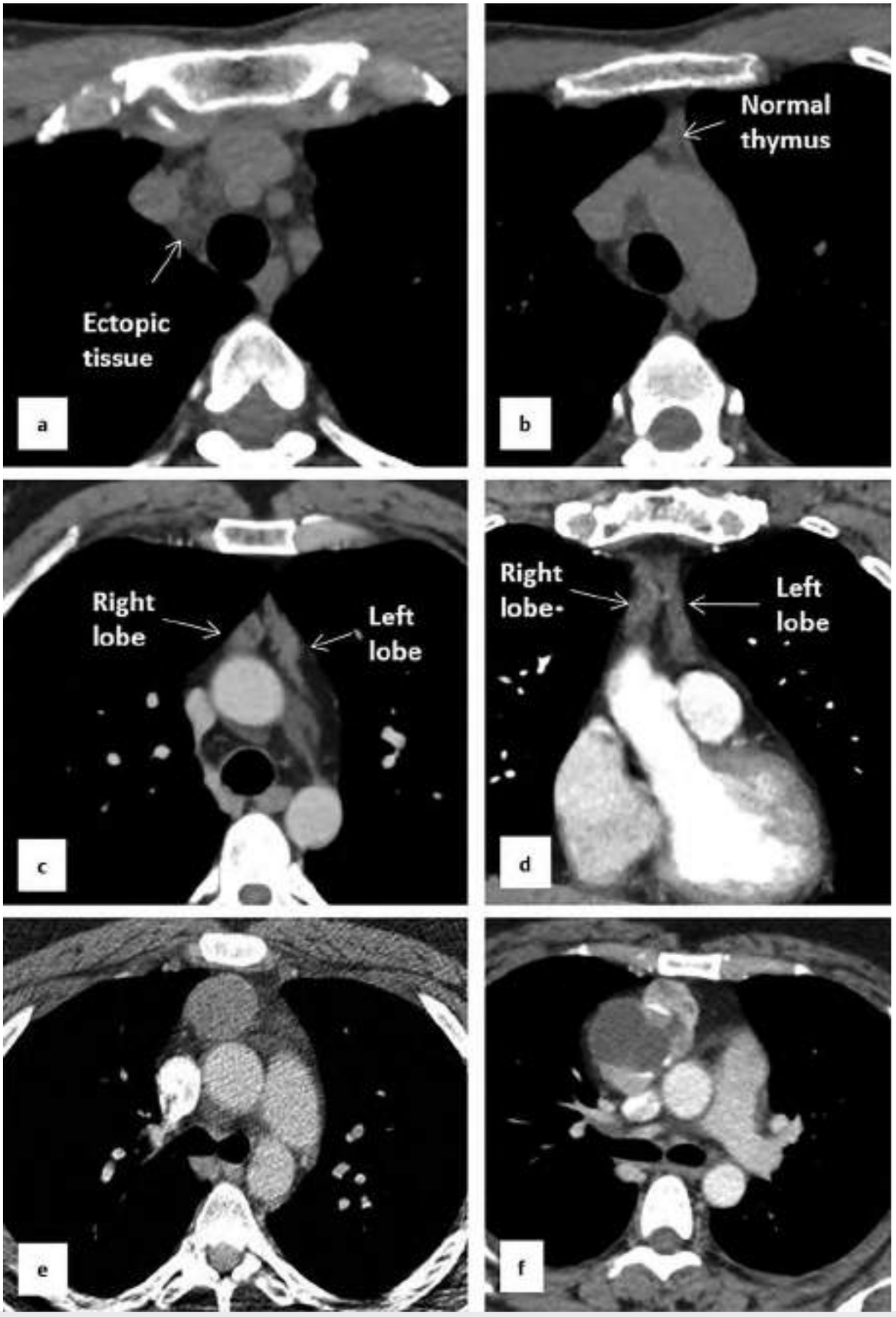

Fig. 3.13 **(a,b)** Axial CT images showing ectopic thymic tissue in the right paratracheal region medial to the superior vena cava in a 22-year-old patient with normal thymus. Ectopic thymus in usually seen in aortopulmonary window in 20% and aortocaval groove in 12% of cases. **(c)** Axial and **(d)** coronal CT showing thymic hyperplasia in a 36-year-old man. The two lobes of the thyroid are nicely shown. **(e)** Thymoma; **(f)** teratoma. Teratoma usually contains different mesenchymal elements such as fat and calcification that makes diagnosis easy. Myasthenia gravis is a distinct clinical presentation of the thymoma and thymic hyperplasia.

space remaining as one continuous structure.[18,19] These lobules and lobes can be appreciated on CT scans readily as a normal finding which distinguishes the thymus from normal and abnormal adjacent structures.

The thymus may also become hyperplastic in patients. When the body is under stress, the thymus may actually shrink with a rebound enlargement after removal of stress. This phenomenon is most common in pediatric and adolescent patients after periods of stress (burns, surgery, infection, steroids) but is also known to happen commonly in adults after chemotherapy or radiotherapy and has also been reported with steroid use, after surgery, and with infection (▶ Fig. 3.13). Common pathologies of the thymus include thymic cyst and thymoma (▶ Fig. 3.13). Thymoma usually presents as a well-defined mass in the prevascular mediastinum. It should be differentiated from other common pathologies in this region such as teratoma or lymphoma. Myasthenia gravis is a distinct clinical presentation of the thymoma and thymic hyperplasia.

The thymus maintains several connections to adjacent structures via ligaments and direct connections to maintain a relatively suspended position in the prevascular space of the mediastinum.[19] Superiorly, a thyrothymic ligament connects directly to the inferior thyroid (▶ Fig. 3.10). Posteriorly, a layer of fascia maintains a connection to the brachiocephalic veins and aorta/great vessels. Inferiorly, connective tissue maintains a connection with the pericardium, a connection which persists from early development.

When discussing thymic arterial or venous anatomy, it is always important to remember that considerable variation exists.[20,21] Thymic arterial blood supply arrives via the superior, lateral, and posterior thymic arteries. The ultimate origin of these arteries is variable; arising from the inferior thyroid artery, internal thoracic artery, pericardiophrenic artery, or anterior intercostal arteries. The superior thymic artery usually arises from the inferior thyroidal artery or middle thyroid artery. The lateral thymic arteries are usually branches of the right and sometimes left internal thoracic artery. When present, the posterior thymic arteries are direct branches of the brachiocephalic artery and aorta. Venous drainage is accomplished by a venous plexus predominating on the posterior side of the thymus (▶ Fig. 3.14). This plexus is drained by two small veins on the posterior side of each thymic lobe. Finally, these smaller veins join to form a larger single thymic vein (sometimes referred to as the great vein of Keynes).[20] This thymic vein ultimately drains into the left brachiocephalic vein. Variant anatomy exists where separate thymic veins drain into the left inferior thyroidal vein, internal thoracic vein, or superior vena cava.

◆ Mediastinal Fat

Mediastinal (pericardial) fat is generally unencapsulated fat which encases the various mediastinal structures without compression or displacement, a characteristic trait of benign mediastinal fat. It should not be confused with the epicardial (subepicardial) fat which is located between the visceral layer of the pericardium and the myocardium (▶ Fig. 3.15).[22,23] Mediastinal fat predominates in the prevascular compartment (i.e., anterior mediastinum). The epicardial adipose tissue is supplied by branches of the coronary arteries, whereas the mediastinal fat is supplied from different sources including the superior pericardial, middle pericardial, and pericardiophrenic arteries, branches of the internal mammary artery.[23] When the amount of fat is abnormally increased, it is usually referred to as mediastinal lipomatosis which is commonly due to obesity, diabetes, and exogenous steroid use (▶ Fig. 3.16). Excess fat in the mediastinum can influence patency of the vessels.[24]

◆ Lymph Nodes

Thoracic mediastinal lymph nodes serve to filter lymph through a series of lymphatic vessels. Lymph nodes play a vital role in filtering infections and debris before entering the bloodstream, but they also act as a conduit to collect malignant cells. In this regard, they serve as an important prognosticator when evaluating lung and other types of cancers.

The pattern of mediastinal lymphadenopathy has become an integral part of lung cancer staging. Chief among the staging systems is the clinical TNM (cTNM) staging system which is typically used before any treatment regimen for lung cancer is begun. This system attempts to reliably stage a patient's cancer based on the extent of disease with local, regional, or distant lymph node involvement as a key determinant of disease stage. Several standardized nomenclature systems have been developed; however, the one adopted by the International Association for the Study of Lung Cancer (IASLC) appears to be the most widely used[25] (▶ Fig. 3.17, ▶ Fig. 3.18, ▶ Fig. 3.19). Lymph node stations of the mediastinum are classified in ▶ Table 3.2.

However, care must be taken when localizing lymph nodes, as not all the mediastinal lymph nodes are classified under the IASLC lymph node map. Lymph node groups that have not been explicitly classified include diaphragmatic lymph nodes, which appear around the diaphragm; some authors may consider these to be prevascular lymph nodes as they are anterior to the pericardium (see Chapter 10, Diaphragm) (▶ Fig. 3.20). Intercostal lymph nodes and internal mammary artery lymph nodes are very close and appear contiguous with the mediastinum but would be considered chest wall structures.[26]

Mediastinal lymph nodes primarily drain lymph from the lungs and pulmonary hila in certain patterns. While we will review some of the most common pathways for lymph node drainage, it should be noted that considerable variability exists between many of studies done to date on this topic.[27,28]

With that said, the right upper lobe tends to drain to the right paratracheal station (level 4R) and prevascular (level 3A) lymph nodes, both of which are above the level of the heart (▶ Fig. 3.20). For example, isolated subcarinal lymphadenopathy is much less common in right upper lobe cancers. From the 4 R level, lymph tends to drain into the high right paratracheal (2R) and then scalene/supraclavicular lymph nodes. The right middle lobe, however, most frequently drains to the subcarinal station (level 7) followed by the lower right paratracheal station (level 4R). The right lower lobe is most commonly seen draining to the subcarinal (level 7) and paraesophageal (level 8) stations.[29]

The left upper lobe malignancies seem to drain to the subaortic and para-aortic lymph nodes (level 5 and 6) and left low paratracheal (4L). Note should be made that the lingula actually drains to

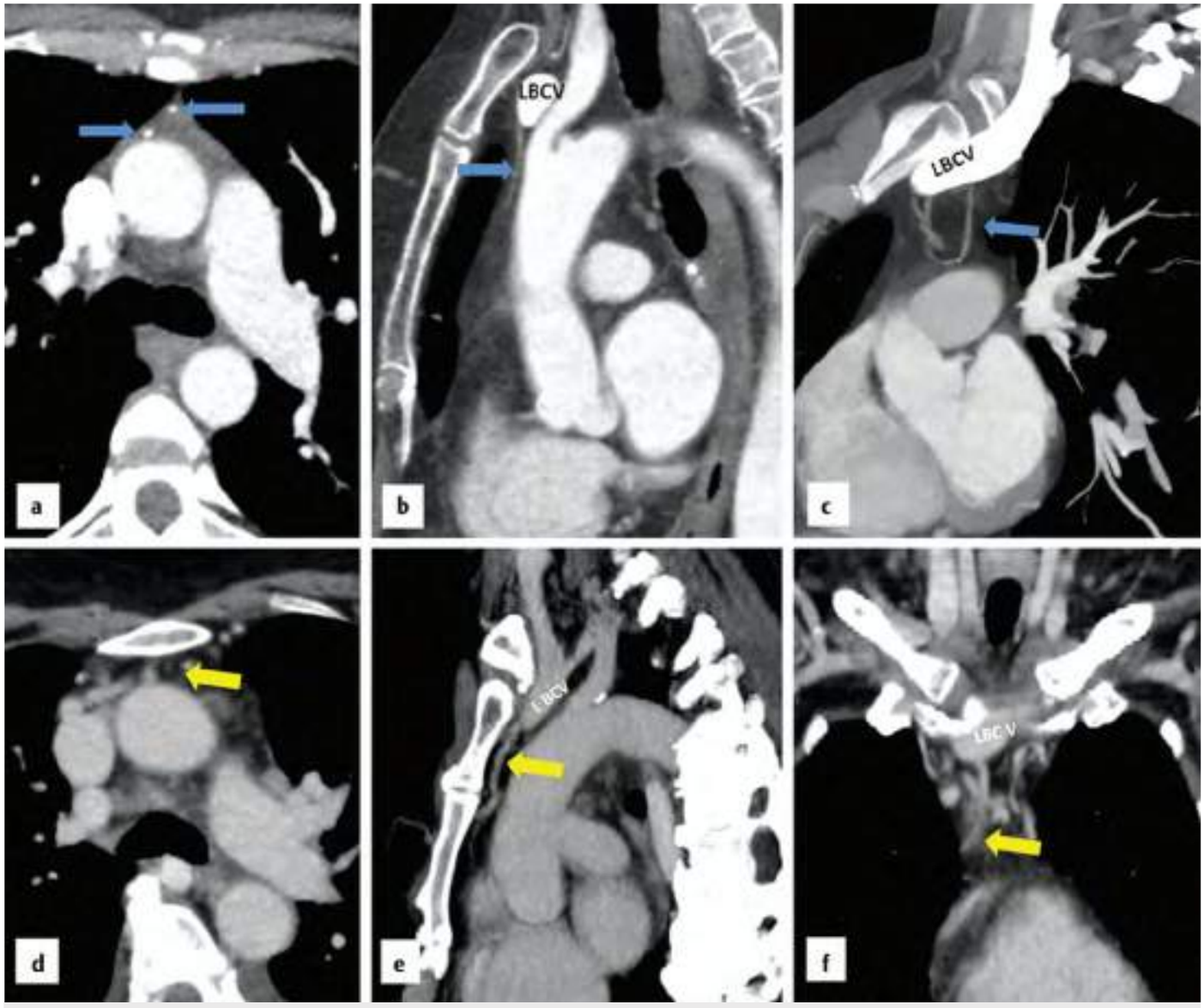

Fig. 3.14 Thymic veins are shown in two different cases. **(a–c)** Axial, sagittal, and coronal CT images. Thymic venous drainage is variable, but a common pattern is of several small veins draining to a dominant great vein of Keynes (*blue arrow*) which then will drain into the left brachiocephalic vein (LBCV) as it crosses the mediastinum. **(b, c)** The great vein of Keynes can be quite tortuous. **(d–f)** Same projections in a different patient showing more extensive venous channels in the anterior mediastinum with the majority draining into the brachiocephalic vein or superior vena cava.

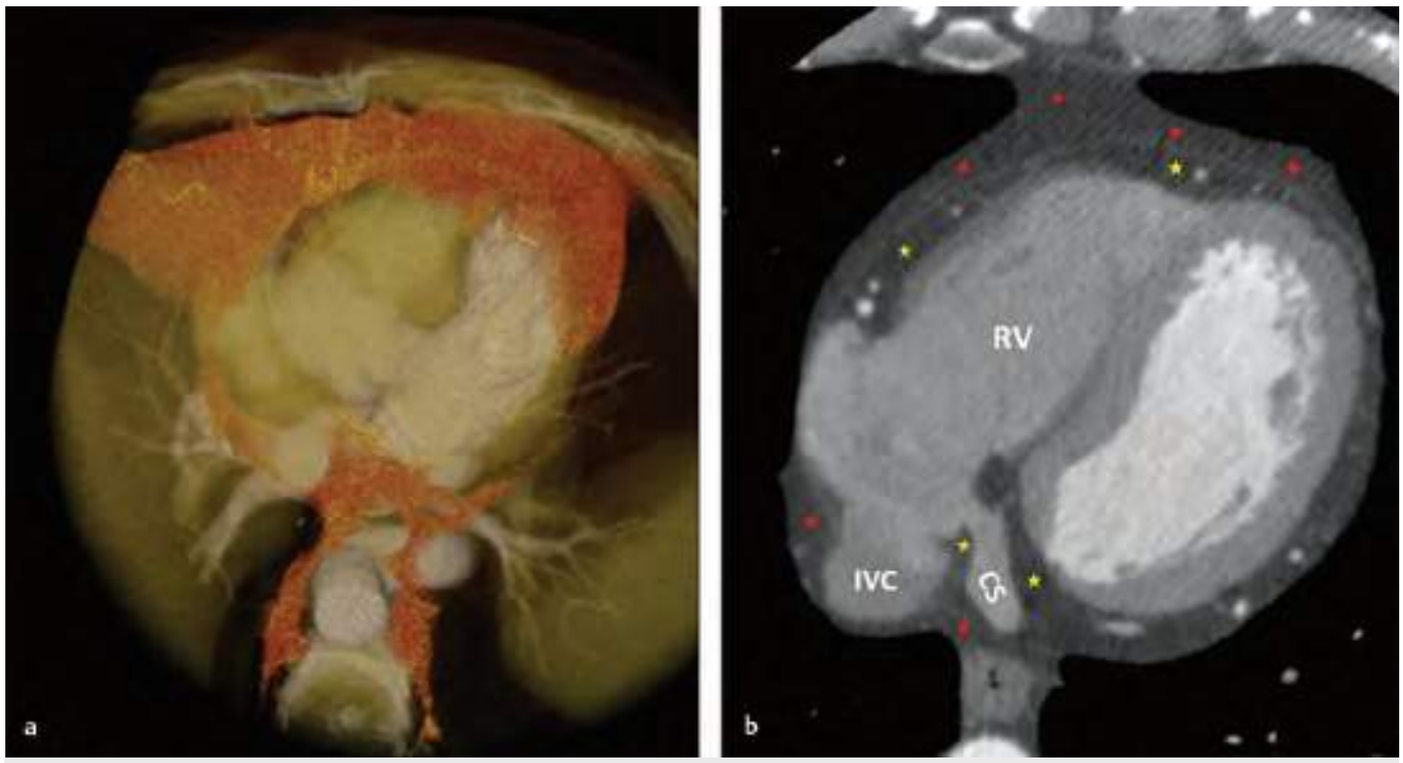

Fig. 3.15 Mediastinal fat: **(a)** Three-dimensional CT color mapping showing the mediastinal fat in orange color. **(b)** Axial image of the heart at the level of the coronary sinus (CS) shows different compartments of the intrathoracic fat including the mediastinal (*red stars*) fat and the epicardial fat (*yellow stars*). The pericardial sac is shown as a thin line between the two compartments. The mediastinal fat is located outside the pericardium and the epicardial fat is located between the pericardial sac and the myocardium. The coronary vessels and the coronary sinus are embedded in the epicardial fat. CS, coronary sinus; IVC, inferior vena cava; RV, right ventricle.

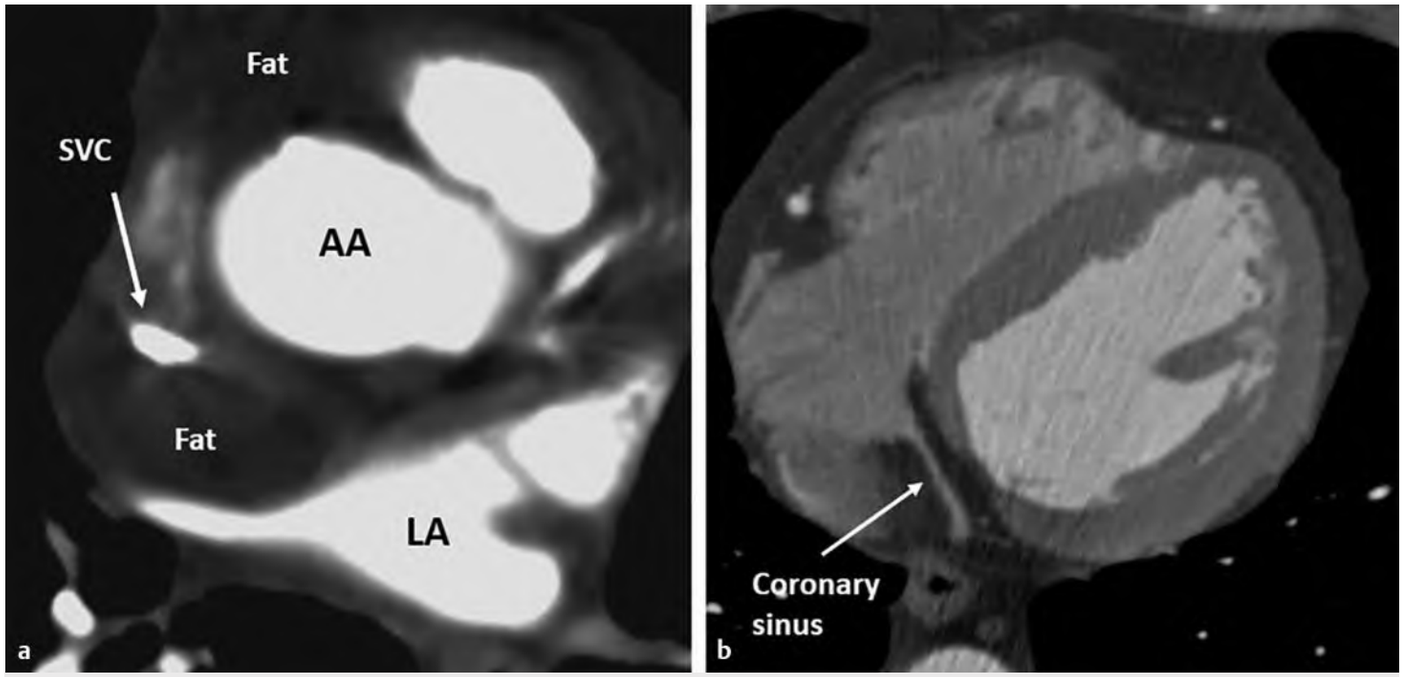

Fig. 3.16 **(a)** Mediastinal lipomatosis compressing vessels. **(b)** Axial image; fatty infiltration around the superior vena cava (SVC) can cause obstruction and difficulty in passing catheters. **(b)** Axial image of the heart showing stenosis of the coronary sinus due to excess fat accumulation AA, ascending aorta; LA, left atrium.

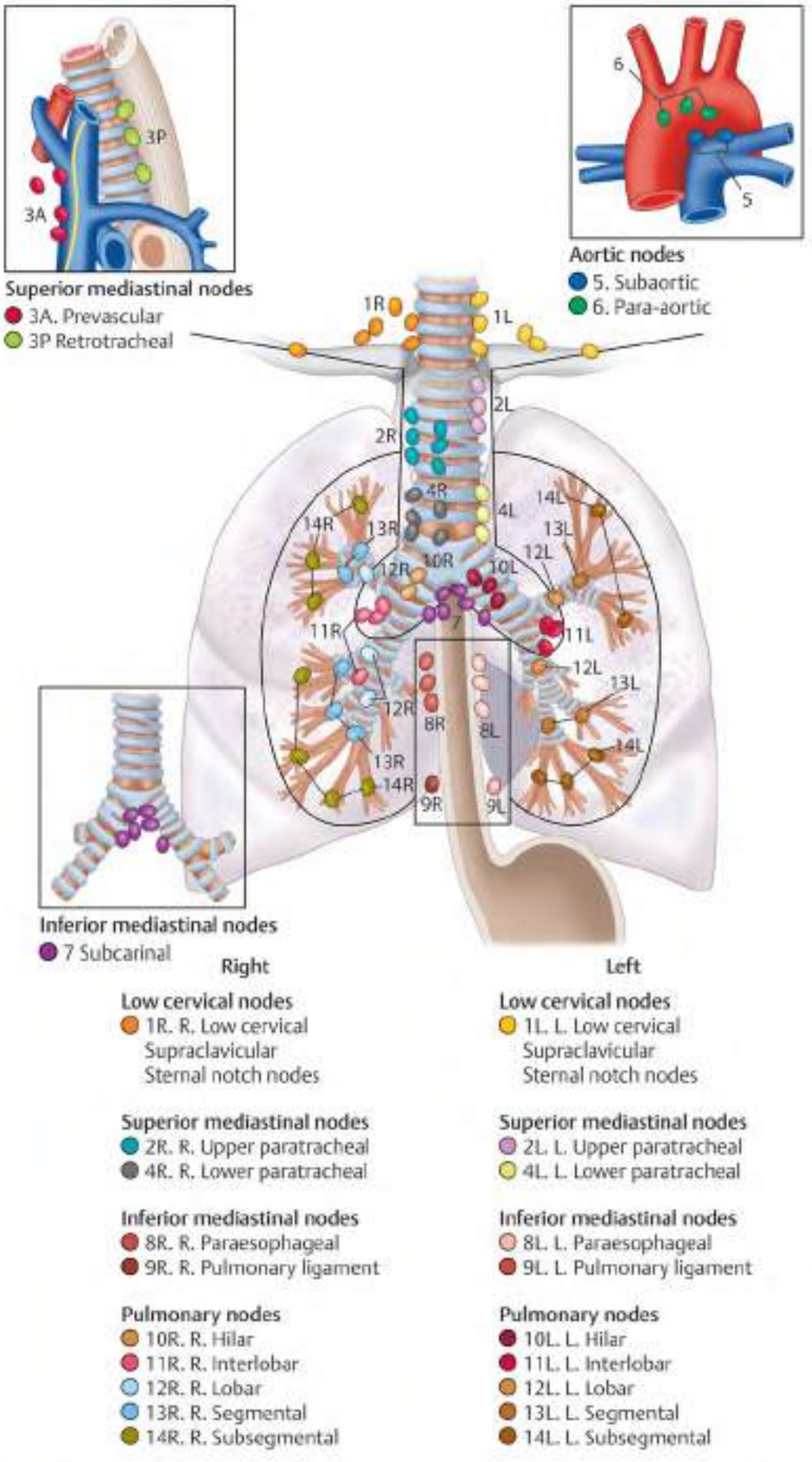

Fig. 3.17 IASLC lymph node map. Adapted from El-Sherief et al 2014.[25]

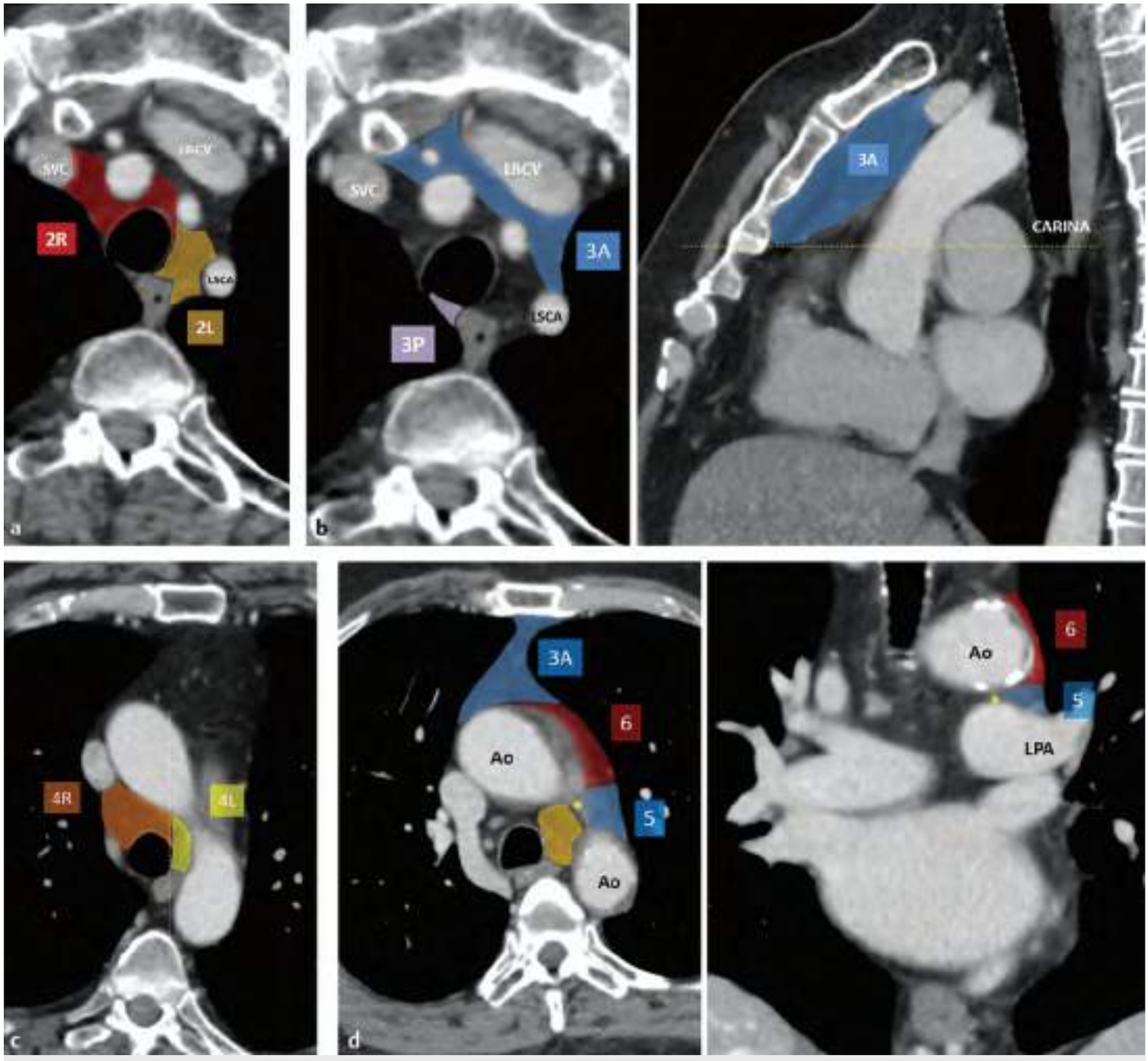

Fig. 3.18 (a–d) Lymph node station based on International Association for the Study of Lung Cancer (IASLC) classification. Border of 4 L and 4 R is the left wall of the trachea. Lateral margins of both the subcarinal and paraesophageal stations are the medial walls of the bronchi. The inferior-most extent of level 7 is the lower border of the bronchus intermedius on the right and left lower lobe bronchus on the left, after which level 8 arises. When the right middle lobe (RML) bronchus (*) or the left lower lobe bronchus is seen, then you are looking at level 8. Level 9 lymph nodes are located at the inferior pulmonary ligament on either side, spanning from the inferior pulmonary vein to the diaphragm. Ao, aortic arch; LBCV, left brachiocephalic vein; LSCA, left subclavian artery; LPA, left pulmonary artery; SVC, superior vena cava.

(*Continued*)

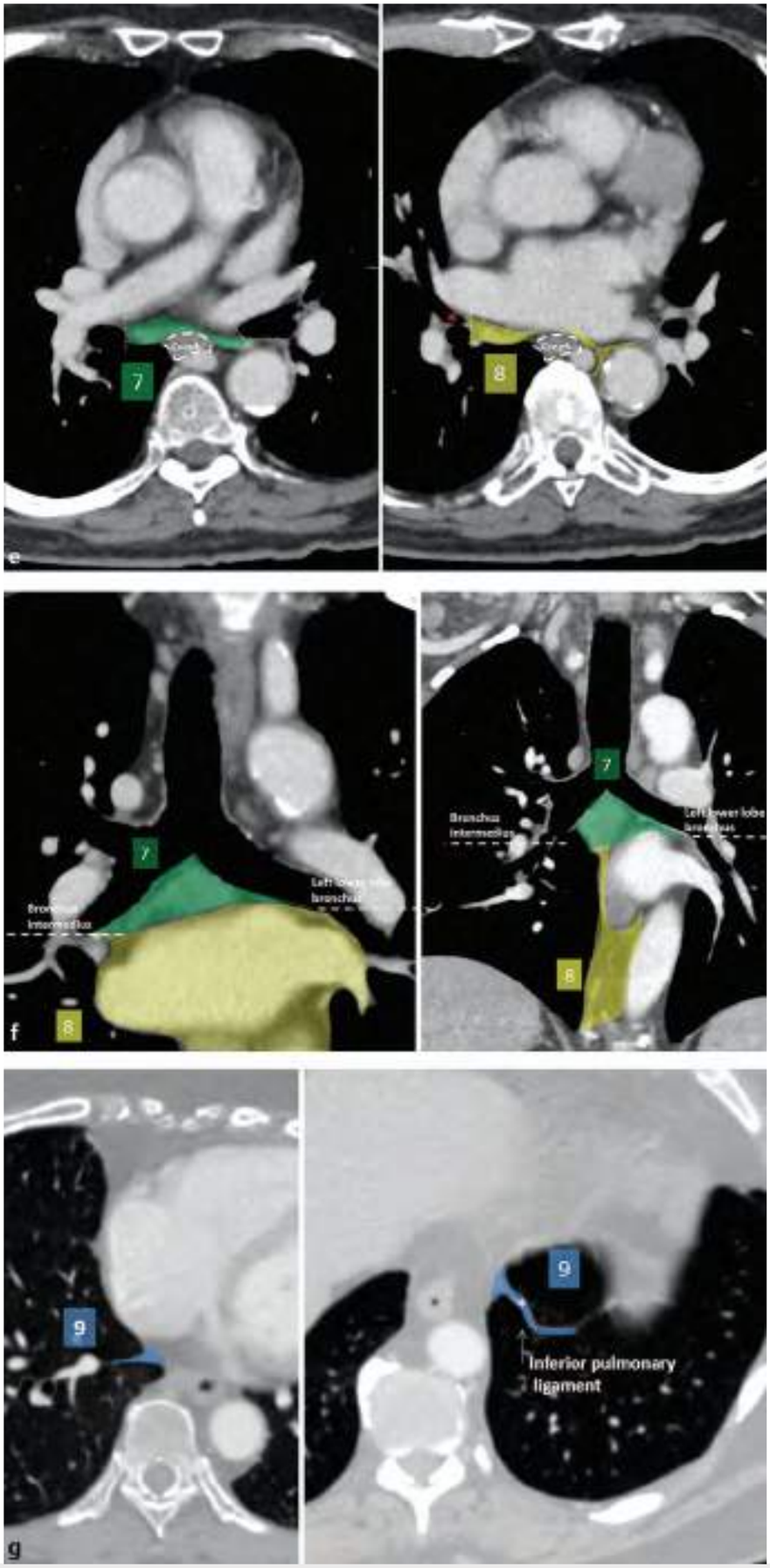
7
8
e
7
Bronchus intermedius
8
f
9
9
Inferior pulmonary ligament
g

Fig. 3.18 (e–g)

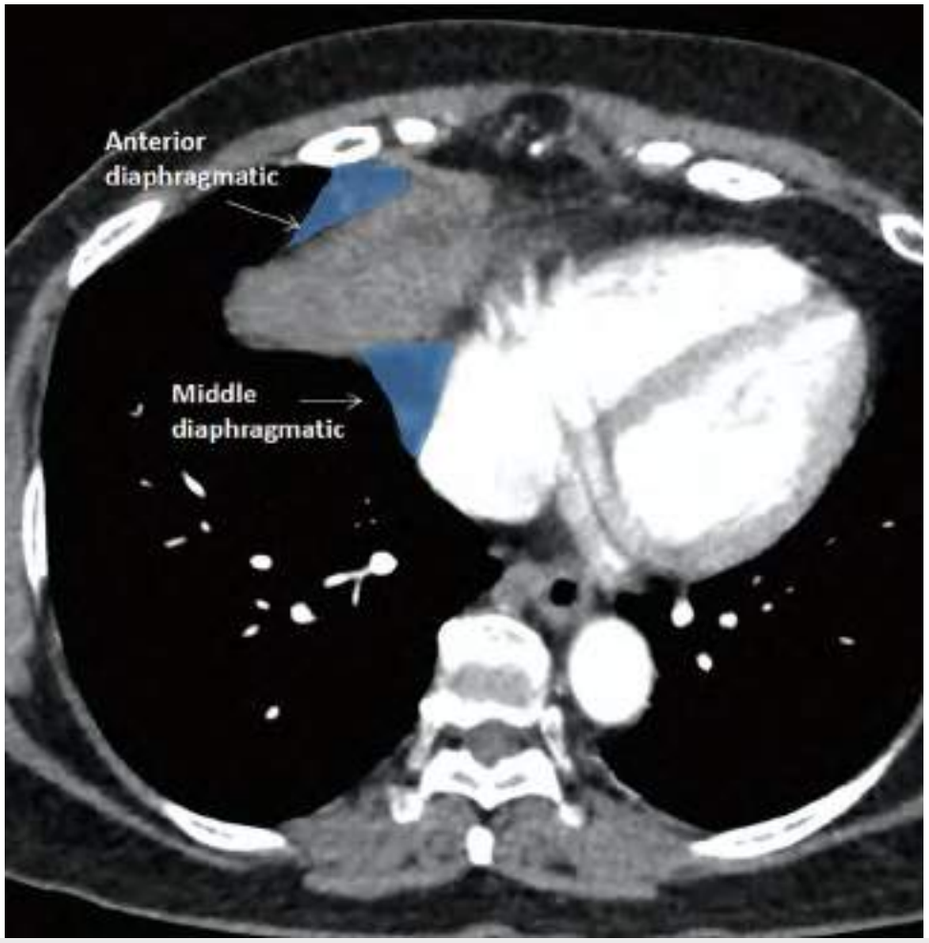

Fig. 3.19 Mediastinal lymph nodes that do not fall into the current IASLC map, anterior and midline diaphragmatic lymph nodes.

the subcarinal lymph nodes first, then to the subaortic and paraaortic stations.

Finally, the left lower lobe tends to drain to the subcarinal station[7] followed by subaortic,[5] left paratracheal (4L), paraesophageal,[8] and inferior pulmonary ligament[9] lymph nodes. The left lower lobe is notable as it tends to drain to contralateral mediastinal lymph nodes more frequently than any other lobe (▶ Fig. 3.20).

The mediastinal lymph nodes receive vessels from the lungs, thymus, thyroid, esophagus, diaphragm, liver, pericardium, and heart.

◆ Lymphatic Vessels

Lymphatic vessels refer to small lymphatic veins and even smaller lymphatic capillaries. These are specialized vessels with higher levels of permeability, allowing them to collect protein-rich fluids, which are called lymph. These small lymphatic vessels in the neck, thorax, and abdomen eventually merge to form the thoracic duct, which has a long portion of its course in the visceral compartment of the mediastinum (middle mediastinum). Lymph vessels contain numerous valves and have smooth muscle in their walls to aid in lymph drainage. This smooth muscle becomes important in certain disease states such as lymphangioleiomyomatosis.

Before entering the mediastinum from the abdomen, four major lymph trunks merge to form a large collecting pool of lymph called the cisterna chyli (see Chapter 9, Lymphatics and Nerves of the Thorax). This cisterna chyli is appreciated on CT as a tubular-appearing structure running in the retrocrural space on the right.[30] From this point, the lymph is directed into the thorax in a tubular channel called the thoracic duct. In general, it is best to think of the thoracic lymphatic vessels as draining this lymph toward the mediastinal lymph nodes and the thoracic duct. Lymph is passed into the various mediastinal lymph nodes where it intermixes with cells of the immune system.

Thoracic Duct

The thoracic duct is the largest lymphatic vessel, measuring 38 to 45 mm in length and 2 to 5 mm in diameter. Aside from the right head/neck, right upper thorax and right upper extremity, it is the end point of much of the lymph drainage in the body.[30] The thoracic duct starts at the superior pole of the cisterna chyli, at the level of the diaphragmatic crus just anterior to the vertebral bodies, travels into the posterior mediastinum via the aortic hiatus of the diaphragm (▶ Fig. 3.21). Usually at the T5 vertebral level, the thoracic duct arcs to the left of the thoracic spine as it continues cranially into the neck. Along its course through the mediastinum, the thoracic duct drains tributaries from various sites in the

Table 3.2 Mediastinal lymph node stations

Name	Station	Borders
Right upper paratracheal	2R	**Superior:** Apex of the right lung/pleural space and the upper border of manubrium
		Inferior: Intersection of left innominate vein with trachea
		Left: Left border or trachea
		Right: Mediastinal pleura
Left upper paratracheal	2L	**Superior:** Apex of the right lung/pleural space and upper border of manubrium
		Inferior: Superior margin of aortic arch
		Left: Mediastinal pleura
		Right: Left lateral border of trachea
Prevascular	3A	**Superior:** Upper border of manubrium
		Inferior: Carina
		Anterior: Posterior aspect of sternum
		Posterior: Anterior border of SVC, great vessels, and pericardium
		Left: Left pleura
		Right: Right pleura
Retrotracheal	3P	**Superior:** Apex of chest
		Inferior: Carina
		Anterior: Posterior aspect of trachea
Right lower paratracheal	4R	**Superior:** Intersection of left innominate vein with trachea
		Inferior: Lower border of azygous vein
		Left: Left lateral border of trachea
Left lower paratracheal	4L	**Superior:** Superior border of the aortic arch
		Inferior: Upper border of the main pulmonary artery
		Left: Ligamentum arteriosum
		Right: Left lateral border of trachea
Subaortic (AP windows)	5	**Superior:** Lower border of aortic arch
		Inferior: Upper border of left main pulmonary artery
		Right: Ligamentum arteriosum
Para-aortic	6	**Superior:** Line tangential to the upper border of the aortic arch
		Inferior: Lower border of the aortic arch
		Anterior: Imaginary horizontal line from the anterior wall of aortic arch
Subcarinal	7	**Superior:** Carina of the trachea
		Inferior: Upper border of the lower lobe bronchus and lower border of the bronchus intermedius
		Left: Medial margin of the main bronchus
		Right: Medial margin of the right main bronchus and bronchus intermedius
Paraesophageal	8	**Superior:** Upper border of the left lower lobe bronchus and lower border of the bronchus intermedius
		Inferior: Diaphragm
Inferior pulmonary ligament	9	**Superior:** Inferior pulmonary vein
		Inferior: Diaphragm

Abbreviation: SVC, superior vena cava.

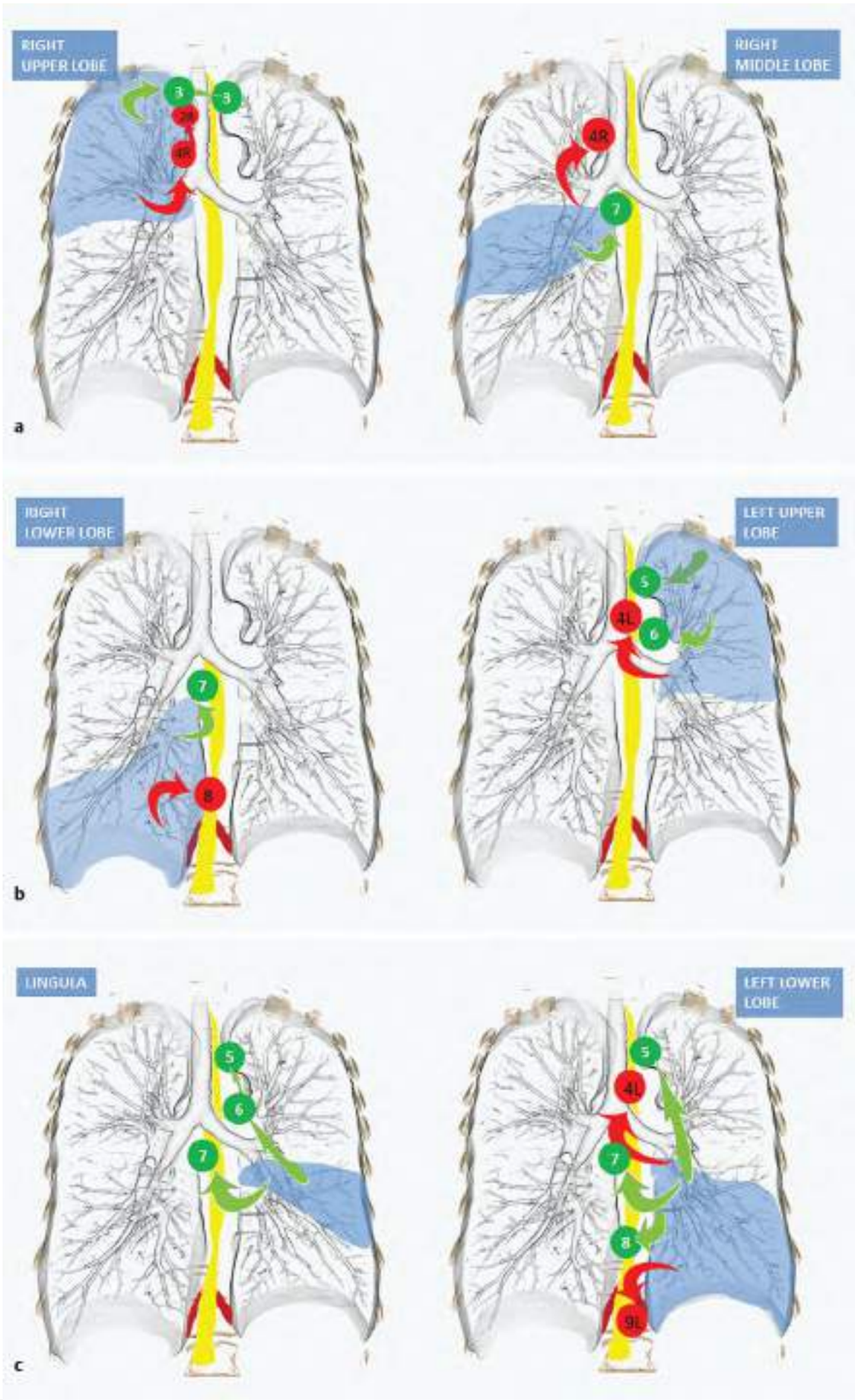

Fig. 3.20 (a–c) Common patterns of lymph drainage from the lung lobes.

thorax such as intercostal lymph channels, left subclavian, and sometimes the left bronchomediastinal trunk. Some lymphatic channels take an anodal course to empty into the thoracic duct, meaning that lymph channels directly drain lymph from an organ into the thoracic duct bypassing any lymph nodes en route. The diaphragm, esophagus, and lower lobes of the lungs have been known to take an anodal pathway into the thoracic duct.[31,32] This anodal route is thought to be an important reason why cancers arising at these locations have poorer prognosis, as their metastases can more easily travel systemically.

◆ Nerves

Nerves of the mediastinum are often overlooked when evaluating with CT and MRI images, due to their small size and unremarkable appearance.[33,34] This is ironic as the nerves which intervene the mediastinum have critical, sometimes life-sustaining functions ranging from diaphragmatic function/breathing via the phrenic nerve to vocal cord function via the recurrent laryngeal nerve. Knowledge of these nerves becomes more important in postoperative cases or when dealing with malignancies, in which cases the nerves may be disrupted or damaged. The major nerves within the mediastinum are the vagus and phrenic nerves, sympathetic trunks and ganglia, autonomic plexuses, and the thoracic spinal nerves.

Phrenic Nerves

There are two phrenic nerves, one on the right and one on the left. The phrenic nerves are primarily responsible for diaphragmatic motor function as well as sensory supply to the diaphragm, mediastinal pleura, and pericardium.

The phrenic nerves originate in the neck from the C3–C5 nerve roots and pass into the mediastinum through the thoracic inlet (▶ Fig. 3.22). The right phrenic nerve enters between the right subclavian artery and vein and travels along the posterolateral side of the right brachiocephalic vein. The left nerve enters the thoracic inlet between the left subclavian artery and vein and travels between the left subclavian artery and left common carotid arteries. As they pass into the mediastinum, both nerves are usually located in the prevascular compartment, although they usually do pass laterally in a very small space between the pericardium and the mediastinal pleural surface. Both phrenic nerves pass anterior to the pulmonary hila and ultimately subdivide into many terminal branches at each hemidiaphragm, on both the cranial and caudal surfaces of the muscle (▶ Fig. 3.23▶ Fig. 3.24). The phrenic nerves derive arterial blood supply from the pericardiophrenic artery.

The phrenic nerves themselves are usually not seen at CT, unless they are encased or adjoined by a layer of pleura, which then makes them apparent.[35,36] The right phrenic nerve is usually appreciated as a rounded structure measuring 1 to 3 mm adjacent to the pericardium and seen in at least two contiguous sections. It is many times identified lateral to the vena cava as opposed to posterior or anterior to it[37] (▶ Fig. 3.24). One of the major results of injury or impairment of the phrenic nerve is diaphragmatic paralysis. This can be the result of common surgical procedures such as coronary artery bypass grafting, and also lung and mediastinal procedures, including complication of radiofrequency catheter ablation for arrhythmia.[38]

Pericardiophrenic Bundle

The pericardiophrenic artery, the pericardiophrenic vein, and the pericardiophrenic nerve collectively form the pericardiophrenic bundle (PCB) (▶ Fig. 3.25). The PCB is an important landmark for preoperative planning of radiofrequency catheter ablation for arrhythmia and pulmonary vein isolation. In these procedures the phrenic nerve can be injured and identifying the location of this nerve can identify patient who are more vulnerable to injury. Identifying the vessels in the bundle can be used as a reliable proxy for the phrenic nerve. The pericardiophrenic bundle can be identified on contrast-enhanced CT, in up to 74% of patients on the left and 47% of patients on the right. Variability in the amount of mediastinal fatty tissue and phase of contrast during imaging has been implicated as reasons for why these bundles are sometimes seen and sometimes not seen. Intravenous contrast is essential as the artery and vein within the bundle must be highlighted. The PCB should be imaged with gated CT and will enhance late relative to the coronary arteries. The left bundle is most apparent on CT when it comes into contract with the aortic arch, left atrial appendage, and along the lateral wall of left ventricle.[36] The right phrenic is most apparent on CT at the level of the right atrium and at the angle of the IVC with the right hemidiaphragm (▶ Fig. 3.24).

Vagus Nerves

There are two vagus nerves, one on the right and another on the left. Each nerve enters the mediastinum behind the sternoclavicular joint and the brachiocephalic vein.[34] Above the heart, the right vagus nerve (RVN) travels to the right of the trachea, somewhat posteriorly (▶ Fig. 3.24). As it travels through the thorax, it passes posterolateral to the great vessels, superior vena cava, and right hilum. At the level of the right hilum, the RVN gives branches to the right pulmonary plexuses. As the RVN continues along the posterolateral aspect of the heart, more branches arise to form the esophageal plexuses, after which the RVN continues into the abdomen. The left vagus nerve (LVN) travels between the left common carotid artery and left subclavian artery after entering the thorax, turning laterally as it reaches the aortic arch (▶ Fig. 3.23, ▶ Fig. 3.24). At the level of the aortic arch, the LVN gives rise to the left recurrent laryngeal nerve, which travels posteriorly curving along the posterior side of the aortic arch. It continues to travel along the left lateral mediastinum near the esophagus and where it gives branches to pulmonary and esophageal plexus, similar to the RVN, before ultimately traveling into the abdomen.

◆ Sympathetic Chains

The sympathetic chain consists of fibers and ganglia that are located in the paravertebral region on each side along a vertical

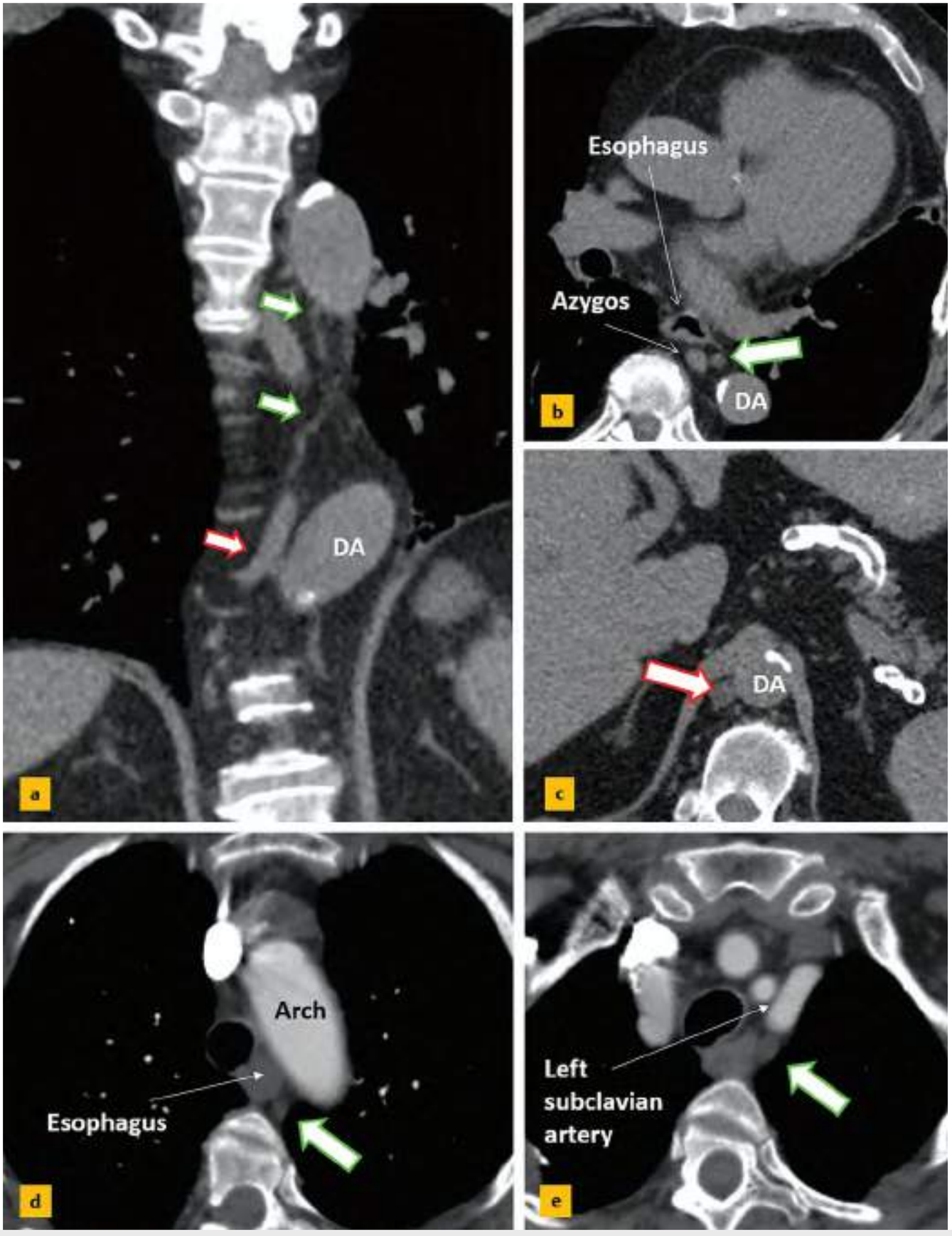

Fig. 3.21 (a–e) Thoracic duct (*arrows*) along its proximal course in the retrocrural region and in the posterior mediastinum. The duct starts at the superior pole of the cisterna chyli, at the level of the diaphragmatic crus (*red white arrows*) just anterior to the vertebral bodies, travels into the posterior mediastinum via the aortic hiatus of the diaphragm, adjacent to the descending thoracic aorta (DA) (*other arrows*).

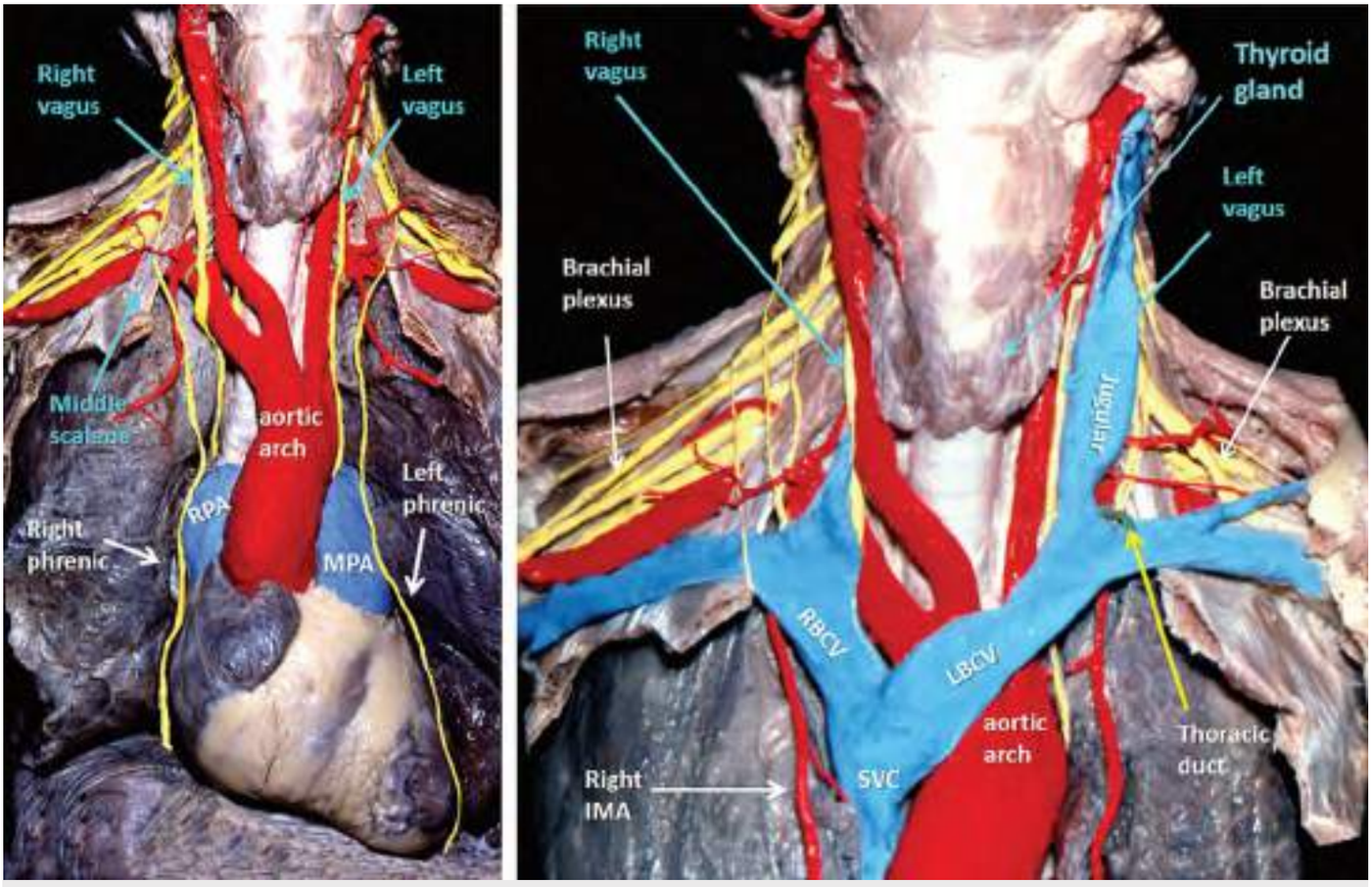

Fig. 3.22 Phrenic and vagal nerves. LBCV, left brachiocephalic vein; MPA, main pulmonary artery; RBCV, right brachiocephalic vein; RPA, right pulmonary artery; SVC, superior cava vena.

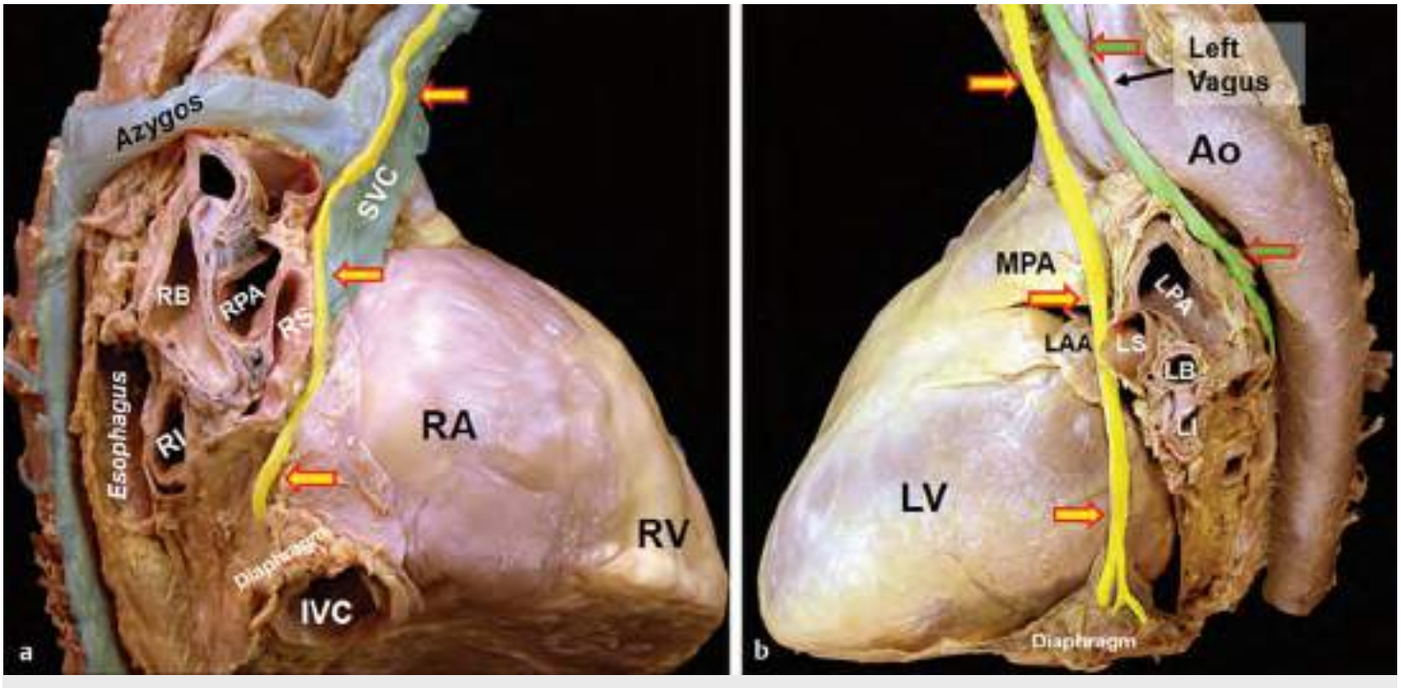

Fig. 3.23 Phrenic and vagal nerves. **(a)** The course of the right phrenic nerve is shown by yellow arrows extending to the right hemidiaphragm. It is closely related to the superior cava vena (SVC), right superior pulmonary vein (RS), and the diaphragm at the level of the inferior vena cava (IVC). **(b)** Dissection of the left phrenic nerve (*yellow arrows*) which descends on the fibrous pericardium anterior and lateral to the aortic arch (Ao), alongside the distal part of main pulmonary artery (MPA), left atrial appendage (LAA), and the lateral wall of the left ventricle (LV) to penetrate the left part of the diaphragm. Note left vagus nerve (*green arrows*) passing close to the aortic arch E and behind the left pulmonary artery (LPA). LB, left bronchus; LI, left inferior pulmonary vein; LS, left superior pulmonary vein; RA, right atrium; RB, right bronchus; RI, right inferior pulmonary vein; RPA, right pulmonary artery; RV, right ventricle; S, esophagus.

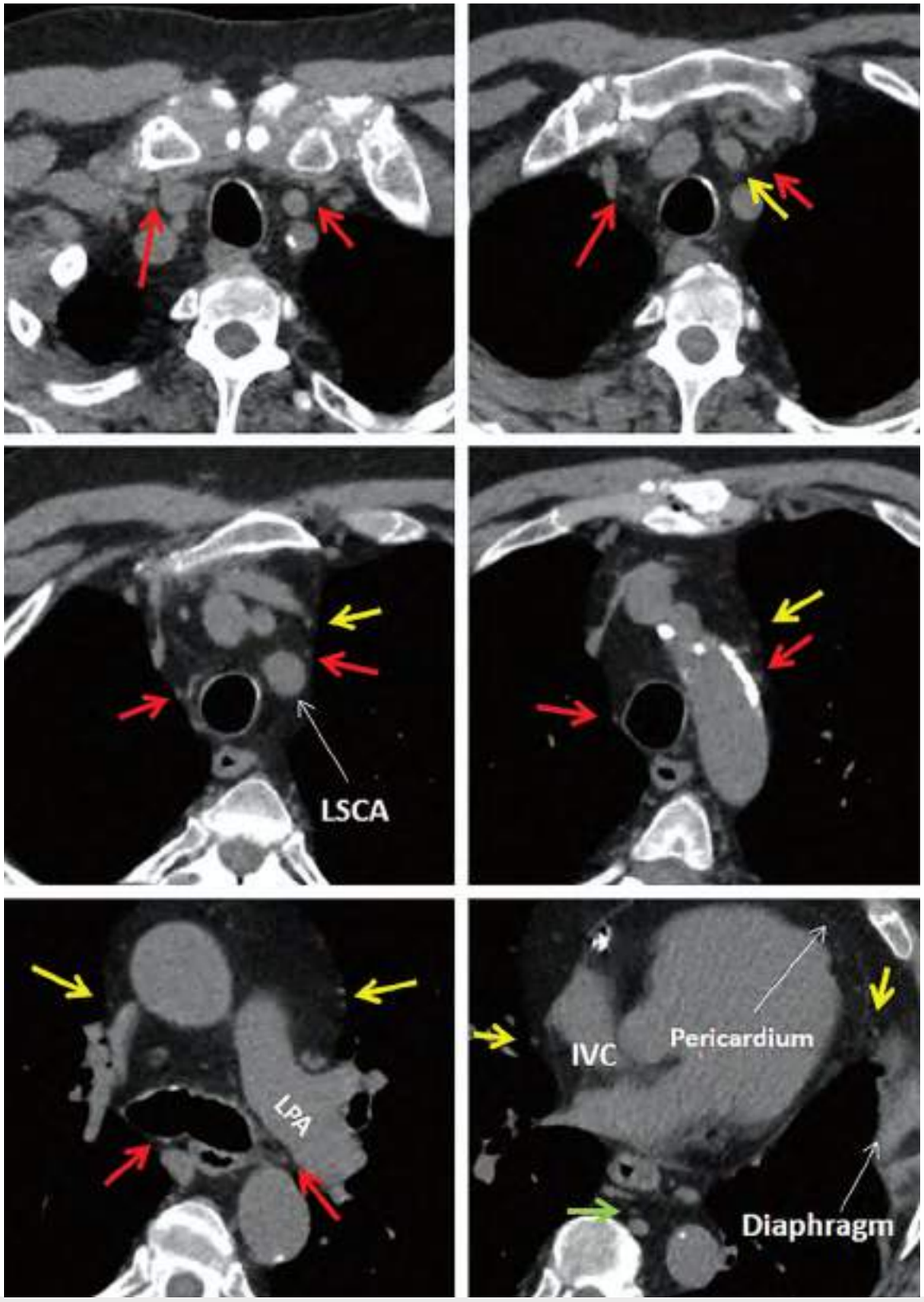

Fig. 3.24 Anatomical course of the phrenic (*yellow arrows*) and vagus (*red arrows*) nerves and their relationship with adjacent structures are shown using axial CT scans. Generally, it would be difficult to show these nerves in routine CT scans except for the left phrenic which is seen in approximately two-thirds of CT angiography studies. In this case, abundant mediastinal fat has helped to see these nerves. Green arrow points to the thoracic duct above the diaphragm. The left neurovascular phrenic bundle is most apparent on CT when it comes into contact with the aortic arch, left atrial appendage, and along the lateral wall of left ventricle. The right phrenic is most apparent on CT at the level of the right atrium and at the angel of the inferior vena cava (IVC) with the right hemidiaphragm. The right vagus nerve is best seen along the lateral margin of the trachea and the left vagus is best seen near the aortic arch. LPA, left pulmonary artery; LSCA, left subclavian artery.

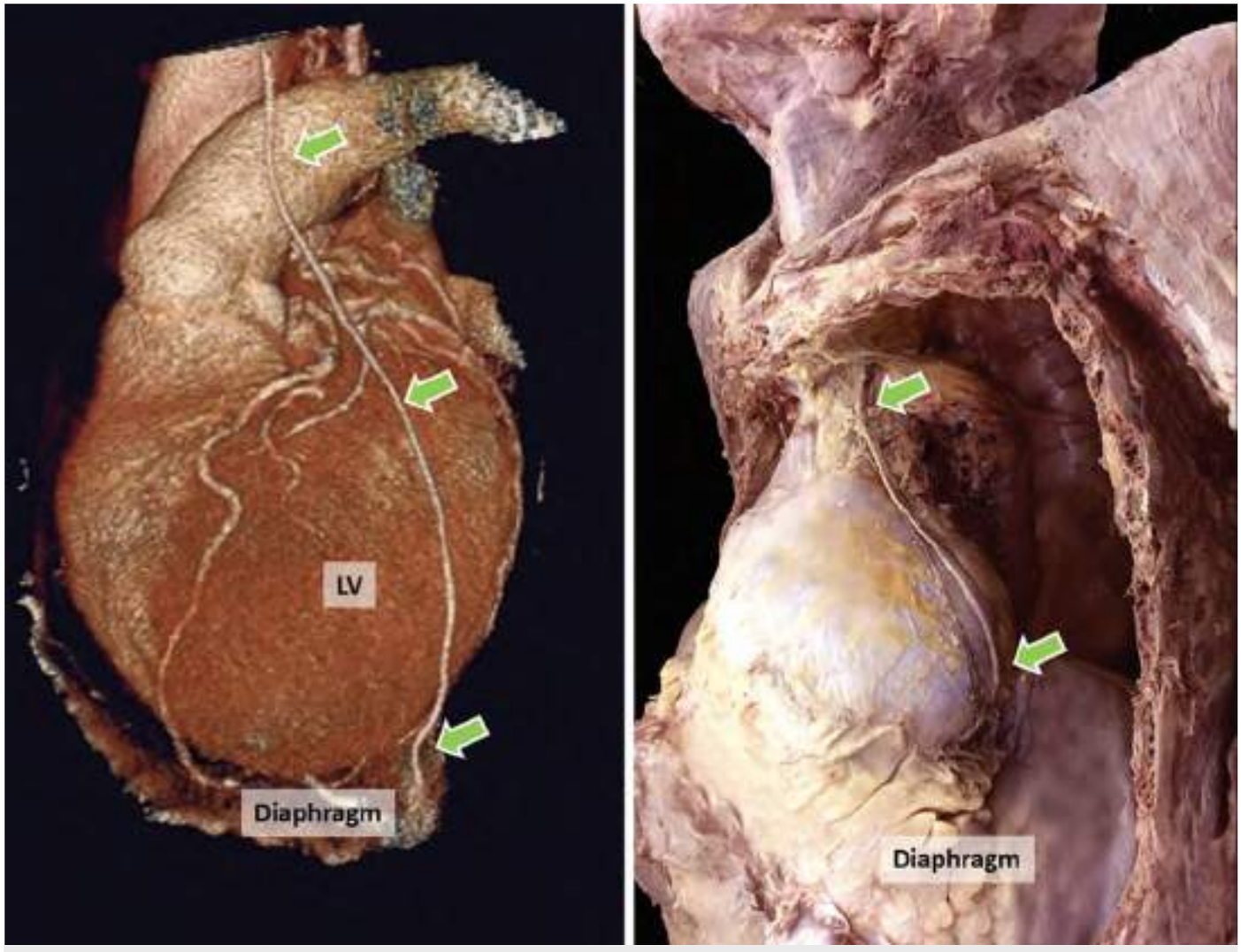

Fig. 3.25 Anatomical course of the left phrenic neurovascular bundle (pericardiophrenic bundle). Left lateral view of 3D CT and cadaveric dissection show the left phrenic nerve running outside pericardium over the left ventricle (LV) and coronary vessels toward the diaphragm (*green arrows*).

line that crosses the necks of the ribs from the thoracic inlet to the diaphragm. Three splanchnic branches arise from each chain and pass medially to the abdominal sympathetic ganglia.[34] Masses arising from these chains present as a solid well-defined tumor in the paravertebral area. CT localization of the sympathetic nerves and ganglia is important for percutaneous thoracic sympathectomy using ethanol injection (▶ Fig. 3.26). This technique is used for treatment of the upper limb hyperhidrosis or Raynaud's disease.[39]

Superior Pulmonary Sulcus

An important disease to involve the thoracic sympathetic system at the thoracic inlet is Pancoast's tumor. The vast majority of Pancoast's tumors are bronchogenic carcinomas, typically a squamous cell carcinoma or adenocarcinoma. Tumor invasion to the superior cervical ganglion of the sympathetic system causes Horner's syndrome. Patients present with ptosis of the eyelid, pupil miosis, facial anhidrosis (▶ Fig. 3.27). The unique characteristic of Pancoast's tumors lies in the anatomy of the region where these tumors occur. The precise anatomical definition of superior pulmonary sulcus remains unclear as most anatomy textbooks do not include it as a defined anatomical area.

Pancoast first described the superior sulcus at the most cephalad extent of the costovertebral gutter.[40] Other investigators defined the superior sulcus as the area in the apical hemithorax posterior to where the subclavian artery crosses the lung apex[41] (Fig. 3.28; Fig. 3.29). In another perspective, the area can be described as the posterior compartment of the thoracic inlet. The thoracic inlet (superior thoracic aperture) is bounded by the T1 posteriorly, the first ribs laterally, and the superior border of the manubrium anteriorly (see Chapter 1, Chest Wall) and can be divided into three compartments by the attachments of the scalene muscles on the superior margin of the first rib.

The anterior compartment is delimitated between the sternum and the anterior scalene containing sternocleidomastoid and omohyoid muscles, subclavian and jugular veins, and scalene fat pad. The middle compartment is located between the anterior and middle scalene muscles; subclavian artery, phrenic nerve, and trunks of the brachial plexus cross it. The posterior compartment lies behind the middle scalene muscle and subclavian artery. It contains the posterior scalene muscle, costocervical

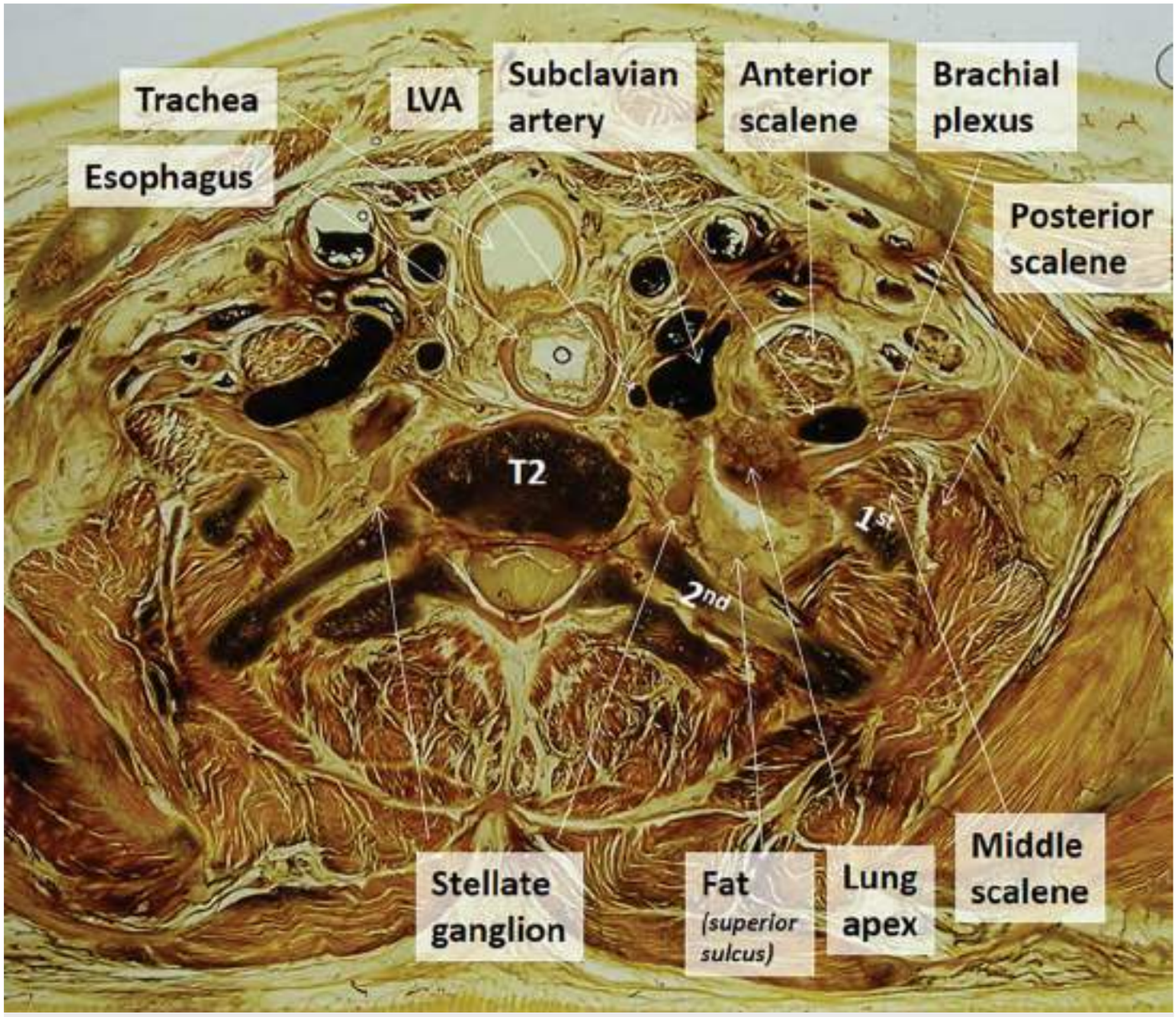

Fig. 3.26 Anatomy of the superior sulcus. LVA, left vertebral artery.

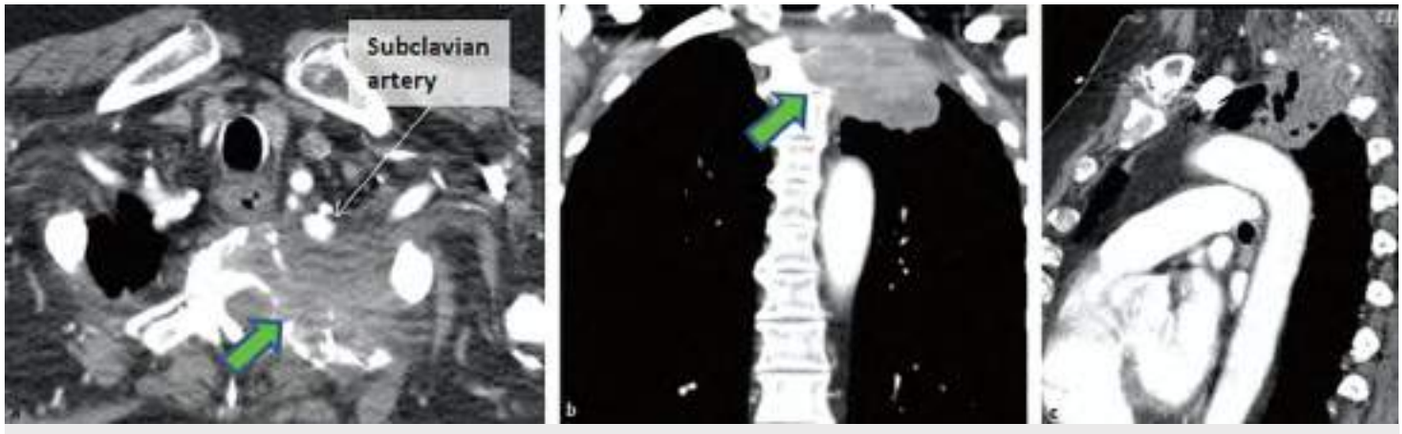

Fig. 3.27 Pancoast's tumor. **(a)** Axial, **(b)** coronal, **(c)** and sagittal CT images show a left apical lung mass posterior to the left subclavian artery with destruction of adjacent first rib and vertebral bodies of T1 and T2 (*arrows*).

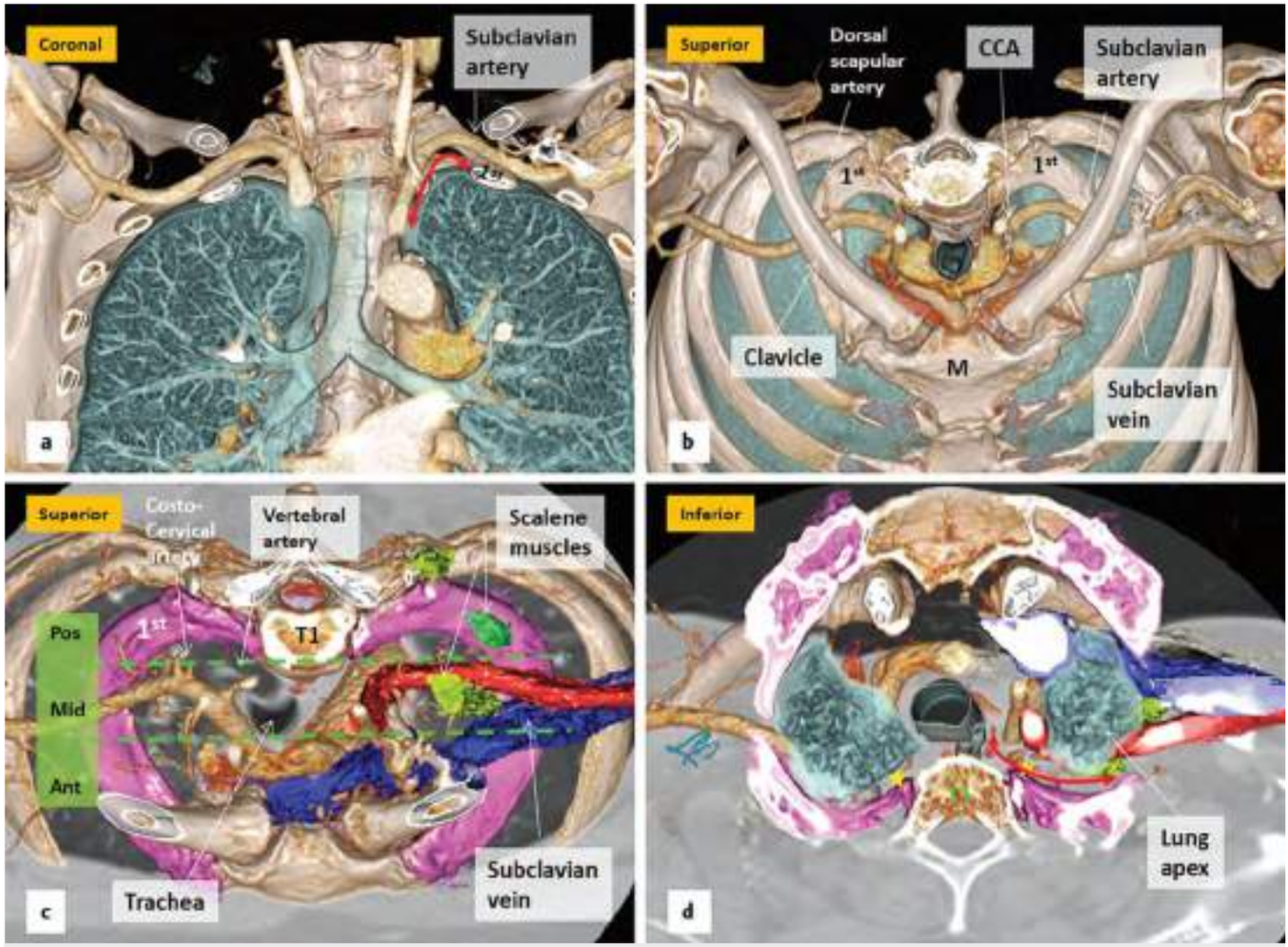

Fig. 3.28 (a–d) Anatomy of the thoracic inlet and superior sulcus. The superior sulcus is at the most cephalad extent of the costovertebral gutter, the area behind the subclavian artery (double-headed red line in **(a)** and **(d)**. In other words, the superior sulcus can be described as the posterior compartment of the thoracic inlet. **(c)** The thoracic inlet is bounded by the T1, the first ribs (1st), and the superior border of the manubrium (M) and divided into three compartments. The anterior compartment (Ant) is delimited between the sternum and the anterior scalene. The middle compartment (mid) is located between the anterior and middle scalene muscles. The posterior compartment lies behind the middle scalene muscle and subclavian artery. It contains the posterior scalene muscle, stellate ganglion (*yellow stars*), sympathetic chain, long thoracic and accessory nerves, neural foramina, and T1/T2 vertebral bodies. CCA, common carotid artery.

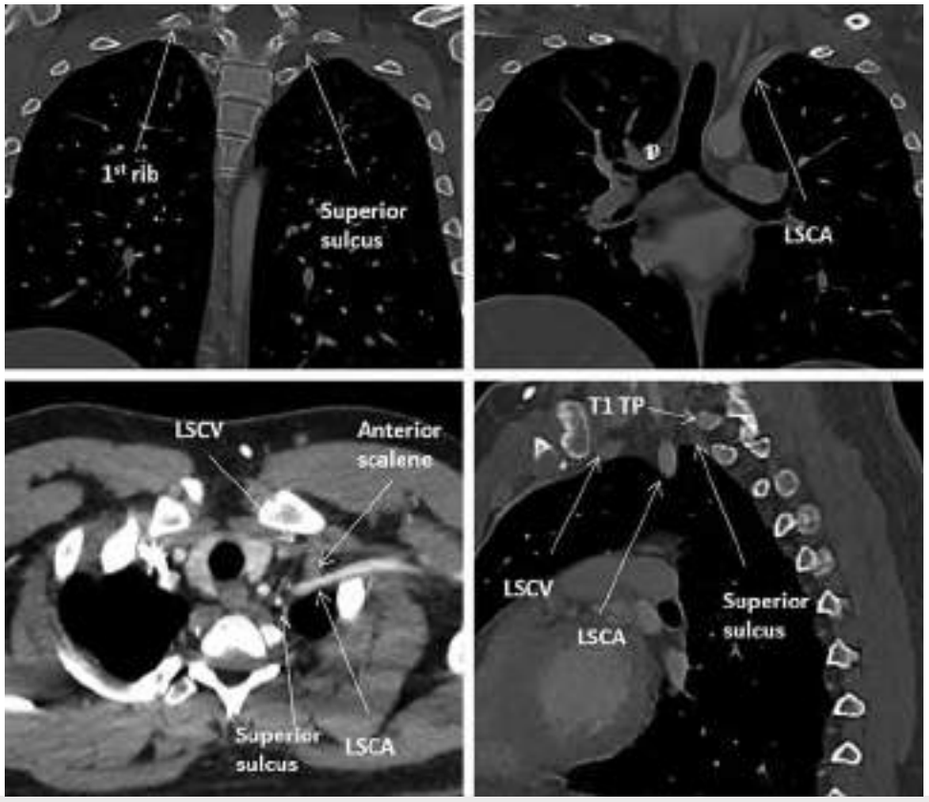

Fig. 3.29 Anatomy of the superior sulcus. LSCA, left subclavian artery; LSCV, left subclavian vein.

artery, stellate ganglion, sympathetic chain, long thoracic and accessory nerves, neural foramina, and T1/T2 vertebral bodies. Invasion of this complex anatomical area accounts for the classic symptoms of Pancoast's tumors.[42]

◆ Mediastinal Pathways of Communication with Neck and Abdomen

The mediastinum communicates with structures beyond the confines established by previous definitions through the perivascular spaces and interfascial planes. There are several pathways of communication between the mediastinum and the neck, pleura, chest wall, and abdomen. For example, air and edema may dissect in any direction between the neck, mediastinum, and abdominal wall (▶ Fig. 3.30). Superiorly, the mediastinum communicates with the retropharyngeal space, vascular sheaths in the neck, and submandibular space.[43,44,45] Inferiorly and anteriorly, the mediastinum communicates with the anterior extraperitoneal space through small defects in the sternocostal attachment of the diaphragm (i.e., foramen of Morgagni) that continues more inferiorly with the flanks laterally and the space of Retzius of the pelvis[46] (▶ Fig. 3.30). Here, endothoracic fascia which lines the ribs and diaphragm and transversalis fascia of the abdomen which lines the underneath of diaphragm become contiguous allowing for communication between the upper abdomen and the mediastinum. The mediastinum also communicates directly with the retroperitoneum by way of the aortic hiatus and with the peritoneum through the esophageal hiatus.[47,48] The vena cava hiatus is also considered a possible pathway of communication between the abdomen and mediastinum, however, the wall of the cava is adherent to the walls of the foramen. Finally, direct transphrenic communication has been reported via either tiny defects through the tendinous or muscular portions of the diaphragm and via transdiaphragmatic lymphatics.[49]

Presence of free air in the mediastinum is called pneumomediastinum. Pneumomediastinum may be due to intrathoracic or extrathoracic sources, when extrathoracic it is due to dissection of air along the pathways explained above. For example, extrathoracic sources of pneumomediastinum include pharyngeal perforation during intubation, sinus fracture, dental extraction.[50] In addition, air may dissect into the mediastinum from the retroperitoneal space. Presence of free air in the mediastinum without any apparent cause is defined as spontaneous pneumomediastinum. The terminal bronchioles of the lung are the most common source of pneumomediastinum. Perforation of small bronchioles and alveoli following mechanical ventilation, acute asthma attack, or intense sport activity results in dissection of air into the peribronchial/perivascular interstitial space (interstitial emphysema) which finally enters into the mediastinum[46] (▶ Fig. 3.31). If the mediastinal parietal pleura subsequently rupture, a pneumothorax results but is unusual.

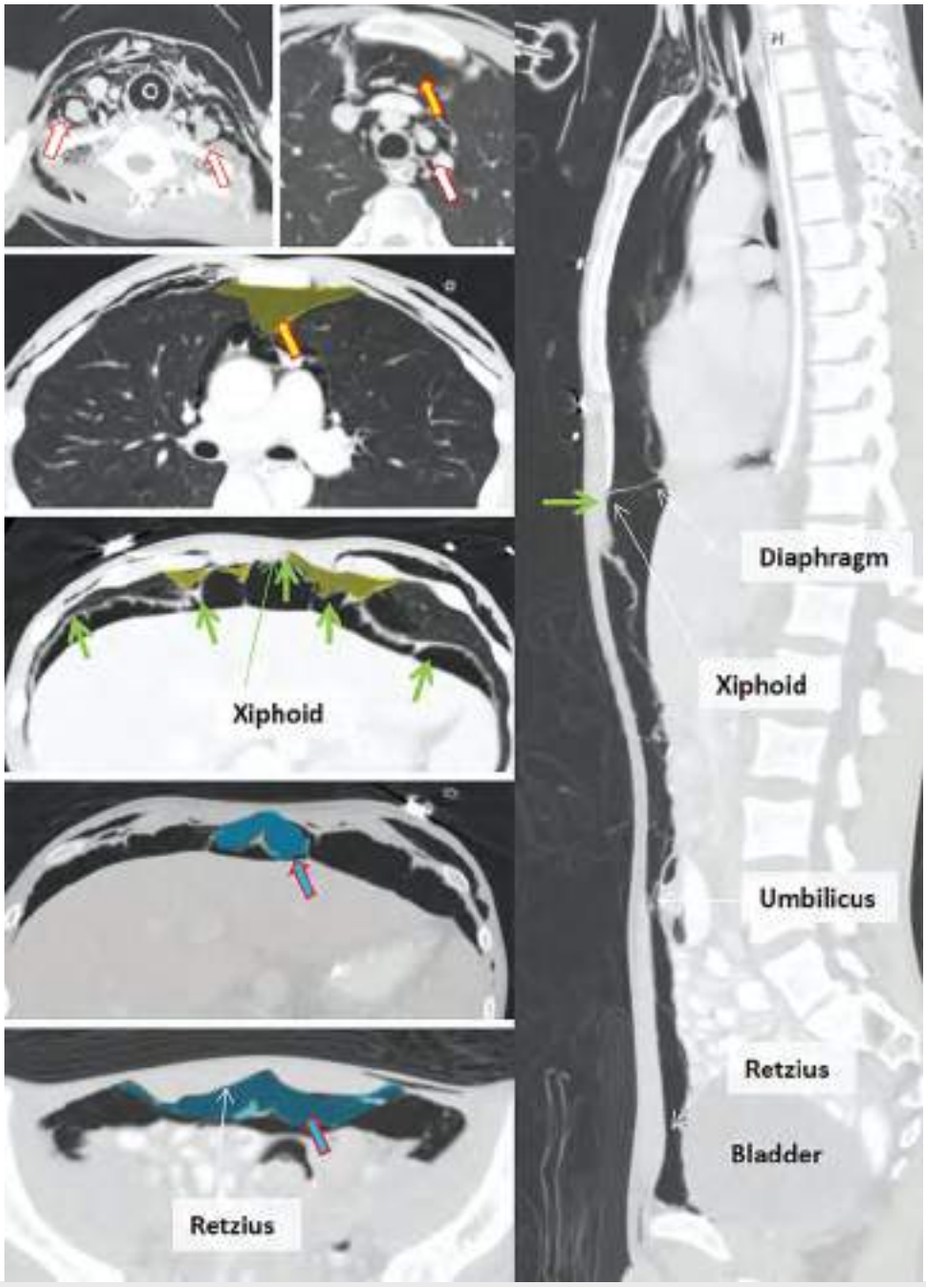

Fig. 3.30 Mediastinal communication with neck and abdomen. In this patient with pneumomediastinum, air is dissected into the neck through soft tissue planes and perivascular sheaths (*white arrows*). Anterior mediastinal air (*yellow arrows* and *yellow areas*) is dissected into the anterior extraperitoneal space (*blue arrows* and *blue areas*) of the abdomen through diaphragmatic tissue planes connecting to the xiphoid of the sternum, the anterior attachments of the respiratory diaphragm. The line of anterior attachments of each hemidiaphragm is shown by green arrows extending cranially and medially to meet at the xiphoid process. The anterior extraperitoneal space is continuous with the flanks laterally and extends to the space of Retzius of the pelvis inferiorly.

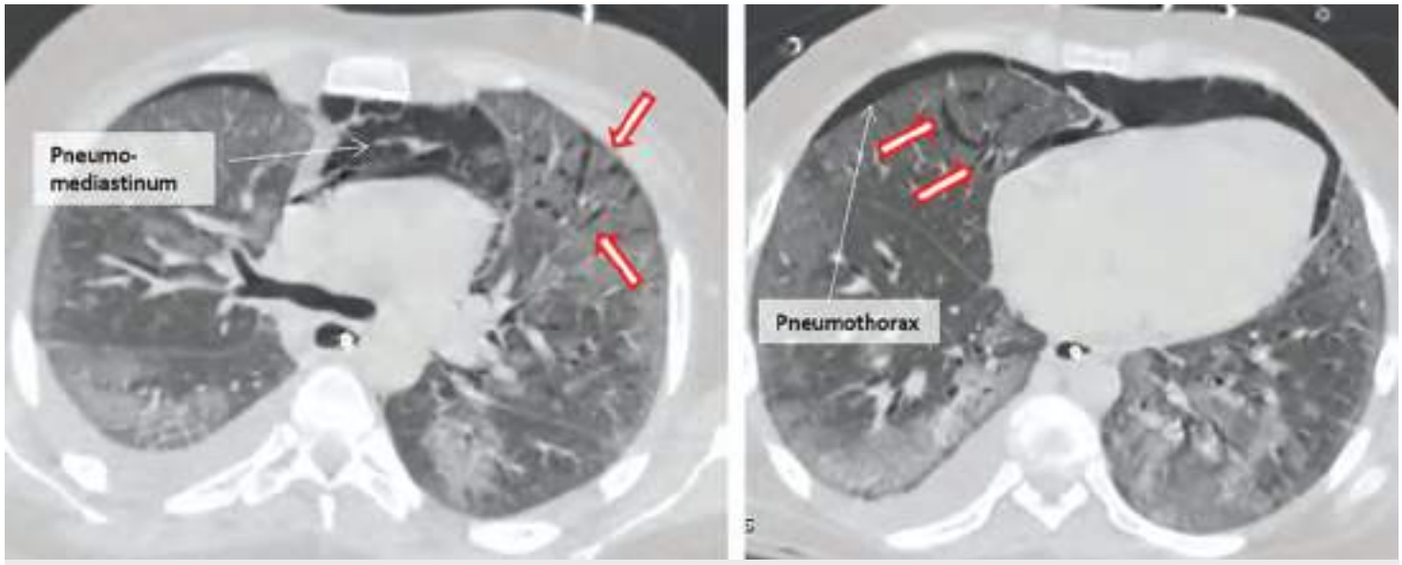

Fig. 3.31 Interstitial emphysema causing pneumomediastinum and a small right pneumothorax after mechanical ventilation in a patient with hypoxia and pulmonary edema. Interstitial emphysema manifests as air in the sheaths surrounding the bronchi, pulmonary arteries, and veins (*arrows*).

References

[1] Thacker PG, Mahani MG, Heider A, Lee EY. Imaging evaluation of mediastinal masses in children and adults: practical diagnostic approach based on a new classification system. J Thorac Imaging.; 30(4):247–267

[2] Carter BW, Tomiyama N, Bhora FY, et al. A modern definition of mediastinal compartments. J Thorac Oncol.; 9(9) Suppl 2:S97–S101

[3] Fujimoto K, Hara M, Tomiyama N, Kusumoto M, Sakai F, Fujii Y. Proposal for a new mediastinal compartment classification of transverse plane images according to the Japanese Association for Research on the Thymus (JART) General Rules for the Study of Mediastinal Tumors. Oncol Rep.; 31(2):565–572

[4] Aquino SL, Duncan G, Taber KH, Sharma A, Hayman LA. Reconciliation of the anatomic, surgical, and radiographic classifications of the mediastinum. J Comput Assist Tomogr.; 25(3):489–492

[5] Gibbs JM, Chandrasekhar CA, Ferguson EC, Oldham SA. Lines and stripes: where did they go?—From conventional radiography to CT. Radiographics.; 27(1):33–48

[6] Shields TW. Primary tumors and cysts of the mediastinum. General Thoracic Surgery. Philadelphia, PA: Lea & Febiger; 1983:927–954

[7] Fraser RS, Müller NL, Colman N, Paré PD. The mediastinum. Fraser and Paré's Diagnosis of Diseases of the Chest. 4th ed. Philadelphia, PA: WB Saunders; 1999:196–234

[8] Cooper C, Moss AA, Buy JN, Stark DD. CT appearance of the normal inferior pulmonary ligament. AJR Am J Roentgenol.; 141(2):237–240

[9] Godwin JD, Vock P, Osborne DR. CT of the pulmonary ligament. AJR Am J Roentgenol.; 141(2):231–236

[10] Rost RC, Jr, Proto AV. Inferior pulmonary ligament: computed tomographic appearance. Radiology.; 148(2):479–483

[11] Wimpfheimer O, Haramati LB, Haramati N. Calcification of the ligamentum arteriosum in adults: CT features. J Comput Assist Tomogr.; 20(1):34–37

[12] Bisceglia M, Donaldson JS. Calcification of the ligamentum arteriosum in children: a normal finding on CT. AJR Am J Roentgenol.; 156(2):351–352

[13] Nasseri F, Eftekhari F. Clinical and radiologic review of the normal and abnormal thymus: pearls and pitfalls. Radiographics.; 30(2):413–428

[14] Nishino M, Ashiku SK, Kocher ON, Thurer RL, Boiselle PM, Hatabu H. The thymus: a comprehensive review. Radiographics.; 26(2):335–348

[15] Aw D, Palmer DB. The origin and implication of thymic involution. Aging Dis.; 2(5):437–443

[16] Lynch HE, Goldberg GL, Chidgey A, Van den Brink MRM, Boyd R, Sempowski GD. Thymic involution and immune reconstitution. Trends Immunol.; 30 (7):366–373

[17] Kong FK, Chen CL, Cooper MD. Reversible disruption of thymic function by steroid treatment. J Immunol.; 168(12):6500–6505

[18] Safieddine N, Keshavjee S. Anatomy of the thymus gland. Thorac Surg Clin.; 21(2):191–195, viii

[19] Di Marino V, Argème M, Brunet C, Coppens R, Bonnoit J. Macroscopic study of the adult thymus. Surg Radiol Anat.; 9(1):51–62

[20] Keynes G. The thymic vein. BMJ.; 1(5540):634

[21] Cahill DR. Anomalous thymic branch of the right common carotid artery. Clin Anat.; 11(5):346–348

[22] Marchington JM, Mattacks CA, Pond CM. Adipose tissue in the mammalian heart and pericardium: structure, foetal development and biochemical properties. Comp Biochem Physiol B.; 94(2):225–232

[23] Iacobellis G, Corradi D, Sharma AM. Epicardial adipose tissue: anatomic, biomolecular and clinical relationships with the heart. Nat Clin Pract Cardiovasc Med.; 2(10):536–543

[24] Mohapatra PR, Janmeja AK. Images in clinical medicine. Asymptomatic mediastinal lipomatosis. N Engl J Med.; 363(13):1265

[25] El-Sherief AH, Lau CT, Wu CC, Drake RL, Abbott GF, Rice TW. International association for the study of lung cancer (IASLC) lymph node map: radiologic review with CT illustration. Radiographics.; 34(6):1680–1691

[26] Ndiaye A, Di-Marino V, Ba PS, Ndiaye A, Gaye M, Nazarian S. Anatomical variations in lymphatic drainage of the right lung: applications in lung cancer surgery. Surg Radiol Anat.; 38(10):1143–1151

[27] Kim AW. Lymph node drainage patterns and micrometastasis in lung cancer. Semin Thorac Cardiovasc Surg.; 21(4):298–308

[28] Ichinose Y, Kato H, Koike T, et al. Japanese Clinical Oncology Group. Completely resected stage IIIA non-small cell lung cancer: the significance of primary tumor location and N2 station. J Thorac Cardiovasc Surg.; 122 (4):803–808

[29] Takahashi K, Stanford W, Van Beek E, Thompson B, Mullan B, Sato Y. Mediastinal lymphatic drainage from pulmonary lobe based on CT observations of histoplasmosis: implications for minimal N2 disease of non-small-cell lung cancer. Radiat Med.; 25(8):393–401

[30] Hematti H, Mehran RJ. Anatomy of the thoracic duct. Thorac Surg Clin.; 21 (2):229–238, ix

[31] Kuge K, Murakami G, Mizobuchi S, Hata Y, Aikou T, Sasaguri S. Submucosal territory of the direct lymphatic drainage system to the thoracic duct in the human esophagus. J Thorac Cardiovasc Surg.; 125(6):1343–1349

[32] Murakami G, Sato I, Shimada K, Dong C, Kato Y, Imazeki T. Direct lymphatic drainage from the esophagus into the thoracic duct. Surg Radiol Anat.; 16 (4):399–407

[33] Fukumoto K, Takatsuki S, Jinzaki M, et al. Three-dimensional imaging and mapping of the right and left phrenic nerves: relevance to interventional cardiovascular therapy. Europace.; 15(7):937–943
[34] Aquino SL, Duncan GR, Hayman LA. Nerves of the thorax: atlas of normal and pathologic findings. Radiographics.; 21(5):1275–1281
[35] Horton R, Di Biase L, Reddy V, et al. Locating the right phrenic nerve by imaging the right pericardiophrenic artery with computerized tomographic angiography: implications for balloon-based procedures. Heart Rhythm.; 7 (7):937–941
[36] Matsumoto Y, Krishnan S, Fowler SJ, et al. Detection of phrenic nerves and their relation to cardiac anatomy using 64-slice multidetector computed tomography. Am J Cardiol.; 100(1):133–137
[37] Berkmen YM, Davis SD, Kazam E, Auh YH, Yankelevitz D, Girgis FG. Right phrenic nerve: anatomy, CT appearance, and differentiation from the pulmonary ligament. Radiology.; 173(1):43–46
[38] Roka A, Heist EK, Refaat M, Ruskin J, Mansour M. Novel technique to prevent phrenic nerve injury during pulmonary vein isolation using preprocedural imaging. J Cardiovasc Electrophysiol.; 26(10):1057–1062
[39] Lee KS, Chuang CL, Lin CL, Tsai LC, Hwang SL, Howng SL. Percutaneous CT-guided chemical thoracic sympathectomy for patients with palmar hyperhidrosis after transthoracic endoscopic sympathectomy. Surg Neurol.; 62 (6):501–505, discussion 505
[40] Pancoast HK. Superior pulmonary sulcus tumor. Tumor characterized by pain, Horner's syndrome, destruction of bone and atrophy of hand muscles. JAMA.; 99:1391–1396
[41] Paulson DL. Carcinomas in the superior pulmonary sulcus. J Thorac Cardiovasc Surg.; 70(6):1095–1104
[42] Marulli G, Battistella L, Mammana M, Calabrese F, Rea F. Superior sulcus tumors (Pancoast tumors). Ann Transl Med.; 4(12):239
[43] Marchand P. The anatomy and applied anatomy of the mediastinal fascia. Thorax.; 6(4):359–368
[44] Maunder RJ, Pierson DJ, Hudson LD. Subcutaneous and mediastinal emphysema. Pathophysiology, diagnosis, and management. Arch Intern Med.; 144 (7):1447–1453
[45] Frias Vilaça A, Reis AM, Vidal IM. The anatomical compartments and their connections as demonstrated by ectopic air. Insights Imaging.; 4(6):759–772
[46] Kleinman PK, Brill PW, Whalen JP. Anterior pathway for transdiaphragmatic extension of pneumomediastinum. AJR Am J Roentgenol.; 131(2):271–275
[47] Joannides M. The etiology of interstitial and mediastinal emphysema. Arch Surg.; 21:333–341
[48] Macklin C. Transport of air along sheaths of pulmonic blood vessels from alveoli to mediastinum: clinical implications. Arch Intern Med (Chic).; 64:913–929
[49] Lidid L, Valenzuela J, Villarroel C, Alegria J. Crossing the barrier: when the diaphragm is not a limit. AJR Am J Roentgenol.; 200(1):W62–W70
[50] Zylak CM, Standen JR, Barnes GR, Zylak CJ. Pneumomediastinum revisited. Radiographics.; 20(4):1043–1057

4 Lungs

Leah Lin and Farhood Saremi

◆ Introduction

The respiratory tract is divided into upper and lower parts. The upper respiratory tract includes the organs outside the thorax including the nose, pharynx, and larynx which are discussed in other chapters. The lower respiratory tract contains the organs within the thorax including the trachea, bronchi, bronchioles, alveolar duct, and alveoli. This chapter reviews the anatomy of the lung with emphasis on the lobes, segments, subsegments, and pulmonary lobules.

◆ Embryology

During weeks 3 to 4 of gestation, the respiratory system develops from the ventral wall of the foregut. The epithelium of the trachea, bronchi, and alveoli originate from the endoderm, and the muscle, cartilage, and connective tissue originate from the mesoderm.[1,2,3,4] The tracheobronchial tree develops between days 24 to 36 of gestation during which a median bulge develops on the ventral wall of the pharynx at the laryngotracheal groove (▶ Fig. 4.1). By day 28, the bulge has formed into the right and left lung buds. These buds continue to elongate forming the primary and segmental bronchi. The human lung develops through multiple stages during gestation: the embryonic, pseudoglandular, canalicular, saccular, and alveolar. The alveoli continue to proliferate until 300 million (32 m^2) have formed, usually by age 8.[1] All preacinar (conducting) airways will develop by week 17 which is the end of the pseudoglandular stage. Acinar contents develop mainly during the canalicular and saccular stages. Development of the pulmonary circulation occurs in parallel with lung development (see Chapter 2, Tracheobronchial System). The pulmonary artery develops from the sixth aortic arch. The distal right pulmonary artery loses its connection with the arch, whereas on the left it maintains connection by the ductus arteriosus. The pulmonary veins derive from the splanchnic mesoderm that overlies the foregut and their development is closely related to the development of the lung buds. Blood returning from the lung buds initially drains into the splanchnic plexus but later a primitive common pulmonary vein appears and connects the lung venous network to the left atrium along with obliteration of the majority of the splanchnic pulmonary connections. Four pulmonary venous tributaries of the primitive pulmonary vein subsequently develop and incorporate into the left atrium.

◆ Anatomy

Lobes and Segmental Anatomy

Knowledge of the normal lobar and segmental anatomy is essential for understanding their variable appearances on chest radiography and CT imaging and for localizing various abnormal findings (▶ Fig. 4.2, ▶ Fig. 4.3). Typically, the right lung consists of three lobes: the upper, middle, and lower lobes. The right upper and middle lobes are separated by the minor or horizontal fissure, and the right middle and lower lobes are separated by the major or oblique fissure. The left lung typically has two lobes: the upper and lower lobes, which are separated by the major or oblique fissure. A fissure is made up of a double layer of visceral pleura that separates pulmonary lobes, however, it may be incomplete or absent. An incomplete major fissure may lead to disease spread because the lung parenchyma of the adjacent pulmonary lobes fuse.[5] The major fissures are usually incomplete toward the mediastinal side near the hilar area and in the upper parts.

Each lobe is divided into bronchopulmonary segments, based on the tertiary (segmental) bronchi supplying each segment

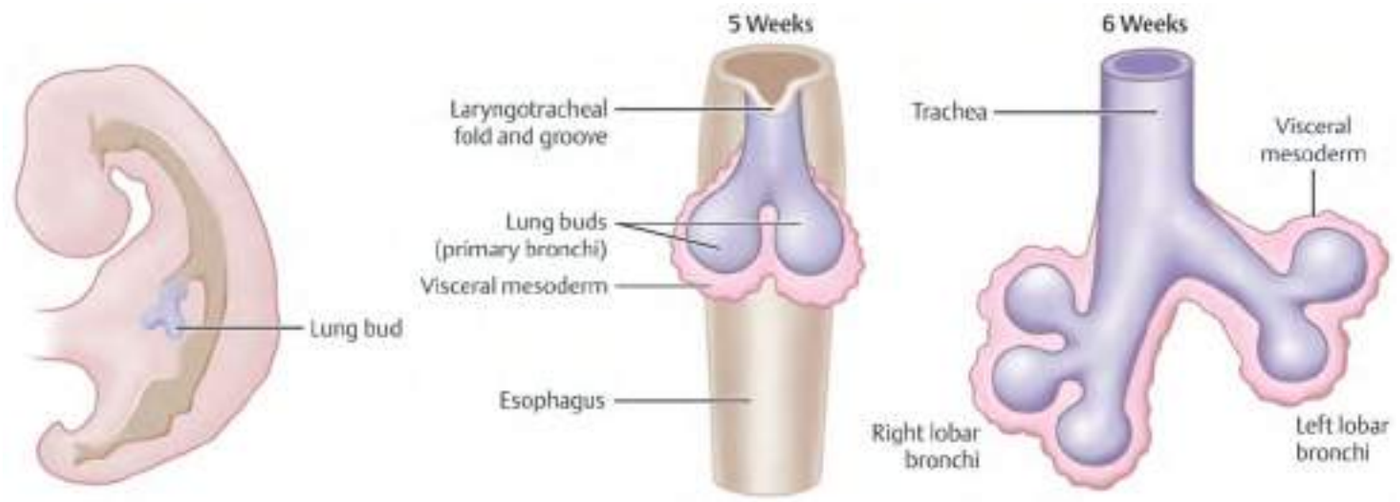

Fig. 4.1 The tracheobronchial tree develops between days 24 and 36 of gestation during which a median bulge develops on the ventral wall of the pharynx at the laryngotracheal groove. By day 28, the bulge has formed into the right and left lung buds. These buds continue to elongate forming the primary and segmental bronchi.

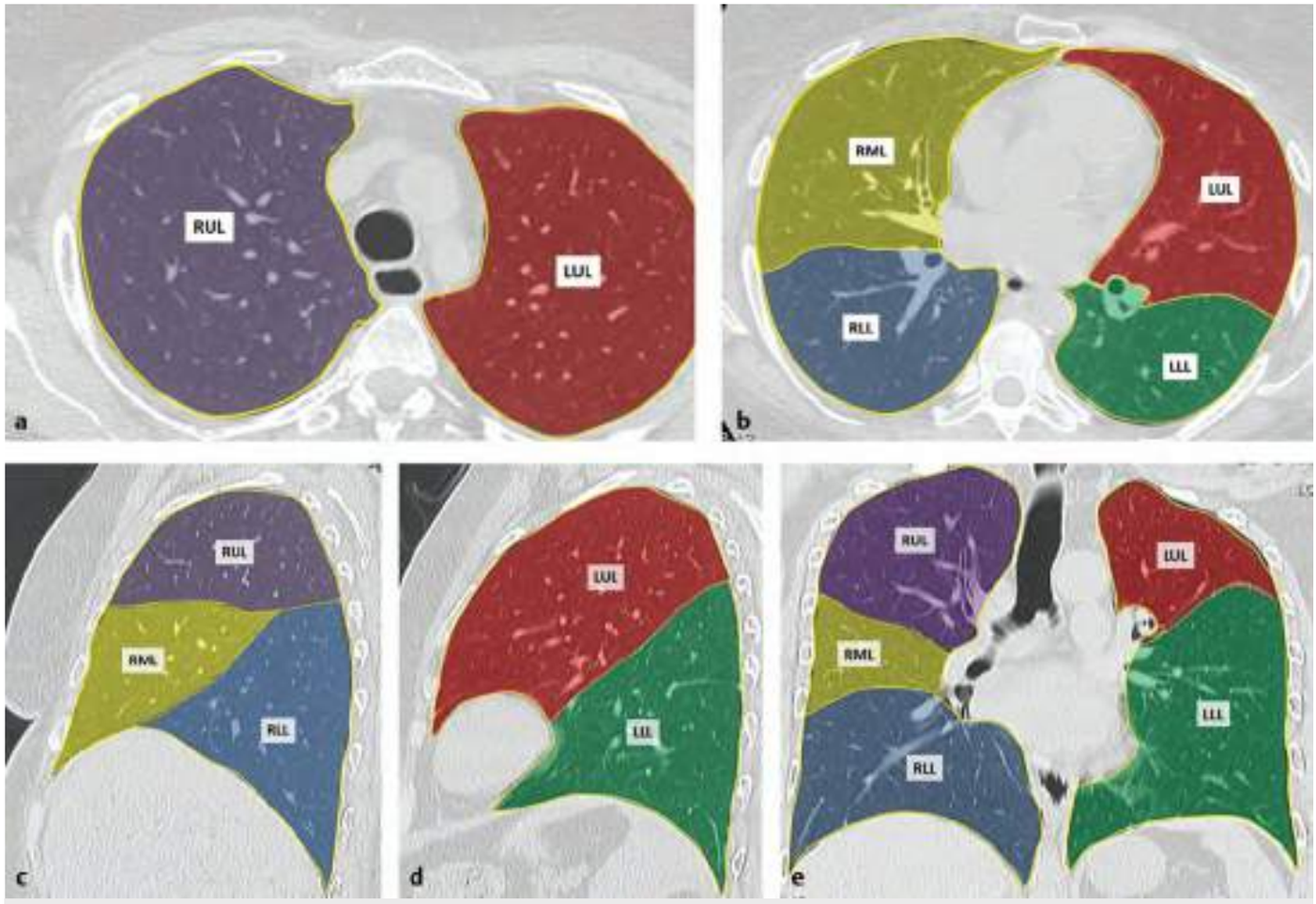

Fig. 4.2 (a–e) Pulmonary lobes. LLL, left lower lung; LML, left middle lung; LUL, left upper lung; RLL, right lower lung; RML, right middle lung; RUL, right upper lung.

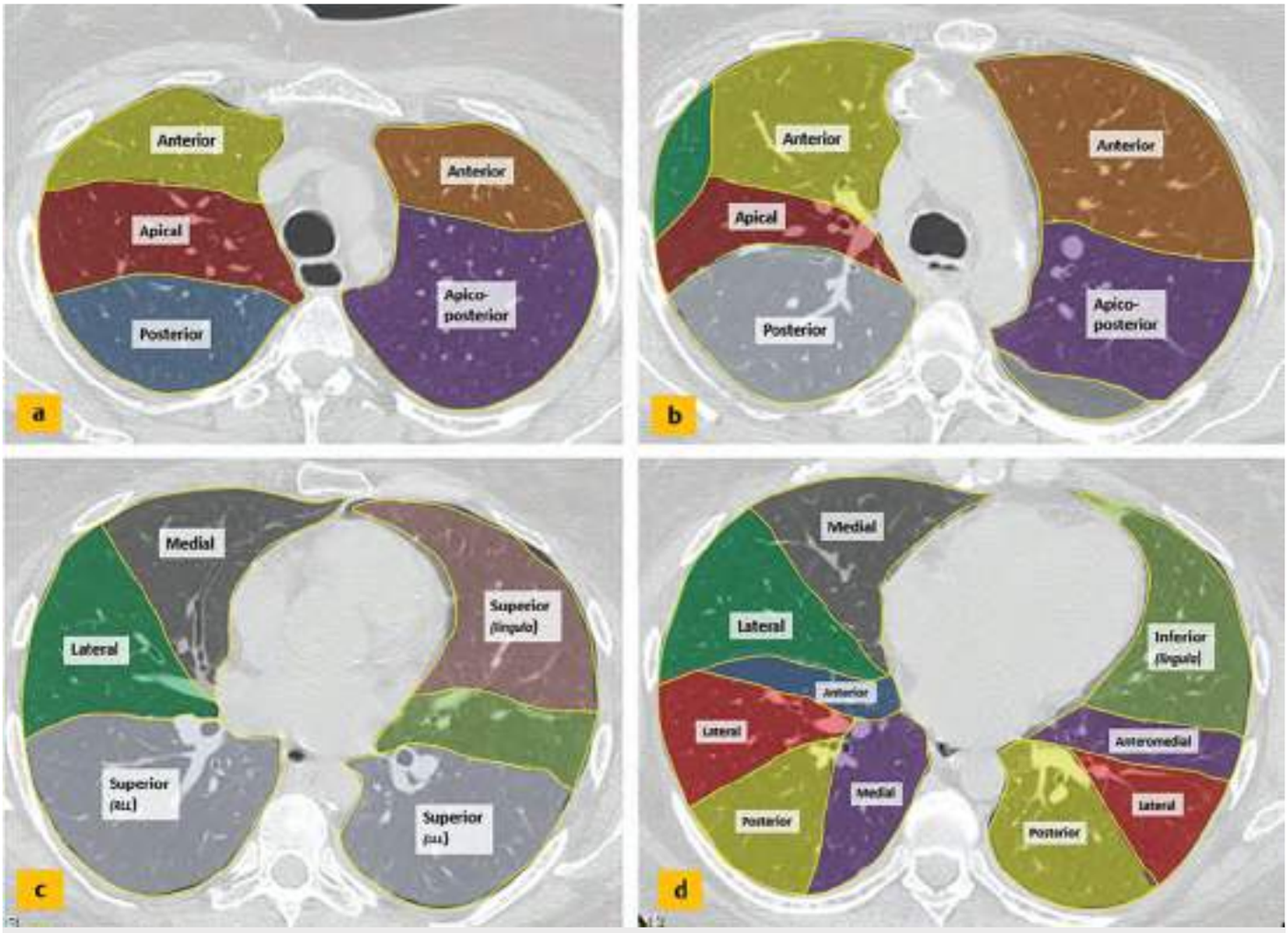

Fig. 4.3 (a–d) Pulmonary segments.

(▶ Fig. 4.3). Each segment is supplied by its own artery and bronchus. The segmental anatomy is somewhat symmetric, even though the right lung consists of three lobes and the left consists of two lobes. There are 10 bronchopulmonary segments in each lung, but in left lung, some of these segments fuse to form 8 segments total. The bronchi continue to divide into smaller and smaller bronchi up to 23 generations of divisions from the main bronchus. On the right, the right upper lobe consists of the apical, posterior, and anterior segments, the right middle lobe consists of the lateral and medial segments, and the right lower lobe consists of the superior, medial, anterior, lateral, and posterior segments. The left upper lobe consists of the apicoposterior, anterior, superior lingula, and inferior lingula segments, and the left lower lobe consists of the superior, anteromedial, lateral, and posterior segments.[6]

Secondary Pulmonary Lobule and Pulmonary Acini

The secondary pulmonary lobule (SPL) is a fundamental structure of the lung, and knowledge of its anatomy helps in the interpretation of both normal and abnormal CT scans. The tertiary bronchi subdivide into the bronchioles down to the level of the secondary lobules where 3-5 terminal bronchioles are located. The terminal bronchioles (final section of the conducting airway) are lined with simple cuboidal epithelium. The diameter of bronchioles is approximately 0.3 to 2 mm. The respiratory bronchioles are subdivisions of the terminal bronchioles which connect with the alveolar ducts and sacs that are responsible for gas exchange. The SPL is the smallest unit of lung structure marginated by connective tissue septa,[7] and each bronchopulmonary segment is made up of multiple SPLs. The SPL is generally polyhedral in shape and varies in size, from 1 to 2.5 cm.[7] At the center of the SPL, run a lobular (preterminal) centrilobular bronchiole and a small pulmonary artery branch. Within the connective tissue septa that marginate the SPL run the veins and the lymphatics[8,9,10] (▶ Fig. 4.4, ▶ Fig. 4.5). It should be noted that the size and shape of the SPL on CT images are affected by the orientation of the lobules in relation to axial slice.

A SPL is made up of smaller structural units called acini. The pulmonary acinus is defined as the structure distal to a terminal bronchiole. It is supplied by a first-order respiratory bronchiole. The number of acini forming the lobules ranges from 3 to 24.[10] Since respiratory bronchioles contain alveoli in their walls, an acinus is described as a unit of lung structure in which all airways participate in gas exchange. Acini can range in size from 6 to 10 mm with a mean acinar volume of 187 mm^3.[11,12] The size of vessels supplying this unit is less than 150 µm.

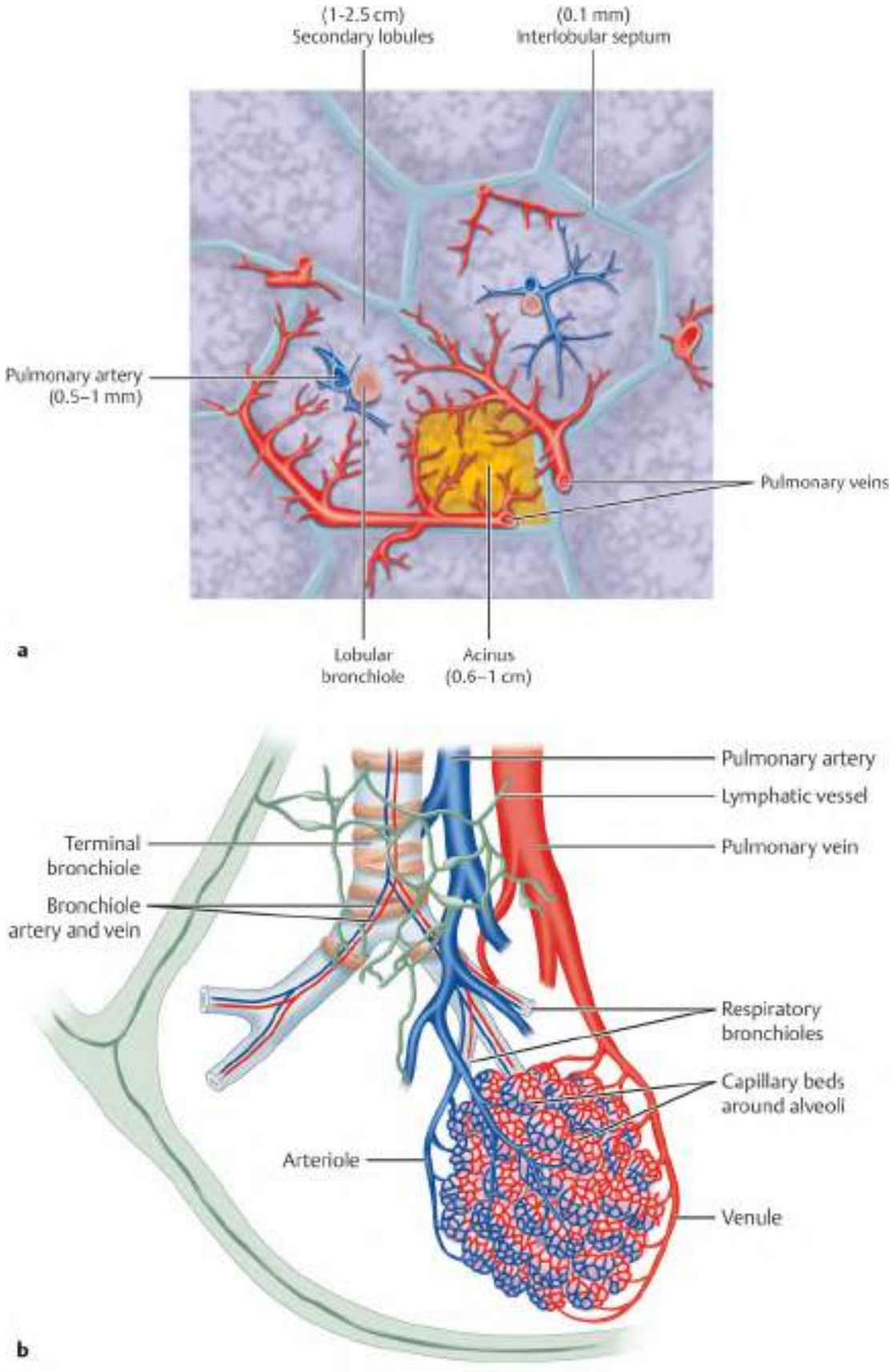

Fig. 4.4 **(a)** Diagram shows anatomy and dimensions of secondary lobule and pulmonary acinus. **(b)** Perfusion of the secondary lobule.

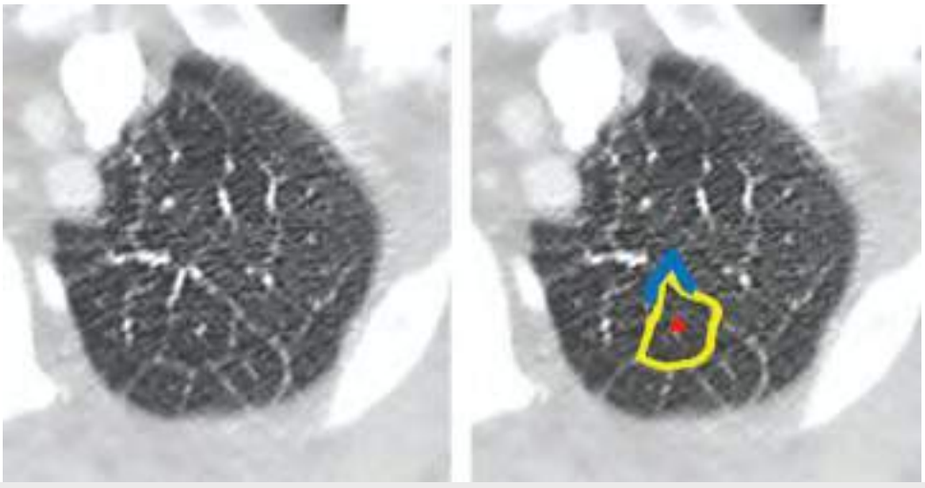

Fig. 4.5 Anatomy of the secondary pulmonary lobule. Transverse CT image of a patient with pulmonary edema. The thickened interlobular septa and pulmonary veins are visible. Interlobular septa (*yellow*), centrilobular artery (*red*), pulmonary vein (*blue*).

Interalveolar Air Drift

In 1931 Van Allen and Lindskog showed intercommunication at the periphery of the bronchial tree allowing transfer of gases and fluid between alveoli.[13] These collateral channels are called pores of Kohn which connect alveoli to adjacent alveoli and the canals of Lambert which connect terminal bronchioles to the alveoli (▶ Fig. 4.6). Collateral channels prevent collapse of the alveoli in case of proximal bronchial obstruction and lung can preserve its ventilation function. Collateral air drift can also occur in the fused lungs at the areas with defective fissures.[14]

Interfissural collateral air drift becomes evident if one lobe is collapsed due to obstruction of the lobar bronchus. The portion of the collapsed lobe fused with the unobstructed lobe remains aerated by the airflow across the incomplete major fissure (▶ Fig. 4.6). The middle lobe has reduced collateral ventilation which predisposes it to complete atelectasis and disease[15] (▶ Fig. 4.7).

Collateral ventilation does not substantially contribute to lung function in the normal lung because of the considerably high resistance to collateral ventilation in the normal lung.[16] On the contrary, the resistance to collateral ventilation will be diminished when bronchial obstruction exists, which facilitates collateral ventilation to the diseased lung.[17] In patients with bronchiolitis obliterans, collateral aeration can persist over a period of years causing emphysema and hyperlucent lung.[18] Collateral ventilation through an incomplete fissure may cause problems during bronchoscopic lung volume reduction by hampering the collapse of a nonfunctioning lung segment.[17] Recognition of an accessory fissure may alter the surgical strategies for a lung lesion, because an incomplete fissure may contribute to postoperative air leakage.

◆ Pulmonary Function

Understanding of lung volumes, lung compliance, pulmonary perfusion, microcirculation, and ventilation–perfusion relationship are essential for clinical application of respiratory physiology. The main function of the lung is establishing a highly effective gas exchange. For this purpose, ventilation and perfusion of the lung need to match. The portion of ventilation which reaches the alveoli and participates in the gas exchange is called alveolar ventilation. Normal value of alveolar ventilation matches the cardiac output and both are approximately 5 L/min.

Lung Ventilation

Gas moves from the outside to the acinus by convection and diffusion. Convective transportation of gas occurs within the conducting airways. At the acinus level, conductive gas transport stops as gas transport is primarily by diffusion and alveolar ventilation. The location of this transition is called the diffusive front.[19]

Normal tidal ventilation which is approximately 4-8 ml/kg-m is required for normal gas exchange.[20,21] Vital capacity of the lung is defined as a full inspiratory breath followed by expiration to reserve volume which is approximately 4 to 5 L in an average 70-kg individual. The residual volume of air remaining in the alveoli after vital capacity breath is called residual volume. Functional residual capacity (FRC) is the amount of air in the lungs after a normal expiration which is the residual volume plus expiratory reserve volume and measures between 2.8 and 3.1 L in standing position. Gases remaining in the lungs at the end of expiration not only prevent alveolar collapse but also continue to oxygenate the pulmonary blood.

Compliance is the ability of lung to distend. It is expressed as the distension of lung for a given level of transpulmonary pressure. In normal respiration, negative pleural pressure is sufficient to distend the lungs during inspiratory phase. Compliance depends on the volume of the lung. Compliance is minimum at extremes of FRC. In other words, an expanded lung or a completely deflated lung has the lower capacity to distend to a given pressure. In the upright lung, the intrapleural pressure becomes positive from apex to base of lung. It is –8 cm of H_2O at the apex and –1.5 cm H_2O at the base. As a result, in upright position apical lungs are less compliant and therefore less ventilated. Ventilation pattern changes with the position of individual because of the change of pleural pressure with gravity. Change in body position from upright to supine, lateral, or prone reduces FRC in dependent lungs which promotes early airway closure and

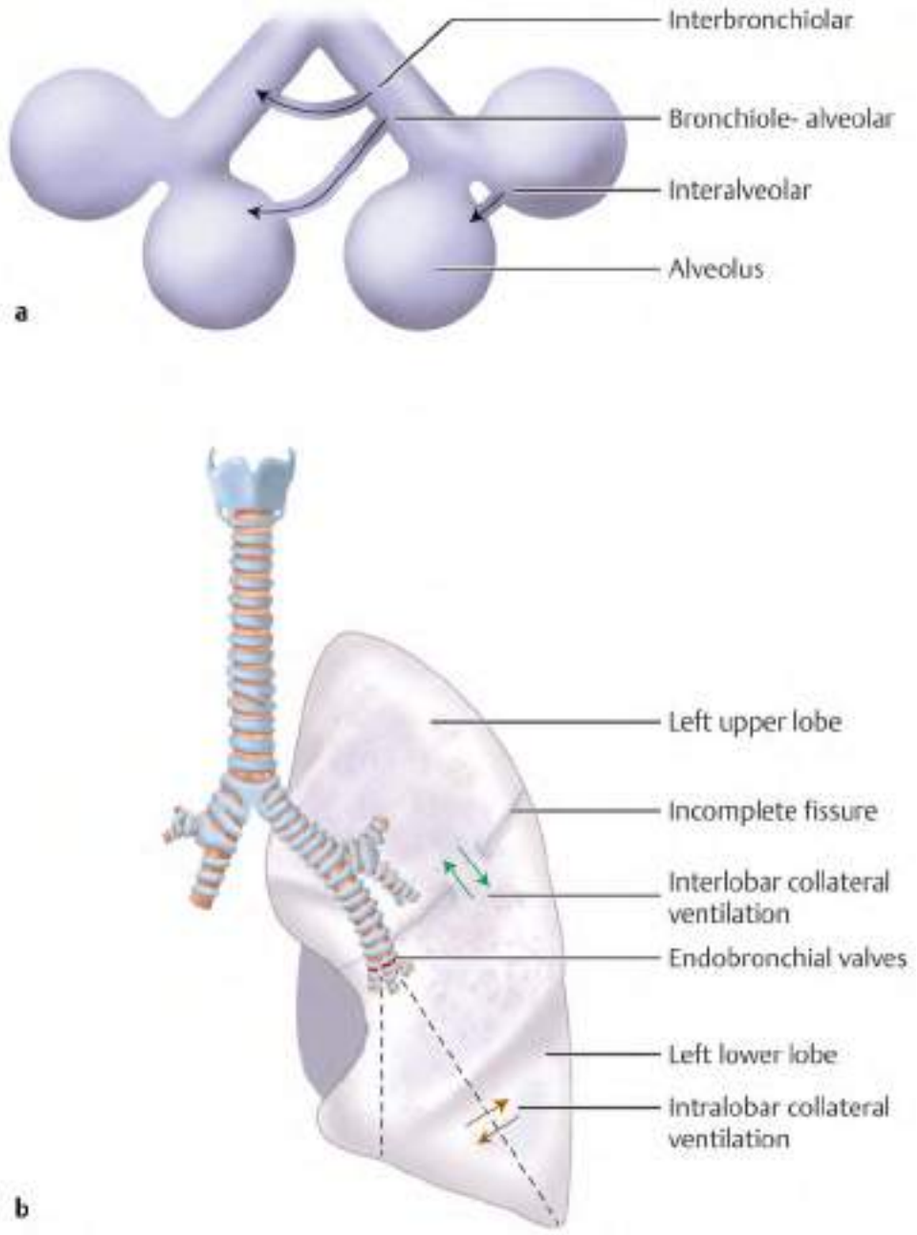

Fig. 4.6 **(a)** Different pathways for collateral ventilation are shown including interalveolar ventilation through the pores of Kohn, Bronchiole–alveolar ventilation through canals of Lambert, and interbronchiolar ventilation through channels of Martin. **(b)** Schematic figure illustrating the role of intra- and interlobar collateral ventilation, and the implications for bronchoscopic lung volume reduction using one-way endobronchial valves. The interlobar collateral ventilation from the left upper to the left lower lobe impedes the desired atelectasis of the lower lobe. Because all segments of the left lower lobe have endobronchial valves, intralobar collateral ventilation does not influence the development of atelectasis. Adapted from Koster and Slebos 2016.[18]

decreases ventilation in the dependent regions. Since lung blood flow passes preferentially to dependent regions, ventilation and perfusion mismatch occurs in these regions.[21]

Lung Circulation

The flow of blood between the heart and the lungs is achieved by two separate pathways, the pulmonary circulation and the bronchial circulation.[22,23] Pulmonary circulation develops early. By day 34 in embryogenesis, circulation exists between the primitive heart and the lung buds. The pulmonary circulation primarily provides blood oxygenation, whereas the systemic (bronchial) circulation is the major supply to nourish the airways and lungs. This dual input perfusion concept is important for imaging analysis of pulmonary perfusion and characterization of intrapulmonary pathologies especially lung masses. Malignant tumors, especially larger ones, may be supplied by both bronchial and pulmonary circulations. It is therefore suggested that including both arterial flows in perfusion measurements of lung tumors may be more accurate. Many conditions, including pulmonary embolism, pulmonary hypertension, chronic obstructive disease and tumors, alter pulmonary perfusion. Furthermore, pulmonary perfusion changes after surgical lung resection and during physiological processes, such as change of body position or during

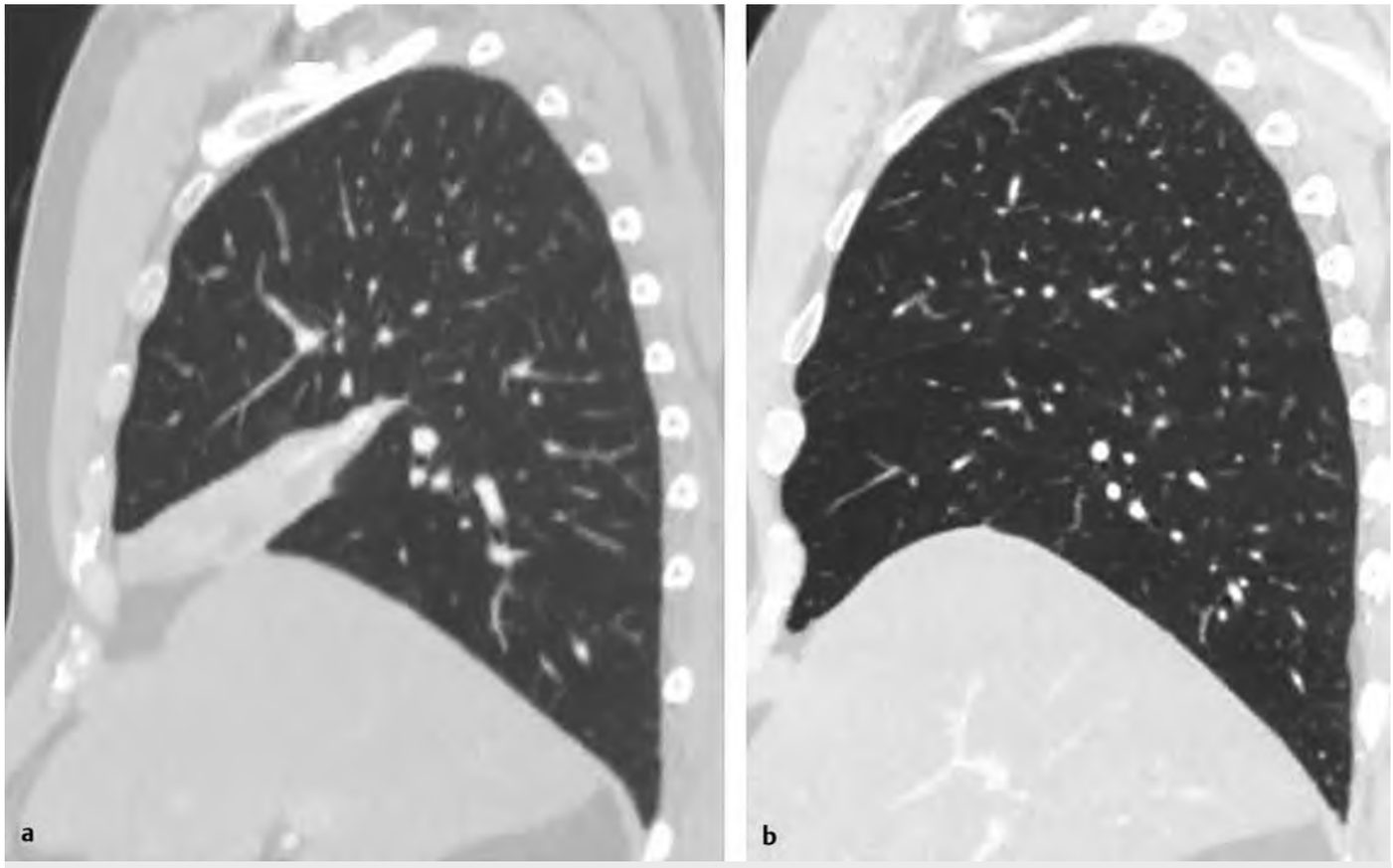

Fig. 4.7 Right middle lobe atelectasis **(a)** which is resolved after removal of the bronchial obstruction **(b)**. Atelectasis of the right middle lobe is usually complete and persistent unless the obstruction is removed. This is due to reduced collateral ventilation that would predispose it to reaeration.

physical activity. Therefore, assessment of the pulmonary perfusion is of physiological and clinical importance. It is important to know that large vessels serve to conduct blood flow throughout the lung, do not participate in gas exchange, and therefore do not represent pulmonary perfusion. Multiple approaches to assess pulmonary perfusion have been used. Computed tomography (CT), magnetic resonance imaging (MRI), and single-photon emission computed tomography (SPECT) all have been successfully used to measure lung perfusion.

The pulmonary vascular circuit runs in parallel to the systemic arterial circuit but in much lower pressure than the systemic circuit. The pulmonary vessels are thin-walled and have less musculature to assist fast diffusion of gases. Despite their low pressure, pulmonary circuit is a high-flow circuit, receiving the entire volume of cardiac output with each stroke. The low pressure of the pulmonary circuit is the effect of low resistance of the pulmonary microcirculation, thanks to its denser vascular network, offering a larger surface area compared to systemic circulation. Because of low pressure and structural differences of pulmonary vasculature, they change with gravity.

The distribution of blood flow in the pulmonary arteries depends on three factors: alveolar pressure, pulmonary arterial pressure, and pulmonary venous pressure. In apical regions, alveolar pressure is higher and arterial blood flow is lower, and this zone is considered as physiological dead space. The patients on positive pressure ventilation with positive end-expiratory pressure (PEEP) may have larger apical zone due to high alveolar pressure. Pulmonary artery pressure is high during exercise, eliminating any existing dead space in the apical regions. Hypoxic pulmonary vasoconstriction is a compensatory mechanism that shifts blood flow away from hypoxic lung regions to better oxygenated regions.

The relative contribution of blood within the lung tissue is high. The lung density at functional residual capacity is approximately one-third of that of the brain and the blood volume itself contributes to more than one-half of the weight of the lung. The lung density is even higher (more capillaries) in dependent lungs compared to nondependent regions.

Pulmonary Artery Microcirculation

Pulmonary microcirculation consists of small arterioles and capillaries (▶ Fig. 4.4). This microcirculation network comprises approximately 25% of lung volume and is designed to handle the entire cardiac stroke volume which permits proper gas exchange.[24]

Small pulmonary arterioles contain smooth muscle fibers and thus have a level of control over blood distribution, acting as resistance vessels and allowing for the shunting of blood within the microcirculation. Even smaller capillaries arise from the branching arterioles, which then form a network of vessels surrounding the alveoli. These capillaries have very thin walls, less than 0.1-µm thick, permitting gas exchange and oxygenation of blood. In addition to gas exchange, the capillaries play a vital role

in chemical substance exchange, such as water and electrolytes, as well as biochemical destruction and synthesis. For example, the vasoconstrictive hormone angiotensin I is converted to the active angiotensin II at the pulmonary capillary level. After gas exchange occurs, blood then continues within the pulmonary venous system for ultimate return to the heart.

Bronchial Artery Circulation

Bronchial circulation differs from pulmonary circulation in that it carries oxygenated blood on the arterial side, arising from the aorta. Bronchial circulation supplies the trachea and bronchi, bronchovascular bundles, pulmonary interstitium, lymph nodes, visceral pleura and the vasa vasorum of the aorta, pulmonary artery, and pulmonary vein.[25]

Bronchopulmonary Arterial Collateral Flow

Several studies have demonstrated the presence of collateral circulatory pathways between the pulmonary arterial system and bronchial arterial system early in life, but in the normal adult lung, this system recedes.[26] While likely still present, there is no demonstrable flow within the collateral vessels.

However, anastomotic flow has been observed in cases of diseased lung, such as in cases of fibrotic interstitial lung disease,[25] atypical mycobacterial infection, or lung cancer. The result is much higher-pressure systemic blood flows (bronchial) entering the lower-pressure pulmonary circuit. The result of which is vascular breakdown and ultimate hemoptysis. In cases of pulmonary embolism, flow through these channels can compensate for lack of pulmonary flow and explains why pulmonary infarction is seen in only a minority of cases.

Ventilation to Perfusion Matching

The alveolar partial pressure of oxygen and carbon dioxide are determined by the ratio of ventilation (V) to perfusion (Q). The normal mean V/Q ratio is approximately 1.3. Both ventilation and perfusion increase from lung apex to base, but perfusion increases more in comparison to ventilation. The ratio of ventilation to perfusion is higher in upper lungs. In upright position, the apex has more ventilation while base has more perfusion. In lateral position, the nondependent lung receives more ventilation and dependent lung receives higher perfusion.[27]

In supine position especially during expiration or immediately after general anesthesia, dependent lungs may become atelectasis (▶ Fig. 4.8). Atelectasis is less severe toward the lung apices. The area of atelectasis becomes the area of shunt where no gas exchange occurs in spite of perfusion. More extensive atelectasis after surgery is common and promotes ventilation perfusion mismatch ($V/Q < 1$) and impairment of gas exchange. Prone position improves the oxygenation by more uniform gas distribution and less lung compression by the heart. There will be no atelectasis in prone position, probably because the weight of the heart is shifted on the sternum instead of lungs as opposed to supine position.[20] CT scan in prone position is commonly used to differentiate interstitial lung pathologies from dependent lung atelectasis (▶ Fig. 4.9).

Aging is associated with an increase in pulmonary vascular resistance due to vascular stiffness. The pulmonary vascular pressure will increase and pulmonary capillary blood volume will be diminished. Another problem with aging is the loss of lung elastic recoil which limits expiratory airflow and induces pulmonary hyperinflation during exercise. Decrease in alveolar surface area due to hyperinflation (senile emphysema) may influence pulmonary vascular resistance and cardiac output.[28,29,30] Pulmonary overinflation combined with decreased chest wall compliance (barrel chest) leads to an increase in the FRC. Despite these changes, healthy aged adults appear to maintain gas exchange at adequate levels at rest and during exercise. Alteration in the distribution of V/Q ratio is common in many lung diseases. For example, decreased V/Q matching is a hallmark of chronic obstructive pulmonary disease (COPD) in which areas of high and low V/Q ratio coexist (▶ Fig. 4.10, ▶ Fig. 4.11, ▶ Fig. 4.12). In pulmonary embolism, perfusion is disrupted but ventilation may remain normal.[31,32]

◆ Imaging of Lung Function

Ventilation and perfusion can be imaged and analyzed using nuclear scan, CT, MRI, and positron emission tomography (PET)[31,32,33] (▶ Fig. 4.10, ▶ Fig. 4.11, ▶ Fig. 4.12). In contrast to anatomical imaging, functional imaging of the lungs does not require high spatial resolution. Physiological and functional imaging of the lung may be accurately performed with much larger voxel sizes equivalent to size of pulmonary gas exchange unit or an acinus which is approximately 1 cm^3.

◆ Radiological Diagnosis of Pulmonary Abnormalities

Many pulmonary disease processes can highlight the anatomy of the secondary pulmonary lobule, including consolidation, ground-glass opacity, both smooth and nodular interlobular septal thickening, centrilobular and “tree-in-bud” nodularity, and emphysema.

Many acute and chronic pulmonary diseases can cause lobular consolidation, including bronchopneumonia, organizing pneumonia, eosinophilic pneumonia, and low-grade adenocarcinoma.[7] Consolidation fills bronchioles and acini, highlighting bronchial branches (air bronchogram) (▶ Fig. 4.13).

Ground-glass opacity is defined as hazy, increased attenuation in the lungs that does not obscure the underlying vascular or bronchial structures.[34,35,36] Ground-glass opacity can be caused by a variety of acute and chronic lung diseases, such as infection, edema, and chronic infiltrative diseases such as hypersensitivity pneumonitis, alveolar proteinosis, and lipoid pneumonia.[7]

As discussed previously, the secondary pulmonary lobule is marginated by connective tissue septa, within which run venous and lymphatic structures. If the interlobular septa are visible on thin-section CT, this usually means that they are abnormally thickened. Septal thickening can be seen with interstitial fluid, cellular infiltration, or fibrosis, and can have a smooth or nodular

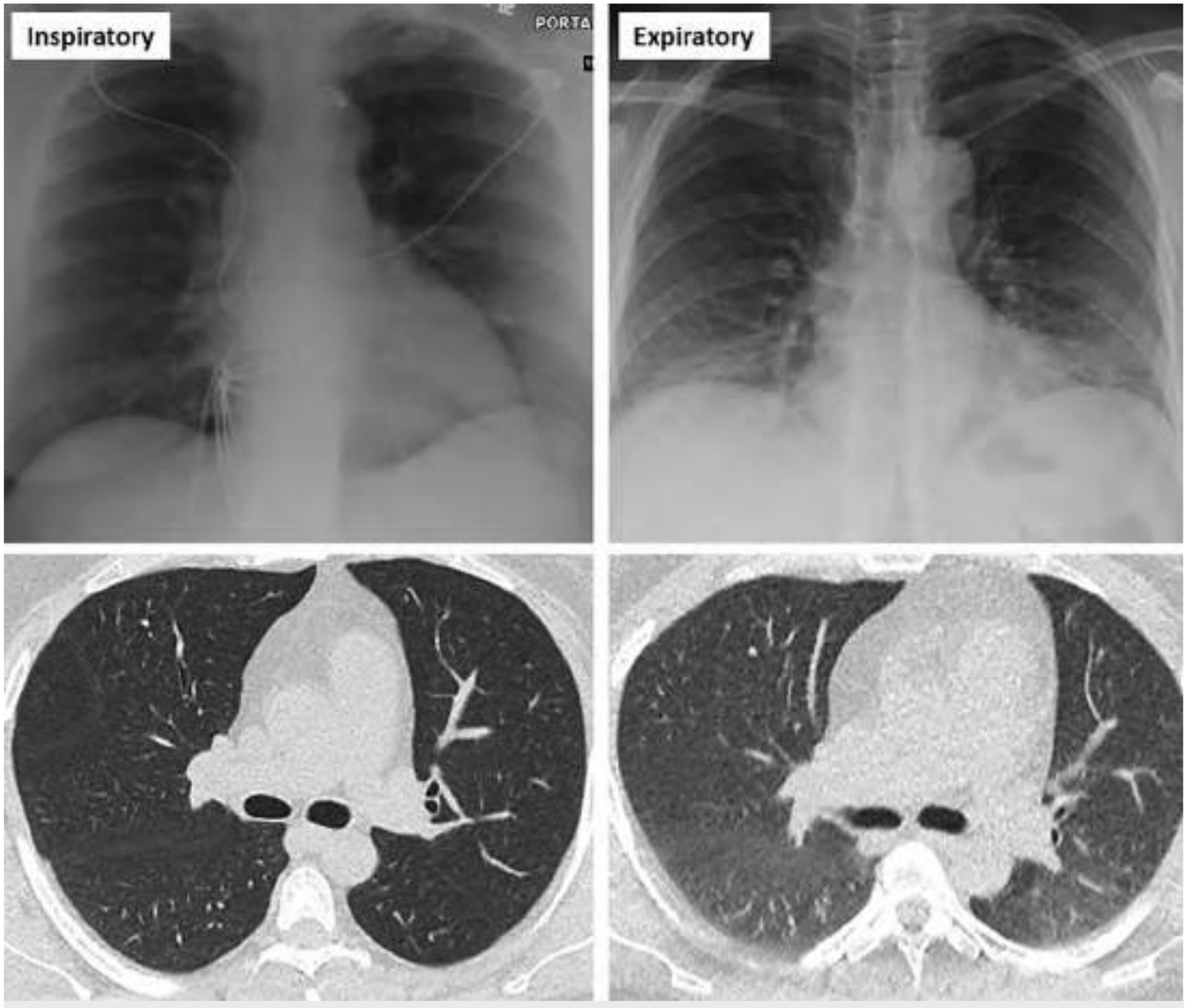

Fig. 4.8 Inspiratory versus expiratory lungs shown by plain radiographs and CT scan. Crowding of vessels and decrease ventilation of the dependent lungs are noted in expiratory phase. The ratio of ventilation to perfusion is higher in upper lungs. In upright position, the apex has more ventilation while base has more perfusion. In supine position, the nondependent lung receives more ventilation and dependent lung receives higher perfusion.

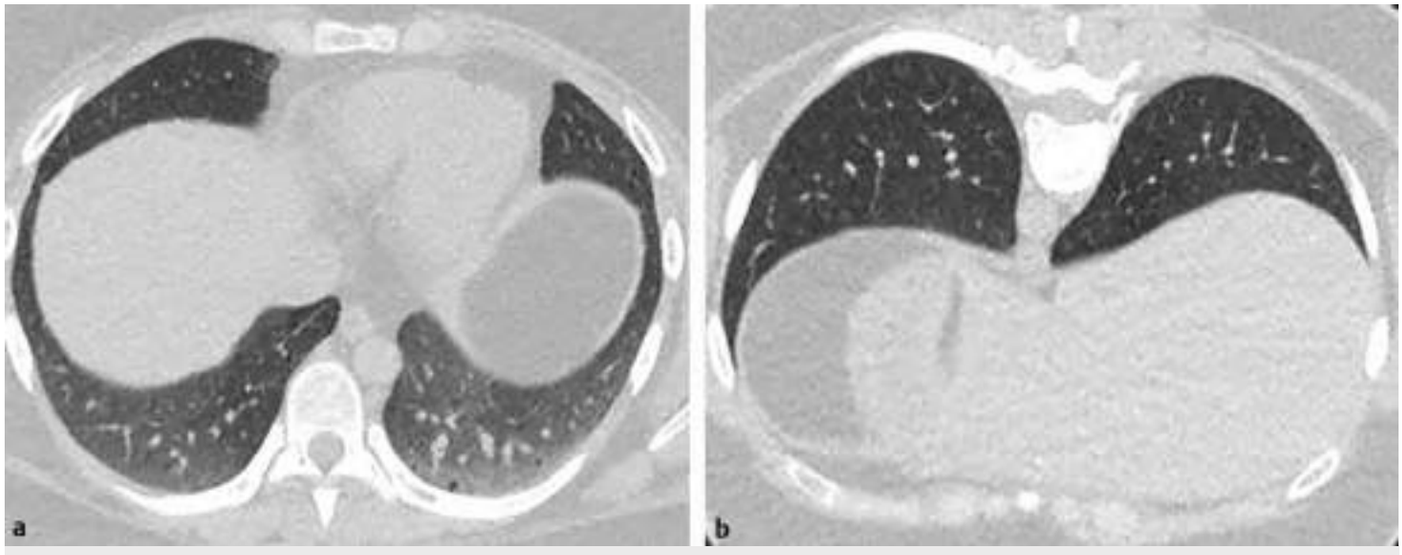

Fig. 4.9 Axial CT scans in **(a)** supine and **(b)** prone positions showing improved dependent atelectasis of the lung bases in prone position.

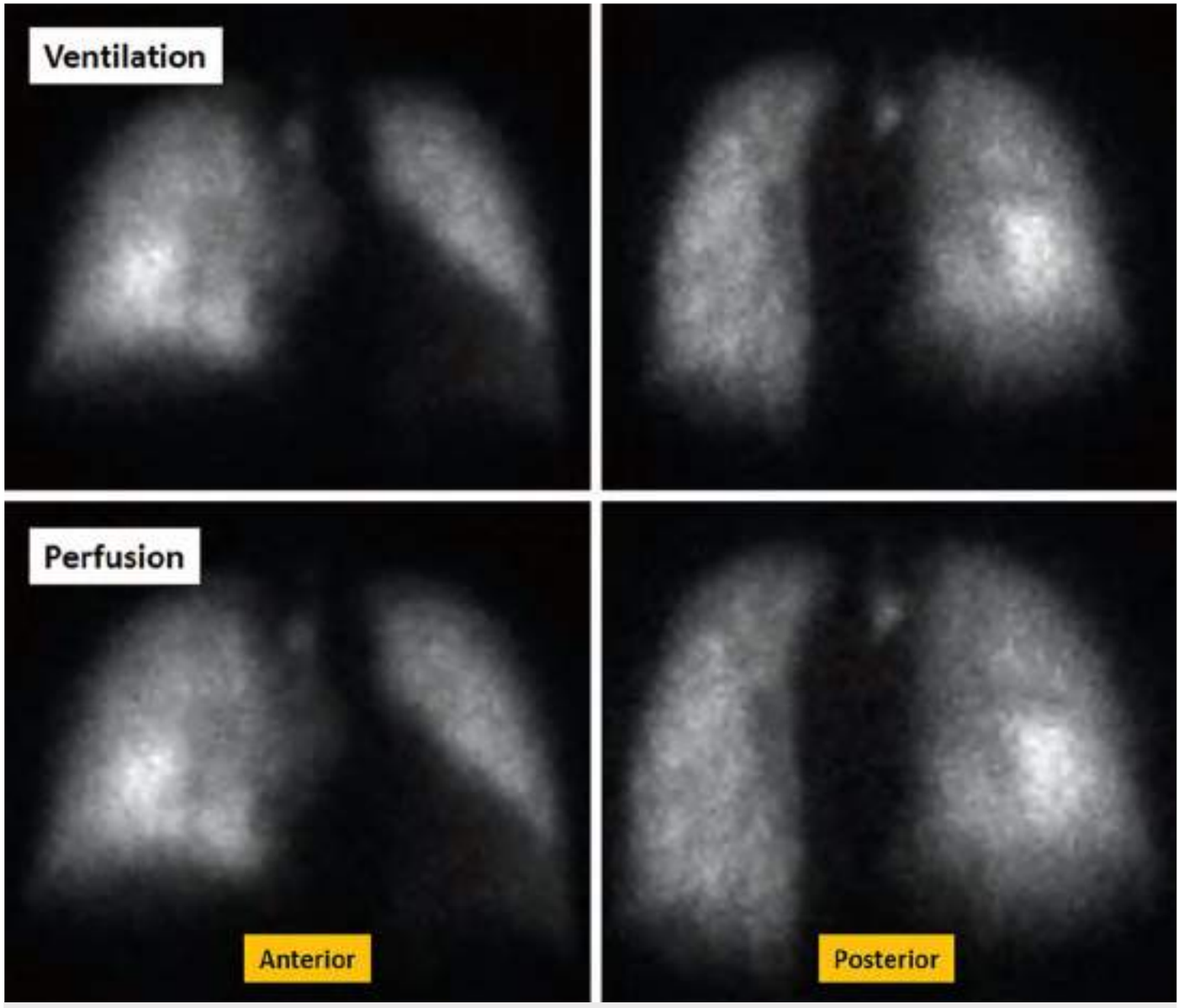

Fig. 4.10 Normal ventilation and perfusion of the lungs are shown by nuclear imaging. Ventilation images are acquired after the administration of approximately Tc-99 m DTPA aerosol. Following the intravenous administration of Tc-99 m MAA, perfusion images of the lung are obtained in different projections. Homogeneous tracer activity throughout both lungs is seen.

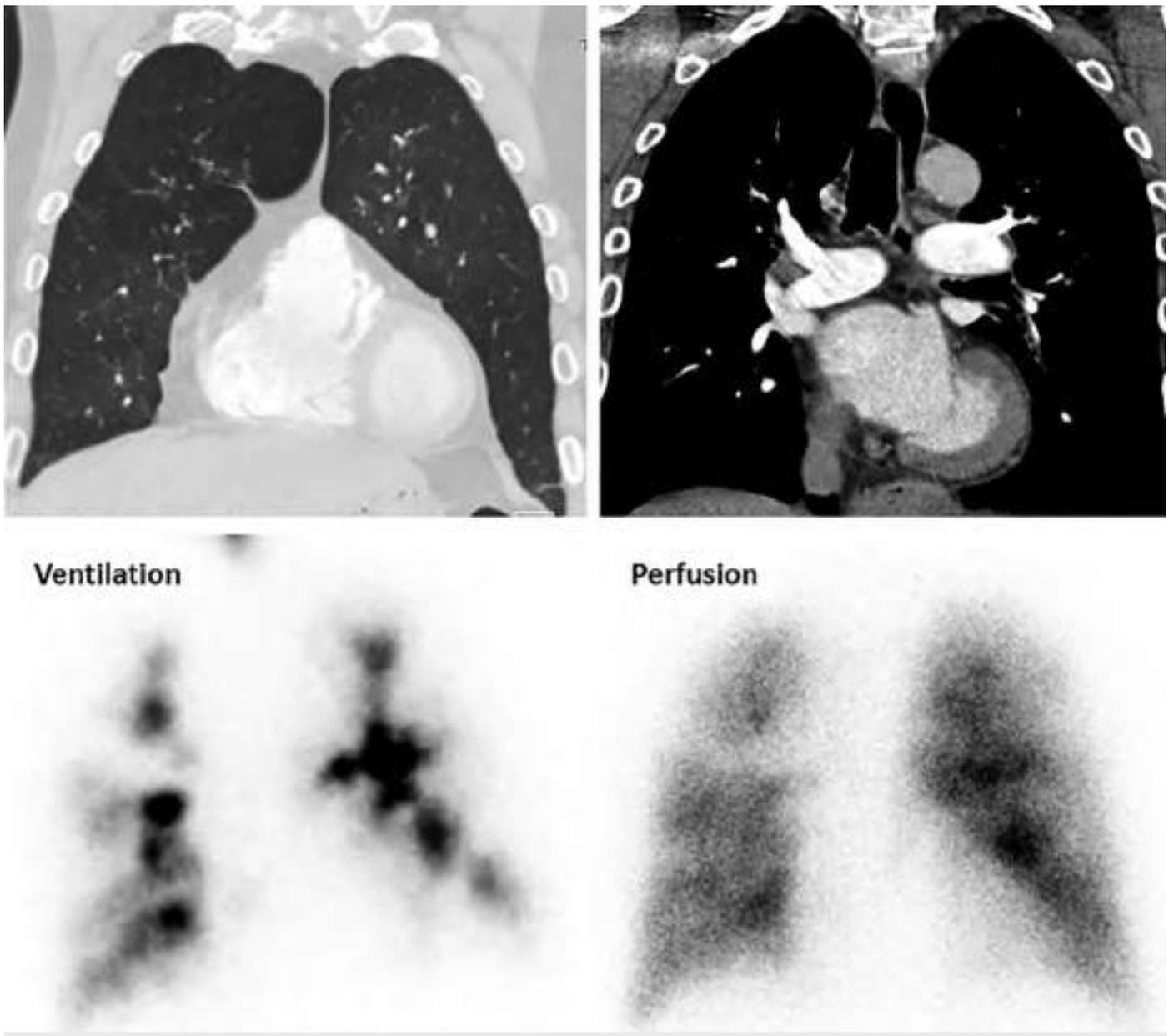

Fig. 4.11 Matched ventilation and perfusion defects in a patient with severe chronic obstructive pulmonary disease (COPD) and pulmonary emphysema. Upper row: CT images showing pulmonary emphysema and normal major pulmonary arteries. Lower row: Multiple matched ventilation–perfusion defects are noted throughout the bilateral lungs. There is patchy distribution of tracer activity throughout both lungs.

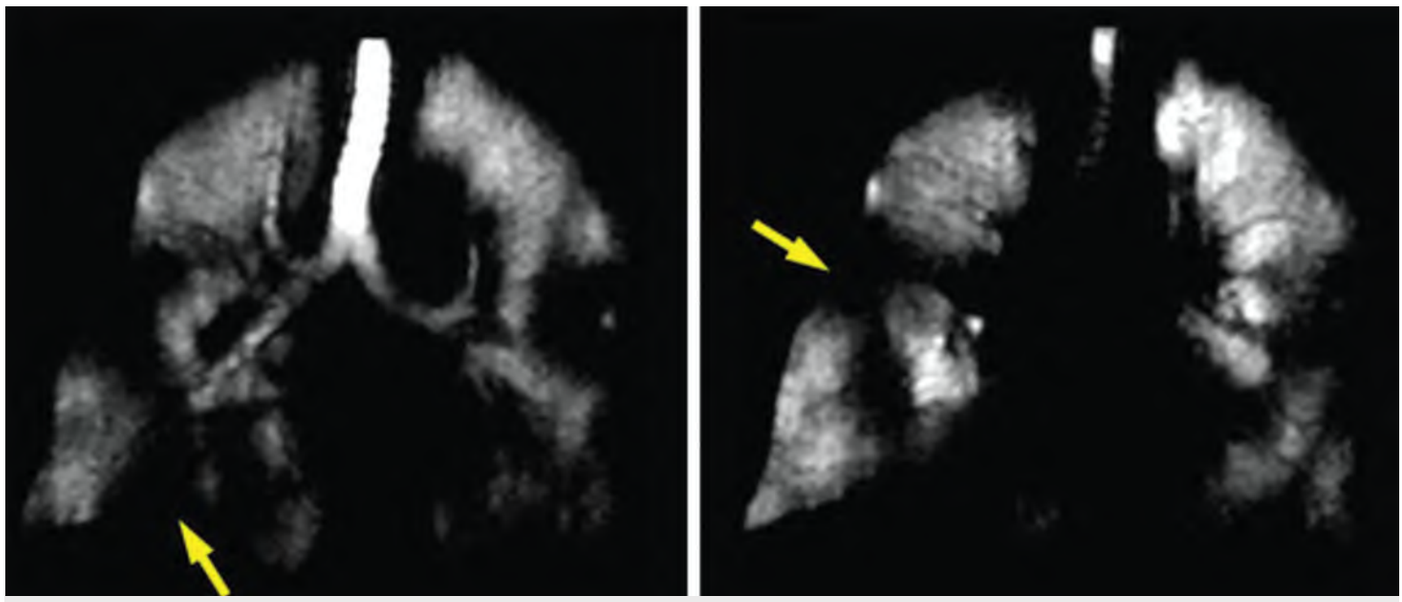

Fig. 4.12 Ventilation defects (*arrows*) shown by hyperpolarized ^{3}He MRI in a patient with chronic obstructive pulmonary disease (COPD). Adapted from Kirby et al 2013.[32]

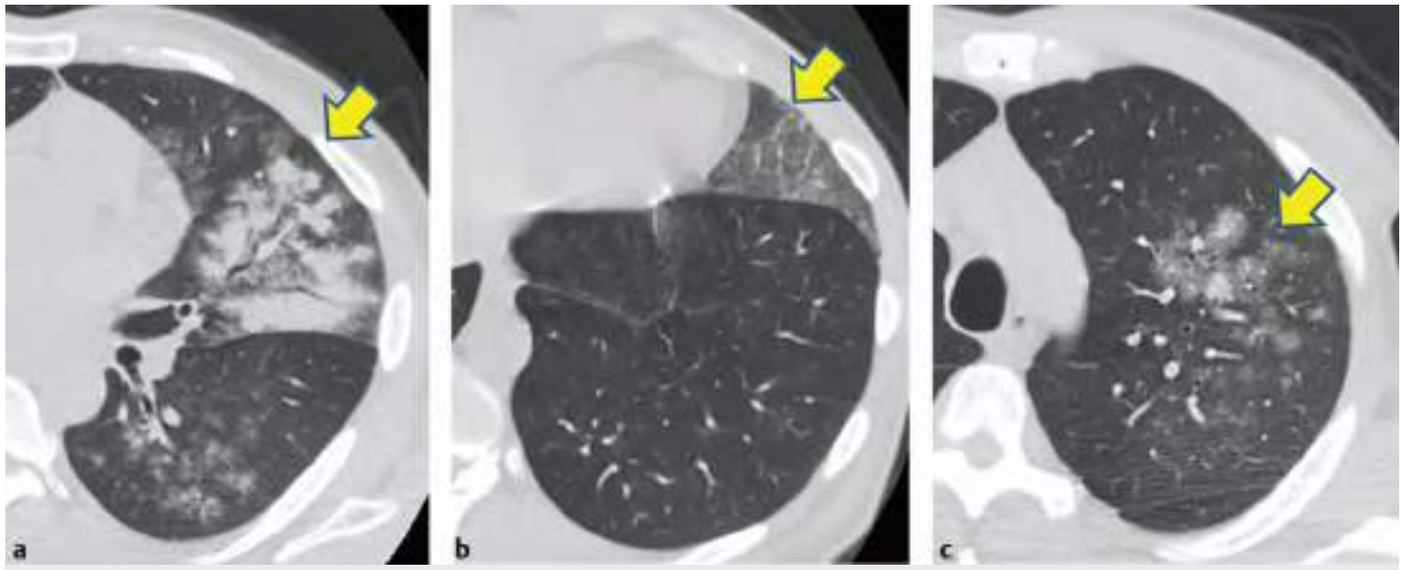

Fig. 4.13 Transverse CT images. **(a)** Thick secretions of bronchopneumonia fill multiple acini; **(b)** ground-glass opacity. Vascular and bronchial structures are visible through ground-glass opacity within the lingula. **(c)** Lobular ground-glass opacity within the left upper lobe.

appearance depending on the pathological process[7,37] (▶ Fig. 4.14).

Smooth interlobular septal thickening is most commonly seen in pulmonary edema and hemorrhage.[38] Nodular interlobular septal thickening is usually secondary to lymphangitic spread of tumor and pulmonary sarcoidosis (▶ Fig. 4.14).

The term centrilobular nodules indicate that the abnormality is related to the centrilobular structures of the secondary pulmonary lobule such as the centrilobular bronchiole, arteriole, lymphatics, and interstitium.[7] Given the location of the centrilobular structures in the secondary pulmonary lobule, on CT, a centrilobular nodule usually appears to be separated from the pleural surfaces, fissures, and interlobular septa by at least several millimeters. Thus, in the periphery of the lung, centrilobular nodules are usually centered approximately 5 to 10 mm from the pleural surface[7] (▶ Fig. 4.14). Centrilobular nodules are usually seen in disease related to the centrilobular bronchiole and can be related to either interstitial or airspace abnormalities. The differential diagnosis is broad, including infection, inflammation, and endobronchial spread of tumor.[39] Tree-in-bud sign usually reflects the presence of dilated centrilobular bronchioles with lumina that are impacted with mucus, fluid, or pus, and it is often associated with peribronchiolar inflammation.[7,40] Because of the branching pattern of the dilated bronchiole, its appearance has been likened to a budding or fruiting tree (▶ Fig. 4.15). The tree-in-bud finding usually represents small airways disease.

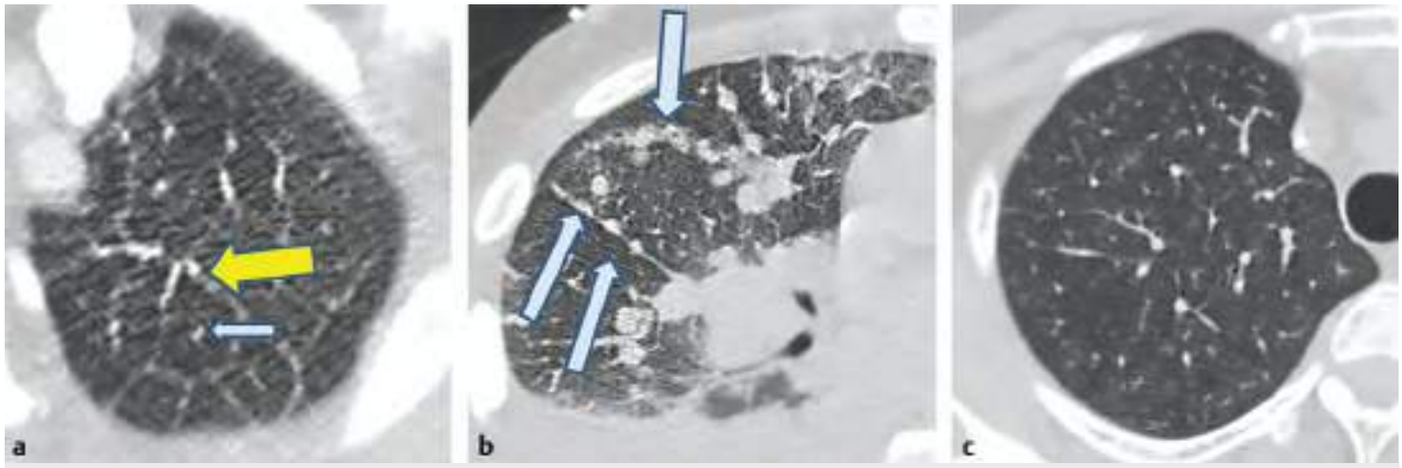

Fig. 4.14 **(a)** Transverse CT shows smooth interlobular septal thickening outlining multiple secondary pulmonary lobules within the upper lobes of a patient with pulmonary edema. Pulmonary veins (*large arrows*) within the septa are visible as branching opacities, lines, or dots. Pulmonary artery is seen in the center of the lobules (*small arrow*). **(b)** Transverse CT image. Nodular interlobular septal thickening (*arrows*) in a patient with metastatic prostate carcinoma, suspicious for lymphangitic carcinomatosis. **(c)** Transverse CT image. Solid and ground-glass centrilobular nodules which may be related to cholesterol granuloma formation in a patient with chronic pulmonary hypertension.

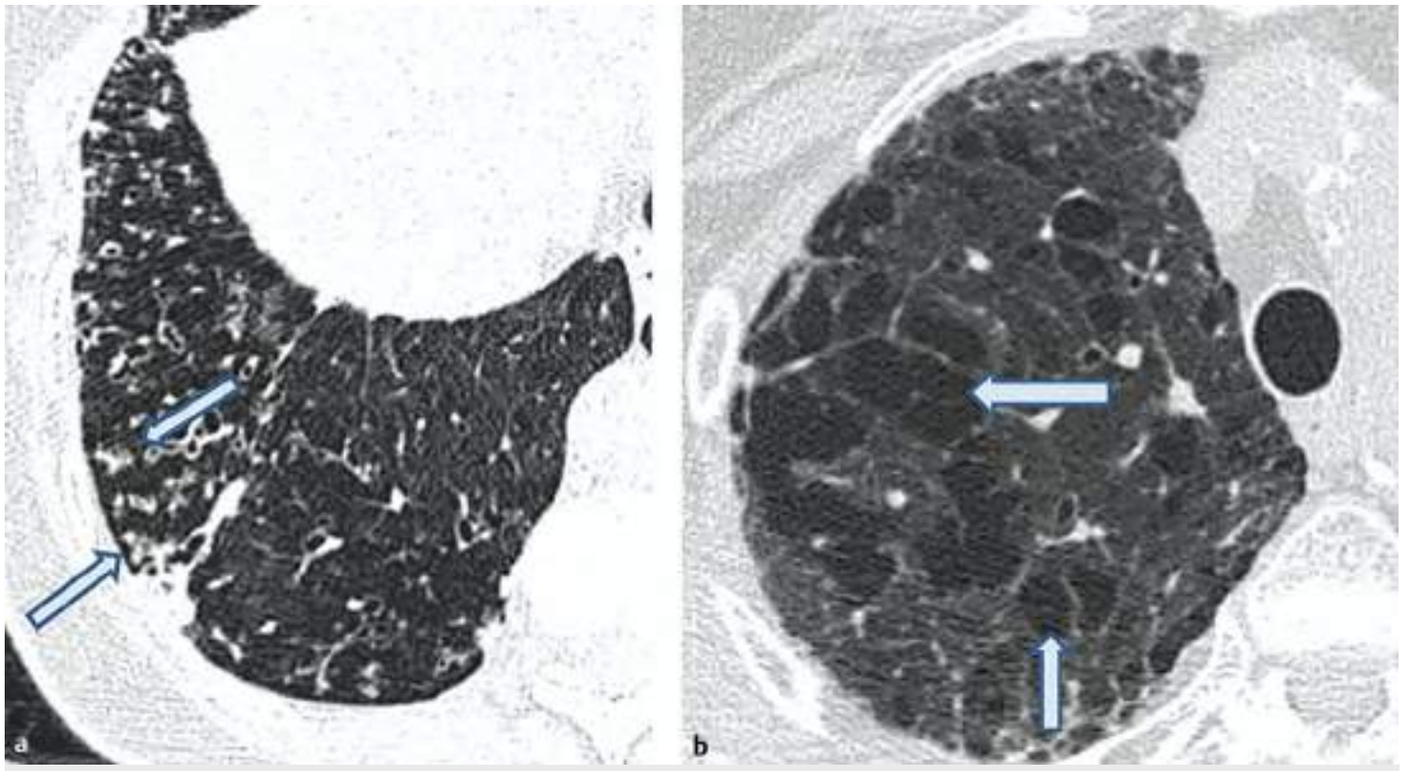

Fig. 4.15 **(a)** Transverse CT image. Bronchiectasis, bronchiectasis, bronchial wall thickening, and centrilobular and tree-in-bud nodularity (*arrows*) in a patient with history of *Mycobacterium avium* complex (MAC) infection. **(b)** Transverse CT image of a patient with centrilobular and paraseptal emphysema shows low attenuation surrounding the centrilobular structures representing destruction in relation to the centriacinar bronchioles. The centrilobular artery is visible in the center of the abnormal secondary pulmonary lobule (*arrows*).

Centrilobular areas of abnormal low attenuation can be seen in emphysema. On histology, centrilobular emphysema is characterized by lung destruction occurring in relation to the centriacinar bronchioles and therefore is located in the center of the secondary pulmonary lobule, surrounding the centrilobular artery. On a CT scan of a patient with centrilobular emphysema, the centrilobular artery is often visible in the center of an area of low attenuation that lacks, in most cases, a visible wall[7] (▶ Fig. 4.15).

References

[1] Berrocal T, Madrid C, Novo S, Gutiérrez J, Arjonilla A, Gómez-León N. Congenital anomalies of the tracheobronchial tree, lung, and mediastinum: embryology, radiology, and pathology. Radiographics.; 24(1):e17

[2] Zylak CJ, Eyler WR, Spizarny DL, Stone CH. Developmental lung anomalies in the adult: radiologic-pathologic correlation. Radiographics.; 22(Spec No): S25–S43

[3] Keslar P, Newman B, Oh KS. Radiographic manifestations of anomalies of the lung. Radiol Clin North Am.; 29(2):255–270

[4] Skandalakis JE, Gray SW, Symbas P. The trachea and the lung. In:S kandalakis JE, Gray SW, eds. Embryology for Surgeons. 3rd ed. Baltimore, MD: Williams and Wilkins; 1994:414–450

[5] Hayashi K, Aziz A, Ashizawa K, Hayashi H, Nagaoki K, Otsuji H. Radiographic and CT appearances of the major fissures. Radiographics.; 21(4):861–874

[6] Sealy WC, Connally SR, Dalton ML. Naming the bronchopulmonary segments and the development of pulmonary surgery. Ann Thorac Surg.; 55(1):184–188

[7] Webb WR. Thin-section CT of the secondary pulmonary lobule: anatomy and the image—the 2004 Fleischner lecture. Radiology.; 239(2):322–338

[8] Heitzman ER, Markarian B, Berger I, Dailey E. The secondary pulmonary lobule: a practical concept for interpretation of chest radiographs. I. Roentgen anatomy of the normal secondary pulmonary lobule. Radiology.; 93(3):507–512

[9] Hansen JE, Ampaya EP. Human air space shapes, sizes, areas, and volumes. J Appl Physiol.; 38(6):990–995

[10] Itoh H, Murata K, Konishi J, Nishimura K, Kitaichi M, Izumi T. Diffuse lung disease: pathologic basis for the high-resolution computed tomography findings. J Thorac Imaging.; 8(3):176–188

[11] Osborne DRS, Effmann EL, Hedlund LW. Postnatal growth and size of the pulmonary acinus and secondary lobule in man. AJR Am J Roentgenol.; 140 (3):449–454

[12] Gamsu G, Thurlbeck WM, Macklem PT, Fraser RG. Peripheral bronchographic morphology in the normal human lung. Invest Radiol.; 6(3):161–170

[13] Reich SB, Abouav J. Interalveolar air drift. Radiology.; 85:80–86

[14] Chae EJ, Seo JB, Kim N, et al. Collateral ventilation in a canine model with bronchial obstruction: assessment with xenon-enhanced dual-energy CT. Radiology.; 255(3):790–798

[15] Terry PB, Traystman RJ. The clinical significance of collateral ventilation. Ann Am Thorac Soc.; 13(12):2251–2257

[16] Cetti EJ, Moore AJ, Geddes DM. Collateral ventilation. Thorax.; 61(5):371–373

[17] Goo HW, Yang DH, Kim N, Park SI, Kim DK, Kim EA. Collateral ventilation to congenital hyperlucent lung lesions assessed on xenon-enhanced dynamic dual-energy CT: an initial experience. Korean J Radiol.; 12(1):25–33

[18] Koster TD, Slebos DJ. The fissure: interlobar collateral ventilation and implications for endoscopic therapy in emphysema. Int J Chron Obstruct Pulmon Dis.; 11:765–773

[19] Levin DL, Schiebler ML, Hopkins SR. Physiology for the pulmonary functional imager. Eur J Radiol.

[20] Patwa A, Shah A. Anatomy and physiology of respiratory system relevant to anaesthesia. Indian J Anaesth.; 59(9):533–541

[21] Hedenstierna G, Baehrendtz S, Klingstedt C, et al. Ventilation and perfusion of each lung during differential ventilation with selective PEEP. Anesthesiology.; 61(4):369–376

[22] Townsley MI. Structure and composition of pulmonary arteries, capillaries, and veins. Compr Physiol.; 2(1):675–709

[23] Murillo H, Cutalo MJ, Jones RP, Lane MJ, Fleischmann D, Restrepo CS. Pulmonary circulation imaging: embryology and normal anatomy. Semin Ultrasound CT MR.; 33(6):473–484

[24] Ivanov KP. Circulation in the lungs and microcirculation in the alveoli. Respir Physiol Neurobiol.; 187(1):26–30

[25] Cauldwell EW, Siekert RG, Lininger RE, Anson BJ. The bronchial arteries; an anatomic study of 150 human cadavers. Surg Gynecol Obstet.; 86(4):395–412

[26] Hasegawa I, Kobayashi K, Kohda E, Hiramatsu K. Bronchopulmonary arterial anastomosis at the precapillary level in human lung. Visualization using CT angiography compared with microangiography of autopsied lung. Acta Radiol.; 40(6):578–584

[27] Rothen HU, Sporre B, Engberg G, Wegenius G, Hedenstierna G. Airway closure, atelectasis and gas exchange during general anaesthesia. Br J Anaesth.; 81 (5):681–686

[28] Taylor BJ, Johnson BD. The pulmonary circulation and exercise responses in the elderly. Semin Respir Crit Care Med.; 31(5):528–538

[29] Roman MA, Rossiter HB, Casaburi R. Exercise, ageing and the lung. Eur Respir J.; 48(5):1471–1486

[30] Oyarzún G M. [Pulmonary function in aging]. Rev Med Chil.; 137(3):411–418

[31] Brudin LH, Rhodes CG, Valind SO, Wollmer P, Hughes JM. Regional lung density and blood volume in nonsmoking and smoking subjects measured by PET. J Appl Physiol (1985).; 63(4):1324–1334

[32] Kirby M, Kanhere N, Etemad-Rezai R, McCormack DG, Parraga G. Hyperpolarized helium-3 magnetic resonance imaging of chronic obstructive pulmonary disease exacerbation. J Magn Reson Imaging.; 37(5):1223–1227

[33] Lee SM, Seo JB, Hwang HJ, et al. Assessment of regional emphysema, air-trapping and Xenon-ventilation using dual-energy computed tomography in chronic obstructive pulmonary disease patients. Eur Radiol.

[34] Naidich DP, Bankier AA, MacMahon H, et al. Recommendations for the management of subsolid pulmonary nodules detected at CT: a statement from the Fleischner Society. Radiology.; 266(1):304–317

[35] Truong MT, Ko JP, Rossi SE, et al. Update in the evaluation of the solitary pulmonary nodule. Radiographics.; 34(6):1658–1679

[36] Lee HY, Choi YL, Lee KS, et al. Pure ground-glass opacity neoplastic lung nodules: histopathology, imaging, and management. AJR Am J Roentgenol.; 202 (3):W224–W233

[37] Kang EY, Grenier P, Laurent F, Müller NL. Interlobular septal thickening: patterns at high-resolution computed tomography. J Thorac Imaging.; 11 (4):260–264

[38] Storto ML, Kee ST, Golden JA, Webb WR. Hydrostatic pulmonary edema: high-resolution CT findings. AJR Am J Roentgenol.; 165(4):817–820

[39] Munk PL, Müller NL, Miller RR, Ostrow DN. Pulmonary lymphangitic carcinomatosis: CT and pathologic findings. Radiology.; 166(3):705–709

[40] Murata K, Itoh H, Todo G, et al. Centrilobular lesions of the lung: demonstration by high-resolution CT and pathologic correlation. Radiology.; 161 (3):641–645

5 The Pleura

Sumuda N. Dissanayake and Farhood Saremi

◆ Introduction

The pleura, derived from the Greek word for *side*, is the serous membrane that covers the lung parenchyma, mediastinum, diaphragm, and rib cage. The pleura allows the lung to expand and contract within the rigid confines of the thoracic cavity by transmitting mechanical forces from the diaphragm and chest wall with minimal friction. They also serve as a protective barrier from infection.[1]

◆ Embryology

The cephalad portion of the embryonic coelomic cavity enlarges during week 4 of development, becoming the pericardial cavity and communicating on each side with the pleural canals. The pleural canals in turn communicate with the peritoneal canals. These compartments of the coelomic cavity are divided by three partitions: (1) the septum transversum serves as an early partial diaphragm, (2) the pleuropericardial membranes divide the pericardial and pleural cavities, and (3) the pleuroperitoneal membranes join with the septum transversum to complete the diaphragm which serves as the partition between each pleural cavity and the peritoneal cavity. The resulting pleural cavity is completely lined by a mesothelial membrane that develops from the somatic mesoderm to become the parietal pleura. The pleural cavity is complete by the third month.[1]

The primordial bronchial buds are recognizable by 24 days and lie together with the trachea in a median mass of mesenchyme that is cranial and dorsal to the peritoneal cavity (▶ Fig. 5.1). This mesenchyme develops into the mediastinum and separates the pleural cavities. The lung buds bulge into the right and left pleural cavities, carrying with them a lining of mesothelium that develops from the splanchnic mesoderm to become the visceral pleura. As the separate lobes of the lung develop, their mesothelial covering is retained as the visceral pleura in the fissures.[1]

◆ The Pleura

The pleura is comprised of the parietal and visceral pleura. The parietal pleura measures 0.1 mm in thickness and is composed of a single layer of mesothelial cells joined with a layer of loose connective tissue containing systemic capillaries, lymphatic vessels, and sensory nerves. The parietal pleura lines the thoracic cavity and is separated from the endothoracic fascia, which lines the inner ribs and innermost intercostal muscles, by a layer of extrapleural fat along most of the chest wall (▶ Fig. 5.2) (see Chapter 1, Thoraic Wall). This extrapleural fat is continuous with the mediastinal fat, therefore mediastinal processes including air,

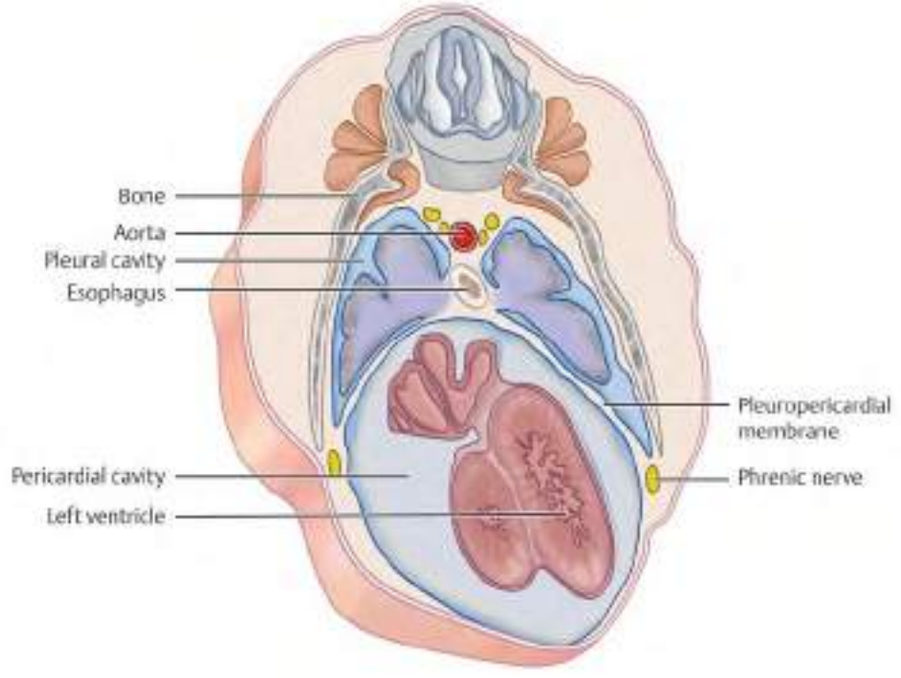

Fig. 5.1 Embryology of the pleura. The primitive lungs grow into the pleural cavity and are covered by the visceral pleura. (Used with permission from Finley and Rusch 2011.[1])

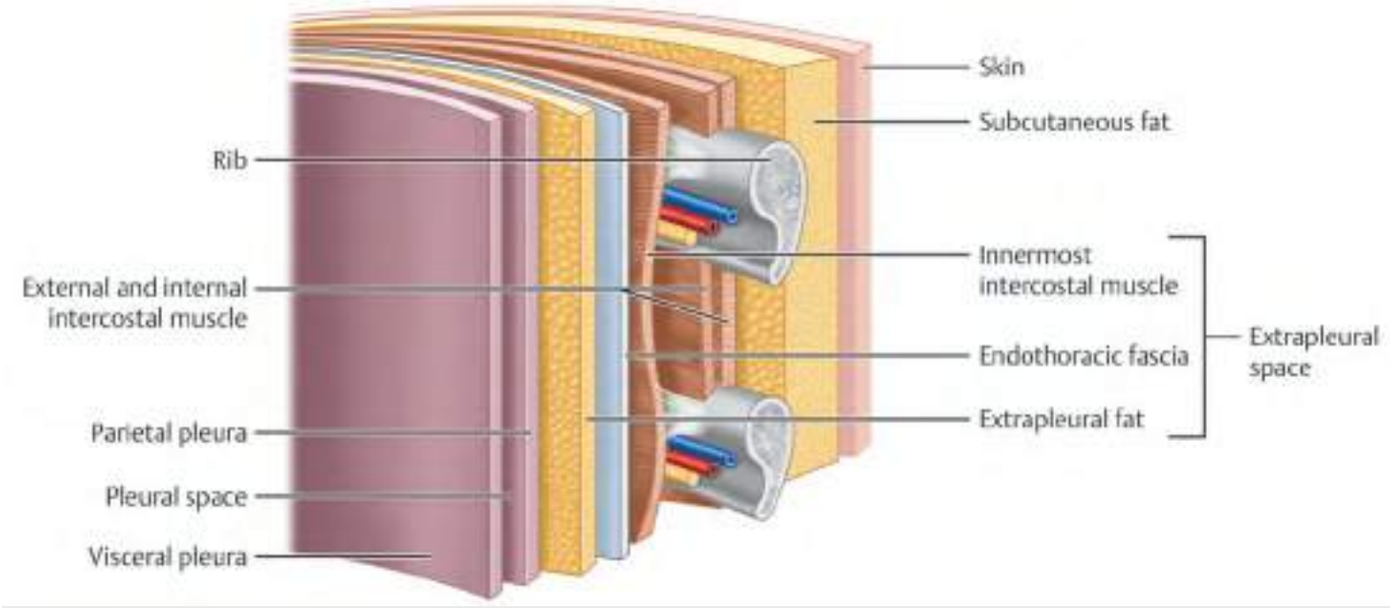

Fig. 5.2 Normal anatomy of the pleura and extrapleural space. The extrapleural space separates the parietal pleura and inner surface of the rib cage. It consists of the innermost intercostal muscle, endothoracic fascia, and extrapleural fat.

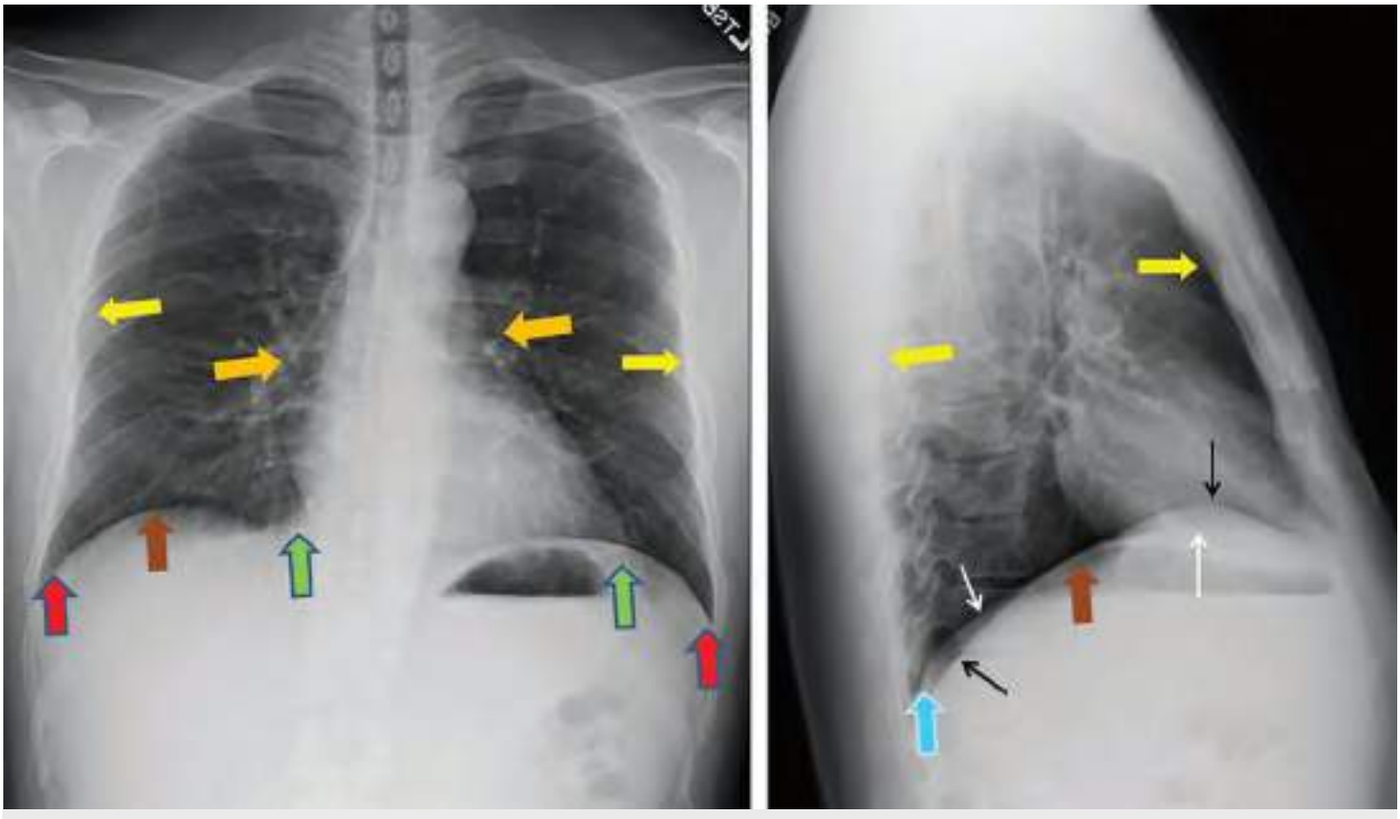

Fig. 5.3 Pleural wall and recesses on frontal and lateral chest radiographs. Red, lateral costophrenic recess; green, mediastinophrenic (cardiophrenic) recess; orange, mediastinal pleura; brown, diaphragmatic pleura; yellow, costal pleura; blue, right and left posterior costophrenic recesses; right diaphragmatic parietal pleura (*black arrow*) (identified by its higher position anteriorly); left diaphragmatic parietal pleura (*white arrow*) (identified by its association with the subjacent gastric bubble and inferior cardiac border).

inflammation, or edema can infiltrate into the extrapleural space. The parietal pleura is subdivided by the surfaces it covers into the mediastinal, costal, and diaphragmatic parietal pleura (▶ Fig. 5.3, ▶ Fig. 5.4). It is strongly adherent to the fibrous pericardium and diaphragm.[2,3]

The visceral pleura measures 0.1 to 0.2 mm in thickness and consists of single layer of mesothelial cells that joins with the fibroelastic fascia of the subpleural interstitium of the lung. It adheres to the lung parenchyma from the hilum outward and lines the interlobar fissures.[2,3] The closed potential space

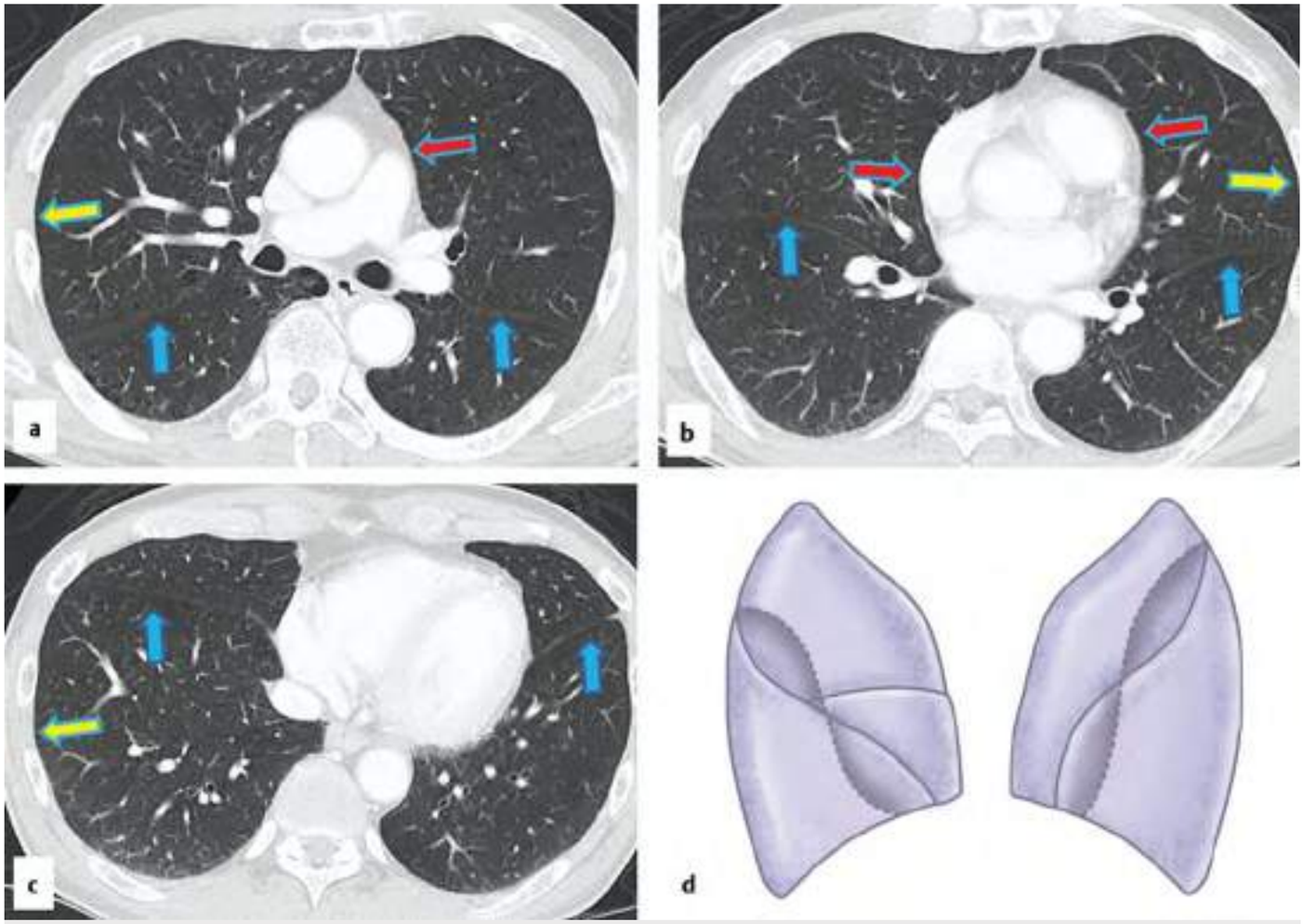

Fig. 5.4 (a–c) Axial noncontrast CT; yellow, costal parietal pleura; red, mediastinal parietal pleura. The major fissures (*blue arrows*) are seen as dense bands. Oblique fissures demonstrate a typical concave anterior configuration in upper thorax and concave posterior configuration in the lower thorax. **(d)** Drawing shows propeller-shaped configuration of the major fissures. (Used with permission from Hayashi et al 2001.[5])

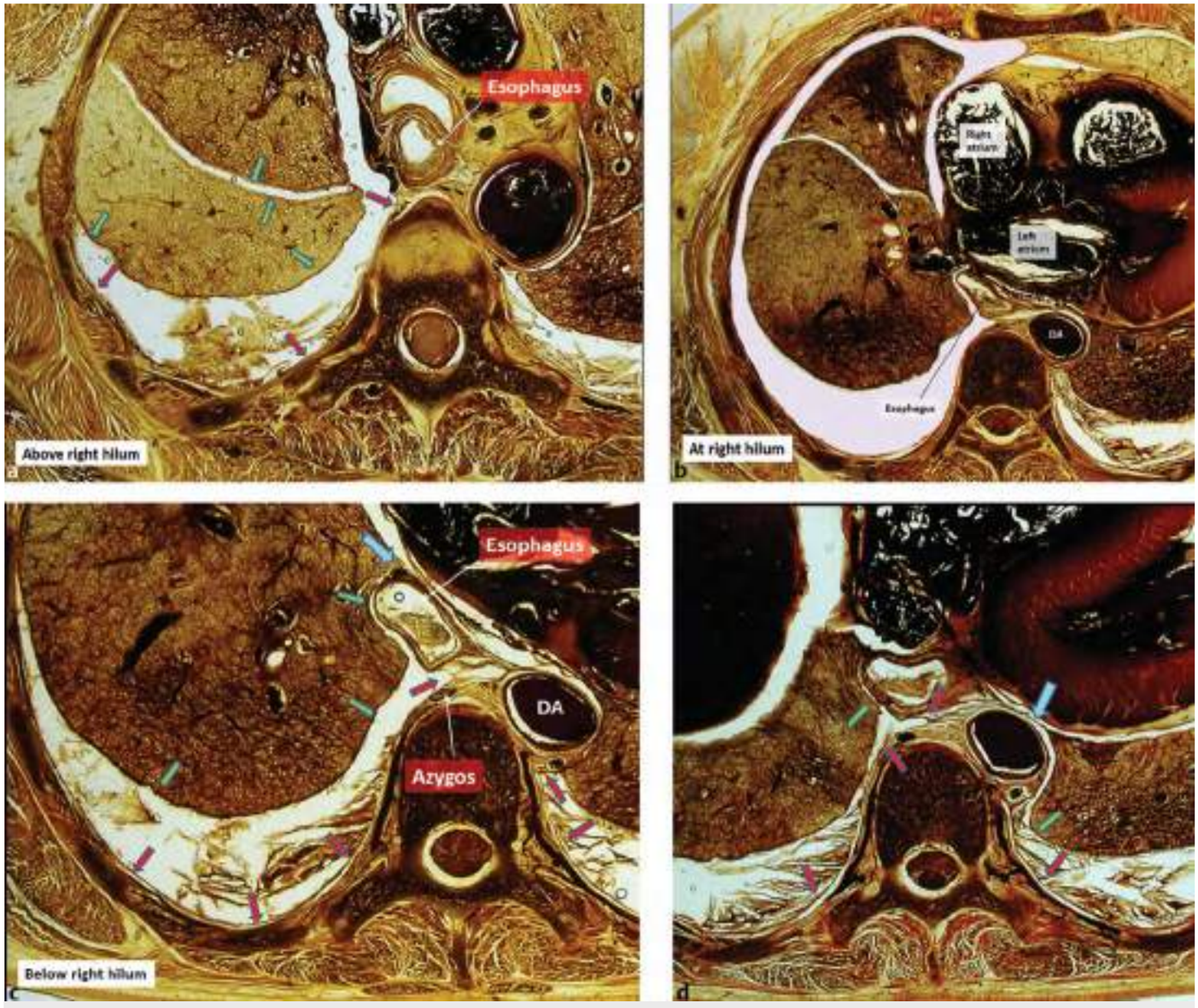

Fig. 5.5 (a–d) Cadaveric axial sections from superior to inferior showing parietal (*red arrows*, *red lining*) and visceral (*green arrows*) pleural surfaces. Above the level of the right hilum, there is no attachment between the two pleural surfaces. The visceral pleura adheres to the lung parenchyma from the hilum outward and lines the interlobar fissures. The visceral pleura merges with mediastinal parietal pleura at pulmonary root and encloses the structures of the pulmonary hilum. Below the hilar level, the reflection of the mediastinal pleura over the visceral pleura continues as a bilayered sheet of both visceral and parietal pleura (total of four layers) in the front and back of the hilar plane to form the inferior pulmonary ligament. Medially, the inferior pulmonary ligament inserts on the right side along the right lateral border of the esophagus (*blue arrow* on the right) and on the left side between the posterior pericardium and anterior margin of the thoracic aorta (*blue arrow* on the left side). Note, azygoesophageal recess is well formed below the hilum **(c)**. DA, descending aorta.

between the parietal and visceral pleura is known as the pleural space. It typically contains a thin film of fluid that acts as lubricant to minimize friction as the visceral pleura slides along the parietal pleura during respiration. Many disease processes can lead to fluid accumulation in the pleural space, known as a pleural effusion. The right and left pleural space are separated by the mediastinum and do not normally communicate.[1]

The visceral pleura merges with mediastinal parietal pleura at pulmonary root and encloses the structures of the pulmonary hilum. At the inferior aspect of the root, the reflection of the mediastinal pleura over the visceral pleura continues as a bilayered sheet of both visceral and parietal pleura (total of four layers) in the front and back of the hilar plane to form the inferior pulmonary ligament (also known as the triangular ligament), that is carried downward and more posteriorly from the medial aspect of the lung to the mediastinum (▶ Fig. 5.5, ▶ Fig. 5.6). Medially, the inferior pulmonary ligament is inserted on the right side along the right lateral border of the esophagus and on the left side on the posterior aspect of the pericardium and thoracic aorta (▶ Fig. 5.5, ▶ Fig. 5.6, ▶ Fig. 5.7). The lower border is located posteriorly, has a variable configuration, and may insert on the diaphragm (▶ Fig. 5.7). The inferior pulmonary ligament contains loose connective tissue, bronchial and esophageal arterial branches, venules that empty into superior diaphragmatic veins, and lymphatic trunks and nodes that drain the lower lobes of the lung and lower third of the esophagus.[4] Blood vessels in the

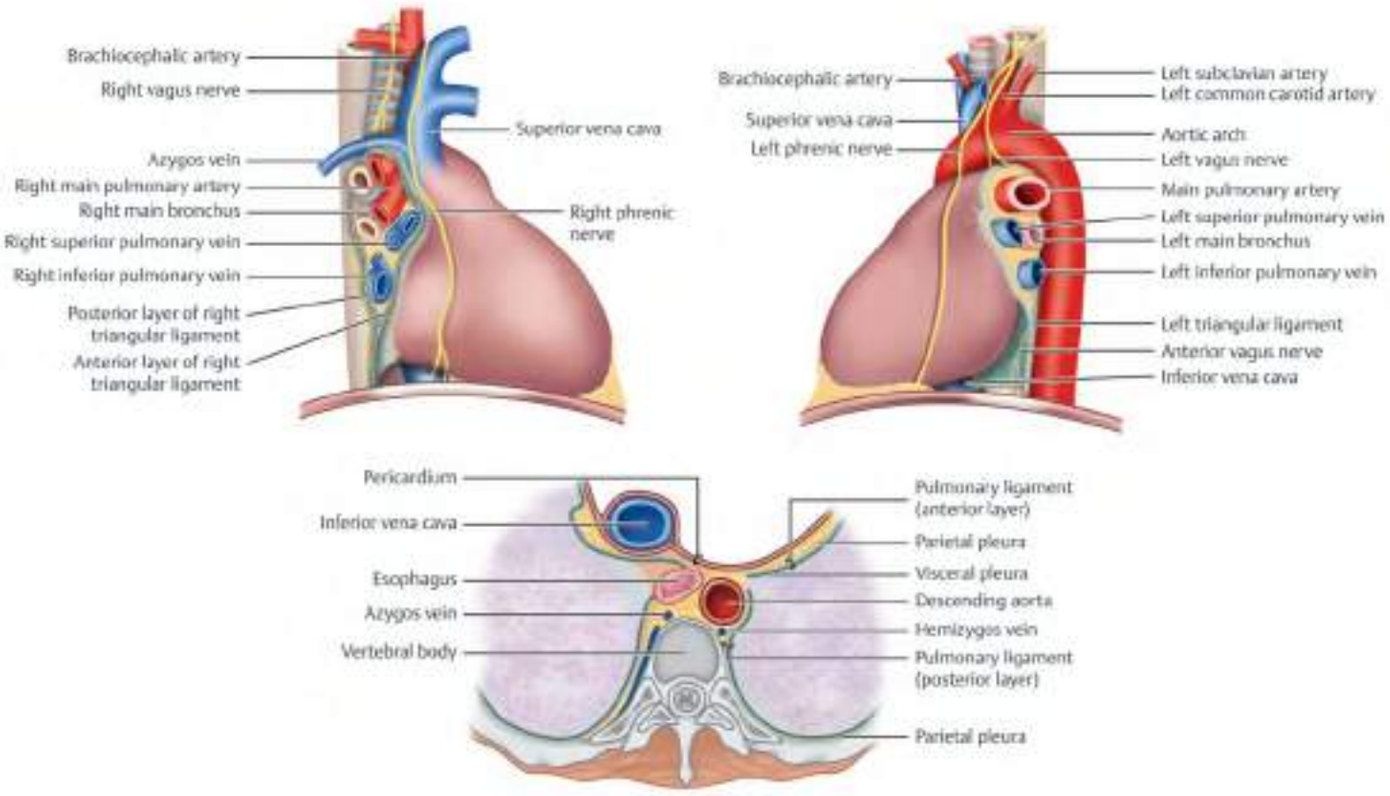

Fig. 5.6 Normal pleural anatomy at hilar level. The visceral pleura encircles the pulmonary hilum and merges with the mediastinal parietal pleura to form the pulmonary ligament. The pulmonary ligament connects to the mediastinum medially and the diaphragm inferiorly.

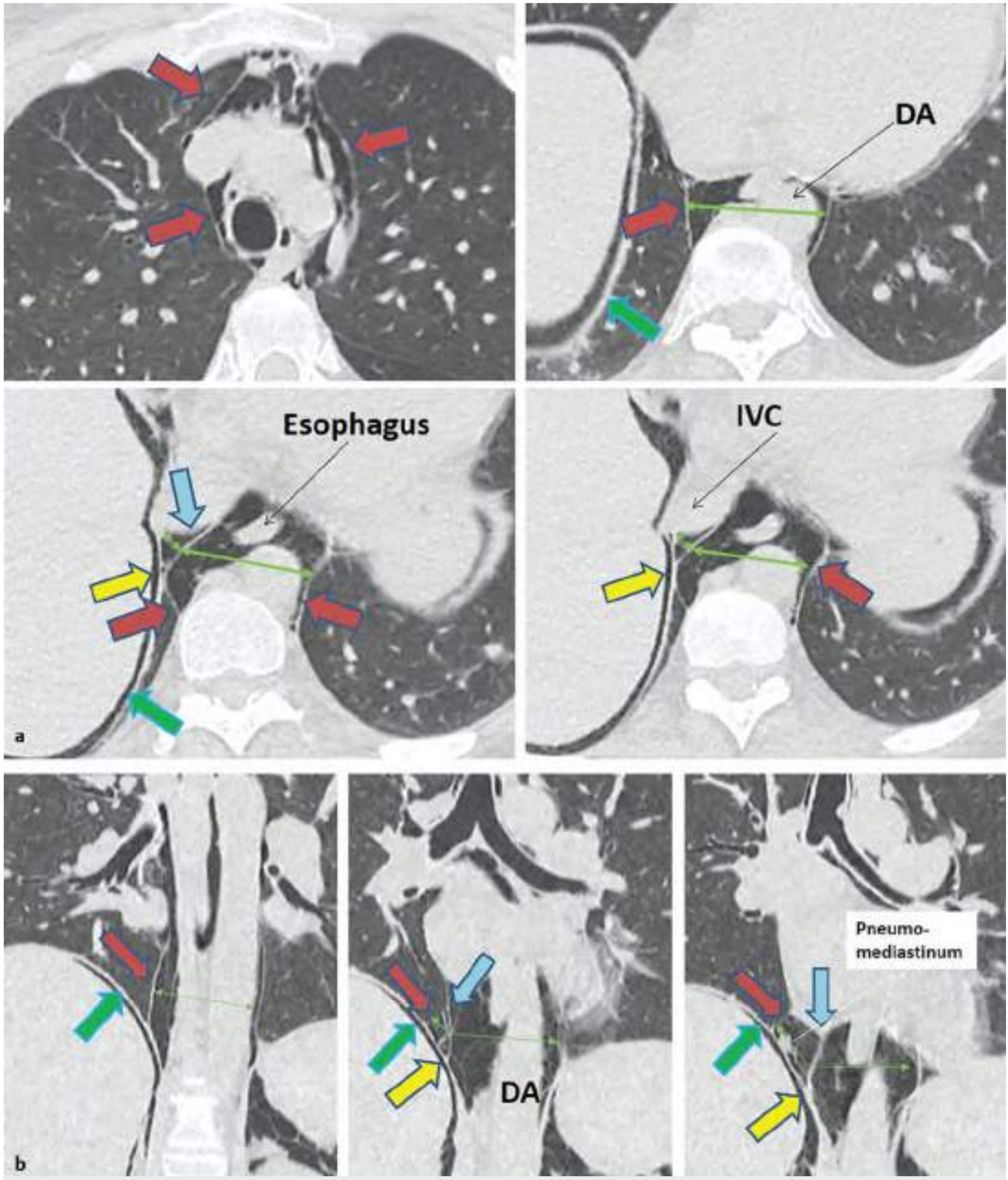

Fig. 5.7 **(a)** Inferior pulmonary ligament is shown on the right side in a patient with extensive pneumomediastinum without pneumothorax. Axial (top to bottom) and coronal (posterior to anterior) CT images are shown. The mediastinal pleura (*red arrows*) is displaced laterally on both sides by the pneumomediastinum. **(b)** The width of the pneumomediastinum is shown by double-headed arrows. The right hemidiaphragm is shown by green arrows. Inferior margin of the diaphragm is outlined by extraperitoneal air inferiorly. The inferior pulmonary ligament (*blue arrows*) is outlined on both sides by the mediastinal air. Its inferior attachment to the diaphragm is shown by yellow arrows. Medially, it extends between the esophagus and the inferior vena cava (IVC). DA, descending aorta.

ligament could be the source of hemorrhage following blunt thoracic injuries. After trauma, air may dissect into the ligament and produce a localized pneumothorax or bleb. Inferior pulmonary ligament is usually seen as a linear or triangular structure at posterior cardiophrenic angles on axial CT images.

The interlobar fissures separate lobes of the lungs and extend from the hilum to the lung surface (▶ Fig. 5.4, ▶ Fig. 5.8). Normal major fissures consist of double layers of infolded invaginations of the visceral pleura. The oblique (major) fissures originate posteriorly near the T4–T5 level and terminate along the anterior diaphragmatic pleura. The right oblique fissure separates the right upper and middle lobes from the right lower lobe. The left oblique fissure separates the left upper and lower lobes. The right major fissure is shorter and wider than the left. The lower part of the left oblique fissure is more posterior due to anterior location of the heart in the left hemithorax. Both fissures have an undulating course with the upper part concave anteriorly and faces laterally, whereas the lower part is convex anteriorly and faces medially (▶ Fig. 5.4, ▶ Fig. 5.5). This configuration is variable. The right minor fissure separates the right middle and upper lobes.[1,2,3] Radiological identification of a lesion in relation to a fissure is important for precise localization of a lesion. Oblique fissures are best identified on lateral chest X-rays and the minor fissure on both lateral and frontal views (▶ Fig. 5.8). The superolateral part of oblique fissure can be identified on frontal X-rays as a curving contour, line, or edge at the upper lateral lung field due to small pleural fluid or extrapleural fat[5] (▶ Fig. 5.9). The superomedial part of the oblique fissure may also be seen on frontal X-ray in the upper paramediastinal lung due to angulation of the medial part of the fissure.

Boundaries and Pleural Recesses

The pleura extends 2 to 3 cm above the first rib, rising beneath the sternocleidomastoid muscle to cover the cupola or dome of the lung. Inferiorly, the pleura follows the line of attachment between the diaphragm and chest wall, ending at the level of the 6th or 7th rib anteriorly, coursing obliquely laterally, and reaching below the 12th rib posteriorly[1,6] (▶ Fig. 5.10). Although predominantly protected by the bony thorax, the pleura is vulnerable to injury above the medial first rib, below the costoxiphisternal angle anteromedially on the right, and posteromedially below the bilateral costovertebral angles.[4]

The pleural recesses are potential spaces located in regions where the parietal pleura changes direction (▶ Fig. 5.10, ▶ Fig. 5.11, ▶ Fig. 5.12). They are present bilaterally at expiration and fill in with lung during inspiration and include the anterior and posterior costomediastinal recess, costophrenic recess, and mediastinophrenic recess[1,4] (▶ Fig. 5.11). The anterior costomediastinal recesses are located between the anterior costal pleura and mediastinal pleura and extend from the sternoclavicular joints down to the seventh costal cartilages (▶ Fig. 5.12). The interpleural triangles denote the spaces separating the right and left anterior costomediastinal recesses superiorly and inferiorly (▶ Fig. 5.12). The left anterior costomediastinal recess may be larger than the right due to the cardiac notch in the left lung. The posterior costomediastinal recesses are located between the mediastinal and posterior costal pleura and extend from the first rib to the 11th intercostal space. Extension of the mediastinal pleura between the hilum or inferior vena cava anteriorly and the vertebral body posteriorly is known as azygoesophageal recess because it is delimited by the esophagus/azygos vein medially (▶ Fig. 5.12). Medial margin of this recess can be seen on frontal chest X-rays as a linear line anterior to the spine (▶ Fig. 5.11). The costophrenic recesses (lateral and posterior) are located at the junction between the costal and diaphragmatic pleura and extend from the 7th costal cartilage anteriorly to the neck of the 12th rib posteriorly (▶ Fig. 5.12). The mediastinophrenic recesses are located between the mediastinal and diaphragmatic pleura and extend from the posterior aspect of the sternum to the posterior 11th intercostal space. The right mediastinophrenic recess is associated with the pericardium, right phrenic nerve, right atrium, inferior vena cava, right border of the esophagus, and right vagus nerve. The left mediastinophrenic recess is associated with the pericardium, left phrenic nerve, left ventricle, esophagus, left vagus nerve, and descending thoracic aorta.[7]

Histology

The pleura consists of a single layer of mesothelial cells laying over connective tissue. The mesothelial cells have a rich endoplasmic reticulum and Golgi complex that facilitates absorption and phagocytosis necessary for active clearance of the pleural space. Microvilli line the mesothelial cells and are coated with surfactant molecules that act as lubricant. The basement membrane is rich in elastic fibers, vasculature, lymphatics, and nerve endings.[8,9]

Blood Supply

The parietal pleura receives blood supply from the systemic arterial system. The intercostal arteries supply the costal pleura, the superior phrenic and musculophrenic arteries supply the diaphragmatic pleura, and the pericardiophrenic artery predominantly supplies the mediastinal pleura. The venous drainage of the parietal pleura is primarily via the intercostal veins which empty into the inferior vena cava or brachiocephalic veins. The diaphragmatic pleura may drain to the inferior phrenic veins to the inferior vena cava or through the superior phrenic veins to the superior vena cava.[3,10]

The visceral pleura receives most of its arterial supply via the bronchial arteries, however, portions adjacent to the diaphragm and costal surfaces are also supplied by the pulmonary arteries. The venous drainage of the visceral pleura is to the pulmonary veins.[10]

Innervation

The parietal pleura has extensive nervous innervation via somatic, sympathetic, and parasympathetic fibers. The costal pleura and periphery of the diaphragmatic pleura are supplied by the intercostal nerves. When these surfaces are stimulated, pain is perceived in the adjacent chest wall. The mediastinal pleura and central diaphragmatic pleura are supplied by the phrenic nerve. Associated stimulation in these areas results in referred

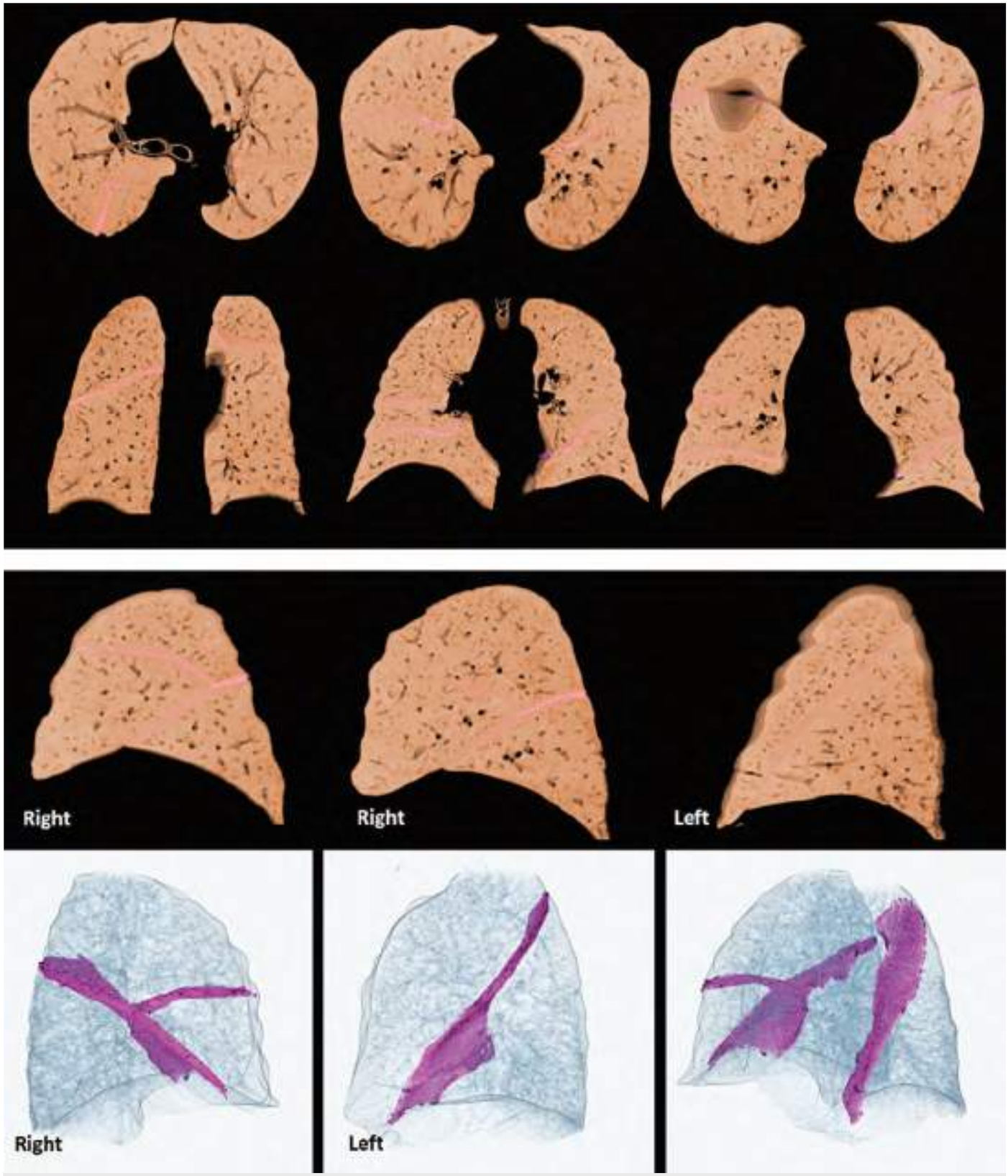

Fig. 5.8 CT images of the lung reconstructed in axial, coronal, and sagittal to show the pleural fissures in 2D and 3D projections.

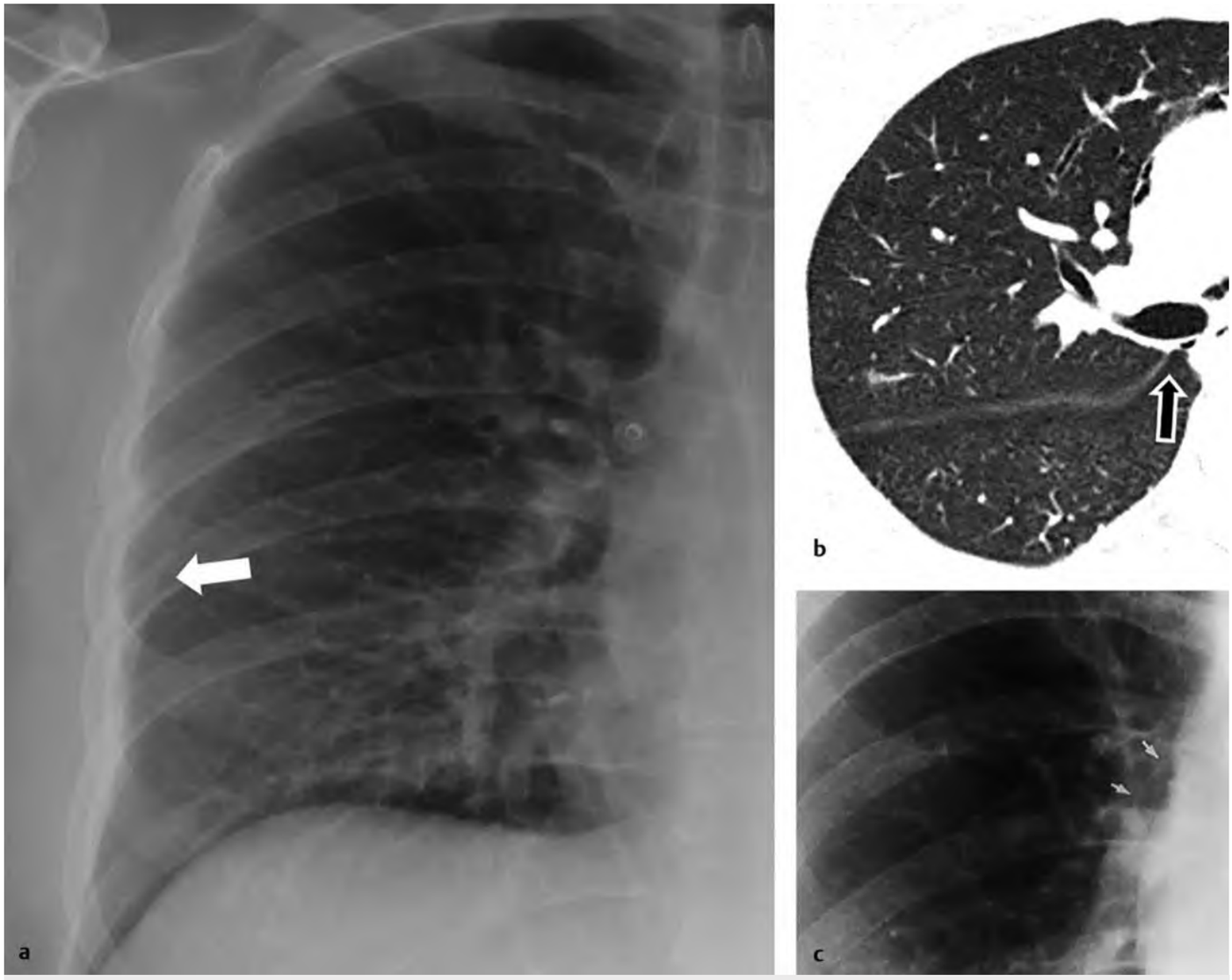

Fig. 5.9 **(a)** Inferior margin of the right major fissure (*arrow*) is demarcated by pleural effusion. **(b, c)** Demonstration of the superomedial part of the oblique fissure on frontal X-ray (*arrows*) in the upper paramediastinal lung due to vertical angulation of the medial part of the fissure (*black arrow*). Similar variation can occur on the lateral margin of the major fissure to make it visible on frontal X-rays.

pain in the ipsilateral shoulder.[1,3] Recent evidence has shown nerve endings in the visceral pleura in animals that are closely associated with the elastic fibers of the lung. Known as visceral pleura receptors, these fibers are believed to mediate sensory transduction of painful or mechanical stimuli and may act in producing reflexive dyspnea in the setting of pleural disease.[1]

Lymphatic Drainage

Lymphatic channels in the parietal pleura communicate with the pleural space via stomas measuring 2 to 12 µm that are found predominantly along the mediastinal parietal pleura and intercostal surfaces, particularly in the lower chest. These stomas are the primary pathway for elimination of material from the pleural space. The visceral pleura does not have stoma and thus does not act in clearance of pleural fluid.[7,9,11]

Lymphatic plexuses in the costal pleura are mainly confined to the intercostal spaces. These channels drain anteriorly toward internal thoracic lymph nodes or posteriorly toward intercostal lymph nodes. The lymphatic channels in the mediastinal pleura drain to tracheobronchial and mediastinal nodes. Diaphragmatic pleural lymphatic channels drain to parasternal, middle phrenic, and posterior mediastinal nodes. Transdiaphragmatic channels are also present which allow seeding of the pleural space by some abdominal malignancies.[1] The visceral pleura has an extensive lymphatic plexus that drains from the lung surface toward the hilum. The plexus also penetrates internally to join lymph channels along the interlobular septa. All drainage from the visceral pleura eventually reaches the lung root.[1]

◆ Incomplete and Accessory Fissures

Extension of the pleura into the fissures allows each individual lobe to expand and contract independently. However, in many individuals the fissures are incomplete which reduces this independence.[12] Accessory fissures are clefts lined by visceral pleura that usually occur at the boundaries between bronchopulmonary segments. They are the most common developmental pulmonary

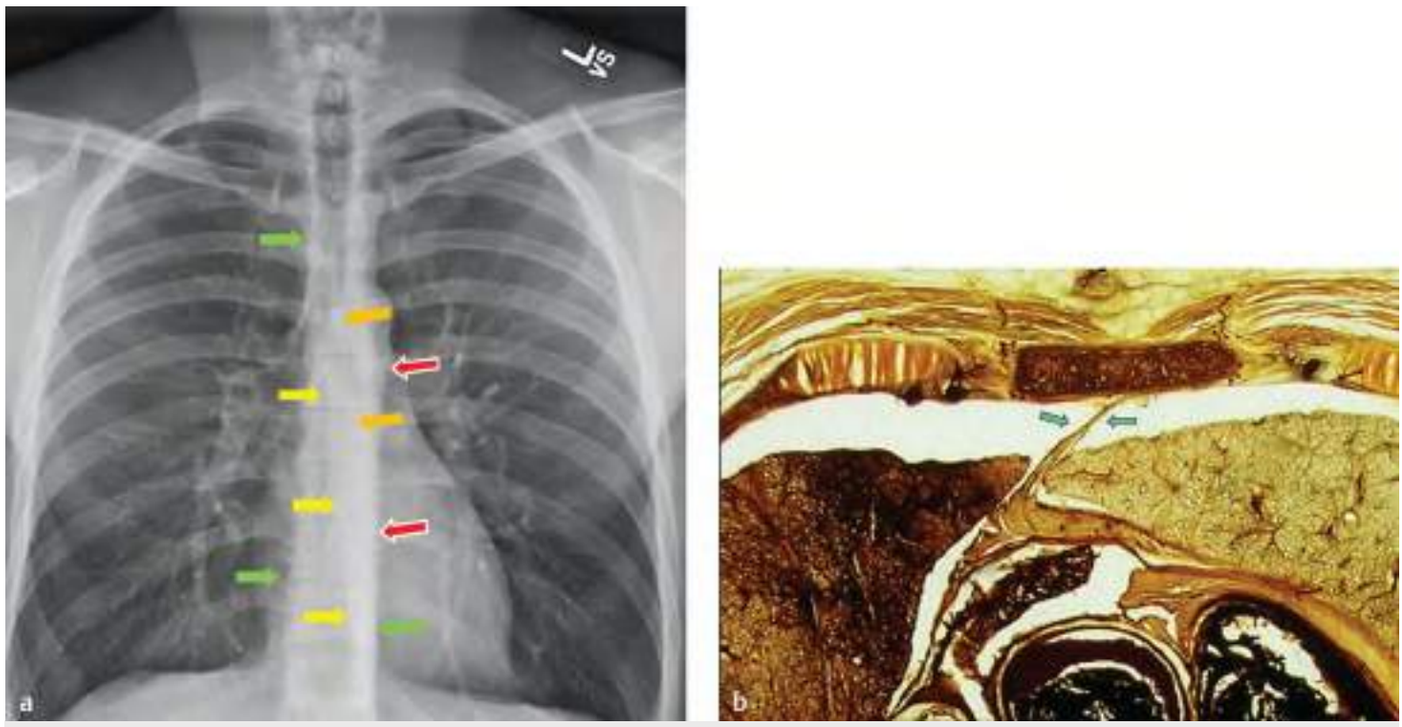

Fig. 5.10 **(a)** Paramediastinal recesses are shown. The anterior costomediastinal recess is formed by apposition of the mediastinal pleura in the anterior mediastinum to form the anterior junctional line (*orange arrows*) on X-ray. The posterior costomediastinal recesses are formed with the vertebra (*green arrows*). Additional recesses along the mediastinal pleura include the azygoesophageal recess (*yellow arrows*) bordered medially by the azygos vein and the descending aortic recesses along the anterior or posterior walls of the aorta. Red arrows demarcate the lateral margin of the descending aorta. In emphysematous lungs the posterior mediastinal pleural surfaces may approach each other to from the posterior junctional line behind the heart. **(b)** Cadaveric section shows the right and left mediastinal parietal pleura approaching each other anterior to the mediastinum (*arrows*) to form the anterior junctional line and recesses.

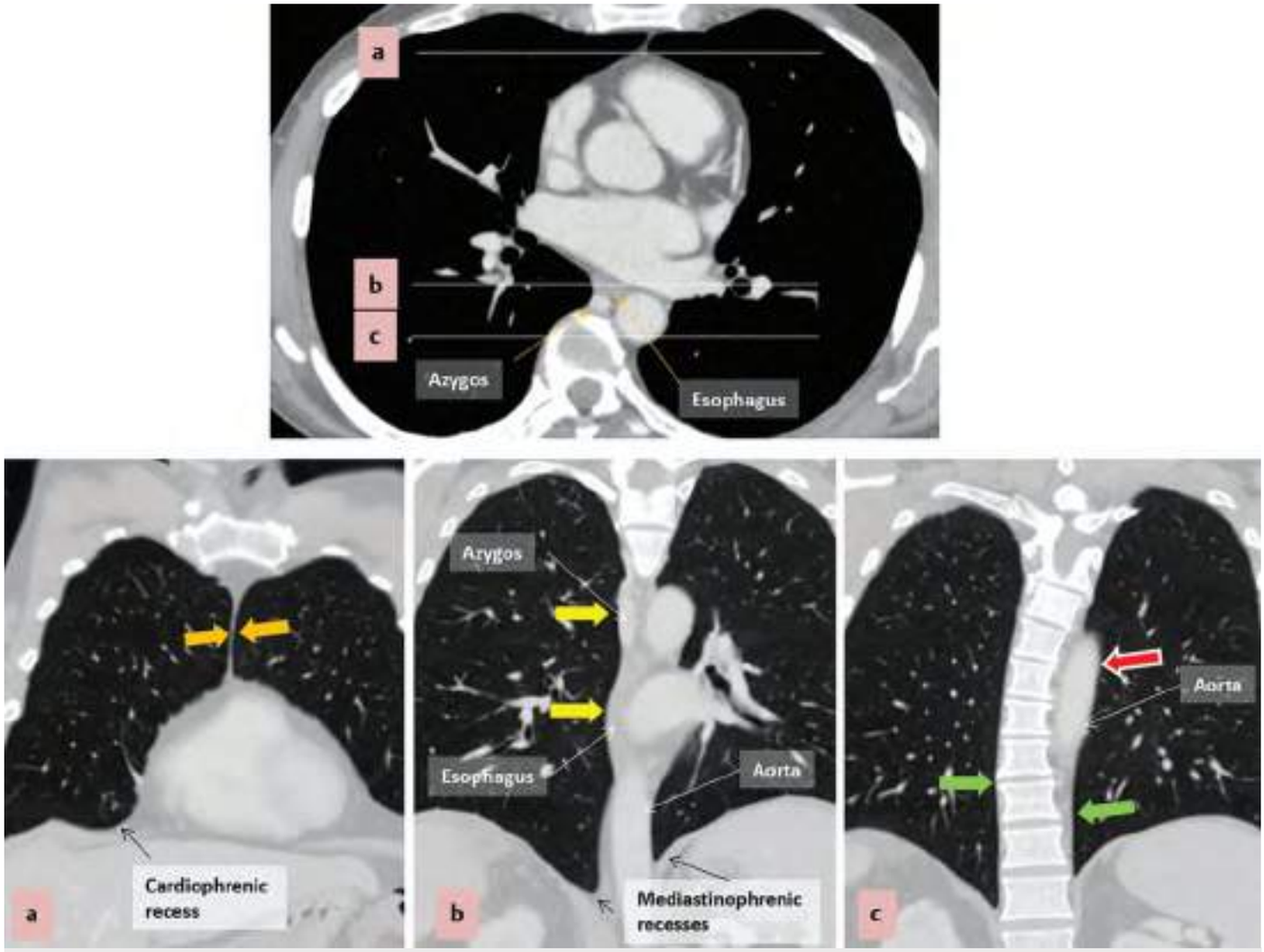

Fig. 5.11 Pleural recesses. Coronal CT scan at three levels showing the **(a)** anterior costomediastinal recess, **(b)** the azygoesophageal recess, and **(c)** posterior costomediastinal (paravertebral and para-aortic) recesses all formed by the mediastinal pleura.

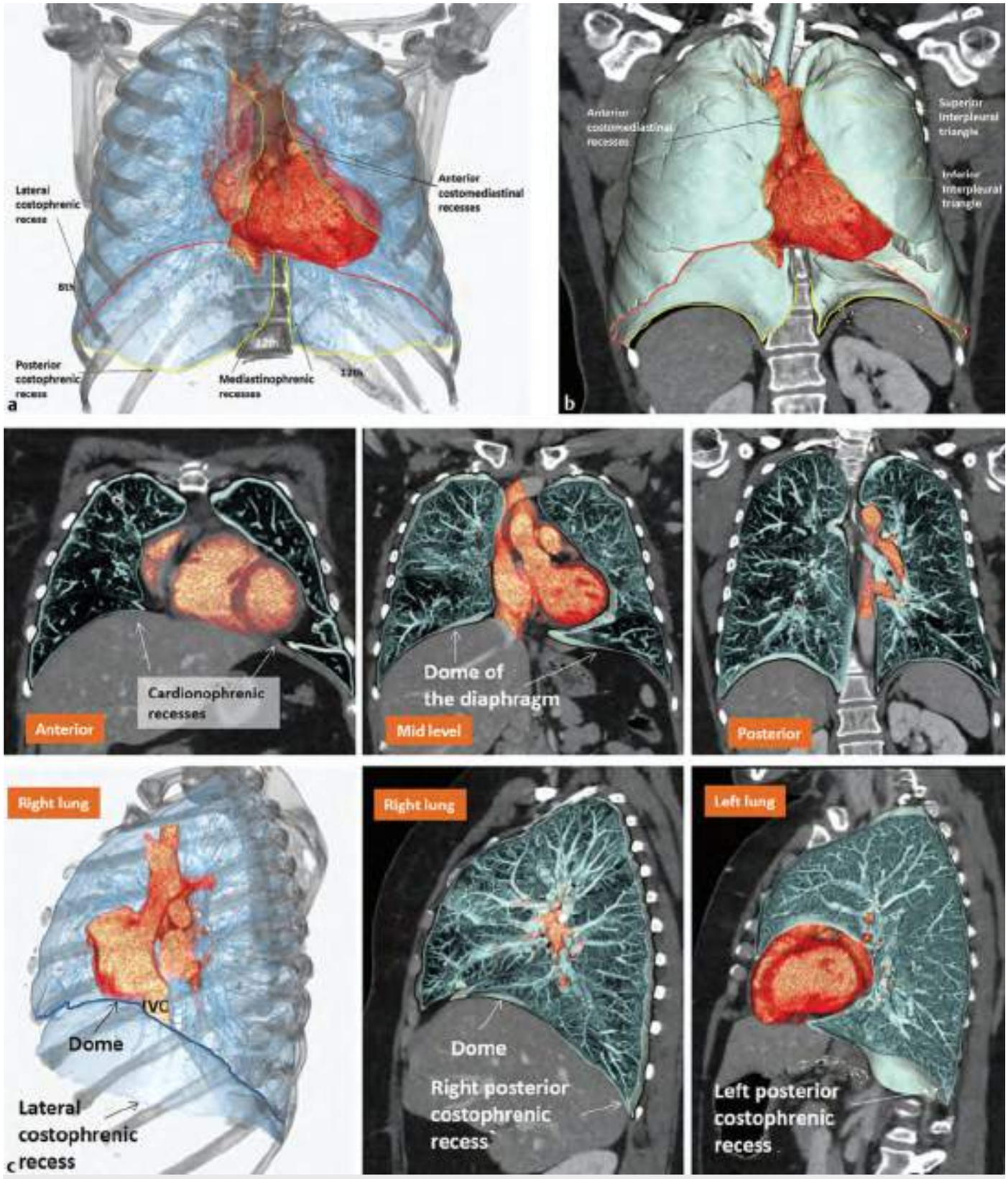

Fig. 5.12 (**a–c**) Pleural recesses. The pleural recesses are potential spaces located in regions where the parietal pleura changes direction. Red line, anterior margin of the diaphragm; yellow line, posterior margin of the diaphragm; green line, anterior mediastinal pleura.

variant. The most common accessory fissures are the inferior accessory fissure, which outlines the medial basal segment, the superior accessory fissure, which outlines the superior segment, and the left minor fissure, which outlines the lingula[13,14] (▶ Fig. 5.13).

The azygos lobe is a variant that results when the right posterior cardinal vein, a precursor to the azygos vein, fails to migrate over the lung apex and instead penetrates it, carrying along pleural layers to entrap a portion of right upper lobe (▶ Fig. 5.14). Two folds of parietal and two folds of visceral pleura form a mesentery termed the azygos fissure which contains the azygos arch in its lowermost portion. The azygos lobe is found in 1% of anatomical specimens.[15] Vertical fissure line is seen as a linear shadow medial to the costophrenic angle and somewhat parallel to the lateral chest wall to end at or below the minor fissure.

◆ Common Diseases of the Pleura

Pleural Effusion

The production and absorption of pleural fluid is maintained in equilibrium. On average, pleural fluid is estimated to be produced at 0.01 mL/kg/h and is cleared at the same rate.[16] As a result, over a 24-hour period, the average 60-kg person will turnover 14.4 mL of pleural fluid. The parietal pleura plays a more significant role in maintaining the equilibrium of pleural fluid due to its closer proximity of vasculature to the pleural space, 10 to 12 µm compared to 20 to 50 µm for the visceral pleura, and its lymphatic stomata that opens directly into the pleural space and facilitates reabsorption of pleural fluid.[17,18] In response to increased fluid production, the rate of reabsorption is believed to increase as high as 0.28 mL/kg/h.[19] A pleural effusion results when production of pleural fluid outpaces fluid reabsorption (▶ Fig. 5.15). Pleural fluid may also accumulate via passage through holes in the diaphragm.[20]

Pleural effusions begin to collect between the inferior surface of the lower lobes and diaphragm. After 75 mL accumulates in this region, fluid begins to spill over to the costophrenic recesses. On chest radiography, obscuration of the posterior costophrenic recess on a lateral view occurs with 75 mL of fluid accumulation while 175 mL of fluid is necessary to obscure a lateral costophrenic recess on a frontal view.[21] Obscuration of the diaphragm occurs with accumulation of 500 mL of fluid and if fluid reaches as high as the anterior fourth rib, the fluid volume has typically reached 1,000 mL. Decubitus radiography is the most sensitive radiographic view for detection of pleural effusion and can detect as little as 5 mL of fluid.[4] Excessive extrapleural and mediastinal fat (*arrows*) can mimic plural effusion or pleural thickening on chest X-ray which can easily be distinguished by computed tomography (CT) (▶ Fig. 5.16). Subpulmonic effusion is an unusual accumulation of fluid in the diaphragmatic surface of the pleural cavity that may be missed on plain films and CT is required to show it (▶ Fig. 5.17). Loculation of pleural fluid can occur at any location (▶ Fig. 5.18). Empyema is defined as the accumulation of pus within the pleural space. It is typically associated with pulmonary infections but can also be seen in relation to surgical procedures and trauma.[4,22]

Pneumothorax

Pneumothorax is defined as the accumulation of gas within the pleural space (▶ Fig. 5.19). The gas may originate from the lung parenchyma or the outside environment. A pneumothorax can be either spontaneous, such as from the rupture of bullae, or the result of trauma. The pressure within the pleural space is normally negative relative to atmospheric pressure throughout respiration. This facilitates the elastic recoil of the lungs. In the setting of a pneumothorax, lung collapse occurs.[23] A tension pneumothorax occurs when air flows into the pleural space during inhalation but cannot exit during exhalation and need to be evacuated immediately. Dissection of air from the mediastinum or anterior extraperitoneal or after traumatic injury of the thoracic wall into extrapleural space occasionally occurs and should not be confused with pneumothorax (▶ Fig. 5.20).

Pleural Masses

Metastatic cancer is the most common cause of tumor involvement of the pleura.[24,25,26] Lung and breast adenocarcinoma are the most common, accounting for 40 and 20% of cases, respectively. Lymphoma accounts for 10% of cases.[22] Mesothelioma is the most common primary malignancy to involve the pleura[24] (▶ Fig. 5.21). Pleural lipomas are benign tumors that arise from the parietal pleura and extend into the subpleural, pleural, or extrapleural space (▶ Fig. 5.22).[25] Pleural pseudotumor refers to pleural fluid that collects within a lung fissure, most commonly in the minor fissure (▶ Fig. 5.18).[24]

Pleural plaques are the most frequent manifestation of asbestos inhalation and occur 20 to 30 years following first exposure (▶ Fig. 5.23).[27,28] The plaques arise in the parietal pleura and are usually asymptomatic and incapable of malignant degeneration. Calcification of plaques is common.[24,27]

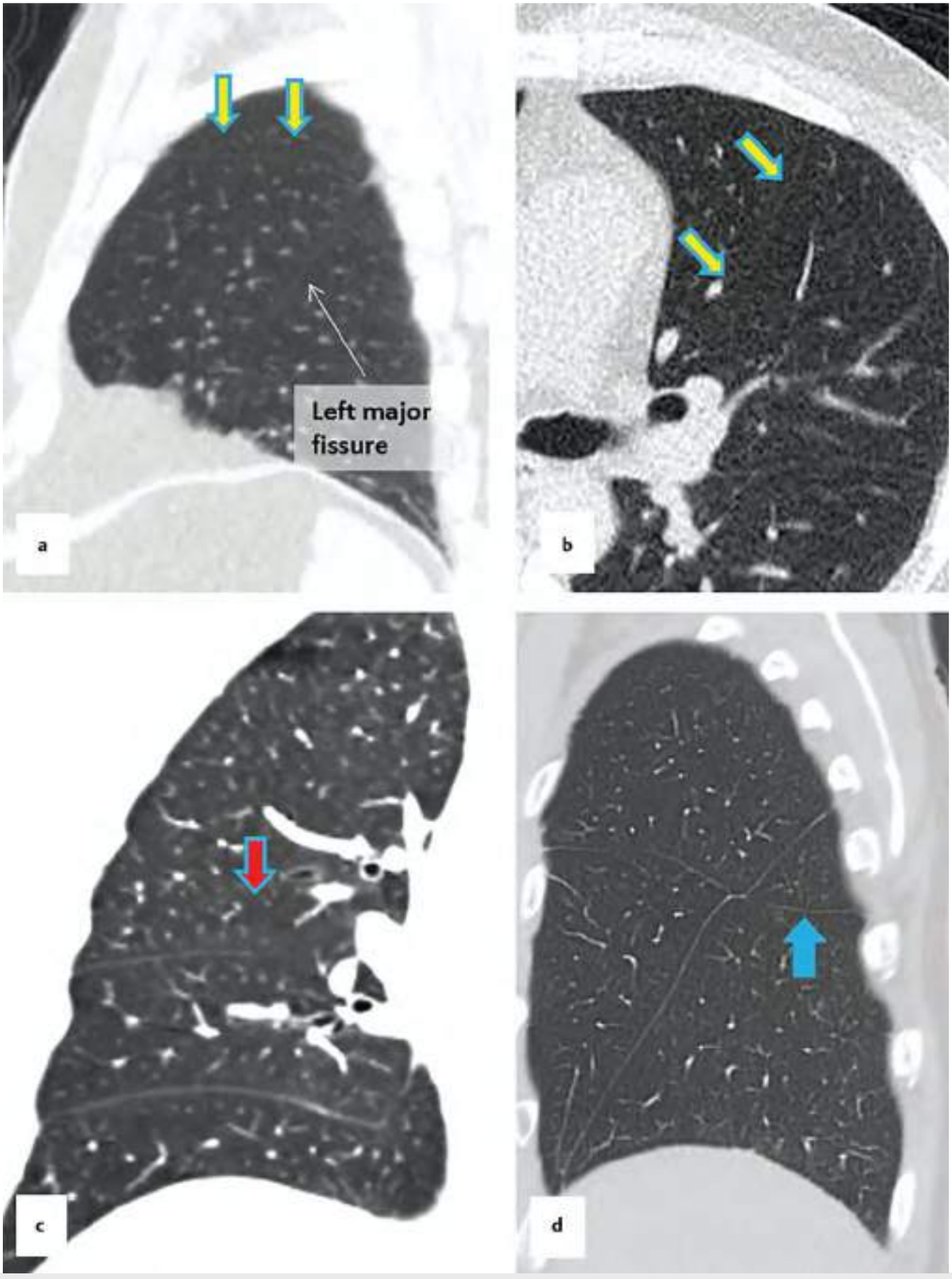

Fig. 5.13 **(a)** Sagittal and **(b)** axial noncontrast CT showing left minor fissure (*yellow arrow*). **(c)** A portion of the right minor fissure (*red arrow*) is incomplete. **(d)** Sagittal CT image of a right superior accessory fissure (*blue arrow*).

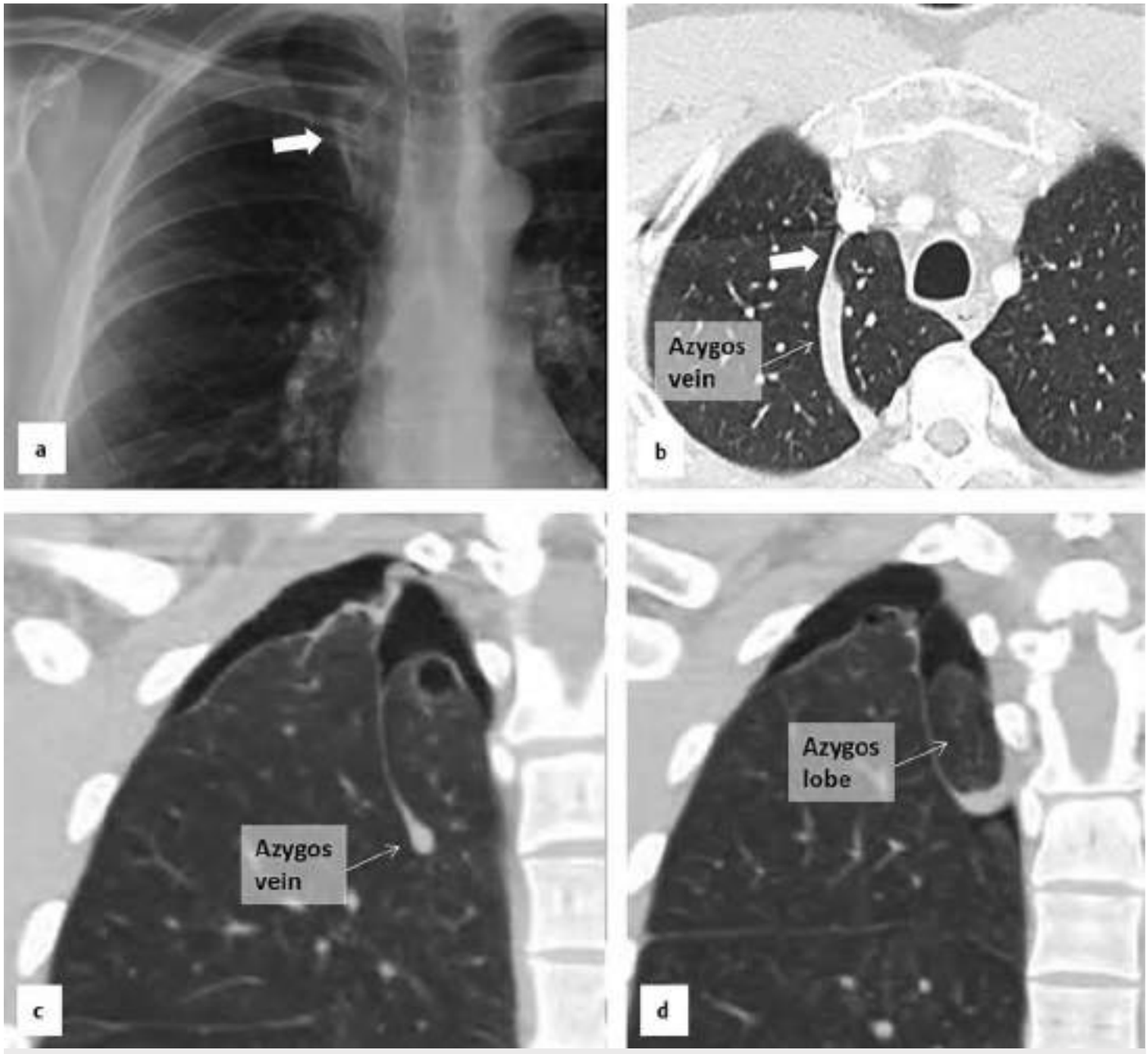

Fig. 5.14 (a, b) Frontal chest radiograph and axial CT show the azygos vein in azygos fissure (*arrows*). **(c, d)** Coronal CT images showing the azygos vein in azygos fissure in a patient with spontaneous pneumothorax due to a subpleural bleb.

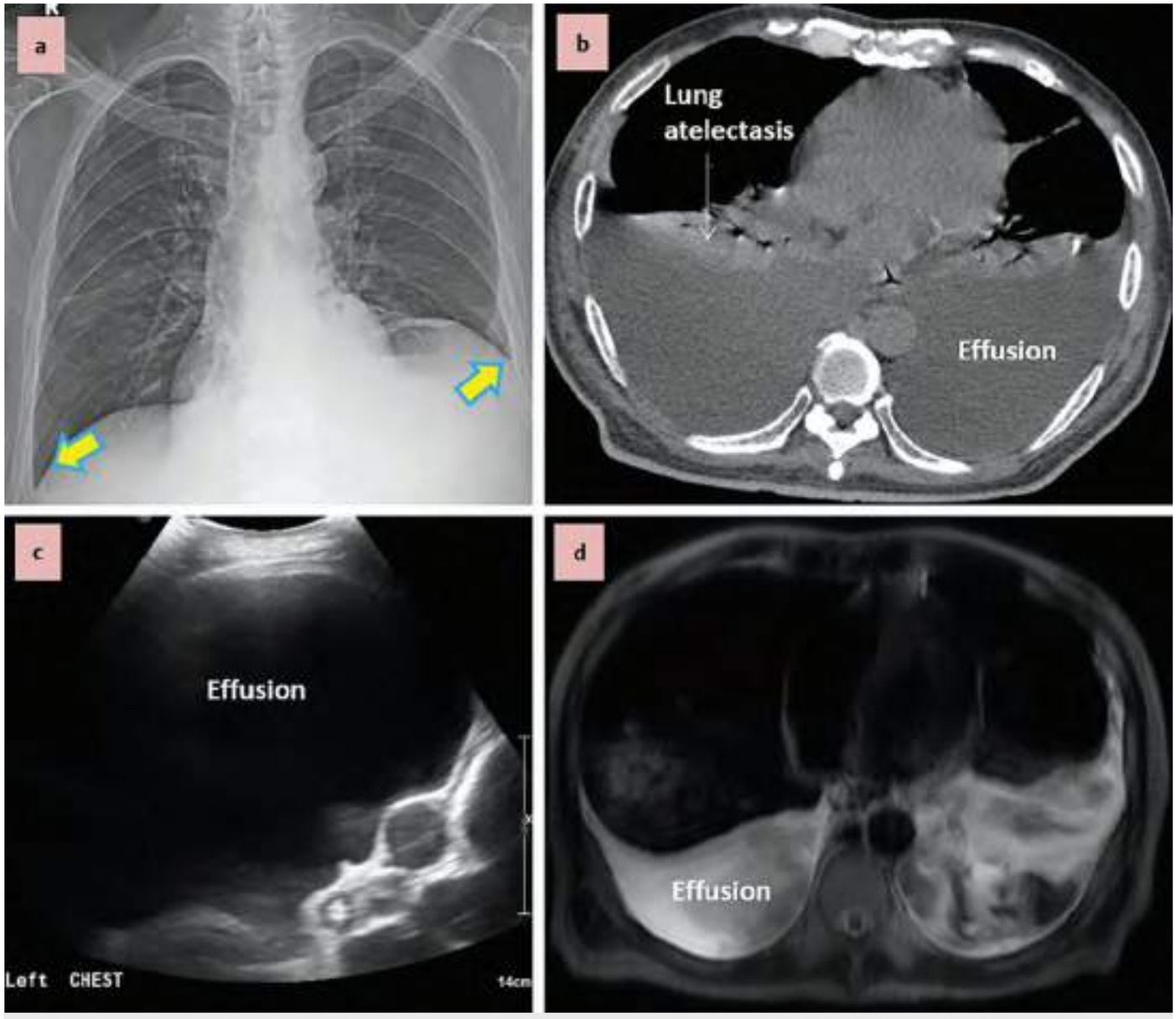

Fig. 5.15 Typical appearance of noncomplicated pleural effusion using different imaging modalities. **(a)** Frontal chest radiograph. Suggestion of bilateral pleural effusions due to blunting of the costophrenic angles. **(b)** Axial CT showing large bilateral pleural effusions which is also clearly shown by ultrasound **(c)** and MRI **(d)**.

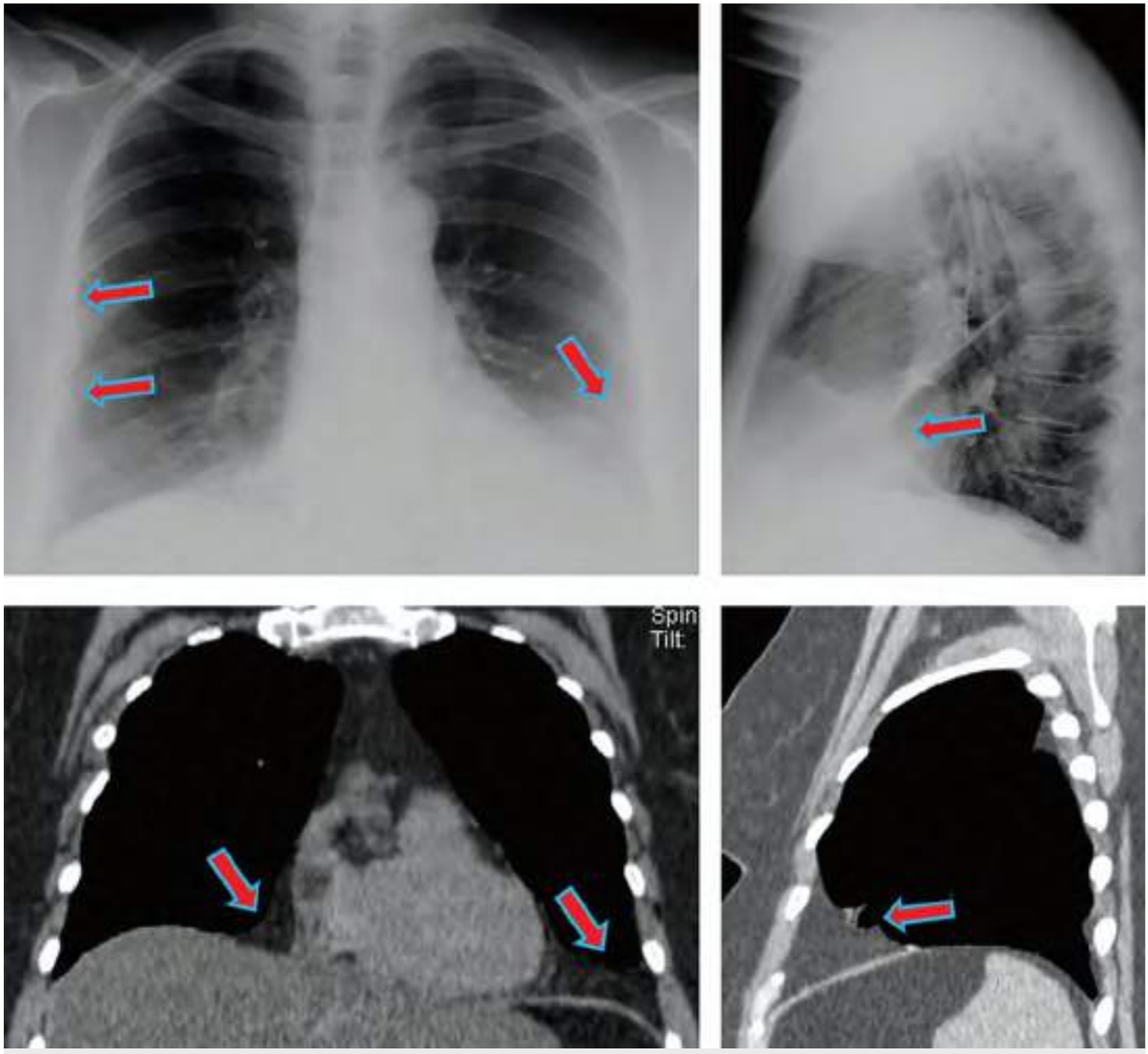

Fig. 5.16 Large amount of extrapleural and mediastinal fat (*arrows*) can mimic pleural effusion or pleural thickening on chest X-ray which can easily be distinguished by CT.

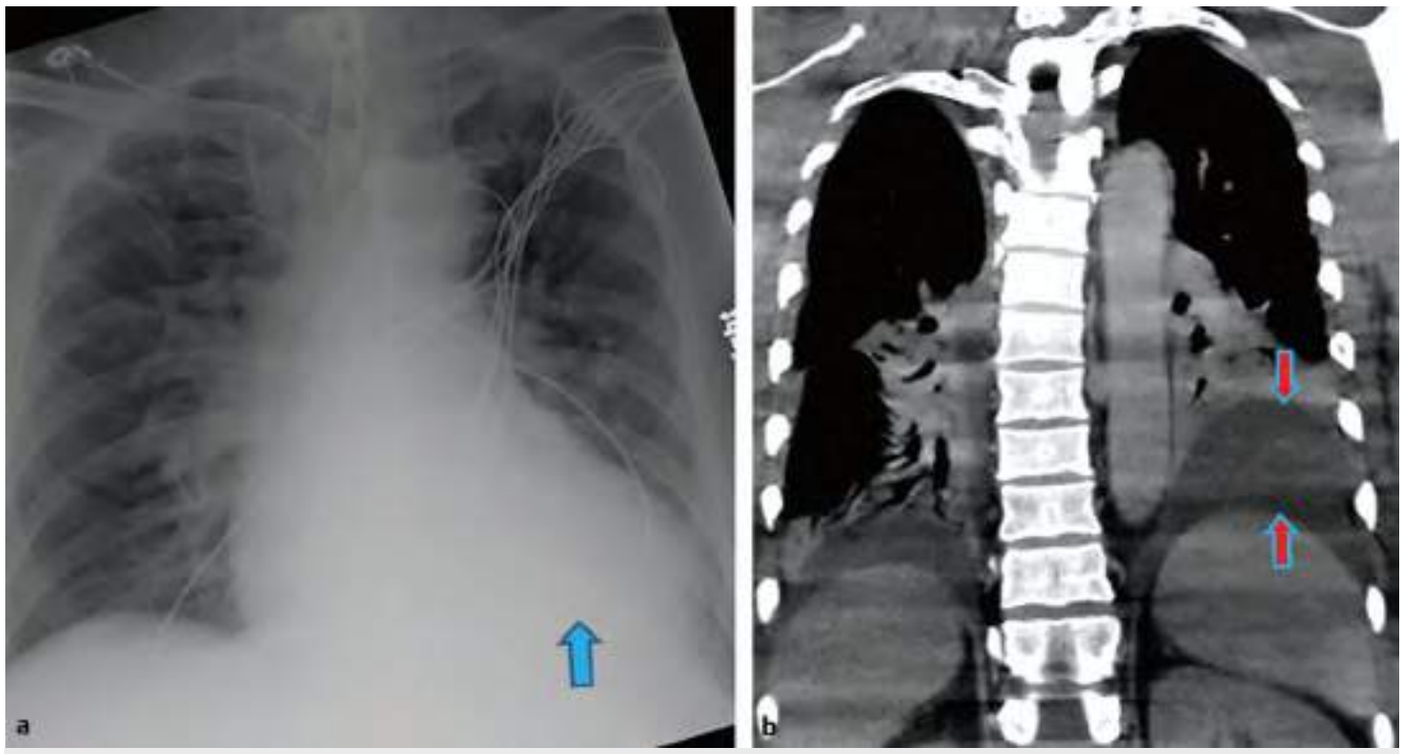

Fig. 5.17 **(a)** Frontal chest radiograph showing loss of definition of the left hemidiaphragm in the retrocardiac region (*blue arrow*). (**b**) Coronal CT shows a right subpulmonic effusion (*between red arrows*) with fluid accumulating in the posterior costophrenic recess between the atelectatic lung base and diaphragm.

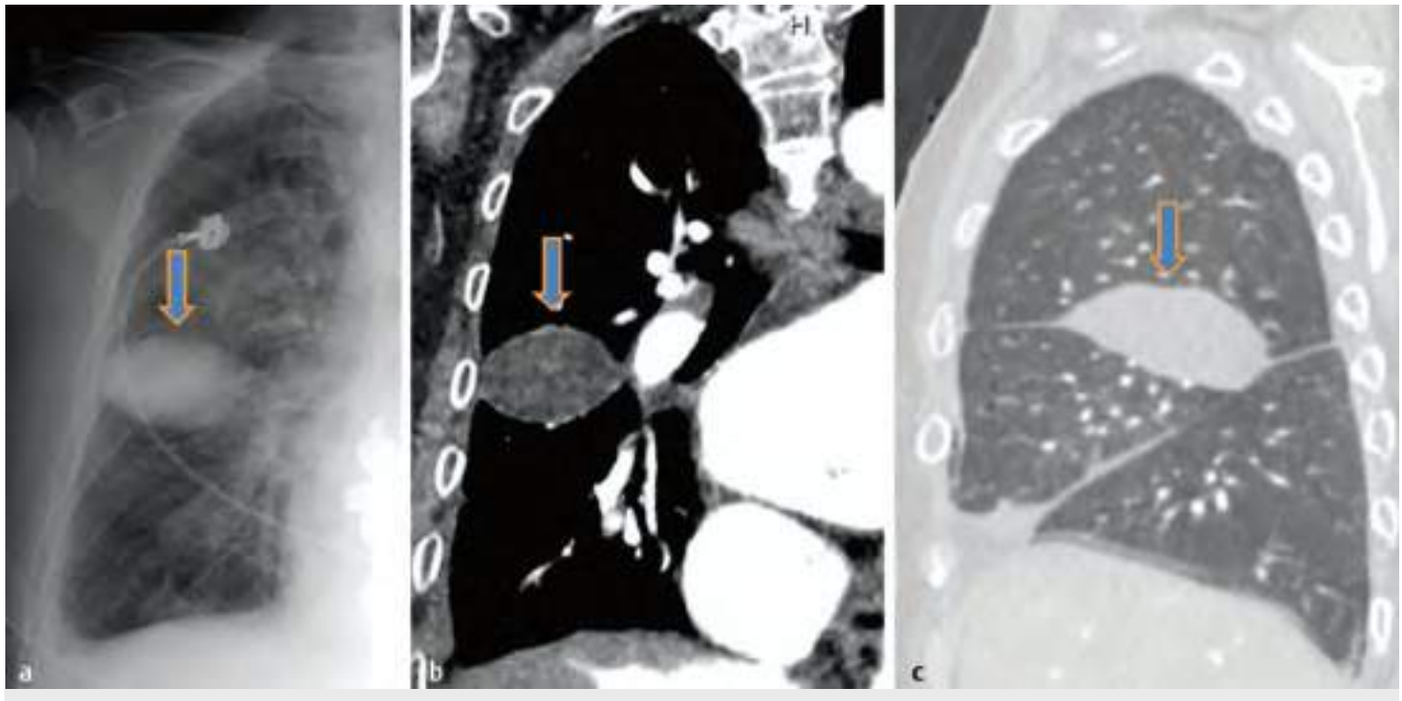

Fig. 5.18 Loculated pleural effusion (also known as pseudotumor) in the minor fissure. **(a)** Frontal X-ray; **(b)** coronal CT; **(c)** sagittal CT in lung window.

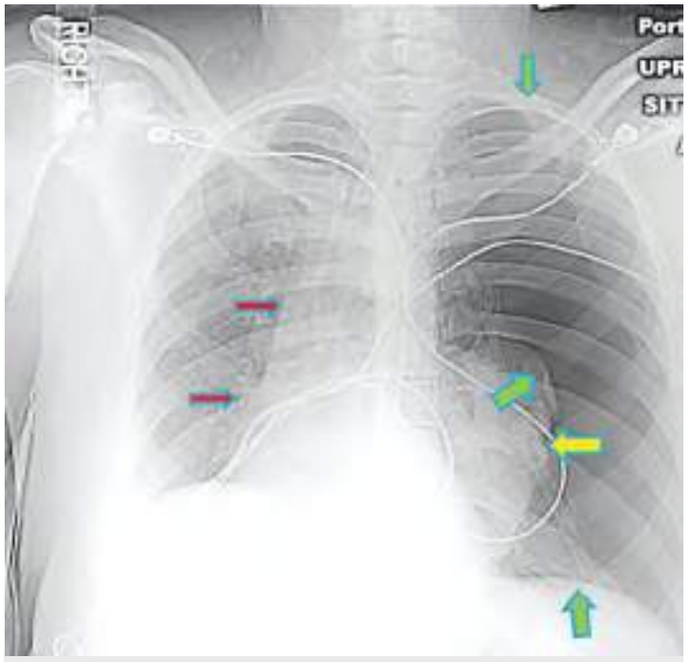

Fig. 5.19 Frontal chest radiograph. Large left tension pneumothorax (*green arrows*). The left lung (*yellow arrow*) is collapsed and the mediastinum (*red arrows*) is shifted rightward.

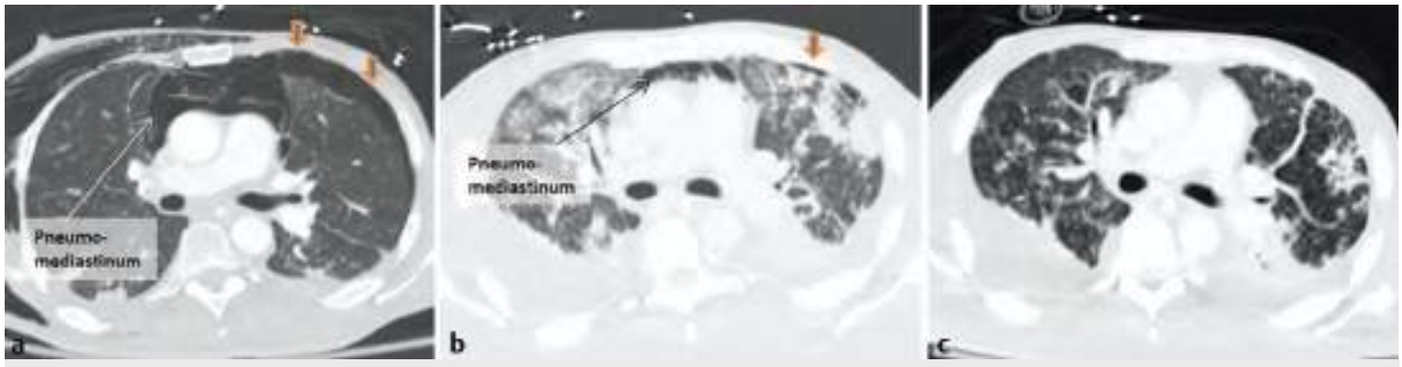

Fig. 5.20 Extrapleural air (*arrows*) resolving in 2 weeks. **(a)** Axial CT shows a large pneumomediastinum dissecting into the left extrapleural fat. A large right chest wall emphysema is also seen. **(b, c)** Spontaneous resolution of air collections in 2 weeks. Extrapleural air should not be confused with pneumothorax.

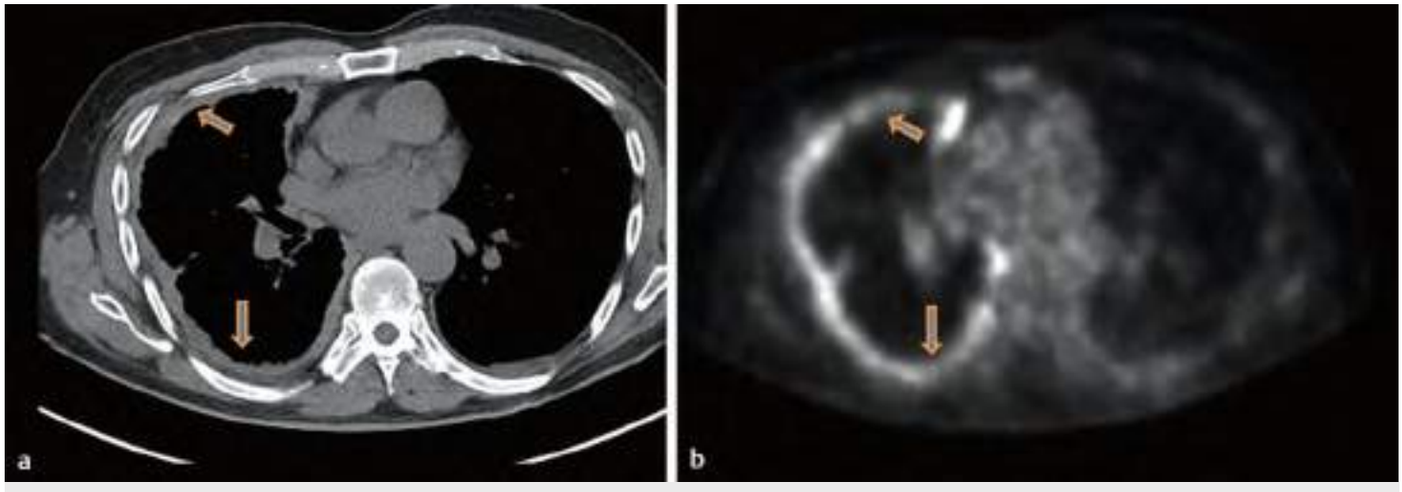

Fig. 5.21 Mesothelioma with circumferential nodular asymmetric pleural thickening (*arrows*) involving the right costal and mediastinal parietal pleura shown by **(a)** axial noncontrast CT and **(b)** attenuation-corrected FDG-18 axial positron emission tomography (PET). There is increased FDG activity in the area of abnormality suggesting malignancy.

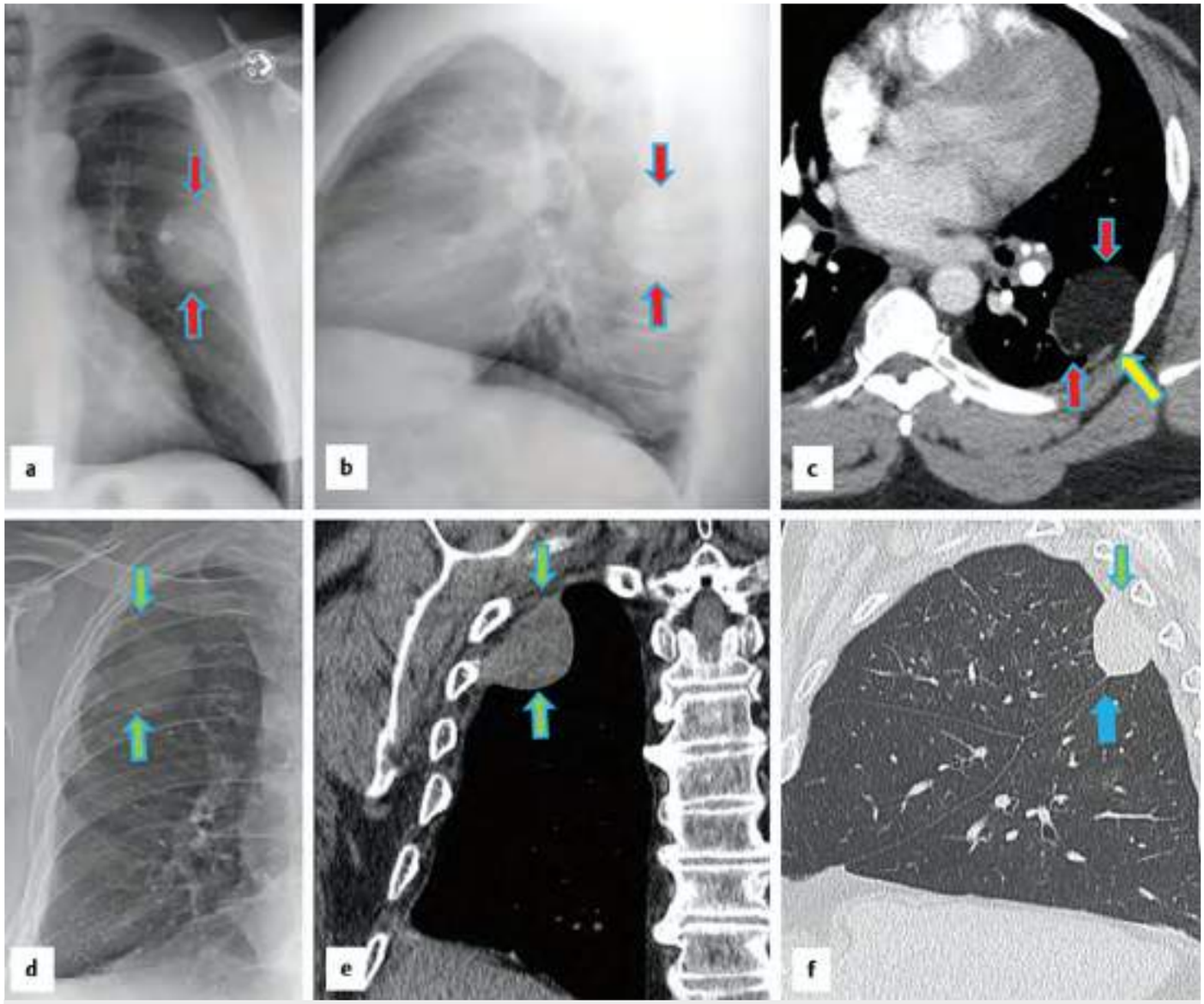

Fig. 5.22 Local extrapleural and pleural masses. **(a–f)** Frontal and lateral chest radiographs and axial CT scan. Rounded mass projecting in the lateral left midlung (*between red arrows*) demonstrates sharp borders medially and indistinct border laterally. The partially indistinct border suggests an extraparenchymal origin. CT scan shows fat-attenuation mass compatible with a pleural lipoma. The mass is contiguous with the extrapleural fat (*yellow*) located superficial to the parietal pleura and deep to the endothoracic fascia. **(d–e)** Frontal chest radiographs and coronal and axial CT images showing a solid mass in the right upper hemithorax consistent with a fibrous tumor of pleura.

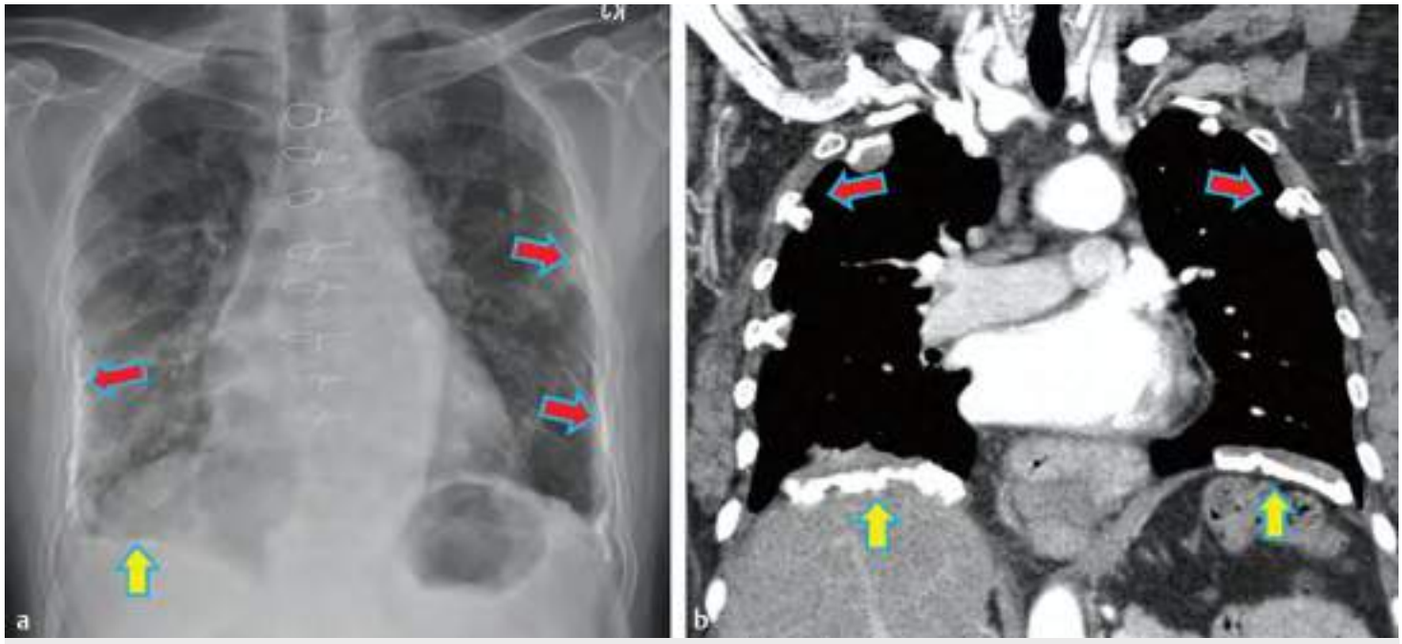

Fig. 5.23 Calcified pleural plaques. **(a)** Frontal chest radiograph and **(b)** CT scan show thick calcified pleural plaques along the costal (*red arrows*) and diaphragmatic (*yellow arrows*) parietal pleura due to prior asbestos exposure.

References

[1] Finley DJ, Rusch VW. Anatomy of the pleura. Thorac Surg Clin.; 21(2):157–163, vii

[2] Light RW. Pleural Diseases. Philadelphia, PA: Lippincott Williams & Wilkins; 2007

[3] Leonard RJ. Human Gross Anatomy: An Outline Text. New York, NY: Oxford UP; 1995

[4] Yalcin NG, Choong CKC, Eizenberg N. Anatomy and pathophysiology of the pleura and pleural space. Thorac Surg Clin.; 23(1):1–10, v

[5] Hayashi K, Aziz A, Ashizawa K, Hayashi H, Nagaoki K, Otsuji H. Radiographic and CT appearances of the major fissures. Radiographics.; 21(4):861–874

[6] Morrissey BM, Bisset RA. The right inferior lung margin: anatomy and clinical implication. Br J Radiol.; 66(786):503–505

[7] Bertin F, Deslauriers J. Anatomy of the pleura: reflection lines and recesses. Thorac Surg Clin.; 21(2):165–171, vii

[8] D'Angelo E, Loring SH, Gioia ME, Pecchiari M, Moscheni C. Friction and lubrication of pleural tissues. Respir Physiol Neurobiol.; 142(1):55–68

[9] Wang NS. Anatomy and physiology of the pleural space. Clin Chest Med.; 6 (1):3–16

[10] Gilbert E, Hakim TS. Relative contribution of bronchial flow to subpleural region in dog lung. J Appl Physiol (1985).; 73(3):855–861

[11] Miura T, Shimada T, Tanaka K, Chujo M, Uchida Y. Lymphatic drainage of carbon particles injected into the pleural cavity of the monkey, as studied by video-assisted thoracoscopy and electron microscopy. J Thorac Cardiovasc Surg.; 120(3):437–447

[12] Wang NS. Anatomy of the pleura. Clin Chest Med.; 19(2):229–240

[13] Godwin JD, Tarver RD. Accessory fissures of the lung. AJR Am J Roentgenol.; 144(1):39–47

[14] Foster-Carter AF. Broncho-pulmonary abnormalities. Br J Tuberc Dis Chest.; 40(4):111–124

[15] Mata J, Cáceres J, Alegret X, Coscojuela P, De Marcos JA. Imaging of the azygos lobe: normal anatomy and variations. AJR Am J Roentgenol.; 156(5):931–937

[16] Wiener-Kronish JP, Albertine KH, Licko V, Staub NC. Protein egress and entry rates in pleural fluid and plasma in sheep. J Appl Physiol.; 56(2):459–463

[17] Broaddus VC, Wiener-Kronish JP, Berthiaume Y, Staub NC. Removal of pleural liquid and protein by lymphatics in awake sheep. J Appl Physiol (1985).; 64 (1):384–390

[18] Albertine KH, Wiener-Kronish JP, Staub NC. The structure of the parietal pleura and its relationship to pleural liquid dynamics in sheep. Anat Rec.; 208 (3):401–409

[19] Sahn SA. The diagnostic value of pleural fluid analysis. Semin Respir Crit Care Med.; 16:269

[20] Lieberman FL, Hidemura R, Peters RL, Reynolds TB. Pathogenesis and treatment of hydrothorax complicating cirrhosis with ascites. Ann Intern Med.; 64 (2):341–351

[21] Stark P. The pleura. In: Taveras JM, Ferrucci JT, eds. Radiology. Diagnosis Imaging, Intervention. Philadelphia, PA: Lippincott; 2000:29

[22] Kuhlman JE, Singha NK. Complex disease of the pleural space: radiographic and CT evaluation. Radiographics.; 17(1):63–79

[23] Pneumothorax CW. Tuberc Respir Dis (Seoul).; 76:99–104

[24] Walker CM, Takasugi JE, Chung JH, et al. Tumorlike conditions of the pleura. Radiographics.; 32(4):971–985

[25] Gaerte SC, Meyer CA, Winer-Muram HT, Tarver RD, Conces DJ, Jr. Fat-containing lesions of the chest. Radiographics.; 22(Spec No):S61–S78

[26] Dynes MC, White EM, Fry WA, Ghahremani GG. Imaging manifestations of pleural tumors. Radiographics.; 12(6):1191–1201

[27] Nishimura SL, Broaddus VC. Asbestos-induced pleural disease. Clin Chest Med.; 19(2):311–329

[28] Peacock C, Copley SJ, Hansell DM. Asbestos-related benign pleural disease. Clin Radiol.; 55(6):422–432

6 Pulmonary Artery and Vein

Hiro Kiyosue and Miyuki Maruno

◆ Pulmonary Artery

The pulmonary trunk (the main pulmonary artery) originates at the base of the right ventricle, and the origin is located anterior to the aortic sinus. It moves posteriorly on the left side of the ascending aorta in the pericardial sac, and divides into the right and left pulmonary arteries in front of the left main bronchus at the level of T5 to T6 vertebra (▶ Fig. 6.1). The diameters of the pulmonary trunk, the right pulmonary artery, and the left pulmonary artery are approximately 24, 16, and 18 mm, respectively. Their upper limits are about 30, 20, and 22 mm, respectively.[1] The left pulmonary artery is slightly larger than the right pulmonary artery. The mean pressure of the pulmonary artery is 9 to 18 mm Hg in normal conditions, and it is elevated greater than 25 mm Hg in pulmonary hypertension. The wedge pressure, representing left atrial pressure, is 6 to 12 mm Hg, which is elevated in several pathological conditions such as left heart failure and mitral valve stenosis. The right pulmonary artery runs transversely behind the ascending aorta and superior vena cava to reach the root of the right lung (▶ Fig. 6.1, ▶ Fig. 6.2, ▶ Fig. 6.3). The right pulmonary artery divides into a superior and an inferior trunk (interlobar artery) behind the superior vena cava in the mediastinum (▶ Fig. 6.2, ▶ Fig. 6.3). The superior trunk generally gives off segmental arteries supplying the upper lobe. The inferior trunk (interlobar artery) runs laterally and inferiorly between the superior pulmonary vein and the right main bronchus, which gives off segmental arteries to the middle lobe and the inferior lobe. The segmental pulmonary arterial branches run along the accompanying branches of the bronchial tree. The left pulmonary artery ascends posteriorly, and arches over the left main bronchus laterally to the root of the left lung (▶ Fig. 6.1, ▶ Fig. 6.2). It gives off several superior lobar arteries (the number varies from two to seven branches) to supply the superior lobe, then it becomes interlobar artery which branches off into the segmental arteries to feed the left lower lung lobe. In both lungs, segmental and subsegmental branches are usually located in the vicinity of corresponding bronchi, however, branching patterns of the segmental/ subsegmental arteries are variable especially in upper lobes (▶ Fig. 6.2). The segmental and subsegmental arteries of both the pulmonary arteries are summarized in ▶ Table 6.1.

For the right upper lobe, the apical (A1: A1a, apical; and A1b, anterior) segmental/subsegmental artery arises from the superior trunk. The anterior subsegmental artery (A3b) of the anterior segmental artery (A3) usually arises from the superior trunk. The posterior (A2: A2a, posterior; and A2b, lateral) segmental/subsegmental arteries and lateral subsegmental artery (A3a) of A3 can originate from either the superior trunk or the interlobar artery (so-called ascending pulmonary artery).[2,3] The segmental arteries of the right middle lobe (A4, lateral; A5, medial) arise from the anterior aspect of the interlobar artery independently or from a common trunk. These segmental arteries further divide into subsegmental arteries (A4a, lateral; A4b, medial; A5a, superior; and A5b, inferior). The middle lobe segmental arteries occasionally originate from the artery to the basal segments (▶ Fig. 6.2).[4,5] The middle lobe arteries rarely give off a branch to the lower lobe. The lower lobe apical segmental artery (A6) originates from the posterolateral aspect of the interlobar artery opposite to the middle lobe artery. It runs posteriorly, accompanying the corresponding bronchus (B6), and divides into three subsegmental arteries (A6a, superior; A6b, lateral; and A6c, medial). One of these subsegmental arteries can rarely originate independently from the interlobar artery. After branching the A6, the left pulmonary artery divides into basal segmental arteries (A7, medial; A8, anterior; A9, lateral; and A10, posterior). They originate from the inferior pulmonary trunk either independently or via an anterior (A7 and A8) or a posterior trunk (A9 and A10). Each basal segmental artery subdivides into the following subsegmental arteries: A7a, dorsal; A7b, ventral; A8a, lateral; A8b, basal; A9a, lateral; A9b, basal; A10a, posterior; A10b, lateral; and A10c, basal. The basal segmental arteries are occasionally duplicated or even triplicated surrounding a corresponding bronchus.[6]

For the left upper lobe, the anterior segmental artery (A3) arises from the anterosuperior aspect of the left pulmonary artery at the arch, and then the apicoposterior segmental (A1 + 2) or the subsegmental arteries (A1 + 2a, apical; A1 + 2b, posterior; and A1 + 2c, lateral) arise independently or with a common trunk from the posterosuperior aspect of the left pulmonary artery. The anterior segmental artery (A3) further subdivides into three subsegmental arteries (A3a, lateral; A3b medial; and A3c, superior). The left pulmonary artery enters the major fissure, becoming interlobar artery, and runs on the side of the lower lobe bronchus. The lingular segmental arteries (A4, superior; and A5, inferior) arise from the anterior aspect of the interlobar artery independently or as a single trunk. The lingular arteries rarely originate from the other upper lobe arteries or the basal segmental arteries. Branching pattern and course of the segmental arteries to the left lower lobe are similar to the right pulmonary artery. The apical segmental artery of the left lower lobe (A6) usually originates at slightly higher portion of the interlobar artery compared to its fellow on the right side. Medial basal segmental artery (A7) is often subtle or unidentified on the left side.

Intrapulmonary arteries divide and subdivide along the bronchi and bronchioles which lie in the central portion of the secondary and then the primary pulmonary lobules. There, they become arterioles proceeding along the respiratory bronchioles and alveolar ducts to form capillary networks in the alveolar walls for gas exchange.[7] These capillary networks continue to the pulmonary venules which join the pulmonary veins which are located in the interlobular septa.

◆ Pulmonary Vein

The pulmonary vein in the interlobular septa join together to form segmental pulmonary veins. Unlike the segmental pulmonary arteries, the segmental pulmonary veins are not close to the bronchi, instead they run within the intersegmental septa. The

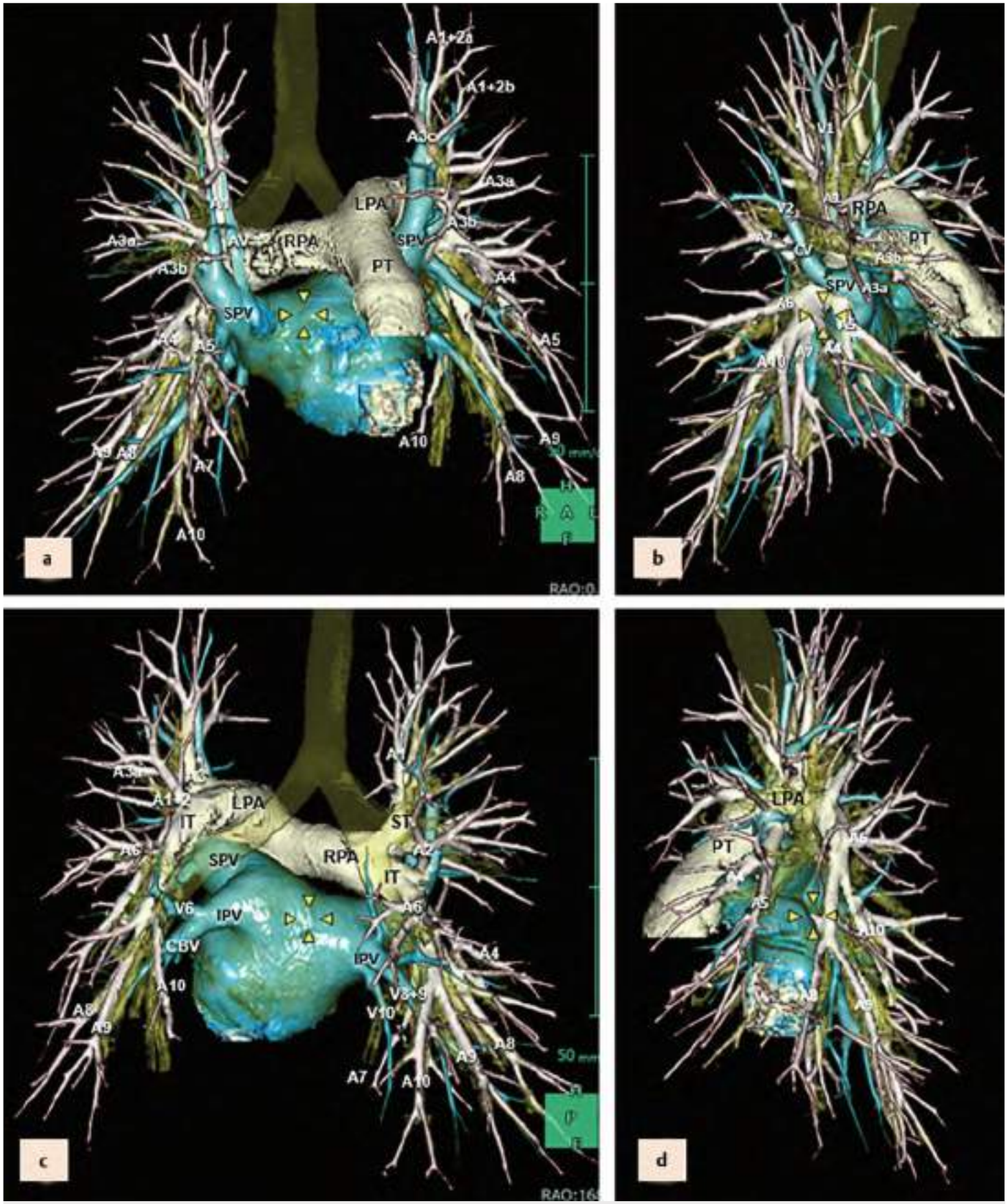

Fig. 6.1 Normal CT Anatomy of the pulmonary artery and vein. Anterior **(a)**, right lateral **(b)**, posterior **(c)**, and left lateral **(d)** views of 3D CT angiography (3DCTA). AV, anterior vein; CBV, common basal vein; CV, central vein; IPV, inferior pulmonary vein; IT, inferior trunk; LPA, left pulmonary artery; PT, pulmonary trunk; RPA, right pulmonary artery; SPV, superior pulmonary vein; ST, superior trunk.

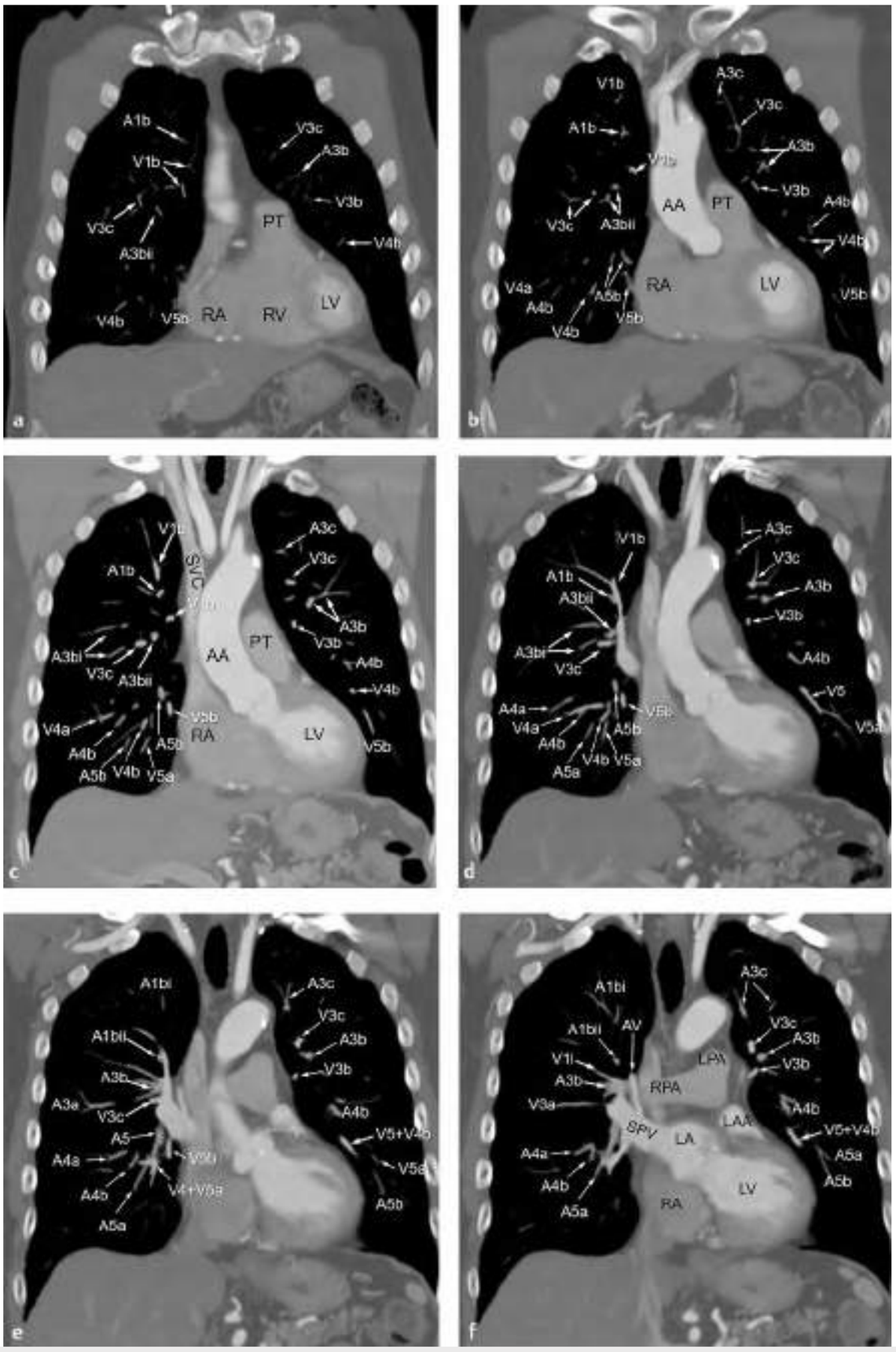

Fig. 6.2 Coronal multiplanar reconstruction (MPR) images showing pulmonary arterial and venous branches. AA, ascending aorta; AV, anterior vein; CV, central vein; IT, inferior trunk; LA, left atrium; LAA, left atrial auricle; LIPV, left inferior pulmonary vein; LPA, left pulmonary artery; LSPV, left superior pulmonary vein; LV, left ventricle; RA, right atrium; RV, right ventricle; RPA, right pulmonary artery; SVC, superior vena cava.

(*Continued*)

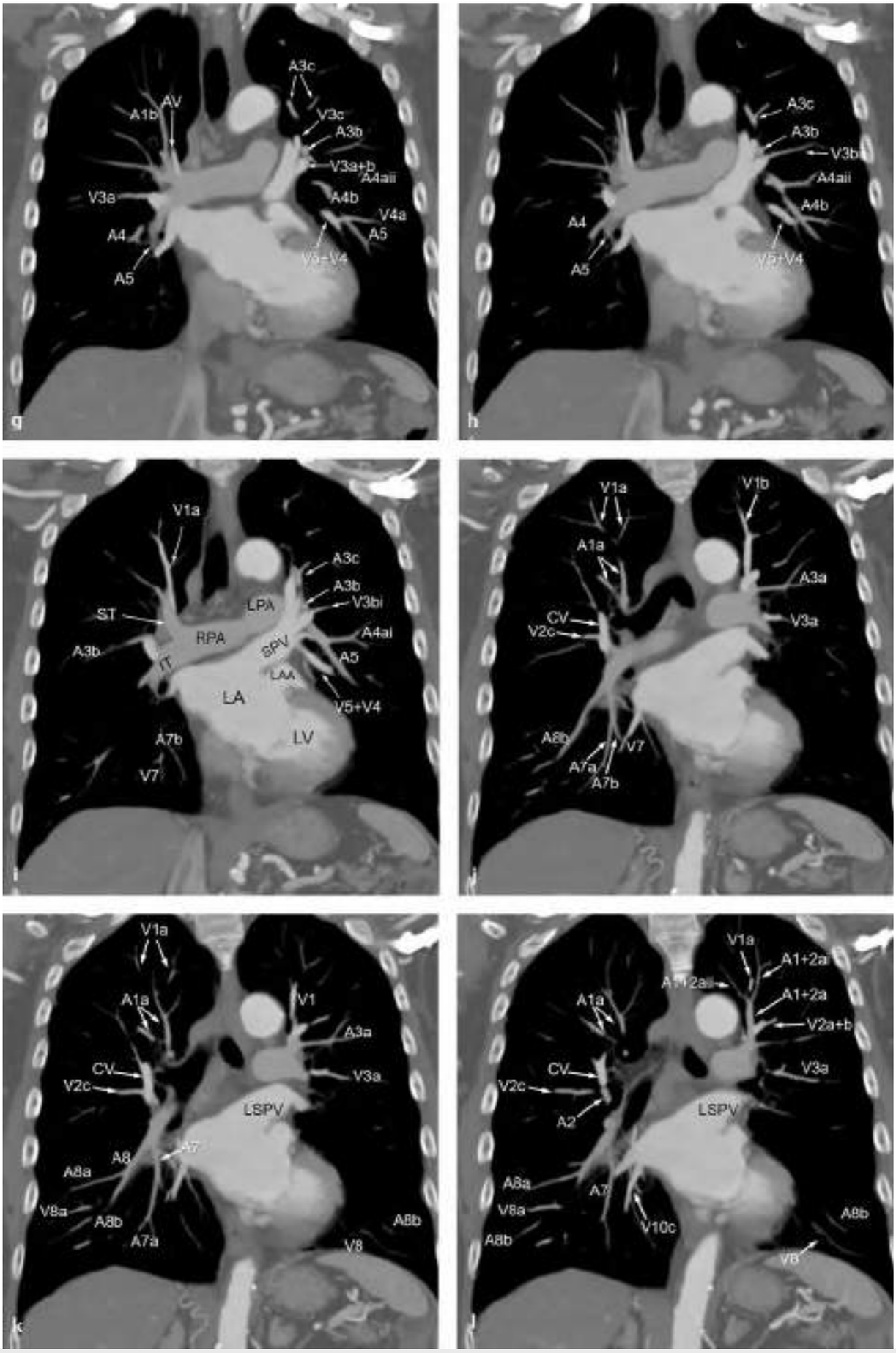

Fig. 6.2 (*Continued*) **(g–l)**

(*Continued*)

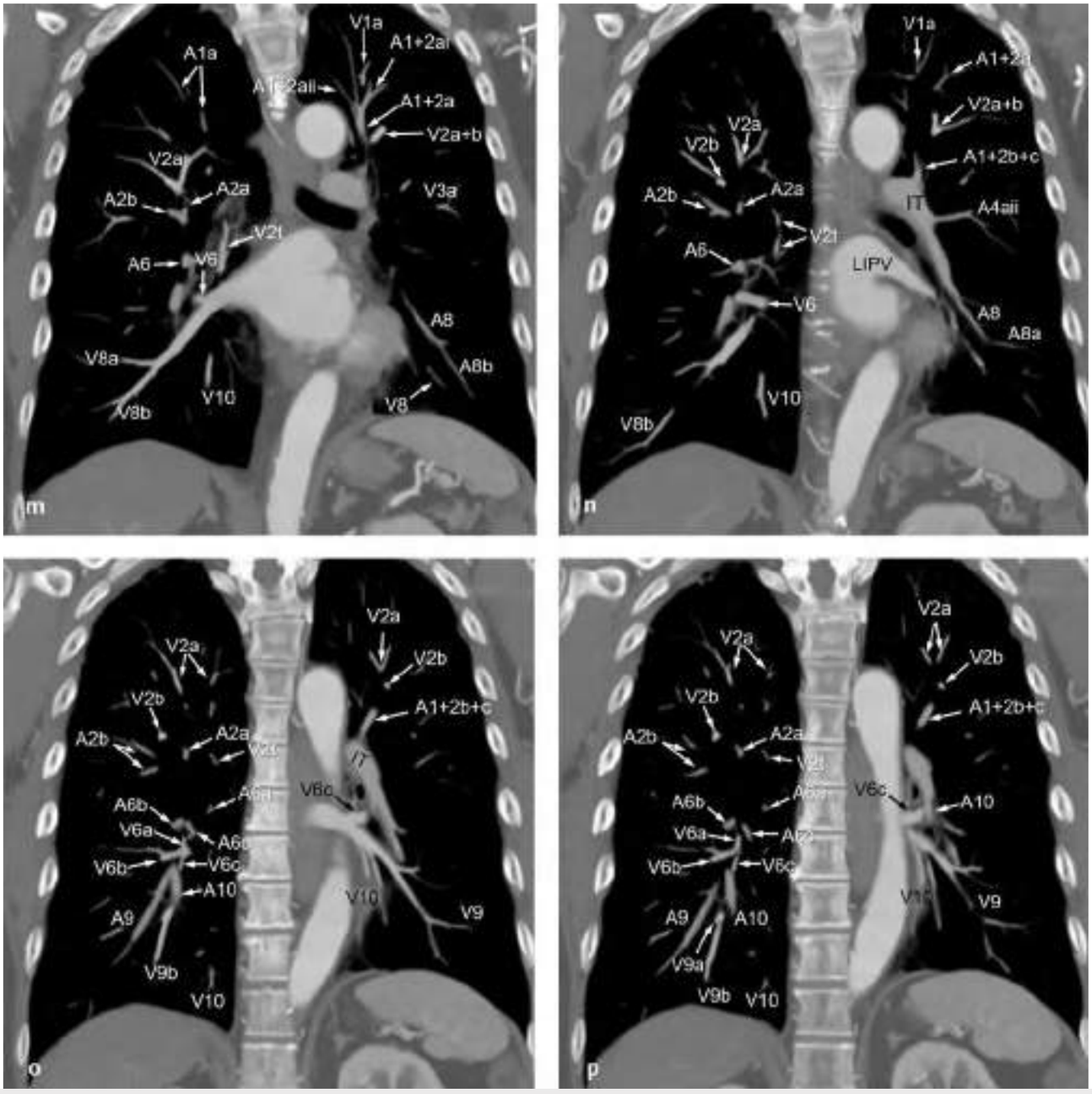

Fig. 6.2 (*Continued*) **(m–p)**

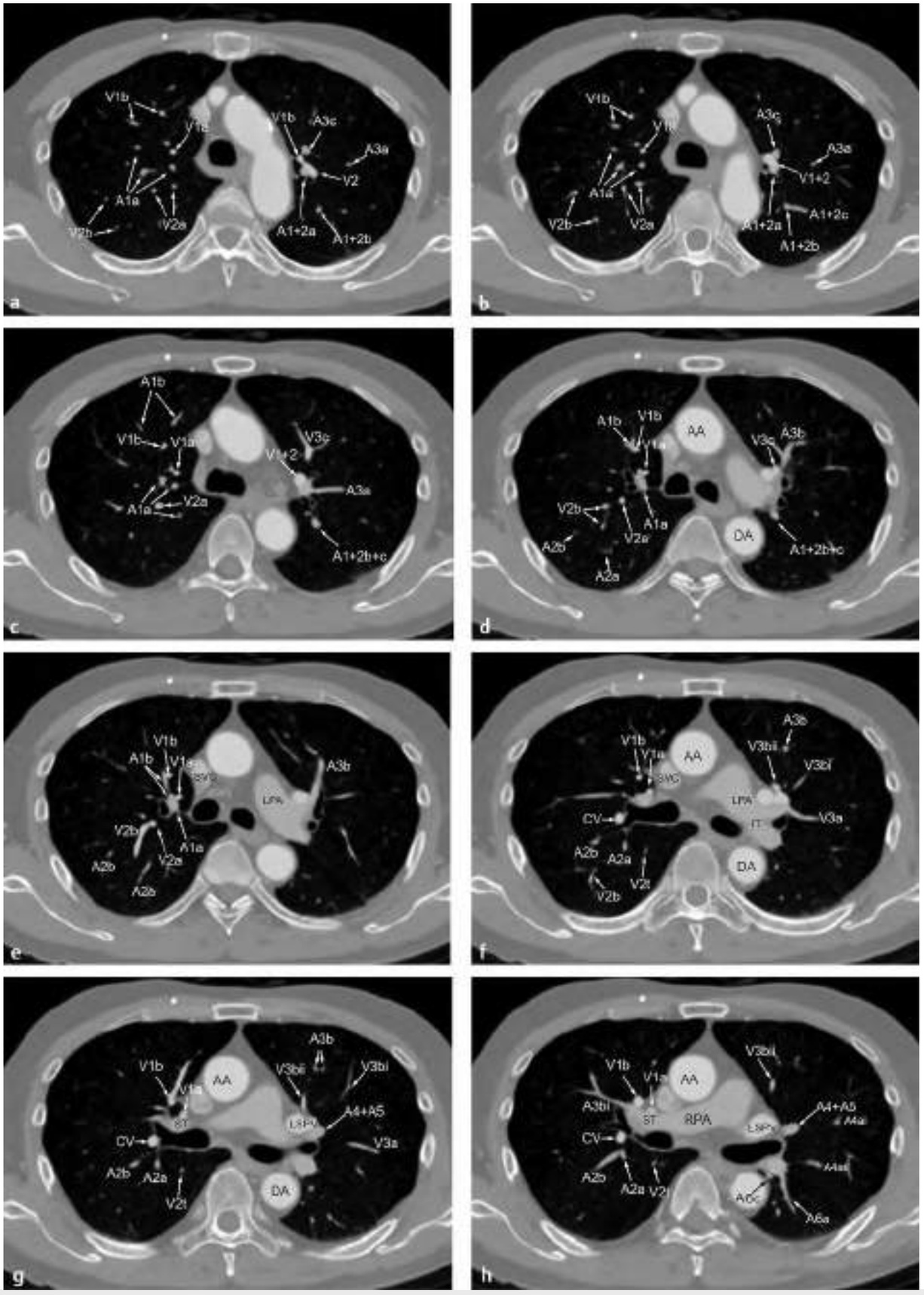

Fig. 6.3 Axial multiplanar reconstruction (MPR) CT images showing arterial and venous branches. AA, ascending aorta; CBV, common basal vein; CV, central vein; DA, descending aorta; IT, Inferior trunk; LAA, left atrial auricle; LIPV, left inferior pulmonary vein; LPA, left pulmonary artery; LSPV, left superior pulmonary vein; PT, pulmonary trunk; RPA, right pulmonary artery; RSPV, right superior pulmonary vein; ST, superior trunk; SVC, superior vena cava.

(*Continued*)

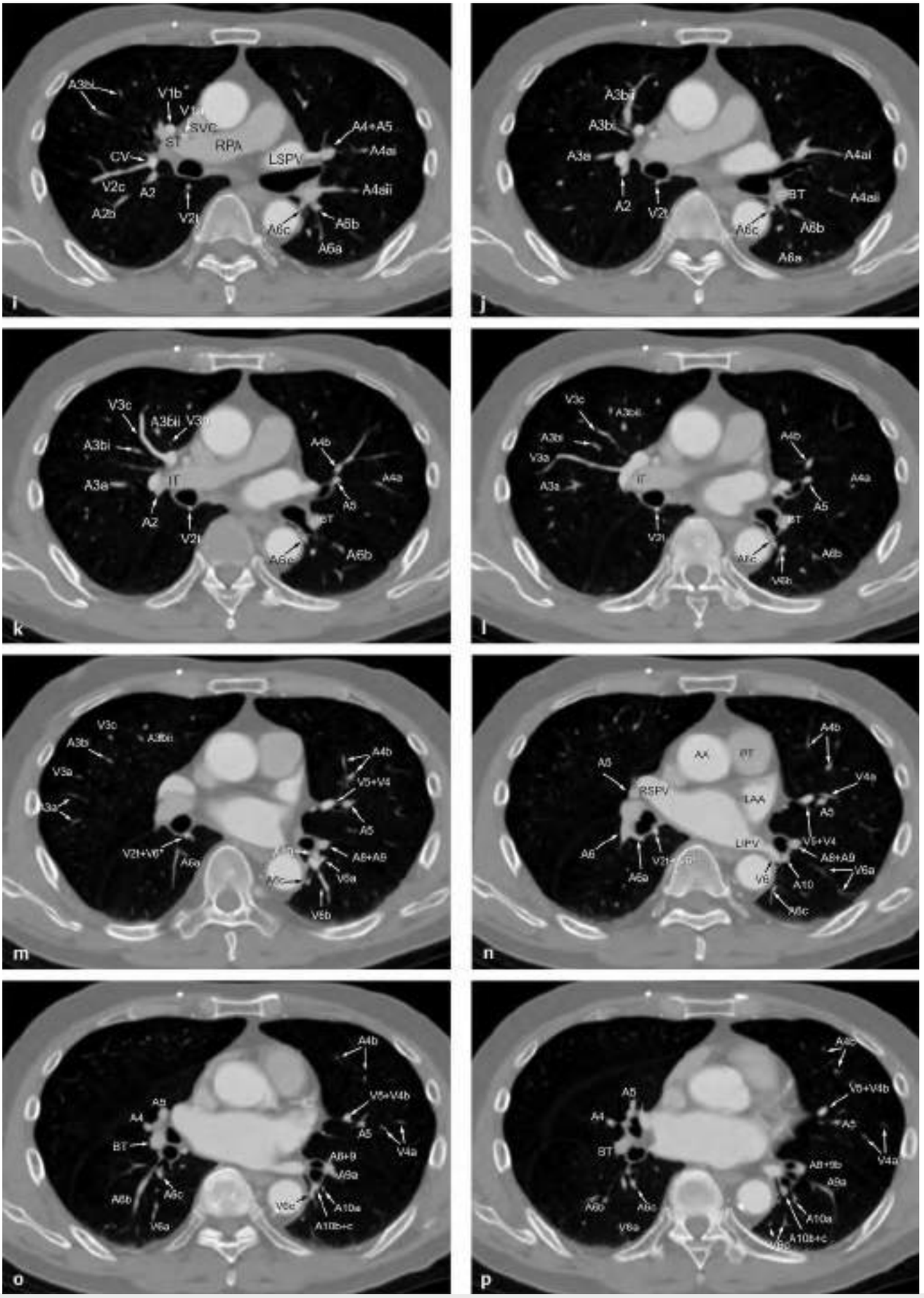

Fig. 6.3 (*Continued*) **(i–p)**

(*Continued*)

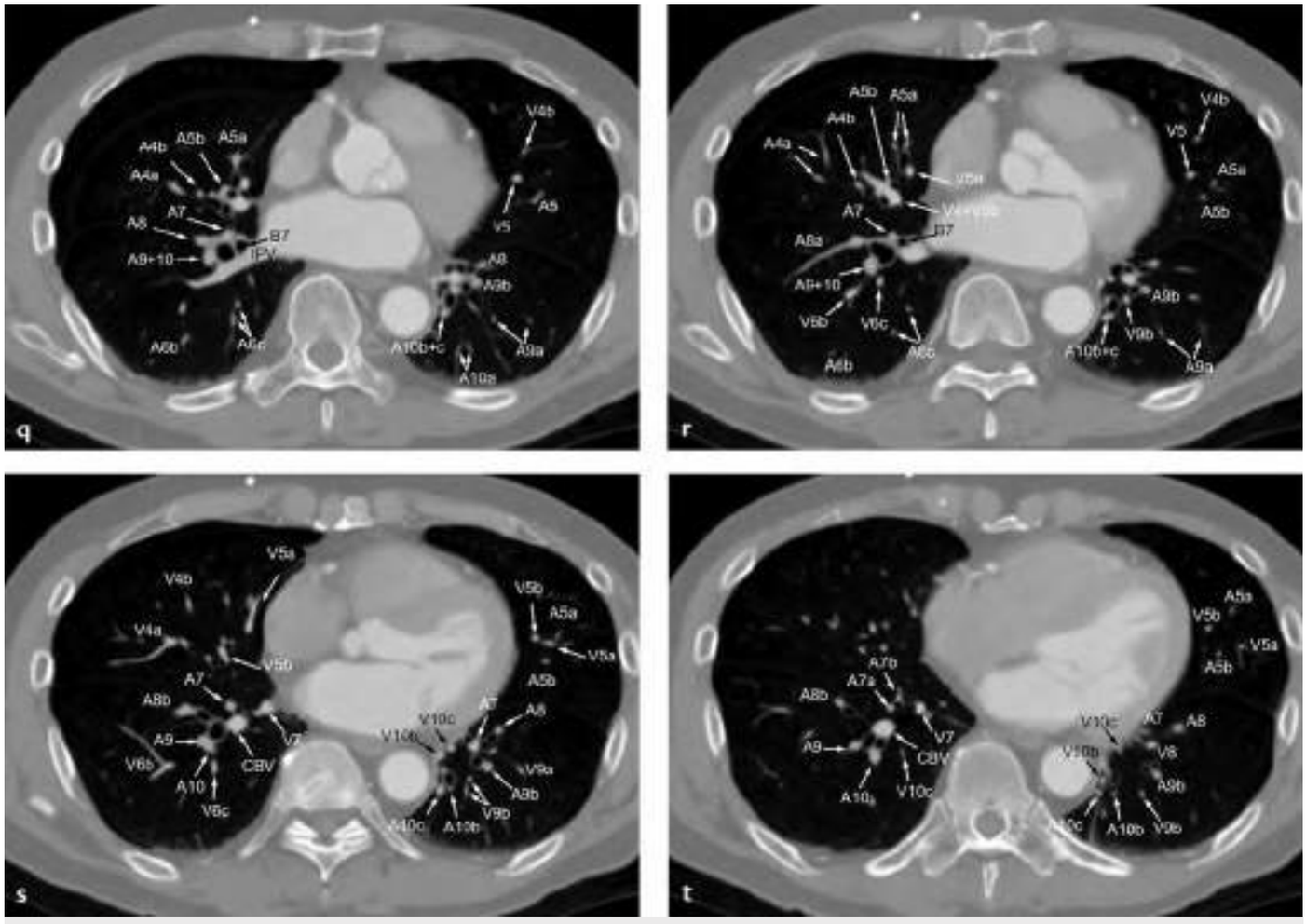

Fig. 6.3 (*Continued*) **(q–t)**

segmental pulmonary veins join to form two common trunks of the superior pulmonary vein and the inferior pulmonary vein which connect to the left atrium on each side. The orifices of the inferior pulmonary veins are more dorsal than those of the superior pulmonary veins (▶ Fig. 6.2).[8] The orifices of the left pulmonary veins are located more superiorly than those of the right pulmonary veins (▶ Fig. 6.1).[9,10] There are some variations of the pulmonary veins. The left superior and inferior pulmonary veins occasionally form a single common trunk before entering the left atrium (▶ Fig. 6.4). Other variations are accessory pulmonary veins, including one or more accessory middle pulmonary veins and the upper pulmonary vein which directly connect to the left atrium (▶ Fig. 6.5, ▶ Fig. 6.6). Recognition of these variations of the pulmonary veins is important for thoracic surgery and catheter ablation treatment of arrhythmic cardiac diseases.

Subsegmental pulmonary veins and their relationship to the pulmonary (sub)segments are summarized on ▶ Table 6.2.

The right superior pulmonary vein usually receives the segmental or lobar veins from the right upper lobe and the middle lobe, which are located anterior and inferior to the right pulmonary artery. The subsegmental veins of posterior segment (V2a, apical; V2b, posterolateral; and V2c, horizontal) join to form the central vein which is located at the central portion of the upper lobe and descend between the B2 (posterior) and B3 (anterior) segmental bronchi (central vein type), and then join to the superior pulmonary vein superiorly (▶ Fig. 6.2, ▶ Fig. 6.6). At the right lung apex, the apical (V1a) and the anterior (V1b) subsegmental veins of the apical segment join to form apical segmental vein (V1) which runs downward. These V1 subsegmental veins totally or partially join to form the central vein or descend anteromedial to the central vein (anterior vein) joining the superior pulmonary vein anterosuperiorly. Subsegmental veins of anterior segment (V3) can join the central vein, the anterior vein, or independently to the superior pulmonary vein. V3d (lateral) subsegmental vein generally joins the central vein. In some cases, the common trunk of V1 and V2 subsegmental veins runs anteriorly far above the bifurcation of the B2 and B3, which descend anteromedially to the upper bronchi (semicentral vein type) (▶ Fig. 6.7). This type of upper lobe venous drainage is more frequently seen in the left lobe. One or two subsegmental veins of the V2 (especially V2 t, terminal) occasionally descend on the posterior surface of the bronchus intermedius, which drain either into the superior pulmonary vein or the inferior pulmonary vein.[11] In the right middle lobe, two segmental veins of V4 (lateral) and V5 (medial) are generally formed by the subsegmental veins. The V4a (posterior) and V4b (anterior) join to form the V4, and the V5a (superior) and V5b (inferior) form the V5, respectively. The segmental veins join together to form the middle lobe vein which usually joins the superior pulmonary vein. In some cases, the segmental veins or subsegmental veins independently join to

Table 6.1 Segmental and subsegmental arteries of the pulmonary artery

Right pulmonary artery		Left pulmonary artery	
Segmental artery	**Subsegmental artery**	**Segmental artery**	**Subsegmental artery**
Upper lobe		**Upper lobe**	
A1, apical	A1a, apical	A1 + 2, apicoposterior	A1 + 2a, apical
	A1b, anterior		A1 + 2b, posterior
A2, posterior	A2a, posterior		A1 + 2c, lateral
	A2b, lateral	A3, anterior	A3a, lateral
A3, anterior	A3a, lateral		A3b, anterior
	A3b, anterior		A3c, superior
Middle lobe		A4, superior lingula	A4a, lateral
A4, lateral	A4a, superior		A4b, medial
	A4b, lateral	A5, inferior lingula	A5a, superior
A5, medial	A5a, superior		A5b, inferior
	A5b, inferior	**Lower lobe**	
Lower lobe		A6, apical	A6a, superior
	A6a, superior		A6b, lateral
	A6b, lateral		A6c, medial
	A6c, medial	A7, medial	
A7, medial	A7a, posterior	A8, anterior	A8a, lateral
	A7b, anterior		A8b, basal
A8, anterior	A8a, lateral	A9, lateral	A9a, lateral
	A8b, basal		A9b, basal
A9, lateral	A9a, lateral	A10, posterior	A10a, posterior
	A9b, basal		A10b, lateral
A10, posterior	A10a, posterior		A10c, basal
	A10b, lateral		
	A10c, basal		

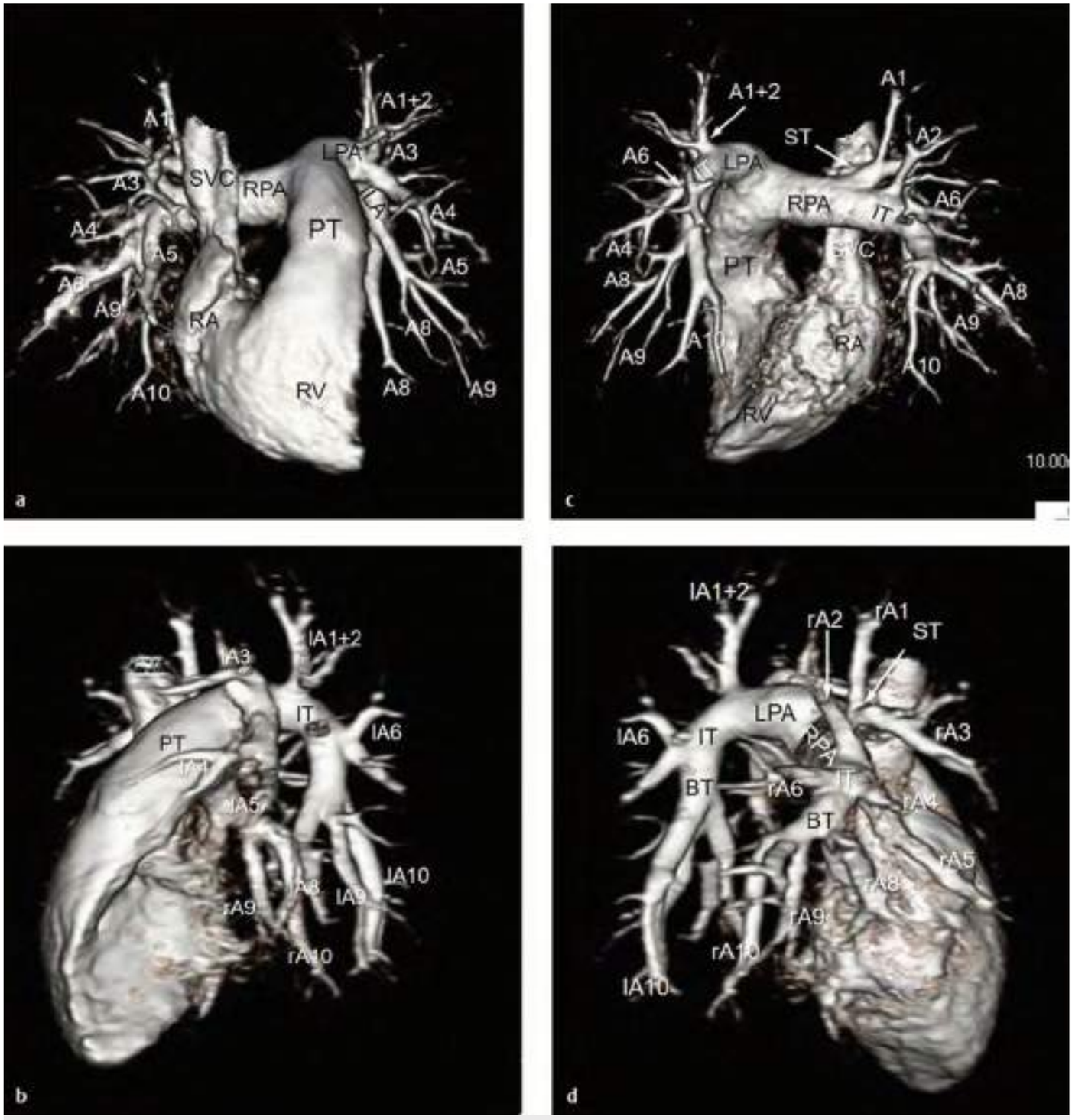

Fig. 6.4 3D-MR angiographic images of the pulmonary artery **(a)** anterior view, **(b)** left lateral view, **(c)** posterior view, and **(d)** right lateral view. BT, basal trunk; ILA, inferior lobar artery; IT, inferior trunk; LPA, left pulmonary artery; PT, pulmonary trunk; RA, right atrium; RPA, right pulmonary artery; RV, right ventricle; ST, superior trunk; SVC, superior vena cava.

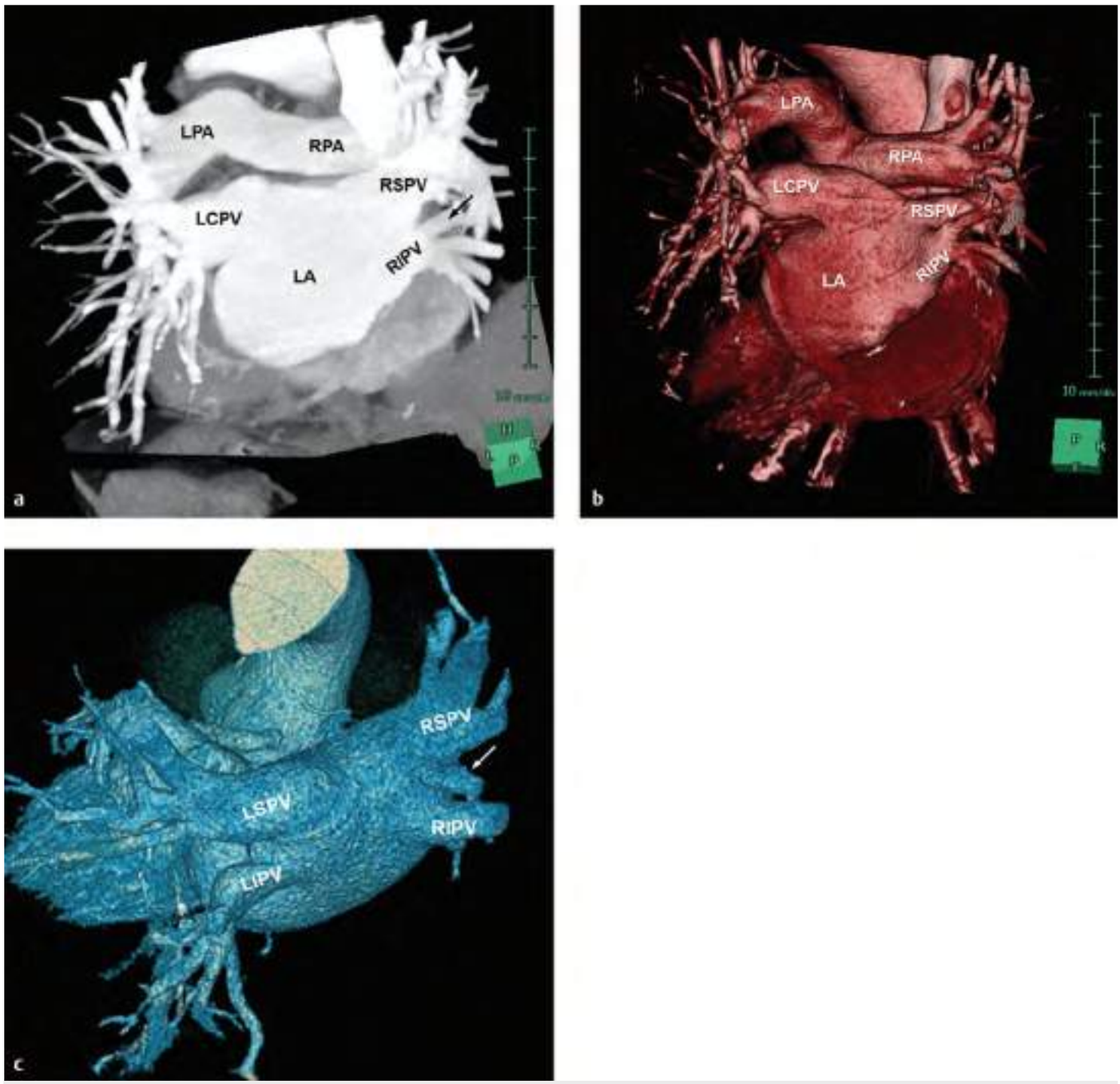

Fig. 6.5 Left common pulmonary vein. Coronal maximum intensity projection (MIP image) **(a)** and posterior view of the volume rendering (VR) image **(b)** of 3DCTA show left pulmonary vein joints to form a single pulmonary vein (left common pulmonary vein [LCPV]) draining to the left atrium. An accessory pulmonary vein (*black arrow*) from the right middle lobe draining directly into the left atrium (LA) between the right superior pulmonary vein (RSPV) and the right inferior pulmonary vein (RIPV). **(c)** Right accessory pulmonary vein. VR image of 3DCTA shows an accessory pulmonary vein (*white arrow*) from the right middle lobe draining directly into the left atrium between the RSPV and the right inferior pulmonary vein (RIPV). LIPV, left inferior pulmonary vein; LPA, left pulmonary artery; LSPV, left superior pulmonary vein; RPA, right pulmonary artery.

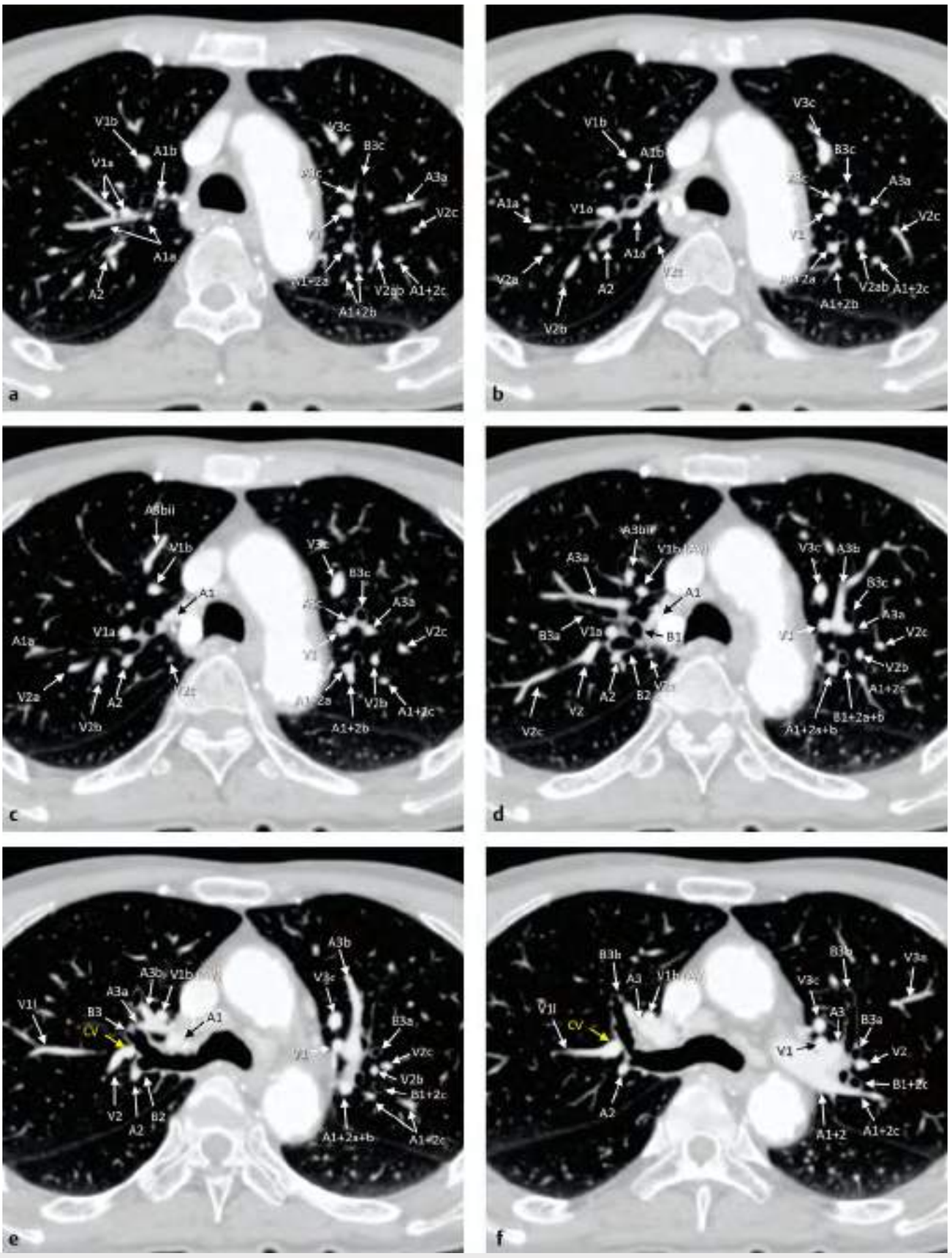

Fig. 6.6 Axial CT anatomy of the pulmonary segmental vessels of the upper and middle lobes CT images show "central venous drainage type" of the upper veins in both lungs. The central vein (CV) is formed by V2 (and V1) subsegmental veins, runs inferiorly through the angle formed by the bifurcation of the right upper lobe bronchus into B2 and B3. Note a variation of an accessory pulmonary vein (Acc PV) from the right middle lobe joining directly to the left atrium. AV, anterior vein; IPV, inferior pulmonary vein; IT, inferior trunk; LA, left atrium; LAA, left atrial auricle; SPV, superior pulmonary vein; ST, superior trunk.

(*Continued*)

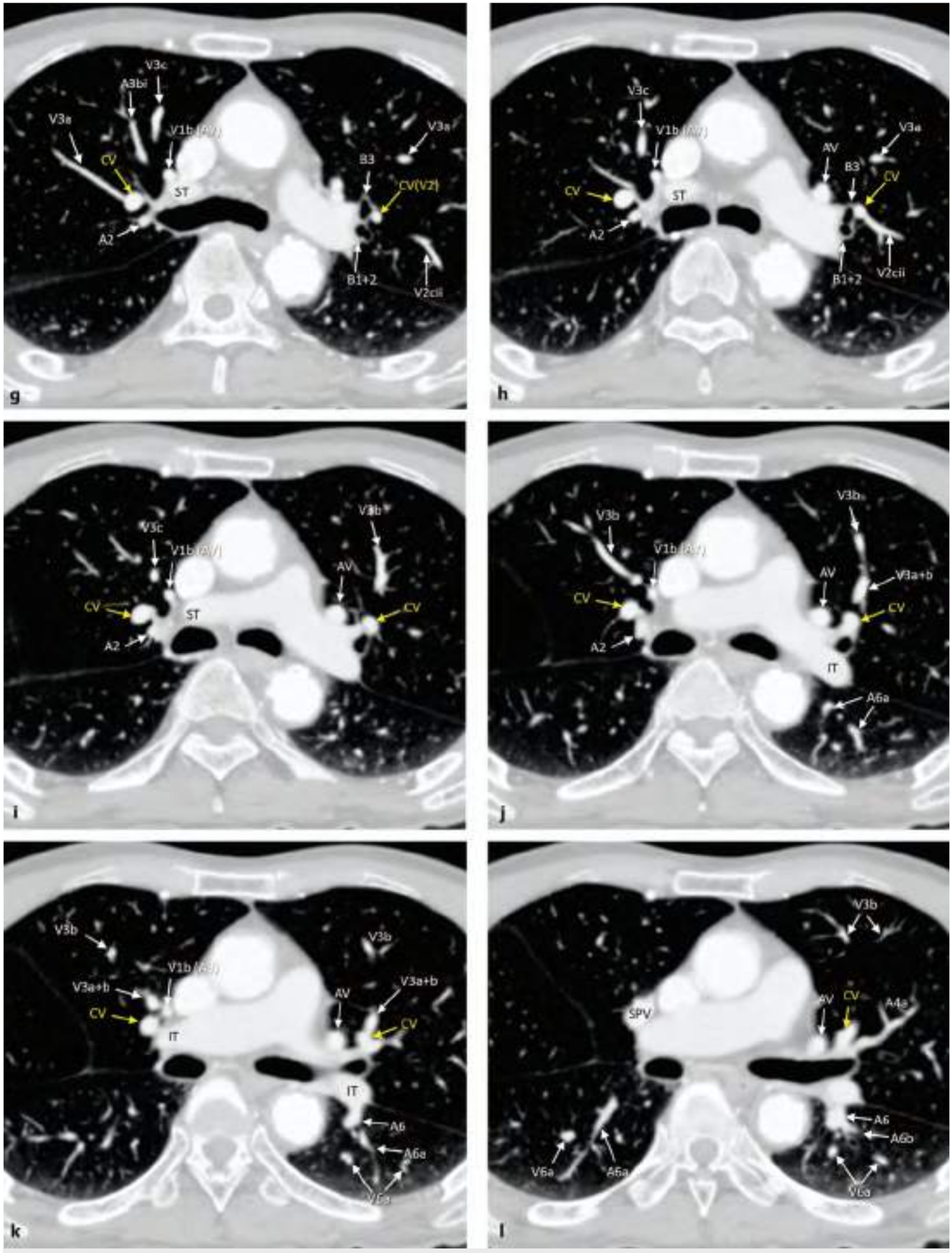

Fig. 6.6 (*Continued*) **(g–l)**

(*Continued*)

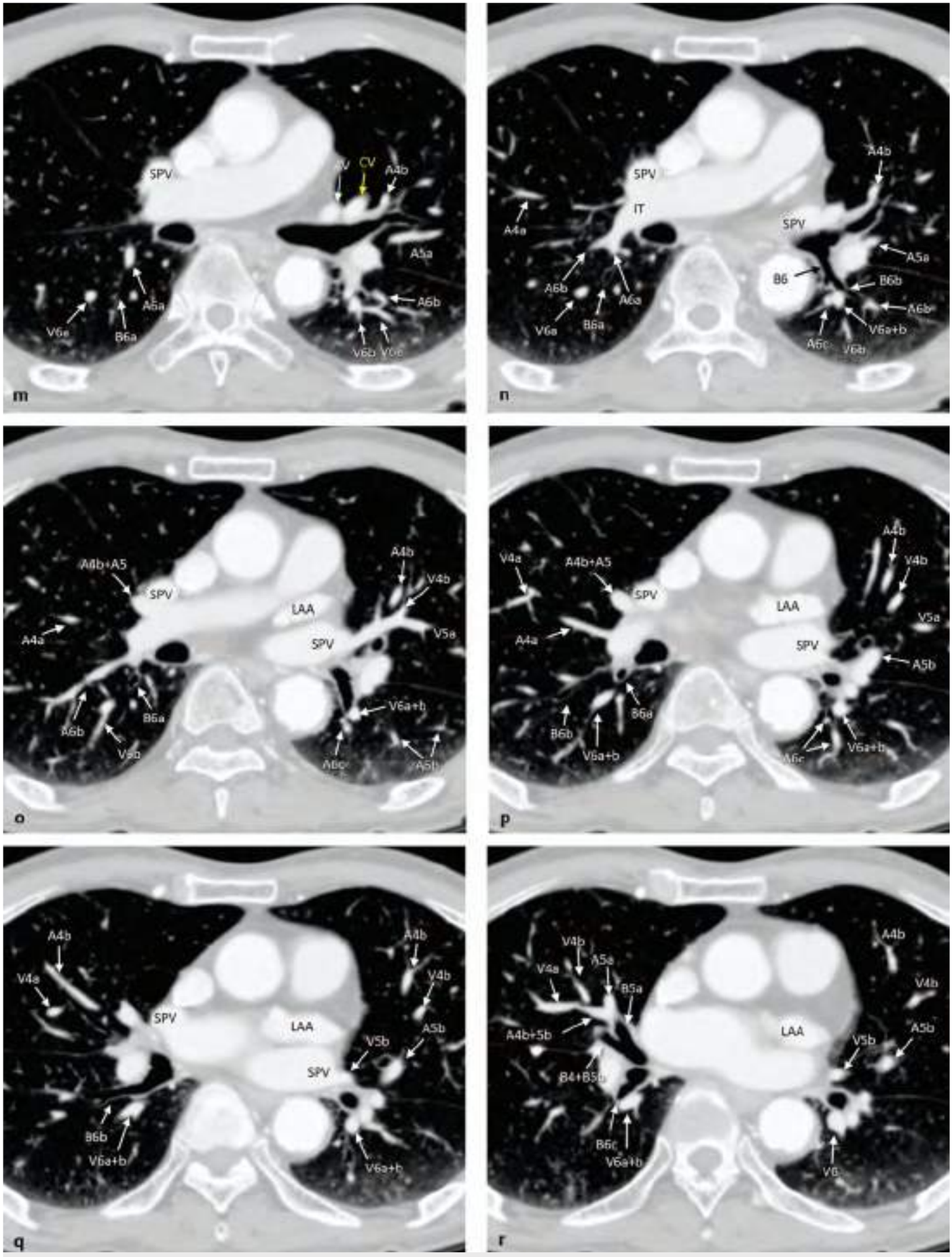

Fig. 6.6 (*Continued*) (m–r)

(*Continued*)

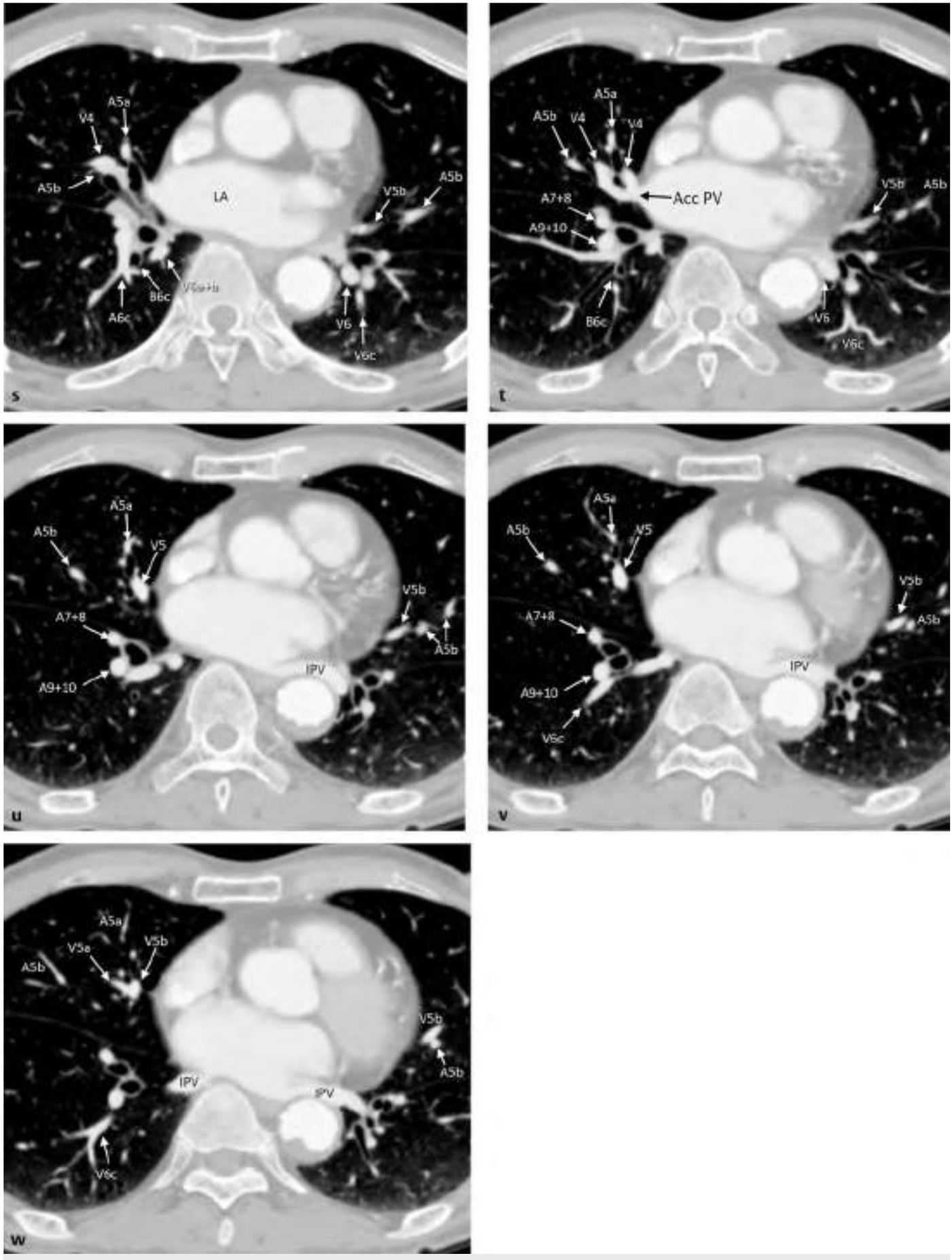

Fig. 6.6 (*Continued*) (s–w)

Table 6.2 Subsegmental pulmonary veins and relevant subsegments

Right pulmonary veins		Left pulmonary veins	
Subsegmental vein	**Bounded (sub)segments**	**Subsegmental vein**	**Bounded (sub)segments**
Upper lobe		**Upper lobe**	
V1a	S1a/b	V1a	S1 + 2a subsubsegments
V1b	S1b/S3b	V1b	S1 + 2a/S3c
V1l	S1/S2,3	V2a	S1 + 2a/b
V2a	S1a/S2a	V2b	S1 + 2b/c
V2b	S2a/b	V2c	S1 + 2c/S3a
V2c	S2a/S3a	V3a	S3a/S4a
V2t	S2 /S6	V3b	S3b/S4b
V3a	S3a/b	V3c	S3b/c
V3b	S3b/S4	V4a	S4a/S5
V3c	S3b subsubsegments	V4b	S4b/S5
Middle lobe		V5a	S5a/b
V4a	S4a/b	V5b	S5b
V4b	S4b/S5		
V5a	S5a/b		
V5b	S5b		
Lower lobe		**Lower lobe**	
V6a	S6a/b, c	V6a	S6a/b, c
V6b	S6b/c	V6b	S6b/c
V6c	S6c/S10a	V6c	S6c/S10a
V7	S7/S8,10	V7	S7/S8,10
V8a	S8a/b	V8a	S8a/b
V8b	S8b/S9b	V8b	S8b/S9b
V9a	S9a/b	V9a	S9a/b
V9b	S9b/S10b	V9b	S9b/S10b
V10a	S10a/b, c	V10a	S10a/b, c
V10b	S10b/c	V10b	S10b/c
V10c	S10c/S7	V10c	S10c/S7

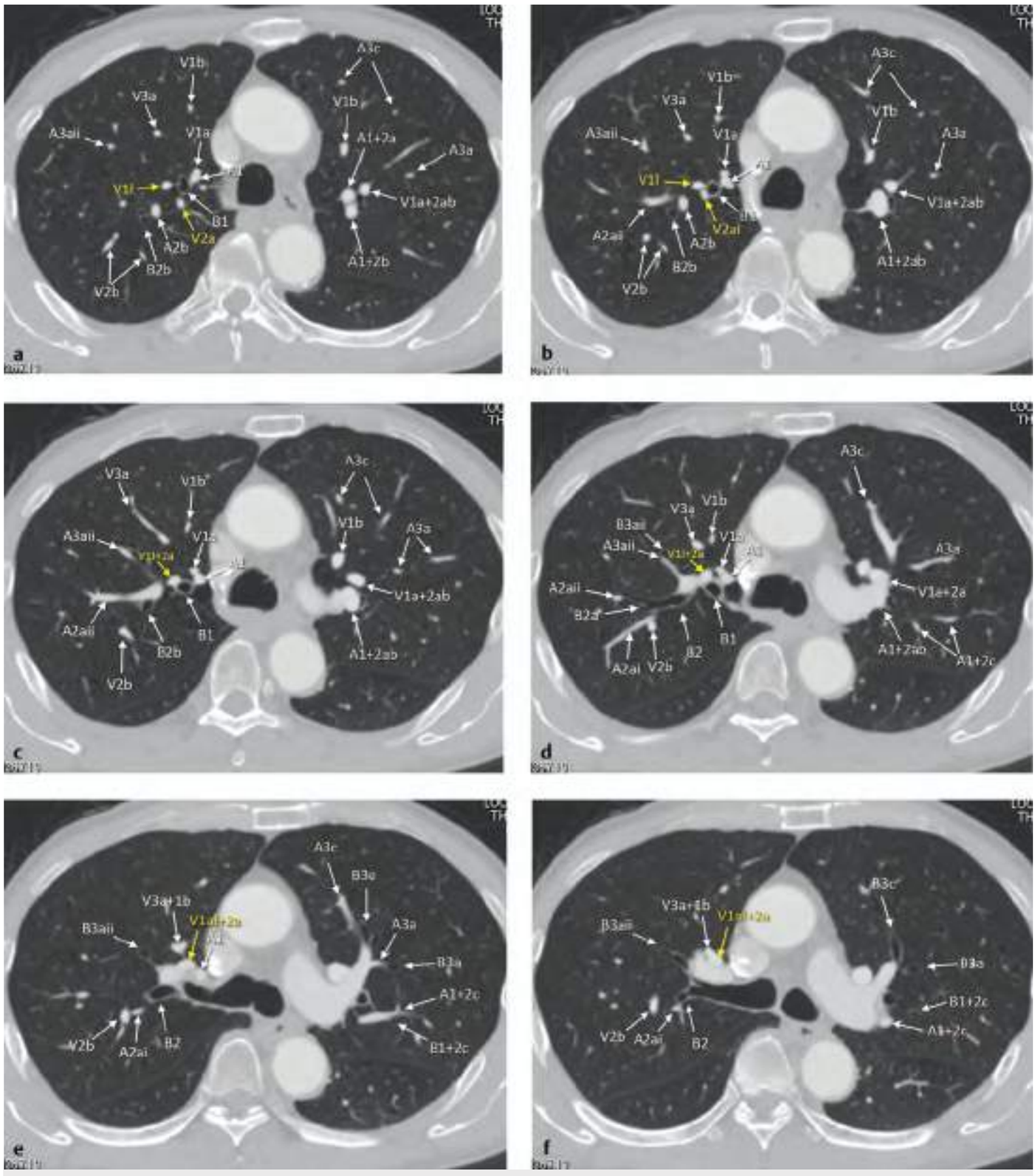

Fig. 6.7 "Semicentral vein" type upper lobe venous drainage. Axial CT images show V2 subsegmental veins and V1 running anteroinferiorly around the B1 and join to form a venous trunk at the anteromedial aspect of the B2-B3 bifurcation in the right upper lobe. SPV, superior pulmonary vein; ST, superior trunk.

(*Continued*)

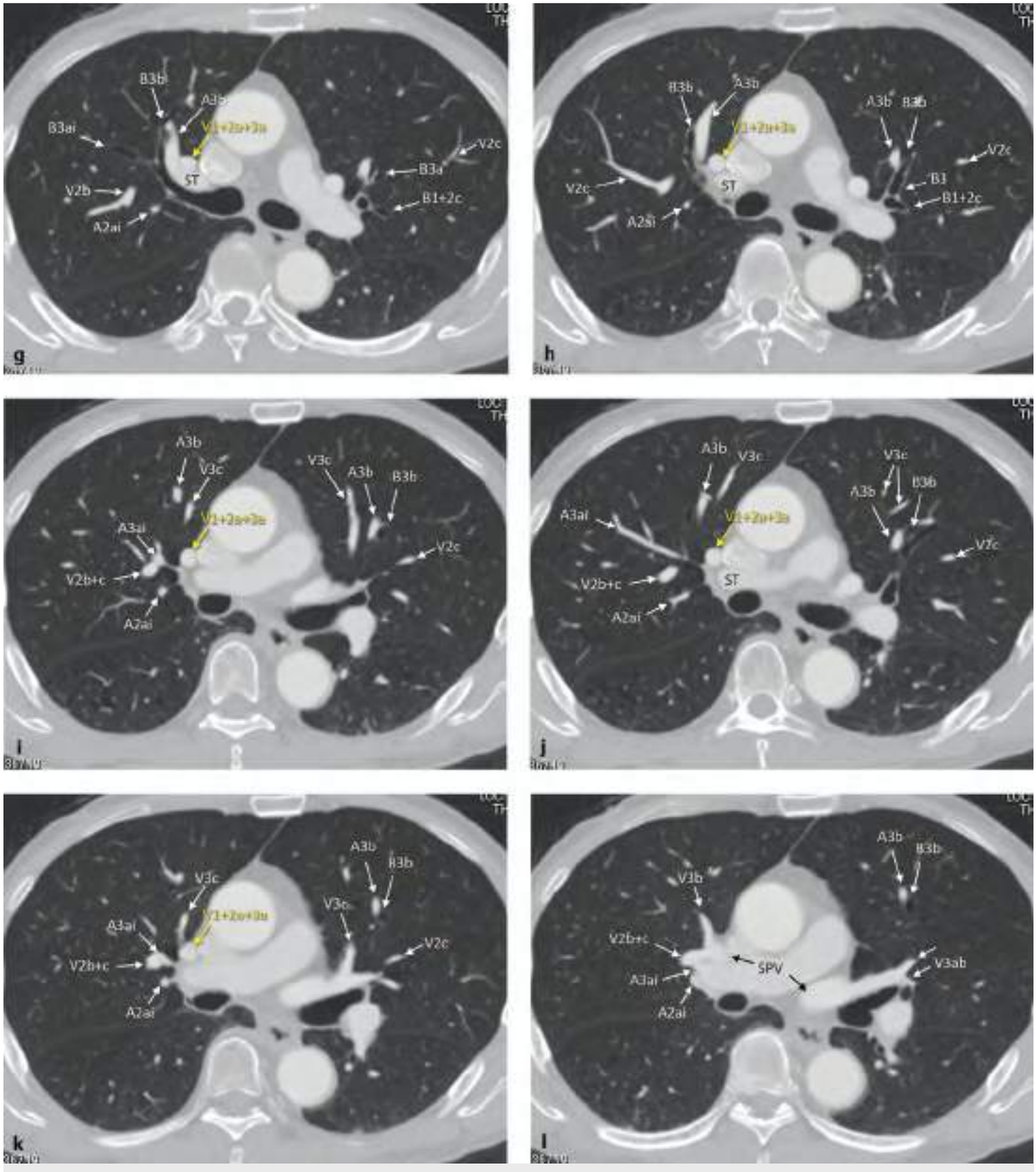

Fig. 6.7 (*Continued*) **(g–l)**

the superior pulmonary vein. The middle lobe vein or the segmental vein occasionally drains directly into the left atrium or the inferior pulmonary vein (▶ Fig. 6.5, ▶ Fig. 6.6, ▶ Fig. 6.8).[12] Exceptionally, the lateral segmental vein (V4) or its subsegmental vein empties into the anterior segmental vein (V3) of the upper lobe.[13]

The right inferior pulmonary vein is formed by all five segmental veins of the right lower lobe. It occasionally receives segmental or subsegmental veins from the middle lobe or the upper lobe (V2). Three basal segmental veins of the V8 (anterior), the V9 (lateral), and the V10 (posterior) ascend medially by crossing behind their respective bronchi to form the common basal vein. The V7

(medial) basal segmental vein is a small intersegmental vein which ascends posteriorly to join the common basal vein at the anteroinferior aspect. The V6 (lower lobe apical segmental vein) descends from the apex of the lower lobe, crosses behind the basal bronchus to join the common basal vein to form the inferior pulmonary vein. The V6 segmental vein rarely receives a V2 subsegmental vein and ends directly into the left atrium.

Branching pattern of the left pulmonary veins is similar to that of the right pulmonary veins. As mentioned before, semicentral type of venous drainage of the upper lobe vein is more frequent in the left lung. One or both lingular veins may, like the middle lobe veins, empty into the inferior pulmonary vein or directly into the left atrium. However, the direct drainage of lingular vein into the left atrium is much less frequently on the left side.

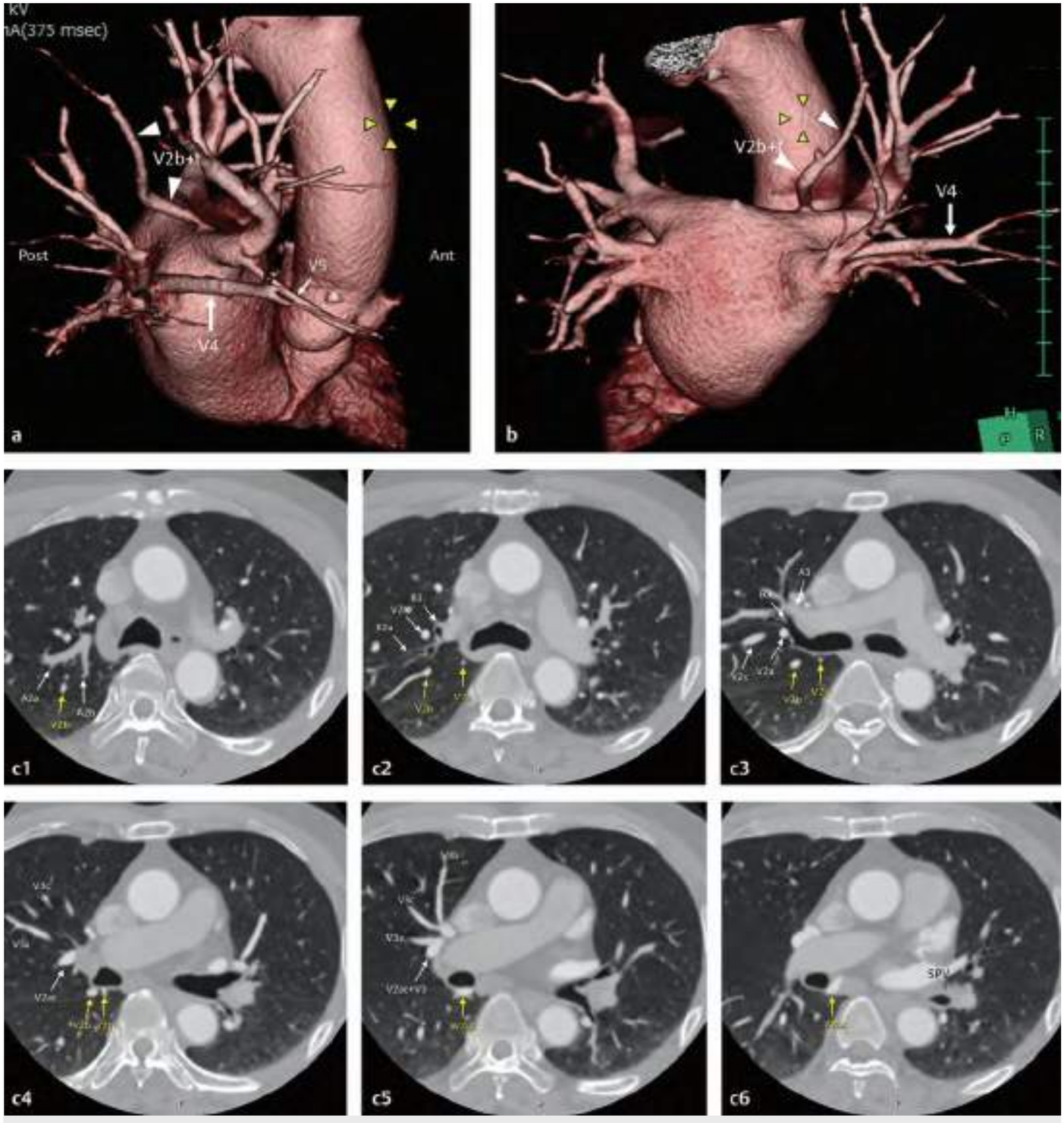

Fig. 6.8 Uncommon variation of the segmental pulmonary veins of V2 and V4. Right lateral **(a)** and posterior **(b)** 3DVR images and sequential axial images **(c)** of the CTA show uncommon variations of the subsegmental veins of the right lung. V2b runs inferomedially and joins with V2 t to form V2b + (*white arrowheads*) which runs inferiorly along the posterior surface of the bronchus intermedius. It then runs inferomedially in the mediastinum and terminates at the superior aspect of the junction between the right superior pulmonary vein and the left atrium. The other V2 subsegmental veins (V2a and V2c) run anteroinferiorly and join the superior pulmonary vein. Another uncommon variation is also noted in the right middle lobe veins. V4 (*arrow*) extends posteriorly and joins the right inferior pulmonary vein. IPV, inferior pulmonary vein; LA, left atrium; LAA, left atrial auricle; LLB, lower lobe bronchus; MLB, middle lobe bronchus; SPV, superior pulmonary vein.

(*Continued*)

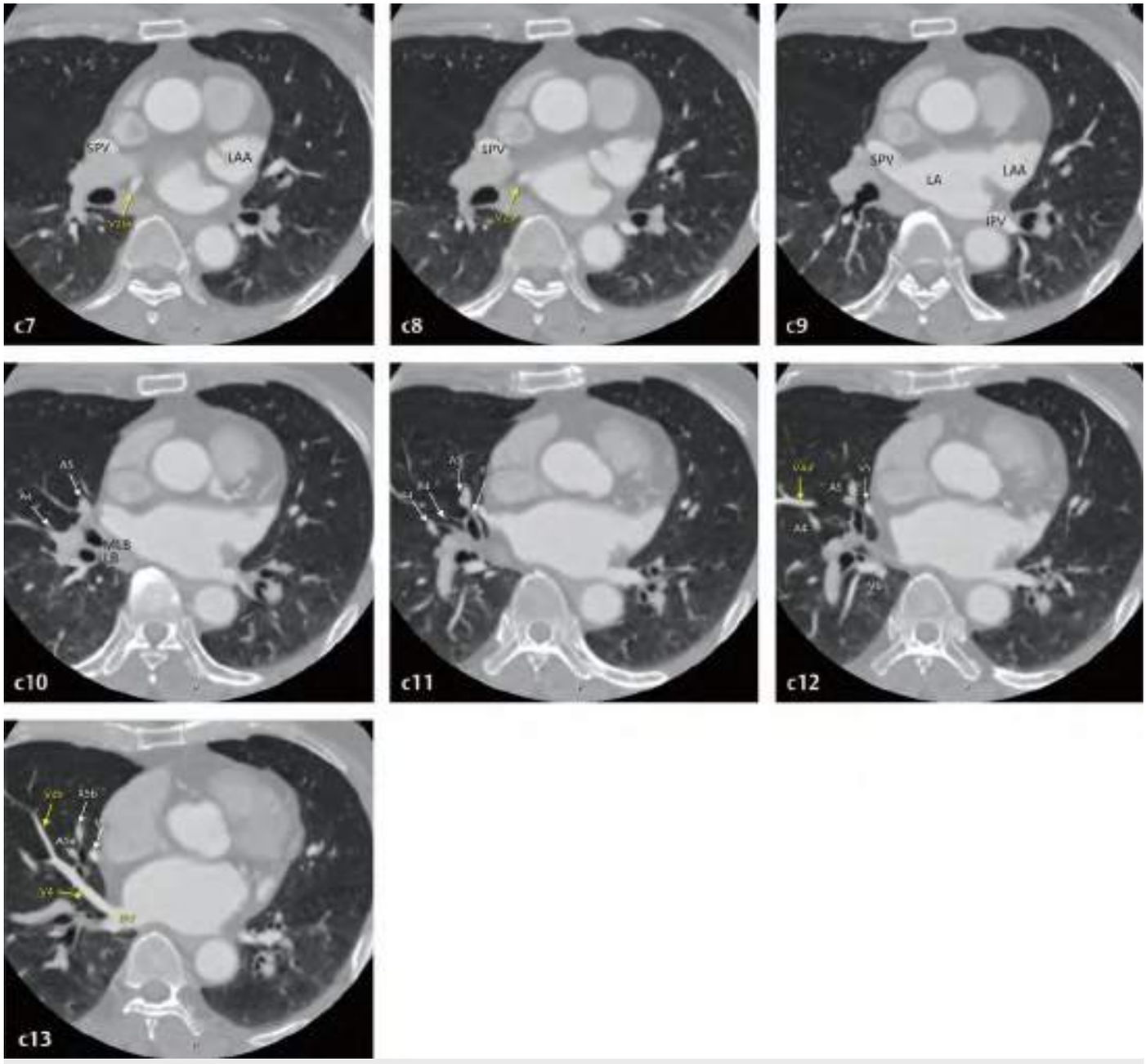

Fig. 6.8 (*Continued*) **(c7–c13)**

◆ Embryology

Pulmonary Arteries

In early embryo, a single diverticulum is derived from the foregut in the common mesenchymal sheath, which divides to form the left and right lung buds. Before the development of the sixth aortic arch (pulmonary arch), the capillary plexus develops from the aortic sinus extend backward caudal to the fourth aortic arch, some of which run caudally to develop into the primitive lung bud and the primitive esophagus (▶ Fig. 6.9**a, b**).[14,15] At the same time, another vascular plexus extends from the dorsal aorta to the primitive esophagus. Both vascular plexuses connect together to form vascular net surrounding the lung buds in the mesenchymal sheath. A pair of pulmonary arches develops in both sides thereafter, which connect the aortic sinus and the dorsal aorta under the fourth aortic arch. The pulmonary arch is constructed from the proximal parts of the vascular plexus, but the peripheral portion of the plexus (net surrounding the lung buds) transforms into the intrapulmonary arteries (▶ Fig. 6.9**c**).[14] The connection of the pulmonary plexus with the dorsal aorta regresses and disappears. Along with the development of the heart, the aortic sinus becomes the truncus arteriosus, and divides into two great arteries of ascending aorta and the pulmonary trunk as described in Chapter 8. The pulmonary trunk directly continued to the pulmonary arches on each side. The proximal portion of the pulmonary arches becomes the main trunk of the right and the left pulmonary artery. The distal part of the right pulmonary arch beyond the origin of the primitive pulmonary artery will regress and disappear (▶ Fig. 6.9**d**). The distal portion of the left pulmonary arch remains as the ductus arteriosus until birth.

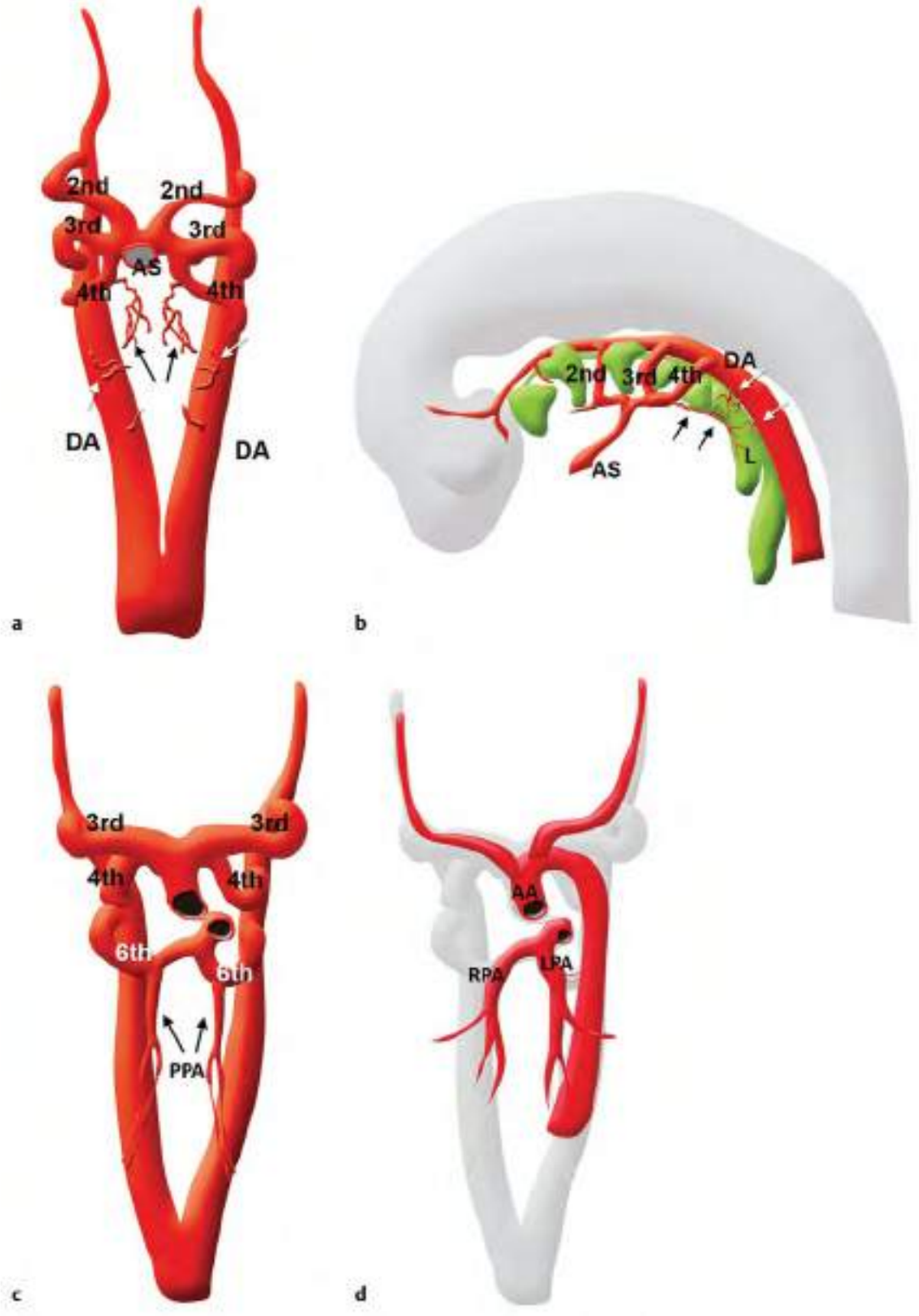

Fig. 6.9 Schematic drawing of the development of the pulmonary artery. Frontal **(a)** and lateral **(b)** images of the embryo. Vascular plexus (*arrows*) arising from the proximal portion of the fourth aortic arch supply of the primitive lung bud (L) at early embryo stage before forming sixth aortic arch. Another vascular plexus (*white arrows*) from the dorsal aorta (DA) also supplies the lung bud as well as the primitive esophagus. One of these plexuses may develop to form the sixth aortic arch (pulmonary arch). **(c)** After development of the sixth aortic arch, the primitive pulmonary arteries (PPA) arise from the sixth arches using remnants of the vascular plexus. The vascular plexus from the dorsal aorta has already disappeared. The pulmonary trunk and ascending aorta (AA) are now separated by the septum. **(d)** The distal portion of the sixth aortic arches and the primitive pulmonary arteries form the right and the left pulmonary arteries (RPA and LPA). The distal portion of the left pulmonary arch remains as the ductus arteriosus until birth. 2nd, second aortic arch; 3rd, third aortic arch; 4th, fourth aortic arch; 6th, sixth aortic arch (pulmonary arch); AA, ascending aorta; AS, aortic sinus; DA, descending aorta; LPA, left pulmonary artery; PPA, primitive pulmonary artery; RPA, right pulmonary artery.

Pulmonary Veins

The pulmonary venous system develops from the mesenchyme. The primitive lung bud is drained via the venous plexus of the foregut (splanchnic plexus) which connect to both common cardinal veins, and umbilicovitelline venous system (▶ Fig. 6.10**a**). A solitary vein develops in the dorsal mesocardium, which forms a new drainage route connecting the pulmonary venous plexus to the left atrium.[16] The solitary vein (the primitive pulmonary vein) is incorporated into the left atrium by growth of the vestibular spine which is a mesenchymal condensation extending from the mediastinum and covers the leading edge of the primary atrial septum. The old drainage route from the pulmonary venous plexus to the cardinal and umbilicovitelline venous system regresses and disappears. Along with further development of the heart, more of the primitive pulmonary venous tributes will be incorporated into the left atrium, and finally four independent pulmonary veins, receiving all pulmonary venous blood, empty into the left atrium.

◆ Developmental Failure

Developmental failure of any of the above steps can cause several anomalies. Some of the anomalies are briefly described here.

Persistent Truncus Arteriosus

Persistent truncus arteriosus is caused by a failure of division of truncus arteriosus into the ascending aorta and the pulmonary trunk (▶ Fig. 6.11). It is a rare anomaly approximately 1 to 2% of infant with congenital heart diseases, and it is often associated with other various abnormalities such as dysplastic valve (the truncal valve), interruption of the aortic arch, and atrial septal defect.[17,18] Typical clinical manifestation includes cyanosis and tachypnea at birth, and heart failure within weeks. Mortality rate would be high up as 100% by 1 year unless the surgical repair. Persistent truncus arteriosus are classified into four types mainly by the origin of the pulmonary artery and other abnormalities.[17,19]

Aberrant Left Pulmonary Artery

Aberrant left pulmonary artery (pulmonary artery sling) is a rare anomaly, in which the left pulmonary artery arises from the posterior aspect of the right pulmonary artery to the left lung by passing between the trachea and esophagus (▶ Fig. 6.12, ▶ Fig. 6.13). It is thought to be caused by a failure of formation of the sixth aortic arch (pulmonary arch). The anomalous left pulmonary artery compresses the lower trachea, right main bronchus and esophagus, and can cause upper airway symptoms. About 40 to 50% of cases are associated with other abnormalities.[20,21,22] Severity of symptoms and prognosis are varied from asymptomatic to fatal, which would be related to the severity of tracheobronchial stenosis. In rare examples, the anomaly remains asymptomatic until found incidentally in adulthood (▶ Fig. 6.13).

Systemic Arterial Supply to the Lung

Systemic arterial supply to the lung can be seen in various congenital and acquired diseases.[23,24] Congenital lesions include pulmonary atresia, interruption of the unilateral pulmonary arteries (unilateral pulmonary artery atresia), pulmonary sequestration, and aberrant systemic artery supplying to the lung base (▶ Fig. 6.14).[25,26,27] Acquired lesions are mainly due to acquired lung diseases, such as bronchiectasis and inflammatory lung disease. There are three routes of systemic arterial supply. First, patent ductus arteriosus which is the main route of systemic–pulmonary arterial supply in case of pulmonary atresia and interruption of the left pulmonary artery. Second, an aberrant systemic artery from the descending aorta supplying to the lung which is the main route in cases of pulmonary sequestration and the aberrant systemic artery supplying the lung base (▶ Fig. 6.14). This route can be seen in cases of pulmonary atresia or interruption of the pulmonary artery, too. Origin of the aberrant systemic artery is thought to be the remnant of an embryonic vessels connecting to the lung plexus from the dorsal aorta. Third, multiple potential anastomoses of pulmonary artery with the well-developed systemic arteries including the bronchial artery, the intercostal arteries, the inferior phrenic artery, and other arteries of the thorax, which develop secondary due to angiogenesis in the acquired lesion but can develop as a collateral pathway in cases of pulmonary atresia. Pulmonary atresia is caused by atresia of the pulmonary valve, and it is frequently associated with ventricular septal defect. In the past, it was classified as a type of persistent truncus arteriosus (type 4 in a classification by Collett and Edwards). Interruption of the pulmonary artery is caused by a failure of connection between the pulmonary arch and the pulmonary trunk (dysplasia of the proximal portion of the pulmonary arch) and/or between the pulmonary arch and the primitive pulmonary artery, which are often associated with other anomalies of heart and the aortic arch.

Pulmonary Arteriovenous Malformation

Pulmonary arteriovenous malformations are abnormal connection between the pulmonary arteries and veins without capillary bed (▶ Fig. 6.15). Approximately 70 to 80% of cases of pulmonary arteriovenous malformation are associated with hereditary hemorrhagic telangiectasia which is an autosomal dominant disease involving vessels of multiple organs skin, mucosal tissue, liver, lung, and central nerves system.[28,29] Pathogeneses of pulmonary arteriovenous malformations is unknown, but it is generally thought that the pulmonary arteriovenous malformation may be congenital lesion caused by remnant of physiological anastomoses between the arterial and venous plexus during fetal development. It can cause paradoxical embolization through the pulmonary arteriovenous shunt, and it also cause hypoxia, and pulmonary hemorrhage.

Cerebral symptoms including cerebral infarction, transit ischemic attack, and cerebral abscess can occur approximately 50% of patients with the pulmonary arteriovenous malformation. Majority of the pulmonary arteriovenous malformation can be successfully treated by transcatheter embolization. Generally, catheterization for the lesion fed by the left A3b is more difficult than those of the other locations because of the acute angle of the origin of A3b from the left pulmonary artery (▶ Fig. 6.15).

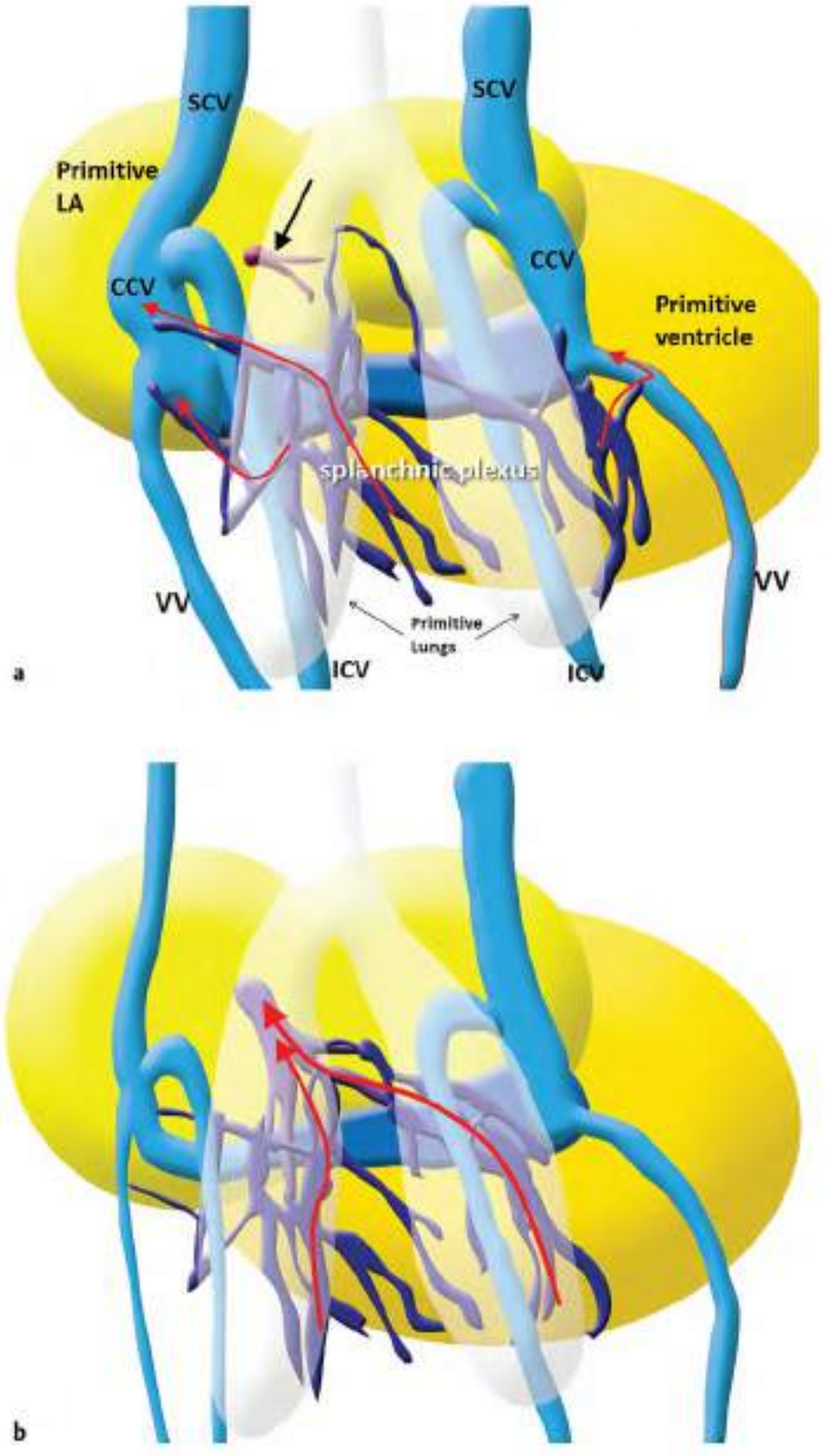

Fig. 6.10 Development of the pulmonary veins. **(a)** Primitive lung bud is drained via the splanchnic venous plexus into the common cardinal vein (CCV), superior cardinal vein (SCV), and/or the vitelline vein (VV) in both the sides. A solitary vein develops in the dorsal mesocardium (*black arrow*), which further develops to connect the left atrium to the splanchnic plexus. **(b)** The solitary vein develops and venous blood from the lung bud is now drained (*red arrows*) via the plexus and solitary vein (becoming pulmonary vein) into the left atrium. The connection of the pulmonary venous plexus with cardinal and vitelline veins regresses and disappears. ICV, inferior cardinal vein; LA, left atrium.

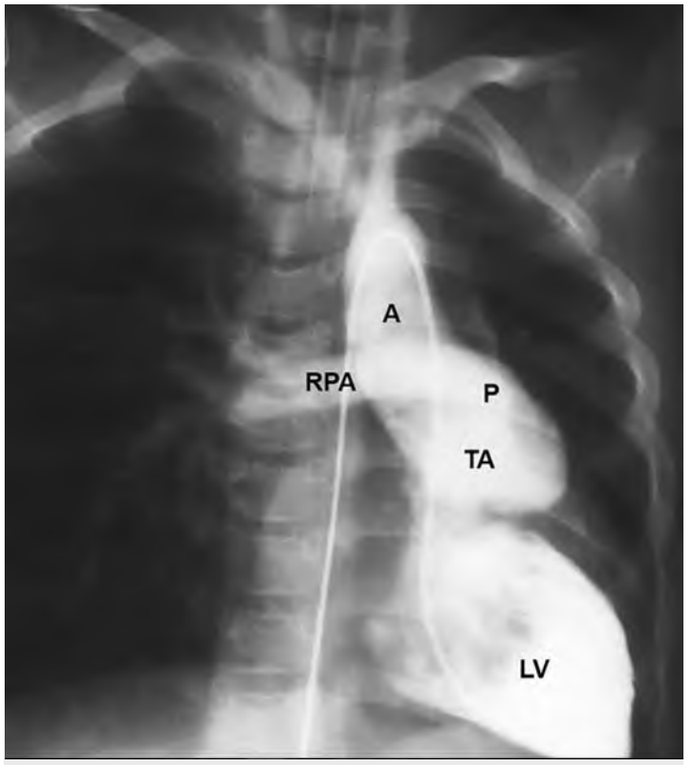

Fig. 6.11 Persistent trunk arteriosus. Left ventriculography shows that both the aorta (a) and the pulmonary artery (P) arising from a large arterial trunk (TA). LV, left ventricle; RPA, right pulmonary artery.

Therefore, knowledge of pulmonary vascular anatomy and variations is essential for the treatment.

Anomalous Pulmonary Venous Return

Anomalous pulmonary venous return comprises a group of developmental abnormalities in which blood is returned to the right atrium or its tributaries. It is caused by a failure of connection between the primitive pulmonary vein and the pulmonary venous plexus, and persistent embryonic drainage of the pulmonary venous plexus to the cardinal venous system or umbilicovitelline venous system. Anomalous pulmonary venous return can be divided into total anomalous pulmonary venous return (TAPVR) and partial anomalous pulmonary venous return (PAPVR) (▶ Fig. 6.16; see Chapter 7). All pulmonary venous vessels drain into the systemic vein or the right atrium in TAPVR. TAPVR is classified into four types according to the venous drainage as follows: type1 (supracardiac type), the four pulmonary vein draining via a common vein into the right or left superior vena cava or their tributaries; type 2 (cardiac type), the pulmonary veins draining into the right atrium and/or coronary sinus; type 3 (infradiaphragmatic type), the common pulmonary vein draining into the portal venous system; and type 4 (mixed type), the pulmonary veins draining into different venous systems. TAPVR is found in 1.5% of cardiovascular malformations.[30] In PAPVR, one or a few pulmonary veins connect to the right superior vena cava, the right atrium, the left innominate vein, or the inferior vena cava. Among them, the most common form of PAPVR is the right upper pulmonary vein draining to the right atrium or the superior vena cava. The prevalence of a PAPVR reported is 0.2 to 0.7%.[31] A specific type of PAPVR in which the right pulmonary vein draining into the inferior vena cava and coexistence of pulmonary sequestration is well known as Scimitar syndrome. Patients with PAPVR are often asymptomatic or show few symptoms. However, PAPVR including Scimitar syndrome can be often associated with systemic arterial supply to the affected lung, and therefore, it may present pulmonary hypertension and hemorrhage.[32,33]

◆ Pulmonary Artery Diameters in Pathologies

Pulmonary artery diameters vary with age and gender. Enlargement of the pulmonary arteries is common in pulmonary hypertension, chronic pulmonary embolism, chronic interstitial lung disease, and chronic obstructive pulmonary disease (COPD). Normal diameters of the pulmonary arteries in adults are 29 ± 4 mm for the main pulmonary artery, 23 ± 3 for the left pulmonary artery, and 23.5 ± 3.7 for the right pulmonary artery. Pulmonary hypertension is defined as a mean pulmonary arterial pressure of at least 25 mm Hg.[34,35] Right heart catheterization is currently the gold standard method for detecting pulmonary hypertension, but it is an invasive test. Computed tomography (CT) scan is commonly used for scanning of the lung and mediastinum and pulmonary artery measurements are usually used to diagnose patient with pulmonary hypertension. A cutoff main pulmonary artery of greater than 33 mm has a very high accuracy for diagnosis of pulmonary hypertension. Diameters less than 27 mm are always normal. A CT-demonstrated distal main pulmonary artery diameter exceeding that of the ascending aorta is 71% sensitive and 76% specific for pulmonary hypertension.[36] A segmental artery-to-bronchus ratio greater than 1:1 is abnormal, but this is a very nonspecific finding. In pulmonary artery hypertension, the arteries become more pulsatile and the right pulmonary artery wall distensibility is used as a criterion to find patients with pulmonary hypertension. Distensibility as measured with magnetic resonance imaging (MRI) or CT is calculated by dividing the difference between the maximum cross-sectional area and the minimum cross-sectional area by the maximum cross-sectional area and multiplying the result by 100. The best pulmonary artery distensibility cutoff for distinguishing between patients with pulmonary hypertension is calculated at 16.5%.[37]

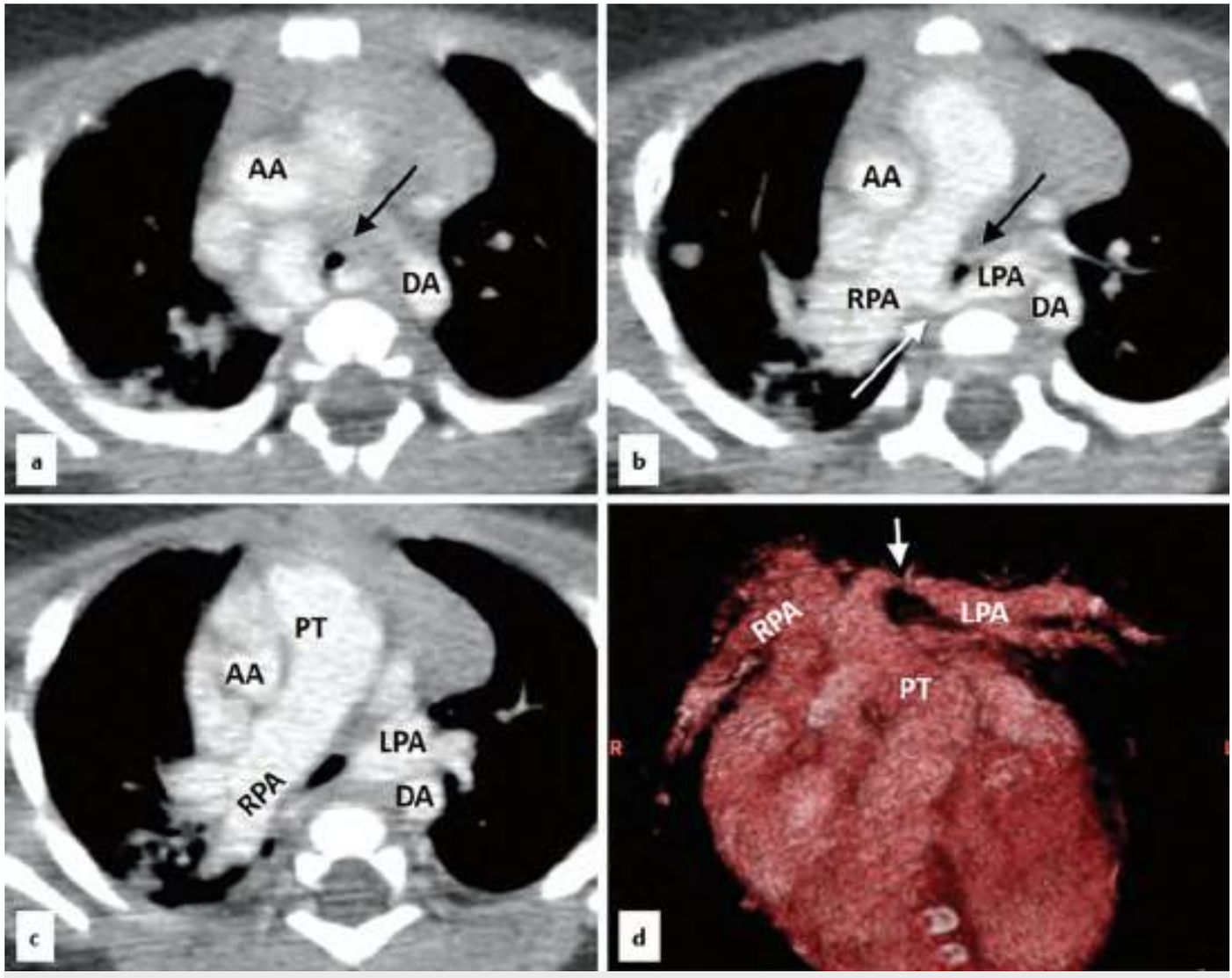

Fig. 6.12 Pulmonary sling (aberrant left pulmonary artery). Axial images **(a-c)** and 3D image **(d)** of contrast-enhanced CT in a child show an aberrant left pulmonary artery (LPA) arising from the right pulmonary artery (RPA). The aberrant left pulmonary artery runs between the trachea and esophagus to the left lung. Narrowing of the trachea (*black arrow*) and stenosis of the proximal portion of the left pulmonary artery (*white arrow*). AA, ascending aorta; DA, descending aorta; PT, pulmonary trunk.

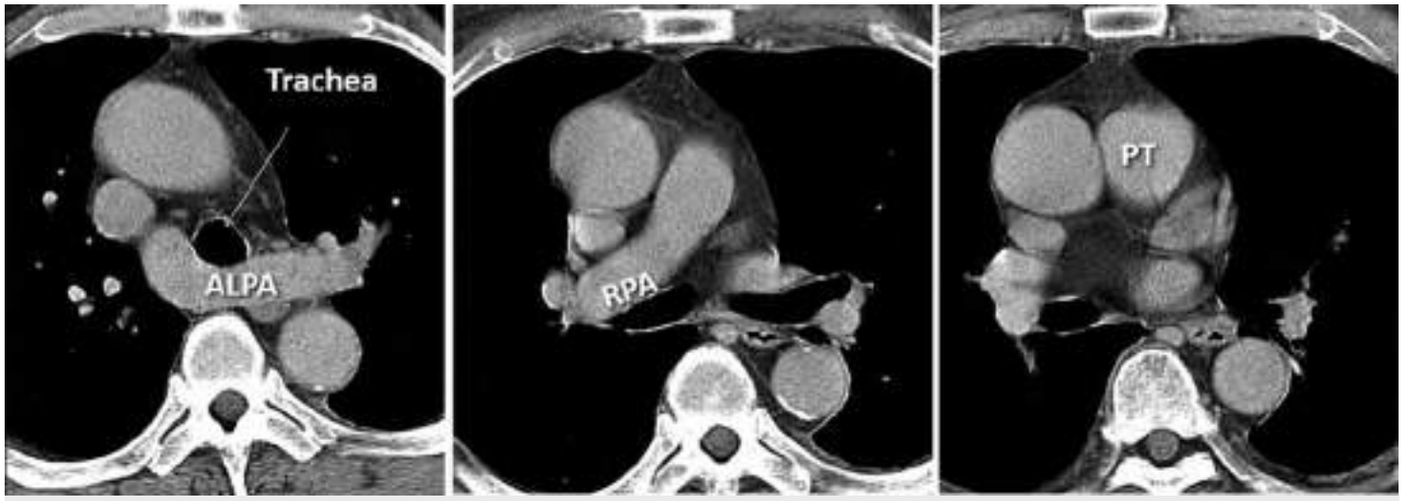

Fig. 6.13 Pulmonary sling incidentally found in an adult patient. Axial CT images show an aberrant left pulmonary artery (ALPA) without tracheal stenosis. PT, pulmonary trunk; RPA, right pulmonary artery.

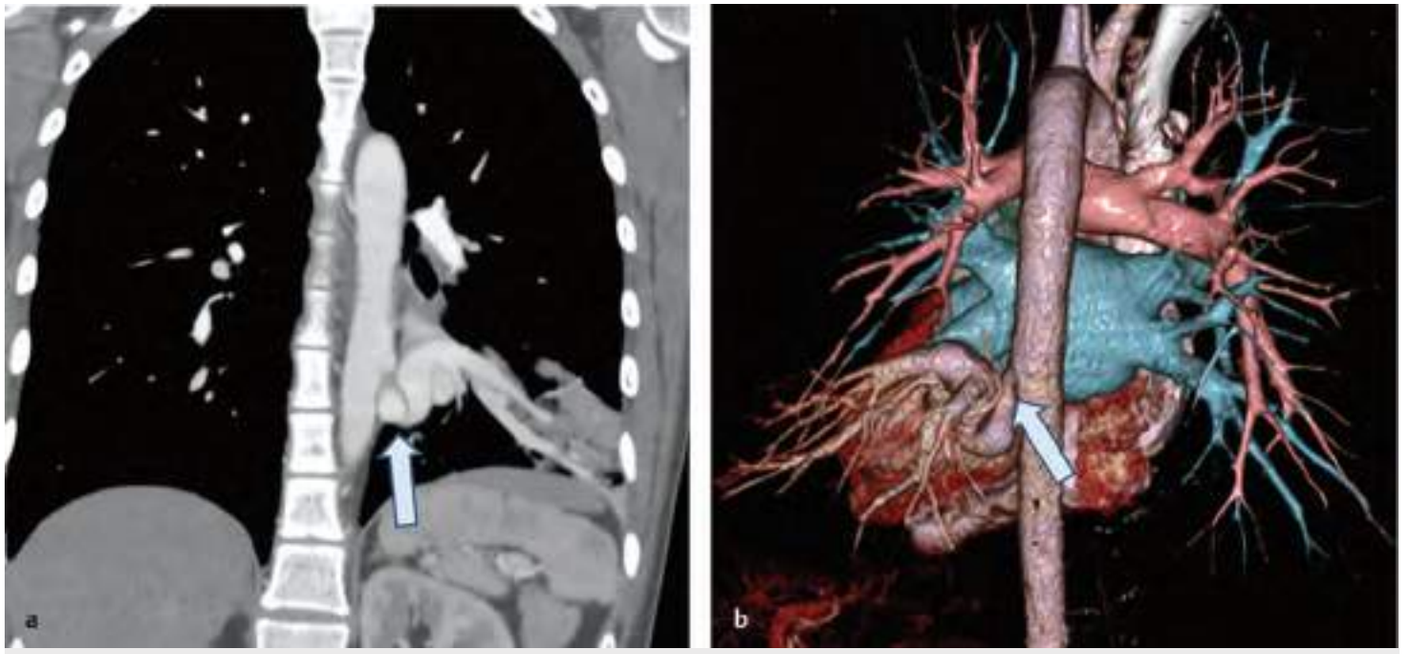

Fig. 6.14 Systemic arterial supply to the left basal lung (*arrow*). Coronal MPR image **(a)** and posterior view of the 3D CT angiography **(b)** show that an enlarged artery originating from the descending aorta supplies the basal segments of the left lung.

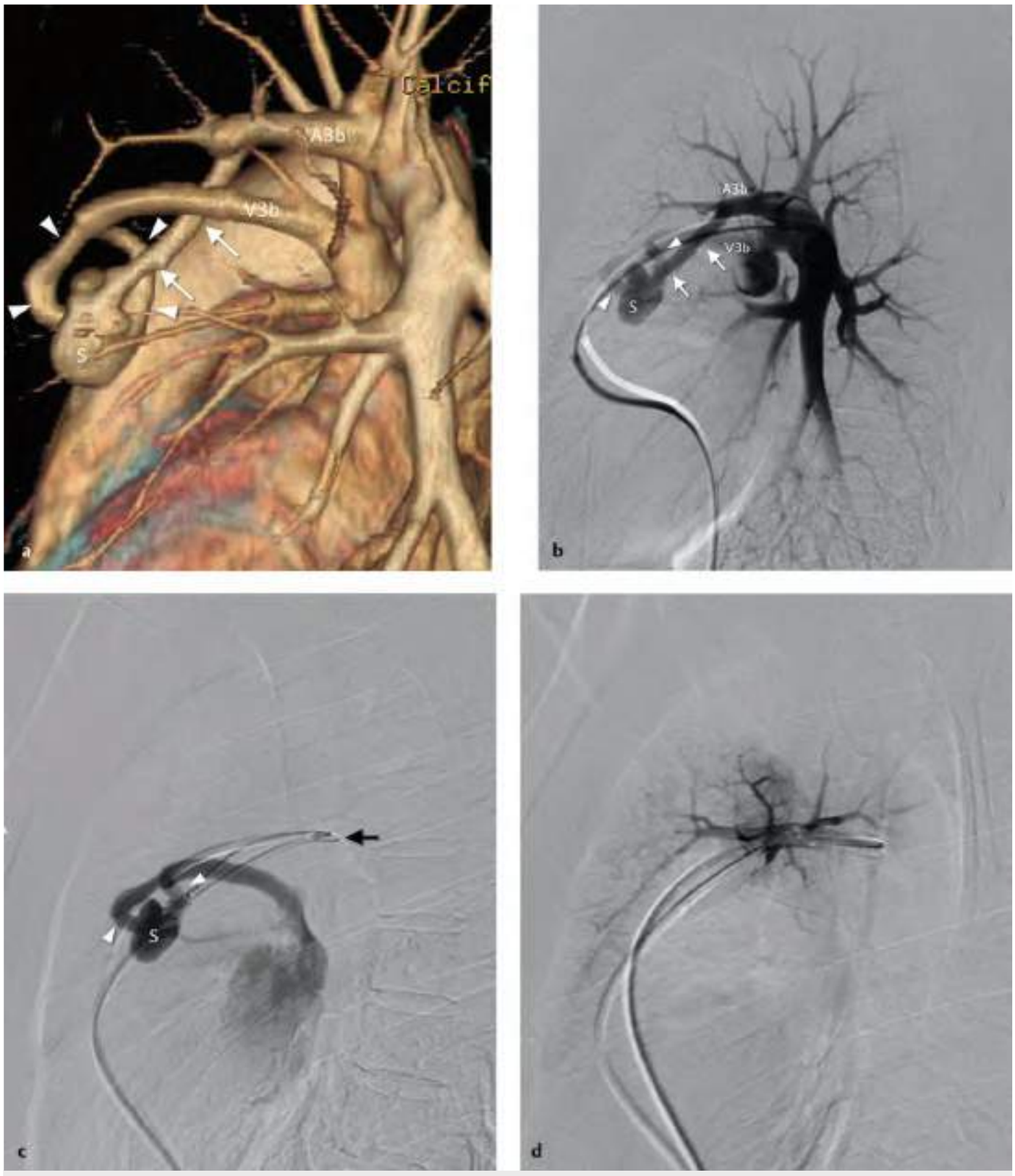

Fig. 6.15 Pulmonary arteriovenous malformation (AVF) at the S3 of the left lung. The arteriovenous malformation was treated by transcatheter embolization. Image of systemic arterial supply **(a)** and lateral view of the pulmonary angiography **(b)** show an arteriovenous malformation consists of a large fistulous sac draining into V3b via the two drainage veins (*white arrowheads*). **(c)** Selective angiography of the feeding artery at the just proximal portion of the fistulous sac (S) clearly demonstrates the fistulous (S) and the two drainage veins (*white arrowheads*). Note an acute angle of the catheter (*arrow*) at the origin of A3b. **(d)** Selective angiography of the left A3 segmental artery immediately after coil embolization shows disappearance of the AVF.

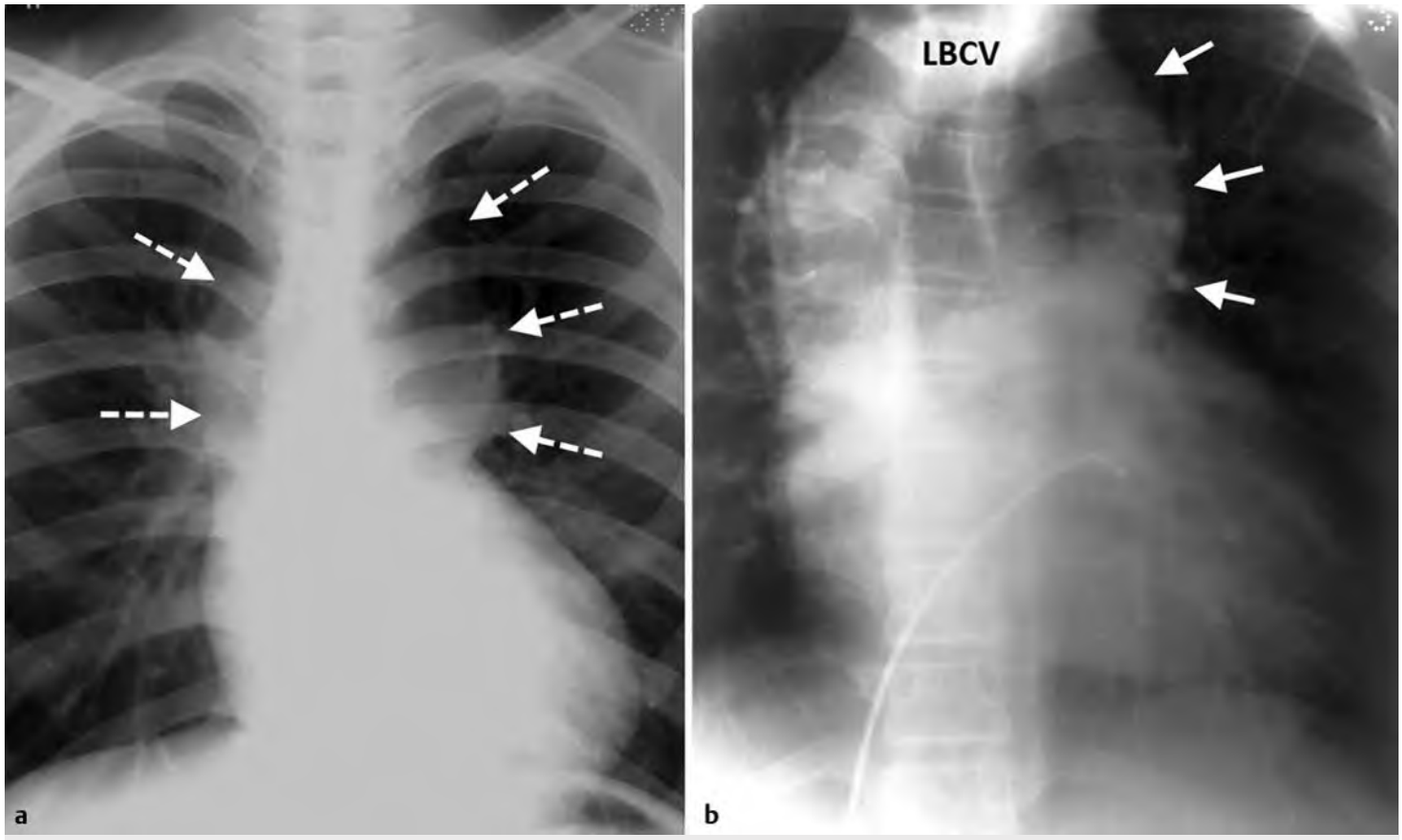

Fig. 6.16 Supracardiac type (type 1) total pulmonary venous return. **(a)** Frontal view of the chest X-ray shows typical findings of the "snowman appearance" (*arrows*). (**b**) Right ventricular angiography at venous phase shows all pulmonary veins join to an enlarged anomalous vein (*white arrows*) draining into the left brachiocephalic vein (LBCV).

References

[1] Bozlar U, Ors F, Deniz O, et al. Pulmonary artery diameters measured by multidetector-row computed tomography in healthy adults. Acta Radiol.; 48 (10):1086–1091

[2] Lee KS, Bae WK, Lee BH, Kim IY, Choi EW, Lee BH. Bronchovascular anatomy of the upper lobes: evaluation with thin-section CT. Radiology.; 181(3):765–772

[3] Van Der Spuy JC. The surgical anatomy of the pulmonary vessels. Thorax.; 8 (3):189–194

[4] Subotich D, Mandarich D, Milisavljevich M, Filipovich B, Nikolich V. Variations of pulmonary vessels: some practical implications for lung resections. Clin Anat.; 22(6):698–705

[5] Okumura Y, Suzuki M, Takemura A, Takahashi S. Radioanatomical study of the bronchovascular anomalies of the middle and lower lobes of the right lung using multidetector computed tomography. J Comput Assist Tomogr.; 33 (4):529–534

[6] Jardin M, Remy J. Segmental bronchovascular anatomy of the lower lobes: CT analysis. AJR Am J Roentgenol.; 147(3):457–468

[7] Frazier AA, Galvin JR, Franks TJ, Rosado-De-Christenson ML. From the archives of the AFIP: pulmonary vasculature: hypertension and infarction. Radiographics.; 20(2):491–524, quiz 530–531, 532

[8] Demos TC, Posniak HV, Pierce KL, Olson MC, Muscato M. Venous anomalies of the thorax. AJR Am J Roentgenol.; 182(5):1139–1150

[9] Kato R, Lickfett L, Meininger G, et al. Pulmonary vein anatomy in patients undergoing catheter ablation of atrial fibrillation: lessons learned by use of magnetic resonance imaging. Circulation.; 107(15):2004–2010

[10] Marom EM, Herndon JE, Kim YH, McAdams HP. Variations in pulmonary venous drainage to the left atrium: implications for radiofrequency ablation. Radiology.; 230(3):824–829

[11] Asai K, Urabe N, Yajima K, Suzuki K, Kazui T. Right upper lobe venous drainage posterior to the bronchus intermedius: preoperative identification by computed tomography. Ann Thorac Surg.; 79(6):1866–1871

[12] Sugimoto S, Izumiyama O, Yamashita A, Baba M, Hasegawa T. Anatomy of inferior pulmonary vein should be clarified in lower lobectomy. Ann Thorac Surg.; 66(5):1799–1800

[13] Ryba S, Topol M. Venous drainage of the middle lobe of the right lung in man. Folia Morphol (Warsz).; 63(3):303–308

[14] Congdon ED. Transformation of the aortic-arch system during the development of the human embryo. Contrib Embryol.; 14:47–110

[15] Hall SM, Hislop AA, Pierce CM, Haworth SG. Prenatal origins of human intrapulmonary arteries: formation and smooth muscle maturation. Am J Respir Cell Mol Biol.; 23(2):194–203

[16] Anderson RH, Brown NA, Moorman AFM. Development and structures of the venous pole of the heart. Dev Dyn.; 235(1):2–9

[17] Collett RW, Edwards JE. Persistent truncus arteriosus; a classification according to anatomic types. Surg Clin North Am.; 29(4):1245–1270

[18] Egbe A, Uppu S, Lee S, Ho D, Srivastava S. Changing prevalence of severe congenital heart disease: a population-based study. Pediatr Cardiol.; 35(7):1232–1238

[19] Van Praagh R, Van Praagh S. The anatomy of common aorticopulmonary trunk (truncus arteriosus communis) and its embryologic implications. A study of 57 necropsy cases. Am J Cardiol.; 16(3):406–425

[20] Jue KL, Raghib G, Amplatz K, Adams P, Jr, Edwards JE. Anomalous origin of the left pulmonary artery from the right pulmonary artery. Report of 2 cases and review of the literature. Am J Roentgenol Radium Ther Nucl Med.; 95(3):598–610

[21] Clarkson PM, Ritter DG, Rahimtoola SH, Hallermann FJ, McGoon DC. Aberrant left pulmonary artery. Am J Dis Child.; 113(3):373–377

[22] Backer CL, Russell HM, Kaushal S, Rastatter JC, Rigsby CK, Holinger LD. Pulmonary artery sling: current results with cardiopulmonary bypass. J Thorac Cardiovasc Surg.; 143(1):144–151

[23] Castañer E, Gallardo X, Rimola J, et al. Congenital and acquired pulmonary artery anomalies in the adult: radiologic overview. Radiographics.; 26 (2):349–371

[24] Do KH, Goo JM, Im JG, Kim KW, Chung JW, Park JH. Systemic arterial supply to the lungs in adults: spiral CT findings. Radiographics.; 21(2):387–402
[25] Jefferson K, Rees S, Somerville J. Systemic arterial supply to the lungs in pulmonary atresia and its relation to pulmonary artery development. Br Heart J.; 34(4):418–427
[26] Kruzliak P, Syamasundar RP, Novak M, Pechanova O, Kovacova G. Unilateral absence of pulmonary artery: pathophysiology, symptoms, diagnosis and current treatment. Arch Cardiovasc Dis.; 106(8-)(9):448–454
[27] Kieffer SA, Amplatz K, Anderson RC, Lillehei CW. Proximal interruption of a pulmonary artery. Am J Roentgenol Radium Ther Nucl Med.; 95(3):592–597
[28] Mager JJ, Overtoom TTC, Blauw H, Lammers JWJ, Westermann CJJ. Embolotherapy of pulmonary arteriovenous malformations: long-term results in 112 patients. J Vasc Interv Radiol.; 15(5):451–456
[29] Cartin-Ceba R, Swanson KL, Krowka MJ. Pulmonary arteriovenous malformations. Chest.; 144(3):1033–1044
[30] Correa-Villaseñor A, Ferencz C, Boughman JA, Neill CA, The Baltimore-Washington Infant Study Group. Total anomalous pulmonary venous return: familial and environmental factors. Teratology.; 44(4):415–428
[31] Haramati LB, Moche IE, Rivera VT, et al. Computed tomography of partial anomalous pulmonary venous connection in adults. J Comput Assist Tomogr.; 27(5):743–749
[32] Haworth SG, Sauer U, Bühlmeyer K. Pulmonary hypertension in scimitar syndrome in infancy. Br Heart J.; 50(2):182–189
[33] Dickinson DF, Galloway RW, Massey R, Sankey R, Arnold R. Scimitar syndrome in infancy. Role of embolisation of systemic arterial supply to right lung. Br Heart J.; 47(5):468–472
[34] Kam JC, Pi J, Doraiswamy V, et al. CT scanning in the evaluation of pulmonary hypertension. Lung.; 191(4):321–326
[35] Chan AL, Juarez MM, Shelton DK, et al. Novel computed tomographic chest metrics to detect pulmonary hypertension. BMC Med Imaging.; 11:7
[36] Mahammedi A, Oshmyansky A, Hassoun PM, Thiemann DR, Siegelman SS. Pulmonary artery measurements in pulmonary hypertension: the role of computed tomography. J Thorac Imaging.; 28(2):96–103
[37] Revel MP, Faivre JB, Remy-Jardin M, Delannoy-Deken V, Duhamel A, Remy J. Pulmonary hypertension: ECG-gated 64-section CT angiographic evaluation of new functional parameters as diagnostic criteria. Radiology.; 250(2):558–566

7 Pulmonary and Systemic Veins

Farhood Saremi

◆ Introduction

Intrathoracic veins can be categorized into the systemic and pulmonary veins (PVs). The systemic veins return deoxygenated blood into the right atrium (RA) and the PVs forward the oxygenated lung blood into the left atrium (LA). Anatomical variation and congenital anomalies of these vessels are common. Knowing anatomy of these vessels is very important for correct recognition of the variants of these vessels which may have important clinical and surgical implications. Thrombosis of the brachiocephalic veins and occasionally superior vena cava (SVC) is seen after catheter insertion, a common intervention in many patients admitted to hospitals. Congenital abnormalities of the major mediastinal venous structures occur in less than 2% of people who have no other abnormalities. Although many congenital anomalies have been described, they occur with sufficient frequency without significant adverse clinical consequence: persistence of a left SVC with and without a coexisting right SVC, azygos or hemiazygos continuation of an interrupted inferior vena cava (IVC), and partial anomalous pulmonary venous return (PAPVR).

◆ Systemic Veins

The systemic veins of the thorax include the SVC and its tributaries and the azygos system. Only the suprahepatic portion of the IVC before its entrance into the RA is located within the thorax.

Superior Vena Cava

The SVC starts at the confluence of the right and left brachiocephalic veins. It travels 5 to 7 cm on the right anterior aspect of the upper mediastinum from the level of the first sternocostal junction to the superior cavoatrial junction. At the junction with the RA, the SVC is located posterolateral to the ascending aorta, anterior to the right pulmonary artery and anteromedial to the right superior PV (▶ Fig. 7.1). The right phrenic neurovascular bundle travels along the lateral wall of the SVC. The sinoatrial node (SA) artery encircles the SVC at the superior cavoatrial junction before entering the SA node region. The distal 2 cm of the SVC is intrapericardial and the azygos vein enters the SVC posteriorly above the pericardial reflection. Deoxygenated blood from upper extremity, head, neck, and azygos system enters the SVC. The SVC is the major conduit for passage of indwelling catheters, pacer leads, and transvenous interventional devices.

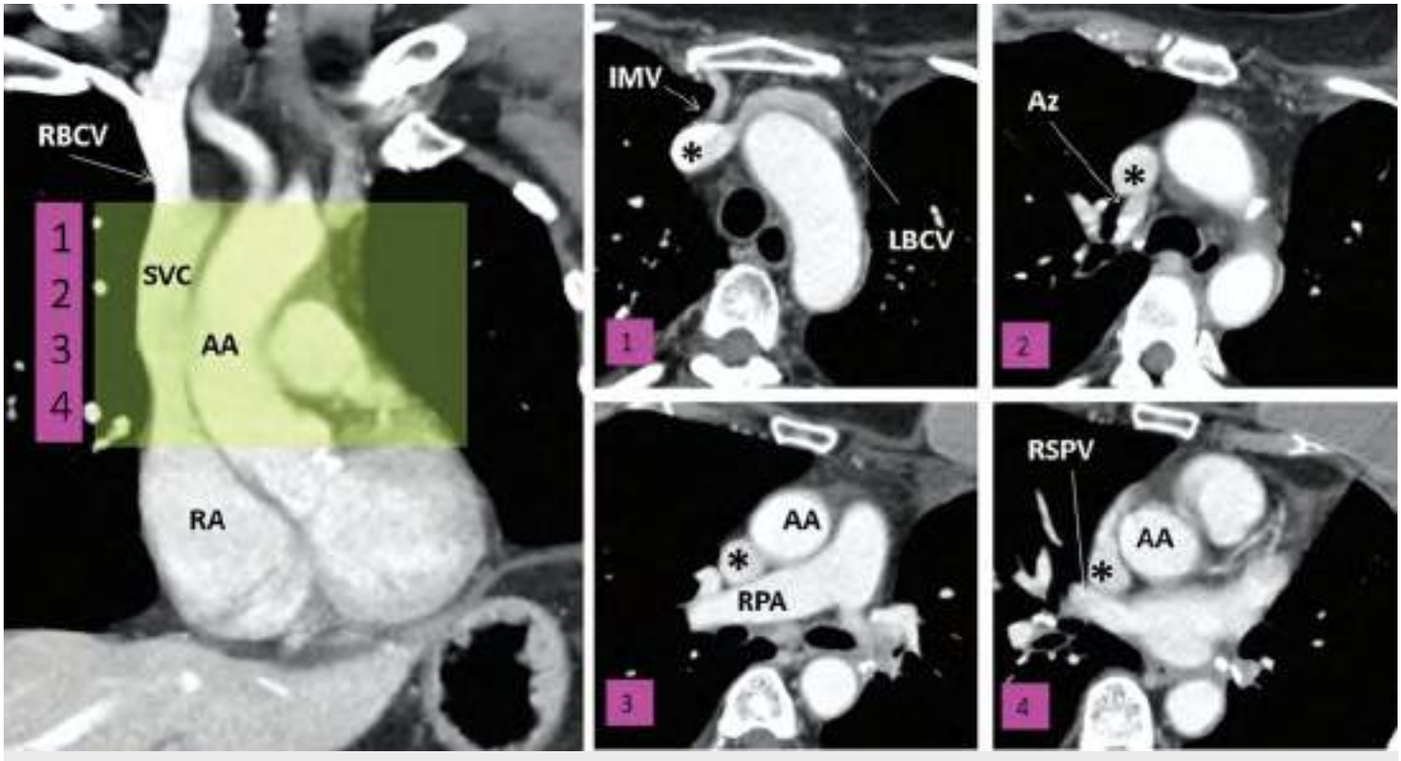

Fig. 7.1 Superior vena cava (SVC). CT images showing the relationship of the SVC with adjacent structures. The azygos vein (AZ) enters the SVC posteriorly above the pericardial reflection. At the junction with the right atrium (RA), the SVC (asterisks) is located posterolateral to the ascending aorta (AA), anterior to the right pulmonary artery (RPA), and anteromedial to the right superior pulmonary vein (RSPV). IMV, internal mammary vein; LBCV, left brachiocephalic vein; RBCV, right brachiocephalic vein.

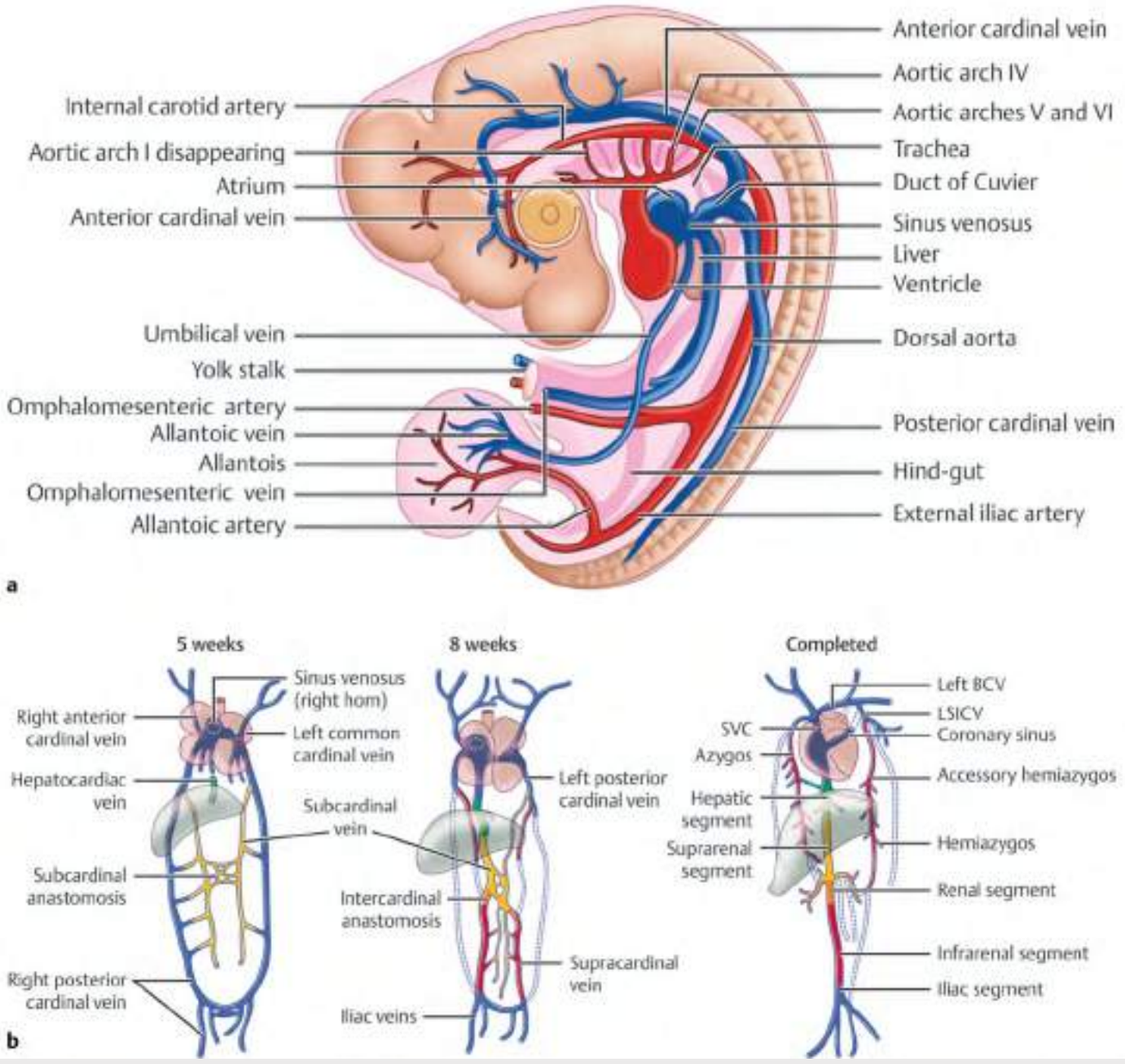

Fig. 7.2 **(a)** Three pairs of venous channels during the first 4 weeks of fetal development draining into the sinus venosus. (1) The omphalomesenteric (vitelline) veins, carrying blood from the yolk sac; (2) the umbilical vein, originating in the chorionic villi and carrying oxygenated blood from the placenta; and (3) the common cardinal veins (ducts of Cuvier), draining the body of the embryo.[1,2,3,4,5,6] **(b)** Development of the cardinal veins. Anterior views. BCV, brachiocephalic vein; LSICV, left superior intercostal vein; SVC, superior vena cava.

Embryology

The formation and anatomical variations of the systemic venous of the thorax are the result of complex pattern in persistence and regression of the segments of three pairs of venous channels during the first 4 weeks of fetal development: (1) the omphalomesenteric (vitelline) veins, carrying blood from the yolk sac; (2) the umbilical vein, originating in the chorionic villi and carrying oxygenated blood from the placenta; and (3) the common cardinal veins (ducts of Cuvier), draining the body of the embryo.[1,2,3,4,5,6] All these three venous channels drain into the sinus venosus (▶ Fig. 7.2**a**). The sinus venosus or systemic venous sinus, which connects to the right RA, is formed by myocardial differentiation of the mesenchyme that surrounds the common cardinal veins at the junction between the splanchnic and somatic mesoderm. Its opening into the RA is marked by the so-called "venous valves."

The right and left common cardinal veins are formed by the confluence of the anterior and posterior cardinal veins[1,2] (▶ Fig. 7.2). The anterior cardinal vein drains the cephalic portion of the embryo and the posterior cardinal vein drains the remainder of its body. The left cardinal vein and terminal segment of the left vitelline vein regress during embryogenesis. The right horn of the sinus venosus further develops and eventually forms the posterior wall of the RA. The right anterior and common cardinal veins persist and form the SVC. The left horn of the sinus venosus,

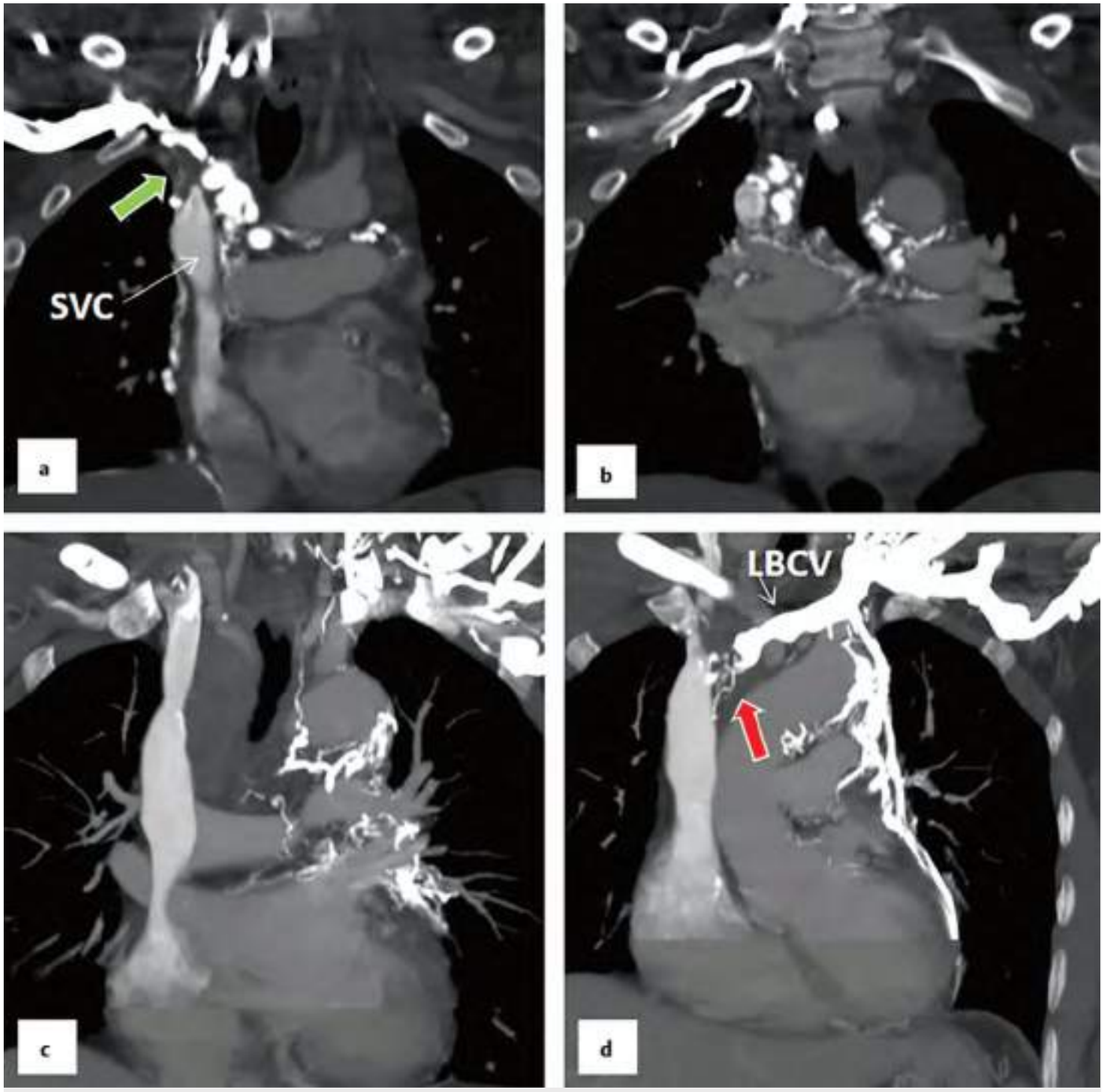

Fig. 7.3 (**a**, **b**) Coronal CT images showing obstruction (*green arrow*) of the superior vena cava (SVC) due to a small cell lung cancer. **(c**, **d)** Focal stenosis (*red arrow*) of the left brachiocephalic vein (LBCV). Both cases have developed extensive mediastinal collaterals.

in conjunction with the regressing left common cardinal vein, form the coronary sinus (CS) that opens into the RA and the left anterior cardinal venous system remains as the ligament or oblique vein of the LA (vein of Marshall) draining into the CS (▶ Fig. 7.2). A bridging venous plexus which was formed between the right and left anterior cardinal veins around 24-mm crown-rump embryonic stage develops to be the left brachiocephalic vein.[7] The left anterior cardinal vein below this connection gradually obliterates. Its upper portion remains as part of the left superior intercostal vein (SICV). The right sinus valve persists as the valve of the IVC (Eustachian valve) and the valve of the coronary sinus (Thebesian valve).[2] The right vitelline vein forms the hepatic segment of the IVC (hepatocardiac channel) (▶ Fig. 7.2). Various abnormal venous connections can occur if any of these processes fails to occur properly.

Pathologies

Obstruction of the SVC is usually secondary to tumor infiltrates or intrinsic thrombosis after long-term catheter insertion (▶ Fig. 7.3).

Isolated anomalies of the right SVC are rare.[8] Anomalous low insertion of the right SVC into the RA can be seen as an isolated anomaly. Congenital aneurysmal dilation of the SVC may be

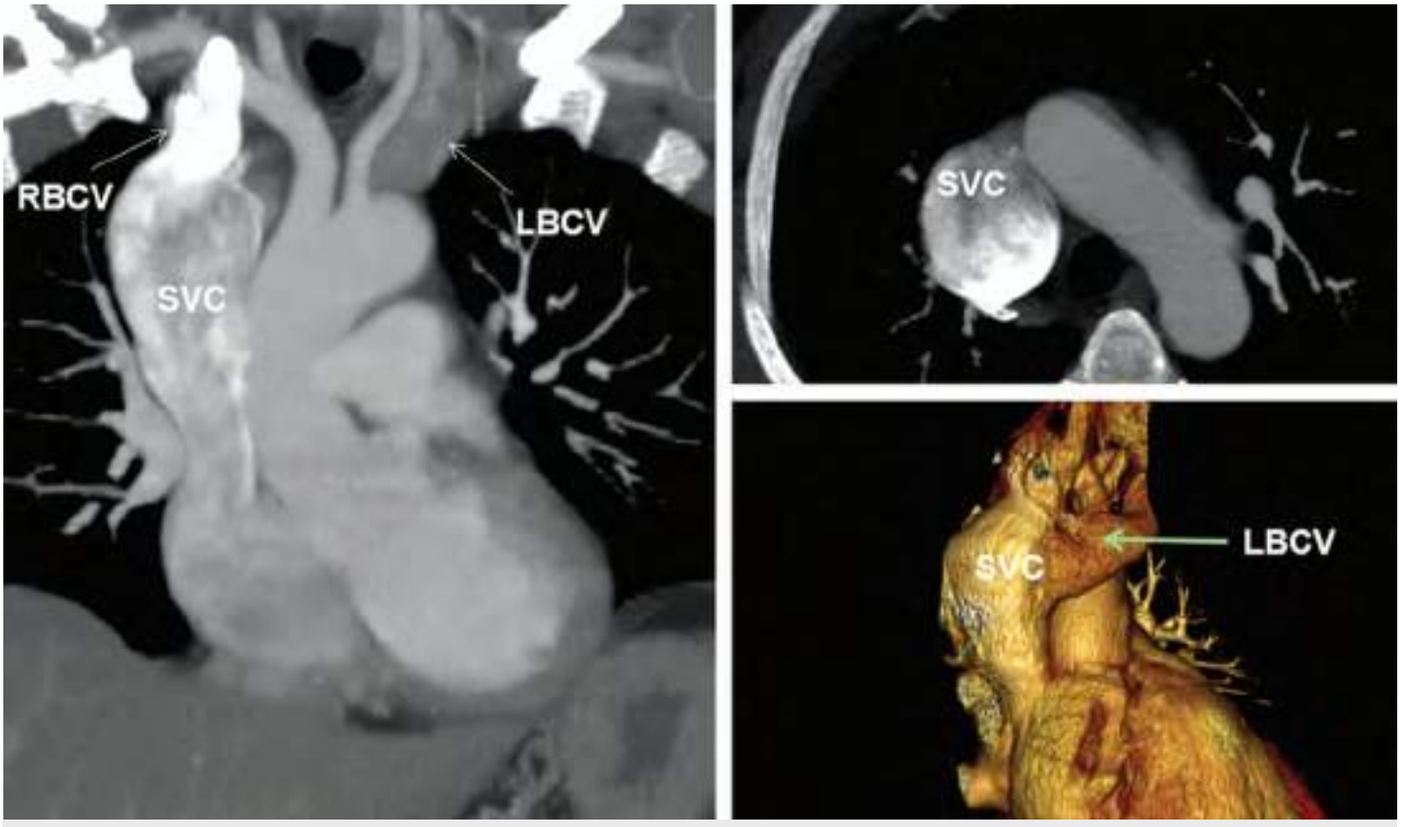

Fig. 7.4 Superior vena cava (SVC) aneurysm above the confluence with the azygos vein shown by CT. The azygos vein was normal sized. The left brachiocephalic vein (LBCV) is mildly enlarged. The patient referred to CT for possible mass seen on chest X-ray. RBCV, right brachiocephalic vein.

mistaken with a mass[9] (▶ Fig. 7.4). It may involve the SVC only or multiple veins in the upper mediastinum.

The left SVC is the most common anomalous systemic vein drainage in thorax, incidentally found in 1 out of 200 (0.5%) of computed tomography (CT) or magnetic resonance imaging (MRI) studies of chest (▶ Fig. 7.5). Prevalence is higher in patients with congenital heart malformation and may be seen in 5 to 10% of patients.[10,11] It results from failure of parts of the left anterior and common cardinal veins to regress. Isolated left SVC is less common than duplicated SVC (▶ Fig. 7.2). The left SVC drains the tributaries of the left subclavian and jugular veins into the coronary sinus via the oblique vein of the LA. The left SVC is closely sandwiched between the left superior PV and the left atrial appendage wall. This is a benign condition, but rarely the left SVC connects to the LA causing a right-to-left shunt.

◆ Brachiocephalic Veins

The brachiocephalic veins are formed by the confluence of the internal jugular and subclavian veins behind the sternoclavicular joint (▶ Fig. 7.1). The left brachiocephalic vein passes obliquely from left to right and the right brachiocephalic vein moves downward behind the manubrium. They unite to form the SVC. The left brachiocephalic vein is longer than the right; neither has a valve. The brachiocephalic veins receive the internal thoracic and inferior thyroid veins. The left brachiocephalic vein also receives the left SICV.

Anomalous brachiocephalic vein is uncommon, accounting for approximately 1% of congenital cardiovascular anomalies.[7,12] The cause of an anomalous brachiocephalic vein remains controversial and is related to abnormal regression of the anterior cardinal anastomosis. The presence of two or more (a plexus) transverse precardinal anastomoses is proposed to explain three patterns of anomalous brachiocephalic vein development: anomalous subaortic left brachiocephalic vein, persistent left SVC with a hypoplastic left brachiocephalic vein connecting to the right SVC, double SVC with agenesis of the left brachiocephalic vein,[7] and circumarctic left brachiocephalic vein (▶ Fig. 7.6). An anomalous subaortic left brachiocephalic vein is a benign anatomical variant. This vein, rather than joining the right brachiocephalic vein ventral to the aorta, crosses the midline dorsal to the ascending aorta to join the SVC caudal to the azygos vein (▶ Fig. 7.6). Recognition of the brachiocephalic vein anomalies is important to avoid misdiagnosis and prevent technical difficulty in a left arm approach for the insertion of a central venous catheter and cardiovascular intervention.

Stenosis or occlusion of the brachiocephalic vein is a common complication of long-term central venous catheter insertion (▶ Fig. 7.3).

◆ Left Superior Intercostal Vein

The residuals of an obliterated left anterior cardinal vein are seen as the oblique vein of the LA (Marshall) on the cardiac end and as a small vertical vein on the venous end between the left SICV and the left brachiocephalic vein[3,11] (▶ Fig. 7.7). The left SICV is a bridging vessel that links the posteriorly located azygos–hemiazygos systems with the anteriorly located left

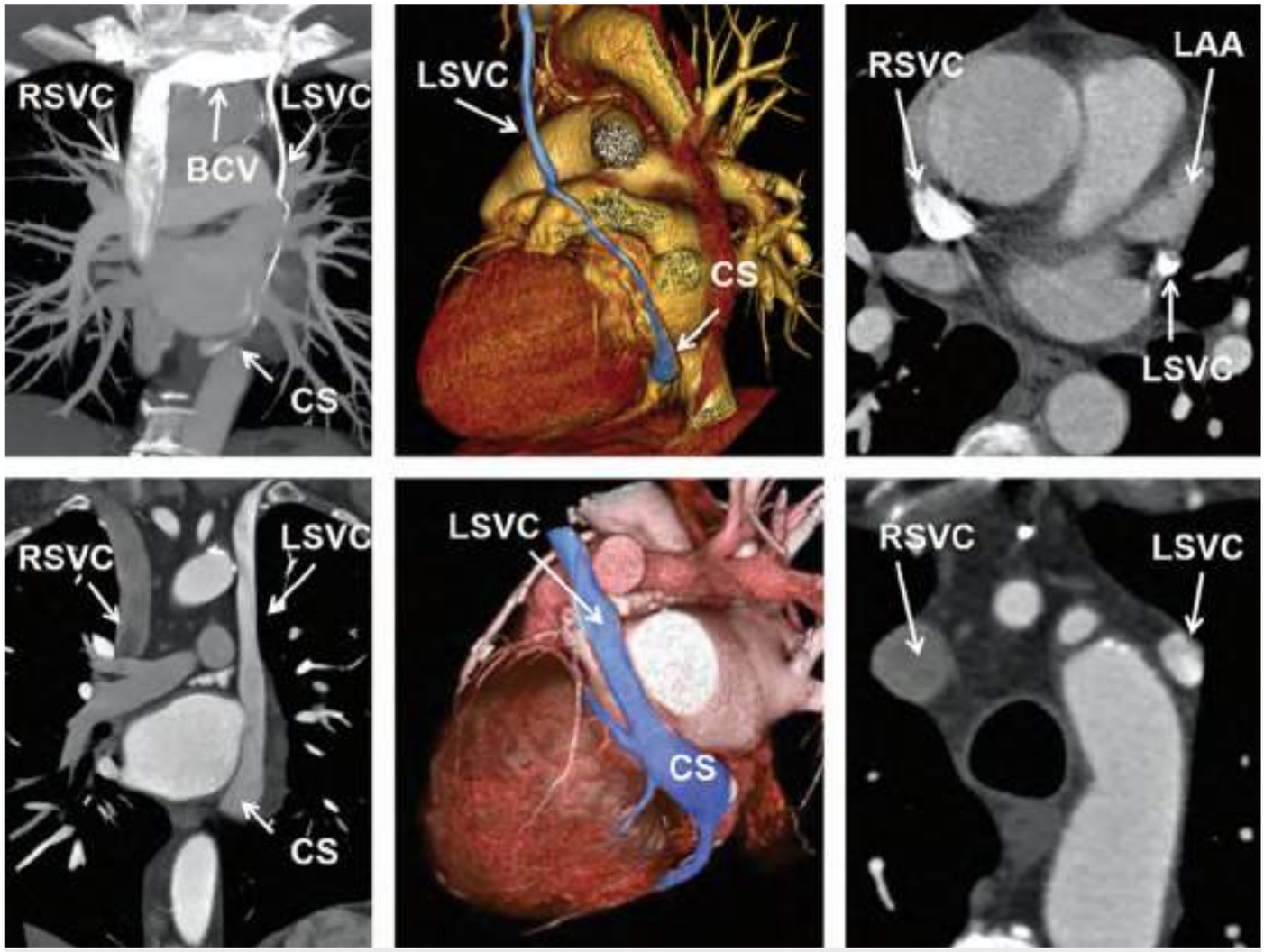

Fig. 7.5 Double superior vena cava (SVC) system with (upper row) and without (lower row) presence of a left brachiocephalic vein (BCV). Note the coronary sinus (CS) is generally larger in the absence of left brachiocephalic vein. The size of left SVC (LSVC) is variable in the presence of left brachiocephalic vein, but it is generally smaller than the right SVC (RSVC). LAA, left atrial appendage.

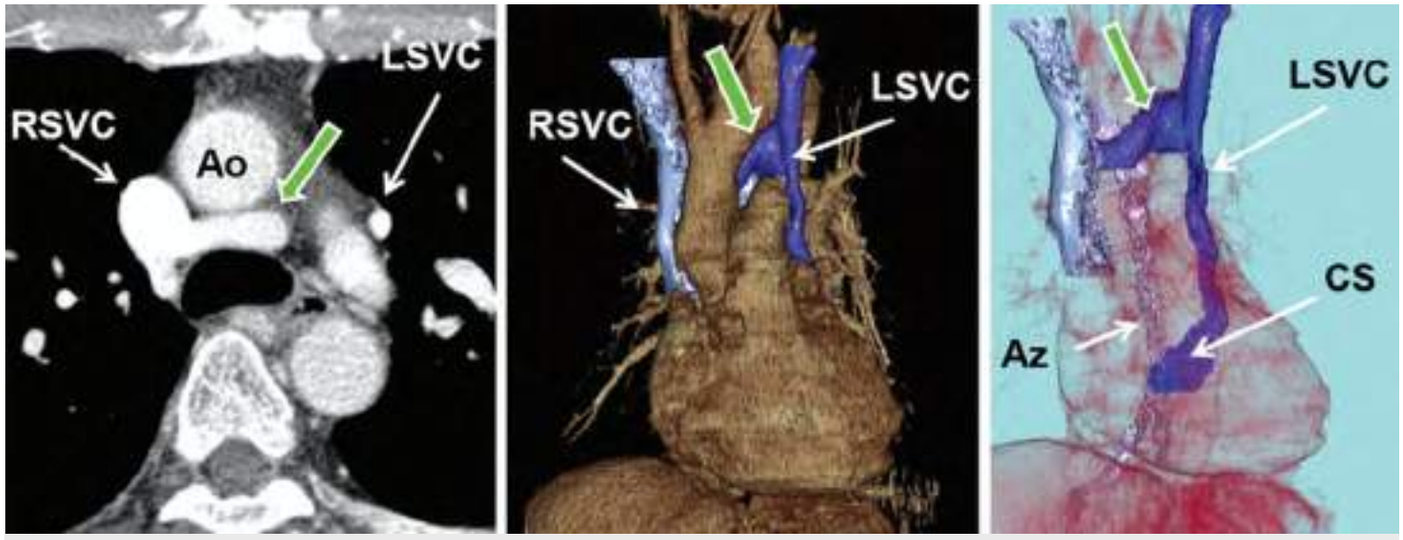

Fig. 7.6 Retroaortic left brachiocephalic vein (*green arrow*) with persistent left superior vena cava (LSVC). The azygos vein (Az) enters normally into the right SVC (RSVC). Ao, aorta; CS, coronary sinus.

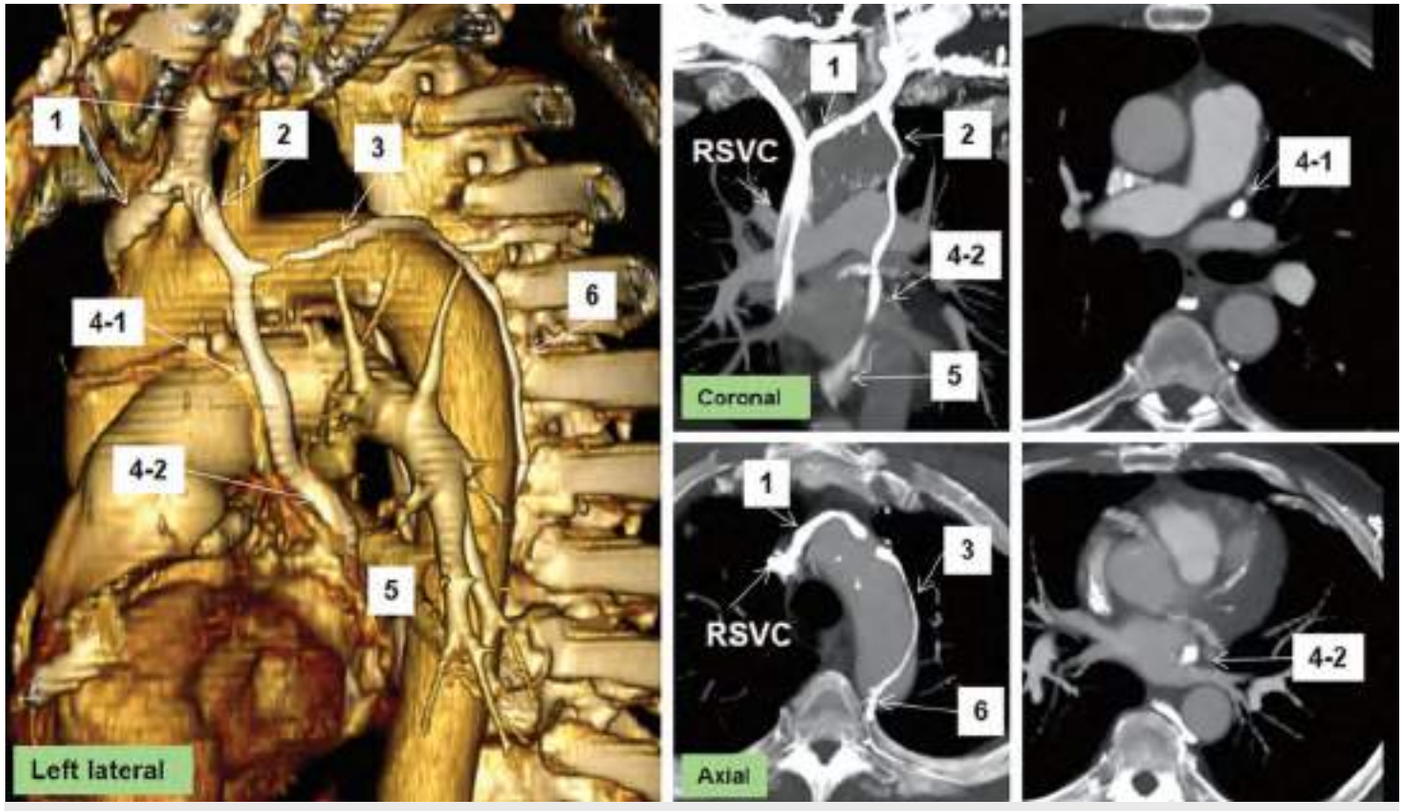

Fig. 7.7 Left superior intercostal vein (LSICV). The LSICV is a bridging vessel (#3) that links the posteriorly located azygos–hemiazygos systems (#6) with the anteriorly located left brachiocephalic vein (#1). It passes along the left margin of the aortic arch. As shown in this case, the LSICV may connect to a persistent left superior vena cava (#4) and from there to the coronary sinus (#5). #2, vertical vein (proximal part of the left SVC); RSVC, right superior vena cava.

brachiocephalic vein. The left SICV drains the second, third, and fourth posterior intercostal veins, then passes forward and upward along the aortic arch to drain into the left brachiocephalic vein near the venous angle. In two-thirds, the vein connects to the accessory hemiazygos vein which is recognizable in most CT angiographies[13,14] (▶ Fig. 7.8). The left SICV is described as "aortic nipple" in up to 10%[13] of chest radiographs. Obviously, in CT scans it can be seen more frequently (45%) along the lateral side of aortic arch. This bridging venous pathway has the potential of creating a right-to-left shunt when the SVC and left brachiocephalic vein are narrowed or obstructed. In these situations, venous connections develop between the mediastinal veins or tributaries of the left SICV on the systemic side and the superior PVs (rarely the LA) on the pulmonary side.[15]

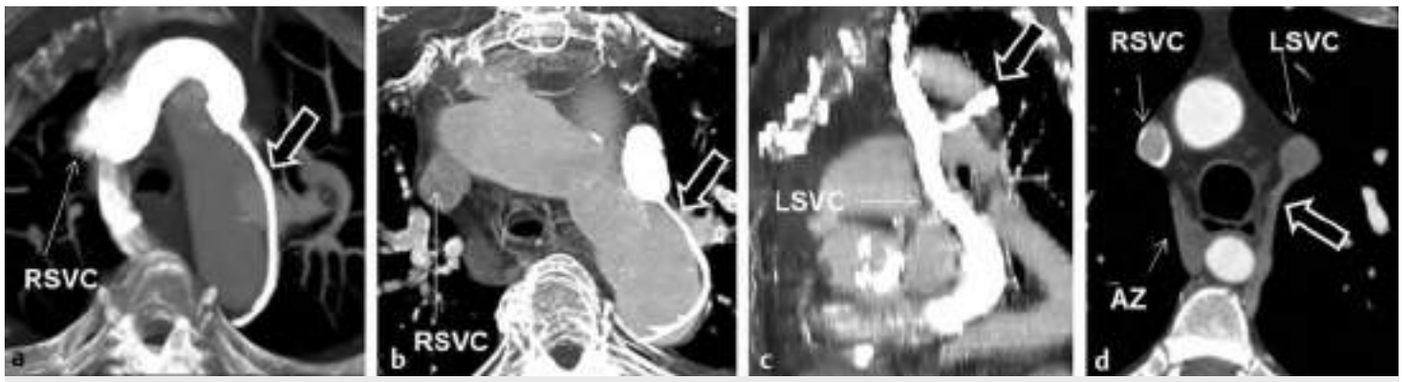

Fig. 7.8 Different connection patterns of left superior intercostal vein (LSICV) (*arrows*). **(a)** Normal with right SVC only. **(b)** Duplicated SVC and small LSICV. **(c)** Left SVC with a large LSICV. **(d)** Duplicated SVC with the LSICV entering the left and the azygos (AZ) entering the right SVC. LSVC, left superior vena cava; RSVC, right superior vena cava.

◆ Azygos System and Inferior Vena Cava

In the thorax, the azygos system receives blood from the posterior intercostal and mediastinal venous tributaries. The SICV drains the second through the fourth intercostal spaces. The right SICV communicates with the azygos knob (▶ Fig. 7.9). The left SICV drains into the left brachiocephalic vein along the lateral margin of the aortic arch and may connect to the accessory hemiazygos in 70 to 80% of cases. The azygos vein drains into the SVC just cephalad to the right main bronchus. In many cases, a valve exists at the confluence of the azygos vein with the SVC (▶ Fig. 7.9). The hemiazygos vein crosses midline at T8 to T9 level and behind the descending thoracic aorta to join the azygos vein (▶ Fig. 7.9). From this point, the accessory hemiazygos vein extends further cephalad in a left paravertebral position and communicate with the azygos and paravertebral veins at different levels.

Embryology

During the fourth to sixth weeks of embryological development, a pair of posterior cardinal veins drain all but the cephalic portion of the embryo.[11,16,17] Later at the sixth week, a second new pair of vein, the subcardinal veins, develop which become dominant at seventh weeks while most of the posterior cardinal veins gradually disappear (▶ Fig. 7.2). Important anastomoses develop between the right and left subcardinal veins anterior to the aorta. The right subcardinal vein further develops to the renal and suprarenal portions of the IVC which connect with the hepatic segment of the IVC (derived from the termination of the right omphalomesenteric vein). At the eighth week, the posterior cardinal veins will be replaced proximally by a third pair of veins, the supracardinal veins, which develop medial and dorsal to the posterior cardinal veins and later anastomose each other behind the aorta. The azygos vein derives mainly from the upper right supracardinal vein, but the azygos arch seems to originate from the remaining of the upper cranial segment of the right posterior cardinal vein. Similarly, upper left supracardinal vein turns into the hemiazygos vein and residual of the cranial segment of the left posterior cardinal vein may form the posterior portion of left SICV. The IVC development is complex and five embryological segments contribute to its composition. In caudal–cranial order, these segments include posterior cardinal veins (iliac segment); right supracardinal vein (infrarenal segment); anastomosis between the right supra- and subcardinal veins (renal segment); right subcardinal vein (suprarenal segment); and hepatocardiac canal (hepatic segment).

Variants and Pathologies

Dilation of the azygos system is a common finding in patients with obstruction of the SVC, acting as collateral pathway to direct blood into the LA. Azygos will also be dilated in cirrhosis due to abnormal portosystemic shunting (▶ Fig. 7.10).

Azygos and Hemiazygos Continuation of the IVC

Abnormal connection of the hepatic segment to the suprarenal segment of the IVC results in azygos or hemiazygos continuation of the venous system from abdomen into the thorax[16] (▶ Fig. 7.11). Therefore, although a large azygos or hemiazygos vein is the predominant finding in these venous anomalies, the primary anomaly is the IVC maldevelopment. These anomalies may be isolated or associated with other anomalies. It can be part of situs anomalies with left isomerism (polysplenia syndrome), in which the liver and stomach are located in midline, multiple spleens are found along the greater curvature of the stomach, and the minor fissure of the right lung is absent.[18] Azygos continuation is rare in patients with asplenia (right isomerism).

The imaging features of azygos continuation of the IVC include dilation of the azygos vein, azygos arch, and SVC caused by increased flow. The hepatic veins drain into the RA via the suprahepatic IVC (▶ Fig. 7.11). The hepatic segment of the IVC is absent or hypoplastic, and this condition must be documented to exclude other causes of an enlarged azygos vein. Hemiazygos continuation of a left-sided IVC is a rare anomaly in which a dilated hemiazygos vein drains into the azygos vein at T8 to T9. Alternatively, the hemiazygos vein continues cephalad to connect with the accessory hemiazygos vein and a left SVC, all of which are dilated.

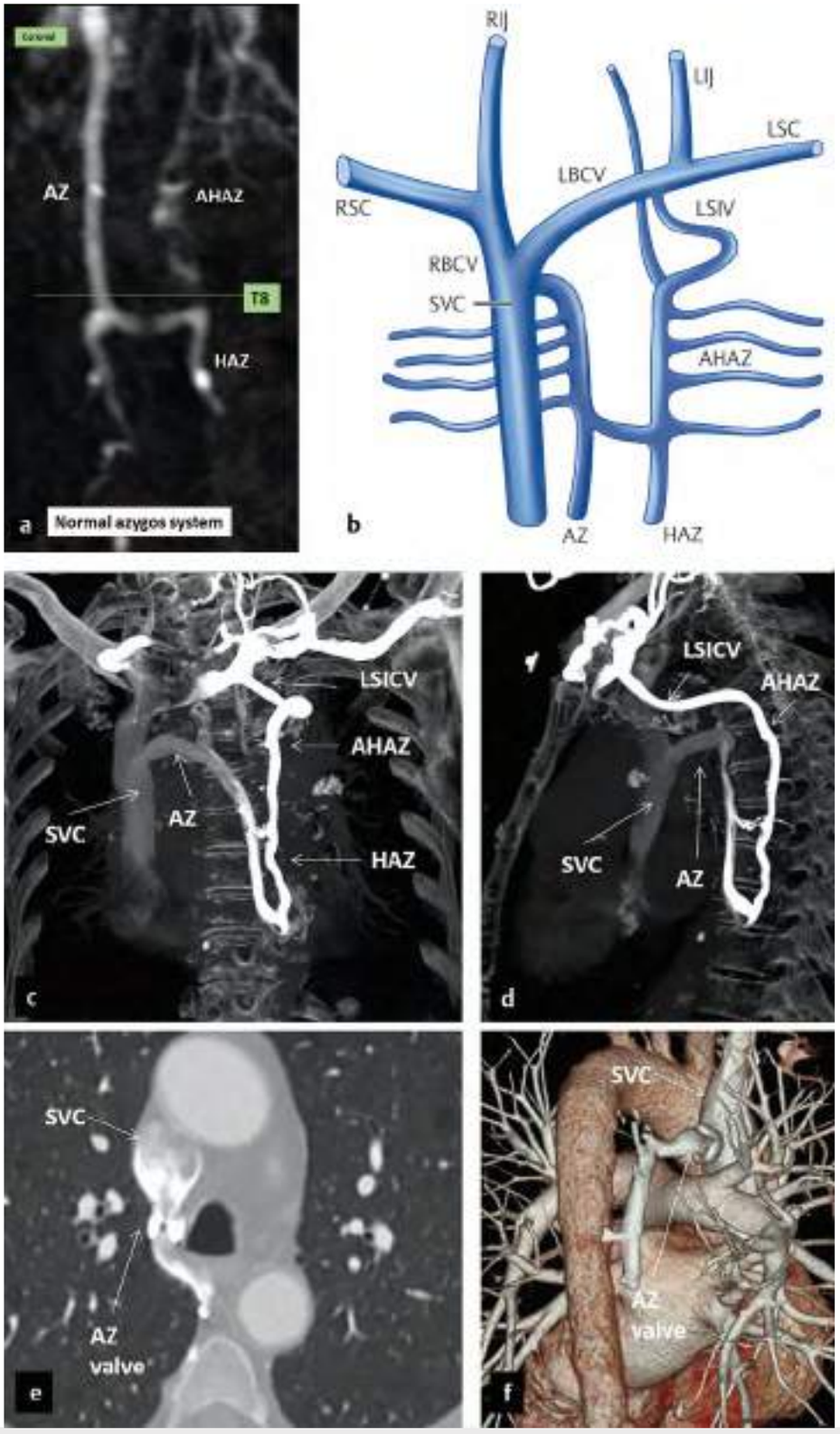

Fig. 7.9 **(a)** Normal azygos system is shown in MR angiography. The hemiazygos (HAZ) and accessory HAZ (AHAZ) connect each other approximately at T8 level and cross-link with the azygos (AZ) at the same level. **(b)** Schematic drawing of the normal venous drainage in the upper thorax. **(c)** Coronal and **(d)** sagittal left subclavian venograms showing filling of the azygos system through the left superior intercostal vein (LSICV). **(e)** Axial and **(f)** volume-rendered CT showing the azygos valve at the connection to the superior vena cava (SVC). AZ, azygos vein; AHAZ, accessory hemiazygos vein; HAZ, hemiazygos vein; LBCV, left brachiocephalic vein; LIJ, left internal jugular vein; LSC, left subclavian vein; RIJ, right internal jugular vein; RSC, right subclavian vein; SVC, superior vena cava.

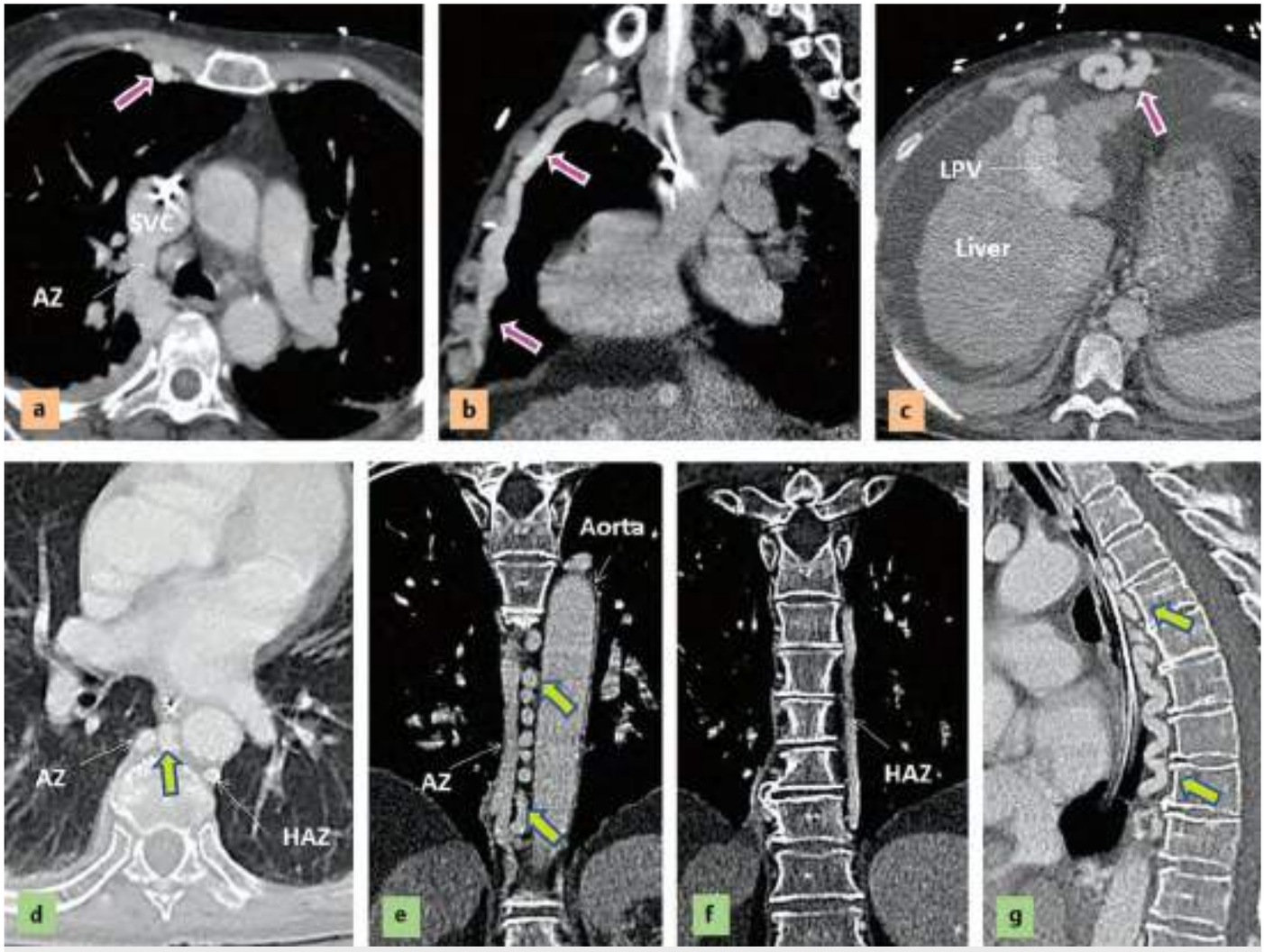

Fig. 7.10 (**a–c**) Portal hypertension causing enlarged internal mammary vein (*arrows*) bridging between the superior vena cava (SVC) and left portal vein (LPV) in a patient with severe cirrhosis. Azygos (AZ) vein is also enlarged. (**d–g**) Dilated azygos (AZ) and hemiazygos (HAZ), and a tortuous paraesophageal veins (*arrows*) in a patient with cirrhosis and portal hypertension.

Fig. 7.11 Azygos (AZ) continuation of inferior vena cava (IVC), an incidental finding in CT of the patient. The azygos (asterisks) is markedly enlarged and enters posterior aspect of the superior vena cava (SVC) The hemiazygos (HAZ) vein is diminutive. The intrahepatic segment of the IVC is absent, but the suprahepatic segment is present.

Other Variants or Anomalies of the Azygos Vein

Azygos lobe of the right lung apex occurs in 1% of population as a result of malposition of terminal part of the azygos vein.[19] It occurs when the right posterior cardinal vein, one of the precursors of the azygos vein, fails to migrate over the apex of the lung and penetrates it instead, carrying along pleural layers that entrap a portion of the right upper lobe. This is a benign anatomical variant and should not be mistaken with major anomalies. Left azygos lobe is rare and is caused by a malpositioned left SICV draining into the left brachiocephalic vein.[20]

In rare occasions, the azygos vein enters the right brachiocephalic vein, right subclavian vein, intrapericardial SVC, or RA. Total absence of the azygos vein, a very rare anomaly, arises when the cranial segment of the right supracardinal vein fails to develop.[21] It is usually asymptomatic. Normal drainage of the right and left intercostal veins by the hemiazygos and accessory hemiazygos veins will be compromised causing unusual enlargement of these veins.

◆ Pulmonary Veins

Anatomy

Normal PV anatomy consists of two right-sided and two left-sided veins with separate ostia (▶ Fig. 7.12). The pulmonary venous system carries oxygenated blood from capillaries toward the LA. The capillaries arise from the branching arterioles, which then form a network of vessels in the wall of alveoli (▶ Fig. 7.13). These capillaries have very thin walls, less than 0.1 µm thick, permitting gas exchange and oxygenation of blood. Arteriovenous shunting can occur normally near the terminal bronchioles that let passage of small particles less than 500 µm.[22]

The pulmonary venules run in the interlobular septa, between lung segments, in the visceral pleura, and along the interlobar fissures (▶ Fig. 7.13). Segmental tributaries coalesce to form lobar veins.

The anatomy and size of the LA and PVs are commonly variable. The superior PVs typically drain the upper and middle lung lobes, whereas the inferior PVs originate from the lower lobes (▶ Fig. 7.14). The right superior PV has a vertical course, initially passing along the lateral side of the SVC and anterior to the right pulmonary artery and then behind the superior cavoatrial junction and inferior to the right pulmonary artery before entering the LA. In contrast, the left superior PV has a more horizontal course superior and then anterior to the left mainstem bronchus and inferior to the main pulmonary artery before connecting to the LA. The inferior PV courses horizontally in the lower hemithorax. The left inferior PV passes anterior to the descending aorta and medial to the left lower lobe bronchus before reaching the LA. Its ostium may lie anterior to the esophagus.

Embryology

The primary heart tube is formed from fusion of vitelline veins which differentiate into myocardium (▶ Fig. 7.15). The vitelline veins also fuse to form the portal vein. Later, development of other systemic venous systems including the cardinal and the umbilical venous systems occurs. Together with the umbilical veins, the portal vein contributes to the hepatic vascular bed. The PVs are the fourth venous system that becomes connected to the

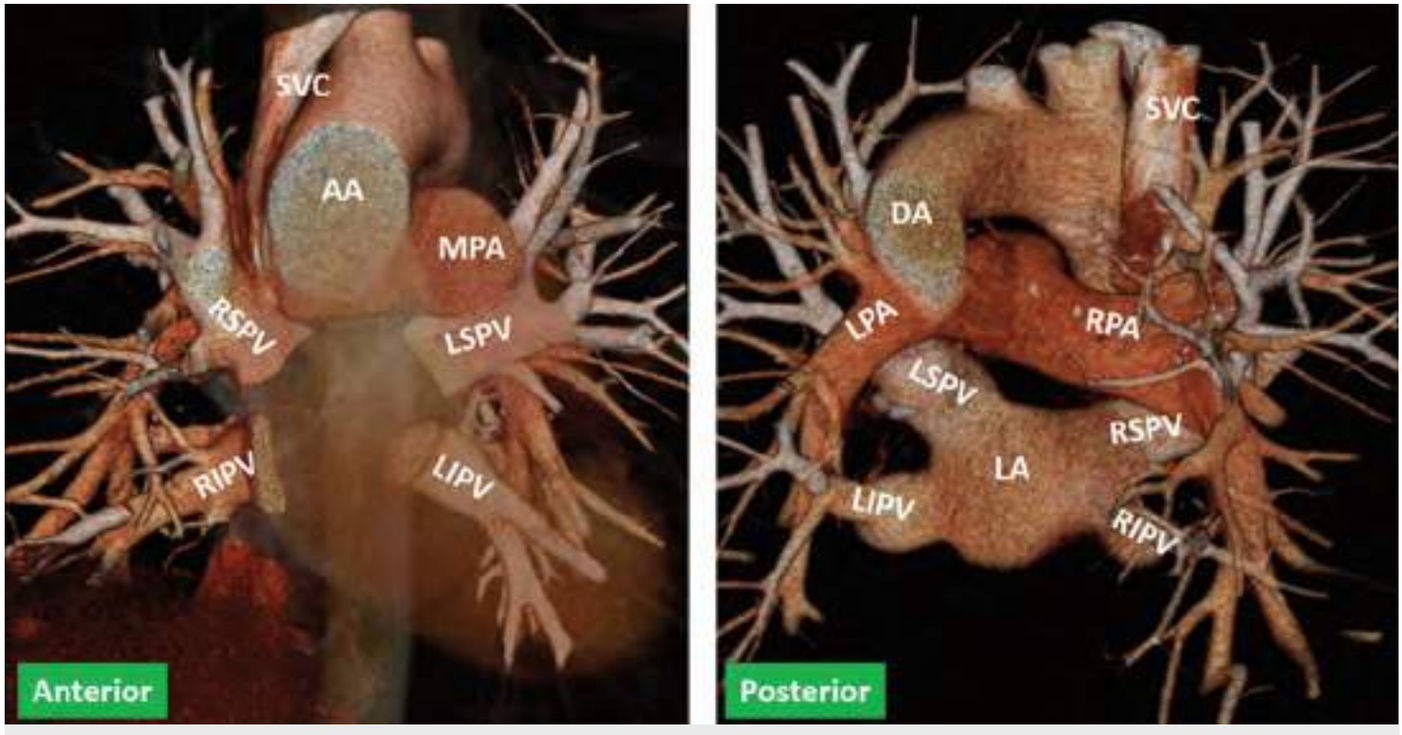

Fig. 7.12 Normal arrangement of the pulmonary veins. AA, ascending aorta; DA, descending aorta; LA, left atrium; LIPV, left inferior pulmonary vein; LPA, left pulmonary artery; LSPV, left superior pulmonary vein; RIPV, right inferior pulmonary vein, RPA, right pulmonary artery; RSPV, right superior pulmonary vein; SVC, superior vena cava.

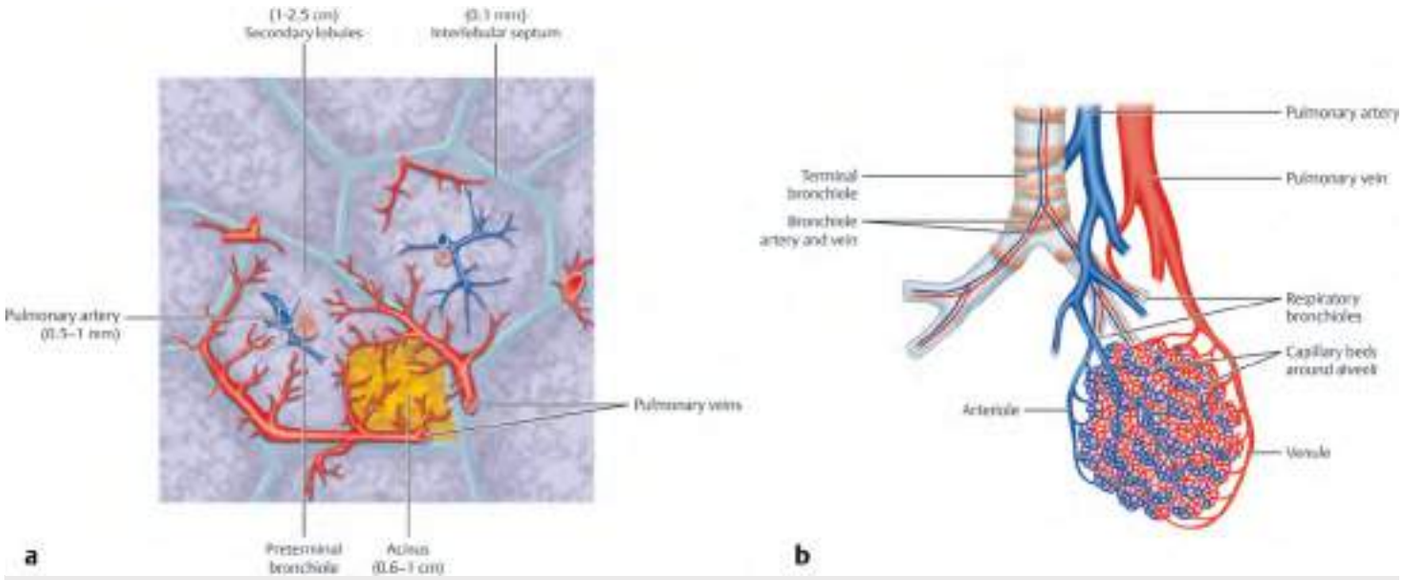

Fig. 7.13 (a, b) Pulmonary microvasculature and their relationship with the pulmonary lobules. The pulmonary venules run in the interlobular septa. Bronchial circulation contributes to the pulmonary microvasculature by supplying blood to the bronchovascular bundles, pulmonary interstitium, and the vasa vasorum of the pulmonary arteries and veins.

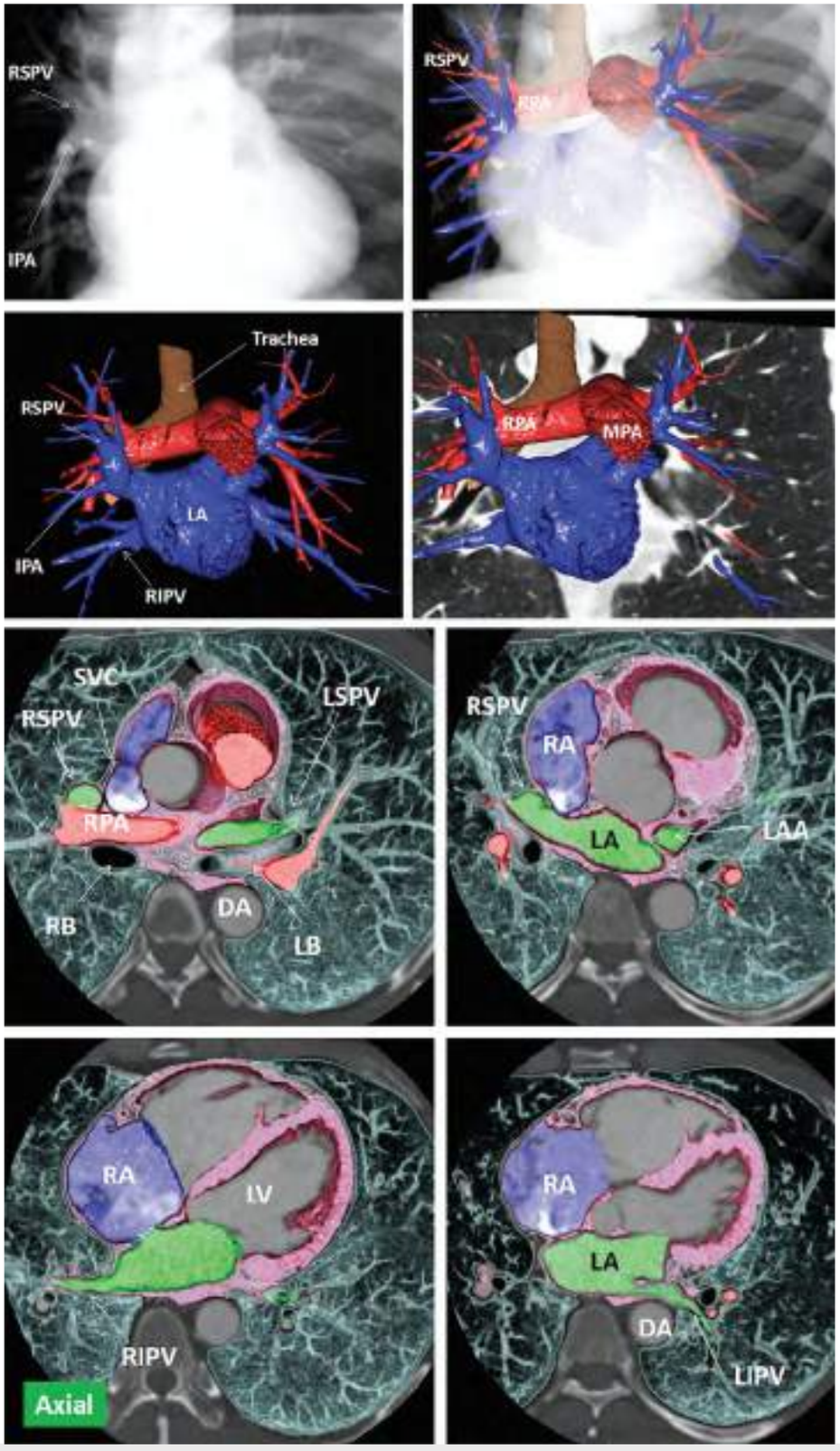

Fig. 7.14 Arrangement of the central pulmonary veins in the thorax shown by frontal, axial, sagittal, and coronal series. Central pulmonary veins (shown in green) arrangement in the thorax. The right superior pulmonary vein (RSPV) has a vertical course, initially passing along the lateral side of the superior vena cava (SVC) and anterior to the right pulmonary artery (RPA) and then behind the superior cavoatrial junction and inferior to the right pulmonary artery before entering the left atrium (LA). The RSPV forms the superior margin of the right hilar angle (best shown on plain radiograph). The inferior margin of the hilar angle is formed by the interlobar pulmonary artery (IPA). The left superior PV (LSPV) has a more horizontal course superior and then anterior to the left main stem bronchus (LB) and inferior to the main pulmonary artery (MPA) before connecting to the LA. The inferior PV courses horizontally in the lower hemithorax. The left inferior PV (LIPV) passes anterior to the descending aorta (DA) and medial to the left lower lobe bronchus before reaching the LA. Its ostium may pass anterior to the esophagus. LAA, left atrial appendage; LV, left ventricle; LPA, left pulmonary artery; RB, right bronchus; RA, right atrium; RV, right ventricle.

(*Continued*)

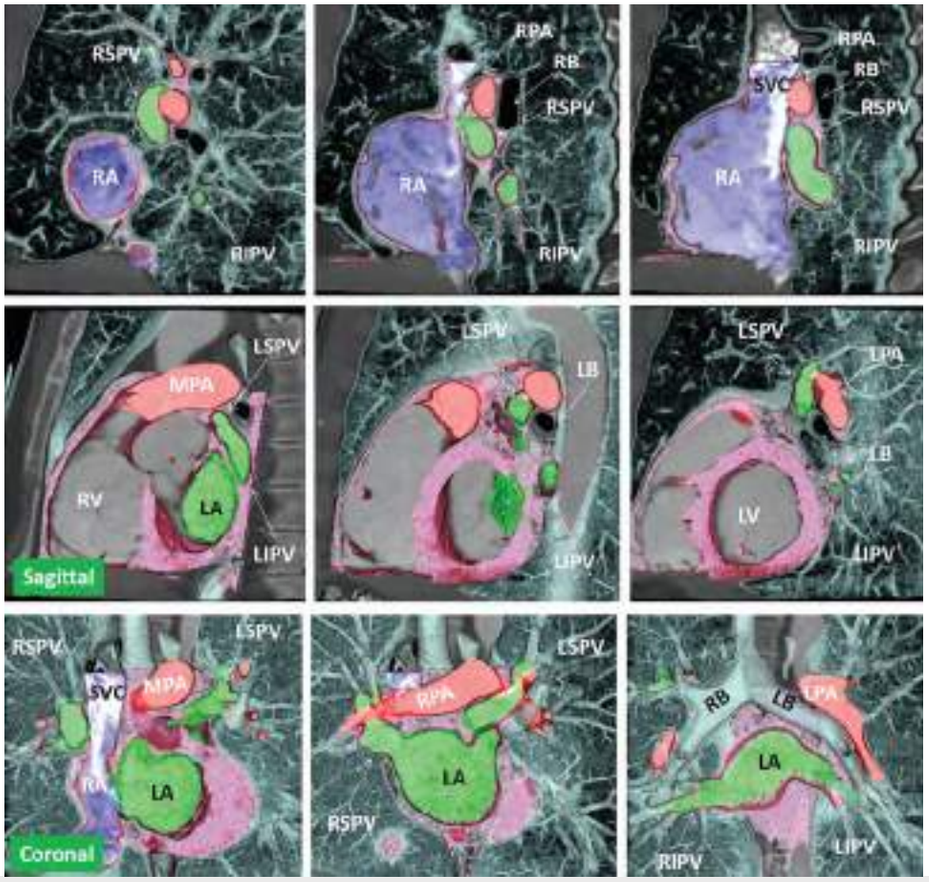

Fig. 7.14 (*continued*)

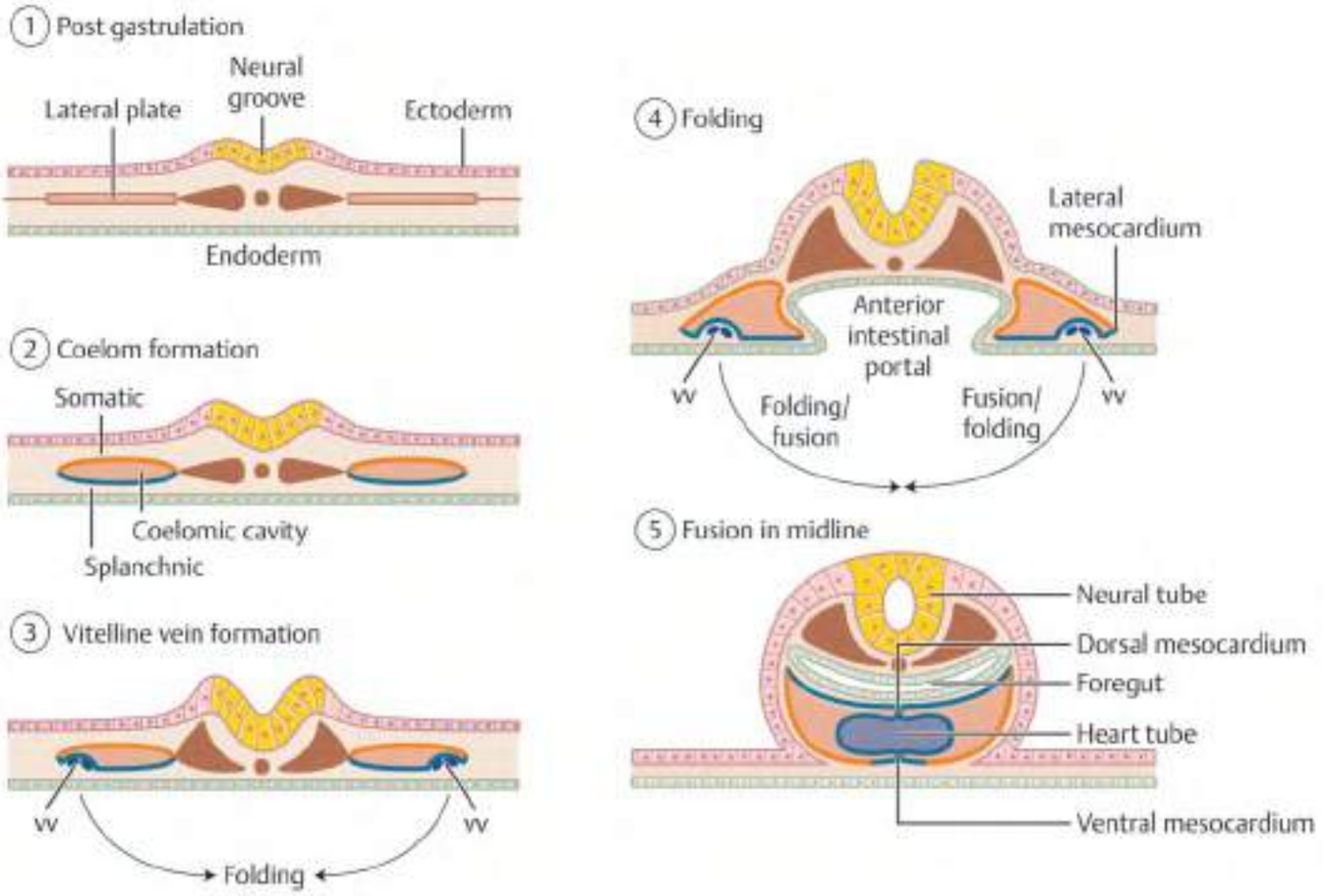

Fig. 7.15 Development of the heart tube. After gastrulation, the embryo can be represented as a trilaminar disk made up of endoderm, mesoderm, and ectoderm. The heart tube and its venous tributaries are derivatives of the mesoderm. With formation of the coelomic cavity, lateral plate mesoderm separates into splanchnic and somatic mesoderm layers, which line the endoderm and the ectoderm, respectively. The lateral edges of the splanchnic mesoderm gradually lumenize to form the vitelline veins. Besides playing an important role in separating the embryonic coelomic cavity, these lateral mesocardial connections also envelop the forming common cardinal veins. Fusion of the bilateral vitelline veins generates the primary heart tube. The point of fusion is recognized as the ventral mesocardium. The medial splanchnic mesoderm becomes the pericardial back wall, which is connected to the heart tube via the dorsal mesocardium. The dorsal mesocardium connects the heart to the splanchnic mesoderm that overlies the embryonic pharynx. This mesocardium is the only site through which vessels (i.e., pulmonary vein) or additional tissue can dorsally enter the heart. (Used with permission from van den Berg et al 2011.[23])

primary heart. In contrast to the SVC and coronary sinus which arise from the sinus venosus, the PV does not originate from the primary myocardium surrounding the orifices of the systemic venous tributaries. It derives from the splanchnic mesoderm that overlies the foregut and their development is closely related to the development of the lung buds[5] (▶ Fig. 7.16. During the first 2 months in utero, the lung buds develop from the foregut. Blood returning from the lung buds initially drains into the splanchnic plexus. The splanchnic venous plexus which extends from the heart to the liver communicates with the paired cardinal veins as well as the umbilicovitelline veins. Within the mediastinal splanchnic mesoderm, a midpharyngeal strand vascular plexus canalizes to form the primitive PV. This primitive common PV connects the lung venous network to the LA close to the atrioventricular junction where the primary dorsal mesocardium was connected.[23,24] Later, the pulmonary venous connections to the cardinal and umbilicovitelline veins disappear.[24] Along with growth of the primary atrial septum on the right side of the pulmonary venous orifice, final location of the PV orifice is determined within the morphologically LA. Four pulmonary venous tributaries of the primitive PV subsequently develop and assimilate into the LA.

Various abnormal systemic or pulmonary venous connections develop if any of these processes fails to occur properly.[25] If the common PV fails to properly incorporate into the posterior left atrial wall, PV stenosis/atresia or cor triatriatum will occur.[24] Anomalous PV return is total if the entire PV return is directed to the RA and partial if only a portion of the PV circulation is affected. The proportion of anomalous PV return influences the extent of physiological blood flow compromise and the age of presentation. In general, the sites of anomalous connections are divided into (1) direct right atrial wall; (2) the derivatives of the right common cardinal systems including the SVC and azygos vein; (3) the derivatives of the left common cardinal system, specifically the coronary sinus; and (4) the derivatives of the umbilicovitelline system such the portal vein.[23] Abnormal opening of the right superior PV at right superior cavoatrial junction results in a sinus venosus type of atrial septal defect (ASD).

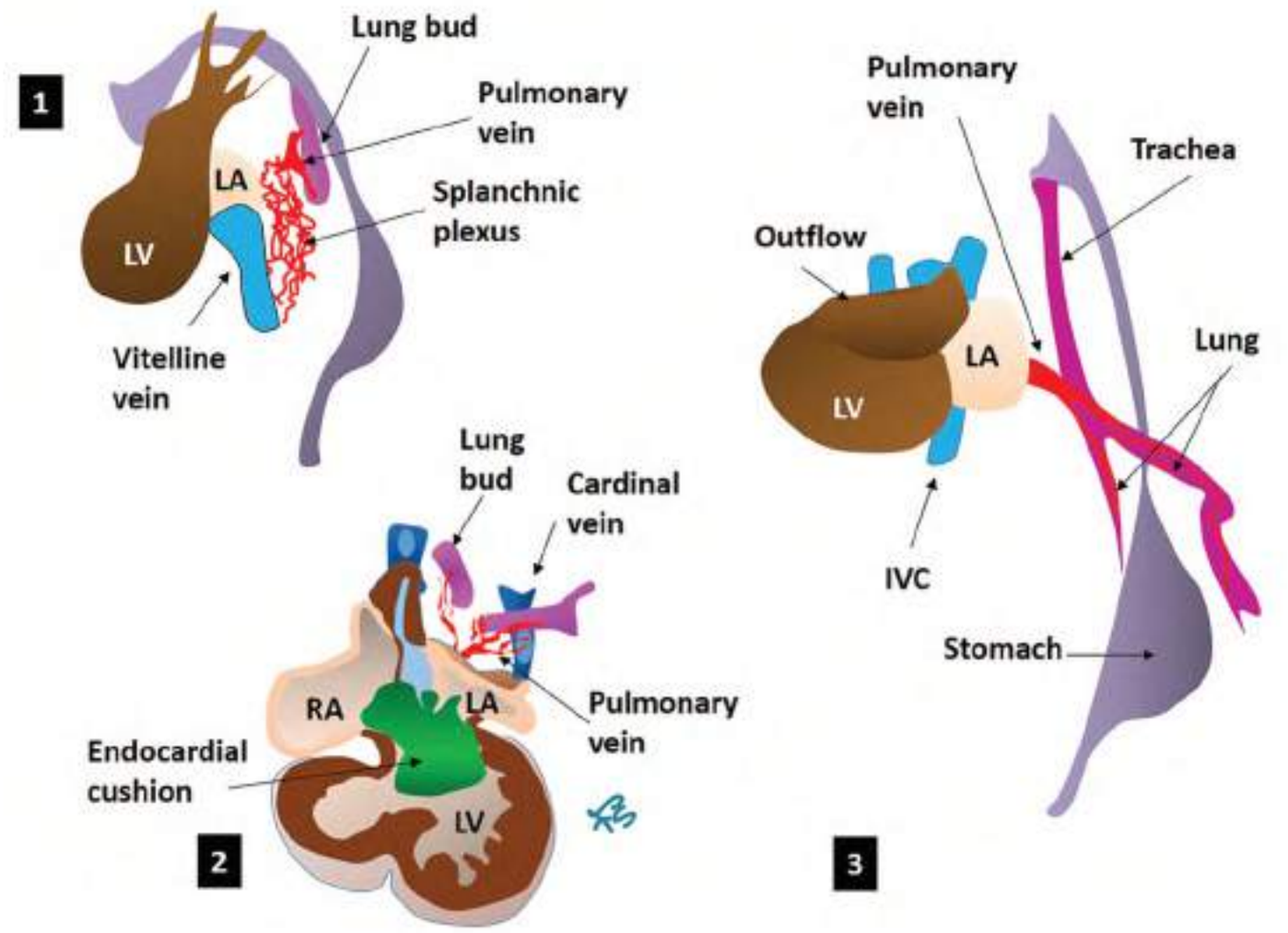

Fig. 7.16 Development of the pulmonary vein. The pulmonary vein develops from the vascular plexus in the splanchnic mesoderm and enters the dorsal heart tube (left atrium) through the dorsal mesocardium. (2) Lateral view and (3) long axis cut of the heart region of stage 16 embryo. Blood returning from the lung buds initially drains into the splanchnic plexus. The splanchnic venous plexus which extends from the heart to the liver communicates with the paired cardinal veins as well as the umbilicovitelline veins. The primitive pulmonary vein is formed within the mediastinal splanchnic mesoderm and later connects to the left atrium (#3). (4) Later, the pulmonary venous connections to the cardinal and umbilicovitelline veins disappear. Four pulmonary venous tributaries of the primitive pulmonary vein subsequently develop and assimilate into the left atrium (LA). IVC, inferior vena cava; LV, left ventricle; RA, right atrium.

Ostial Pulmonary Vein

The significance of the ostial PVs is in connection with higher rate of arrhythmogenic trigger foci in this region causing atrial fibrillation (AF). These foci have been successfully treated using catheter ablation techniques. In 70 to 80%, four PV ostia exist; a superior–inferior ostium on the right and a superior–inferior ostium on the left.[26,27] Conjoined (common) PV is seen 25 to 30% of individuals and it is more common on the left side (▶ Fig. 7.17). Supernumerary veins are also frequently seen. In 12 to 25% the vein of the middle lobe drains directly into the right wall of LA with a cross-sectional diameter of less than 8 mm.[27,28] In the remainder the middle lobe PV drains into the right superior PV or less commonly the right inferior PV. It is not uncommon to find a supernumerary PV draining the posterior segment of the right upper lobe or superior segment of right lower lobe. This vein usually connects to the right superior aspect of the LA (▶ Fig. 7.18). Absence of one PV requires careful examination of all intrathoracic venous system as it can be associated with partial anomalous venous return.

The PV ostia are ellipsoid with a longer superior–inferior dimension. The superior PV ostia are usually larger than the inferior PV ostia. The diameter, cross-sectional area, and shape of the distal PVs before confluence with the LA as shown by cadaveric and in vivo CT or MR examinations vary. In postmortem studies, the diameter of the PVs ranges from 5 to 30 mm with mean diameter of the superior PVs around 18 mm and for the inferior PVs around 16.5 mm. Similar measurements have been obtained with CT scan.[27] The caliber of the PVs gradually increased as they approached the LA. On the other hand, the distal left inferior PV caliber may decrease as entering the LA very close to the descending aorta, as a result it may show a focal narrowing that should not be mistaken for stenosis (▶ Fig. 7.17). Medial insertion of left inferior PV near posterior midline is occasionally seen (▶ Fig. 7.17). The length of PVs prior to bifurcation ranges from 10 to 54 mm and the thickness of the PV wall in this region

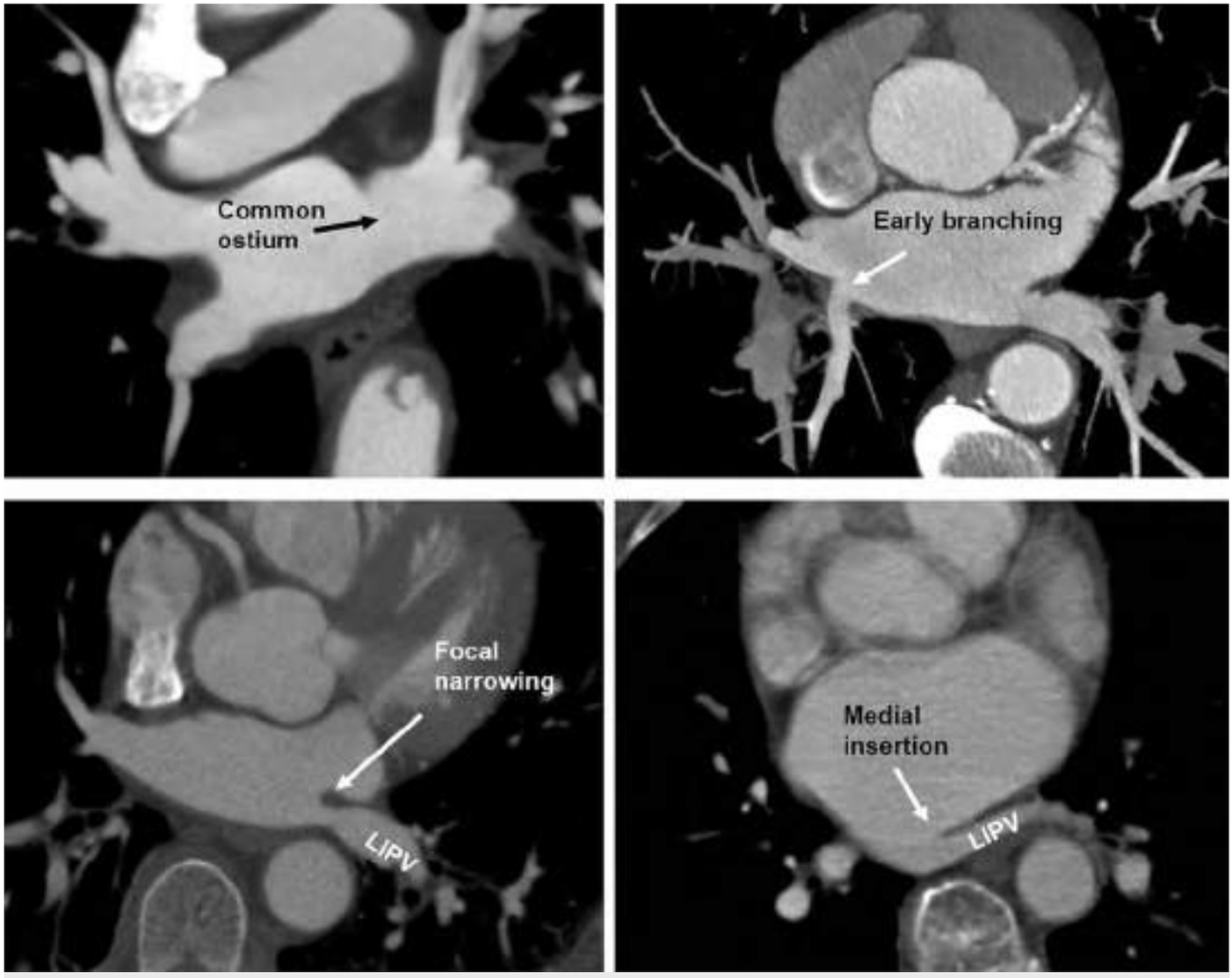

Fig. 7.17 Anatomical variants of the pulmonary vein (PV) insertion. Conjoined (common) PV is seen 25 to 30% of individuals and it is more common on left side. Medial insertion of the left inferior pulmonary vein (LIPV) is relatively uncommon and may cause difficulty in circumferential PV isolation. It is not uncommon to see mild narrowing of the LIPV at its confluence with the left atrium. This is most likely secondary to the compressive effect of the pulsating aorta and should not be mistaken for stenosis. Early branching is also common and usually is seen with right upper lobe pulmonary vein entering near the confluence of right superior PV with the left atrium.

measures 0.3 to 0.8 mm.[26] Mean distance to first bifurcation as measured by CT include right superior 14.5 mm; left superior 17.5 mm; right inferior 7 mm; left inferior 13.5 mm; and independent middle lobe 8.5 mm.[27] For ablation purposes, any measurement of the PVs should take place in the same phase of the cardiac cycle during the follow-up studies of patients. Generally, the PV ostia enlarge at the end of ventricular systole compared with end of ventricular diastole, by the factors of 1.25 to 1.5.[29]

Structure of the Pulmonary Vein Ostia

Although different mechanisms of AF exist, it is well established that the myocardial sleeve of the PVs is an underlying source of triggers that initiates AF.[30,31] AF is the most common sustained cardiac arrhythmia that is characterized by uncoordinated contraction of the atrium. It can be treated by radiofrequency (RF) catheter ablation designed to electrically isolate initiating foci within the PVs from the LA. Because of the clinical importance of the PVs in the initiation of chronic and paroxysmal AF and the increasingly widespread application of catheter ablation techniques in these veins as a treatment for AF, over past decade, investigators initiated a widespread effort to explain the relationship of the AF with the structural elements in the wall of the PV ostium. Their findings demonstrated that the left atrial myocardium extends for variable distances into the PVs in more than 90% of individuals especially in the superior left PV, which in some clinical series has been found to be the most frequent site of focal triggers. Investigations have also shown variable amount of fibrosis, scarring, and amyloid deposition within the myocardial ostium of the PVs especially in the elderly and patients with paroxysmal AF[32,33] (▶ Fig. 7.19).

Histological examinations have shown that the smooth muscle of the pulmonary venous ostial wall is separated by a thin plane of fibrofatty tissue from an outer layer of myocardial bundles (▶ Fig. 7.19). This intermediate myocardial layer, between the adventitia and the venous media, is the myocardial continuity

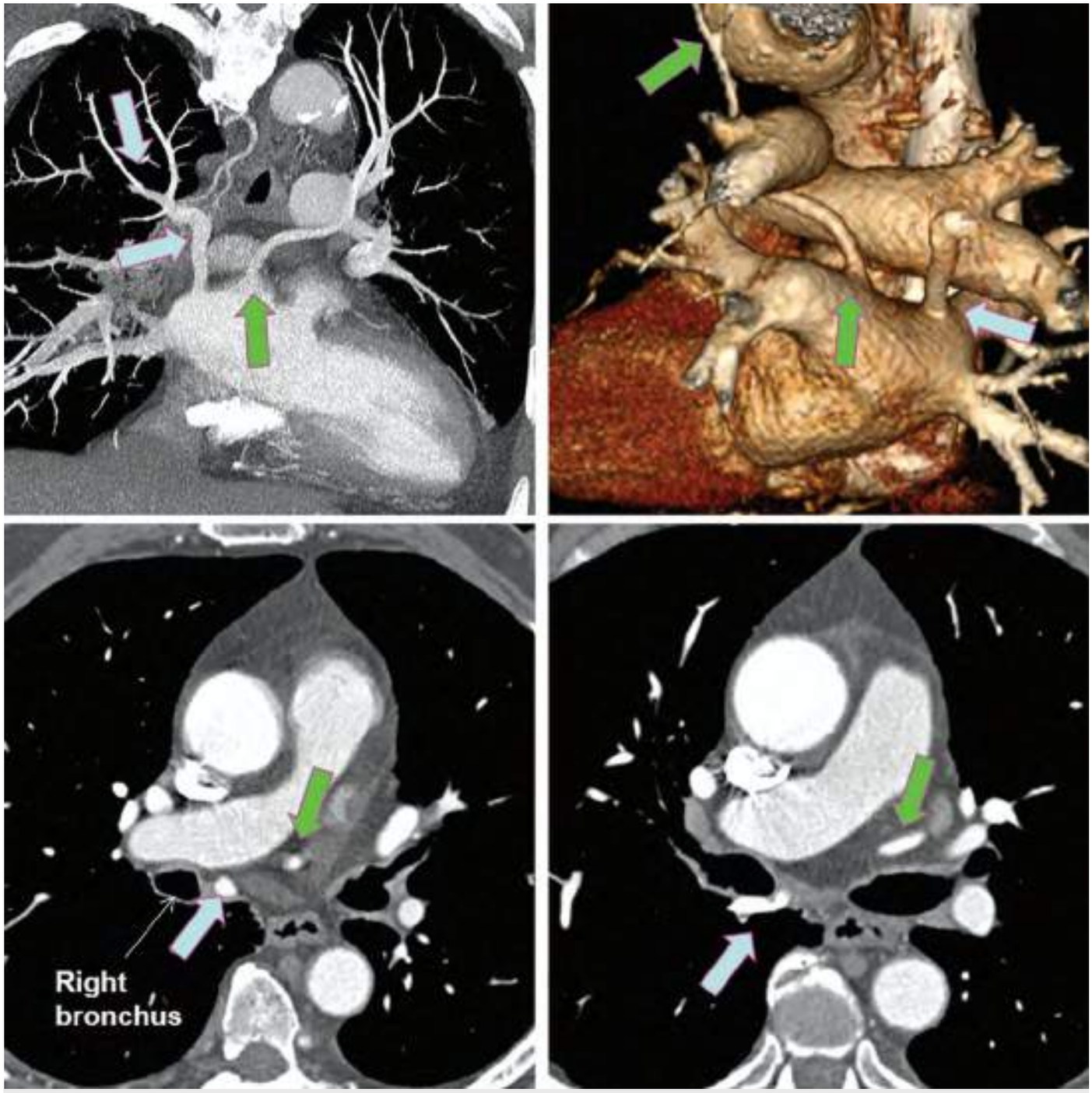

Fig. 7.18 Supernumerary pulmonary vein. A rare example showing two supernumerary veins. The right one draining the superior right upper lobe (*blue arrows*) and the left one (*green arrows*) draining the superior left upper lobe. Right-sided supernumerary vein is more common. As seen in this example, it passes behind the right mainstem bronchus, draining the posterior segment of the right upper lobe or superior segment of right lower lobe. These veins usually connect to the superior aspect of the left atrium.

from the left atrial wall known as "myocardial sleeves."[34,35] Therefore, myocardial sleeve lies external to the venous wall and within the epicardium/adventitia (▶ Fig. 7.18). The thickness of the myocardial sleeve ranges from 1.2 to 2.8 mm and covers up to 1 cm of the PV ostium. The inferior veins tend to have less myocardial coverage than the superior veins.[36] The thickest sleeve is in the left superior vein. The orientation of these myocardial fibers within human PVs is complex and composed of spiral, longitudinal, and transverse fibers.[34] It is also shown that myocardial fibers cross the angle (carina) between the superior and inferior venous orifices especially on the left side.[35] This venous angle muscle appears particularly important in the development of AF. Most triggers for initiating AF appear to originate from PV carina[37] and many suggest circumferential ablation of both vessels to achieve complete PV electrical disconnection.

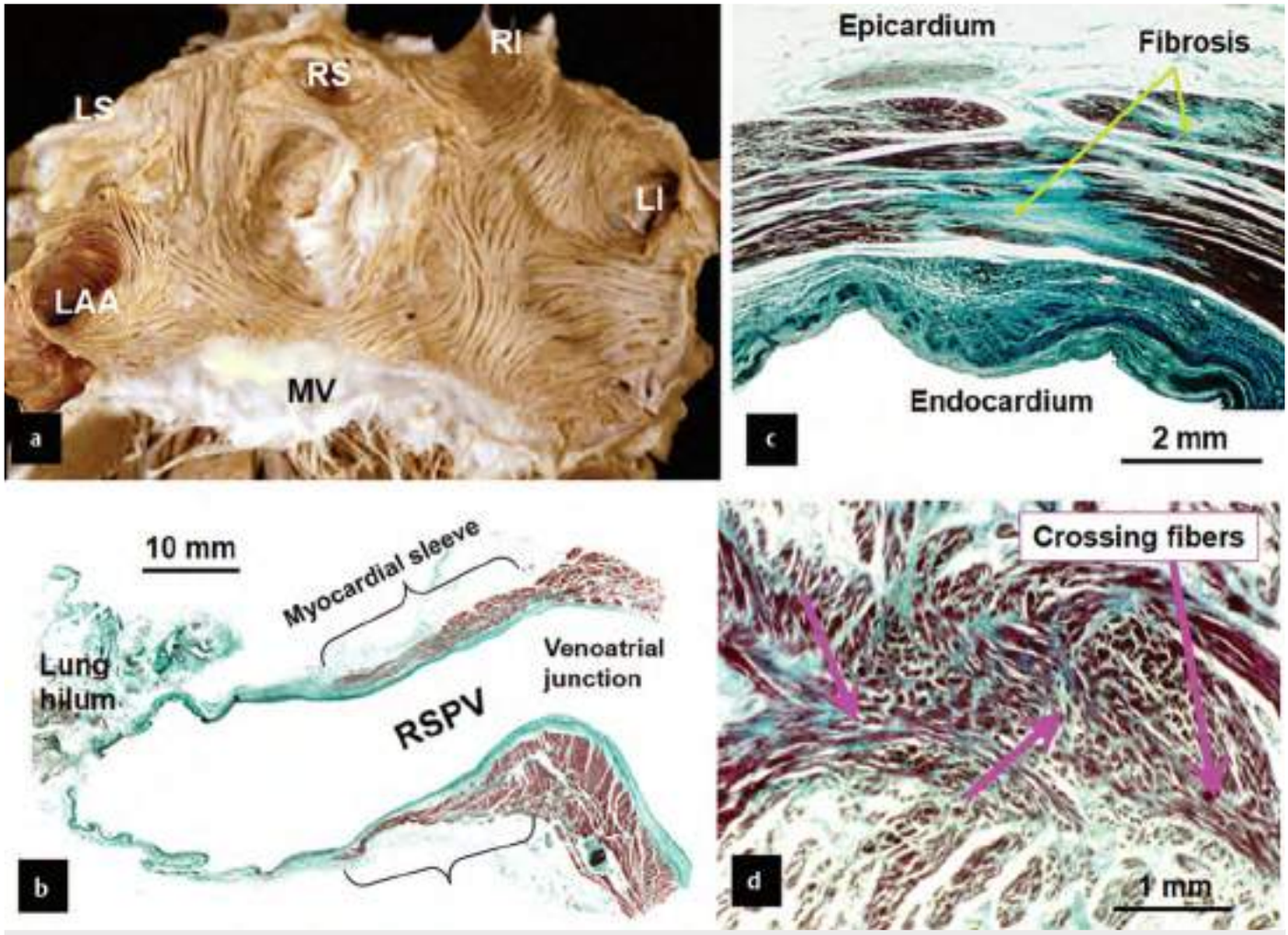

Fig. 7.19 **(a)** Dissection of the left atrium shows the entrances and myocardial sleeves of the four pulmonary veins. (**b**) Longitudinal sections through the right superior pulmonary veins (RSPV). The myocardial sleeve completely surrounding the superior vein and extending from the venoatrial junction. **(c)** The myocardial sleeve of a left superior PV shows extensive fibrotic replacement. **(d)** Longitudinal sections of the myocardial sleeve of the right superior pulmonary vein showing a complex arrangement of circular and longitudinal bundles of myocytes. LAA, left atrial appendage; LI, left inferior pulmonary vein; LS, left superior pulmonary vein; MV, mitral valve; RI, right inferior pulmonary vein; RS, right superior pulmonary vein.

Techniques for Catheter Ablation of Atrial Fibrillation

Historically, the most common ablation strategy for treatment of paroxysmal AF has been electrical isolation of the PVs by creating circumferential ablation lines around the individual PV ostia. The lines are either guided by fluoroscopy, 3D electroanatomical mapping, or intracardiac echocardiography.[38,39] Because of high rate of recurrence and complications such as PV stenosis, ablation strategies have been modified to include the atrial walls. For example, circumferential line of ablation shifted proximally to cover both of the PV ostia on each aside and antrum ablation introduced to treat non-PV trigger points for AF[40] (▶ Fig. 7.20). In antrum ablation, the most common sites are the LA "roof" connecting the superior aspects of the left and right upper PV isolation lesions, the region of tissue between the mitral valve and the left inferior PV (the mitral isthmus)[41] (▶ Fig. 7.20). These techniques result in success rate of more than 90% with long-term success rate ranging from 60 to 90% in patients with paroxysmal AF but lower rates in those with chronic AF.[38,42]

Cardiac Autonomic Nervous System and Atrial Fibrillation

Vagal stimulation shortens the atrial effective refractory period that facilitate the initiation and maintenance of AF. Cardiac ganglia are generally located in the epicardial layer of the base of the heart and are surrounded by adipose tissue.[43] The largest populations are concentrated along the interatrial groove near the junction of the right superior PV and the SVC (PV–SVC far pad) and the junction of the IVC and the LA (IVC–LA fat pad). Adding LA ganglion plexus to other ablation targets may improve ablation success in patients undergoing circumferential PV ablation for paroxysmal AF.[39]

Pathology

Pulmonary veins can be occluded in hypercoagulable state, tumor invasion, mediastinal fibrosis, chronic inflammatory processes, vasculitis, and iatrogenic (ablation procedures, surgery) (▶ Fig. 7.21). It is not unusual to see some stenosis at PV anastomosis after lung transplantation (▶ Fig. 7.22). The incidence of PV

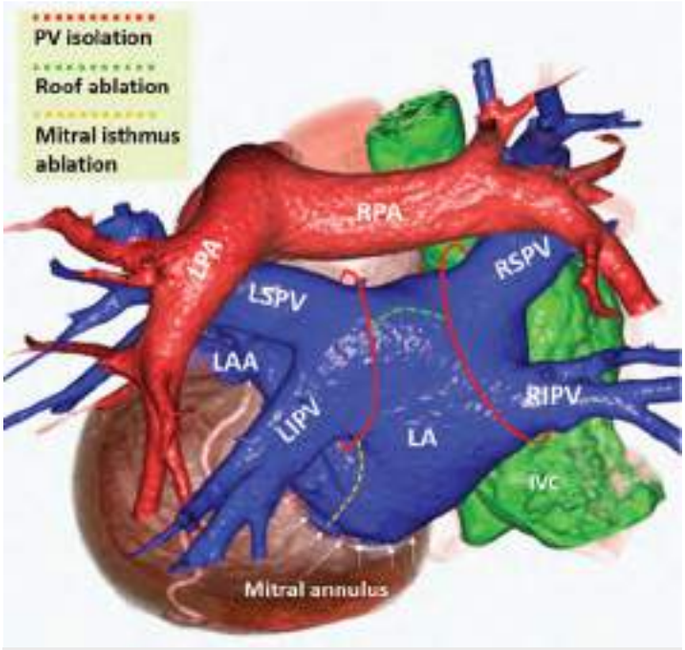

Fig. 7.20 Ablation of atrial fibrillation. Circumferential pulmonary vein ablation. Posterior 3D view of the left atrium (LA) and pulmonary veins is shown. The two encircling pulmonary vein lesions (*red circles*) are connected with an ablation line in the roof (*green line*). Another ablation line is created along the mitral isthmus (*orange arrow*), between the left inferior pulmonary vein (LIPV) and the lateral mitral annulus. IVC, inferior vena cava; LAA, left atrial appendage; LPA, left pulmonary artery; LSPV, left superior pulmonary vein; MV, mitral valve; RIPV, right inferior pulmonary vein; RPA, right pulmonary artery; RSPV, right superior pulmonary vein.

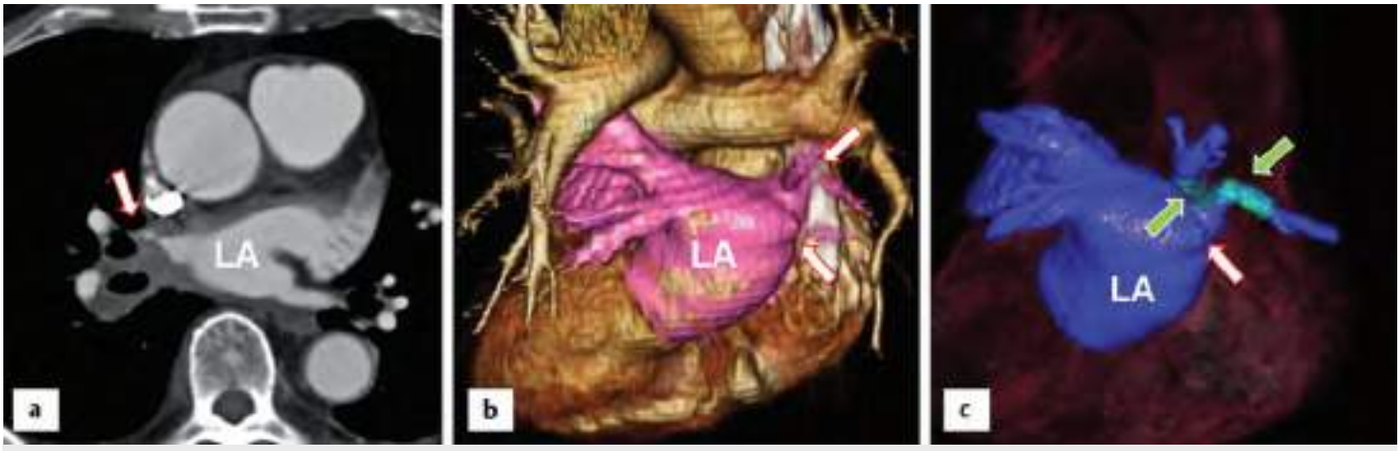

Fig. 7.21 Pulmonary vein stenosis after catheter ablation. **(a)** Axial CT shows severe stenosis (*arrow*) of the right superior pulmonary vein. **(b)** Inferior view of the heart showing focal narrowing of the right superior and inferior pulmonary veins (*arrows*). **(c)** Left atrium (LA) view showing stented branches of the right superior pulmonary vein. The left inferior pulmonary vein is occluded.

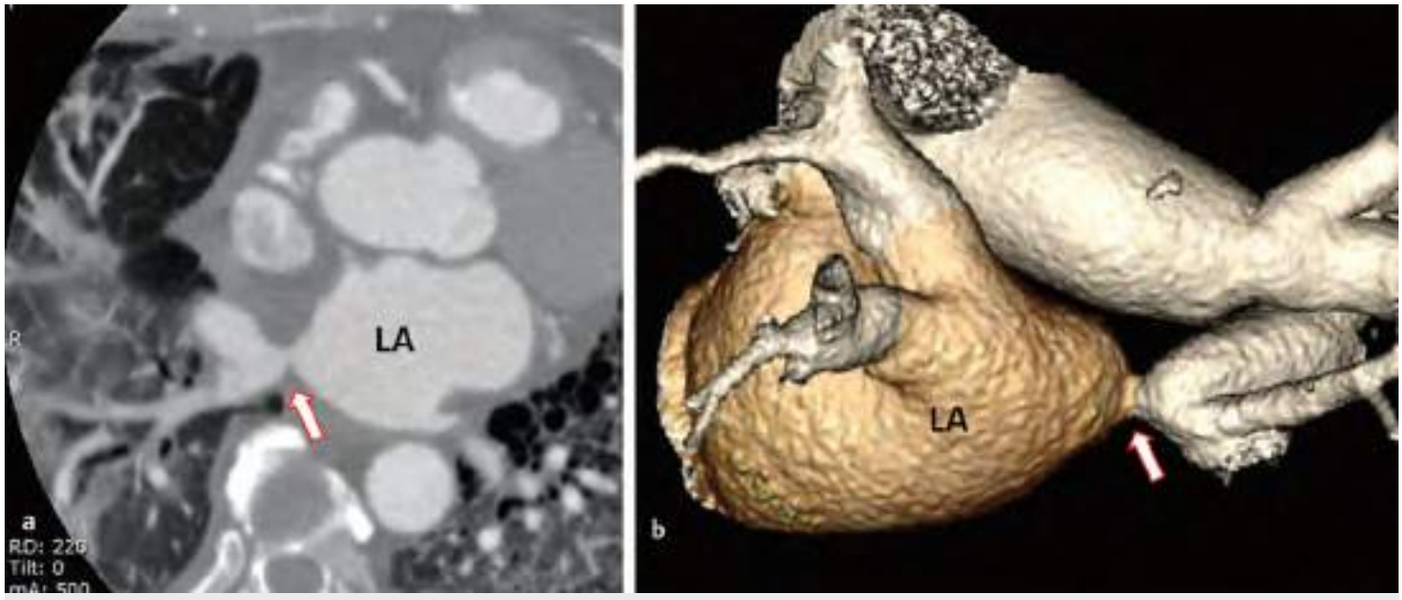

Fig. 7.22 Pulmonary vein stenosis after right lung transplant. **(a, b)** Axial and volume-rendered CT of the left atrium showing stenosis of the right pulmonary vein (*arrows*). The right lung transplant appears edematous. LA, left atrium.

stenosis caused by AF ablation has decreased to less than 1% due to improved techniques.[44,45,46,] Symptoms such as cough, hemoptysis, or recurrent lung infection, are more likely seen with severe stenosis (> 70%). However, even severe PV stenosis or complete PV occlusion in one lobe may be asymptomatic[46] (▶ Fig. 7.21). CT or chest X-ray may show interstitial or airspace edema of the involved lobe. As stated above, mild narrowing of the left inferior PV at its confluence with the LA is common and should not be mistaken with postablation stenosis (▶ Fig. 7.17). Patients with symptomatic and severe PV stenosis will require therapeutic procedures, such as stenting and balloon angioplasty (▶ Fig. 7.21). Thus, follow-up imaging study postablation is crucial in early detection and prompt treatment of PV stenosis.

Anomalies

Congenital PV stenosis and hypoplasia/atresia are rare and usually seen in children with heart malformations.[47]

Partial anomalous pulmonary venous return (connection) is probably the most common PV anomaly in which one or more of the PVs drain into the RA or one of its tributaries instead of the LA, creating a left-to-right shunt which is usually hemodynamically insignificant[48,49,50] (▶ Fig. 7.23). PAPVR alone can be symptomatic when 50% or more of the pulmonary blood flow returns abnormally into the systemic side. In adults, PAPVR is an incidental finding in imaging studies of the chest with normal hearts and usually seen in adult cases, involves left upper lobe PAPVR or isolated right upper lobe PAPVR without ASD (▶ Fig. 7.22**a**,**b**). The anomaly should be suspected if the tip of a central venous catheter seen on chest X-ray extends beyond the normal cardiovascular margin in to the lung paraenchyma (▶ Fig. 7.24). Among cases of right upper lobe PAPVR, 42% are associated with sinus venosus ASD.[50] Differentiation of the left upper lobe PAPVR with persistent left SVC can be confusing to an inexperienced imager. Both anomalies are caused by a persistent left anterior cardinal vein. In PAPVR of the left upper lobe, the anomalous vein interposed between the parenchymal veins of the left upper lobe and the left brachiocephalic vein is described as the “vertical vein” because unlike a persistent left SVC, it does not drain caudally into the coronary sinus (▶ Fig. 7.23**a**). In PAPVR of the right lower lobe the anomalous vein usually drains into the subdiaphragmatic IVC and resembles a curved Turkish sword or Scimitar (Scimitar or venolobar syndrome) (▶ Fig. 7.23**f**). Total anomalous pulmonary venous connection is very rare in adults but accounts for approximately 1 to 5% of cardiovascular congenital anomalies in children.

Pulmonary venous varices are usually incidental findings on imaging studies and should not be confused with a mediastinal mass or a lung nodule (▶ Fig. 7.25). These relatively rare lesions may be congenital due to abnormal development of the primitive splanchnic or acquired secondary to increased pressure of the pulmonary veins (i.e., in mitral valve disease). Lesions usually present as a focal saccular dilatation or less commonly as tortuous elongated dilated veins, in the lung or more frequently at the confluences to the left atrium. The latter type rarely is associated with focal atrial tachycardia and atrial fibrillation.

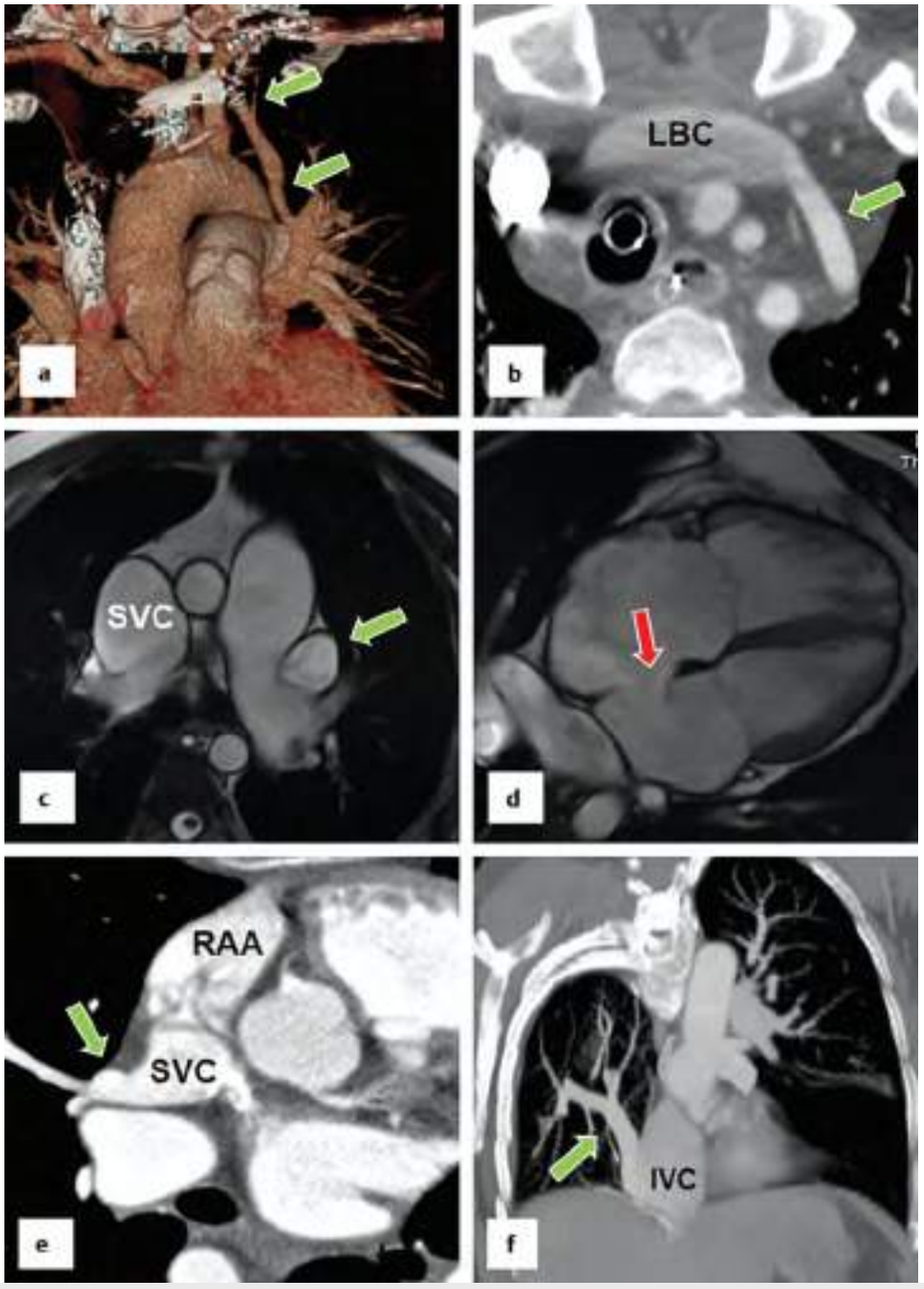

Fig. 7.23 Variants of partial anomalous pulmonary venous return. **(a, b)** Partial anomalous pulmonary venous return (*green arrows*) draining part of the left upper lung into the left brachiocephalic (LBC) vein. The vertical vein is shown on volume-rendered image (*arrows*). **(c, d)** Partial anomalous pulmonary venous return (*green arrows*) draining most of the left upper lung. The superior vena cava (SVC) is enlarged and a large atrial septal defect (ASD, *red arrow*) exists. Cardiomegaly due to large left-to-right shunt is seen. **(e)** Partial anomalous pulmonary venous (*green arrow*) return draining part of the right upper lung into the SVC. **(f)** Scimitar syndrome. Anomalous drainage of the right lower lobe into the suprahepatic inferior vena cava (IVC). RAA, right atrial appendage.

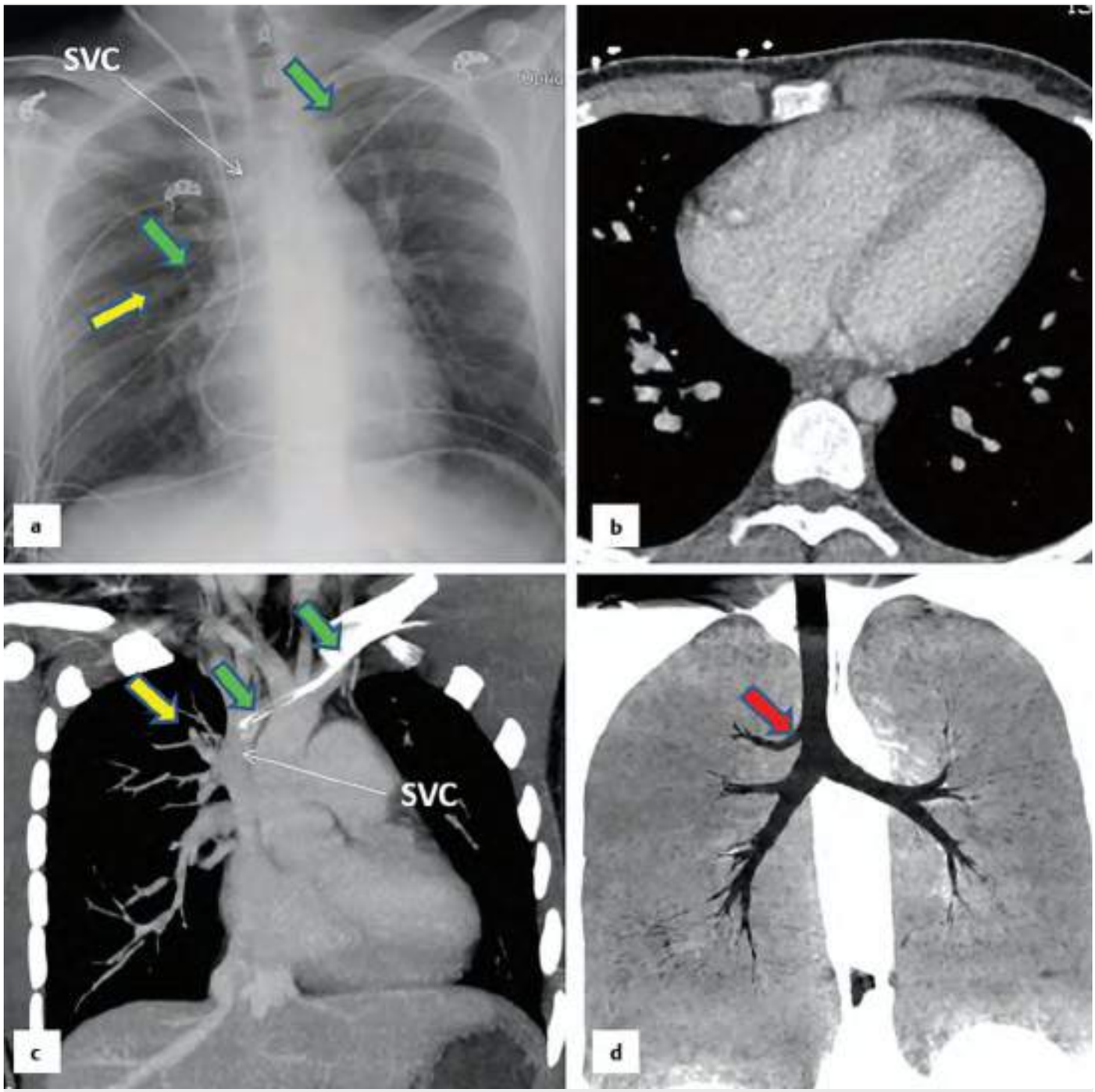

Fig. 7.24 Partial anomalous pulmonary venous return. **(a)** X-ray showing misplaced left central venous catheter (PICC line) into an anolmous right pulmonary vein which is draining into the superior vena cava (SVC). **(b)** No intra cardiac shunt was seen. **(c)** Follow-up CT scan showing left PICC line pulled backed into the SVC. The anomalous right pulmonary vein is also seen (*yellow arrow*). **(d)** Incidentally noted a right tracheal bronchus (*arrow*).

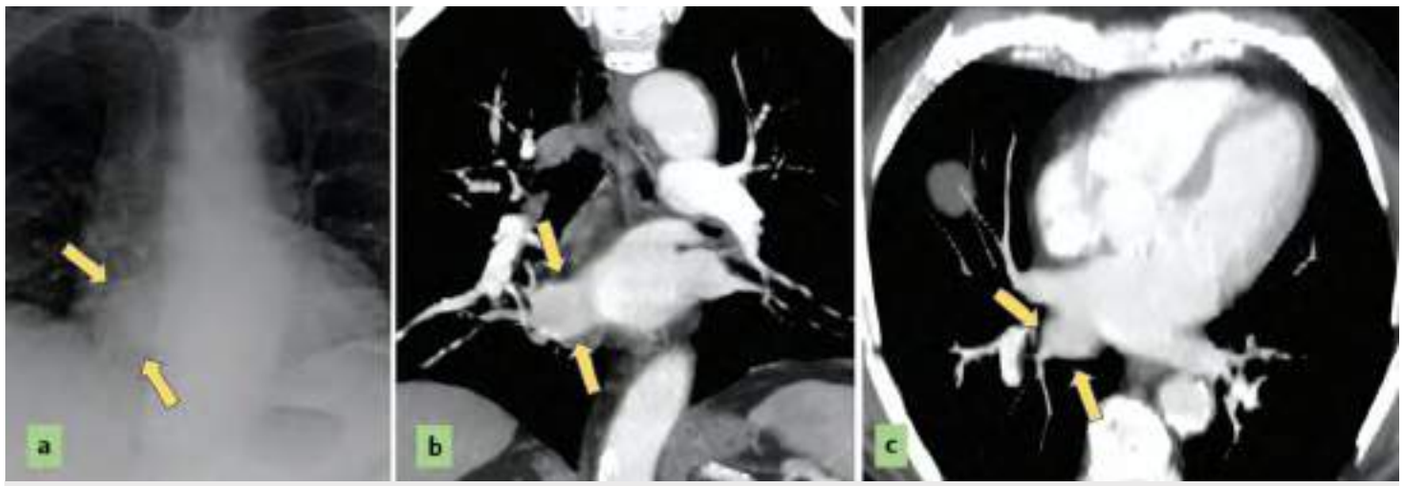

Fig. 7.25 (a–c) Pulmonary vein varix. Varicoid dilatation of the of the right inferior pulmonary vein (*arrows*) before confluence with the left atrium presented as a right paramediastinal pseudomass on chest X-ray.

References

[1] Minniti S, Visentini S, Procacci C. Congenital anomalies of the venae cavae: embryological origin, imaging features and report of three new variants. Eur Radiol.; 12(8):2040–2055

[2] Steding G, Xu JW, Seidl W, Männer J, Xia H. Developmental aspects of the sinus valves and the sinus venosus septum of the right atrium in human embryos. Anat Embryol (Berl).; 181(5):469–475

[3] Kellman GM, Alpern MB, Sandler MA, Craig BM. Computed tomography of vena caval anomalies with embryologic correlation. Radiographics.; 8(3):533–556

[4] Webb S, Kanani M, Anderson RH, Richardson MK, Brown NA. Development of the human pulmonary vein and its incorporation in the morphologically left atrium. Cardiol Young.; 11(6):632–642

[5] Anderson RH, Brown NA, Moorman AFM. Development and structures of the venous pole of the heart. Dev Dyn.; 235(1):2–9

[6] Anderson RH, Webb S, Brown NA. Clinical anatomy of the atrial septum with reference to its developmental components. Clin Anat.; 12(5):362–374

[7] Chen SJ, Liu KL, Chen HY, et al. Anomalous brachiocephalic vein: CT, embryology, and clinical implications. AJR Am J Roentgenol.; 184(4):1235–1240

[8] Takeda K, Matsumura K, Ito T, Nakagawa T, Yamaguchi N. Anomalous insertion of the superior or the inferior vena cava into the right atrium. Pediatr Cardiol.; 19(6):474–476

[9] Moncada R, Demos TC, Marsan RM, Churchill RJ, Reynes C, Love L. CT diagnosis of aneurysms of the thoracic venous system. J Comput Assist Tomogr.; 9:305–309

[10] Buirski G, Jordan SC, Joffe HS, Wilde P. Superior vena caval abnormalities: their occurrence rate, associated cardiac abnormalities and angiographic classification in a paediatric population with congenital heart disease. Clin Radiol.; 37(2):131–138

[11] Webb WR, Gamsu G, Speckman JM, Kaiser JA, Federle MP, Lipton MJ. Computed tomographic demonstration of mediastinal venous anomalies. AJR Am J Roentgenol.; 139(1):157–161

[12] Takada Y, Narimatsu A, Kohno A, et al. Anomalous left brachiocephalic vein: CT findings. J Comput Assist Tomogr.; 16(6):893–896

[13] Ball JB, Jr, Proto AV. The variable appearance of the left superior intercostal vein. Radiology.; 144(3):445–452

[14] McDonald CJ, Castellino RA, Blank N. The aortic "nipple". The left superior intercostal vein. Radiology.; 96(3):533–536

[15] Gilkeson RC, Nyberg EM, Sachs PB, Wiant AM, Zahka KG, Siwik ES. Systemic to pulmonary venous shunt: imaging findings and clinical presentations. J Thorac Imaging.; 23(3):170–177

[16] Dudiak CM, Olson MC, Posniak HV. Abnormalities of the azygos system: CT evaluation. Semin Roentgenol.; 24(1):47–55

[17] Dudiak CM, Olson MC, Posniak HV. CT evaluation of congenital and acquired abnormalities of the azygos system. Radiographics.; 11(2):233–246

[18] Jelinek JS, Stuart PL, Done SL, Ghaed N, Rudd SA. MRI of polysplenia syndrome. Magn Reson Imaging.; 7(6):681–686

[19] Mata J, Cáceres J, Alegret X, Coscojuela P, De Marcos JA. Imaging of the azygos lobe: normal anatomy and variations. AJR Am J Roentgenol.; 156(5):931–937

[20] Takasugi JE, Godwin JD. Left azygos lobe. Radiology.; 171(1):133–134

[21] Hatfield MK, Vyborny CJ, MacMahon H, Chessare JW. Congenital absence of the azygos vein: a cause for "aortic nipple" enlargement. AJR Am J Roentgenol.; 149(2):273–274

[22] Dorfmüller P, Günther S, Ghigna MR, et al. Microvascular disease in chronic thromboembolic pulmonary hypertension: a role for pulmonary veins and systemic vasculature. Eur Respir J.; 44(5):1275–1288

[23] van den Berg G, Moorman AF. Development of the pulmonary vein and the systemic venous sinus: an interactive 3D overview. PLoS One.; 6(7):e22055

[24] Blom NA, Gittenberger-de Groot AC, Jongeneel TH, DeRuiter MC, Poelmann RE, Ottenkamp J. Normal development of the pulmonary veins in human embryos and formulation of a morphogenetic concept for sinus venosus defects. Am J Cardiol.; 87(3):305–309

[25] White CS, Baffa JM, Haney PJ, Campbell AB, NessAiver M. Anomalies of pulmonary veins: usefulness of spin-echo and gradient-echo MR images. AJR Am J Roentgenol.; 170(5):1365–1368

[26] Hassink RJ, Aretz HT, Ruskin J, Keane D. Morphology of atrial myocardium in human pulmonary veins: a postmortem analysis in patients with and without atrial fibrillation. J Am Coll Cardiol.; 42(6):1108–1114

[27] Cronin P, Kelly AM, Desjardins B, et al. Normative analysis of pulmonary vein drainage patterns on multidetector CT with measurements of pulmonary vein ostial diameter and distance to first bifurcation. Acad Radiol.; 14(2):178–188

[28] Kim YH, Marom EM, Herndon JE, II, McAdams HP. Pulmonary vein diameter, cross-sectional area, and shape: CT analysis. Radiology.; 235(1):43–49, discussion 49–50

[29] Choi SI, Seo JB, Choi SH, et al. Variation of the size of pulmonary venous ostia during the cardiac cycle: optimal reconstruction window at ECG-gated multidetector row CT. Eur Radiol.; 15(7):1441–1445

[30] Nathan H, Eliakim M. The junction between the left atrium and the pulmonary veins. An anatomic study of human hearts. Circulation.; 34(3):412–422

[31] Haissaguerre M, Jais P, Shah DC, et al. Spontaneous initiation of AF by ectopic beats originating in the pulmonary veins. N Engl J Med.; 339:659–666

[32] Steiner I, Hájková P, Kvasnicka J, Kholová I. Myocardial sleeves of pulmonary veins and atrial fibrillation: a postmortem histopathological study of 100 subjects. Virchows Arch.; 449(1):88–95

[33] Becker AE. How structurally normal are human atria in patients with atrial fibrillation? Heart Rhythm.; 1(5):627–631

[34] Ho SY, Cabrera JA, Tran VH, Farré J, Anderson RH, Sánchez-Quintana D. Architecture of the pulmonary veins: relevance to radiofrequency ablation. Heart.; 86(3):265–270

[35] Cabrera JA, Ho SY, Climent V, Fuertes B, Murillo M, Sánchez-Quintana D. Morphological evidence of muscular connections between contiguous pulmonary

venous orifices: relevance of the interpulmonary isthmus for catheter ablation in atrial fibrillation. Heart Rhythm.; 6(8):1192–1198

[36] Sánchez-Quintana D, Doblado-Calatrava M, Cabrera JA, Macías Y, Saremi F. Anatomical Basis for the Cardiac Interventional Electrophysiologist. BioMed Res Int.; 2015:547364

[37] Valles E, Fan R, Roux JF, et al. Localization of atrial fibrillation triggers in patients undergoing pulmonary vein isolation: importance of the carina region. J Am Coll Cardiol.; 52(17):1413–1420

[38] Haïssaguerre M, Hocini M, Sanders P, et al. Catheter ablation of long-lasting persistent atrial fibrillation: clinical outcome and mechanisms of subsequent arrhythmias. J Cardiovasc Electrophysiol.; 16(11):1138–1147

[39] Pappone C, Santinelli V, Manguso F, et al. Pulmonary vein denervation enhances long-term benefit after circumferential ablation for paroxysmal atrial fibrillation. Circulation.; 109(3):327–334

[40] Ouyang F, Bänsch D, Ernst S, et al. Complete isolation of left atrium surrounding the pulmonary veins: new insights from the double-Lasso technique in paroxysmal atrial fibrillation. Circulation.; 110(15):2090–2096

[41] Ernst S, Ouyang F, Löber F, Antz M, Kuck KH. Catheter-induced linear lesions in the left atrium in patients with atrial fibrillation: an electroanatomic study. J Am Coll Cardiol.; 42(7):1271–1282

[42] Nademanee K, McKenzie J, Kosar E, et al. A new approach for catheter ablation of atrial fibrillation: mapping of the electrophysiologic substrate. J Am Coll Cardiol.; 43(11):2044–2053

[43] Singh S, Johnson PI, Lee RE, et al. Topography of cardiac ganglia in the adult human heart. J Thorac Cardiovasc Surg.; 112(4):943–953

[44] Takahashi A, Kuwahara T, Takahashi Y. Complications in the catheter ablation of atrial fibrillation: incidence and management. Circ J.; 73(2):221–226

[45] Cappato R, Calkins H, Chen SA, et al. Worldwide survey on the methods, efficacy, and safety of catheter ablation for human atrial fibrillation. Circulation.; 111(9):1100–1105

[46] Saad EB, Rossillo A, Saad CP, et al. Pulmonary vein stenosis after radiofrequency ablation of atrial fibrillation: functional characterization, evolution, and influence of the ablation strategy. Circulation.; 108(25):3102–3107

[47] Heyneman LE, Nolan RL, Harrison JK, McAdams HP. Congenital unilateral pulmonary vein atresia: radiologic findings in three adult patients. AJR Am J Roentgenol.; 177(3):681–685

[48] Kalke BR, Carlson RG, Ferlic RM, Sellers RD, Lillehei CW. Partial anomalous pulmonary venous connections. Am J Cardiol.; 20(1):91–101

[49] Haramati LB, Moche IE, Rivera VT, et al. Computed tomography of partial anomalous pulmonary venous connection in adults. J Comput Assist Tomogr.; 27(5):743–749

[50] Ho ML, Bhalla S, Bierhals A, Gutierrez F. MDCT of partial anomalous pulmonary venous return (PAPVR) in adults. J Thorac Imaging.; 24(2):89–95

8 Thoracic Aorta and Major Branches

Hiro Kiyosue, Miyuki Maruno, and Norio Hongo

◆ Anatomy

The aorta is the largest artery originating at the upper part of the left ventricle. It can be divided into four sections: the ascending aorta, the aortic arch, the thoracic (descending) aorta, and the abdominal aorta (▶ Fig. 8.1). The aorta ascends obliquely to the right within the pericardium, between the superior vena cava and main pulmonary artery, and anterior to the right pulmonary artery and trachea (ascending aorta). At T3 to T4 level, it turns backward to form the aortic arch. It descends within the thorax on the left side of the vertebral column (descending aorta) into the abdomen through the aortic hiatus in the diaphragm (abdominal aorta).

◆ Ascending Aorta

The origin of the ascending aorta (the aortic root) shows anatomical dilation just above each of the aortic valve leaflets known as the sinuses of Valsalva. These three aortic sinuses include the left coronary, the right coronary, and the noncoronary (nonadjacent) sinuses.[1] The left aortic sinus and right aortic sinus, give rise to the left and right coronary arteries (RCAs), respectively (▶ Fig. 8.2). The transverse diameter of the aorta at the level of the sinus is usually less than 3.5 cm. A diameter above 4 cm is abnormal. Sinuses of Valsalva are equal in size but rarely one or all can become aneurysmal.[2] Aneurysm of the sinus of Valsalva can be congenital or acquired, more common in men, and rarely

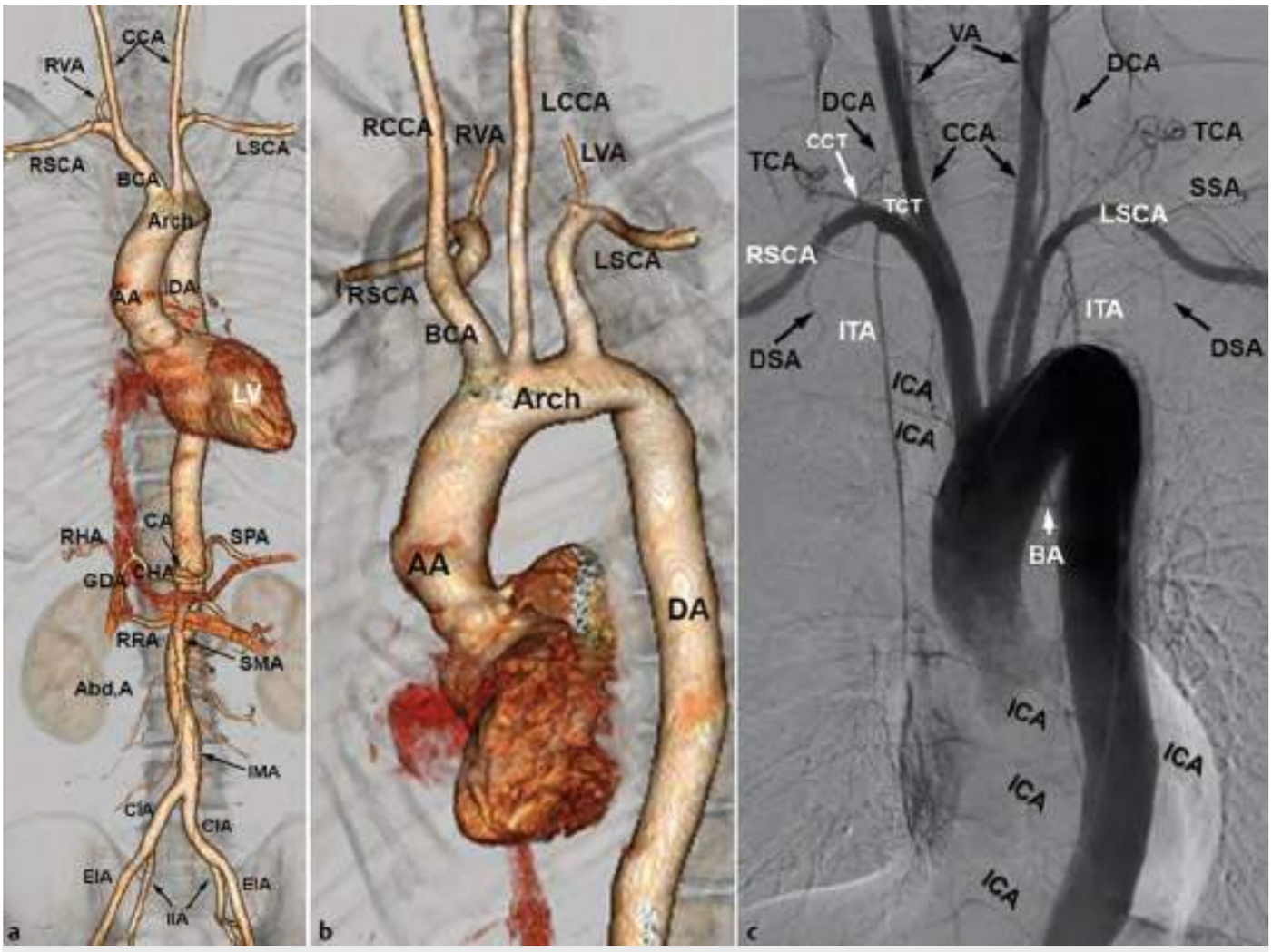

Fig. 8.1 Aorta and its major branches. **(a)** Anterior view and **(b)** left anterior oblique view of the 3D CT angiography of the aorta and its branches with volume-rendering reconstruction. **(c)** Anterior view of aortography. AA, ascending aorta; Arch, aortic arch; BA, bronchial artery; CA, celiac artery; CHA, common hepatic artery; DA, descending aorta; Abd A, abdominal aorta; BCA, brachiocephalic artery; CCA, common carotid artery; CIA, common iliac artery; DCA, deep cervical artery; DSA, dorsal scapular artery; EIA, external iliac artery; GDA, gastroduodenal artery; ITA, internal thoracic artery; ICA, intercostal artery; IMA, inferior mesenteric artery; IIA, internal iliac artery; LV, left ventricle; R(L)CCA, right (left) common carotid artery; R(L)SCA, right (left) subclavian artery; R(L)VA, right (left) vertebral artery; RRA, right renal artery; RHA, right hepatic artery; SMA, superior mesenteric artery; SPA, splenic artery; SSA, suprascapular artery; TCA, transverse cervical artery; TCT, thyrocervical trunk; VA, vertebral artery.

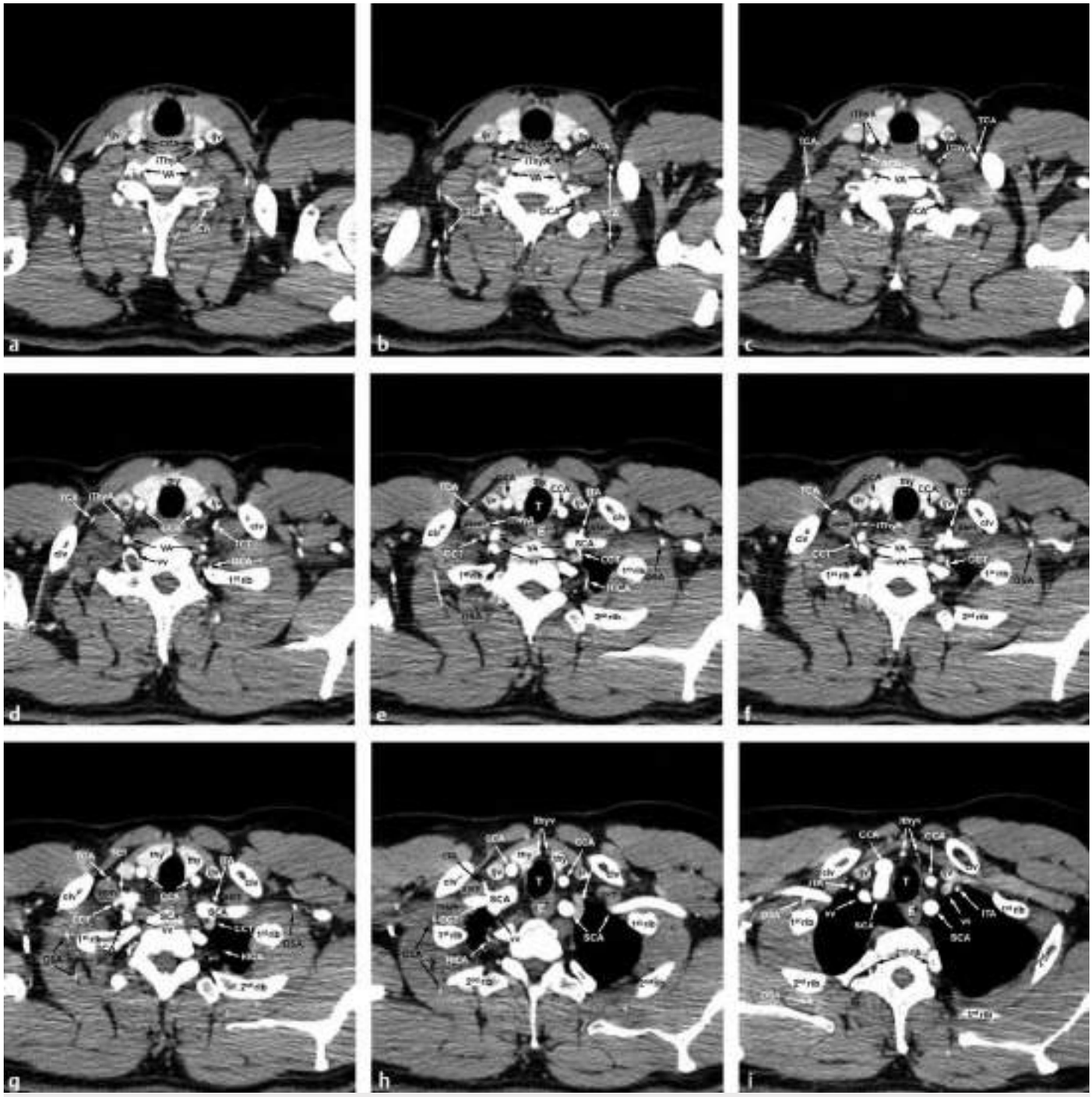

Fig. 8.2 Axial contrast-enhanced images of the chest showing the aorta and its major branches. AA, ascending aorta; ACA, ascending cervical artery; Arch, aortic arch; asm, anterior scalene muscle; azv, azygos vein; BCA, brachiocephalic artery; CCA, common carotid artery; CCT, costocervical trunk; clv, clavicle; CX, circumflex artery; DCA, deep cervical artery; DD, descending aorta; DSA, dorsal scapular artery; E, esophagus; HICA, highest intercostal artery; ILA, interlobar artery; ITA, internal thoracic artery; iv, innominate vein; iThyA, inferior thyroid artery; ithyv, inferior thyroid vein; ijv, internal jugular vein; LPA, left pulmonary artery; lspv, left superior pulmonary vein; LBA, left bronchial artery; LA, left atrium; LPVAA, longitudinal paravertebral anastomotic artery; LCA, left coronary artery; LAD, left anterior descending artery; LAA, left atrial appendage; L(R)BT, left (right) basal trunk; lipv, left inferior pulmonary vein; msm, middle scalene muscle; PAT, pulmonary artery trunk; rspv, right superior pulmonary vein; RPA, right pulmonary artery; r(l)mb, right (left) main bronchus; RCA, right coronary artery; RA, right atrium; ripv, right inferior pulmonary vein; SCA, subclavian artery; svc, superior vena cava; TCA, transverse cervical artery; TCT, thyrocervical trunk; thy, thyroid; T, trachea; VA, vertebral artery; vv, vertebral vein; 2nd ICA, second intercostal artery; 3rd ICA, third intercostal artery; 4th ICA, fourth intercostal artery; 5th ICA, fifth intercostal artery; 6th ICA, sixth intercostal artery.

(*Continued*)

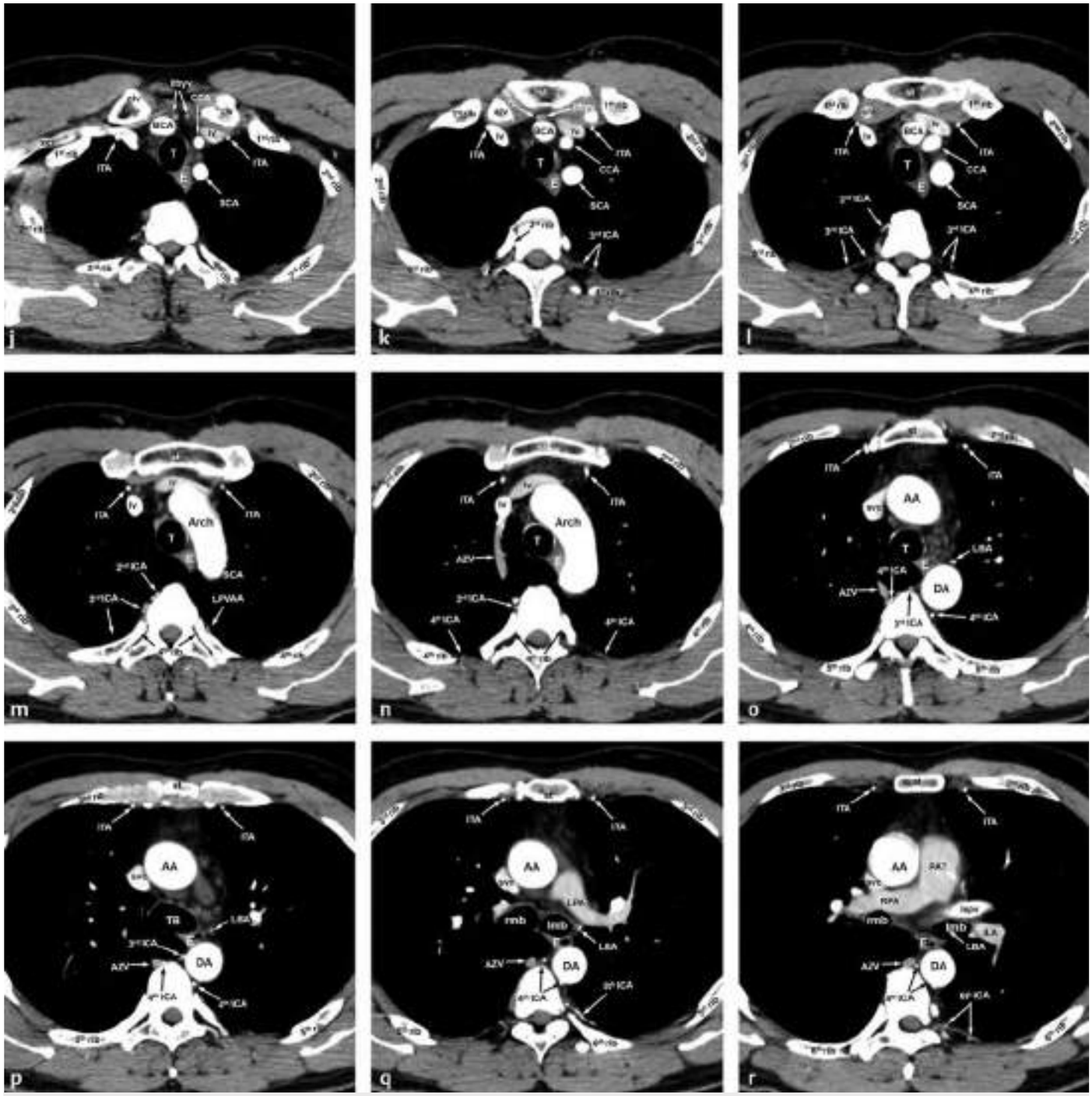

Fig. 8.2 (*Continued*) **(j–r)**

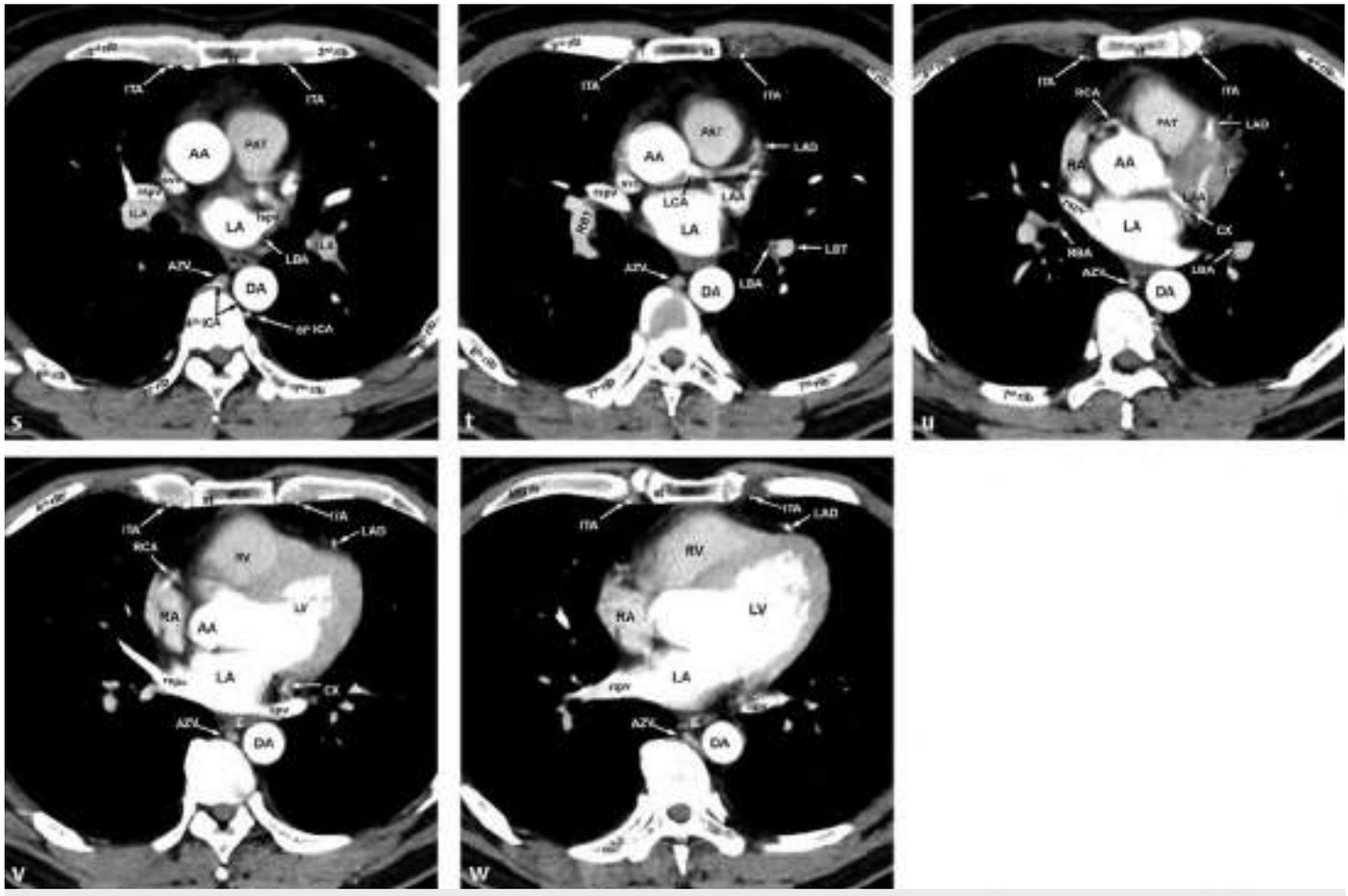

Fig. 8.2 (s–w)

can rupture. The ascending aorta is about 33 mm in diameter and 5 cm in length in adult human. The upper limit of normal diameter of the ascending aorta is about 41 mm.[3]

Branches from the Ascending Aorta

Right Coronary Artery

Detail of the anatomy of the coronary arteries is described in Chapter 18. The RCA runs between the right ventricular outflow tract and the right atrial appendage and descends through the right atrioventricular groove (▶ Fig. 8.2). It curves posteriorly toward the crux of the heart and continues downward in the posterior interventricular sulcus.[4] The RCA gives off branches to the right ventricular outflow tract (conus branch), sinoatrial node (sinoatrial nodal artery), the right atrium, and the right ventricle (the right marginal branch is the largest one). It also gives branches to the inferior wall of the left ventricle which adjoins the posterior interventricular sulcus.

Left Coronary Artery

The left coronary artery passes between the pulmonary trunk and the left atrial appendage, and it divides into the left anterior descending artery (LAD) and the left circumflex artery (LCx) (▶ Fig. 8.1, ▶ Fig. 8.3). The LAD runs downward along the anterior interventricular groove, which gives branches to the ventricles and interventricular septum. The largest branch of the LAD is the diagonal branch supplying blood to the anterolateral portion of the left ventricle. The LCx travels in the left atrioventricular groove to reach the back of the heart. It gives off branches to supply the left atrium and the posterior and lateral free walls of the left ventricle.

Coronary artery anomalies such as anomalous in origin, course, and number are relatively common with higher frequency in congenital cardiac diseases.[5,6] Coronary artery fistulas, including coronary–pulmonary arterial fistulas, coronary–bronchial arterial anastomoses, coronary artery–cardiac chamber fistulas, and coronary artery–systemic venous fistulas, are found in 0.9 % of patients undergone coronary computed tomography (CT) angiography.[7] Majority of coronary artery anomalies are asymptomatic, but they can cause angina, ischemic heart attack, sudden death, heart failure, pulmonary hypertension, and pulmonary hemorrhage.

◆ Aortic Arch

The aortic arch begins at the level of the second sternocostal joint. It runs upward and bends posteriorly to the left, and then descends to connect to the descending aorta at the level of the T4 vertebra. Three major branches originating from aortic arch include the brachiocephalic artery, the left common carotid artery, and the left subclavian artery (▶ Fig. 8.1, ▶ Fig. 8.3). The aortopulmonary ligament (ligamentum arteriosus), an

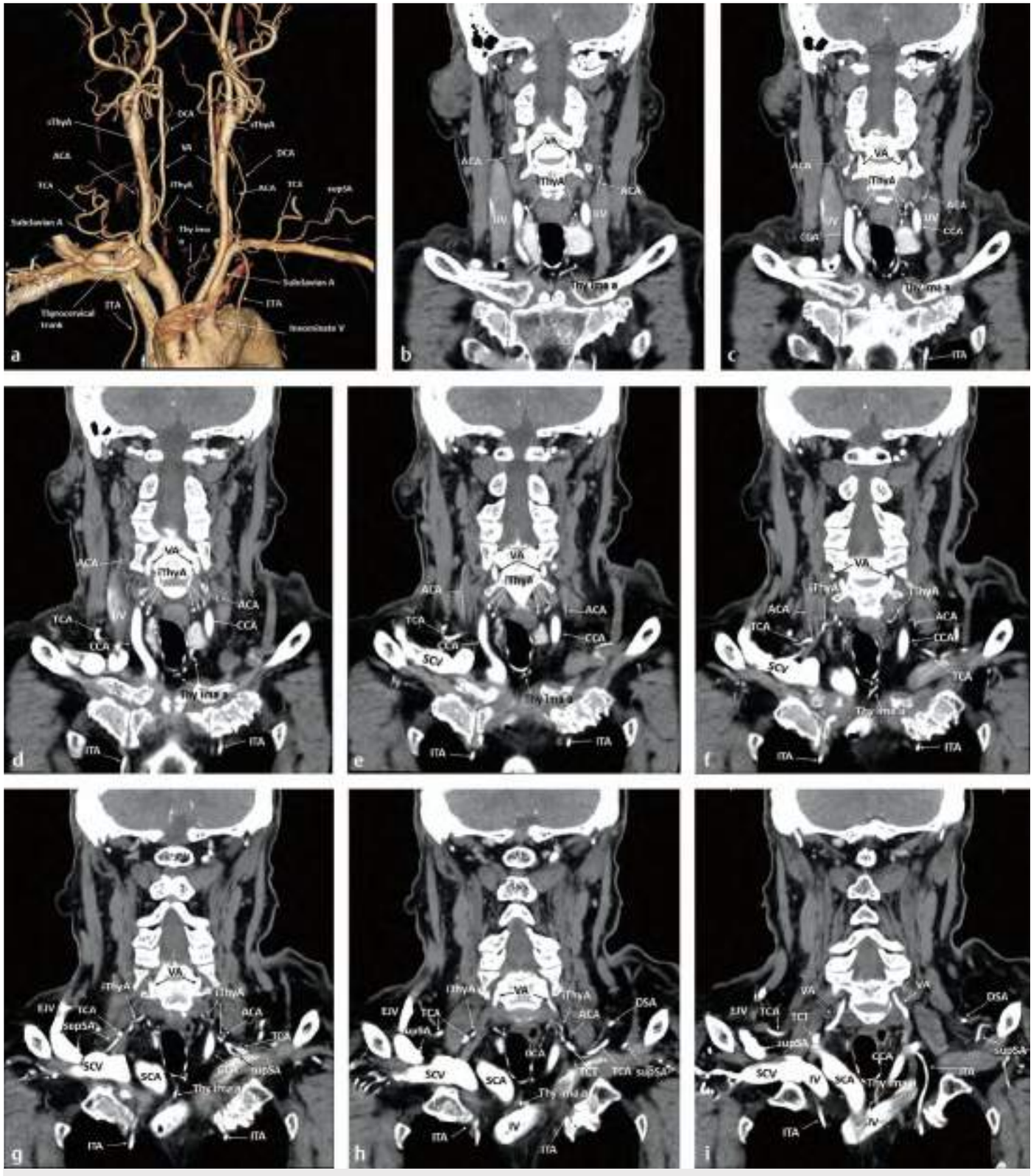

Fig. 8.3 Branches of the aortic arch shown on frontal 3D CT angiography **(a)**, coronal **(b-l)** 2D images from anterior to posterior, and sagittal **(m-u)** views on the right side from lateral to medial. ACA, ascending cervical artery; BCA, brachiocephalic artery; CCA, common carotid artery; CCT, costocervical artery; DCA, deep cervical artery; DSA, dorsal scapular artery; EJV, external jugular vein; HIA, highest intercostal artery; IJV, internal jugular vein; IV, innominate vein; ITA, internal thoracic artery; iThyA, inferior thyroid artery; SCV, subclavian vein; sThyA, superior thyroid artery; supSA, suprascapular artery; SCA, subclavian artery; TCA, transverse cervical artery; TCT, thyrocervical trunk; Thy ima a, thyroid ima artery; VA, vertebral artery.

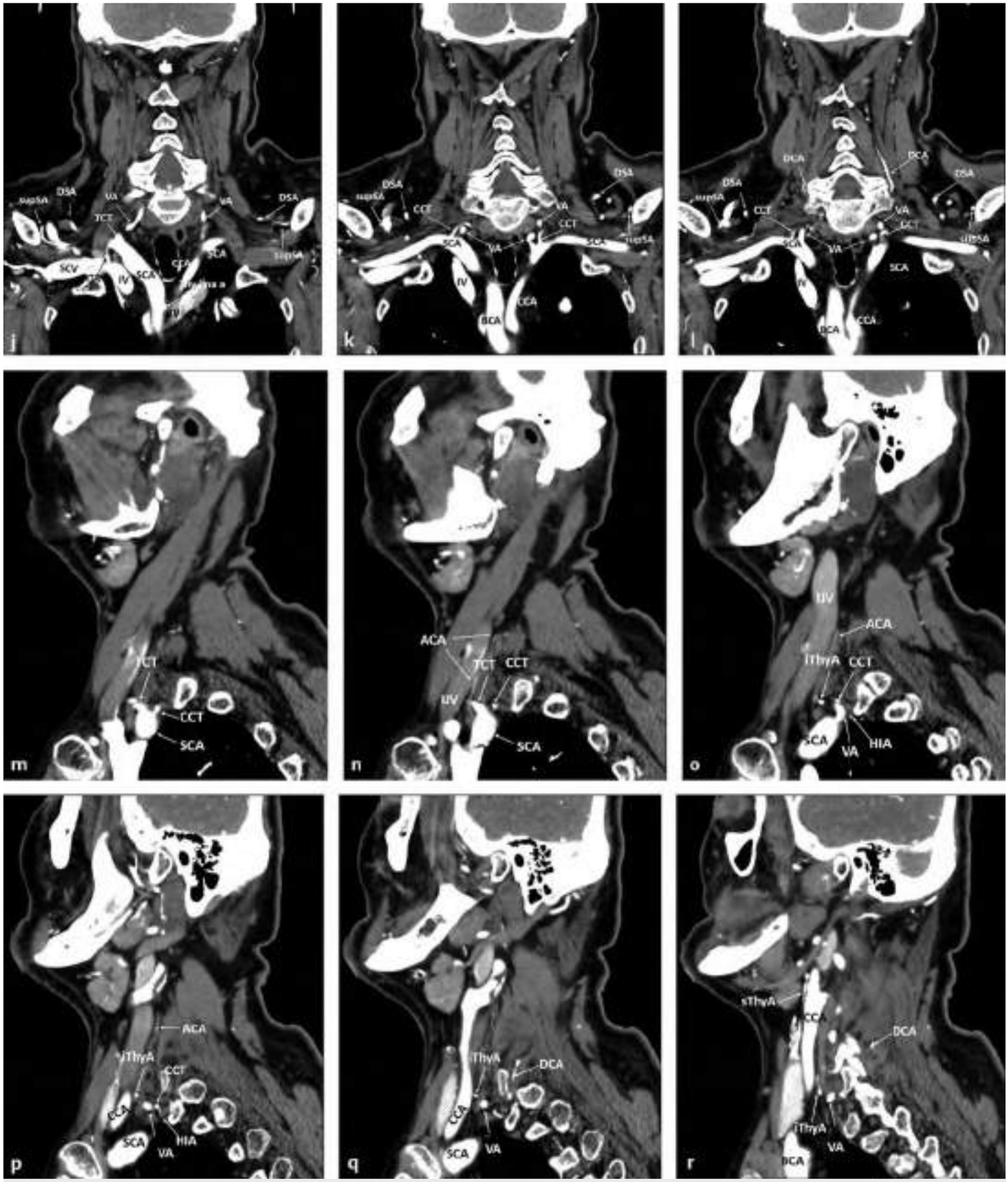

Fig. 8.3 (j–r)

(*Continued*)

Fig. 8.3 *(Continued)* **(s–u)**

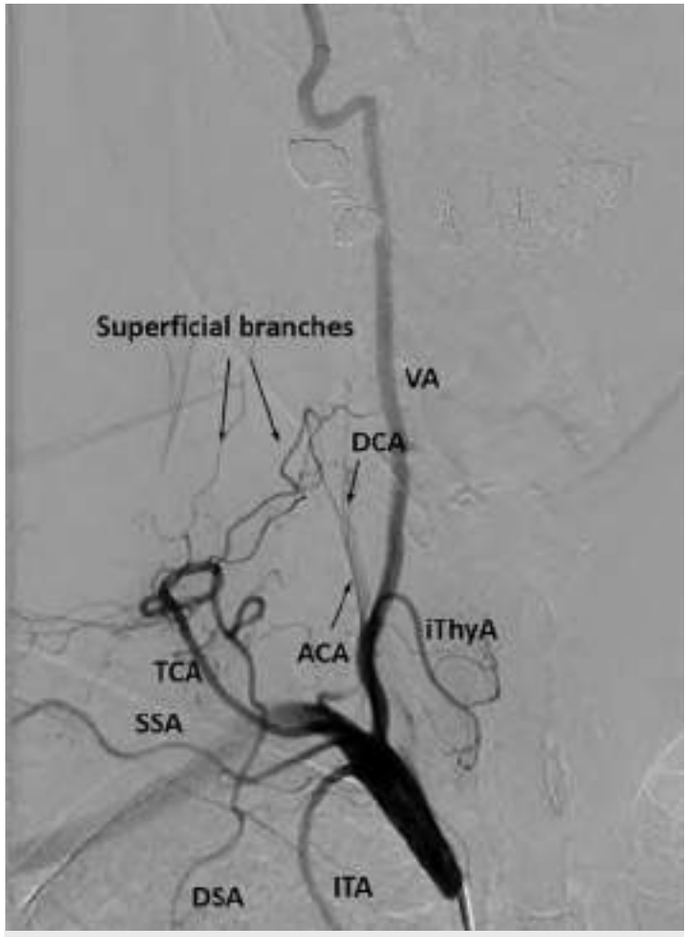

Fig. 8.4 Right subclavian angiography (frontal view). ACA, ascending cervical artery; DCA, deep cervical artery; DSA, dorsal scapular artery; iThyA, inferior thyroidal artery; ITA, internal thoracic artery; TCA, transverse cervical artery; SSA, suprascapular artery; VA, vertebral artery.

embryological remnant of the ductus arteriosus, connects the distal portion of the aortic arch with the pulmonary trunk. Blunt aortic injuries often result in disruption of the aorta near the aortopulmonary ligament.[8] The left recurrent laryngeal nerve, a branch of the vagus nerve, hooks around the aortic arch to the left of the aortopulmonary ligamentum and ascends between the trachea and esophagus.[9] The right recurrent laryngeal nerve hooks around the right subclavian artery and ascends into the neck.

Branches from the Aortic Arch

Brachiocephalic Artery

The brachiocephalic artery (the innominate artery) is the first and the largest branch arising from the aortic arch. It runs obliquely upward to the right to the level of the right sternoclavicular joint where it divides into the right common carotid artery and the right subclavian artery. The length of the brachiocephalic artery varies and can elongate with age and arteriosclerosis causing widening of the superior mediastinum on plain radiographs. The brachiocephalic artery occasionally gives off the thyroid ima artery, a branch supplying the inferior part of the thyroid gland (▶ Fig. 8.3).[10,11]

A tracheal artery and/or bronchial artery may also arise from the brachiocephalic artery either as a single branch or a common trunk with the thyroid ima artery.[12]

Right Common Carotid Artery

The right common carotid artery, originating from the brachiocephalic artery, runs upward in the deep cervical space and divides into the external and internal carotid arteries at the level of the upper border of the thyroid cartilage (▶ Fig. 8.3). It is contained in the carotid sheath together with the internal jugular vein and the vagus nerve. The common carotid artery lies medial to the internal jugular vein, and the vagus nerve runs posteriorly between the two vessels. The superior thyroidal artery occasionally arises from the distal portion of the common carotid artery.

Right Subclavian Artery

The right subclavian artery, originating from the brachiocephalic artery, runs superolaterally, passing between anterior and middle scalene muscles, and then runs inferolaterally (▶ Fig. 8.3, ▶ Fig. 8.4). The subclavian artery becomes the axillary artery at

Fig. 8.5 "Bovine arch" branching type of the left common carotid artery. Left anterior oblique view of the 3D CT angiography shows the left common carotid artery (LCCA) (*white arrow*) originating from a common trunk with the brachiocephalic artery (BCA). LSA, left subclavian artery; RCC, right common carotid artery; RSA, right subclavian artery.

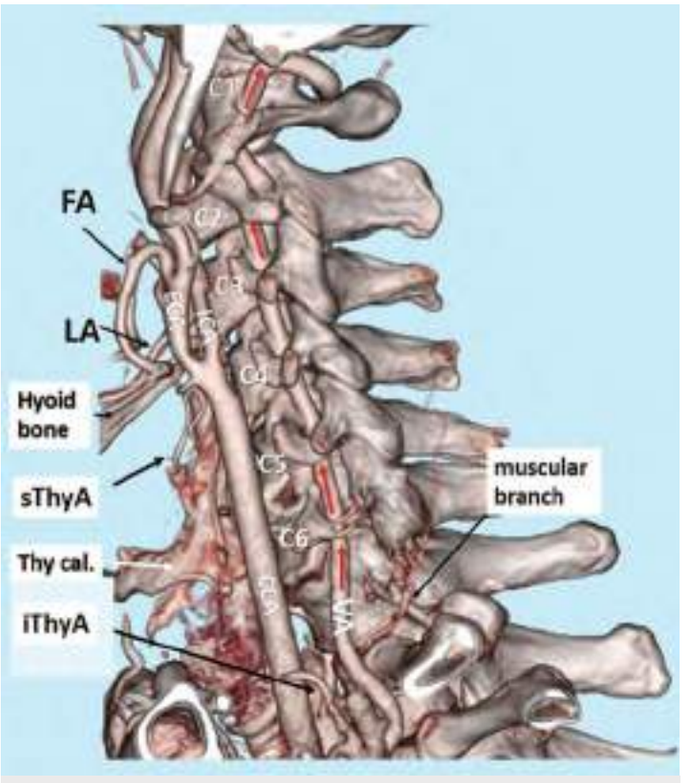

Fig. 8.6 Lateral view of the 3D CT angiography at the cervical portion of the vertebral and carotid arteries. The vertebral artery (VA) runs upward through the transverse foramens of the C6–C1 vertebrae (*arrows*), and into the intracranial space through the foramen magnum. FA, facial artery; iThyA, inferior thyroid artery; LA, lingual artery; sThyA, superior thyroid artery; Thy cal, thyroid cartilage.

the outer margin of the first rib. The brachial plexus also passes between anterior and middle scalene muscles and runs along the subclavian artery. Thoracic outlet syndrome can occur by compression of the subclavian artery and/or the brachial plexus between the anterior and middle scalene muscles and/or between the first rib and clavicle causing pain, weakness of the hand and arm, and discoloration of the hand.[13]

Left Common Carotid Artery and the Left Subclavian Artery

The left common carotid artery and the left subclavian artery are the second and the third branches originating from aortic arch, respectively. Both run superolaterally from the superior mediastinum to the neck, and then run on a path similar to the contralateral side. The left common carotid artery can originate from the brachiocephalic artery in 10% of cases. This branching type is called "bovine arch" (▶ Fig. 8.5).[14]

Branches of the Subclavian Arteries

The subclavian arteries give off various branches supplying the neck, shoulder, chest wall, and brain.

The Vertebral Artery

The vertebral artery is the first branch arising from the upper part of the proximal portion of the subclavian artery, which ascends through the transverse foramen of the sixth cervical vertebra (▶ Fig. 8.6, ▶ Fig. 8.7). It runs upward into the posterior fossa through the foramen magnum and joins the contralateral vertebral artery to form the basilar artery. The cervical portion of the vertebral artery gives off branches to the adjacent muscles (muscular branches), vertebrae (vertebral branches), spinal cord (anterior and posterior spinal arteries), and cervical nerves (radicular arteries) (▶ Fig. 8.7).[15] The posterior meningeal artery supplying the dura matter of the posterior fossa, and the posterior inferior cerebellar artery supplying the medulla and cerebellum arise from distal portion of the vertebral artery around the craniocervical junction.

The Internal Thoracic Artery

The internal thoracic artery (internal mammary artery) originates from the proximal portion of the subclavian artery across the origin of the thyrocervical trunk (▶ Fig. 8.3). It passes behind the subclavian vein and the first rib and descends in the anterior chest wall along the lateral margin of the sternum. It supplies the anterior chest wall, mediastinum, sternum, and thymus, before terminating into the musculophrenic and superior epigastric arteries (▶ Fig. 8.8).[16] It may arise from a common trunk with the suprascapular or inferior thyroid arteries.

The Thyrocervical Trunk

The thyrocervical trunk, the second ascending branch of the subclavian artery, originates at the inner border of the anterior

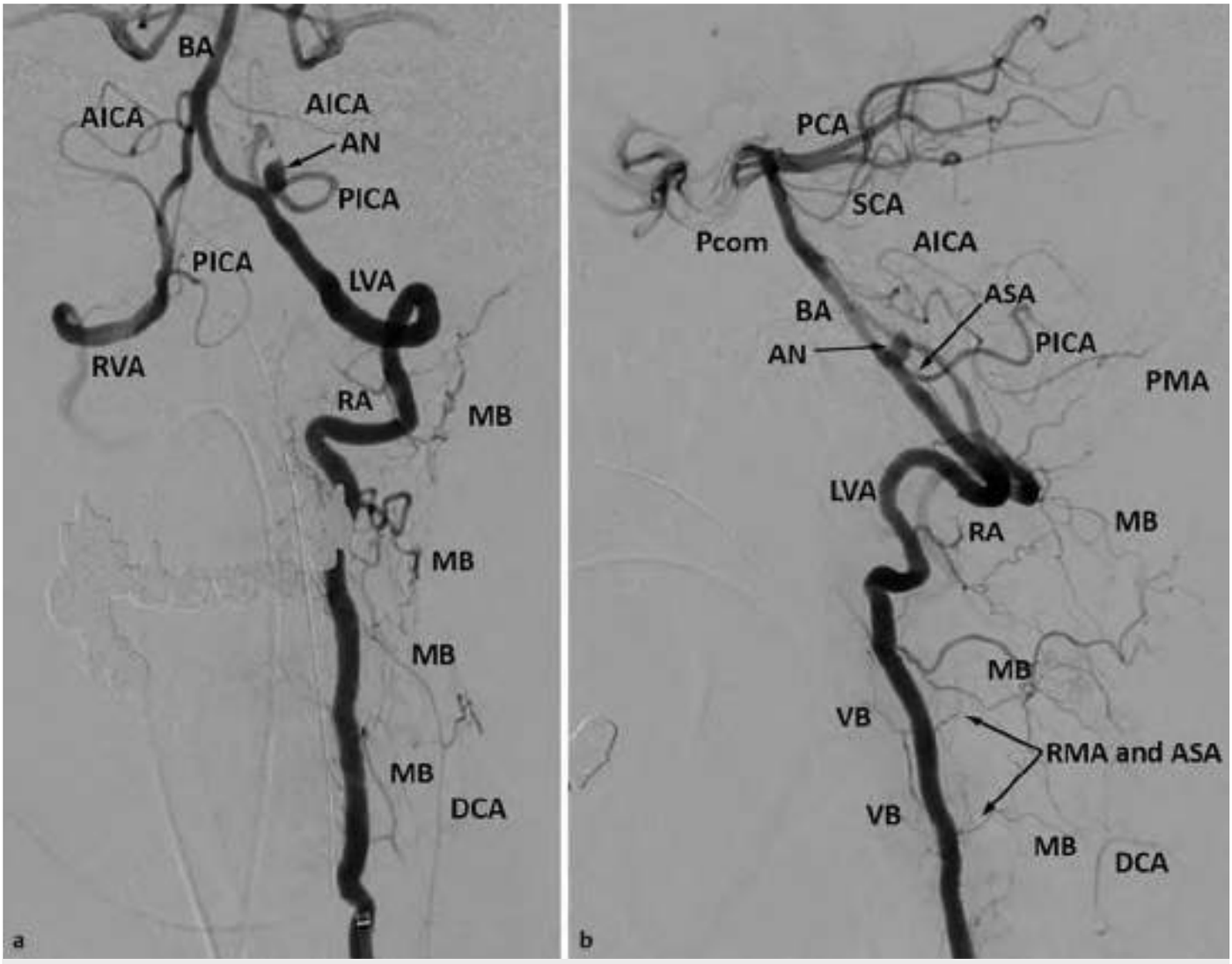

Fig. 8.7 **(a)** Frontal and **(b)** lateral views of the left vertebral angiography in a patient with an aneurysm at the posterior inferior cerebellar artery (PICA). The left vertebral artery runs upward with forming two bends at the C1 and C2 vertebrae, and then it moves medially and joins the right vertebral artery to form the basilar artery. Multiple muscular branches (MB) originate from the cervical portion of the vertebral artery, some of which anastomose with the deep cervical artery (DCA), the ascending cervical artery, and the occipital artery. Vertebral branches (VB) and epidural branches supplying the vertebral body and epidural space arise from the vertebral artery at each segment. The vertebral artery also gives off branches of radicular artery (RA) supplying the cervical nerves, and the radiculomedullary artery (RMA) and the radiculopial artery contiguous with the anterior spinal artery (ASA) and the posterior spinal artery, respectively. The posterior meningeal artery arising at the craniocervical junction distributes to the dura matter of the posterior fossa. The PICA usually originates at the intracranial portion of the vertebral artery, which supplies the medulla, cerebellar tonsil, vermis, and inferior portion of the cerebellar hemisphere. A small aneurysm (AN) at the origin of the PICA is noted. AICA, anterior inferior cerebellar artery; BA, basilar artery; LVA, left vertebral artery; PCA, posterior cerebral artery; Pcom, posterior communicating artery; PMA, posterior meningeal artery; RVA, right vertebral artery; SCA, superior cerebellar artery.

scalene muscle. The thyrocervical trunk is the short common trunk for four important arterial branches including the inferior thyroid artery, the ascending cervical artery, the suprascapular artery, and the transverse cervical artery (▶ Fig. 8.3, ▶ Fig. 8.9). The inferior thyroid artery runs superomedially and gives off branches to the inferior part of the thyroid gland, larynx, trachea, and the esophagus. The ascending cervical artery ascends behind the carotid sheath to the transverse process of the cervical vertebra. The ascending cervical artery gives off small muscular and vertebral branches and provides anastomotic arteries with branches of the vertebral artery. It may give off a branch to the spinal cord, an anterior or posterior spinal artery. The suprascapular artery and the transverse cervical artery run laterally and supply the surrounding muscles and bony structures. These arteries occasionally arise independently from the subclavian artery at its distal portion. The dorsal scapular artery can arise from the transverse cervical artery in approximately 30% of cases.[17]

The Costocervical Trunk

The costocervical trunk arises from posterosuperior aspect of the subclavian artery. It divides into the deep cervical artery and the highest (superior) intercostal artery (▶ Fig. 8.1, ▶ Fig. 8.10). The deep cervical artery runs posteriorly between the first rib and transverse process of the seventh cervical vertebra, and then ascends deeply in the posterior cervical space (▶ Fig. 8.3,

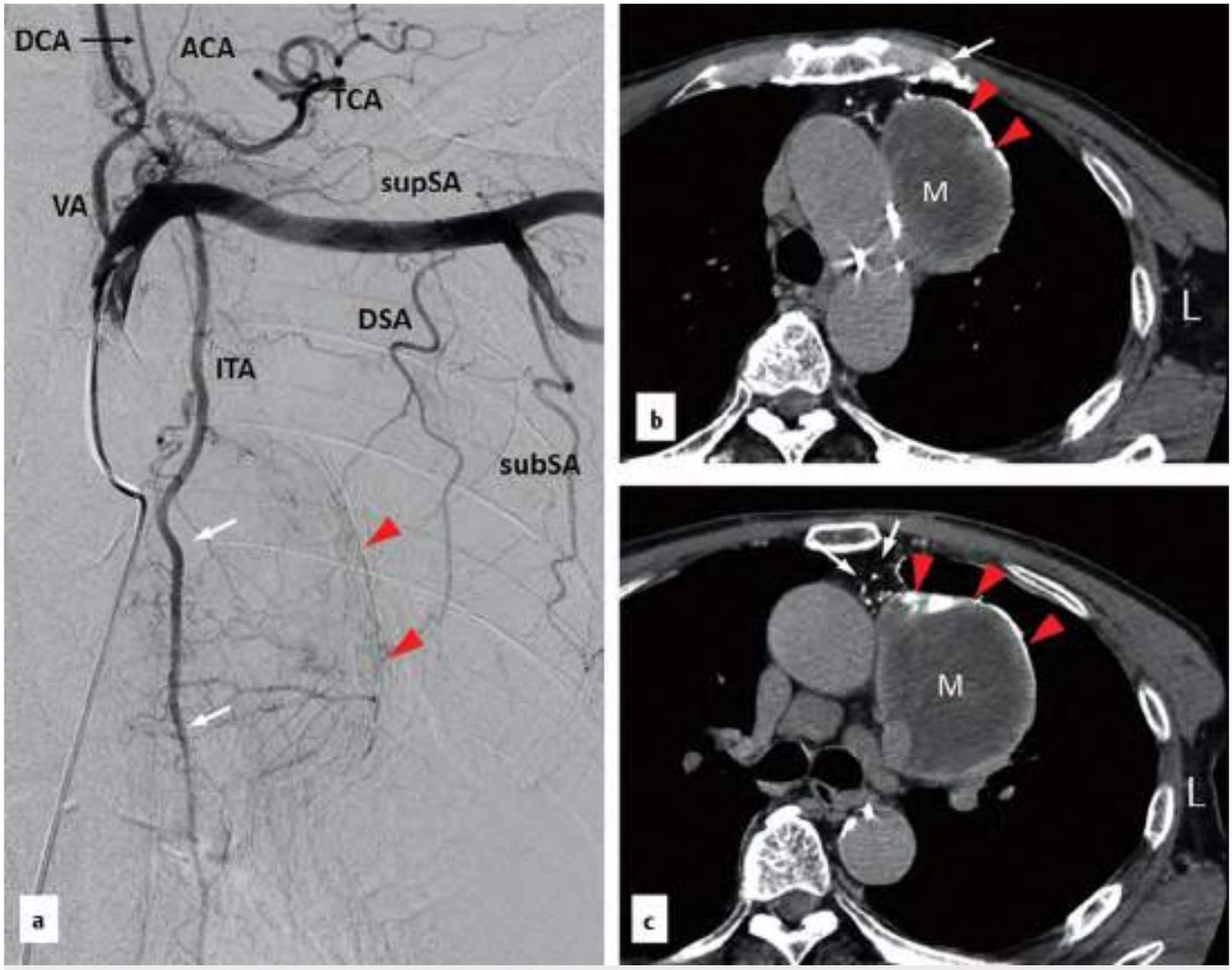

Fig. 8.8 The internal thoracic artery (*white arrows*) and arterial territory. **(a)** Left subclavian angiography and **(b, c)** CT during internal thoracic angiography in a patient with a large mediastinal tumor (*red arrows*). Left subclavian angiography demonstrates that the internal thoracic artery (*white arrows*) gives off multiple mediastinal branches supplying a large mass. The internal thoracic artery also supplies the anterior mediastinum, parietal pleura, and sternocostal junction. ACA, ascending cervical artery; DCA, deep cervical artery; DSA, dorsal scapular artery; ITA, internal thoracic artery; subSA, subscapular artery; supSA, suprascapular artery; TCA, transverse cervical artery; VA, vertebral artery.

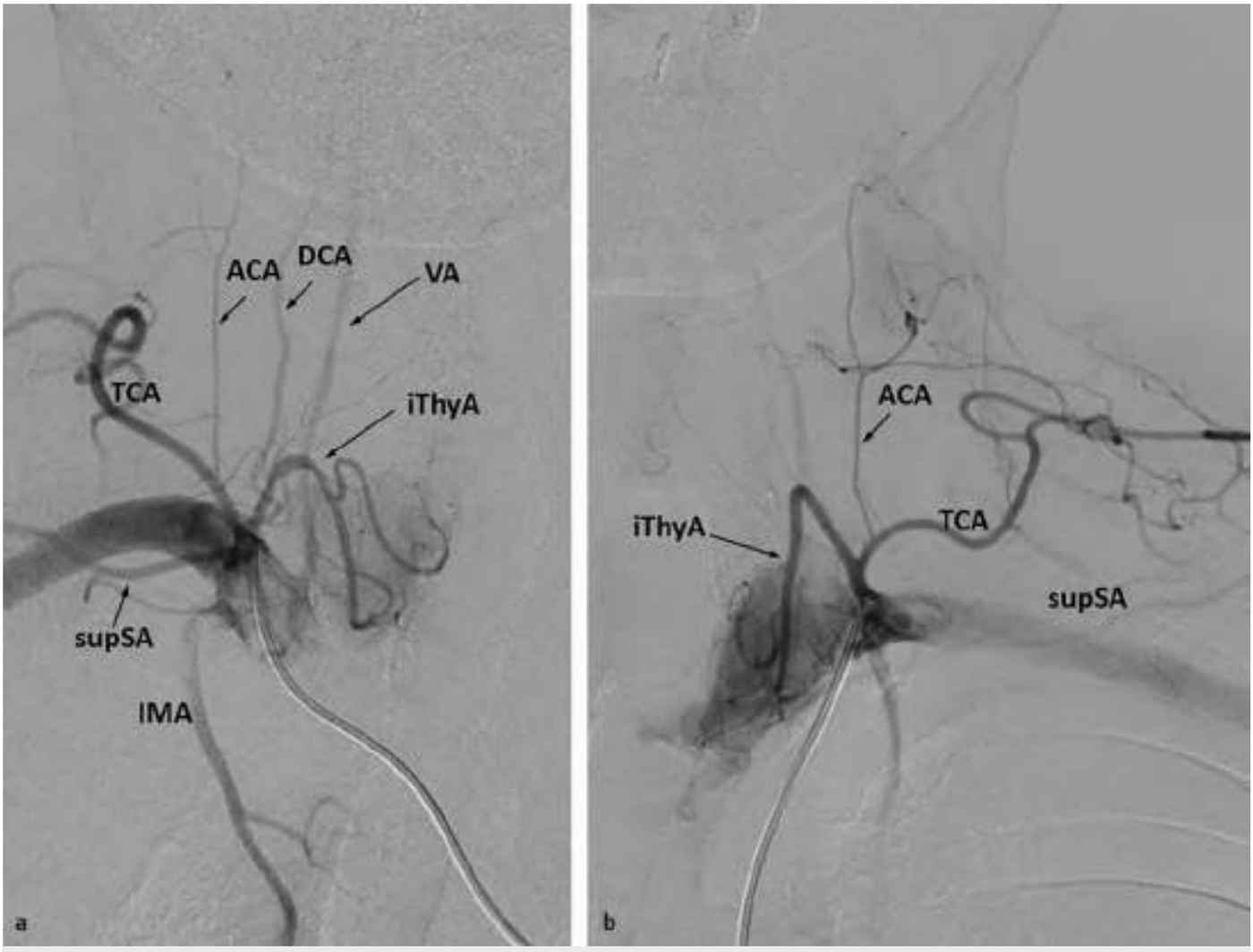

Fig. 8.9 Selective angiography of the thyrocervical trunk. **(a)** Right thyrocervical trunk and **(b)** left thyrocervical trunk. The thyrocervical trunk consists of three major branches of inferior thyroid artery (iThyA), transverse cervical artery (TCA), and the suprascapular artery (supSA). In both sides, the ascending cervical artery (ACA) arises from the transverse cervical artery. Note the contrast brush of the thyroid gland supplied by the inferior thyroid artery. DCA, deep cervical artery; VA, vertebral artery.

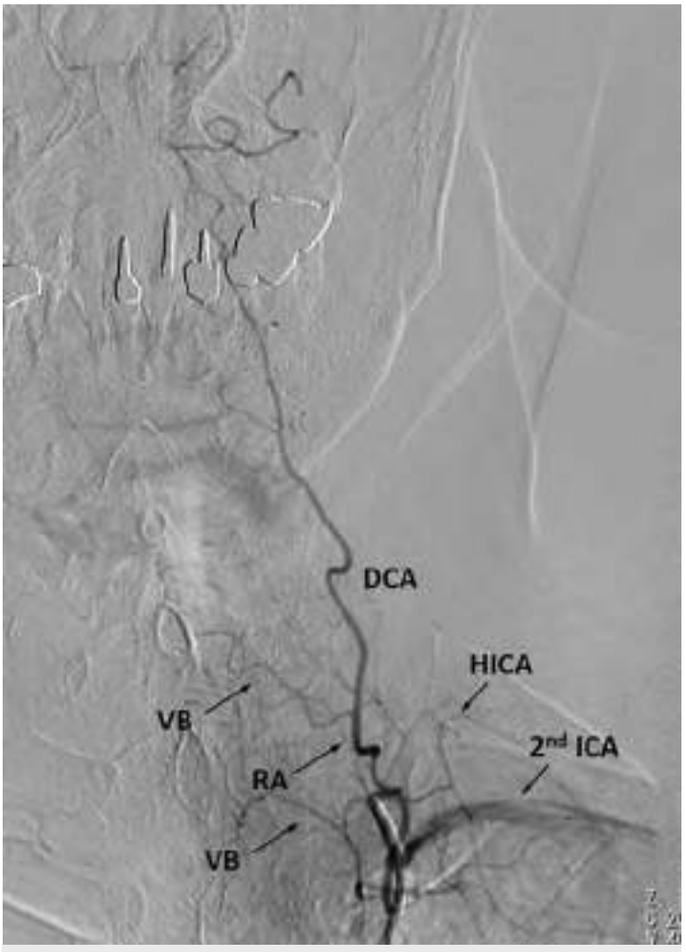

Fig. 8.10 Selective angiography of the left costocervical trunk. DCA, deep cervical artery; HICA, highest intercostal artery; 2nd ICA, second intercostal artery; VB, vertebral body branch; RA, radicular artery.

▶ Fig. 8.10). It supplies the posterior cervical muscles and anastomoses with the muscular branches of the vertebral and occipital arteries (▶ Fig. 8.7). It may give off an anterior or posterior spinal artery between the seventh cervical and first thoracic vertebrae (▶ Fig. 8.11). The deep cervical artery is occasionally absent, which can be replaced by other branches such as the superficial branches of the transverse cervical artery. The highest intercostal artery descends in front of the first and second ribs and often anastomoses with an intercostal artery from descending aorta (▶ Fig. 8.10). It supplies adjacent muscles, bony structures, and gives off small spinal branches.

The Dorsal Scapular Artery

The dorsal scapular artery arises from the distal portion of the subclavian artery in more than 60% of cases. It runs posteriorly to supply the levator scapulae muscle and the rhomboid muscle (▶ Fig. 8.1, ▶ Fig. 8.8). The dorsal scapular artery may originate from the transverse cervical artery in 30% of cases (▶ Fig. 8.4).[17] It then descends to supply the medial part of the scapula and anastomoses with the intercostal arteries and branches of the subscapular artery from the axillar artery.

◆ Descending Thoracic Aorta

The descending thoracic aorta is continuous with the aortic arch at the level of the fourth thoracic vertebra. It descends in the posterior mediastinum to reach the aortic hiatus of the diaphragm at the lower border of the 12th thoracic vertebra where it becomes the abdominal aorta. The descending aorta lies on the left of the vertebral column at its beginning, and it descends medially. It lies in front of the vertebral column at its termination. It gives off segmental intercostal arteries, and arteries to the bronchi and esophagus (▶ Fig. 8.1).

Branches from Descending Aorta

Intercostal and Subcostal Arteries

The nine paired segmental arteries from the 3rd to 11th intercostal artery originate from the descending aorta, which supply the intercostal spaces, vertebral body, paravertebral muscle, nerve roots, and spinal cord (▶ Fig. 8.12). The subcostal arteries below the 12th ribs supply the flat abdominal wall muscles. There are longitudinal paravertebral and epidural anastomoses between the intercostal arteries at consecutive levels. There are also transverse anastomoses between the paraspinal and epidural arteries on each side communicating the intercostal arteries with the contralateral ones (▶ Fig. 8.13).[14]

The intercostal artery divides into two branches named intercostal/lateral muscular branch and the dorsal spinal branch. The dorsal spinal branch further divides into the dorsal, epidural, meningeal, and radiculomeningeal branches, and sometimes radiculopial (posterior spinal) or radiculomedullary (anterior spinal) arteries (▶ Fig. 8.12). The artery of Adamkiewicz is the name given to the largest radiculomedullary artery that supplies the spinal cord.[14,18] It ascends medially to the anterior surface of the spinal cord along with the nerve root, and then continues along the anterior spinal artery forming a typical “hairpin turn” at the midline (▶ Fig. 8.14). The artery of Adamkiewicz originates between T8 and L1 in 92% of cases. It is seen predominantly on the left side (70%).[19]

Bronchial Artery

Paired bronchial arteries usually arise from the descending aorta, which supply the bronchial and peribronchial tissues and visceral pleura (▶ Fig. 8.1, ▶ Fig. 8.15).[20] The left bronchial arteries most commonly arise directly from the descending aorta. The right bronchial arteries often originate from a common trunk with an intercostal artery. Common trunk of the bilateral bronchial arteries is also seen in about 35% of cases (▶ Fig. 8.15**b**).[12] Some individuals show ectopic bronchial arteries which most often originate from inferior aspect of the aortic arch, followed by the brachiocephalic, and coronary arteries (▶ Fig. 8.16, ▶ Fig. 8.17). Knowledge of the ectopic origin of the bronchial artery is important for successful bronchial artery embolization for a massive hemoptysis (▶ Fig. 8.16).

Fig. 8.11 Radiculomedullary artery arising from the costocervical trunk. **(a)** Frontal view of the selective angiography and **(b)** coronal maximum intensity projection (MIP) image of the rotational angiography of the costocervical trunk. The radiculomedullary artery (RMA) arising at the origin of the deep cervical artery (DCA) runs superomedially into the intervertebral foramen between the C7 and Th1 vertebrae, and then continues to the anterior spinal artery (ASA, *arrowheads*). Note a radiculomeningeal branch (Mening B) running parallel to the radiculomedullary artery and terminating at the dural sleeve.

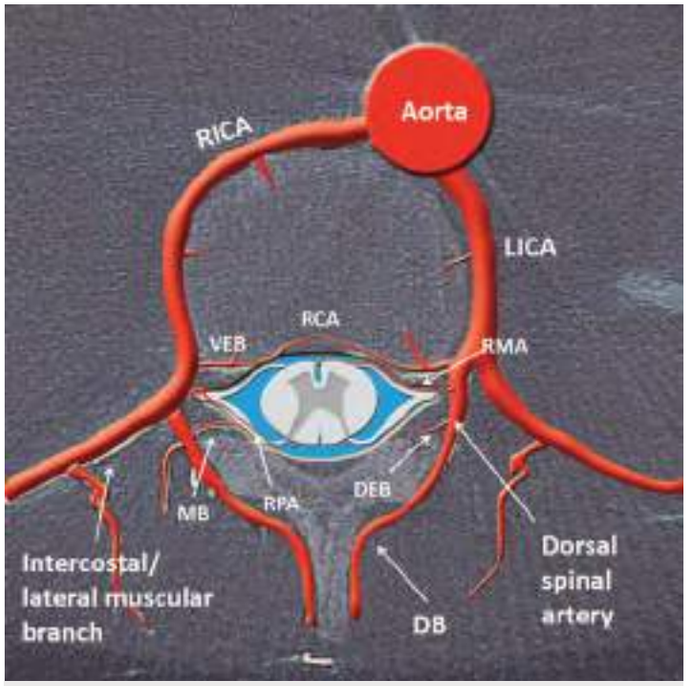

Fig. 8.12 Schematic drawing of the branches of the intercostal/lumbar artery. MB, meningeal branch; DEB, dorsal epidural branch; DB, dorsal branch; R(L)ICA, right (left) intercostal artery; RCA, retrocorporeal anastomosis; RMA, radiculomedullary artery; RPA, radiculopial artery; VEB, ventral epidural branch (image being drawn.)

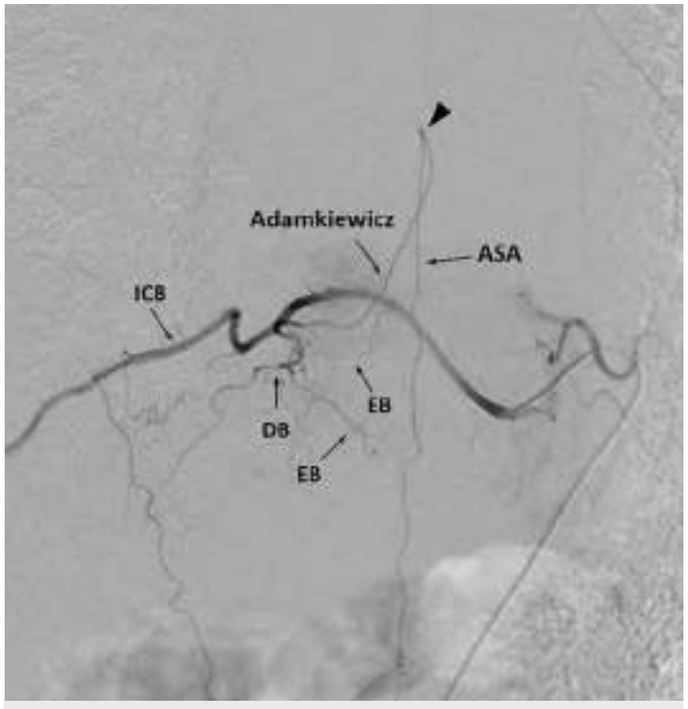

Fig. 8.14 Adamkiewicz artery. Right 10th intercostal artery gives off the artery of Adamkiewicz (the largest radiculomedullary artery) continuous with the anterior spinal artery (ASA) with an acute curvature ("hairpin turn") (arrowhead). EB, epidural branch; DB, dorsal branch; ICB, intercostal branch.

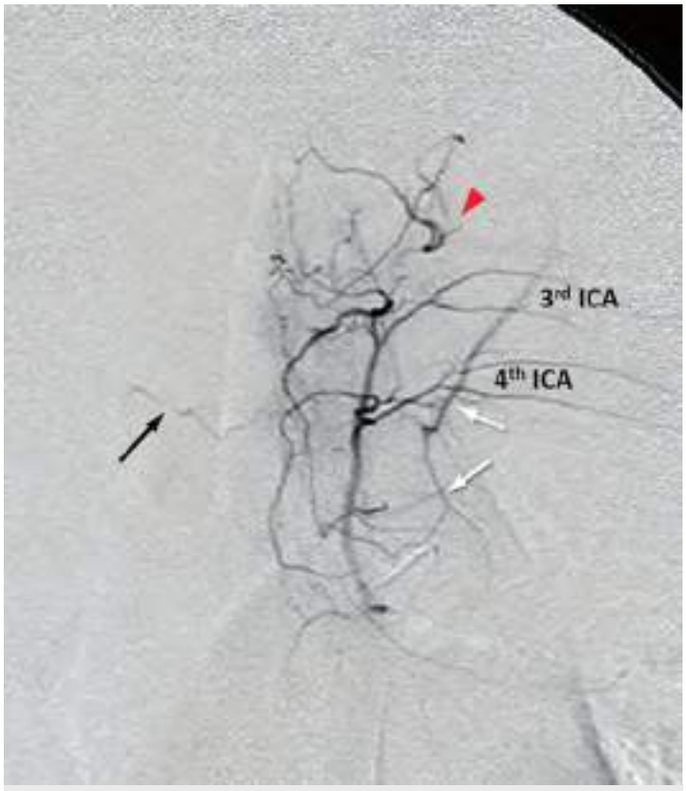

Fig. 8.13 Longitudinal paravertebral anastomosis of the intercostal arteries. Selective angiography of the left fourth intercostal angiography shows the left fourth and third intercostal arteries (fourth ICA and third ICA) with a large longitudinal anastomosis. The left second intercostal artery (*arrowhead*) and the right fourth intercostal artery (*black arrow*) are also partially opacified via the dorsal paravertebral anastomosis and the retrocorporeal epidural anastomosis, respectively. Note opacification of left bronchial artery (*white arrows*) via paravertebral anastomoses.

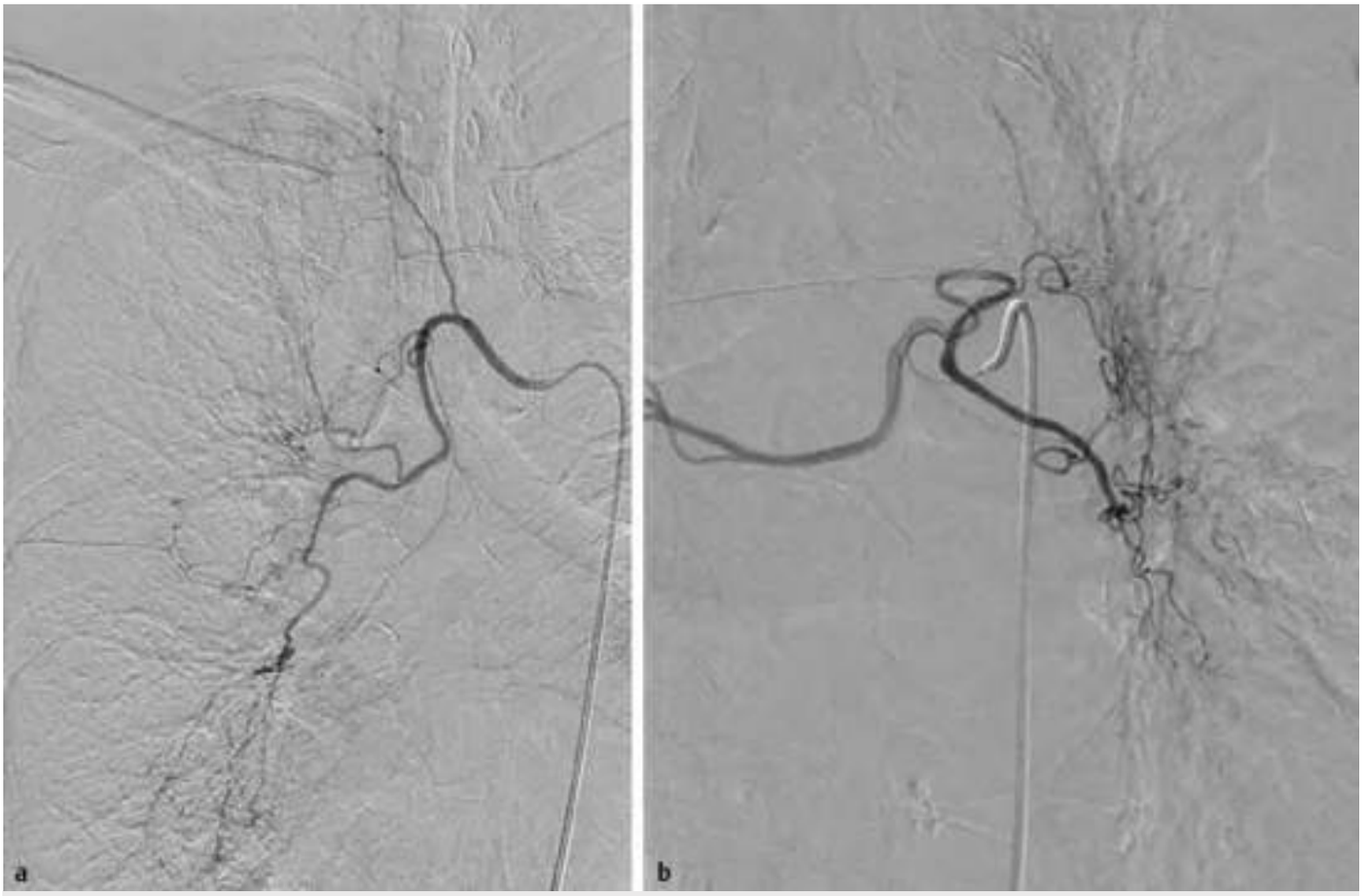

Fig. 8.15 **(a)** Right bronchial artery in a patient with chronic bronchitis. Selective right bronchial angiography shows the right bronchial artery originating directly from the descending aorta at the level of the tracheal bifurcation. The right bronchial artery is enlarged and form multiple bronchial–pulmonary arterial shunts. **(b)** Common trunk of the right and left bronchial arteries. Selective bronchial angiography shows both bronchial arteries originating at a common trunk.

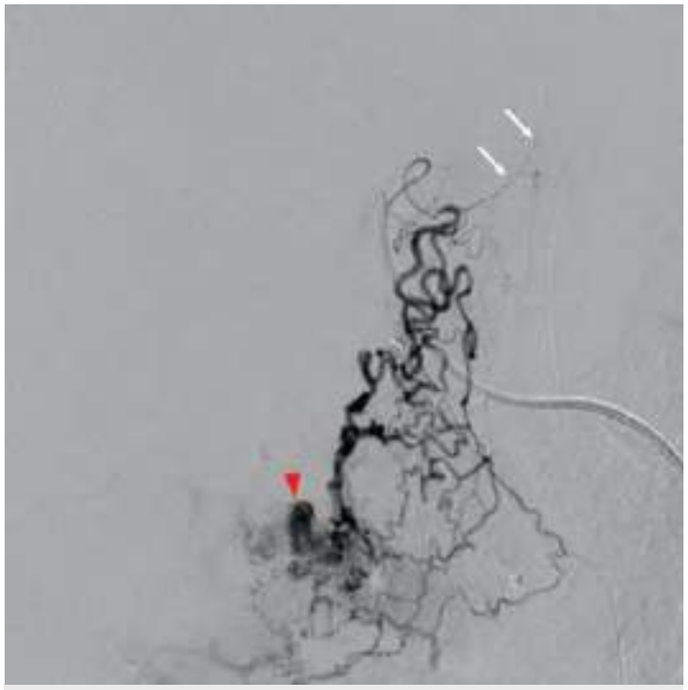

Fig. 8.16 Bronchial artery originating from the brachiocephalic artery in a patient with massive hemoptysis due to bronchiectasis and chronic bronchitis. Selective angiography of the bronchial artery originating from the brachiocephalic artery shows the dilated branches shunting to the pulmonary arterial branches. A pseudoaneurysm (*arrowhead*) is noted. Arrows indicate partial opacification of the thyroid ima artery.

Other Small Branches of Descending Aorta

Other small branches can arise from the descending aorta. These arteries, usually too small to be resolved using current imaging techniques, can only be seen when become dilated: the mediastinal arteries supplying the lymph nodes and loose areolar tissue in the posterior mediastinum, the esophageal arteries arising anteriorly to supply the esophagus, the pericardial branches supplying the dorsal pericardium, and the superior phrenic arteries supplying the superior surface of the diaphragm.

◆ Embryological Development

The two endocardial heart tube and dorsal aorta are formed in mesodermal layer of the cranial end of the embryonic disc on around 19 days. Subsequently, the two endocardial tubes fuse to form the primitive heart tube by lateral folding of the embryonic disc (▶ Fig. 8.18).[21,22] On day 21, longitudinal folding of the embryo occurs, which results in 180-degree turn in the cephalic region (▶ Fig. 8.19).[21] Because of the longitudinal folding, the brain comes to lie in the most cranial portion of the embryo, followed by the pharynx, heart, and diaphragm. The longitudinal folding also creates a loop in the dorsal aorta and rotates it from the caudal end to the cranial end of the heart tube. The primitive heart tube can be divided into five parts including the sinus venosus, the primitive atrium, the primitive ventricle, the bulbus cordis, and the truncus arteriosus. The bulbus cordis extends cranially into the truncus arteriosus through which is connected to

Fig. 8.17 Bronchial artery aneurysm originating from aortic arch in a patient with bronchiectasis. **(a)** Left lateral oblique view of CT angiography and **(b)** selective angiography of the bronchial artery show a large aneurysm at the origin of the bronchial artery which is arising at the inferior aspect of the aortic arch. The aneurysm located just below the aortic arch, and the distal portion of the bronchial artery and its branches are also enlarged and tortuous.

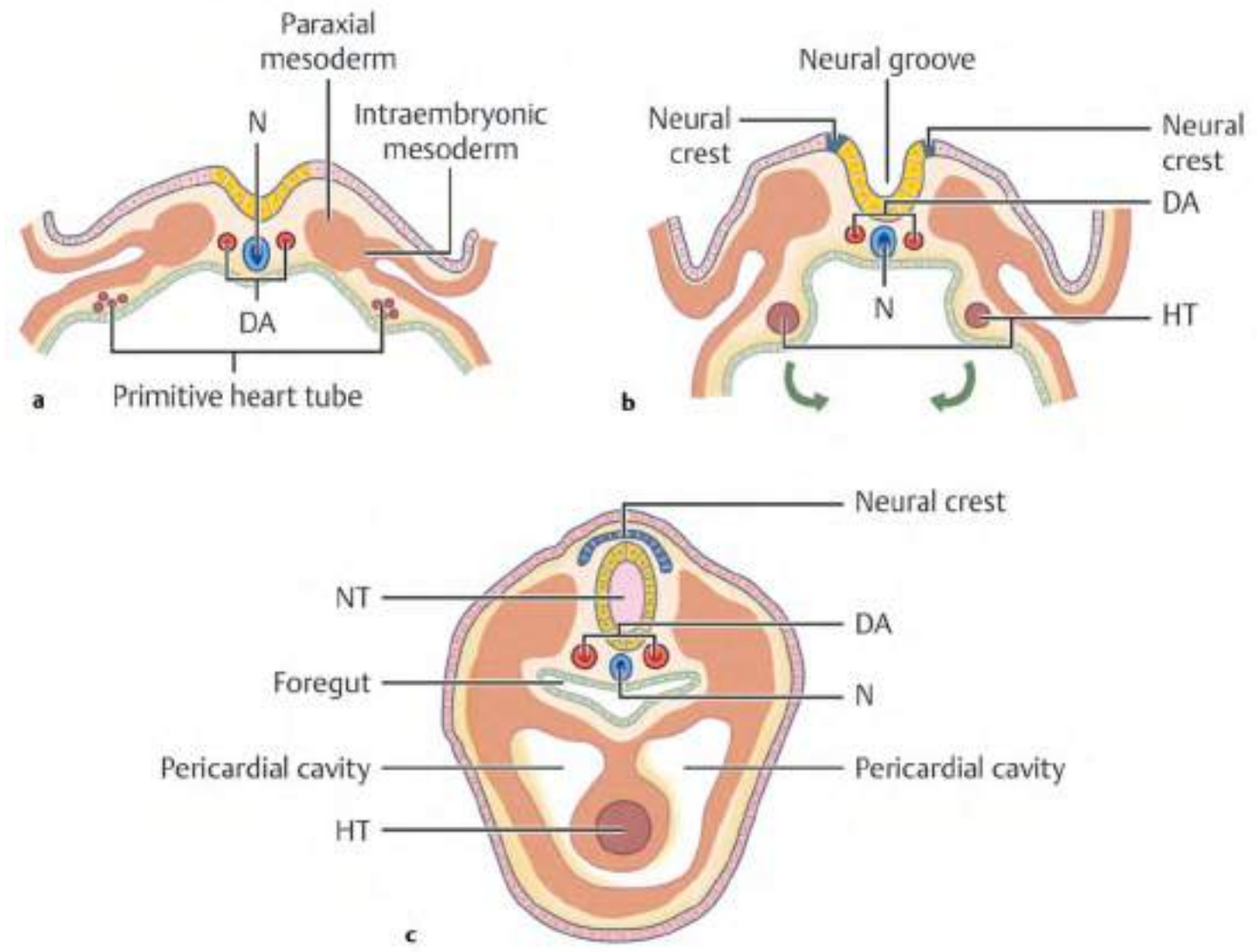

Fig. 8.18 Schematic drawing of development of heart tube on axial plane during lateral folding. **(a)** Capillaries forming future primitive heart tube appear in the mesoderm of the cranial end of the flat embryonic disc on each side. These capillaries fuse and four vascular channels appear on both sides which form the dorsal aortas (DA) and heart tubes. **(b)** The flat embryonic disc transforms into a tubular structure during the fourth week of development. With lateral folding, the lateral edges of the germ disk approach each other and the two heart tubes (HT) approach each other in midline. **(c)** Two heart tubes are fused and form a single heart tube. N, notochord.

the aortic sac. The aortic sac is connected to the dorsal aorta through the aortic arches. Looping of the primitive heart tube occurs within the pericardial sac on approximately day 23. The cranial parts of the heart tube bend ventrally and caudally and to the right, and the caudal part of the tube including the atrium and sinus venosus come to lie dorsal to the bulbus cordis, truncus arteriosus, and ventricle (▶ Fig. 8.20). Reversal of the heart looping can occur, which results in dextrocardia where the left ventricle ends up locating to the right rather than the left.

The truncus arteriosus is continuous with the aortic sac from which six arch arteries arise on each side. Each of the arch arteries runs in the corresponding pharyngeal arch and connects to the dorsal aorta. Among the arch arteries, the fifth arch arteries disappear bilaterally. The first and the second arch arteries regress and their remnants form distal branches of the external carotid artery including the maxillomandibular arteries, and the middle meningeal artery.[23] The third arch arteries form the common carotid artery and the origin of the internal carotid artery. The left fourth arch artery forms the distal main part of the aortic arch, and the right fourth arch artery forms the right subclavian artery (▶ Fig. 8.21). The left seventh segmental artery forms the left subclavian artery. The proximal part of the sixth arch arteries forms the pulmonary artery on each side. The distal part of the left sixth arch forms the ductus arteriosus while it disappears on the right side. The ductus arteriosus obliterates after birth. The aortic sac divides into two horns with the left horn forming the proximal part of the aortic arch, and the right horn forming the brachiocephalic artery. The ascending aorta and the most proximal part of the aortic arch, and the pulmonary trunk are formed by division of the truncus arteriosus. Two truncobulbar (outflow tract) cushions, derived from neural crest cells, in association with the pharyngeal arches 4 and 6, grow toward each other and fuse to form a spiral-shaped septum throughout the outflow tract (truncus arteriosus and bulbus cordis), which divides it into the aorta and main pulmonary artery. The distal part of the main pulmonary artery is located left laterally to the aorta, and the

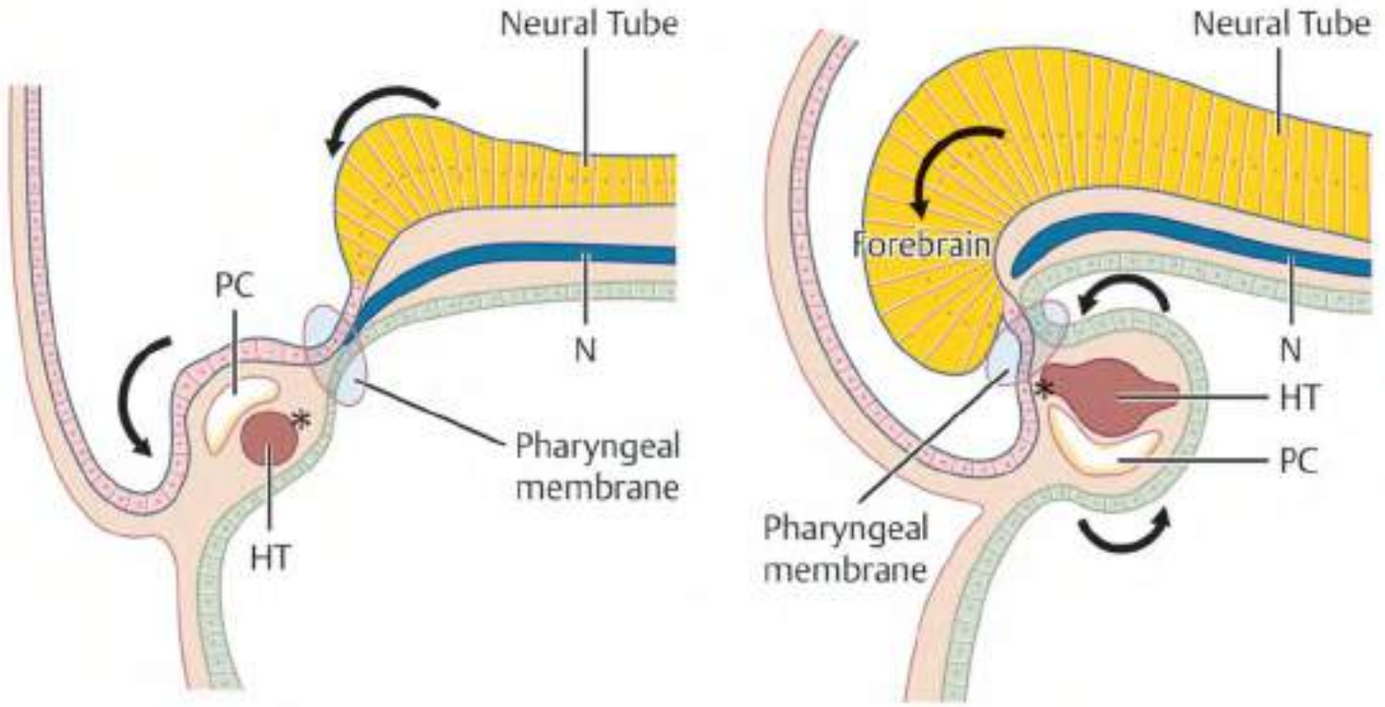

Fig. 8.19 Schematic drawing of longitudinal folding and rotation of the heart tube. Because of rapid growing of the embryo in long axis especially in the dorsal region, the embryo forms a C-shaped curve. As a result of longitudinal folding, the brain (forebrain) comes to lie in most cranial portion of the embryo, and followed by the pharyngeal membrane, heart tube (HT), and diaphragm. The junction between the heart tube and the dorsal aorta (asterisk) rotates from caudal end to the cranial end of the heart tube.

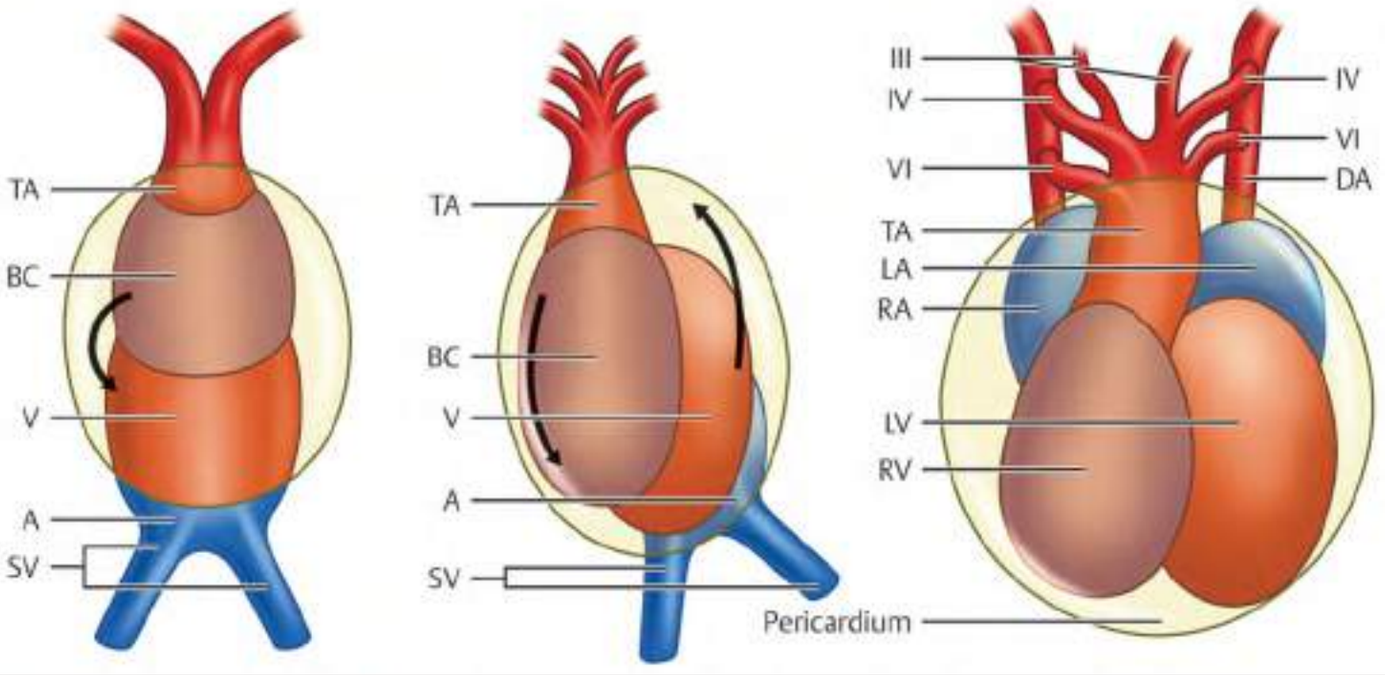

Fig. 8.20 Schematic drawing of formation of the heart loop from 22nd to 24th days. The cranial parts of the tube such as bulbus cordis bends ventrally and caudally and to the right, and the caudal parts (atrium and sinus venosus) move dorsally. Finally, four chambers of heart are arranged in their final position within the pericardium. A, primitive atrium; BC, bulbus cordis; SV, sinus venosus; TA, truncus arteriosus; V, primitive ventricle.

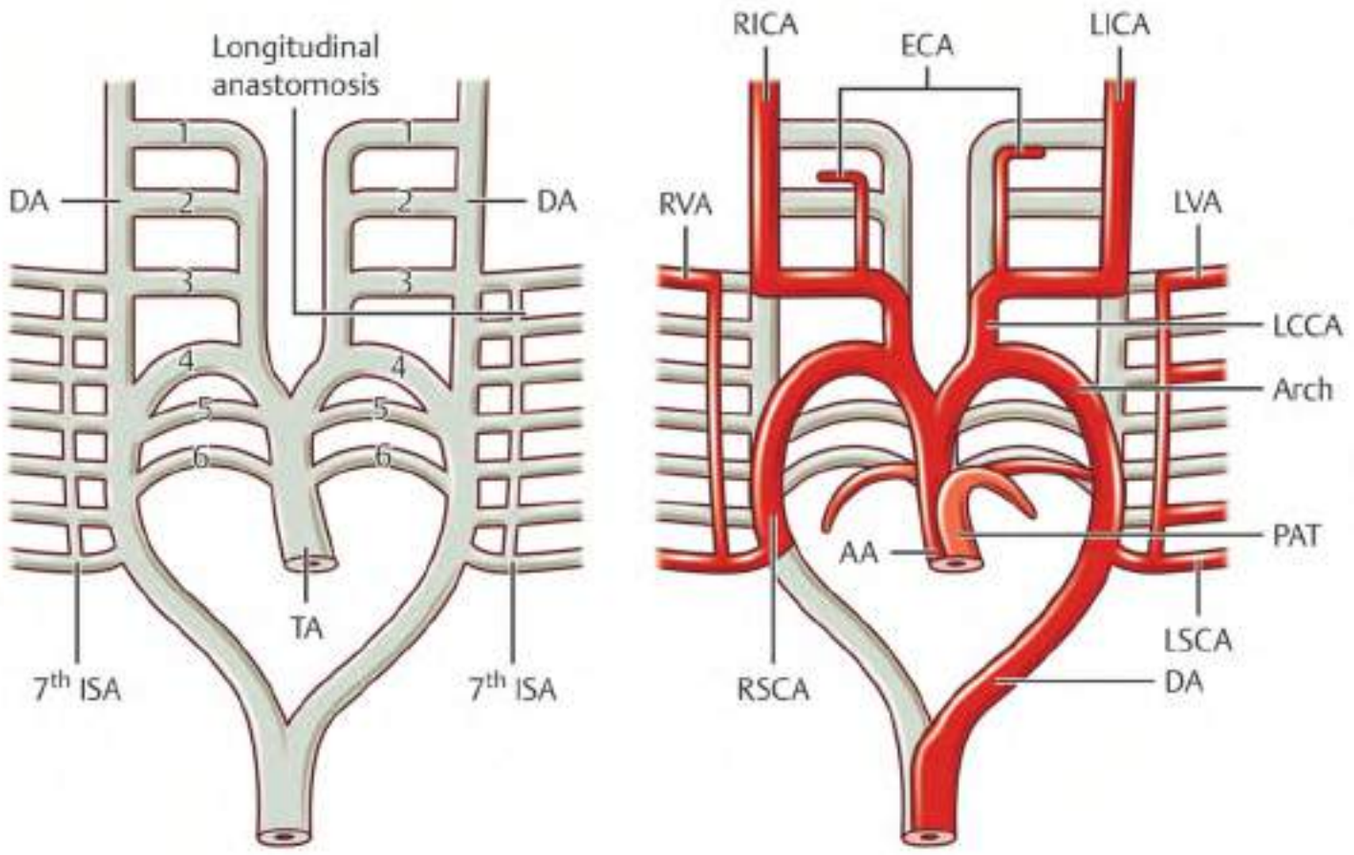

Fig. 8.21 Schematic drawing of primitive aortic arches and dorsal aorta, and normal developmental pattern of the aortic arches after the transformation. 1–6, first to sixth primitive aortic arch; DA, dorsal aorta; TA, truncus arteriosus; 7th ISA, seventh intersegmental artery. R(L)ICA, right (left) internal carotid artery; R(L)CCA, right (left) common carotid artery; ECA, external carotid artery; Arch, aortic arch; R(L)SCA, right (left) subclavian artery; R(L)VA, right (left) vertebral artery; AA, ascending aorta; PAT, pulmonary arterial trunk; DA, descending aorta.

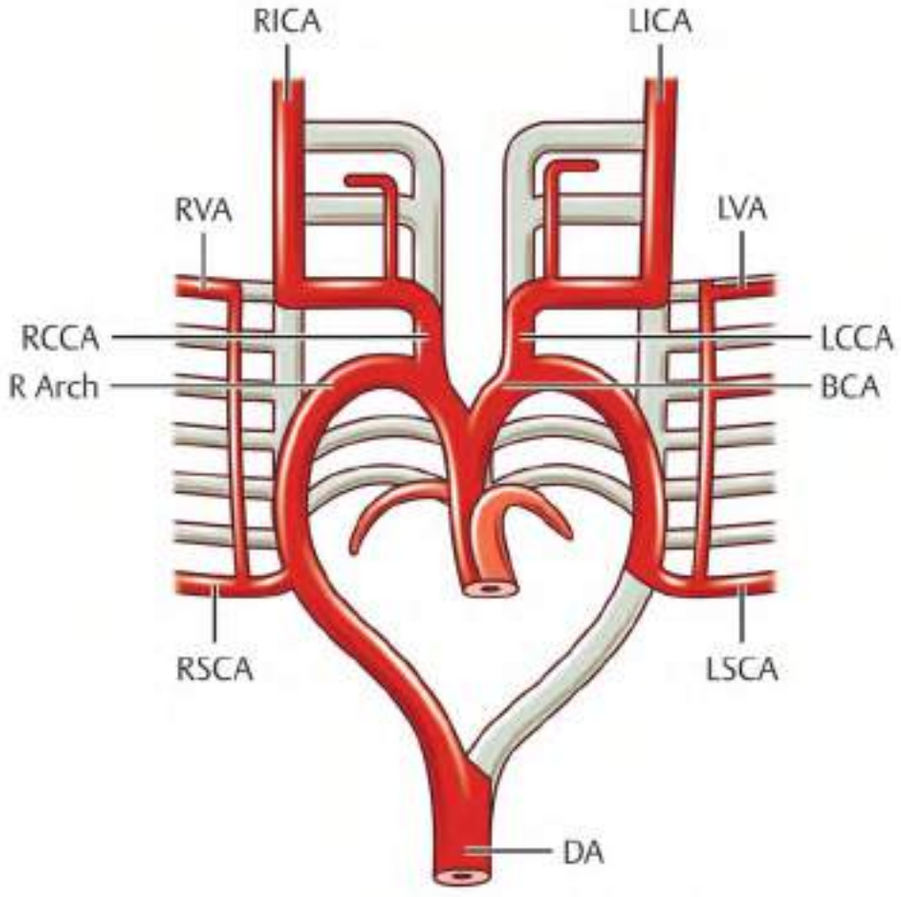

Fig. 8.22 Right aortic arch type 1. schematic drawing of development of the right aortic arch (type 1: mirror image branching pattern). Type 1 right aortic arch is caused by abnormal regression of the left dorsal aorta distally to the origin of the seventh intersegmental artery (further left subclavian artery). R(L)ICA, right (left) internal carotid artery; R(L)CCA, right (left) common carotid artery; R Arch, right aortic arch; R(L)SCA, right (left) subclavian artery; R(L)VA, right (left) vertebral artery; DA, descending aorta.

proximal part is located right anterolaterally to the aorta. Pulmonary and aortic valves are formed via cavitation of the truncobulbar cushion tissue in each of the outflow arteries.

Failure of this partition of outflow can cause several anomalies such as persistent truncus arteriosus, and transposition of the great vessels.[21,24] Abnormal arrangement of the regression of the arch arteries can cause several variations of aortic arch and the relevant major arteries.[25]

◆ Anatomical Variations and Anomalies

Right Aortic Arch

Right aortic arch accounts for 0.05 to 0.14% of population, caused by persistence of the right fourth arch artery and caudal part of the right dorsal aorta with abnormal regression of those of the left side.[26,27] Right aortic arch can be divided into the following three types: type 1, right-sided aortic arch with mirror image branching (▶ Fig. 8.22, ▶ Fig. 8.23); type 2, right-sided aortic arch with aberrant left subclavian artery (▶ Fig. 8.24, ▶ Fig. 8.25); and type 3, right-sided aortic arch with isolation of the left subclavian artery. Type 1 is the most common type approximately 59% of aortic arch, which is caused by interruption of the dorsal segment of the left arch between the seventh segmental artery (left subclavian artery) and the descending aorta. It is often associated with other anomalies such as persistent truncus arteriosus, or transposition of the great vessels. Type 2 is the second common type approximately 40% of right aortic arches, which is caused by interruption of the dorsal segment of the left arch between the left fourth arch artery (left common carotid artery) and the seventh segmental artery (left subclavian artery). Type 2 is often associated with an aneurysmal dilation at the origin of an aberrant left subclavian artery, the so-called "Kommerell's diverticulum," which is thought to be a remnant of the distal portion of the left arch (▶ Fig. 8.25). This type can cause symptoms due to compression of the esophagus. Type 3 is rare, less than 1%, which is caused by interruption of the left arch at two levels, with one level between the left fourth arch artery (common carotid artery) and the left seventh segmental artery (left subclavian artery) and the other level distal to the attachment of the left ductus.

Double Aortic Arch

Double aortic arch is the second common arch anomaly, caused by persistent right side arch artery (▶ Fig. 8.26). It often causes symptoms in childhood due to compression of trachea and esophagus. Approximately 20% of cases are associated with congenital heart diseases.[25]

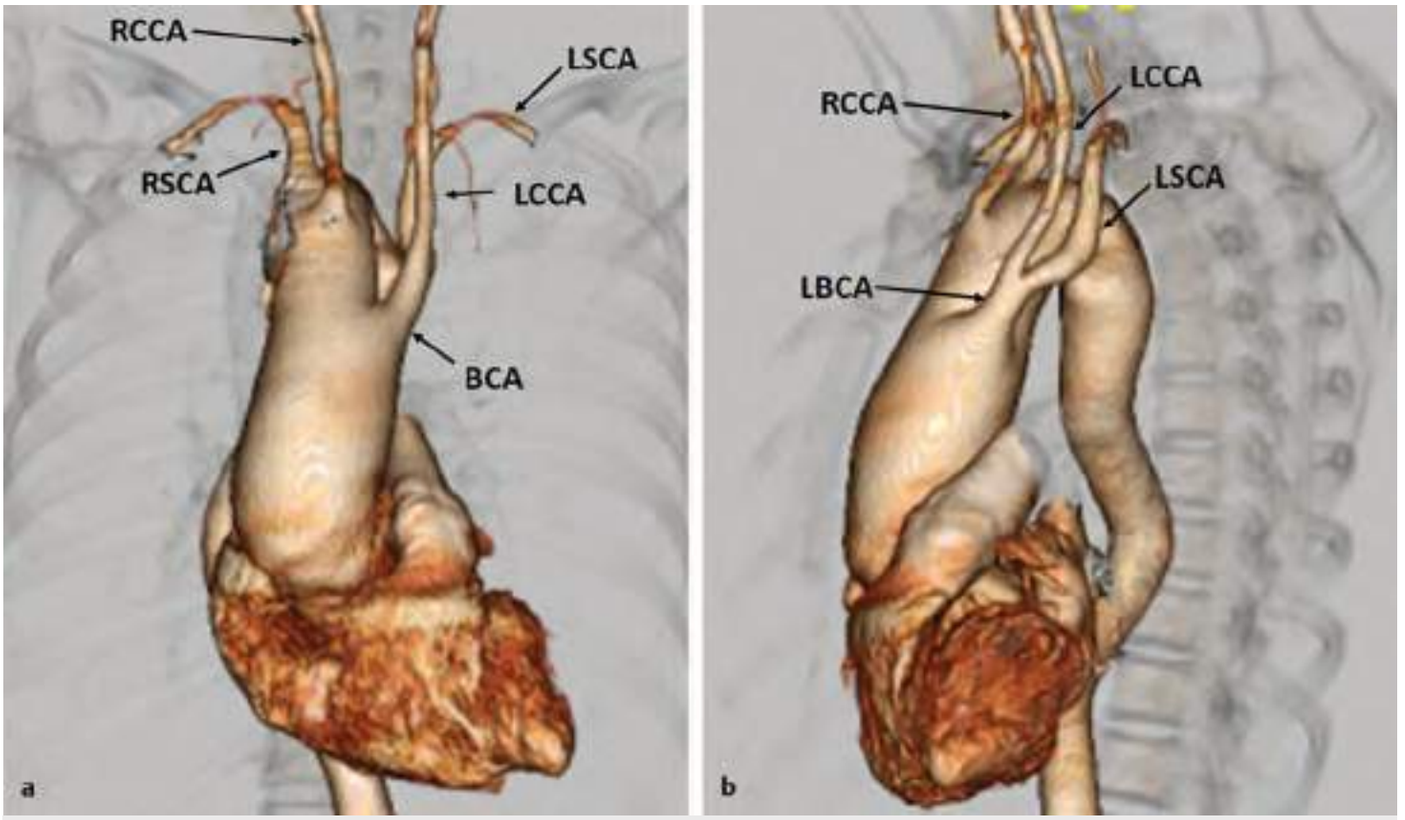

Fig. 8.23 Right aortic arch (type 1). **(a)** Frontal and **(b)** left anterior lateral views of the 3D CT angiography images show a right side aortic arch with major aortic branches ordered from proximal to distal as, the left brachiocephalic artery (LBCA), the right common carotid artery (RCCA), and the right subclavian artery (RSCA).

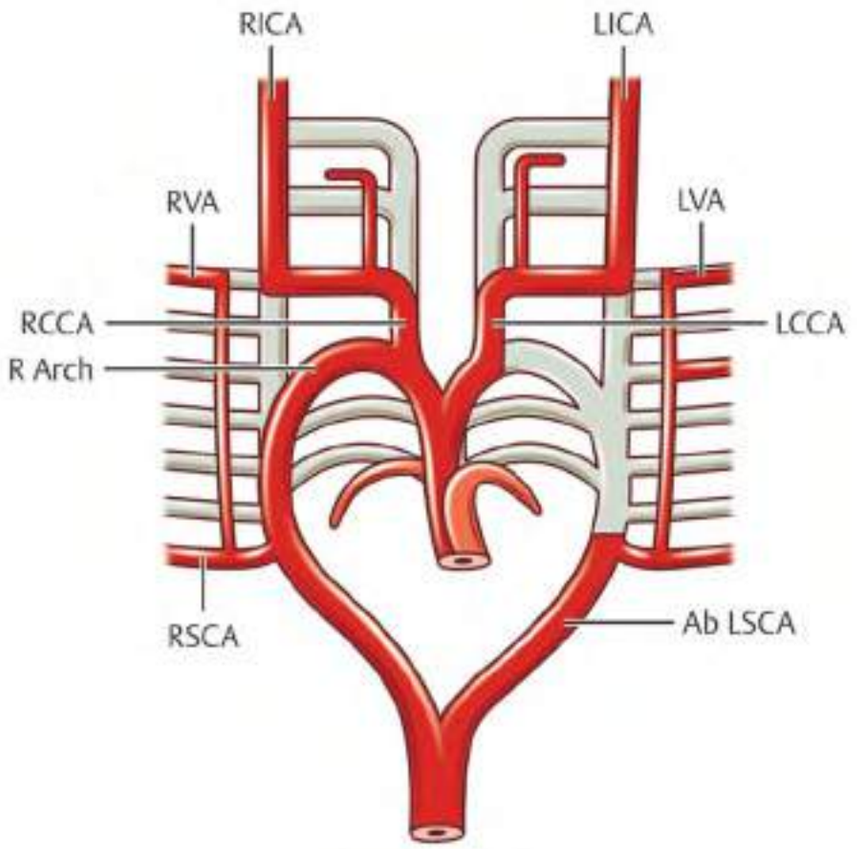

Fig. 8.24 Right aortic arch type 2 coexistence with aberrant left subclavian artery. Schematic drawing of development of the right aortic arch (type 2: mirror aberrant left subclavian artery pattern). Type 2 right aortic arch is caused by abnormal regression of the left fourth arch. The left subclavian artery is formed from the seventh intersegmental artery supplied via the remnant of the distal portion of the dorsal aorta. R(L)ICA, right (left) internal carotid artery; R(L)CCA, right (left) common carotid artery; R Arch, right aortic arch; RSCA, right subclavian artery; R(L)VA, right (left) vertebral artery; Ab LSCA, aberrant left subclavian artery.

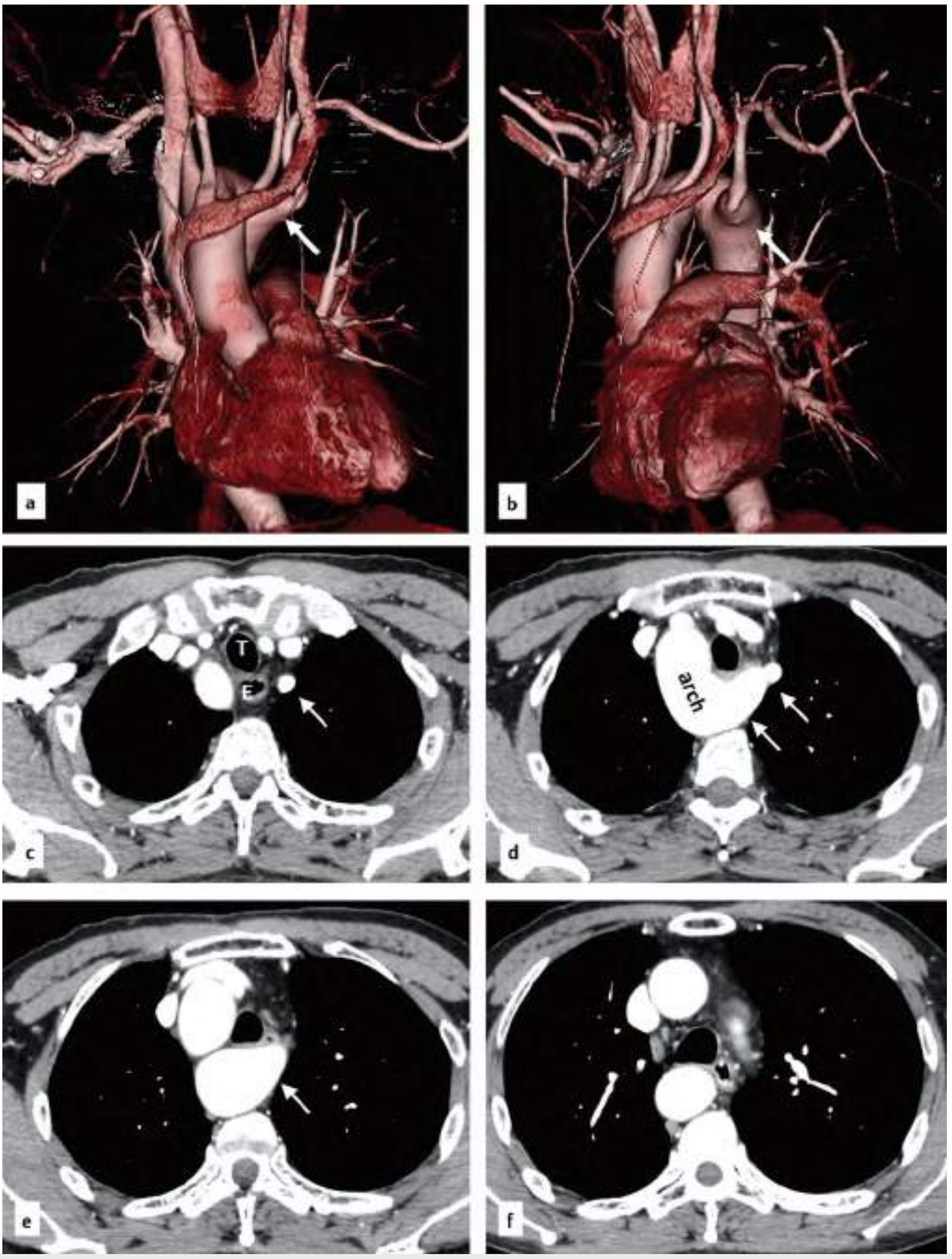

Fig. 8.25 Right aortic arch type 2 with aberrant left subclavian artery. **(a)** Frontal and **(b)** lateral views of the 3D CT angiography show the right-sided aortic arch with an aberrant left subclavian artery. Kommerell's diverticulum (*white arrow*) at the origin of the aberrant subclavian artery is noted. (**c–f**) Axial images of the contrast-enhanced CT shows that the aortic arch (arch) located on the right side to the trachea (T). The aberrant left subclavian artery (*arrows*), originating at the right-sided descending aorta with Kommerell's diverticulum, runs transversely to the left side behind the trachea (T) and esophagus (E). The esophagus is displaced anteriorly.

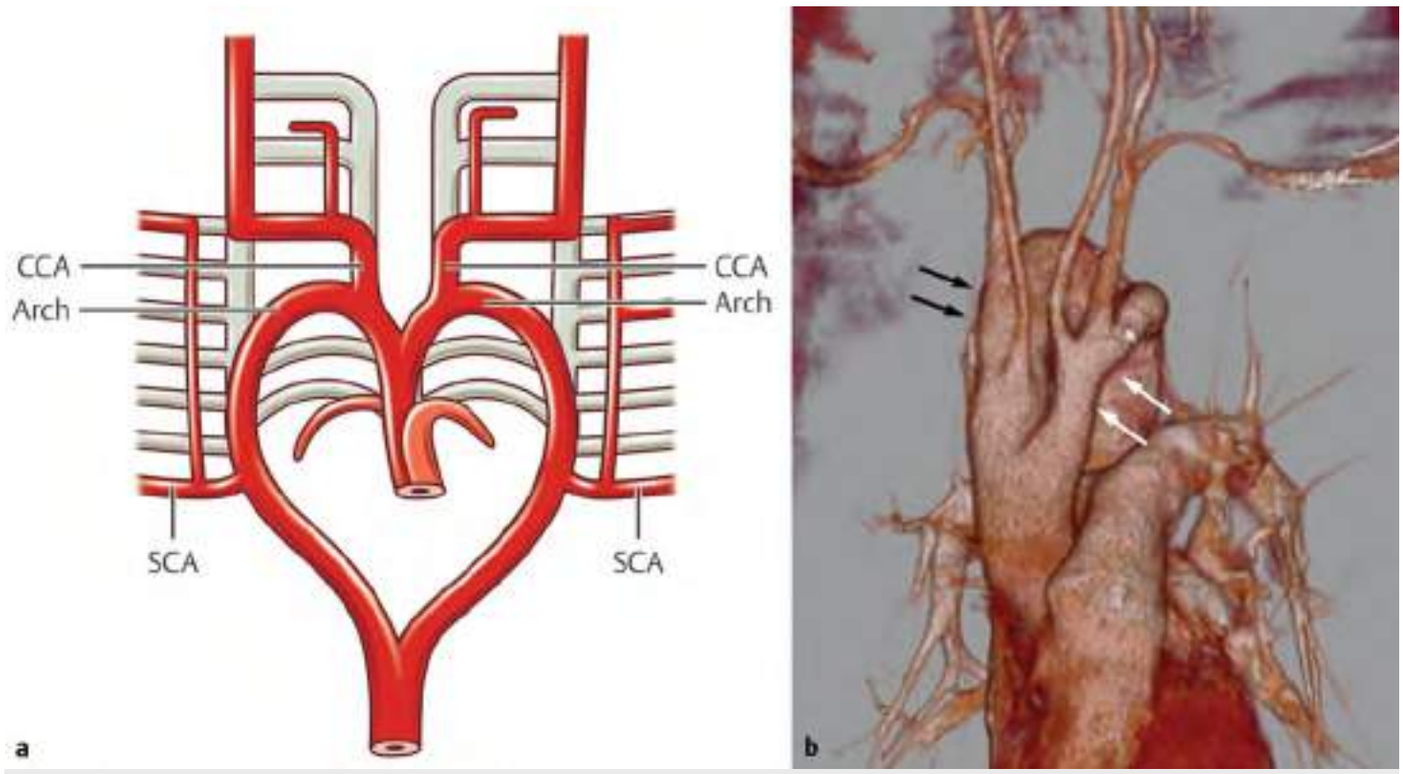

Fig. 8.26 Double aortic arch. **(a)** Schematic drawing of the development of the double aortic arch due to persistent connection between the fourth aortic arch (arch) and the dorsal aorta (DA) on both sides. **(b)** Frontal view of the 3D CT angiography shows the two aortic arches on both sides. The common carotid artery (CCA) and the subclavian artery (SCA) originate separately from each aortic arch.

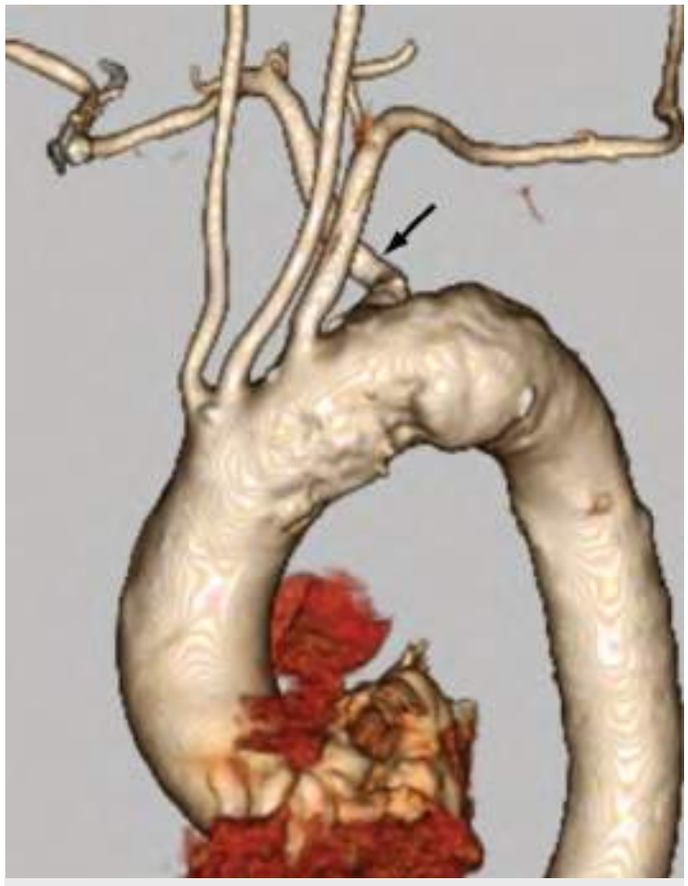

Fig. 8.27 Aberrant right subclavian artery. Left lateral view of the 3D CT angiography shows the right subclavian artery originating at the distal portion of the aortic arch.

Aberrant Right Subclavian Artery

Aberrant right subclavian artery is a very common incidental finding on CT studies of chest. It is caused by interruption of the dorsal segment of the fourth arch artery and a remnant of the right seventh segmental artery, which accounts for 0.5 to 2% in population. It is usually asymptomatic but can cause dysphagia and dyspnea due to compression of esophagus or trachea (▶ Fig. 8.27). Similar to the left aberrant subclavian artery, it can be associated with Kommerell's diverticulum.[28,29]

Patent Ductus Arteriosus

The ductus arteriosus is a fetal blood vessel of the left sixth arch artery that closes soon after birth. Although the ductus arteriosus is narrowed within 12 to 24 hours after birth and seals completely after 3 weeks in normal situation, it does not close in a case of patent ductus arteriosus. It can cause several symptoms such as volume overload, dyspnea, and poor growth. However, in some newborn patients with severe congenital heart disease such as transposition of the great vessels, persistent ductus arteriosus can be vital in supplying oxygenated blood. Aneurysmal dilation of the patent ductus arteriosus can rarely occur in approximately 1.5%, and rarely can rupture (▶ Fig. 8.28).[30]

Left Vertebral Artery Originating from Aortic Arch

Left vertebral artery can originate from aortic arch between the origins of the left common carotid artery and the left subclavian

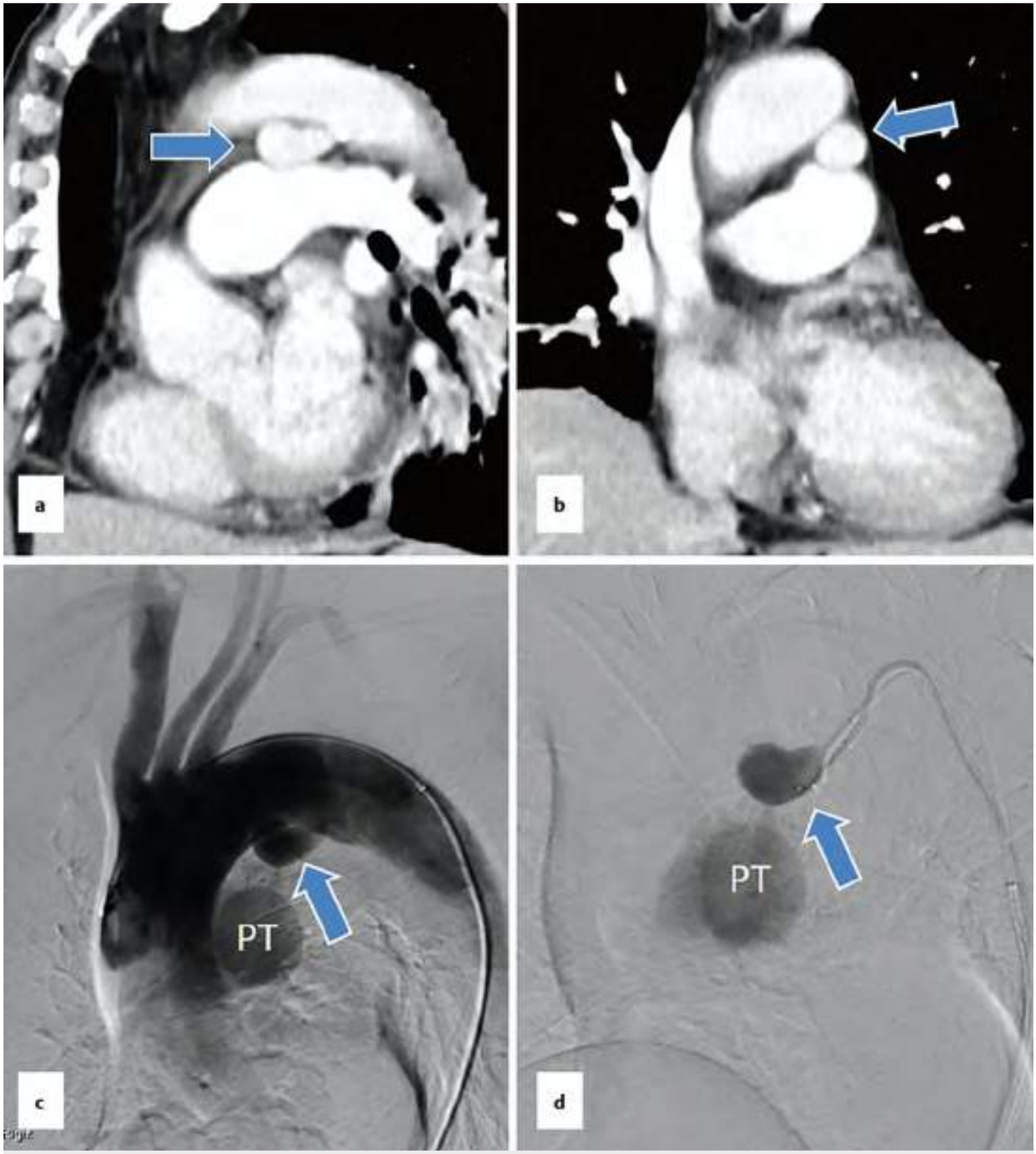

Fig. 8.28 Aneurysm of the patent ductus arteriosus. **(a)** Sagittal and **(b)** coronal multiplanar reconstruction (MPR) images of the 3D CT angiography show an aneurysm (*blue arrow*) at the aortopulmonary window. Dilation of the pulmonary trunk and main pulmonary arteries are also noted. **(c)** Lateral views of aortography and **(d)** selective angiography of the ductus arteriosus show an aneurysm formation of the ductus arteriosus (*arrow*) located just below the aortic arch, which shunts to the pulmonary trunk (PT).

Fig. 8.29 Left vertebral artery originating from the aortic arch. Anterior view of the aortogram shows the left vertebral artery (*arrowheads*) originating independently from the aortic arch between the origins of the left common carotid artery and the left subclavian artery.

artery (▶ Fig. 8.29). This variation can be observed in approximately 6% of cases. The vertebral artery is formed by longitudinal anastomosis between the segmental arteries from first to seventh segmental artery. In normal situation, the vertebral artery originates from the subclavian artery (the left seventh segmental artery). When arising from the aortic arch, the sixth segmental artery is likely its origin. Aberrant origin of the right vertebral artery from the aorta distal to the origin of the left subclavian artery is very rare. It courses behind the esophagus and may have a diverticulum at its origin (vertebral lusoria).

Coarctation of the Aorta

Coarctation of the aorta is defined as a discrete obstructive narrowing in the proximal descending aorta close to the aortic isthmus, an area between the left subclavian artery and ligamentum arteriosum. The majority of cases of aortic coarctation are sporadic; however, several studies have identified clear genetic associations between aortic coarctation and other types of congenital heart disease.[31] The time of presentation depends on the severity of the stenosis as well as the presence or absence of sufficient collateral circulation. In untreated aortic coarctation, lower body systemic perfusion will be decreased, resulting in diminished peripheral pulses in the lower body. Common collateral pathways include intercostal, internal thoracic (mammary), cervical, scapular, and thoracodorsal arteries (▶ Fig. 8.30).

Pseudocoarctation of the Aorta

Pseudocoarctation (kinking, buckling) of the aorta is an uncommon isolated anomaly of the aortic arch characterized by elongation of the aortic arch and acute anterior angulation of the aortic arch at the level of the ligamentum arteriosum with little or no obstruction and absence of increased collateral circulation

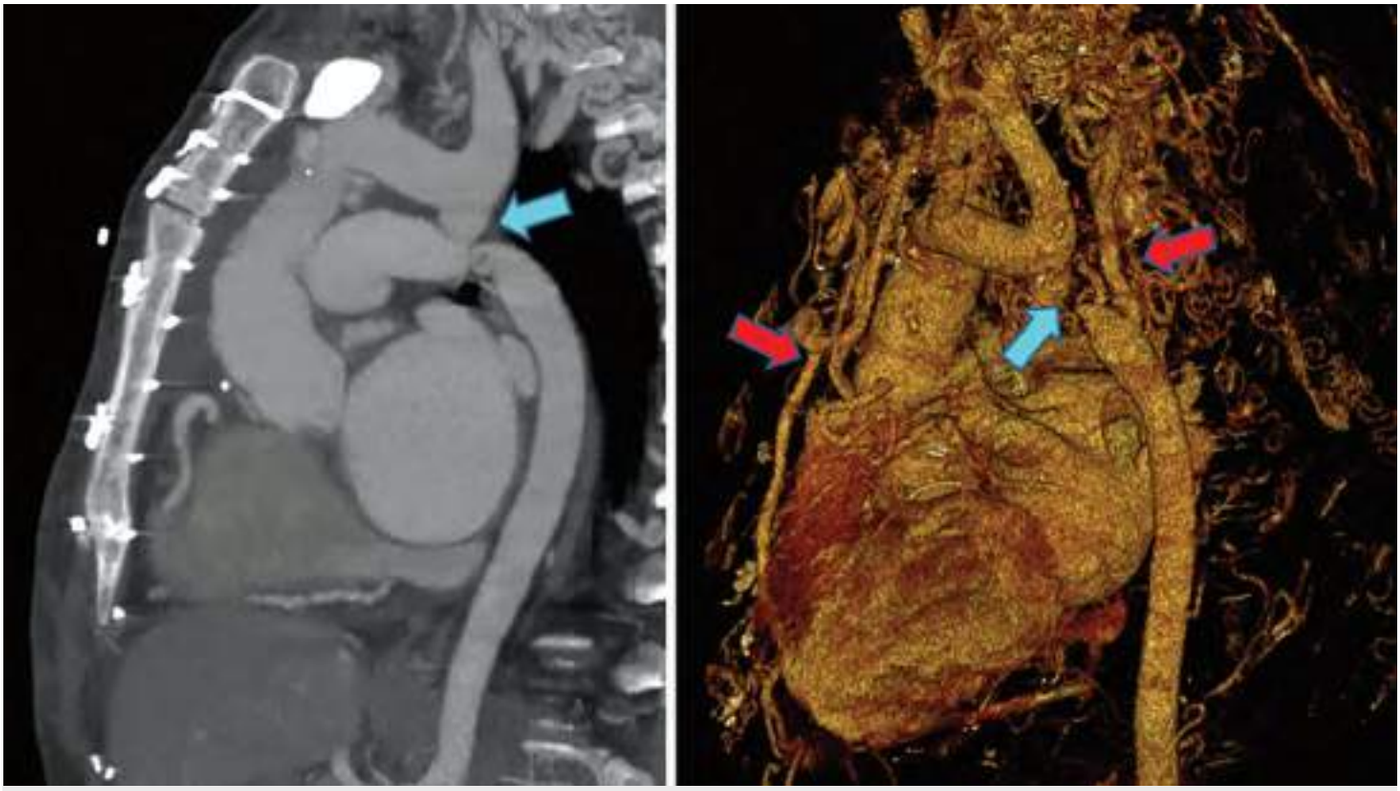

Fig. 8.30 Severe isthmic coarctation (*blue arrows*) of the aorta shown by CT angiography. Extensive intercostal and internal mammary collaterals (*red arrows*) are shown providing blood flow to the distal aorta.

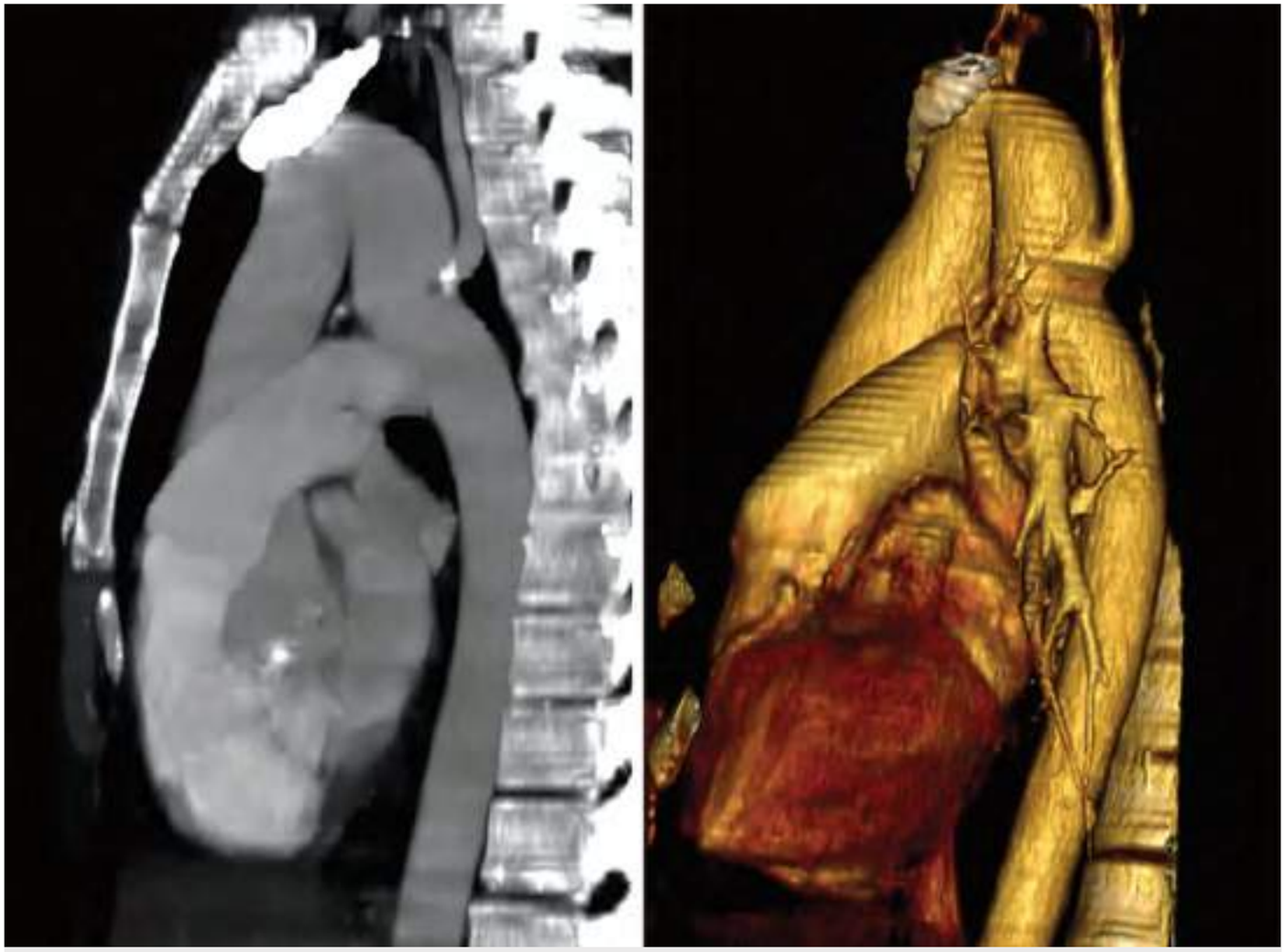

Fig. 8.31 Pseudocoarctation. Note anterior angulation of the aortic arch at the level of the ligamentum arteriosum.

(▶ Fig. 8.31). Reduction of the isthmic segment cross-sectional diameter may exist but it is usually less the 50% of that of the transverse arch.[32]

References

[1] Moore KL, Dalley AF, Agur A. Clinically Oriented Anatomy. 4th ed. Philadelphia, PA: Lippincott Williams & Wilkins; 1999:130–133

[2] Bricker AO, Avutu B, Mohammed TL, et al. Valsalva sinus aneurysms: findings at CT and MR imaging. Radiographics.; 30(1):99–110

[3] Wolak A, Gransar H, Thomson LE, et al. Aortic size assessment by noncontrast cardiac computed tomography: normal limits by age, gender, and body surface area. JACC Cardiovasc Imaging.; 1(2):200–209

[4] Zimmermann E, Schnapauff D, Dewey M. Cardiac and coronary anatomy in computed tomography. Semin Ultrasound CT MR.; 29(3):176–181

[5] Gupta R, Marwah A, Shrivastva S. Anomalous origin of right coronary artery from pulmonary artery. Ann Pediatr Cardiol.; 5(1):95–96

[6] Goo HW, Seo DM, Yun TJ, et al. Coronary artery anomalies and clinically important anatomy in patients with congenital heart disease: multislice CT findings. Pediatr Radiol.; 39(3):265–273

[7] Lim JJ, Jung JI, Lee BY, Lee HG. Prevalence and types of coronary artery fistulas detected with coronary CT angiography. AJR Am J Roentgenol.; 203(3):W237–43

[8] Ripple MG, Grant JR, Mealey J, Fowler DR. Evaluation of aortic injury in driver fatalities occurring in motor vehicle accidents in the State of Maryland for 2003 and 2004. Am J Forensic Med Pathol.; 29(2):123–127

[9] Haller JM, Iwanik M, Shen FH. Clinically relevant anatomy of recurrent laryngeal nerve. Spine.; 37(2):97–100

[10] Yamasaki M. Comparative anatomical studies on the thyroid and thymic arteries. III. Guinea pig (Cavia cobaya). J Anat.; 186(Pt 2):383–393

[11] Ozlugedik S, Ozcan M, Unal A, Yalcin F, Tezer MS. Surgical importance of highly located innominate artery in neck surgery. Am J Otolaryngol.; 26 (5):330–332

[12] Hartmann IJ, Remy-Jardin M, Menchini L, Teisseire A, Khalil C, Remy J. Ectopic origin of bronchial arteries: assessment with multidetector helical CT angiography. Eur Radiol.; 17(8):1943–1953

[13] Raptis CA, Sridhar S, Thompson RW, Fowler KJ, Bhalla S. Imaging of the patient with thoracic outlet syndrome. Radiographics.; 36(4):984–1000

[14] Uchino A, Saito N, Okada Y, et al. Variation of the origin of the left common carotid artery diagnosed by CT angiography. Surg Radiol Anat.; 35(4):339–342

[15] Lasjaunias P, Berenstein A, ter Brugge KG. Spinal and spinal cord arteries and vein. Surgical Neuroangiography, Volume 1. 2nd ed. Springer; 2001:73–146

[16] Pietrasik K, Bakon L, Zdunek P, Wojda-Gradowska U, Dobosz P, Kolesnik A. Clinical anatomy of internal thoracic artery branches. Clin Anat.; 12(5):307–314

[17] Huelke DF. A study of the transverse cervical and dorsal scapular arteries. Anat Rec.; 132(3):233–245

[18] Rodriguez-Baeza A, Muset-Lara A, Rodriguez-Pazos M, Domenech-Mateu JM. The arterial supply of the human spinal cord: a new approach to the arteria radicularis magna of Adamkiewicz. Acta Neurochir (Wien).; 109(1–2):57–62

[19] Takase K, Sawamura Y, Igarashi K, et al. Demonstration of the artery of Adamkiewicz at multi- detector row helical CT. Radiology.; 223(1):39–45

[20] Walker CM, Rosado-de-Christenson ML, Martínez-Jiménez S, Kunin JR, Wible BC. Bronchial arteries: anatomy, function, hypertrophy, and anomalies. Radiographics.; 35(1):32–49
[21] Sadlar TW. Chamter13 cardiovascular system. Langman's Medical Embryology. 12th ed. Lippincott Williams & Wlkins; 2012:162–195
[22] Abdulla R, Blew GA, Holterman MJ. Cardiovascular embryology. Pediatr Cardiol.; 25(3):191–200
[23] Hiruma T, Nakajima Y, Nakamura H. Development of pharyngeal arch arteries in early mouse embryo. J Anat.; 201(1):15–29
[24] Sharma A, Priya S, Jagia P. Persistent truncus arteriosus on dual source CT. Jpn J Radiol.; 34(7):486–493
[25] McLoughlin MJ, Weisbrod G, Wise DJ, Yeung HP. Computed tomography in congenital anomalies of the aortic arch and great vessels. Radiology.; 138 (2):399–403
[26] Hastreiter AR, D'Cruz IA, Cantez T, Namin EP, Licata R. Right-sided aorta. I. Occurrence of right aortic arch in various types of congenital heart disease. II. Right aortic arch, right descending aorta, and associated anomalies. Br Heart J.; 28(6):722–739
[27] Shuford WH, Sybers RG, Gordon IJ, Baron MG, Carson GC. Circumflex retroesophageal right aortic arch simulating mediastinal tumor or dissecting aneurysm. AJR Am J Roentgenol.; 146(3):491–496
[28] Barone C, Carucci NS, Romano C. A rare case of esophageal dysphagia in children: aberrant right subclavian artery. Case Rep Pediatr.; 2016:2539374
[29] Polguj M, Chrzanowski A, Kasprzak JD, Stefaczyk L, Topol M, Majos A. The aberrant right subclavian artery (arteria lusoria): the morphological and clinical aspects of one of the most important variations—a systematic study of 141 reports. Sci World J.; 2014:292734
[30] Ohtsuka S, Kakihana M, Ishikawa T, et al. Aneurysm of patent ductus arteriosus in an adult case: findings of cardiac catheterization, angiography, and pathology. Clin Cardiol.; 10(9):537–540
[31] Bruneau BG. The developmental genetics of congenital heart disease. Nature.; 451(7181):943–948
[32] Atalay MK, Kochilas LK. Familial pseudocoarctation of the aorta. Pediatr Cardiol.; 32(5):692–695

9 Lymphatics and Nerves of the Thorax

Gina Cavallo, R. Shane Tubbs, and Farhood Saremi

◆ Introduction

The thorax is an irregular cylinder with a narrow superior opening, the superior thoracic aperture, and a relatively large inferior opening, the inferior thoracic aperture. The superior thoracic aperture is open, allowing continuity with the neck, while the inferior thoracic aperture is covered by the diaphragm. The thorax houses and protects the heart, lungs, and great vessels along with their corresponding lymphatics and nerves. The mediastinum acts as a conduit for structures that (a) pass completely through the thorax from one body region to another or (b) connect organs in the thorax to other body regions.[1]

Although the nerves of the thorax are rarely identified at cross-sectional imaging, their location can be inferred by localizing easily identified anatomical landmarks. Familiarity with the functional anatomy and clinical significance of the nerves of the thorax is important for interpreting thoracic images correctly.[2] However, various noninvasive diagnostic techniques such as chest radiography, computed tomography (CT), positron emission tomography (PET), and magnetic resonance imaging (MRI) are currently available for assessing the intrathoracic lymphatic system. The lymph nodes distributed through the mediastinum and hila are best understood by correlation with CT and MR cross-sectional images.[3]

◆ Nerves

Innervation of Thoracic Wall

Innervation of the thoracic wall is primarily by the intercostal nerves, which are the anterior rami of spinal nerves T1 to T11 and lie in the intercostal spaces between adjacent ribs (▶ Fig. 9.1). The ventral ramus of spinal nerve T12 (the subcostal) is inferior to the 12th rib.

These nerves innervate the thoracic wall, related parietal pleura, and associated skin. A typical intercostal nerve passes

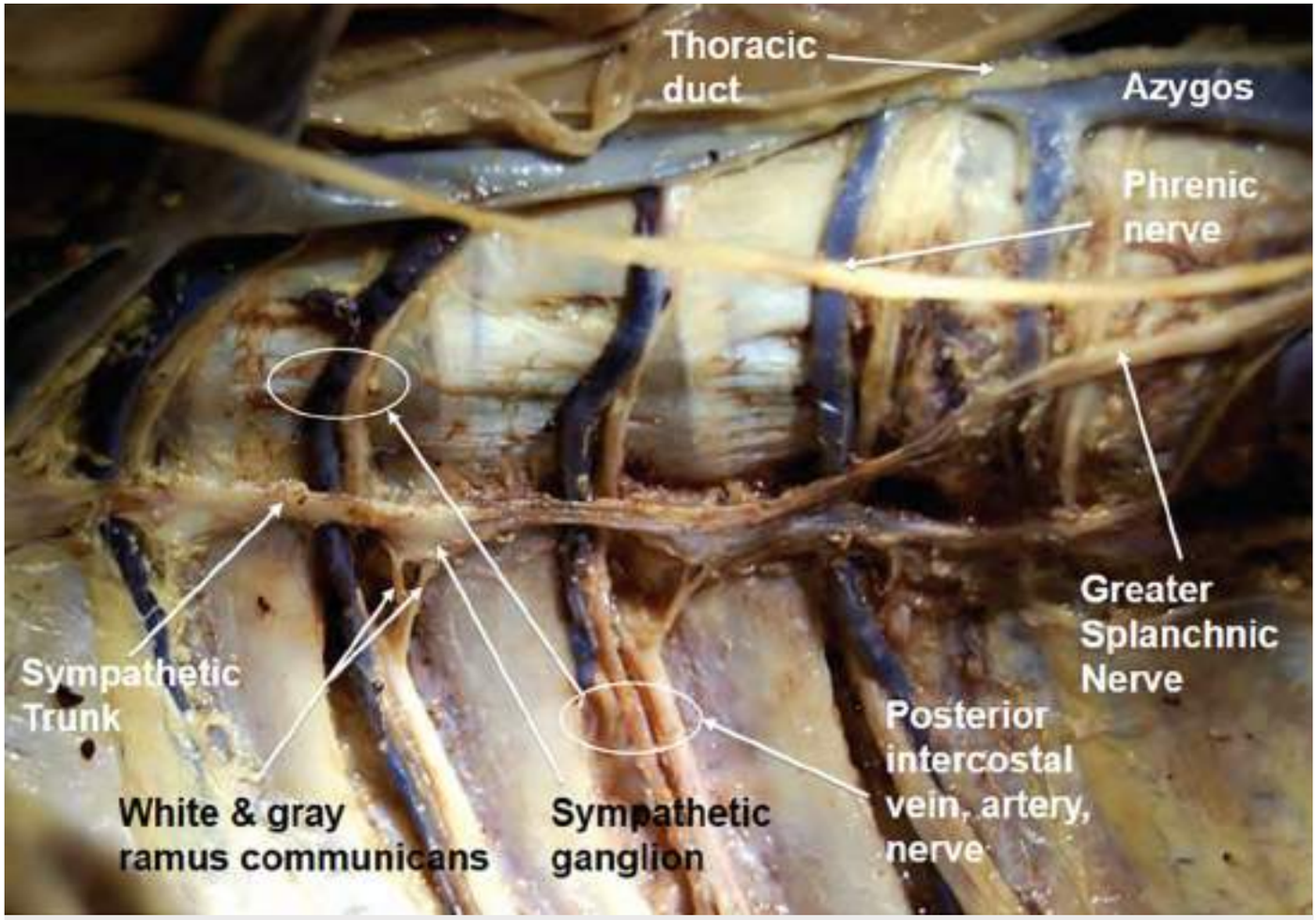

Fig. 9.1 View of the right paraspinal structures. Posterior intercostal neurovascular bundle is shown. Note the intercostal vein superior to the artery and the intercostal nerve passing inferior to the artery. The intercostal veins originating from the azygos vein. The white (myelinated) ramus communicans is the preganglionic sympathetic outflow from the spinal cord and the gray ramus communicans is the postganglionic sympathetic inflow to the spinal cord. Both pass through the paravertebral ganglion of the sympathetic trunk.

laterally around the thoracic wall in an intercostal space. The largest branch is the lateral cutaneous, which pierces the lateral thoracic wall and divides into anterior and a posterior branch that innervate the overlying skin.[1]

In addition to the thoracic wall, the intercostal nerves innervate other regions; for example, the ventral ramus of T1 contributes to the brachial plexus, the lateral cutaneous branch of the second intercostal nerve (the intercostobrachial) contributes to cutaneous innervation of the medial upper arm, and the lower intercostal nerves supply muscles, skin, and peritoneum of the abdominal wall.[1]

The intercostal nerves end as anterior cutaneous branches, which emerge either parasternally, between adjacent costal cartilages, or laterally to the midline, on the anterior abdominal wall, to supply the skin. In addition to these major branches, small collateral branches run in the intercostal space along the superior border of the lower rib.[1]

The dermatomes of the thorax generally reflect the segmental organization of the thoracic spinal nerves (see Volume II, Chapter 1, Abdominopelvic Wall). The exception, anteriorly and superiorly, is the first thoracic dermatome, which is located mostly in the upper limb, not on the trunk. The anterosuperior region of the trunk receives branches from the ventral ramus of C4 via supraclavicular branches of the cervical plexus. The highest thoracic dermatome on the anterior chest wall is T2, which also extends into the upper limb. At the midline, the skin over the xiphoid process is innervated by branches of the T6 spinal nerve. The dermatomes of T7 to T12 follow the contour of the ribs onto the anterior abdominal wall.

In the thorax, the intercostal nerves carry somatic motor innervation to the muscles of the thoracic wall (intercostal, subcostal, and transversus thoracis), somatic sensory innervation from the skin and parietal pleura, and postganglionic sympathetic fibers to the periphery.[1]

Vagus Nerves

The vagus nerves pass through the superior and posterior divisions of the mediastinum on their way to the abdominal cavity. They pass through the diaphragm with the esophagus. En route through the thorax, they provide parasympathetic innervation to the thoracic viscera and carry visceral afferents from them.[1] In brief, the right and left vagus nerves enter the thorax between their respective brachiocephalic veins and the subclavian artery, medial to the mediastinal pleura (▶ Fig. 9.2, ▶ Fig. 9.3). In good-quality CT images, the vagus nerve may be seen at the thoracic inlet behind the brachiocephalic veins. They descend posterior to their respective pulmonary hila, ramify to form the esophageal

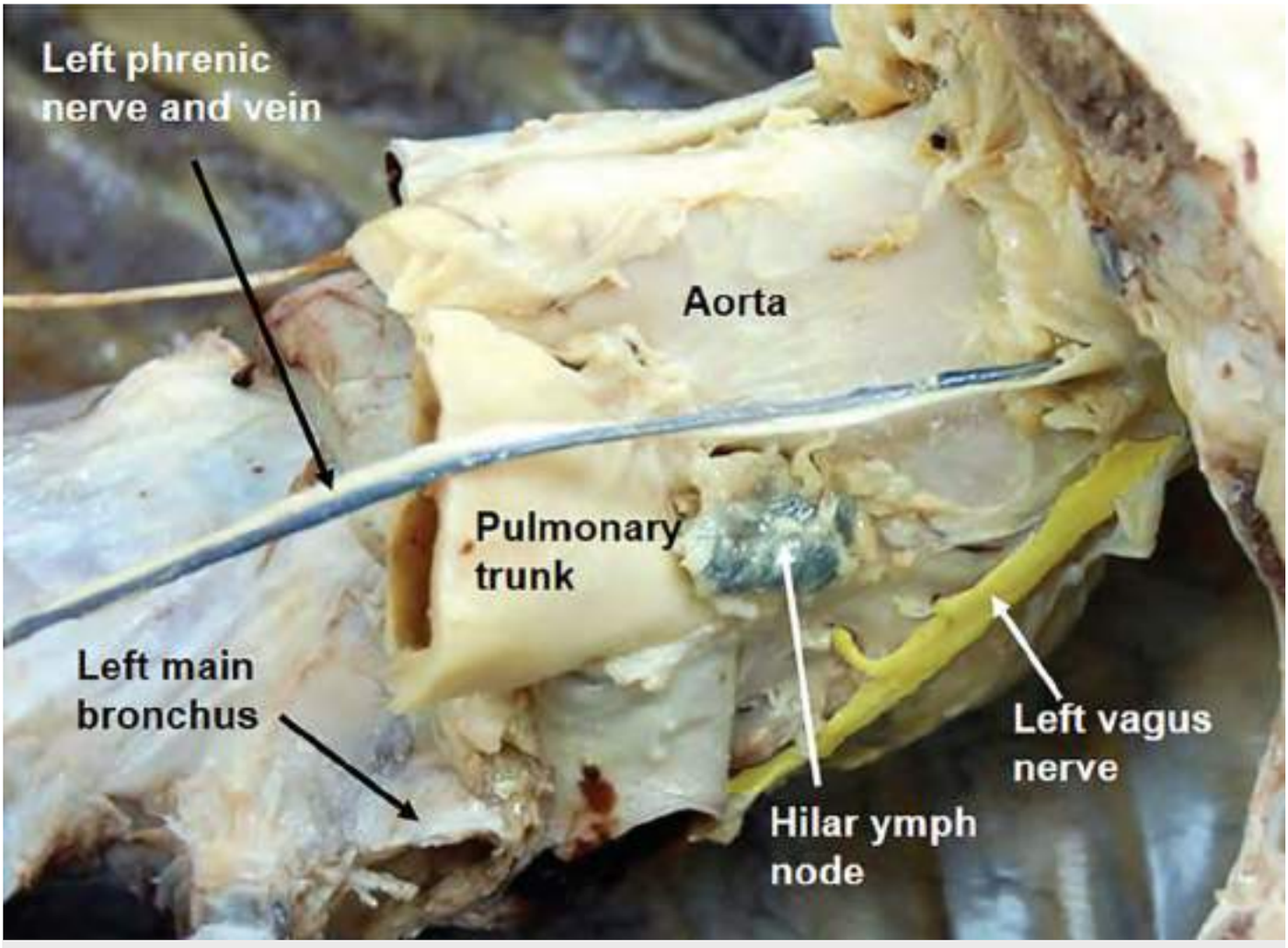

Fig. 9.2 Left view of the upper mediastinum. The left vagus nerve is seen passing behind the left hilum and ramifies to form the esophageal plexus.

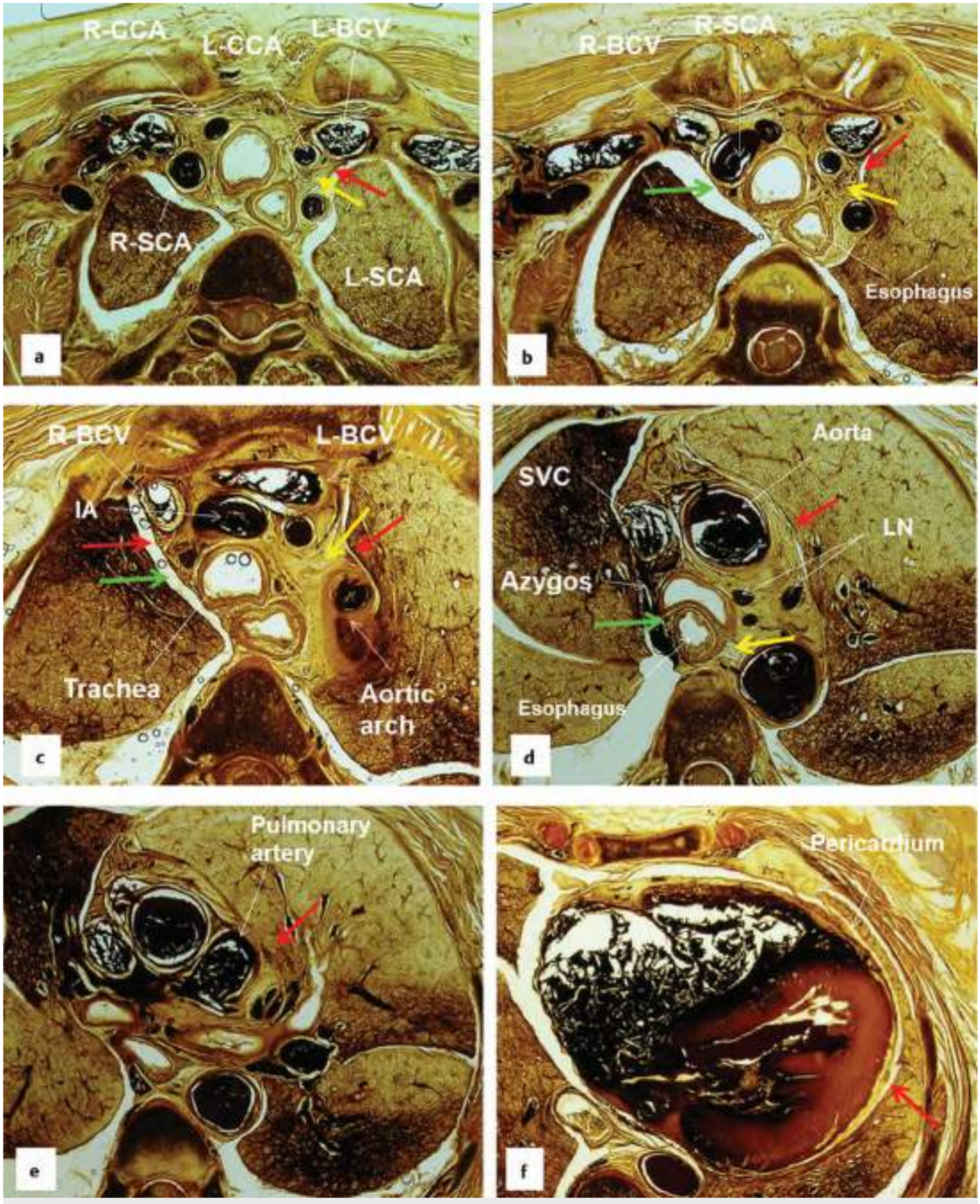

Fig. 9.3 (**a–f**) Vagus and phrenic nerves from superior to inferior. (**a–c**) The right vagus nerve (*green arrows*) enters the superior mediastinum and lies between the right brachiocephalic vein (R-BCV) and the innominate artery (IA). The left vagus nerve (*yellow arrows*) enters the superior mediastinum posterior to the left brachiocephalic vein and between the left common carotid artery (L-CCA) and left subclavian artery (L-SCA). Both phrenic nerves are lateral to the vagus nerve at the thoracic inlet (*red arrows*). (**d**) Shows the anatomical location of the left phrenic neurovascular bundle (*red arrow*) as it passes along the pericardium. LN, lymph nodes, SVC, superior vena cava.

Fig. 9.4 Frontal view of the mediastinum showing the left vagus nerve and the recurrent laryngeal nerve on that side. The left recurrent laryngeal nerve arises from it at the inferior margin of the arch of aorta just lateral to the ligamentum arteriosum.

plexus, and then pass through the esophageal hiatus of the diaphragm as the anterior and posterior vagal trunks.[2]

Right Vagus Nerve

The right vagus nerve enters the superior mediastinum and lies between the right brachiocephalic vein and the innominate artery. It descends in a posterior direction toward the trachea, crosses the lateral surface of the trachea, and passes posteriorly to the root of the right lung to reach the esophagus. Just before the esophagus, the arch of the azygos vein crosses it. As it passes through the superior mediastinum, it gives branches to the esophagus, cardiac plexus, and pulmonary plexus.[1,2]

Left Vagus Nerve

The left vagus nerve enters the superior mediastinum posterior to the left brachiocephalic vein and between the left common carotid and left subclavian arteries. As it passes into the superior mediastinum, it lies just deep to the mediastinal part of the parietal pleura and crosses the left side of the arch of aorta. Inferiorly, it runs lateral to the trachea and esophagus. It continues to descend in a posterior direction and passes posterior to the root of the left lung to reach the esophagus in the posterior mediastinum.[1,2]

As the left vagus nerve passes through the superior mediastinum, it gives branches to the esophagus, the cardiac plexus, and the pulmonary plexus. Also, the left recurrent laryngeal nerve arises from it at the inferior margin of the arch of aorta just lateral to the ligamentum arteriosum (▶ Fig. 9.4). The left recurrent laryngeal nerve passes inferior to the arch of aorta before ascending on its medial surface. Entering a groove between the trachea and esophagus, it continues superiorly to enter the neck and terminates in the larynx.[1]

Recurrent Laryngeal Nerves

The recurrent laryngeal nerves follow an asymmetric pathway through the upper chest. The right recurrent laryngeal nerve originates from the right vagus nerve at the level of the right subclavian artery and loops under this artery to ascend out of the thorax. The left recurrent laryngeal nerve originates from the left vagus nerve at the level of the transverse aortic arch and loops under it immediately posterior to the ligamentum arteriosum to ascend along the posterolateral tracheal margin and exit the thorax (▶ Fig. 9.4). The recurrent laryngeal nerves provide ipsilateral motor innervation to the intrinsic laryngeal muscles for vocalization and sensory innervation to the upper esophagus. They also mediate airway sensation from the level of the true vocal cords to the carina.[2]

Phrenic Nerves

The phrenic nerves lie along the lateral mediastinum and run from the thoracic inlet to the diaphragm (▶ Fig. 9.5, ▶ Fig. 9.6). They course through the upper chest, medial to the mediastinal pleura and the apex of the right or left lung. They provide motor innervation to the diaphragm and sensory innervation to its central intrathoracic and peritoneal surfaces. They also innervate the pericardium and mediastinal pleura and mediate pain from these areas to the neck and shoulder. Manifestations of phrenic nerve disease include diaphragmatic paralysis with elevation or persistent hiccups. The phrenic nerves in their neurovascular bundle can occasionally be visualized on cross-sectional imaging.[2] It is

Fig. 9.5 Left view of the pericardial sac and overlying mediastinal pleura. The phrenic nerves course through the upper chest, medial to the mediastinal pleura and the apex of the right or left lung.

Fig. 9.6 In brief, the right and left vagus nerves enter the thorax between their respective brachiocephalic veins and the subclavian artery, medial to the mediastinal pleura. They descend posterior to their respective pulmonary hila, ramify to form the esophageal plexus, and then pass through the esophageal hiatus of the diaphragm as the anterior and posterior vagal trunks. Greater and lesser thoracic splanchnic nerves are splanchnic nerves that arise from the sympathetic trunk in the thorax and travel inferiorly to provide sympathetic innervation to the abdomen. The greater thoracic splanchnic nerve passes through the diaphragm and synapses at the celiac ganglia. The inferior thoracic splanchnic nerve also travels inferiorly and synapse with postganglionic fibers in the superior mesenteric ganglia.

easier to see the left phrenic neurovascular bundle as it passes over the left pericardium.

Right Phrenic Nerve

The right phrenic nerve enters the superior mediastinum lateral to the right vagus nerve and lateral and slightly posterior to the beginning of the right brachiocephalic vein. It continues inferiorly along the right side of this vein and the right side of the superior vena cava (▶ Fig. 9.6). On entering the middle mediastinum, it descends along the right side of the pericardial sac, within the fibrous pericardium, anterior to the root of the right lung. The pericardiacophrenic vessels accompany it through most of its course in the thorax. It leaves the thorax by passing through the diaphragm with the inferior vena cava.[1]

Left Phrenic Nerve

The left phrenic nerve enters the superior mediastinum in a position similar to the path taken by the right phrenic nerve. It lies lateral to the left vagus nerve and lateral and slightly posterior to the beginning of the left brachiocephalic vein and continues to descend across the left lateral surface of the arch of aorta, passing superficially to the left vagus nerve and the left superior intercostal vein. On entering the middle mediastinum, it follows the left side of the pericardial sac, within the fibrous pericardium, anterior to the root of the left lung, and is accompanied by the pericardiacophrenic vessels (▶ Fig. 9.3, ▶ Fig. 9.5). It leaves the thorax by piercing the diaphragm near the apex of the heart.[1]

Sympathetic Nerves

The sympathetic trunks (chains) of the thorax are paired, symmetric structures that extend from the thoracic inlet to the diaphragm (▶ Fig. 9.6, ▶ Fig. 9.7, ▶ Fig. 9.8). These fibers and ganglia run in a vertical line that crosses the necks of the ribs. They are covered by the parietal pleura, except for the most inferior segment of the right trunk. Preganglionic nerves from the spinal cord synapse at the sympathetic ganglia, and the postganglionic fibers emerge from the ganglia to a visceral organ.

Fig. 9.7 Paravertebral view showing the thoracic duct, esophageal plexus, and azygos vein.

All preganglionic nerve fibers of the sympathetic system are carried out of the spinal cord in spinal nerves T1 to L2. This means that sympathetic fibers found anywhere in the body ultimately emerge from the spinal cord as components of those spinal nerves. Preganglionic sympathetic fibers destined for the head are carried out in spinal nerve T1.[1] The sympathetic ganglia of the thorax are symmetric bilateral chains of 11 ganglia in the paravertebral soft tissue and in continuity with the neck and abdominal chains. Three splanchnic branches emerge from each trunk and pass medially to the abdominal sympathetic ganglia.[2]

Motor Innervation of the Diaphragm

The diaphragm is innervated by the two phrenic nerves that originate, one on each side, as branches of the cervical plexus in the neck. They arise from the anterior rami of cervical nerves C3, C4, and C5, the main contribution coming from C4. They penetrate the diaphragm and innervate it from its abdominal surface (▶ Fig. 9.8).

The phrenic nerves pass vertically through the neck, the superior thoracic aperture, and the mediastinum to supply motor innervation to the entire diaphragm, including the crura (muscular extensions that attach the diaphragm to the upper lumbar vertebrae). In the mediastinum, they pass anteriorly to the roots of the lungs. Spinal cord injuries below the level of origin of the phrenic nerve do not affect movement of the diaphragm.[1]

Pulmonary Innervation

Structures of the lung, and the visceral pleura, are supplied by visceral afferents and efferents distributed through the anterior pulmonary plexus and posterior pulmonary plexus. These interconnected plexuses lie anteriorly and posteriorly to the tracheal bifurcation and main bronchi. The anterior plexus is much smaller than the posterior. Branches of these plexuses, which ultimately originate from the sympathetic trunks and vagus nerves, are distributed along branches of the airway and vessels. Visceral efferents from the vagus nerves constrict the bronchioles while the sympathetic system dilates them.[1]

Esophageal Innervation

The thoracic part of the esophagus lies between the trachea and the vertebral column in the superior mediastinum. On its way down, the esophagus passes behind the aortic arch, and enters the posterior mediastinum at the level of T4/T5 intervertebral discs. The thoracic duct lies on the left side, and the left recurrent laryngeal nerve lies in the left tracheoesophageal groove. Laterally, on the left side, it is related to the aorta and left subclavian artery; on the right side, it is related to the azygos vein. Anteriorly, the esophagus is related to the trachea, right pulmonary artery, left bronchus, pericardium with left atrium, and diaphragm. Posteriorly, it is related to the vertebral column, right posterior intercostal arteries, thoracic duct, thoracic part of the

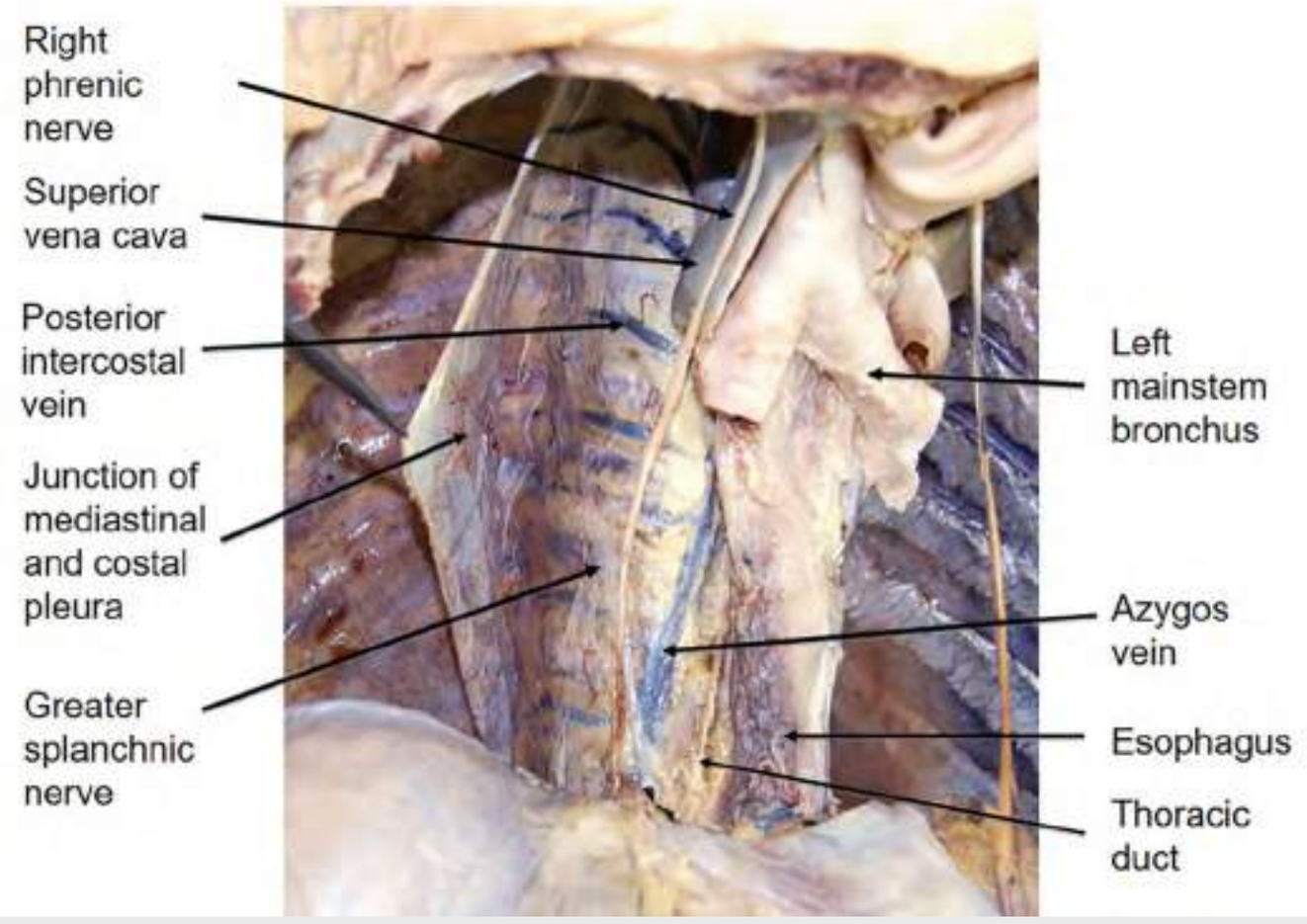

Fig. 9.8 The right phrenic nerve descends along the right side of the superior vena cava.

aorta, and diaphragm. In the posterior mediastinum, the esophagus is related to the descending thoracic aorta, left mediastinal pleura, azygos vein, and cardiac and pulmonary plexus.[4]

In general, innervation of the esophagus is complex. Esophageal branches arise from the vagus nerves and sympathetic trunks to form the esophageal plexus (▶ Fig. 9.6, ▶ Fig. 9.7). Striated muscle fibers in the superior portion of the esophagus originate from the branchial arches and are innervated by branchial efferents from the vagus nerves. Smooth muscle fibers are innervated by components of the parasympathetic part of the autonomic division of the peripheral nervous system, visceral efferents from the vagus nerves. These are preganglionic fibers that synapse in the myenteric and submucosal plexuses of the enteric nervous system in the esophageal wall. Sensory innervation of the esophagus involves visceral afferent fibers originating in the vagus nerves, sympathetic trunks, and splanchnic nerves.[1]

Cardiac Innervation

The fibrous pericardium is a cone-shaped bag with its base on the diaphragm and its apex continuous with the adventitia of the great vessels. Nerves supplying the pericardium arise from the vagus nerve, the sympathetic trunks, and the phrenic nerves. The phrenic nerves, which innervate the diaphragm and originate from spinal cord levels C3 to C5, pass through the fibrous pericardium and innervate it as they travel toward their final destination. The source of somatic sensation (pain) from the parietal pericardium is carried by somatic afferent fibers in the phrenic nerves. Therefore, "pain" related to a pericardial problem can be referred to the supraclavicular region of the shoulder or lateral neck area, the dermatomes for spinal cord segments C3, C4, and C5.

The autonomic division of the peripheral nervous system is directly responsible for regulating heart rate, the force of each contraction and cardiac output. Branches from both the parasympathetic (vagus) and sympathetic systems contribute to forming the cardiac plexus. This plexus consists of a superficial part, inferior to the aortic arch and between it and the pulmonary trunk, and a deep part, between the aortic arch and the tracheal bifurcation.

From the cardiac plexus, small branches that contain both sympathetic and parasympathetic fibers supply the heart. They affect nodal tissue and other components of the conduction system, the coronary blood vessels, and the atrial and ventricular musculature.[1]

Parasympathetic Innervation

Stimulation of the parasympathetic system decreases the heart rate, reduces the force of contraction, and constricts the coronary arteries. The preganglionic parasympathetic fibers reach the

heart as cardiac branches from the right and left vagus nerves.[1] They enter the cardiac plexus and synapse in ganglia located either within the plexus or in the walls of the atria primarily over the superior aspect and posterior surfaces of the atria near the posterior atrioventricular groove.

Sympathetic Innervation

Stimulation of the sympathetic system increases both the heart rate and the force of contraction. There are three sympathetic cardiac nerves, superior, middle, and inferior, arising from the superior, middle, and inferior sympathetic cervical ganglia, respectively. The inferior cervical and the first thoracic ganglia usually fuse to form the cervicothoracic (stellate) ganglion. The stellate ganglion is located anterior to the transverse process of C7 just below the subclavian artery and could be visualized in some CT scans.

Sympathetic fibers reach the cardiac plexus through the cardiac nerves from the sympathetic trunk. Preganglionic sympathetic fibers from the upper four or five segments of the thoracic spinal cord enter and move through the sympathetic trunk. They synapse in cervical and upper thoracic sympathetic ganglia, and postganglionic fibers proceed as bilateral branches from the sympathetic trunk to the cardiac plexus.[1]

Visceral Afferents

The cardiac plexus also contains visceral afferents from the heart. These fibers pass through the cardiac plexus and return to the central nervous system in the cardiac nerves from the sympathetic trunk and in the vagal cardiac branches. The afferents associated with the vagal cardiac nerves return to the vagus nerve. They sense alterations in blood pressure and blood chemistry and are therefore primarily concerned with cardiac reflexes.

The afferents associated with the cardiac nerves from the sympathetic trunks return to either the cervical or the thoracic portions of the sympathetic trunk. If they are in the cervical portion, they normally descend to the thoracic region where they reenter the upper four or five thoracic spinal cord segments along with afferents from the thoracic region of the sympathetic trunk.

Visceral afferents associated with the sympathetic system conduct pain sensation from the heart, detected at the cellular level as tissue-injuring events (i.e., cardiac ischemia). This pain is often “referred” to cutaneous regions supplied by the same spinal cord levels.[1]

◆ Lymphatics

Thoracic lymphatics are involved in the immune system of such intrathoracic organs as the lungs, pleura, esophagus, and mediastinum. The network of lymphatic vessels carries interstitial fluid from the lungs, chyle from the digestive system and white blood cells, and other immune components. The thoracic lymphatics include the thymus and bone marrow, which are lymphoid tissues dedicated to lymphocyte production and circulation. All lymphatic collectors flow into lymph nodes, which are important parts of the lymphatic system. Pathways called lymph node chains eventually drain into the systemic circulation either through direct connections at the level of the cervical venous confluence or indirectly via the thoracic duct. The number, size, and locations of the collecting channels and lymph nodes differ among individuals and such variability must be taken into account in a clinical setting.[5]

During embryonic period, the lymphatic channels connect to six primitive lymph sacs; two jugular lymph sacs, two iliac lymph sacs, one retroperitoneal lymph sac, and one cisterna chyli. The jugular lymph sacs connect with the cisterna chyli via two lymphatic trunks. These two trunks are interconnected across the midline by numerous collateral. Only after regression of the inferior portion of the right trunk and the superior portion of the left trunk, the definitive thoracic duct forms. Except for the superior part of the cisterna chyli, other lymph sacs will be transformed into groups of lymph nodes.

Lymphatic Drainage of the Thoracic Wall

The lymphatic vessels of the thoracic wall drain mainly into lymph nodes associated with the internal thoracic arteries (parasternal nodes), with the heads and necks of ribs (intercostal nodes), and with the diaphragm (diaphragmatic nodes). Lateral chest wall and breast drain into the axillary lymph nodes. The medial breast also drains into the internal thoracic chain.

The anterior part of each intercostal space drains into parasternal node located at the anterior end of that space along the internal mammary artery, whereas their efferents unite with those of the tracheobronchial and brachiocephalic nodes. The posterior part drains into the intercostal node located near the head and neck of the rib. Efferents of the lower four to seven spaces unite to form a common trunk that descends to the intra-abdominal cisterna chili or drains directly at the origin of the thoracic duct. Efferents of the left upper spaces end in the thoracic duct, whereas those of the right upper spaces end in one of the right lymphatic trunks.[5]

The parasternal nodes drain into bronchomediastinal trunks. The intercostal nodes in the upper thorax also drain into bronchomediastinal trunks, whereas those in the lower thorax drain into the thoracic duct.

Nodes associated with the diaphragm interconnect with the parasternal, prevertebral, juxtaesophageal, brachiocephalic (anterior to the brachiocephalic veins in the superior mediastinum), and lateral aortic/lumbar (in the abdomen) nodes.

There are three sets of diaphragmatic lymph nodes: anterior, middle, and posterior. The anterior set (also known as anterior cardiophrenic or pericardial lymph nodes) comprises two or three small glands behind the base of the xiphoid process, which receive afferents from the convex surface of the liver and the lower thoracic wall. It also contains one or two glands on either side near the junction of the seventh rib with its cartilage, which receives lymphatic vessels from the front part of the diaphragm (▶ Fig. 9.9). The efferent vessels of the anterior set pass to the internal thoracic glands (▶ Fig. 9.9). Lymphoma is the most common malignancy involving the anterior lymph nodes followed by metastasis from breast, lung, and liver tumors. The middle set of diaphragmatic lymph nodes consists of two or three glands on either side close to the phrenic nerves entering the diaphragm,

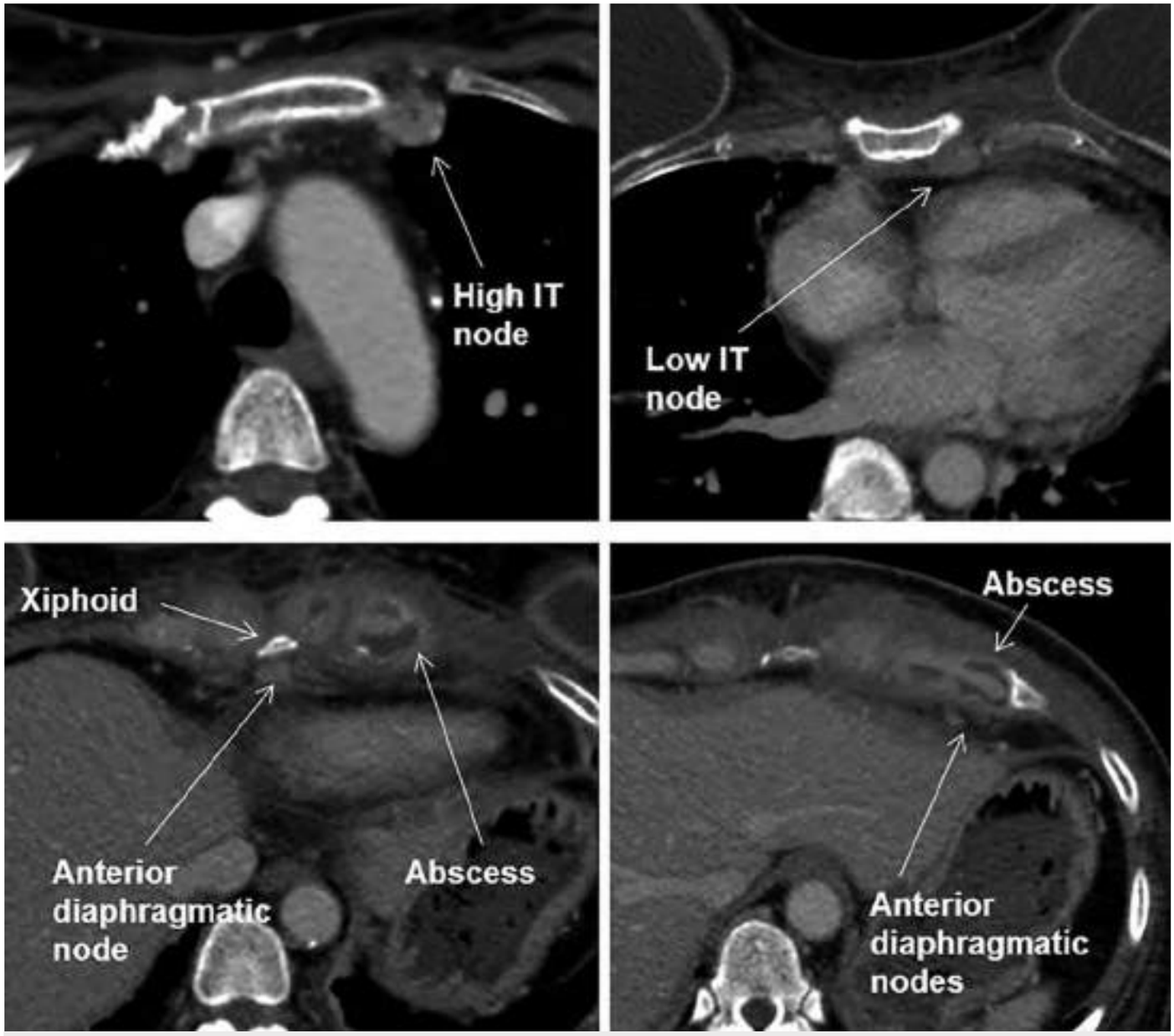

Fig. 9.9 Axial CT images showing mediastinal node enlargement in a patient with infective chondritis and abscess formation around the left anterior seventh costal cartilage. Anterior diaphragmatic nodes and left internal thoracic (IT) chain are involved.

around the fibrous pericardium and the inferior vena cava. Their efferent vessels pass to the posterior mediastinal glands. The posterior set consists of a few glands situated on the back of the crura of the diaphragm. They are connected with both the lumbar glands and the posterior mediastinal glands. The superficial regions of the thoracic wall drain mainly into axillary lymph nodes in the axilla or parasternal nodes.[1]

Lymphatic Drainage of the Lungs

Pleura and Pleural Spaces

The pleura is the serous membrane that is divided into the visceral pleura, which covers the lung parenchyma and interlobar fissures, and the parietal pleura that lines the inner surface of each hemithorax along the chest wall and the diaphragm. These pleura fuse at the hilum where they form the pulmonary ligament.

The pleural space is on the boundary of two lymphatic systems, both of which are important in fluid resorption and removal of foreign particles, cells, and proteins from that space.[5]

The visceral pleura is very rich in lymphatic vessels. In the subpleural space of the visceral pleura, large lymphatic capillaries form a meshed network that drains into the pulmonary lymphatic system and is called the superficial lymphatic plexus of the lung. These capillaries are more abundant over the lower lobes and are connected to the deep pulmonary plexus located in the interlobular and peribronchial spaces.[5]

The lymphatic drainage of the parietal pleura is more elaborate, with direct communications between the pleural space and the parietal lymphatic channels. These communications, called stomata, are the major route for pleural fluid resorption and the removal of foreign particles and cells. Over the costal pleura, the collecting vessels run parallel to the ribs to reach the internal mammary (thoracic) nodal chain anteriorly and the intercostal nodal chain posteriorly. At the level of the diaphragm, drainage is to the retrosternal, mediastinal, and celiac nodes. These transdiaphragmatic anastomoses allow for the passage of fluid and foreign particles from the peritoneal cavity into the pleural space.[5]

Lungs

Among human organs, the lungs have by far the largest surface exposed to an environment containing particulates, toxic matter, and pathogens; in addition, it is constantly supplied by large volumes of blood arising from a highly specialized vascular system. The lungs require an efficient lymphatic system not only to keep them dry in the event of massive fluid challenges but also in order to clear toxins that could penetrate the epithelium. The interstitial space and thin epithelium are exposed to osmotic, hydrostatic, and hydrodynamic forces from the tissues and bloodstream, and must adapt to a continual shifting of fluid, protein, and cells. All of these challenges are met at least in part by the lung lymphatics.[5,6] There are two main groups of pulmonary lymphatics in human. The superficial lymphatics begin at the periphery of the lung lobules near the pleura or interlobular septa (▶ Fig. 9.10). The second group originates as blind-ended tubes in the center of acini around the alveolar ducts. There are no lymphatics in the walls of alveoli. These vessels give rise to the peribronchial lymphatics which form a network around the bronchoarterial bundles to reach the hilum.

The superficial (subpleural) and deep lymphatics of the lung drain into lymph nodes called tracheobronchial nodes around the roots of the lobes and main bronchi and along the sides of the trachea. As a group, these lymph nodes extend from within the lung, through the hilum and root, and into the mediastinum.

The tracheobronchial lymph nodes form four main groups: tracheal, bronchial, bronchopulmonary, and pulmonary. The tracheal nodes (paratracheal) are located on either side of the trachea (▶ Fig. 9.11). The bronchial glands (precarinal, subcarinal) are between the lower part of the trachea and bronchi and between the two bronchi. The bronchopulmonary (hilar) glands are found in the hilum of each lung. The pulmonary glands (interlobar, lobar, segmental, parenchymal) are in the lung parenchyma and are found on the larger branches of the bronchi. Glands in this group drain the lungs, bronchi, trachea, and heart.

Efferent vessels from these nodes pass superiorly along the trachea to unite with similar vessels from the parasternal and brachiocephalic nodes, which are anterior to the brachiocephalic veins in the superior mediastinum, to form the right and left bronchomediastinal trunks. These trunks drain directly into deep veins at the base of the neck, or possibly into the right lymphatic trunk or thoracic duct.[1]

Thoracic Duct

The thoracic duct is the largest lymphatic vessel in the body and the principal channel through which lymph from most of the body is returned to the venous system (▶ Fig. 9.6, ▶ Fig. 9.7). It is approximately 45 cm in length and 2 to 5 mm in diameter. The flow rate through the thoracic duct is between 60 and 190 mL/h, and, like all the larger lymph collectors, it has a media made of smooth muscle fibers that contract periodically to aid antegrade flow, and a system of valves that prevent retrograde flow.[5,7]

It begins as a confluence of lymph trunks in the abdomen (the right and left lumbar trunks, the intestinal trunk, and the lowest intercostal vessels), and in 80% of individuals forming a saccular dilation referred to as the cisterna chyli, which drains the abdominal viscera and walls, pelvis, perineum, and lower limbs (▶ Fig. 9.11). The cisterna chyli is an elongated cystic structure located at L1–L2 in 60% of individuals. It is located in the retrocrural space to the right of the abdominal aorta in 75% of the cases.[8] Demonstration of the normal cisterna chyli is common in routine CT or MR studies of the abdomen (▶ Fig. 9.12).

Entering the thorax posterior to the aorta through the aortic hiatus of the diaphragm, the thoracic duct ascends through the posterior mediastinum to the right of the midline between the thoracic aorta on the left and the azygos vein on the right. It lies posterior to the diaphragm and the esophagus and anterior to the bodies of the vertebrae (▶ Fig. 9.6, ▶ Fig. 9.7).

The thoracic duct extends from vertebra L2 to the root of the neck. At vertebral level T5, it moves to the left of midline and enters the superior mediastinum. It continues through the superior mediastinum and into the neck. It is usually joined by the left jugular trunk, which drains the left side of the head and neck,

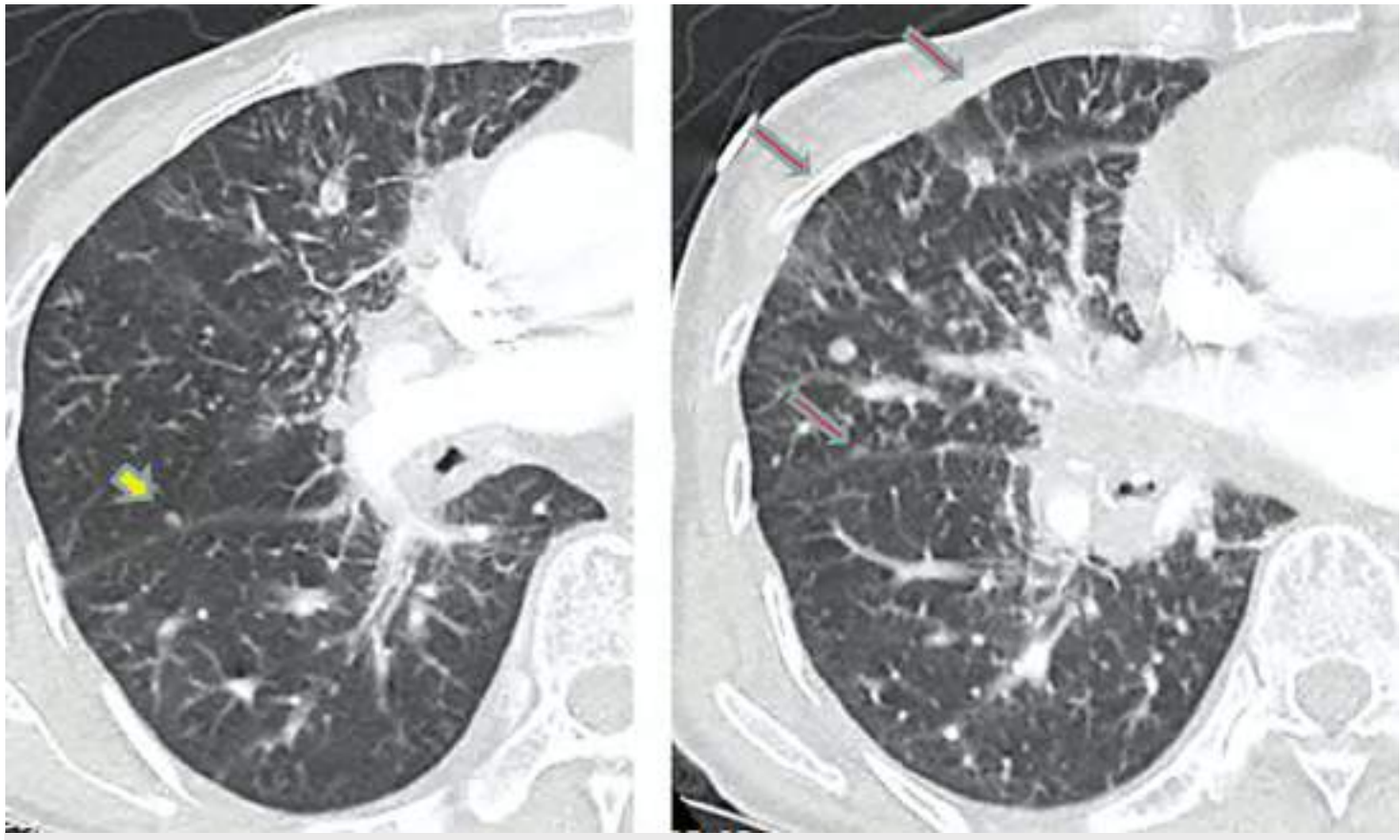

Fig. 9.10 Thickening of the lung lymphatics involving the interlobular septa, pleural surfaces (*red arrows*), and bronchovascular bundles due to lymphangitic carcinomatosis. A small subpleural node is shown (*yellow arrow*). There are two main groups of pulmonary lymphatics in human. The superficial lymphatics begin at the periphery of the lung lobules near the pleura or interlobular septa. The deep lymphatics give rise to the peribronchial lymphatics which form a network around the bronchoarterial bundles to reach the hilum.

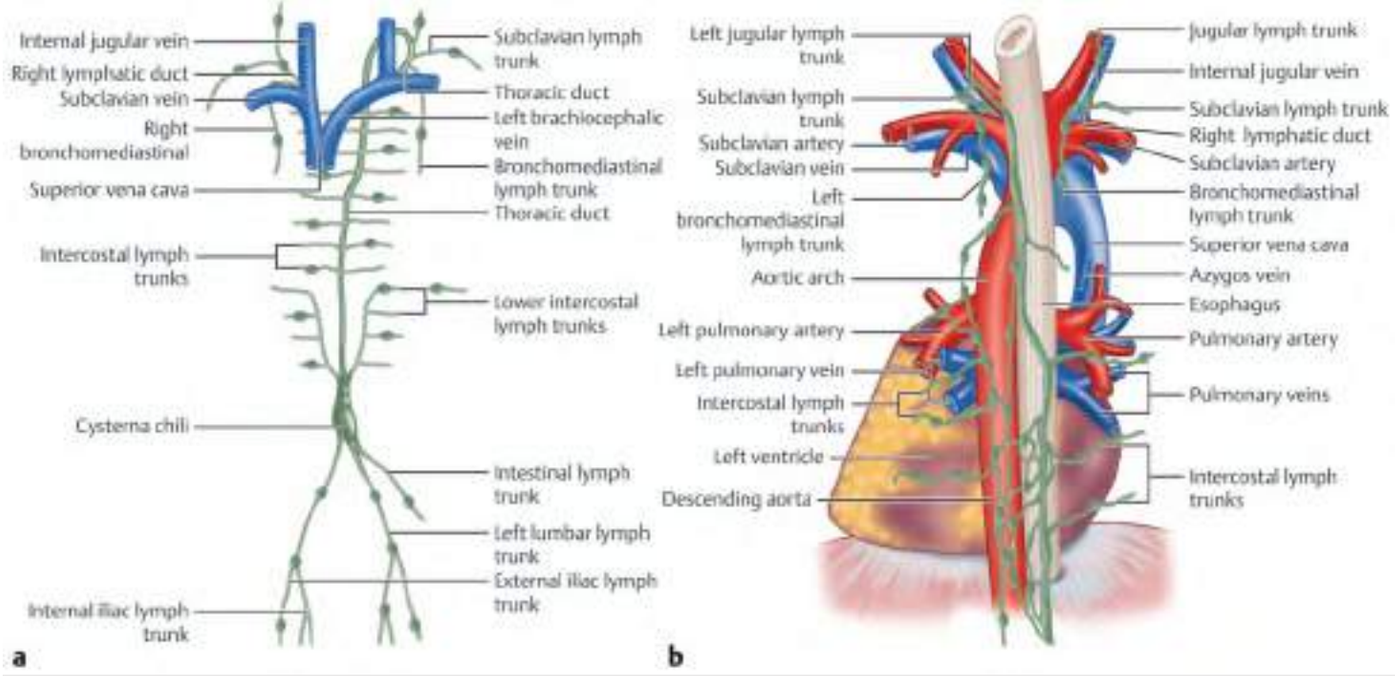

Fig. 9.11 (a, b) The lymphatic system. Several tributaries join the thoracic duct at various places along its length. Note that the right lymphatic duct in the neck forms from the union of three lymphatic trunks: right jugular, right subclavian, and right bronchomediastinal trunks.

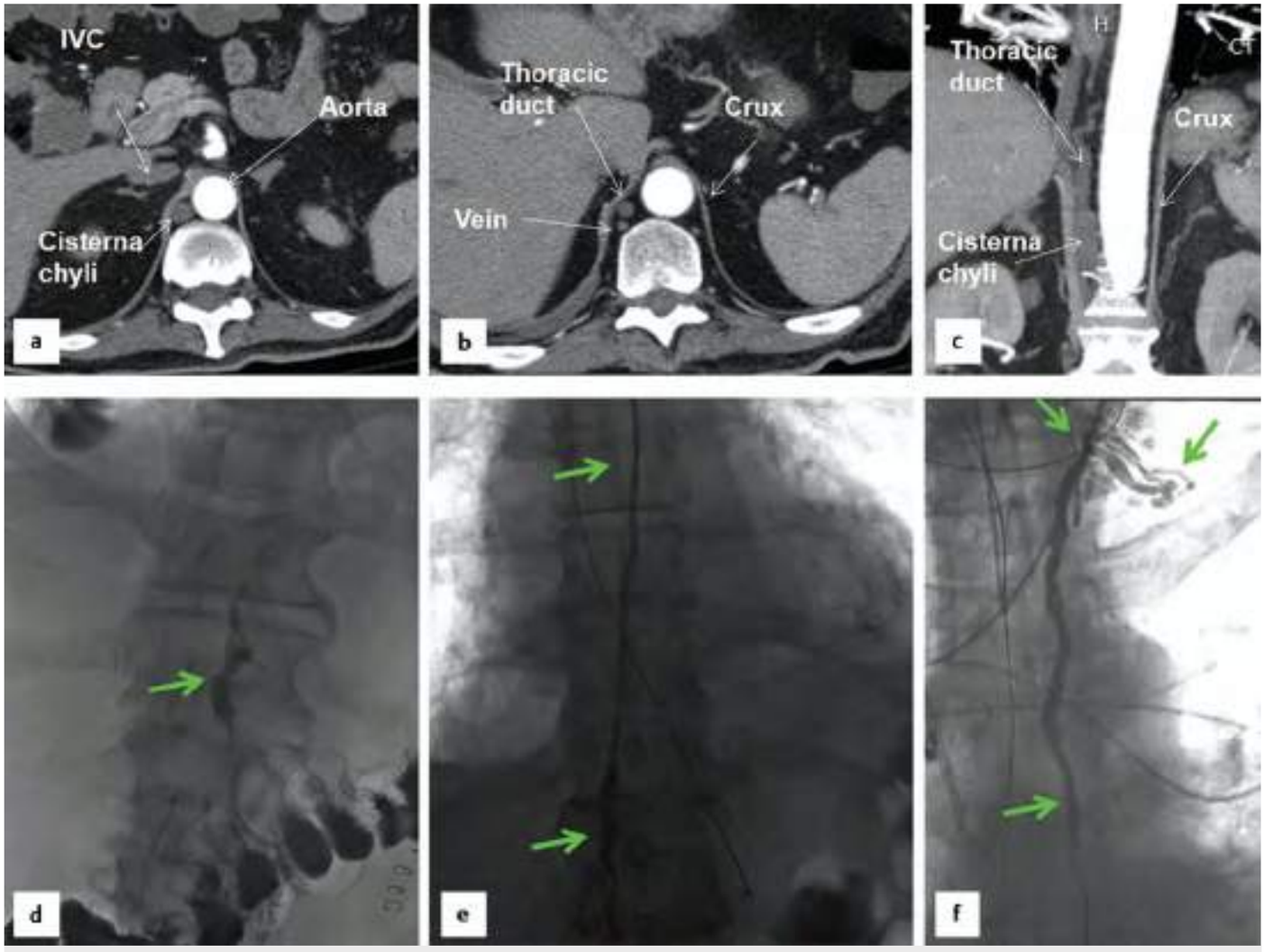

Fig. 9.12 Upper row. (**a, b**) Axial and **(c)** coronal CT scan shows the cisterna chyli and the proximal part of the thoracic duct (*arrows*). Lower row. (**d–f**) Lymphangiogram showing normal cisterna chyli and the thoracic duct through its course into the left brachiocephalic vein. IVC, inferior vena cava.

and the left subclavian trunk, which drains the left upper limb, and then it empties into the posterior aspect of the internal jugular vein or at junction of the left subclavian and left internal jugular veins.[1,7,9] A terminal valve prevents venous reflux.

The thoracic duct is the main lymphatic vessel to which all lymphatic networks eventually drain. It usually receives the contents from the confluence of lymph trunks in the abdomen, descending thoracic lymph trunks draining the lower six or seven intercostal spaces on both sides, upper intercostal lymph trunks draining the upper left five or six intercostal spaces, ducts from posterior mediastinal nodes, and ducts from posterior diaphragmatic nodes. The thoracic duct and all lymphatic channels, except the smallest ones, have several valves.

The anatomy of the thoracic duct is variable; 40 to 60% of individuals have anomalous venous connections with the azygos, intercostal, and lumbar veins and as many as 25 to 30% have multiple ducts at the diaphragmatic level. The termination of the thoracic duct at the cervical venous confluence is also highly variable[10] (▶ Fig. 9.13). The thoracic duct terminates as a single vessel in 70 to 85% of cases. Other forms of termination include two, three, or more ducts.[10,11] Occasionally, a prominent bulging is seen at the cervical venous confluence (▶ Fig. 9.14). Rarely, injury to the thoracic duct can happen after cannulation of the jugular or subclavian veins. In radiology, the thoracic duct can be visualized with standard contrast-enhanced lymphangiography or MR lymphography. The thoracic duct may be injured after trauma where it crosses the midline. Enlargement of the thoracic duct may occur in right heart failure and portal hypertension.

Multiple tributaries join the thoracic duct. The ascending lumbar lymph trunks from both sides pass through the diaphragmatic crura to join the thoracic duct. The intercostal lymph nodes of the lower six or seven intercostal spaces from the descending thoracic lymph trunks that passes the aortic hiatus and join the origin of the thoracic duct in the upper abdomen (▶ Fig. 9.11). The upper five or six left intercostal spaces form upper intercostal trunk that drains into the thoracic duct. Occasionally, the left subclavian and left bronchomediastinal trunks connect the thoracic duct.

The right bronchomediastinal trunk is the vestigial portion of the embryological right thoracic duct (▶ Fig. 9.11). It may drain directly into the right subclavian vein or connect with the right jugular and right subclavian trunks to form the right lymphatic trunk. Enlarged supraclavicular lymph node at the confluence of the thoracic duct is called Virchow's nodes, named after German

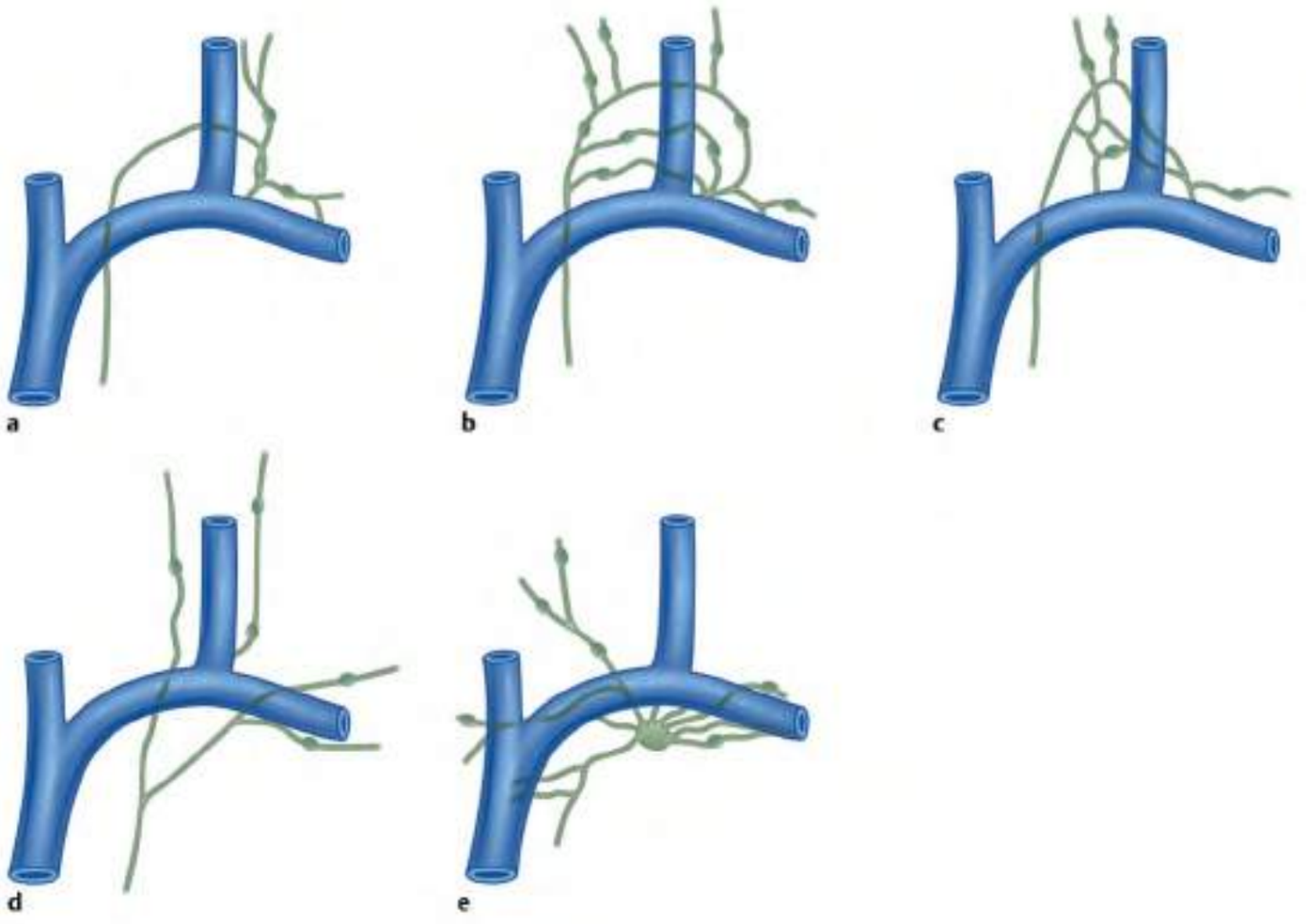

Fig. 9.13 Variations of the entry of the thoracic duct into the venous system. **(a)** A single thoracic duct and a simple junction. **(b)** Plexiform ramification of the final segment of a thoracic duct, but with a simple junction. **(c)** Delta-like entry of the thoracic duct. **(d)** Duplication of the final segment of the thoracic duct and two separate junctions. **(e)** Ampullary enlargement of the thoracic duct with multiple terminal branches. (Used with permission from Baumeister RGH. Surgical anatomy of the lymphatic system. In: Heberer G, van Dongen RJAM, eds. Vascular Surgery. New York, NY: Springer-Verlag; 1989:37; with permission of Springer Science and Business Media.)

pathologist Rudolf Virchow (1821–1902). It is usually caused by metastatic gastric carcinoma, although it can also be seen in other gastrointestinal, thoracic, and pelvic cancers.

Thymus Lymphatics

As a primary lymphatic organ, the thymus does not have afferent lymphatics. Three groups of efferent vessels have been identified: superior lymphatic vessels draining directly into the internal jugular, innominate, or anterior mediastinal nodes; anterior lymphatic ducts draining into the parasternal nodes; and posterior lymphatic ducts draining into the tracheobronchial nodes.[5]

Esophageal Lymphatics

There are lymphatic plexuses in every esophageal layer, but the lymphatic network is more abundant in the submucosa and less developed in the muscular layer. In general, the upper two-thirds of the esophagus drain cephalad and the lower third drains caudad.

In the thorax, most nodes draining the esophagus are located in the region of the tracheobronchial bifurcation and pulmonary hilum.[5] Some lymphatics of the esophagus may directly drain lymph into the thoracic duct without crossing any lymph node. This anodal route can be the source of distant metastases in esophageal cancer in spite of normal nearby lymph nodes.[11]

Mediastinum

The lymphatic collectors and the nodes located along their course form pathways called lymph node chains. The lymphatic collectors of the mediastinum originate from the deep lymphatic channels of the lungs. Their drainage is generally ipsilateral, but anomalies can be encountered. In general, lymphatic collectors of the inferior mediastinum travel upstream within the inferior pulmonary ligaments and ascend toward the carina. On occasion, collectors from the inferior mediastinum travel downstream, traversing the diaphragm. There are numerous lymphatic collectors in the superior mediastinum and most ascend along the lateral and anterior aspect of the trachea. On the right side (right

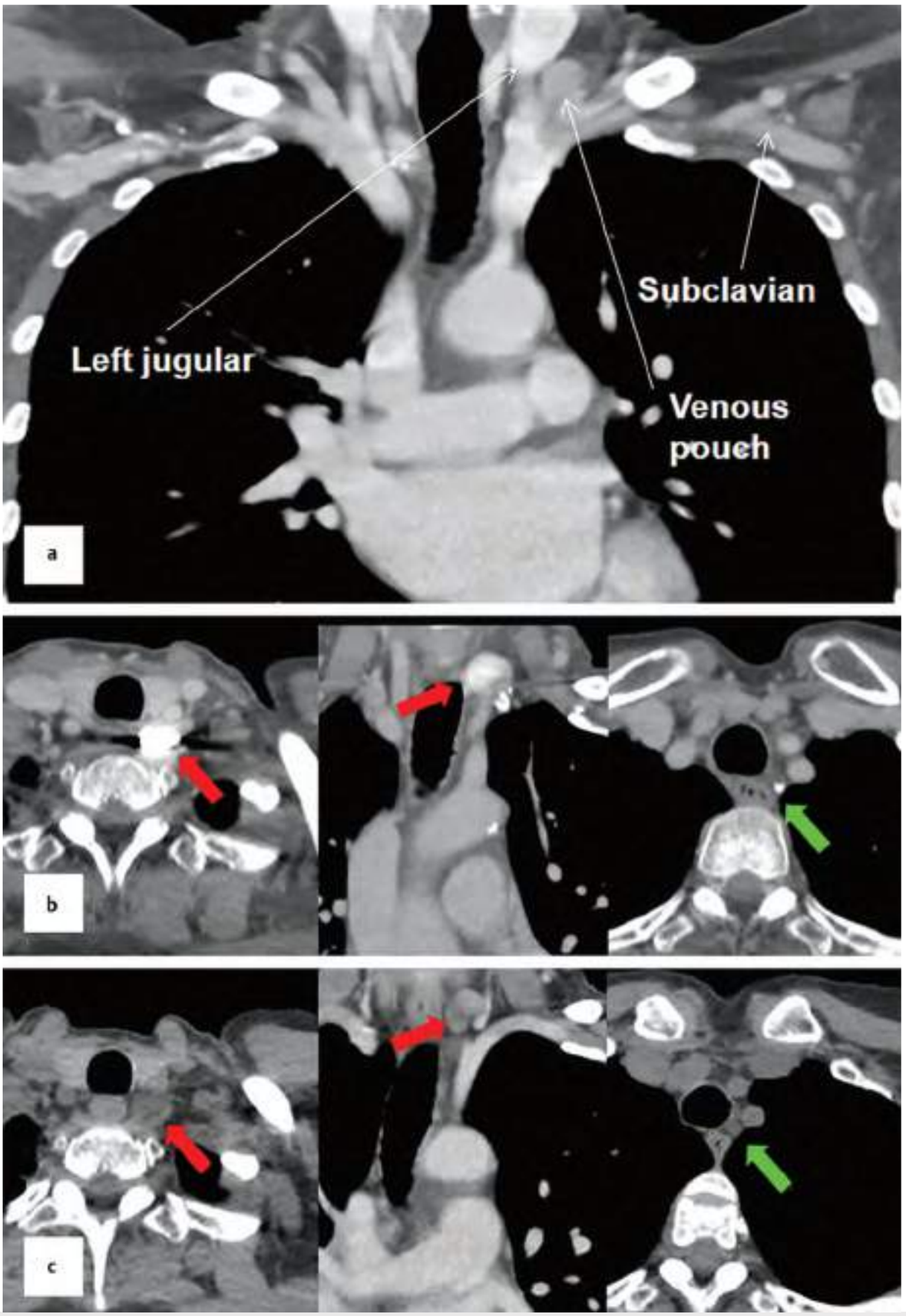

Fig. 9.14 **(a)** Venous pouch at the confluence of the left subclavian and internal jugular veins where the thoracic duct enters. **(b)** Delayed postcontrast CT images showing residual contrast (*red arrows*) in the venous pouch located between the left subclavian vein and the thoracic duct. Reflux of the contrast into the thoracic duct is also seen (*green arrows*). **(c)** Follow-up precontrast CT images showing clearance of the contrast (*green arrow*).

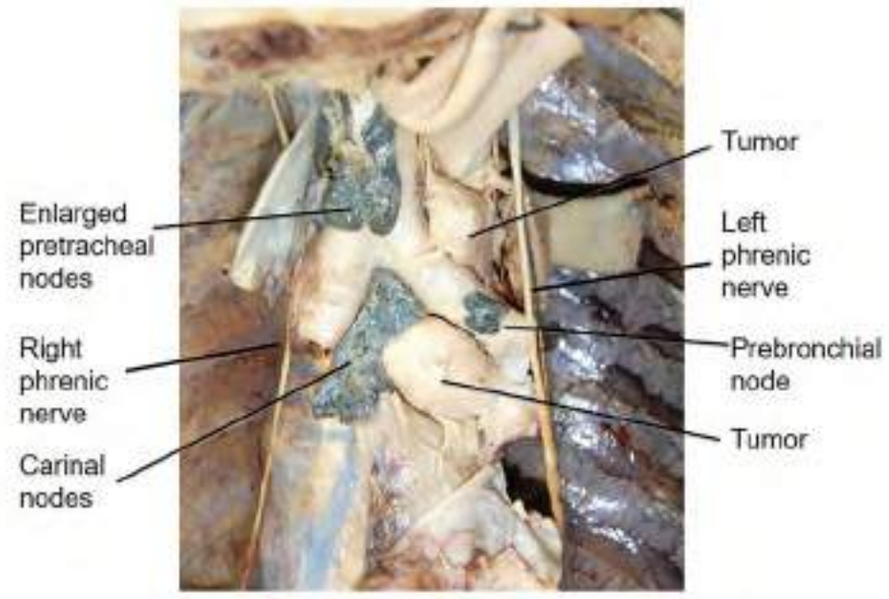

Fig. 9.15 View of the anterior mediastinum showing tumors and metastatic lymph nodes.

pretracheal lymphatic collector) they terminate in the venous circulation, whereas on the left side (left pretracheal lymphatic collector), they travel cephalad along the left recurrent nerve to terminate eventually at the left jugular–subclavian venous confluence. Additional important lymphatic collectors of the superior mediastinum include a right posterior lymphatic collector (tracheoesophageal collector), which ascends between the right lateral aspect of the trachea and lateral border of the esophagus, and a group of left preaortic collectors, which are located in the anterior mediastinum and run upward along the aortic arch to terminate into the left internal jugular subclavian vein confluence.[5]

In the thorax, there are three main lymphatic pathways: a posterior parietal chain ascending in the posterior mediastinum along the spine, an anterior parietal chain ascending along the internal mammary vessels, and a median visceral chain ascending along the tracheobronchial tree and the phrenic nerves[5] (▶ Fig. 9.15, ▶ Fig. 9.16, ▶ Fig. 9.17, ▶ Fig. 9.18).

The posterior parietal chain collects intercostal lymphatics draining the chest wall, the posterior parietal pleura, and the posterior part of the diaphragm. Over the course of these lymphatics, lymph nodes are located in the extrapleural fat adjacent to the heads of the ribs (posterior intercostal nodes).[5]

The anterior thoracic chain drains the anterior chest wall, the anterior and lateral diaphragm, and the medial breast. The internal mammary nodes are found in the intercostal spaces along the sternum and usually present from the fifth intercostal spaces to the clavicles. There are connections between the left and right anterior thoracic chains through intercostal channels.[5]

The median visceral chain collects branches from the posterior paraesophageal chain, some from the anterior chain along the phrenic nerves and, most importantly, from the median tracheobronchial chain, which essentially drains the lungs.[5]

Although the anatomy of thoracic lymph nodes has long been known, these nodes have recently been regrouped in terms of nodal stations. The modification was intended to correlate basic anatomy with new imaging techniques such as computed tomographic scanning. In this regional classification, lymph nodes located within the lung (bronchopulmonary nodes) are classed as being in stations 11 to 14, those located in the hilum (hilar nodes) are included in station 10, and those from the mediastinum are classed as being in stations 1 to 9 depending on their location. The anatomical boundary between the hilar and mediastinal nodes is the mediastinal pleura.[5]

Nodes of the posteroinferior mediastinum (stations 7, 8, 9) are largely paraesophageal (station 8) and subcarinal (station 7). Nodes of the inferior pulmonary ligament (station 9) are few and lie in close proximity to the inferior pulmonary vein. They can connect with the para-aortic nodes in the abdomen. The lymph nodes of the tracheal bifurcation (station 7) are variable in number and size, and they are arranged in clusters, one located anteriorly and one more posteriorly and extending laterally to the main bronchi. The paraesophageal nodes (station 8) are mostly involved with esophageal lymph drainage.[5]

Nodes of the superior mediastinum (stations 1, 2, 4) constitute the most important group of mediastinal nodes. The tracheobronchial nodes (station 4) are located in the angle between the trachea and corresponding main bronchus (▶ Fig. 9.16, ▶ Fig. 9.17). On the right side, they are situated medial to the arch of the azygos vein and above the right pulmonary artery; on the left, they lie in the concavity of the aortic arch. The superior paratracheal nodes (station 2) are located higher up along the anterolateral wall of the trachea. Those on the right side are more numerous than those on the left, and they lie inferior and to the right of the innominate artery. Still higher lymph nodes are located in station 1 where they lie about a horizontal line at the upper rim of the innominate artery. These nodes form the link between the tracheobronchial nodes and interior deep cervical nodes.[5]

The nodes of the anterior mediastinum (stations 5, 6) are numerous and overlie the upper portion of the pericardium. The nodes of station 5 are located in the aortopulmonary window

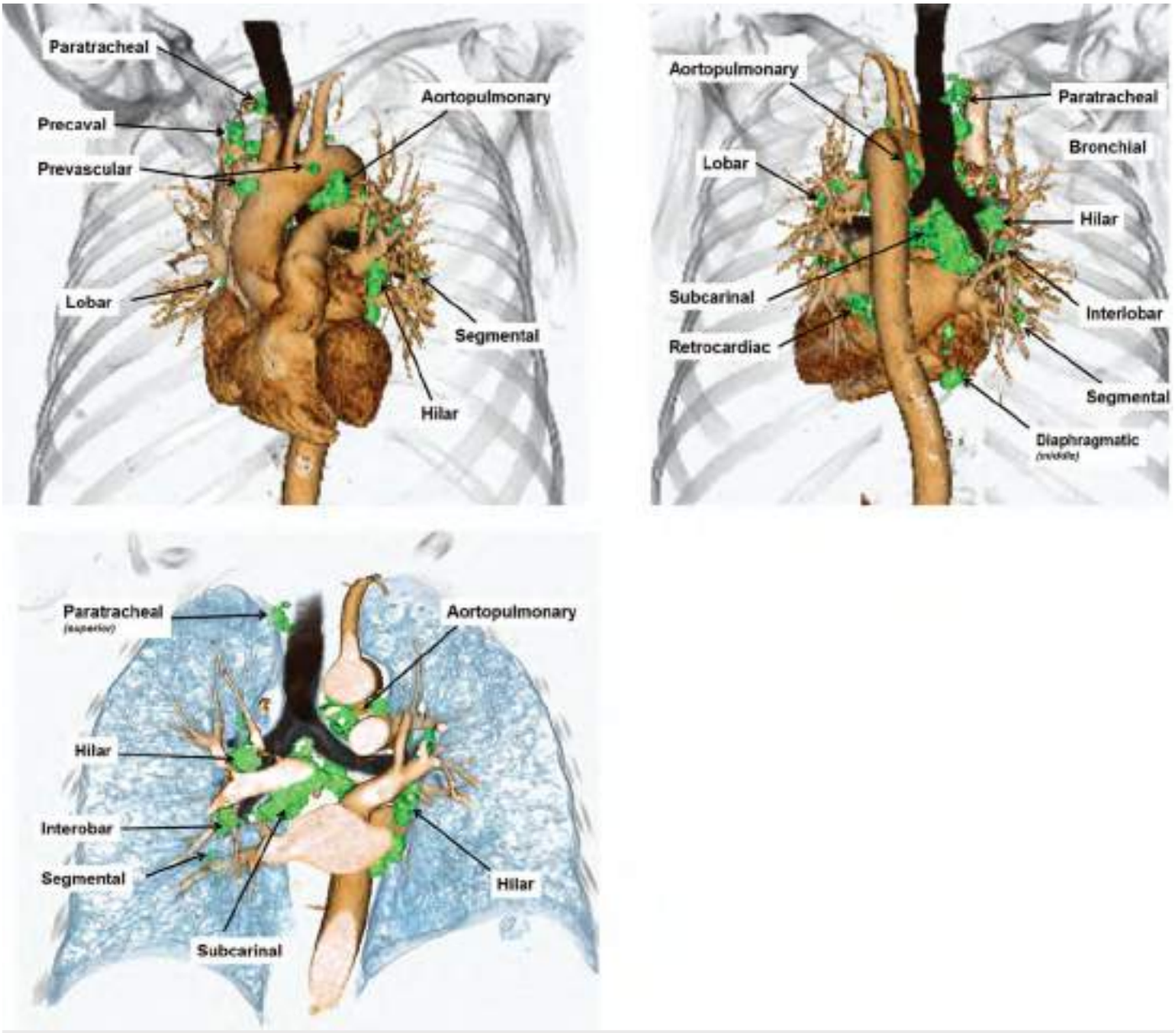

Fig. 9.16 (**a–c**) Tracheobronchial and bronchopulmonary lymph nodes are shown by volume-rendered CT. In radiology, lymph nodes are usually named in relation to the nearby anatomical structure. The pulmonary nodes include interlobar, lobar, segmental, and parenchymal.

close to the origin of the left pulmonary artery and the ligamentum arteriosum, whereas those of station 6 are deeply embedded between the origins of the left carotid and left subclavian arteries. These nodes, which are particularly important in the lymphatic drainage of the left upper lobe, lie underneath the mediastinal pleura between the phrenic and vagus nerves.[5]

CT has become the imaging modality of choice for assessing patients with bronchogenic carcinoma. Its efficacy in assessing mediastinal nodal status is limited by a relatively low sensitivity and specificity. Despite its limitations, CT remains important by aiding in the selection of the most appropriate procedure for staging, by guiding biopsies, and by providing anatomical information for visual correlation with FDG-PET images. CT-guided transthoracic needle biopsy of mediastinal nodes is occasionally performed for staging purposes, either alone or in conjunction with other procedures. Virtual bronchoscopy, an advanced visualization technique in which helical CT data and virtual reality computing are used to create three-dimensional endobronchial simulations, can help to guide transbronchial needle aspiration. The ability of virtual bronchoscopy to generate mediastinal lymph node maps in order to demonstrate complex three-dimensional anatomical relationships can help determine the most direct approach to transbronchial needle aspiration.[12]

Pericardial and Cardiac Lymphatics

The pericardium consists of two layers of mesothelial cells with lymphatic stomata scattered in the inner layer. Pericardial stomata connect with submesothelial lymphatic vessels, and the drainage is eventually directed toward the tracheobronchial nodes for the lateral pericardium and the paraesophagael nodes for the posterior pericardium. The lymphatic vessels of the anterior pericardium most often pass along the phrenic nerves to terminate in the nodes of the anterior mediastinum.[13]

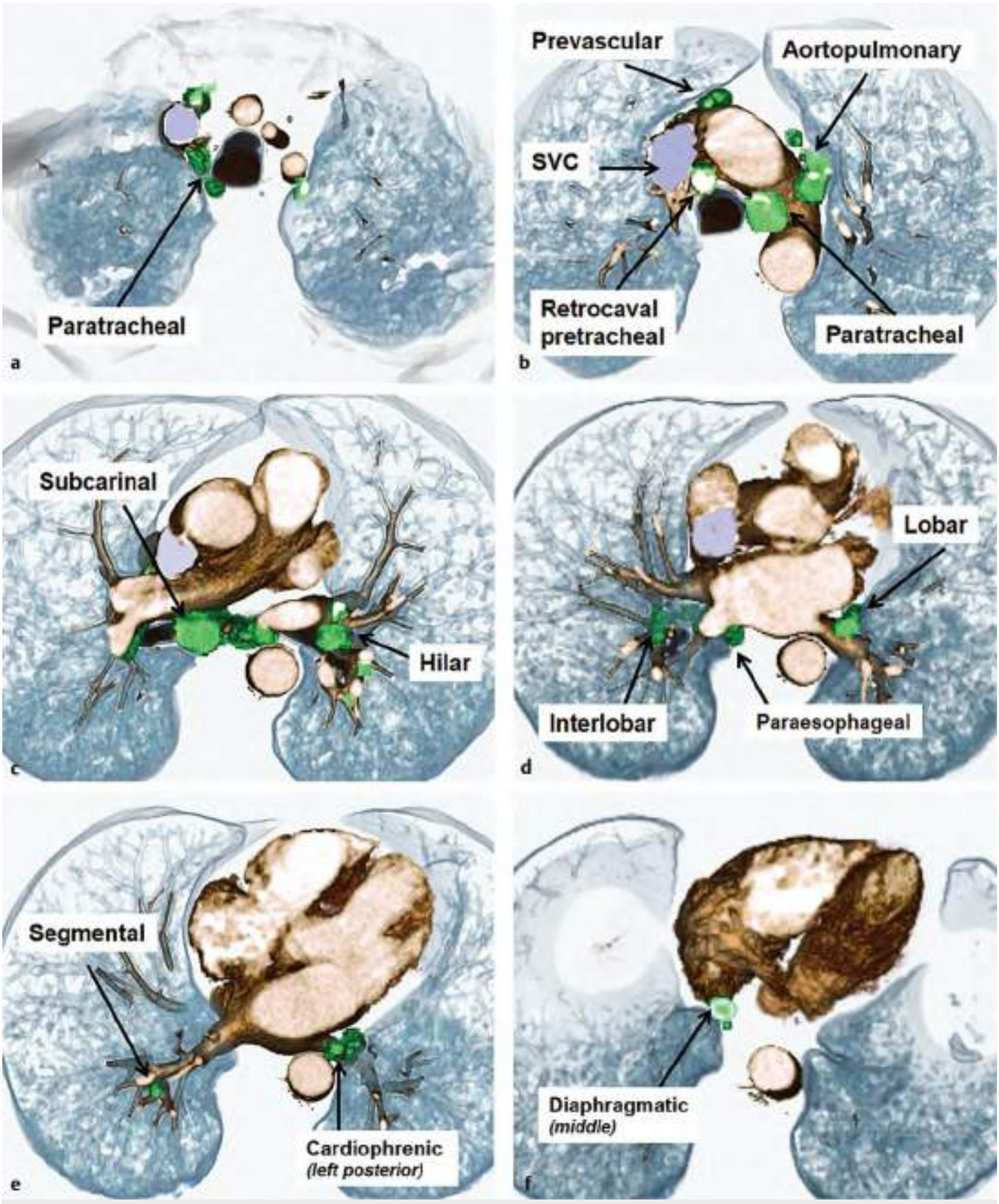

Fig. 9.17 Axial color-coded CT images showing mediastinal lymph nodes.

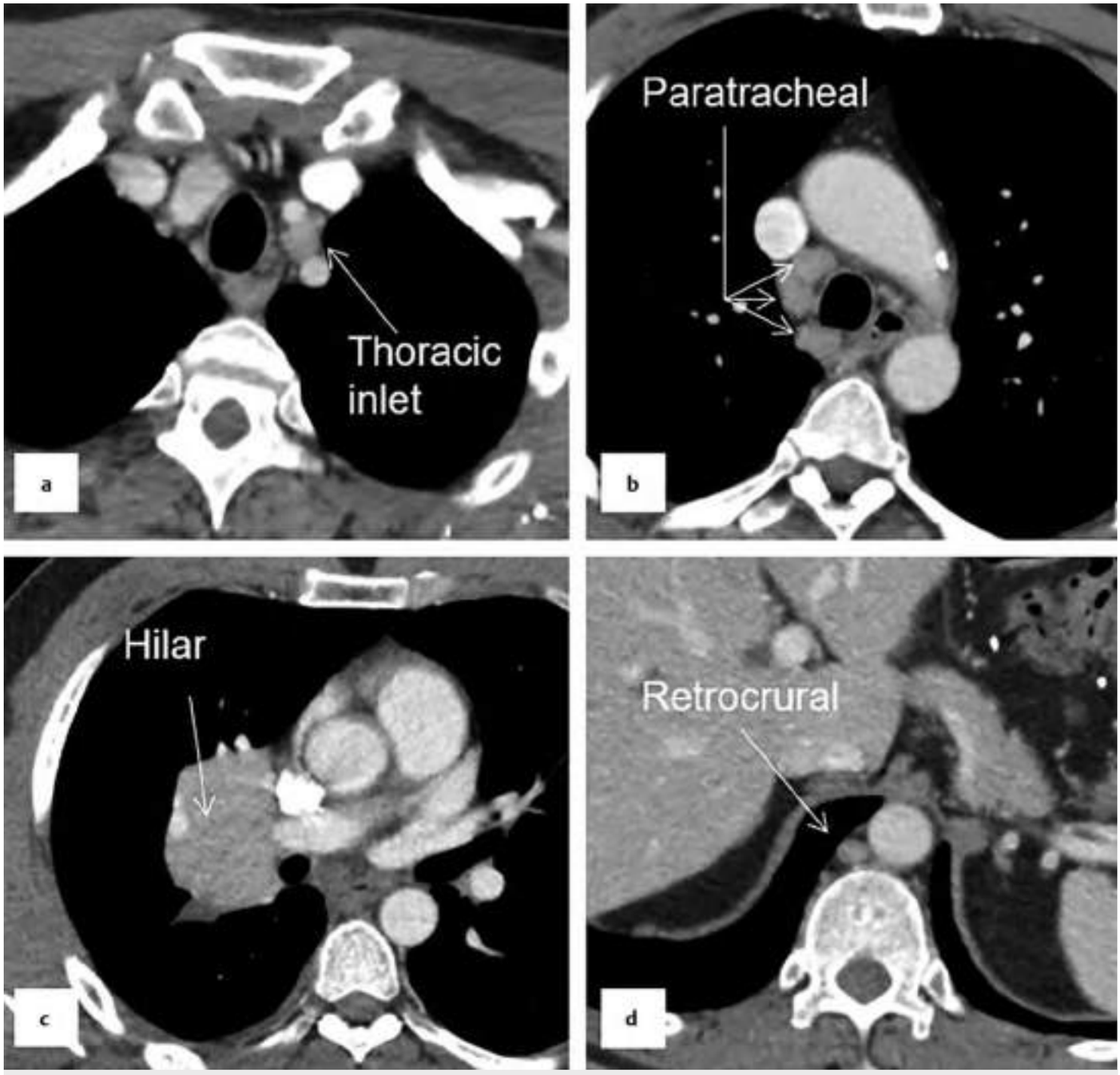

Fig. 9.18 Examples of abnormal mediastinal lymph nodes. **(a)** Left high paratracheal at the thoracic inlet. **(b)** Right paratracheal enlarged nodes. **(c)** Right hilar large confluent nodes in a patient with Castleman disease. **(d)** Retrocrural (posterior diaphragmatic). SVC, superior vena cava.

The lymphatic vessels of the heart follow the coronary arteries and drain mainly into the brachiocephalic nodes, anterior to the brachiocephalic veins and tracheobronchial nodes, at the inferior end of the trachea.[1]

The lymphatic system of the heart consists of three plexuses. The endocardial plexus is a network of small lymphatic capillaries located below the basal membrane of the endocardium and drains into the myocardial plexus, which has a drainage pattern that generally follows the coronary blood vessels. The third plexus, the epicardial plexus, collects effluents from the subendocardial and myocardial plexuses and is a loosely interconnected network located in the subepicardial connective tissue. It reaches the collector lymphatic channels over the surface of the heart and eventually coalesces into the cardiac lymphatic trunks.[5]

The left main cardiac lymphatic trunk collects lymph from a left branch (anterior surface of the left ventricle) and a right branch (posterior surface of the left ventricle and left atrium). It runs behind and along the left main pulmonary artery and eventually passes to the left of the aortic root and ascending aorta toward the aortic arch.[5]

The right main cardiac lymphatic trunk, which collects lymph from the right ventricle and the right atrium, is located over the posterior surface of the heart. It runs along the interventricular groove toward the base of the heart and, like the right coronary

artery, curves toward the anterior surface of the right ventricle in the direction of the right atrium and ascending aorta. The right main cardiac lymphatic trunk then travels in the direction of the aortopulmonary window where it unites with the left trunk to reach the nodes in that area.[5]

References

[1] Drake R, Vogl AW, Mitchell AW. Grays Anatomy for Students'. 2nd ed. 2009

[2] Aquino SL, D, uncan GR, Hayman LA. Nerves of the thorax: atlas of normal and pathologic findings. Radiographics.; 21(5):1275–1281

[3] Mennini ML, Catalano C, Del Monte M, Fraioli F. Computed tomography and magnetic resonance imaging of the thoracic lymphatic system. Thorac Surg Clin.; 22(2):155–160

[4] Beasley P. Anatomy of the pharynx and esophagus. In: Kerr AG, Gleeson M, eds. Scott-Browns Otolaryngology. 6th ed. Oxford, UK: Butterworth-Heinemann; 1997

[5] Brotons ML, Bolca C, Fréchette E, Deslauriers J. Anatomy and physiology of the thoracic lymphatic system. Thorac Surg Clin.; 22(2):139–153

[6] Schraufnagel DE. Lung lymphatic anatomy and correlates. Pathophysiology.; 17(4):337–343

[7] Gossner J. Appearance and visibility of the thoracic duct on computed tomography of the chest. Internet J Radiol..; 12:2

[8] Loukas M, Wartmann CT, Louis RG, Jr, et al. Cisterna chyli: a detailed anatomic investigation. Clin Anat.; 20(6):683–688

[9] Phang K, Bowman M, Phillips A, Windsor J. Review of thoracic duct anatomical variations and clinical implications. Clin Anat.; 27(4):637–644

[10] Kinnaert P. Anatomical variations of the cervical portion of the thoracic duct in man. J Anat.; 115(Pt 1):45–52

[11] Hematti H, Mehran RJ. Anatomy of the thoracic duct. Thorac Surg Clin.; 21 (2):229–238, ix

[12] Boiselle PM, Patz EF, Jr, Vining DJ, Weissleder R, Shepard JA, McLoud TC. Imaging of mediastinal lymph nodes: CT, MR, and FDG PET. Radiographics.; 18 (5):1061–1069

[13] Eliskova M, Eliska O, Miller AJ. The lymphatic drainage of the parietal pericardium in man. Lymphology.; 28(4):208–217

10 Diaphragm

Ashley Prosper and Farhood Saremi

◆ Introduction

The diaphragm is a musculotendinous dome-shaped sheet between the thoracic and abdominal cavities. More than just a geographical boundary between the thoracic and abdominal cavities, the diaphragm is the most important muscle of respiration and vital to human life. Understanding its embryology, anatomy, and mechanism of action is key to interpretation of its pathologies.

◆ Embryology

Four embryological structures give rise to the mature diaphragm during weeks 4 to 12 of human development: the transverse septum anteriorly, two pleuroperitoneal folds (membranes) laterally, the dorsal mesentery (aka the esophageal mesentery) dorsomedially, and muscular ingrowth from the lateral body walls (▶ Fig. 10.1). These primitive structures together form the mature diaphragm's two parts: a fibrous central tendon and peripherally arising muscular bundles, which will be described in detail later.

The transverse septum is the first diaphragmatic precursor to develop, arising from the mesenchymal coelomic wall at the level of the C3 cervical somites during weeks 3 to 4 of gestation. As the head folds ventrally during the fourth week of gestation, the transverse septum forms a partition between the pericardial and abdominal cavities anteriorly, separating the heart from the liver. During weeks 4 to 8 this mesoderm descends from the cervical level to its final position at the junction of the thoracic and abdominal cavities.[1,2,3,4] During this descent through the neck, myogenous stem cells are able to migrate from cervical somites into the transverse septum. The transverse septum forms major parts of the diaphragm; therefore, innervation of the diaphragm is mainly supplied from the phrenic nerve, derived from C3, C4, and C5.[3] The pleuroperitoneal membranes are the next diaphragmatic precursors to develop. Arising during week 6 of development from the lateral body wall, they grow medially to flank the

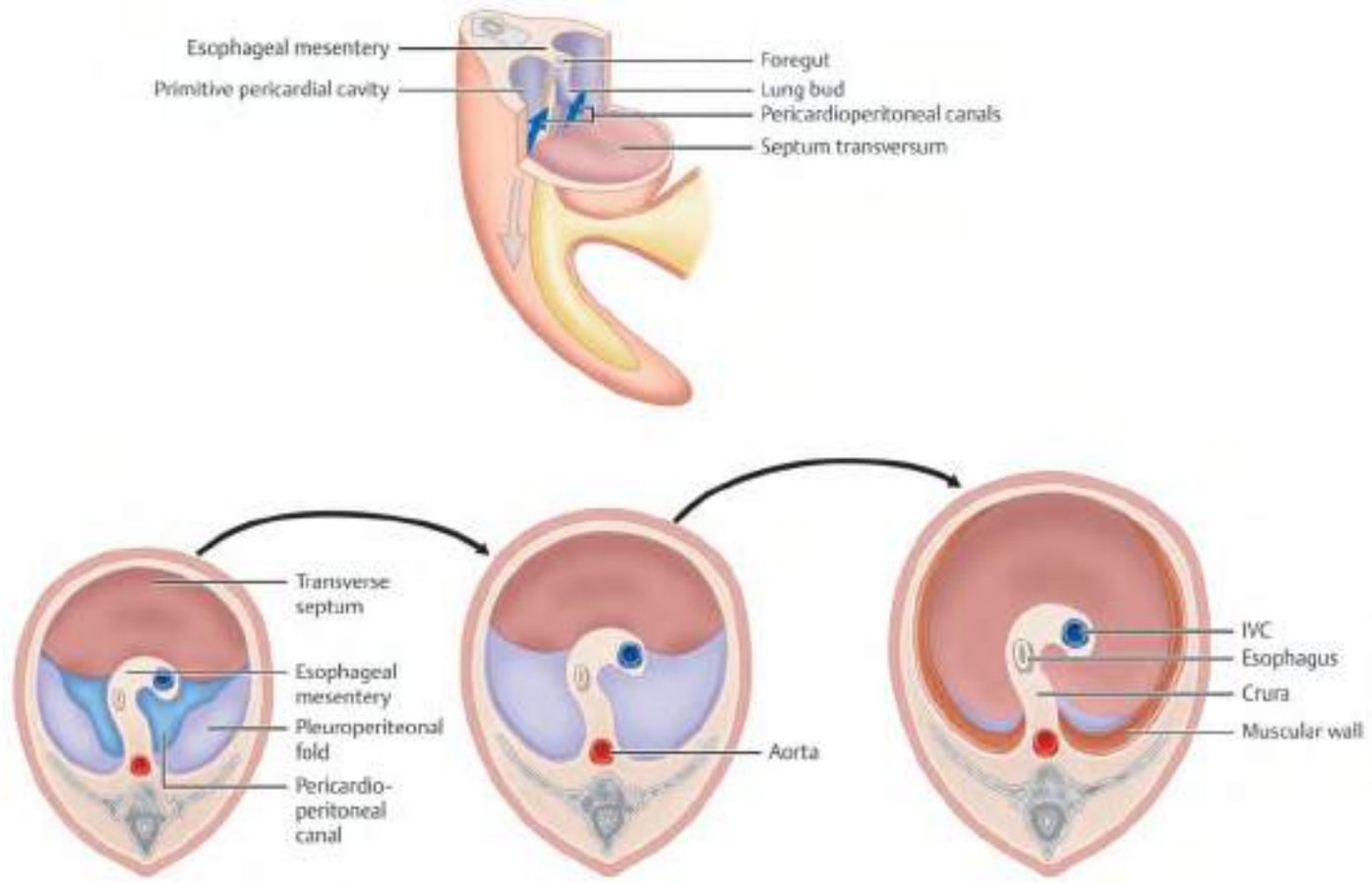

Fig. 10.1 Development of the diaphragm. Four embryological structures give rise to the mature diaphragm during weeks 4 to 12 of human development: the transverse septum anteriorly, two pleuroperitoneal folds (membranes) laterally, the dorsal mesentery dorsomedially, and muscular ingrowth from the lateral body walls. The two pleuroperitoneal folds fuse with the transverse septum and the dorsal mesentery around 7 to 8 weeks and close the pericardioperitoneal (pleuroperitoneal) canals. The transverse septum forms major part of the central tendon and ventral part of the diaphragm. The dorsal/esophageal mesentery forms the diaphragmatic crura. Muscle bundles derived from cervical myotomes form the muscular portion of the diaphragm. Late growth of other structures decreases the relative contribution of the pleuroperitoneal membranes to a small area. IVC, inferior vena cava. Used with permission from Fisher and Bodenstein 2006.[2]

esophagus, meet the transverse septum and the dorsal mesentery. The dorsal/esophageal mesentery anchors the foregut to the body wall and eventually forms the diaphragmatic crura. After the pleuroperitoneal membranes have fused to the transverse septum and dorsal mesentery, muscle bundles derived from myotomes of the 7th to 12th segments begin to develop between the primitive pleura and peritoneum, forming the muscular portion of the diaphragm and give the final dome-shaped appearance of the diaphragm. These muscle bundles are categorized into three groups based on their origins from the peripheral body wall: the pars lumbalis, costalis, and sternalis. Therefore, innervation of the peripheral part of the diaphragm is by the lower intercostal nerves. The diaphragm in newborn is relatively flat and moves mainly in its posterior part whereas in the adult it is dome-shaped and move centrally.

◆ Anatomy

The diaphragm is domed-shaped peripherally and is relatively flat in its central portion (▶ Fig. 10.2). It is approximately 2 to 4 mm in thickness. The right hemidiaphragm is located higher on the right than the left. The overall configuration and position of the diaphragm is influenced by the status of respiration, patient position, and pathologies. In supine position, the diaphragm remains high than standing position.[4,5,6] Hyperinflated lungs or large pleural effusion can depress the diaphragm. The slope of the diaphragm from the dome to the periphery is greatest in the posterior region forming the posterior costophrenic angle where pleural fluid accumulates first (▶ Fig. 10.2, ▶ Fig. 10.3).

The superior surface of the diaphragm is covered by the endothoracic fascia, parietal diaphragmatic pleura, and pericardium. The diaphragmatic pleura and the fibrous pericardium are firmly attached to the endothoracic fascia and diaphragm.

The anteroinferior surface of the diaphragm is covered by the diaphragmatic fascia, an extension of the transversalis fascia, extraperitoneal fat, and in part by the peritoneum (▶ Fig. 10.4). The posteroinferior surface of the diaphragm is not covered completely by the peritoneum and faces the retroperitoneal fat. The diaphragmatic attachment of the falciform ligament and bare area of the liver also are not covered by the peritoneum (▶ Fig. 10.4). The falciform ligament is the remnant of the primitive ventral mesentery, extending between the anterior abdominal wall and the diaphragm and the anterior surface of the liver.[4]

The round ligament of the liver and the obliterated left umbilical vein run in the free edge of the falciform ligament facing the peritoneum.

The diaphragm is comprised of two parts: a central tendinous and a peripheral muscular (▶ Fig. 10.5). The diaphragm muscle is composed of two regions. The costal diaphragm which is a thin striated muscle in the periphery of the diaphragm and the crural diaphragm which is thicker and located more posteriorly in the paravertebral area.

Central Tendon

The central tendon of the diaphragm is an aponeurosis to which the diaphragmatic muscles project from the body wall. This central tendon is positioned anteriorly along the diaphragmatic dome and subjacent to the fibrous pericardium. The tendon is most commonly V-shaped. Three leaflets comprise the central tendon: right, middle, and left, listed here in order of decreasing size.[7] Superior surface of the central tendon is adhered to the fibrous pericardium (▶ Fig. 10.3).

Peripheral muscular attachments of the central tendon are divided into (1) sternal or anterior, (2) costal or lateral, and (3) lumbar or posterior. The tendon area is smaller than the muscle area in most individuals.[7] Diaphragmatic attachments on the sides are symmetric. The crural attachment of the diaphragm is asymmetric when comparing the left and right sides.

Muscular Attachments

Anterior/Sternal and Lateral Attachments

Anteriorly, the diaphragm attaches to the xiphoid process, aponeurosis of the transverse abdominal muscle (▶ Fig. 10.4, ▶ Fig. 10.5). The anterolateral diaphragm attaches to the medial aspects of the 7th and 8th ribs and their anterior costochondral junctions anteriorly and the 9th and 10th ribs laterally. The xiphoid slip attachment, or the sternal part of the diaphragm, being the most central and superior anterior attachment, results in an inverted V- or U-shaped configuration to the diaphragm when viewed in the frontal (coronal) projection[8] (▶ Fig. 10.6, ▶ Fig. 10.7). Small triangular spaces known as "foramina of Morgagni" separate the sternal attachment slips from the costal fibers on each side (▶ Fig. 10.5).

Posterior/Lumbar Attachments

Posteriorly and medially, the diaphragm attaches to the body wall via the left and right crura, which are anchored to the superior aspect of the lumbar spine. Posterolaterally, the diaphragm attaches to the 11th and 12th ribs. This part of diaphragm blends with aponeurosis of the transverse abdominal muscle and the deep layer of the thoracodorsal fascia.

Variable Appearance of the Diaphragmatic Muscular Slips

As described earlier, muscle bundles forming the muscular part of the diaphragm are categorized by their origin: lumbar, costal, and sternal or the pars lumbalis, costalis, and sternalis.[8,9] These muscle bundles course from their peripheral origins, centrally and superiorly, toward the diaphragm's central tendon. Diaphragmatic muscle bundles vary in morphology (▶ Fig. 10.6, ▶ Fig. 10.7). Thickened slips may pose a diagnostic challenge on imaging. Prominent slips may indent or invaginate the hepatic surface. Multiple slips invaginating the liver surface can mimic cirrhosis, though hepatic surface nodularity in cirrhosis is more irregular (▶ Fig. 10.7). In some cases, a particularly prominent slip may mimic a hepatic mass on some projections, particularly on ultrasound. Slips have also been shown to mimic abdominal adenopathy. In patients with abundant fat in the mediastinum and anterior abdominal wall, the sternal slips of the diaphragm may be displaced laterally. These laterally displaced slips with adjacent fat should not be mistaken with Morgagni hernia

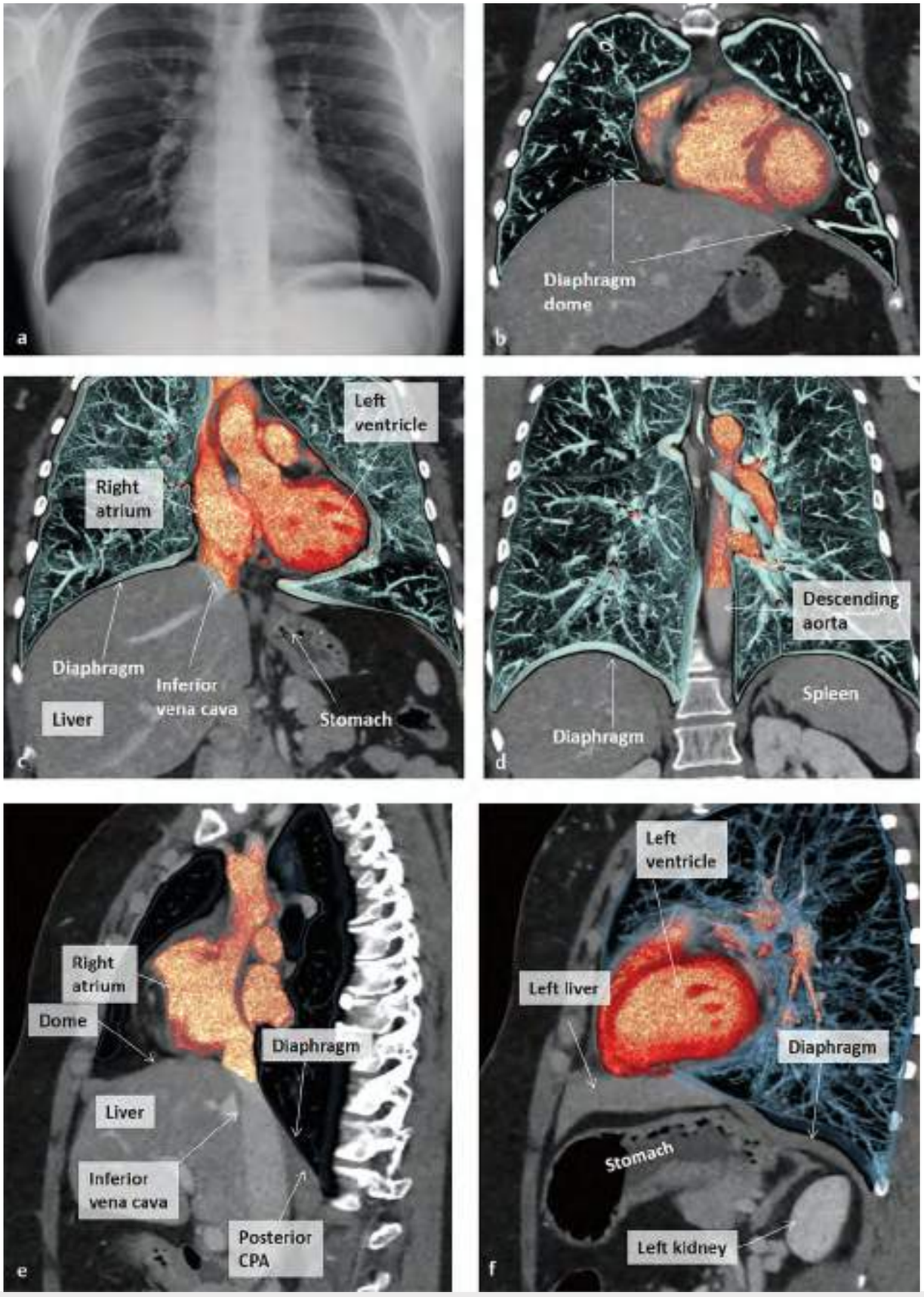

Fig. 10.2 (a–f) Normal appearance of the diaphragm on posteroanterior plain X-ray and coronal CT scan at three levels: anterior, midlevel (through the inferior vena cava), and posterior. Also shown are sagittal views (lower row) at the level of the inferior vena cava and medial spleen. The slope of the diaphragm from the dome to the periphery is greatest in the posterior region where the posterior costophrenic angles (CPA) of the pleura are located.

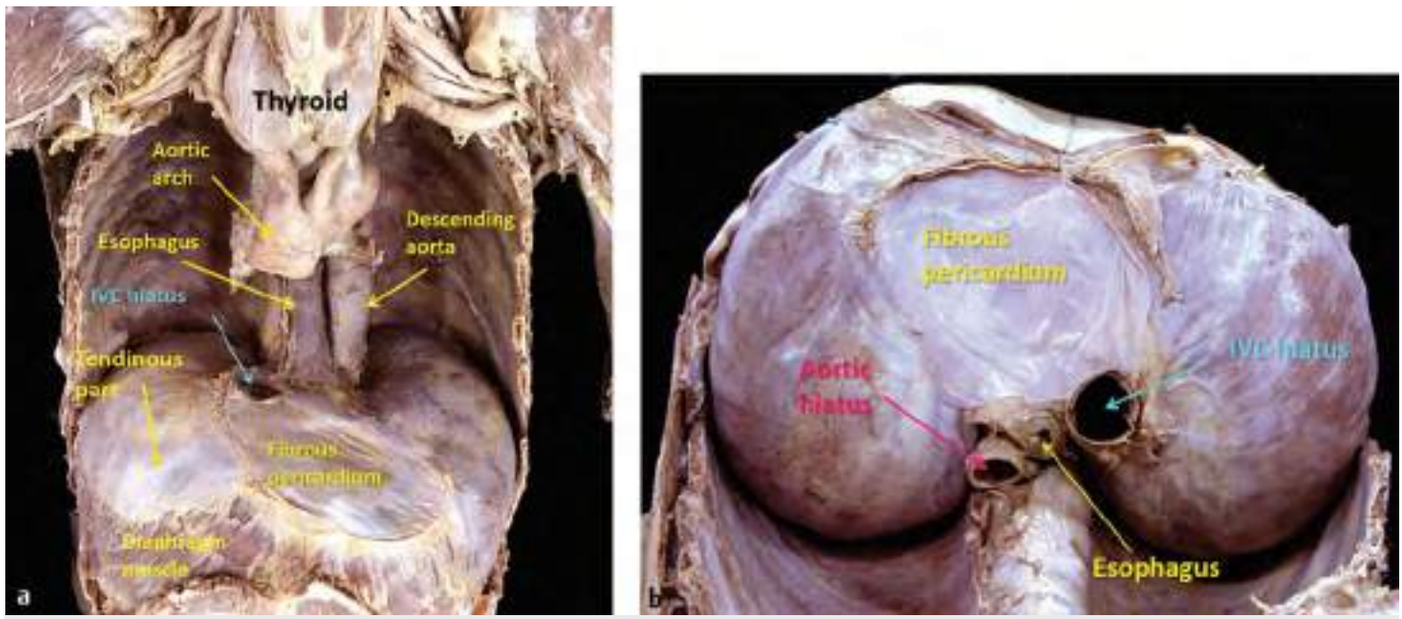

Fig. 10.3 **(a)** Superior views of the diaphragm. **(b)** Hiatuses. The diaphragm provides three openings or hiatuses, namely the aortic, esophageal, and vena caval hiatuses. IVC, inferior vena cava.

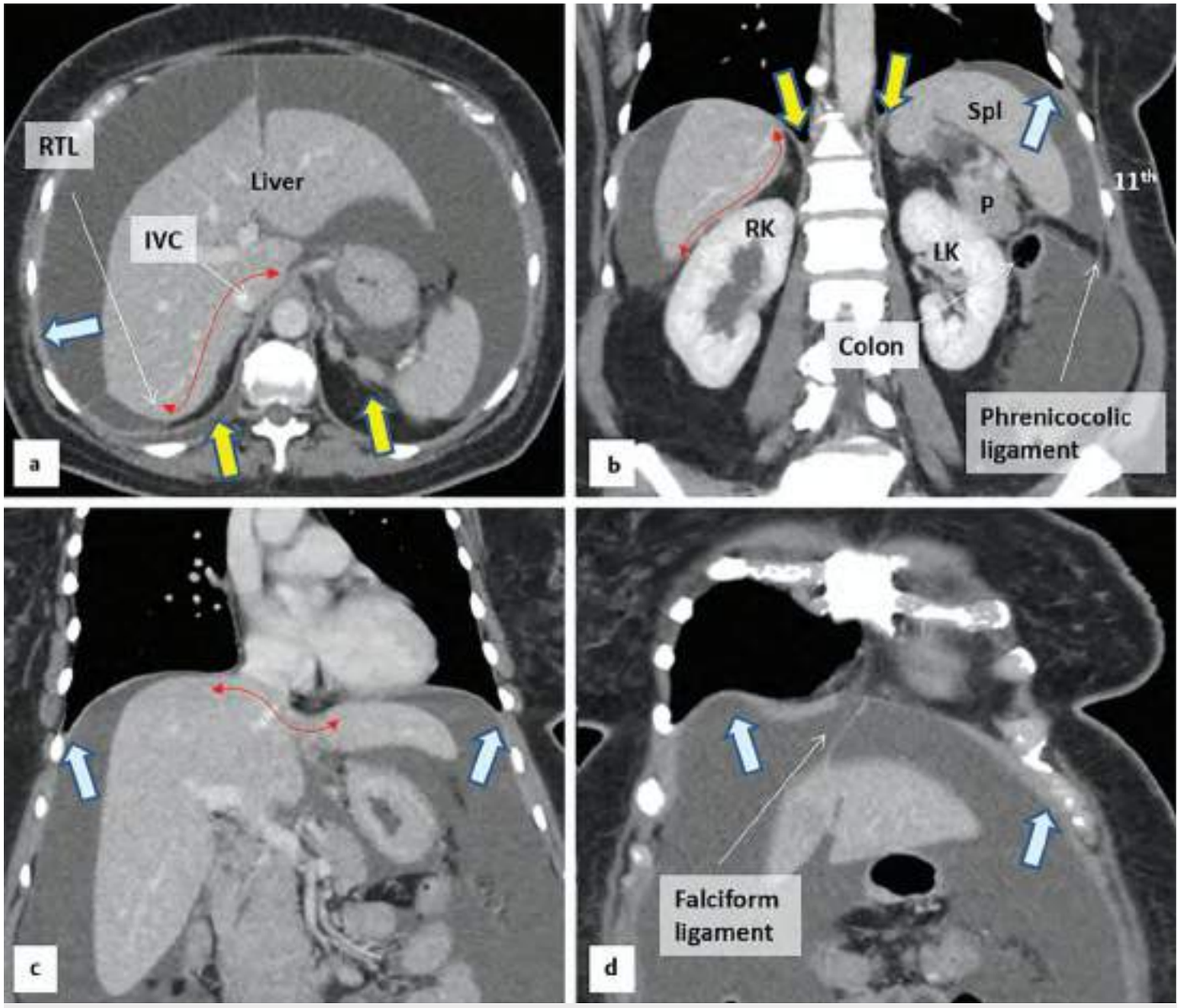

Fig. 10.4 Inferior diaphragm borders shown in a patient with ascites. **(a)** Axial CT. **(b-d)** Coronal CT from posterior to anterior. The inferior surface of the diaphragm is facing the peritoneal cavity (*blue arrows*) except along its posterior margin where it is facing the extraperitoneal fat (*yellow arrows*), at the bare area of the liver, and where ligaments are attached (*yellow arrows*) such as the gastrophrenic ligament and the phrenicocolic ligament. The bare area of the liver (*double-headed red arrows*) faces the inferior vena cava (IVC), right adrenal, superior pole of the right kidney, right crus, and vertebrae. The diaphragmatic attachment of the falciform ligament also is not covered by the peritoneum. The phrenicocolic ligament connects the splenic flexure of the colon to the diaphragm at the level of the 11th rib. LK, left kidney; RK, right kidney; P, pancreas; Spl, spleen; RTL, right triangular ligament.

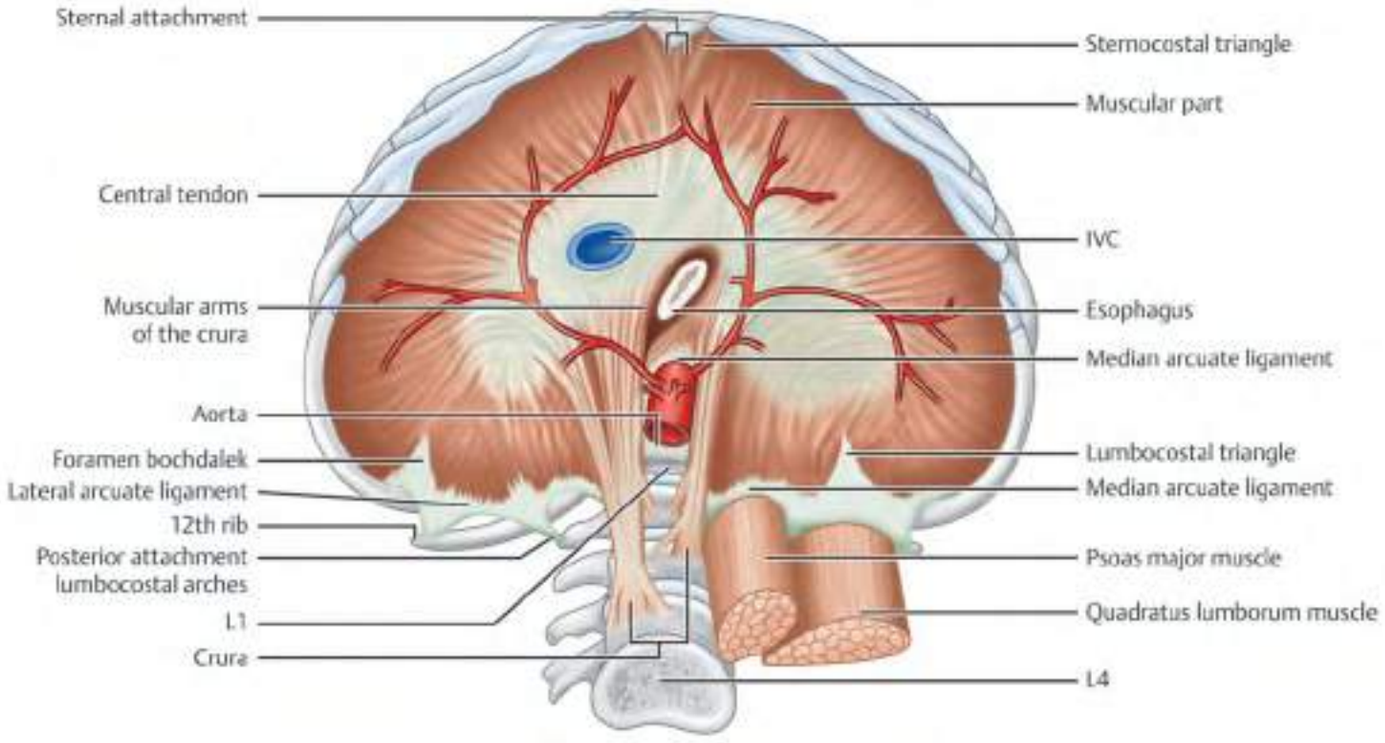

Fig. 10.5 Inferior surface of the diaphragm. Hiatus and arcuate ligaments are shown. The lumbocostal triangles (Bochdalek's foramen) are where the diaphragm attaches to the anterior margin of the 12th rib. The sternocostal triangles (Morgagni's foramen) are bilateral muscular fat-filled defects through which the superior epigastric artery, veins, and lymphatics pass. IVC, inferior vena cava.

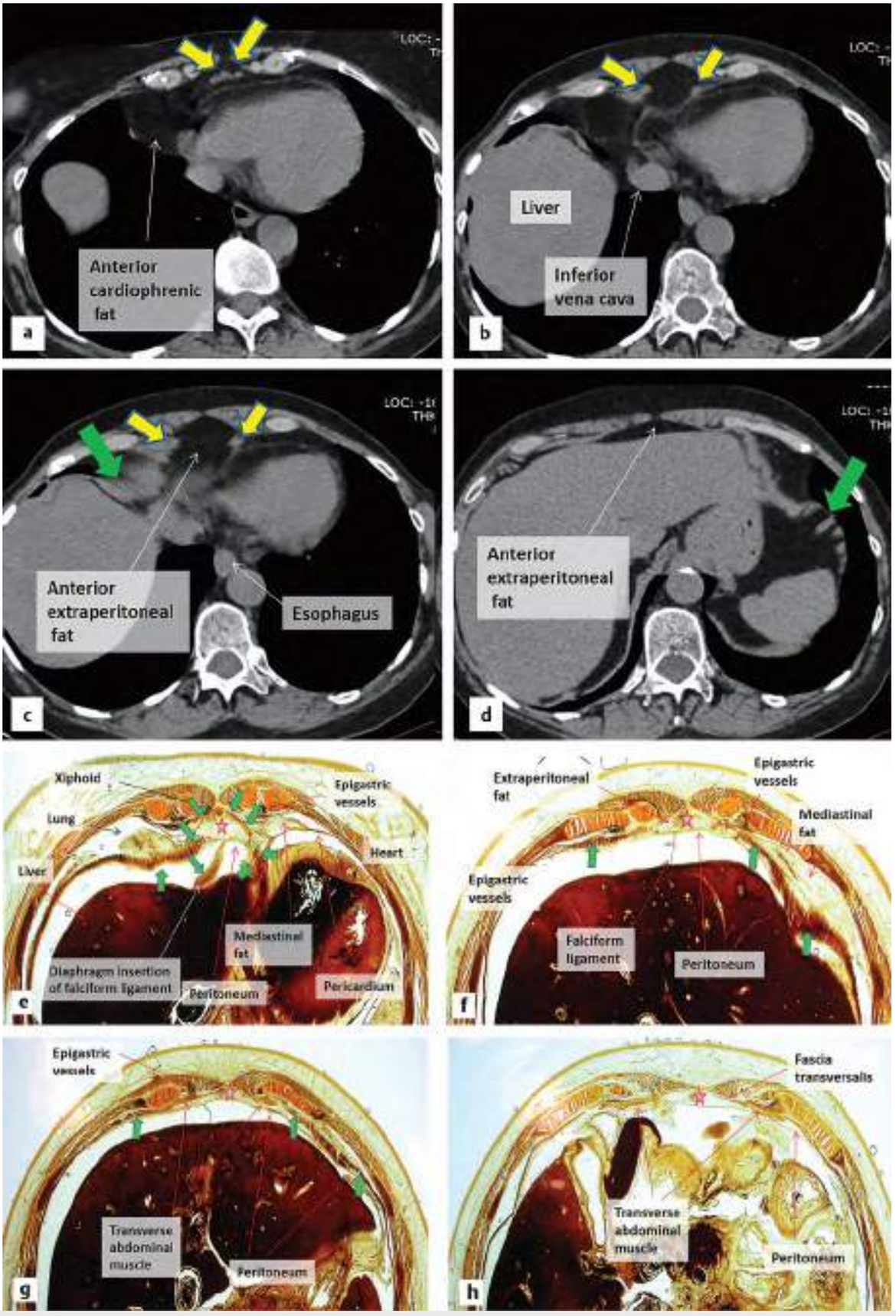

Fig. 10.6 Anterior diaphragmatic attachments. (**a–d**) The xiphoid slip attachment, or the sternal part of the diaphragm (*yellow arrows*) is the most central and superior anterior attachment. These anterior slips are separated from each other by large amount of fat in anterior cardiophrenic angle of the mediastinum which is continuous with the fat in the anterior extraperitoneal space. This configuration should not be mistaken with hernia of the peritoneal fat through the Morgagni foramen. Note large muscle slips of the diaphragm (*green arrows*). **(e**, **f)** Cadaveric axial cuts from superior to inferior. Anterior diaphragmatic attachments (*green arrows*) are shown. Note most epigastric vessels travel outside the attachments of the diaphragm. **(g**, **h)** The origins of the transverse abdominal muscle slips from the costochondral junctions anterior to the diaphragmatic slips are shown. The anterior extraperitoneal space (*stars*) containing fat is seen arising below the anterior diaphragmatic attachments to the xiphoid (*stars*). This space can communicate with the anterior mediastinal fat through fenestrations in the diaphragmatic attachments to the xiphoid.

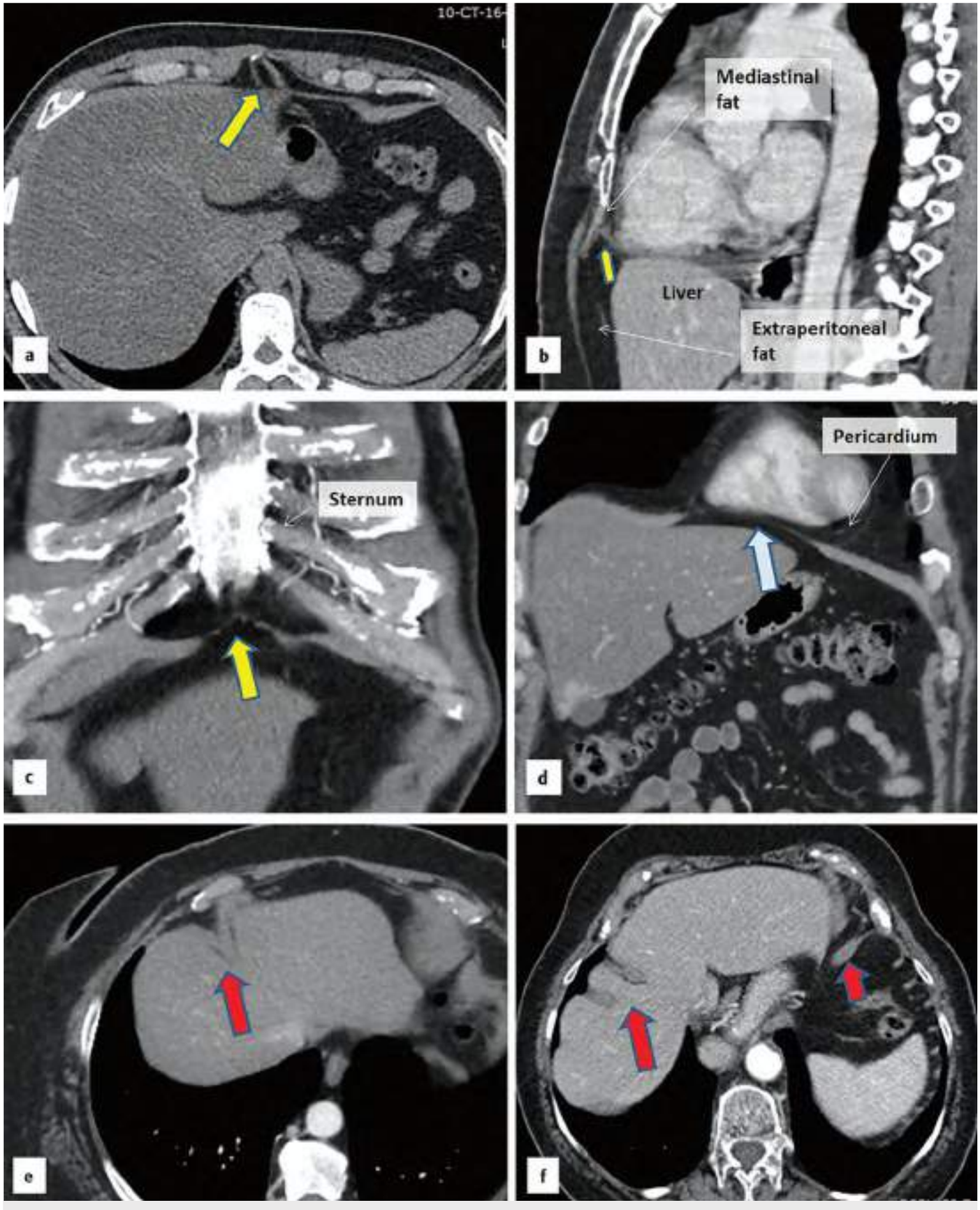

Fig. 10.7 Variable appearance of the diaphragmatic muscular slips. **(a)** Axial, **(b)** sagittal, and **(c)** coronal views show the anterior slip attachments with an inverted V- or U-shaped configuration (*yellow arrows*). **(d)** Coronal CT showing the central tendon (*blue arrow*) where the pericardium is attached. **(e, f)** Large muscle slips (*red arrows*) indenting the liver should not be mistaken with pathology.

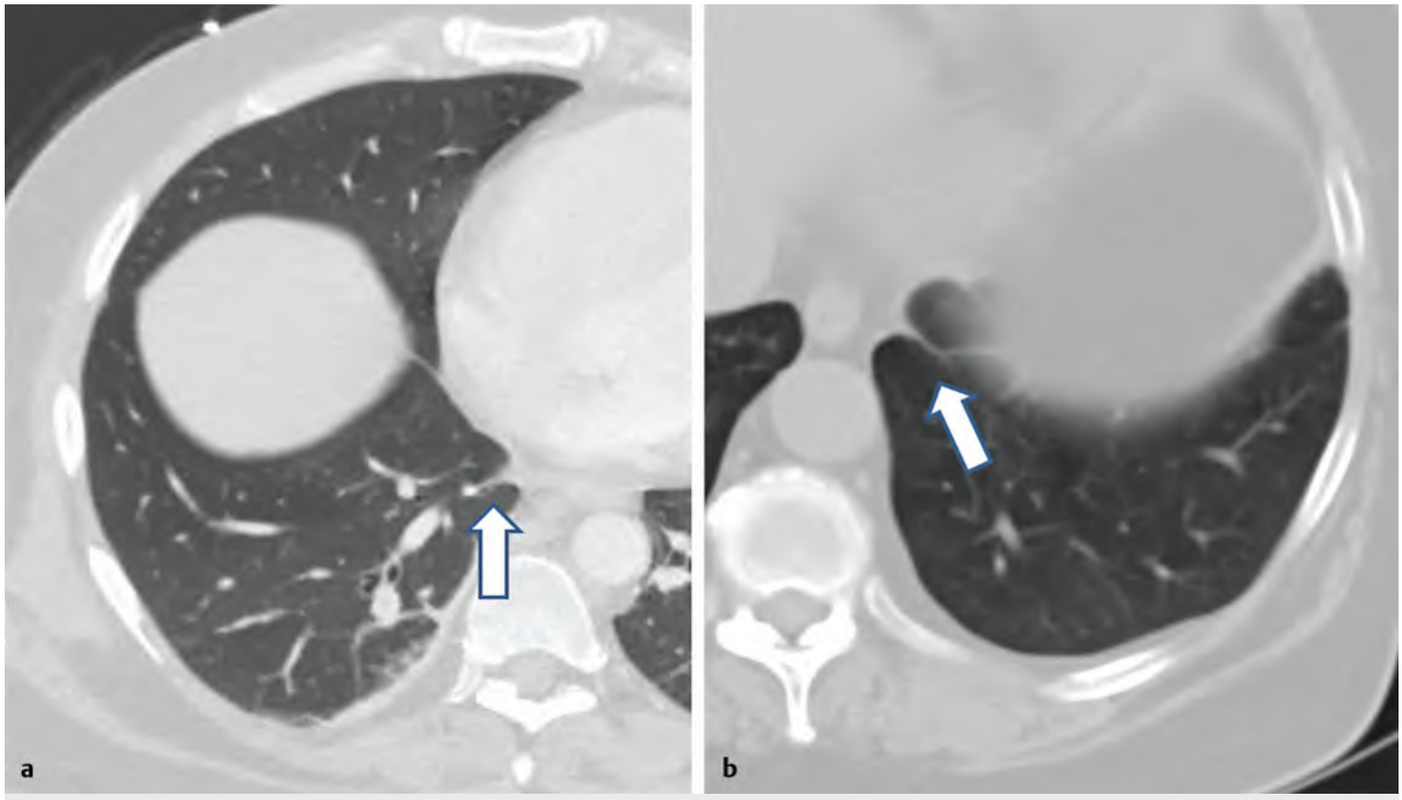

Fig. 10.8 Inferior pulmonary ligament (*arrows*). **(a)** Right. **(b)** Left. The inferior pulmonary ligament is a pleural thickening connecting the diaphragm to the hila of the lungs. In axial views it may be seen as linear structures in paravertebral region surrounded by lower lobe lung immediately cephalad to its termination on the left hemidiaphragm.

(▶ Fig. 10.6). On computed tomography (CT), identifying contiguity with the diaphragm on multiple transaxial CT images can help distinguish a slip from abdominal pathology.[8]

Diaphragm Ligaments

Several ligaments composed of loose connective tissue are attached to the superior or inferior surface of the diaphragm. Above, the phrenopericardial ligament connects the diaphragm to the fibrous pericardium (see Chapter 5). The phrenicoesophageal ligaments join the esophagus and the left and right hemidiaphragms.[10] The inferior pulmonary ligament is a pleural thickening connecting the diaphragm to the hila of the lungs (see Chapter 5). In patients with hyperinflated lung volumes, the lower lobe engulfs the ligament on both sides, causing the ligament to appear to be located within the paravertebral lung on axial CT sections (▶ Fig. 10.8). The right ligament is located near the inferior vena cava (IVC) and the left ligament near the descending aorta.[8]

Inferior to the diaphragm the two layers of the falciform ligament are continuous with the peritoneal reflections between the liver and diaphragm.[4] These peritoneal reflections form the anterior and posterior layers of the coronary ligament on the right and left. The anterior and posterior coronary ligaments meet to enclose the bare area on each side. Their confluence points form the right and left triangular ligaments. The bare area of the liver faces the IVC, right adrenal, superior pole of the right kidney, right crus, and vertebrae (▶ Fig. 10.4, ▶ Fig. 10.9). There is also a small bare area behind the abdominal esophagus facing the diaphragm and at the attachment of gastrophrenic ligament. The phrenicocolic ligament connects the splenic flexure of the colon to the diaphragm at the level of the 11th rib (▶ Fig. 10.4). The ligament of Treitz connects the duodenojejunal junction to the right crus.

Arcuate ligaments are thickened fascia along the posterior margin of the diaphragm. Posteriorly and laterally, the diaphragm forms two arcuate ligaments on each side.[11] The lateral arcuate ligament spans the quadratus lumborum, whereas the medial arcuate ligament spans the psoas muscles (▶ Fig. 10.5). The lateral arcuate ligament extends between the transverse process of L1 and the inferior edge of the 12th rib. The medial arcuate ligament extends between the transverse process of L1 and the corresponding crus. The medial arcuate ligaments are separated from each other by the crura and the vertebral bodies.

The median arcuate ligament joints the crura in midline. It usually passes superior to the origin of the celiac axis. Low-lying variations of the median arcuate ligament's attachments to the lumbar spine can compress the celiac artery in 10 to 24% of people, in some cases resulting in symptoms including abdominal pain, nausea and vomiting, or median arcuate ligament syndrome[12] (▶ Fig. 10.10).

Diaphragmatic Crus

The term crura, the plural of crus, is derived from the Latin word cruralis, meaning "leg." There are two diaphragmatic crura on the sides of the vertebral bodies that encircle the gastroesophageal (GE) junction and forms the hiatus of the diaphragm.[13,14] The

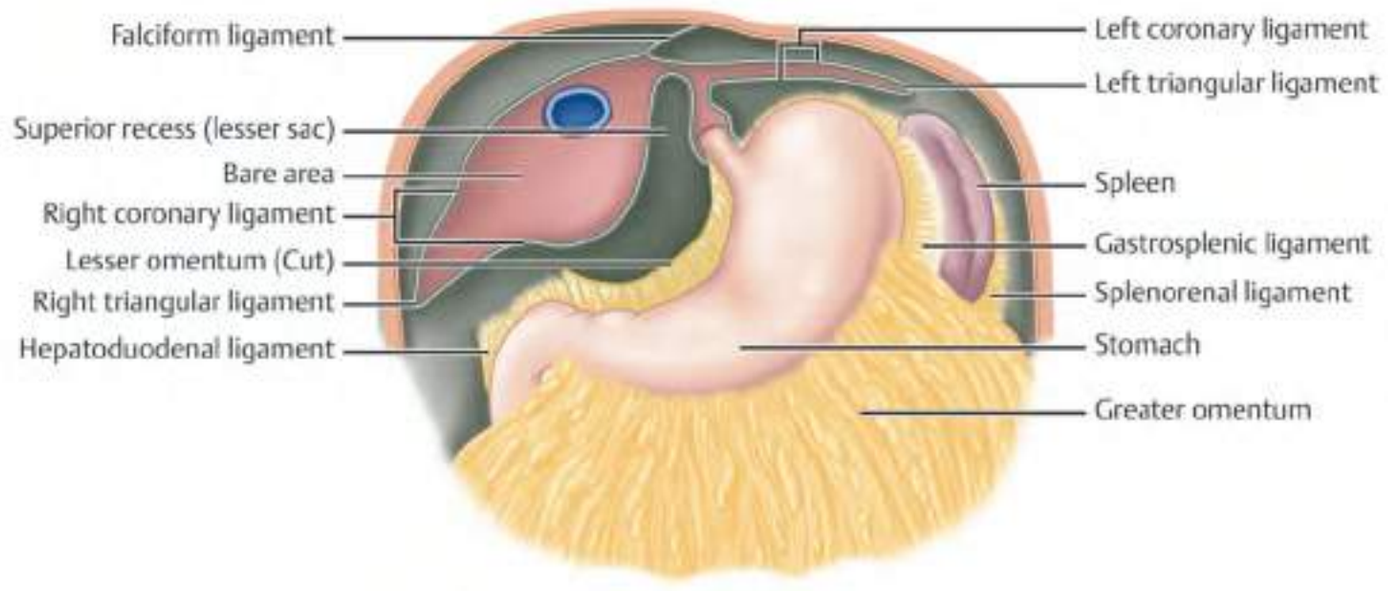

Fig. 10.9 Inferior surface of diaphragm and peritoneal reflections on it forming the bare area of the liver. The margins of the bare area are peritoneal reflections that form the falciform, coronary, and triangular ligaments of the liver.

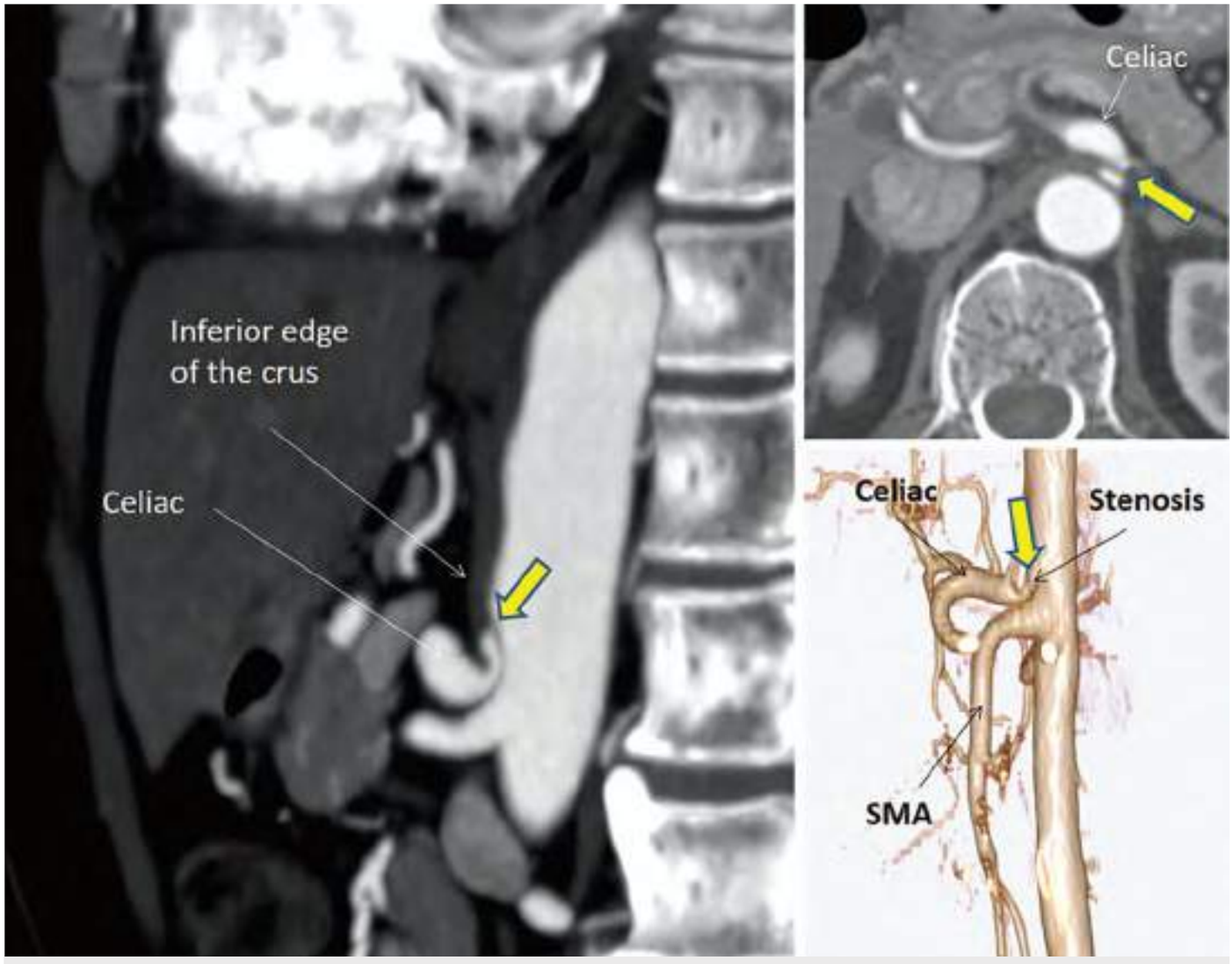

Fig. 10.10 Median arcuate ligament forms the inferior margin of a bridge jointing the crura in midline. It usually passes superior to the origin of the celiac axis (*yellow arrows*). Low-lying variations of the median arcuate ligament can compress the celiac artery in 10 to 24% of people. SMA, superior mesentric artery.

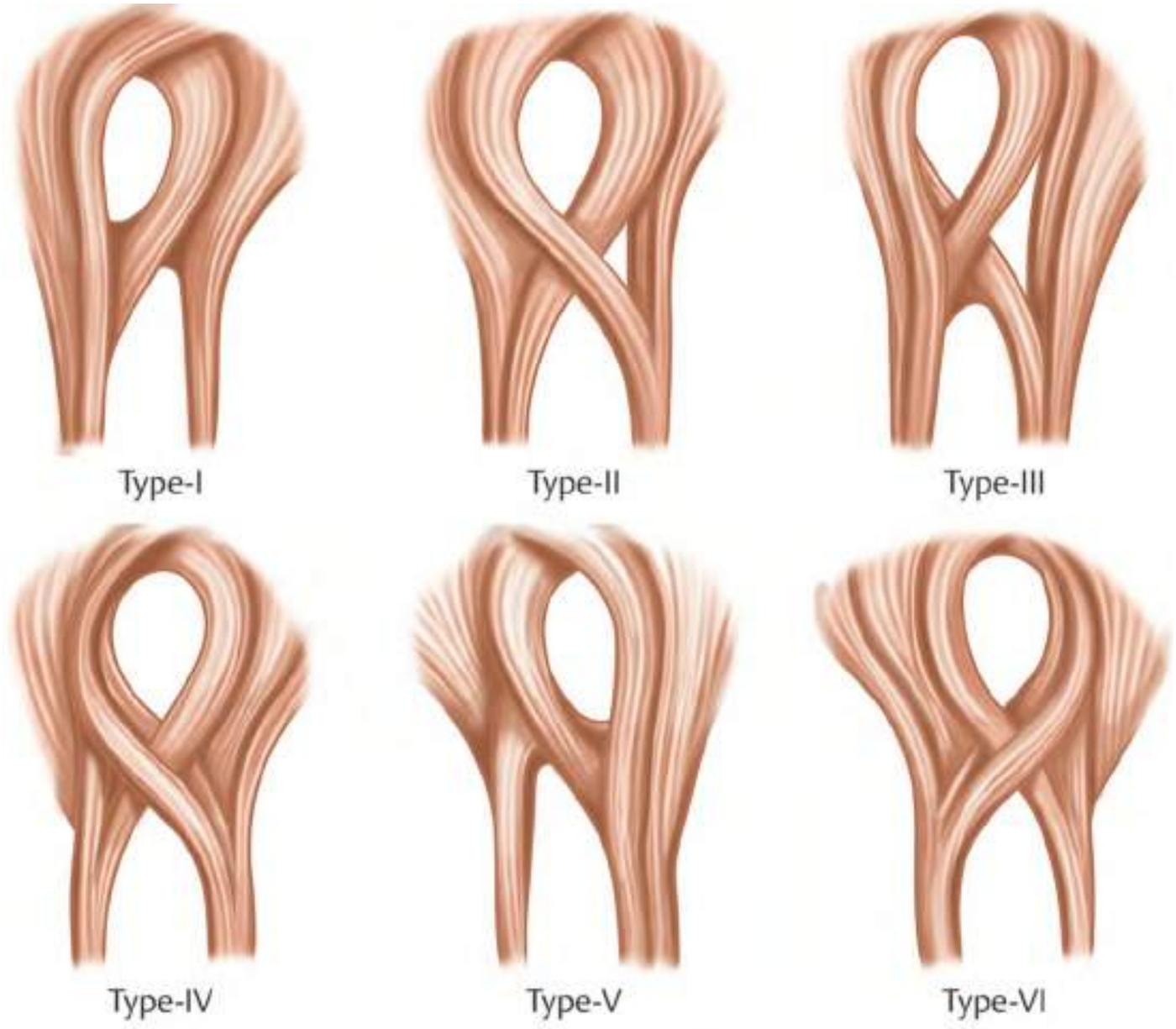

Fig. 10.11 Diagrammatic representation of the different types of diaphragmatic crura. In 45% the esophageal hiatus is formed from muscular contributions of the right crus only (Type I). (Used with permission from Loukas 2008.[14])

crura arise from the anterior surface of the lumbar vertebral bodies and the anterior longitudinal ligament from L1 through L3 and insert on the central tendon. It is longer on the right side. The origin of the crura near the bone is tendinous but the crura become increasingly muscular as they ascend into the diaphragm. Only the tendinous parts hold sutures after surgery. Each crus has two parts, a vertical part that moves along the vertebrae and a transverse part along the diaphragm proper. The pattern of the transverse part of the crus at esophageal hiatus is variable. In many cases, especially on the right side, two arms exist, one anterior and one posterior to the GE junction, that encircle the esophageal hiatus. In a recent study by Loukas et al, it is shown that in 45% the esophageal hiatus is formed from muscular contributions of the right crus only (▶ Fig. 10.5).[14] This pattern is very common in CT studies of the abdomen. In 20 to 30% the left arm arises from the right crus, and the right arm arises from both crura or the right side. Extra bands may be seen in the remainder of cases (▶ Fig. 10.11). There is a wide range of normal variants of the diaphragmatic crura.

The phrenicoesophageal ligaments (membrane) attach the lower esophageal segment to the diaphragmatic crura within the esophageal hiatus and indirectly prevent GE reflux. Its fibers are continuous with the transversalis and endothoracic fascia covering the diaphragm and penetrate superiorly and inferiorly in the adventitia and intermuscular connective tissue of the distal esophagus.[15] In adults, the ligament is attenuated as subperitoneal fat accumulates in the hiatus and in hiatal hernia the ligament is either torn or disappeared.

Retrocrural Space

The retrocrural space is a small triangular region posterior to the two diaphragmatic crura and anterior to the spine.[16] Normal structures within the retrocrural region include the aorta, nerves,

the azygos and hemiazygos veins, the cisterna chyli with the thoracic duct, fat, and lymph nodes (▶ Fig. 10.12). It is a common location for passage of abnormalities from the abdomen into the posterior mediastinum including lymph node metastasis, hernia of fat, and primary tumors. Aortic aneurysm and azygos and hemiazygos continuation of the IVC are among vascular abnormalities in this region. Enlarged azygos and hemiazygos veins in this region are a common finding in cirrhosis with portal hypertension and those with thrombosis of the IVC (▶ Fig. 10.12).

◆ Diaphragmatic Hiatuses

While serving as a boundary between the thoracic and abdominal cavities, the diaphragm must allow, structures important to both cavities, to pass from one side to the other[17] (▶ Fig. 10.3, ▶ Fig. 10.5). The diaphragm thus provides three major openings, or hiatuses, named after the principal structures traveling through them, namely the aortic, esophageal, and vena caval hiatuses. Smaller hiatuses exist and will be described below. Communication occurs between structures above and below the diaphragm through the hiatuses. The aortic and esophageal hiatuses are the most common diaphragmatic communication pathways through which inflammatory, infectious, and malignant processes can spread from one cavity to another. Through small porous defects or perivascular sheaths air or fluid can travel between the thorax (mediastinum or pleura) and the abdomen (abdominal wall, peritoneum, or retroperitoneum).

10

Vena Cava Hiatus

The most cephalad hiatus is the vena caval hiatus, located at the T8 level approximately 2 cm to the right of the midline. In addition to the IVC, this diaphragmatic opening also provides a passage for branches of the right phrenic nerve and pericardiophrenic vessels. It is not uncommon to see the retroperitoneal fat entering this region causing narrowing of the IVC (▶ Fig. 10.13).

Esophageal Hiatus

At the T10 level, the esophagus with its vessels, vagal nerve, and additional sympathetic nerve fibers pass through the diaphragm at the esophageal hiatus. The anterolateral margins of the hiatus are formed by the crura and the posterior margin is formed by the median arcuate ligament. Given the common occurrence and poorly understood etiology of hiatal hernias, many authors have studied the anatomical variants of the esophageal hiatus. As described earlier, in the most common configuration, the esophageal hiatus is encircled by the dorsal and ventral arm of the right diaphragmatic crus, alone.[18] Of note, in a surgical electrophysiological stimulation study of 14 patients, Shafik et al suggested that the muscular loop encircling the distal esophagus was not crural in origin at all, but an entirely separate muscle, which he named the "striated GE sphincter."[19] The normal size of the esophageal hiatus is variable. Mean hiatal surface area is reportedly 5.84 cm^2.[20] It may become larger in patients with a large amount of visceral fat and increases with age as the space fills with loose connective tissue and fat (see Volume II, Chapter 2, Esophagus).[21]

Aortic Hiatus

The aorta finds its way through the diaphragm at the T12 level along with the thoracic duct and azygos and hemiazygos veins.

Sternocostal Triangle (Larrey's Space, Morgagni's Foramen)

Not true foramens, the sternocostal triangles are bilateral muscular defects through which the superior epigastric artery and veins, anterior branch of the phrenic nerve, and lymphatics pass (▶ Fig. 10.5). As the pars sternalis and costalis form, they do not completely fuse. This incomplete fusion results a muscle-free trigone in the diaphragm. Many processes, including extraperitoneal or mediastinal air can travel this way.

Lumbocostal Triangle (Bochdalek's Foramen)

It is located where the diaphragm attaches to the anterior margin of the 12th rib. It may remain membranous with few muscle fibers (▶ Fig. 10.5). Defects of this potential space results in Bochdalek's hernia. On routine CT scan of the abdomen, it is not uncommon to find a small defect or membranous bulge containing retroperitoneal fat in this region (▶ Fig. 10.14).

Tiny Diaphragmatic Fenestrations

Tiny focal defects in the diaphragm especially in the tendinous part of the diaphragm are described that allows transphrenic migration of fluid, gas, or neoplasm (porous diaphragm syndrome). Clinical examples include left-sided lymphangitic spread of the gastric cancer into the left pleural space or lung, development of pleural effusion in ovarian fibroma (Meigs syndrome), right pleural effusion in liver disease with ascites (hepatic hydrothorax), and spontaneous (catamenial) pneumothorax with the onset of menses.

◆ Diaphragmatic Hernias

Hiatal Hernia

The exact etiology of hiatal hernias remains unknown. Several theories have been proposed. A literature review performed by Gryglewski et al[18] of all English language studies discussing hiatal hernia development highlighted several leading theories including the following:

- Inheritance: One study by Carre et al suggested an autosomal dominant inheritance across a large five-generation family.[22]
- Increased intra-abdominal pressure either via obesity or activities such as weightlifting.
- Inflammatory reaction from gastroesophageal reflux resulting in esophageal contraction and shortening, as suggested by Mittal and Kassab.[23]

In patients with hiatal hernia widening of the esophageal hiatus is common and can readily demonstrated by CT as a separation

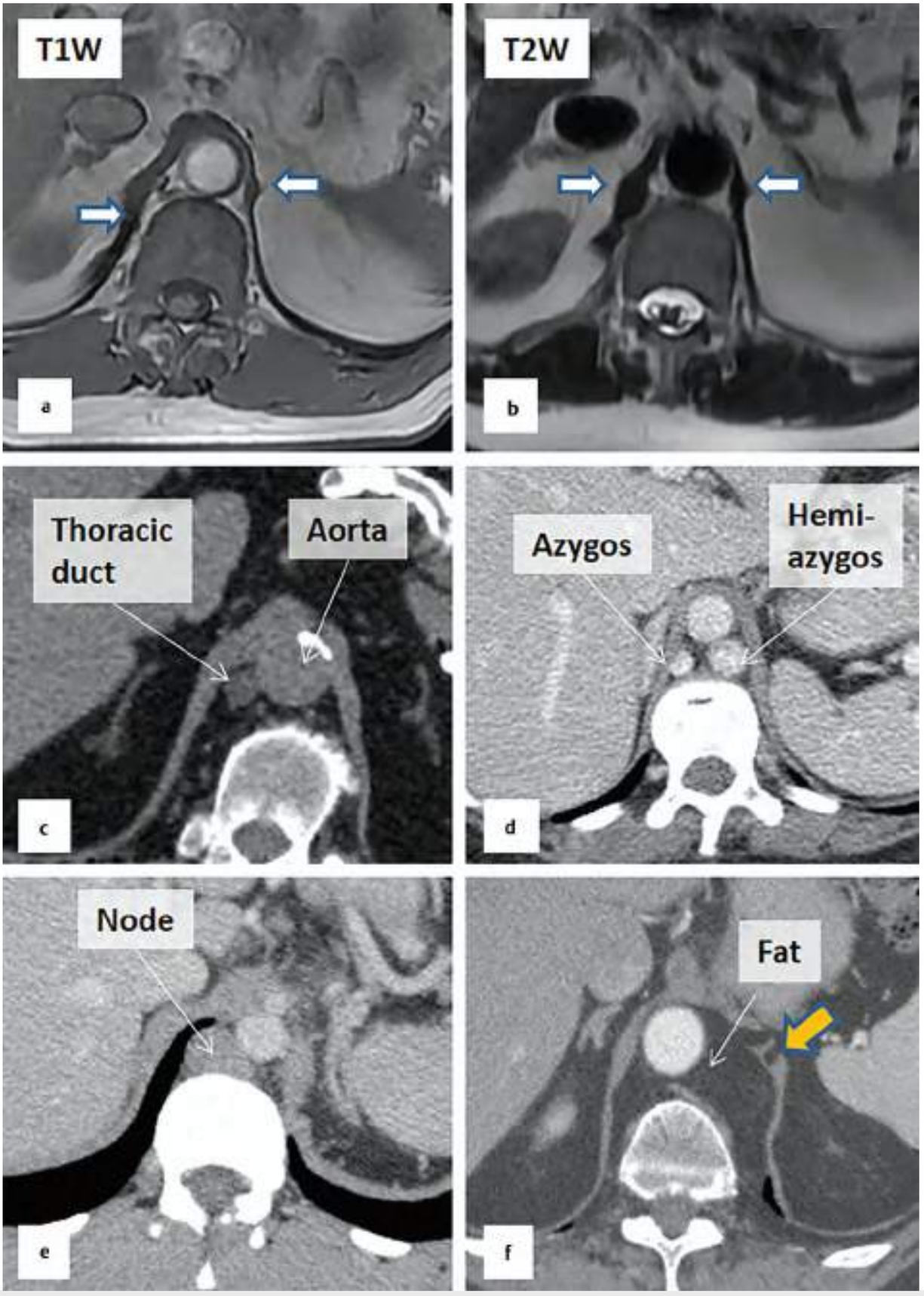

Fig. 10.12 Retrocrural space. **(a, b)** Normal appearance of the crus in MRI. It looks gray on T1 W and dark on T2 W related to fibrous content. **(c, d)** Normal structures within the retrocrural region include the aorta, nerves, the azygos and hemiazygos veins, the cisterna chyli with the thoracic duct, fat, and lymph nodes. **(e)** Enlarged retrocrural lymph nodes. Orange arrow in **(f)** shows small defects in the left crus which is a common finding. Large amount of fat is seen in the retrocrural region.

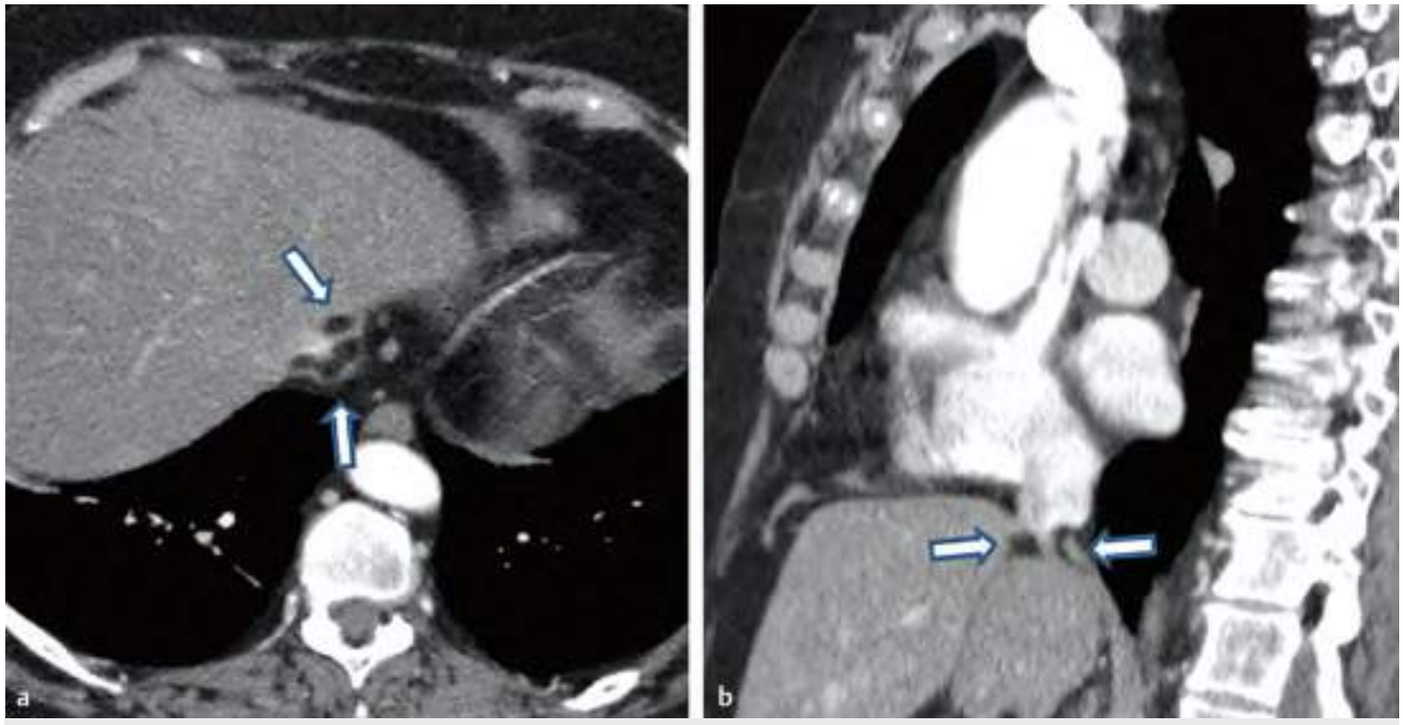

Fig. 10.13 **(a)** Axial and **(b)** sagittal CT show accumulation of fat in the vena cava hiatus causing narrowing of the inferior vena cava in that area.

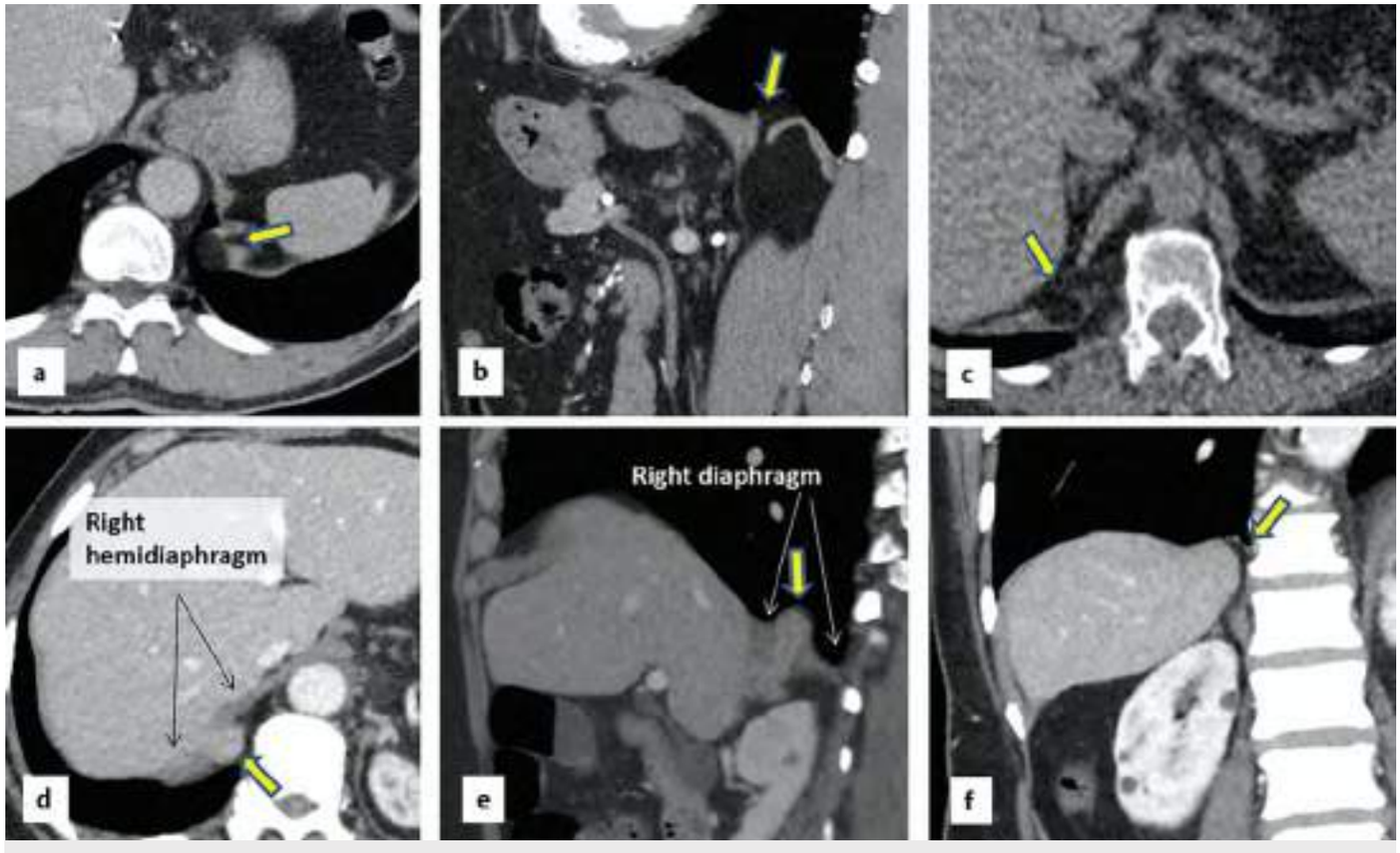

Fig. 10.14 Small diaphragmatic defects with fat herniation (*arrows*). **(a)** Axial and **(b)** sagittal CT showing defect in the left posterior diaphragm. **(c)** Axial CT showing defect in the right posterior diaphragm. On routine CT scan of the abdomen, it is not uncommon to find a small defect or a membranous bulge containing retroperitoneal fat in the posterior diaphragm. **(d-f)** Liver herniation (*arrows*). **(d)** Axial, **(e)** sagittal, and **(f)** coronal CT images showing a small portion of the liver herniating through a small diaphragmatic defect mimicking a lung lesion.

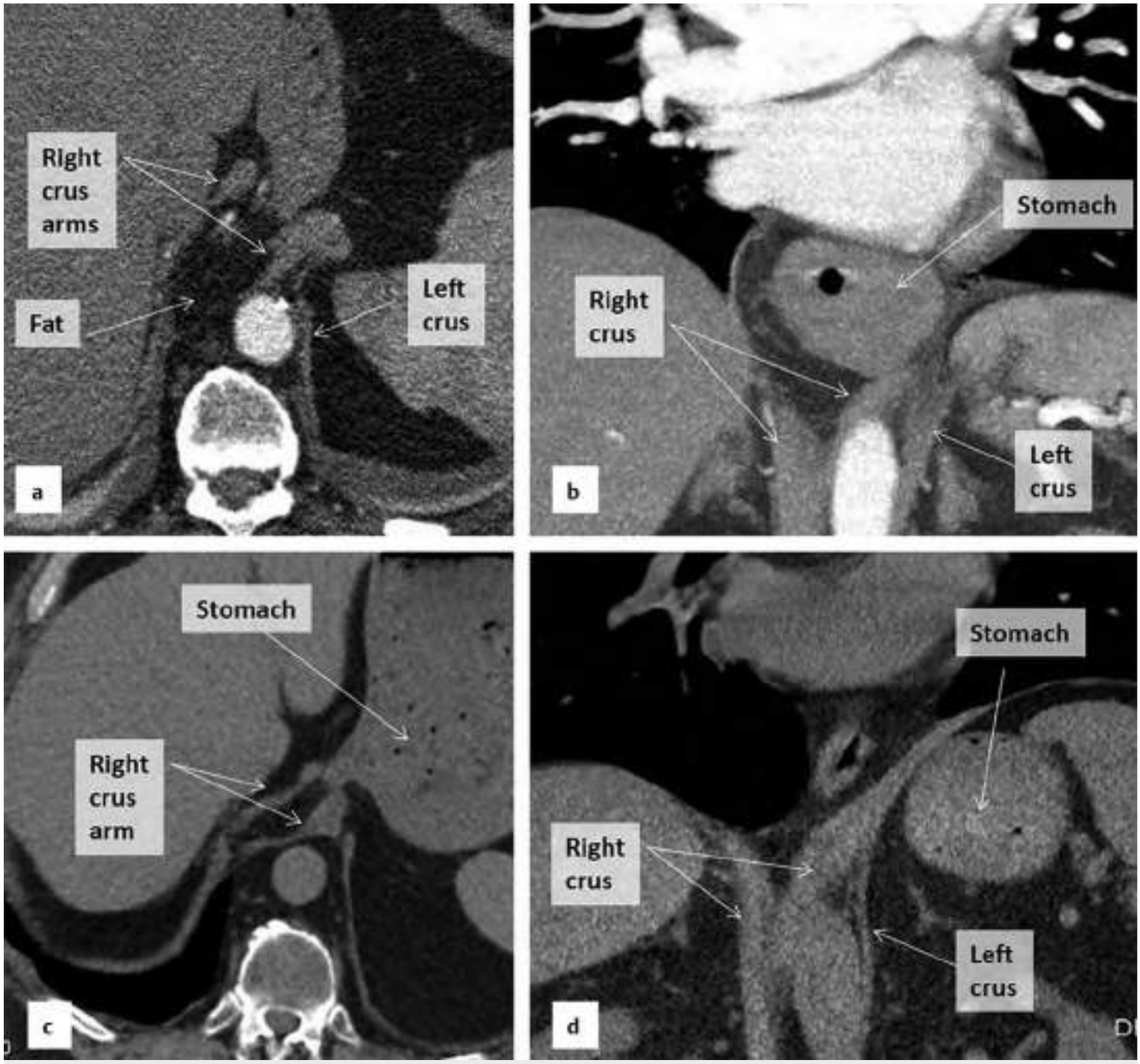

Fig. 10.15 (**a**) Axial CT shows widening of the esophageal hiatus due to herniation of the lesser omentum fat causing separation of the two arms of the right crus. (**b**) Coronal CT shows herniation of the stomach above the esophageal hiatus. (**c**) Axial and (**d**) coronal CT in a normal hiatus are shown for comparison.

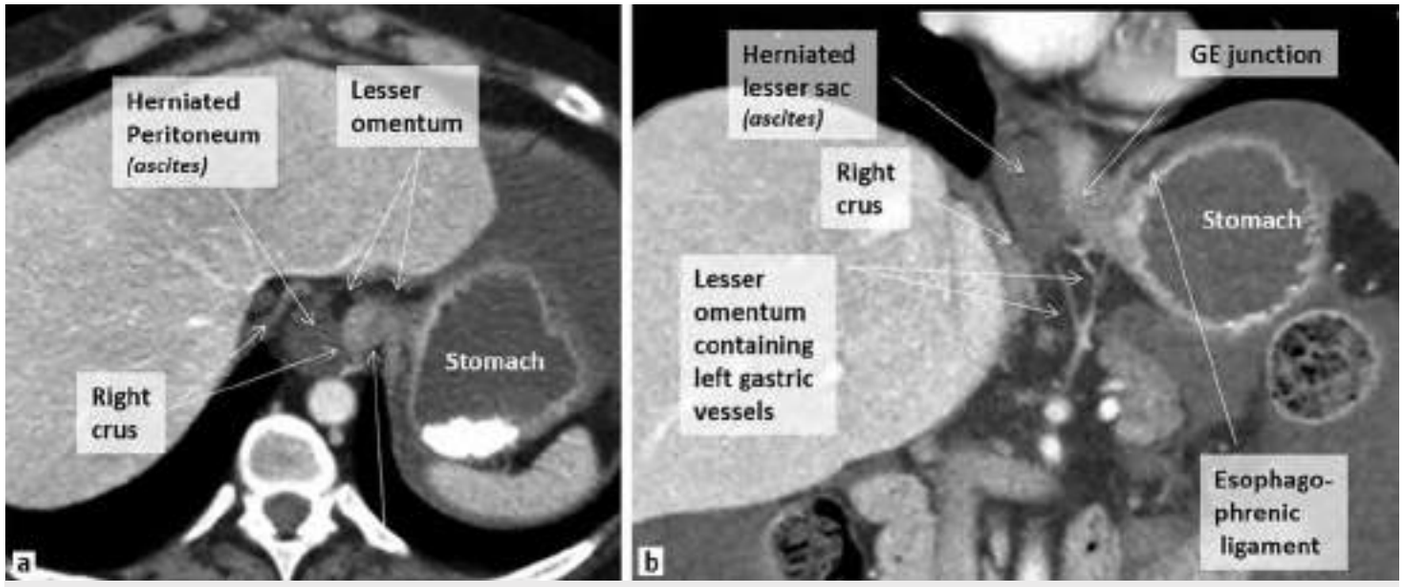

Fig. 10.16 (**a**) Axial and (**b**) coronal CT images showing herniation of the peritoneal sac containing ascetic fluid through the esophageal hiatus. There are also small bare areas behind the abdominal esophagus facing the diaphragm and at the attachment of gastrophrenic ligament. GE, gastroesophageal.

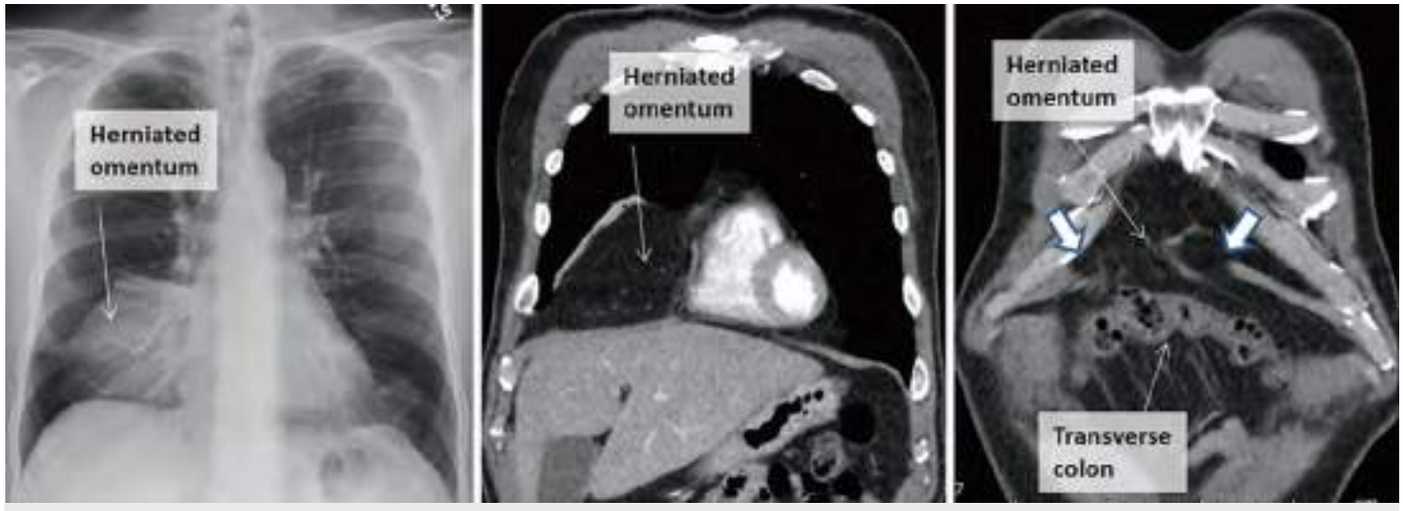

Fig. 10.17 Morgagni's hernia. A large defect in the Morgagni foramen (*arrows*) is seen causing herniation of the omental fat in the right anterior cardiophrenic angle.

of the diaphragmatic crura and an increased distance between the crura and esophageal wall (▶ Fig. 10.15, ▶ Fig. 10.16). Crural closure accompanied by fundoplication is an important part of surgical treatment of GE reflux disease and hiatal hernias.

Morgagni's Hernia

The aforementioned Morgagni's foramen, or sternocostal triangle, is a muscle-free area in the diaphragm, resulting from failure in fusion of the transverse septum to the lateral body wall. In the absence of hernia, this space is protected by fat and is flanked by pleura superiorly and peritoneum inferiorly. Hernias occur when peritoneal contents protrude through this space in the diaphragm. It is usually on the right side, containing omental fat in most cases (▶ Fig. 10.17).

Bochdalek's Hernia

Congenital defect in the pleuroperitoneal folds or failure of the pleuroperitoneal folds to fuse with the transverse septum and to the intercostal muscles. In the majority of cases, 80% to 90%, this defect is located on the left posterolateral diaphragm. Of the two congenital diaphragmatic hernias, Bochdalek's hernias are by far the most common, comprising 90% of congenital diaphragmatic hernias. There are several theories as to the pathophysiology behind congenital, Bochdalek's, diaphragmatic defects. These include premature gut migration from the yolk sac into the abdominal cavity, primary pulmonary hypoplasia, and phrenic nerve abnormalities.[24] A large portion of the stomach and small bowel herniate into the left hemithorax in prenatal period. Left lung development is impaired resulting in a hypoplastic lung (▶ Fig. 10.18).

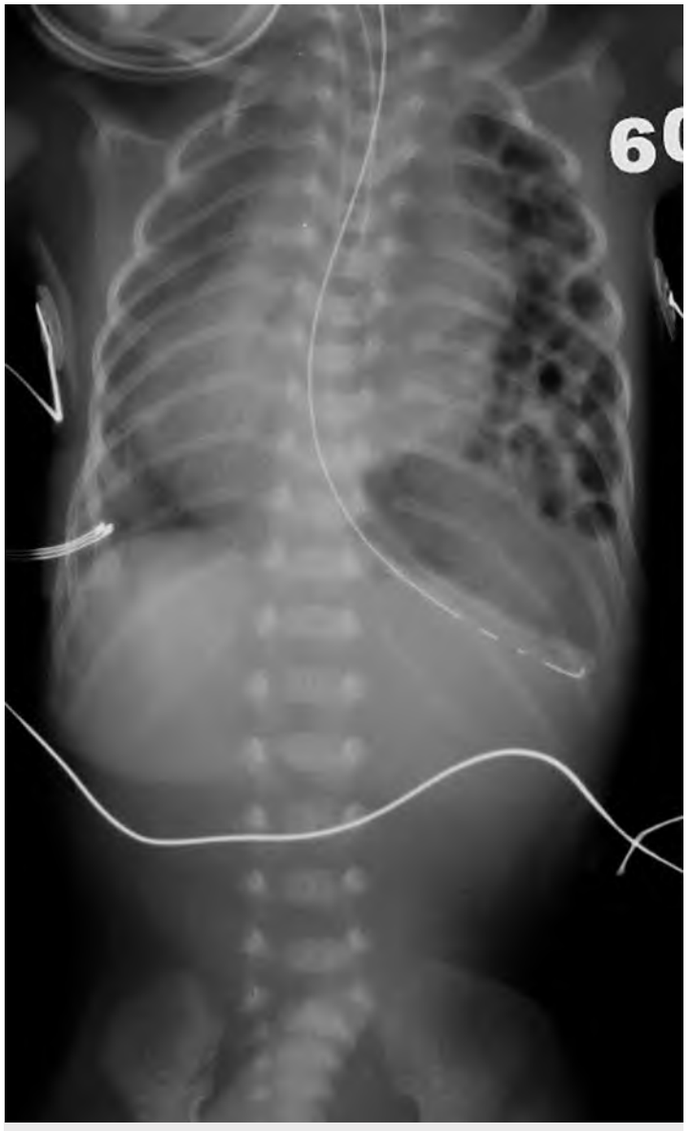

Fig. 10.18 Bochdalek's hernia; Kidney, ureter, bladder (KUB) at birth showing large portion of the stomach and small bowel herniated into the left hemithorax in prenatal period. As a result of compression the left lung development will be impaired resulting in a hypoplastic lung.

◆ Innervation

As the diaphragm's embryological precursor travels from its initial location in the cervical spine to its final destination at the boundary between the thoracic and abdominal cavities, it acquires innervation from the C3 to C5 ventral rami with C4 serving as the largest contributor.[25] The ventral rami of C3 to C5 descend caudally with the internal jugular vein, anterior to the scalene muscles, between the pericardium and mediastinal pleura, forming the left and right phrenic nerves. An accessory phrenic nerve is seen in 60%. It usually originates from the nerve to subclavius or ansa cervicalis and joins the phrenic nerve somewhere at the base of the neck.[26]

The right phrenic nerve has a more direct course than the left, remaining nearly vertical in its descent. On its path to the diaphragm, the right phrenic nerve innervates the pericardium overlying the right atrium and the mediastinal pleura. The left phrenic nerve has a variable course superiorly within the neck, eventually crossing over the left apical pleura, between the branch points of the left common carotid and subclavian arteries, along the aortic arch toward the left hilum to reach the left ventricular pericardium and mediastinal pleura. On its way, the phrenic nerve is accompanied by the phrenic vessels and together they are called phrenic neurovascular bundle.

Once at the level of the diaphragm, the phrenic nerve travels through the diaphragmatic muscles, sending sensory branches superiorly to the parietal pleura and inferiorly to the parietal peritoneum.[17] The larger motor branches separate within the diaphragm into three or four major nerve trunks: sternal, anterolateral, posterolateral, and crural.[4] Inferior to diaphragm, the right phrenic nerve has communications with the celiac plexus and phrenic ganglion. Phrenic nerves specially on the right extends below the diaphragm and form the phrenic ganglion in 20 to 50% before connecting the celiac ganglion. Phrenic ganglia are close to the diaphragmatic crura and may be damaged during placement of sutures to approximate the crura for repair of hiatal hernias.[27]

◆ Blood Supply

Arteries

The diaphragm is vascularized by the inferior phrenic, superior phrenic, pericardiacophrenic, musculophrenic, and lower intercostal arteries. Two inferior phrenic arteries supply the diaphragm (▶ Fig. 10.19). These arteries are variable in the origins with possible origination including[28,29]:

- Directly from the aorta (40%), superior to the celiac access, via a common origin or individually.
- As a branch from the celiac trunk (with almost equal frequency as direct origination from the aorta).
- From a renal artery (17%).
- In rare cases from the left gastric, superior mesenteric, hepatic artery proper, spermatic and contralateral inferior phrenic arteries[29] (▶ Fig. 10.19).

These inferior phrenic arteries then course anterior to the diaphragmatic crura, along the medial limb of the adrenal gland. The left courses behind the esophagus and then superiorly through the left side of the esophageal hiatus. The right courses behind the vena cava and then superiorly along the right side of the vena caval hiatus. At the level of the central tendon, each phrenic artery yields medial and lateral branches. The medial branches jointly supply the central tendon. The lateral branches independently supply their respective sides as they course toward the thoracic wall. The margin of the hiatus is supplied by a branch of the left inferior phrenic artery. The inferior phrenic artery also gives rise to the inferior vena caval, distal esophageal, and accessory splenic branches.[28] The inferior phrenic artery is the most common source of extrahepatic collateral blood supply for hepatocellular carcinoma.

In contrast to the well-described inferior phrenic arteries, the anatomical description of the superior phrenic arteries, which supplies the superior aspect of the diaphragm, is less well defined. Historically, the pericardiacophrenic artery also known as superior phrenic artery is an artery originating from the proximal internal thoracic artery and accompanying the phrenic nerve

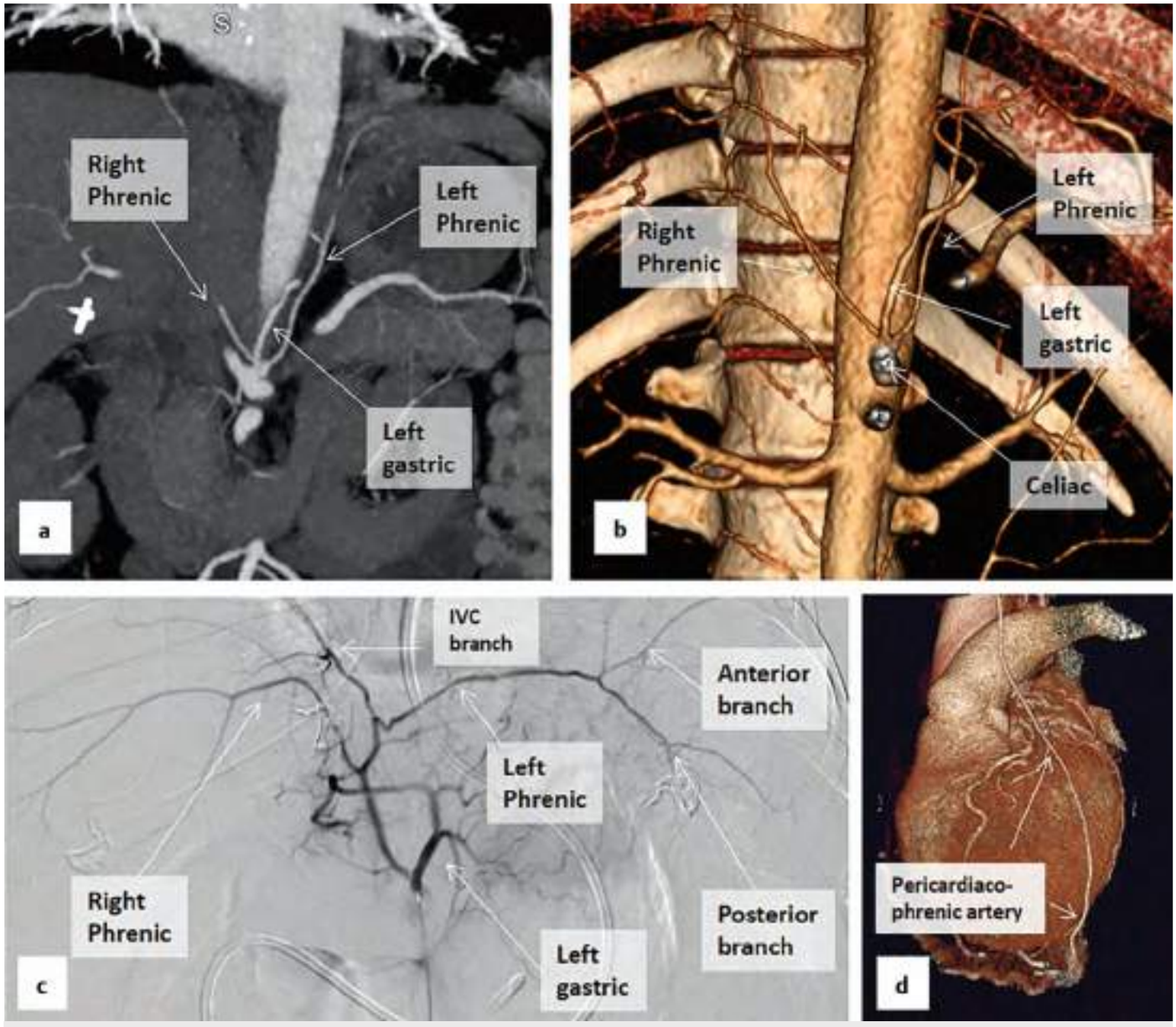

Fig. 10.19 (**a–c**) Inferior phrenic artery. (**a**, **b**) CT images showing the phrenic arteries as branches of the celiac trunk. (**c**) Angiogram showing common trunk of the phrenic proper and left gastric arteries. The phrenic artery is then divided into the right and left branches. (**d**) Cardiac CT shows the left pericardiacophrenic artery and vein moving in a bundle with the phrenic nerve. IVC, inferior vena cava.

along its course to the diaphragm, later anastomosing with the inferior phrenic and musculophrenic arteries (▶ Fig. 10.19). More recent texts describe the superior phrenic artery as paired arteries originating from the thoracic aorta superior to the aortic hiatus and supplying the superior diaphragmatic surface. In their cadaveric study of 100 subjects in an effort to delineate variant arterial supply of hepatocellular carcinoma, Loukas et al found the right superior phrenic artery to originate most commonly from the aorta (42% of cases) followed by the proximal 10th intercostals artery (33%) and distal 10th intercostals artery (25%). The left superior phrenic artery also most commonly originated from the aorta (51%) and less likely from the proximal left 10th intercostal artery (40%) versus distal left 10th intercostals artery (9%).[29] In most cadaveric specimens, the superior phrenic artery terminated within the medial and posterosuperior surface of diaphragm versus the less likely terminus along the posterior diaphragmatic surface. The musculophrenic artery is terminal branch of the internal thoracic artery, running laterally near the attachment of the diaphragm to the lower ribs. It gives branches to the anterior margin of the diaphragm.

Veins

Accompanying the diaphragmatic arteries are their venous counterparts, with separate venous drainage for the superior and inferior diaphragmatic surfaces. Tributaries of the pericardiophrenic and musculophrenic veins drain the superior diaphragmatic surface.[30]

The right inferior phrenic vein travels through the vena caval hiatus, draining into the IVC. There are often two left inferior phrenic veins emptying variably into the left renal or adrenal veins as well as connecting with a tributary through the esophageal

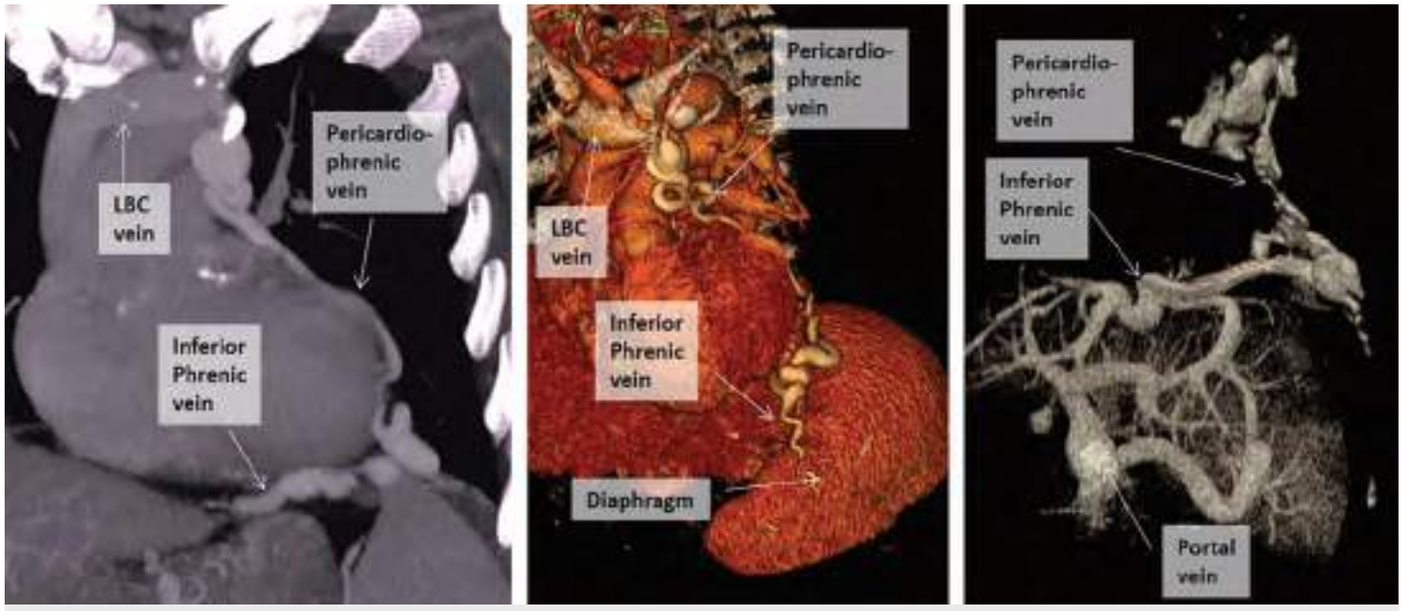

Fig. 10.20 Cirrhosis and portal hypertension showing a large connection between the paraumbilical vein and the left phrenic vein. The left phrenic vein also connected with the left brachiocephalic (LBC) vein through the left inferior superior phrenic venous system causing a portosystemic shunt. Tributaries of the pericardiophrenic vein drains normally the superior diaphragmatic surface.

hiatus or emptying into the IVC. The variable anatomy of the inferior phrenic veins has been a focus of recent interest given a rise in variceal embolization in portal hypertension. For example, the left gastric vein, a major portosystemic collateral supply for distal esophageal varices, drains into the IVC via the left inferior phrenic vein. In portal hypertension, the left gastric vein can connect with the left brachiocephalic vein (portosystemic shunt) through the left inferior superior phrenic venous system (▶ Fig. 10.20).

Lymphatics

There are three groups lymph nodes on the superior surface of the diaphragm: anterior, middle, and posterior[4,31,32] (▶ Fig. 10.21). Both pleural and peritoneal serosal surfaces of the diaphragm are connected by small lymphatic channels passing through the diaphragm. These small communications may be the source of lymphangitic spread of the abdominal malignancy (i.e., gastric cancer) into the lung or pleural space.

The anterior group (also known as anterior cardiophrenic or anterior pericardial lymph nodes) comprises two or three small glands on either sides of the sternum near the junction of the seventh costochondral junction cartilage. They receive lymphatic vessels from the anterior part of the diaphragm, the convex surface of the liver, and the lower thoracic wall and finally drain into the internal thoracic glands (▶ Fig. 10.21). Lymphoma (especially after recurrence) is the most common malignancy involving anterior lymph nodes followed by metastasis from liver, breast, and lung tumors (▶ Fig. 10.22). The middle group of the diaphragmatic lymph nodes consists of two or three glands on either sides close to the phrenic nerves entering the diaphragm, around the fibrous pericardium and the IVC. This group drains into the node around the inferior pulmonary ligaments, the posterior mediastinal nodes, and the peritracheobronchial nodes. The posterior set consists of a few glands situated on the back of the crura of the diaphragm. They are connected with the paravertebral, posterior mediastinal, and retrocrural glands. The peripheral margin of the diaphragm drains into the thoracic wall, paravertebral, and parasternal nodes.

◆ Physiology

The diaphragm muscle has more than one single respiratory function, and has several links with other parts of the body. It modulates cardiovascular function, helps in urination, and defecation by increasing intra-abdominal pressure, and helps prevent GE reflux. Respiration is a coordinated effort with participation from the diaphragm, the intercostal muscles, as well as the accessory muscles of respiration including, but not limited to, the scalene and sternocleidomastoid muscles. At rest, the diaphragm assumes a dome-shape and the intercostal muscles are relaxed. Once triggered by the neurologic system to take a breath, the diaphragm contracts resulting in a flattened configuration and increasing the thoracic cavity's volume. At the same time, the intercostal muscles tighten, lifting the downward sloping ribs anteriorly, thus increasing the depth of the thoracic cavity. In total, the craniocaudal expansion from the diaphragm and anteroposterior expansion by the intercostal muscles increase thoracic cavity volume by 0.5 L.[33]

Respiration is somewhat unique in that it is regulated by both voluntary and involuntary neurologic control.

- Voluntary respiration: Take a deep breath. As you will yourself have to do so, an electrical impulse travels from your cerebral cortex along the corticospinal tracks to the motor neurons in the cervical spinal cord. The phrenic nerve, originating from C3 to C5, continues the impulse to the diaphragm, triggering its contraction and flattening.
- Involuntary respiration: While reading the paragraph above, your involuntary respiratory regulation resumed control. A complicated system of spontaneously discharging pacemaker cells in the medulla, dorsal and ventral medullary respiratory

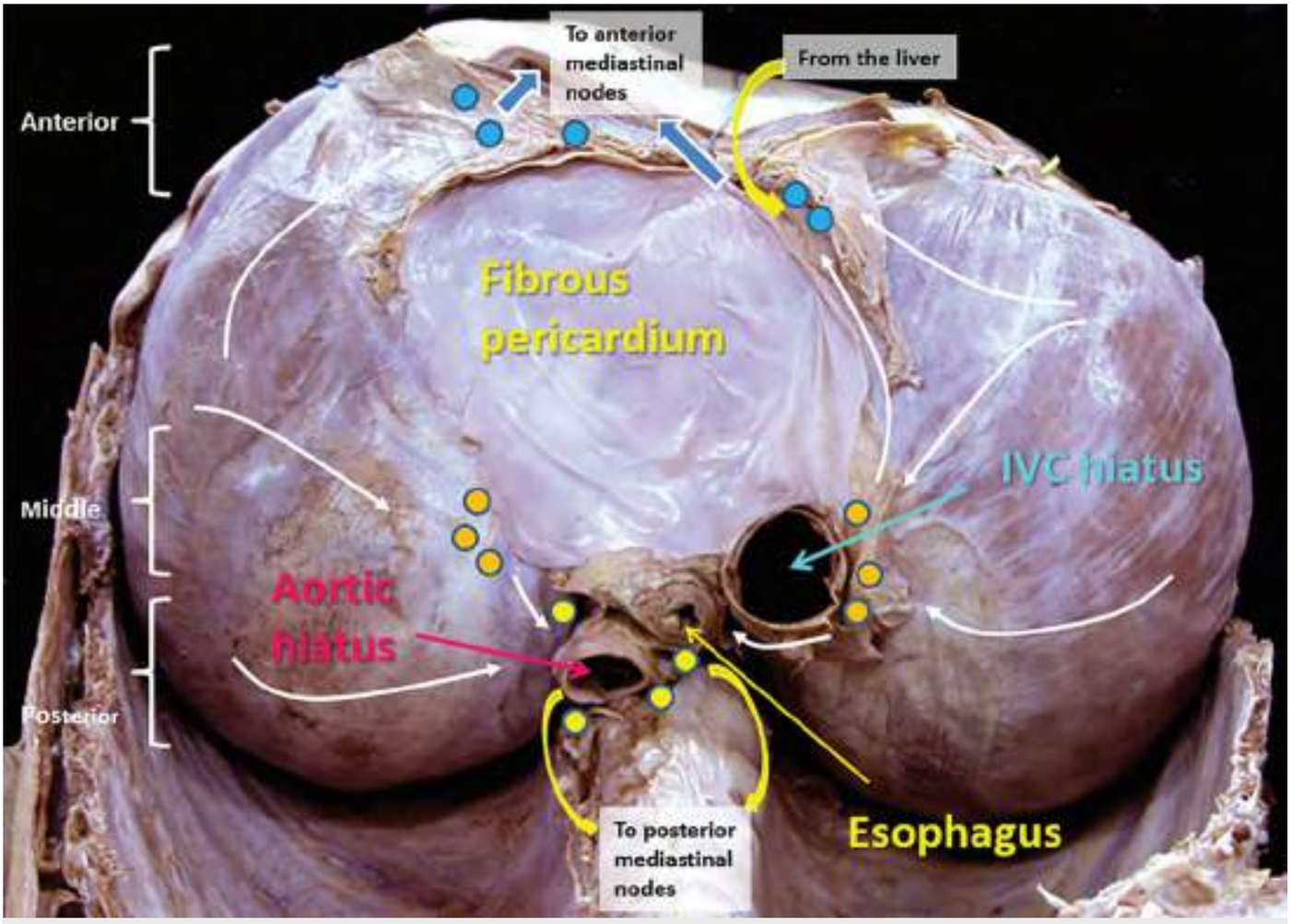

Fig. 10.21 Normal lymphatic drainage of the diaphragm (superior view). There are three group lymph nodes on the superior surface of the diaphragm: anterior, middle, and posterior. The anterior group (also known as anterior cardiophrenic or anterior pericardial lymph nodes) receives lymphatic vessels from the anterior part and also from the liver and drains into the internal thoracic glands and anterior mediastinal nodes. The middle group nodes consist are close to the phrenic nerves entering the diaphragm, around the fibrous pericardium and the inferior vena cava (IVC). The posterior set consists of a few glands situated on the back of the crura of the diaphragm. They are connected with the paravertebral, posterior mediastinal, and retrocrural glands.

neurons, modifying neurons in the pons, and vagal feedback from your expanding lungs coordinated to provide an adequate rate and depth of diaphragmatic and intercostal contraction and thus respiration.[34]

◆ Dysfunction of the Diaphragm

Normal function of the diaphragm is essential for life. Abnormal function of the diaphragm occurs as a result of many extrinsic and intrinsic problems including due to phrenic nerve paralysis, brain pathologies, diaphragmatic perforation, or incomplete motion due to large pleural effusion, pregnancy, or abdominal masses. The liver is connected to the diaphragm by the coronary ligaments; therefore, a large liver can interfere with normal function of the diaphragm and its pathologies can easily affect the hemidiaphragm. The diaphragm is also connected to abdominal and chest wall muscles by the fascia including the thoracolumbar fascia, fascia transversalis, or endothoracic fascia, which has proprioceptive properties. It is also directly related to the transverse abdominal, psoas, and quadratus lumborum muscle. These fascial planes and muscle structures are linked together and their pathologies affect each other.[10]

Respiration is a constant and important modulator of the cardiovascular function. Negative pressure within the thoracic cavity with each diaphragmatic contraction is essential for normal venous drainage. Therefore, if there are symptoms of venous stasis, examination of the diaphragm is recommended.[35] Normal lymphatic flow along the diaphragm is maintained only when it functions properly. Further, it is important to know that the function of the cisterna chyli, which is located in the retrocrural region, can be compromised by masses in this region, causing ascites and lymphedema.

Phrenic Nerve Injury

Recognizing its key role in transmitting a neurologic impulse from either the cerebral cortex during voluntary respiration, or the neurons controlling spontaneous respiration in the brainstem, a phrenic nerve injury results in paralysis of the ipsilateral hemidiaphragm. Patients may experience phrenic nerve injury as

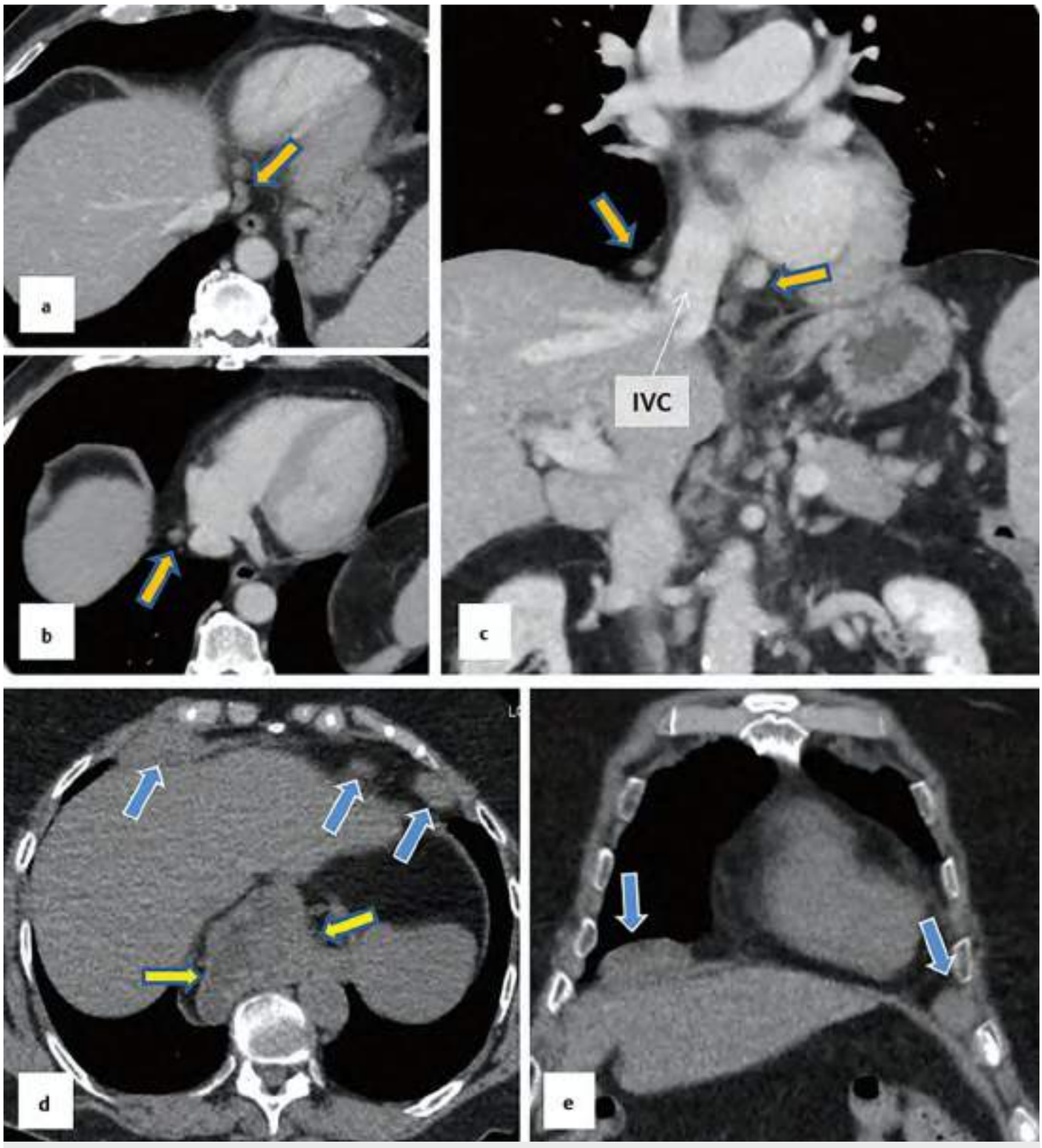

Fig. 10.22 Examples of the diaphragmatic nodes. **(a, b)** Axial and **(c)** coronal CT show the middle chain (posterior cardiophrenic angle) around the inferior vena cava (IVC) and above the diaphragm (*orange arrows*). **(d)** Axial and **(e)** coronal CT. Showing enlarged anterior cardiophrenic angle (*blue arrows*) and retrocrural (*yellow arrows*) lymph nodes in a patient with lymphoma.

a result of iatrogenic injury (i.e., postsurgical), trauma, infection, or intrathoracic malignancy, to name a few.

In otherwise healthy patients, unilateral diaphragmatic paralysis is often asymptomatic, particularly at rest. Detection of unilateral paralysis is often an incidental finding on chest radiography performed for other indications.

Chest Radiograph Evaluation

In the majority of individuals, the right hemidiaphragm is elevated when compared to the right, with approximately one rib space of difference between the two sides. An exaggerated dome configuration of the diaphragm seen on chest radiography with deepened, narrowed cardiophrenic angles is suggestive of

Fig. 10.23 Paralysis of the diaphragm after mediastinal surgery. Chest X-ray before surgery of the right mediastinum showing normal position of the right hemidiaphragm. Sniff fluoroscopy after surgery shows normal left hemidiaphragm excursion but lack of motion of the right side.

diaphragmatic paralysis. However, while detection of diaphragmatic paralysis on chest radiographs has been shown to be highly sensitive, up to 90%, specificity is low, an underwhelming 44%.[36]

Fluoroscopic Sniff Test

Fluoroscopic evaluation allows for real-time imaging of diaphragmatic motion. Normally, both diaphragms contract in synchrony. It is important to note that there is often a slight difference in the timing and extent of diaphragmatic contraction in normal patients, with the right hemidiaphragm most commonly slightly delayed compared to the left. In classic teaching, a paralyzed hemidiaphragm does not move and will occasionally paradoxically contract. This paradoxical motion can be exaggerated by prompting a patient to sniff. However, the sniff test has been shown to result in false positives in 6% of normal patients.[37]

Ultrasound

Benefiting from a lack of ionizing radiation while maintaining the ability for real-time imaging, ultrasound is a useful alternative to fluoroscopy in the evaluation of diaphragmatic motion. Of added benefit is ultrasound's ability to detect and objectively measure the thickening of the diaphragm with contraction.

Most patients with paralysis of hemidiaphragm are asymptomatic. For symptomatic patients plication of the hemidiaphragm may be considered.

◆ Eventration

It is important to not only recognize the signs of phrenic nerve injury and diaphragmatic paralysis, but also to be able to distinguish diaphragmatic elevation as a result of paralysis versus the much more common abnormal morphology known as "eventration." In contrast to diaphragmatic paralysis which results in abnormal motion of a normally formed hemidiaphragm, eventration is a focal thinning and elevation of the diaphragm (▶ Fig. 10.23). Eventration can be congenital or acquired. In congenital eventration, all or part of the diaphragm is replaced by fibroelastic tissue, resulting in diaphragmatic weakening without disruption of the continuity of the diaphragms' attachments.[38] Acquired eventration has been described as a result of birth trauma and postsurgical in etiology.[39] Most often asymptomatic, eventration can be exaggerated by increased intra-abdominal pressure, most commonly in obesity. If small in size, the thinned diaphragmatic eventration will typically move with the rest of the diaphragm, though paradoxical motion can be observed.

◆ Other Pathologies

Diaphragmatic perforation is a rare complication of blunt abdominal injury and usually involves mid-to-posterior portion of the left hemidiaphragm. The diagnosis of diaphragmatic rupture is frequently delayed for months on years. Imaging of the diaphragmatic perforation can mimic simple diaphragmatic elevation/eventration or pleural effusion (▶ Fig. 10.24). Primary masses of

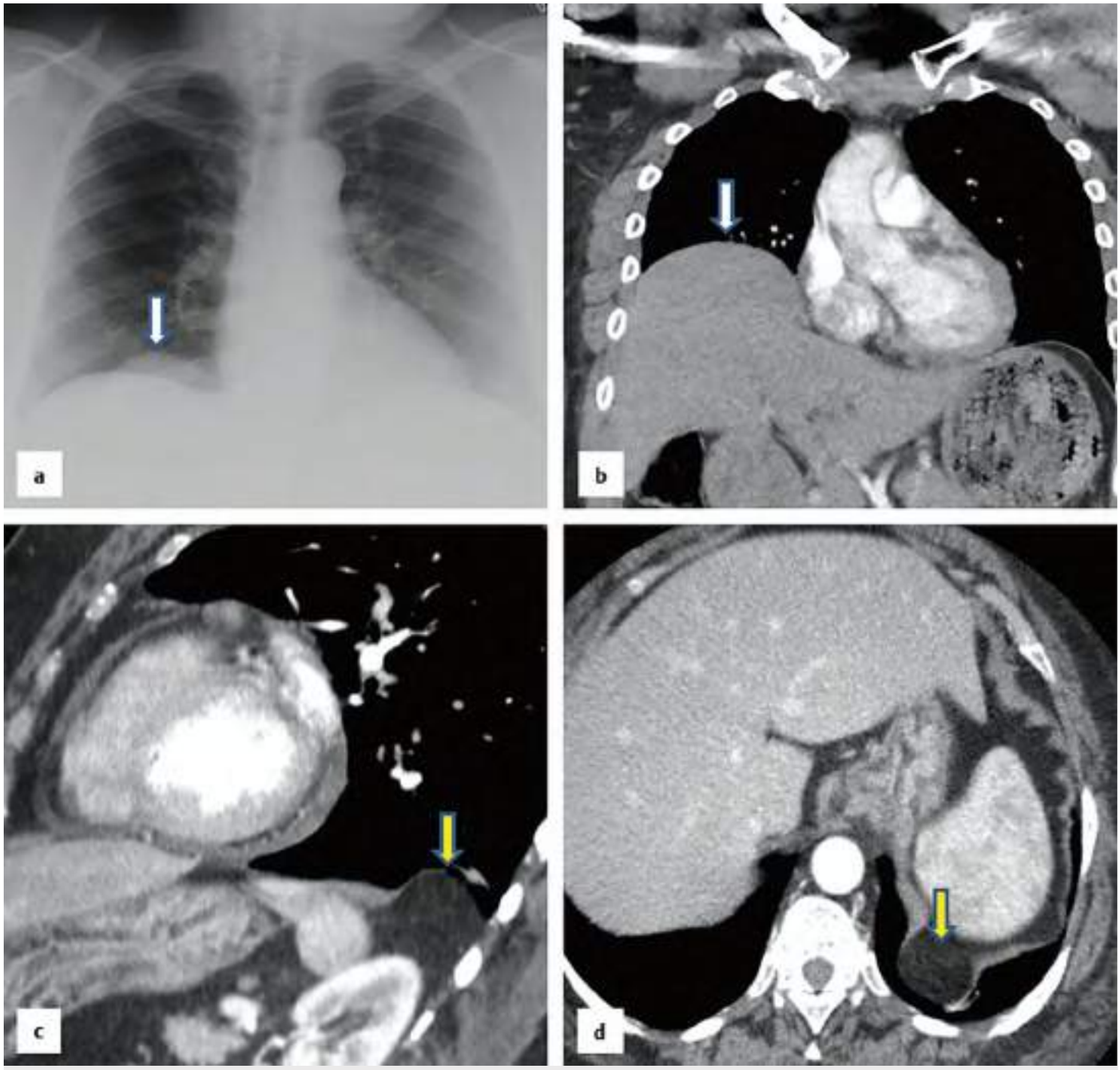

Fig. 10.24 (**a**, **b**) Right hemidiaphragm eventration (*arrow*). (**c**, **d**) Left posterior hemidiaphragm eventration (*arrow*). In eventration, part of the diaphragm is replaced by fibroblastic tissue, resulting in diaphragmatic thinning and weakening.

diaphragm are uncommon and mostly limited to benign masses such as lipoma or duplication cysts (▶ Fig. 10.25, ▶ Fig. 10.26). Subdiaphragmatic fluid collection and abscesses are common after upper abdominal surgery or acute inflammatory processes such as perforated viscus or pancreatitis.

References

[1] Sadler TW. Development of the diaphragm. In: Sadler TW, ed. Langman's Medical Embryology. Baltimore, MD: Lippincott Williams & Wilkins; 2004

[2] Fisher JC, Bodenstein L. Computer simulation analysis of normal and abnormal development of the mammalian diaphragm. Theor Biol Med Model.; 3:9

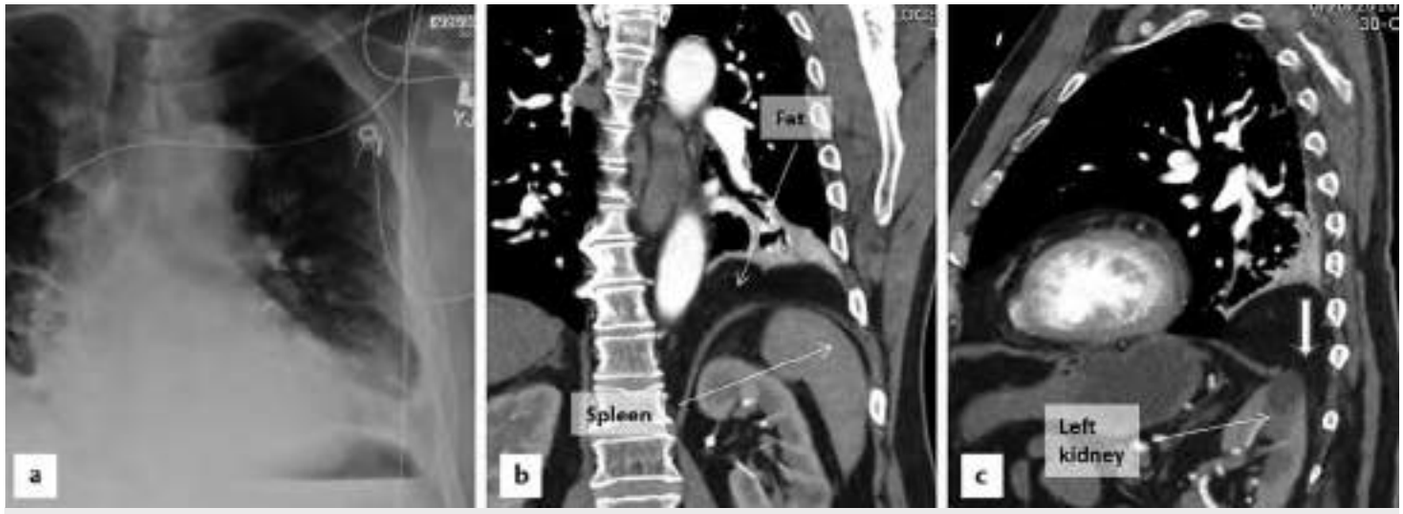

Fig. 10.25 Traumatic diaphragmatic rupture. (**a**) Frontal X-ray shows blunting of the left costophrenic angle suggesting pleural effusion. (**b**) Coronal and (**c**) sagittal CT show perforated diaphragm (*arrow*) causing herniation of the retroperitoneal fat above the diaphragm.

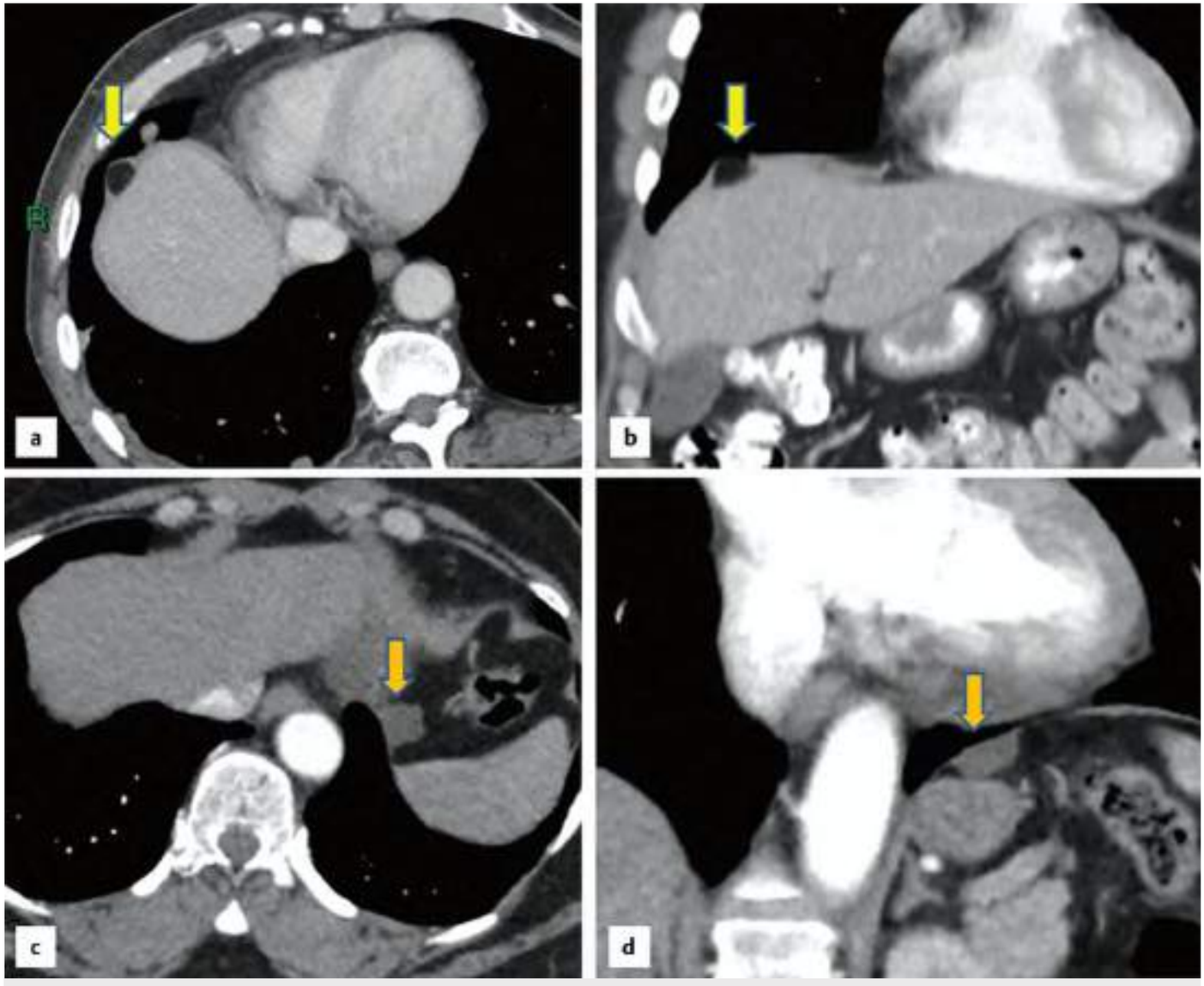

Fig. 10.26 (**a**) Axial and (**b**) coronal CT show a small lipoma of the diaphragm (*arrows*). (**c**) Axial and (**d**) coronal CT show a small cyst of the diaphragm (*arrows*).

[3] Merrell AJ, Kardon G. Development of the diaphragm—a skeletal muscle essential for mammalian respiration. FEBS J.; 280(17):4026–4035
[4] Ricketts RR, Loukas M, Skandalakis LJ, Mcclusky DA III, Mirilas M. Surgical anatomy of the diaphragm. In: Fischer's Mastery of Surgery. Lippincott Williams & Wilkins; 2011
[5] Maish MS. The diaphragm. Surg Clin North Am.; 90(5):955–968
[6] Rives JD, Baker DD. Anatomy of the attachments of the diaphragm: their relation to the problems of the surgery of diaphragmatic hernia. Ann Surg.; 115 (5):745–755
[7] du Plessis M, Ramai D, Shah S, Holland JD, Tubbs RS, Loukas M. The clinical anatomy of the musculotendinous part of the diaphragm. Surg Radiol Anat.; 37(9):1013–1020
[8] Panicek DM, Benson CB, Gottlieb RH, Heitzman ER. The diaphragm: anatomic, pathologic, and radiologic considerations. Radiographics.; 8(3):385–425
[9] Hawkins SP, Hine AL. Diaphragmatic muscular bundles (slips): ultrasound evaluation of incidence and appearance. Clin Radiol.; 44(3):154–157
[10] Bordoni B, Zanier E. Anatomic connections of the diaphragm: influence of respiration on the body system. J Multidiscip Healthc.; 6:281–291
[11] Lindner HH, Kemprud E. A clinicoanatomical study of the arcuate ligament of the diaphragm. Arch Surg.; 103(5):600–605
[12] Horton KM, Talamini MA, Fishman EK. Median arcuate ligament syndrome: evaluation with CT angiography. Radiographics.; 25(5):1177–1182
[13] Dakwar E, Ahmadian A, Uribe JS. The anatomical relationship of the diaphragm to the thoracolumbar junction during the minimally invasive lateral extracoelomic (retropleural/retroperitoneal) approach. J Neurosurg Spine.; 16 (4):359–364
[14] Loukas M, Wartmann ChT, Tubbs RS, et al. Morphologic variation of the diaphragmatic crura: a correlation with pathologic processes of the esophageal hiatus? Folia Morphol (Warsz).; 67(4):273–279
[15] Apaydin N, Uz A, Evirgen O, Loukas M, Tubbs RS, Elhan A. The phrenicoesophageal ligament: an anatomical study. Surg Radiol Anat.; 30(1):29–36
[16] Restrepo CS, Eraso A, Ocazionez D, Lemos J, Martinez S, Lemos DF. The diaphragmatic crura and retrocrural space: normal imaging appearance, variants, and pathologic conditions. Radiographics.; 28(5):1289–1305
[17] Borley N, Collins P, Crossman A, et al. Diaphragm. In: Stranding S, ed. Gray's Anatomy. 40th ed. N.p.: Elsevier; 2008:1007–1012
[18] Gryglewski A, Pena IZ, Tomaszewski KA, Walocha JA. Unsolved questions regarding the role of esophageal hiatus anatomy in the development of esophageal hiatal hernias. Adv Clin Exp Med.; 23(4):639–644
[19] Shafik A, Shafik A, El-Sibai O, Shafik I. Physioanatomic study of the diaphragmatic crura: the identification of autonomous "gastroesophageal sphincter". J Invest Surg.; 18(3):135–142
[20] Shamiyeh A, Szabo K, Granderath FA, Syré G, Wayand W, Zehetner J. The esophageal hiatus: what is the normal size? Surg Endosc.; 24(5):988–991
[21] Ginalski JM, Schnyder P, Moss AA, Brasch RC. Incidence and significance of a widened esophageal hiatus at CT scan. J Clin Gastroenterol.; 6(5):467–470
[22] Carré IJ, Johnston BT, Thomas PS, Morrison PJ. Familial hiatal hernia in a large five generation family confirming true autosomal dominant inheritance. Gut.; 45(5):649–652
[23] Mittal RK, Kassab GS. Esophagogastric junction opening: does it explain the difference between normal subjects and patients with reflux disease? Gastroenterology.; 125(4):1258–1260
[24] Rottier R, Tibboel D. Fetal lung and diaphragm development in congenital diaphragmatic hernia. Semin Perinatol.; 29(2):86–93
[25] Hidayet MA, Wahid HA, Wilson AS. Investigations on the innervation of the human diaphragm. Anat Rec.; 179(4):507–516
[26] Loukas M, Kinsella CR, Jr, Louis RG, Jr, Gandhi S, Curry B. Surgical anatomy of the accessory phrenic nerve. Ann Thorac Surg.; 82(5):1870–1875
[27] Loukas M, Du Plessis M, Louis RG, Jr, Tubbs RS, Wartmann CT, Apaydin N. The subdiaphragmatic part of the phrenic nerve—morphometry and connections to autonomic ganglia. Clin Anat.; 29(1):120–128
[28] Gwon DI, Ko GY, Yoon HK, et al. Inferior phrenic artery: anatomy, variations, pathologic conditions, and interventional management. Radiographics.; 27 (3):687–705
[29] Loukas M, Louis RG Jr, Wartmann CT, et al. Superior phrenic artery: an anatomic study. Surg Radiol Anat 2007;29(1):97–102. Moore, Keith L, Dalley Arthur F, Agur AMR. Clinically Oriented Anatomy. Philadelphia, PA: Lippincott Williams & Wilkins; 2006
[30] Loukas M, Louis RG, Jr, Hullett J, Loiacano M, Skidd P, Wagner T. An anatomical classification of the variations of the inferior phrenic vein. Surg Radiol Anat.; 27(6):566–574
[31] Okiemy G, Foucault C, Avisse C, Hidden G, Riquet M. Lymphatic drainage of the diaphragmatic pleura to the peritracheobronchial lymph nodes. Surg Radiol Anat.; 25(1):32–35
[32] Souilamas R, Hidden G, Riquet M. Mediastinal lymphatic efferents from the diaphragm. Surg Radiol Anat.; 23(3):159–162
[33] Morton DA, Foreman K, Albertine KH. Lungs. In: Morton DA, Foreman K, Albertine KH, eds. The Big Picture: Gross Anatomy. New York, NY: McGraw-Hill; 2011. http://accessmedicine.mhmedical.com/content.aspx?bookid=381&Sectionid=40140009. Accessed July 03, 2016
[34] Barrett KE, Barman SM, Boitano S, Brooks HL. Regulation of respiration. In: Barrett KE, Barman SM, Boitano S, Brooks HL, eds Ganong's Review of Medical Physiology. 25th ed. http://accessmedicine.mhmedical.com/content.aspx?bookid=1587&Sectionid=97166494. Accessed July 03, 2016
[35] Byeon K, Choi JO, Yang JH, et al. The response of the vena cava to abdominal breathing. J Altern Complement Med.; 18(2):153–157
[36] Chetta A, Rehman AK, Moxham J, Carr DH, Polkey MI. Chest radiography cannot predict diaphragm function. Respir Med.; 99(1):39–44
[37] Alexander C. Diaphragm movements and the diagnosis of diaphragmatic paralysis. Clin Radiol.; 17(1):79–83
[38] Deslauriers J. Eventration of the diaphragm. Chest Surg Clin N Am.; 8(2):315–330
[39] Tiryaki T, Livanelioğlu Z, Atayurt H. Eventration of the diaphragm. Asian J Surg.; 29(1):8–10

11 Breast Anatomy

Sandy C. Lee

◆ Introduction

Understanding breast anatomy is important to recognizing the disease processes that may occur within the breast. Mammary glands are unique to mammals and are unlike any other anatomical part of the body. They are essentially modified exocrine glands responsible for lactation, the production of milk. Being knowledgeable about the embryological development and anatomy of the breast is crucial for radiologists to determine radiological–pathological concordance or discordance after a breast biopsy, to understand imaging correlates, and to plan interventional procedures. The historical understanding of breast anatomy is based on Sir Astley Cooper's book which was published in 1840, but significant advances in medicine and imaging have improved our overall understanding of breast anatomy.

◆ Embryology and Development

The breasts develop from an ectodermal milk line running from the axilla to the medial thigh on each side.[1] These paired mammary ridges develop on the ventral surface of the embryo and much of the line atrophies except at the pectoral location.[1,2] The breasts start to develop during the fourth to sixth weeks of embryonic life from the ectoderm, which are skin precursor cells.[3] Under influences of maternal hormones and genetics, the mammary ridges thicken and form the human breasts at the level of the fourth intercostal space bilaterally. Mammary buds are usually formed by the fifth week of gestation. Between the 5th and 12th weeks, the mammary buds continue to grow and form secondary buds and mammary lobules. After the 12th week, the secondary buds continue to develop and branch, and ultimately develop into ducts that extend from the nipple to the breast lobules[3,4] (▶ Fig. 11.1).

The nipple–areolar complex begins to develop between 12th and 16th weeks of gestation. The nipples are inverted at this time but then evert when the fetus is near full term or after birth when the sebaceous glands and erectile tissue of the nipple–areolar complex develop. During this time, the areola increases in pigmentation between 32nd and 40th weeks.[5]

The nipple can fail to evert after birth which is often hereditary and a result of a hypoplastic ductal system. Incomplete regression of the milk line can result in an accessory nipple anywhere along this region. An accessory nipple (polythelia) and/or breast tissue (polymastia) most commonly develop in the axilla or inframammary fold but can occur anywhere along the milk line (▶ Fig. 11.2, ▶ Fig. 11.3). Polythelia can occur in both sexes with the incidence varying greatly in literature. One study reports an incidence of accessory nipples to be 2.5%.[5,6,7]

Other developmental abnormalities can include hypoplasia (underdevelopment of the breast), amastia (absence of one or

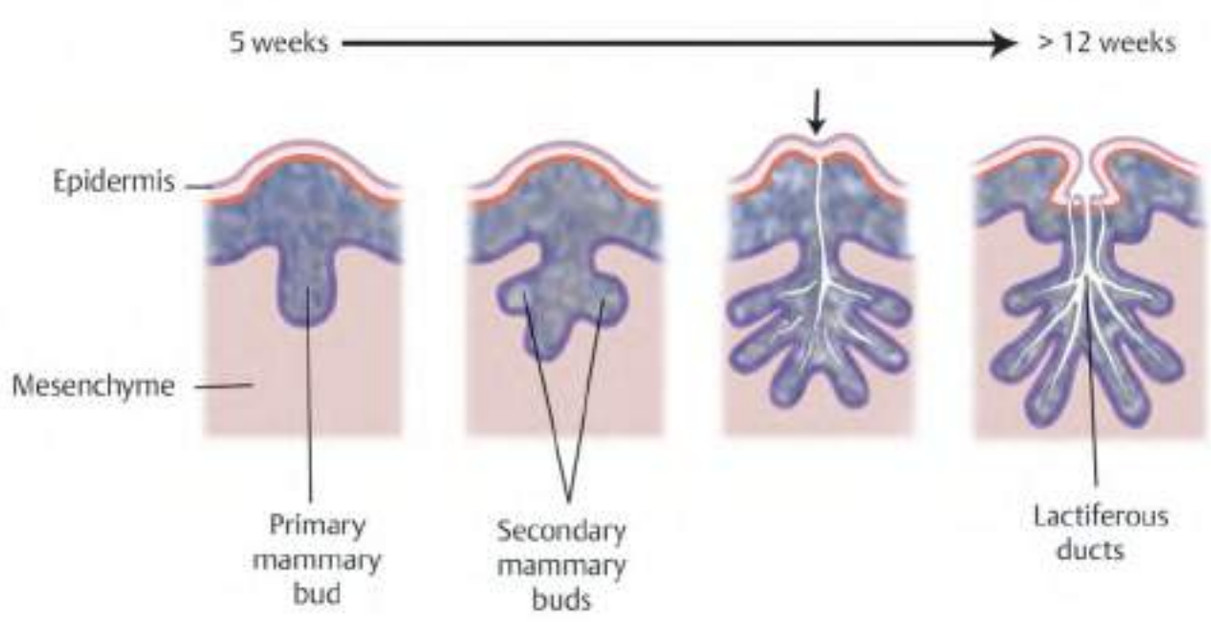

Fig. 11.1 Embryology; the breasts start to develop during the 4th to 6th weeks of embryonic life. Primary breast buds are usually formed by the 5th week of gestation. Between the 5th and 12th weeks, secondary breast buds and mammary lobules start to form. After the 12th week, the secondary buds continue to develop and branch into the ducts that extend from the nipple.

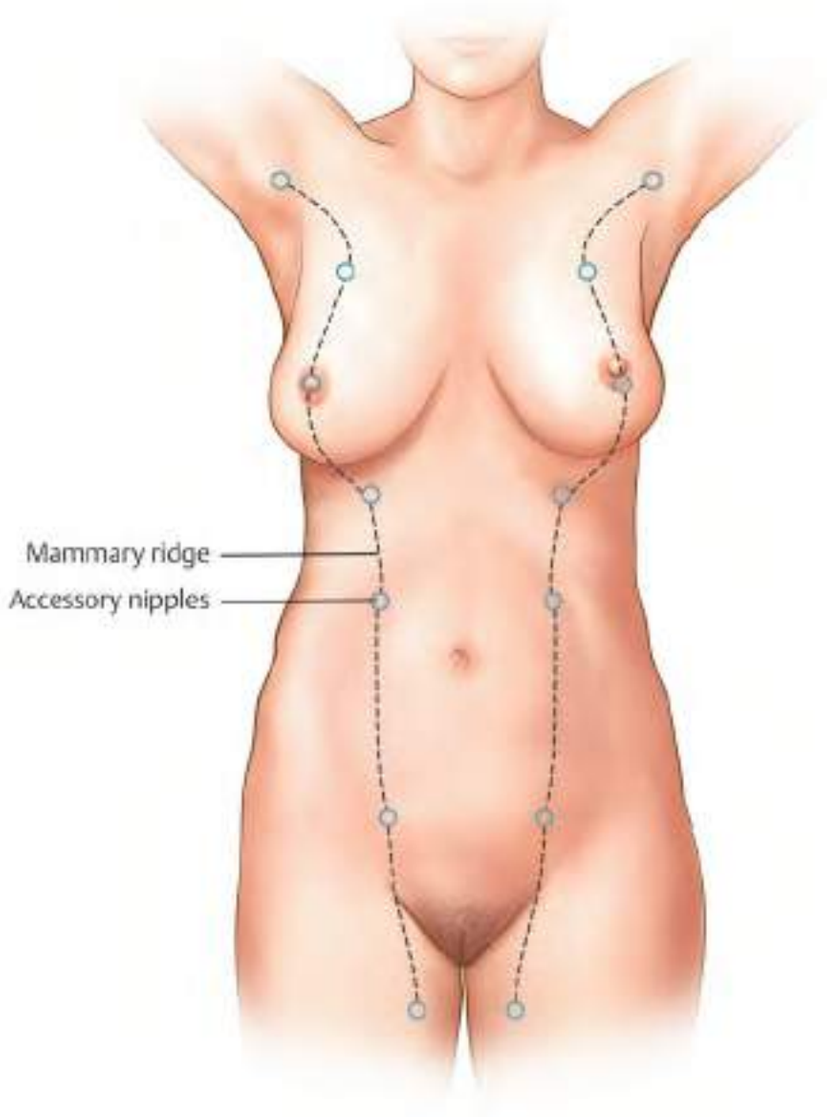

Fig. 11.2 Milk lines. The milk lines are two lines which run from the axilla to the medial thigh on each side. These paired mammary ridges usually atrophy after 6 weeks of embryonic age except at the pectoral location. Incomplete regression of the milk line results in an accessory nipple (polythelia) or breast tissue (polymastia) anywhere along this region.

both breasts), or athelia (absence of one or both nipples).[2] When amastia occurs unilaterally, it is associated with the absence of the pectoralis muscle, while amastia that occurs bilaterally is associated with other birth defects.[7,8] It is important for both clinicians and radiologists to be knowledgeable about the development and appearance of breast buds because the most common cause of amastia is iatrogenic resulting from biopsy of a developing breast bud and leading to a marked deformity later in life.[8]

During this time of growth, the supporting structures and tissues of the breast are developing and maturing under the influence of maternal hormones. While the ducts and alveoli are made from the ectoderm, the connective tissue and vasculature of the breast are formed from mesenchyme. Shortly after birth, when the maternal hormones are no longer present, there is a pause in breast growth and does not restart again until puberty. The developmental period of the breast bud and nipple is the same process for males and females.

When puberty starts, there is a difference in the development of male and female breast tissue. In the male breast during puberty, the ducts and stromal tissues involute and atrophy. Therefore, the male breast is mostly comprised of fat. On the other hand, in the female breast, the estrogenic effects stimulate the growth of the supporting soft tissue structures as well as the ducts and lobules. During puberty in females, the breast mound increases. The subsequent enlargement and outward growth of the areola then result in a secondary mound.[1]

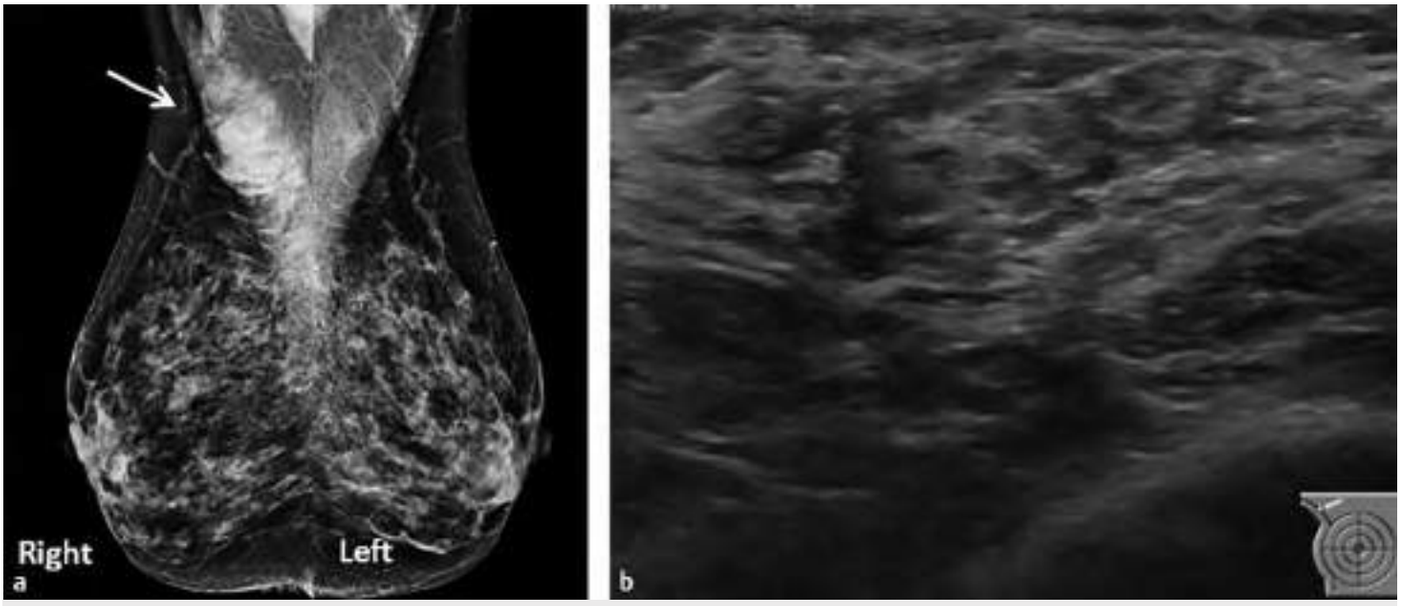

Fig. 11.3 Example of accessory breast tissue. **(a)** Mediolateral oblique (MLO) mammographic views of the breasts demonstrate asymmetric tissue in the right axilla (*arrow*) overlying the pectoralis muscle. **(b)** Corresponding targeted ultrasound of the right axilla shows benign tissue consistent with accessory breast tissue (polymastia). Embryologically, this is a result of incomplete regression of the right mammary ridge at this location.

◆ Breast Parenchyma

The adult breast lies between the second and sixth ribs and has a medial boundary being the sternal edge and a lateral boundary being the midaxillary line. The breast overlies the pectoralis major muscle superiorly, serratus muscle laterally, and upper abdominal oblique muscles inferiorly.[3] The breast is composed of both epithelial and stromal elements. About 10 to 15% of the breast volume is made of epithelial elements while the remainder of the breast is stromal elements.[9] The upper outer quadrant of the breast usually contains the most amount of glandular tissue.

The skin of the breast is thin and contains hair follicles, sebaceous glands, and sweat glands. Two fascial layers are present within the breast. The superficial fascia lies deep to the dermis and the deep fascia lies anterior to the pectoralis major muscle fascia.[9] The superficial pectoral fascia envelops the breast and is continuous with the superficial abdominal fascia of Camper. The undersurface of the breast lies on the deep pectoral fascia which covers the pectoralis major and anterior serratus muscles. Connecting the two fascial layers are the Cooper suspensory ligaments which allow for support of the breast. The suspensory ligaments of Cooper are perpendicular to the orientation of the skin (▶ Fig. 11.4).

There is a retromammary bursa or space (▶ Fig. 11.4) which is filled with loose tissue, and along with the suspensory ligaments of Cooper, allows the breast to move freely against the thoracic wall.[9] The average breast measures 10 to 12 cm in diameter with an average thickness at the center of approximately 5 to 7 cm.

◆ Ducts and Lobules

The breast is composed of approximately 15 to 20 lobes and these lobes are further divided into lobules. The lobules are made up of branched alveolar glands. Each lobe drains into a major lactiferous duct (▶ Fig. 11.5). The lactiferous ducts dilate into a lactiferous sinus beneath the areola and then open through a constricted orifice onto the nipple. The space between the lobes is filled by connective tissue including fat. During the development of the breasts at the time of puberty, the ducts grow and divide and form terminal end buds. The terminal end buds then form new branches and small ductules termed *alveolar buds*. The alveolar buds differentiate into the terminal structure of the resting breast called *acines* or *ductules*.[8] *Alveolus* sometimes refers to the end secretory unit at rest or nonpregnant state while *acines* refers to the fully developed unit in pregnancy or lactation.[8,10] Typically, there are hundreds of acinar cells within each breast. The *terminal ductal–lobular unit* (TDLU) refers to the basic functional unit of the breast with 30 to 50 acinar cells grouped into a lobule and the associated ducts. A normal TDLU ranges between 1 and 4 mm in size (▶ Fig. 11.5, ▶ Fig. 11.6, ▶ Fig. 11.7).

In the immature breast, the ducts and alveoli are lined by a two-layer epithelium that consists of a basal cuboidal layer and flattened surface layer. In the adult breast, the epithelium proliferates and becomes multilayered. The alveolar cell types have been described: superficial (luminal) A cells, basal (chief) B cells, and myoepithelial cells.[8] Myoepithelial cells are located surrounding the alveoli and are contractile units that are stimulated by hormones such as prolactin and oxytocin (▶ Fig. 11.8).

If pregnancy occurs, the breast lobules which are composed of epithelial lobular cells and underlying contractile myoepithelial cells differentiate for lactation.[3] With the presence of prolactin hormones, the lobules are stimulated to produce and secrete milk. In the first 4 weeks of pregnancy, increased levels of estrogen cause the ducts and lobules to form and branch. By the eighth week of pregnancy, the breasts are larger in size with associated increased vascularity and increasing pigmentation of the nipple–areolar complex. During the second trimester, the lobular formation is greater than that of the ductal sprouting due to increased levels of progesterone. The remainder of the pregnancy

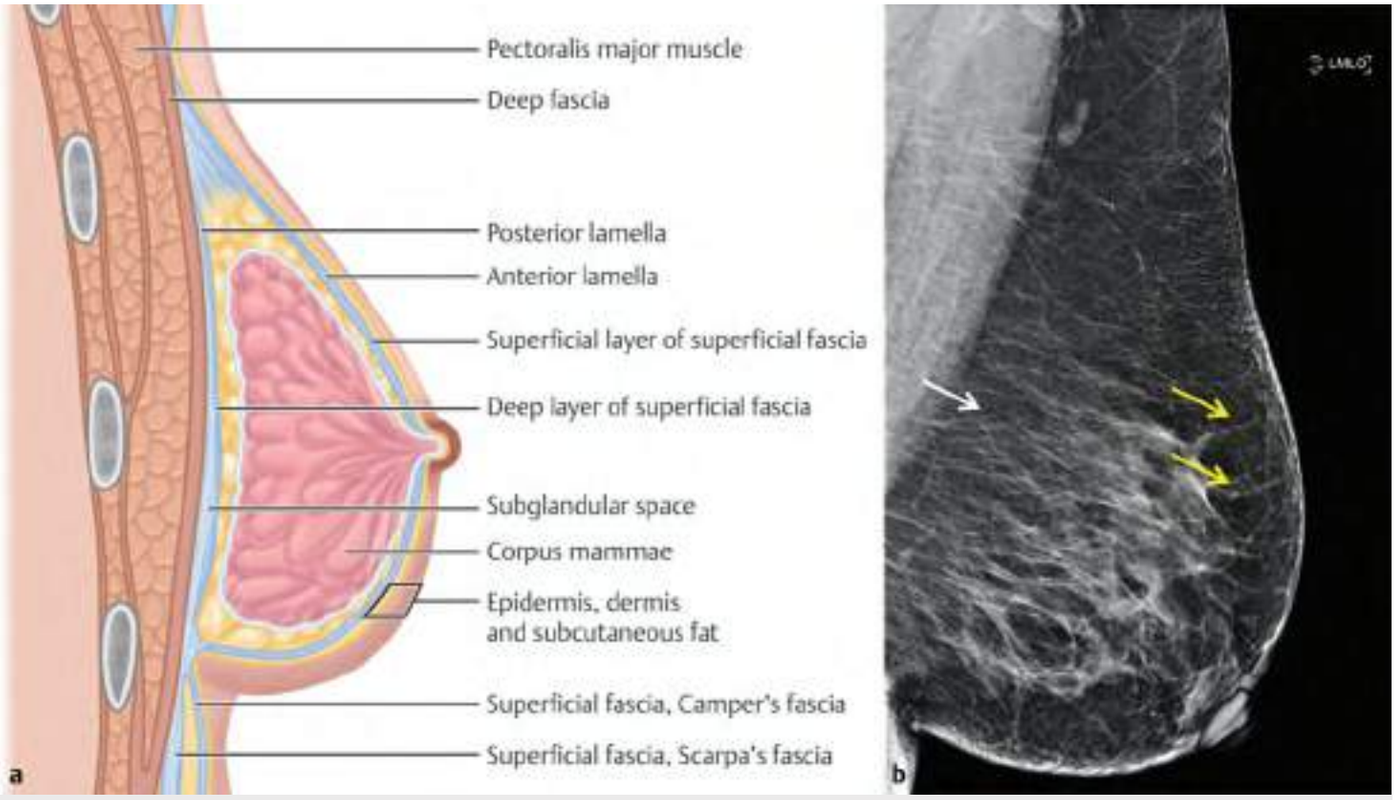

Fig. 11.4 **(a)** Two fascial layers are present (superficial and deep layers of the superficial fascia) which surround the breast parenchyma. The fascia forms septa called Cooper's ligaments, which attach the breast to the skin anteriorly and to the fascia of pectoralis (deep fascia) posteriorly. They also run through the breast, providing a supportive framework between the two fascial layers. If there is malignant tumor which causes infiltration and shortening of the Cooper's ligaments, there will be dimpling of the skin on physical examination. **(b)** Mediolateral oblique (MLO) mammographic view shows Cooper's ligaments (*yellow arrows*) which attach the superficial layer of the superficial fascia to the skin. Also shown is the retromammary/subglandular bursa or space (*white arrow*) which contains loose connective tissue and additional Cooper's ligaments that attach the breast to the chest wall.

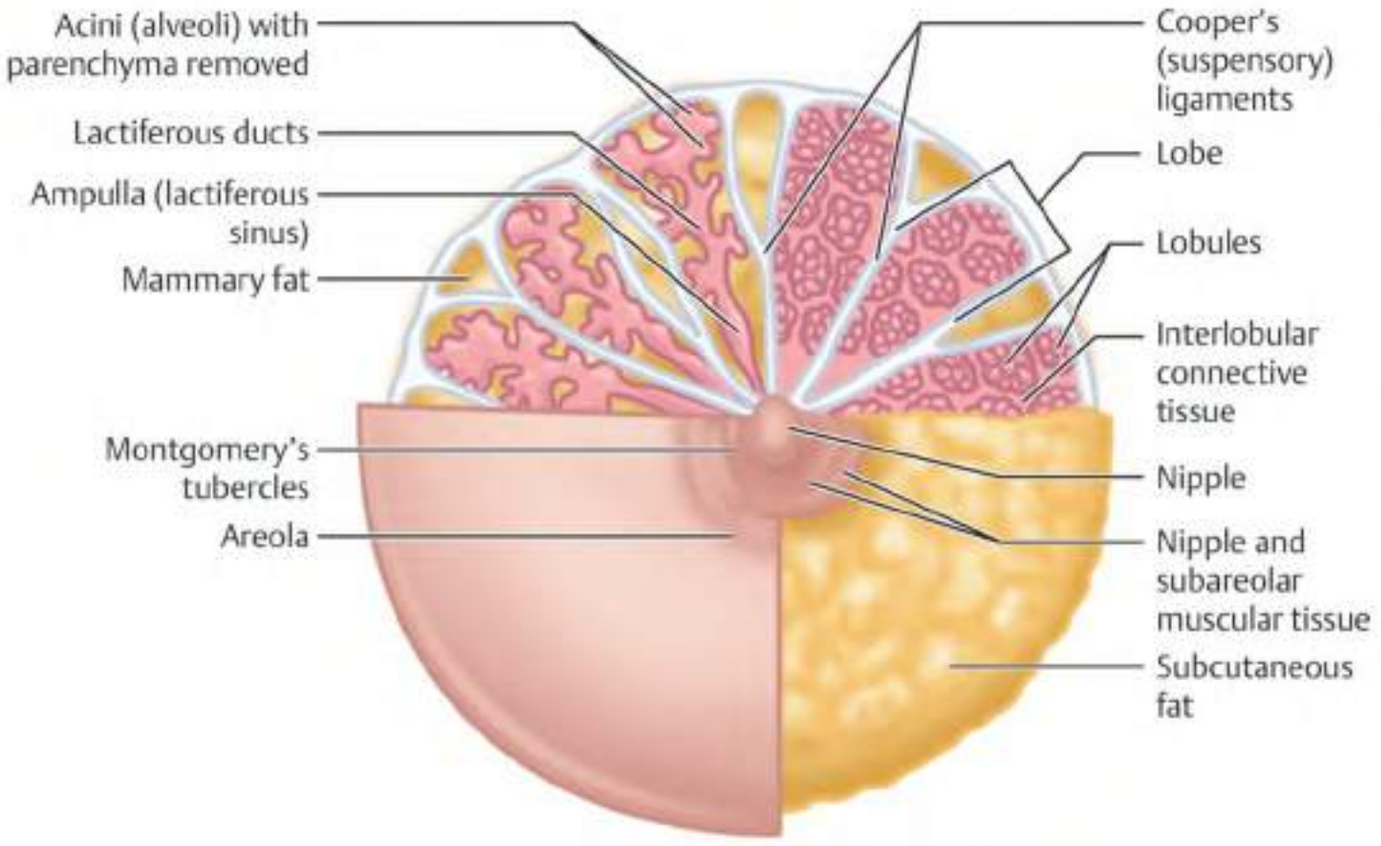

Fig. 11.5 This schematic diagram shows a frontal view of the breast with the different layers: skin, subcutaneous fat, breast ducts, lobes, and lobules containing the acini (alveoli).

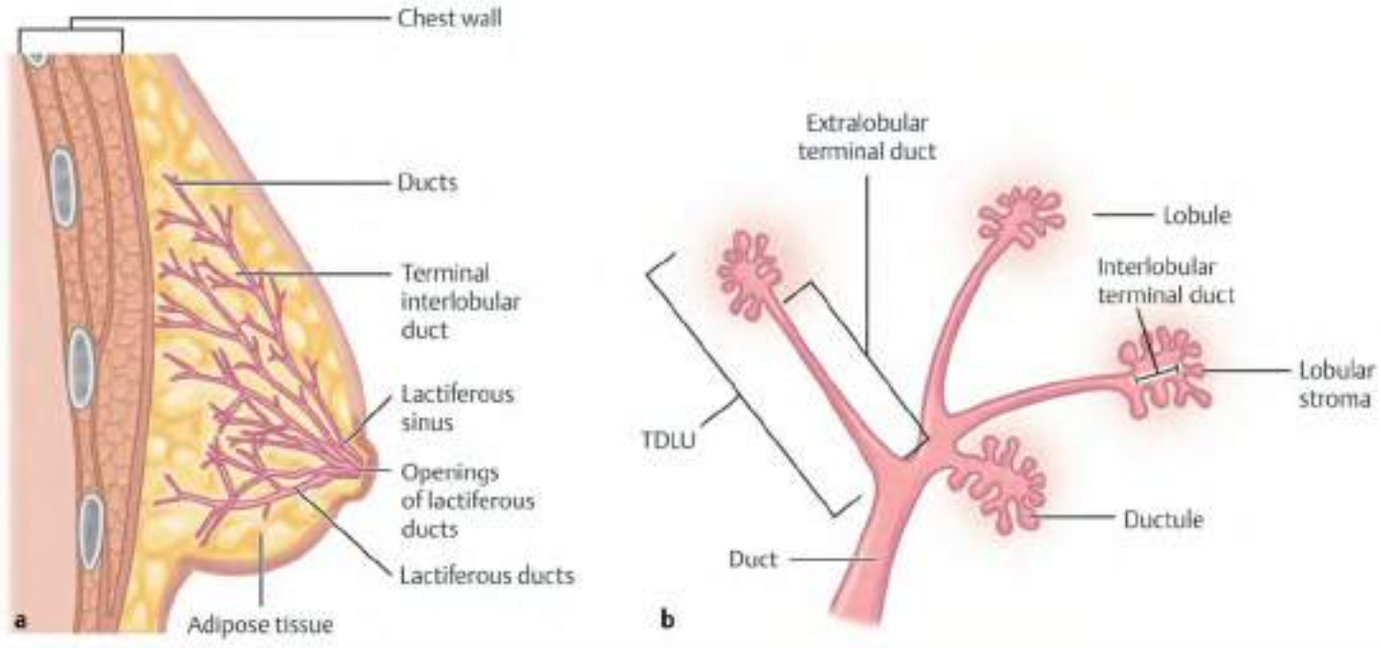

Fig. 11.6 **(a)** The breast is composed of approximately 15 to 20 lobes and these lobes are subdivided into lobules. The lobules are made up of branched alveolar glands. Each lobe drains into a major lactiferous duct. The lactiferous ducts dilate into a lactiferous sinus beneath the areola and then open through a constricted orifice onto the nipple. The diagram shown is the breast in an inactive state. **(b)** The *terminal ductal–lobular unit* (TDLU) refers to the basic functional unit of the breast with 30 to 50 alveolar or acinar cells grouped into a lobule and the associated ducts. A normal terminal ductal lobular unit ranges between 1 and 4 mm in size.

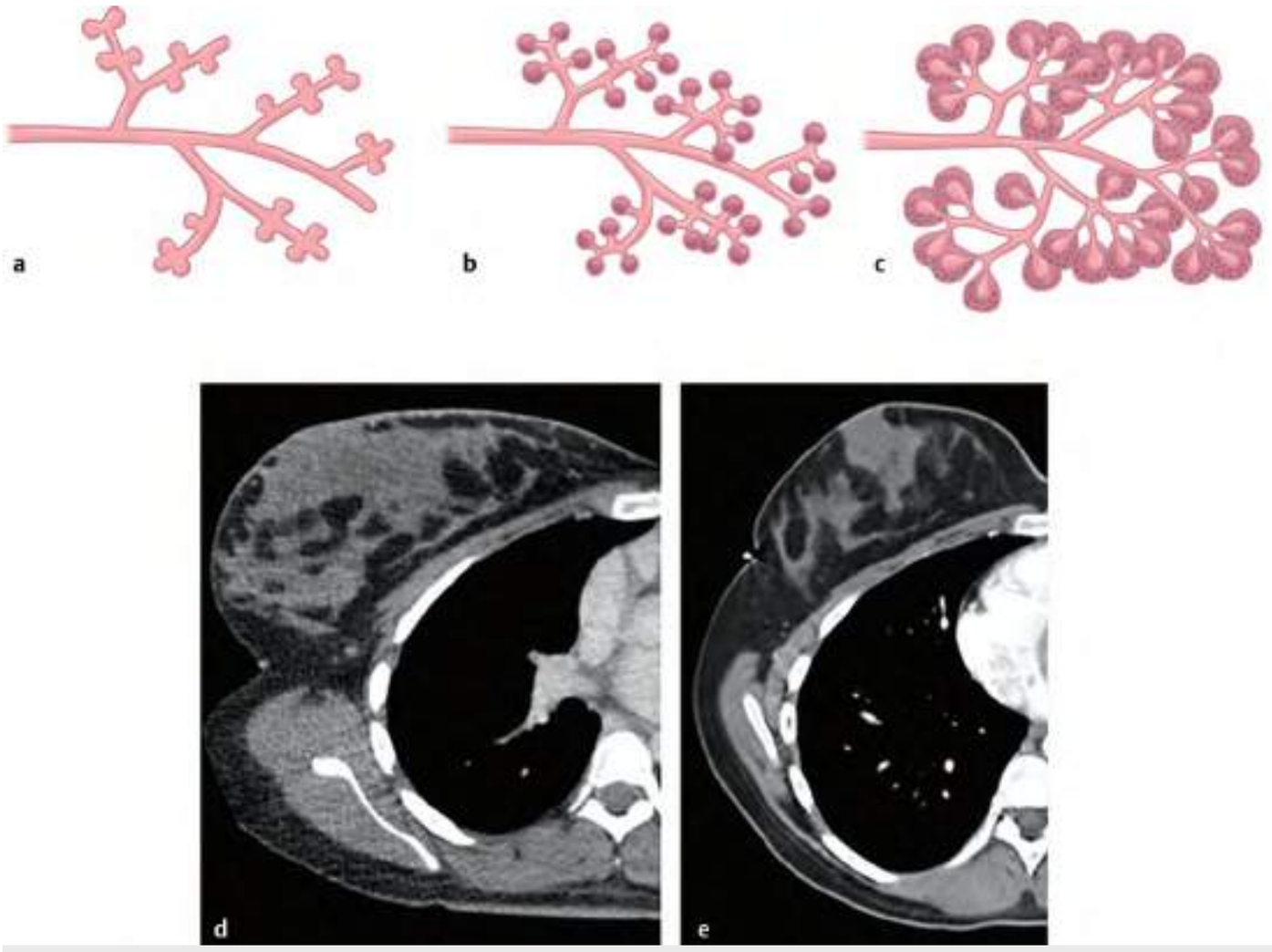

Fig. 11.7 **(a)** The breast in a nonpregnant or inactive state when the ductal system is inactive. **(b)** During pregnancy, the alveoli/acini at the end of the ductal system proliferate and divide in preparation for milk production. **(c)** During the lactational state, milk is produced, secreted, and stored in the lumen of the alveoli/acini. *Alveolus* sometimes refers to the end secretory unit at rest or nonpregnant state while *acines* refers to the fully developed unit in pregnancy or lactation. **(d, e)** Axial CT of the chest during last trimester **(d)** and postpartum state when breastfeeding has ceased **(e)** showing involution of the right breast.

is associated with continued breast enlargement from alveoli being filled with colostrum, and hypertrophy of the myoepithelial cells and connective tissues of the breast[5,8] (▶ Fig. 11.7). If the pregnancy is interrupted early or if breast-feeding is stopped, these lobular cells then return to the nonfunctioning state (▶ Fig. 11.7).

During menopause and the aging process, both the ductal and lobular system of the breast start to atrophy and involute thus decreasing the density of the breast parenchyma. This results in a greater volume of the breast to be composed of fatty elements. This is the result of changes in the circulating hormones and a decrease in ovarian estrogen production. During menopause, ducts, lobules, and lymphatic channels all decrease in number. The ductal system will remain while the lobules shrink and collapse.[5,8]

A wide spectrum of benign and malignant disease processes may occur within the breast that originate from the ducts, lobules, or connective tissues. The most common malignant diseases of the breast include ductal carcinoma in situ (DCIS), invasive ductal carcinoma, and invasive lobular carcinoma. There is evidence that supports the fact that both ductal carcinoma and lobular carcinoma arises in the TDLU.[11] DCIS is "noninvasive" or "preinvasive" ductal carcinoma because the basement membrane of the ducts is not involved by tumor cells. It typically presents on mammogram as suspicious linear or pleomorphic calcifications in a grouped, linear, or segmental distribution (▶ Fig. 11.9, ▶ Fig. 11.10). Invasive cancers usually present as irregular solid masses. About one in five newly diagnosed breast cancers will be DCIS. Invasive or infiltrating ductal carcinomas comprise a majority of newly diagnosed breast cancers (up to 80%) while invasive lobular carcinomas are rarer (about 10%) (▶ Fig. 11.11).

The most common benign breast masses are cysts, fibroadenomas, and papillomas. Breast cysts are derived from the terminal duct lobular unit when there is blockage of the terminal acini with resultant dilation of ducts[12,13] (▶ Fig. 11.12). Fibroadenomas are the most common neoplasm of the breast and is thought to occur in 25% of asymptomatic women.[12] Fibroadenomas develop from the stroma and epithelial components from the breast lobule. Fibroadenomas usually present as a highly mobile, firm, nontender, and often palpable breast mass[12,14] (▶ Fig. 11.13).

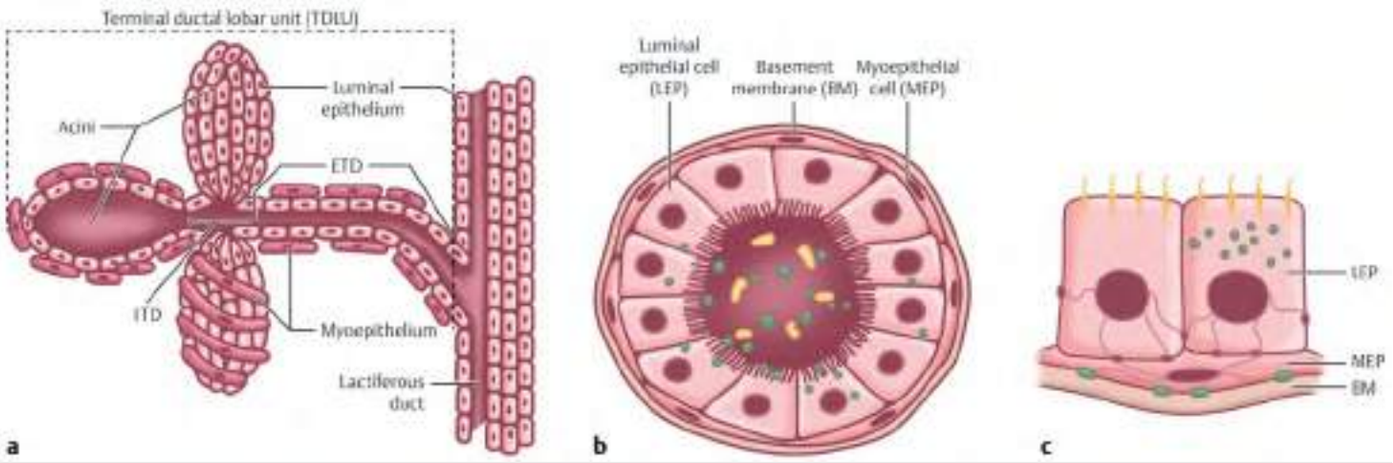

Fig. 11.8 (a–c) Diagrams of the terminal ductal–lobular unit (TDLU) at the cellular level shows the inner secretory luminal epithelial cells (LEP) lining the acini (ductules). The outer layer is made of myoepithelial cells (MEP) which are the contractile units. The basement membrane (BM) is deep to the myoepithelial cell layer. ITD, intralobar terminal duct; ETD, extralobar terminal duct.

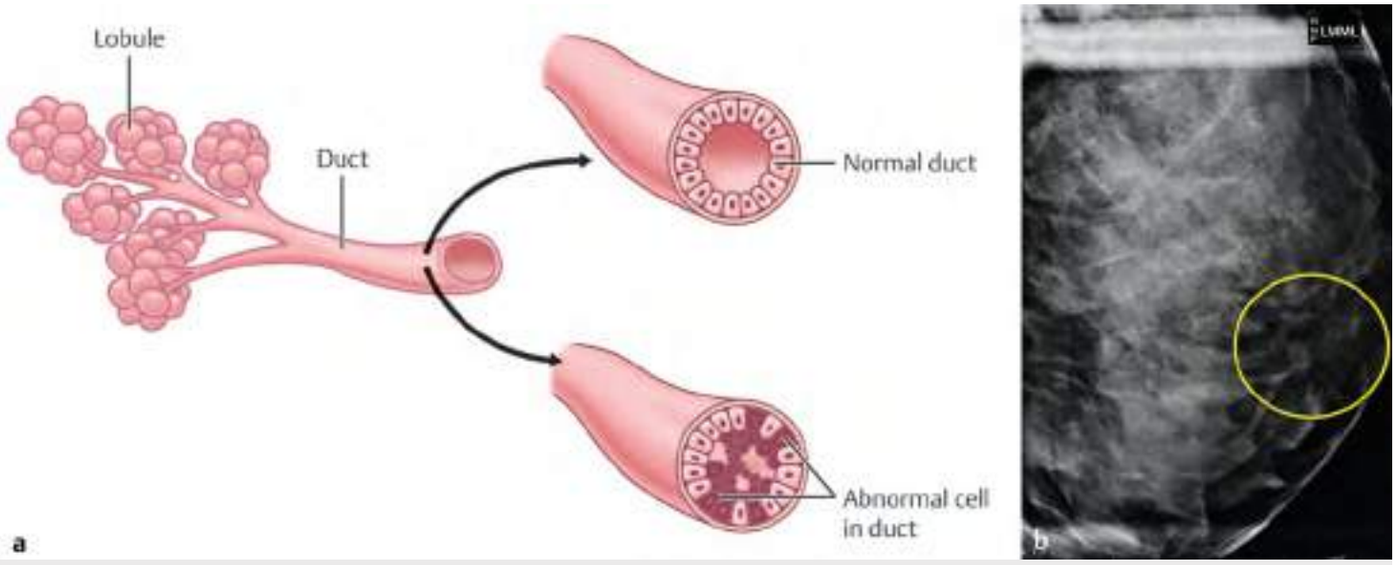

Fig. 11.9 (a) Ductal carcinoma in situ (DCIS). Schematic diagram of where DCIS occurs. DCIS is "noninvasive" or "preinvasive" ductal carcinoma because the basement membrane or walls of the ducts are not involved by tumor cells. It typically presents on mammogram as suspicious linear or pleomorphic calcifications in a grouped, linear, or segmental distribution. **(b)** Spot magnifications view of the left breast demonstrate a group of punctate calcifications which were biopsy-proven DCIS (*yellow circle*).

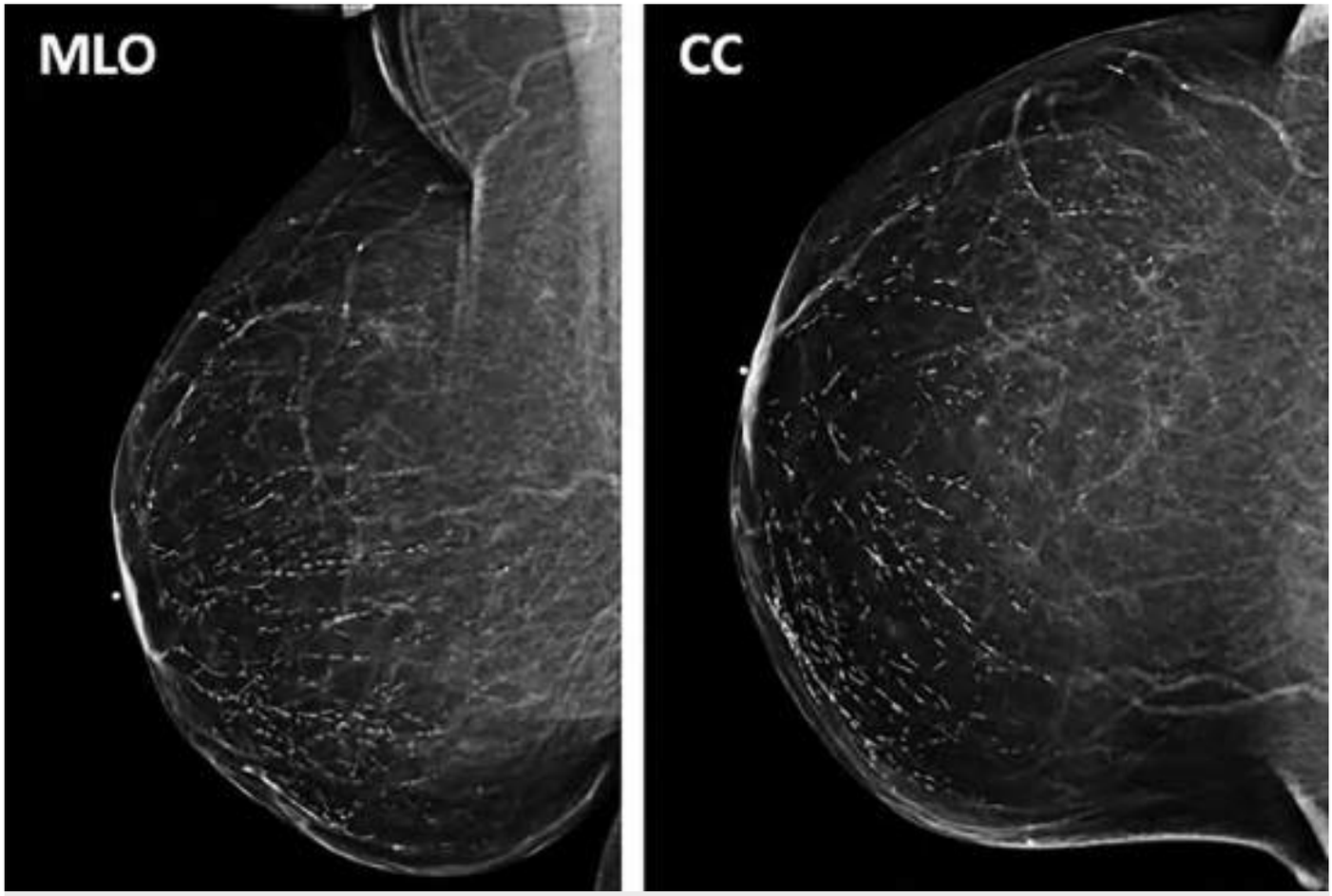

Fig. 11.10 Example of benign secretory calcifications. Mediolateral oblique (MLO) and cranial caudal (CC) mammographic views of the right breast demonstrate large rod-like calcifications in a diffuse distribution radiating from the nipple consistent with benign secretory calcifications. The diffuse distribution suggests a benign process unlike ductal carcinoma in situ (DCIS) which is usually grouped, linear, or segmental in distribution. Benign secretory calcifications are usually a result of intraluminal debris that calcify forming the thick, rod-like calcifications that are deposited within the ducts.

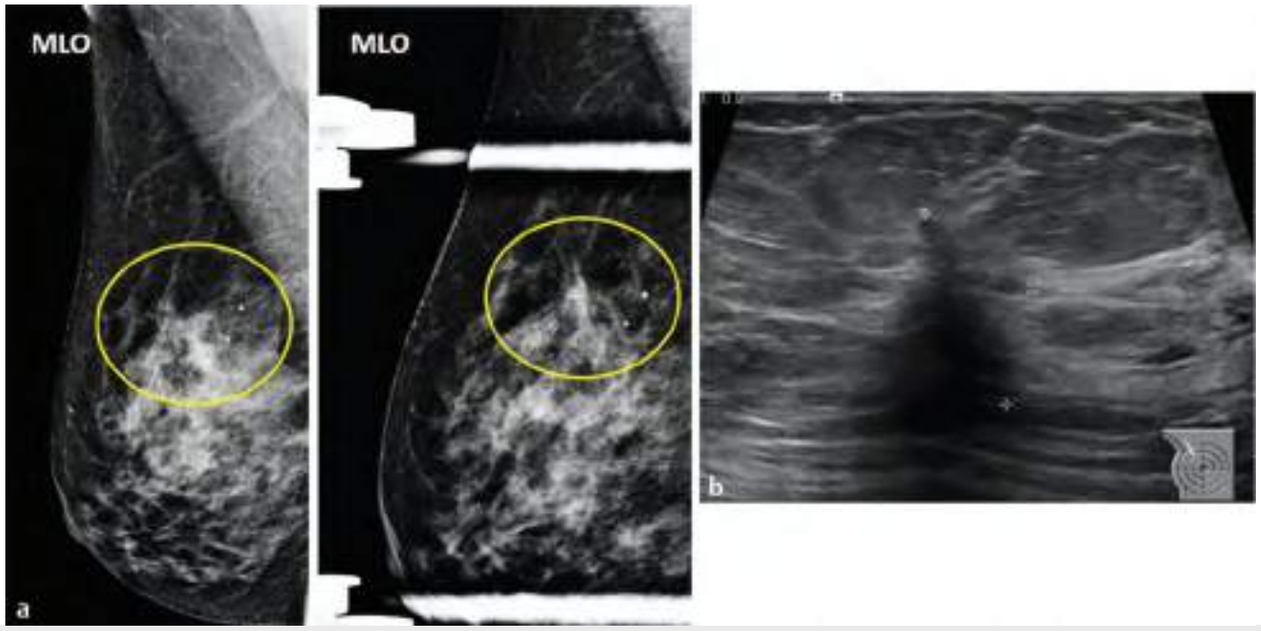

Fig. 11.11 Example of invasive ductal carcinoma. **(a)** Mediolateral oblique (MLO) and spot compression mammographic views of the right breast demonstrate a spiculated irregular mass with associated architectural distortion in the posterior depth of the superior breast (*yellow circles*). **(b)** Targeted ultrasound demonstrates a corresponding irregular hypoechoic antiparallel mass measuring up to 17 mm. This is a biopsy-proven malignant invasive ductal carcinoma.

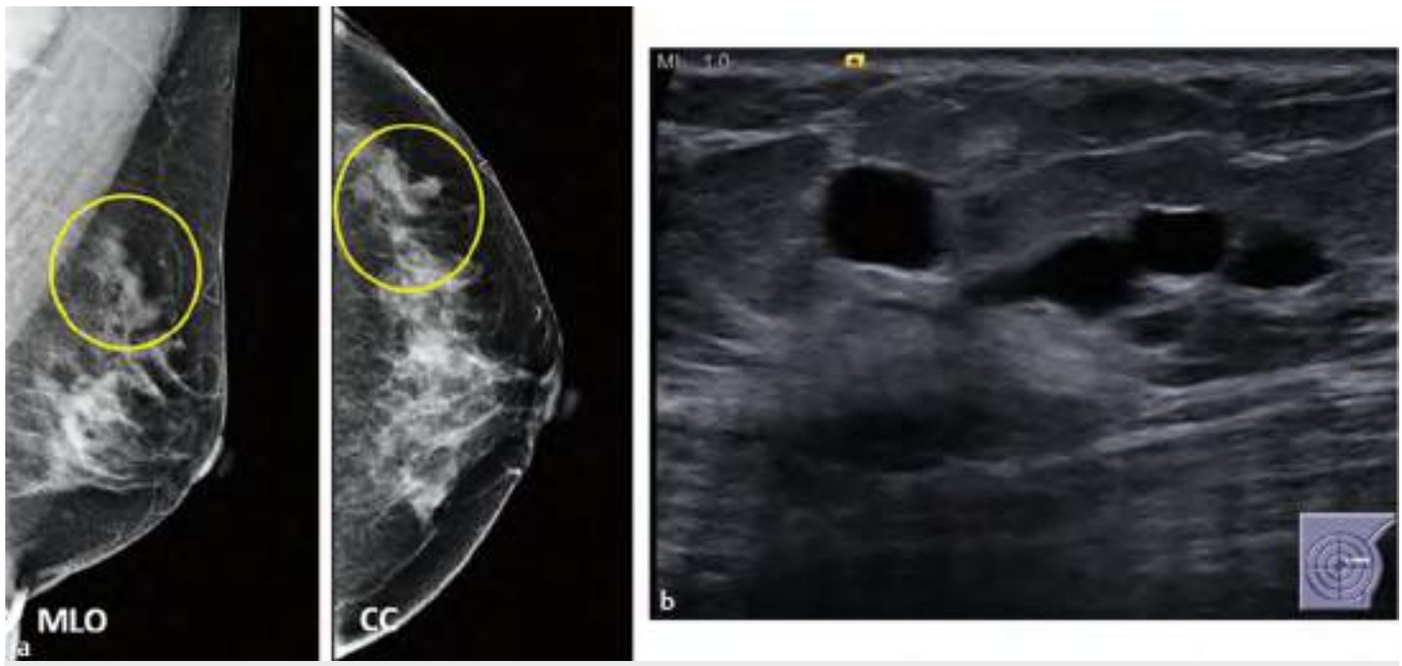

Fig. 11.12 Example of benign simple cyst. **(a)** Mediolateral oblique (MLO) and cranial caudal (CC) mammographic views of the left breast demonstrate several adjacent masses (*yellow circles*) in the posterior depth of the upper outer quadrant corresponding to patient's palpable lump (*triangle skin marker*). **(b)** Targeted ultrasound of the left breast demonstrates several small simple cysts corresponding to the mammographic findings and palpable lump. Breast cysts are derived from the terminal duct lobular unit when there is blockage of the terminal acini resulting in dilation of ducts.

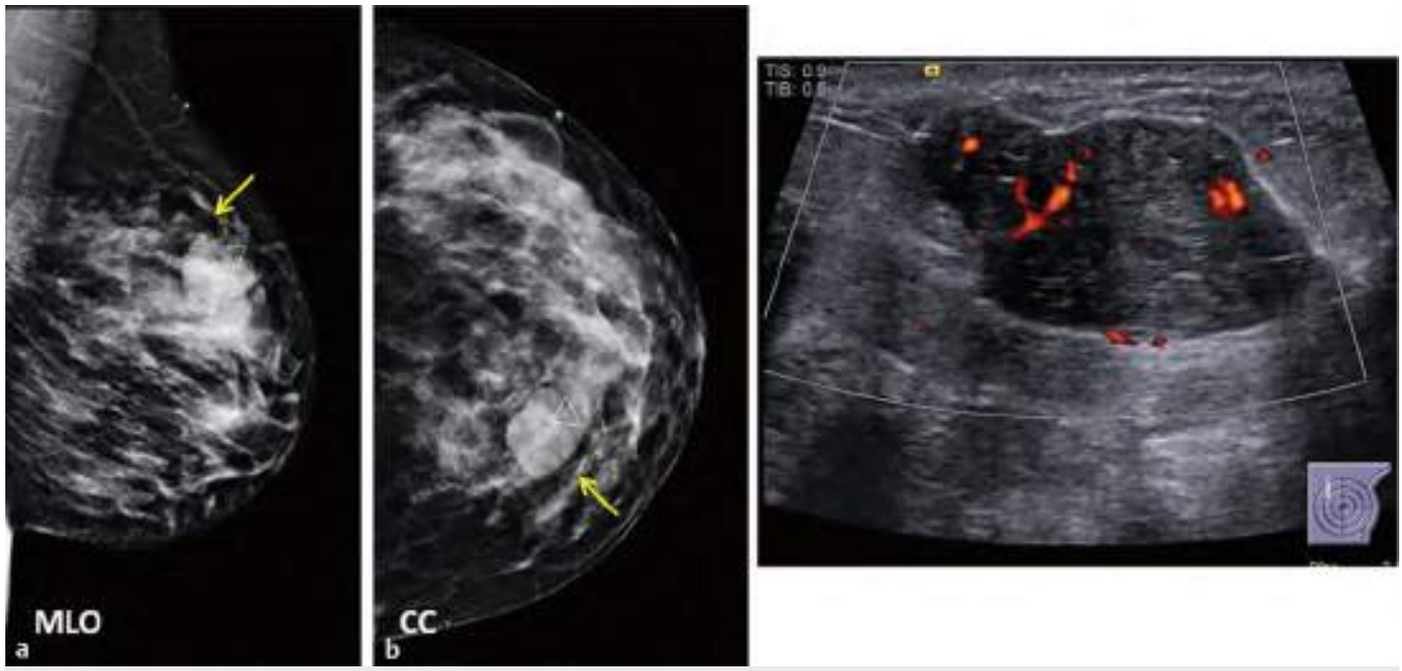

Fig. 11.13 Example of benign fibroadenoma. **(a)** MLO and CC mammographic views of the left breast demonstrate an oval mass (*yellow arrows*) in the middle depth of the upper inner quadrant corresponding to patient's palpable lump (*triangle skin marker*). (**b**) Targeted power Doppler ultrasound of the left breast demonstrates an oval solid circumscribed mass with internal flow corresponding to the mammographic finding and palpable lump. This is a biopsy-proven benign fibroadenoma. Fibroadenomas are the most common solid masses within the breast and can occur in up to 25% of asymptomatic women.

◆ Nipple–Areolar Complex

At full development of the breasts, the nipple–areolar complex most commonly is located at the fourth intercostal space. A mature breast usually is composed of 15 to 20 segments that converge at the nipple in a radial arrangement. The number of segments and the number of mammary ducts may vary.[15,16,17] There may be anywhere between 4 and 18 main mild ducts at the nipple, but the average is about 10 major collecting ducts that open at the nipple.[16] This ductal network can be very complex and heterogeneous and may not always follow a perfect radial pattern as commonly depicted.[3] The ducts are usually 2 mm in diameter but coalesce in the subareolar region into lactiferous sinuses which measure 5 to 8 mm in diameter[17] (▶ Fig. 11.6; ▶ Fig. 11.14).

The nipple–areolar complex contains *Montgomery glands* which are embryologically between sweat glands and mammary glands and are capable of secreting milk.[15] The *Montgomery glands* open at the *Morgagni tubercles*, which are small raised papules on the areola[18] (▶ Fig. 11.5). The skin of the nipple is continuous with the ductal epithelium and therefore disease processes such as malignant neoplasms of the ducts may spread to involve the nipple.[15]

Both nipple retraction and inversion may occur as a congenital or acquired process and may be unilateral and bilateral. Usually, bilateral and slow progressive nipple retraction is a benign process.[17] However, if a woman presents with new onset of unilateral nipple inversion, underlying malignancy or inflammation should be excluded by appropriate clinical and imaging work-up.[17] It is important that during mammographic imaging, the nipple is positioned in profile, because it may be mistaken for a mass. The nipple should be in profile for at least one mammographic view. On contrast-enhanced breast magnetic resonance imaging (MRI), the nipple has variable imaging appearances. Usually, the nipples are surrounded by a smooth thin rim of enhancement and are symmetric.[19] Sometimes the enhancement from an inverted nipple may be mistaken for a mass (▶ Fig. 11.15).

Benign and malignant pathological processes may involve the skin of the nipple. Benign skin diseases involving the nipple include eczema and psoriasis and are usually bilateral. If symptoms do not improve, a biopsy is necessary to exclude Paget's disease of the nipple, a malignant condition involving the epidermis and usually associated with underlying DCIS and occasionally invasive ductal carcinoma.[20]

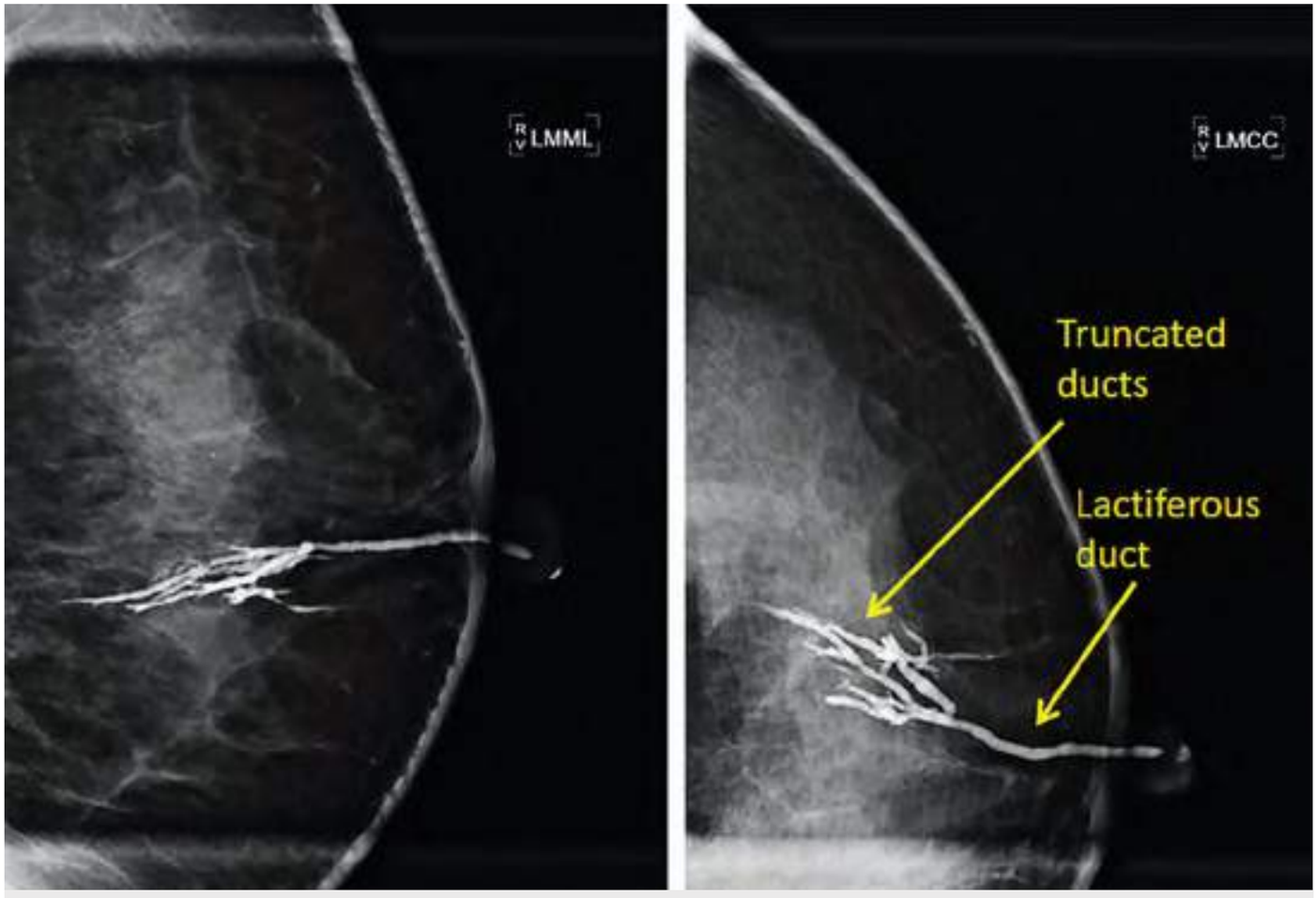

Fig. 11.14 Galactogram of left breast demonstrating truncated ducts. A galactogram was performed on this 40-year-old woman as part of a diagnostic work-up for suspicious bloody nipple discharge from the left breast. After the nipple orifice secreting the bloody nipple discharge was cannulated with a 32-gauge blunt-tipped needle, 1 cc of water-soluble iodinated contrast agent was injected demonstrating opacification of the ductal system of the selected breast lobe extending from the lactiferous duct to the distal ducts which appear abnormally truncated and tapering. The ductules and alveoli do not seem to be opacified in this examination.

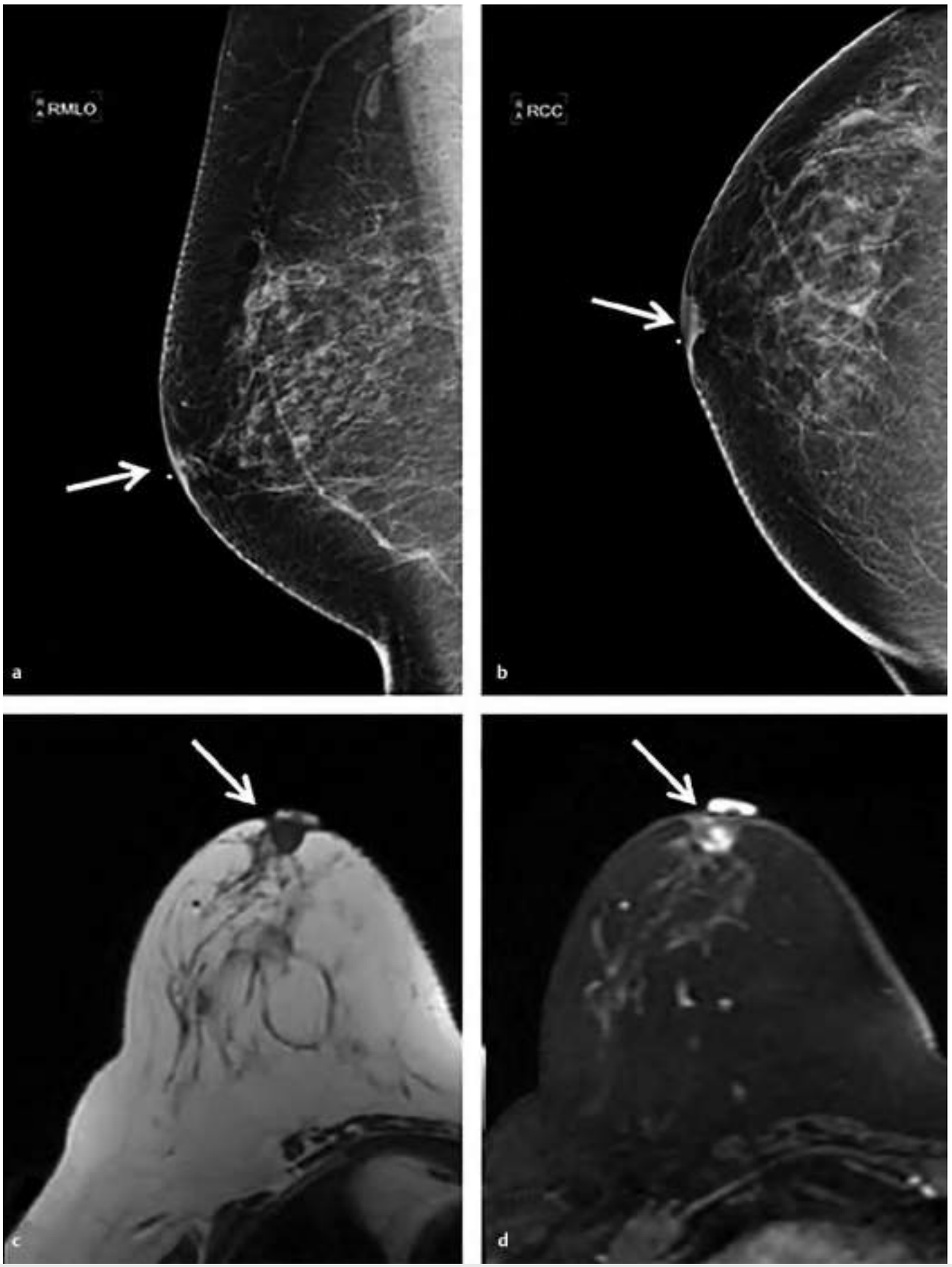

Fig. 11.15 Inverted nipple. **(a)** MLO and **(b)** CC mammographic views of the right breast demonstrate inverted nipple (*arrows*). Metallic BB marker is placed to mark the nipple on the mammogram. **(c)** Axial T1-weighted MR and **(d)** axial T1-postcontrast fat subtracted MR images demonstrate oval area of enhancement in the subareolar region. MR marker is placed to mark the nipple.

◆ Neuromuscular Anatomy and Chest Wall

The major muscles involved with the breast are the pectoralis major, pectoralis minor, serratus anterior, and latissimus dorsi (▶ Fig. 11.16). The aponeurosis of the external oblique and rectus abdominus muscles is also important.[5] Muscle anatomy is described in detail in Chapter 1.

The pectoralis major muscle lies beneath the breast tissue and is a thick fan-shaped muscle. There are two origins with the superior origin arising from the anterior surface of the medial half of the clavicle and the inferior origin extending from the superior sternum extending down to the level of the attachment of the cartilage of the sixth or seventh ribs. The extensive origin of fibers converges toward their insertion into a tendon that is ultimately inserted into the lateral lip of the bicipital groove of the humerus. The pectoralis major is innervated by both the medial anterior thoracic nerve and lateral anterior thoracic nerve. The medial anterior thoracic nerve originates in the C7, C8, and T1 nerve roots from the lower trunk of the brachial plexus. The medial anterior thoracic nerve is responsible for the contraction of the sternalis head of the pectoralis major. The lateral anterior thoracic nerve originates from the C5 and C6 nerve roots, branches off of the lateral cord of the brachial plexus, and is distributed over the deep surface of the pectoralis major. The lateral anterior thoracic nerve provides motor input to the clavicular head of the pectoralis major.[21]

The pectoralis minor muscle is situated underneath the pectoralis major muscle, arises from the outer aspect of the third, fourth, and fifth, and inserts into the medial border of the coracoid process of the scapula. In up to 15% of people, the pectoralis minor muscle can insert onto the head of the humerus as well as the coracoid process of the scapula.[5] The medial pectoral nerve innervates the pectoralis minor muscle which arises from the medial cord of the brachial plexus.[5] The borders of the pectoralis minor muscle are used to assign lymph node levels in breast cancer staging.

The serratus anterior muscle arises from the upper eight ribs laterally and inserts into the vertebral border of the scapula on its costal surface. The serratus anterior muscle is supplied by the long thoracic nerve of Bell which arises from the posterior aspect of the C5, C6, and C7 roots of the brachial plexus. The latissimus dorsi muscle arises from spinous processes and supraspinous ligaments at the levels of T7 and all of the lumbar and sacral vertebrae. The tendon of the latissimus dorsi muscle inserts in the bicipital groove of the humerus. The nerve supplying the latissimus dorsi muscle is the thoracodorsal nerve which arises from the posterior cord of the brachial plexus with segmental origin from C6, C7, and C8.

It is important to note that for staging purposes, chest wall involvement by breast cancer upgrades the tumor stage of breast cancer to at least an overall stage of III regardless of the tumor size. Contrast-enhanced breast MRI is the best imaging modality in determining chest wall involvement. Chest wall involvement specifically refers to the involvement of the ribs, serratus anterior muscle, and/or the intercostal muscles. According to the eighth edition of the American Joint Committee on Cancer staging system, pectoralis major and/or minor muscle involvement alone is not considered chest wall involvement and therefore does not change the clinical stage.[22,23,24,25] Even though pectoralis muscle involvement alone does not change the stage of breast cancer, it is important to know that it can alter the surgical management (▶ Fig. 11.17).

The sternalis muscle is a normal anatomical variant or accessory muscle, which is of uncertain etiology and function and thought to have an embryological origin from the pectoralis major muscle. It is located between the sternal insertion of the sternocleidomastoid muscle and the rectus abdominal muscle and runs from the jugular notch to the inferior portion of the sternum. Cadaveric studies show that it can occur in up to 8% of men and women and are twice as common to be unilateral than

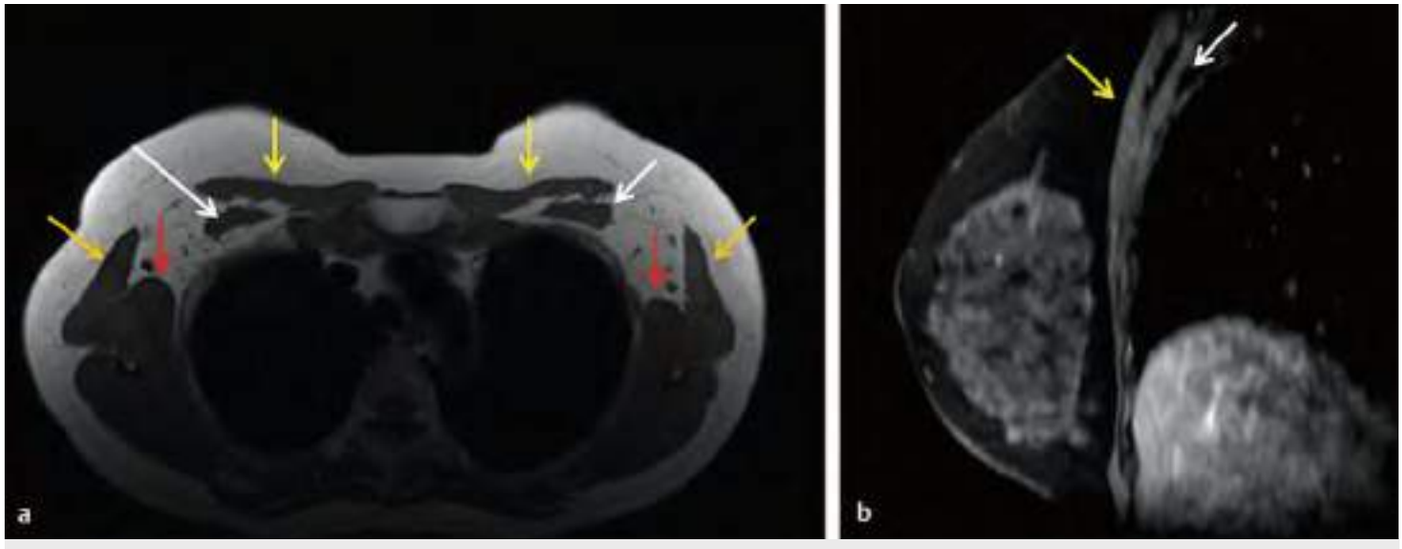

Fig. 11.16 Musculature anatomy on MRI. **(a)** Axial T1-weighted MR image through the cranial aspect of the chest wall. Included are the pectoralis major muscle (*yellow arrows*), pectoralis minor muscle (*white arrows*), serratus anterior muscle (*red arrows*), and latissimus dorsi muscle(*orange arrows*). **(b)** Sagittal postcontrast fat-suppressed T1-weighted MR images through the breasts and chest wall. The pectoralis major (*yellow arrow*) and pectoralis minor (*white arrow*) are shown.

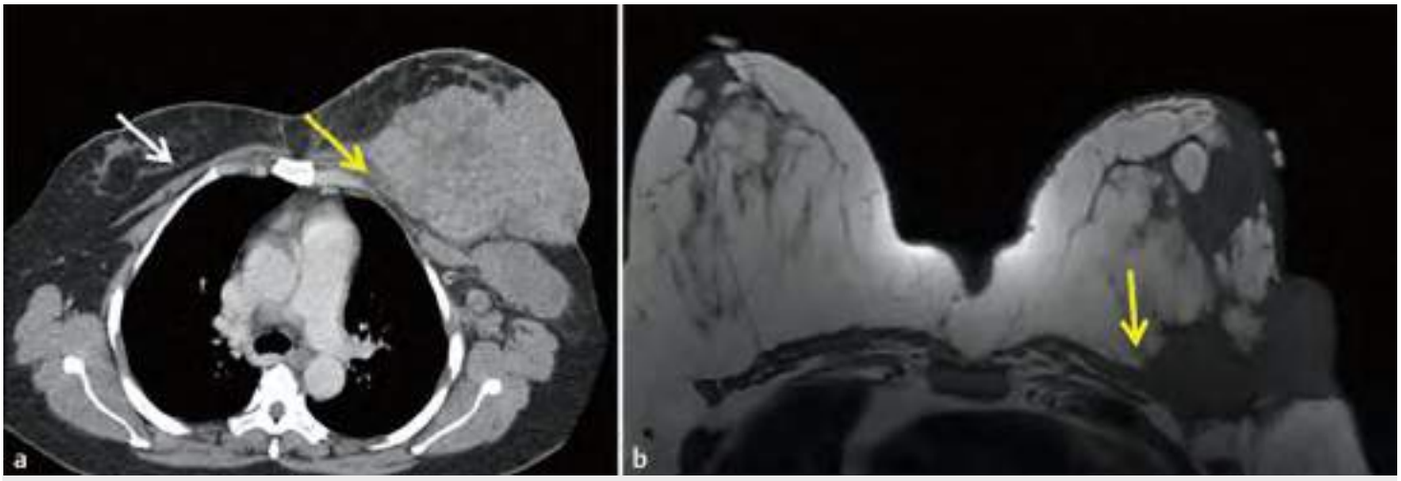

Fig. 11.17 Pectoralis major muscle invasion by tumor. A 47-year-old woman with locally advanced large left breast infiltrating ductal carcinoma with left axillary metastases. **(a)** Axial contrast-enhanced CT demonstrates a large heterogeneous mass invading the left pectoralis muscle posteriorly (*yellow arrow*). Normal pectoralis major muscle is seen on the right (*white arrow*). **(b)** The same patient subsequently received neoadjuvant chemotherapy and axial T1, axial MR image demonstrates residual smaller tumor involving the pectoralis muscle (*yellow arrow*).

bilateral.[26,27] On mammographic imaging, it can be seen in the most posterior aspect of the medial breast anterior to the medial aspect of the pectoralis major muscle. It is important for radiologists to be familiar with this anatomical variant since it can be mistaken for breast pathology. Typically, on mammogram it may present as an asymmetry, or mass with ill-defined margins, or "flame-shaped" appearance[26] (▶ Fig. 11.18).

The sensory innervation of the breast and the anterolateral chest wall comes from the lateral and anterior cutaneous branches of the second through sixth intercostal nerves.[28]

11

◆ Lymphatics and Axilla

Knowledge of the lymphatic system is essential to understanding the drainage pattern and spread of breast malignancies. Sappey first described the breast lymphatics in the 1870s.[29] The lymphatic system of the breast tends to follow the venous anatomy. The lymphatic system within the breast begins in the walls of the mammary ducts from the interlobular connective tissue.[3] The deep lymphatic system that drains the breast communicates with the superficial lymphatic system which drains the surface of the body especially in the subareolar plexus around the nipple.[3] The subareolar plexus drains mainly to the axillary lymph nodes. Flow from the deep subcutaneous and intramammary lymphatic vessels moves toward the axillary and internal mammary lymph nodes. Approximately 3% of the lymphatic drainage from the breast ultimately flows to the internal mammary chain, while 97% flows to the axillary lymph nodes.[30]

Both the breast dermal lymphatics and the breast tissue lymphatics drain to the same axillary lymph nodes.[5] This has been shown by sentinel lymph node studies. Additional lymphoscintigraphic studies have shown that the deeper parenchyma or retromammary lymphatics also tend to drain to the internal mammary lymph nodes and not directly to the axillary lymph nodes.[31,32,33]

Since Sappey's description of drainage of the subareolar plexus, there has been controversy regarding the exact pattern and drainage involving the subareolar plexus. A study from 1959 showed that the lymphatic pathway traveled from the tumor injection site directly to the axilla and not necessarily through the dense network of lymphatic capillaries present in the subareolar plexus.[34] The details of lymphatic drainage of malignant tumors of the breast are still controversial, but studies favor a direct pathway from the injection site to the axilla, and not necessarily through the subareolar complex.

Axillary lymph nodes are the major location and route of regional spread of breast cancer. Axillary lymph nodes can be divided into levels I, II, and III for the purposes of staging and pathological anatomy (▶ Fig. 11.19, ▶ Fig. 11.20).

The levels of the lymph nodes are based on the relationship of the lymph nodes to pectoralis minor muscle. Level I includes lymph nodes that are lateral to the lateral border of the pectoralis minor muscle. Level II refers to lymph nodes that are posterior to and between the lateral and medial borders of the pectoralis minor muscle. Rotter nodes are specifically interpectoral lymph nodes that are located between the pectoralis major and minor muscles along the course of the lateral pectoral nerve. Level III consists of lymph nodes that are medial to the superior border of pectoralis minor and includes subclavicular nodes[22] (▶ Fig. 11.19).

Axillary lymph nodes can also be divided into six main groups which are recognized by the surgeons: axillary vein group (level I), external mammary group (level I), scapular group (level I), central group (level II), interpectoral group (level II), and subclavicular group (level III). The axillary vein and external mammary groups lie lateral to the pectoralis minor muscle (▶ Fig. 11.19). The scapular group lies along the subscapular vessels. The interpectoral nodes are also otherwise known as Rotter's nodes located between the pectoralis major and minor muscles. The central nodes are beneath the lateral border of the pectoralis major muscle and below the pectoralis minor muscle. The subclavicular nodes lie medial to the pectoralis minor muscle and to the lateral extent of the axilla. There are also intramammary lymph nodes and paramammary nodes in the subcutaneous fat in the upper outer quadrant of the breast[28] (▶ Fig. 11.19).

Fig. 11.18 Sternalis muscle. **(a)** MLO and **(b)** CC views of the left breast in a male patient presenting with a left lump. Incidentally seen on the CC view is an apparent mass (*yellow arrow*) in the most posterior aspect of the medial breast anterior to the pectoralis major muscle (*white arrows*). It is important for radiologists to be familiar with this anatomical variant since it can be mistaken for breast pathology. Typically, on mammogram it may present as an asymmetry or mass with ill-defined margins or "flame-shaped" appearance. **(c)** Axial T1-weighted and **(d)** sagittal postcontrast fat-suppressed images demonstrate an accessory muscle anterior to the medial aspect of the pectoralis muscle consistent with a sternalis muscle. This MR demonstrates that the sternalis muscle is present bilaterally.

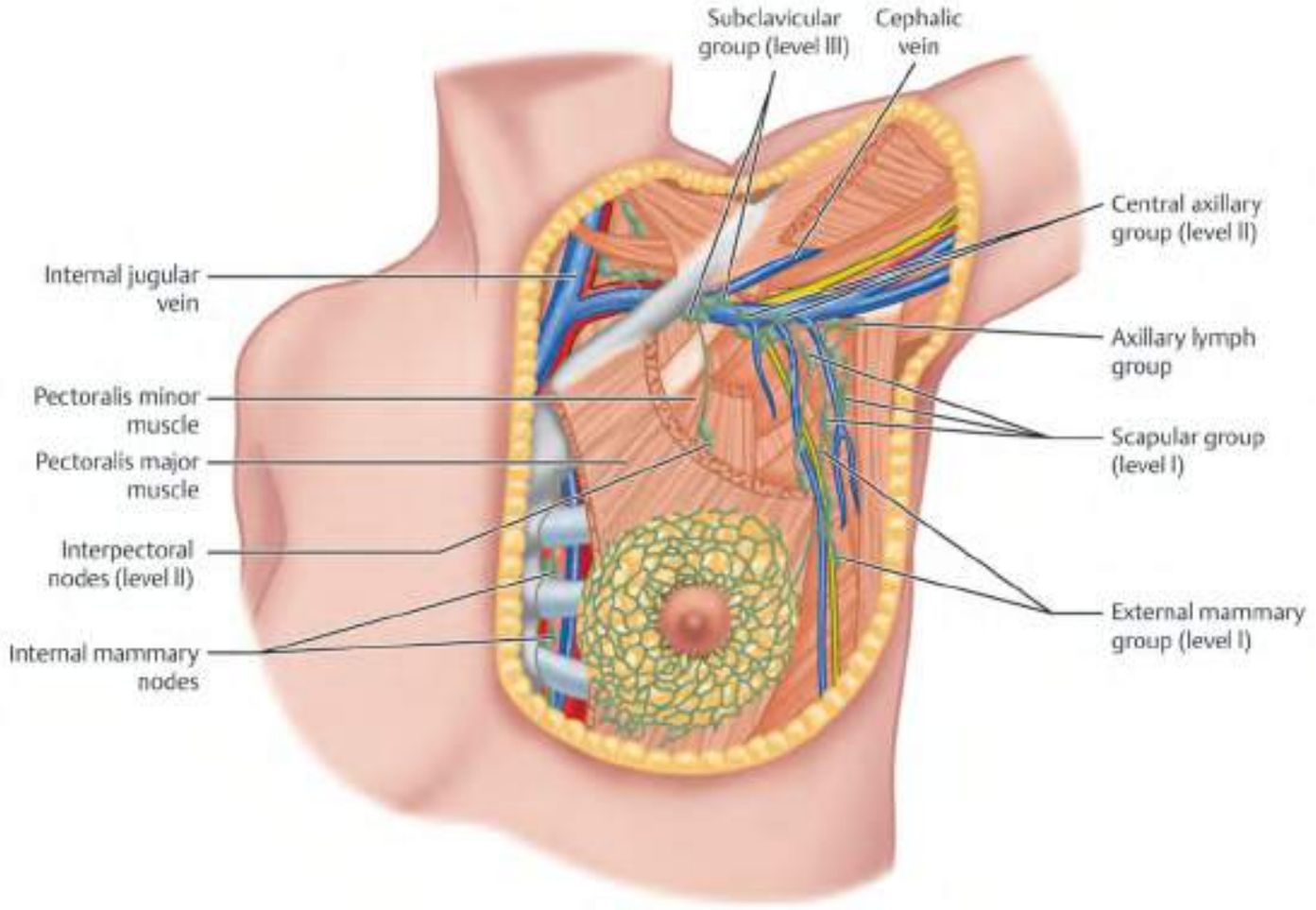

Fig. 11.19 Schematic diagram of the lymphatic drainage of the breast. The lymphatics of the breast drain into three major nodal chains: axillary, internal mammary, and supraclavicular. Approximately 75% of the lymphatic drainage of the breast goes to the axillary lymph nodes while up to 25% may drain to the ipsilateral internal mammary nodal chain.

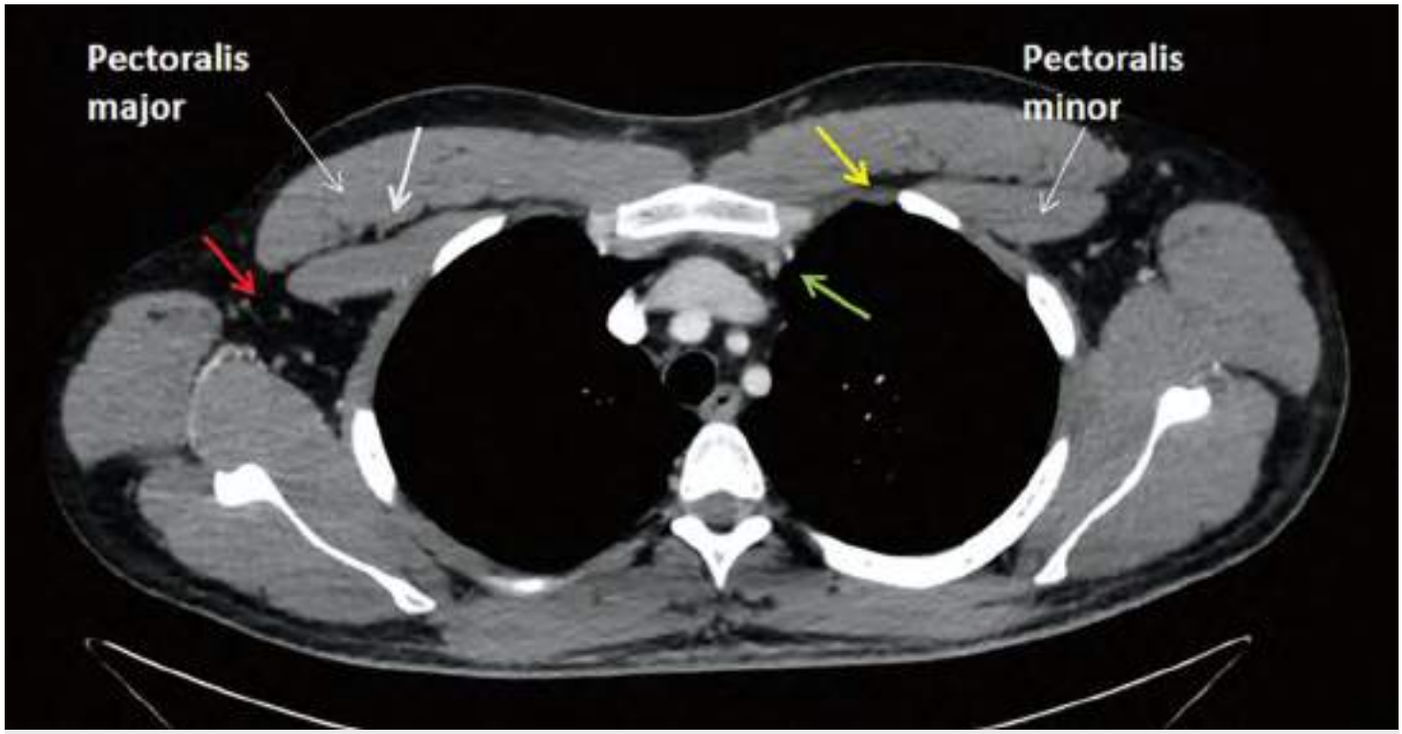

Fig. 11.20 Axillary nodal anatomy. Axial CT of the thorax demonstrating the axillary lymph node levels which are assigned based on relationship to the pectoralis minor muscles. Level I lymph nodes are lateral-to-lateral border of pectoralis minor muscle (*red arrow*). Level II lymph nodes are between medial and lateral borders of pectoralis minor (*light blue arrow*). Rotter's nodes specifically refer to level II nodes that are interpectoral in location. Level III lymph nodes are medial-to-medial margin of pectoralis minor muscle (*yellow arrow*). Internal mammary lymph nodes are located adjacent to the internal mammary vessels (*green arrow*).

Internal mammary lymph nodes are located adjacent to internal mammary vessels in the extrapleural fat in the intercostal spaces.[5] These nodes may be located either medial or lateral to the internal mammary vessels. The number of lymph nodes in the internal mammary chain varies.

When the normal physiological pathways of lymphatic drainage are blocked as in some cases of advanced breast cancer and nodal metastases, alternative routes of lymphatic drainage are possible. They include drainage to the contralateral internal mammary chain, lateral intercostal, and mediastinal drainage. Additionally, they may spread through the rectus abdominus muscle sheath to the subdiaphragmatic and subperitoneal plexus (Gerota's pathway) which can then spread to the liver and retroperitoneal lymph nodes.[35,36]

Mammography typically is suboptimal for complete axillary nodal evaluation. High-resolution ultrasound is a good examination for evaluation of nonpalpable low-level axillary nodes and palpable lymph nodes at all levels; however, results may vary depending on the operator. In addition to the axillary lymph nodes, MRI can detect internal mammary and supraclavicular adenopathy. On imaging studies, the size of the lymph node is not reliable to distinguish between normal and abnormal lymph nodes. Abnormal lymph nodes are determined by the overall shape and the changes in the appearance of the node cortex. Abnormal lymph nodes may appear as loss of reniform shape, focal or diffuse cortical thickening, hilar indentation and compression, and loss of the normal central fatty hilum.[36,37,38] It is important to biopsy the abnormal cortex of the suspicious lymph node for the greatest possible yield to determine if there is metastasis. Nuclear medicine lymphoscintigraphy is important for sentinel lymph node detection and identification at surgery in breast cancer patients (▶ Fig. 11.21).

◆ Vascular Anatomy

Overall, the blood supply to the breast varies with age, menstrual cycle, pregnancy/lactation status, and some medications. For example, increased estrogen levels during the menstrual cycle can cause increased blood flow to the breast 3 to 4 days before menstruation and can even cause an increase in breast volume.[5] During pregnancy and lactation, there is increased blood supply to the breast. Premenopausal women have more blood volume when compared to postmenopausal women. Overall, the largest concentration of blood vessels is at the nipple–areolar complex.[3] Usually, the distribution of blood vessels seems to be symmetric in both breasts, and if there is asymmetry of breast vascularity shown on MRI, this may be a potential sign of breast pathology.[39]

Arterial System

The arterial supply to the breast is mainly from the branches of the internal thoracic (mammary) artery, intercostal arteries, and lateral thoracic artery. Superficially within the breast, there are the branches of the internal and lateral thoracic arteries, which then send perforating branches deep into the breast tissue. Branches of the anterior and posterior intercostal arteries course along the pectoralis and serratus anterior muscles and send perforating branches through the chest wall into the deep breast parenchyma.[3] Overall, the internal thoracic artery is the main arterial supply to the breast and its branches supply the central

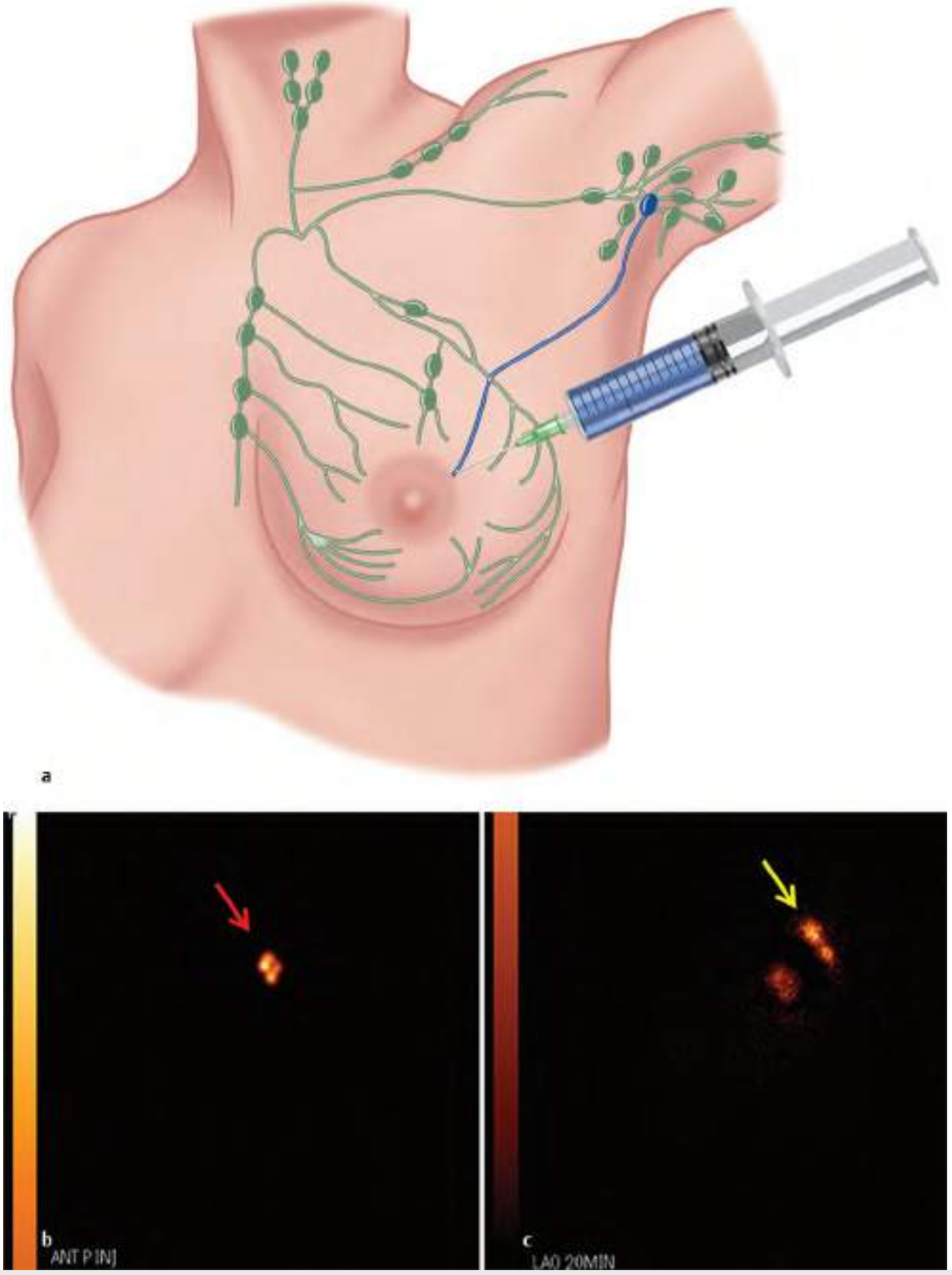

Fig. 11.21 **(a)** Sentinel lymph node identification. During lymphoscintigraphy, a radiative dye is injected into the breast and the radioactive material is carried by the lymphatic system to the sentinel lymph node(s). The sentinel lymph node(s) is identified at the time of surgery and surgically removed to determine if there are tumor metastases. **(b, c)** Breast lymphoscintigraphy: Tc99 m filtered sulfur colloid was administered subcutaneously in a periareolar location in a 47-year-old woman with left breast cancer. Subsequently, images of the left upper thorax and axilla were obtained for localization. Initial image **(b)** shows the injected radioactive material in the periareolar location (*red arrow*). After 20 minutes in the left anterior oblique position, radioactive tracer is now seen in the left axilla (**c**) (*yellow arrow*).

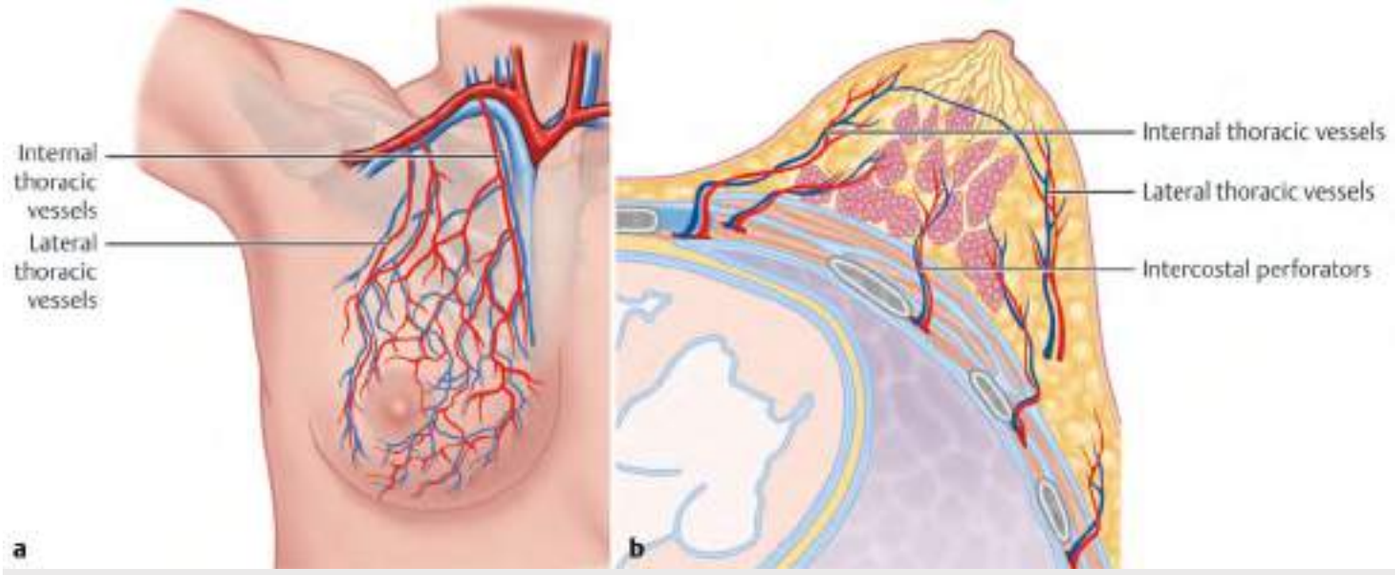

Fig. 11.22 (a, b) Arteries of the breast. Schematic diagram of the arterial blood supply of the breast.

and medial breast. The superolateral breast is supplied by the lateral thoracic artery. The superior breast often is supplied by branches of the subclavian and axillary arteries (thoracoacromial artery, subscapular artery, thoracodorsal artery). The inferior breast is supplied by branches of the musculophrenic artery which is a continuation of the internal thoracic artery but the supply to the inferior breast is variable.[3] The vascular supply to the nipple is complex and studies have shown that there is both a deep and superficial supply to the nipple. One of studies O'Dey[40] found that the internal thoracic artery supplies the nipple–areolar complex but that the lateral thoracic artery can also supply up to three branches to the nipple–areolar complex (▶ Fig. 11.22).

If there are vascular calcifications in the breast, they are usually atherosclerotic calcifications, Monckeberg's medial sclerosis, in the arteries. This finding is frequently encountered on mammograms and has a tram-track configuration.

Venous System

In general, the veins of the breast are larger in size than the arteries. On ultrasound, the veins and arteries can be differentiated based on Doppler waveform analysis. Superficially in the breast, the venous drainage is markedly variable and does not accompany the arterial blood supply. The superficial veins may drain to the center of the breast as well as the periphery. They may also drain to the contralateral breast. When a superficial vein drains centrally, it usually converges at the *circulus venosus of Haller* which is a periareolar circular network of veins. Blood then travels from this venous plexus to the internal thoracic veins medially and into the lateral thoracic veins laterally.[3] In the deep breast tissues, the veins usually parallel the arterial anatomy which includes the posterior intercostal, axillary, and internal thoracic branches (▶ Fig. 11.22). Unlike some other parts of the body, the veins within the breast do not have valves.

Venous congestion and enlarged veins in the breast may be unilateral or bilateral. Unilateral breast vein dilation may be seen as a result of axillary or subclavian obstruction. Superficial collateral veins may drain to the opposite breast. Bilateral enlarged breast veins may be a sign of superior vena cava obstruction or congestive heart failure.[41] Mondor's disease is occlusion of the superficial veins of the breast or chest wall (superficial thrombophlebitis) and presents as a noncompressible "beaded structure" without flow on color Doppler ultrasound. A breast varix is a focally dilated but patent breast vein which may demonstrate a phlebolith on mammogram.[42]

References

[1] Seltzer V. The breast: embryology, development, and anatomy. Clin Obstet Gynecol.; 37(4):879–880

[2] O'Connell RL, Rusby JE. Anatomy relevant to conservative mastectomy. Gland Surg.; 4(6):476–483

[3] Jesinger RA. Breast anatomy for the interventionalist. Tech Vasc Interv Radiol.; 17(1):3–9

[4] Sadler TW. Langman's Medical Embryology. 11th ed. Baltimore, MD: Lippincott Williams & Wilkins; 2009

[5] Osborne M. Breast development and anatomy. In: Harris J, Hellman S, Henderson I, Kinne D, eds. Breast Diseases. 2nd ed. Philadelphia, PA: Lippincott; 1991:1–13

[6] Mimouni F, Merlob P, Reisner SH. Occurrence of supernumerary nipples in newborns. Am J Dis Child.; 137(10):952–953

[7] Perlyn C, Edmiston J, Tunnessen WW, Jr. Picture of the month. Unilateral amastia (Poland syndrome). Arch Pediatr Adolesc Med.; 153(12):1305–1306

[8] Osborne M, Boolbol S. Breast anatomy and development. In: Harris JR, Lippman ME, Morrow M, Osborne CK, eds. Diseases of the Breast. 4th ed. Philadelphia, PA: Lippincott; 2010;1–11

[9] Bland L, Copeland E. The Breast—Comprehensive Management of Benign and Malignant Diseases. 4th ed. Philadelphia, PA: Saunders; 2009

[10] Russo J, Russo IH. Development of human mammary gland. In: Neville MC, Daniel VW, eds. The Mammary Gland. New York, NY: Plenum; 1987:67

[11] Stolier AJ, Wang J. Terminal duct lobular units are scarce in the nipple: implications for prophylactic nipple-sparing mastectomy: terminal duct lobular units in the nipple. Ann Surg Oncol.; 15(2):438–442

[12] Guray M, Sahin AA. Benign breast diseases: classification, diagnosis, and management. Oncologist.; 11(5):435–449

[13] O'Malley FP, Bane AL. The spectrum of apocrine lesions of the breast. Adv Anat Pathol.; 11(1):1–9

[14] El-Wakeel H, Umpleby HC. Systematic review of fibroadenoma as a risk factor for breast cancer. Breast.; 12(5):302–307

[15] Kopans D. Breast anatomy and basic histology, physiology, and pathology. In: Kopans D, ed. Breast Imaging. 3rd ed. Philadelphia, PA: Lippincott Williams & Wilkins; 2007:7–43
[16] Moffat DF, Going JJ. Three dimensional anatomy of complete duct systems in human breast: pathological and developmental implications. J Clin Pathol.; 49 (1):48–52
[17] Nicholson BT, Harvey JA, Cohen MA. Nipple-areolar complex: normal anatomy and benign and malignant processes. Radiographics.; 29(2):509–523
[18] Blech H, Friebe K, Krause W. Inflammation of Montgomery glands. Acta Derm Venereol.; 84(1):93–94
[19] Friedman EP, Hall-Craggs MA, Mumtaz H, Schneidau A. Breast MR and the appearance of the normal and abnormal nipple. Clin Radiol.; 52(11):854–861
[20] Fu W, Mittel VK, Young SC. Paget disease of the breast: analysis of 41 patients. Am J Clin Oncol.; 24(4):397–400
[21] Connell DA, Potter HG, Sherman MF, Wickiewicz TL. Injuries of the pectoralis major muscle: evaluation with MR imaging. Radiology.; 210(3):785–791
[22] Lee SC, Jain PA, Jethwa SC, Tripathy D, Yamashita MW. Radiologist's role in breast cancer staging: providing key information for clinicians. Radiographics.; 34(2):330–342
[23] AJCC (American Joint Committee on Cancer) Cancer Staging Manual; 8th edition, 3rd printing, Amin MB, Edge SB, Greene FL, et al (Eds), Springer, Chicago 2018
[24] Morris EA, Schwartz LH, Drotman MB, et al. Evaluation of pectoralis major muscle in patients with posterior breast tumors on breast MR images: early experience. Radiology.; 214(1):67–72
[25] Kazama T, Nakamura S, Doi O, Suzuki K, Hirose M, Ito H. Prospective evaluation of pectoralis muscle invasion of breast cancer by MR imaging. Breast Cancer.; 12(4):312–316
[26] Bradley FM, Hoover HC, Jr, Hulka CA, et al. The sternalis muscle: an unusual normal finding seen on mammography. AJR Am J Roentgenol.; 166(1):33–36
[27] Barlow RN. The sternalis muscle in American white Negroes. Anat Rec.; 61:413–426
[28] Pandya S, Moore RG. Breast development and anatomy. Clin Obstet Gynecol.; 54(1):91–95
[29] Sappey MP. Anatomie, Physiologie, Pathologie des vasisseaux Lymphatiques consideres chez L'homme at les Vertebres. Paris: A. Delahaye and E. Lecrosnier; 1874
[30] Hultborn KA, Larsson LG, Ragnhult I. The lymph drainage from the breast to the axillary and parasternal lymph nodes, studied with the aid of colloidal Au198. Acta Radiol.; 43(1):52–64
[31] Roumen RM, Geuskens LM, Valkenburg JG. In search of the true sentinel node by different injection techniques in breast cancer patients. Eur J Surg Oncol.; 25(4):347–351
[32] Paganelli G, Galimberti V, Trifirò G, et al. Internal mammary node lymphoscintigraphy and biopsy in breast cancer. Q J Nucl Med.; 46(2):138–144
[33] Estourgie SH, Tanis PJ, Nieweg OE, Valdés Olmos RA, Rutgers EJ, Kroon BB. Should the hunt for internal mammary chain sentinel nodes begin? An evaluation of 150 breast cancer patients. Ann Surg Oncol.; 10(8):935–941
[34] Turner-Warwick RT. The lymphatics of the breast. Br J Surg.; 46:574–582
[35] Ege GN. Internal mammary lymphoscintigraphy. The rationale, technique, interpretation and clinical application: a review based on 848 cases. Radiology.; 118(1):101–107
[36] Thomas JM, Redding WH, Sloane JP. The spread of breast cancer: importance of the intrathoracic lymphatic route and its relevance to treatment. Br J Cancer.; 40(4):540–547
[37] Ahn JH, Son EJ, Kim JA, et al. The role of ultrasonography and FDG-PET in axillary lymph node staging of breast cancer. Acta Radiol.; 51(8):859–865
[38] Yang WT, Ahuja A, Tang A, Suen M, King W, Metreweli C. Ultrasonographic demonstration of normal axillary lymph nodes: a learning curve. J Ultrasound Med.; 14(11):823–827
[39] Kul S, Cansu A, Alhan E, Dinc H, Reis A, Çan G. Contrast-enhanced MR angiography of the breast: evaluation of ipsilateral increased vascularity and adjacent vessel sign in the characterization of breast lesions. AJR Am J Roentgenol.; 195(5):1250–1254
[40] O'Dey Dm, Prescher A, Pallua N. Vascular reliability of nipple-areola complex-bearing pedicles: an anatomical microdissection study. Plast Reconstr Surg.; 119(4):1167–1177
[41] Jesinger RA, Lattin GE, Jr, Ballard EA, Zelasko SM, Glassman LM. Vascular abnormalities of the breast: arterial and venous disorders, vascular masses, and mimic lesions with radiologic-pathologic correlation. Radiographics.; 31 (7):E117–E136
[42] de Lourdes Díaz M, Pina LJ, Alonso A, De Luis E. Phleboliths detected on mammography. Breast J.; 12(5):467–469

12 General Anatomy of the Heart

Farhood Saremi and Damián Sánchez-Quintana

◆ Introduction

This chapter provides a general description of the heart anatomy and offers an outline of the relevant clinical information. Most images are produced using state of the art multidetector computed tomography (MDCT) scanner on living subjects or by meticulous dissection techniques on cadaveric specimens. Anatomical detail of specific heart structures will be presented in the subsequent chapters dedicated to that structure. Imaging study of the heart can be obtained with plain radiographs, computed tomography (CT) scan, magnetic resonance imaging (MRI), echocardiography, and nuclear imaging. Each modality has its own shortcomings or advantages. Plain radiographs are cheap and an easy way of evaluating the heart size and cardiac borders. Anatomical details require further imaging studies. CT with contrast can evaluate details of the heart morphology and the relationship of the heart with the lungs and vessels. MRI has a better contrast resolution and tissue characterization power than CT. Echocardiography has the highest temporal resolution and fast-moving structures such as cardiac valves are best assessed with echocardiography.

◆ Heart Borders in the Thorax

Knowing the radiological borders of the heart in different projections is important for imaging interpretation of heart in normal or pathological states. Plain radiographs are the first step in the imaging evaluation of the heart, lung, and major thoracic vessels.

With plain films, the heart margins can be assessed. Only the margins that are border forming with the lungs or air-containing structures (main stem bronchi, esophagus) can be seen (▶ Fig. 12.1). That is why it would be impossible to see the borders of the cardiac chambers facing the diaphragm or the mediastinum using plain films unless surrounded by air. Showing these borders requires imaging with CT or MRI.

In general, chest X-rays are obtained in frontal and lateral positions. Most X-rays especially in outpatient setting are obtained in posteroanterior (PA) direction while the patient is in upright position while the X-ray cassette placed in front of patients. Chest radiographs especially in bedridden patients are obtained in anteroposterior (AP) direction with the film placed behind the patient and the X-ray tube is positioned anteriorly. On AP films the heart is generally magnified and appears larger. Magnification is also higher in a portable X-ray compared with an upright film. Chest films are generally obtained at deep inspiration. The heart appears larger and more horizontal in expiratory films due to elevation of the diaphragm. Positional and respiratory variations in heart size also are seen in CT scan images but to a lesser degree.

In order to recognize the cardiomediastinal pathologies in plain films, it would be essential to be familiar with radiographic borders of the heart in different projections (▶ Fig. 12.1**a**). On frontal projections (AP or PA views), the right cardiac border is formed by the right atrium (RA) while the left cardiac border is formed by the left ventricle (LV) (▶ Fig. 12.2**a**). The right ventricle (RV) and the left atrium (LA) are not border forming with lungs in PA views and additional projections are required to demonstrate them. The diaphragmatic surface of the heart is formed by the RV. On the lateral projection, the anterior cardiac border is the RV while the posterior cardiac border is composed of both the LV and the LA (▶ Fig. 12.2**b**).

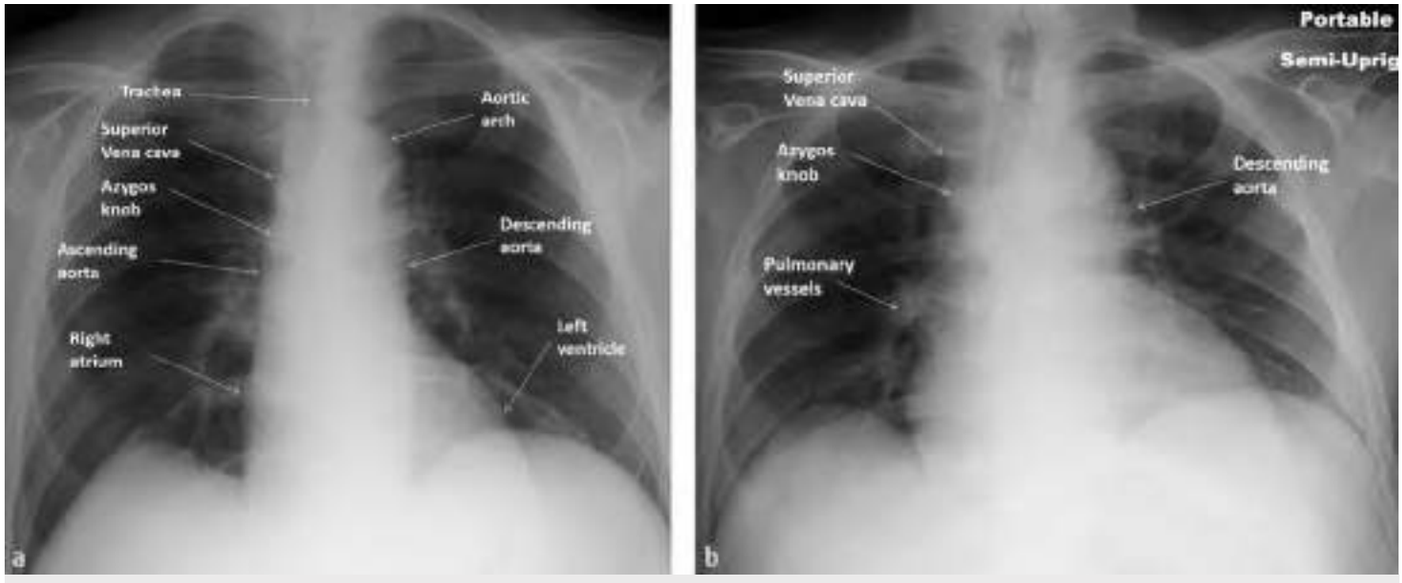

Fig. 12.1 **(a)** Upright inspiratory versus **(b)** sitting chest X-rays. In the sitting and expiratory conditions, the heart and mediastinum appear wider and the lungs are shorter and appear slightly congested. The azygos also appears larger due to increased venous return to the superior vena cava.

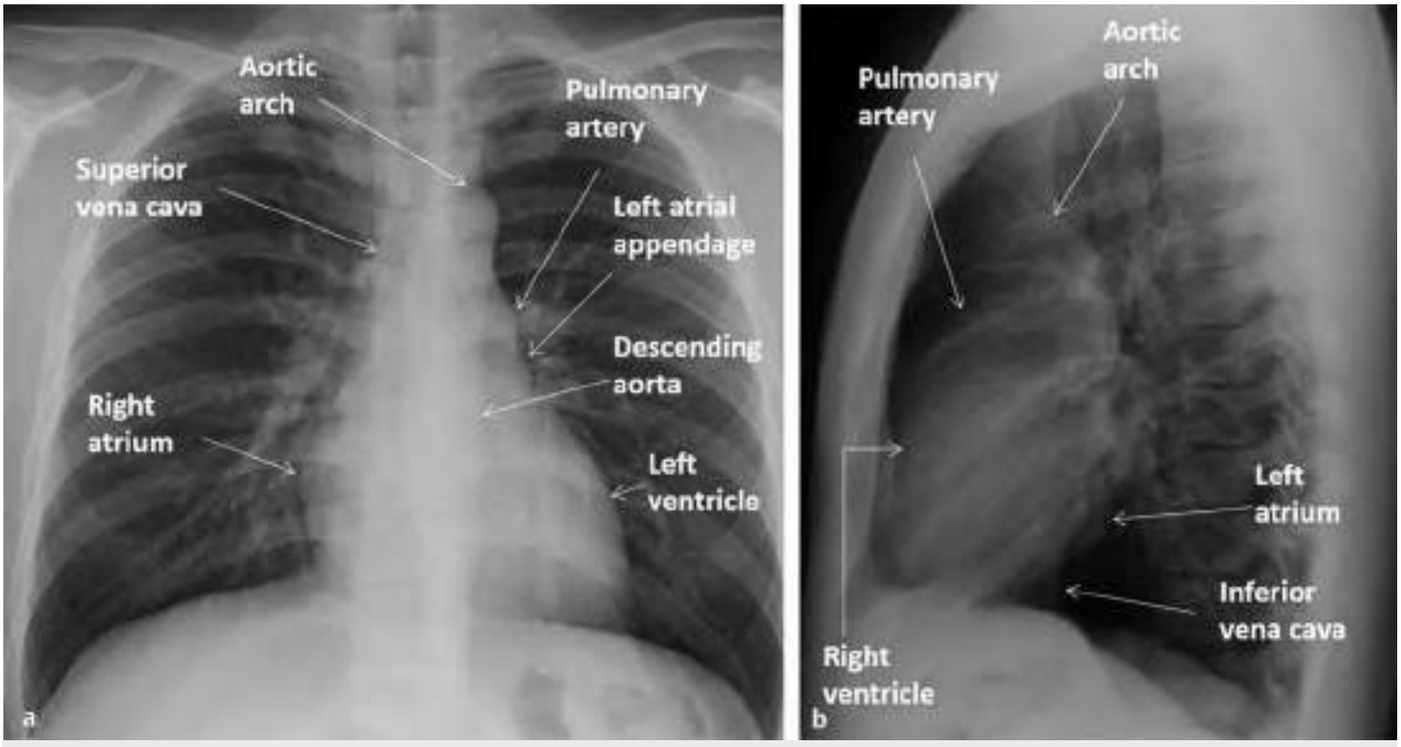

Fig. 12.2 **(a)** Posteroanterior and **(b)** left lateral chest X-ray in standing inspiratory status.

◆ Anatomical Position of the Cardiac Structures

Detail evaluation of the cardiac anatomy and localizing specific structures within the heart require cross-sectional imaging. From these cross-sectional views three-dimensional (3D) (volume-rendered) projections of the heart can be reconstructed. Using CT, MR, or echocardiography cross-sectional images can be obtained or reconstructed in any directions (▶ Fig. 12.3, ▶ Fig. 12.4, ▶ Fig. 12.5, ▶ Fig. 12.6). However, radiologists and cardiologists use certain standard planes in order to define a specific anatomy or pathology of interest. The terminologies used for these views are in reference to the body (chest) and the heart.

Standard planes in reference to the chest (body planes) include three orthogonal cuts in axial (transverse), coronal, and sagittal orientations (▶ Fig. 12.7). Additional body projections commonly used in CT and catheter angiography studies of the heart and coronary arteries include right anterior and left anterior oblique projections in various angles with different caudal or cranial angulations (▶ Fig. 12.8). Heart planes including short axis, horizontal long axis, and vertical long axis also involve three orthogonal planes but in reference to the heart itself[1,2] (▶ Fig. 12.9). Short-axis images, which correspond to a plane parallel to the atrioventricular (AV) groove, are transverse cuts of the heart. Horizontal long-axis (four-chamber) views are double oblique planes of the heart perpendicular to both the interventricular septum and AV planes. Vertical long-axis (two-chamber) views of the heart are parallel to the interventricular septum plane and perpendicular to the AV plane (▶ Fig. 12.9). Taking above concepts into consideration, the location of many of the anatomical structures or a specific pathology of the heart can be addressed using either the heart or the body as the reference. This has caused confusion and discrepancy in the anatomy or radiology nomenclature to localize some anatomical sites. For example, the two papillary muscles of the LV are located superiorly and inferiorly in reference to the body (chest) but positioned anteriorly and posteriorly in reference to the heart (▶ Fig. 12.10).

◆ Anatomical Surfaces and Angles of the Heart

The heart is located in the middle mediastinum. It is surrounded by the epicardial fat and the pericardial sac. The epicardial fat is continuous with the mediastinal fat along the major vessels at the superior aspect of the heart. Superiorly, the heart is connected to the aorta, pulmonary artery, and superior vena cava (SVC). Inferiorly, it is connected to the inferior vena cava (IVC) (▶ Fig. 12.3).

The sternum and costal cartilages are located anterior to the heart and provides rigid protection to the heart during blunt trauma. The heart has an extensive diaphragmatic surface inferiorly (▶ Fig. 12.3). Posteriorly, the heart lies on the esophagus and tracheal bifurcation, and main stem bronchi of the lungs.

The true posterior surface of the heart is commonly referred as the base of the heart which is formed largely by the LA. The term “base of the heart” is not frequently used and should be restricted to the “origin of the great vessels.” The inferior surface of the heart is closely related to the diaphragm and may be called diaphragmatic (▶ Fig. 12.3, ▶ Fig. 12.6). In supine position, along with elevation of the diaphragm, the heart lies horizontally and its lower surface largely faces the diaphragm (▶ Fig. 12.3). However, in upright position, with full inspiration, the heart stands vertically and less walls face inferiorly.[1] Because of differences in morphology of the RV and LV, the diaphragmatic surface of the

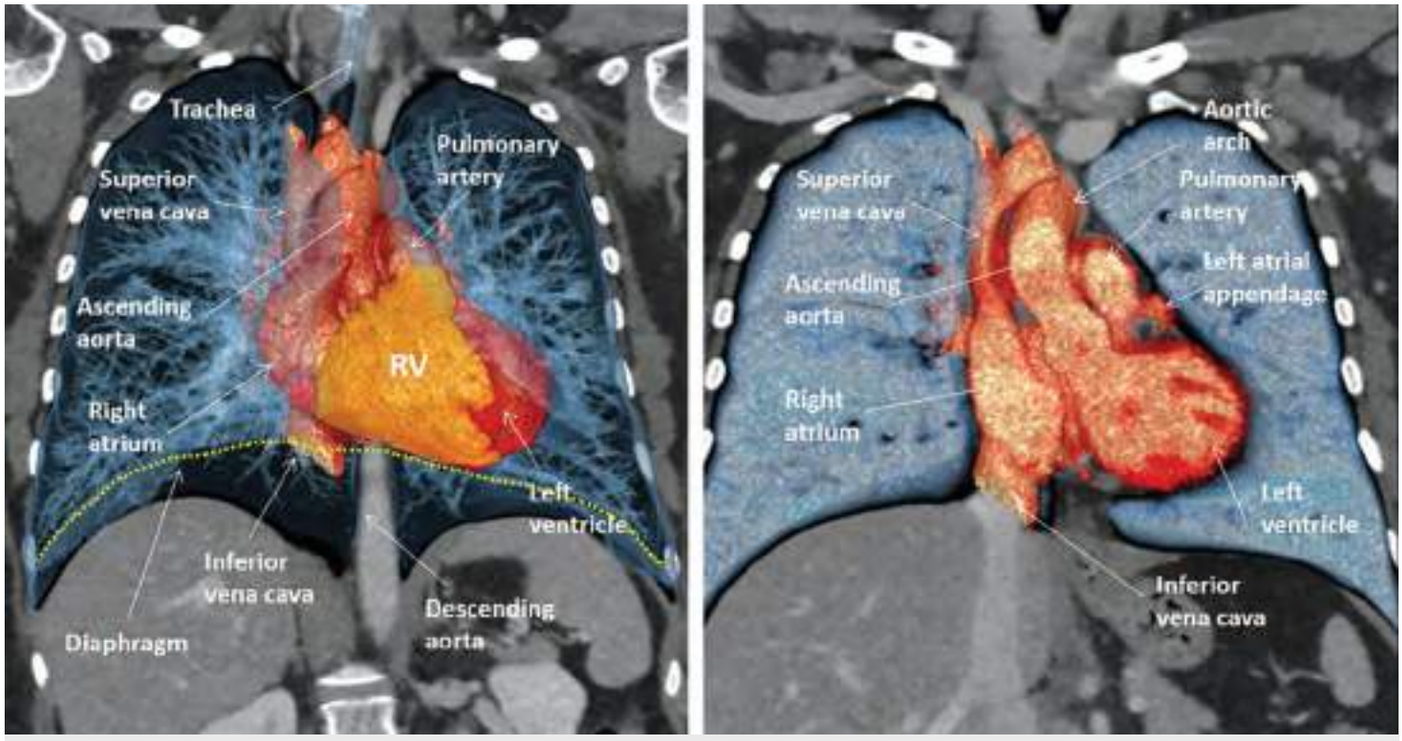

Fig. 12.3 Frontal views of color-coded CT scans of the chest showing cardiac margins. In this example, the ascending aorta does not extend to the lung margin and is not visible on plain X-ray. Instead the superior vena cava and the right atrium are major right heart border-forming structures. On the left side, the aortic arch, main pulmonary artery, left atrial appendage, and left ventricle are border forming. Note in this view, the right ventricle (RV, *in yellow*) is only forming a border with the diaphragm along its inferior margin.

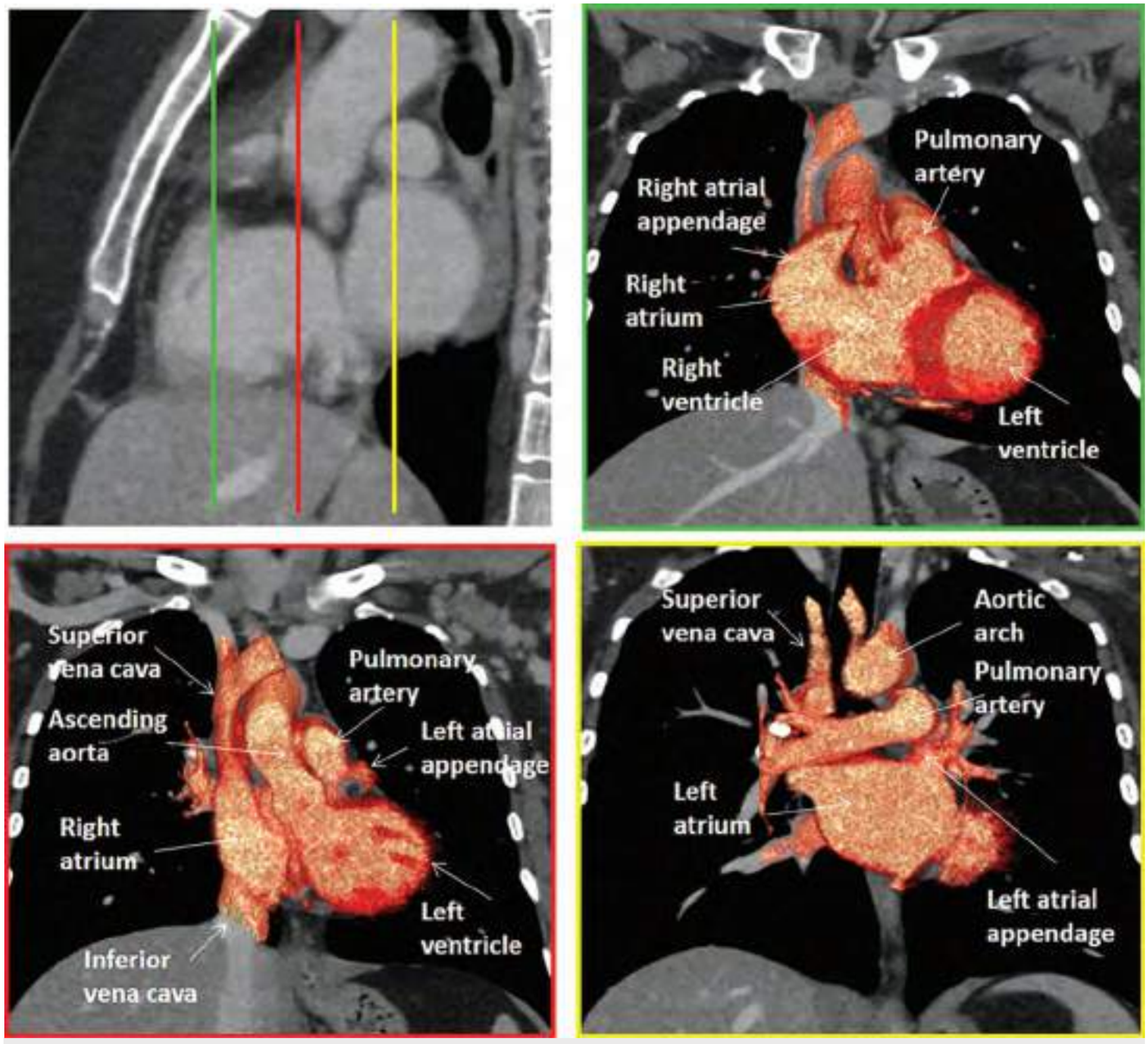

Fig. 12.4 Heart margins in frontal projections. Cross-section at three levels.

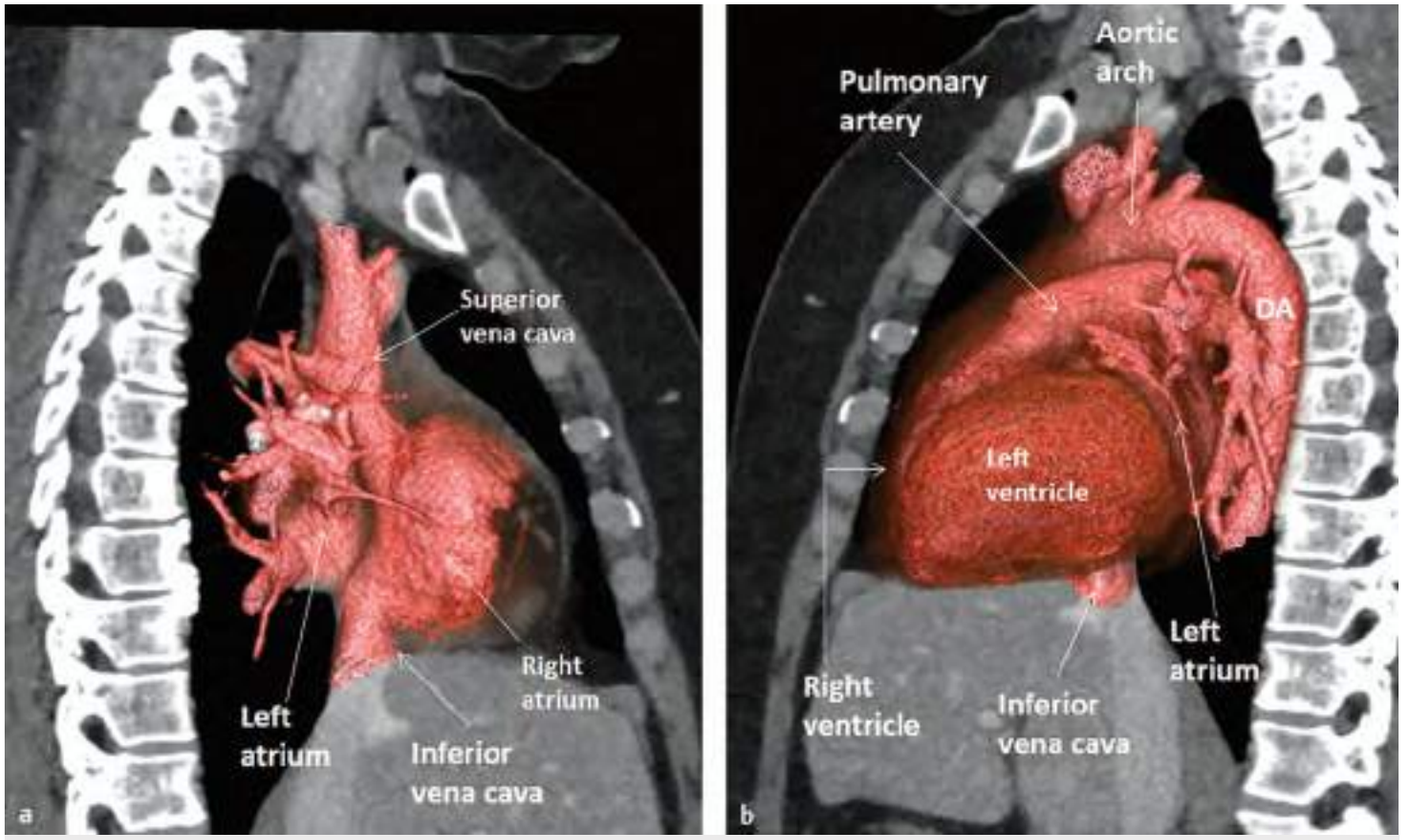

Fig. 12.5 Heart margins in lateral projections. **(a)** Right lateral view and **(b)** left lateral view. DA, descending aorta.

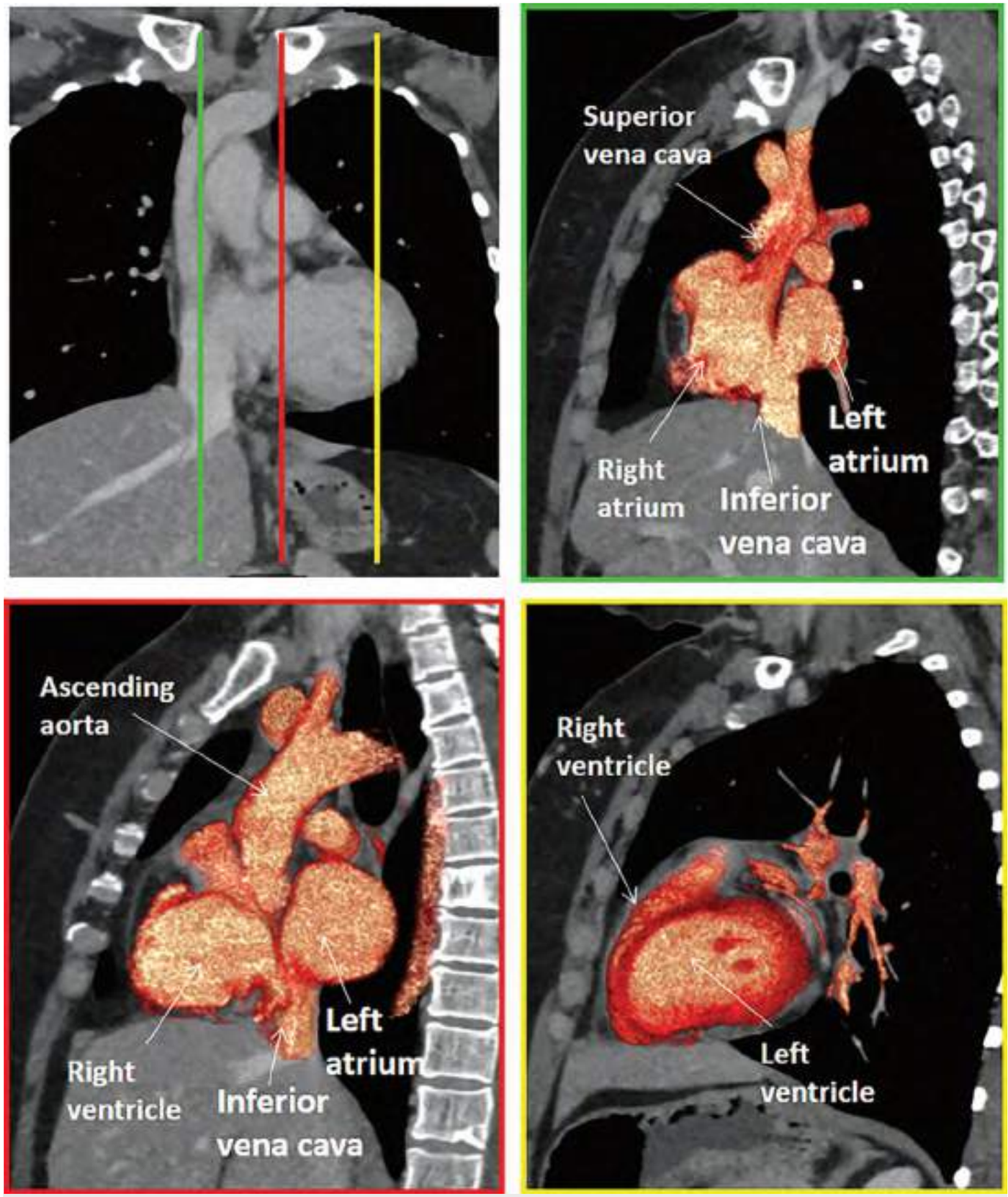

Fig. 12.6 Heart margins in lateral projections. Cross-sections at three levels. The true posterior surface of the heart is commonly referred as the base of the heart which is formed largely by the left atrium. The inferior surface of the heart is closely related to the diaphragm and may be called diaphragmatic.

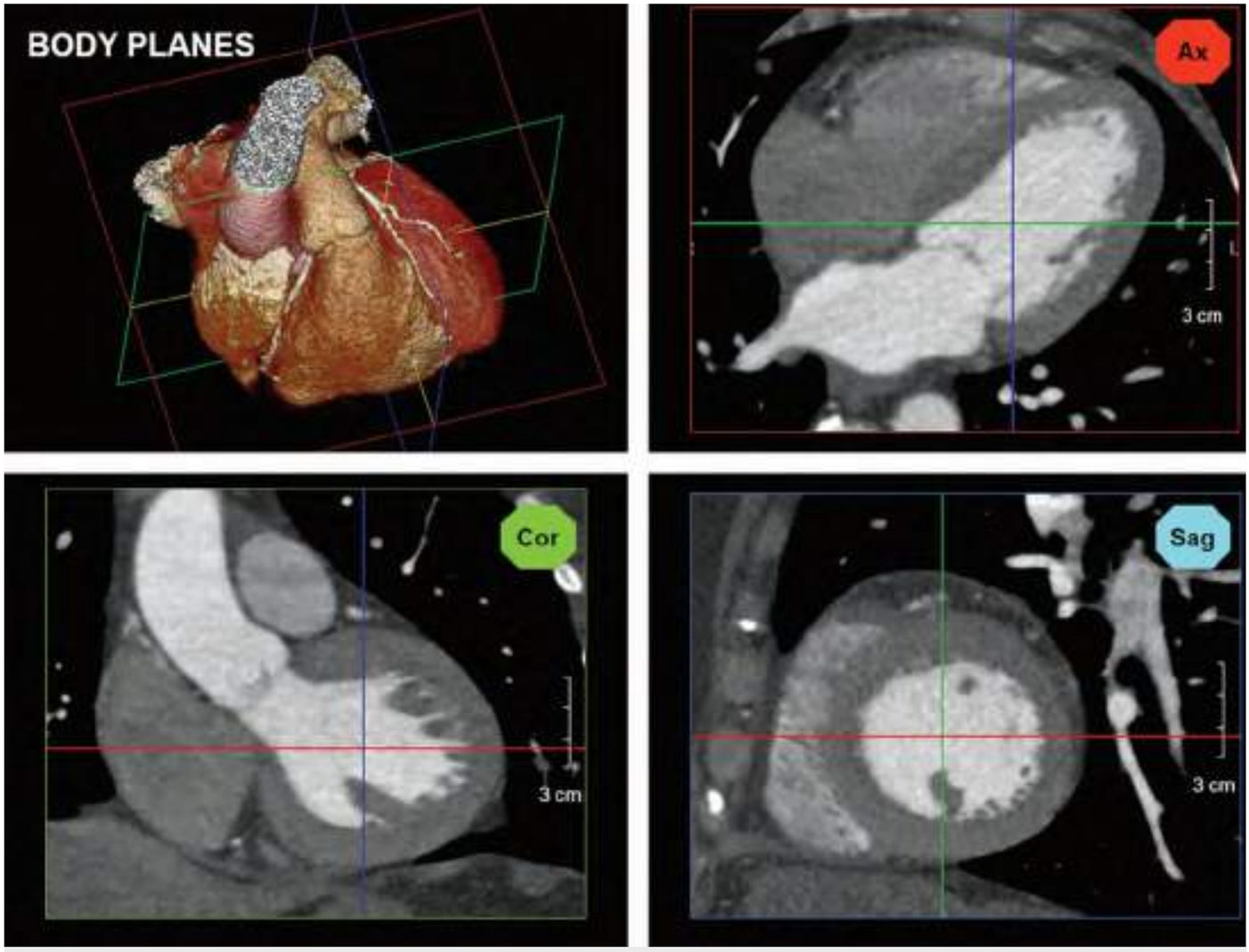

Fig. 12.7 Standard body planes. The heart may be viewed in three standard anatomical planes: transaxial (Ax), coronal (Cor), and sagittal (Sag). Although these planes are perpendicular to one another, the body planes transect the heart obliquely, while the heart planes transect the body almost perpendicularly (▶ Fig. 12.9).

Fig. 12.8 **(a–d)** Common projections of the heart. Images showing the relationship of the heart to the thoracic cage. Angiographic views show the relation of the coronary arteries to the cardiac chambers in different projections. RAO, right anterior oblique; LAO, left anterior oblique.

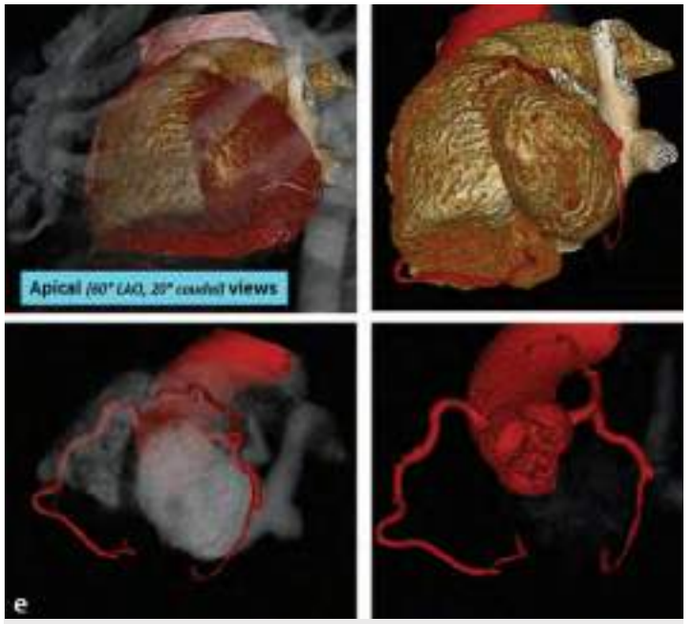

Fig. 12.8 (e)

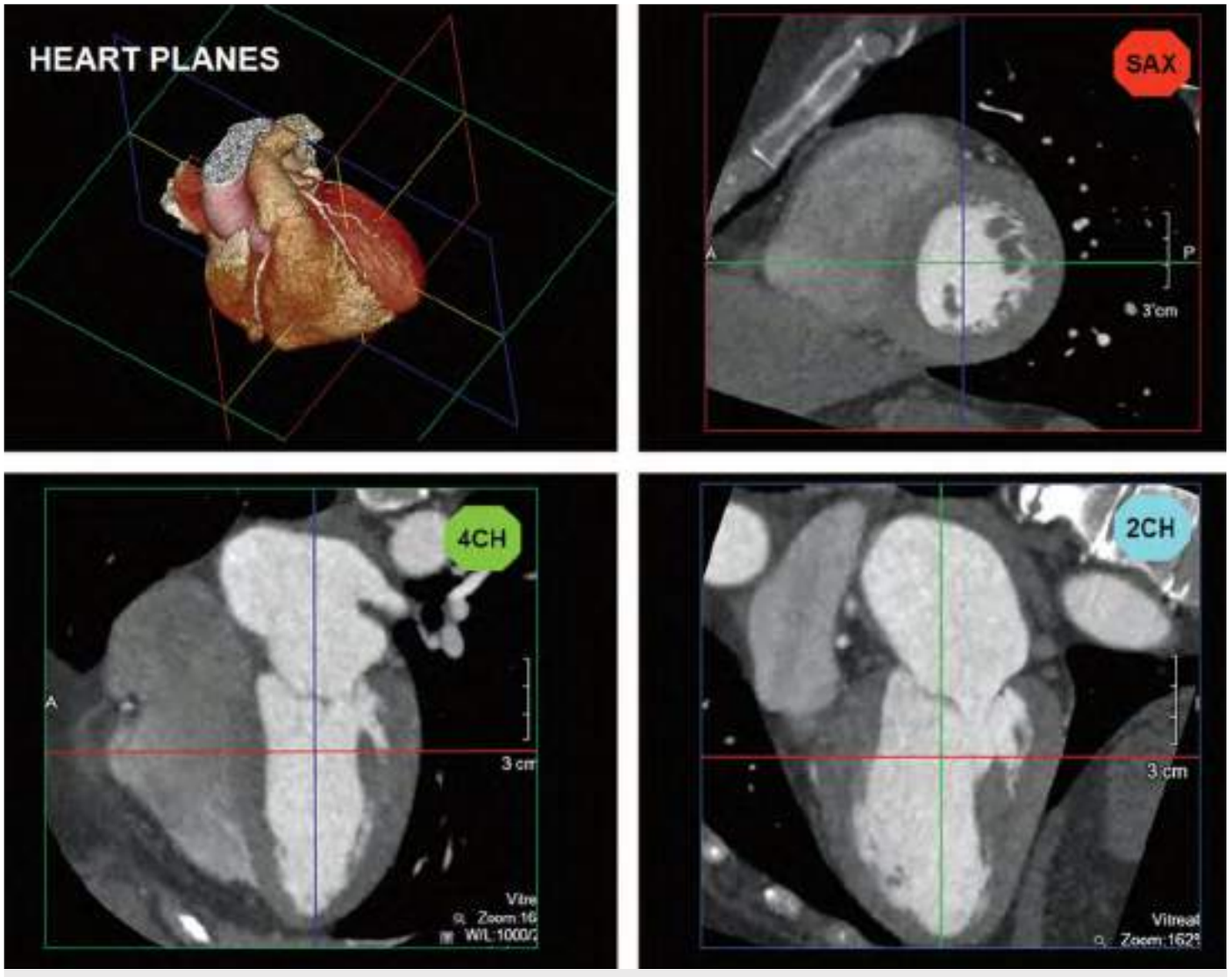

Fig. 12.9 Heart planes. The three major planes of the heart include short axis (SAX), horizontal long axis (4CH, four chamber), and vertical long axis (2CH, two chamber). These planes are approximately perpendicular to one another. The short-axis planes are transaxial planes of the heart and 2CH views are roughly sagittal plane of the heart.

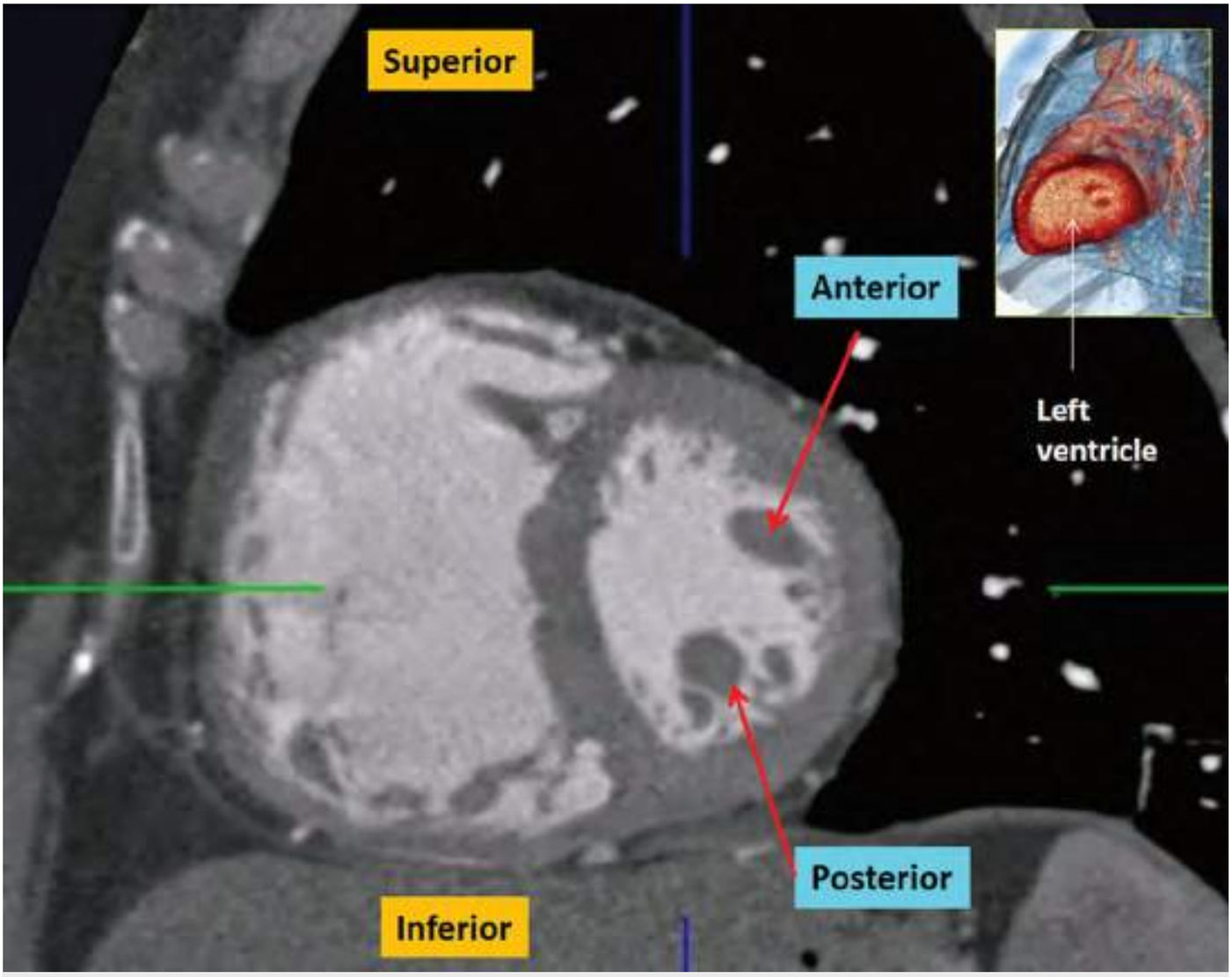

Fig. 12.10 Sagittal CT of the mid-left ventricle. The two papillary muscles of the left ventricle (also shown in the volume rendered in lay image) are located superiorly and inferiorly in reference to the body (attitudinal orientation) but positioned anteriorly and posteriorly in reference to the heart.

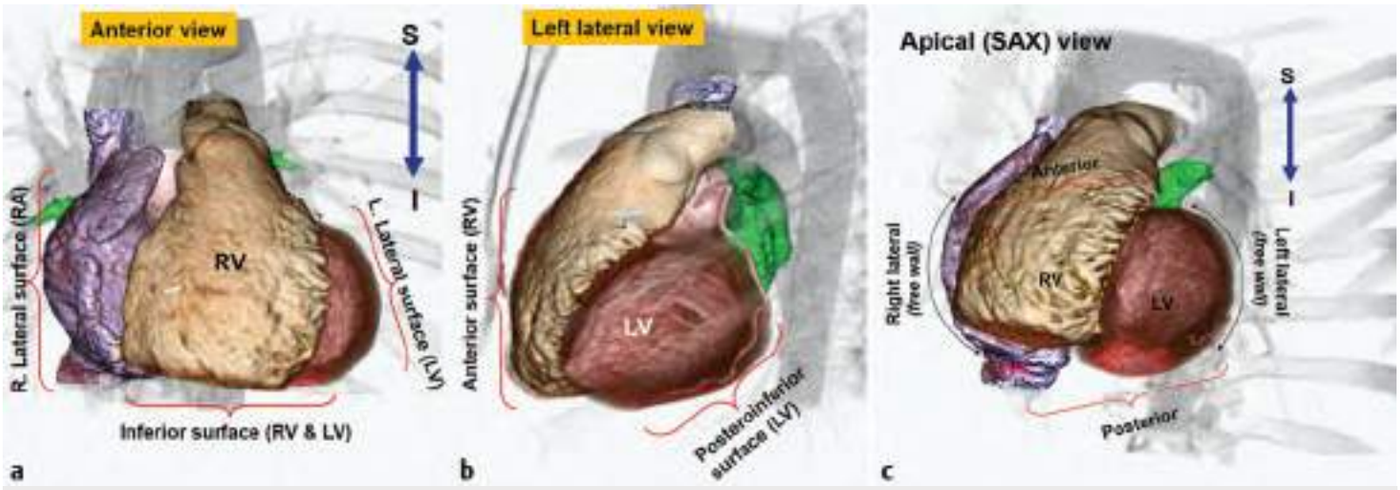

Fig. 12.11 (**a, b**) Ventricular surfaces are shown is relation to the thorax (body) and the heart itself. **(c)** Ventricular surfaces are shown is relation to the heart itself. Dotted yellow line, interventricular groove; L, left; LV, left ventricle; R, right; IVC, inferior vena cava; RV, right ventricle; S, superior; I, inferior.

RV is truly facing inferiorly but the diaphragmatic wall of the LV faces posteroinferiorly (▶ Fig. 12.6, ▶ Fig. 12.11).

The ventricular part of the heart looks like a three-sided pyramid. When viewed from its apex, the three sides of the ventricular mass are readily seen (▶ Fig. 12.12). Two prominent edges are distinguished. The acute margin lies inferiorly and parallel to the diaphragm. It corresponds to a sharp angle between the sternocostal and diaphragmatic surfaces of the RV. The obtuse margin runs posteriorly and superiorly along the lateral (posterior) margin of the LV. It is more or less diffuse in its transition compared with the acute margin.

◆ Right Atrium

The RA is an important chamber with a complicated morphology. It is the chamber of the heart that receives systemic venous blood return from the SVC and IVC and coronary venous return from the coronary sinus.[2] The RA is home to important parts of the cardiac conduction system including, the sinoatrial (SA) node, the AV node, and internodal bundles.

The RA forms the right lower cardiomediastinal border on plain radiographs (▶ Fig. 12.12). Looking at 3D images of the heart from the superior aspect of the chest, the RA is facing anteriorly on the right side of midsagittal plane of the chest, whereas the LA is situated posteriorly and more or less in midline (▶ Fig. 12.13).

The RA has the shape of a rotated box. The longest diameter of the RA box is in superior inferior direction. The SVC connects to the posterior margin of the superior wall of the RA near the interatrial septum. The IVC connects to the posterior margin of the inferior wall of the RA (▶ Fig. 12.14). The superior and inferior connections of the cava are best seen on the lateral CT images of the chest (▶ Fig. 12.13). On axial images, the RA box is rotated along the Z-axis of the body. Therefore, the lateral wall is facing laterally and posteriorly whereas the medial wall facing medially and anteriorly. As a result, the anterolateral corner of the RA, formed by the junction of the anterior and lateral walls, is the major border-forming structure on frontal plain X-rays (▶ Fig. 12.13, ▶ Fig. 12.14). This corner is specifically formed by the right atrial appendage. The tricuspid valve forms the inferior to midpart of the medial wall of the RA and faces medioanteriorly toward the RV (▶ Fig. 12.13, ▶ Fig. 12.15). The plane of the tricuspid is mildly on the right of midsagittal plane. The superior part of the medial RA wall is located next to the aortic root and the inferior part of the medial wall connects to the coronary sinus and forms the right atrial wall of the inferior pyramidal space. The interatrial septum forms part of the posterior wall of the RA (▶ Fig. 12.16, ▶ Fig. 12.17). In general, the anterior and lateral walls are the free walls of the RA. Most surgical approaches to access the intracardiac structures are performed through the anterior and lateral walls.

The RA comprises of three components: the appendage, the venous part (sinus venarum), and the vestibule.[2] The atrial appendage is derived from the primary atrium. The right atrial appendage is the largest component forming the anterolateral aspect of the RA extending between the superior and inferior walls (▶ Fig. 12.15). Its inner surface appears trabeculated formed by multiple pectinate muscles. The venous part of RA is derived from the sinus venosus and is located posterolaterally and connects to the SVC, the IVC, and the coronary sinus (▶ Fig. 12.14, ▶ Fig. 12.15). From the third week after the development of the primitive heart tube, the primary atria are separated from the sinus venosus by a segmentation termed the sinoatrial ring. The sinus venosus has two horns. The right horn gives rise to all the intercaval regions of the RA (sinus venarum) including the crista terminalis, the Eustachian ridge, and the Thebesian valve (▶ Fig. 12.6). The left horn gives rise to the coronary sinus.

The atrial vestibule of the RA is derived from the embryonic AV canal. It is a smooth muscular rim surrounding the tricuspid orifice[1] (▶ Fig. 12.18). The pectinate muscles do not reach this area (▶ Fig. 12.19). The right coronary artery (RCA) runs in the epicardial fat next to the vestibule.

One of the important morphological structures of the RA is the crista terminalis. This C-shaped muscular ridge separates the

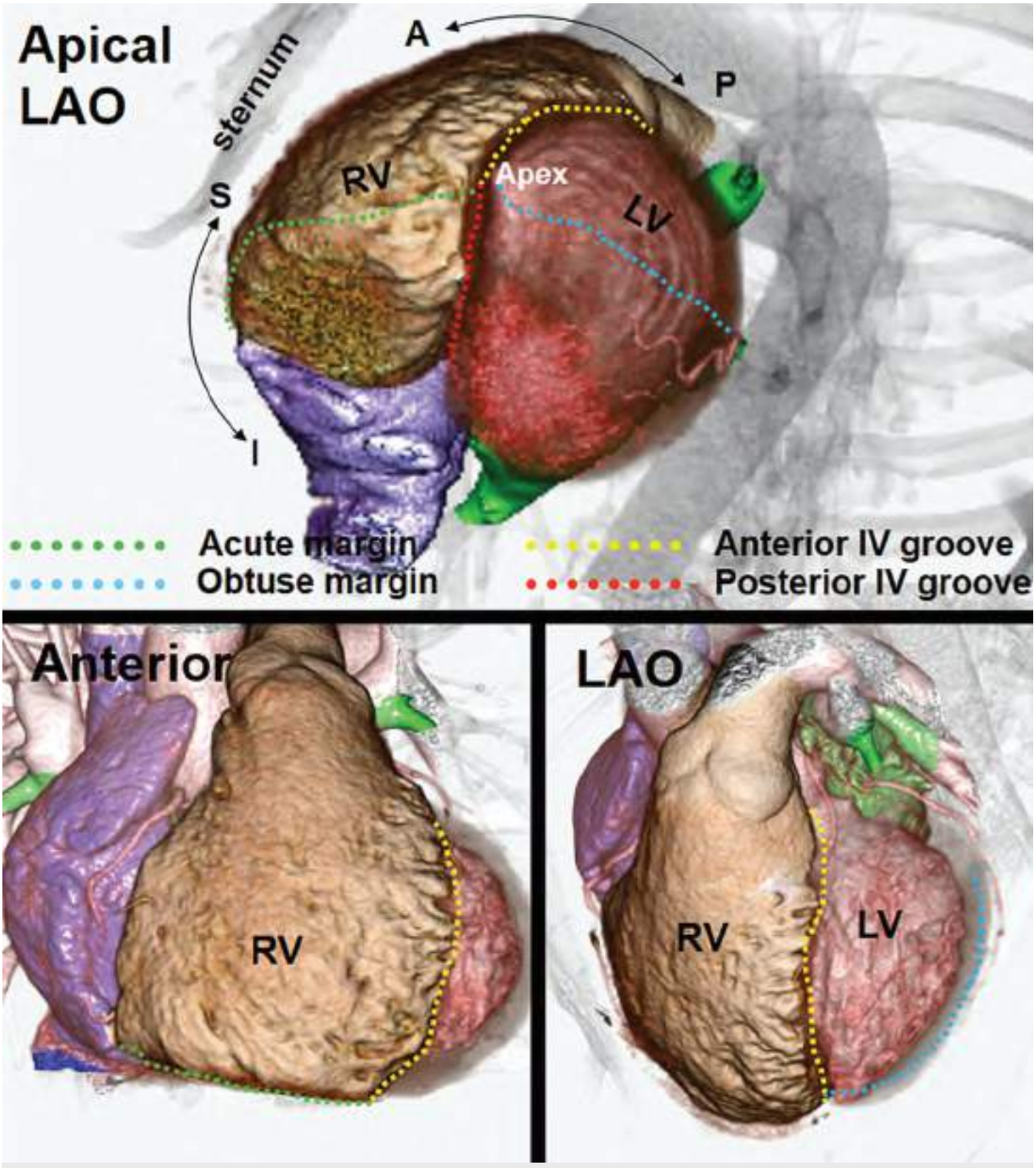

Fig. 12.12 The margins of the heart. The acute margin is applied to the right ventricle (RV) only between the sternocostal (A, anterior) and diaphragmatic (I, inferior) surfaces. In an anterior view, the acute margin forms the lower border and the right atrium forms the right lateral border of the heart. The term "obtuse margin" denotes the posterolateral aspect of the left ventricle (LV) and atrium. It is defined as the junction between the lateral (L) and posterior walls (P) of the LV. In left anterior oblique (LAO) view it forms the left border of the heart. Obtuse margin is a critical anatomical landmark and, in many instances, an artery (obtuse marginal, a branch of the left circumflex artery) runs along it. S, superior.

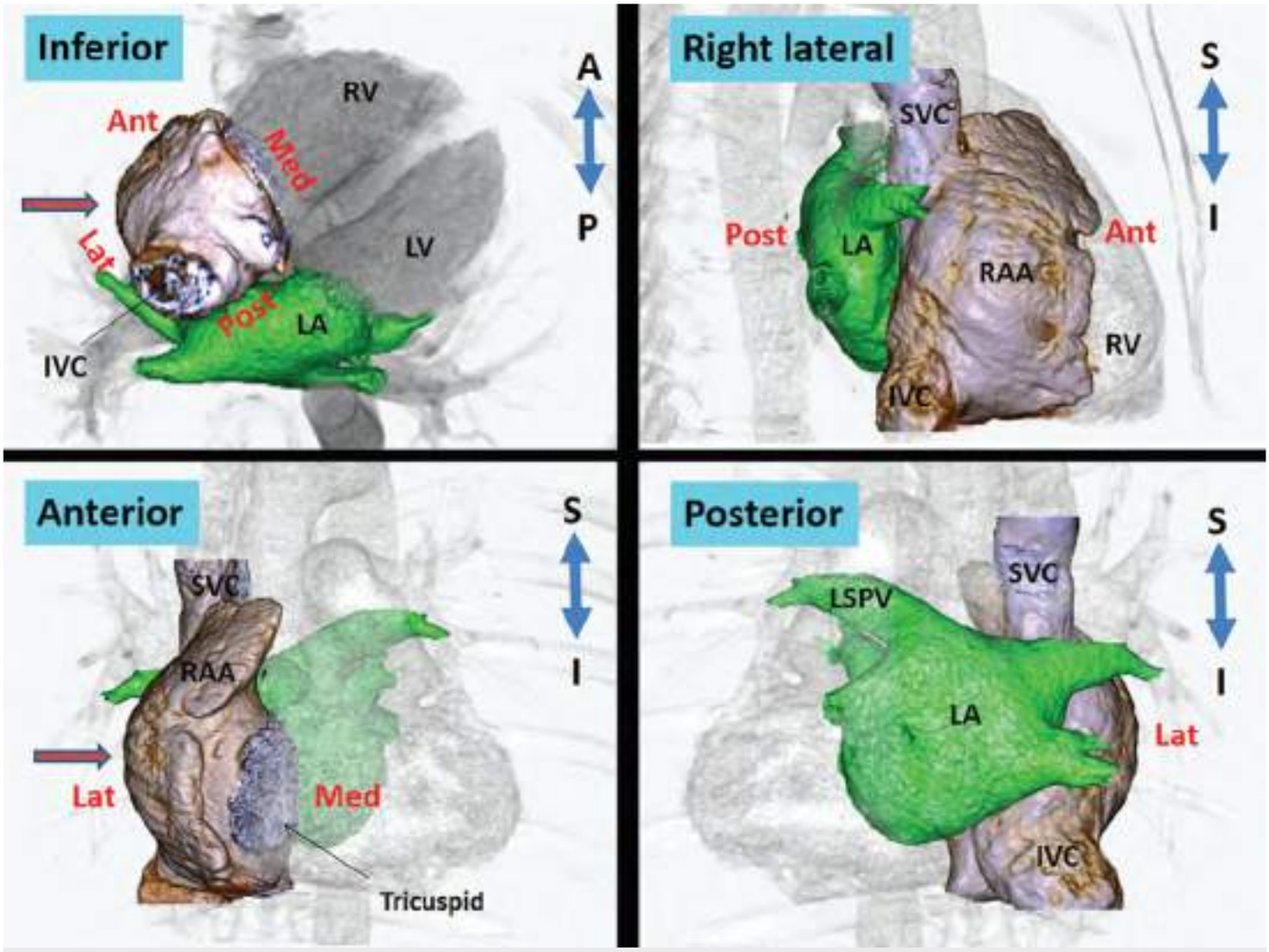

Fig. 12.13 Anatomical lie of the right and left atria in the chest. The right atrium (RA) is facing anteriorly on the right side of midsagittal plane of the chest, whereas the left atrium (LA) is situated posteriorly and more or less in midline. The anterolateral (Ant) corner of the RA, formed by the junction of the anterior and lateral walls, is the major border-forming structure on frontal plain X-rays (*arrows*). The tricuspid valve forms the inferior to mid part of the medial wall of the RA and faces medioanteriorly (Med) toward the right ventricle (RV). The anterior and lateral walls are the free walls of the RA. The left atrium (LA) is divided into five poorly demarcated walls: anterior (anterosuperior), posterior (posteroinferior), superior, left lateral, and septal (anteroinferior). The highest portion of the LA is at the ostium of the left superior pulmonary vein (LSPV). A, anterior; I, inferior; P, posterior; S, superior; IVC, inferior vena cava; RAA, right atrial appendage; LV, left ventricle; SVC, superior vena cava.

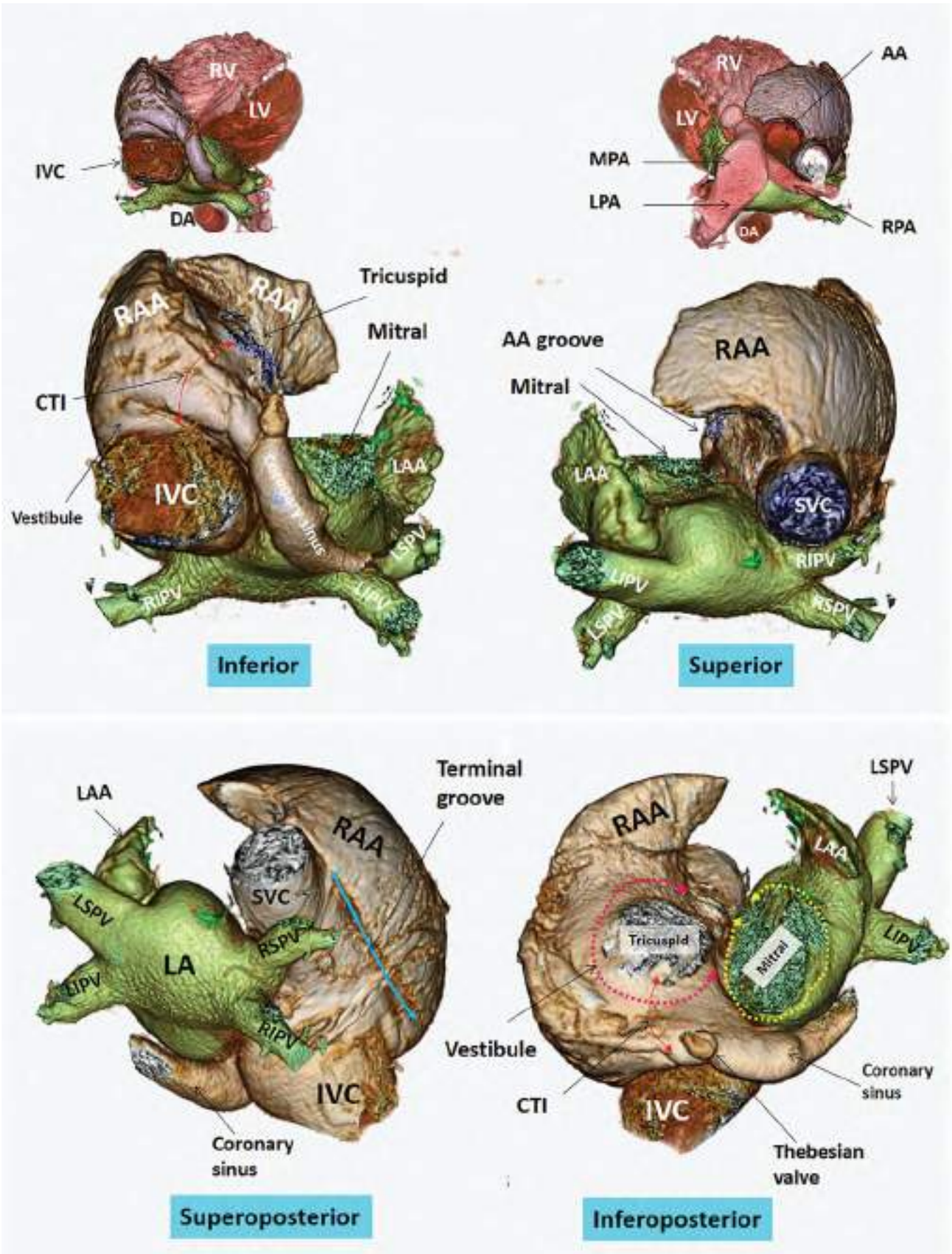

Fig. 12.14 Different views of the atria. The right atrium (RA) is enlarged. The superior part of the medial RA wall is located next to the aortic root and the inferior part of the medial wall connects to the coronary sinus and forms the right atrial wall of the inferior pyramidal space. AA, ascending aorta; CTI, cavotricuspid isthmus; DA, descending aorta; IVC, inferior vena cava; LAA, left atrial appendage; LIPV, left inferior pulmonary vein; LSPV, left superior pulmonary vein; LPA, left pulmonary artery; LV, left ventricle; MPA, main pulmonary artery; RPA, right pulmonary artery; RIPV, right inferior pulmonary vein; RSPV, right superior pulmonary vein; SVC, superior vena cava; RAA, right atrial appendage; RV, right ventricle.

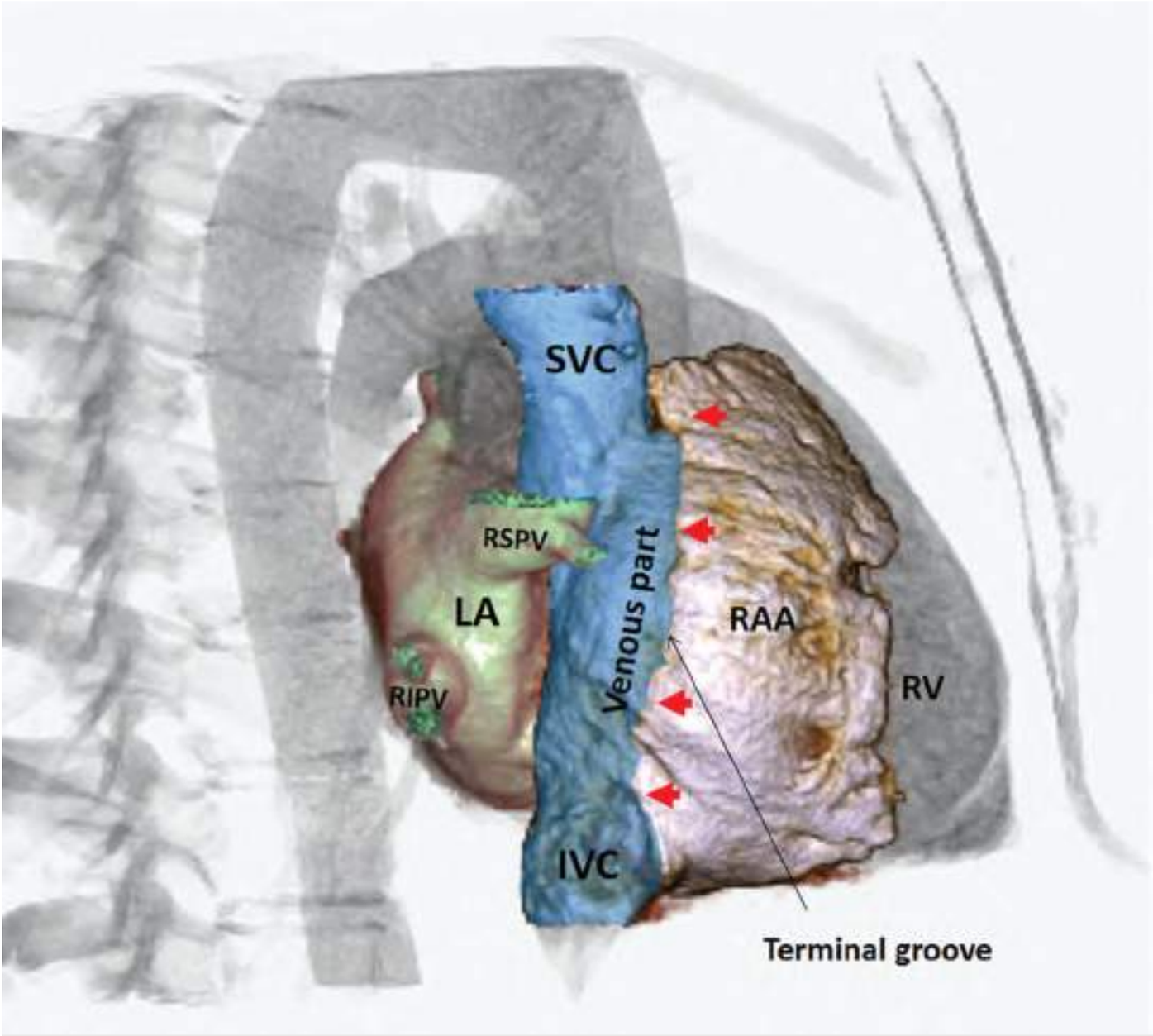

Fig. 12.15 Right lateral view of the heart showing structures of the right atrium. A large part of right atrium is occupied by the right atrial appendage (RAA). The terminal groove (*red arrow*) is a fat-filled sulcus on epicardial side of the RA which corresponds internally to the crista terminalis. IVC, inferior vena cava; LA, left atrium; SVC, superior vena cava; RIPV, right inferior pulmonary vein; RSPV, right superior pulmonary vein; RV, right ventricle.

smooth-walled venous part from the trabeculated appendage.[3] The crista terminalis extends between the superior and inferior walls (▶ Fig. 12.19). It starts anterior to the orifice of the SVC, passes rightward and inferiorly toward the RA vestibule. In front of IVC, the crista terminalis continues as an array of finer bundles that blends in an area of the inferior atrial wall known as the cavotricuspid isthmus. Terminal groove is a fat-filled sulcus on epicardial side of the RA which corresponds internally to crista terminalis (▶ Fig. 12.15). The sinus node and terminal segment of SA node artery are located in this groove, close to the superior cavoatrial junction (see the sinoatrial node).

Superior Right Atrium Landmarks

The most important landmark of the roof of the RA is the superior cavoatrial junction and the structures around it (▶ Fig. 12.14). In this region, the crista terminalis originates anterior to the orifice of the SVC (▶ Fig. 12.19, ▶ Fig. 12.20). Laterally, the crista terminalis continues its normal anatomical course in the lateral RA wall. Medially, the crista terminalis blends with the interatrial muscular bundle commonly known as Bachmann's bundle (▶ Fig. 12.19).

In some CT images of the heart a large pectinate muscle trabeculation band is seen arising from the precaval portion of the

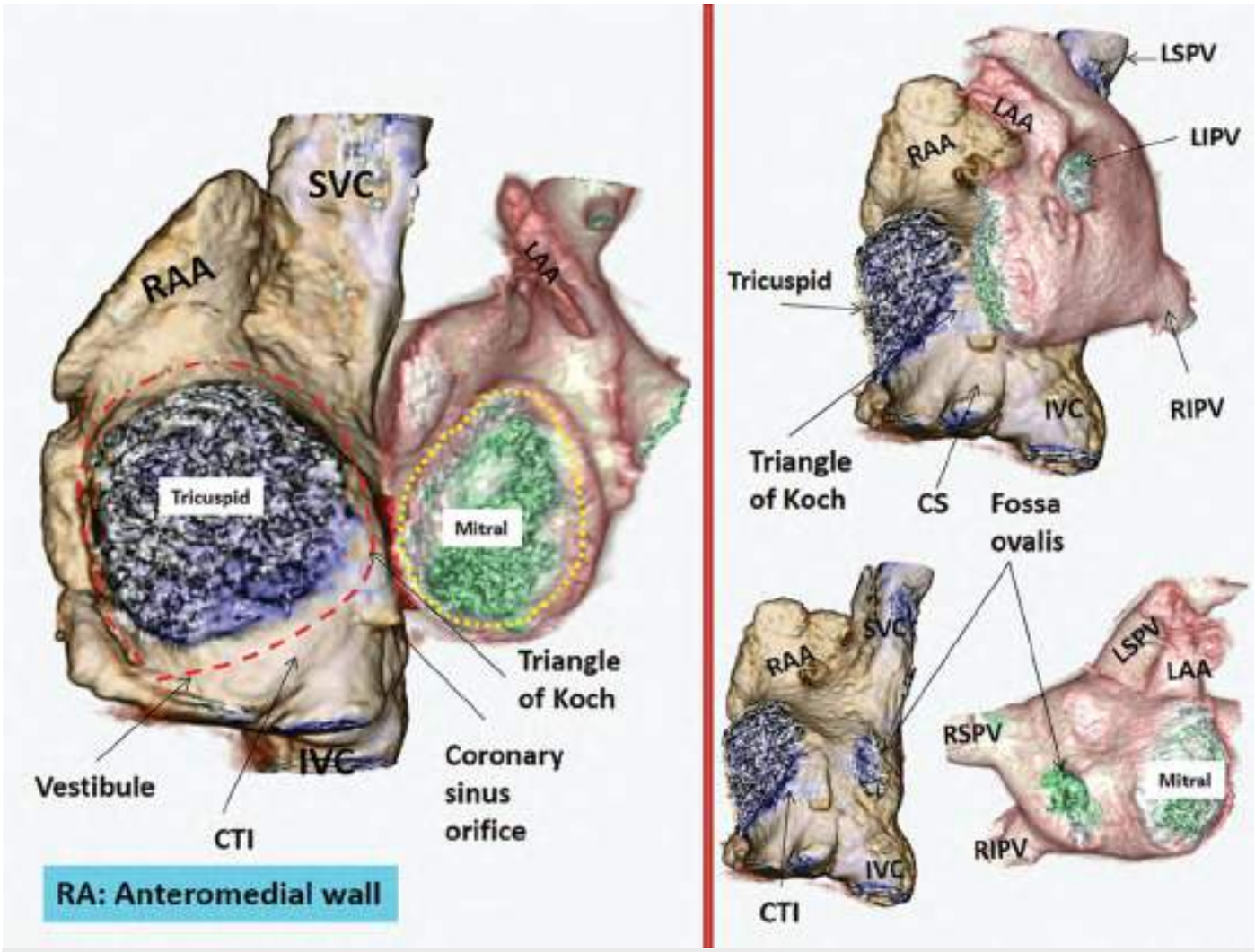

Fig. 12.16 Anteromedial wall of the right atrium (RA). Fossa ovalis and smooth-walled vestibules of the RA (*red circle*) and left atrium (LA, *yellow circle*) are shown. CTI, cavotricuspid isthmus; IVC, inferior vena cava; LAA, left atrial appendage; LIPV, left inferior pulmonary vein; LSPV, left superior pulmonary vein; RIPV, right inferior pulmonary vein; RSPV, right superior pulmonary vein; SVC, superior vena cava; RAA, right atrial appendage.

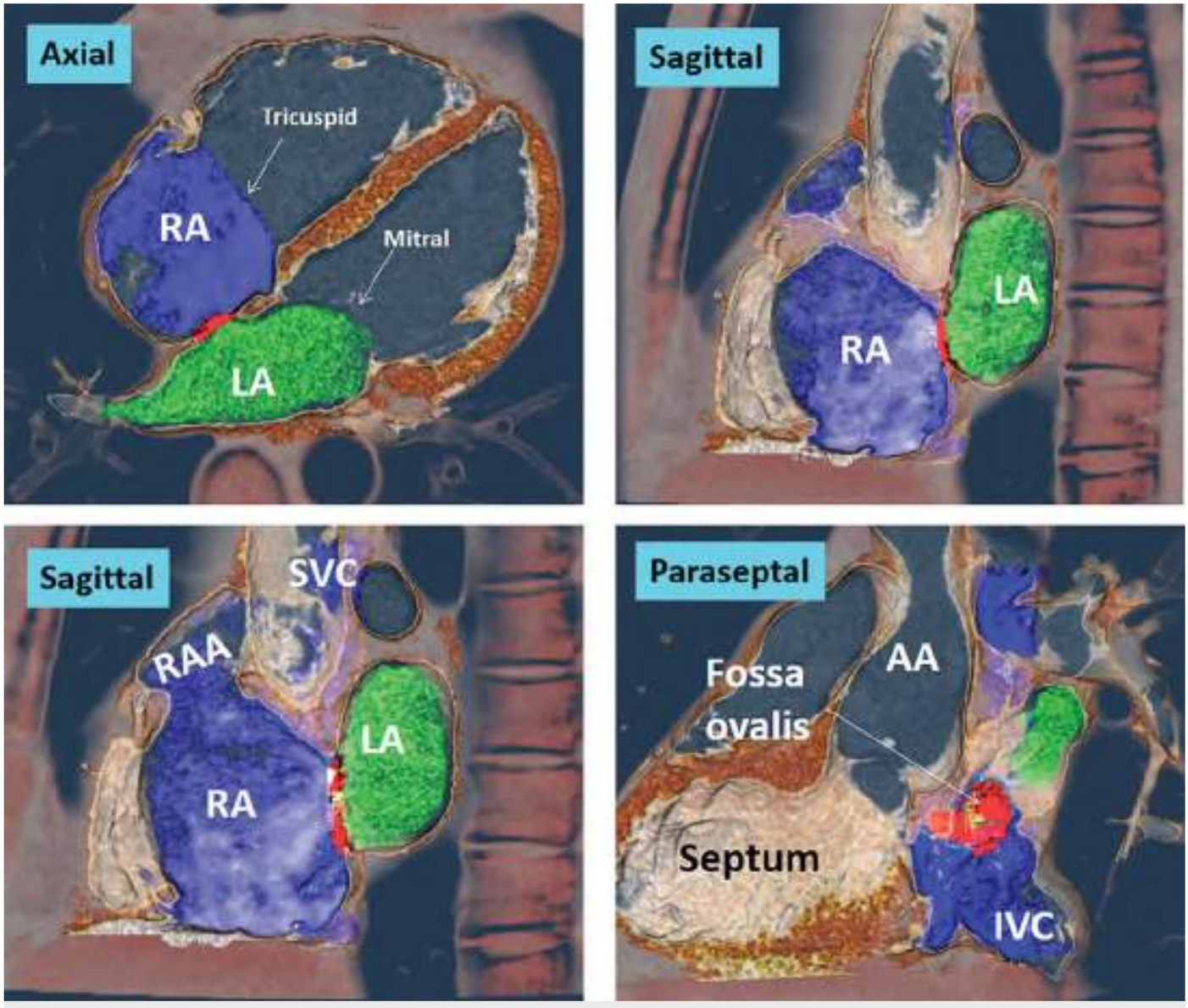

Fig. 12.17 Interatrial septum. The fossa ovalis (*colored in red*) forms the posteromedial wall of the RA and the anteroinferior wall of the LA. The fossa ovalis and the tricuspid valve are located on the right of midsagittal plane. The mitral valve is located anterolaterally at the inferior half of the LA and on the left of midsagittal plane. AA, ascending aorta; IVC, inferior vena cava; LA, left atrium; SVC, superior vena cava; RAA, right atrial appendage; RA, right atrium.

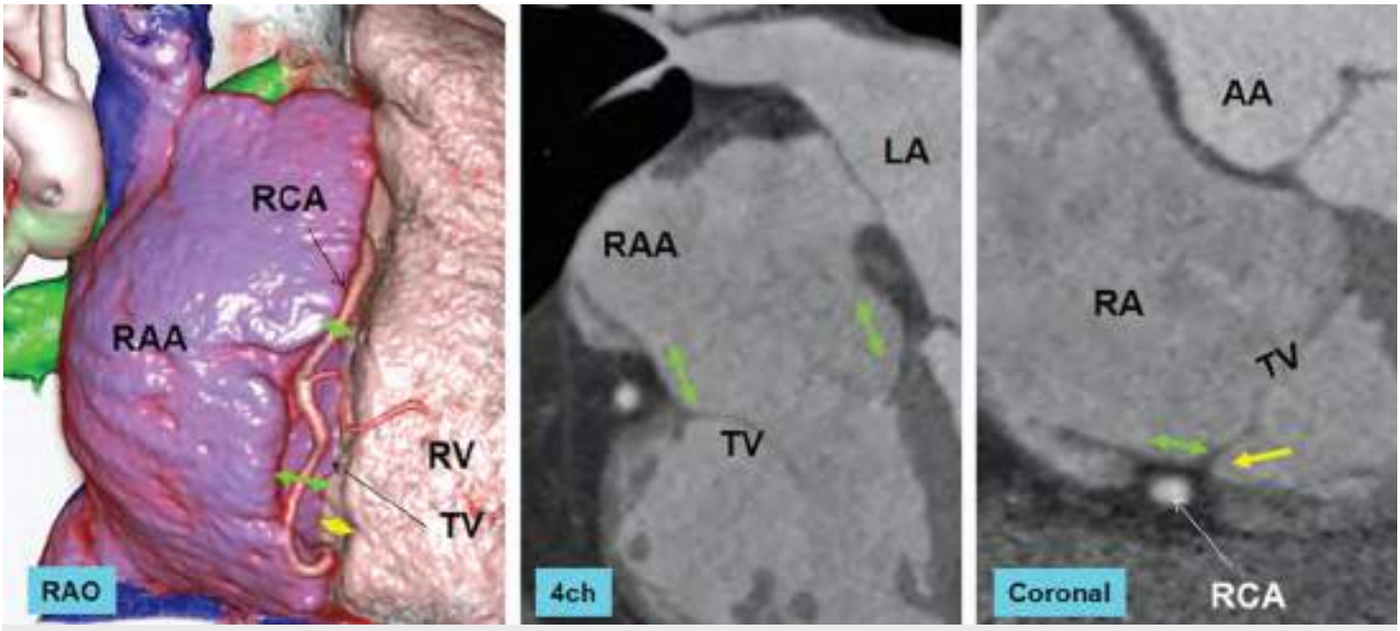

Fig. 12.18 RA vestibule. The vestibule is a smooth muscular rim surrounding the tricuspid orifice (*green arrows*). The pectinate muscles do not reach this area. The right coronary artery (RCA) runs in epicardial fat next to the vestibule. A thin fibrous membrane extends between the tricuspid annulus and the ostium of the right ventricle (RV), known as subvalvular membrane (*yellow arrows*). AA, ascending aorta; LA, left atrium; RAA, right atrial appendage; RA, right atrium; TV, tricuspid valve; RAO, right anterior oblique; 4ch, 4 chamber.

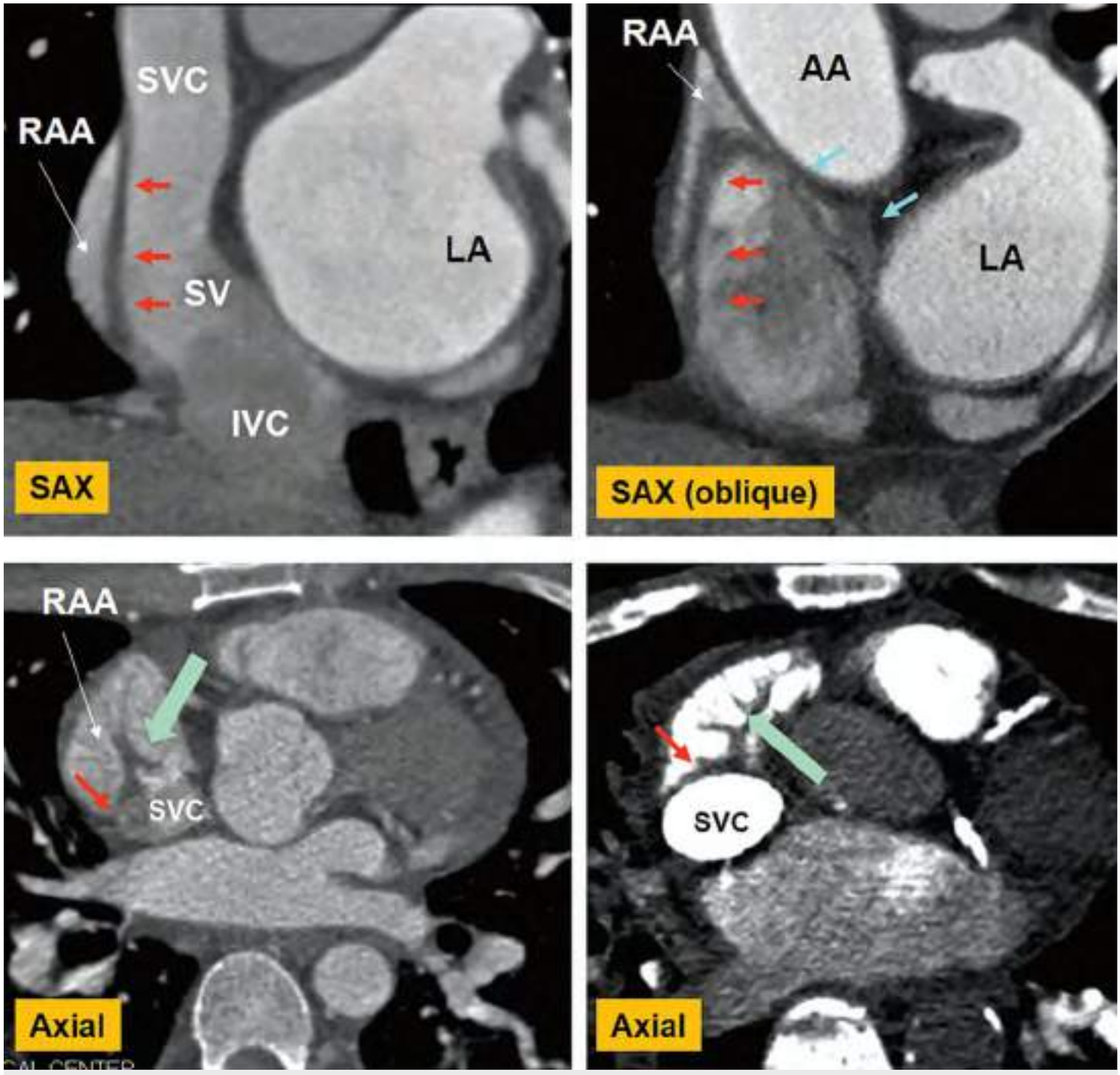

Fig. 12.19 In the upper row, short-axis (SAX) images in two different patients demonstrate the crista terminalis (*red arrows*) as a dark band between right atrial appendage (RAA) and sinus venarum (SV) extending from the superior vena cava (SVC) to the inferior vena cava (IVC). Superiorly, the crista terminalis arches anterior to the orifice of the SVC and extends to the area of the anterior interatrial groove and merges with the interatrial bundle. This part is commonly known as Bachmann's bundle (*blue arrows*). In the lower row, parasagittal band in two different cases. The parasagittal band is seen (*green arrows*) arising from the precaval portion of the crista terminalis (*red arrows*). This large anterior pectinate muscle is a remnant of the septum spurium and should not be mistaken with an intra-atrial thrombus. LA, left atrium; AA, ascending aorta.

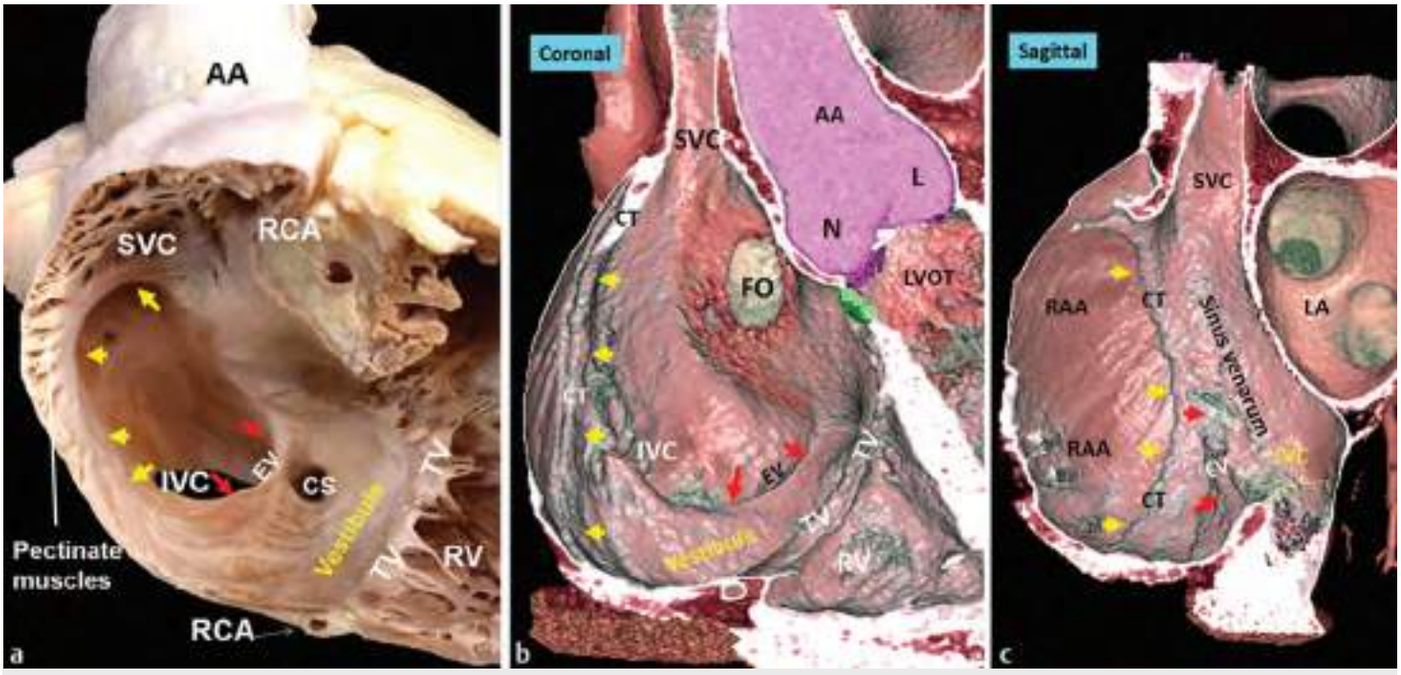

Fig. 12.20 Cadaveric dissection and endoscopy images showing inner views of the right atrium (RA). **(a)** Posterior wall inner view. **(b)** Coronal and **(c)** right lateral wall inner view. C-shaped crista terminalis (CT) is shown extending between the superior vena cava (SVC) and the vestibule of the RA (*yellow arrows*) separating the venous part (sinus venarum) from the right atrial appendage (RAA). Finally, it breaks up into a series of trabeculations around the atrial wall. The entire crista terminalis lies between the pectinate muscles and the sinus venarum. A prominent Eustachian valve/ridge (EV) is shown anterior the orifice of the inferior vena cava (IVC). AA, ascending aorta; CS, coronary sinus; FO, fossa ovalis; LA, left atrium; LVOT, left ventricular outflow tract; L, left coronary sinus; N, noncoronary sinus; RV, right ventricle; RCA, right coronary artery; TV, tricuspid valve.

crista terminalis. This parasagittal band is a remnant of the septum spurium and should not be mistaken with intra-atrial thrombus (▶ Fig. 12.20).

Another important landmark in the superior portion of the RA is the SA node. The SA node is a banana-shaped structure in the subepicardial side of superior cavoatrial junction within the crista terminalis[4] (▶ Fig. 12.21). The mean length of the SA node is reported 20 ± 3 mm[4] and its cross-sectional diameter is usually less than 5 mm.[5] It is the source of the cardiac impulse and composed of specialized cells slightly smaller than normal working cells. With age, the amount of connective and fatty tissue increases with respect to the area occupied by the nodal cells and the node becomes atrophic.[5,6] The SA node can be localized in axial CT images by locating the SA node artery passing along the crista terminalis (▶ Fig. 12.22). The SA node gradually penetrates musculature of the crest to rest in the subendocardium. Because of the vicinity of the SA node to the epicardial surface, it may be damaged in selected cardiac surgeries or extensive pericardial diseases.[7] Modification of the sinus node activity using radiofrequency ablation (RFA) has been established as a treatment for inappropriate sinus tachycardia.[8]

The SA node artery is usually, a single branch, arising from the proximal RCA (60%) or left circumflex (LCx) artery (40%)[7,9] (▶ Fig. 12.23). In an anatomical study of the conduction system arteries by CT scan, single SA node artery from the RCA was seen in 66% and from the LCx artery in 28% of studies.[10] A dual blood supply to SA node was seen in 6%: one from the RCA and the other from the LCx artery. Regardless of its artery of origin, the SA node artery usually courses along the superior interatrial groove toward the superior cavoatrial junction (▶ Fig. 12.23). At the cavoatrial junction, SA node artery course becomes variable and may circle either anteriorly (precaval) or posteriorly (retrocaval) to enter the node[10] (▶ Fig. 12.24).

Anterolateral Right Atrium Landmarks

The body of the crista terminalis is an important structure in the lateral RA wall that could be the source of several forms of atrial tachyarrhythmias.[11] The crista terminalis varies in size and extent in different individuals and should not be mistaken with intra-atrial pathology (▶ Fig. 12.25). Excess epicardial fat can infiltrate around the RA causing marked thickening of the crista terminalis which may mimic a mass (▶ Fig. 12.25, lower row). It may be associated with lipomatous hypertrophy of the interatrial septum.[12] Both conditions are due to excessive accumulation of fat in the epicardial space.[13]

Medially and superiorly, the crista terminalis connects to the interatrial Bachmann bundle (▶ Fig. 12.19). On the right, this broad band of circumferential interatrial myofibers can be traced to the junction of the RA and SVC (▶ Fig. 12.27). On the left, the bundle blends on the epicardial musculature of the LA toward the neck of the left atrial appendage (LAA) (▶ Fig. 12.27).[14,15] This interatrial band ensures rapid interatrial conduction, leading to physiological biatrial contraction. Changes in the musculature of Bachmann's bundle could block or prolong interatrial conduction resulting in abnormal atrial excitability, atrial dysfunction, atrial fibrillation (AF), and other arrhythmias.[16] The principal vascular supply of Bachmann's bundle is believed to stem from the SA node artery and its branches[17] (▶ Fig. 12.26). Anatomical variants of this region are common (▶ Fig. 12.27). An anatomical study of

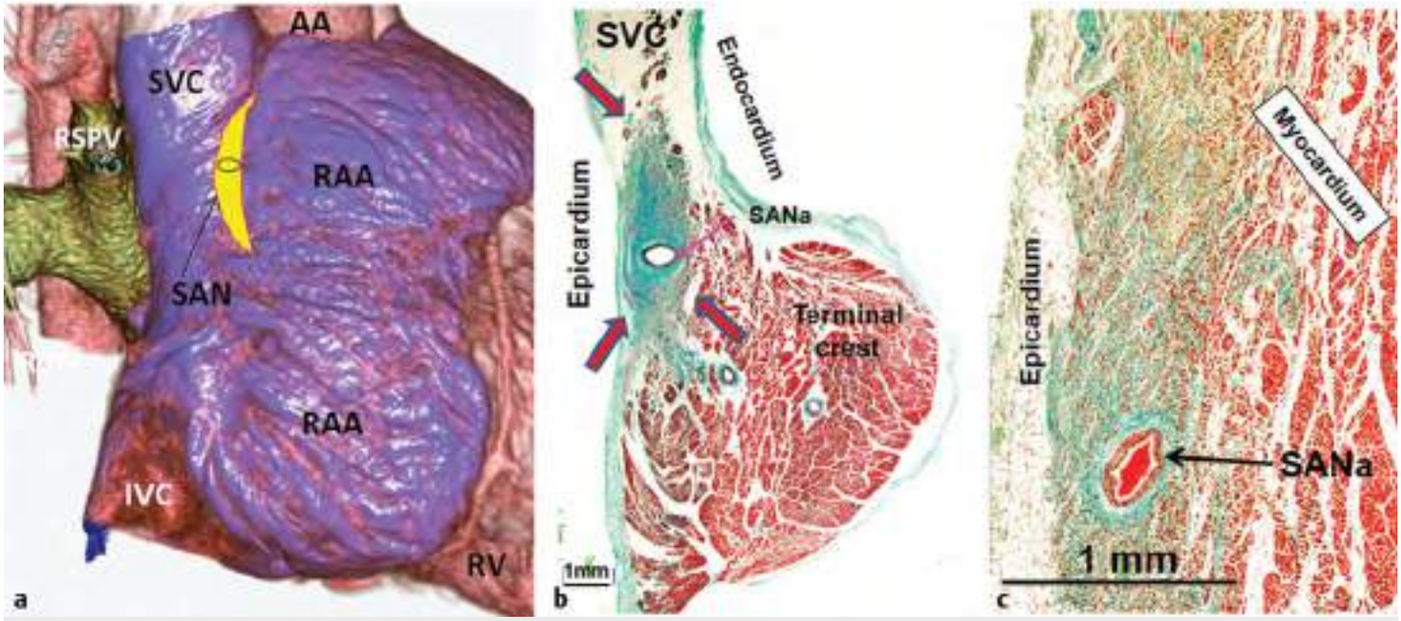

Fig. 12.21 **(a)** Location of the sinus node (crescent) at the lateral aspect of the superior cavoatrial junction. **(b)** Histological section of the sinus node body (Masson's trichrome stain) within a dense matrix of connective tissue (*green color*) showing nodal extensions (*red arrows*) as well as a central position of the sinoatrial node artery (SANa). **(c)** The irregular contour of the sinus node intermingled with the neighboring myocardium without a discrete fibrous border is shown. AA, ascending aorta; RAA, right atrial appendage; SVC, superior vena cava; IVC, inferior vena cava; RSPV, right superior pulmonary vein; RV, right ventricle.

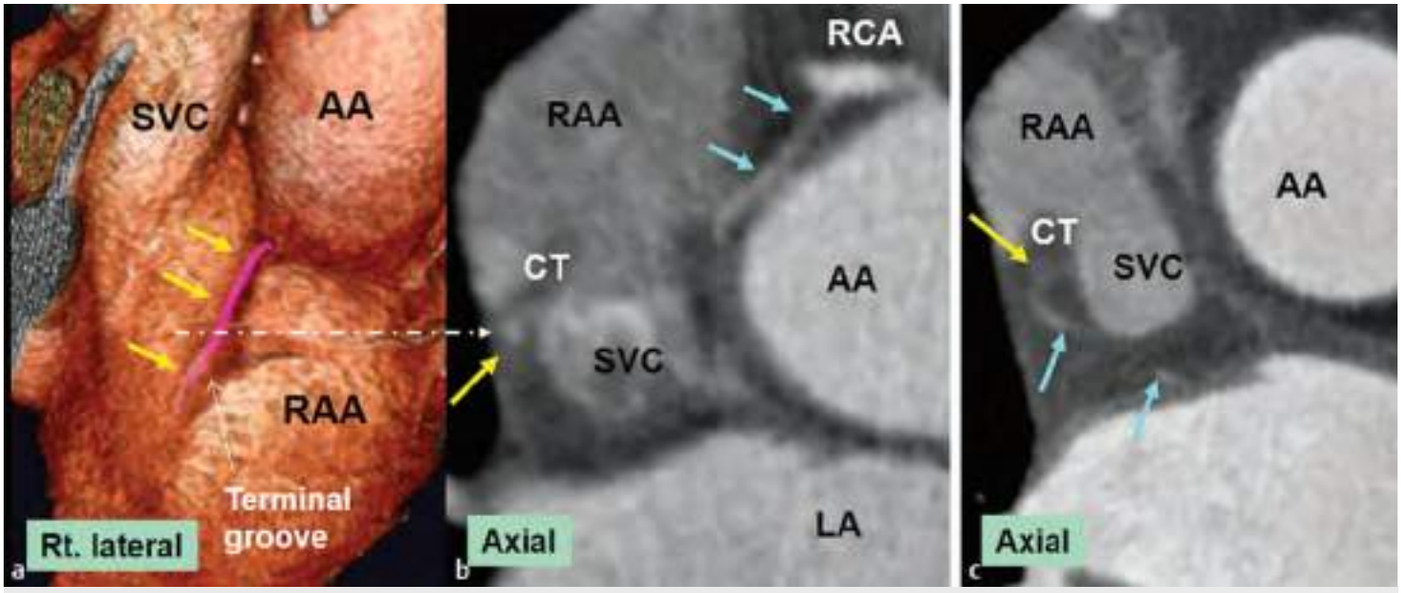

Fig. 12.22 **(a)** Right lateral 3D view of the heart shows the terminal segment of sinoatrial (SA) node artery (*yellow arrows*) in the sulcus terminalis. Axial images at the level of the superior cavoatrial junction (*white dashed line*). The SA node is arranged around the SA node artery (*blue arrows*), which can run centrally inside the node or eccentrically adjacent to it. In the majority of hearts (70%), the SA node artery is located centrally within the node. **(b)** Axial image shows the terminal segment of the SA node artery as a rounded area of enhancement (*yellow arrow*) within the crista terminalis (CT) the anatomical location of SA node. **(c)** Axial image in a different patient again shows the eccentric course of the SA node artery (*blue arrows*) in relation to the SA node (*yellow arrow*) and within the CT. RAA, right atrial appendage; SVC, superior vena cava; LA, left atrium; RCA, right coronary artery.

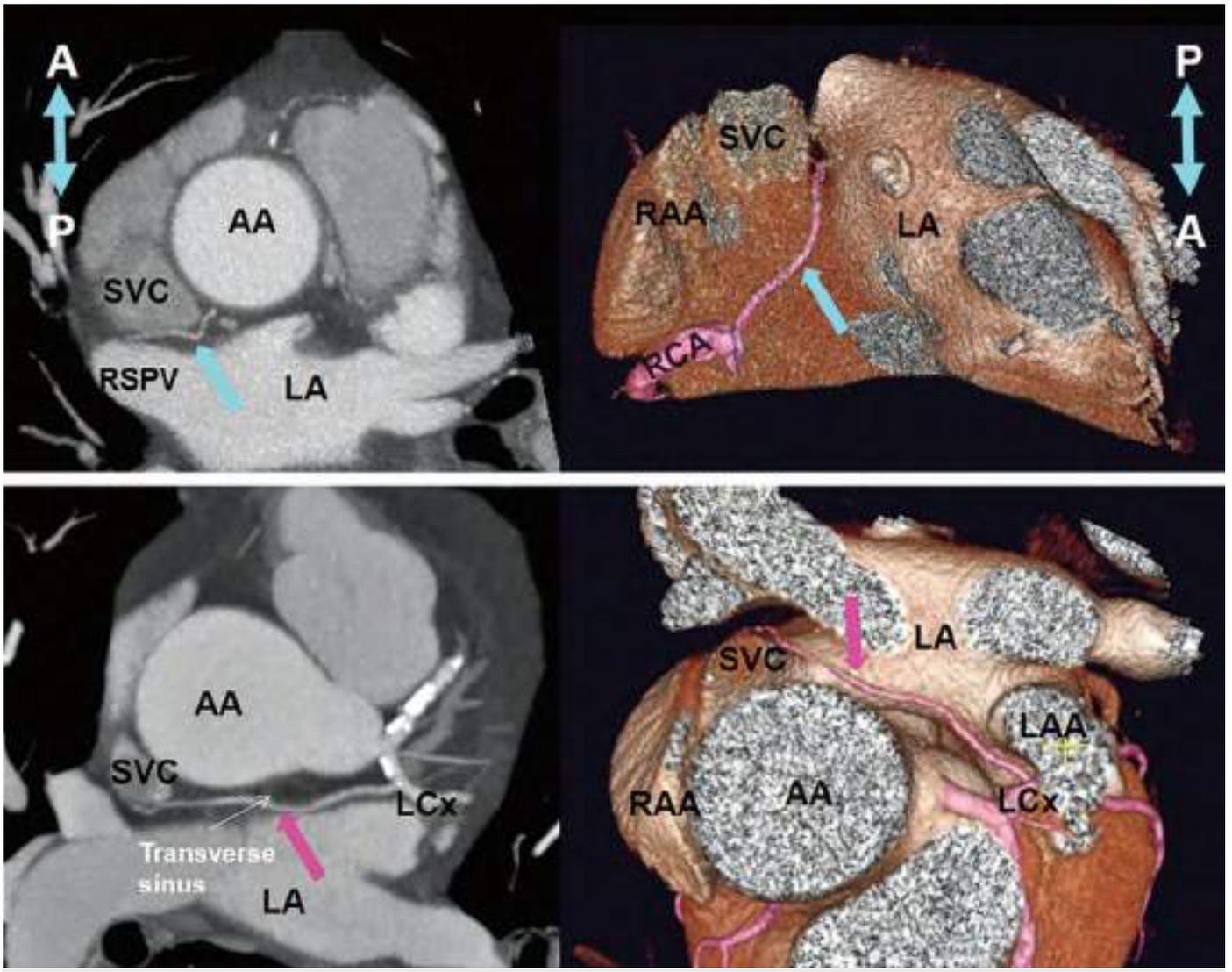

Fig. 12.23 Axial images of coronary CT angiogram (left) and the superior views of the volume-rendered reconstruction of the heart (right) are shown. Blue arrows point to the retrocaval sinoatrial (SA) node artery arising from the RCA (upper images) and from the LCx (lower images). In retrocaval variant of SA node artery, the artery is very close to the interatrial groove and moves posterior wall of the SVC. In the transverse sinus, left SA node artery travels very close to the anterior wall of LA (*red arrows* in lower images) and left atrial appendage (LAA). AA, ascending aorta; LA, left atrium; LCx, left circumflex artery; RAA, right atrial appendage; RCA, right coronary artery; SVC, superior vena cava.

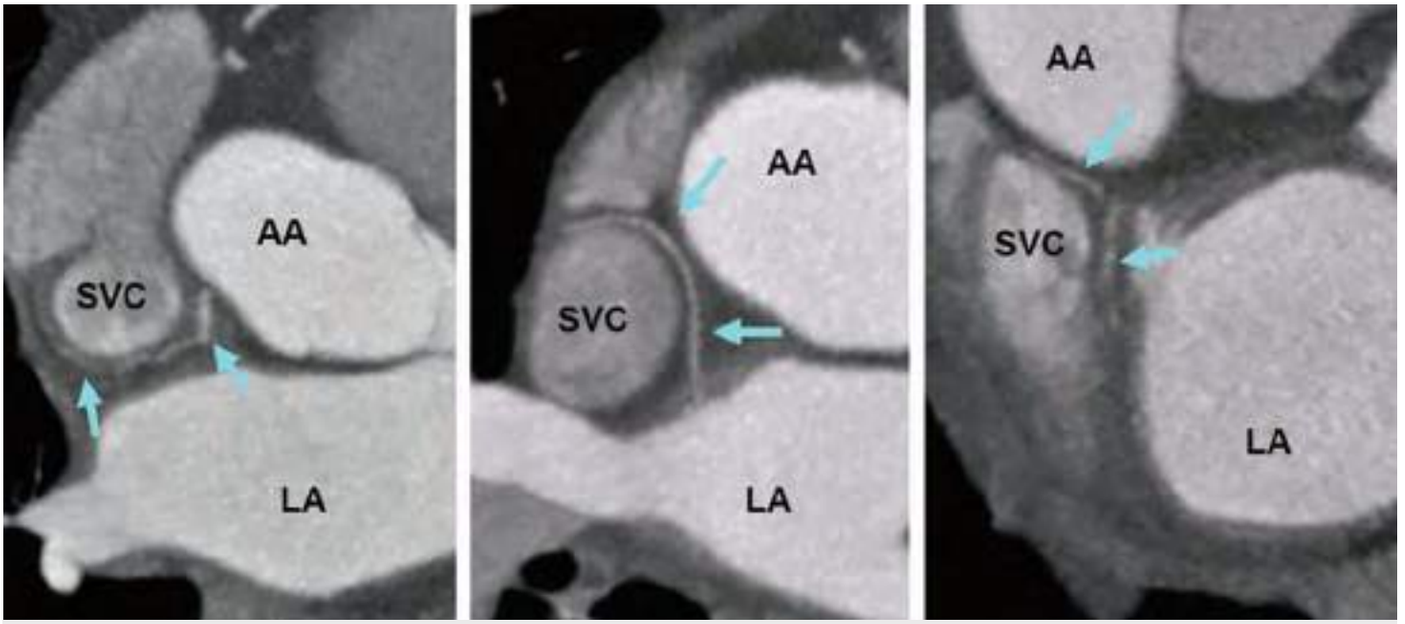

Fig. 12.24 Axial images show different mode of terminations of the sinoatrial (SA) node artery (*arrows*) relative to the SVC. The terminal SA node artery approaches the SA node anterior to the SVC (precaval) in 42%, posterior to the SVC (retrocaval) in 48%, and through multiple branches surrounding the SVC (pericaval) in 10%. AA, ascending aorta; LA, left atrium; SVC, superior vena cava.

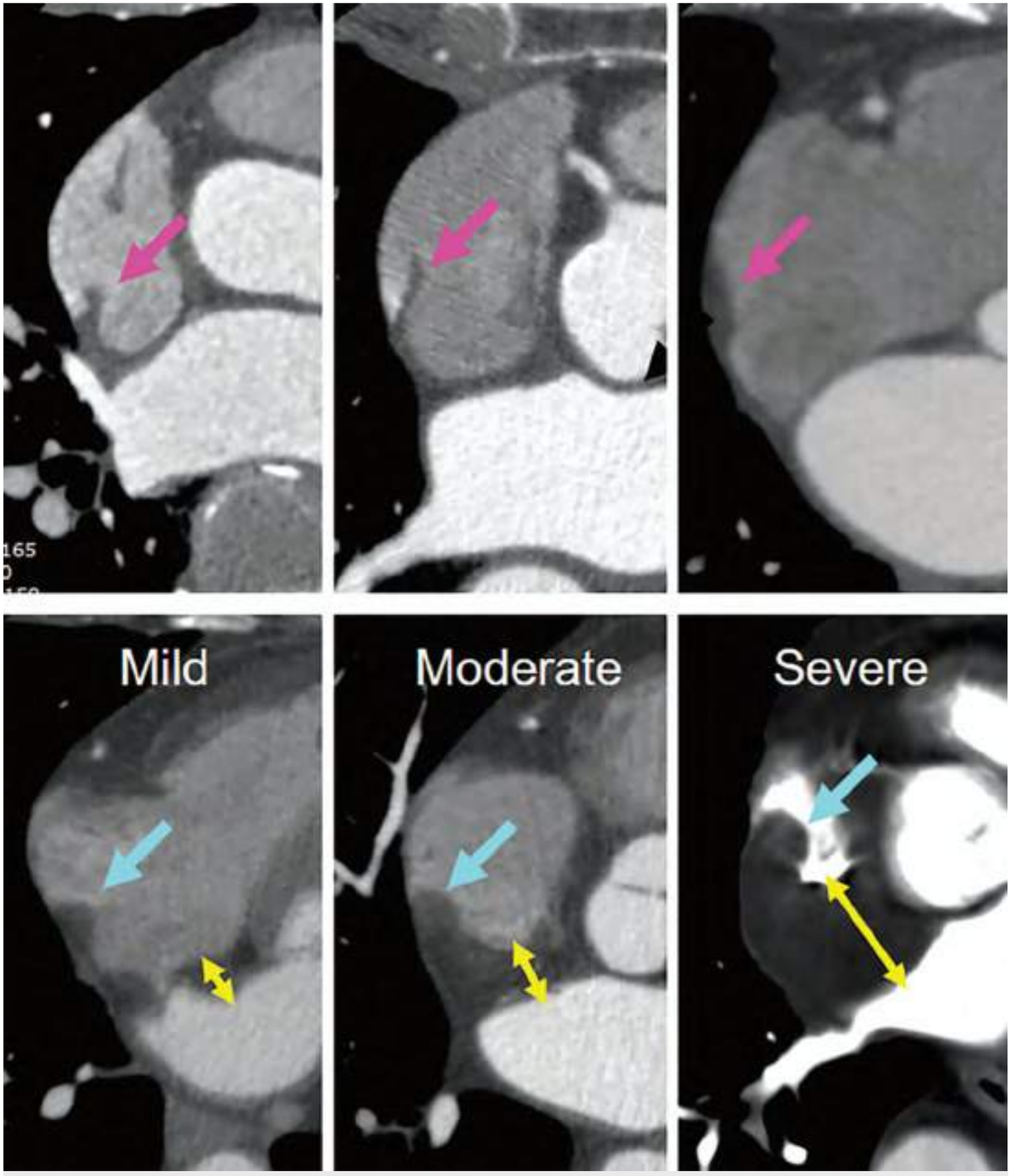

Fig. 12.25 Upper row. The crista terminalis varies in size and extent in different individuals. Axial CT scans show how the crista terminalis (*arrows*) varies in length and thickness. Lower row. Axial CT scans show differing amounts of fat infiltration of the crista terminalis (*blue arrows*) and varying degrees (from mild to severe) of lipomatous hypertrophy of the septum (*yellow arrow*). A large crista terminalis can mimic a mass at echo studies.

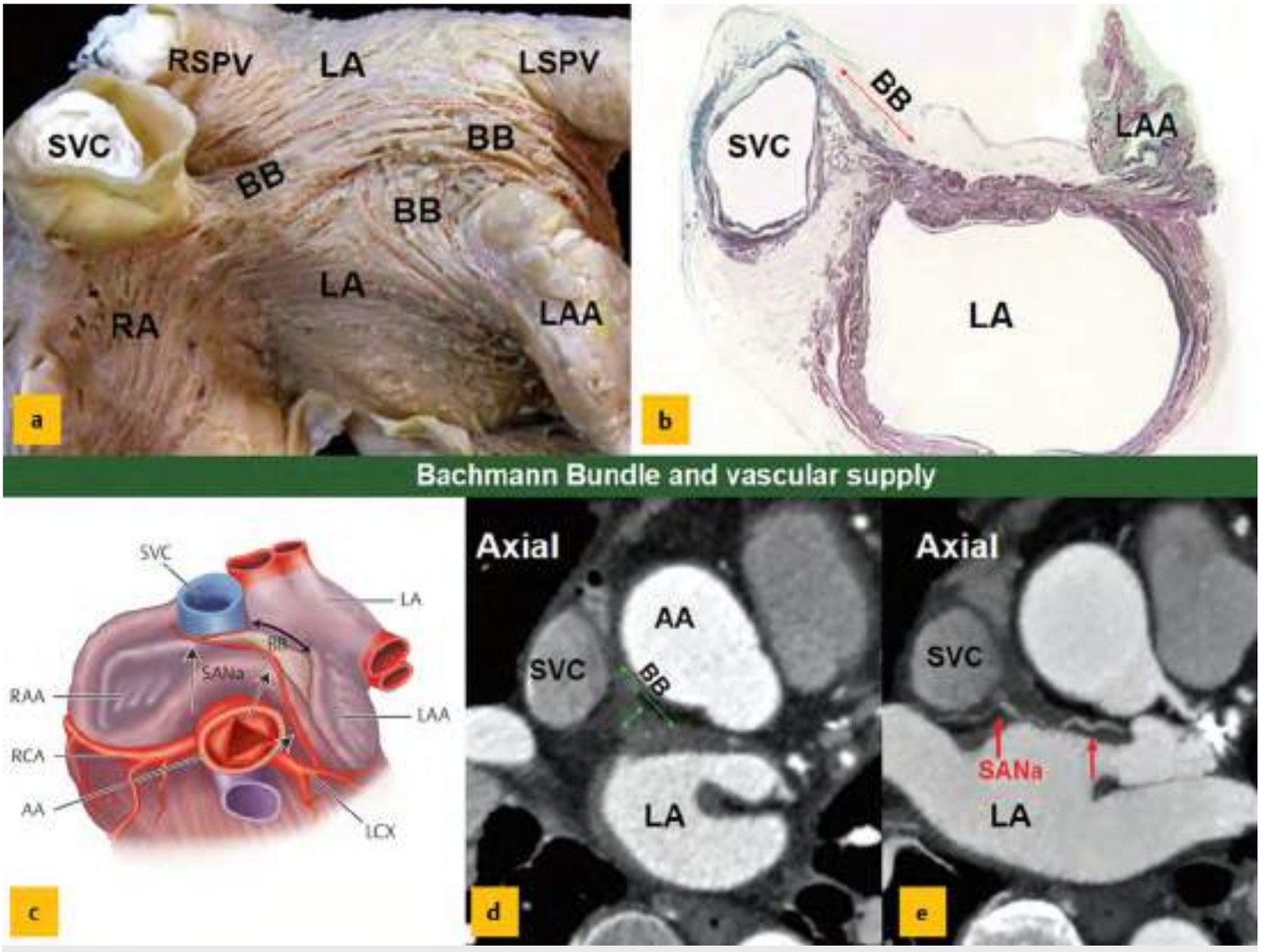

Fig. 12.26 **(a)** Dissection of the subepicardial fibers of the atria viewed from the anterosuperior aspect. Bachmann's bundle (BB), within the red lines crosses the anterior interatrial groove, blends into the circumferential fibers of the anterior wall to encircle the neck of the left atrial appendage (LAA). **(b)** Short-axis cross-section of the left atrium at the interatrial muscle band of Bachmann. **(c)** An illustrative anterosuperior view of the heart showing the anatomical location of BB supplied by the left sinoatrial node artery (SANa) arising from the left circumflex artery (LCx). **(d, e)** Axial CT images showing the length and width of the BB (*green arrows*) and its vascular supply by the left SANa. AA, ascending aorta; LA, left atrium; LSPV, left superior pulmonary vein; RSPV, right superior pulmonary vein; RA, right atrium; RAA, right atrial appendage; RCA, right coronary artery; SVC, superior vena cava.

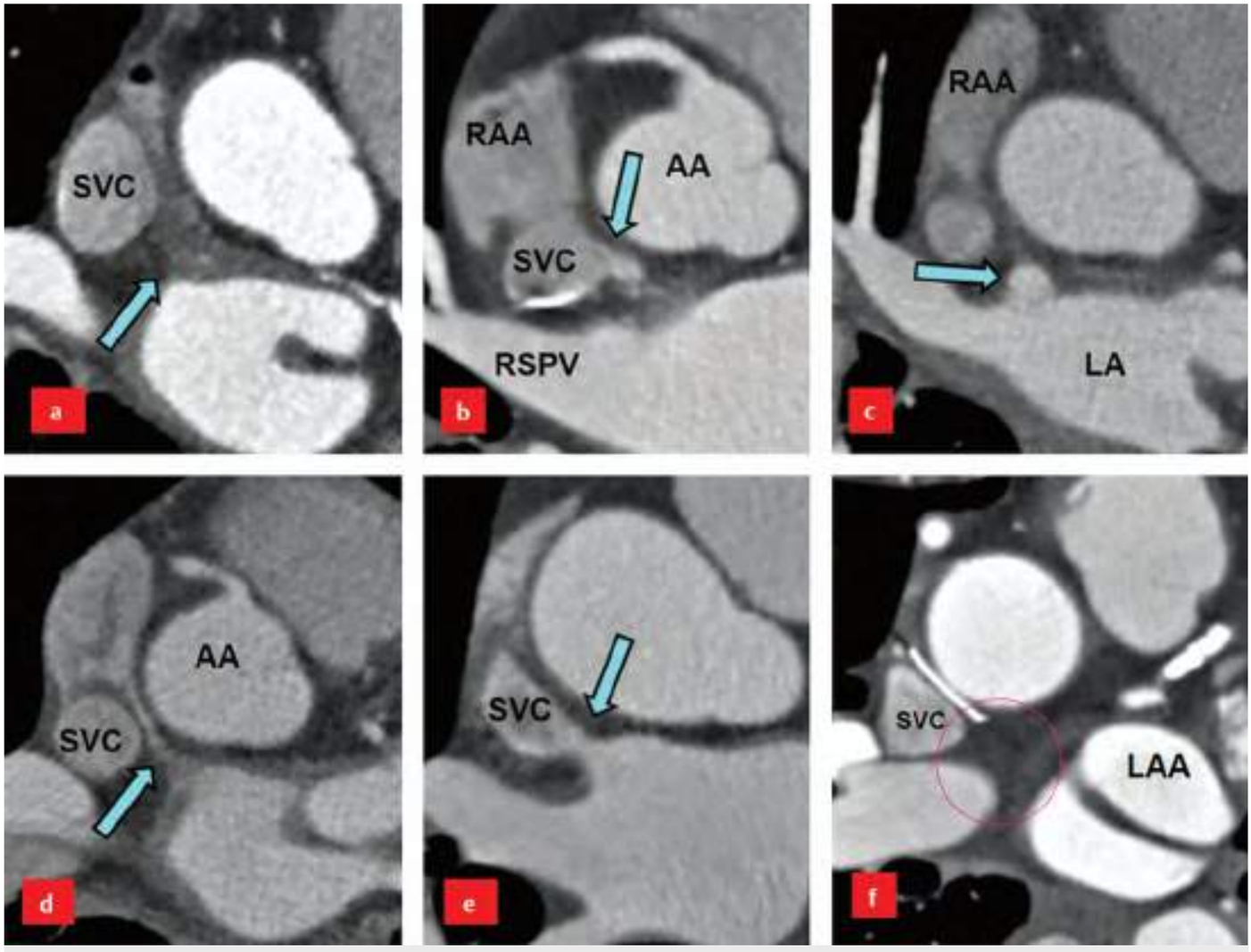

Fig. 12.27 Axial views of the heart in different patients showing anatomical variations of the Bachmann bundle (BB) area (*arrows*). **(a)** Thickened BB, **(b)** BB with contrast-filled protrusion on its right atrial side. **(c)** BB with contrast-filled protrusion on its left atrial side. **(d)** BB filled with contrast. This variation is seen in 11% of the normal individuals and may represent a large Thebesian vein. **(e)** Sinus venosus defect (7 mm). **(f)** Fatty replacement of BB within red circle. Status post-coronary artery bypass graft (CABG) with a sinoatrial (SA) node lead in place. No SA node artery was visualized in this patient. AA, ascending aorta; LA, left atrium; RSPV, right superior pulmonary vein; RAA, right atrial appendage; SVC, superior vena cava.

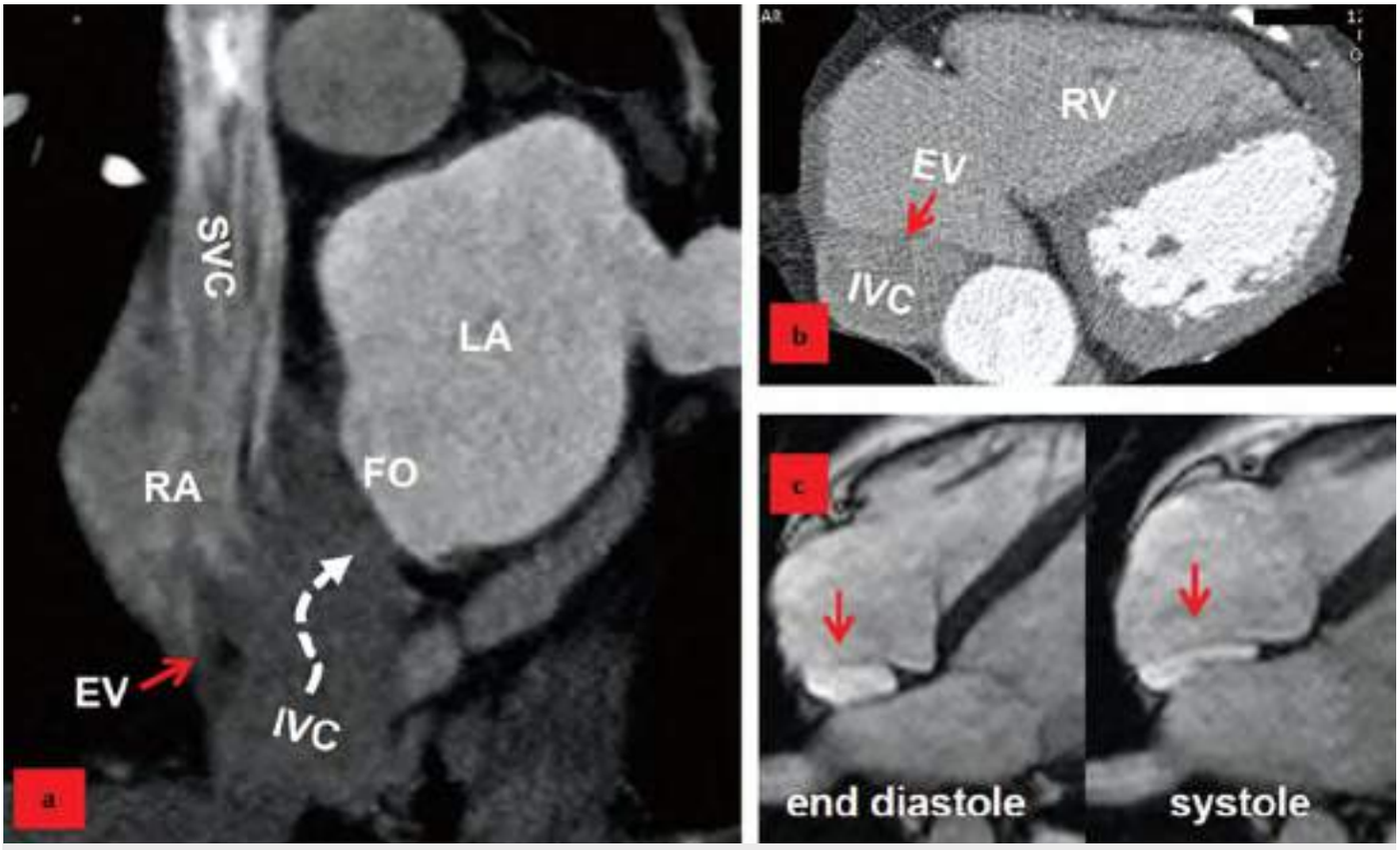

Fig. 12.28 **(a)** Short-axis CT shows preferential inferior vena cava (IVC) flow toward the fossa ovalis (FO) and Eustachian valve (EV). In the posterior half of the right atrial chamber, the blood enters from the IVC, flowing upward and backward through the flap valve of the fossa ovalis, and the EV. The EV has a crucial role in deflecting the blood flow toward the foramen ovale. **(b)** axial CT. **(c)** Axial MR images demonstrate a prominent EV guarding the anterior ostial margin of the IVC. Dynamic changes with diastole and systole are shown in MR images (**c**). LA, left atrium; SVC, superior vena cava.

12

Bachmann's bundle and its vascular supply by CT in normal and abnormal patients showed that Bachmann's bundle was less visible in the patients with severe coronary artery disease as it was replaced with fat[17] (▶ Fig. 12.27).

Inferior Right Atrium Landmarks

The inferior part of the RA is an interesting area with several important anatomical landmarks. The IVC and the coronary sinus connect to this portion of the RA. The Eustachian valve is seen at the anterior margin of the IVC (▶ Fig. 12.28). It is a remnant of the embryonic right valve of the sinus venosus. Embryologically, the Eustachian valve directs oxygenated blood from the IVC across the patent foramen ovale (PFO) into the systemic circulation.[18] It is usually membranous and variably developed. It may look fenestrated or contain muscles. Usually, it inserts medially to the Eustachian ridge at the medial atrial wall. In some cases, the Eustachian valve is large, causing difficulty to pass a catheter (▶ Fig. 12.29). Patients with large Eustachian valve have a higher incidence of PFO.[16]

The inferior wall of the RA between the IVC and the tricuspid valve is a quadrilateral region known as "cavotricuspid isthmus."[19] This part of the right atrial vestibule is the target of catheter ablation techniques for isthmus-dependent atrial flutter.[20] There are variable sizes and morphology that changes with cardiac cycle with the largest diameters during midventricular systole.[21] Obstacles such as large Eustachian ridge/valve, aneurysmal pouches, or even a concave deformation of the entire isthmus may lead to more difficult ablation sessions. Therefore, knowledge of anatomical variants of this region is very important[21] (▶ Fig. 12.30, ▶ Fig. 12.31, ▶ Fig. 12.32).

It is common to observe outpouchings in the medial and lateral margins of the inferior wall of the RA. The medial outpouching inferior to the orifice of the coronary sinus is known as the sub-Eustachian sinus of Keith. It is an extension of a pouch-like isthmus under the orifice of the coronary sinus. Since it is sub-Thebesian rather than sub-Eustachian, some prefer to call it sub-Thebesian sinus/recess[2] (▶ Fig. 12.32, ▶ Fig. 12.33). This anatomical variant is recognized as one of the major procedural difficulties in catheter interventions of the RA and could also be the substrate for reentrant circuit during atrial flutter.

The coronary sinus also connects the inferomedial aspect of the RA. The coronary sinus drains most epicardial coronary venous flow into the RA. Its orifice is guarded by the Thebesian valve. The valve is usually a thin semilunar fold in anteroinferior rim of the ostium and can be seen in most CT angiography studies of the heart[22] (▶ Fig. 12.34). The Thebesian valve is continuous with the Eustachian valve.

The Chiari network represents coarse or fine fibers in the RA, arising from the Eustachian or Thebesian valve, and strands within the RA connecting these valves with the crista terminalis, right atrial wall, or interatrial septum (▶ Fig. 12.35). It is a

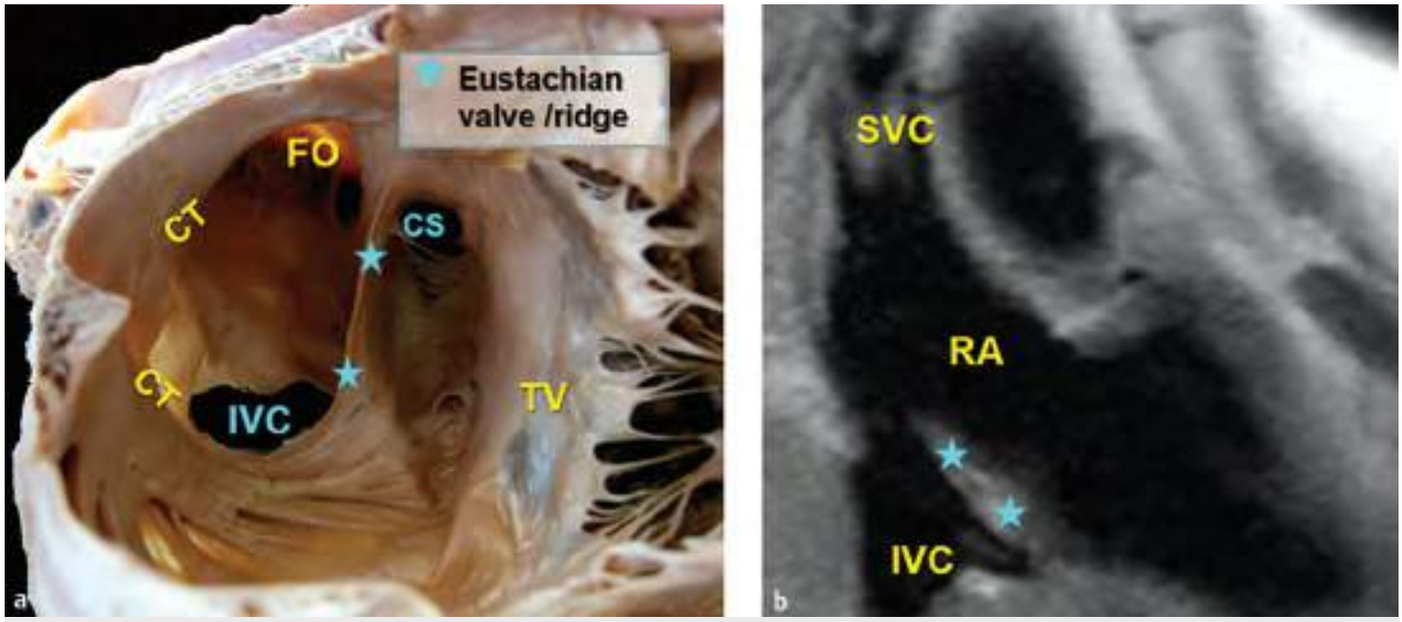

Fig. 12.29 **(a)** Internal view of the right atrium in a cadaveric heart showing a large Eustachian valve/ridge, extending between the inferior vena cava (IVC) and coronary sinus (CS) ostia (*blue stars*). **(b)** Long-axis two-chamber black blood MR view of the right ventricle (RV) shows a large Eustachian valve in the anteroinferior ostial margin of the IVC. CT, crista terminalis; FO, fossa ovalis; RA, right atrium; TV, tricuspid valve; SVC, superior vena cava. Adapted from Saremi 2008.[17]

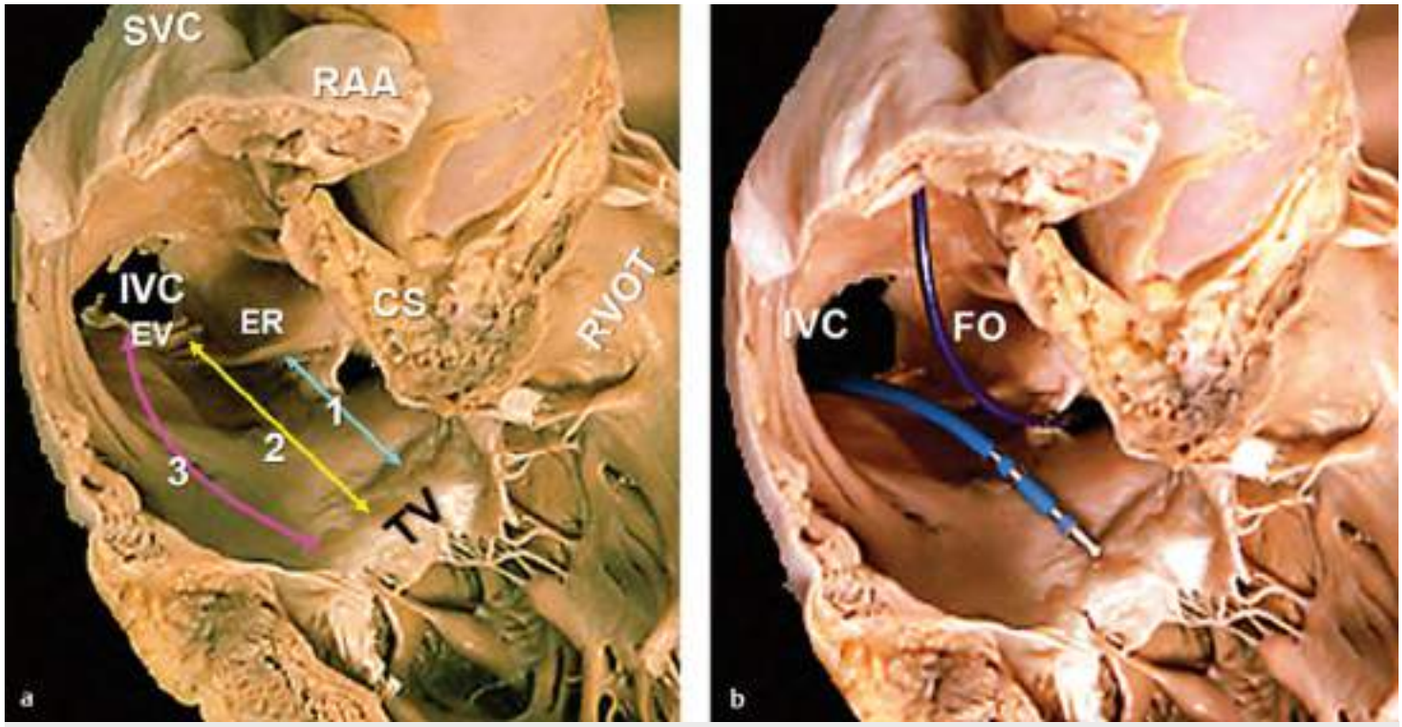

Fig. 12.30 Cavotricuspid isthmus. **(a)** The region of the cavotricuspid isthmus is shown in this right anterior oblique view of the right atrium. The paraseptal, inferior (central), and inferolateral isthmuses are marked 1, 2, and 3, respectively **(b)** showing the position of the radiofrequency ablation catheter at the site of inferior or central isthmus (no. 2). Note the smooth vestibule immediately proximal to the tricuspid valve. CS, coronary sinus orifice; EV, Eustachian valve; ER, Eustachian ridge; IVC, inferior vena cava; FO, fossa ovalis; RAA, right atrial appendage; RVOT, right ventricular outflow tract; SVC, superior vena cava; TV, tricuspid valve.

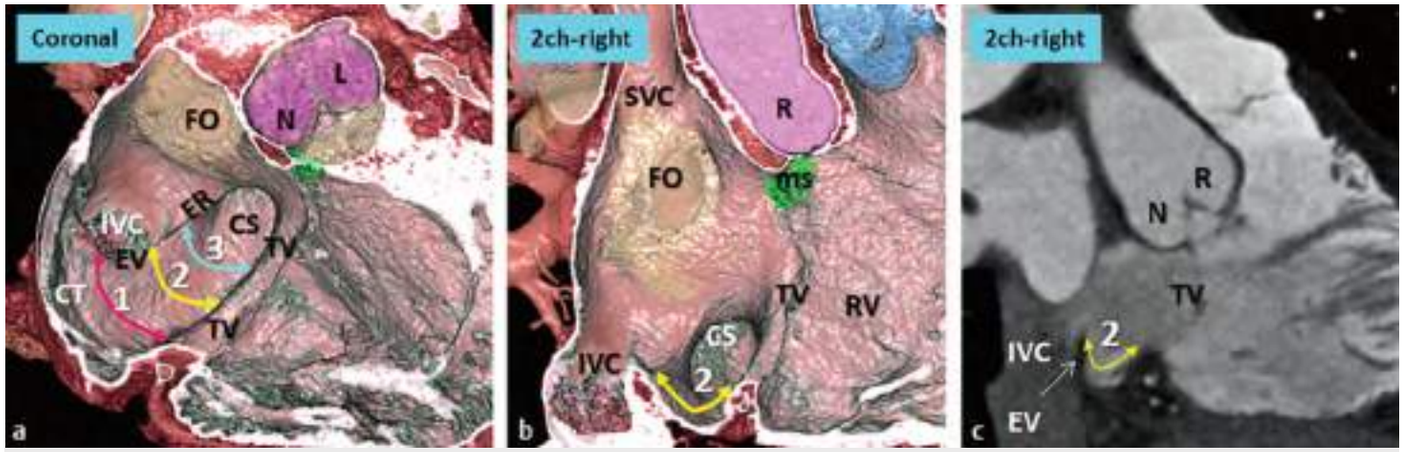

Fig. 12.31 Cavotricuspid isthmus. (**a–c**) CT images demonstrate three locations of the cavotricuspid isthmus including paraseptal (no. 3), inferior (no. 2, central), and inferolateral (no. 1) isthmuses. The cavotricuspid isthmus lies between the Eustachian valve/ridge (EV/ER) and the tricuspid valve (TV) annulus. The central isthmus is usually the part used for radiofrequency ablation of the isthmus-dependent atrial flutter. The central isthmus can be very deep in some cases **(c)**. CS, coronary sinus; CT, crista terminalis; EV, Eustachian valve; ER, Eustachian ridge; IVC, inferior vena cava; FO, fossa ovalis; ms, membranous septum; SVC, superior vena cava; TV, tricuspid valve; L, left coronary sinus; N, noncoronary sinus; R, right coronary sinus.

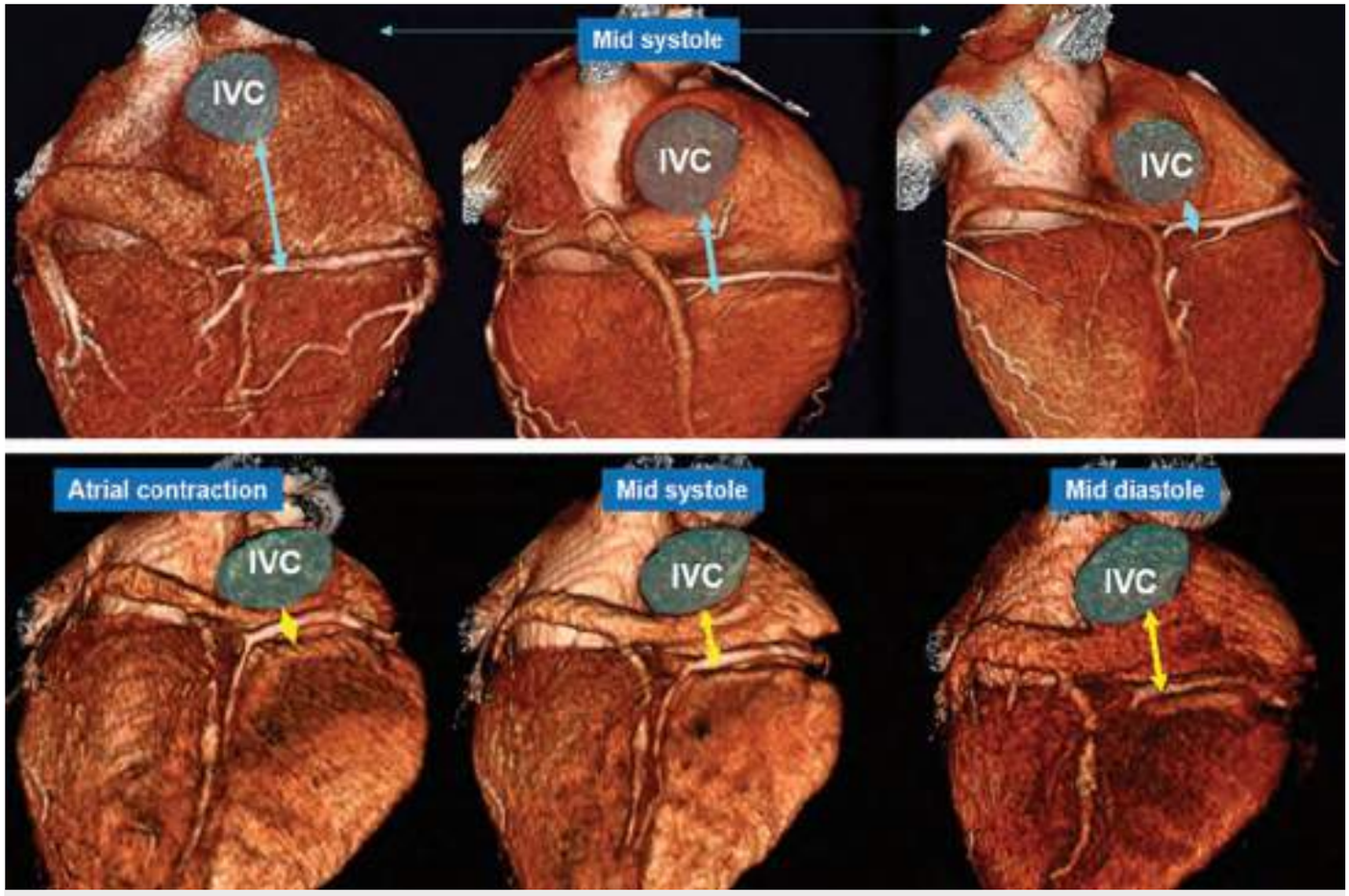

Fig. 12.32 Variation of the cavotricuspid isthmus (CTI). Volume-rendered inferior views of the heart. The length of the CTI varies in different individuals (*upper row*) and different cardiac phases (*lower row*). Knowledge of these anatomical variants prior to catheter ablation will save time and increases the success rate. IVC, inferior vena cava.

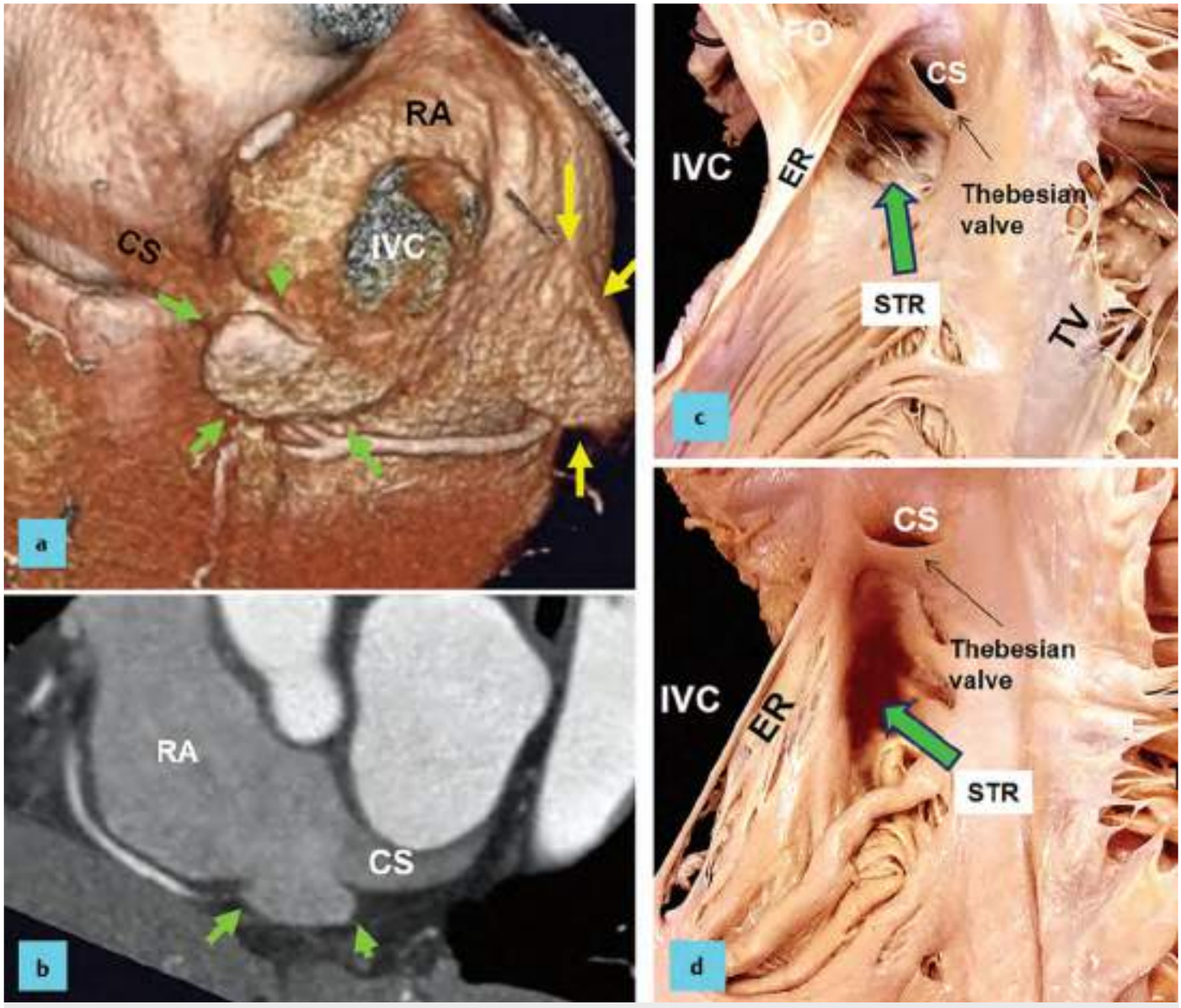

Fig. 12.33 **(a)** Inferior volume-rendered image of the heart demonstrates the inferior wall of the right atrium (RA). It is common to observe two pouches: one medially and one laterally. The inferolateral pouch is usually smaller (*yellow arrows*). The inferomedial pouch is a diverticular extension of cavotricuspid isthmus under the coronary sinus (CS) and has been termed sub-Eustachian sinus of Keith or more correctly sub-Thebesian recess (STR, *green arrows*). **(b)** Short-axis view of the heart showing the STR (*green arrows*). **(c, d)** Internal view of the inferior wall of the RA in two different examples showing the STR. The STR extends below the ostium of the coronary sinus and may interfere with percutaneous catheterization of the coronary sinus. FO, fossa ovalis; ER, Eustachian ridge; IVC, inferior vena cava; TV, tricuspid valve.

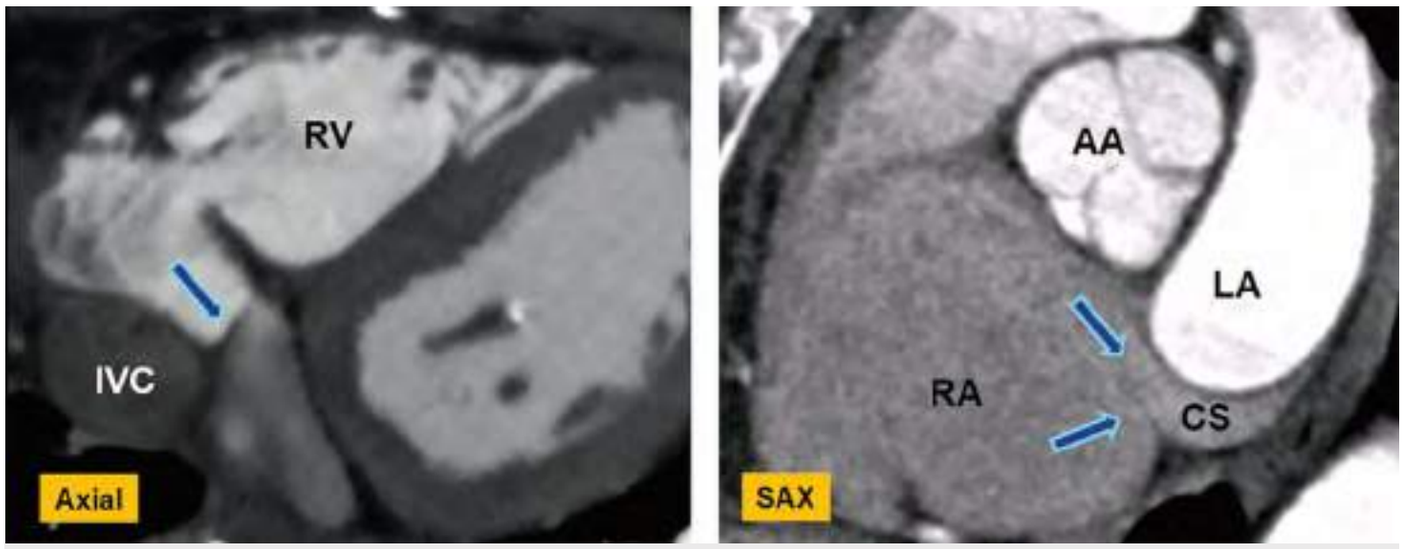

Fig. 12.34 Thebesian valve. Axial and short-axis (SAX) images of two different patients showing the Thebesian valve (*arrows*). AA, ascending aorta; LA, left atrium; IVC, inferior vena cava; RA, right atrium; RV, right ventricle.

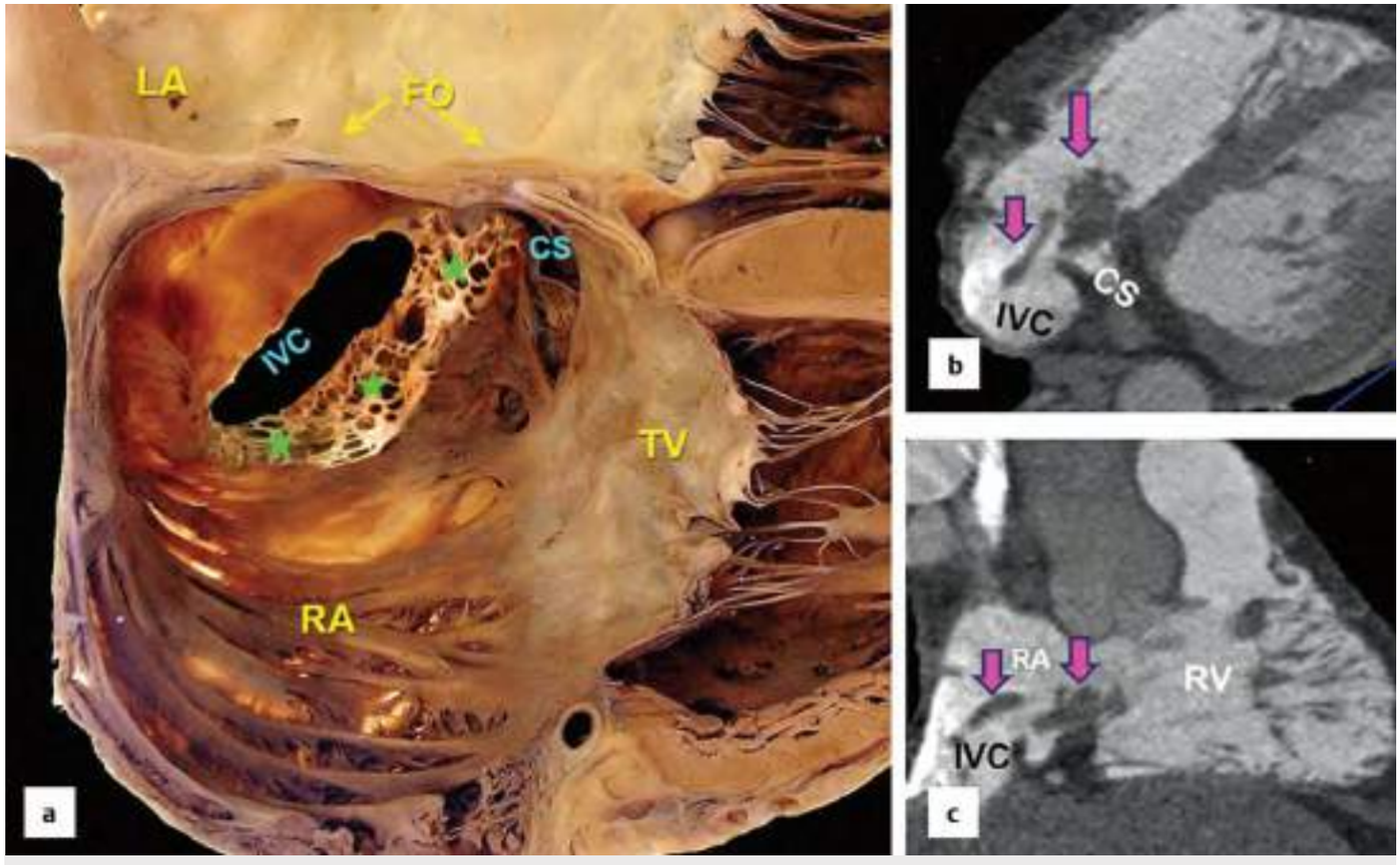

Fig. 12.35 **(a)** Four-chamber views of the inferior wall of the right atrium (RA) in cadaveric heart shows the Chiari network (*green stars*) in the anatomical region of the Eustachian valve, anterior to the inferior vena cava (IVC). It extends to the ostium of the coronary sinus (CS). **(b, c)** Demonstration of the Chiari network with CT angiography of the right heart. **(b)** Axial and **(c)** right ventricle (RV) two-chamber view show rounded and band-like structures (*arrows*) at the inferior cavoatrial junction attaching to the walls of the IVC and CS ostia. This was confirmed by echo which also showed possible thrombus covering the network. Patient had a history of RV endocardial pacemaker. LA, left atrium; FO, fossa ovalis; RA, right atrium; TV, tricuspid valve.

remnant of the embryonic right valve of the sinus venosus,[23,24] and should be differentiated from a large Eustachian valve. The Chiari network fibers may be seen in high-quality CT or MR studies (▶ Fig. 12.35). It could be a risk factor for clot formation.[18]

Medial Right Atrium Landmarks

The inferior part of the medial RA wall above the orifice of the coronary sinus is called the triangle of Koch. It is of significant importance to electrophysiologists because the AV node resides in this triangle and it is the site for catheter ablation procedures which are guided largely by anatomical landmarks (▶ Fig. 12.36, ▶ Fig. 12.37). The AV node consists of a compact portion near the apex and an area of transitional cells near the base of the triangle (▶ Fig. 12.37). The central fibrous body resides in the apex of the triangle and the ostium of the coronary sinus holds its base. When viewed from the RA, the triangle is delimited by the hinge line of the septal tricuspid leaflet on the ventricular side and the Eustachian ridge (tendon of Todaro) on the atrial side.[25] The triangle of Koch is the target of ablation for AV node reentrant tachycardia (AVNRT), septal and paraseptal accessory pathways, and atypical forms of atrial flutter.[26,27] The size of the triangle varies in different individuals with a mean height of 26 ± 8 mm.[28,29] Patients with large triangles require additional ablations of the septal region which may increase the rate of complication.[28]

The vestibular atrial wall between the coronary sinus ostial rim and the hinge line of the septal leaflet of the tricuspid valve is known to electrophysiologists as the septal isthmus (▶ Fig. 12.36). It is one of the targets of ablation of the ”slow pathway” AVNRT. The AV node artery can run very close to the septal isthmus (3.5 ± 1.5 mm) being at risk of coagulation during ablation[28,30] (▶ Fig. 12.14**b**). In general, ablations for slow pathway are performed near the base of triangle where the transitional part of the AV node is located to avoid injury of the compact AV node (fast pathway) or the AV node artery.[29]

The tendon of Todaro runs deep in the atrial musculature (the sinus septum) between the coronary sinus and the fossa ovalis. It extends from the commissure between the Eustachian and

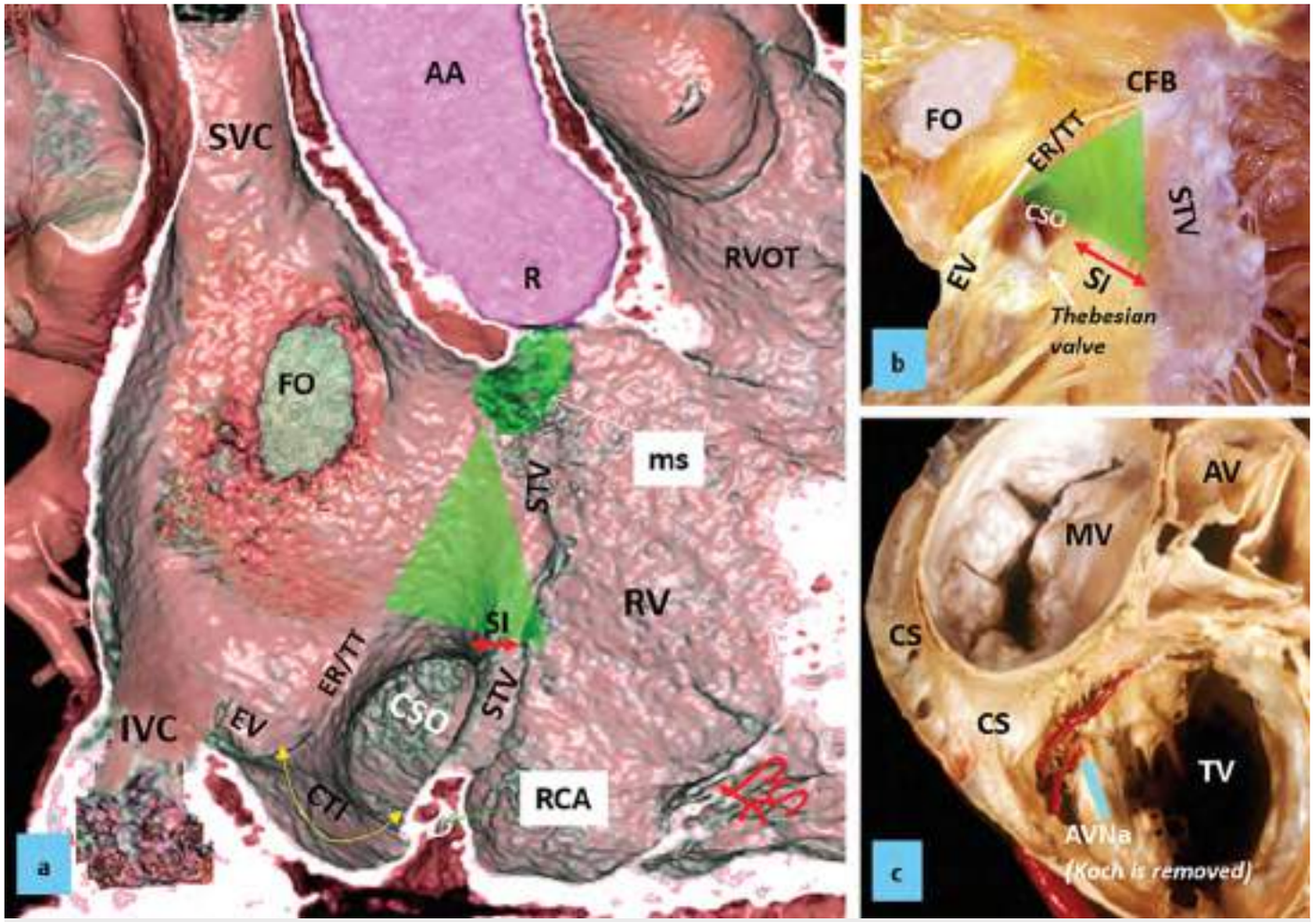

Fig. 12.36 (a, b) Triangle of Koch (medial wall of the right atrium). The posterior border of the triangle is formed by the tendon of Todaro (TT) which is a fibrous extension from the Eustachian valve (EV). The visible part of the TT in the right atrium is a prominent fold called the Eustachian ridge (ER). The anterior border of the triangle is delimited by the septal leaflet of the tricuspid valve (STV) and the base by the ostium of the coronary sinus (CSO). Apex of this triangle corresponds to the central fibrous body (CFB) of the heart. The septal isthmus (SI) is the wall between the CSO and the STV. **(c)** Basal view of the right atrium after removal of the medial wall of right atrium at the triangle of Koch to expose the atrioventricular node artery (AVNa). AA, ascending aorta; CTI, cavotricuspid isthmus; FO, fossa ovalis; MV, mitral valve; ms, membranous septum; RCA, right coronary artery; RV, right ventricle; R, right coronary sinus; RVOT, right ventricular outflow tract; SVC, superior vena cava; TV, tricuspid valve.

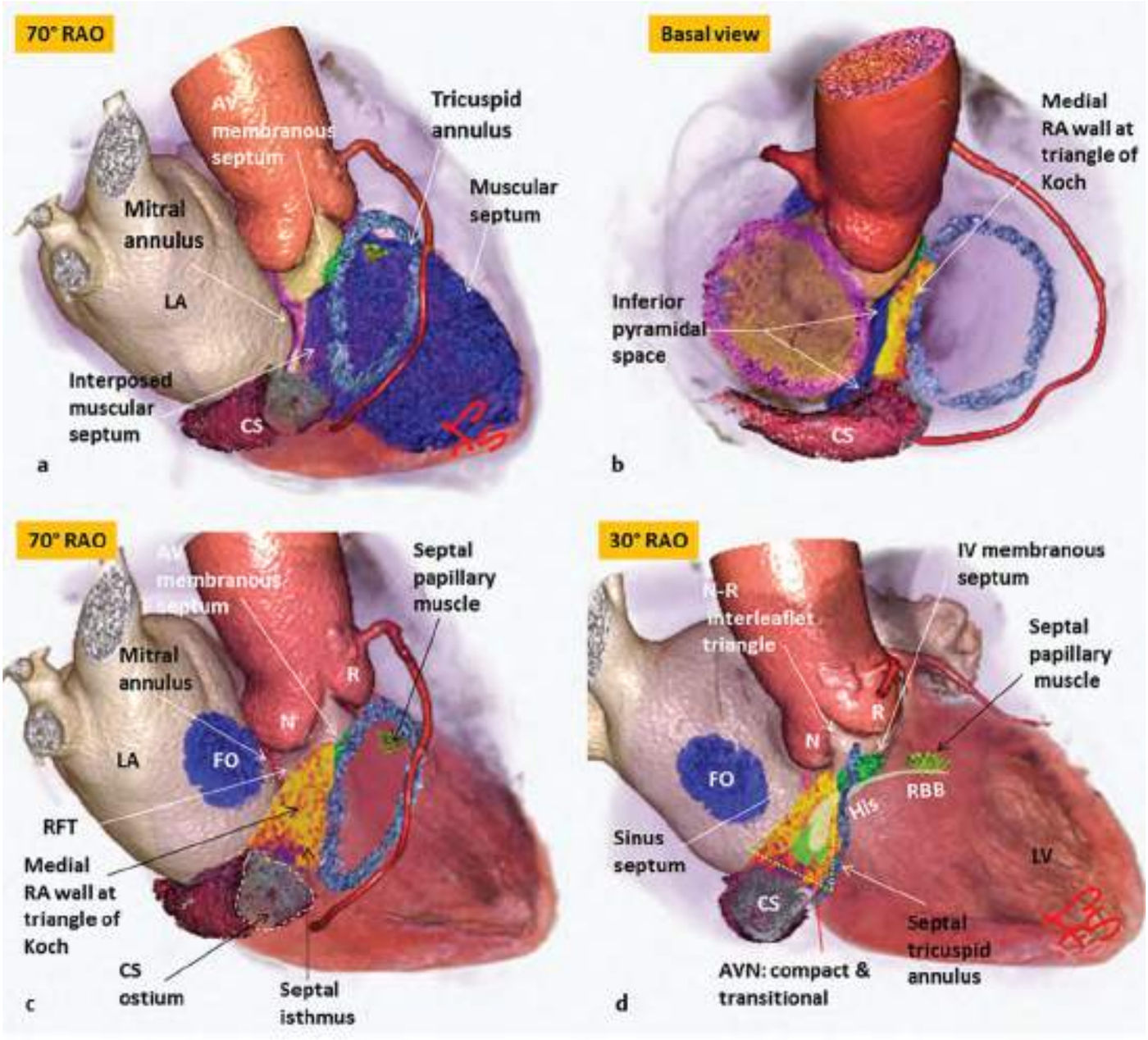

Fig. 12.37 Triangle of Koch. The triangle of Koch is part of medial wall of the right atrium (shown in yellow) which extends between the ostium of the coronary sinus (CS) and the central fibrous body. The central fibrous body is formed by right fibrous trigone (RFT) and the atrioventricular (AV) membranous septum. **(a, b)** The inferior pyramidal space is located outside the heart under the medial wall of the right atrium. **(a)** and **(b)** also show the base of the muscular ventricular septum (shown in blue) interposed between the offset of the attachment of the two AV valves. **(c)** and **(d)** show the enface view of the triangle of Koch. The atrioventricular node (AVN) is located in this region. The His bundle passes under the membranous septum and the right bundle branch (RBB) under the septal papillary muscle. FO, fossa ovalis; LA, left atrium; LV, left ventricle; N, noncoronary sinus; R, right coronary sinus; RAO, right anterior oblique.

Thebesian valves to the central fibrous body[31] (▶ Fig. 12.36). The tendon of Todaro is not visible in the internal view of the RA. Visible representative of it on the internal atrial surface is the Eustachian ridge which can be prominent enough to be visible in CT angiographies in 25% of individual[21] (▶ Fig. 12.31, ▶ Fig. 12.36). The significance of demonstration of a large Eustachian ridge is more related to the need for its catheter ablation to achieve a complete paraseptal isthmus block in patients with atrial flutter.[32] The AVN artery originates from the distal RCA and penetrates into the base of the posterior interatrial septum (inferior pyramidal space) at the level of crux of the heart in 80 to 90% of patients (▶ Fig. 12.38). In the remaining, it originates from the distal LCx artery.[10,33,34,35]

◆ Left Atrium

Over the last decade, there has been tremendous attention by the anatomists and electrophysiologists to the anatomy of the LA. The LA has become the main target of catheter ablation in patients with chronic AF.

The LA is the posterior chamber of the heart that receives pulmonary venous drainage from the four pulmonary veins.[1] The

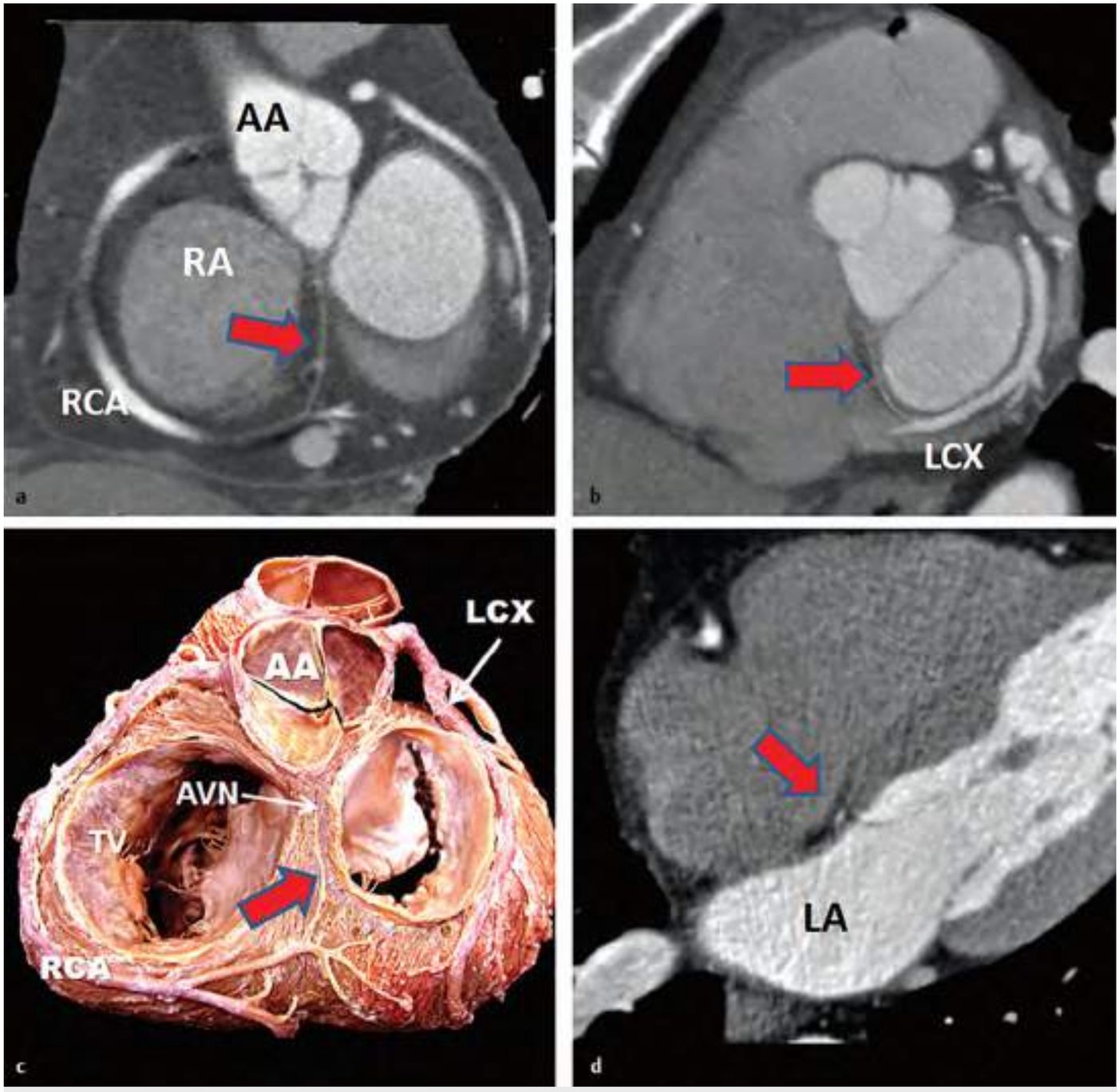

Fig. 12.38 Short-axis views of CT coronary angiography. Arrows point to right atrioventricular nodal (AVN) artery arising from the RCA **(a)** or from the LCx artery **(b)**. **(c)** Cadaveric view of the septal wall of the right atrium after removal of the Koch triangle showing the AVN artery as it moves toward the site of AVN. **(d)** Axial CT showing the AVN artery in the inferior pyramidal space. AA, ascending aorta; RA, right atrium; RCA, right coronary artery; LCx, left circumflex artery; TV, tricuspid valve.

shape of the LA may be compared to box sitting in front of the descending thoracic aorta and the esophagus. The LA is divided into five poorly demarcated walls: anterior (anterosuperior), posterior (posteroinferior), superior, left lateral, and septal (anteroinferior). The relations of the LA to adjacent structures are important (▶ Fig. 12.16, ▶ Fig. 12.39).

The main pulmonary artery and the right pulmonary artery are close to the superior wall of the LA and separated from the LA by the transverse sinus (▶ Fig. 12.13, ▶ Fig. 12.19). The pulmonary veins connect to the posterosuperior aspect of the LA on each side. The ascending aorta is located between the anterior wall of the LA and the medial wall of the RA (▶ Fig. 12.14). They are separated inferiorly by the extracardiac adipose tissue and superiorly by the transverse sinus of the pericardium (▶ Fig. 12.39). The left SA node artery travels in the epicardial fat of the transverse sinus at the junction of the superior and anterior walls of the LA (▶ Fig. 12.23). The noncoronary sinus of the aorta faces the interatrial septum. The posterior wall of the LA is close to the esophagus and the descending aorta. The orifice of the LAA is located anterolaterally at the left superior corner of the LA anterior to the left superior pulmonary vein orifice.

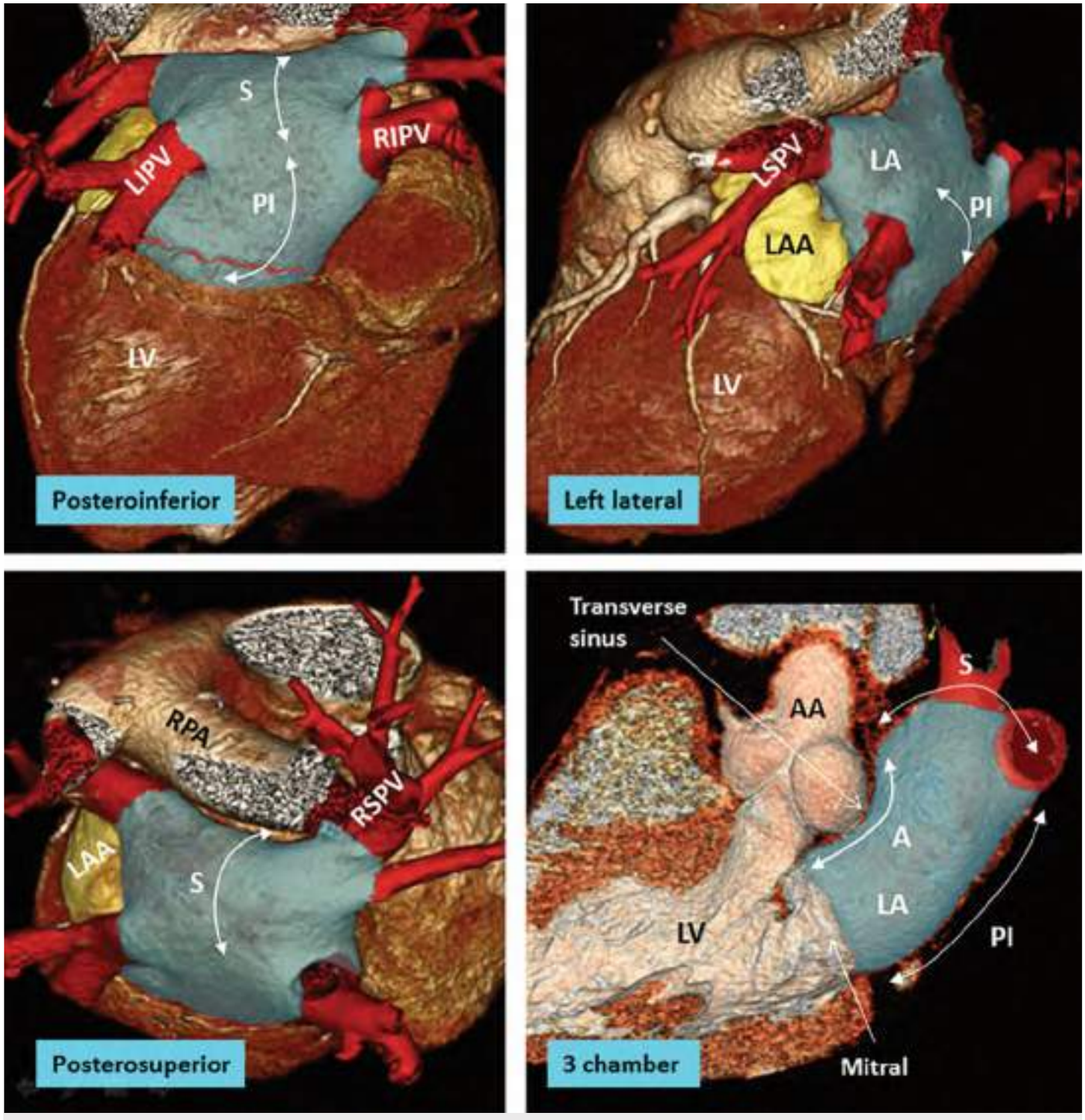

Fig. 12.39 Anatomical relationship of the left atrium (LA). Posteroinferior, left lateral, posterosuperior, and three-chamber views of volume-rendered CT angiographies are shown. The LA (in blue) is located superiorly and posteriorly to the heart. The LA is divided into five poorly demarcated walls: anterior (anterosuperior = A), posterior (posteroinferior = PI), superior, left lateral, and septal (anteroinferior). The anterior (A) wall is closely related to the ascending aorta (AA). The right pulmonary artery (RPA) is close to the superior wall of the LA. The left atrial appendage (LAA) is shown in yellow and the pulmonary veins are shown in red. The four pulmonary veins include LS, left superior; LI, left inferior; RS, right superior; RI, right inferior; LV, left ventricle; PV, pulmonary vein.

The interatrial Bachmann bundle marks the junction of the anterior and superior walls of the LA.

The interatrial septum forms the septal (anteroinferior) wall of the LA facing anteriorly and slightly on the right of midsagittal plane (▶ Fig. 12.17). The mitral valve is the opening of the LA to the LV. It is located anterolaterally at the inferior half of the LA and on the left of midsagittal plane (▶ Fig. 12.17, ▶ Fig. 12.39). The left main stem bronchus passes above the left superior corner of the LV. With LA enlargement, the left bronchus will be pushed superiorly. This causes widening of the tracheal bifurcation angle, a useful sign of LA enlargement on plain films (▶ Fig. 12.40).

The anterior wall thickness measures 3.3 ± 1.2 mm.[36] Part of the anterior wall immediately inferior to the Bachmann bundle and posterior to the aorta can be very thin (1–2 mm). It may

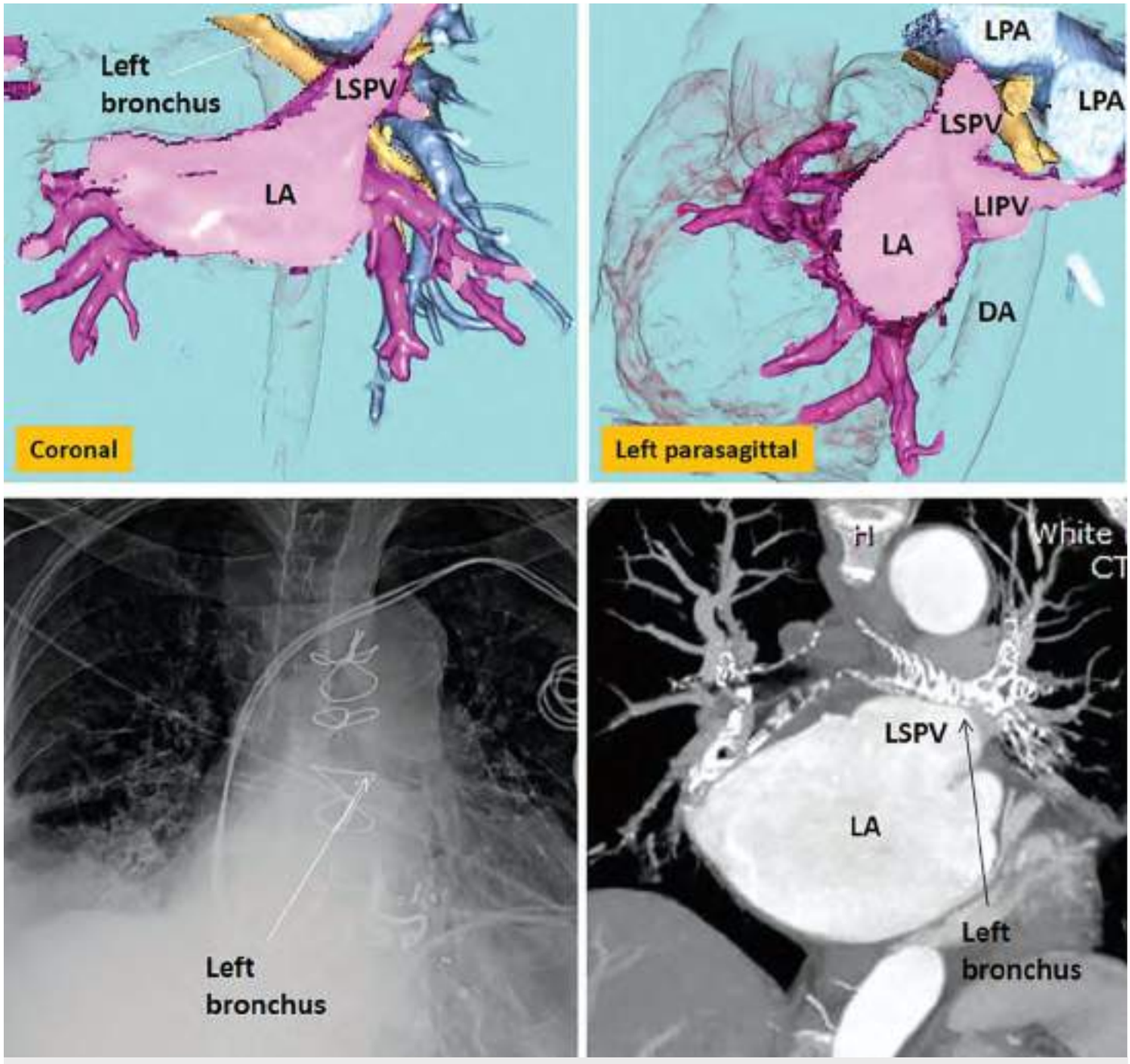

Fig. 12.40 Upper row. Relationship of the left mainstem bronchus to the superior margin of the left atrium (LA). Normal heart. Color-coded CT angiography of chest shows the left main bronchus surrounded by the left pulmonary veins, branches of left pulmonary artery (LPA), and left atrium (LA). The left superior pulmonary vein (LSPV) courses anterior to the left bronchus. An enlarged LA can cause left bronchial compression by elevating the left pulmonary veins. Lower row. Frontal X-ray and coronal CT showing a markedly enlarged LA causing widening of the subcarinal angle by elevating the left bronchus. DA, descending aorta; LIPV, left inferior pulmonary vein.

contain small outpouchings. These features make the anterior wall of the LA susceptible to perforation during catheter interventions. The LA wall is also very thin at the right or left venoatrial junctions.[37,38,39] The superior wall, or dome, is the thickest, measuring 3.5 to 6.5 mm.[2] With the exception of the interatrial muscle bundles (Bachmann's bundle), the muscles of each atrium are confined to its wall. The highest portion of the LA is at the ostium of the left superior pulmonary vein (▶ Fig. 12.13). The left pulmonary veins are usually higher than the right pulmonary veins (▶ Fig. 12.13).

Components of the Left Atrium

As with the RA, the LA consists of a venous component, an appendage and a supravalvular vestibule (▶ Fig. 12.41). Most part of the LA except the appendage is smooth-walled. The superior and posterior walls of the LA form the pulmonary venous component, with the venous orifices at each corner[36] (▶ Fig. 12.39). In early embryonic stage, the pulmonary venous component is a small single vein that opens into the posterior LA adjacent to the developing left AV junction. Subsequent to atrial septation the venous component expands and gradually shifts superiorly to form the roof of the LA with four venous orifices on the sides.

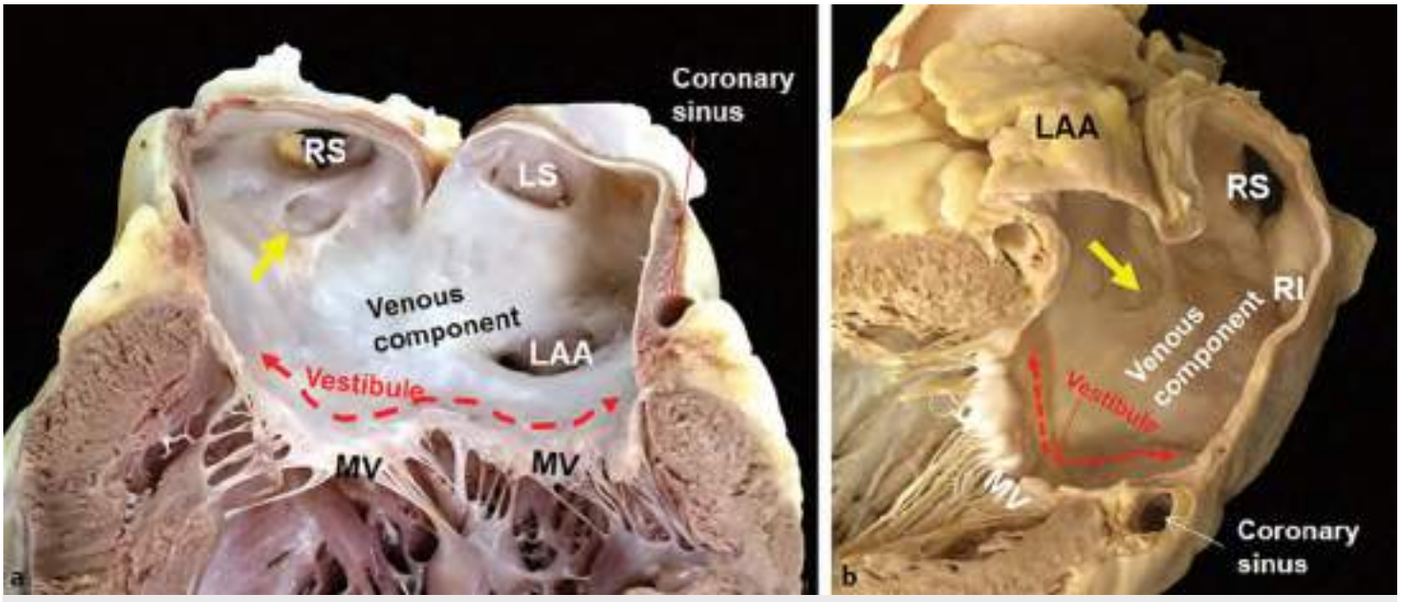

Fig. 12.41 **(a)** Opened view of the LA showing the venous and vestibular components of the LA. The smooth-walled venous component of the LA is the most extensive. The vestibule is also smooth walled and surrounds the mitral orifice. **(b)** Longitudinal sections through the left atrial appendage (LAA) and left ventricle showing the septal wall of the LA. The orifices of the right superior and inferior pulmonary veins (RS and RI) are adjacent to the plane of the septal aspect of the LA. The septal aspect of the LA shows the crescentic edge of the flap valve (*yellow arrows*) against the rim of the oval fossa. LS, left superior; MV, mitral valve.

The vestibular component surrounds the mitral orifice (▶ Fig. 12.16, ▶ Fig. 12.41). As with the developing RA, part of the initial AV canal also forms the vestibule of the mitral valve.[40] Large branches of the LCx artery extend to the posterior aspect of the LA vestibule usually 10 mm above the ostium of the LV. In a dominant LCx artery distal branches can reach to the external crux of the heart. However, exceptions occur and large RCA branches may run in contact with the vestibule. An anatomical area of the vestibule located between the orifice of the left inferior pulmonary vein and the mitral annulus is known as left atrial or mitral isthmus[41] (▶ Fig. 12.42). There is marked variability in the dimensions and wall thickness of the mitral isthmus. This area may be the source of recurrence after circumferential pulmonary vein catheter ablation for AF.[42]

Pulmonary Vein Ostia

Normal pulmonary vein anatomy consists of two right-sided and two left-sided pulmonary veins with separate ostia (▶ Fig. 12.39). This arrangement is commonly variable. The pulmonary vein ostia are ellipsoid with a longer superior–inferior dimension. The right superior pulmonary vein is located close to the SVC, and the right inferior pulmonary vein projects horizontally (▶ Fig. 12.14). The left superior pulmonary vein is close to the LAA and the left inferior pulmonary vein courses near the descending aorta. The veins are larger in men. In patients with enlarged LA or persistent AF veins can be larger. The superior pulmonary vein ostia are larger (19–20 mm) than the inferior ostia (16–17 mm).[43] The ostium of the pulmonary veins is a common location for radiofrequency catheter ablation to treat AF. The ostial diameters influence the selection of the ablation catheter size used. The pulmonary vein trunk is defined as the distance from the ostium to the first-order branch.

Common anomalies include a conjoined (common) left or right pulmonary vein in 25% of individuals.[43] A conjoined pulmonary vein is seen more frequently on the left than the right side.[44] Supernumerary veins are also frequent. The most common is a separate right middle PV, which drains the middle lobe of the lung[45] (▶ Fig. 12.43). One or two middle lobe vein ostia can be seen in 26% of patients.[44] The ostial diameter of the right middle PV is smaller than that of the other veins (mean, 9.9 ± 1.9 mm). The ectopic focus originating from the right middle PV could initiate AF, which is cured by catheter ablation of the right middle PV. In some patients, there is a supernumerary PV that shows an aberrant insertion, with a perpendicular position in relation to the LA posterior wall. The supernumerary branch usually drains the superior or posterior segment of the right upper lobe and characteristically passes behind the bronchus intermedius. In the absence of one pulmonary vein, careful examination of the intrathoracic venous system is required to exclude presence of a partial anomalous pulmonary venous return (▶ Fig. 12.44).

The presence of atrial myocardial tissue extending over the first centimeter of ostial wall of the pulmonary veins has been confirmed both histological examinations.[46] The myocardial sleeve is thickest at the venoatrial junction especially in the left superior pulmonary vein. Although, different mechanisms of AF exist, these myocardial sleeves are believed to be the major source for the development of reentry that triggers AF.[47] In the past, the most common ablation strategy was electrical isolation of the pulmonary veins by creating circumferential ablation lines around the individual or bilateral pulmonary vein ostia. The lines are either guided by fluoroscopy, 3D electroanatomical mapping, or intracardiac echocardiography.[48,49] The focus of radiofrequency or cryoablation strategies shifted from the pulmonary vein to the atrial tissue located in the antrum due to the fact that many nonpulmonary vein trigger points for AF are located in the

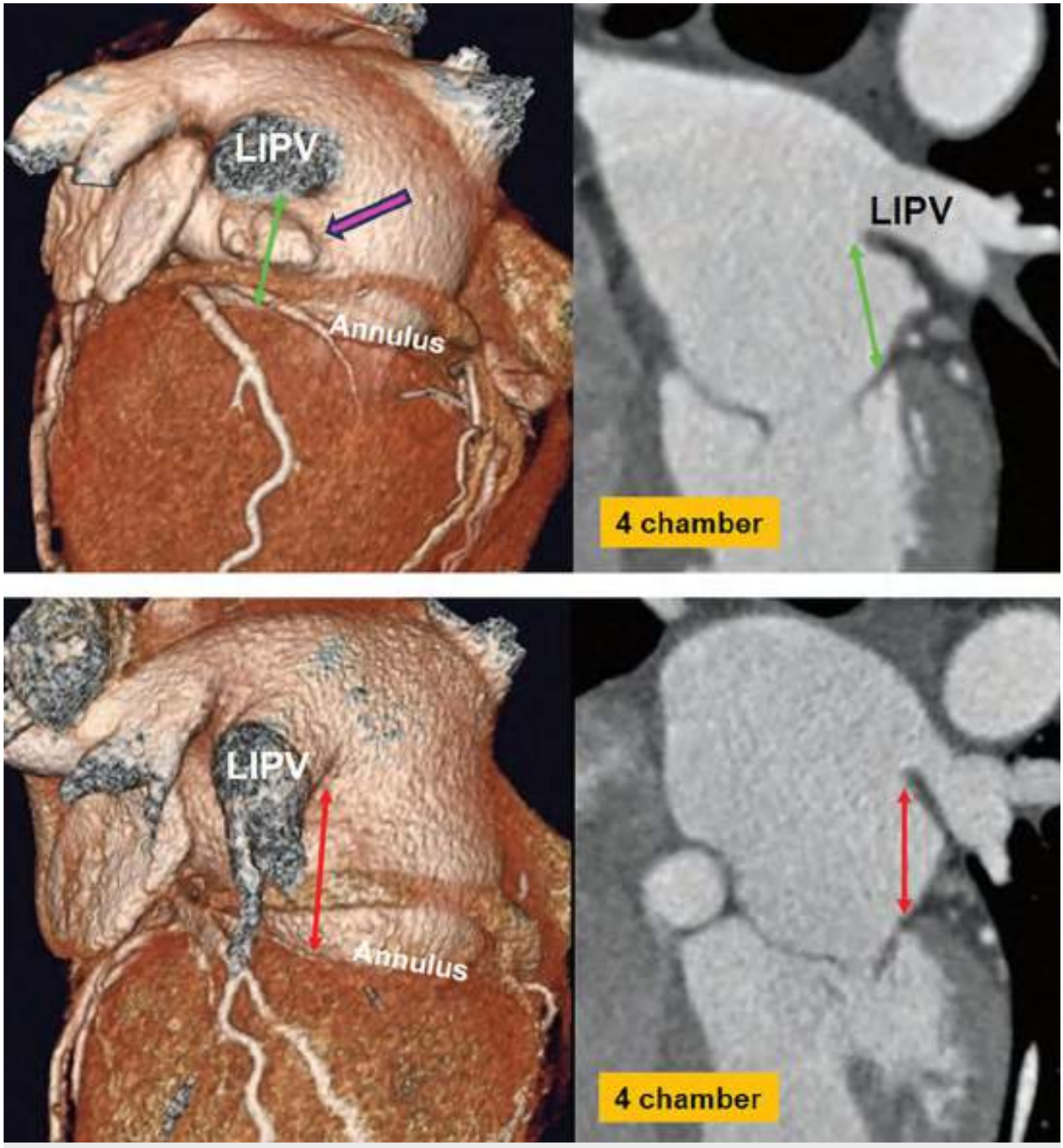

Fig. 12.42 The left atrial isthmus is shown in two different patients. The length of isthmus varies in different individuals. Upper row demonstrates shorter but deeper left isthmus compared to lower images. Left atrial isthmus is the area between the orifice of the left inferior pulmonary vein (LIPV) and the posteroinferior margin of mitral annulus (*double-headed arrows*). CT can easily evaluate the length, depth, and morphological variants of this region. Note, accessory left atrial appendage is common in this anatomical region (*red arrow*).

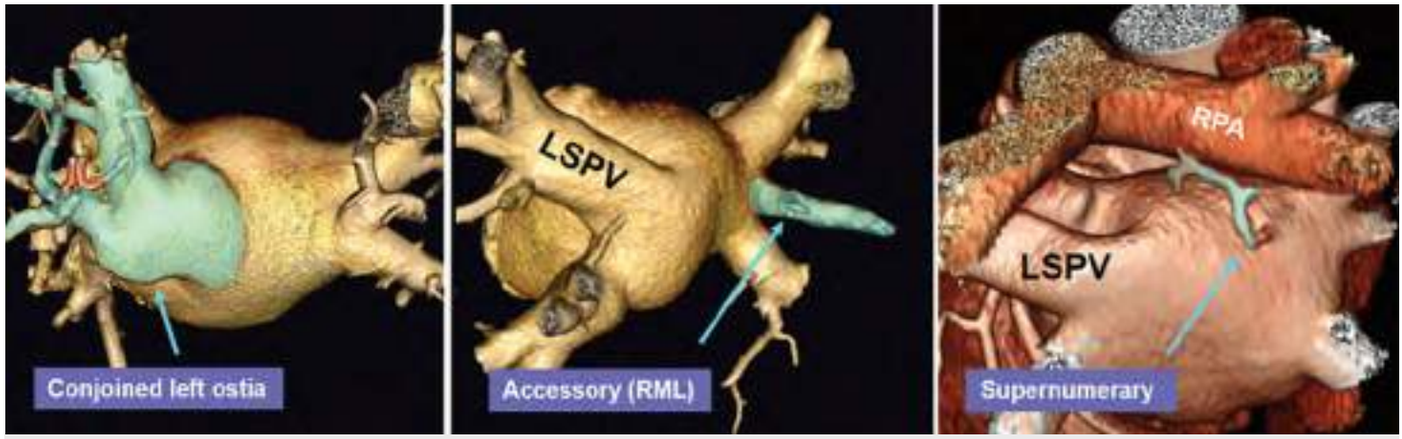

Fig. 12.43 Posterosuperior views of the left atrium showing anatomical variation of the pulmonary veins. Conjoined ostia and accessory right middle lobe (RML) are common and are seen in one-fourth of studies. Accessory branches on the left side are not common. Supernumerary branch is usually a small branch found in 5 to 10% of chest studies. It usually drains the posterior segment of the right upper lobe and consistently travels behind the right main bronchus before entering the left atrium. Rarely, supernumerary branch arises from the superior segment of the right lower lobe and directly connects to the posteroinferior margin of the left atrium. Note close relationship of the right pulmonary artery (RPA) and the superior wall of the left atrium. LSPV, left superior pulmonary vein.

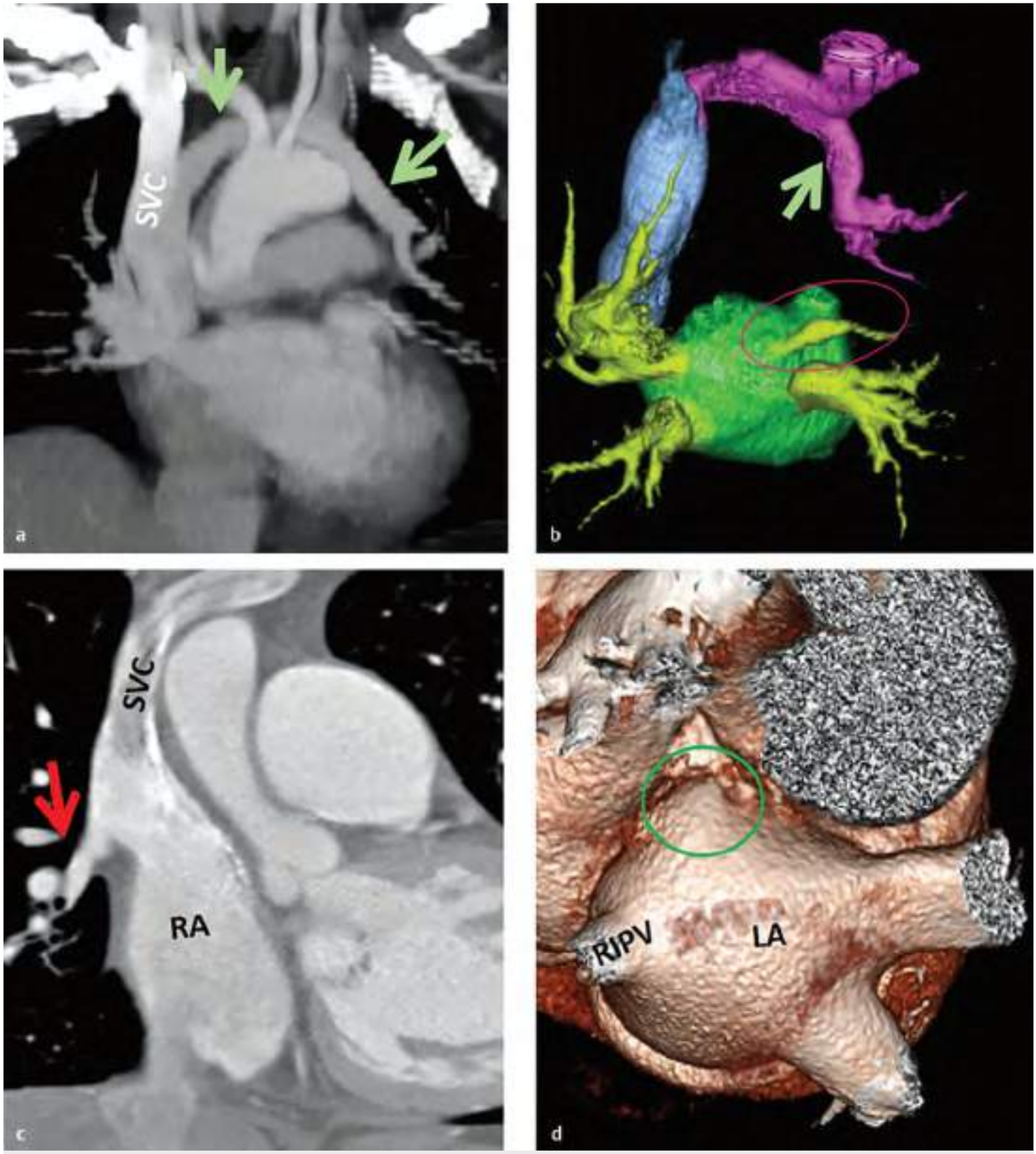

Fig. 12.44 Coronal CT slices and views of volume-rendered CT angiography are shown. **(a, b)** Partial anomalous pulmonary venous return (*green arrows*) draining part of the left upper lung into the superior vena cava (SVC). Note that all four pulmonary veins exist, but the left superior (within *red circle*) appears diminutive. **(c, d)** Partial anomalous pulmonary venous (*red arrow*) return draining part of the right upper lung into the SVC. In this case, the right superior pulmonary vein is absent (*green circle*). RIPV, right inferior pulmonary vein. Image **(d)** is flipped for better orientation. RA, right atrium; LA, left atrium.

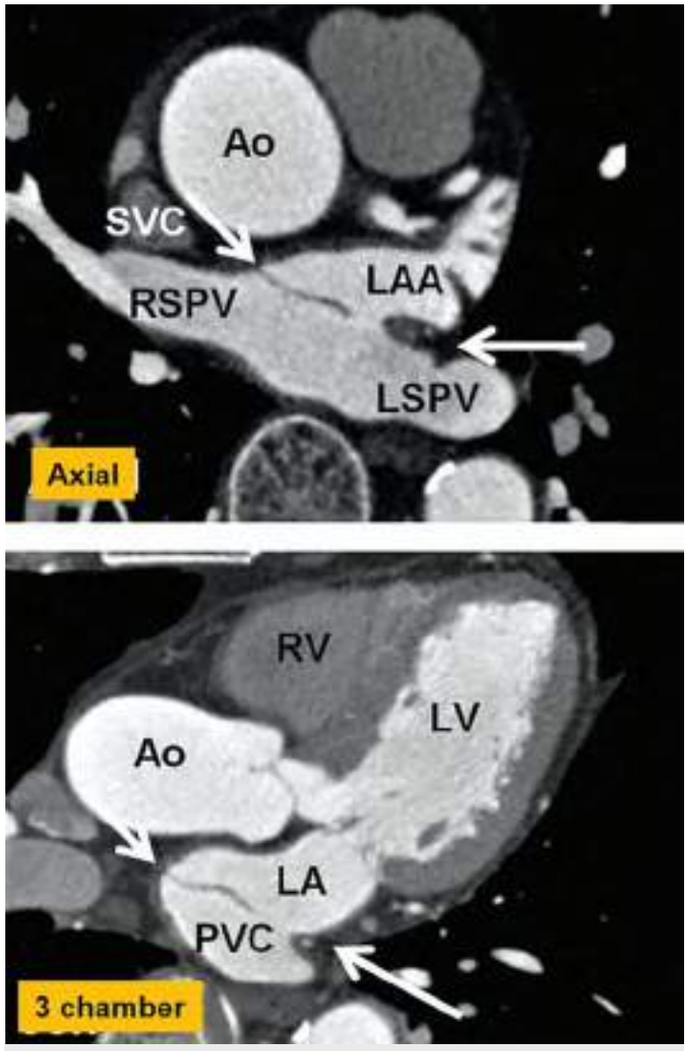

Fig. 12.45 Incidental discovery of a nonobstructive membrane in the LA in an adult. Axial and 3-chamber (3ch) CT images show a membranous septum in the left atrium (LA) extending from the anterior wall of the LA near the orifice of the right superior pulmonary vein (RSPV) to the junction of the left atrial appendage (LAA) and the left superior pulmonary vein (LSPV). This membrane with a 2-cm central perforation separates the pulmonary venous compartment (PVC) of the LA from the main body of the LA. LV, left ventricle; RV, right ventricle; Ao, aorta; SVC, superior vena cava.

antrum rather than the pulmonary veins and that radiofrequency delivery may cause pulmonary vein stenosis.[50] In antrum ablation, the most common sites are the LA "roof" connecting the superior aspects of the left and right upper pulmonary vein isolation lesions and the region of tissue between the mitral valve and the left inferior pulmonary vein (the mitral isthmus).[51]

Incidental discovery of small membranes within the LA near the orifices of the pulmonary veins and adjacent to the superior part of the atrial septum is not rare (▶ Fig. 12.45). Large membranes should raise the possibility of cor triatriatum sinister. This congenital anomaly is rare but surgically correctable.[52]

Left Atrial Appendage

The LAA is derived from the primitive atrium and has a rough trabeculated surface. The LAA interior surface is lined by complicated network of fine pectinate muscles. The LAA is a potential site for deposition of thrombus owing to its narrow neck with the LA.[53] It also appears to be responsible for triggering AF in some patients presenting for repeat procedures of catheter ablation.[54]

There is a wide variation in the configuration of the LAA (▶ Fig. 12.46). The LAA is characteristically a small finger-like extension of the LA with a multilobulated appearance in 80% of hearts[53] (▶ Fig. 12.46). The tip of the LAA can be in a variety of positions, lying over the left anterior descending (LAD) coronary artery, pointing posteriorly, or even directed medially toward the back of the aorta. Using imaging, the LAA morphologies are classified into cactus (30%), chicken wing (48%), windsock (19%), and cauliflower (3%).[54] The rate of thrombus formation is less in nondilated LAA with simple morphology compared with dilated LAAs with complicated shapes. The orifice of the LAA is at the junction of the anterior and the lateral wall, anterior to the left superior pulmonary vein. The axis is directed posteriorly, inferiorly, or anteriorly. It may rotate internally into the transverse sinus (▶ Fig. 12.46c). Rarely, the tip of the LAA may reopen into the anterior wall of the LA (double orifice). The proximal portion of the LCx artery runs in contact with the inferior wall of the LAA. A variable relationship of the coronary arteries to the LAA exists.

The left lateral "ridge" between the LAA and the left pulmonary veins was first described by Keith in 1907 as the "left tenia terminalis." The thickness of the ridge is less than 5 mm in 75% of the hearts (▶ Fig. 12.47, ▶ Fig. 12.48). Thickened ridge can be mistaken for a thrombus or atrial mass. Within the fold runs the remnant of the vein of Marshall, multiple autonomic nerve bundles, and a small atrial artery which, in some cases, is the left SA node artery (S-shaped SA node artery)[55,56] (▶ Fig. 12.47). Persistent left SVC also passes in this region. The S-shaped SA node artery is an anatomical variant of the SA node artery in 14% of coronary CT angiographies. It originates from the posterolateral part of the LCx artery[57] (▶ Fig. 12.47). Surgical or catheter ablation interventions of the LA may pose this artery at risk of injury.

Accessory LAA or LA diverticula are common anatomical variants in 30% of the hearts[58,59] These outpouchings are seen in two anatomical locations: the anterior wall of the LA (projects into the transverse sinus) and the left atrial isthmus (▶ Fig. 12.49). Description of this anatomical variant in radiology reports is required as they may interfere with ablation procedures or be a potential cause of thrombus formation.

Important Periatrial Structures

Important periatrial structures include the esophagus, vagus nerves, phrenic nerves, and descending thoracic aorta. Posterior to the posterior left atrial wall is a layer of fibrous pericardium and fibrofatty tissue of irregular thickness that contains esophageal arteries and the vagus nerve plexus (▶ Fig. 12.50). These anatomical structures may be affected by RFA. The esophagus follows a variable course along the posterior aspect of the LA and it is a movable structure.[60] In 40% of cases, it passes along the middle portion of the posterior LA wall[37,60] (▶ Fig. 12.51). Damage to the esophageal wall may rarely result in the formation of an atrial esophageal fistula.

The vagus nerves pass behind the root of the lungs and form right and left posterior pulmonary plexuses (▶ Fig. 12.50).

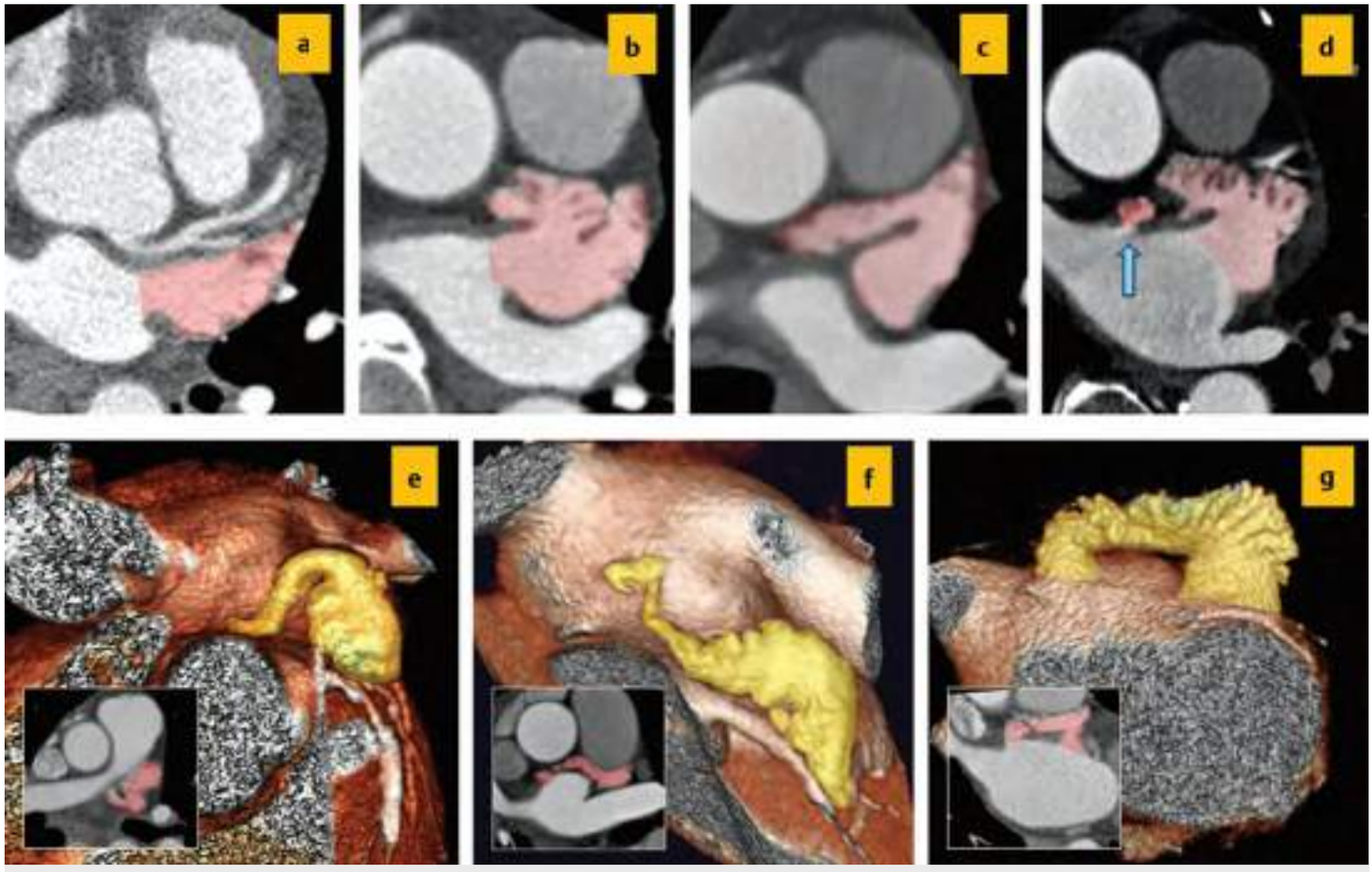

Fig. 12.46 Morphological variation of the left atrial appendage (LAA). **(a–d)** Axial CT images at the level of the LAA showing common variants of the LAA. **(e–g)** Sculpted volume-rendered CT views of the left atrium along with inlay axial 2D images at the level of LAA showing three rare variants of the LAA. The LAA is color coded. The most common variant is the LAA with two lobes (**b**, **d**). It is not uncommon to see that the tip of LAA is medially rotated **(c, e)**. Small accessory appendages arising from the anterior wall are not uncommon (*arrow* in **d**) and in rare instances may connect to the tip of a medially rotated LAA **(f, g)**. **(c)**, **(e)**, and **(f)** are not candidates for an epicardial approach to percutaneous LAA exclusion. The rate of thrombus formation is less in nondilated LAA with simple morphology.

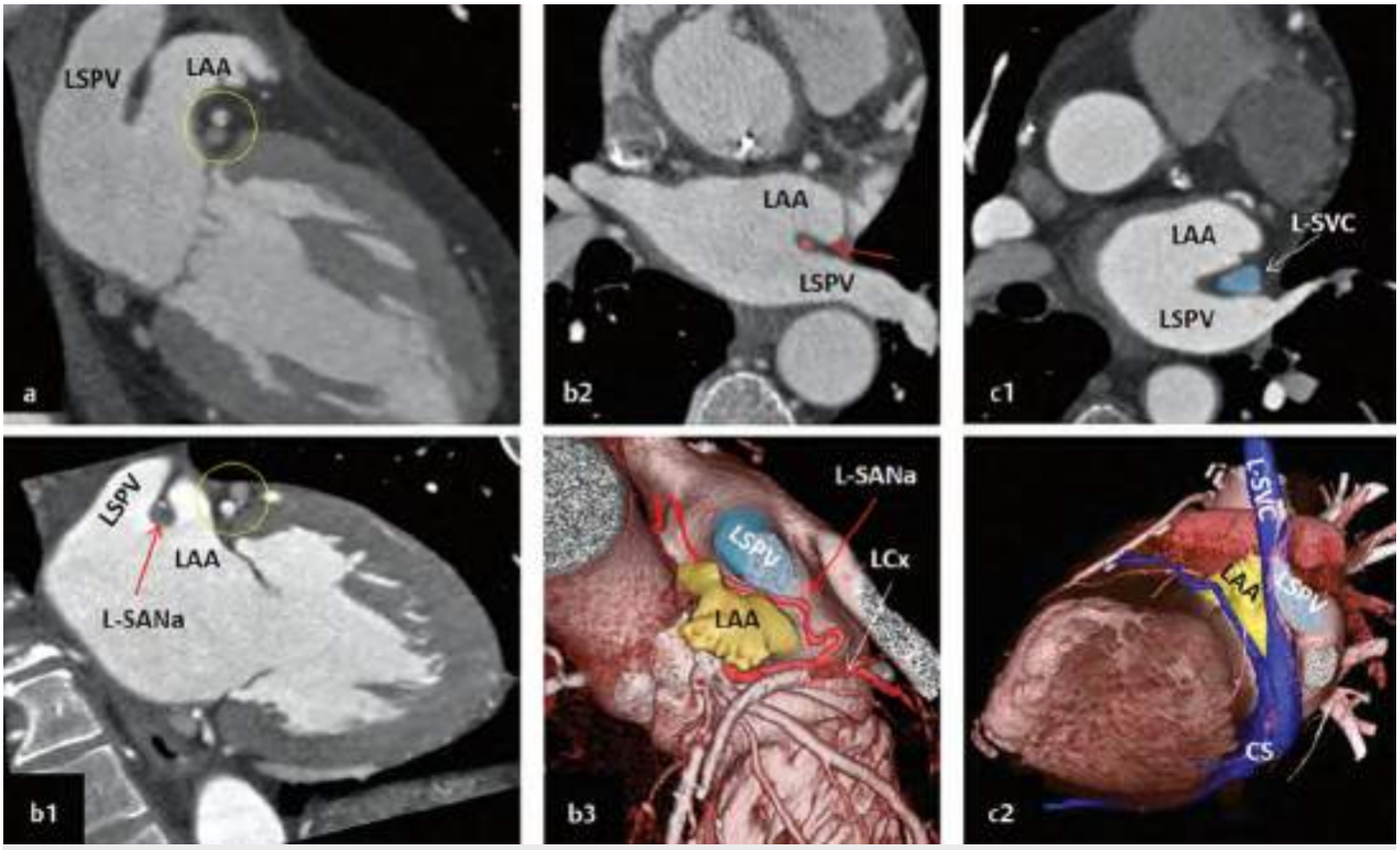

Fig. 12.47 Relationship of vessels with the left atrial appendage (LAA). (**a**) and (**b1**) show the left two-chamber CT images showing the anatomical course of the left circumflex artery and great cardinal vein (*within the yellow circle*) in the atrioventricular groove and inferior to the neck of LAA. **(b1, b2, b3)** In the order, two chambers, axial, and left lateral volume-rendered CT images showing the anatomical course of the S-shaped left sinoatrial node artery (L-SANa) in the groove between the LAA and the left superior pulmonary vein (LSPV) (*red arrows*). The S-shaped variant of the left SANa is seen in 14% of individual and comprises 30% of the left SANa. **(c1, c2)** Axial and left lateral volume-rendered CT images showing a persistent left superior vena cava (L-SVC) passing between the LAA and LSPV until it connects to the coronary sinus (CS). This variant is seen in less than 1% of population but is more common in congenital heart disease.

12

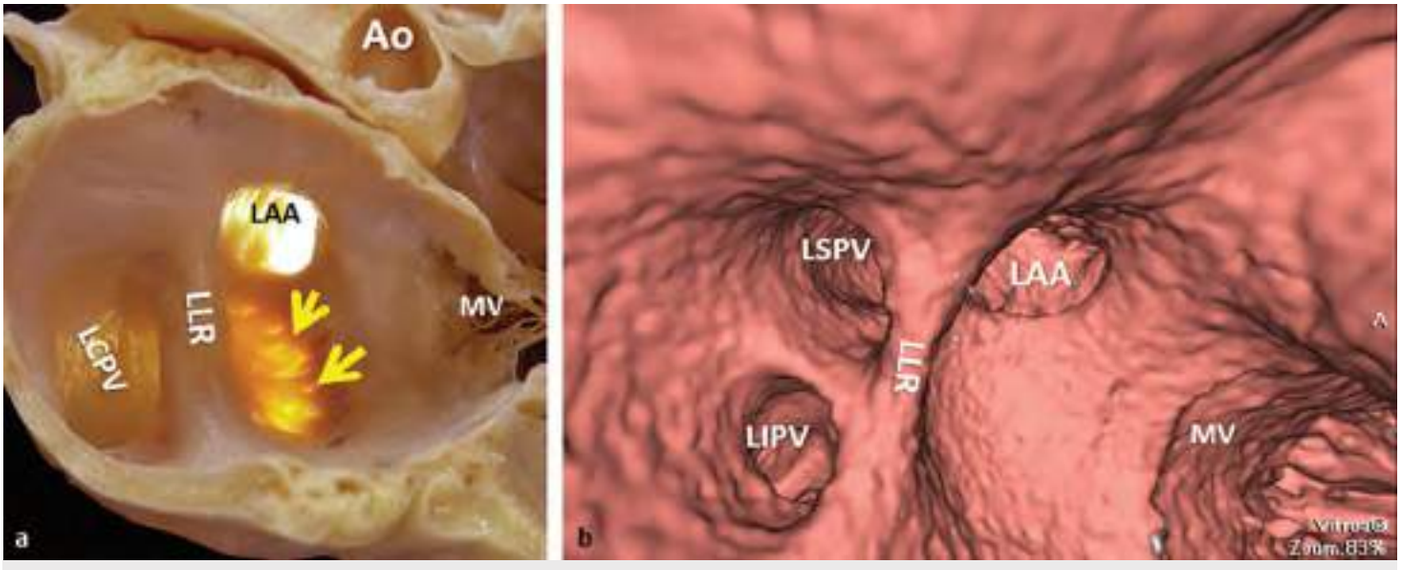

Fig. 12.48 Internal views of the left lateral aspect of the left atrium. (a) Endocardial visualization of the left posterolateral wall showing prominent left lateral ridge (LLR) and pectinate muscle trabeculations (*yellow arrows*) extending inferiorly from the left atrial appendage (LAA) to the vestibule of the mitral valve (MV). Transillumination in this specimen shows the atrial wall becoming exceptionally thin. **(b)** Endoscopic CT angiography view of the left posterolateral wall shows the relationship of the left superior pulmonary vein (LSPV) and the ostium of the LAA. In this example, both are located at the same level. The LLR is relatively thin. Ao, aorta; LIPV, left inferior pulmonary vein; MV, mitral valve; LCPV, left common pulmonary vein.

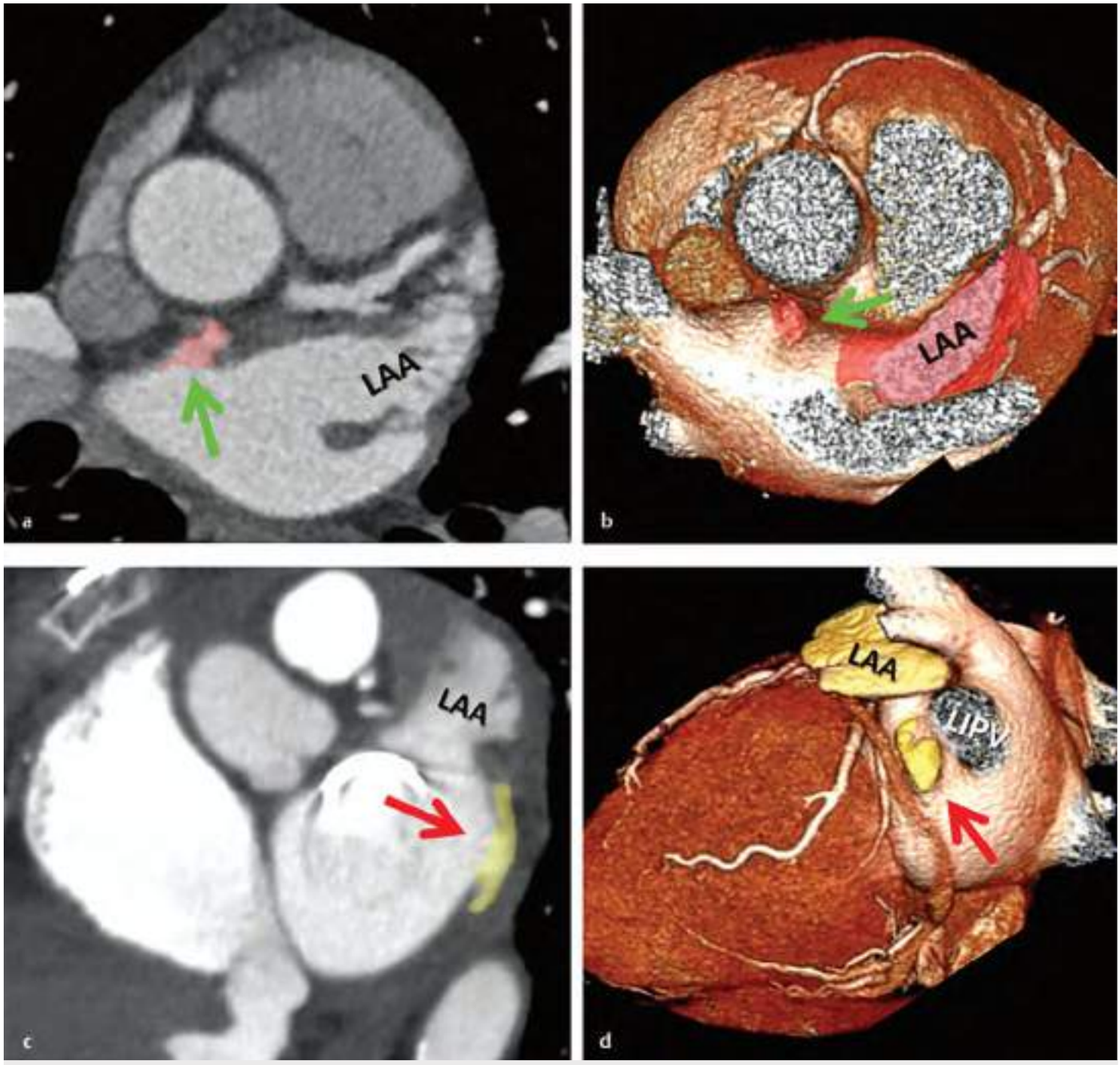

Fig. 12.49 Small accessory appendages are common findings in the left atrial wall presenting as small outpouchings with irregular margin in the left atrial wall arising **(a)** and **(b)**. from the anterior wall (*green arrow*) of the left atrium or **(c)** and **(d)** the mitral isthmus (*red arrows*). The left atrial isthmus is the area between the orifice of the left inferior pulmonary vein (LIPV) and the posteroinferior margin of mitral annulus.

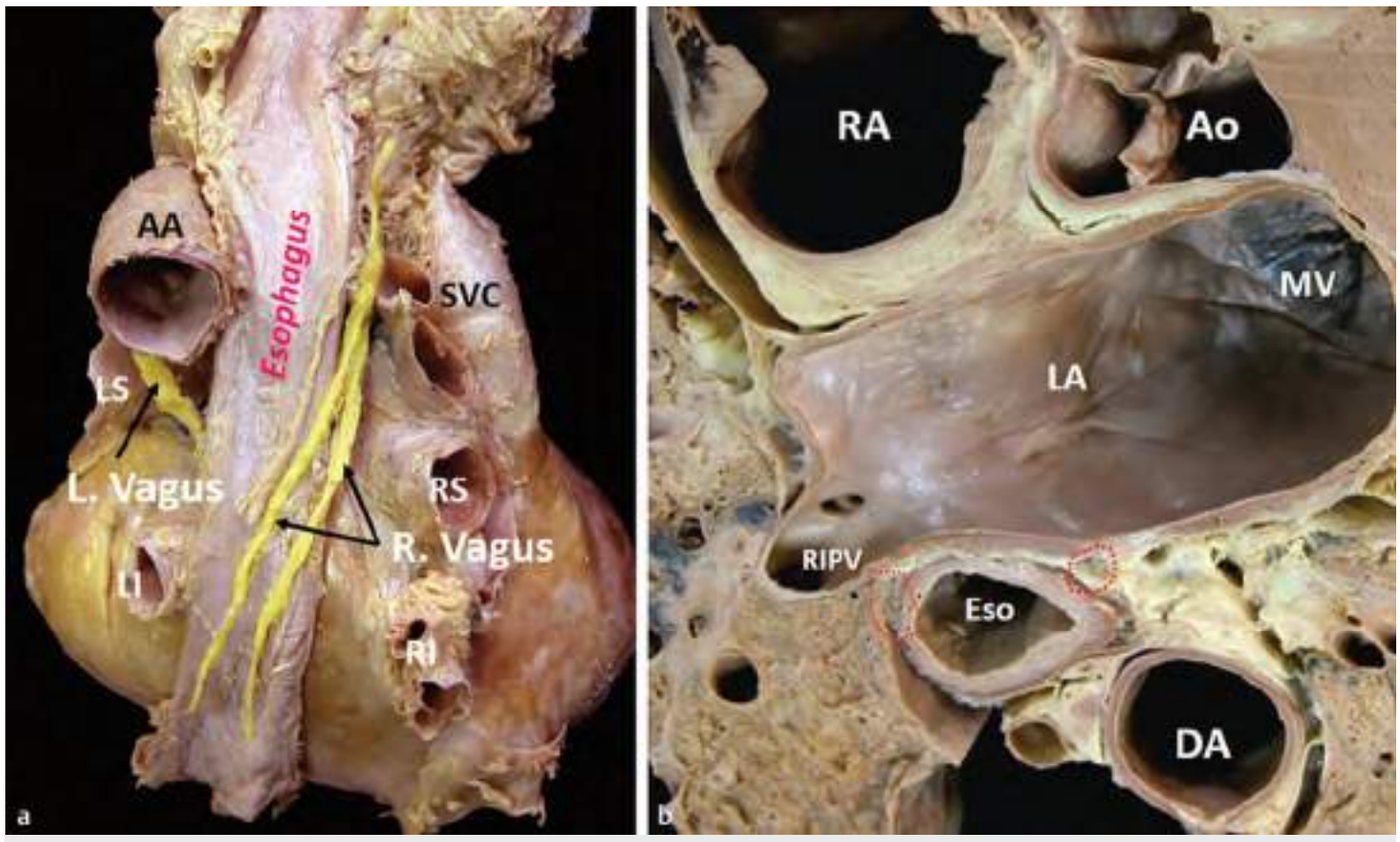

Fig. 12.50 (a) Thoracic organs viewed from the back after removal of the descending thoracic aorta to show the course of the esophagus in situ and its relationship to the right (R) and left (L) vagus nerves. **(b)** Transthoracic section through a cadaver showing the locations of the esophagus, the descending aorta, and the vagus nerves (*red dashed circles*). Note the minimal distance between the endocardial surface of the right inferior pulmonary vein (RIPV). Ablation procedures of the left atrium can damage the esophagus and vagal nerves. Pulmonary veins: LS, left superior; LI, left inferior; RS, right superior; RI, right inferior; Ao, aorta; AA, ascending aorta; DA, descending aorta; SVC, superior vena cava; LA, left atrium; RA, right atrium.

12

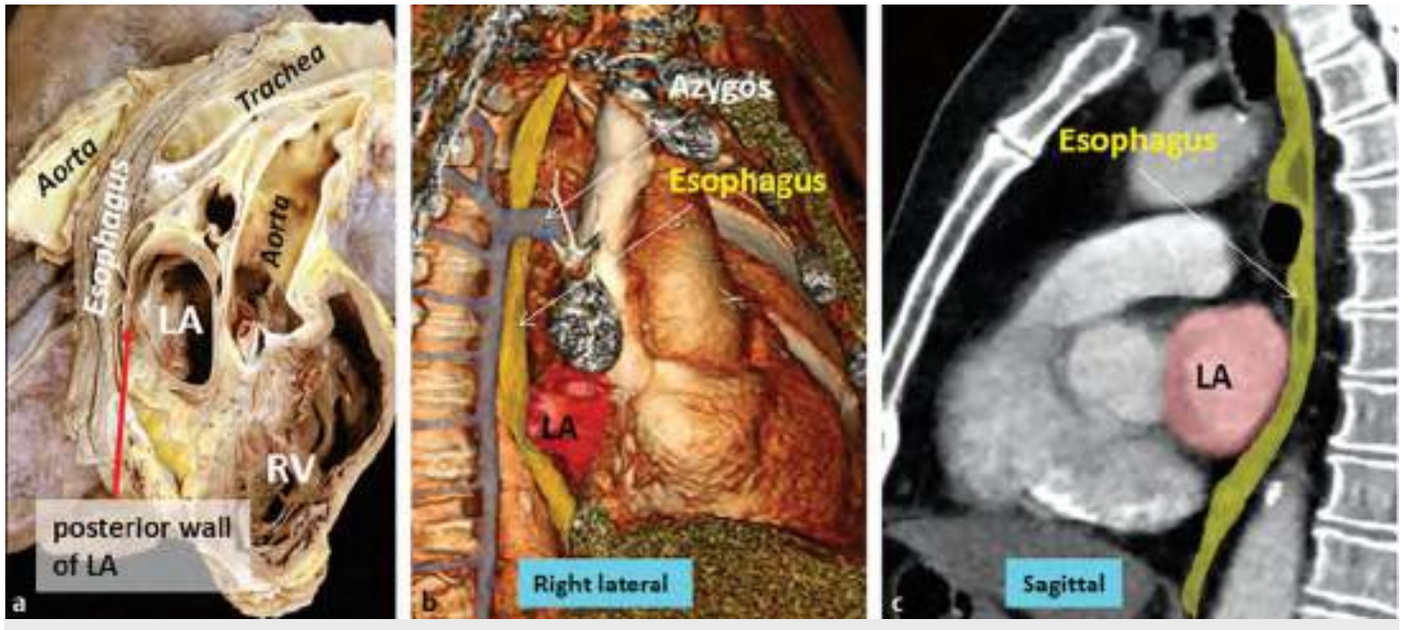

Fig. 12.51 **(a)** Sagittal section through the heart and esophagus showing the relationship of the posterior wall of the left atrium (LA) and the esophagus. **(b)** Right lateral volume-rendered CT angiography and **(c)** sagittal CT of chest show the relationship of the esophagus (*yellow*) to the left atrium (*red*). The azygos is shown in blue. RV, right ventricle.

Branches of the pulmonary plexuses form the posterior and anterior esophageal plexuses which enter the abdomen through the esophageal diaphragmatic opening to become the posterior and anterior vagal trunks that innervate the stomach and pyloric canal and the digestive tract as far as the proximal part of the colon.[61] Thermal injury may involve the periesophageal vagal nerves resulting in a syndrome of acute delayed gastric emptying.[62]

The phrenic nerves lie along the lateral mediastinum and run from the thoracic inlet to the diaphragm (▶ Fig. 12.52). Phrenic nerve injury results from direct thermal injury, usually to the right phrenic nerve, which is located lateral to the SVC and anterior to the right superior pulmonary vein.[63,64] Less frequently, ablation within the LAA can result in the left phrenic nerve damage which may pass close to the apex of the LAA in 30% of the hearts.[63] On the other hand, the left phrenic nerve passes close to the LV. CT coronary angiography can demonstrate the left phrenic neurovascular bundle as it passes over the LV pericardium in two-thirds of the studies[65] (▶ Fig. 12.52).

◆ Interatrial Septum

The true atrial septum is limited to the floor of the membranous fossa ovalis and its immediate muscular rim at the anteroinferior margin, which is confluent with the apical part of Koch's triangle. The floor of the fossa ovalis represents the embryonic primary atrial septum (septum primum) which fuses to the remainder of the septal wall within the first 2 years of life. Fusion is incomplete in about 25% of people, leaving a PFO[66] (▶ Fig. 12.53). The muscular rim (also known as the limbus) of the superior, inferior, and posterior margins of the fossa ovalis is formed by the infolding of the right and left atrial walls. The epicardial fat fills the interatrial groove between the infolding walls. To understand the above concepts, a review of the embryology of the septum is necessary.

Atrial septation is a complex process involving several tissue components.[67] Atrial septation starts with the appearance of a ridge in the atrial roof called primary atrial septum (septum primum). The primary septum grows toward the cushions of the AV canal. The leading edge of the primary septum (mesenchymal cap) connects to another structure known as "vestibular spine" (▶ Fig. 12.54). The vestibular spine is a mesenchymal protrusion from the mediastinum into the common atrium that closes the gap of the primary atrial foramen (ostium primum) between the primary septum and the inferior endocardial cushions of the AV canal. Later muscularization of the vestibular spine and the mesenchymal cap occur, producing the secondary component of the real atrial septum. Along with above developments, the attachment of the primary septum to the atrial roof begins to break down to form the secondary atrial foramen (foramen ovale/ostium secundum).[68] The remainder of the primary atrial septum becomes the flap valve of the foramen which is attached to the vestibular spine anteriorly (▶ Fig. 12.54). With further development, infolding of the posterosuperior wall of RA close to pulmonary venous sinus of the LA occurs to form a wall previously known as septum secundum. As the name implies, this infolding only represents invagination of the atrial wall with epicardial fat sandwiched between the infolded walls (▶ Fig. 12.55). Therefore, the superior, posterior, and inferior muscular rims of the fossa ovalis are formed by infolded atrial wall (▶ Fig. 12.56). These rims are not real septum and more correctly defined as the "interatrial groove" and the rim attached to the membranous fossa ovalis commonly named as the "limbus" (▶ Fig. 12.55). Only the anterior/anteroinferior rim formed by the vestibular spine is a real muscularized septum buttressing the atrial septum to the AV junctions (ventral atrial buttress) (▶ Fig. 12.54). Therefore, inadvertent needle or catheter puncture outside the limited margins of the limbus during transseptal interventions results in perforation into the pericardial sinuses. At particular risk is the puncture of the anterior rim of the interatrial groove, which is in close aortic valve (▶ Fig. 12.56). Excess accumulation of the epicardial fat in the interatrial grooves results in thickening of the atrial wall which may reach up to 2 cm in thickness. Thickness of more than 2 cm is defined as lipomatous hypertrophy (▶ Fig. 12.56).

Defect in the primary atrial septum is called "ostium secundum" defect. Defect in the vestibular spine is called vestibular defect.[69] Abnormal growth of the vestibular spine and mesenchymal cap can lead to ostium primum atrial septal defect (ASD). Ostium primum ASD is now categorized in AV canal defects because of associated AV cushions defects.

Patent Foramen Ovale

Closure of the septum primum is complete when the valve becomes adherent to the rim to form the fossa ovalis. The size of fossa ovalis and its margins may vary greatly. In 25 to 35% in autopsy studies,[66,70] the seal is incomplete leaving a crevice at the anterosuperior quadrant of the rim that allows a probe to be passed obliquely from the RA into the LA (PFO) (▶ Fig. 12.57). This nonfusion creates the tunnel-like PFO orientated in a craniocaudal, PA, and right-to-left axis.[71] The incidence and size of PFO do not differ with gender but varies significantly with age; 34% of PFOs occurs in the first three decades, 25% in the 4th to 8th decades, and 20% in the 9th and 10th decades.[66] The size of PFO increases progressively from a mean of 3.4 mm in the first decade to 5.8 mm in the tenth decade (possibly because smaller defects seal with age).

Normally, the PFO is closed by the higher left atrial-to-right atrial pressure gradient. If the left atrial pressures rise (i.e., pulmonary hypertension), a small clot may pass directly from the RA into the left side and resides in different organs such as brain to cause a stroke. This condition is called paradoxical embolism. The presence of shunting through the PFO not only depends on the transatrial pressure gradient, but also likely relates to anatomical features of the PFO. These include the size of opening into the RA, length of the PFO tunnel, and the extent of excursion of the flap membrane. Moreover, the risk of stroke appears to increase in the presence of structures that direct flow toward a PFO (i.e., prominent Eustachian valve) or hemodynamic changes that increase right-sided pressure (i.e., large pulmonary embolism) (▶ Fig. 12.28, ▶ Fig. 12.29). PFO tunnel length is another important factor in increasing the chance of right-to-left shunting. In a recent MDCT study of asymptomatic individuals, 92% of the shunts occurred with a PFO tunnel length of 6 mm or less.[70] This information may be important in patients being evaluated for possible candidates of percutaneous closure. When the flap length is very short, a bidirectional shunt is more probable. In a

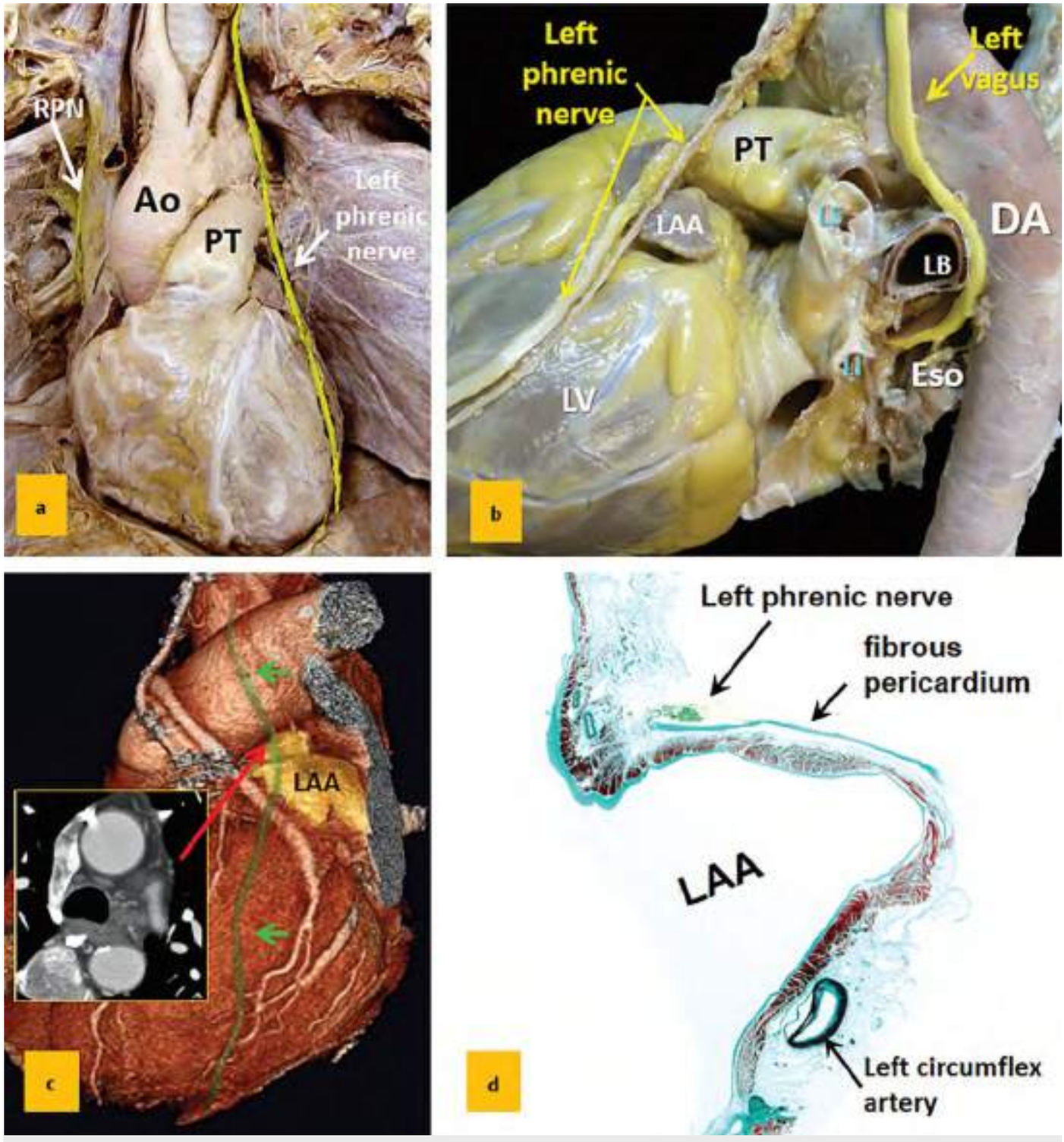

Fig. 12.52 Phrenic nerves. **(a)** Frontal view of a cadaver dissection shows the course of the right and left phrenic nerves. **(b)** Dissection of the left phrenic nerve, which descends onto the fibrous pericardium anterior and lateral to the aortic arch, alongside the distal part of pulmonary trunk (PT), left atrial appendage (LAA), and the lateral wall of the left ventricle (LV). **(c)** Left lateral volume-rendered CT image of the heart showing the anatomical course of left phrenic neurovascular bundle (shown in *green* and demarcated by *green arrows*) in relation to the LAA. Corresponding two-dimensional axial CT at the superior margin of the LAA (*red arrow*) is also shown (*inlay image*). Neurovascular bundle is usually seen as a single trunk anterior or over the body of LAA. In 23% of individual the nerve moves over the neck of LAA. **(d)** Microscopic cross-section of the LAA showing the left phrenic nerve outside the fibrous pericardium. LS, left superior pulmonary vein; Ao, aorta; Eso, esophagus; DA, descending aorta; LB, left bronchus; RPN, right phrenic nerve; LI, left inferior pulmonary vein.

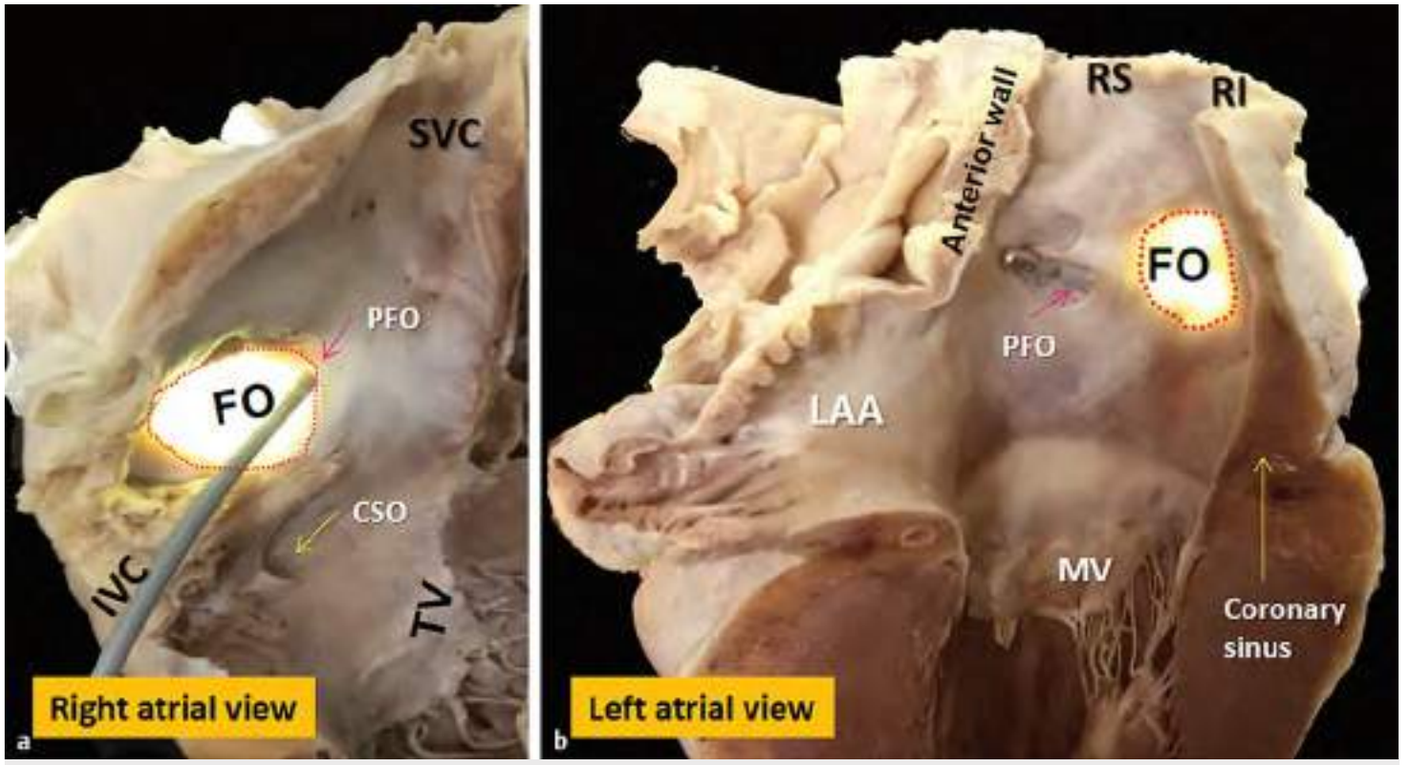

Fig. 12.53 Views of the atrial septum from the right and left sides showing patent foramen ovale. **(a)** Right septal view of the right atrium showing by transillumination the flap valve of the fossa ovalis (FO) and the muscular rim that surrounds it on the right atrial aspect. In this heart, there is probe patency of the oval fossa, leaving a gap in the anterosuperior. The gap can allow a catheter to be slipped between the rim and the valve to enter the left atrium. **(b)** Note by transillumination the location of the FO in the left side of the septum. CSO, coronary sinus ostium; LAA, left atrial appendage; MV, mitral valve; PFO, patent foramen oval; RS, right superior pulmonary vein; RI, right inferior pulmonary vein; SVC, superior vena cava.

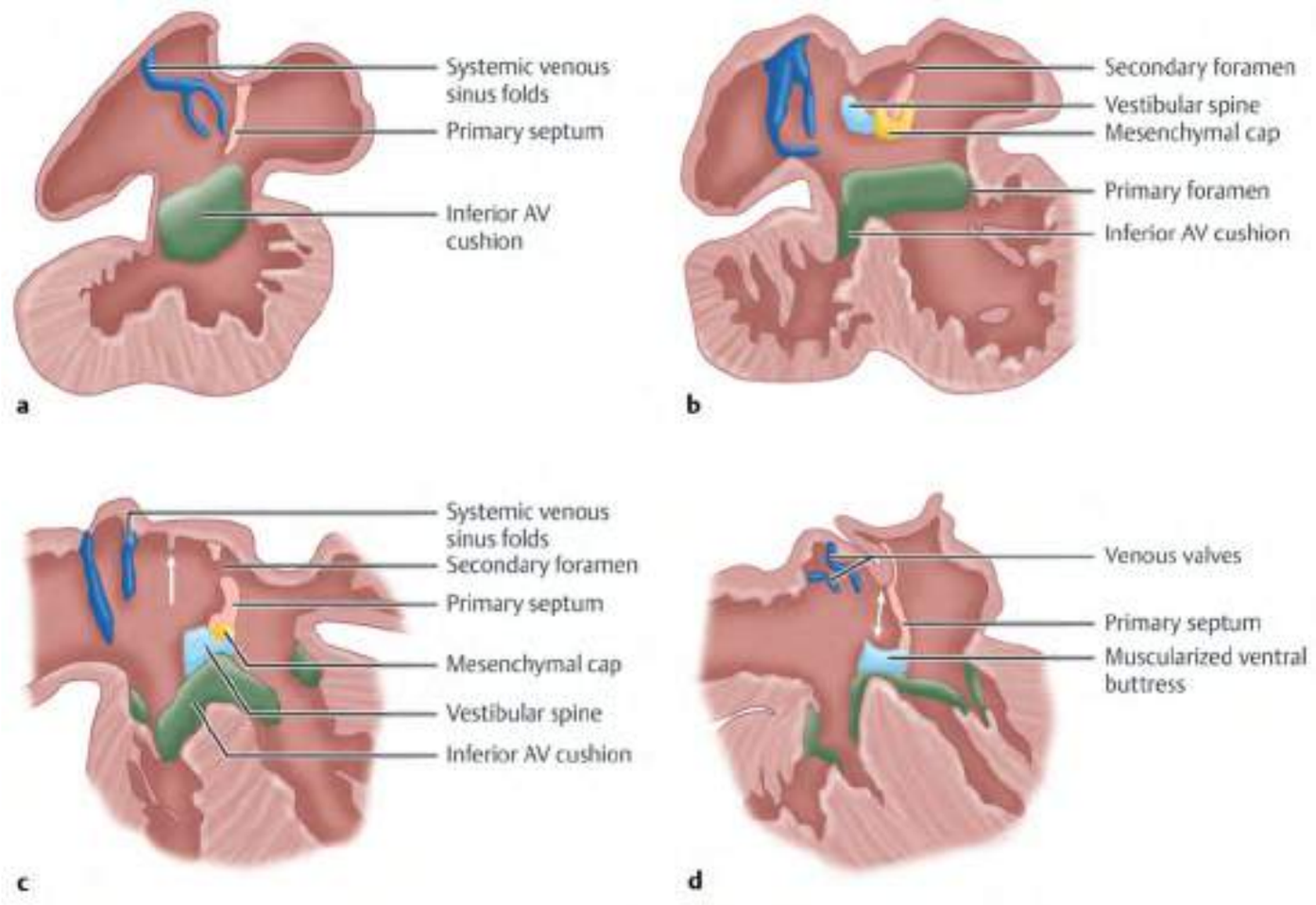

Fig. 12.54 Illustrations of four chambers of the heart showing development of the atrial septum. **(a)** The sections are from episcopic datasets of developing mouse embryos at embryonic day E11.5. The primary septum arising from the atrial roof. **(b)** E13.5, breakdown of the primary septum occurs at the atrial roof side. The ventral and caudal margins of the primary septum is formed by the muscularized vestibular spine (green) and mesenchymal cap (orange). **(c)** Later phase. The primary foramen is now closed by the vestibular spine. The secondary foramen remains open. Cranial rim is seen at the atrial roof (*arrow*). **(d)** E18.5. The opening of the oval fossa is seen (*double-headed arrow*). Its dorsal rim is formed by an infolding of the atrial walls at the level of the muscular ridge seen in the atrial roof forming the interatrial groove filled with extracardiac fat **(c)**. The walls of the interatrial groove are formed by the right atrium on the right and the pulmonary veins on the left. This fold closes the secondary foramen.

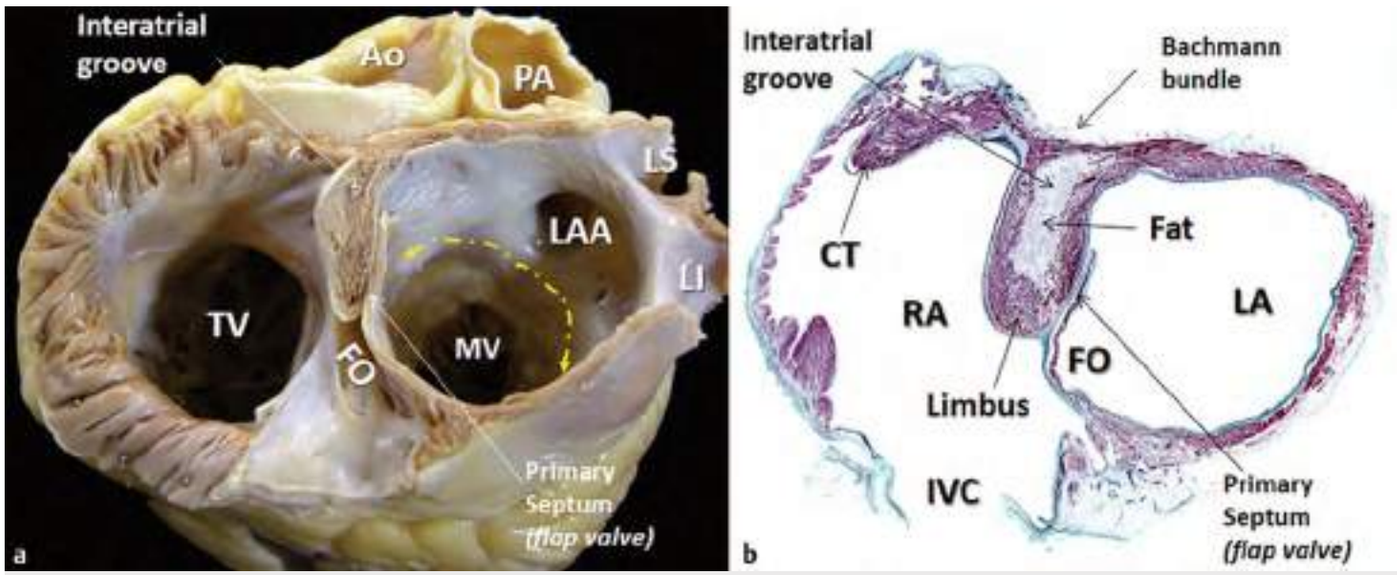

Fig. 12.55 **(a)** Short-axis section across the atrial chambers above the atrioventricular valves. The vestibule (*dotted yellow line*) of the left atrium (LA) and the nonuniform thickness of the left atrial wall are seen. **(b)** Cross-section at the level of the fossa ovalis (FO). Interatrial muscle of Bachmann's bundle is nicely shown. Ao, aorta; CT, crista terminalis; IVC, inferior vena cava; LAA, left atrial appendage; LI, left inferior pulmonary vein; LS, left superior pulmonary vein; MV, mitral valve; PA, pulmonary artery; RA, right atrium; TV, tricuspid valve.

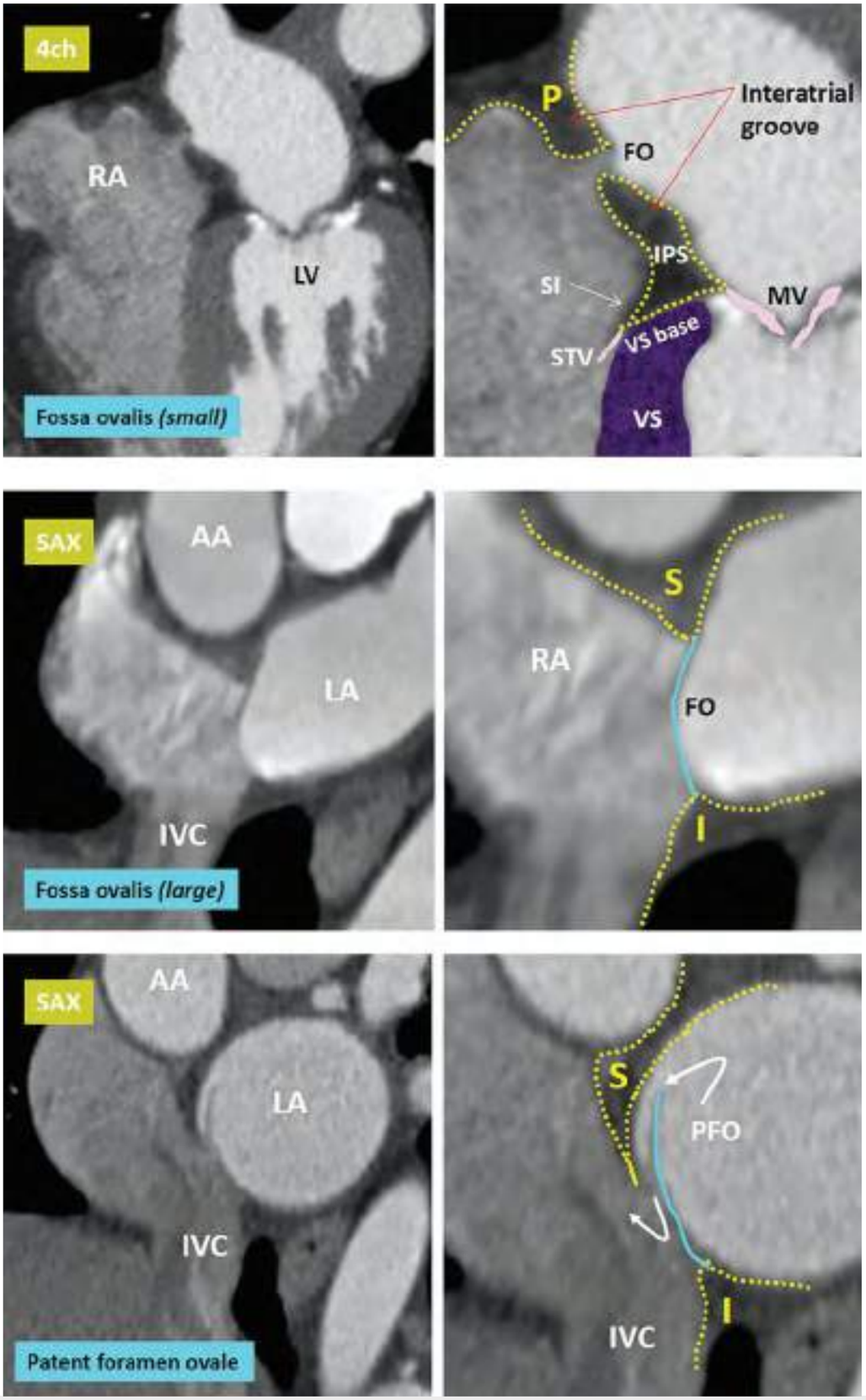

Fig. 12.56 Anatomy of the interatrial septum, fossa ovalis (FO), and patent foramen ovale (PFO). Four-chamber (4ch) and short-axis (SAX) views of the heart in different patients. Magnified views with highlighted margins are shown on the left side. 4ch images show a small FO. The interatrial groove is large and filled with fat (lipomatous hypertrophy of septum). Middle row SAX images show a large FO with completely sealed margin. Lower row SAX images show a well-structured PFO. The septum primum (*blue line*) is fused to the inferior rim of the FO and extends superiorly as a flap. The superior (S) and the inferior (I) rims of the FO are formed by infolding of the right atrial wall (interatrial groove) filled with extracardiac fat. The infolding of the right atrial wall overlaps the flap of septum primum, forming a narrow tunnel (*white arrows*) through which a probe can be passed called PFO. AA, ascending aorta; IVC, inferior vena cava; IPS, inferior pyramidal space; LA, left atrium; LV, left ventricle; MV, mitral valve; P, posterior; RA, right atrium; SI, septal isthmus; STV, septal tricuspid isthmus; VS, ventricular septum.

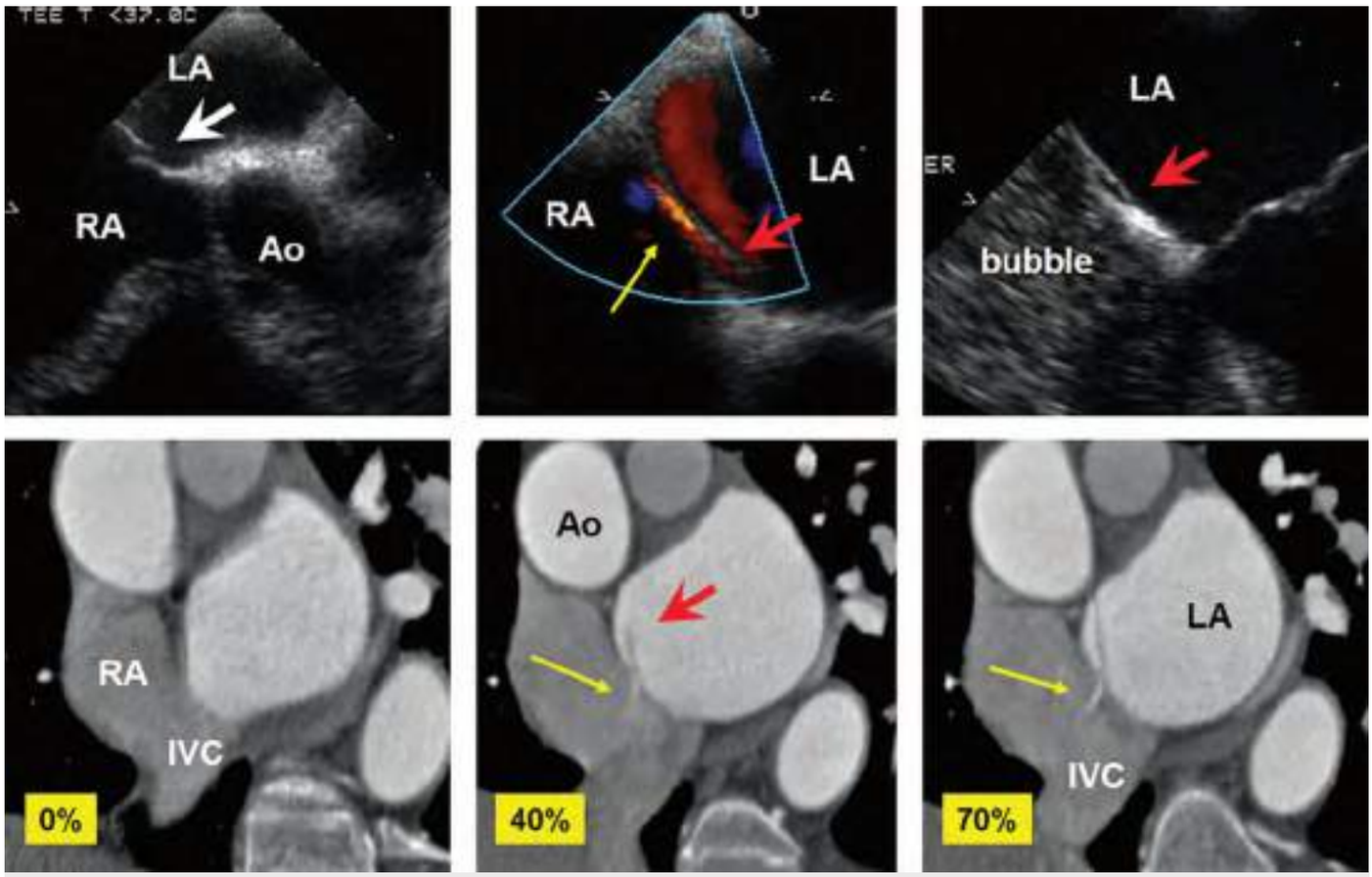

Fig. 12.57 Patent foramen ovale (PFO) and flow dynamics through it shown by echocardiography and CT. Comparison of transesophageal echocardiography (TEE) and CT angiogram in a patient with small interatrial left-to-right shunt. Upper row panel demonstrates recorded TEE images obtained before contrast injection (*left*), with color Doppler (*middle*), and after injection of agitated saline (*right*). The flap valve is shown by thick red arrows. PFO is shown on precontrast and color Doppler images but no right-to-left shunt was detected on the bubble study. Note, the jet of color flow indicating a left-to-right shunt (*thin yellow arrow*). Lower row images are short-axis views of the CT angiogram in the same patient. The jet of left-to-right PFO shunt (*yellow thin arrow*) is shown at 40% (systole) and 70% (mid-diastole) intervals but is not shown during 0% (atrial contraction) phase interval. With atrial contraction, the PFO flap valve is pushed against the atrial septum causing occlusion of the PFO tunnel. In the evaluation of PFO shunt with CT it is important to review all recorded phases of cardiac cycle. Ao, aorta; IVC, inferior vena cava; LA, left atrium; RA, right atrium.

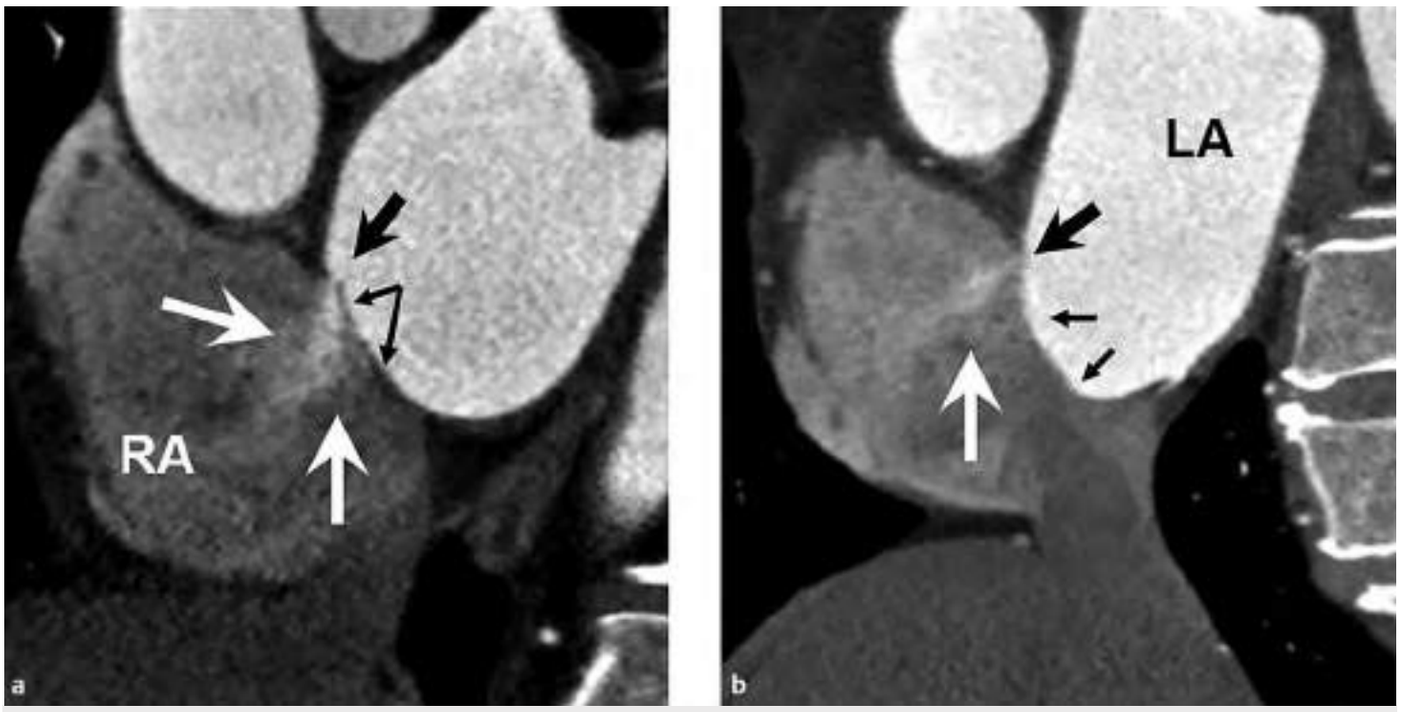

Fig. 12.58 Short-axis images show incompetent valves in patent foramen ovale (PFO) with free flow of contrast through the opening (*white arrows*). **(a)** The free flap valve is too short to cover the superior rim of the fossa ovalis (*large black arrow*). **(b)** Atrial septal aneurysm (*small arrows*) also demonstrates very short PFO tunnel (*large black arrow*) causing a left-to-right shunt (*white arrow*). LA, left atrium; RA, right atrium.

recent postmortem study by Ho et al,[72] two types of PFO were described: valve-competent and valve-incompetent. PFOs with a short, overlapping flap with an atrial septal aneurysm were classified as incompetent with high likelihood of bidirectional flow. Similar incompetent morphology has also been described using CT scanning in patients with a short PFO tunnel length or those with an atrial septal aneurysm[70] (▶ Fig. 12.58).

Atrial Septal Aneurysm

Atrial septal aneurysm is another important anatomical feature to consider in evaluating PFO. An atrial septal aneurysm is defined as a bulging of greater than 15 mm beyond the plane of the atrial septum[73] (▶ Fig. 12.59). Generally, protrusion in the RA is the more common (76%) and usually shows transient motion toward the LA during systole or with the Valsalva maneuver.[74] The incidence of atrial septal aneurysm is 4.6 to 10% by transesophageal echocardiography.[73,74] The prevalence of PFO is higher when an atrial septal aneurysm exists and may reach up to 30 to 60% (▶ Fig. 12.58). An atrial septal aneurysm can easily be assessed by CT and MRI. In one study with MDCT, an atrial septal aneurysm was seen in 4% of patients, and 63% of patients with atrial septal aneurysm were found to have a left-to-right shunt.[70]

◆ Right Ventricle

The RV in the normal heart lies behind the sternum. It is the most anteriorly located cardiac chamber and also forms the inferior border of the cardiac silhouette. In contrast to the near conical shape of the LV, the RV is more triangular in shape and wraps around the LV giving it a crescent-shaped appearance when viewed in short axis (▶ Fig. 12.3, ▶ Fig. 12.8, ▶ Fig. 12.60). The superior aspect of the RV is connected to the pulmonary valve. The anterior and inferior walls are the free walls of the RV facing the sternum and the diaphragm, respectively (▶ Fig. 12.61). The right lateral wall is connected to the tricuspid valve and RA in its posterior–inferior margin and appears free, facing the right lung, along its anterior superior margin. The medial and posterior RV walls are formed by the ventricular septum.

Traditionally, the RV is divided into the sinus and conus parts. The lower margin of the moderator band is designated as the border between the smooth conus and the trabeculated sinus (▶ Fig. 12.62, ▶ Fig. 12.63). The RV has also been divided into basal-, mid-, and apical levels and each level is subdivided into the anterior, lateral, and inferior wall segments. This segmental classification is primarily used for imaging purposes to address a specific vascular territory or perfusion abnormality or simply describe regional/segmental RV function/dysfunction.[75]

Current literature divides the RV and LV into three anatomical and functional subunits portions: the inlet, apical trabecular, and outlet portions[76,77] (▶ Fig. 12.62, ▶ Fig. 12.63). The inlet portion of the RV surrounds and supports the tricuspid valve and its tension apparatus. Therefore, the inlet extends from the tricuspid valve to the insertions of the papillary muscles onto the ventricular wall. The trabecular portion of the RV involves the distal body and apex and is characterized by coarse trabeculations, a typical feature of the RV. At the apex, the wall of the ventricle is quite thin and vulnerable to perforation by cardiac catheters and pacemaker electrodes. The right outflow tract or infundibular portion extends to the pulmonary valve and is generally free of trabeculations (▶ Fig. 12.64).

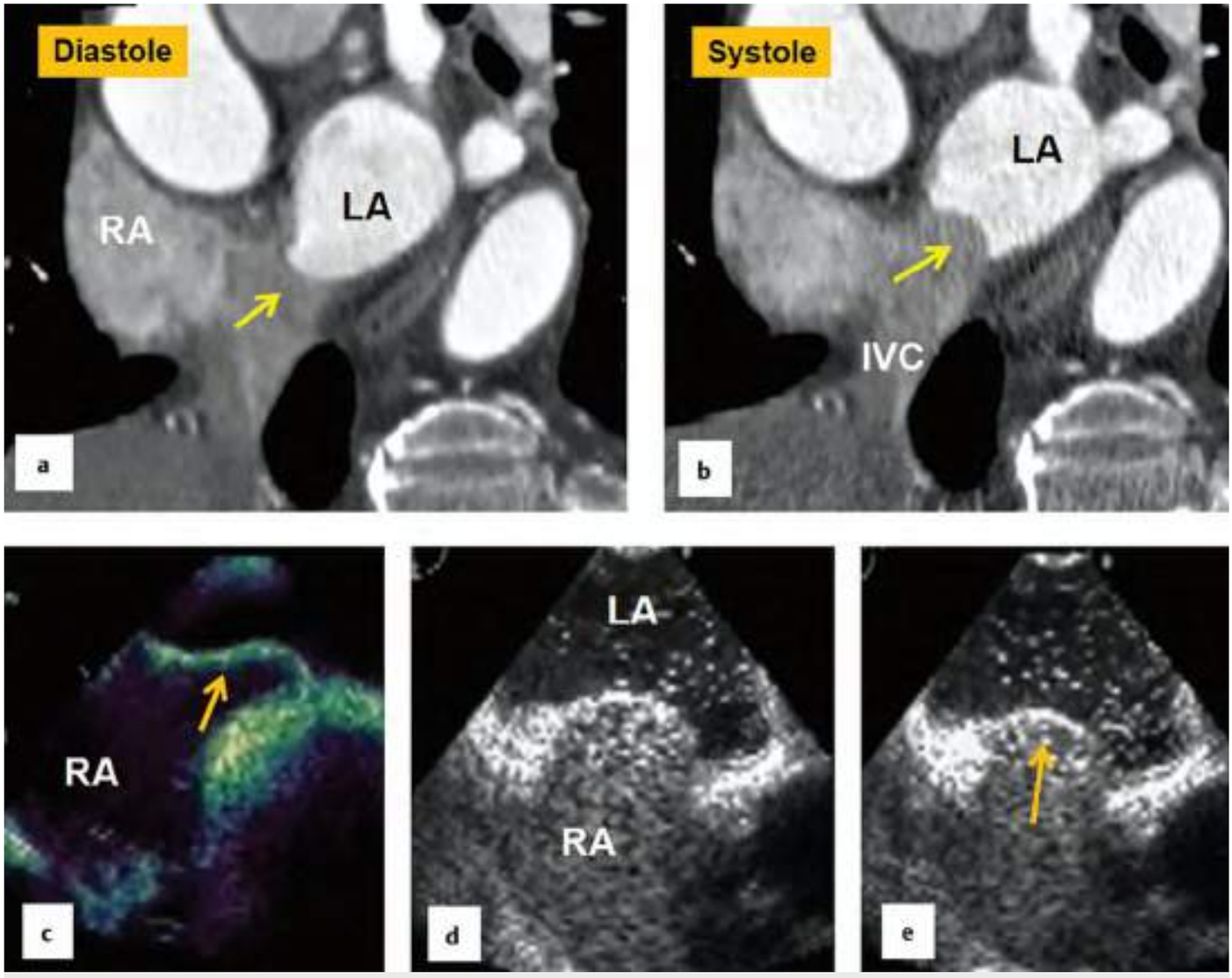

Fig. 12.59 Atrial septal aneurysm (ASA). **(a, b)** Short-axis CT angiograms demonstrate an ASA (*arrows*) protruding into the right atrium (RA) in diastole and toward the left atrium in systole. Right atrial protrusion of ASA is the most common morphology and usually shows transient motion toward the left atrium (LA) during systole (*arrow*) or with the Valsalva. **(c)**, **(d)**, and **(e)** are transesophageal echocardiography (TEE) images of ASA (*arrows*) with a right-to-left shunting during agitated saline contrast study showing bubble entered into the LA **(d)** and **(e)**.

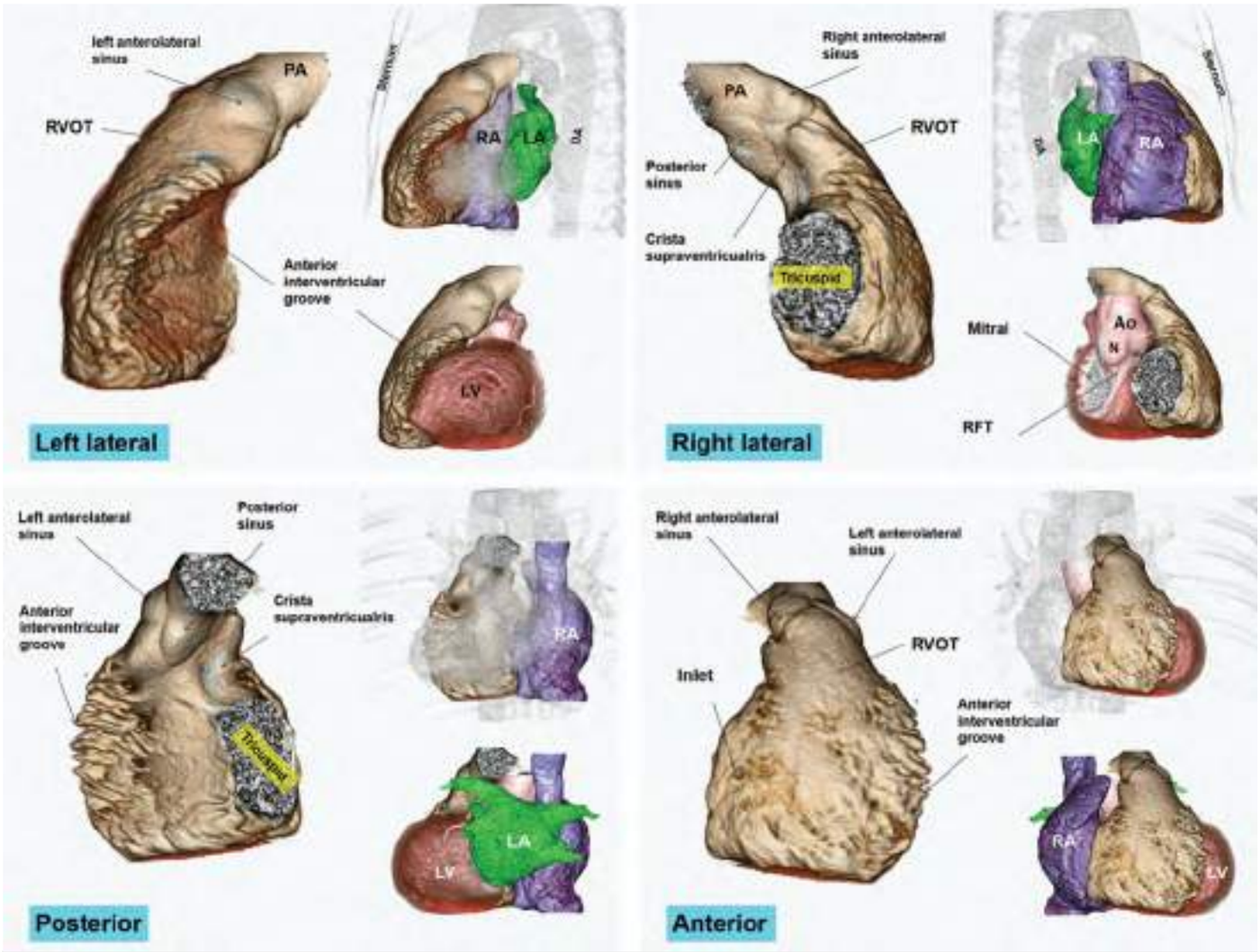

Fig. 12.60 Right ventricular walls. Ao, aorta; DA, descending aorta; LA, left atrium; LV, left ventricle; N, noncoronary sinus; RA, right atrium; RV, right ventricle; RVOT, right ventricular outflow tract; RFT, right fibrous trigone; PA, main pulmonary artery.

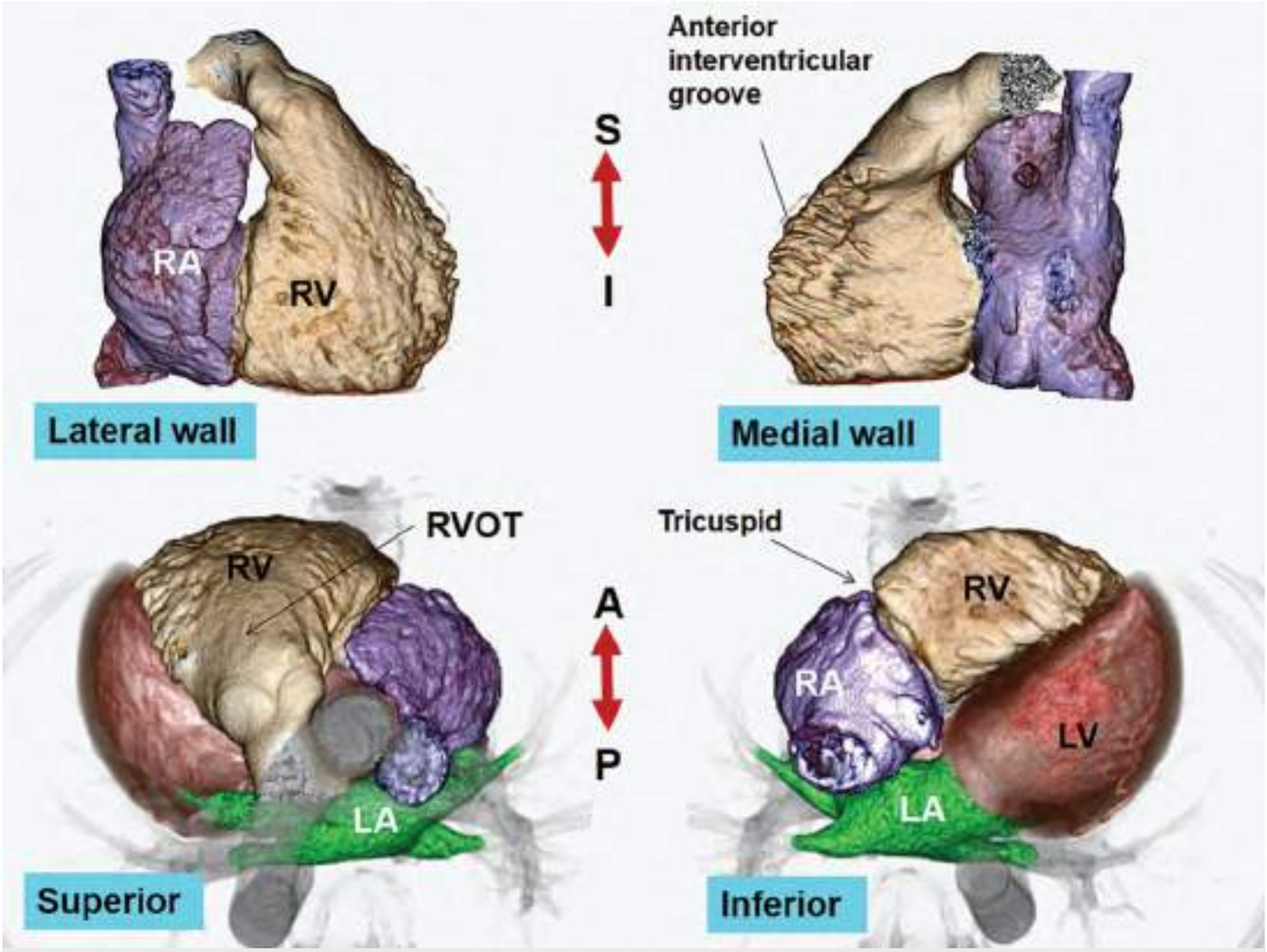

Fig. 12.61 Anatomical position of the cardiac chamber in the chest. Walls of the right ventricle are shown in different projections. The anterior and inferior walls are the free walls of the RV facing the sternum and the diaphragm, respectively. The right lateral wall is connected to the tricuspid valve inferiorly. The medial and posterior RV walls are formed by the ventricular septum. LA, left atrium; LV, left ventricle; RA, right atrium; RV, right ventricle; RVOT, right ventricular outflow tract; A, anterior; I, inferior; P, posterior; S, superior.

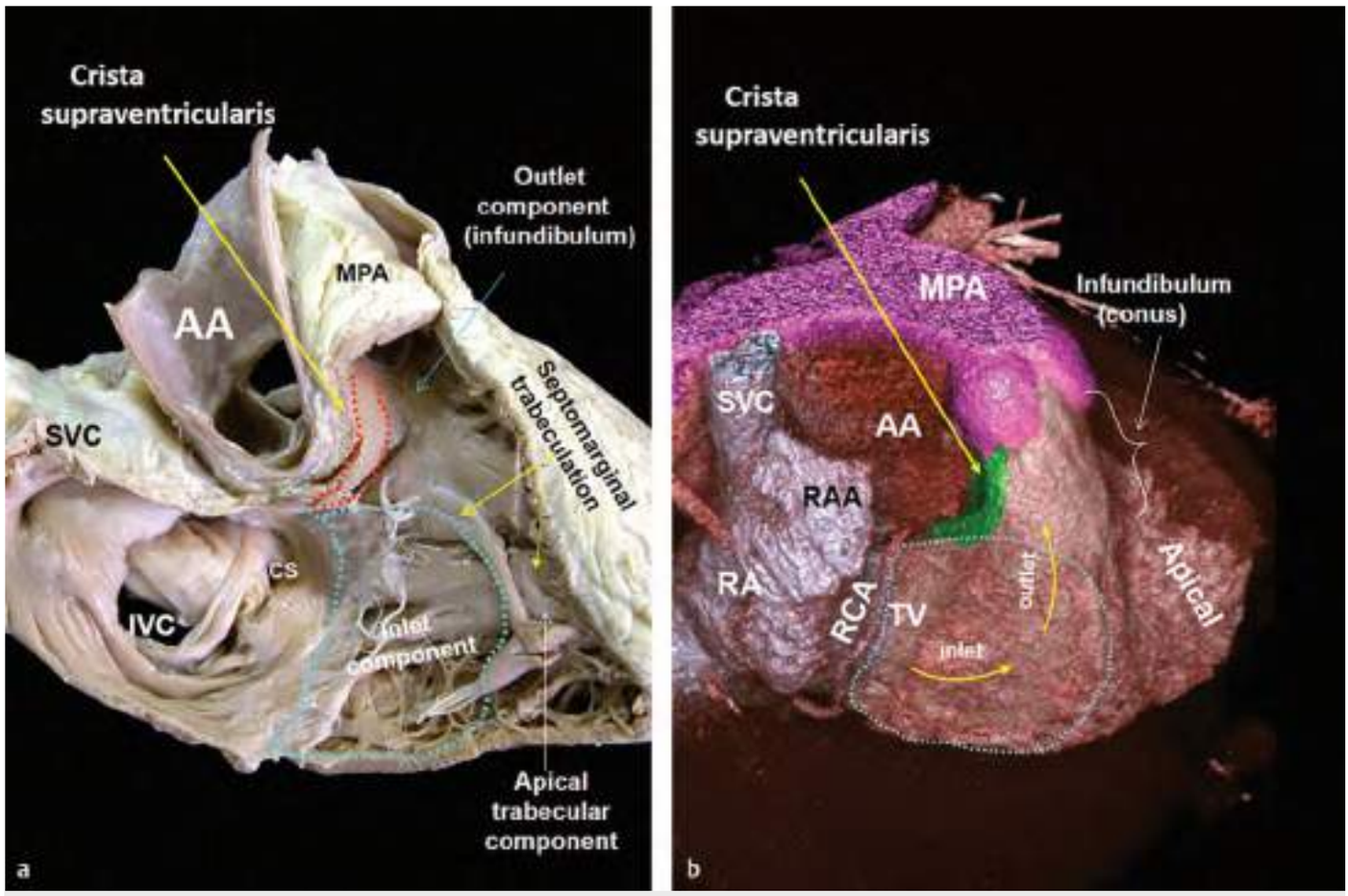

Fig. 12.62 Right anterior oblique views (two chamber) of the right heart are shown. **(a)** Cadaveric specimen. **(b)** Volume-rendered CT image of the right heart. The right ventricle comprises of three components: the inlet, apical trabecular, and outlet portions. The outflow tract separates the tricuspid and pulmonary valves. The crista supraventricular is posterior wall of the infundibulum at the ventriculoinfundibular fold which is cradled between limbs of septomarginal trabeculation. It is separated from the right aortic sinus by epicardial fat. AA, ascending aorta; CS, coronary sinus; IVC, inferior vena cava; MPA, main pulmonary artery; RA, right atrium; RCA, right coronary artery; RAA, right atrial appendage; SVC, superior vena cava; TV, tricuspid valve.

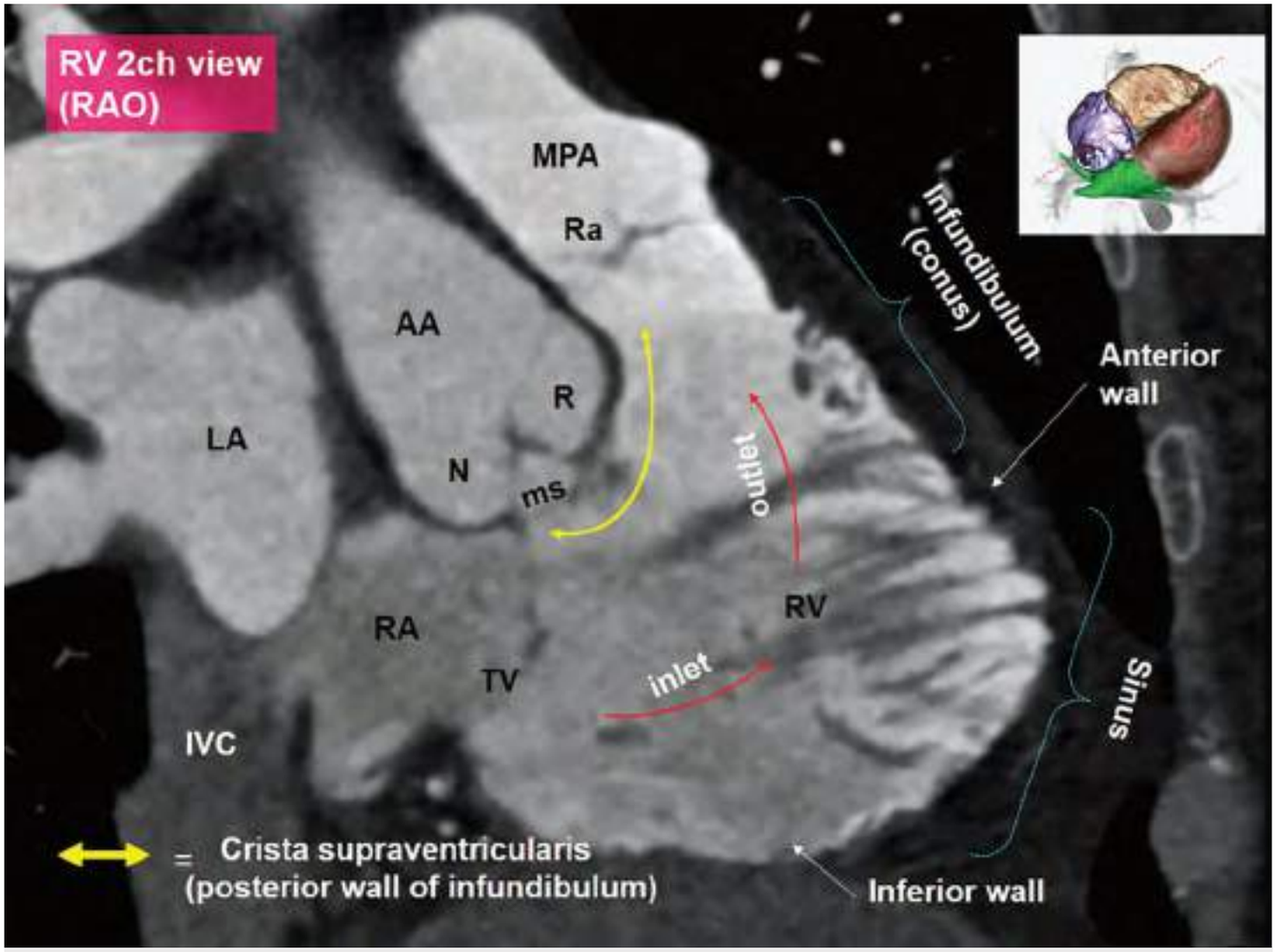

Fig. 12.63 Right ventricle components. Right anterior oblique view (two chamber) of the right heart is shown. The right ventricle (RV) can be divided into inflow and outflow segments. The outflow tract (the infundibulum or conus), separates the inflow and outflow valves. The axis of the orifices of the two segments roughly forms an angle of 60 degrees. The posterior wall of the infundibulum extends between the septal papillary muscle and the right anterior pulmonary sinus (Ra). It is in contact with the right coronary aortic sinus (R) but separated from it by the epicardial fat. Focal membranous segment of the posterolateral of the conus may exist in some cases causing of a focal aneurysmal bulge in this region when pressure in the RV is high. AA, ascending aorta; LA, left atrium; MS, membranous septum; MPA, main pulmonary artery; N, noncoronary aortic sinus; TV, tricuspid valve; RA, right atrium; IVC, inferior vena cava.

Fig. 12.64 Anatomical review of the right ventricular outflow tract (RVOT). Short-axis views of this region are shown at the pulmonary valve (PV) and two levels below it. Reference cuts are shown by different colors on the two-chamber view of the right ventricle (2ch-RV). The RVOT extends between the moderator band and the pulmonary valve (PV). It is a smooth-walled conduit and characterized on the side by the septoparietal muscle trabeculations (*yellow arrows*) with variable thickness. AA, ascending aorta; AV, aortic valve; LVOT, left ventricular outflow tract; LA, left atrium; MV, mitral valve; RA, right atrium.

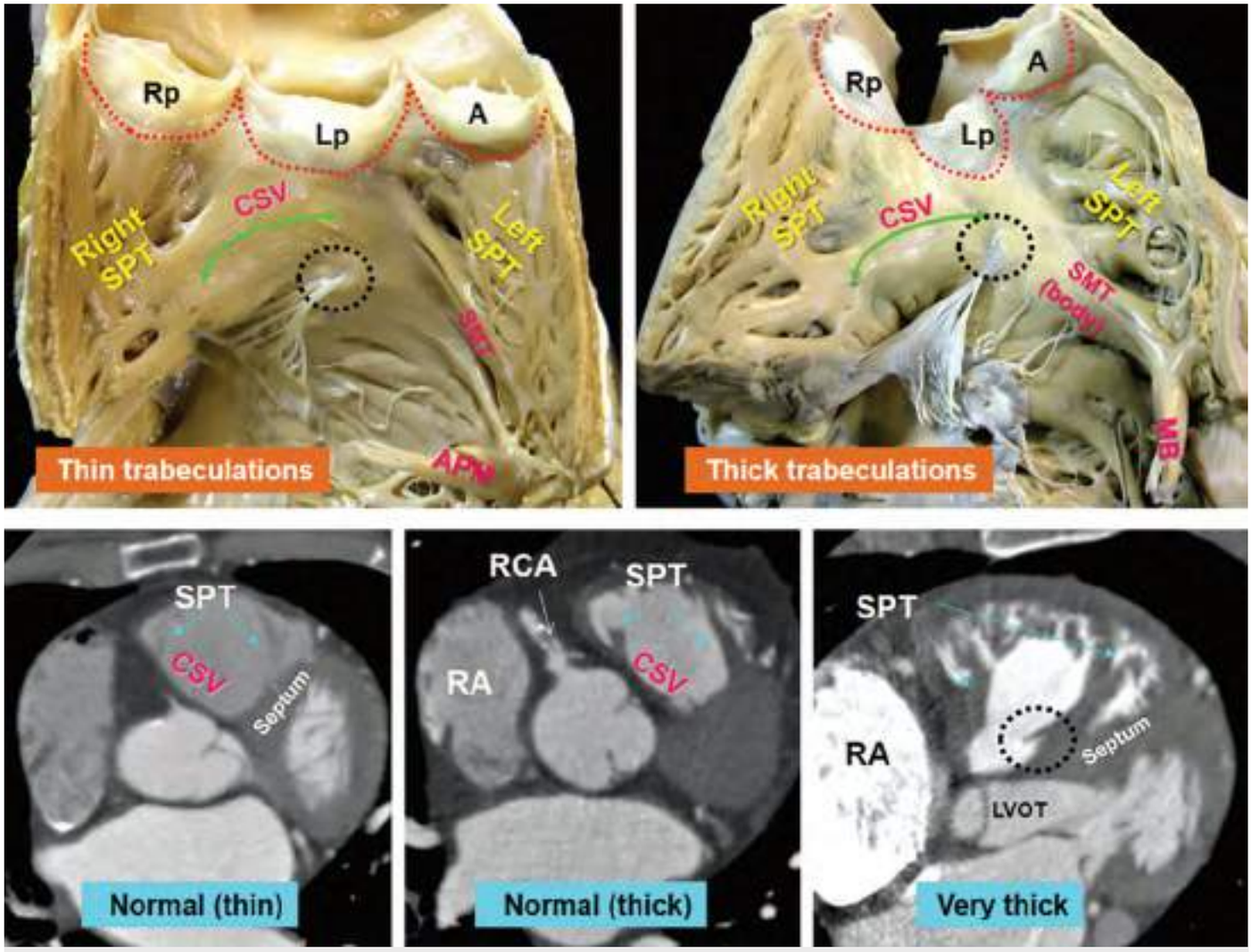

Fig. 12.65 Variation of trabeculations in RVOT. Upper panel: RVOT open book dissection views. The septomarginal trabeculation (SMT), is a muscle strap plastered onto the septal part. The crista supraventricularis (CSV) extends between SMT and the pulmonary valve and forms the paraseptal wall of the RVOT (*double-headed green arrows*). The septoparietal trabeculations (SPT) originate from the anterior margin of the SMT and run around the parietal quadrant of the endocardial infundibulum along the right and left septoparietal walls of the RVOT. These trabeculations vary in number (5–22 trabeculations) and thickness (2–10 mm). The SPTs can be flat or prominent and may be hypertrophied as in pulmonary hypertension or tetralogy of Fallot, contributing to muscular subpulmonary stenosis. The SMT continues to apex and turns into the moderator band (MB) and anterior papillary muscle. Lower panel: demonstrates variable thickness of the SPTs on axial CT angiograms. Note marked thickening of the RVOT in the last image in a patient with pulmonary valve stenosis. The right atrium (RA) is markedly enlarged. Black circles demarcate medial papillary muscle. A, anterior; Rp, right posterior; Lp, left posterior are pulmonary sinuses; LVOT, left ventricle outflow tract; RA, right atrium; RCA, right coronary artery.

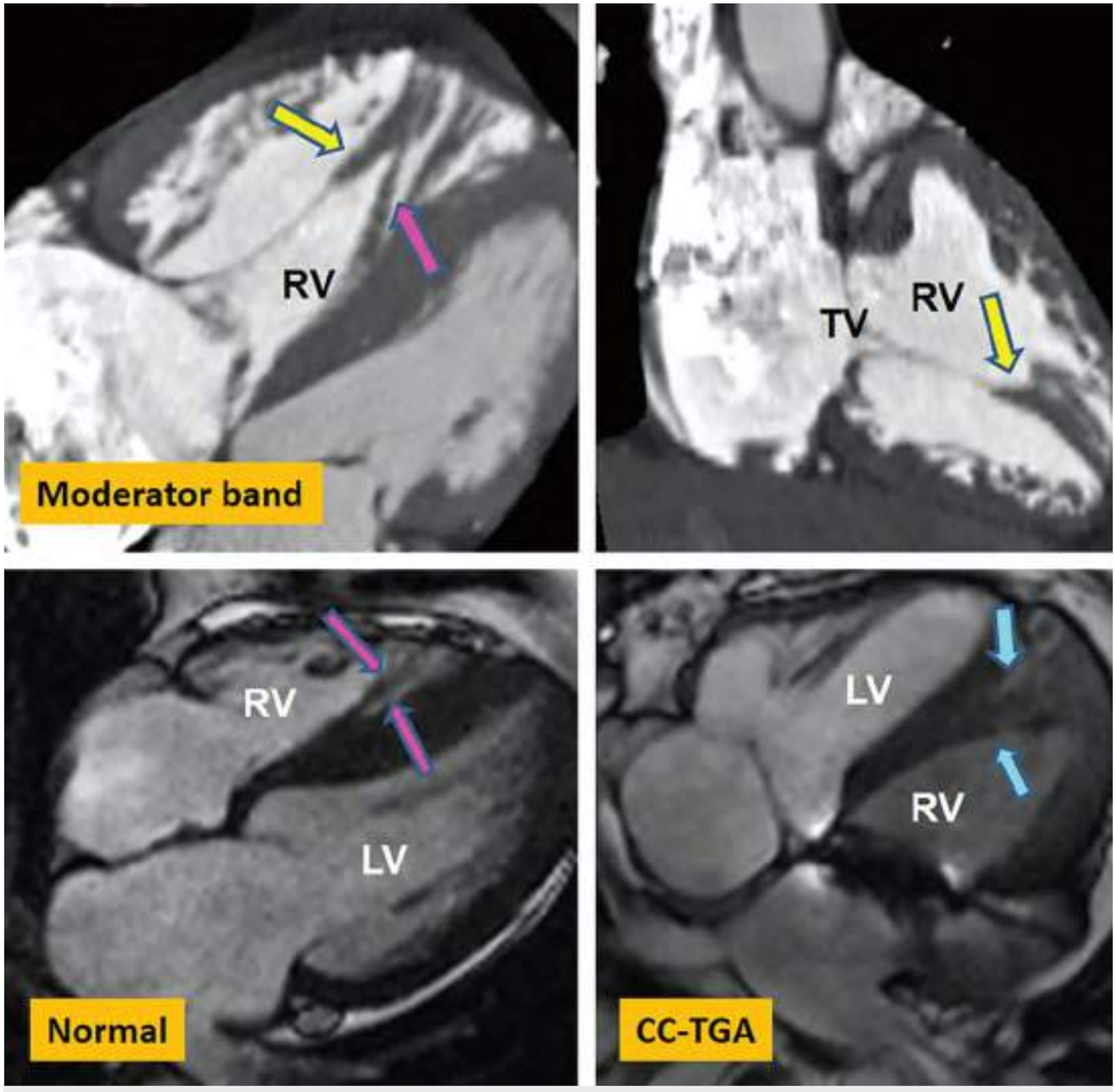

Fig. 12.66 Upper row CT images in axial and two-chamber right ventricular views showing the moderator band (*pink arrow*) arising from the septal wall. The moderator band continues toward the parietal (free) wall of the right ventricle (RV) and gives rise to the anterior papillary muscle (*yellow arrow*). Lower row shows a thin moderator band in a normal heart and a thickened band in a patient with congenitally corrected transposition of the great arteries (CCTGA) in which the ventricles are switched. LV, left ventricle; TV, tricuspid valve.

Right Ventricular Outflow Tract

The proximal border of the right ventricular outflow tract (RVOT) is characterized by a prominent Y-shaped muscle column referred to as "septomarginal trabeculation" or "septal band" (▶ Fig. 12.62, ▶ Fig. 12.65). The septomarginal trabeculation consists of a proximal body and two distal limbs; the anterosuperior and posteroinferior limbs. The anterosuperior limb extends along the infundibulum wall to the leaflets of the pulmonary valve.[2] The posteroinferior limb runs proximally and inferiorly toward the right ventricular inlet (▶ Fig. 12.65). The body of the septomarginal trabeculation is attached to the ventricular septum and runs toward the apex of the RV, where it divides into smaller trabeculations including the "moderator band." The moderator band continues to the parietal (free) wall of the RV and gives rise to the anterior papillary muscle (▶ Fig. 12.66). Anatomical localization of the moderator band is important to characterize the morphological RV in congenital heart disease (▶ Fig. 12.66). The moderator band is variable in size (▶ Fig. 12.66). It is usually located equidistant from the tricuspid valve and the apex. The mean thickness of the band is 4.5 ± 2 mm, and its mean length is 16 ± 2 mm, ranging from 11 to

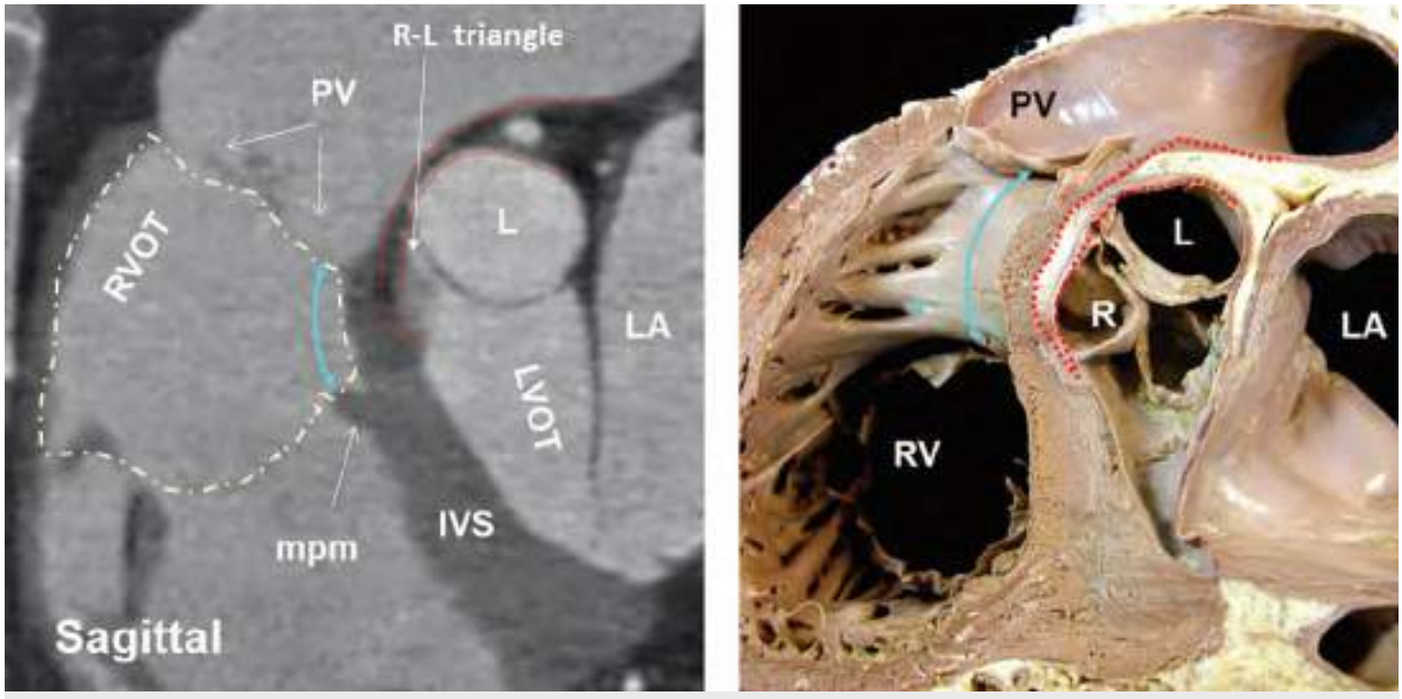

Fig. 12.67 Right ventricular outflow tract (RVOT) shown by corresponding saggital CT and cadaveric cut. The posterior wall of the RV infundibulum (supraventricular crest) (*blue arrows*) and the anterior wall of ascending aorta are separate making the infundibulum resectable during surgery. The height of supraventricular crest varies from patient to patient, however, most of it is separated from the aorta by the epicardial fat (*dotted red line*) and can be surgically removed without entering the left ventricular cavity. The term supraventricular crest is replaced by ventriculoinfundibular fold, representing any muscular structure interposed between the attachments of the leaflets of the atrioventricular and arterial valves. The inferior central part of it is called outlet septum which is part of septomarginal trabeculation above the level of medial papillary muscle (mpm). True existence of the outlet septum in normal hearts is debatable and even if exists should be very small. The intervalvular triangle between the right and left (R–L triangle) coronary sinuses of the aorta forms the uppermost part of the LVOT. PV, pulmonary valve; L, left aortic sinus; R, right aortic sinus; RV, right ventricle; LA, left atrium; IVS, interventricular septum; LVOT, left ventricle outflow tract.

24 mm.[78] Arterial supply to the moderator band originates from septal branches of the LAD artery.[79] Anastomotic vessels with the RCA exist at the level of the anterior papillary muscle. The body of the Y-shaped septomarginal trabeculation is adherent to the septum and in sectional imaging, it appears as a bump on the septum. When abnormally formed or hypertrophied, the septomarginal band can form a ring and divide the RV into two chambers (double-chambered RV).[80]

The body of the RVOT is formed by the pulmonary infundibulum (conus) which is a tubular muscular structure that supports the leaflets of the pulmonary valve. The length, size, and angle of the infundibulum vary (▶ Fig. 12.64, ▶ Fig. 12.65). The size and thickness of the infundibulum is relatively independent of the general size of the RV, but it can be enlarged in both RV volume overload and RV pressure overload.[1] One determinant of the size of the infundibulum is the axis of the pulmonary trunk. The infundibulum may be less developed in the presence of a horizontal axis of the pulmonary trunk.

The posterior wall of the infundibulum is formed by a prominent muscular ridge, known as the "crista supraventricularis (supraventricular crest, infundibular septum)." Although it looks like a ridge, the supraventricular crest is in fact an infolding of the ventricular wall (the "ventriculoinfundibular fold") inserting into the ventricular septum.[81] The crista supraventricularis is located between the two limbs of the septomarginal trabeculation and separates the tricuspid and pulmonary valves (▶ Fig. 12.62). This is in contrast to what is seen in the LV where the aortic and mitral valves are in fibrous continuity. The length of crista supraventricularis varies from patient to patient. The crista supraventricularis is separated from the aortic root by the epicardial fat and can be surgically removed without entering the left ventricular cavity[4] (▶ Fig. 12.67). Only a small central portion of its basal part, at the bifurcation of the two limbs of the septomarginal trabeculation, may form part of the interventricular septum.[76] Incisions through the crista supraventricularis should be made carefully as it may injure the RCA (▶ Fig. 12.65).

One imaging characteristics of the RVOT in normal hearts is its anterocephalad position relative to the left ventricular outflow tract (LVOT) resulting in a characteristic "cross-over" relationship between the two ventricular outflows (▶ Fig. 12.68**a**). This important spatial relationship can be lost in congenital heart malformations such as transposition of the great arteries (▶ Fig. 12.68**b**). Morphologically, the RV is distinguished from the LV by having coarser trabeculae, a moderator band, septal papillary muscles, and a lack of fibrous continuity between its tricuspid and pulmonary valve leaflets.[81]

Right Ventricle Size

The muscular wall of the normal RV is usually thin, but in conditions of pressure overload (i.e., pulmonary hypertension), the RV wall can reach up to 10 mm (▶ Fig. 12.65). The PA chest radiograph could be misleading in the assessment of the RV size because the RV is located anteriorly and may not increase the size

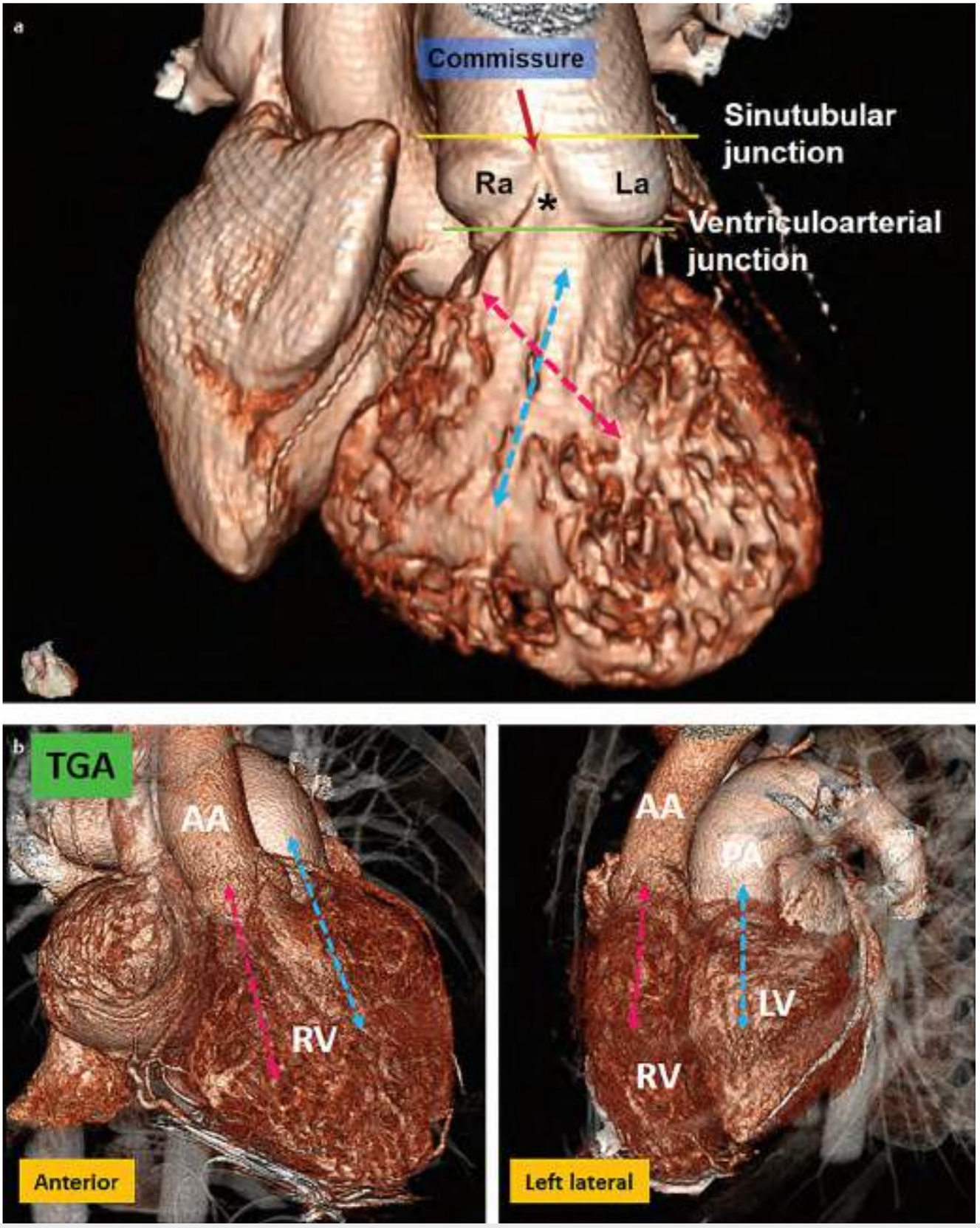

Fig. 12.68 **(a)** Anterior view showing the crossover arrangement between left and right ventricular outflow tracts (*red and blue arrows*, respectively). The pulmonary sinuses including the right anterior (Ra) and left anterior (La) sinuses are seen. The ventriculoarterial junction is demarcated by the green line. Intervalvular fibrous triangle is shown (*black star*). The commissure between the annuli is marked by arrow indicating peripheral apposition of the leaflets. The yellow line connecting the commissures marks the sinotubular junction. **(b)** Parallel arrangement between the functional left and right ventricular outflow tracts (*red and blue arrows*, respectively) in two views in patient with transposition of the great arteries (TGA). Note the normal anterior/posterior arrangement of the morphological ventricles in TGA. AA, ascending aorta; LV, left ventricle; PA, pulmonary artery; RV, right ventricle.

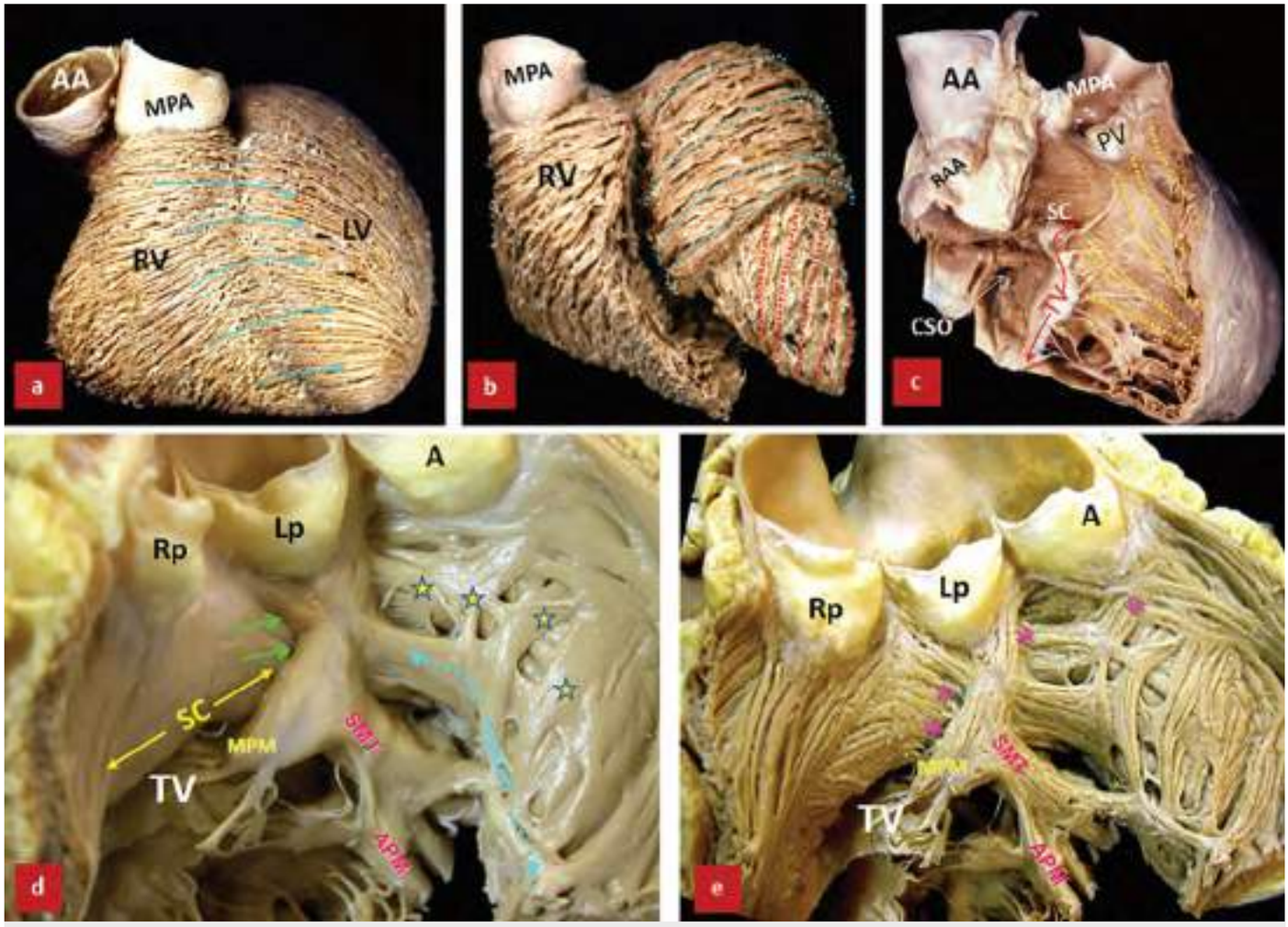

Fig. 12.69 Heart dissections show the change in the myocardial fiber orientation. **(a)** Slightly oblique or circumferential orientation of the myocardial strands in the epicardial or superficial region of the right ventricular walls. Note that there is continuity between the superficial fibers of the right and left ventricle (*arrows*). **(b)** Demonstrates prominent circumferential middle of the left ventricle (*blue dotted lines*) which is absent within the normal right ventricle. **(c)** Demonstrates the deep or subendocardial region in an opened right ventricle (*yellow dotted lines*). This deep region can also be seen in the left ventricle (*red dots*) in **(b)**. Note subendocardial myocardial strands are longitudinally or obliquely arranged at right angles with respect to epicardial strands. **(d, e)** Endocardial view of the RVOT. The endocardial infundibular sleeve consists of septoparietal trabeculations (*stars*) arising from the septomarginal trabeculation (SMT), the medial papillary muscle (MPM), and the junction (*green arrows*) between the supraventricular crest (SC) and the SMT. **(e)** Same specimen showing the RVOT subendocardial myofiber arrangements. Note the crossing architecture pattern of the myocardial strands between the SMT with the septoparietal trabeculations and supraventricular crest below the pulmonary valve (*asterisks*). APM, anterior papillary muscle; AA, ascending aorta; CSO, coronary sinus orifice; LV, left ventricle; RV, right ventricle; RAA, right atrial appendage; TV, tricuspid valve; PV, pulmonary valve; MPA, main pulmonary artery; Lp, left posterior; A, anterior; Rp, right posterior.

of heart. On the other hand, a lateral chest radiograph may help by showing a decrease in the retrosternal clear margin when the RV is enlarged. Overall, precise measurement of the RV sizes is challenging because of its complex shape.[76] The 3D nature and complex anatomy of the RV make cross-sectional CT and MR imaging ideal for assessing its sizes. The RV must be imaged in multiple planes, although the short-axis view is usually the most helpful. Visually, the RV size can be described as either normal or mildly, moderately, or severely enlarged. If the RV is as big as the LV, it is usually characterized as moderately enlarged, and if larger than the LV, it is called severely enlarged.[82]

Right Ventricle Function

The RV is a subpulmonary ventricle which pumps into a low-resistance circuit. Therefore, the RV functions at a lower ejection fraction (EF) than the LV. The myocardial fiber arrangements of the LV and RV are fundamentally different. Circumferential strands are predominant in the mesocardium of the LV, particularly at the basal level, and are covered by longitudinally directed strands in the subendocardium and obliquely arranged strands in the subepicardium (▶ Fig. 12.69). The RV contraction, on the other hand, relies more heavily on longitudinal shortening than the circumferential fiber arrangement of the LV. In the normal heart, the muscular wall of the RV, not including the trabeculations, is 3- to 5-mm thick.[83,84,85] In this relatively thin wall of the RV the outer circumferential and inner longitudinal myofiber layers predominate. A hypertrophied RV (as in tetralogy of Fallot) can change its architecture to resemble the sandwich pattern seen in the normal LV.[86] Myocardial strands are aligned in circumferential fashion in the subepicardium of the RV infundibulum and form the bulk of the wall (▶ Fig. 12.69**a**). At the

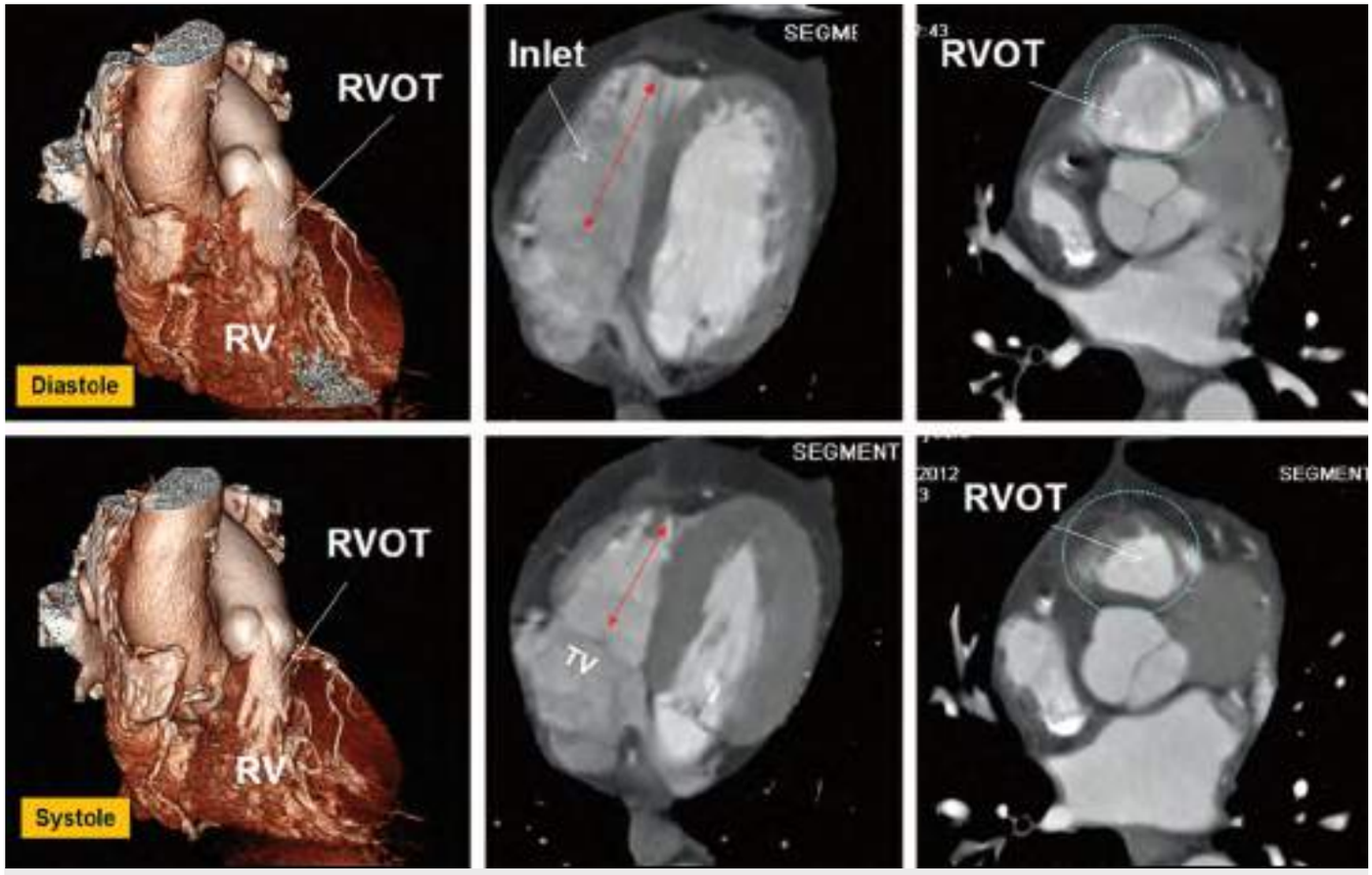

Fig. 12.70 CT images showing right ventricle (RV) function at inlet and outlet (RVOT) levels. The RV inlet has a greater contribution compared with the outlet in RV function. Note prominent longitudinal contraction (*red arrows*) in the inlet (*middle images*) and circumferential contraction (*blue circles*) in the right ventricular outflow tract (RVOT). TV, tricuspid valve.

subendocardium of the infundibulum, there are a series of longitudinally aligned muscle column branching laterally from the septomarginal trabeculation. These muscle columns form the so-called "septoparietal trabeculations" (▶ Fig. 12.65). The septoparietal trabeculations can be flat or prominent and may be hypertrophied as seen in pulmonary hypertension or tetralogy of Fallot, causing muscular subpulmonary stenosis (▶ Fig. 12.65).

From a functional standpoint, it is important to mention that the RV inlet has a greater contribution compared with the infundibulum[87,88,89] (▶ Fig. 12.70). The infundibulum functions as a propulsive exit from the RV and contributes to less than 20% of total RV function.[87] In contrast to the normal LV, the ventricular torsion is essentially absent and strain rate is reduced in the RV. As mentioned above, with constant RV pressure overload, myocardial hypertrophy and circumferential contraction may develop as an adaptive response to the systemic load, however, in the long run, due to the lack of torsion and reduced strain rate, the RV may become dysfunctional.

Tricuspid Valve

The tricuspid valve is located to right and anterior of the mitral valve (▶ Fig. 12.71). The ostium of the tricuspid valve is elliptical. The tricuspid annulus is almost completely muscular and there is no well-formed fibrous annulus. Therefore, some investigators have replaced the term "fibrous annulus" with "valvar attachments." Instead, the vestibule of the RA is separated from the ventricular ostium by the fibrofatty tissue of the AV groove. The three leaflets of the tricuspid valve are named for their anatomical location: septal (medial, conal), anterosuperior, and inferior (posterior) (▶ Fig. 12.72, ▶ Fig. 12.73). The number of leaflets is variable. The largest is usually the anterosuperior. The inferior leaflet may be very small or absent. The septal leaflet attaches to the septum and in part the inferior wall of the RV. Septal attachment over the membranous septum is a distinguishing feature of the tricuspid valve and divides the membranous septum into the AV and interventricular components.[76] (▶ Fig. 12.74). However, presence of a gap in the leaflet at the attachment site to the membranous septum is not infrequent.[76] The entire parietal attachment of the tricuspid valve usually is encircled by the RCA (▶ Fig. 12.58) running within the AV groove.

The papillary muscles (PM) of the tricuspid valve include the septal, anterior, and inferior (posterior).[52,90] The anterior (single or bifid) and inferior (one or two) papillary muscles are attached to the anterior and inferior walls of the RV, respectively (▶ Fig. 12.65, ▶ Fig. 12.66, ▶ Fig. 12.73). They provide insertions for the chordae from the parietal leaflets of the tricuspid valve. A second inferior papillary muscle may be attached to the septum (▶ Fig. 12.73). The septal PM usually arises from the body or posterior limb of the septomarginal trabeculation. The one arising

Fig. 12.71 Orientation of the atrioventricular valves on anterior and 65-degree left anterior oblique (LAO) views. The tricuspid valve (*blue*) is anterior and to the right of the mitral valve (*green*).

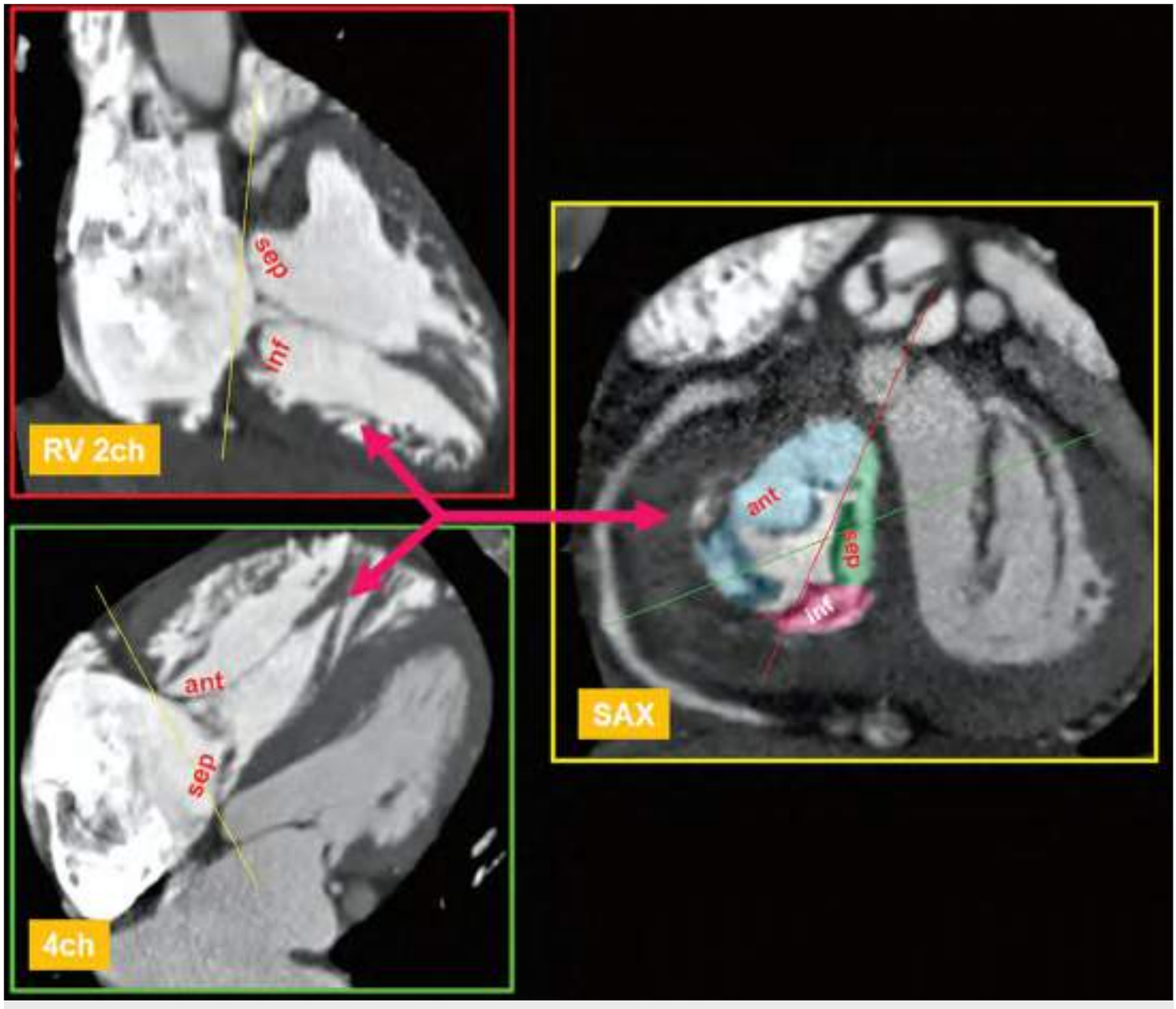

Fig. 12.72 The three leaflets of the tricuspid valve are named for their anatomical location: septal (medial, conal), anterosuperior, and inferior (posterior). Ant, anterior; Inf, inferior; Sep, septal; RV 2ch, right ventricle 2 chamber; 4ch, 4 chamber; SAX, short axis.

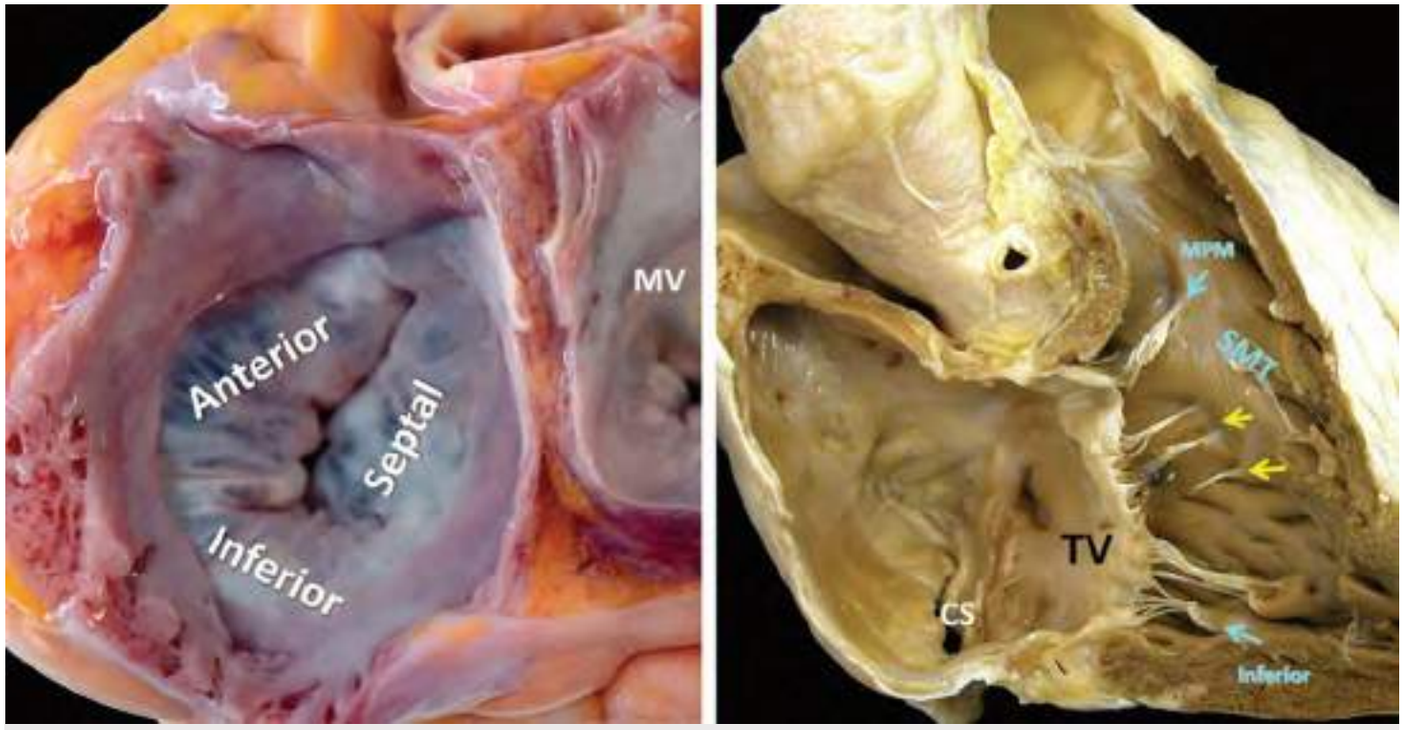

Fig. 12.73 Tricuspid valve apparatus. The three leaflets of the tricuspid valve are named for their anatomical location. The septal leaflet attaches to the septum and in part the inferior wall of the RV. The papillary muscles (PM) of the tricuspid valve include the medial (septal), anterior, and inferior (posterior). Small accessory papillary muscles may also be attached to the septum (*yellow arrows*). The medial PM usually arises from the body (MPM) or posterior limb of the septomarginal trabeculation (SMT). The one arising from the posterior limb is called conal (or Luschka) PM. MPM, medial papillary muscle; CS, coronary sinus; MV, mitral valve; TV, tricuspid valve.

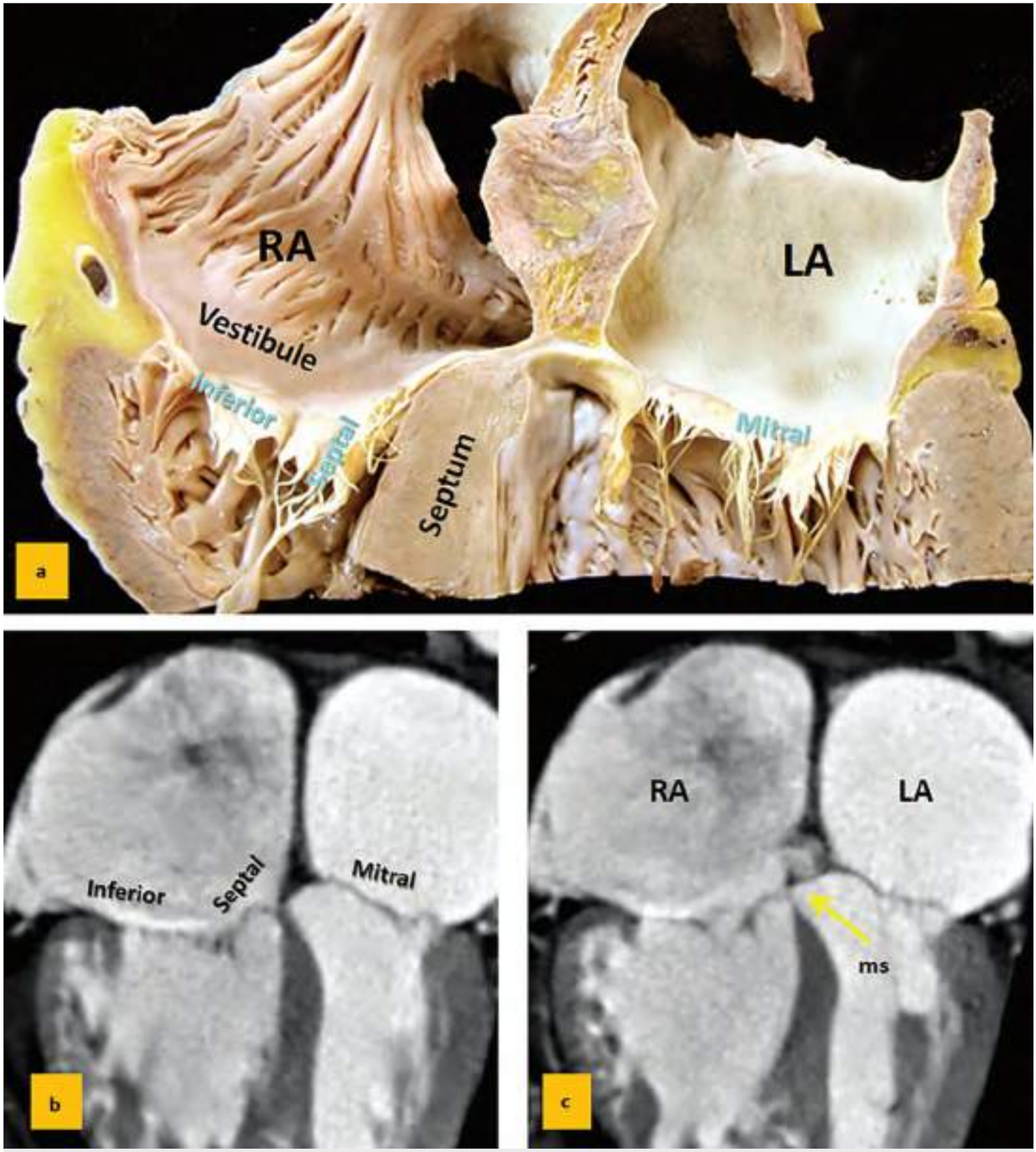

Fig. 12.74 (a) Four-chamber cut inferior to the membranous septum showing the offset between the mitral and septal tricuspid attachments (usually < 10 mm). The septal leaflet is attached to the base of the ventricular septum. Note thickened interatrial septum filled with fat. **(b)** Four-chamber cut of CT image at the same level the cadaveric cut was obtained. **(a)** Slice anterior to **(b)** at the level of the membranous septum (ms). Septal attachment over the membranous septum is a distinguishing feature of the tricuspid valve and divides the membranous septum into the atrioventricular and interventricular components as seen in image **(c)**. LA, left atrium; RA, right atrium.

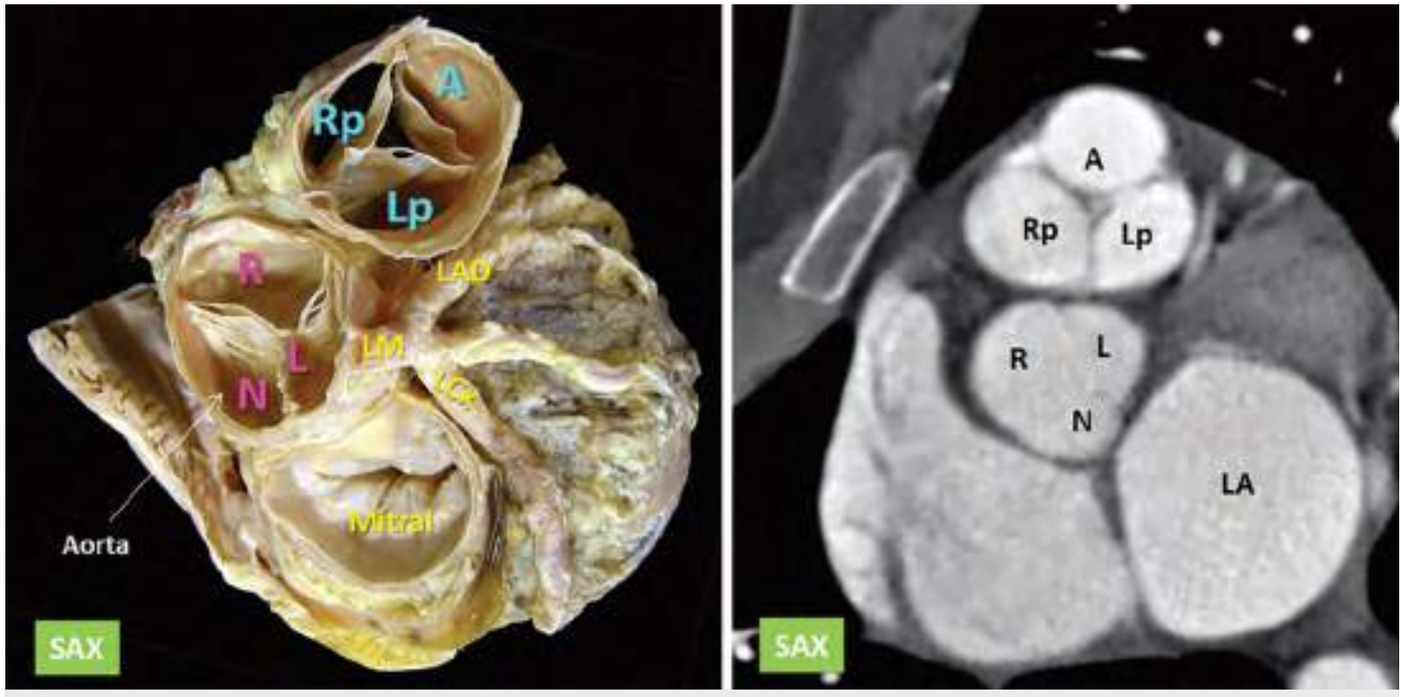

Fig. 12.75 Pulmonary valve sinuses shown in short-axis (SAX) views. In relation to the heart, the pulmonary sinuses can be named anterior (A, nonadjacent), left posterior (Lp), and right posterior (Rp). The commissures form where the leaflets join together at their peripheral ends. However, the three leaflets are not always well separated and their commissures may be poorly developed. R, right; L, left; N, noncoronary; LAD, left anterior descending artery; LM, left main artery; LCx, left circumflex artery; LA, left atrium.

from the posterior limb is called conal (or Luschka) PM.[2] It is absent in 20% of the hearts.[52] The right bundle branch of cardiac conduction system passes immediately beneath the septal papillary muscle and then within the body of the septomarginal trabeculation before entering the moderator band.[91]

12

Pulmonary Valve

When heart is viewed in attitudinal anatomical position as sitting in the thorax, the pulmonary valve leaflets and sinuses are seen to be posterior, right anterolateral, and left anterolateral[1] (▶ Fig. 12.68). However, in relation to the heart, the pulmonary sinuses can be named anterior (nonadjacent), left posterior, and right posterior. The commissures form where the leaflets join together at their peripheral ends. However, the three leaflets are not always well separated and their commissures may be poorly developed. Because of the semilunar shape of the pulmonary leaflets (similar to the aortic valve) this valve does not have a ring-like annulus (▶ Fig. 12.75). The sinotubular junction of the pulmonary trunk marks the level of the commissures between the sinuses (▶ Fig. 12.68). A second junction exists at the anatomical ventriculoarterial junction, localized by a circular line which connects the bases (nadir) of the sinuses[85] (▶ Fig. 12.68).

The leaflets of the pulmonary and aortic valves have different levels of attachments and there is an extracardiac tissue plane between the walls of the aorta and the pulmonary trunk (▶ Fig. 12.67). This anatomical feature makes possible the safe separation of the pulmonary valve and the infundibulum from the rest of the RVOT for use as a valve autograft (i.e., the Ross procedure).[92]

◆ Left Ventricle

The LV is a conical structure with the mitral valve at its base which narrows down to a rounded apex (▶ Fig. 12.76). The proximal two-thirds of the LV are covered by the RV anteriorly (▶ Fig. 12.76). The apical part is free anteriorly and faces the left anterior chest wall. Superiorly, the LV (the anterior wall of the LV) faces the mediastinum and the lung. The LAD artery branches pass close to the superior wall (called anterior wall in heart views) of the LV. The aorta originates at the medial superior aspect of the LV near the base of the LV. The inferior wall of the LV is sitting on the left hemidiaphragm. The lateral wall of the LV is free facing the left lung and the medial and anterior walls are formed by the septum. Based on recommendation of American Heart Association, a standardized segmental model is proposed for tomographic imaging of the heart.[93] In this model, the muscle and cavity of the LV are divided into 17 segments which are assigned to coronary arterial territories. In this model, the superior wall of the LV is called the anterior wall and the anterior wall of the LV is called the septal wall. The lateral and inferior walls face the left lung and the diaphragm, respectively (▶ Fig. 12.77).

The opening (base) of the LV is located posteriorly and is called the ostium.[1] The ostium of the LV is covered by the aortoventricular membrane, a tough fibrous structure which is connected to the aortic sinuses superiorly and the mitral valve posteriorly.[94] The anatomical concept of the LV ostium and the aortoventricular membrane are based on the pioneering work of McAlpine.[1] The highest point (summit) of the ostium is at the level of interleaflet triangle between the left and right coronary sinuses of the aorta (▶ Fig. 12.78, ▶ Fig. 12.79). The lowest point of the ostium is approximately 1.5 cm posterior to the inferior commissure of the

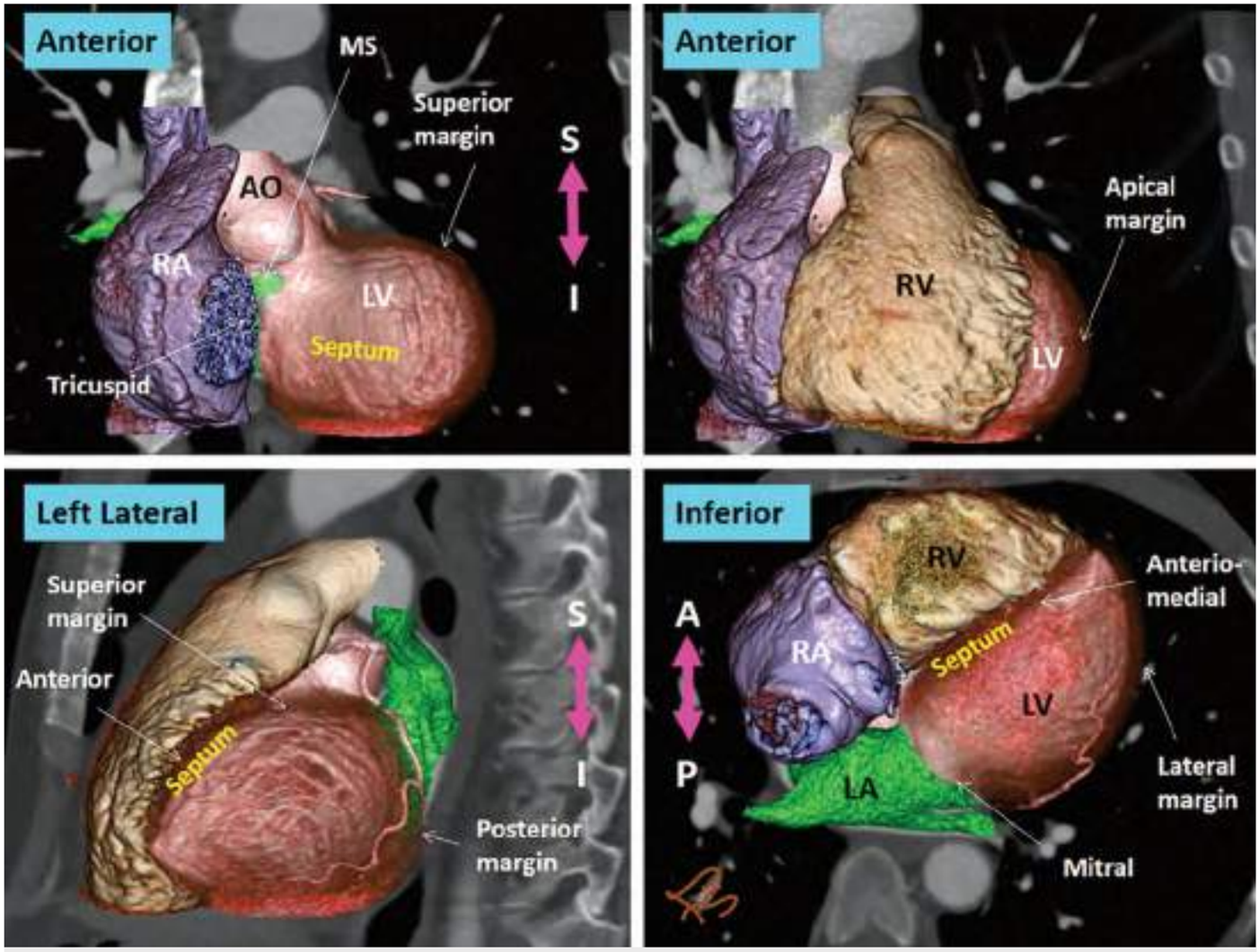

Fig. 12.76 Left ventricle (LV) walls and boundaries. The proximal two-thirds of the LV are covered by the RV anteriorly. The apical part is free anteriorly and faces the left anterior chest wall. Superiorly, the LV (the anterior wall of the LV) faces the mediastinum and the lung. The aorta (Ao) originates at the medial superior aspect of the LV near the base of the LV. The inferior wall of the LV is sitting on the left hemidiaphragm. The lateral wall of the LV is free facing the left lung and the medial and anterior walls are formed by the septum. Ao, aorta; LA, left atrium; LV, left ventricle; RA, right atrium; RV, right ventricle; A, anterior; P, posterior; I, inferior; S, superior.

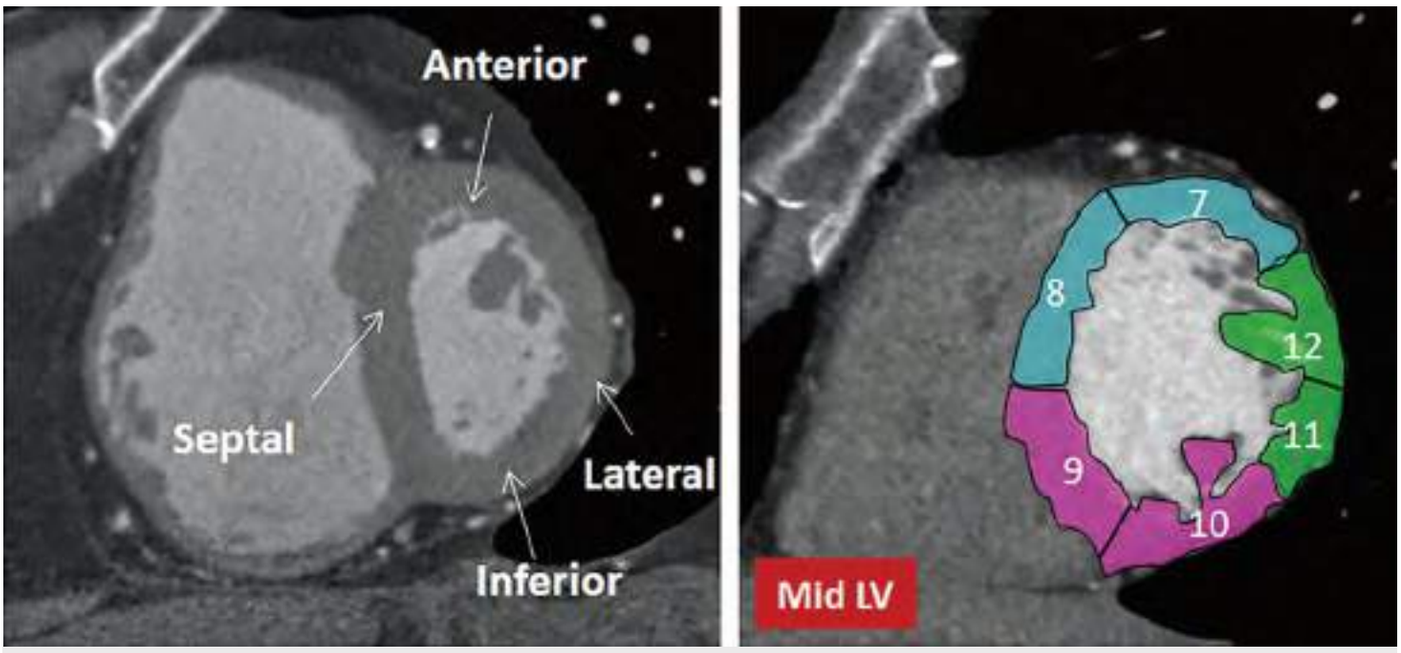

Fig. 12.77 Standardized 17 segmental model is proposed for tomographic imaging of the heart. Mid-left ventricle (LV) segments are shown. In this model, the superior wall of the LV is called the anterior wall and the anterior wall of the LV is called the septal wall. The lateral and inferior walls face the left lung and the diaphragm, respectively.

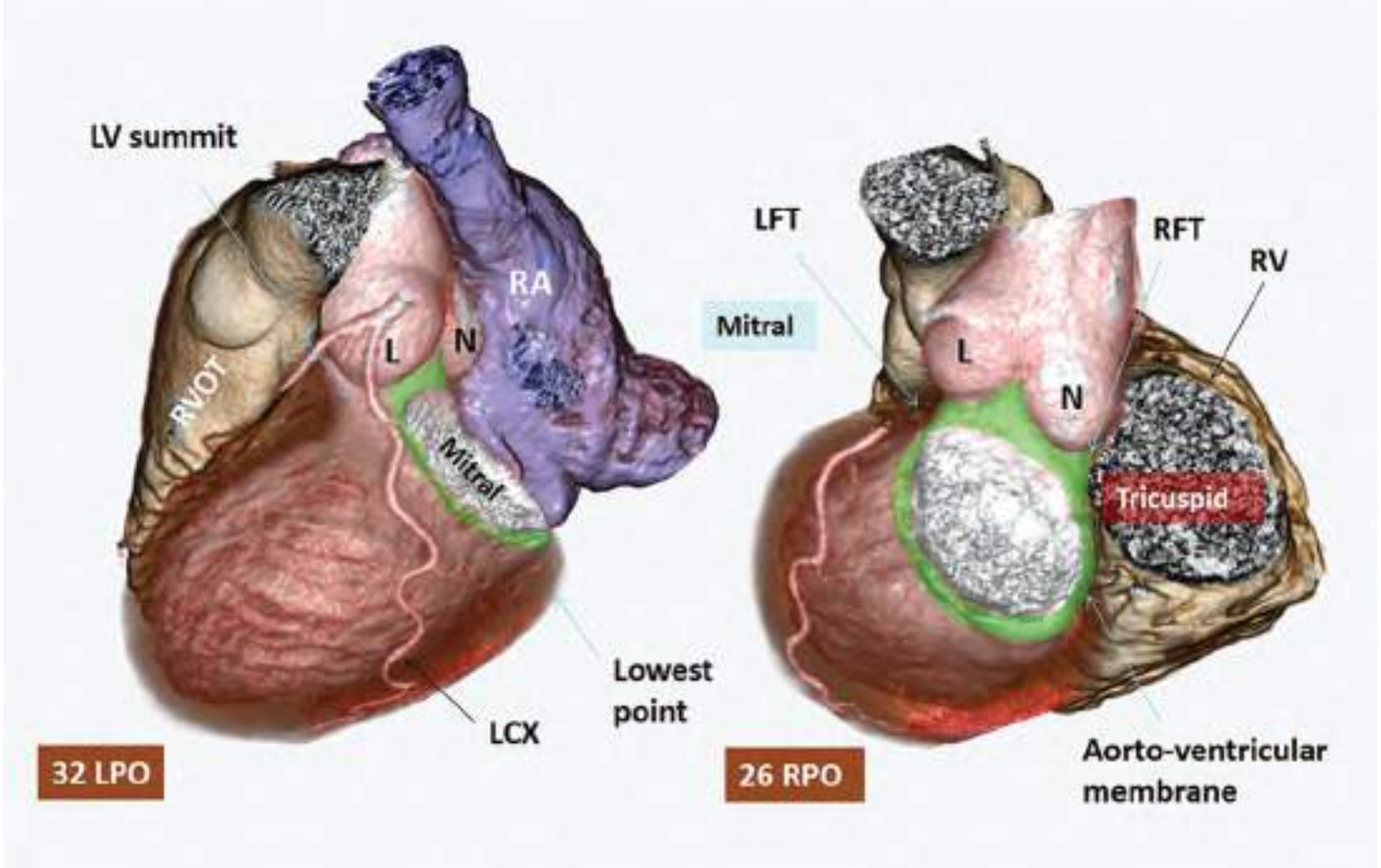

Fig. 12.78 Left ventricle (LV) anatomy. The ostium of the LV is covered by the aortoventricular membrane (*green area*), a tough fibrous structure which is connected to the aortic sinuses superiorly and the mitral valve posteriorly. Note aortomitral fibrous continuity between the left and noncoronary (N) aortic sinuses which together with the mitral annulus form a saddle-shaped appearance. The right fibrous trigone (RFT) and left fibrous trigone (LFT) are also part of the aortoventricular membrane. Also seen is the highest point (summit) of the ostium at the level of interleaflet triangle between the left (L) and right coronary sinuses of the aorta. LPO, left posterior oblique; LCx, left circumflex artery; RV, right ventricle; RVOT, right ventricular outflow tract; RPO, right posterior oblique.

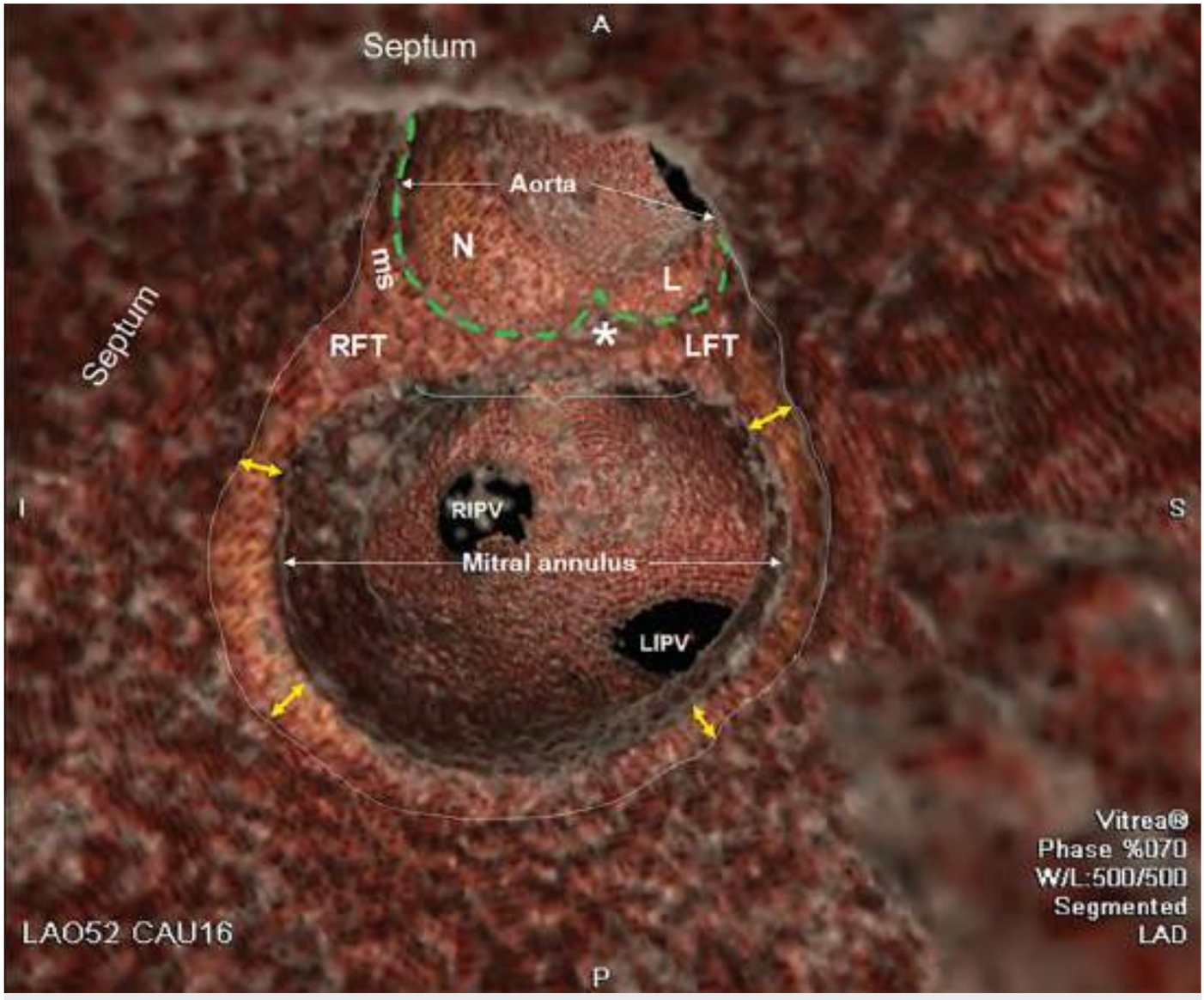

Fig. 12.79 Components of the aortoventricular membrane are shown in this virtual endoscopy view of the left ventricle (LV). The ostium of the LV consists of aortic and mitral divisions. The width of the attachment between the anterior mitral leaflet and the aortic valve (left and noncoronary sinuses) is approximately 3 cm extending between the left and right fibrous trigones. This fibrous membrane is known as the aortomitral fibrous continuity (*blue bracket*). The right fibrous trigone (RFT) is in continuity with the membranous septum (ms). Intervalvular triangle (*marked by "star"*) between the aortic annuli is also continuous with the rest of fibrous membrane. Note the subvalvular membrane around the mitral ring (*small double-headed yellow arrows*) meets the left and right fibrous trigones anteriorly. LFT, left fibrous trigone; L, left coronary sinus; N, noncoronary sinus; RIPV, right inferior pulmonary vein; LIPV, left inferior pulmonary vein.

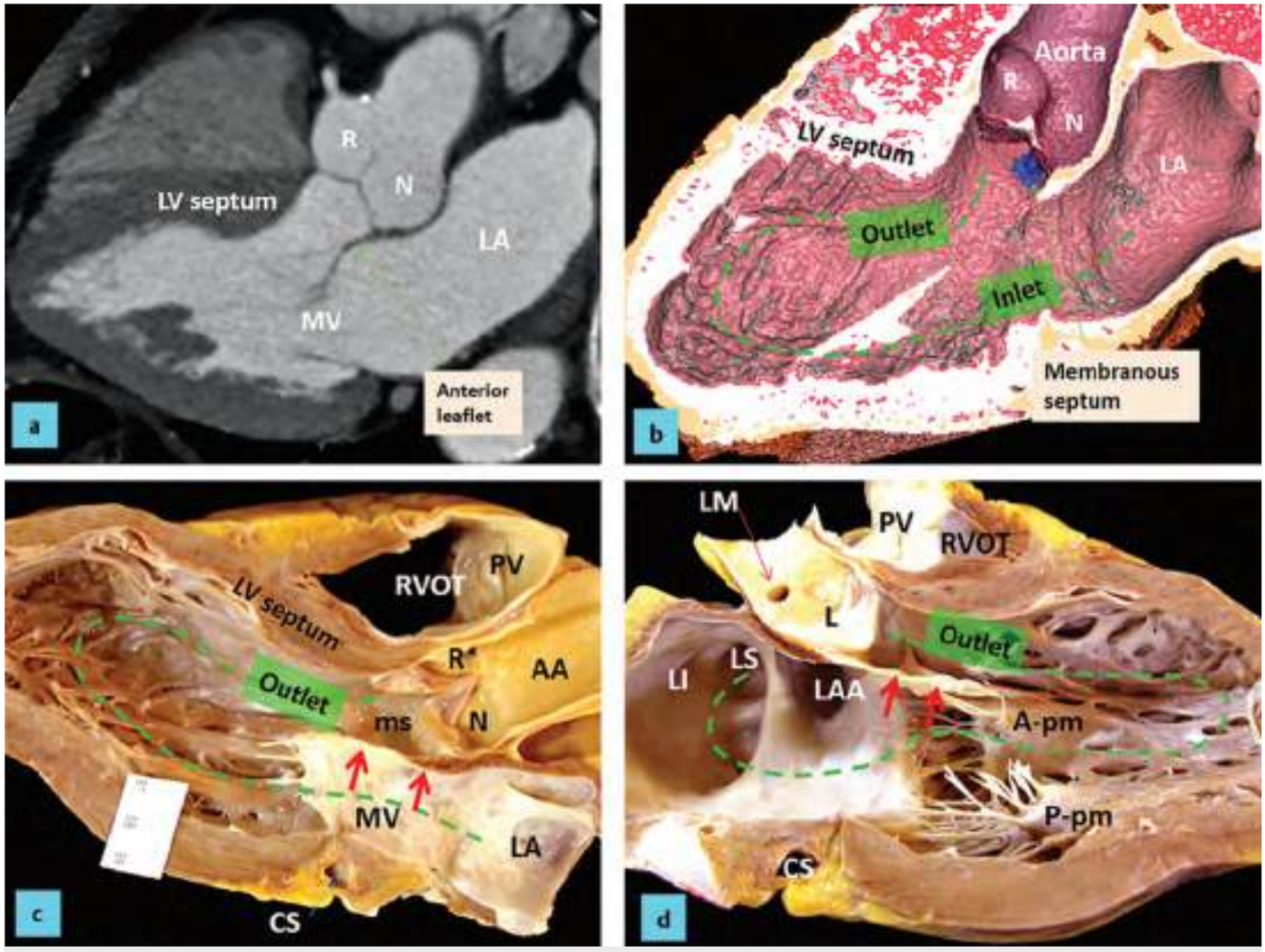

Fig. 12.80 LV components. **(a, b)** Three-chamber views of the left heart showing the inlet and outlet components of the left ventricle (LV). **(c, d)** Two halves of a heart are bisected longitudinally to show the three aortic sinuses and the papillary muscles of the mitral valve. Note the muscular subpulmonary infundibulum of the right ventricular outflow tract (RVOT) abuts the right (R) and left (L) coronary aortic sinuses. Anterior leaflet of the mitral valve is shown by red arrows. AA, ascending aorta; A-pm, anterior papillary muscle; CS, coronary sinus; LA, left atrium; MV, mitral valve; N, noncoronary aortic sinus; L, left coronary sinus; LAA, left atrial appendage; LI, left inferior pulmonary vein; LM, left main coronary artery orifice; LS, left superior pulmonary vein; P, posterior coronary sinus; PV, pulmonary valve; P-pm, posterior papillary muscle; R, right coronary sinus.

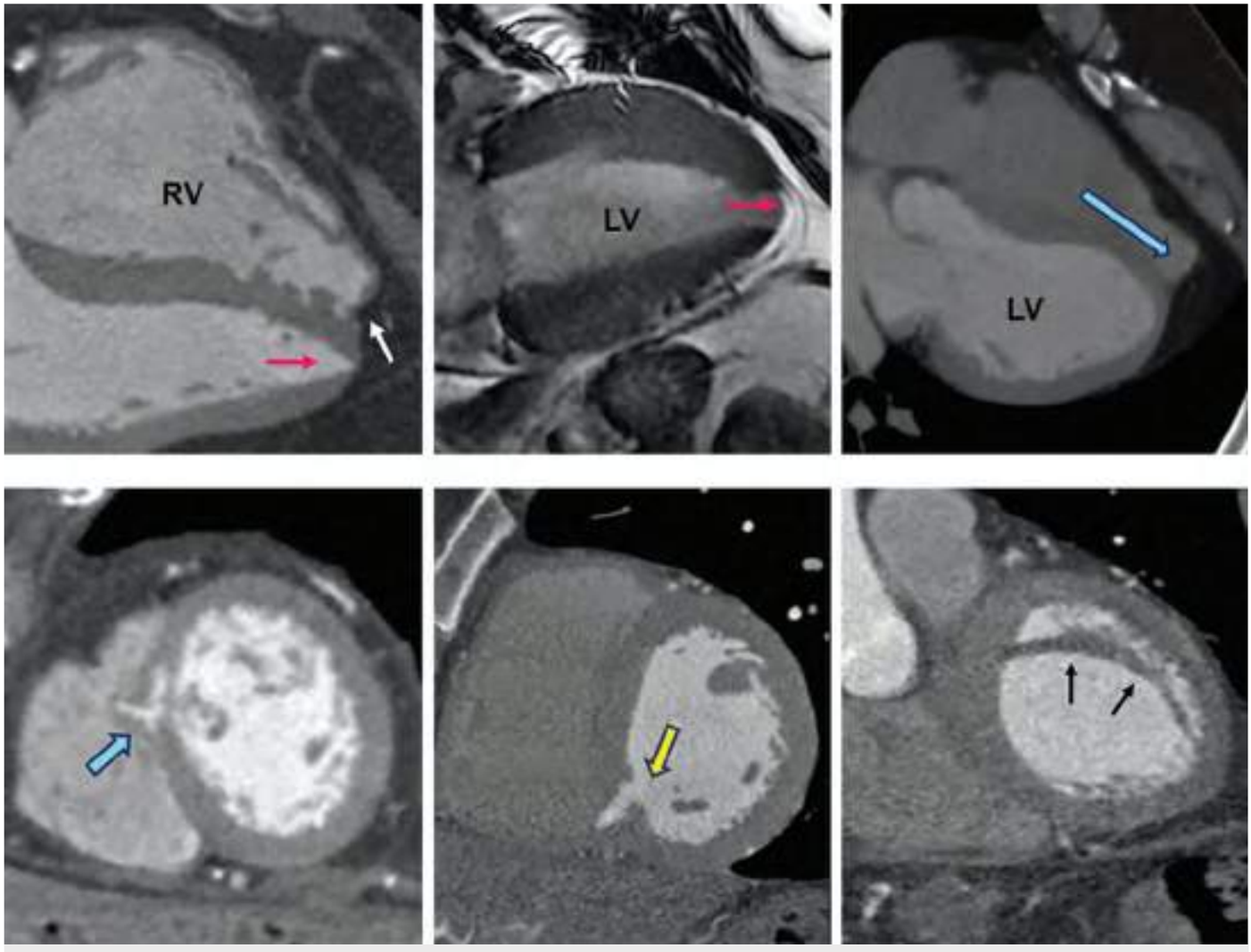

Fig. 12.81 Upper row: Cardiac views demonstrate varying shape of the apices in four different examples. The apex of the left ventricle (LV) may be sharply angular or smooth and spherical. In some cases, the LV apex is paper thin (*red arrows*). The location of the RV apex is important during right heart catheterization. It is anterior to the left apex and can be demarcated from the left apex by an incisura (*white arrow*). In some cases, the apex of the RV is thin and shapely angulated, which results in vulnerability to perforation. Ballooning of the RV apex is seen in some cases (*blue arrow*). Perforation of the LV apex is surprisingly uncommon in contrast to perforation of the apex of the RV during catheterizations or biopsy procedures. Lower row: Short-axis images of the left ventricle showing common anatomical variants including large Thebesian sinuses (*blue arrow*), myocardial cleft (*yellow arrow*), and intraventricular muscular bridge (false tendon) extending between septum and lateral wall of the LV (*small arrows*). False tendons are bands of fibrous or fibromuscular that traverse the cavity of the left ventricle with no connection to the valve leaflets.

mitral valve (▶ Fig. 12.78). Similar to the RV, the LV cavity can be subdivided into three components: the inlet, the apical trabecular, and the outlet. The inlet component is surrounded by the mitral valve and its tension apparatus and the outlet supports the aortic valve (▶ Fig. 12.80). The anterior leaflet of the mitral valve separates the inlet from the outlet. The leaflets of the aortic and mitral valves approach each other and remain in fibrous continuity (▶ Fig. 12.80). The apical trabecular component of the LV extends to the apex where the myocardium is very thin (▶ Fig. 12.81). Perforation of the LV apex is surprisingly uncommon in contrast to perforation of the apex of the RV during catheter insertion or pacemaker and implantable cardioverter defibrillator (ICD) implant placements.[95] The relation of the apices of the ventricles to each other is not without clinical significance. The apex of the RV may be demarcated from the left, producing an incisura (▶ Fig. 12.81). However, it is the apex of the LV (not the RV) which is readily identified at fluoroscopy. The RV apex may appear aneurysmal in some normal individuals, especially in axial views of CT of the thorax (▶ Fig. 12.81).

The trabeculations of the LV including its septal wall are quite fine compared with those of the RV, a useful characteristic in diagnosis of ventricular morphology in congenital heart disease (▶ Fig. 12.81). The outlet part of the septum is usually smooth (▶ Fig. 12.80). Normal LV myocardial thickness is between 7 and 11 mm. Heavy trabeculation of the LV is not normal and may indicate a congenital malformation known as noncompaction. Common anatomical variants such as large Thebesian sinusoids, myocardial cleft, or muscle bridges within the LV cavity should not be confused with pathologies[96,97] (▶ Fig. 12.81).

There are two papillary muscles arising from the inferior and superolateral aspects of the LV at the midventricular level and are named posteromedial and anterolateral, respectively. However, better terminologies to address the location of the two papillary muscles using correct attitudinal anatomical location would be

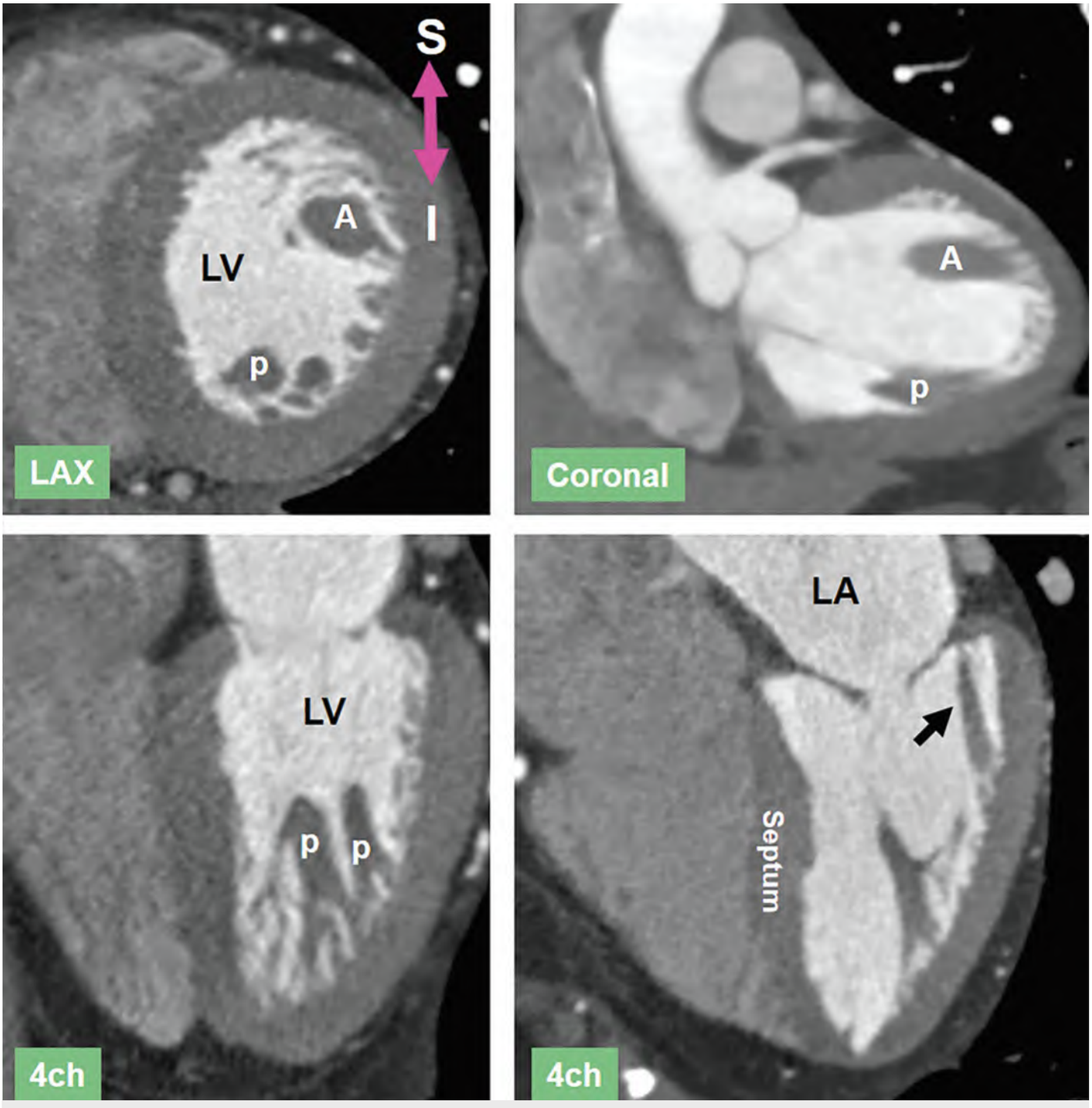

Fig. 12.82 Left ventricle (LV) papillary muscles are shown. Short-axis (LAX) image at midventricular level shows the anterolateral (A) and the posteromedial (P) papillary muscles. The anterior PM is larger and less tethered to the LV wall than the posterior. In approximately two-thirds of people, the anterior PM is a single structure and the posterior consists of one or two based columns with one or two heads (lower left image). Usually, no papillary muscle attaches to the left side of the ventricular septum. An accessory papillary muscle is seen in last image (*small arrow*). 4ch, 4 chamber; S, superior; I, inferior; LA, left atrium; LV, left ventricle.

the "inferior" and "superolateral" PMs (▶ Fig. 12.82). Usually, no papillary muscle attaches to the left side of the ventricular septum. The papillary muscles are extensions of the ventricular muscle and their function relates to the integrity of LV function and geometry. Knowledge of the variation in the location and number of papillary muscles is useful in mitral valve surgery and reconstruction of the LV wall aneurysm. Accessory, duplicated, bifid, basal, or apical PMs may be present (▶ Fig. 12.82). The superolateral papillary muscle is supplied by branches of the LAD artery and the inferior papillary muscles by the branches of the dominant RCA or the LCx artery. Damage and perforation of the inferior papillary muscles after myocardial infarctions may result in mitral regurgitation. The chordae tendineae (tendinous chords) are strong, fibrous connections between the valve leaflets and the papillary muscles. They are important component of AV valve (mitral and tricuspid) complex and prevent the cusps from inverting into the atrial cavity during systole. Chordae tendineae may originate from the papillary muscle or the wall of LV.[98,99]

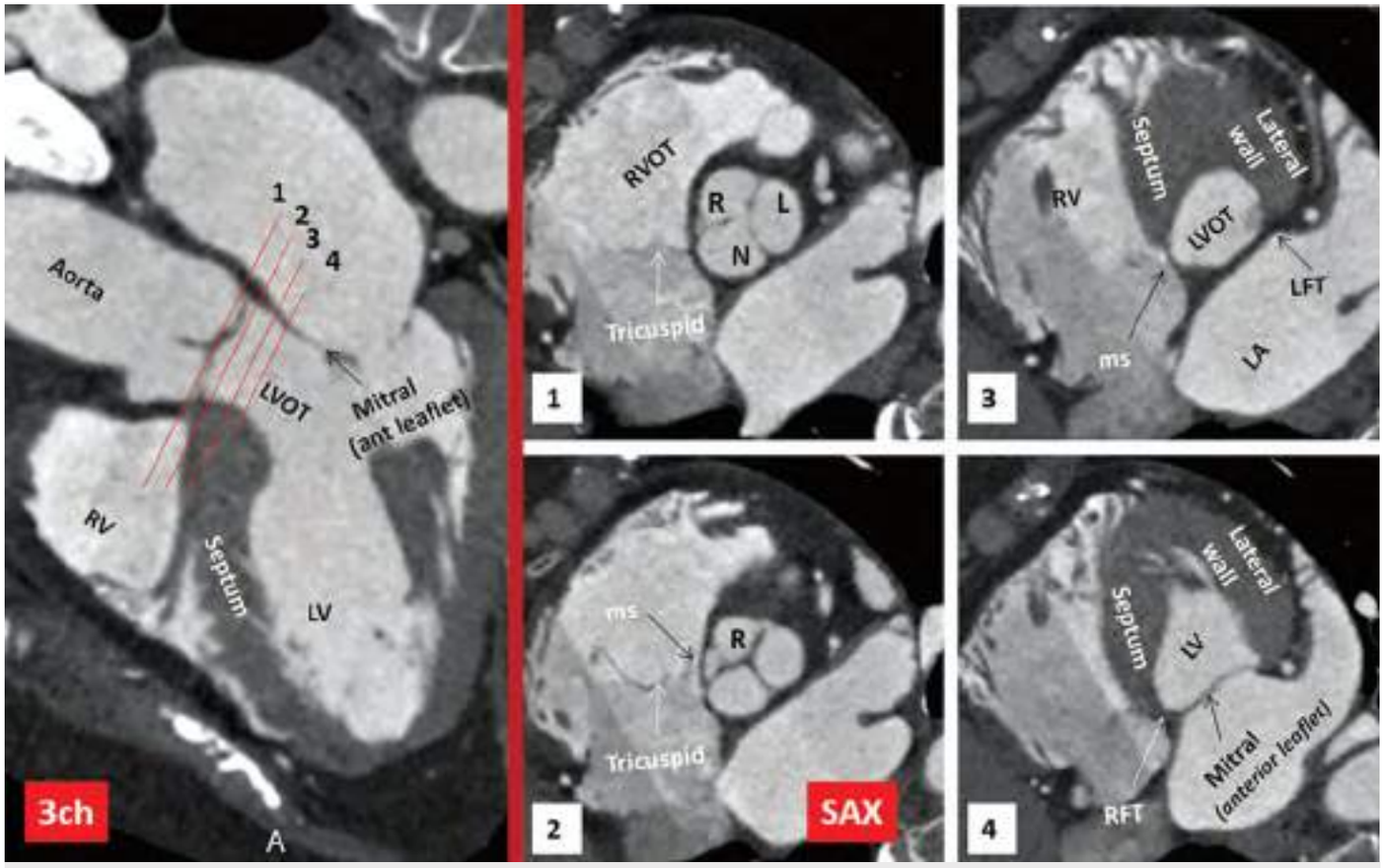

Fig. 12.83 Left ventricular outflow tract (LVOT). When viewed in short-axis cross-section, the posterior wall of the LVOT is formed by the interleaflet fibrous triangle between the noncoronary (N) and left coronary (L) aortic sinuses which is in fibrous continuity with the anterior leaflet of the mitral valve. This aortomitral valvar fibrous curtain (part of the aortoventricular membrane) is thicker on the sides and forms the right fibrous trigone (RFT) and left fibrous trigone (LFT) at the nadir of the noncoronary and left coronary sinuses, respectively. The anterior wall of the LVOT is primarily formed by the muscular ventricular septum. The anteromedial wall of the LVOT is formed by the membranous septum (ms). LA, left atrium; LV, left ventricle; RV, right ventricle; R, right coronary sinus; RVOT, right ventricular outflow tract.

The origin, insertion, attachments, and branching patterns of the chordae tendineae vary. Mean number of chordae arising from apical half of a single papillary muscle is 9 with the range of 3 to 18.[98] Elongation or rupture of the chords affects the function of the mitral valve.

Left Ventricular Outflow Tract

The LVOT supports the aortic valve (▶ Fig. 12.83). The LVOT area appears ellipsoid in its axial view. The longer diameter is around 20 to 23 mm. Dynamic changes of the LVOT area during cardiac cycle are detectable in normal individuals. It becomes larger at late systole. When viewed in short-axis cross-section, the posterior wall of the LVOT is formed by the interleaflet fibrous triangle between the noncoronary and left coronary sinuses which is in fibrous continuity with the anterior leaflet of the mitral valve. This aortomitral valvar fibrous curtain is thicker on the sides and forms the right and left fibrous trigones at the nadir of the noncoronary and left coronary sinuses, respectively (▶ Fig. 12.79, ▶ Fig. 12.83). The anterior wall of the LVOT is primarily formed by the muscular ventricular septum (▶ Fig. 12.83). The anteromedial wall of the LVOT is formed by the membranous septum and the interleaflet fibrous triangle between the noncoronary and right coronary sinuses (▶ Fig. 12.83). The anterolateral wall of the LVOT is formed by free wall of the LV and the interleaflet fibrous triangle between the left and right coronary sinuses (▶ Fig. 12.83). Therefore, in contrast to the RV infundibulum, which is composed entirely of muscle, the LVOT consists of both muscular and fibrous components.

Mitral Valve

The mitral valve components include valvular apparatus (annulus, leaflets, and commissures) and tension apparatus (papillary muscles and chordae tendineae)[100,101] (▶ Fig. 12.84, ▶ Fig. 12.85, ▶ Fig. 12.86, ▶ Fig. 12.87). The mitral valve is formed by two leaflets approaching one another at the commissures. The attachment site of the aortic (also called anterior or superior) leaflet is shorter than the mural (also called posterior or inferior) leaflet and comprises approximately one-third of the circumference of the mitral annulus (▶ Fig. 12.84). The two leaflets of the mitral valve have different morphologies. The anterior leaflet is in fibrous continuity with the aortic sinuses extending between the nadirs of the left and noncoronary aortic sinuses with the right and left fibrous trigones formed at each corner of this fibrous curtain (▶ Fig. 12.79). When the valve is closed, the surface area of the anterior leaflet is larger than the posterior leaflet (3/1 or 2/1) (▶ Fig. 12.84). The posterior leaflet has a scalloped margin with three or more segments separated by clefts.[101]

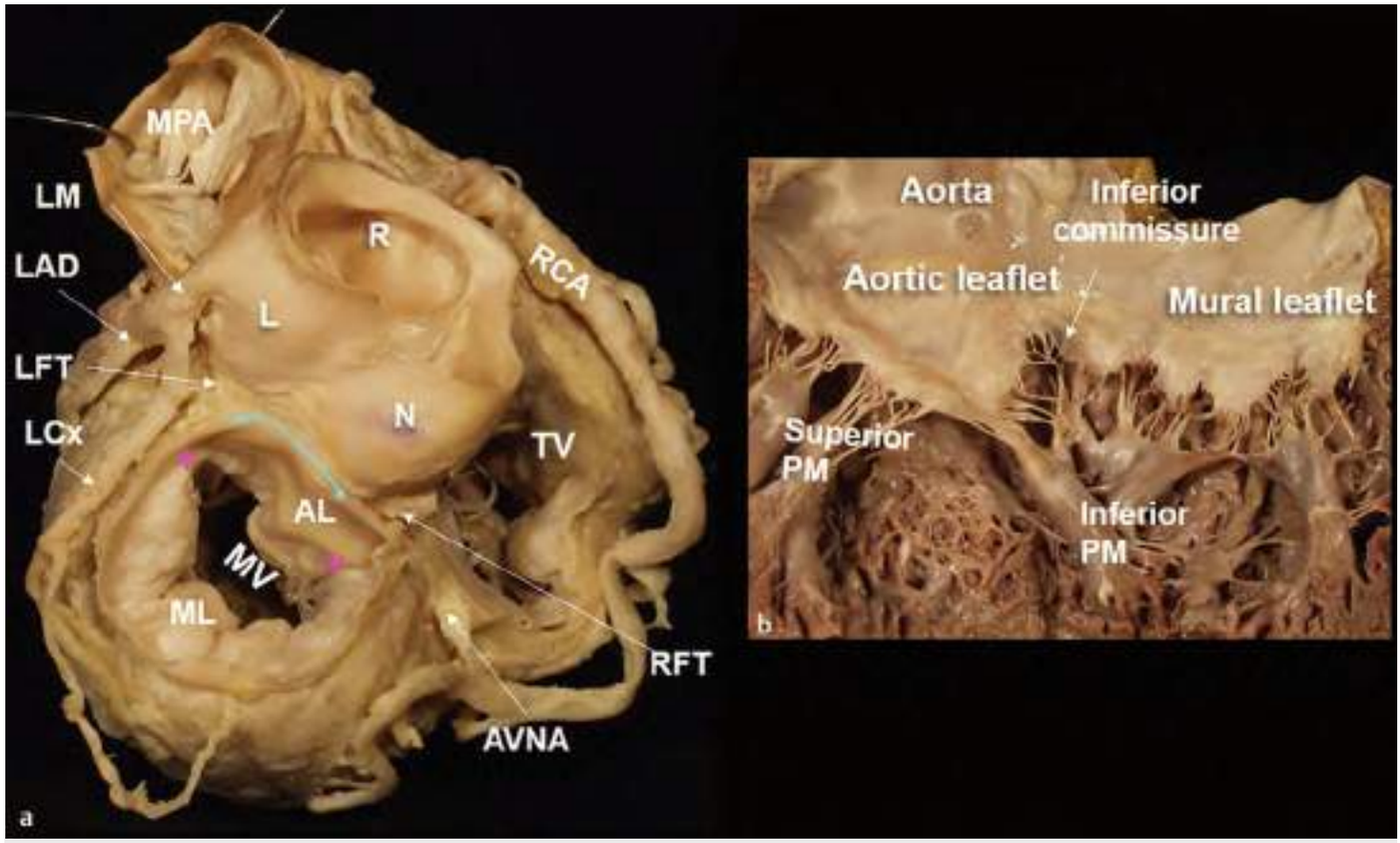

Fig. 12.84 Mitral valve. **(a)** The mitral valve is shown from the atrial side. The attachment site of the aortic leaflet (AL) is shorter than the mural leaflet (ML) and comprises approximately one-third of the circumference of the mitral annulus. Three segments of the aortic leaflet are seen. The middle segment is between the right and left fibrous trigones. The anterior and posterior segments of the anterior leaflet are attached to the ostium of the LV and each extends between a mitral commissure (*red asterisks*) and the right or left fibrous trigone. Note the central location of the aortic root, with the three sinuses: R, right; L, left, and NF, nonfacing ("noncoronary") and the two fibrous trigones (LFT and RFT). The left main (LM) coronary artery and its circumflex branch (LCx) wind around the mitral valve (MV) orifice; in an analogous manner, the right coronary artery (RCA) winds around the tricuspid valve (TV) orifice. **(b)** Opened view of the mitral valve apparatus. Each leaflet has a thinner clear zone and a tauter rough zone. The valve leaflets coapt at the level of their rough zones. MPA, main pulmonary artery; ML, mural leaflet; AL, aortic leaflet of mitral valve. (Adapted from Muresian 2009.[101])

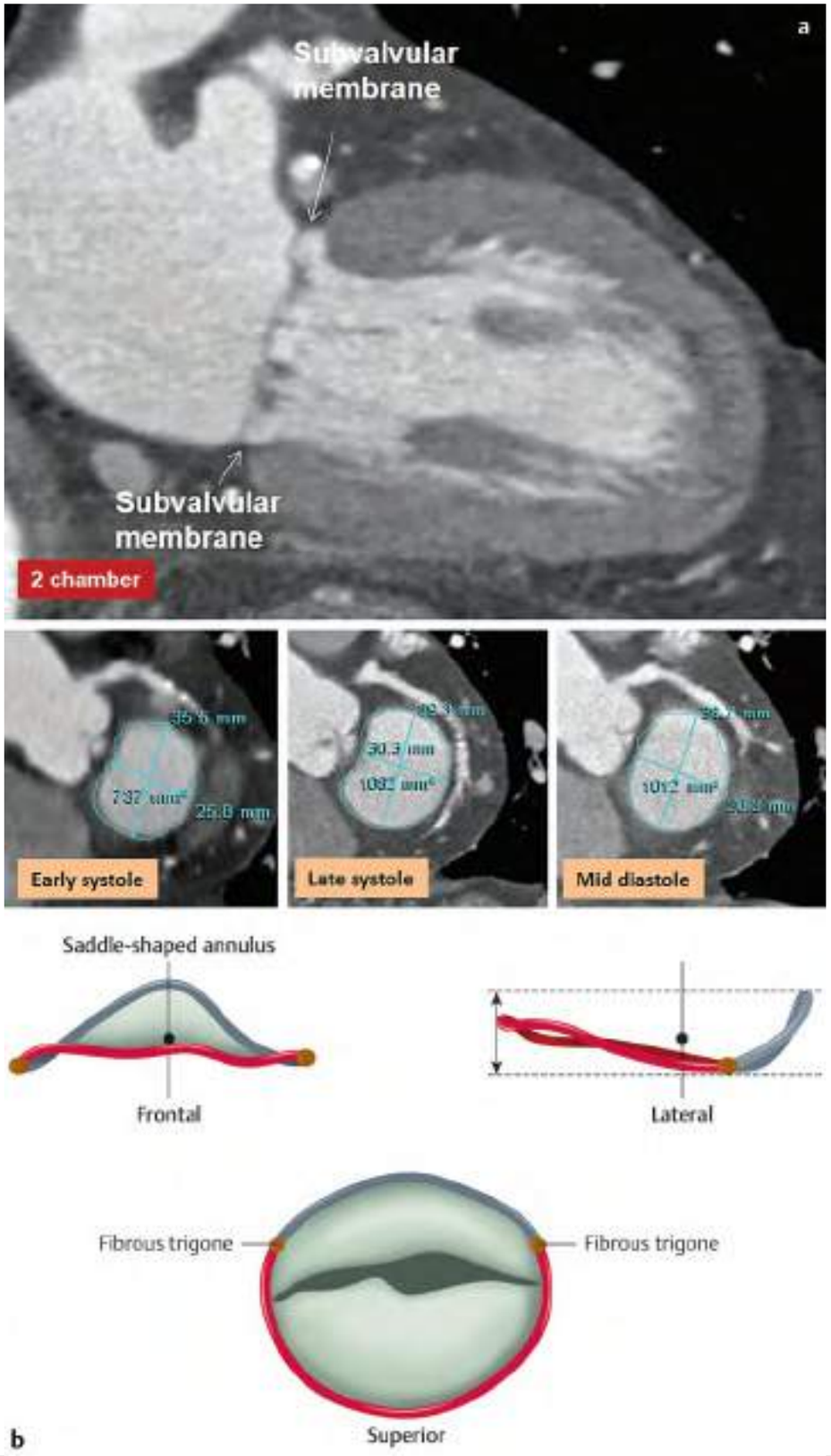

Fig. 12.85 Mitral annulus. **(a, b)** The mitral valve leaflets are supported by a rather band-like dense collagenous annulus, also known as subvalvular membrane. The mitral valve annulus is a functional unit and demonstrates a nonplanar saddle-shaped morphology which varies with cardiac cycle. No change occurs at aortomitral continuity. Annular contraction occurs in early systole and a deeper saddle-shaped morphology occurs followed by gradual annular area increase until end systole. The difference is minimal during late systole and diastole.

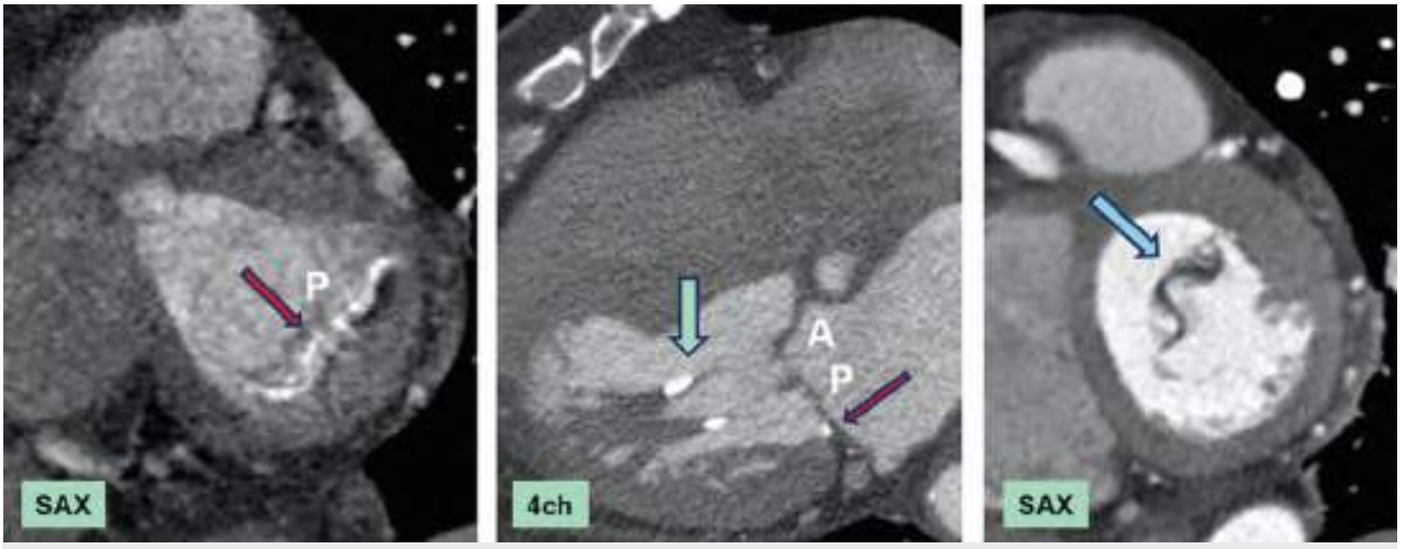

Fig. 12.86 Calcification of the mitral annulus is common and usually involves the posterior leaflet, subvalvular membrane, and LV ostium (*red arrows*). Papillary muscles may calcify too (*green arrow*). At the midpoint of the posterior leaflet (P) of the mitral valve, the subvalvular segment of the aortoventricular membrane narrows and in some cases is not visible. This is the region where calcification of the annulus develops the most. Mild calcifications do not cause serious functional abnormality. Thickening and fatty degeneration of free edge of the mitral leaflets may develop with aging (*blue arrow*). A, anterior mitral leaflet; P, posterior (inferior) mitral leaflet; 4ch, four-chamber view; SAX, short-axis view.

Unlike the tricuspid valve, the mitral valve leaflets are supported by a rather dense collagenous annulus, also known as subvalvular membrane.[1] The annulus is a band-like structure, not a ring- or cord-like structure, and extends peripherally from the fibrous trigones (▶ Fig. 12.79, ▶ Fig. 12.85). It is deficient toward the aorta at the level of mitral–aortic valvar fibrous continuity extending between the left and right trigones.[101] For surgical purposes, the annulus is considered the area of the attachment of the valve leaflets to the myocardial muscle.

The mitral valve annulus is a functional unit and demonstrates a nonplanar saddle-shaped morphology[102] (▶ Fig. 12.85, ▶ Fig. 12.87). The complex 3D geometry of the mitral annulus may play an important physiological role in the proper and durable function of the valvular complex. The saddle morphology of the annulus imposes leaflet curvature that—in combination with leaflet bulging—reduces stress on valve components during systole and may contribute to valve competence.[103] During systole in normal hearts the annulus height to intercommissural width ratio will be increased which leads to a deeper saddle shape. The annulus height is approximately 6 mm and will increase to 8 mm in early systole. Normally the mitral annulus appears oval-shaped in short-axis view and the intercommissural length (superior–inferior) is longer than the aortomural (septolateral) diameter. Diameters are usually less than 40 mm. In early systole, mild annular contraction may also occur in aortomural diameter which approximates anterior and posterior leaflets. Diameters in late systole and diastole are not different.[104] This normal dynamic change in morphology is altered in myxomatous valve disease, acute posterior wall ischemia, or in patients with dilated cardiomyopathy. Flattening and dilation of the annulus in these conditions lead to mitral insufficiency.[104] Calcifications of the mitral annulus are common and usually involve the posterior mitral annulus (▶ Fig. 12.86). In mitral valve replacement, the attached border of the posterior leaflet is of particular interest because of the danger of periprosthetic leak when the annulus is heavily calcified.[105] This complication is less common in relation to the anterior leaflet as its attachments to the fibrous trigones are stronger and less involved with calcifications.

The LCx artery and the coronary sinus run close to the posterior mitral annulus (▶ Fig. 12.87).

In contrast to the tricuspid valve, there is no direct attachment of the mitral valve to the ventricular septum, although the papillary muscles are frequently connected to the septum or to the right fibrous trigone by the false cords.[99] The attached border of the anterior leaflet is divisible into three segments. The middle segment is the longest and in fibrous continuity with the aortic valve. This segment extends between the right and left fibrous trigones (▶ Fig. 12.84). This relation is important in aortic valve replacement surgery. The anterior and posterior segments of the anterior leaflet are attached to the ostium of the LV and each extends between a mitral commissure and the right or left fibrous trigone (▶ Fig. 12.84).

Aortic Valve

The aortic valve is a semilunar valve and a functional unit composed of three structures: (A) the functional aortic annulus, comprising of the ventriculoaortic junction (VAJ) and the sinotubular junction (STJ); (B) the leaflets with their attachment; and (D) the sinuses. Behind each leaflet, the aortic wall bulges outward to form the three sinuses of Valsalva designated as right coronary, left coronary, and noncoronary (nonadjacent) sinuses[106] (▶ Fig. 12.88, ▶ Fig. 12.89). Between the sinuses, the commissures are formed marking the level of the sinotubular junction. Because of the semilunar nature of the attachments of the aortic sinus, there are three interleaflet fibrous triangles that reach to the level of the STJ of the aorta (▶ Fig. 12.89, ▶ Fig. 12.90). From an imaging point of view, the aortic annulus (imaging VAJ) corresponds to the plane passing through the nadir of the leaflet hinge lines. Surgical annulus is generally referred to the leaflet hinge lines

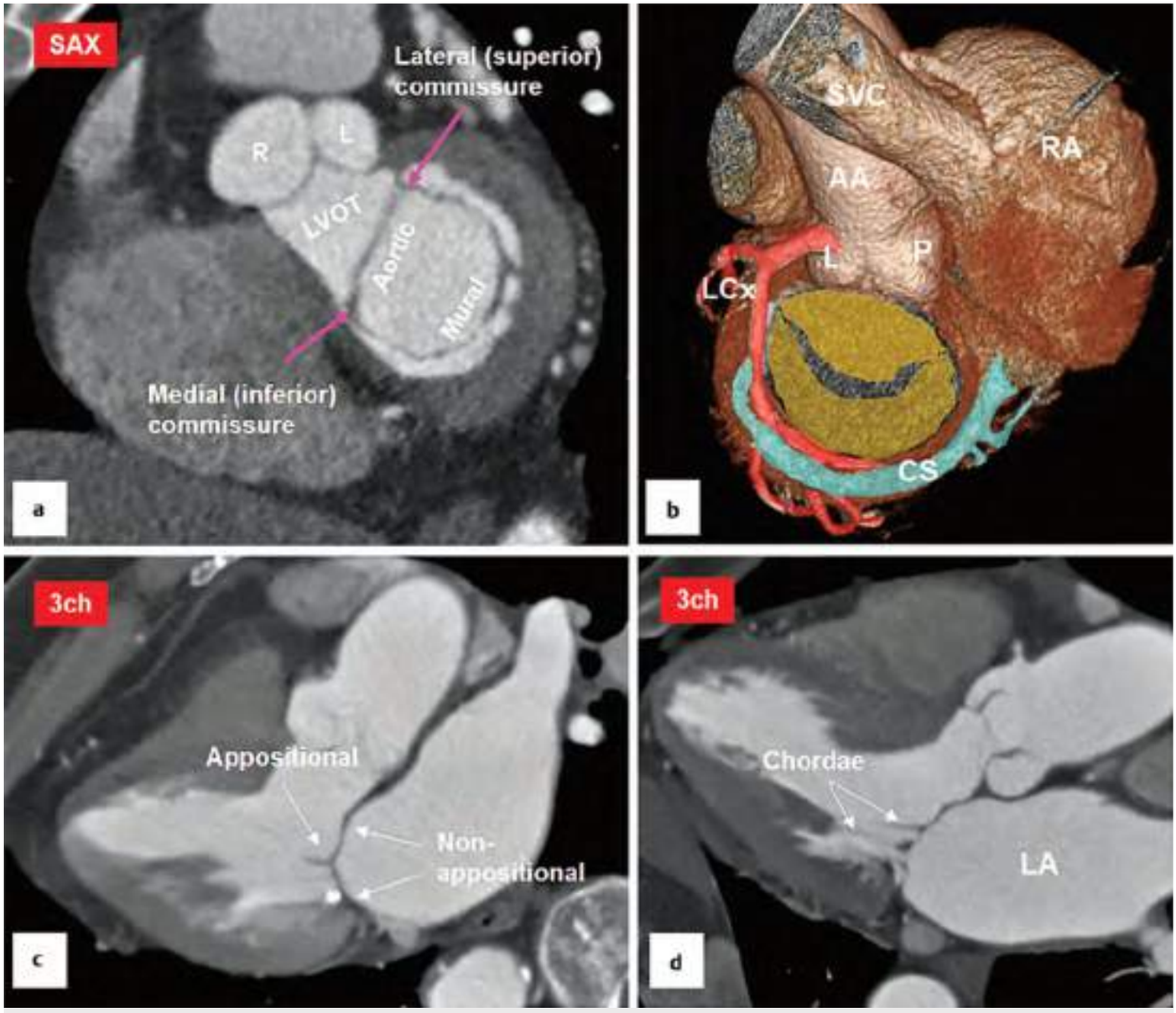

Fig. 12.87 **(a)** Short-axis view of the two leaflets of the mitral valve. The commissure is defined as the junction of the mitral leaflets. The anterior (superior, aortic) and posterior (inferior, mural) leaflets are confluent at the commissures and do not reach the annulus. At the commissures the valve is approximately 1 cm in width. **(b)** The relationship of the posterior mitral ring with coronary vessels is shown in this 3D image of the heart. The left atrium is removed from the image. The left circumflex artery (LCx) runs adjacent to the superior margin of the posterior leaflet, whereas the coronary sinus (CS) is adjacent to the inferior margin of the mitral annulus. These structures can be damaged during surgical or percutaneous mitral valve interventions. When the LCx is dominant, the entire attachment of the posterior leaflet may be closely related to this artery. **(c)** The appositional (coaptation) and nonappositional zones of the mitral leaflets are shown in this three-chamber view (3ch) obtained by CT during systole. The mitral leaflets overlap at the coaptation surface between 6 and 8 mm which is important for normal valve function. Short coaptation length can increase rate of regurgitation when the ventricle is dilated. **(d)** 3ch view showing the chordae tendineae. SVC, superior vena cava; AA, ascending aorta; LVOT, left ventricular outflow tract; P, posterior coronary sinus; L, left coronary sinus; LA, left atrium; R, right coronary sinus; RA, right atrium.

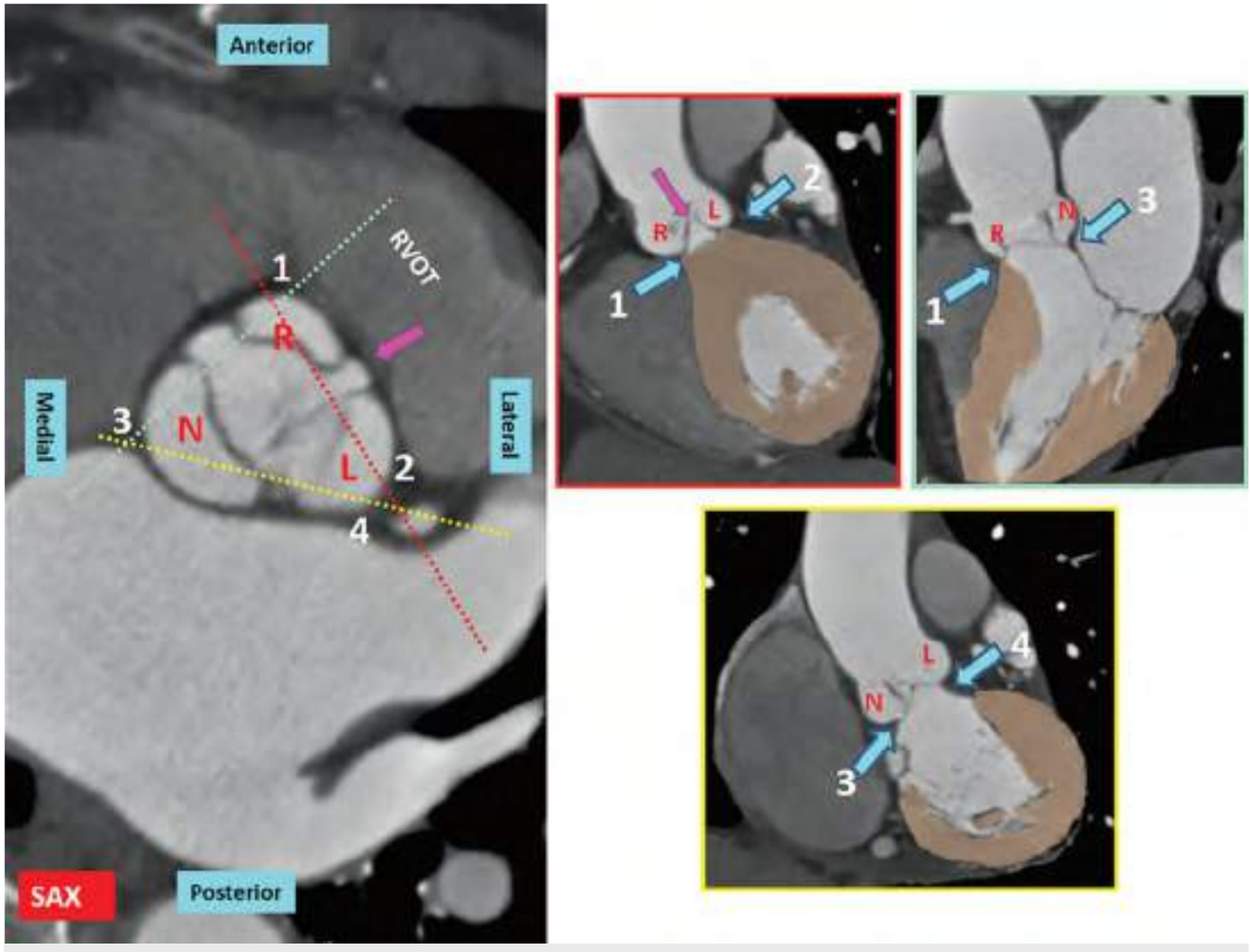

Fig. 12.88 Anatomical contacts of the left ventricle (LV) ostial muscle with the aortic sinuses. Using short-axis (SAX) reference through the aortic valve three long axis images are obtained along the anterolateral (red), anteromedial (blue), and posterior (yellow) walls of the left ventricular outflow tract. The nadir of both the right (R) and left (L) coronary sinuses is in contact with the LV ostium muscle. The intervalvular fibrous triangle between the right and left coronary sinuses of the aorta forms the uppermost part of the LVOT (*red arrow*). It faces the space between the aortic root and the right ventricular outflow tract (RVOT). N, noncoronary sinus.

12

onto which the prosthetic valve is sewn. For the anatomist, the VAJ is where the ventricular myocardium terminates.

The aorta is connected to the superior aspect of LVOT at an angle of 30% above the horizontal plane with the noncoronary sinus most inferiorly and the left coronary sinus most superiorly (▶ Fig. 12.88). Similar to the pulmonary valve, the aortic valve does not have a discrete annulus. The fibrous annuli conform to the shape of sinuses. They provide attachment to both the aortic wall and leaflets of the aortic valve. Both the aortic and the pulmonary roots have ventricular musculature at the base of their sinuses (VAJ). Ventricular musculature is circumferential in the pulmonary root, but it involves only 50% of the aortic annulus and the rest fibrous. On the other hand, ventricular musculature is absent or incomplete in the aortic root at the level of the noncoronary sinus due to the fibrous continuity between the leaflets of the aortic and mitral valves and the presence of the membranous septum.[107] The nadir of both the right and left coronary sinuses is in contact with the LV ostium (▶ Fig. 12.88, ▶ Fig. 12.89, ▶ Fig. 12.90). The right coronary sinus is in contact with the LV ostial myocardium over a distance of 16 mm.[94] The left coronary sinus is in contact with the LV ostium in the anterolateral portion of the sinus for only 7.5 mm, significantly less than for the right coronary sinus. The posterior portion of the left coronary sinus is not in direct contact with LV myocardium but is attached to the left fibrous trigone and faces the LA (▶ Fig. 12.89). Therefore, an electrocardiographic catheter positioned in the anterolateral portion of the left coronary sinus will record a ventricular electrogram whereas a catheter moved in the more posterior portion of this sinus will often record an atrial electrogram. A large left fibrous trigone results in minimal muscular attachment of the left coronary sinus to the LV. In contrast, muscular replacement of the left coronary sinus may rarely exist, causing direct attachment of the left coronary sinus to the LV muscle. Particular care is necessary in placing sutures in the muscular portion or paravalvular leak may result. The inferior margin of the noncoronary sinus is in contact with the membranous portion of the interventricular septum where it comes in close apposition to the penetrating bundle of His (▶ Fig. 12.37**d**). Because of this close proximity, a catheter

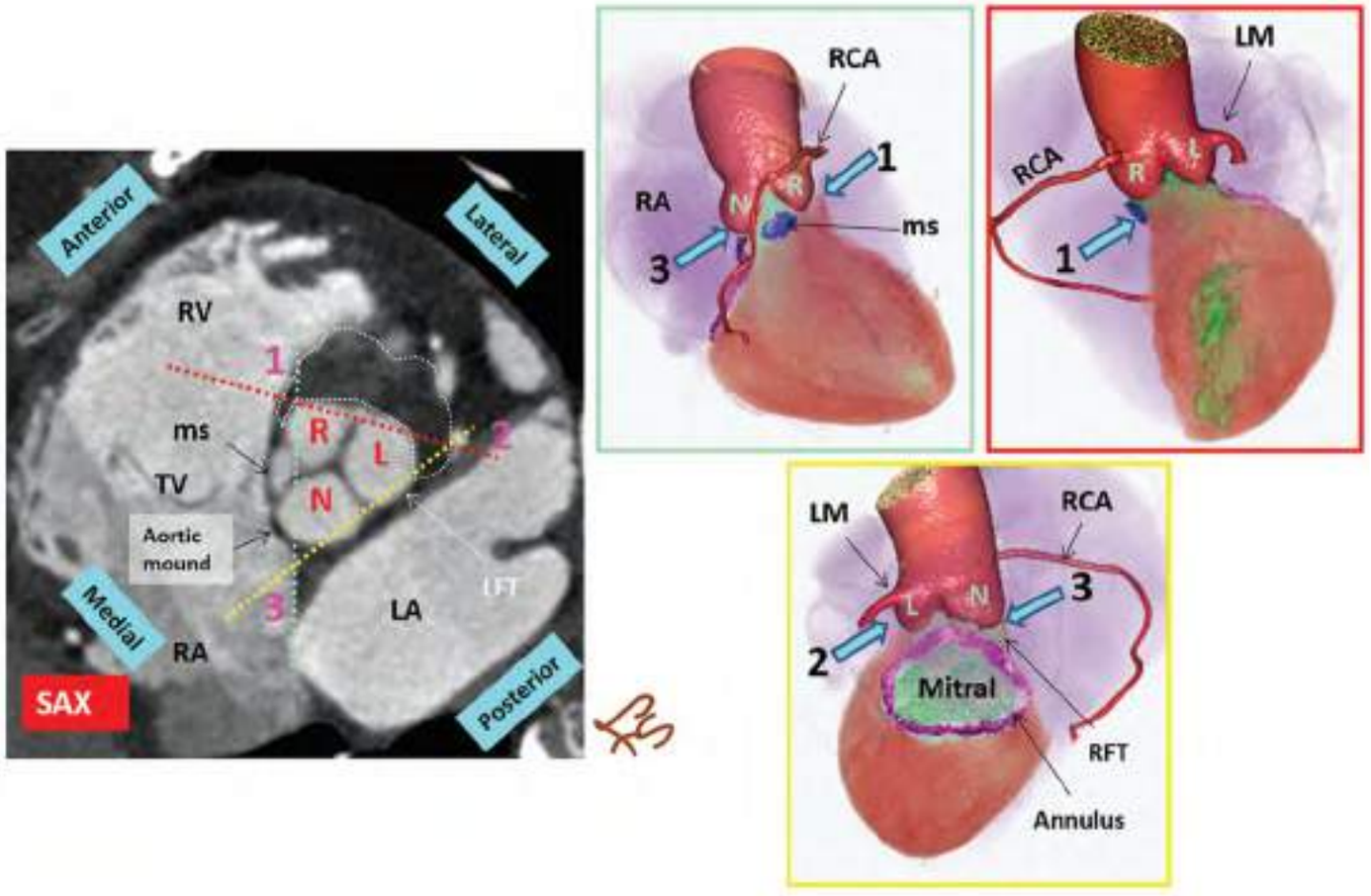

Fig. 12.89 Anatomical contacts of the left ventricle (LV) muscle with the aortic sinuses. Using short-axis (SAX) reference through the aortic valve, three volume-rendered images of the left heart are obtained along the anterolateral (red), anteromedial (blue), and posterior (yellow) walls of the left ventricular outflow tract. The muscular part of the LVOT is demarcated by dotted white line. The LV muscle is shown in brown on color-coded images. The nadir of the right (R) and sometimes left (L) coronary sinuses is in contact with the LV ostium muscle. The posterior portion of the left coronary sinus is not in direct contact with LV myocardium but is attached to the left fibrous trigone (LFT) and faces the left atrium (LA). Therefore, surgeons cannot dissect to the surgical ventriculoarterial junction where the nadir of the right coronary sinus is located. This does not apply to the nadirs of the noncoronary and in many cases the left coronary sinuses. There are three interleaflet fibrous triangles that reach to the level of the sinotubular junction of the aorta. LM, left main, ms, membranous septum; RCA, right coronary artery; RFT, right fibrous trigone; RV, right ventricle; TV, tricuspid valve.

recording His bundle activation across the tricuspid annulus marks the inferior extent of the noncoronary sinus.

The ostium of the RCA is located approximately 15 to 20 mm from the nadir of the sinus. The left main coronary artery ostium is located 12 to 17 mm above the nadir of the left coronary sinus. The aortic valve is related to each of the cardiac chambers and valves (▶ Fig. 12.89). These relationships are very important for understanding of the aortic valve pathological extensions and diagnosis of some conotruncal congenital heart malformations. The adjoining halves of the noncoronary and left coronary aortic sinuses are anterior to the LA with the transverse sinus of the pericardium located between them (▶ Fig. 12.89). The anterior half of the noncoronary sinus (adjoining the right coronary sinus) bulges toward the medial wall of the RA and is called "atrial mound" (▶ Fig. 12.89). The midpoint of the noncoronary sinus faces the interatrial junction (▶ Fig. 12.89). However, this relationship commonly changes with clockwise or counterclockwise rotation of the aortic root (▶ Fig. 12.91). The right coronary sinus of the aorta is in close proximity to the posterior wall of RVOT (crista supraventricularis) (▶ Fig. 12.63). The two walls are separated by the epicardial fat. The fibrous triangle between the noncoronary and right coronary sinuses is located directly above the membranous ventricular septum and the penetrating AV bundle of His (▶ Fig. 12.37). The intervalvular triangle between the right and left coronary sinuses of the aorta is located anterior to the left fibrous trigone and forms the uppermost part of the LVOT (▶ Fig. 12.88, ▶ Fig. 12.89). An incision through this area passes into the space between the aortic root and the RVOT. Only a small basal part of this area in some normal heart stands as a true outlet septum (infundibular septum). Thus, although the outlet components of the RV and LV face each other, an incision below the aortic valve may enter low into the infundibulum of the RV.

Membranous Septum

The membranous septum is located centrally within the cardiac base between the crest of the muscular ventricular septum and the interleaflet fibrous triangle, an area that separates the noncoronary sinus from the right coronary sinus (▶ Fig. 12.92, ▶ Fig. 12.93). The membranous septum is a thin fibrous septum

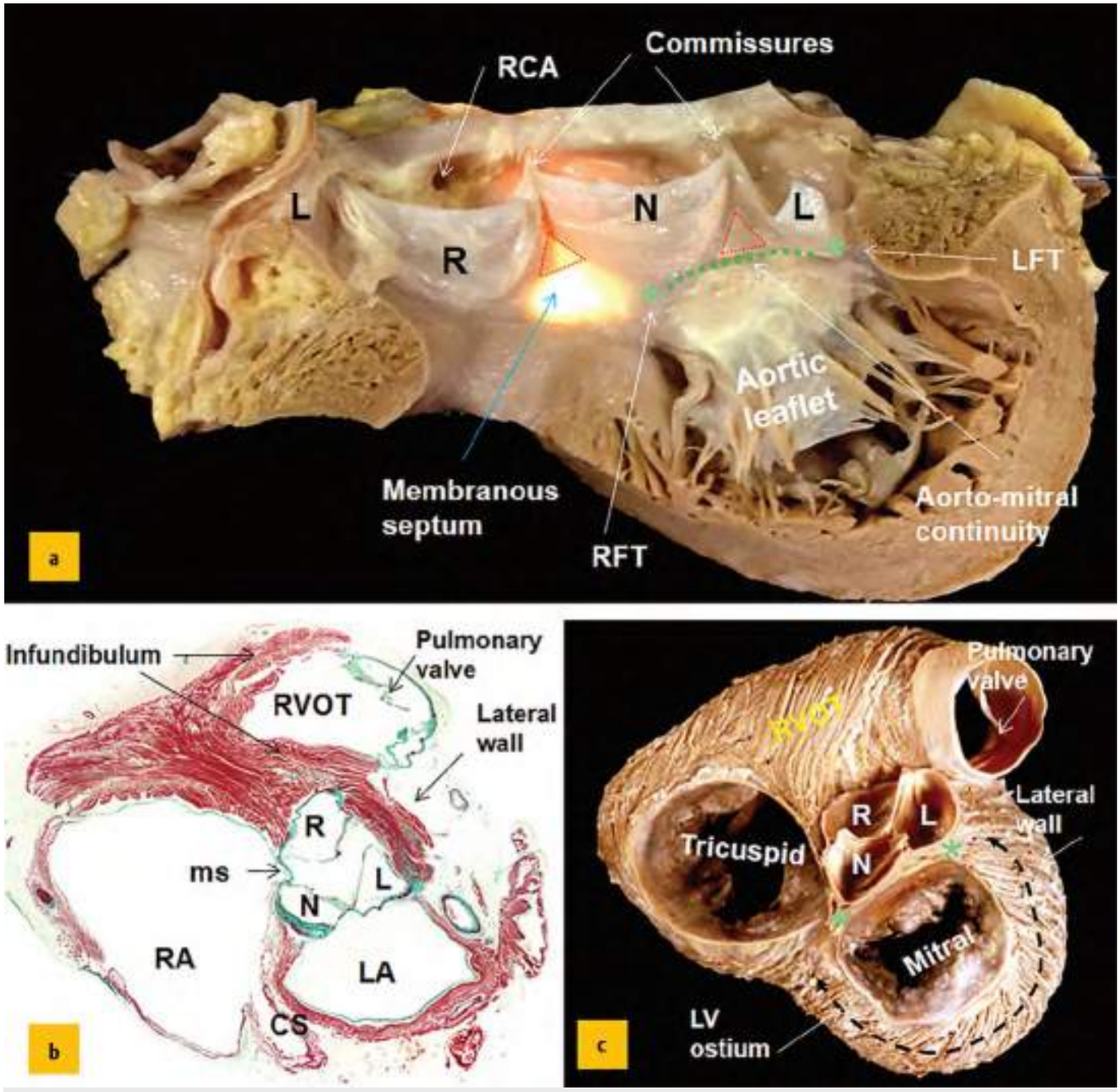

Fig. 12.90 **(a)** Aortic sinuses. Longitudinal open book dissection shows the three aortic sinuses. The fibrous continuity between the aortic leaflet of the mitral valve and left coronary (L) and noncoronary (N) of the aortic sinuses is shown with the junction demarcated by dashed green line. Two of the three interleaflet fibrous triangles (*red triangles*) and the membranous septum (ms) are shown. Note that the right fibrous trigone (RFT) is continuous with the membranous septum. The atrioventricular conduction axis penetrates through this fibrous area. The two fibrous structures together form the so-called central fibrous body **(b)** cross-section of the heart at the aortic sinuses. The muscular subpulmonary infundibulum of the right ventricular outflow tract (RVOT) and the muscle of the left ventricle (LV) ostium abut the right coronary (R) and left coronary (L) sinuses. Note that, while all the leaflets of the pulmonary valve are supported by infundibular musculature, only two of the leaflets of the aortic valve have muscular support. (**c**) Base of heart. The vestibule of the mitral and tricuspid valves is shown from the atrial side. The ostium of the LV is shown by back dashed line. Green stars, fibrous trigones; CS, coronary sinus; LFT, left fibrous trigone; Ao, aorta; MV, mitral valve; LVOT, left ventricular outflow tract; PT, pulmonary trunk; RVOT, right ventricular outflow tract; RCA, right coronary artery; TV, tricuspid valve.

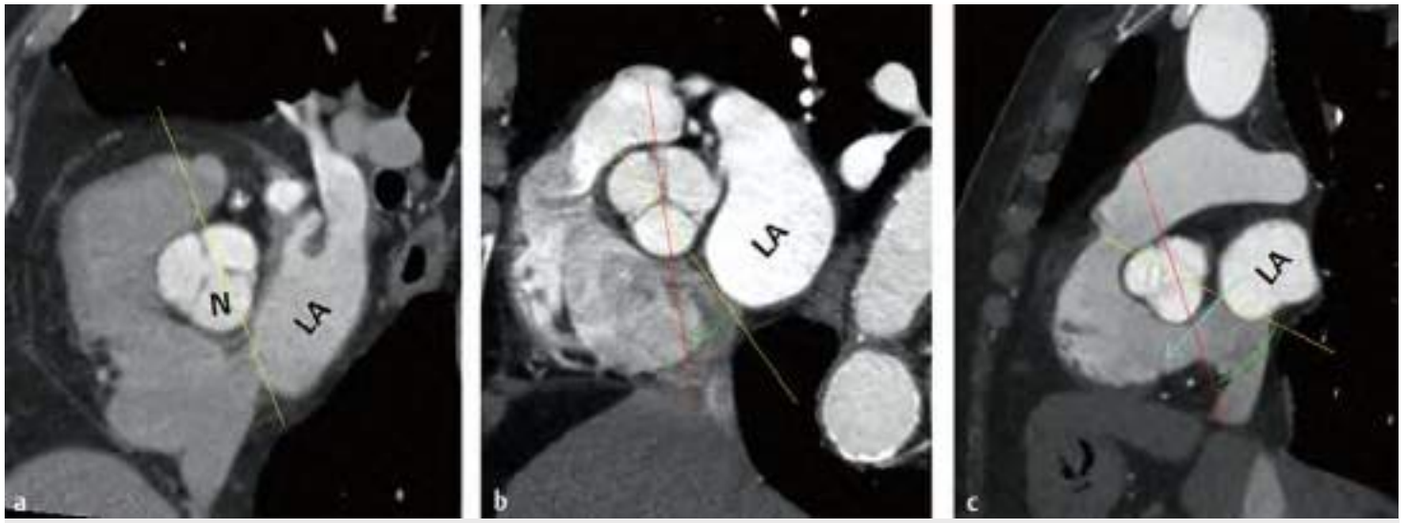

Fig. 12.91 **(a)** In most individuals, the midportion of the noncoronary aortic sinus (N) faces the interatrial septum. **(b)** In some cases, it is slightly rotated clockwise. **(c)** In rare examples, the aortic root shows marked clockwise rotation and translocation (*arrow*). LA, left atrium.

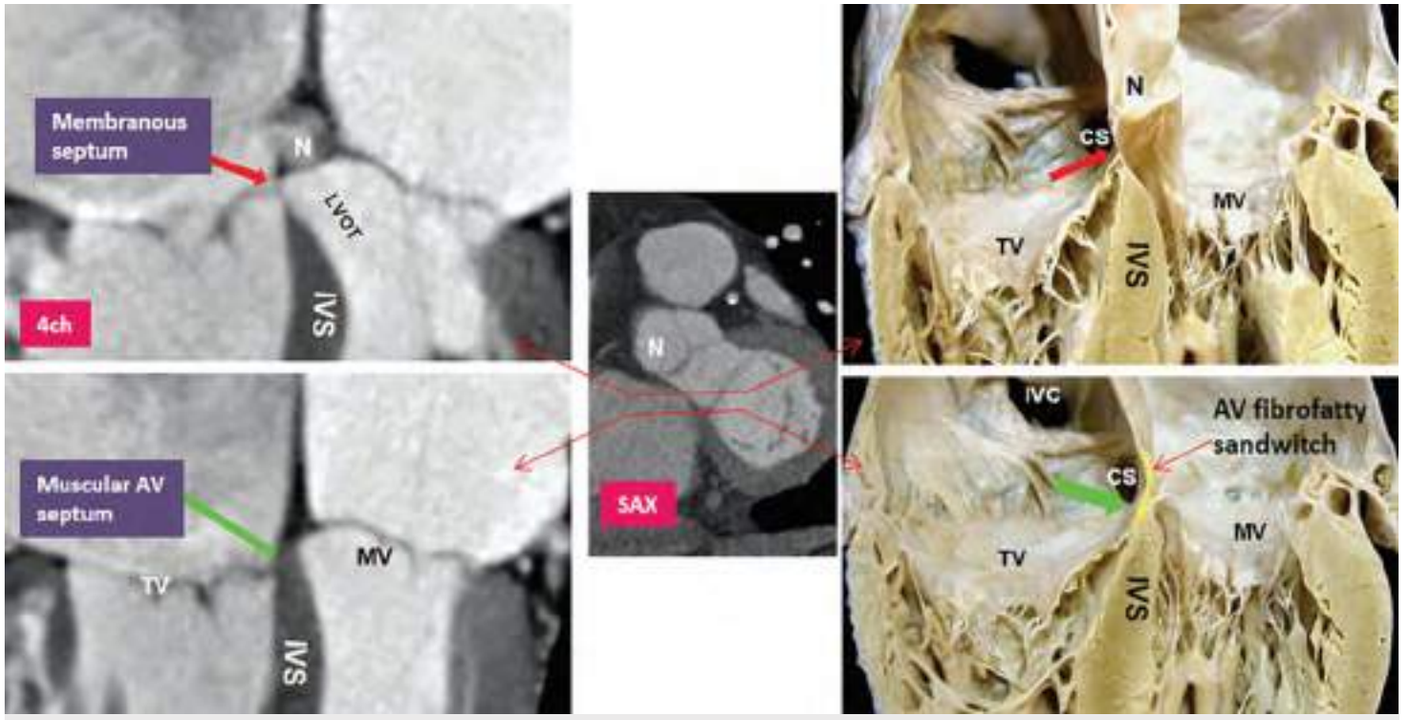

Fig. 12.92 Membranous septum (*red arrows*) versus muscular atrioventricular (AV) septum (*green arrows*). The membranous septum is clearly shown on both CT and cadaveric sections. On the other hand, CT shows a muscular AV septum inferior to the membranous septum whereas the cadaveric cut shows a sliver of fat interposed between the atrium and ventricular walls at the same anatomical level. Therefore, current resolution of CT may not be sufficient to show the small fat interposed between the two walls. CS, coronary sinus; IVC, inferior vena cava; IVS, interventricular septum; LVOT, left ventricular outflow tract; N, noncoronary sinus; MV, mitral valve; SAX, short axis; TV, tricuspid valve; 4ch, four chamber.

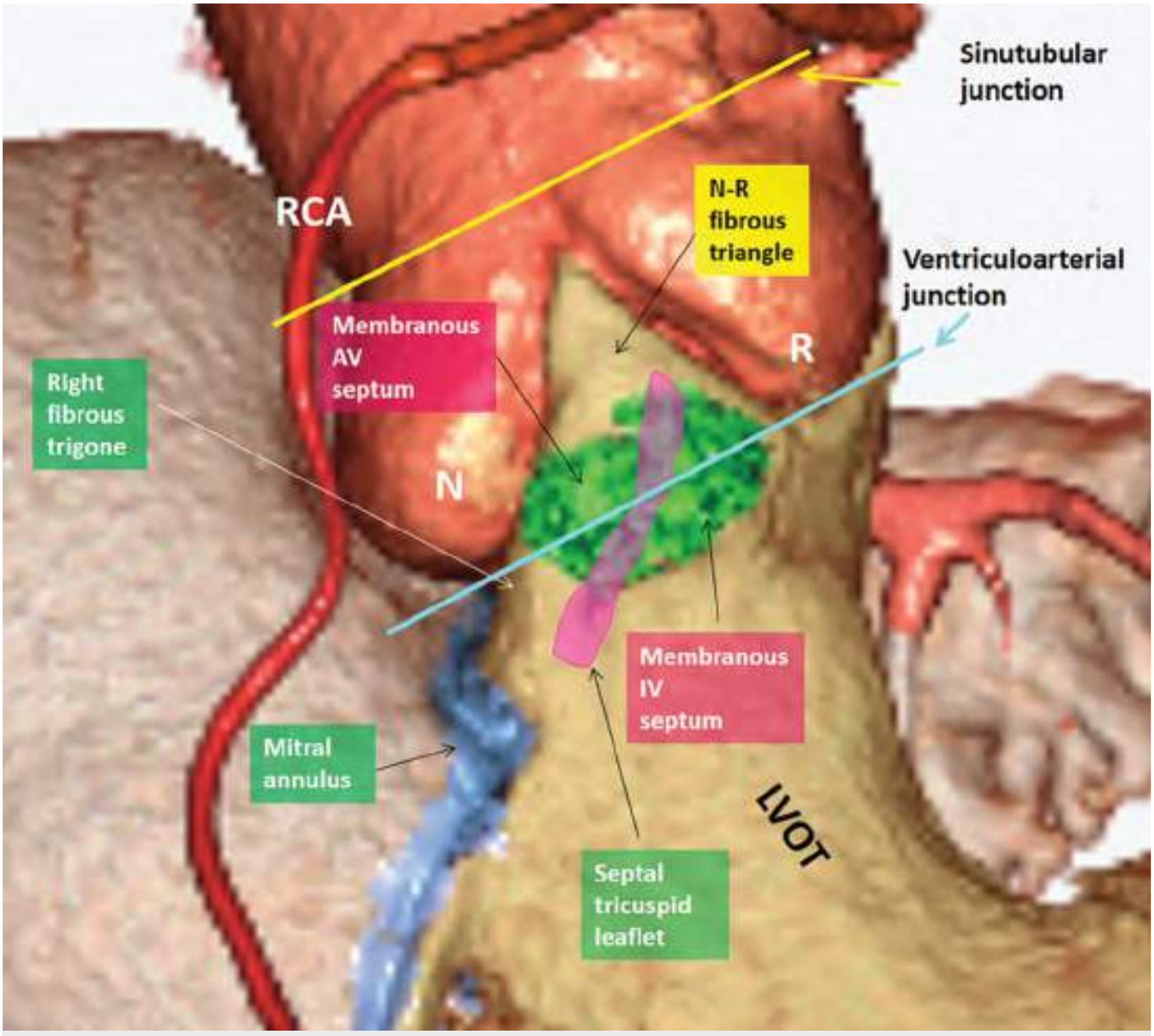

Fig. 12.93 Right anterior oblique color-coded volume-rendered CT images show the relationship of the membranous septum with the septal leaflet of the tricuspid annulus. Also shown are the sinotubular junction, ventriculoarterial junction, also called basal ring or surgical annulus, and the sinuses of Valsalva. The membranous septum is located between the muscular ventricular septum and the interleaflet triangle between the noncoronary (N) and right (R) coronary sinuses. The right fibrous trigone (RFT), where the mitral leaflet meets the nadir of the noncoronary sinus at the central fibrous body, lies inferior and posterior to the membranous septum and together form the central fibrous body.

with an irregular quadrangular shape, about 1-cm long.[68] As opposed to the muscular AV septum, the membranous septum is a true septum. The membranous septum has two components relative to the attachment of the septal tricuspid leaflet (▶ Fig. 12.37**d**):

1. AV component: between the RA and the LV.
2. Interventricular (IV) component: between the RV and LV.

The right fibrous trigone is continuous with the membranous interventricular septum (▶ Fig. 12.90). The septal attachment of the tricuspid valve demarcates the AV and interventricular divisions of the membranous septum (▶ Fig. 12.93). As mentioned, the left bundle of the cardiac conduction system enters the LVOT posterior to the membranous septum (▶ Fig. 12.36; ▶ Fig. 12.94).

Left Ventricular Function

The heart is a muscular pump that supplies blood to the body. This goal is achieved by electric excitation that produces sequential ventricular emptying and filling. The terms *systole* and *diastole*, have been derived from the Greek words "stello" (reduction, shortening) and "diastello" (augmentation, lengthening), respectively.[108] ▶ Fig. 12.95 shows pressure changes of the aorta, LV, and LA during cardiac cycle.

According to the classical mechanical concept the ventricular systole is from the initial increase of the ventricular pressure to the appearance of the aortic incisura. In this period, the initial isovolumetric contraction phase is followed by rapid and slow ejection, with consecutive reduction of the ventricular cavities'

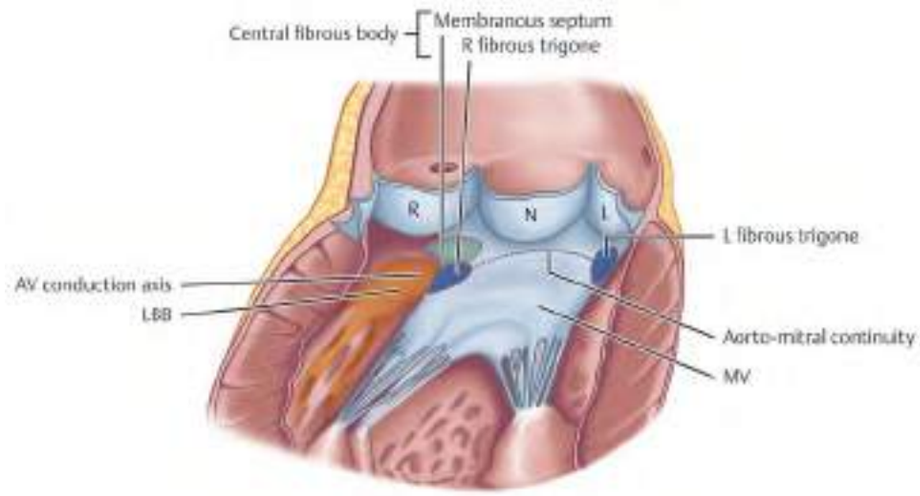

Fig. 12.94 Left ventricular view showing the atrioventricular (AV) conduction axis connecting the left bundle branch (LBB) posterior to the membranous septum. R, right; L, left; N, nonfacing ("noncoronary") aortic sinuses; MV, mitral valve.

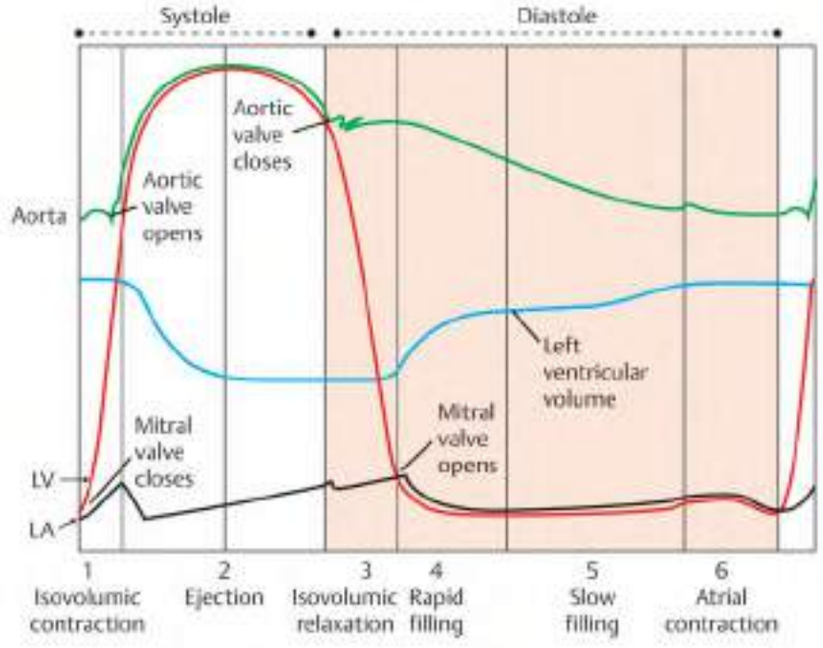

Fig. 12.95 Currently accepted time frames of systole and diastole, with measurements of intravascular pressure in the aorta, left ventricle (LV), left atrium (LA), and LV volume, together with their impact on the mitral and aortic valves. Aortic flow occurs between the two intervals that define ejection. The physiological phases of cardiac cycle that include isovolumic contraction, ejection, isovolumic relaxation, rapid and slow filling, and atrial contraction are shown. The LV volume decreases rapidly early in systole and slowly thereafter. The LV volume then increases rapidly in early filling and more slowly during late filling. The time interval during which this initial pressure decrease occurs is approximately 120 ms in the normal human heart. (Adapted from Buckberg et al 2008.[109])

volume and their long-axis shortening. The ventricular diastole is from the appearance of the aortic incisura to the end of atrial contraction. Diastole starts with isovolumetric relaxation phase and followed by the auxotonic relaxation phases (i.e., rapid filling, diastasis, and atrial contraction). In this period with the ventricular volume increases and lengthening along long axes occurs. It is believed that the term "isovolumic diastolic relaxation," is not correct and that it should be replaced with term "late systolic contraction" because of ongoing contraction (~90 ms) of the ascending segment of the apical myocardial loop occurs during this interval.[109]

Three muscle layers are classically described in the LV myocardial wall. A middle circumferential muscle strands (especially at the base) which is covered by obliquely arranged strands on the epicardial side and longitudinally directed strands on the endocardial side[83] (▶ Fig. 12.69). These muscle layers provide a complex myocardial contraction in all axes of the LV. The classical concept that the LV muscle is homogeneous, with all of its fibers contracting or relaxing simultaneously has changed. Torsion (twisting) is now believed to be the predominant movement that ejects the blood. Despite rapid progress in technology, it is still unclear how the end-to-end longitudinal chains of cardiomyocytes are arranged. Some believe that similar to skeletal muscles, myocardial cells are arranged as a continuous spiral (helical) muscle band that forms both RV and LV. In this new concept first introduced by Torrent-Guasp, the ventricular muscle is composed of two muscle loops, termed the *transverse basal and oblique apical loops*[108] (▶ Fig. 12.96).

The basal loop is circumferential and wraps around both the LV and RV but does not involve the septum. Therefore, at basal level, three groups of fibers are seen: inner and outer fibers that tend to run obliquely to the equatorial plane and a middle set that runs more horizontally. The apical loop shows a figure 8 configuration and is formed by two obliquely oriented muscle fibers: a descending segment and an ascending segment which form a vortex at the cardiac apex (▶ Fig. 12.96**e**). In this helical pattern the septum belongs to the LV. Dynamic change in length and diameters of the LV during cardiac cycle is facilitated by torsion of the LV around its long axis.

Other scientists disregard the helical loop concept and believe that ventricular myocardium is not analogous to skeletal muscles, instead it contains complex myocytic chains that form a 3D interconnected meshwork with a heterogeneous branching lamellar architecture, which facilitates the complex internal deformations of the ventricular wall.[110]

During initial isovolumic contraction, the apex shows a brief clockwise rotation and the base shows a brief counterclockwise rotation (▶ Fig. 12.97). Later in systole during ejection, the base changes direction and starts to rotate in a clockwise direction and the apex starts to rotate in counterclockwise direction.[111] In diastole, recoil of twist deformation (untwisting) is associated with the release of restoring forces, which contributes to LV diastolic relaxation and early diastolic filling.

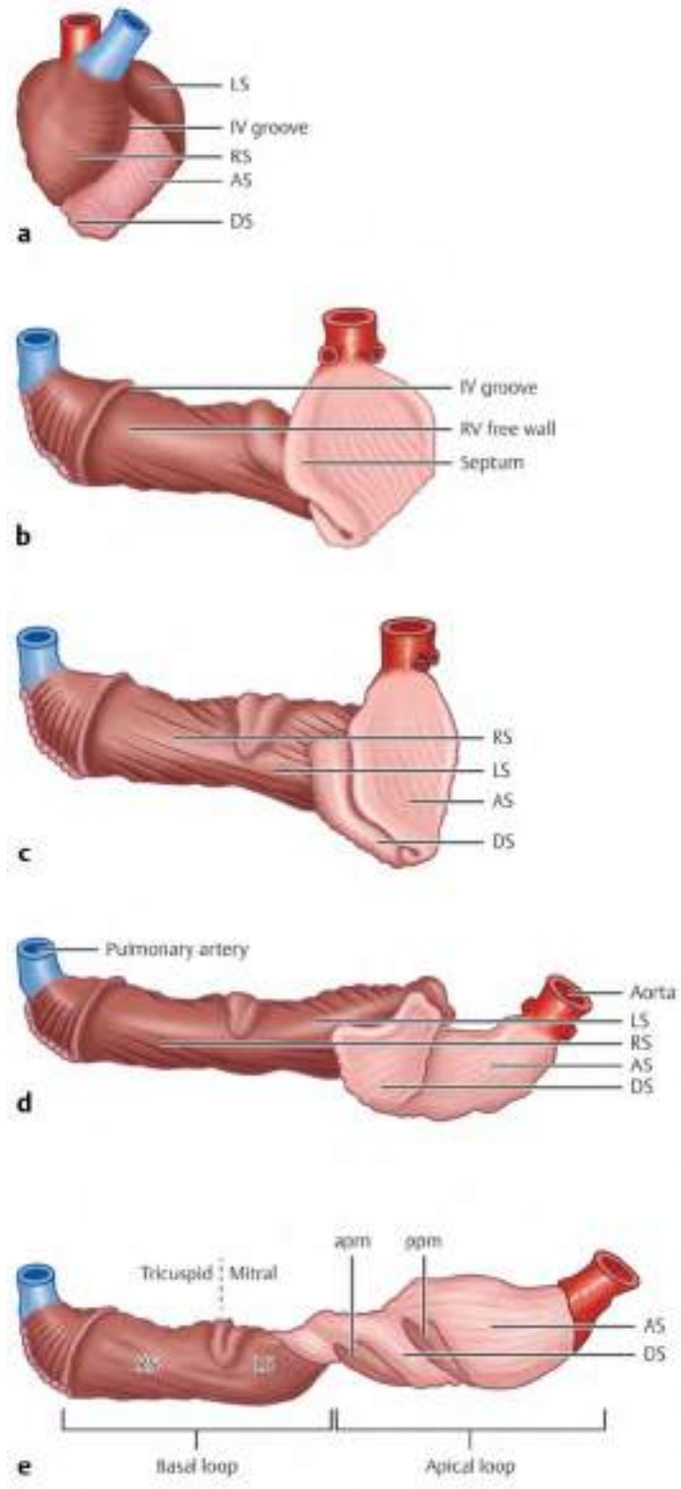

Fig. 12.96 (a–e) Unscrolling of Torrent-Guasp's myocardial band model, whereby the intact heart is unwrapped into define the stretched-out band. The myocardial band extends between the pulmonary artery and the aorta. Note the helix of the apical loop that contains predominantly oblique fibers and the twisting nature of the helix at the junction of the basal and apical loops. RS, right segment; LS, left segment; DS, descending segment; AS, ascending segment. (Adapted from Buckberg G et al 2008.[109])

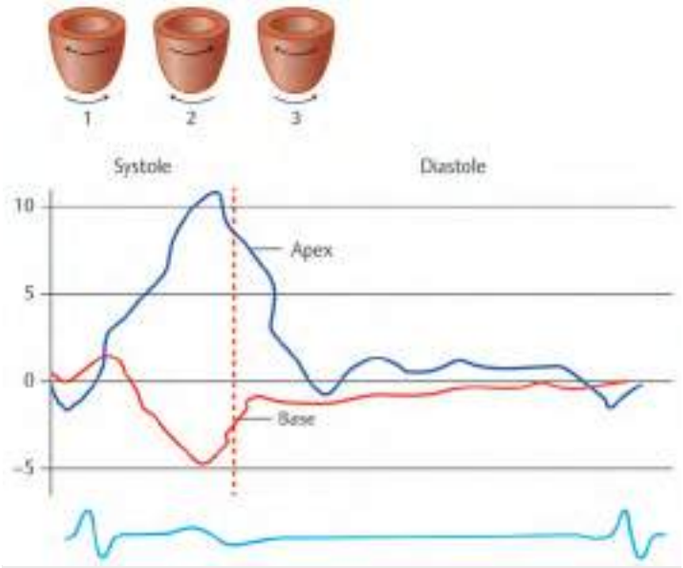

Fig. 12.97 Temporal sequences of the left ventricle (LV) twist during a cardiac cycle of normal heart. Clockwise (below baseline) and counterclockwise (above baseline) twists of the base and apex are shown. During isovolumic contraction (phase 1), the apex shows a brief clockwise rotation and the base shows a brief counterclockwise rotation. During ejection (phase 2), the direction of rotation changes and the LV apex rotates counterclockwise and the base rotates clockwise. Diastolic recoil of the LV twist (phase 3) occurs predominantly during the phase of isovolumic relaxation and early diastolic filling. (Adapted from Sengupta et al 2008.[111])

◆ Ventricular Septum

The ventricular septum is a thick muscle wall that separates the LVs and RVs and contributes to the cardiac function. The weight of septum is approximately 40% of ventricular myocardial mass. Although the septum anatomy contains two predominant muscle layers, it functions as a single unit. Therefore, there is no functional left- and right-sided septum.[112]

In helical loop model, the septum and the free wall of the LV is formed by the ascending segment of the apical loop. The free wall of the RV is formed from the wrapping of the right segment of the basal loop which is attached to the anterior margin of the septum at the anterior AV groove (▶ Fig. 12.96).

For an efficient EF based on twisting action, the orientation of the muscle fibers is important. In free wall of the RV the fibers are transverse, therefore, EF is 30% whereas in the septum and free wall of the LV oblique fiber orientation predominates that increases the EF to 60%. The septum is responsible for approximately 40% of left ventricular output. During systole, the septum twists and shortens in order to eject the blood forcefully out of both ventricular cavities. Therefore, normal function of the septum is pivotal for normal function of both ventricles.

The twisting action of the septum diminishes when the LV or RV dilates. Dilation of one ventricle will result in elevation of end diastolic pressure causing diastolic bowing of the septum into the contralateral chamber. Bowing of the septum into the ventricle changes the orientation of its muscle fibers into transverse hence lowering the ejection power of the septum. The RV can function properly as long as the septum is normal. With severe pulmonary hypertension and bowing of the septum into the RV, the function of the RV can rapidly decline. In the absence of septal twisting due to septal damage, ventricular ejection is produced by circumferential constriction caused by contraction of the basal wall that contains predominantly transverse fibers. Conversely, septal dysfunction does not usually cause severe LV dysfunction as long as the oblique fibers in the LV free wall are intact to retain the capacity to twist.

◆ Atrioventricular Conduction Axis

The AV conduction axis is an essential component of the septal AV junction. The AV node lies within the triangle of Koch just below the atrial side of the central fibrous body, approximately at the nadir of the noncoronary sinus of the aortic valve.[91,113] It measures 5 mm in length, 2.5 to 3.5 mm in width, and 1 mm in thickness.[113,114] The superior margin of the AV node is adherent to the central fibrous body but, it is neither encased by the fibrous tissue nor insulated from the working atrial myocardium (▶ Fig. 12.15). The AV node has two parts[1]: a compact part and[2] an area of transitional cells. The compact part is semioval shaped at the mid- to apical portion of the triangle of Koch. Transitional cells are located toward the orifice of the coronary sinus (▶ Fig. 12.37; ▶ Fig. 12.98).

The AV bundle of His exits the AV node, penetrates the right fibrous trigone, and runs along the inferior margin of the IV component of the membranous septum underneath the septal attachment of the tricuspid valve before dividing into the left and right bundle branches[114] (▶ Fig. 12.94, ▶ Fig. 12.98). The left bundle branch divides into the posterior, septal, and anterior branches while the right bundle branch courses as a single cord-like trunk below the medial (septal) papillary muscle complex to enter the inferior arm of the septomarginal trabeculation and from there into the moderator band. The arterial supply to the posterior interventricular septum, interatrial septum (including the AV node), and penetrating His bundle is largely provided by the AV node artery.[115,116] The right superior septal artery and the left first septal artery may provide collateral vascular supply especially when the flow to the AV node artery is compromised (Fig. 12[?]99).

The AV conduction axis cannot be visualized by clinical imaging methods. However, certain landmarks allow us to approximately localize this axis on CT. These key landmarks include the posteroinferior margin of the AV membranous septum, the right fibrous trigone and the medial papillary muscle.[91] The His bundle runs underneath the membranous septum and the right bundle branch runs underneath the medial papillary muscle (▶ Fig. 12.37; ▶ Fig. 12.98). Therefore, a line connecting these two locations demarcates the location of the AV conduction axis.[117]

The right fibrous trigone and the IV component of the membranous septum are collectively called the “central fibrous body” where fibrous union of the aortic noncoronary sinus, anterior leaflet of mitral valve, and septal leaflet of the tricuspid valve occurs[114] (▶ Fig. 12.90). At the central fibrous body, the penetrating bundle of His is directly related to the above valves and the membranous septum. This close association increases the risk of damage during surgical or percutaneous manipulation of any of

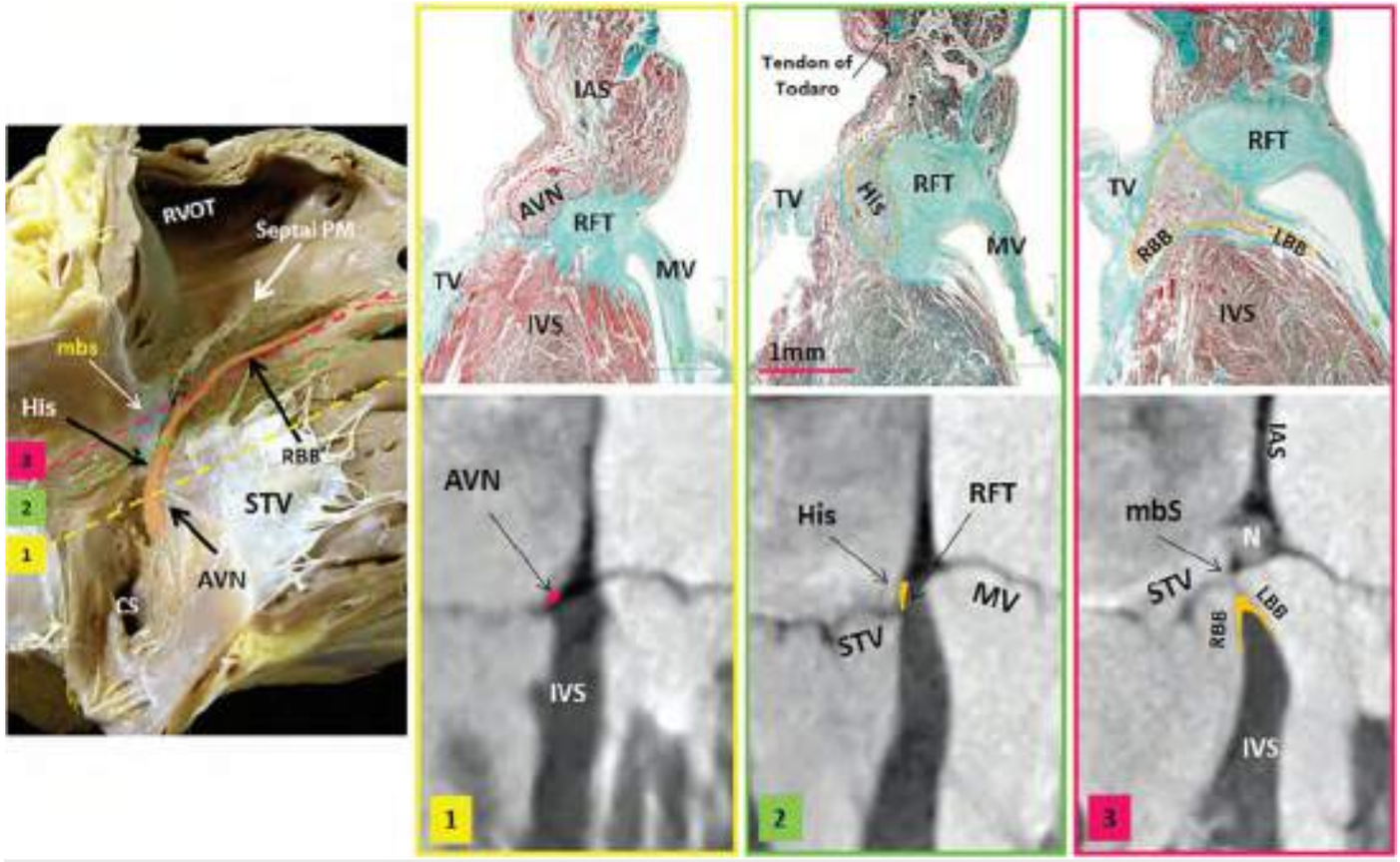

Fig. 12.98 Atrioventricular (AV) conduction axis. Long-axis four-chamber cadaveric cuts with corresponding CT images at three levels showing anatomical location of the cardiac conduction system at the AV junction. The levels of three reference cuts are shown in different colors on cadaveric inner view of the triangle of Koch. The anatomical course of the AV conduction axis is nicely dissected in this view. Section 1 above the coronary sinus (CS), is where the AV node (AVN) resides. The AVN is 5 mm is length and extends to the inferior margin of the membranous septum (mbs) where the right fibrous trigone (RFT) is located. Section 2 shows the bundle of His (1–2 cm in length) penetrating the right fibrous trigone and passing below the membranous septum. In section 3, the His bundle has divided into bundle branches at the base of the interventricular septum (IVS). The right bundle branch passes below the septal papillary muscle (PM). Therefore, a line connecting the superior edge of the CS, inferior margin of the mbs, and inferior edge of the septal MP demarcates the approximate location of the AV conduction axis. These three landmarks can easily be shown in most high-quality CT angiographies of the heart. IAS, interatrial septum; LBB, left bundle branch; MV, mitral valve; RVOT, right ventricular outflow tract; STV, septal tricuspid valve; TV, tricuspid valve.

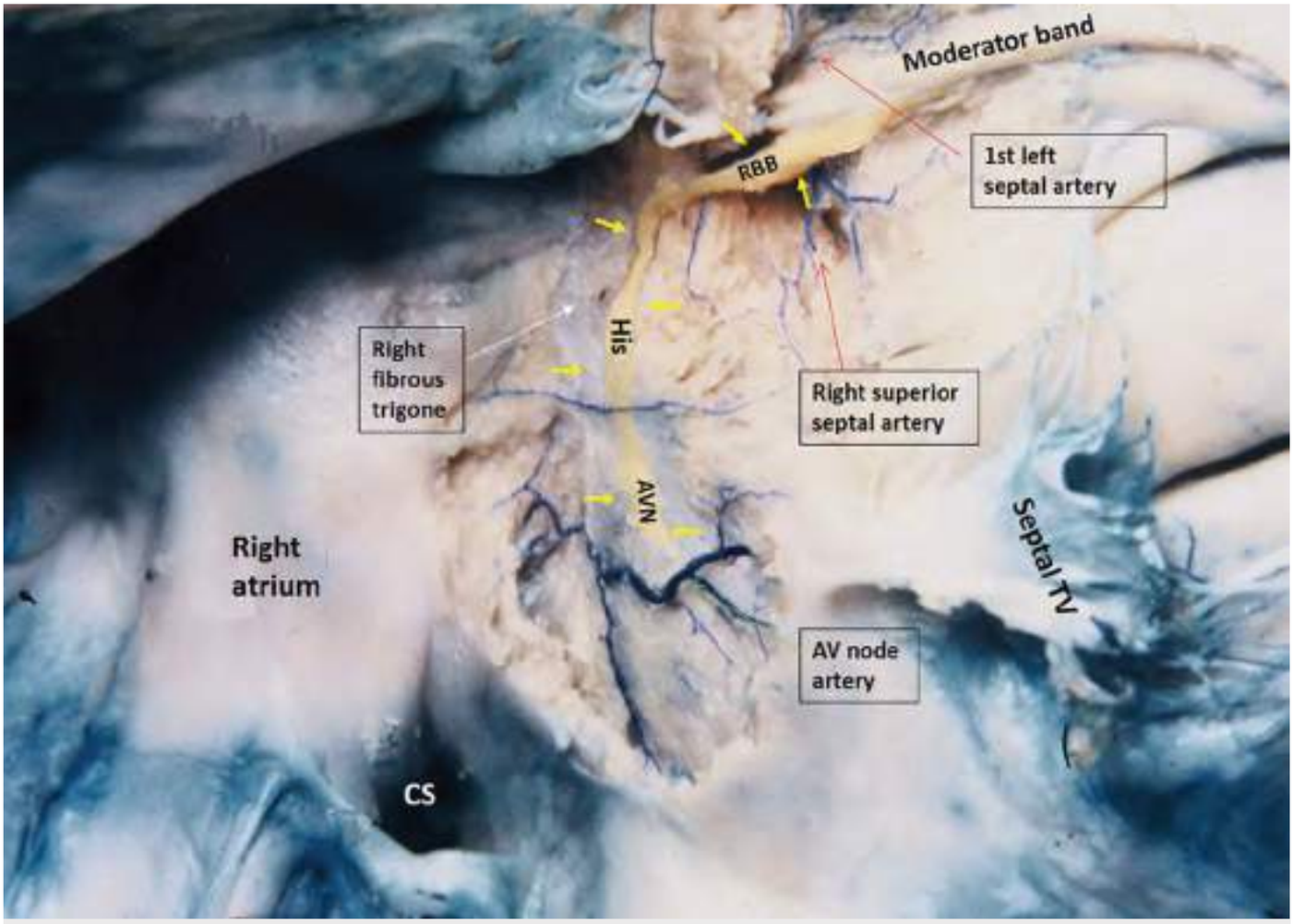

Fig. 12.99 Cadaveric view from the right atrium medial wall showing the arterial supply of the atrioventricular (AV) conduction axis. The AV node (AVN), penetrating bundle of His (His), right bundle branch (RBB), and AV node artery are exposed. Yellow arrows demarcate the conduction axis. The AVN artery is the main supplier of the AVN. Distal branches of the right superior septal artery (a branch of the right coronary artery) nourish the His bundle and communicate with the AVN artery. Branches of the first septal artery (branch of left anterior descending artery) extend to the RBB and moderator band. CS, coronary sinus; TV, tricuspid valve. Adapted from Abuin and Nieponice A 1998.[116]

these structures. Because of the close proximity of these structures, large calcifications within the anteromedial aspect mitral annulus or at the noncoronary sinus of the aortic valve may damage the His bundle resulting in AV conduction block[118,119] (▶ Fig. 12.17**a**). AV conduction block is a known common complication after transcatheter aortic valve implantation involving a heavily calcified valve.[119,120] Primary calcification of the AV node is very rare but has been reported. Invasive neoplasm, and marked epicardial lipomatosis can interfere with normal function of the AV conduction axis. In congenital heart disease, the conduction pathway can be anatomically normal but misplaced due to a congenital defect.

References

[1] McAlpine WA. Heart and Coronary Arteries: An Anatomical Atlas for Clinical Diagnosis, Radiological Investigation, and Surgical Treatment. New York, NY: Springer-Verlag; 1975;160–178

[2] Anderson RH, Brown NA. The anatomy of the heart revisited. Anat Rec.; 246 (1):1–7

[3] Sánchez-Quintana D, Anderson RH, Cabrera JA, et al. The terminal crest: morphological features relevant to electrophysiology. Heart.; 88(4):406–411

[4] Sánchez-Quintana D, Cabrera JA, Farré J, Climent V, Anderson RH, Ho SY. Sinus node revisited in the era of electroanatomical mapping and catheter ablation. Heart.; 91(2):189–194

[5] Matsuyama TA, Inoue S, Kobayashi Y, et al. Anatomical diversity and age-related histological changes in the human right atrial posterolateral wall. Europace.; 6(4):307–315

[6] Shiraishi I, Takamatsu T, Minamikawa T, Onouchi Z, Fujita S. Quantitative histological analysis of the human sinoatrial node during growth and aging. Circulation.; 85(6):2176–2184

[7] Sow ML, Ndoye JM, Lô EA. The artery of the sinoatrial node: anatomic considerations based on 45 injection-dissections of the heart. Surg Radiol Anat.; 18 (2):103–109

[8] Man KC, Knight B, Tse HF, et al. Radiofrequency catheter ablation of inappropriate sinus tachycardia guided by activation mapping. J Am Coll Cardiol.; 35 (2):451–457

[9] Berdajs D, Patonay L, Turina MI. The clinical anatomy of the sinus node artery. Ann Thorac Surg.; 76(3):732–735, discussion 735–736

[10] Saremi F, Abolhoda A, Ashikyan O, et al. Arterial supply to sinuatrial and atrioventricular nodes: imaging with multidetector CT. Radiology.; 246 (1):99–107, discussion 108–109

[11] Kalman JM, Olgin JE, Karch MR, Hamdan M, Lee RJ, Lesh MD. "Cristal tachycardias": origin of right atrial tachycardias from the crista terminalis identified by intracardiac echocardiography. J Am Coll Cardiol.; 31(2):451–459
[12] Heyer CM, Kagel T, Lemburg SP, Bauer TT, Nicolas V. Lipomatous hypertrophy of the interatrial septum: a prospective study of incidence, imaging findings, and clinical symptoms. Chest.; 124(6):2068–2073
[13] Saremi F, Krishnan S. Cardiac conduction system: anatomic landmarks relevant to interventional electrophysiologic techniques demonstrated with 64-detector CT. Radiographics.; 27(6):1539–1565, discussion 1566–1567
[14] Lemery R, Guiraudon G, Veinot JP. Anatomic description of Bachmann's bundle and its relation to the atrial septum. Am J Cardiol.; 91(12):1482–1485, A8
[15] Leier CV, Meacham JA, Schaal SF. Prolonged atrial conduction. A major predisposing factor for the development of atrial flutter. Circulation.; 57 (2):213–216
[16] Schuchlenz HW, Saurer G, Weihs W, Rehak P. Persisting eustachian valve in adults: relation to patent foramen ovale and cerebrovascular events. J Am Soc Echocardiogr.; 17(3):231–233
[17] Saremi F, Channual S, Krishnan S, Gurudevan SV, Narula J, Abolhoda A. Bachmann bundle and its arterial supply: imaging with multidetector CT—implications for interatrial conduction abnormalities and arrhythmias. Radiology.; 248(2):447–457
[18] Saremi F, Emmanuel N, Wu PF, et al. Paradoxical embolism: role of imaging in diagnosis and treatment planning. Radiographics.; 34(6):1571–1592
[19] Cabrera JA, Sánchez-Quintana D, Farré J, Rubio JM, Ho SY. The inferior right atrial isthmus: further architectural insights for current and coming ablation technologies. J Cardiovasc Electrophysiol.; 16(4):402–408
[20] Olgin JE, Kalman JM, Fitzpatrick AP, Lesh MD. Role of right atrial endocardial structures as barriers to conduction during human type I atrial flutter. Activation and entrainment mapping guided by intracardiac echocardiography. Circulation.; 92(7):1839–1848
[21] Saremi F, Pourzand L, Krishnan S, et al. Right atrial cavotricuspid isthmus: anatomic characterization with multi-detector row CT. Radiology.; 247 (3):658–668
[22] Silver MA, Rowley NE. The functional anatomy of the human coronary sinus. Am Heart J.; 115(5):1080–1084
[23] Bhatnagar KP, Nettleton GS, Campbell FR, Wagner CE, Kuwabara N, Muresian H. Chiari anomalies in the human right atrium. Clin Anat.; 19(6):510–516
[24] Schneider B, Hofmann T, Justen MH, Meinertz T. Chiari's network: normal anatomic variant or risk factor for arterial embolic events? J Am Coll Cardiol.; 26(1):203–210
[25] Sanchez-Quintana D, Davies DW, Ho SY, Oslizlok P, Anderson RH. Architecture of the atrial musculature in and around the triangle of Koch: its potential relevance to atrioventricular nodal reentry. J Cardiovasc Electrophysiol.; 8(12):1396–1407
[26] Jazayeri MR, Hempe SL, Sra JS, et al. Selective transcatheter ablation of the fast and slow pathways using radiofrequency energy in patients with atrioventricular nodal reentrant tachycardia. Circulation.; 85(4):1318–1328
[27] Coffey JO, d'Avila A, Dukkipati S, et al. Catheter ablation of scar-related atypical atrial flutter. Europace.; 15(3):414–419
[28] Ueng KC, Chen SA, Chiang CE, et al. Dimension and related anatomical distance of Koch's triangle in patients with atrioventricular nodal reentrant tachycardia. J Cardiovasc Electrophysiol.; 7(11):1017–1023
[29] Delise P, Bonso A, Coro L, et al. Pacemapping of the triangle of Koch: a simple method to reduce the risk of atrioventricular block during radiofrequency ablation of atrioventricular node reentrant tachycardia. Pacing Clin Electrophysiol.; 24(12):1725–1731
[30] Anderson RH, Webb S, Brown NA. Clinical anatomy of the atrial septum with reference to its developmental components. Clin Anat.; 12(5):362–374
[31] Ho SY, Anderson RH. How constant anatomically is the tendon of Todaro as a marker for the triangle of Koch? J Cardiovasc Electrophysiol.; 11(1):83–89
[32] Chang SL, Tai CT, Lin YJ, et al. The electroanatomic characteristics of the cavotricuspid isthmus: implications for the catheter ablation of atrial flutter. J Cardiovasc Electrophysiol.; 18(1):18–22
[33] Sánchez-Quintana D, Ho SY, Cabrera JA, Farré J, Anderson RH. Topographic anatomy of the inferior pyramidal space: relevance to radiofrequency catheter ablation. J Cardiovasc Electrophysiol.; 12(2):210–217
[34] Anderson KR, Murphy JG. The atrio-ventricular node artery in the human heart. Angiology.; 34(11):711–716
[35] Arid JM, Armstrong O, Rogez JM, Robert R, Lardoux MC, Leborgne J. Arterial vascularisation of the atrioventricular node. Surg Radiol Anat.; 22(2):93–96
[36] Ho SY, Sánchez-Quintana D, Cabrera JA, Anderson RH. Anatomy of the left atrium: implications for radiofrequency ablation of atrial fibrillation. J Cardiovasc Electrophysiol.; 10(11):1525–1533
[37] Sánchez-Quintana D, Cabrera JA, Climent V, Farré J, Mendonça MC, Ho SY. Anatomic relations between the esophagus and left atrium and relevance for ablation of atrial fibrillation. Circulation.; 112(10):1400–1405
[38] Sánchez-Quintana D, Pizarro G, López-Mínguez JR, Ho SY, Cabrera JA. Standardized review of atrial anatomy for cardiac electrophysiologists. J Cardiovasc Transl Res.; 6(2):124–144
[39] Sánchez-Quintana D, Doblado-Calatrava M, Cabrera JA, Macías Y, Saremi F. Anatomical Basis for the Cardiac Interventional Electrophysiologist. BioMed Res Int.; 2015:547364
[40] Moorman A, Webb S, Brown NA, Lamers W, Anderson RH. Development of the heart: (1) formation of the cardiac chambers and arterial trunks. Heart.; 89(7):806–814
[41] Becker AE. Left atrial isthmus: anatomic aspects relevant for linear catheter ablation procedures in humans. J Cardiovasc Electrophysiol.; 15(7):809–812
[42] Jaïs P, Hocini M, Hsu LF, et al. Technique and results of linear ablation at the mitral isthmus. Circulation.; 110(19):2996–3002
[43] Cronin P, Sneider MB, Kazerooni EA, et al. MDCT of the left atrium and pulmonary veins in planning radiofrequency ablation for atrial fibrillation: a how-to guide. AJR Am J Roentgenol.; 183(3):767–778
[44] Marom EM, Herndon JE, Kim YH, McAdams HP. Variations in pulmonary venous drainage to the left atrium: implications for radiofrequency ablation. Radiology.; 230(3):824–829
[45] Jongbloed MR, Lamb HJ, Bax JJ, et al. Noninvasive visualization of the cardiac venous system using multislice computed tomography. J Am Coll Cardiol.; 45 (5):749–753
[46] Ho SY, Cabrera JA, Tran VH, Farré J, Anderson RH, Sánchez-Quintana D. Architecture of the pulmonary veins: relevance to radiofrequency ablation. Heart.; 86(3):265–270
[47] Sánchez JE, Plumb VJ, Epstein AE, Kay GN. Evidence for longitudinal and transverse fiber conduction in human pulmonary veins: relevance for catheter ablation. Circulation.; 108(5):590–597
[48] Pappone C, Oreto G, Rosanio S, et al. Atrial electroanatomic remodeling after circumferential radiofrequency pulmonary vein ablation: efficacy of an anatomic approach in a large cohort of patients with atrial fibrillation. Circulation.; 104(21):2539–2544
[49] Marrouche NF, Martin DO, Wazni O, et al. Phased-array intracardiac echocardiography monitoring during pulmonary vein isolation in patients with atrial fibrillation: impact on outcome and complications. Circulation.; 107 (21):2710–2716
[50] Ouyang F, Bänsch D, Ernst S, et al. Complete isolation of left atrium surrounding the pulmonary veins: new insights from the double-Lasso technique in paroxysmal atrial fibrillation. Circulation.; 110(15):2090–2096
[51] Ernst S, Ouyang F, Löber F, Antz M, Kuck KH. Catheter-induced linear lesions in the left atrium in patients with atrial fibrillation: an electroanatomic study. J Am Coll Cardiol.; 42(7):1271–1282
[52] Nigri GR, Di Dio LJ, Baptista CA. Papillary muscles and tendinous cords of the right ventricle of the human heart: morphological characteristics. Surg Radiol Anat.; 23(1):45–49
[53] Veinot JP, Harrity PJ, Gentile F, et al. Anatomy of the normal left atrial appendage: a quantitative study of age-related changes in 500 autopsy hearts: implications for echocardiographic examination. Circulation.; 96 (9):3112–3115
[54] Di Biase L, Santangeli P, Anselmino M, et al. Does the left atrial appendage morphology correlate with the risk of stroke in patients with atrial fibrillation? Results from a multicenter study. J Am Coll Cardiol.; 60(6):531–538
[55] Cabrera JA, Saremi F, Sánchez-Quintana D. Left atrial appendage: anatomy and imaging landmarks pertinent to percutaneous transcatheter occlusion. Heart.; 100(20):1636–1650
[56] Kim DT, Lai AC, Hwang C, et al. The ligament of Marshall: a structural analysis in human hearts with implications for atrial arrhythmias. J Am Coll Cardiol.; 36(4):1324–1327
[57] Saremi F, Channual S, Abolhoda A, Gurudevan SV, Narula J, Milliken JC. MDCT of the S-shaped sinoatrial node artery. AJR Am J Roentgenol.; 190(6):1569–1575

[58] Duerinckx AJ, Vanovermeire O. Accessory appendages of the left atrium as seen during 64-slice coronary CT angiography. Int J Cardiovasc Imaging.; 24 (2):215–221
[59] Peng LQ, Yu JQ, Yang ZG, et al. Left atrial diverticula in patients referred for radiofrequency ablation of atrial fibrillation: assessment of prevalence and morphologic characteristics by dual-source computed tomography. Circ Arrhythm Electrophysiol.; 5(2):345–350
[60] Lemola K, Sneider M, Desjardins B, et al. Computed tomographic analysis of the anatomy of the left atrium and the esophagus: implications for left atrial catheter ablation. Circulation.; 110(24):3655–3660
[61] Ho SY, Cabrera JA, Sánchez-Quintana D. Vagaries of the vagus nerve: relevance to ablationists. J Cardiovasc Electrophysiol.; 17(3):330–331
[62] Shah D, Dumonceau JM, Burri H, et al. Acute pyloric spasm and gastric hypomotility: an extracardiac adverse effect of percutaneous radiofrequency ablation for atrial fibrillation. J Am Coll Cardiol.; 46(2):327–330
[63] Sánchez-Quintana D, Ho SY, Climent V, Murillo M, Cabrera JA. Anatomic evaluation of the left phrenic nerve relevant to epicardial and endocardial catheter ablation: implications for phrenic nerve injury. Heart Rhythm.; 6(6):764–768
[64] Sacher F, Monahan KH, Thomas SP, et al. Phrenic nerve injury after atrial fibrillation catheter ablation: characterization and outcome in a multicenter study. J Am Coll Cardiol.; 47(12):2498–2503
[65] Matsumoto Y, Krishnan S, Fowler SJ, et al. Detection of phrenic nerves and their relation to cardiac anatomy using 64-slice multidetector computed tomography. Am J Cardiol.; 100(1):133–137
[66] Hagen PT, Scholz DG, Edwards WD. Incidence and size of patent foramen ovale during the first 10 decades of life: an autopsy study of 965 normal hearts. Mayo Clin Proc.; 59(1):17–20
[67] Anderson RH, Brown NA, Webb S. Development and structure of the atrial septum. Heart.; 88(1):104–110
[68] Anderson RH, Spicer DE, Brown NA, Mohun TJ. The development of septation in the four-chambered heart. Anat Rec (Hoboken).; 297(8):1414–1429
[69] Sharratt GP, Webb S, Anderson RH. The vestibular defect: an interatrial communication due to a deficiency in the atrial septal component derived from the vestibular spine. Cardiol Young.; 13(2):184–190
[70] Saremi F, Channual S, Raney A, et al. Imaging of patent foramen ovale with 64-section multidetector CT. Radiology.; 249(2):483–492
[71] Thompson T, Evans W. Paradoxical embolism. Q J Med.; 23:135–0
[72] Ho SY, McCarthy KP, Rigby ML. Morphological features pertinent to interventional closure of patent oval foramen. J Interv Cardiol.; 16(1):33–38
[73] Hanley PC, Tajik AJ, Hynes JK, et al. Diagnosis and classification of atrial septal aneurysm by two-dimensional echocardiography: report of 80 consecutive cases. J Am Coll Cardiol.; 6(6):1370–1382
[74] Pearson AC, Nagelhout D, Castello R, Gomez CR, Labovitz AJ. Atrial septal aneurysm and stroke: a transesophageal echocardiographic study. J Am Coll Cardiol.; 18(5):1223–1229
[75] Raney AR, Saremi F, Kenchaiah S, et al. Multidetector computed tomography shows intramyocardial fat deposition. J Cardiovasc Comput Tomogr.; 2 (3):152–163
[76] Ho SY, Nihoyannopoulos P. Anatomy, echocardiography, and normal right ventricular dimensions. Heart.; 92 Suppl 1:i2–i13
[77] Haddad F, Hunt SA, Rosenthal DN, Murphy DJ. Right ventricular function in cardiovascular disease, part I: Anatomy, physiology, aging, and functional assessment of the right ventricle. Circulation.; 117(11):1436–1448
[78] Loukas M, Klaassen Z, Tubbs RS, et al. Anatomical observations of the moderator band. Clin Anat.; 23(4):443–450
[79] Reig J, Albertí N, Petit M. Arterial vascularization of the human moderator band: an analysis of this structure's role as a collateral circulation route. Clin Anat.; 13(4):244–250
[80] Alva C, Ho SY, Lincoln CR, Rigby ML, Wright A, Anderson RH. The nature of the obstructive muscular bundles in double-chambered right ventricle. J Thorac Cardiovasc Surg.; 117(6):1180–1189
[81] Anderson RH, Razavi R, Taylor AM. Cardiac anatomy revisited. J Anat.; 205 (3):159–177
[82] Warnes CA. Adult congenital heart disease importance of the right ventricle. J Am Coll Cardiol.; 54(21):1903–1910
[83] Sanchez-Quintana D, Anderson RH, Ho SY. Ventricular myoarchitecture in tetralogy of Fallot. Heart.; 76(3):280–286
[84] Anderson RH, Smerup M, Sanchez-Quintana D, Loukas M, Lunkenheimer PP. The three-dimensional arrangement of the myocytes in the ventricular walls. Clin Anat.; 22(1):64–76
[85] Nielsen E, Smerup M, Agger P, et al. Normal right ventricular three-dimensional architecture, as assessed with diffusion tensor magnetic resonance imaging, is preserved during experimentally induced right ventricular hypertrophy. Anat Rec (Hoboken).; 292(5):640–651
[86] Anderson RH, Ho SY, Redmann K, Sanchez-Quintana D, Lunkenheimer PP. The anatomical arrangement of the myocardial cells making up the ventricular mass. Eur J Cardiothorac Surg.; 28(4):517–525
[87] Geva T, Powell AJ, Crawford EC, Chung T, Colan SD. Evaluation of regional differences in right ventricular systolic function by acoustic quantification echocardiography and cine magnetic resonance imaging. Circulation.; 98 (4):339–345
[88] Lindqvist P, Henein M, Kazzam E. Right ventricular outflow-tract fractional shortening: an applicable measure of right ventricular systolic function. Eur J Echocardiogr.; 4(1):29–35
[89] Calcutteea A, Chung R, Lindqvist P, Hodson M, Henein MY. Differential right ventricular regional function and the effect of pulmonary hypertension: three-dimensional echo study. Heart.; 97(12):1004–1011
[90] Loukas M, Tubbs RS, Louis RG, Jr, et al. An endoscopic and anatomical approach to the septal papillary muscle of the conus. Surg Radiol Anat.; 31 (9):701–706
[91] Anderson RH, Yanni J, Boyett MR, Chandler NJ, Dobrzynski H. The anatomy of the cardiac conduction system. Clin Anat.; 22(1):99–113
[92] Luciani GB, Favaro A, Casali G, Santini F, Mazzucco A. Ross operation in the young: a ten-year experience. Ann Thorac Surg.; 80(6):2271–2277
[93] Cerqueira MD, Weissman NJ, Dilsizian V, et al. American Heart Association Writing Group on Myocardial Segmentation and Registration for Cardiac Imaging. Standardized myocardial segmentation and nomenclature for tomographic imaging of the heart. A statement for healthcare professionals from the Cardiac Imaging Committee of the Council on Clinical Cardiology of the American Heart Association. Circulation.; 105(4):539–542
[94] Yamada T, Litovsky SH, Kay GN. The left ventricular ostium: an anatomic concept relevant to idiopathic ventricular arrhythmias. Circ Arrhythm Electrophysiol.; 1(5):396–404
[95] Migliore F, Zorzi A, Bertaglia E, et al. Incidence, management, and prevention of right ventricular perforation by pacemaker and implantable cardioverter defibrillator leads. Pacing Clin Electrophysiol.; 37(12):1602–1609
[96] Johansson B, Maceira AM, Babu-Narayan SV, Moon JC, Pennell DJ, Kilner PJ. Clefts can be seen in the basal inferior wall of the left ventricle and the interventricular septum in healthy volunteers as well as patients by cardiovascular magnetic resonance. J Am Coll Cardiol.; 50(13):1294–1295
[97] von Lüdinghausen M. The venous drainage of the human myocardium. Adv Anat Embryol Cell Biol.; 168:I–VIII, 1–104
[98] Gunnal SA, Wabale RN, Farooqui MS. Morphological study of chordae tendinae in human cadaveric hearts. Heart Views.; 16(1):1–12
[99] Loukas M, Louis RG, Jr, Black B, Pham D, Fudalej M, Sharkees M. False tendons: an endoscopic cadaveric approach. Clin Anat.; 20(2):163–169
[100] Anderson RH, Frater RW. How can we best describe the components of the mitral valve? J Heart Valve Dis.; 15(6):736–739
[101] Muresian H. The clinical anatomy of the mitral valve. Clin Anat.; 22(1):85–98
[102] Levine RA, Handschumacher MD, Sanfilippo AJ, et al. Three-dimensional echocardiographic reconstruction of the mitral valve, with implications for the diagnosis of mitral valve prolapse. Circulation.; 80(3):589–598
[103] Salgo IS, Gorman JH, III, Gorman RC, et al. Effect of annular shape on leaflet curvature in reducing mitral leaflet stress. Circulation.; 106(6):711–717
[104] Grewal J, Suri R, Mankad S, et al. Mitral annular dynamics in myxomatous valve disease: new insights with real-time 3-dimensional echocardiography. Circulation.; 121(12):1423–1431
[105] Blanke P, Dvir D, Cheung A, et al. Mitral annular evaluation with CT in the context of transcatheter mitral valve replacement. JACC Cardiovasc Imaging.; 8(5):612–615
[106] Anderson RH. Clinical anatomy of the aortic root. Heart.; 84(6):670–673
[107] Hasdemir C, Aktas S, Govsa F, et al. Demonstration of ventricular myocardial extensions into the pulmonary artery and aorta beyond the ventriculo-arterial junction. Pacing Clin Electrophysiol.; 30(4):534–539
[108] Torrent-Guasp F, Kocica MJ, Corno A, et al. Systolic ventricular filling. Eur J Cardiothorac Surg.; 25(3):376–386

[109] Buckberg G, Hoffman JI, Mahajan A, Saleh S, Coghlan C. Cardiac mechanics revisited: the relationship of cardiac architecture to ventricular function. Circulation.; 118(24):2571–2587
[110] Stephenson RS, Agger P, Lunkenheimer PP, et al. The functional architecture of skeletal compared to cardiac musculature: myocyte orientation, lamellar unit morphology, and the helical ventricular myocardial band. Clin Anat.; 29 (3):316–332
[111] Sengupta PP, Tajik AJ, Chandrasekaran K, Khandheria BK. Twist mechanics of the left ventricle: principles and application. JACC Cardiovasc Imaging.; 1 (3):366–376
[112] Saleh S, Liakopoulos OJ, Buckberg GD. The septal motor of biventricular function. Eur J Cardiothorac Surg.; 29 Suppl 1:S126–S138
[113] Anderson RH, Ho SY. The architecture of the sinus node, the atrioventricular conduction axis, and the internodal atrial myocardium. J Cardiovasc Electrophysiol.; 9(11):1233–1248
[114] Sánchez-Quintana D, Yen Ho S. [Anatomy of cardiac nodes and atrioventricular specialized conduction system]. Rev Esp Cardiol.; 56(11):1085–1092
[115] Berdajs D, Künzli A, Shurr U, Zünd G, Turina MI, Genonni M. Clinical anatomy of the atrioventricular node artery. J Heart Valve Dis.; 15(2):225–229
[116] Abuin G, Nieponice A. New findings on the origin of the blood supply to the atrioventricular node. Clinical and surgical significance. Tex Heart Inst J.; 25 (2):113–117
[117] Mori S, Spicer DE, Anderson RH. Revisiting the Anatomy of the Living Heart. Circ J.; 80(1):24–33
[118] Montemurro D, Ronzani G, Defilippi G, Pizzuti A, Brusca A. [Conduction disorders and sites of calcification of the mitral ring: 2-dimensional echocardiographic study]. G Ital Cardiol.; 16(4):308–312
[119] Takamoto T, Popp RL. Conduction disturbances related to the site and severity of mitral anular calcification: a 2-dimensional echocardiographic and electrocardiographic correlative study. Am J Cardiol.; 51(10):1644–1649
[120] Hamdan A, Guetta V, Klempfner R, et al. Inverse relationship between membranous septal length and the risk of atrioventricular block in patients undergoing transcatheter aortic valve implantation. JACC Cardiovasc Interv.; 8(9):1218–1228

13 Atrioventricular Septal Region

Shumpei Mori, Diane E. Spicer, and Robert H. Anderson

◆ Introduction

The anatomy of the base of the ventricular mass is markedly complex. Several important structures, including the hinges of the leaflets of the cardiac valves, the inferior pyramidal space, the membranous septum, the basal components of the atrial septum, the paraseptal areas, the atrioventricular conduction axis, and the arterial roots are all concentrated around or within the base of the ventricles.[1,2,3,4,5,6,7] Even with the heart in one's hands, it can be remarkably difficult to provide a simple description of the relationships of the various components. For example, because the hinge of the septal leaflet of the tricuspid valve is located apically relative to the mitral valvar attachment, the cavity of the right atrium faces that of the left ventricle. There is, therefore, seemingly an extensive atrioventricular septal area.[1] In fact, because a cranial extension of the inferior atrioventricular groove interposes between the right atrial wall and the crest of the muscular ventricular septum, the larger part of the area is a sandwich rather than a true septum.[7] It has recently been shown that these subtle relationships are better illustrated using virtual dissection of three-dimensional datasets obtained during life using computed tomography (CT).[8,9,10] Such virtual dissections also place the related structures into the heart as seen in the living individual, providing attitudinally appropriate images.[11,12] In this chapter, we use such datasets to show the precise anatomical relationships of all these cardiac components. We begin, however, by illustrating the advantages to be gained in the clinical setting by describing the components using attitudinally appropriate nomenclature.

◆ Anatomical Arrangement of the Base of the Ventricular Mass

The base of the ventricular mass surrounds and supports the atrioventricular and ventriculoarterial junctions (▶ Fig. 13.1). Within the roof of the left ventricle, the atrioventricular and ventriculoarterial junctions are adjacent to one another, sharing a common area of aortic-to-mitral valvar continuity. The aortic root is deeply wedged between the orifice of the mitral valve and the basal extent of the muscular ventricular septum (▶ Fig. 13.1, ▶ Fig. 13.2). Within the right ventricle, in contrast, the atrioventricular and arterial valves are supported by discrete and separate junctions, with the muscular subpulmonary infundibulum lifting the leaflets of the pulmonary valve away from the remainder of the ventricular base (▶ Fig. 13.1). When viewed from the right and from posterior, it can be seen that the inferior components of the atrioventricular junctions diverge from one another, with the inferior pyramidal space filling the area between the junctions (▶ Fig. 13.1). The inferior pyramidal space is an extracardiac space separating the atrial and ventricular myocardial components (▶ Fig. 13.3). It is filled with epicardial fibroadipose tissue. The

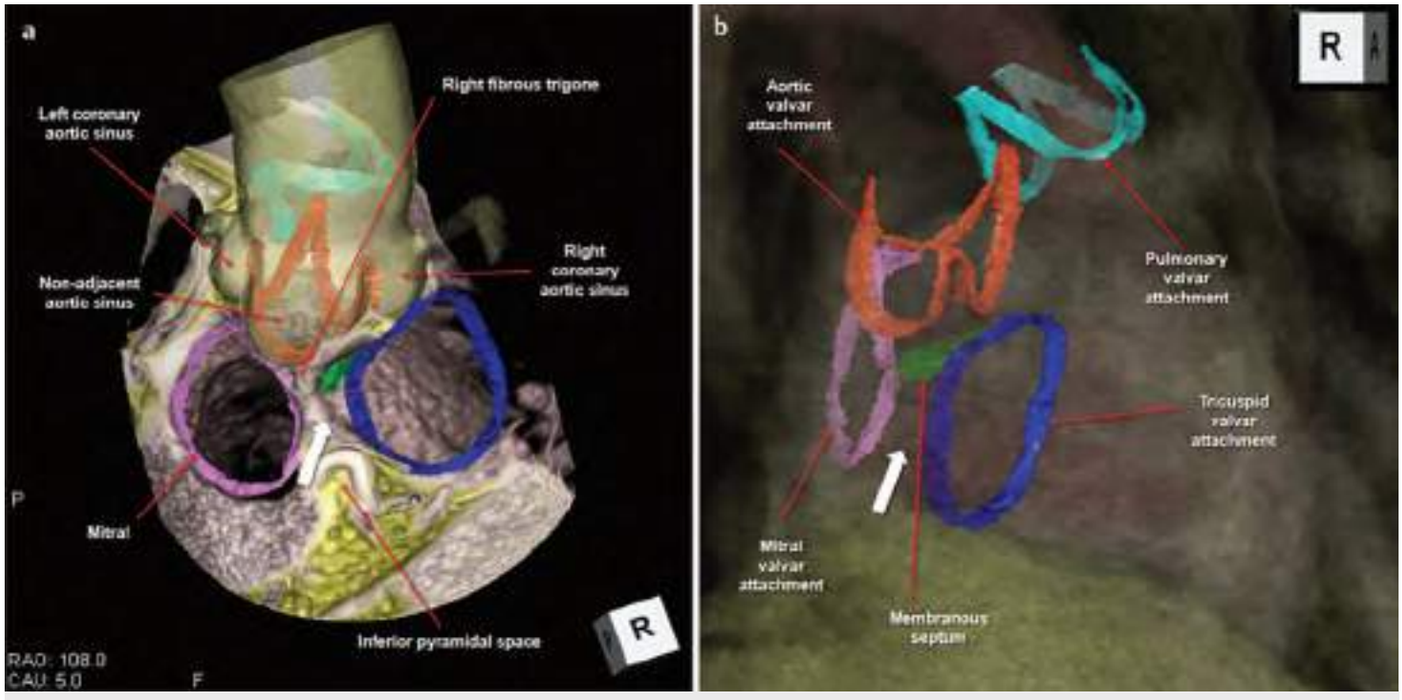

Fig. 13.1 The reconstructions show the three-dimensional anatomy of the base of the ventricular mass, which surrounds and supports the atrioventricular and the ventriculoarterial junctions. The attachments of the leaflets of the aortic, pulmonary, mitral, and tricuspid valves, are shown in red, sky blue, pink, and blue, respectively **(a, b)**. Green shows the membranous septum. The tricuspid valvar attachment (*blue*) is located slightly inferiorly and apically with respect to the mitral valvar attachment (*pink*). The resultant gap between the mitral and tricuspid valvar attachments (*white arrow*) corresponds to the atrioventricular sandwich.

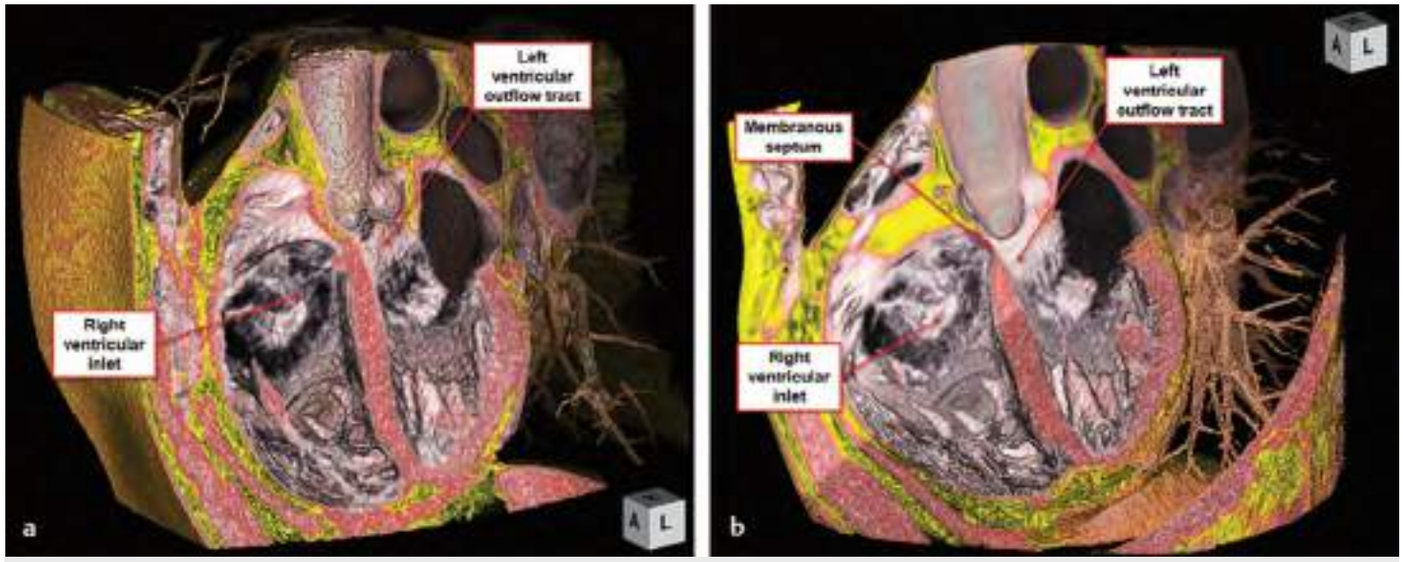

Fig. 13.2 The reconstruction shows how the aortic root being deeply wedged between the orifice of the mitral valve and the basal extent of the muscular ventricular septum forming the left ventricular outflow tract. **(a)** More posterior image **(b)** shows that the posterior part of the ventricular septum interposes between the right ventricular inlet and the left ventricular outlet.

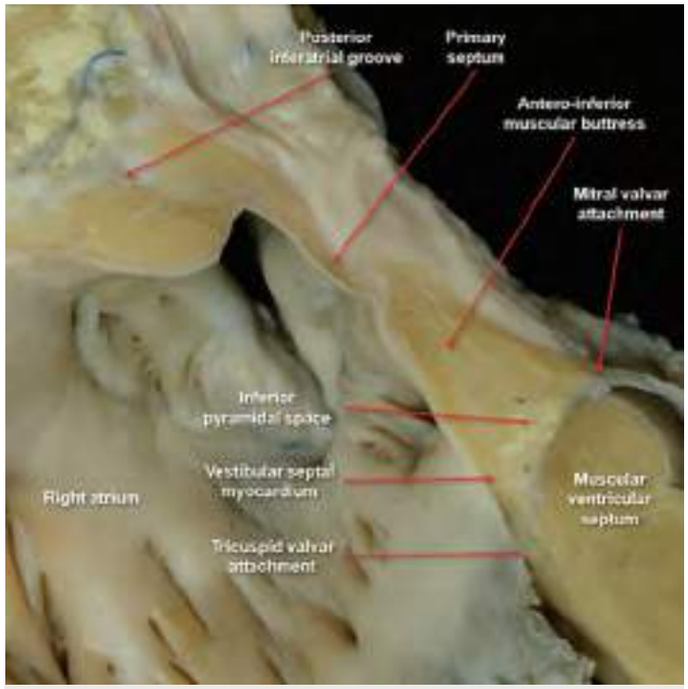

Fig. 13.3 Longitudinal sectional plane of the dissection image showing the fat plane in the inferior pyramidal space. The right atrial vestibular septal myocardium continues apically to overlap the crest of the muscular ventricular septum, producing the atrial surface of the inferior pyramidal space.

anteroinferior muscular buttress of the atrial septum provides the cranial and posterior margin of the inferior pyramidal space and the right atrial vestibular myocardium continues apically to overlap the crest of the muscular ventricular septum. At the apex of the inferior pyramidal space, the orifices of the atrioventricular valves and the aortic root are in conjunction (▶ Fig. 13.1, ▶ Fig. 13.4). This area, known as the central fibrous body, is made up of the right fibrous trigone and the membranous septum (▶ Fig. 13.4). The right fibrous trigone is the rightward end of the area of fibrous continuity between the leaflets of the mitral and aortic valves (▶ Fig. 13.4). The central fibrous body produces the most obvious and strongest part of the so-called cardiac skeleton. Understanding its relations is key to the appreciation of the overall arrangement. The hinge of the septal leaflet of the tricuspid valve divides the membranous septum into its atrioventricular and interventricular components (▶ Fig. 13.5). On the ventricular aspect of the tricuspid valvar hinge, and inferior to the interventricular portion of the membranous septum, by virtue of the wedged position of the subaortic outflow tract, the basal part of the muscular ventricular septum interposes between the right ventricular inlet and the left ventricular outlet (▶ Fig. 13.2). The atrioventricular conduction axis[13,14,15,16,17] is carried on the crest of this part of the muscular ventricular septum, with the wedged location of the aortic root making it possible for the penetrating part of the axis to extend directly from the apex of the inferior pyramidal space to the septal crest (▶ Fig. 13.6).

◆ The Cardiac Valvar Attachments

When describing the location of the hinges of cardiac valves within the ventricular base, we prefer to use the term “attachment” instead of the more popular “annulus,” since there are no discrete anatomical rings to be found encircling the orifices of the arterial valves. In recognition of common usage, nonetheless, when labeling our images, we have used “annulus” to describe the attachments of the leaflets of the mitral valve. Even the rings representing the attachments of the atrioventricular valves, however, are no more than the valvar hinges, with fibroadipose tissues occupying the larger parts of the so-called atrioventricular valvar annuluses. The reconstructions made possible by analysis of the three-dimensional datasets, furthermore, demonstrate the inadequacy of illustrating the attachments of all four valvar leaflets in the same plane. As is shown, the attachments of the leaflets guarding all four valvar orifices occupy markedly different planes (▶ Fig. 13.1). The attachments of the arterial valvar leaflets

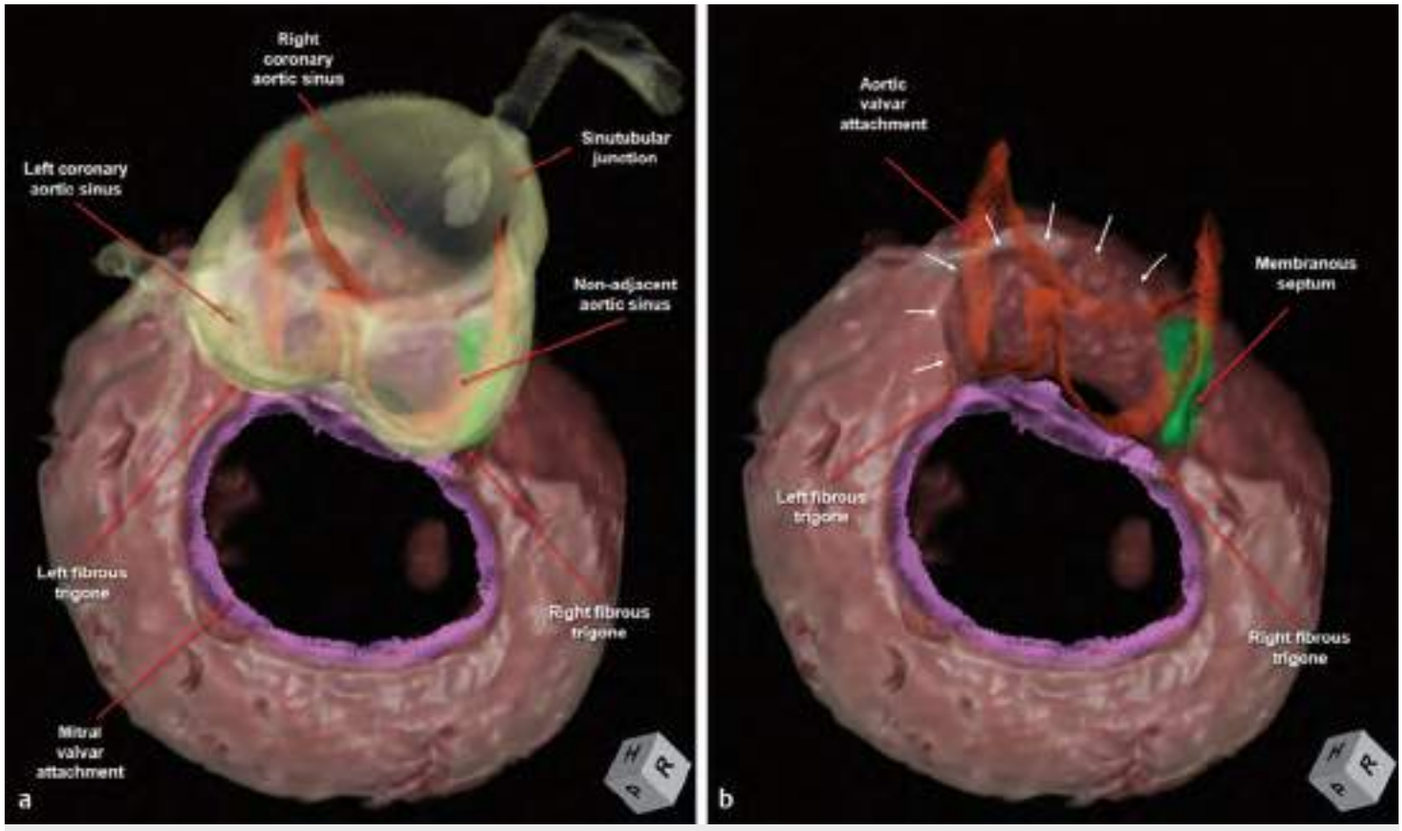

Fig. 13.4 The mitral valvar attachments, and the aortic root, are shown from the left atrial side. The central fibrous body is made up of the right fibrous trigone, which is the rightward end of the area of aortic-to-mitral valvar continuity **(a)** and the membranous septum **(b)**. White arrows in **(b)** show the extent of the left ventricular myocardial crescents found at the bases of the two aortic valvar sinuses that give rise to the coronary arteries.

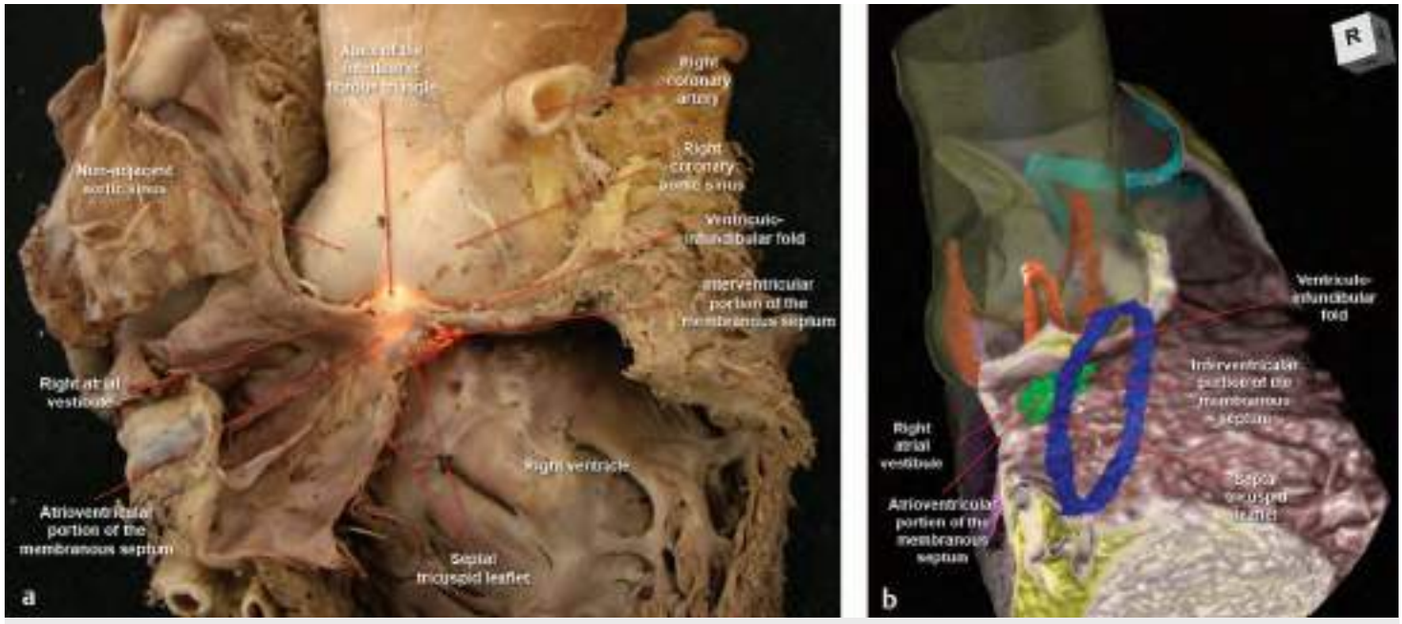

Fig. 13.5 **(a)** The interleaflet fibrous triangle between the right coronary and nonadjacent aortic sinuses is viewed from the right ventricular side. It is divided by the ventriculoinfundibular fold and the right atrial vestibule into an apical portion and the membranous septum. The latter is crossed by the attachment of the septal leaflet of the tricuspid valve to separate it into atrioventricular and interventricular components. **(b)** The membranous septum (*green*) is divided into atrioventricular and interventricular portions by the septal attachment of the septal tricuspid valvar leaflet (*blue*).

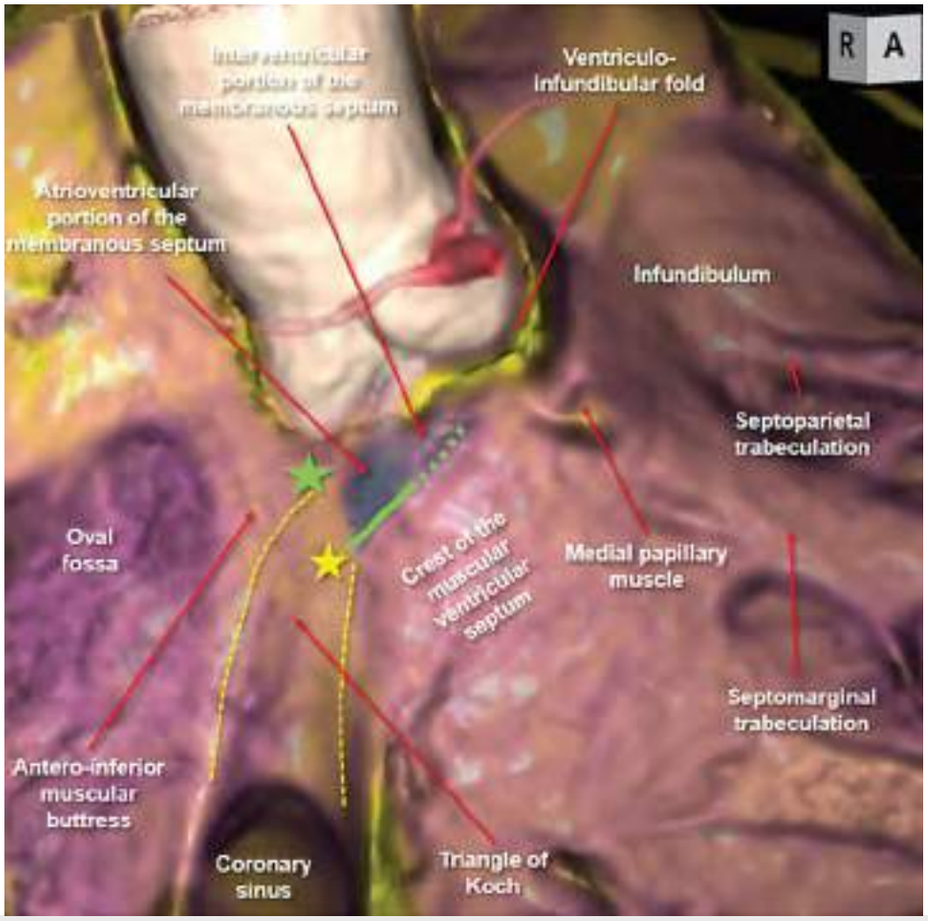

Fig. 13.6 Volume-rendered CT image of the inner wall of the right heart showing the structural anatomy of the right heart in relation to the atrioventricular conduction axis. The triangle of Koch floors the area between the tendon of Todaro and the septal attachment of the septal tricuspid valvar leaflet (*dotted yellow lines*). The atrioventricular node (*yellow star*) is located at the apex of the triangle of Koch adjacent to the crest of muscular ventricular septum, just inferior to the atrioventricular portion of the membranous septum. The bundle of His runs along the inferior rim of the membranous septum, penetrating the central fibrous body to reach the left ventricular side (penetrating portion is shown by *solid green line*) at the inferior rim of the atrioventricular portion of the membranous septum. It then branches into the left and right bundle branches (branching portion is shown by *green dotted lines*). The right fibrous trigone (*green star*) is located close to the nadir of the nonadjacent aortic sinus. This site marks the conjunction of the anteroinferior muscular buttress, the atrioventricular sandwich, the crest of the muscular ventricular septum, and the atrioventricular portion of the membranous septum.

13

reconstruct in the form of three-pointed coronets, rather than little rings. The pulmonary valvar coronet is located most superiorly, having a marked obliquity relative to the aortic valvar coronet. The hinges of the mitral and tricuspid valvar leaflets, in contrast, do produce ring-like configurations. They are positioned close together in relatively planar fashion, although the mitral valvar hinges produce a saddle-like configuration, and the tricuspid valvar attachment is located slightly inferiorly and apically (▶ Fig. 13.7). It is the resulting inferior gap between the mitral and tricuspid valvar attachments that encloses the inferior pyramidal space, with the membranous septum at its apex (▶ Fig. 13.7).

As we have already emphasized, the aortic root is deeply wedged between the mitral valvar orifice, the muscular ventricular septum, and the tricuspid valvar attachment (▶ Fig. 13.7). The basal part of the ventricular septum, therefore, is interposed between the right ventricular inlet and left ventricular outlet (▶ Fig. 13.2). Even though the leaflets of the aortic and mitral valves are in fibrous continuity, the planes of the two valvar orifices are obtuse rather than parallel (▶ Fig. 13.1), producing the so-called aortoseptal angle between the aortic root and the left ventricle, as routinely visualized in echocardiography.[18] It is the fibrous continuity between the leaflets of the aortic and mitral valves that makes up the roof of the left ventricle (▶ Fig. 13.4), with the ends of the fibrous area thickened to form the right and left fibrous trigones. The leaflets of the tricuspid valve are hinged from the right atrial vestibule at all points except where the septal leaflet crosses the membranous septum (▶ Fig. 13.5, ▶ Fig. 13.7). As we have discussed, both valvar orifices are relatively planar, although that of the mitral valve is somewhat saddle-shaped (▶ Fig. 13.7). This shape of mitral ring is considered important in reducing the stress placed on the valvar leaflets during the cardiac cycle.[19,20]

◆ The Inaccurate Notion of a "Cardiac Skeleton"

It is the central fibrous body that constitutes the strongest part of the so-called cardiac skeleton. As we have shown, this structure is

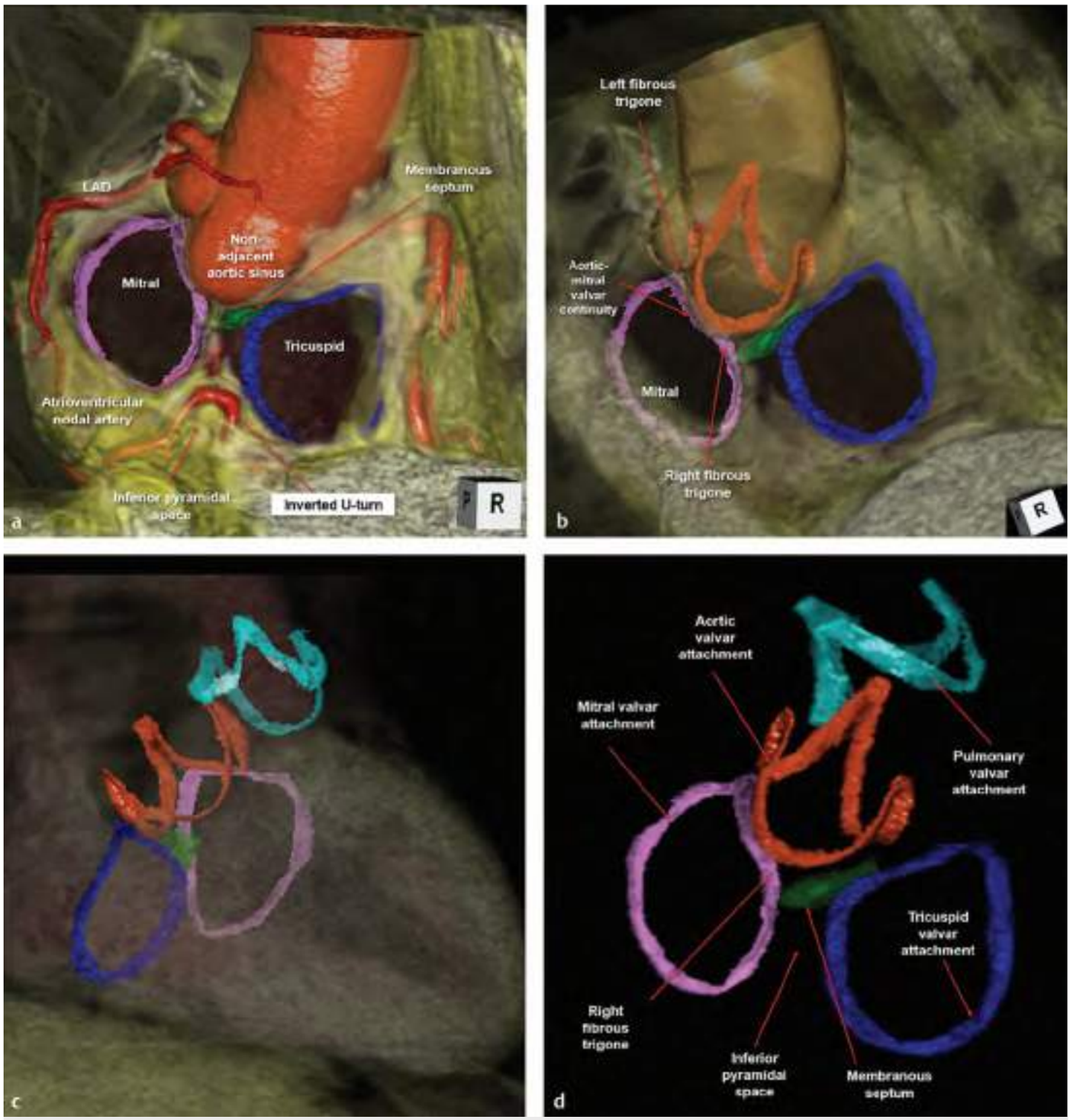

Fig. 13.7 (a, b) The aortic root wedges between the attachments of the atrioventricular valves from the top of the heart. On the other hand, the inferior pyramidal space wedges from the bottom of the heart. The structures are tightly connected by the firm fibrous tissue known as the central fibrous body, composed of the right fibrous trigone and membranous septum (*green*). **(c)** Shows the frontal view of the heart. The anatomical alignment and configuration of each valvar attachment is emphasized by different colors. The pulmonary valvar coronet (*sky blue*) is located most superiorly, having a marked obliquity relative to the aortic valvar coronet (*red*), whereas the hinges of the mitral (*pink*) and tricuspid (*blue*) valvar leaflets produce ring-like configurations, located together in close to relatively planar fashion, although the tricuspid valvar attachment is located slightly inferiorly and apically. Note, the mitral valvar hinges producing a saddle-like configuration. Green shows the membranous septum. **(d)** Shows the inferior gap between the mitral and tricuspid valvar attachments that encloses the inferior pyramidal space, with the membranous septum at its apex. LAD, left anterior descending artery.

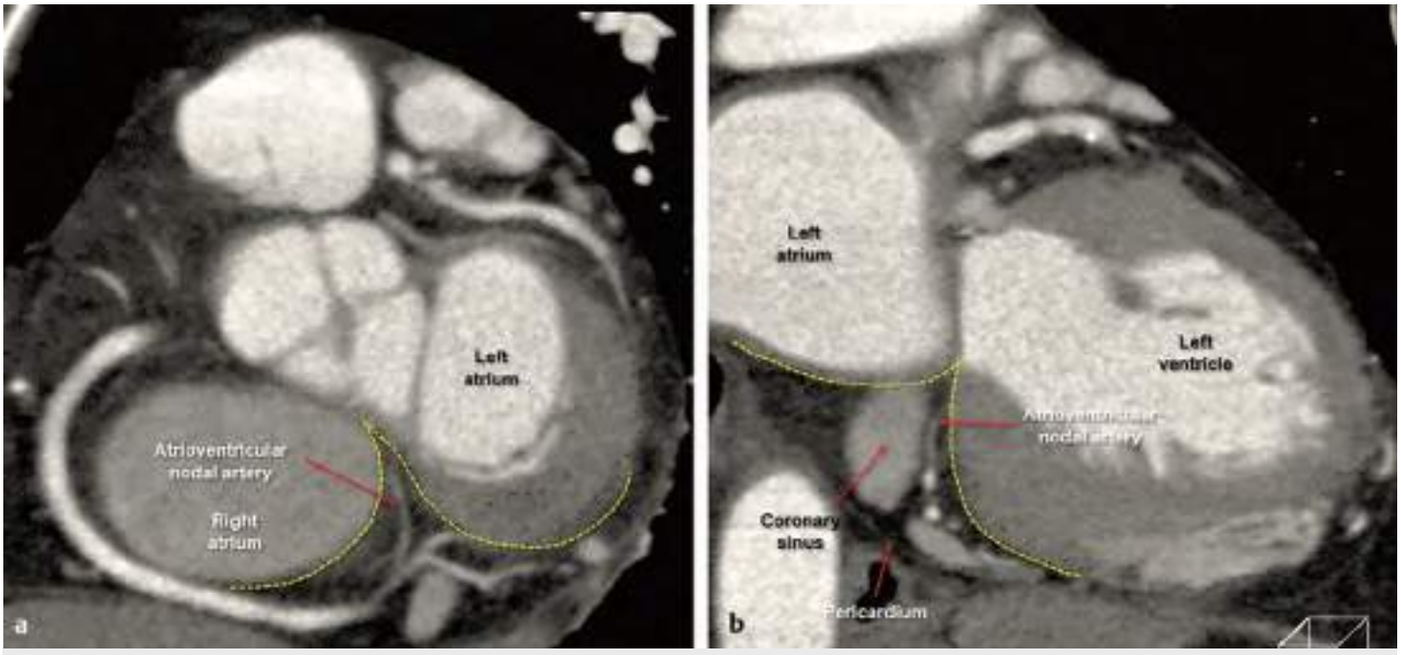

Fig. 13.8 Multiplanar reconstructions are shown of the left ventricular short-axis **(a)** and long-axis **(b)** images. The inferior pyramidal space (area surrounded by yellow dotted line) is recognized as a triangular fibroadipose tissue wedged into the heart, which contains the coronary sinus, the right coronary artery, and the atrioventricular nodal artery.

the combination of the membranous septum and the right fibrous trigone (▶ Fig. 13.4). Aside from the central fibrous body, there is no "skeleton." Even the central fibrous body is part of the insulating tissues of the heart, rather than functioning as part of a "skeleton" in the sense of the musculoskeletal system. The notion of the so-called cardiac skeleton, therefore, has been greatly exaggerated. The hinges of the valvar leaflets are supported by the ventricular myocardium, rather than providing origins and insertions for the ventricular cardiomyocytes. It is the fibroadipose tissue contained within the atrioventricular junctions, furthermore, which serves to separate the atrial and ventricular muscular masses at all points except the penetration of the atrioventricular conduction axis. As far as the arterial valves are concerned, it is the semilunar attachments of the leaflets that conventionally are considered to represent part of the "skeleton." These lines are no more than the hinges of the semilunar leaflets, with the free-standing subpulmonary infundibular sleeve serving to lift the leaflets of the pulmonary valve away from the cardiac base (▶ Fig. 13.1).

◆ The Inferior Pyramidal Space

The triangular inferior pyramidal space is filled by the cranial extension of fibroadipose tissue from the inferior atrioventricular groove (▶ Fig. 13.7, ▶ Fig. 13.8). In certain individuals, during the fluoroscopic examination, it is sometimes possible to recognize the space as filled by an extensive fat pad. Its location can also be recognized in some patients during routine coronary angiography, when an inverted U-turn of the distal part of the right coronary artery gives rise to the artery of the atrioventricular node (▶ Fig. 13.7). The sides of the pyramid are bordered by the inferior rim of the atrial septum, the inferior rim of the ventricular septum, and the inferior attachments of the tricuspid and mitral valves (▶ Fig. 13.7, ▶ Fig. 13.8). As we have already established, the hinge of the septal leaflet of the tricuspid valve is positioned apically relative to the attachments of the mitral valve (▶ Fig. 13.1, ▶ Fig. 13.7). Between these two hinges, the septal component of the right atrial vestibule, overlapping the crest of the basal part of the ventricular septum, forms the atrial surface of the triangle of Koch (▶ Fig. 13.6, ▶ Fig. 13.9). And, as we have already discussed, this overlapping was previously considered to represent a muscular atrioventricular septum.[21] The area, however, cannot be removed without creating a communication with the extracardiac adipose tissue contained within the inferior pyramidal space. That is why the "septum" is best considered as an atrioventricular sandwich, with "meat" of the sandwich provided by the insulating tissues which interpose between the atrial and ventricular muscular layers (▶ Fig. 13.10).

◆ The Membranous Septum

The atrioventricular component of the membranous septum, located at the apex of the inferior pyramidal space, where the cavity of the right atrium faces directly with the left ventricle, is a true atrioventricular septal structure (▶ Fig. 13.5, ▶ Fig. 13.11). Since the membranous septum, in most individuals, is crossed by the hinge of the septal leaflet of the tricuspid valve, its anterior component is an interventricular septal structure (▶ Fig. 13.5, ▶ Fig. 13.11, ▶ Fig. 13.12). The entirety of the membranous septum, when viewed from its left side, is seen to occupy the base of the triangle between the right coronary and nonadjacent aortic sinuses. It forms part of the medial wall of the left ventricular outflow tract (▶ Fig. 13.5, ▶ Fig. 13.12).

◆ The Atrial Septum

At first sight, the atrial septum seems extensive, being made up of the oval fossa and its surrounding rims. Of these structures,

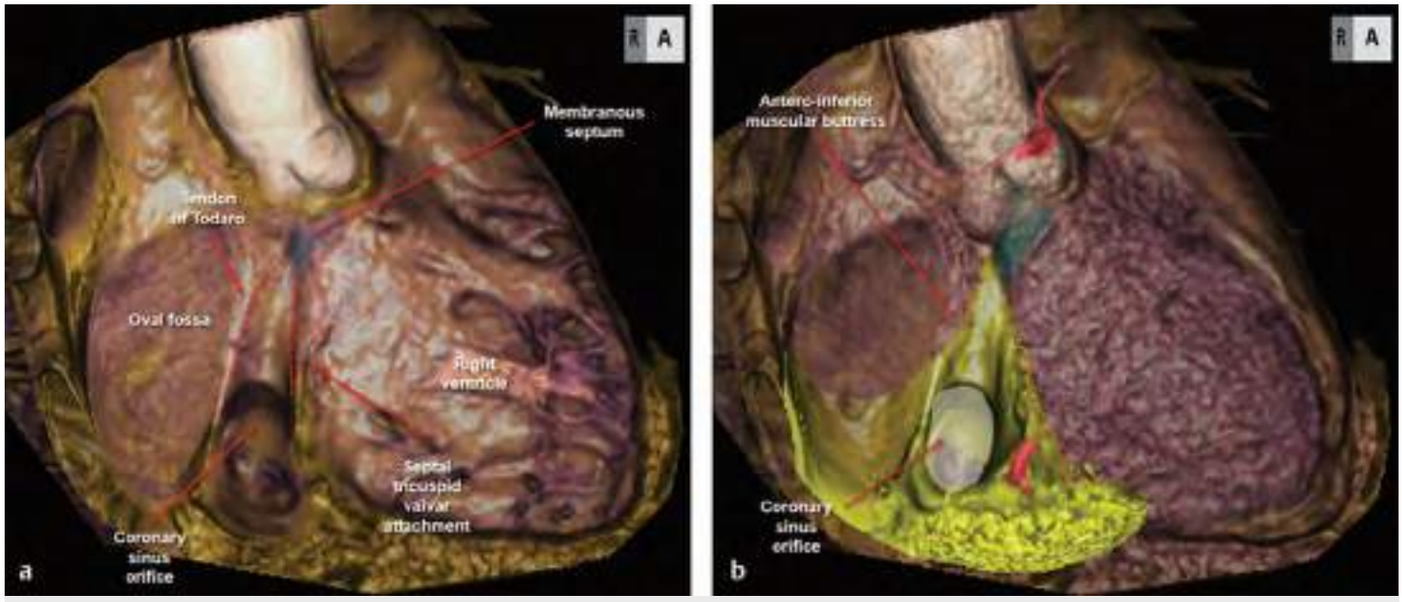

Fig. 13.9 As shown in panel **(a)**, the triangle of Koch floors the area between the tendon of Todaro and the septal attachment of the septal tricuspid valvar leaflet (*dotted red lines*). In panel **(b)** the anatomical extension of the epicardial fat including the part in the inferior pyramidal space is projected in yellow over the image in panel **(a)**. The septal component of the right atrial vestibule forms the atrial surface of the triangle of Koch, overlapping the crest of the muscular ventricular septum.

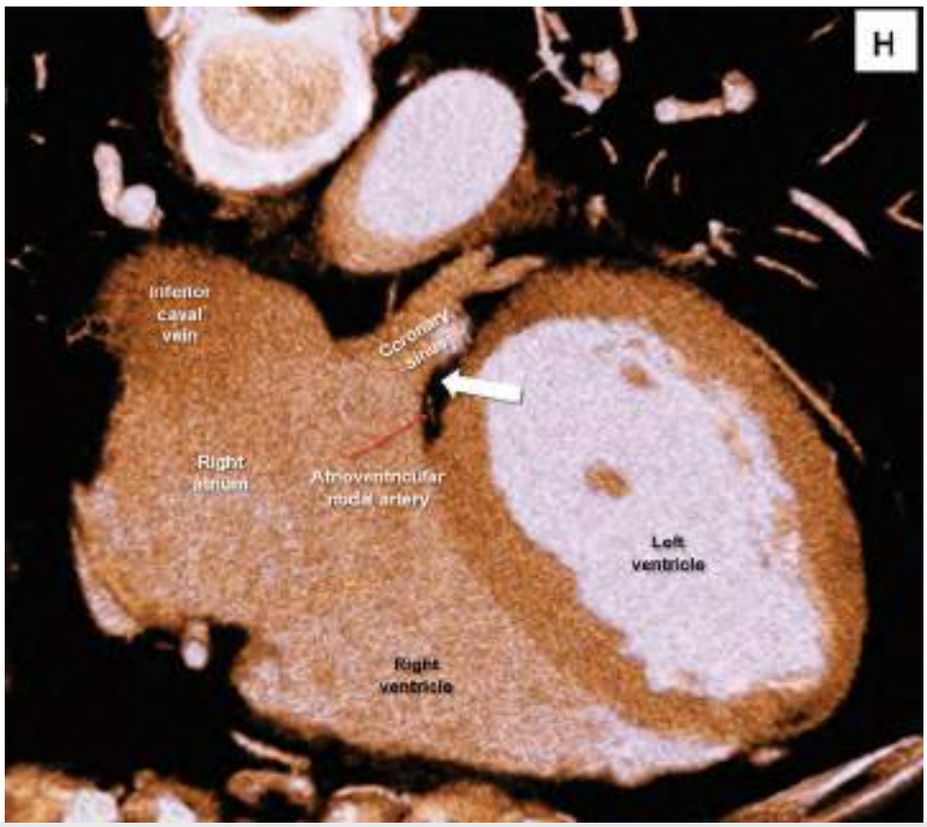

Fig. 13.10 Four-chamber CT image at the level of the coronary sinus. Fibroadipose tissue of the inferior pyramidal space (*white arrow*) interposes between the septal component of the right atrial vestibule and the crest of the muscular ventricular septum (atrioventricular sandwich).

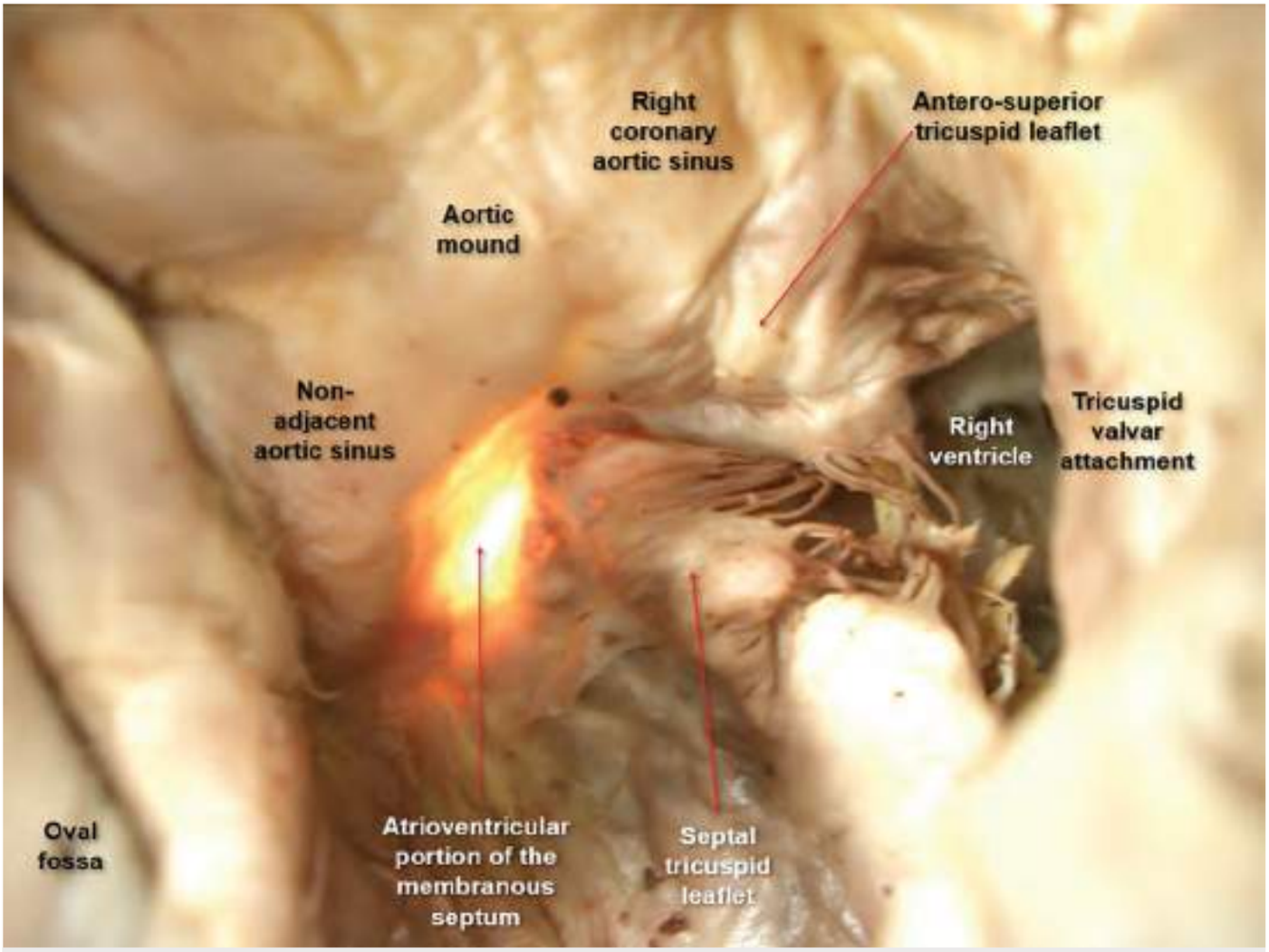

Fig. 13.11 The membranous septum is divided into atrioventricular and interventricular portions by the septal attachment of the septal tricuspid valvar leaflet. The membranous septum is located at the commissure between the septal and anterosuperior tricuspid valvar leaflets. The right atrium directly faces the left ventricular outflow tract at this atrioventricular portion of the membranous septum.

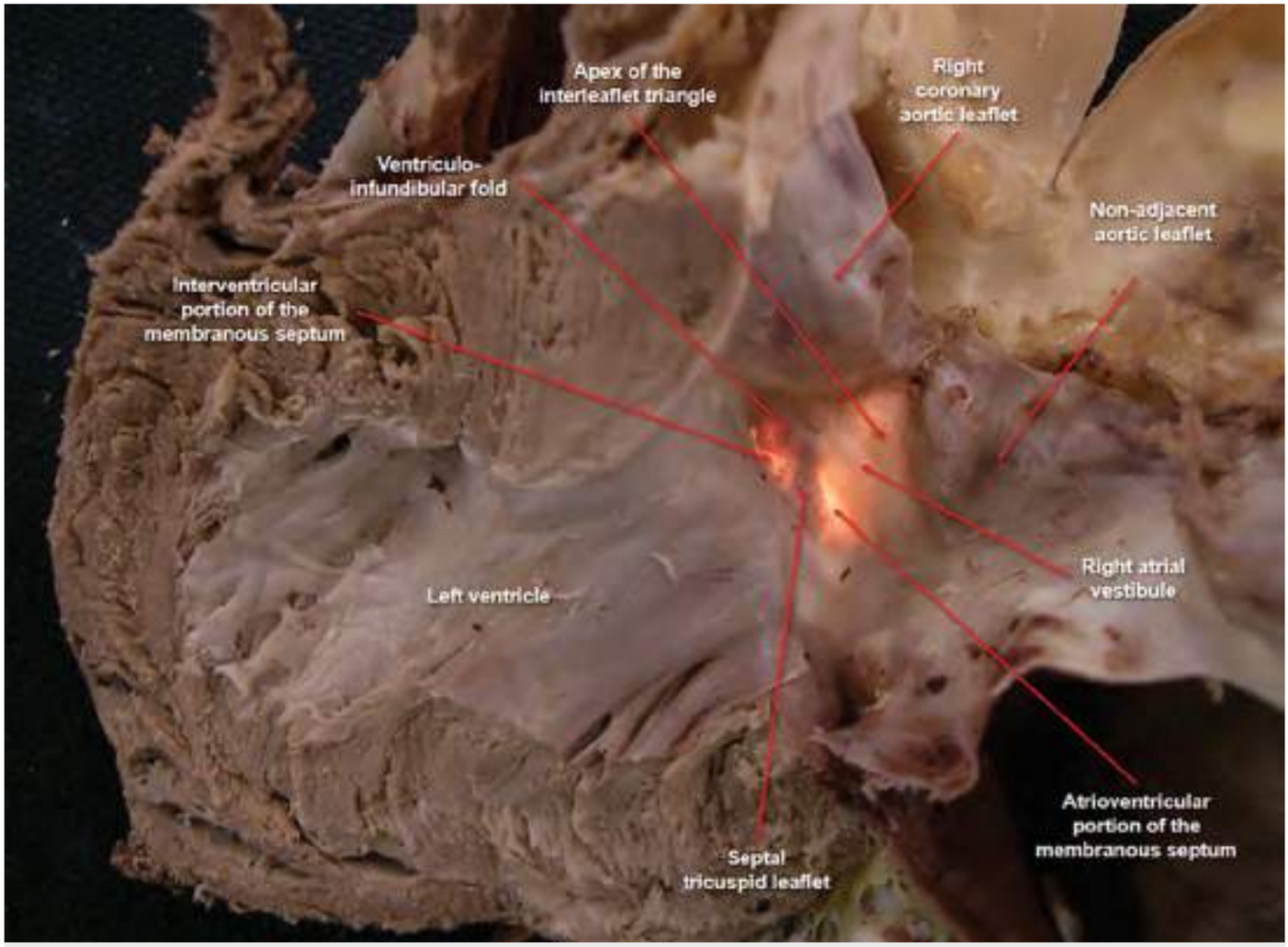

Fig. 13.12 The interleaflet fibrous triangle between the right coronary and nonadjacent aortic sinuses is shown from the left ventricular side. It is divided on the right side by the ventriculoinfundibular fold and the right atrial vestibule into an apical portion and the membranous septum. The latter part is crossed by the attachment of the septal leaflet of the tricuspid valve, thus separating it into atrioventricular and interventricular components.

however, it is only the floor of the oval fossa, derived from the primary atrial septum, and the anteroinferior muscular buttress, which anchors the oval fossa to the atrioventricular junctions, which are true septums (▶ Fig. 13.3, ▶ Fig. 13.13). Only these parts can be removed without exiting from the cardiac cavities.[22] The posterosuperior rim of the oval fossa is often described as the "secondary septum." This is not the case, since the rim is no more than an extensive fold between the attachments of the caval veins to the right atrium and the right pulmonary veins to the left atrium (▶ Fig. 13.3, ▶ Fig. 13.13). The anterosuperior rim of the fossa is also a fold, separated by the transverse sinus of the pericardium from the nonadjacent aortic sinus, also known as the noncoronary aortic sinus, although very rarely it can give rise to a coronary artery. The nonadjacent aortic sinus, therefore, when images are viewed in the right anterior oblique projection, serves as a useful landmark in recognizing the anterosuperior margin of the atrial septum. The oval fossa itself has been measured as having average dimensions of 14.7 by 12.0 mm.[23] In up to one-third of normal individuals, there is persistent patency of the oval foramen, which is seen as a slit-like tunnel.[24] When assessed using cardiac CT in an American population, persistent patency of the foramen was found in just under one-quarter of individuals.[24] Assessment of autopsied specimens, in contrast, revealed prevalence of only one-eighth in the Japanese population.[25] A comparable assessment of autopsied specimens in North America had revealed probe patency in up to one-third,[26] so these differences in prevalence are likely to be real.

When viewing the anatomy in right anterior oblique fluoroscopy projections, note should be taken of the relations of an obvious radiolucent band to the orifices of the coronary sinus and the right coronary artery (▶ Fig. 13.14**a**). This band is produced by the right atrioventricular groove. Its position is useful when locating the site of the right atrial appendage (▶ Fig. 13.14**c**), and in distinguishing the right coronary from the nonadjacent aortic sinuses (▶ Fig. 13.14**b**). These relationships are significant when assessing the progress of a catheter or pacing lead from the right atrium into the right ventricle (▶ Fig. 13.14**c**).

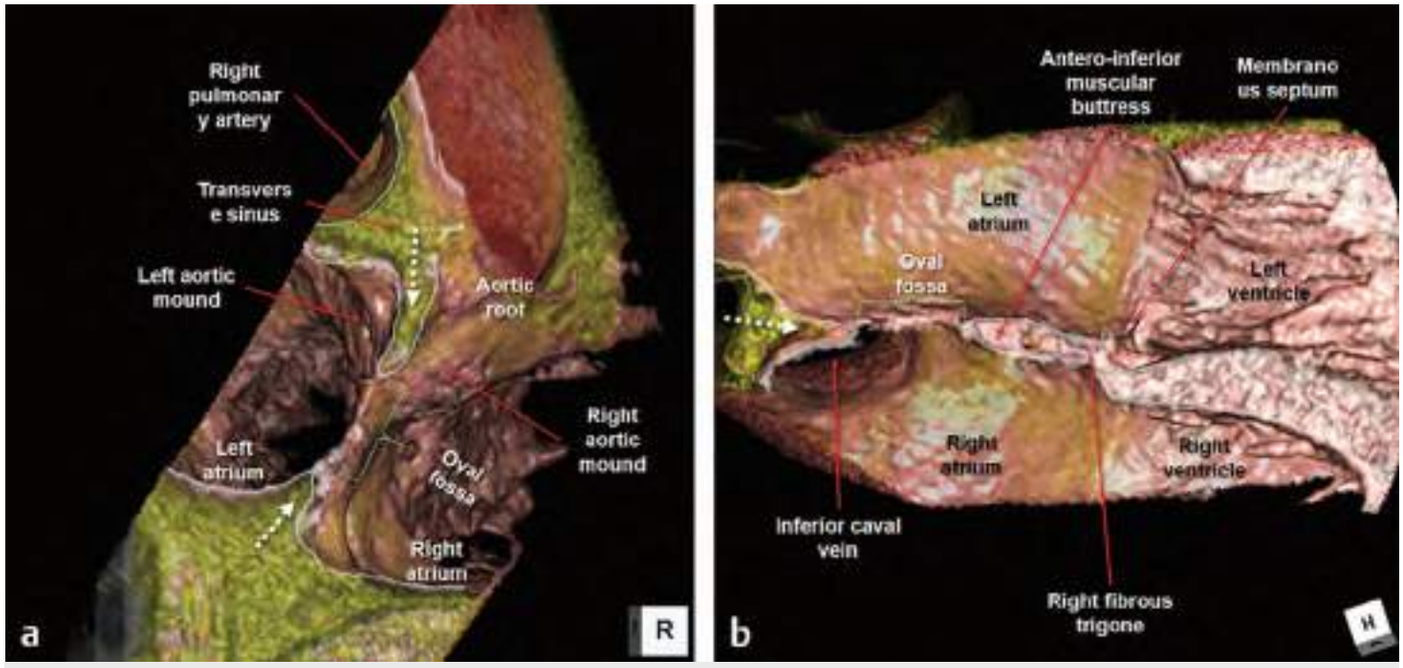

Fig. 13.13 Short-axis **(a)** and long-axis **(b)** views of the atrial septum. The superior, inferior, and posterior rims of the oval fossa are not true anatomical septums, but folds in the atrial walls filled with epicardial fat (*white arrows*).

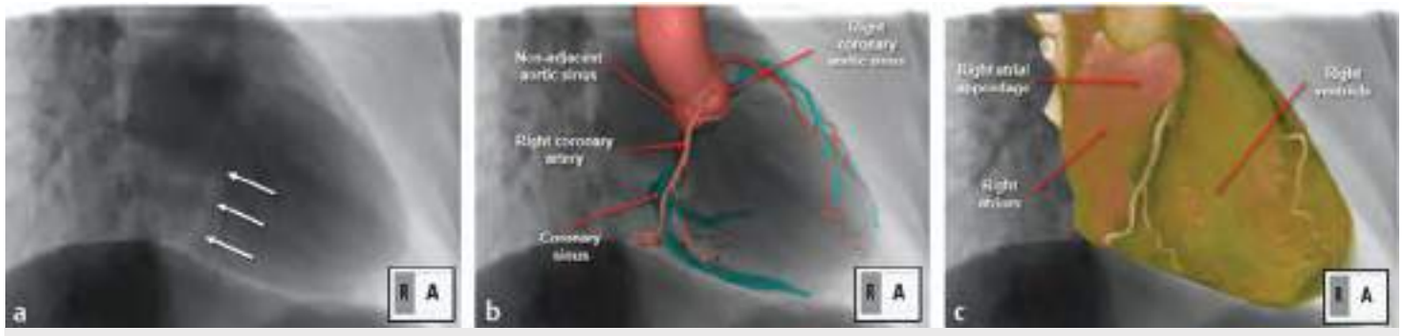

Fig. 13.14 (**a–c**) Right anterior oblique images, presence of a radiolucent band (*white arrows*) in **(a)** is a useful landmark during cardiac intervention. The ascending aorta, right coronary artery, coronary sinus, and right atrial appendage are close to this region. Demonstration of this radiolucent band is useful in locating these structures.

13

◆ The Atrioventricular Conduction Axis

The atrioventricular node is located at the apex of the inferior pyramidal space, with the atrial surface of the space being recognized in the opened heart as the triangle of Koch (▶ Fig. 13.6, ▶ Fig. 13.9). The location of the node can be determined by tracing the course of the nodal artery, which ascends in the insulating fibroadipose tissues of the inferior pyramidal space,[27] usually taking its origin from the distal right coronary artery (▶ Fig. 13.8). Having reached the central fibrous body, the conduction axis becomes insulated from the atrial myocardium as it enters the atrioventricular portion of the membranous septum. Although there are individual variations,[16] the nonbranching component of the conduction axis, having entered the subaortic outflow tract, is usually sandwiched between the inferior rim of the membranous septum and the crest of the muscular ventricular septum. The axis then gives rise to the left and right bundle branches, with the left branch cascading in fan-like fashion down the smooth left ventricular surface of the ventricular septum.[13] The right bundle branch, in contrast, is a thin cord-like fascicle, which passes through the muscular crest, surfacing in the right ventricle beneath the medial papillary muscle (▶ Fig. 13.6). A line drawn from the apex of the triangle of Koch to the medial papillary muscle serves as the landmark to the location of the conduction axis.[17] The inferior rim of the membranous septum, therefore, can serve as the landmark for electrophysiologists aiming to locate the His-bundle electrode, marking as it does the penetrating portion of the axis. When viewed in left anterior oblique projection, this site is seen inferior to the aortic root at the dimple of the medial tricuspid valvar attachment (▶ Fig. 13.15).

◆ The Right-Sided Paraseptal Areas

Electrophysiologists investigating the substrates for the Wolff–Parkinson–White variants of ventricular preexcitation have long

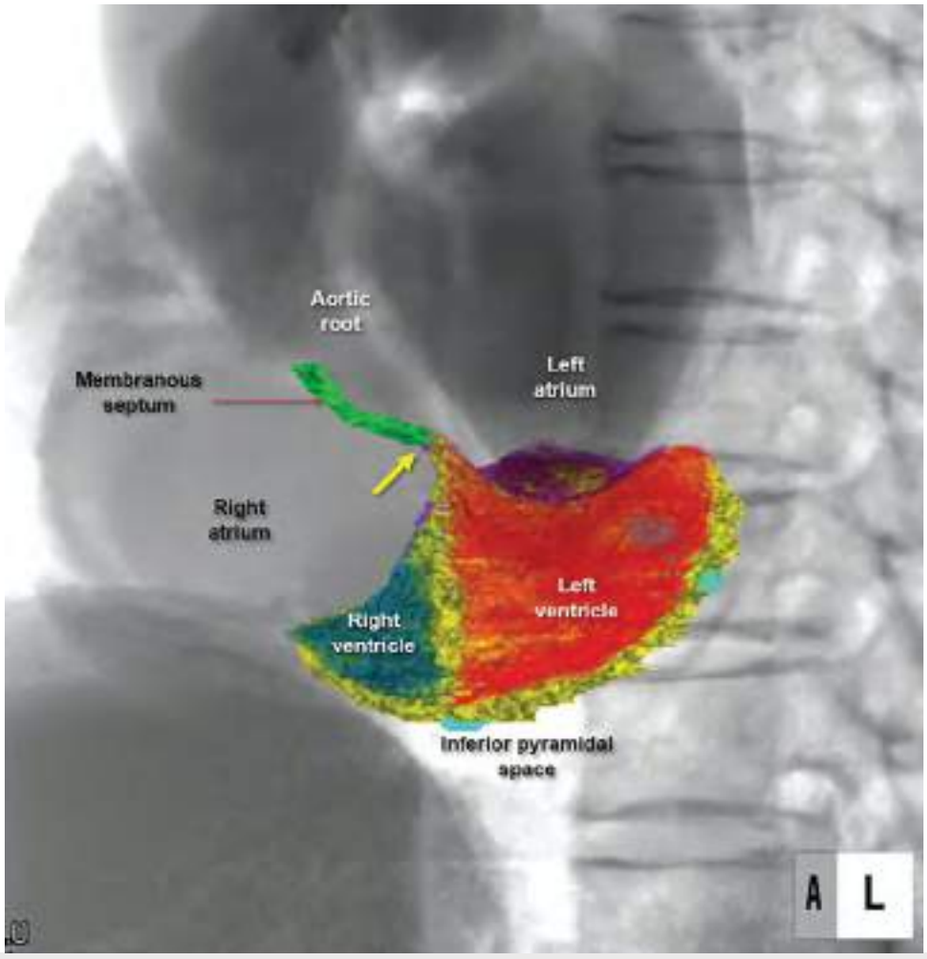

Fig. 13.15 The inferior rim of the membranous septum can serve as the landmark for electrophysiologists to locate the His-bundle electrode. The dimple (*yellow arrow*) formed by the membranous septum at the attachment of the medial tricuspid leaflet is seen on left anterior oblique view, denoting the routine site for fixation of the His-bundle electrode.

distinguished between left-sided, right-sided, and allegedly "septal" accessory muscular connections. In reality, all the accessory muscular connections are located within the epicardial fibroadipose tissues that separate the atrial and ventricular muscular masses. As such, therefore, none of the pathways are truly septal, since as we have already shown, it is only the caudal component of the membranous septum that produces a true atrioventricular septum. The accessory muscular connections are more accurately described as being paraseptal. Further problems arise in their current descriptions, since the location of the pathways has traditionally been described with the heart viewed in Valentine's position,[28] rather than in attitudinally appropriate fashion.[29] In ▶ Fig. 13.16, we show how the so-called "anterior" pathways are superiorly located relative to the hinge of the anterosuperior leaflet of the tricuspid valve. The accessory connections in this area run from the superior vestibular component of the right atrioventricular junction, adjacent to the right coronary aortic sinus, and insert into the supraventricular crest. The so-called "midseptal" connections run within the fibroadipose tissue in the middle third of the inferior pyramidal space, while the so-called "posterior" connections, in reality positioned inferiorly, extend from the septal isthmus to insert in the underlying ventricular myocardium. The midparaseptal and inferior paraseptal connections, therefore, are running within the confines of the triangle of Koch, which forms the atrial surface of the inferior pyramidal space (▶ Fig. 13.9, ▶ Fig. 13.16). When viewed in attitudinal fashion, its posterior anatomical boundary is the tendon of Todaro (▶ Fig. 13.9). This structure cannot be directly visualized in the clinical setting. It is the cranial continuation of the Eustachian valve. It runs within the so-called "sinus septum" to insert into the atrioventricular component of the membranous septum, with the latter structure forming the apex of the triangle. The anterior boundary is the attachment of the septal leaflet of the tricuspid valve, with the orifice of the coronary sinus forming the base of the triangle (▶ Fig. 13.9, ▶ Fig. 13.16). When viewed in attitudinally appropriate fashion, the apex of the triangle points upward. When viewed in left anterior oblique projection, a large part of the septal isthmus at the base of the triangle faces onto the eye of the observer, with the membranous septum is being seen in tangential orientation (▶ Fig. 13.16**c**). Appreciation of these arrangements is important when seeking to modify the slow pathway during radiofrequency catheter ablation. Although the tendon of Todaro is not directly visible in the clinical setting, it may be possible to identify the Eustachian valve. Guarding the orifice of the inferior caval vein during fetal life, and persisting to variable degree postnatally, it is positioned between the anterior rim of the inferior caval vein and the posterior rim of the orifice of the coronary sinus (▶ Fig. 13.17). The so-called sinus septum,

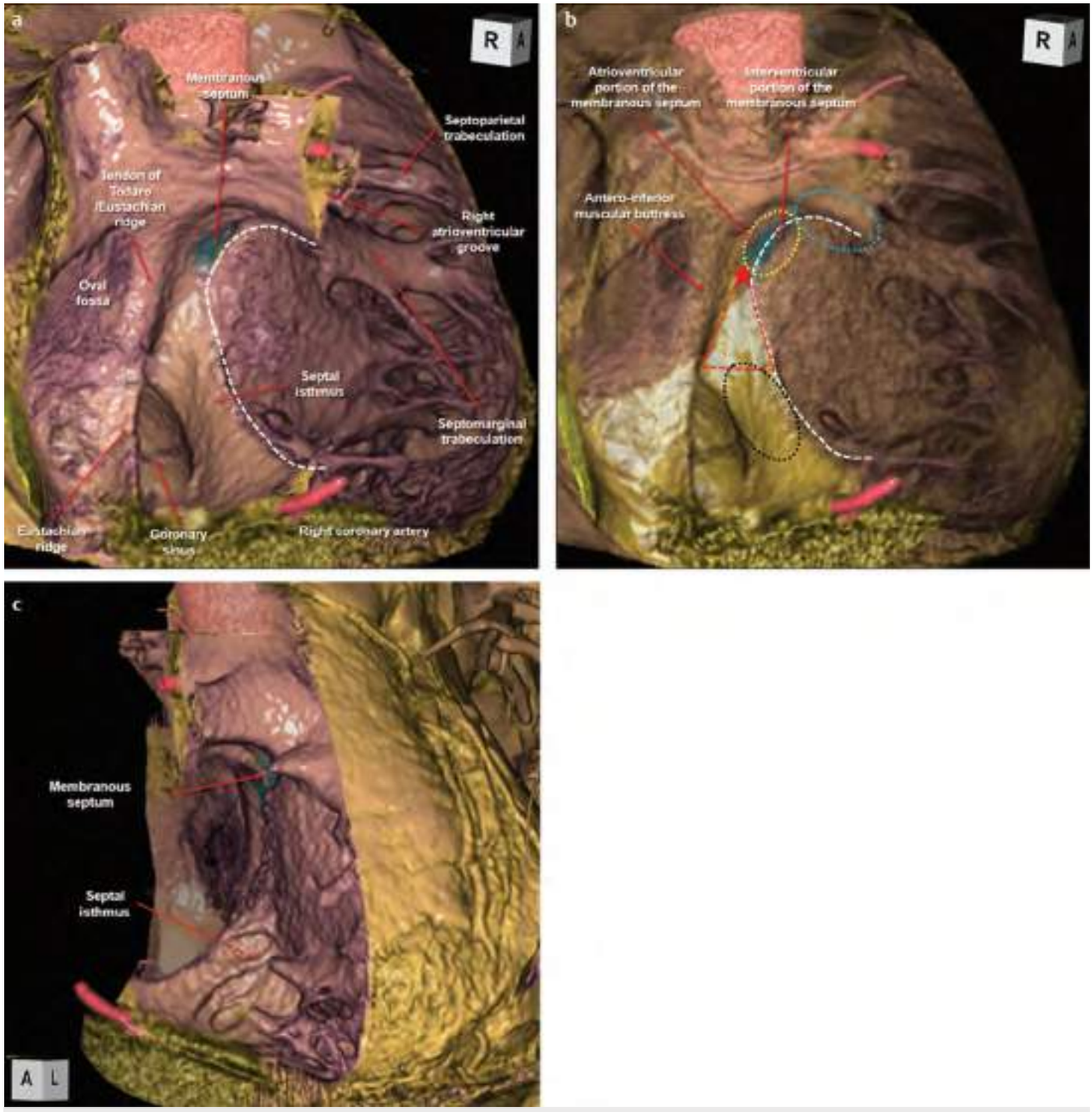

Fig. 13.16 The volume-rendered image viewed from the right anterior oblique cranial direction **(a)** shows the morphology of the right-sided paraseptal areas along the tricuspid valvar attachment (*white dotted line*). The membranous septum is visualized (*sky blue*). In **(b)** the anatomical extension of the inferior pyramidal space (*yellow*) behind the atrial wall is shown. The red star indicates the location of the atrioventricular node. The sky blue dotted circle indicates the superior paraseptal area. The yellow dotted circle indicates the superior septal area, corresponding to the membranous septum. The red dotted triangle indicates the midparaseptal area corresponding to the triangle of Koch. Note the apex of the triangle of Koch points upward. The black dotted circle indicates the inferior paraseptal area. The relationship between the membranous septum and septal isthmus is also shown in **(a)**. **(c)** Shows the relationship in left anterior oblique projection. The membranous septum and septal isthmus are located in perpendicular fashion relative to each other. Accordingly, if viewed from the left anterior oblique direction, a large part of the septal isthmus is not tangential, rather faces onto the eye of the observer, whereas the membranous septum is tangential.

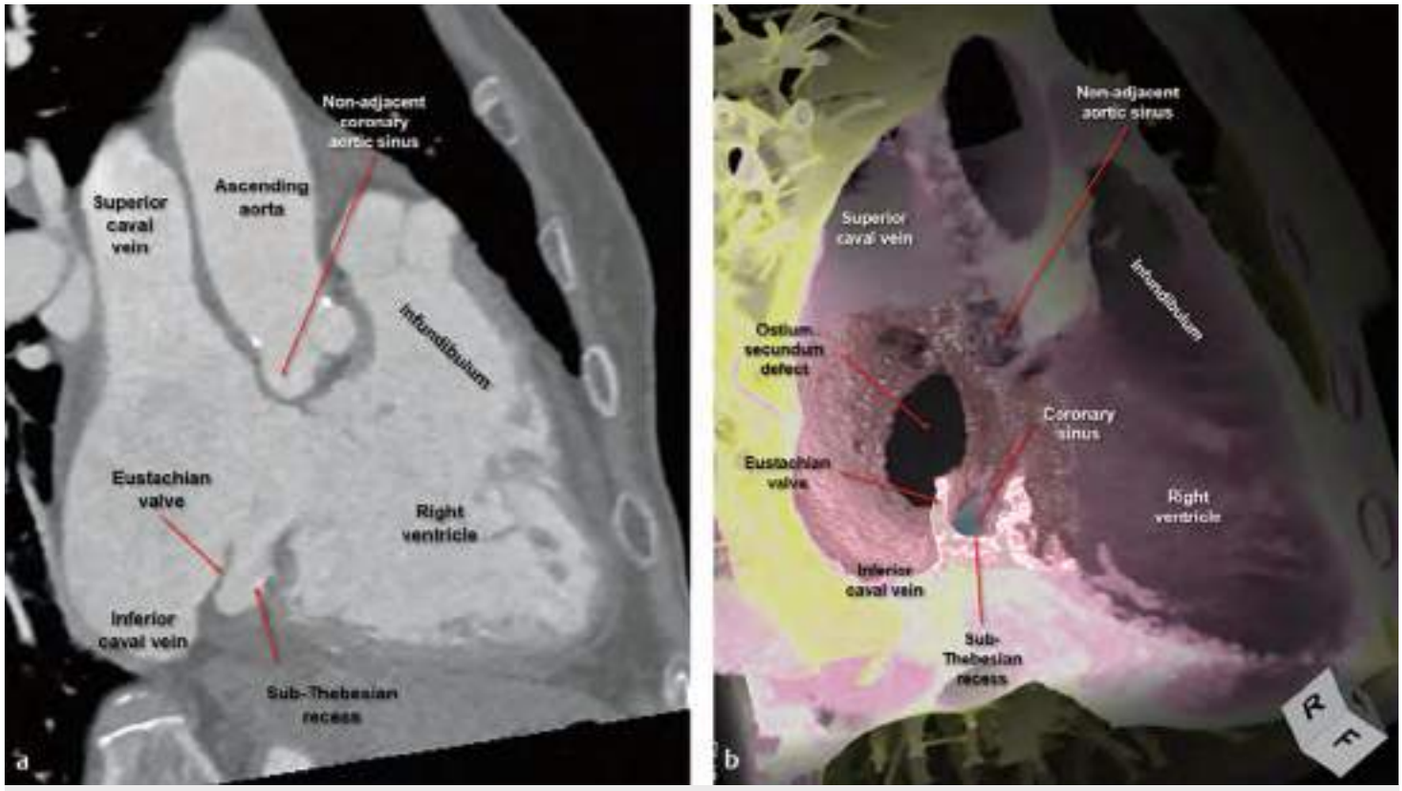

Fig. 13.17 The images are from a patient known to have a so-called "ostium secundum" atrial defect, in other words a defect within the oval fossa. **(a)** Shows a prominent Eustachian valve reconstructed from a patient with an oval fossa defect in multiplanar fashion, with **(b)** showing a volume-rendered image. The Eustachian valve is located at the junction of the anterior rim of the inferior caval vein and the posterior rim of the coronary sinus orifice. A large sub-Thebesian recess is also seen.

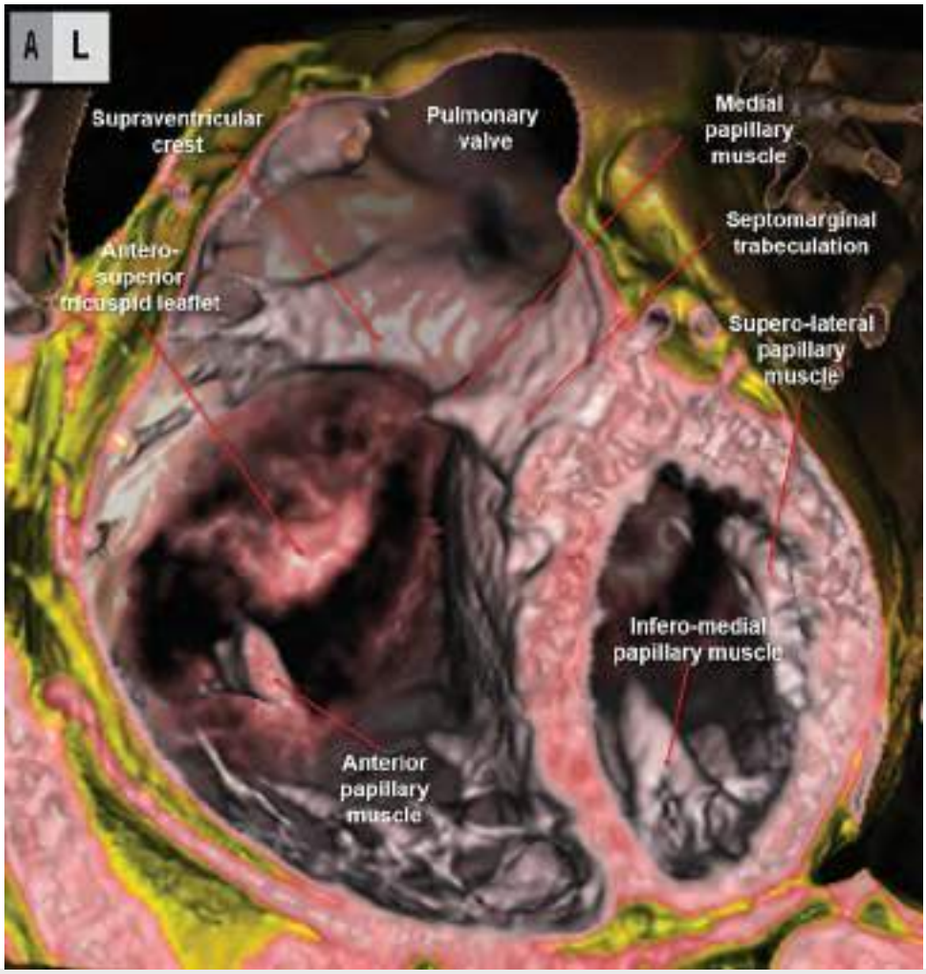

Fig. 13.18 The reconstruction shows that the papillary muscles of the mitral valve are positioned inferomedially, and superolaterally.

through which the tendon of Todaro runs, is made up of the infolded atrial walls between the atrial terminations of these venous channels. Another vestige of the valves of the embryonic systemic venous sinus typically persists to guard the orifice of the coronary sinus. This is the Thebesian valve. An extensive diverticulum is usually found inferior to the orifice of the coronary sinus. Often called the "sub-Eustachian sinus," the structure is seen to be sub-Thebesian when the heart is viewed in attitudinally appropriate fashion (▶ Fig. 13.17). Should the embryonic valves of the systemic venous sinus persist postnatally in exuberant fashion, they produce the so-called Chiari network.[30]

◆ The Atrioventricular Valves and Papillary Muscles

We have emphasized the problems that currently exist in describing correctly the locations of the accessory muscular connections responsible for the Wolff–Parkinson–White variants of ventricular preexcitation.[29] These problems are then further exemplified when we consider the traditional names given to the leaflets of the atrioventricular valves, along with their supporting papillary muscles. When viewed in attitudinally appropriate fashion, there is no question but that the papillary muscles supporting the ends of the solitary zone of apposition between the leaflets of the mitral valve are positioned inferoseptally (inferomedially) and superolaterally (▶ Fig. 13.18). They are not located in posteromedial and anterolateral positions, as is suggested by current terminology. The muscles supporting the leaflets of the tricuspid valve are located medially, anteriorly, and inferiorly, with multiple additional tendinous cords attaching the septal leaflet of the valve directly to the basal part of the ventricular septum (▶ Fig. 13.19). With regard to the leaflets themselves, we again encounter major problems in the current terms used for the tricuspid valve. This is because the alleged "posterior" leaflet is positioned inferiorly when the heart is viewed in attitudinally appropriate fashion (▶ Fig. 13.20). It is the septal leaflet of the tricuspid valve that is located posteriorly, with the prominent third leaflet positioned anterosuperiorly. In the mitral valve, there are fewer problems with current nomenclature, since the two leaflets are located more-or-less anteriorly and posteriorly, albeit with a degree of obliquity relative to the bodily axes (▶ Fig. 13.20). We prefer, nonetheless, to describe the leaflets as being aortic and mural, since in this way we are able to emphasize their locations relative to the zone of fibrous continuity with the aortic valve, and the left atrioventricular junction, respectively (▶ Fig. 13.20).

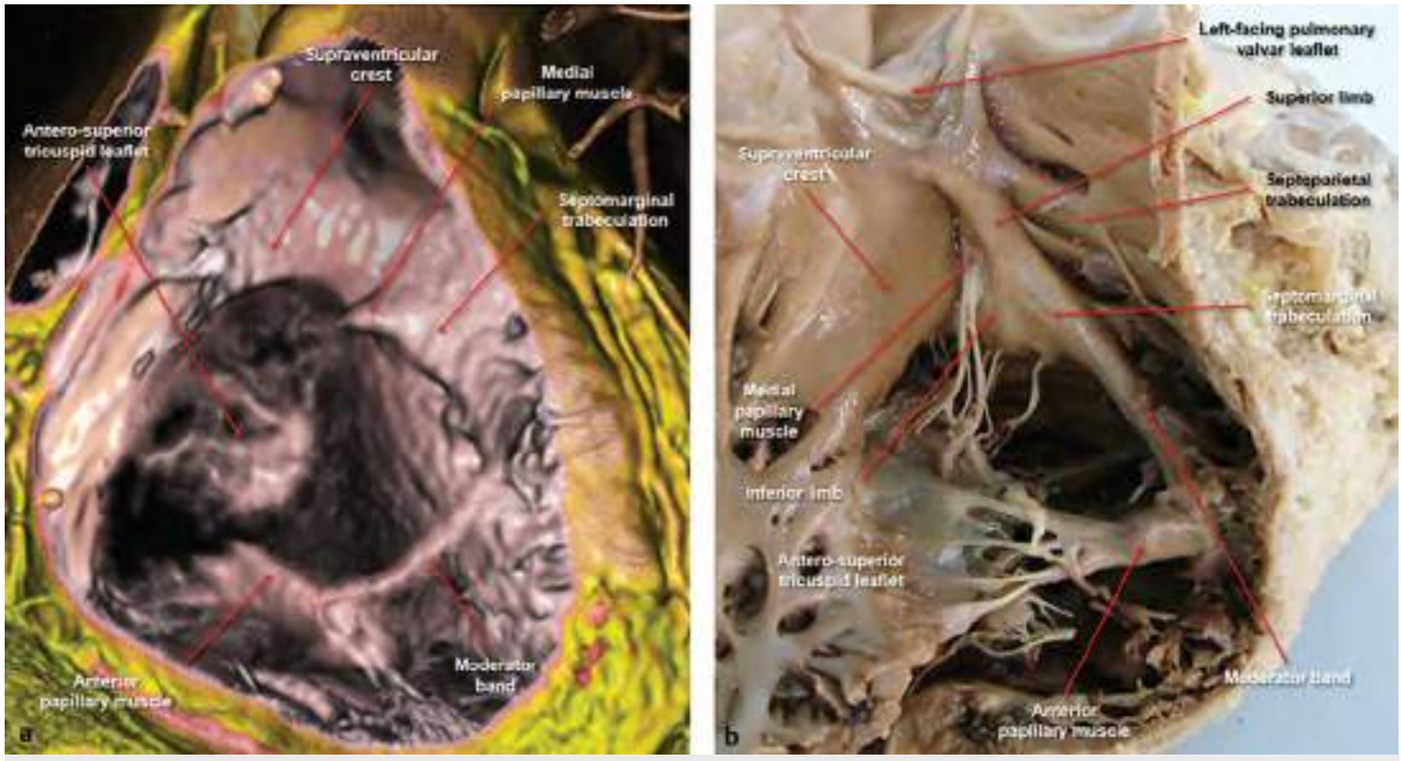

Fig. 13.19 The virtual dissection shown in **(a)** and the dissection of an autopsied heart shown in **(b)** reveal the components of the supraventricular crest and its relationship to the septomarginal trabeculation and papillary muscles.

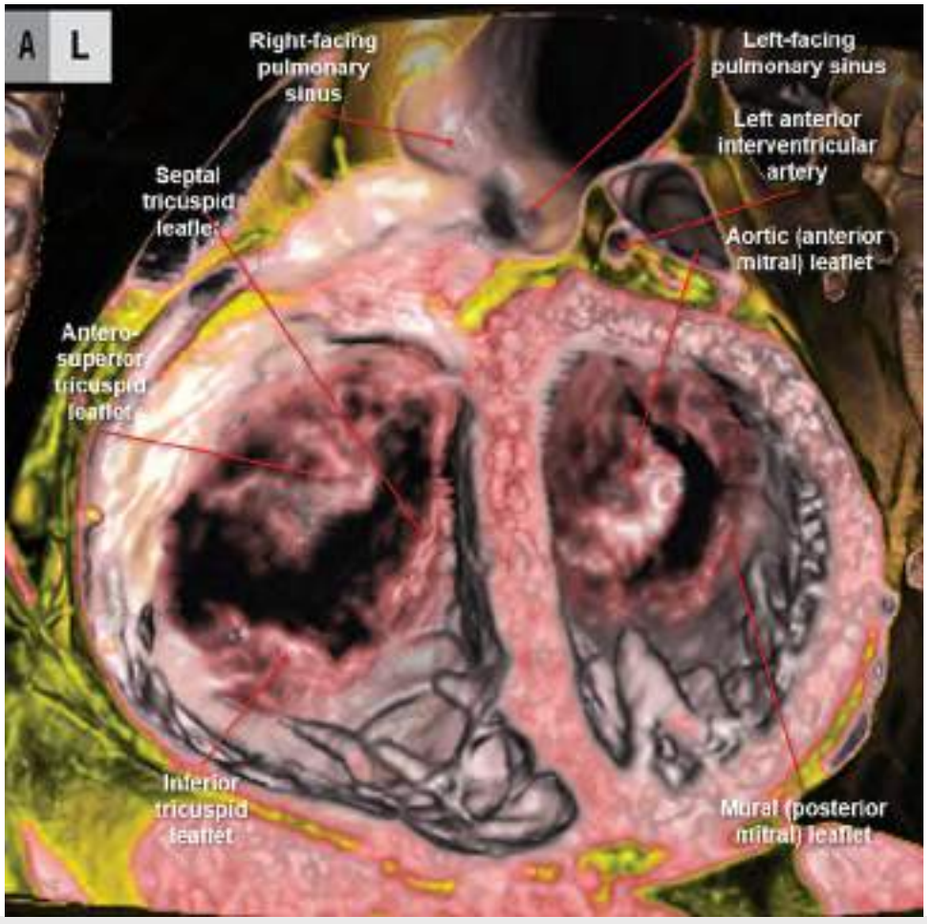

Fig. 13.20 The short axis of the ventricular mass is viewed from the apex in attitudinally appropriate fashion. The alignment of the anterior (aortic) mitral valvar leaflet and posterior (mural) mitral valvar leaflet is visualized. Note also that the leaflets of the tricuspid valve occupy anterosuperior, inferior, and septal locations within the right atrioventricular junction.

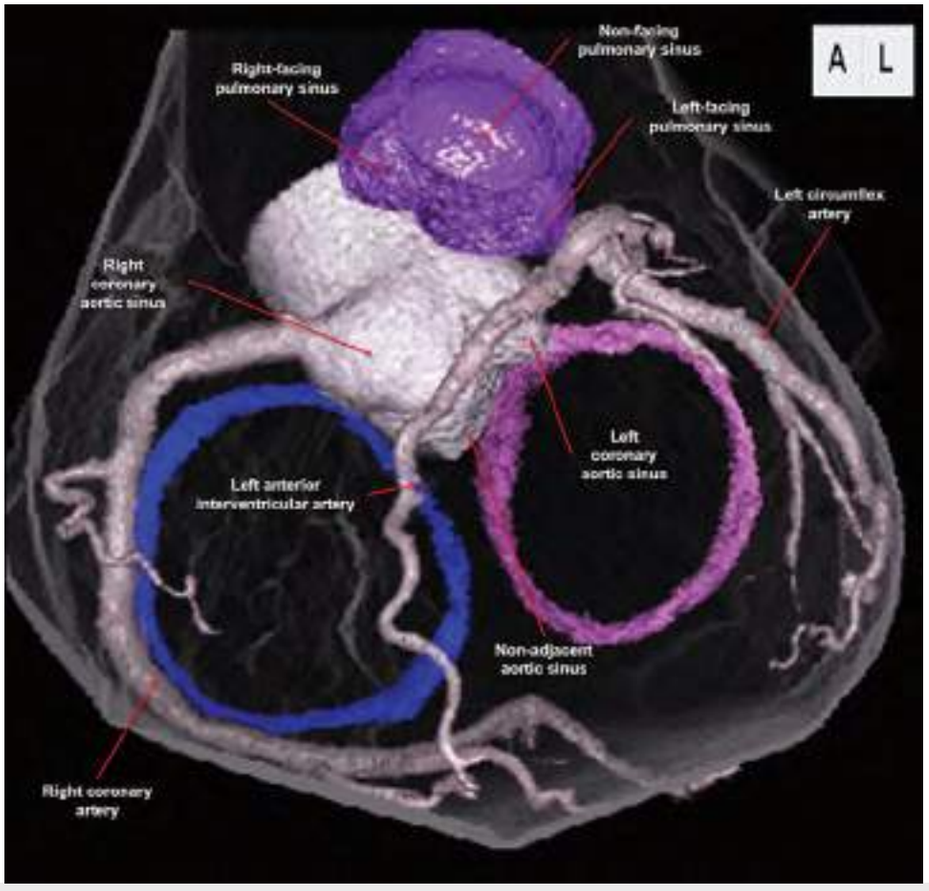

Fig. 13.21 The arterial roots are located within the superior half of the cardiac base, with the recess of the aortic root insinuating itself between the basal part of the muscular ventricular septum and the orifices of the atrioventricular valves. The pulmonary valvar sinuses are best described as right (-facing), left (-facing), and nonadjacent, respectively.

◆ The Arterial Roots

When viewed in frontal projection, the arterial roots are seen to be located within the superior half of the cardiac base, although as we have shown, a recess of the aortic root extends inferiorly, insinuating itself between the basal part of the muscular ventricular septum and the orifices of both atrioventricular valves (▶ Fig. 13.21). The aortic root is the centerpiece of the cardiac base. When describing the anatomical arrangement of the roots, we currently encounter problems not only in accounting for their location relative to the bodily coordinates, but also in adequately describing their components. In no small part, this is because the term "cusp" is currently used indiscriminately in accounting for either the moving components of the roots, or the walls that support them in semilunar fashion.[31] When defined literally, a "cusp" is either an elevation, or else describes the crossing point of two curves. The word is poorly suited for description of either the moving components of the roots, or their supporting structures. Our preference is to describe the supporting structures as the valvar sinuses. We use "leaflet" to account for the moving components, employing the word in this context for the moving parts of both the atrioventricular and arterial valves.[32] When seen in three-dimensional fashion, the arterial valvar leaflets are hinged in semilunar fashion, thus producing three-pointed coronets in both aortic and pulmonary positions (▶ Fig. 13.1, ▶ Fig. 13.7). The semilunar attachments are attached distally at the sinotubular junctions, which are discrete anatomical entities. Their proximal borders, however, are imaginary planes formed by joining together their basal attachments (▶ Fig. 13.22). These most proximal attachments, furthermore, extend on the ventricular aspects of the anatomical ventriculoarterial junctions. This means that, potentially, there are crescents of myocardium incorporated at the bases of the sinuses in both arterial roots, although the myocardium within the sinuses is covered by a layer of fibrous tissue. Because of the fibrous continuity between the leaflets of the aortic and mitral valves in the left ventricular outflow tract, however, the myocardial crescents in the left ventricular outlet are found at the bases of only the two aortic valvar sinuses that give rise to the coronary arteries (▶ Fig. 13.4, ▶ Fig. 13.23). All three sinuses of the pulmonary root, in contrast, incorporate myocardial crescents at their bases.[33] This is because, by virtue of the presence of the circumferential free-standing subpulmonary infundibular sleeve, the leaflets of the pulmonary valve are elevated away from the cardiac base. The entirety of the pulmonary root, therefore, can be removed, and is used as an aortic autograft in the Ross procedure.[34] When viewed in frontal fashion, the subpulmonary infundibular sleeve, along with the inner heart curvature, is seen as the supraventricular crest, which interposes between the leaflets of the tricuspid and pulmonary valves (▶ Fig. 13.19). The supraventricular crest itself inserts into the septal surface of the right ventricle between the limbs of the septomarginal trabeculation, with the latter structure also known as the septal band (▶ Fig. 13.19). The supraventricular crest is a

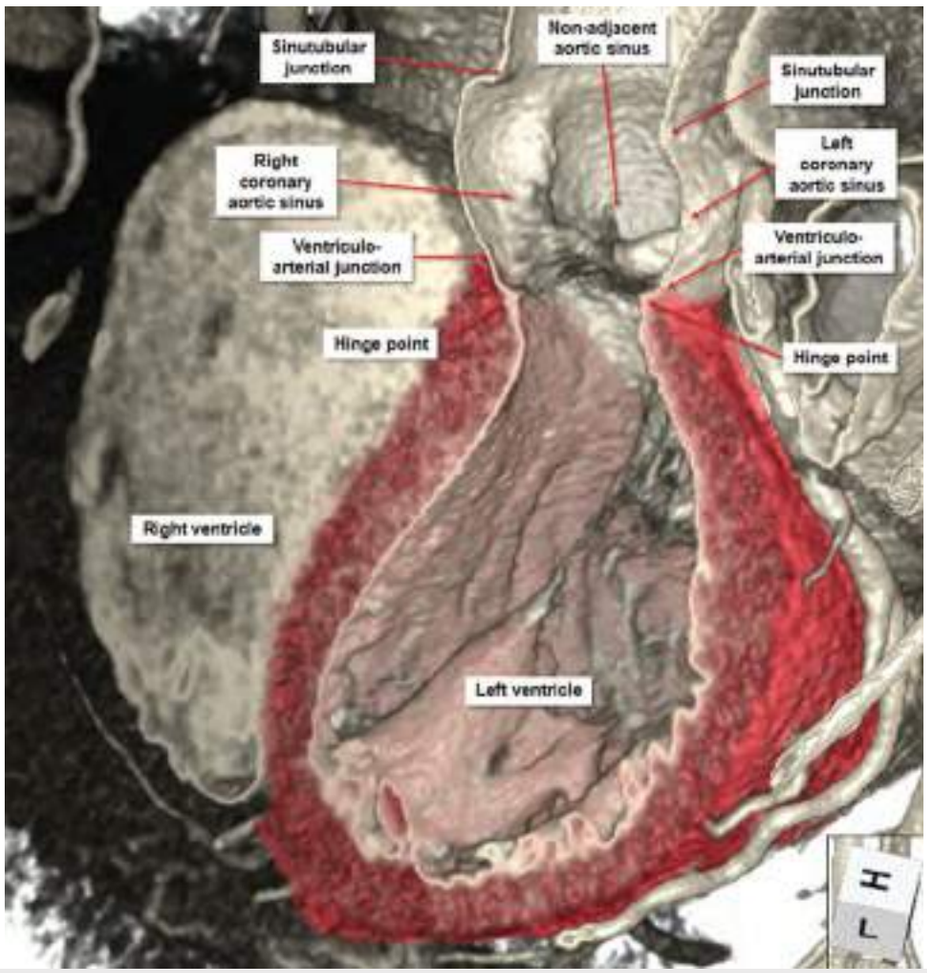

Fig. 13.22 The reconstruction of the aortic root shows the myocardium of the crest of the muscular ventricular septum and left ventricular free wall incorporated at the bases of the right and left coronary aortic sinuses. Note that the hinge points attach proximal to the anatomical ventriculoarterial junction.

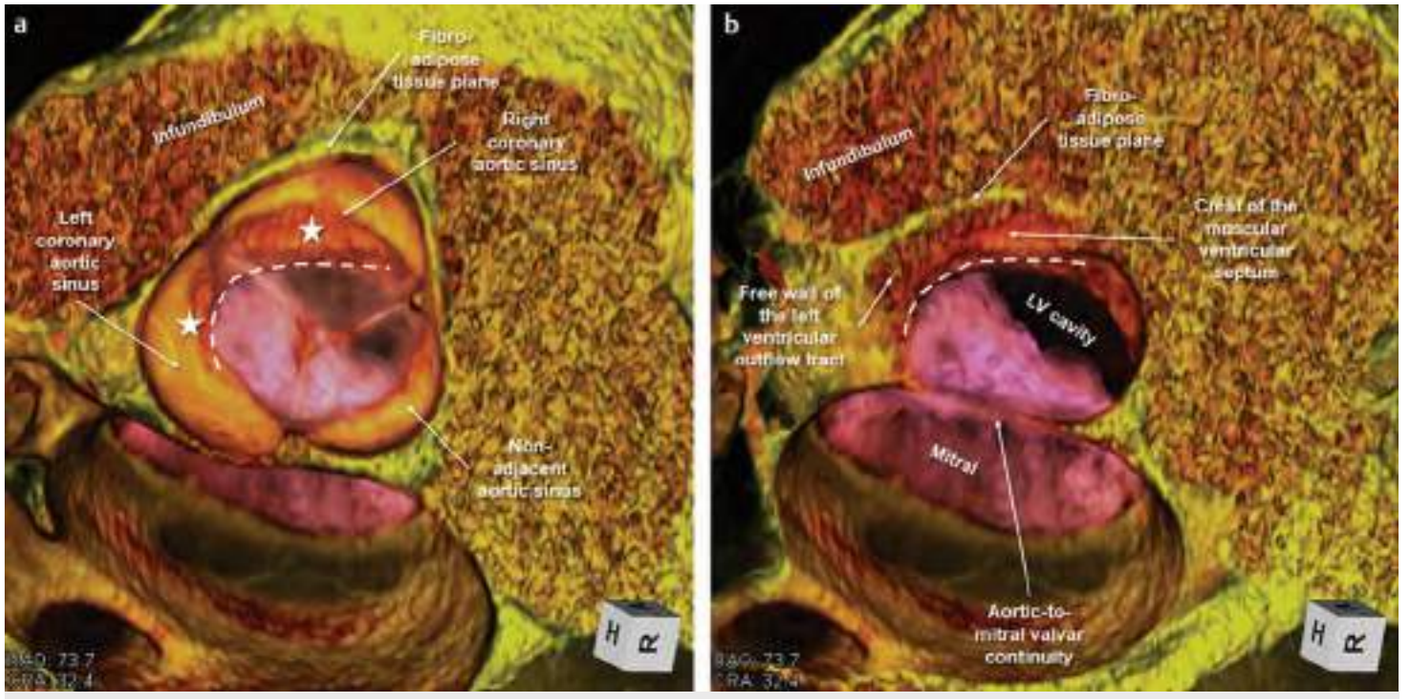

Fig. 13.23 The short-axis views of the aortic valve as seen from the arterial aspect are shown at the level of the sinuses of Valsalva **(a)** and left ventricular outflow tract **(b)**. The white stars show the crescents of myocardium incorporated into the base of the right coronary aortic sinus and anterior half of the left coronary aortic sinus. White dashed lines indicated the extent of incorporated left ventricular myocardium.

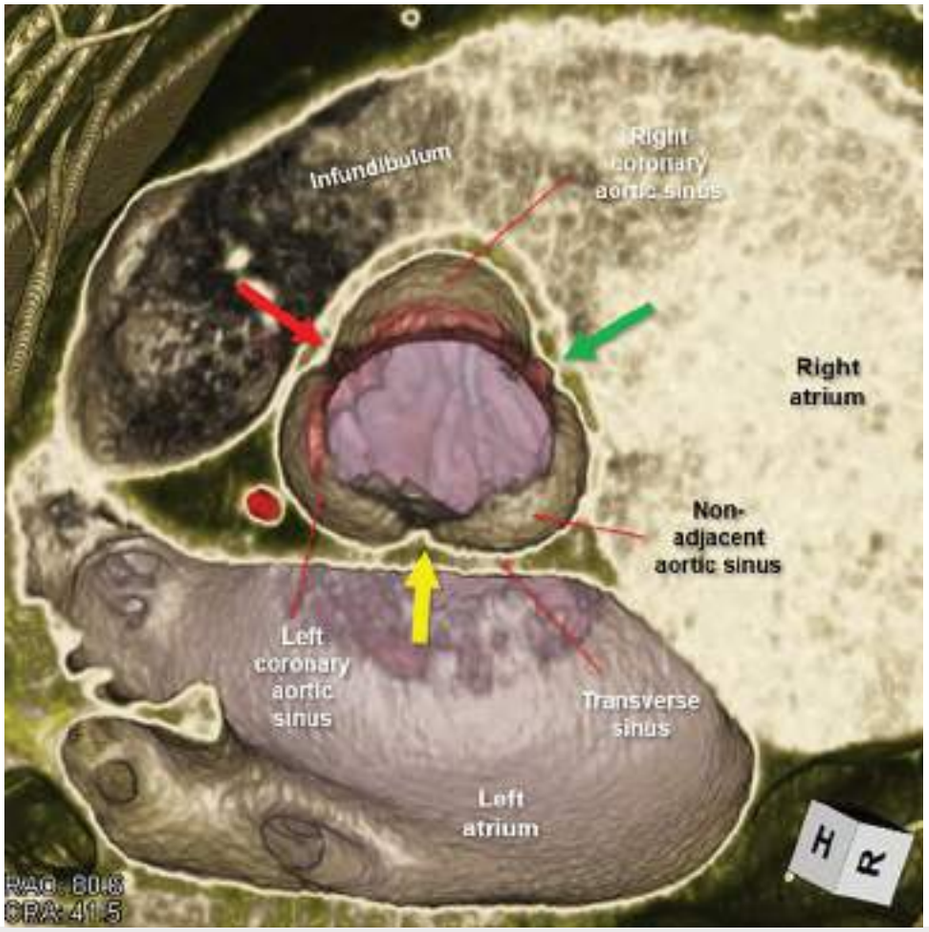

Fig. 13.24 The short-axis section of the aortic root is shown just below the level of the sinotubular junction. Red, green, and yellow arrows indicate the apex of the interleaflet fibrous triangles between each coronary aortic sinus, showing their potential continuity with the pericardial cavity. The yellow arrow denotes the interleaflet fibrous triangle between the left coronary and the nonadjacent aortic sinuses facing the transverse sinus. The red arrow shows the interleaflet fibrous triangle between the right and left coronary aortic sinuses facing the fibroadipose tissue plane behind the posterior free-standing subpulmonary infundibulum. The green arrow shows the interleaflet fibrous triangle between the right coronary and nonadjacent aortic sinuses facing the periaortic pericardial space.

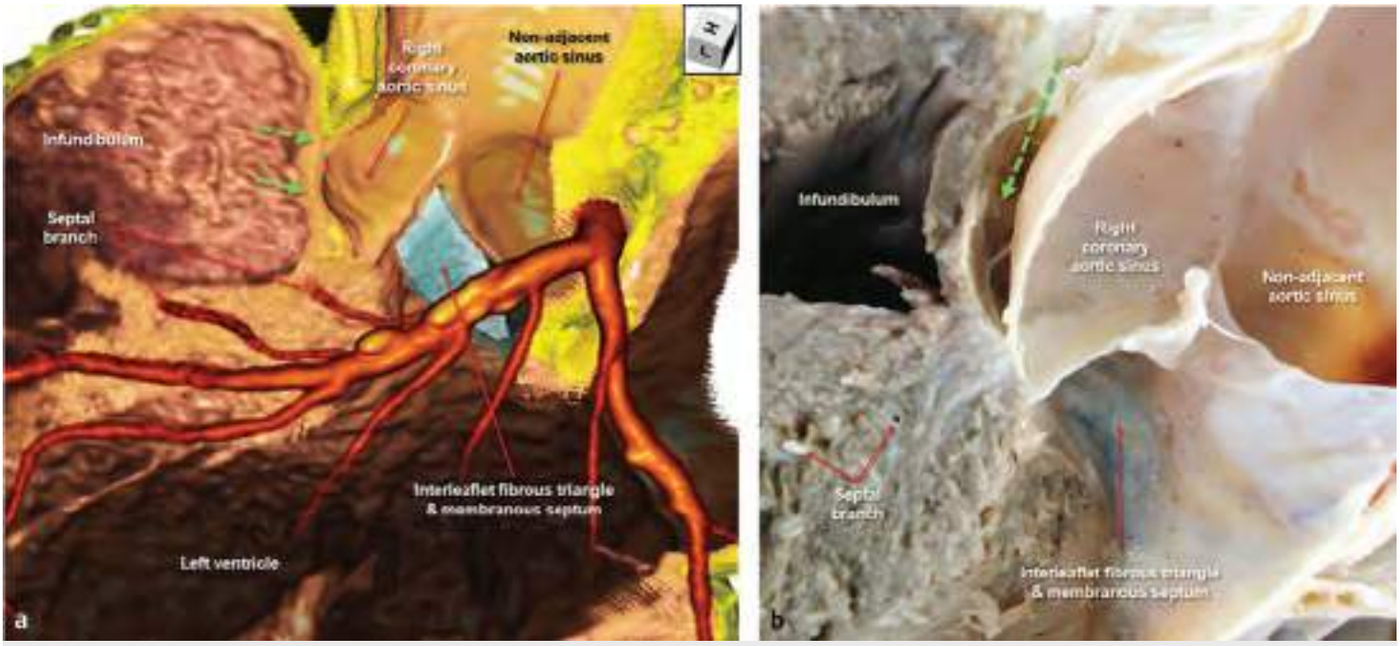

Fig. 13.25 **(a)** Long-axis section through the aortic root shows the yellowish extracardiac fibroadipose tissue plane (*green dotted arrows*), which interposes between the free-standing subpulmonary infundibulum and the anterior right coronary aortic sinus. **(b)** In the autopsied heart, a dissection has been made into the tissue plane (*green dotted arrow*). Note, the major septal branch from the anterior interventricular artery enters the septal crest through this tissue plane.

free-standing structure, and not a "muscular outlet septum" as previously thought. A fibroadipose tissue plane interposes between the posterior aspect of the free-standing subpulmonary infundibulum and the entirety of the right coronary aortic sinus (▶ Fig. 13.24, ▶ Fig. 13.25). Previous analysis using cardiac CT has already shown that, if a muscular outlet septum did indeed exist in the normal heart, it would be very small.[35] Our cardiac CT study suggests that, in the normal heart, there is no muscular outlet septum. The discrepancy may be due to limited spatial resolution of current clinical scanners, as in some cases it would be difficult to distinguish apposing walls of the supraventricular crest from the ventricular septum. We are unable currently to demonstrate the precise extent of the tissue planes relative to the ventricular septal crest using CT, but it is equally difficult to show this feature when dissecting the normal heart in the autopsy room. Using CT, nonetheless, we are able to demonstrate the extent of the muscular ventricular septum relative to the cardiac contour (▶ Fig. 13.26). In this way, we show how, when assessed using the right anterior oblique view, it is possible to recognize the notch in the ventricular septum made by the right coronary aortic sinus. This corresponds posteroinferiorly with the ventriculoinfundibular fold, derived from the initial muscular inner heart curvature. The anterosuperior component of the ventriculoinfundibular fold is the posterior part of the free-standing subpulmonary infundibulum, formed during development by muscularization of the proximal outflow cushions.[36] Distinction of these components by the electrophysiologist could well prove important when seeking to establish the substrates for ventricular arrhythmias, known frequently to arise from the right ventricular outflow tract.

Unlike the right ventricular outflow tract, which is exclusively muscular, the subaortic outflow tract of the left ventricle has partly fibrous borders. These are located medially and posteriorly, and are formed by the membranous septum, the right fibrous trigone, the area of fibrous continuity with the aortic leaflet of the mitral valve, and the left fibrous trigone (▶ Fig. 13.4, ▶ Fig. 13.7). The anterior muscular components are formed by the crest of the muscular ventricular septum. The muscular components continue laterally to incorporate a small part of the parietal ventricular wall at the base of the left coronary aortic sinus (▶ Fig. 13.23, ▶ Fig. 13.27). In cardiac electrophysiology, this area just beneath the anterior half of the left coronary aortic sinus is called the left ventricular summit.[37] It is also well recognized as a potentially vulnerable area during transcatheter aortic valve replacement.[38] Calcification at this region (▶ Fig. 13.28) is reported to be a possible risk factor for rupture of the aortic root.[39]

There is no myocardium within the aortic root supporting the posterior part of right side of the right coronary aortic sinus, the entirety of the nonadjacent aortic sinus, or the posterior half of the left coronary aortic sinus (▶ Fig. 13.27). During embryonic development, nonetheless, the larger part of these areas was also initially made up by the muscular tissue of the inner heart curvature. In early development, therefore, the aortic valve, like the pulmonary valve, possesses a completely muscular infundibulum. It is only subsequent to closure of the embryonic interventricular communication, when the aortic root has completed its transfer into the left ventricle, that the muscular tissue of the inner heart curvature becomes converted to fibrous tissue.[36]

During its development, furthermore, the entirety of the aortic root is initially encased with a turret of outflow tract myocardium. It is the regression of the distal margin of this turret during normal development that places the apexes of the interleaflet fibrous triangles, the fibrous structures found on the ventricular aspect of the valvar sinuses,[40] in potential continuity with the pericardial cavity (▶ Fig. 13.24). The apex of the triangle that

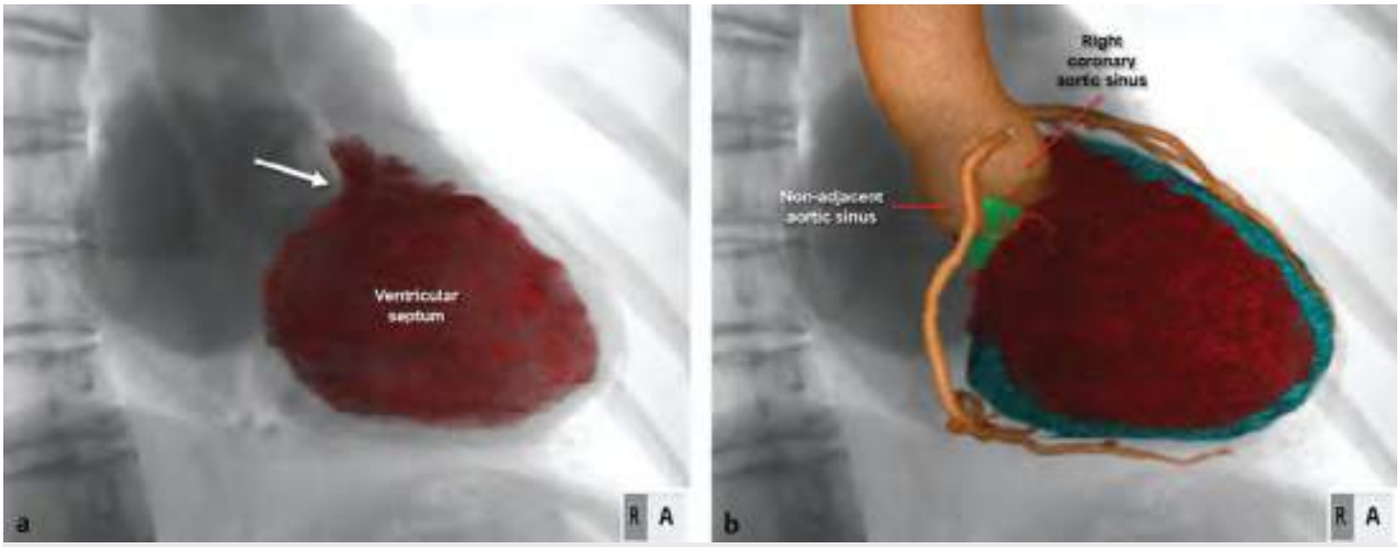

Fig. 13.26 From the right anterior oblique view, the notch in the ventricular septum made by the right coronary aortic sinus is recognizable (*white arrow*) in **(a)**. It corresponds to the ventriculoinfundibular fold. The internal surface of the fold is the supraventricular crest **(b)**. Sky blue indicates the left ventricular free wall. Green denotes the interleaf let fibrous triangle and membranous septum.

interposes between the non- and the left coronary aortic sinuses faces the transverse pericardial sinus (▶ Fig. 13.24). The apex of the triangle between the right and left coronary aortic sinuses faces the fibroadipose tissue plane separating the free-standing subpulmonary infundibulum from the aortic root (▶ Fig. 13.23, ▶ Fig. 13.24). The basal part of the triangle between the right coronary and nonadjacent aortic sinuses is the membranous component of the ventricular septum (▶ Fig. 13.5, ▶ Fig. 13.12, ▶ Fig. 13.27). The location of the ventriculoinfundibular fold on the right side of the septum, however, divides the triangle into intracardiac and extracardiac components. The extracardiac component is the apex of the triangle. This part points to the rightward margin of the transverse sinus above the superior paraseptal area. Since the membranous septum itself is further divided into two portions by the septal attachment of the septal tricuspid leaflet, it follows that there are three discrete components of the fibrous triangle separating the right coronary and nonadjacent aortic sinuses. The apex of the triangle faces the right side of the transverse sinus between the aortic root and the right atrial appendage. Its other parts are the atrioventricular and interventricular portions of the membranous septum (▶ Fig. 13.5, ▶ Fig. 13.12, ▶ Fig. 13.29). It is because the apex of the triangle separates the left ventricular outflow tract from the transverse pericardial sinus that is not a true anatomical septum.

◆ Conclusion

By using virtual dissection of computed tomographic datasets obtained during clinical investigations, we have shown that we are now able to demonstrate the anatomy of the heart with just as much, if not more, accuracy as when we hold the heart in our hands in the dissection room. The use of virtual dissections, furthermore, permits us to retain the heart in its appropriate location within the body, thus facilitating the use of attitudinally appropriate terminology. These techniques now provide the gold standard for the understanding and interpretation of the more subtle aspects of cardiac anatomy.

◆ Acknowledgments

We thank Prof. Ken-ichi Hirata for placing his scientific expertise at our disposal during the preparation of the manuscript. We also thank Prof. Toshio Terashima, Associate Prof. Takamitsu Arakawa, and Tomiyoshi Setsu for their assistance in providing the facilities for the standard dissections that provided the necessary basis for the virtual dissections. We also thank our colleagues in cardiology—Sei Fujiwara, Tomofumi Takaya, Takayoshi Toba, Tatsuro Ito, Akira Kasamatsu, Kazuhiro Kashio—and in radiology—Atsushi Kono, Tatsuya Nishii, Yoshiaki Watanabe—for their cooperation in

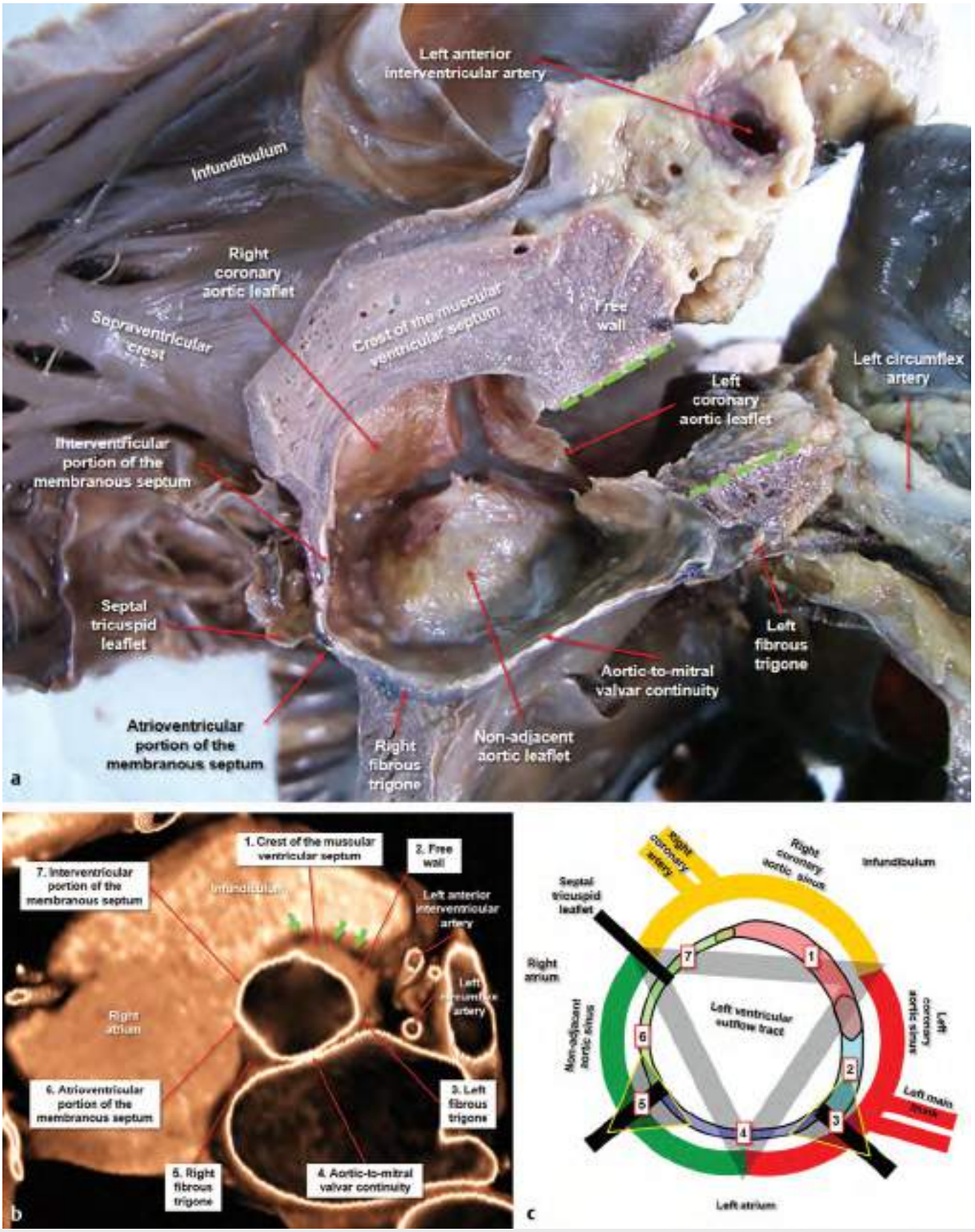

Fig. 13.27 **(a)** The components of the left ventricular outflow tract in short axis are demonstrated in the autopsied heart. The left ventricular outflow tract is made up of the crest of the muscular ventricular septum, the ventricular free wall, left fibrous trigone, aortic-to-mitral valvar continuity, right fibrous trigone, atrioventricular portion of the membranous septum, and the interventricular portion of the membranous septum, as traced in clockwise fashion. Green dotted lines indicate the sectional plane from the free wall to the left coronary aortic sinus. **(b)** The alignment and segmentation of the left ventricular outflow tract is demonstrated in the living heart in a schematic diagram **(b)**. Each number in **(b)** corresponds to the same number in **(c)**. In this patient, the fibroadipose tissue plane (*green arrows*) extends apically below the ventriculoarterial junction to the level of left ventricular outflow tract.

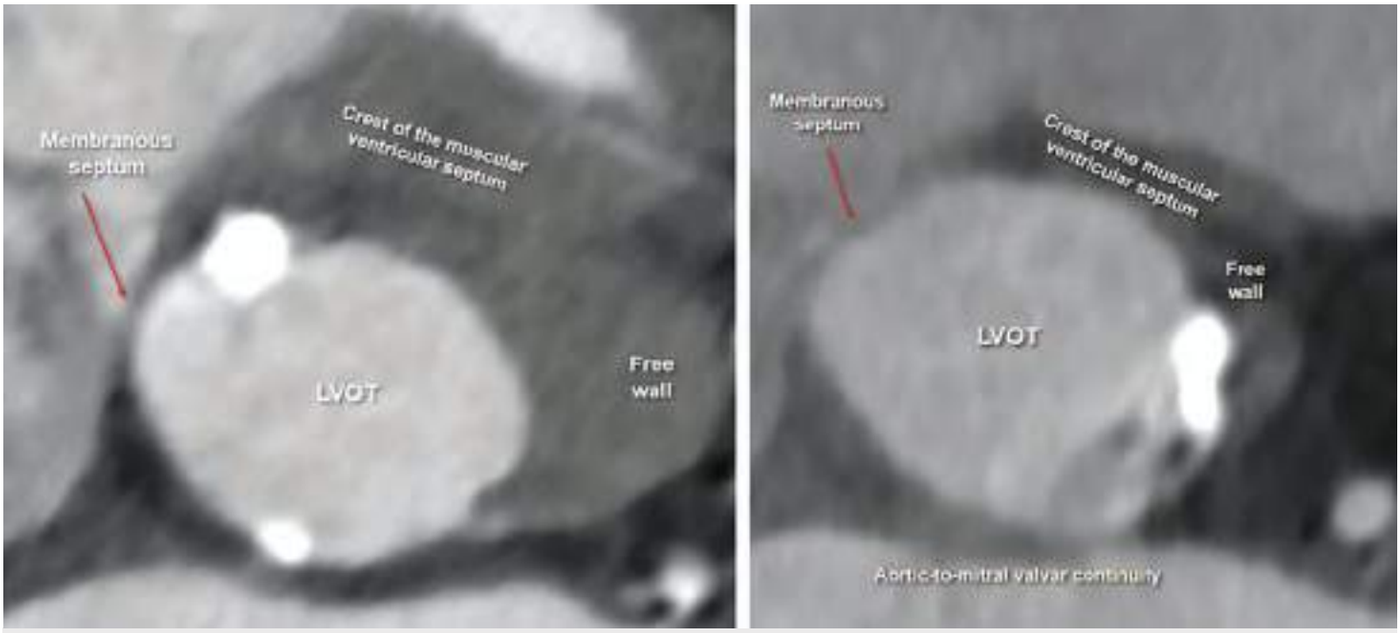

Fig. 13.28 The short-axis views of the left ventricular outflow tract (LVOT) shows calcifications found at the level of virtual basal ring, at the crest of the ventricular septum, at the left ventricular free wall, and around aortic-to-mitral valvar continuity, in a patient with aortic stenosis.

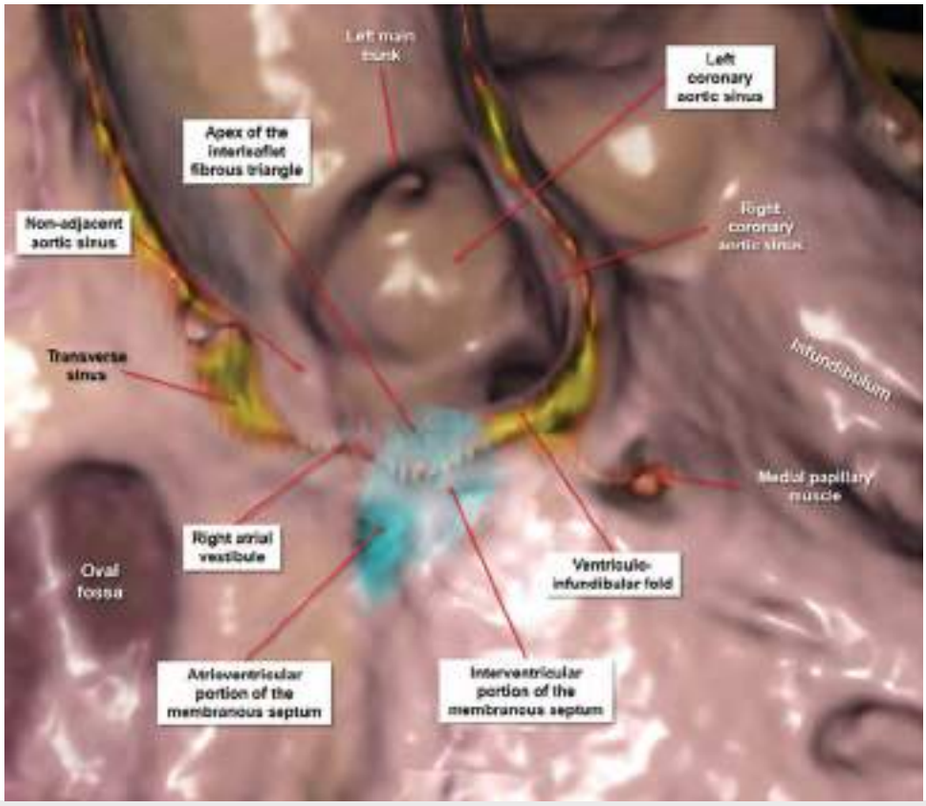

Fig. 13.29 Inner view of the right heart showing the membranous septum and associated structures. The reconstruction is made by removing the right coronary aortic valvar sinus. The image shows how the interleaflet triangle between the right coronary and nonadjacent sinuses is divided by the ventriculoinfundibular fold and the right atrial vestibule into an apical portion and the membranous septum. The latter is crossed by the attachment of the septal leaflet of the tricuspid valve, separating it into the atrioventricular and interventricular components.

image reconstruction and manuscript editing. The images could not have been produced without the technical support provided by our radiological technologists: Tomoki Maebayashi, Erina Suehiro, Wakiko Tani, Toshinori Sekitani, Kiyosumi Kagawa, Noriyuki Negi, Tohru Murakami, and Hideaki Kawamitsu.

References

[1] Sealy WC, Gallagher JJ. The surgical approach to the septal area of the heart based on experiences with 45 patients with Kent bundles. J Thorac Cardiovasc Surg.; 79(4):542–551
[2] Dean JW, Ho SY, Rowland E, Mann J, Anderson RH. Clinical anatomy of the atrioventricular junctions. J Am Coll Cardiol.; 24(7):1725–1731
[3] Anderson RH, Ho SY, Becker AE. Anatomy of the human atrioventricular junctions revisited. Anat Rec.; 260(1):81–91
[4] Sánchez-Quintana D, Ho SY, Cabrera JA, Farré J, Anderson RH. Topographic anatomy of the inferior pyramidal space: relevance to radiofrequency catheter ablation. J Cardiovasc Electrophysiol.; 12(2):210–217
[5] Anderson RH, Webb S, Brown NA, Lamers W, Moorman A. Development of the heart: (2) Septation of the atriums and ventricles. Heart.; 89(8):949–958
[6] Anderson RH, Razavi R, Taylor AM. Cardiac anatomy revisited. J Anat.; 205 (3):159–177
[7] Farré J, Anderson RH, Cabrera JA, et al. Cardiac anatomy for the interventional arrhythmologist: I. terminology and fluoroscopic projections. Pacing Clin Electrophysiol.; 33(4):497–507
[8] Saremi F, Krishnan S. Cardiac conduction system: anatomic landmarks relevant to interventional electrophysiologic techniques demonstrated with 64-detector CT. Radiographics.; 27(6):1539–1565, discussion 1566–1567
[9] Mori S, Nishii T, Takaya T, et al. Clinical structural anatomy of the inferior pyramidal space reconstructed from the living heart: three-dimensional visualization using multidetector-row computed tomography. Clin Anat.; 28 (7):878–887
[10] Mori S, Fukuzawa K, Takaya T, et al. Clinical structural anatomy of the inferior pyramidal space reconstructed within the cardiac contour using multidetector-row computed tomography. J Cardiovasc Electrophysiol.; 26(7):705–712
[11] Anderson RH, Loukas M. The importance of attitudinally appropriate description of cardiac anatomy. Clin Anat.; 22(1):47–51
[12] Anderson RH, Spicer DE, Hlavacek AJ, Hill A, Loukas M. Describing the cardiac components—attitudinally appropriate nomenclature. J Cardiovasc Transl Res.; 6(2):118–123
[13] Tawara S. Das Reizleitungssystem des Saugetierherzens: Eine anatomisch-histologische Studie uber das Atrioventrikularbundel und die Purkinjeschen Faden. Jena, Germany: Gustav Fischer; 1906:9–70, 114–156
[14] Widran J, Lev M. The dissection of the atrioventricular node, bundle and bundle branches in the human heart. Circulation.; 4(6):863–867
[15] Titus JL. Cardiac arrhythmias. 1. Anatomy of the conduction system. Circulation.; 47(1):170–177
[16] Massing GK, James TN. Anatomical configuration of the His bundle and bundle branches in the human heart. Circulation.; 53(4):609–621
[17] Anderson RH, Boyett MR, Dobrzynski H, Moorman AF. The anatomy of the conduction system: implications for the clinical cardiologist. J Cardiovasc Transl Res.; 6(2):187–196
[18] Kleinert S, Geva T. Echocardiographic morphometry and geometry of the left ventricular outflow tract in fixed subaortic stenosis. J Am Coll Cardiol.; 22 (5):1501–1508
[19] Levine RA, Handschumacher MD, Sanfilippo AJ, et al. Three-dimensional echocardiographic reconstruction of the mitral valve, with implications for the diagnosis of mitral valve prolapse. Circulation.; 80(3):589–598
[20] Salgo IS, Gorman JH, III, Gorman RC, et al. Effect of annular shape on leaflet curvature in reducing mitral leaflet stress. Circulation.; 106(6):711–717
[21] Becker AE, Anderson RH. Atrioventricular septal defects: What's in a name? J Thorac Cardiovasc Surg.; 83(3):461–469
[22] Anderson RH, Webb S, Brown NA. Clinical anatomy of the atrial septum with reference to its developmental components. Clin Anat.; 12(5):362–374
[23] Verma S, Adler S, Berman A, Duran A, Loar D. Localization of fossa ovalis and Brockenbrough needle prior to left atrial ablation using three-dimensional mapping with EnSite Fusion. J Interv Card Electrophysiol.; 30(1):37–44
[24] Saremi F, Channual S, Raney A, et al. Imaging of patent foramen ovale with 64-section multidetector CT. Radiology.; 249(2):483–492
[25] Kuramoto J, Kawamura A, Dembo T, Kimura T, Fukuda K, Okada Y. Prevalence of patent foramen ovale in the Japanese population—autopsy study. Circ J.; 79 (9):2038–2042
[26] Hagen PT, Scholz DG, Edwards WD. Incidence and size of patent foramen ovale during the first 10 decades of life: an autopsy study of 965 normal hearts. Mayo Clin Proc.; 59(1):17–20
[27] Anderson RH, Spicer DE, Hlavacek AM, Cook AC, Backer CL. Surgical anatomy of the conduction system. Wilcox's Surgical Anatomy of the Heart. 4th ed. Cambridge: Cambridge University Press; 2013:111–127
[28] Scheinman MM, Wang YS, Van Hare GF, Lesh MD. Electrocardiographic and electrophysiologic characteristics of anterior, midseptal and right anterior free wall accessory pathways. J Am Coll Cardiol.; 20(5):1220–1229
[29] Cosío FG, Anderson RH, Kuck KH, et al. Living anatomy of the atrioventricular junctions. A guide to electrophysiologic mapping. A Consensus Statement from the Cardiac Nomenclature Study Group, Working Group of Arrhythmias, European Society of Cardiology, and the Task Force on Cardiac Nomenclature from NASPE. Circulation.; 100(5):e31–e37
[30] Bhatnagar KP, Nettleton GS, Campbell FR, Wagner CE, Kuwabara N, Muresian H. Chiari anomalies in the human right atrium. Clin Anat.; 19(6):510–516
[31] Anderson RH. Demolishing the tower of babel. Eur J Cardiothorac Surg.; 41 (3):483–484
[32] Anderson RH. Clinical anatomy of the aortic root. Heart.; 84(6):670–673
[33] Stamm C, Anderson RH, Ho SY. Clinical anatomy of the normal pulmonary root compared with that in isolated pulmonary valvular stenosis. J Am Coll Cardiol.; 31(6):1420–1425
[34] Merrick AF, Yacoub MH, Ho SY, Anderson RH. Anatomy of the muscular subpulmonary infundibulum with regard to the Ross procedure. Ann Thorac Surg.; 69(2):556–561
[35] Saremi F, Gera A, Ho SY, Hijazi ZM, Sánchez-Quintana D. CT and MR imaging of the pulmonary valve. Radiographics.; 34(1):51–71
[36] Anderson RH, Mohun TJ, Spicer DE, et al. Myths and realities relating to development of the arterial valves. Cardiovasc Dev Dis.; 1:177–200
[37] Yamada T, McElderry HT, Doppalapudi H, et al. Idiopathic ventricular arrhythmias originating from the left ventricular summit: anatomic concepts relevant to ablation. Circ Arrhythm Electrophysiol.; 3(6):616–623
[38] Piazza N, de Jaegere P, Schultz C, Becker AE, Serruys PW, Anderson RH. Anatomy of the aortic valvar complex and its implications for transcatheter implantation of the aortic valve. Circ Cardiovasc Interv.; 1(1):74–81
[39] Hayashida K, Bouvier E, Lefèvre T, et al. Potential mechanism of annulus rupture during transcatheter aortic valve implantation. Catheter Cardiovasc Interv.; 82(5):E742–E746
[40] Sutton JP, III, Ho SY, Anderson RH. The forgotten interleaflet triangles: a review of the surgical anatomy of the aortic valve. Ann Thorac Surg.; 59 (2):419–427

14 The Aortic Valve

Francesco F. Faletra and Farhood Saremi

◆ Introduction

The aortic valve is a complex structure, which consists of different highly specialized components that interact with each other, modifying their shape and size during the cardiac cycle. Following the direction of the flow, we encounter the ventriculoarterial junction, leaflets, sinuses, the crown-shaped annulus, the interleaflet triangles, the commissures, the coronary ostia, and sinotubular junction.[1,2] Although in anatomical books this complex apparatus takes often the name of aortic valve, we prefer to use the more inclusive name of the "aortic root." The job of the aortic root is definitely one of the most difficult. It (a) allows forward passage of 70 to 100 mL of blood with each systole in a low ventricle–aorta gradient, (b) prevents diastolic reflux, (c) assures wide flow variations (up to five times), and (d) maintains an optimal coronary perfusion.

The most important component of the aortic root is the aortic leaflets. The aortic leaflets open and close about 3 billion of times in the course of an average lifetime. Despite their delicate and flexible tissue structure, the leaflets have a strong structural skeleton that withstands the diastolic aortic pressure. This constant workload would certainly cause premature degeneration of the leaflets, if the protective effect of the "aortic root" did not exist. The aortic root helps to preserve leaflets by distributing the stress between the various components. Because of its conical–cylindrical shape and its pivotal role in cardiac function role, the aortic root could be considered the "fifth chamber" of the heart (▶ Fig. 14.1). This chapter describes the anatomy of various component of the aortic root.

◆ Anatomy

Ventriculoarterial Junction

The ventriculoarterial junction is a circumferential line which demarcates the site of connection of the left ventricle to the nadir of the aortic sinuses. The ventriculoarterial junction should not be confused with the aortic annulus. During aortic valve replacement, surgeons suture the basal ring of the prosthetic valve to the contour of the base of the aortic root describing this boundary as the "annulus." No matter of what terminology used, it should be noted the ventriculoarterial junction as an anatomically rigid ring-like fibrous structure does not exist, otherwise it would create a gradient similar to that produced by prosthetic valves. On the contrary, the ventriculoarterial junction is able to expand and twist during isovolumic contraction and early phase of ejection to minimize pressure gradient across the valve. Therefore, the ventriculoarterial junction can be more precisely defined as the "boundary" between the fibroelastic wall of the aorta and the partly muscular and partly fibrous rim of the left ventricular outflow tract. The ventriculoarterial junction is not a rigid structure and similar to the other parts of the aortic root and the leaflets, it has a specific kinematics during the cardiac cycle. During the ejection phase, the ventriculoarterial junction contracts, while the sinotubular junction expands; together, they form a truncated cone with the smaller surface toward the left ventricle. This transient morphology facilitates the progression of the column of blood toward the ascending aorta.

Aortic Leaflets

The aortic leaflets represent the "core" of the aortic root. Describing them as a simple flap of thin fibrous tissue is incorrect. On the contrary, they are "live" structures with an architecture formed by three inner layers (fibrosa, spongiosa, and ventricularis) that are covered on both sides by the endothelial cells. The aortic leaflets contain cells that secrete proteins that form an extracellular matrix, nerve endings, blood vessels, and possibly some contractile activity (documented only by anecdotal observations). In other words, aortic leaflets are metabolically "alive" with the potential to *self-regenerate*. One of the secret of their longevity is probably the ability to repair.

The shape of aortic leaflets resembles a "bird's nest." In each leaflet, one can distinguish a hinge line, which is the line of insertion of the leaflet on the wall, a body, and a free edge of coaptation. At the center of the leaflet free margin a fibrous nodule exist which is called the nodule of "Arantius." When the valve closes, the leaflets approach one another along the surface of coaptation, which takes the name of "lunula" (▶ Fig. 14.2).

The impact that the leaflets have in the act of closure certainly would cause severe wear and tear. The reason that this does not occur prematurely is because when the pressure in the aorta exceeds that of the ventricle, leaflets are almost closed. Vortices formed within the sinuses of Valsalva promote the closure during systole when the flow starts to decelerate. In other words, the closure of the leaflets begins during ejection (▶ Fig. 14.3).

Aortic Annulus

The term "annulus" of a valve would simply apply to a circular structure formed by a thick fibrous ring that sustains leaflets.[3] This is not the case for the aortic annulus. The "true" aortic annulus (i.e., fibrous structure that permits tight attachment of the leaflet to the aortic wall) has a "trident" or "crown-shaped" configuration. The lowest part of insertion (nadir) corresponds to ventriculoarterial junction and the highest part (commissure) to the sinotubular junction. At this level, the insertion of one cusp meets and continues with that of the adjacent cusps. As mentioned above, many use the term "annulus" to denote the location of the ventriculoarterial junction. For example, in the transcutaneous aortic valve implantation, the *virtual annulus* measurement is obtained by connecting the nadirs of the three leaflets at or slightly below the ventriculoarterial junction for selecting the right prosthesis size. In normal subjects, the *virtual annulus* is elliptical in diastole and circular in systole (▶ Fig. 14.4).

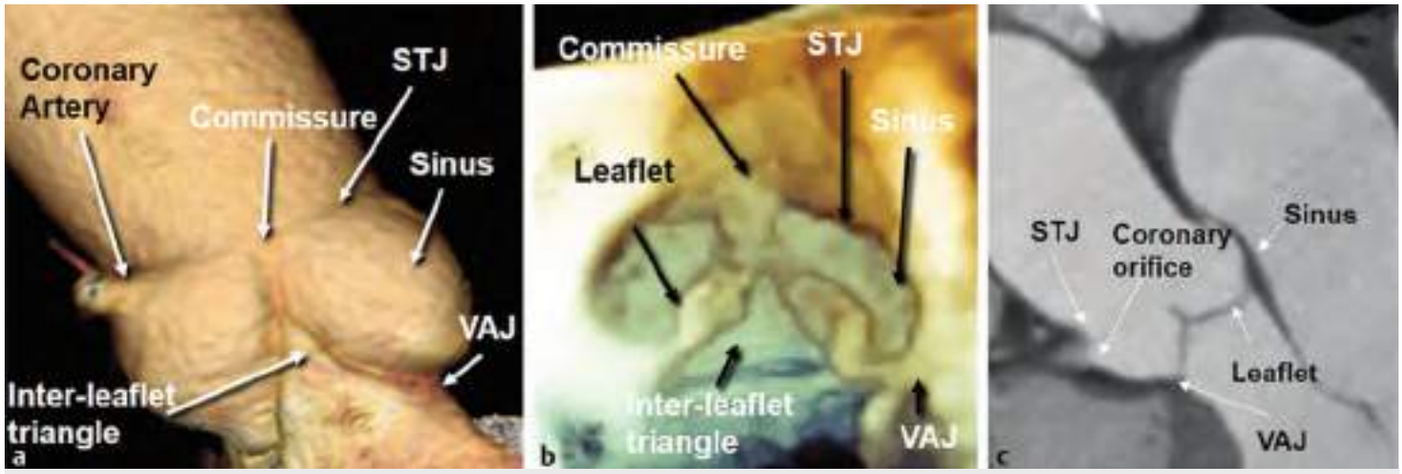

Fig. 14.1 Images of aortic root and its components using **(a)** volume-rendered CT scan, **(b)** 3D transesophageal echocardiography, and (**c**) CT multiplanar reconstruction. STJ, sinotubular junction; VAJ, ventriculoarterial junction.

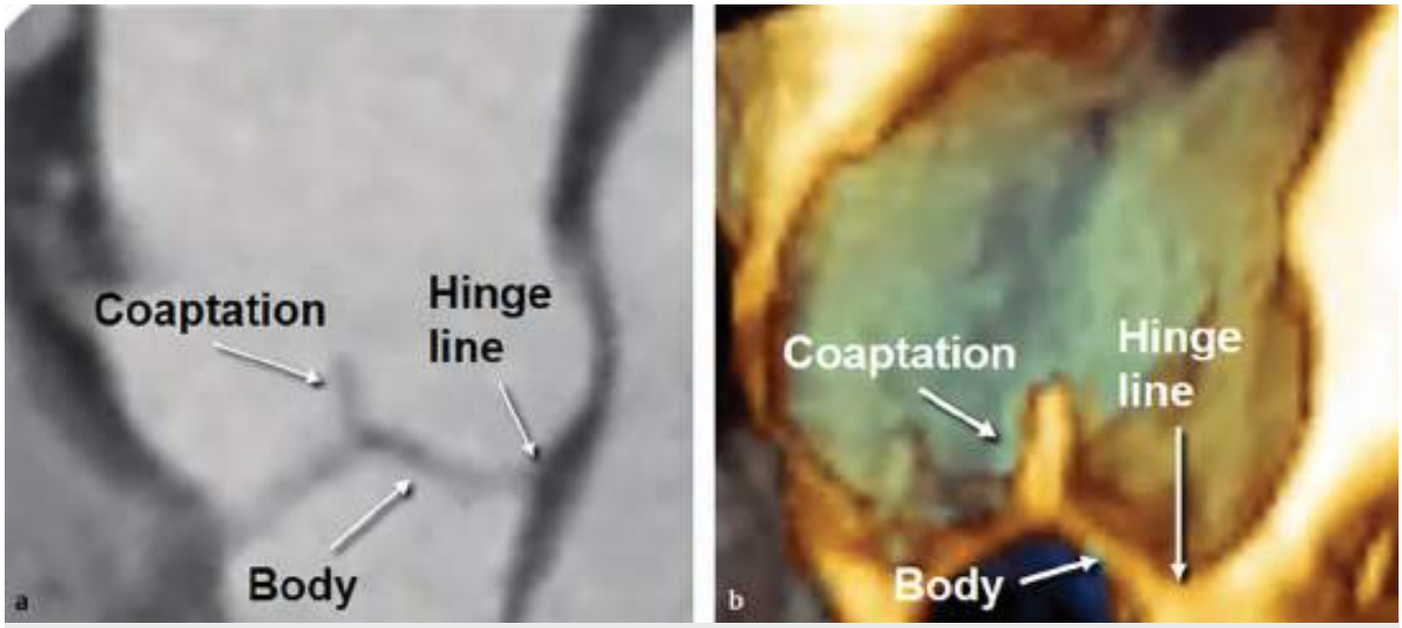

Fig. 14.2 Images of a longitudinal cut of aortic root in **(a)** multiplanar CT and **(b)** 3D transesophageal echocardiography showing the coaptation surface, the hinge line, and the body of leaflets. The area of leaflet coaptation reduces stress on leaflets in a sort of "mutual aid." The radial forces acting on them abolish, in fact, each other.

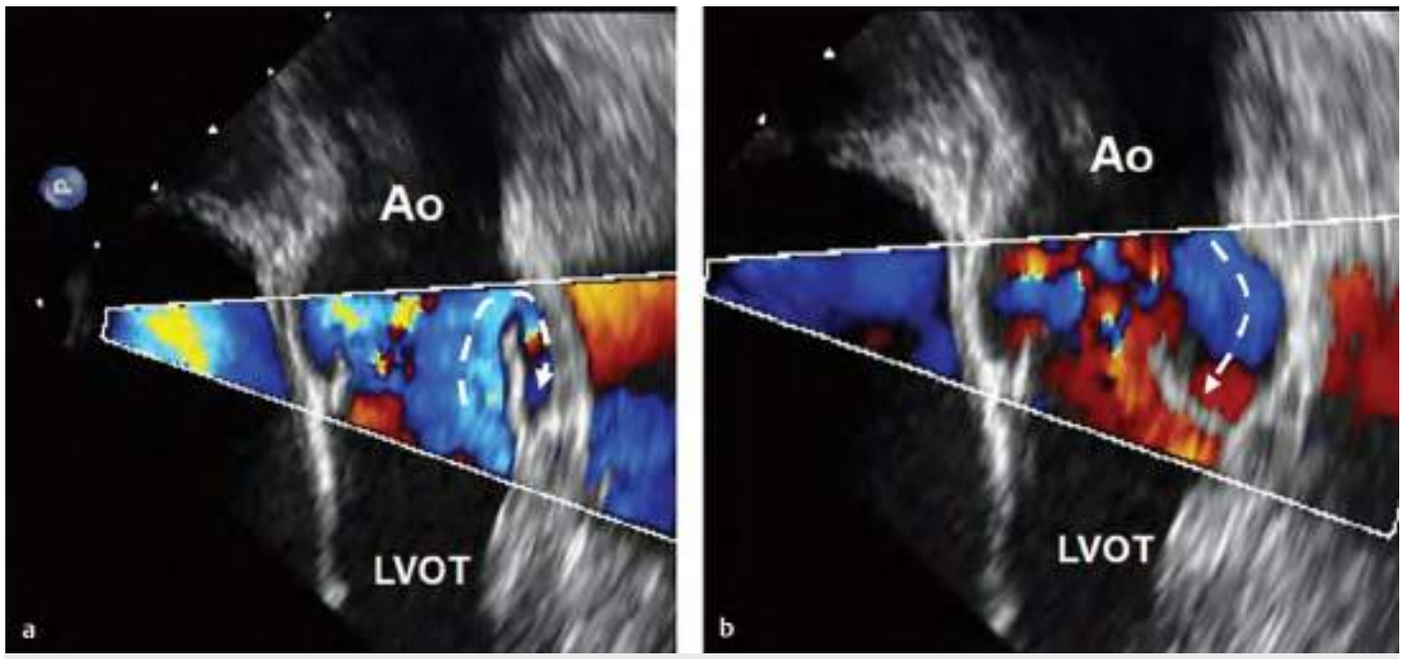

Fig. 14.3 2D transesophageal color Doppler imaging showing the vortex (*curved arrow*) that the complex leaflets–sinuses create. **(a)** In early systole, the vortex prevents the complete apposition of the leaflets on the aortic wall, which may cause the occlusion of coronary ostia (*curved dotted arrow*). **(b)** In late systole, the vortices push leaflets toward one another promoting the closure (*curved dotted arrow*). Ao, aorta; LVOT, left ventricular outflow tract.

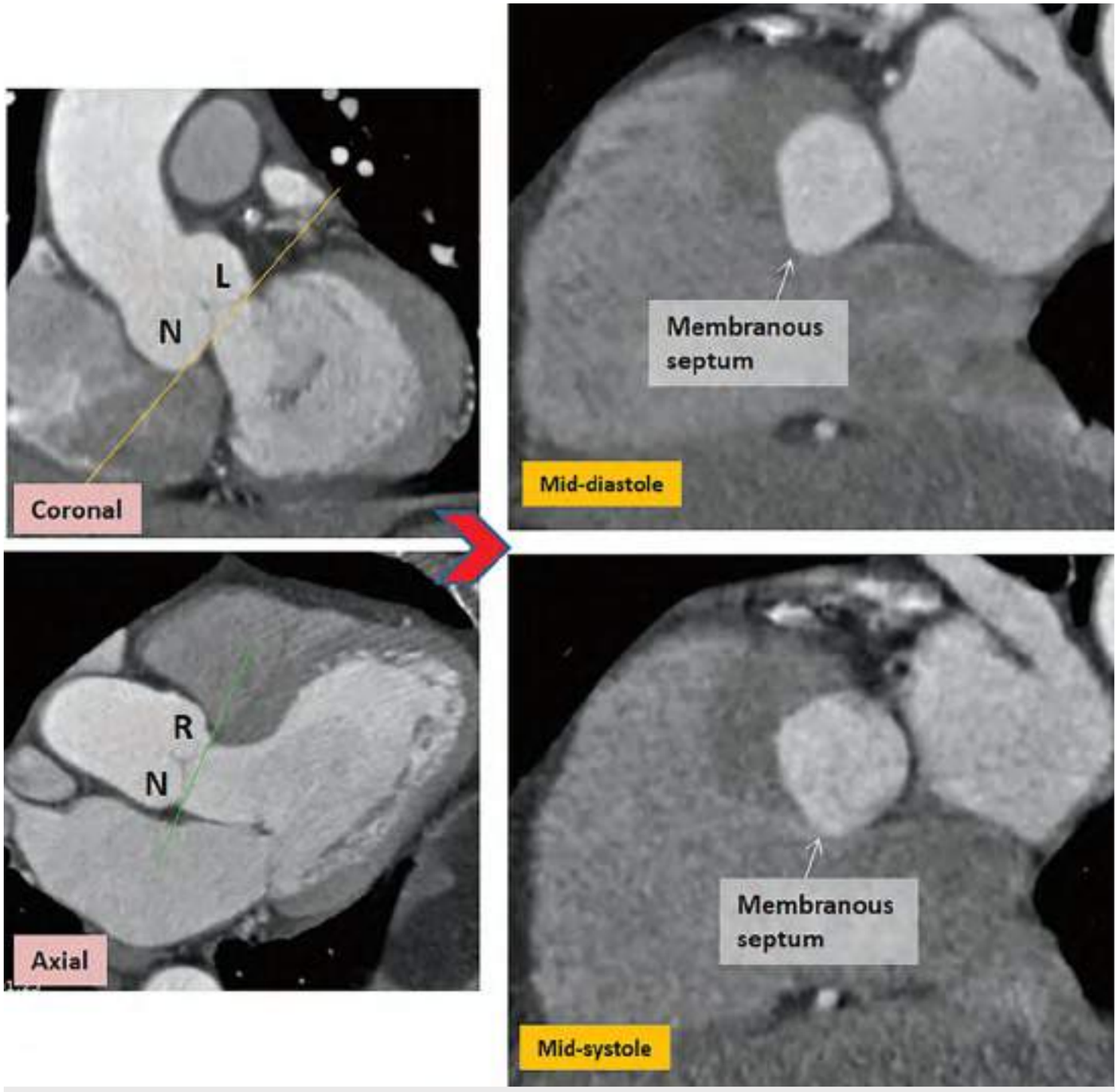

Fig. 14.4 Method of measuring the virtual annulus of the aortic valve. Using two orthogonal views (i.e., coronal and axial), short-axis images of the left ventricular outflow tract will be obtained at the level of the ventriculoarterial junction (VAJ). Measurements of the annulus (perimeter, area, diameters) are usually obtained at midsystole when the annulus is largest. Note that in diastole the annulus is oval-shaped while in systole it is more circular. The VAJ area reaches a maximal expansion during first third of the ejection but decreases during the last two-thirds of the ejection. The difference in diameters during cardiac cycle is less than 10%. In adults, VAJ diameter has a mean of 23 mm in women and 26 mm in men; indexed value is 13 mm/m^2 in both genders. The VAJ may be enlarged in aortic regurgitations. In aortic stenosis, the VAJ is more oval-shaped. L, left coronary sinus; N, noncoronary sinus; R, right coronary sinus.

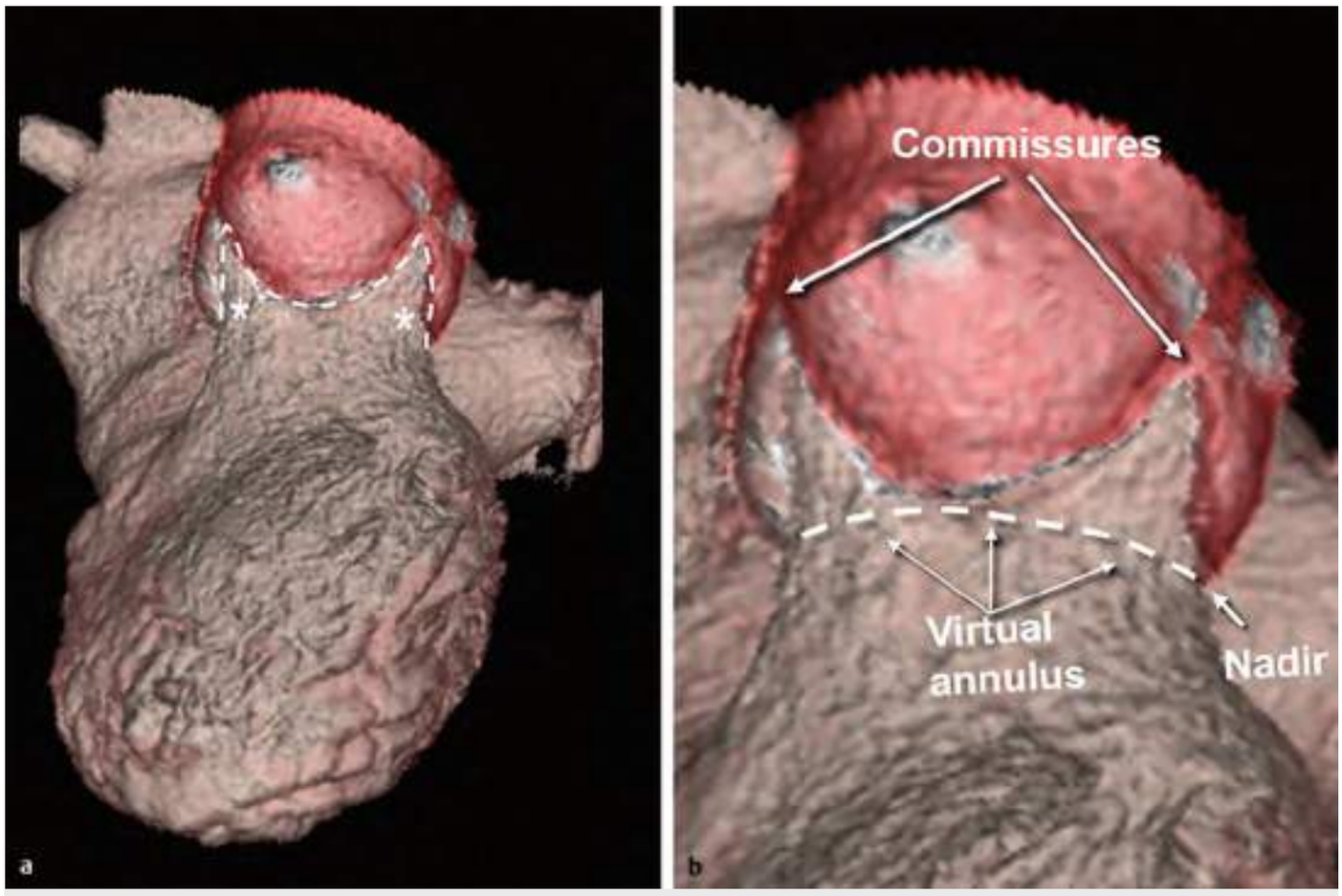

Fig. 14.5 **(a)** Computed tomographic volume-rendered image of the aortic root (*pink color*) showing the "crown-shaped" annulus (*dotted line*) and two interleaflet triangles (*asterisks*). **(b)** Magnified image showing the commissures and nadirs. The dotted line marks the virtual annulus. This circumference of this area is obtained by joining the nadirs of the three leaflets.

Interleaflet Triangles

Given the particular crown-shaped configuration of the aortic annulus, three triangles of fibrous and muscular tissue, named *interleaflet triangles* (ILTs), arise from the left ventricular outflow tract between the sinuses.[4] The ILT between the right and left coronary sinuses may contain ventricular muscular tissue. The ILT between the left coronary and the noncoronary sinuses is a fibrous sheet that continues with the anterior leaflet of mitral valve (the mitral–aortic curtain). Finally, the ILTs between the noncoronary and right coronary sinuses comprise of fibrous tissue which is continuous with the membranous septum. Interestingly, the ILTs, which are unmistakably considered part of the aortic root, are, in fact, under the ventricular pressure (▶ Fig. 14.5, ▶ Fig. 14.6).

Sinuses of Valsalva

The sinuses of Valsalva are three protrusions at the aortic root. Similar to the valve leaflets, the aortic sinuses are named right, left, and noncoronary. The first two include the origin of the coronary arteries. The wall of the sinuses is mainly composed of an elastic lamina and smooth muscle cells and oftentimes it would not be easy to distinguish between the tunica media and tunica intima. Collagen and elastic fibers form the adventitia. In diastole, the aortic root assumes, when seen in cross-section at level of the midpoint of Valsalva's sinuses, a trilobate conformation. In this way, each sinus becomes more spherical and with the correspondent leaflet forms a single, roughly hemispherical, functional unit.[5] Anatomists call this functional unit *cusp*. This trilobate conformation allows homogeneous distribution of the aortic pressure between the leaflets and the sinuses (▶ Fig. 14.7).

Sinotubular Junction

The sinotubular junction is the only fibrous ring of the aortic root and marks the border between the aortic root and the ascending aorta. This ring supports the cranial insertion of the leaflets: the commissures. The diameter of the sinotubular junction is 10 to 15% smaller than the diameter of the ventriculoarterial junction. However, during ventricular ejection the sinotubular junction dilates giving the aortic root the conformation of a truncated cone with the smaller circumference facing the ventricle.

◆ Aortic Diseases

In this chapter, we will briefly discuss the most common pathologies affecting the aortic leaflets such as papillary fibroelastomas, bicuspid valve, aortic stenosis, aortic insufficiency and aortic endocarditis, and the most frequent disease affecting the aortic

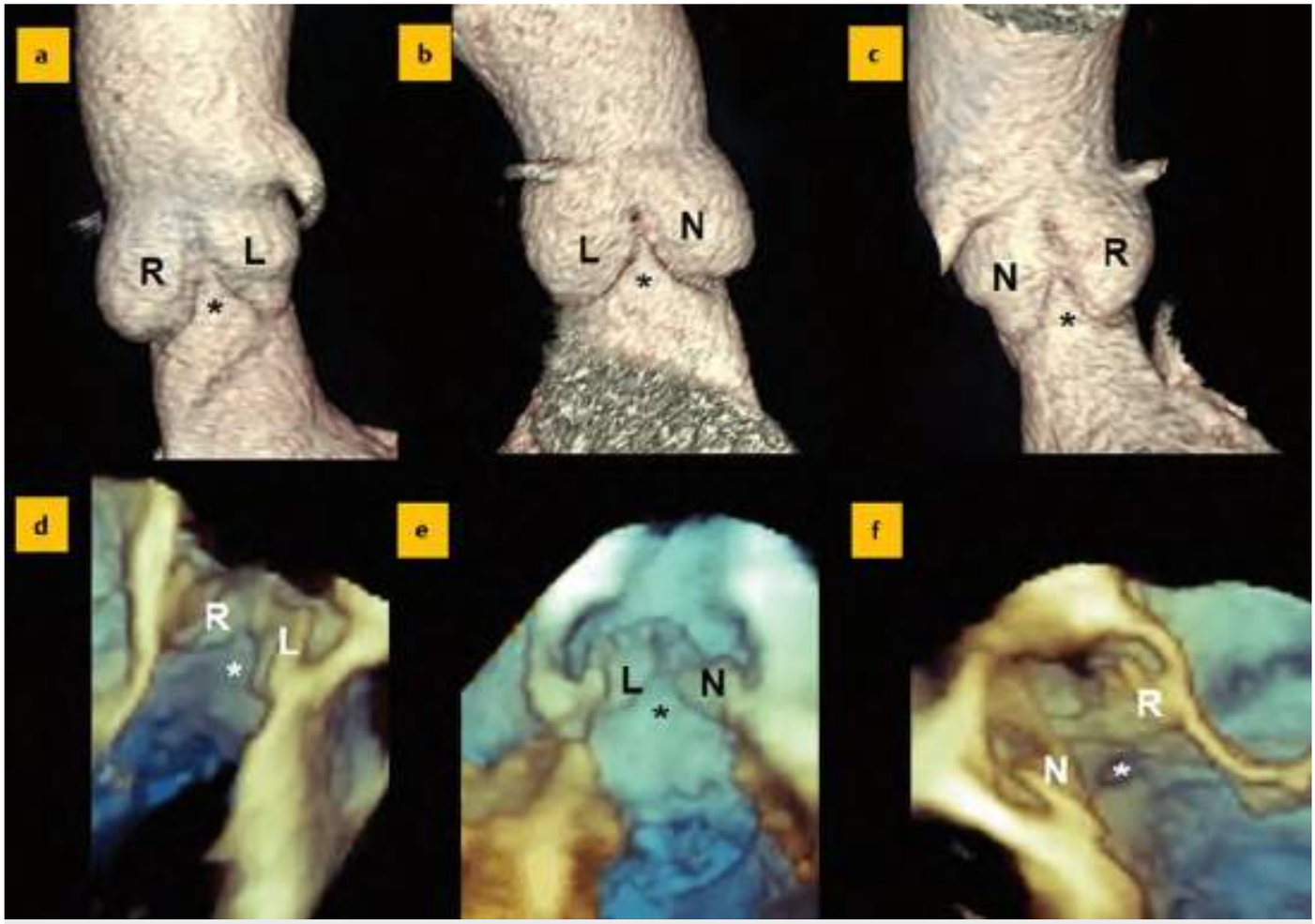

Fig. 14.6 Computed tomographic volume-rendered images of the aortic root and interleaflet triangles (ILTs). **(a)** The ILT (*stars*) situated between the right and left coronary leaflets consists of muscular tissue. **(b)** The ILT between the left and the noncoronary leaflet is a fibrous sheet that continues with the anterior leaflet of mitral valve (the mitral–aortic curtain). **(c)** The ILT between the noncoronary and right coronary sinuses is continuous with the membranous septum. **(d–f)** 3D transesophageal echo images showing the internal perspectives of ILT. From this perspective, ILTs are sited between leaflets. L, left coronary sinus; N, noncoronary sinus; R, right coronary sinus.

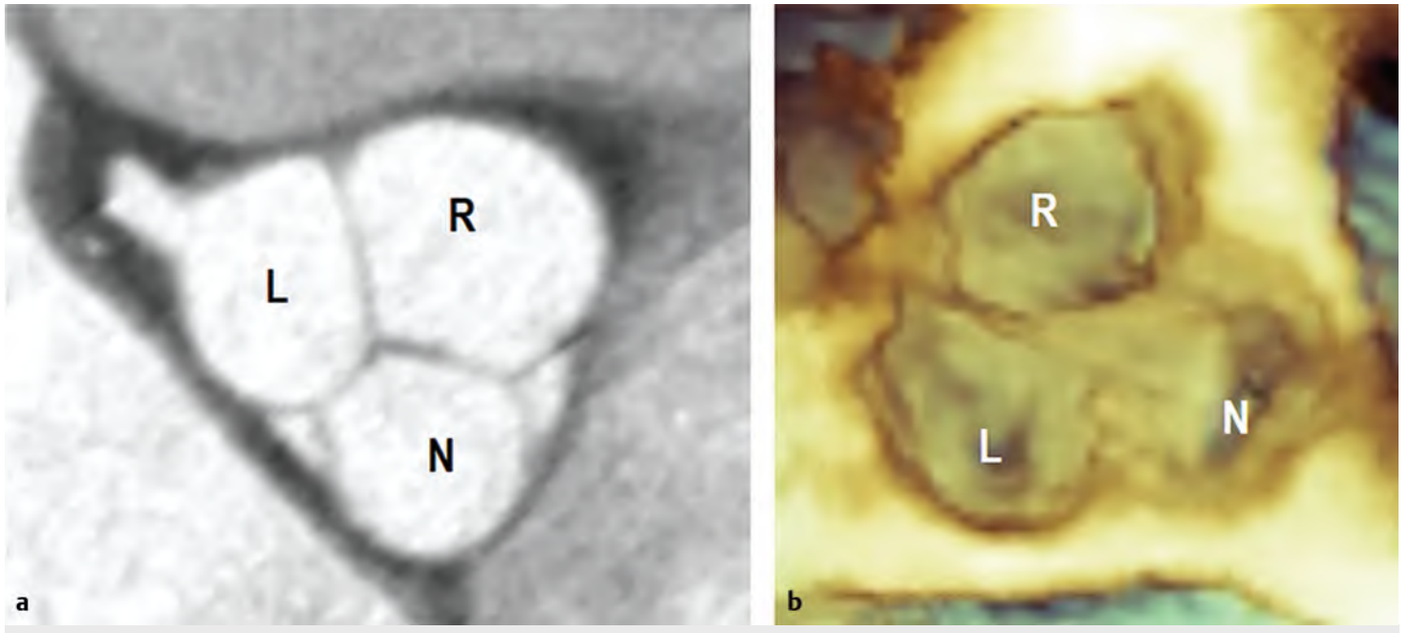

Fig. 14.7 A trilobate configuration of the aortic root in diastole imaged by **(a)** 2D CT and **(b)** 3D transesophageal echo. In diastole, the sinuses of Valsalva become more spherical (*smaller radius*) in order to lower wall stress on the cusps. According to the law of Laplace, wall stress is directly proportional to the pressure and the radius of curvature, and inversely proportional to the thickness of the wall. L, left coronary sinus; N, noncoronary sinus; R, right coronary sinus.

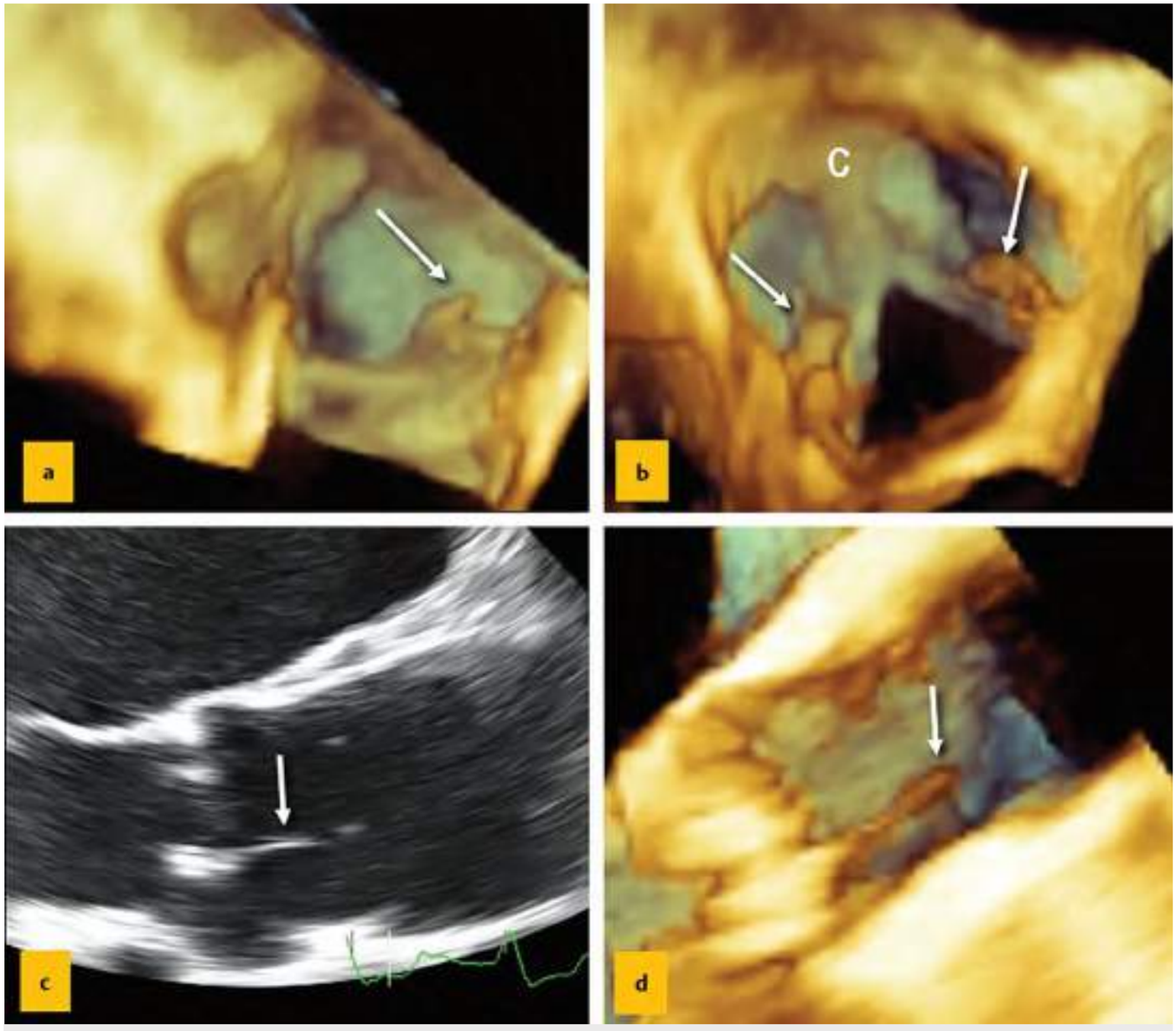

Fig. 14.8 (**a**, **b**) 3D transesophageal echo (TEE) images showing Lambl's excrescences (*arrows*) from two different perspectives. Long filiform Lambl's excrescency in **(c)** 2D and **(d)** 3D TEE in a patient with calcified leaflets. C, commissure.

root and the aorta namely aortic aneurysm, and aortic dissection. We start with an aspect of the aortic leaflets that is between anatomical variant and disease: Lambl's excrescences.

Lambl's Excrescences

Lambl's excrescences are filiform fibrous structures attached along the coaptation surface of the aortic leaflets, often at level of the nodules of Arantius, where the wear and tear may cause endothelial exfoliations and promote fibrin and small thrombi formation, which eventually heal in collagen filiform organization.[6] Usually asymptomatic and present in older individuals, Lambl's excrescences are considered a benign age-related process. Lambl's excrescences may occur in normal or calcified leaflets (▶ Fig. 14.8**c, d**). However, occasionally, these excrescences may detach and reside in remote vessels (▶ Fig. 14.8**a, b**).

Papillary Fibroelastoma

Papillary fibroelastoma (PFE) is a rare benign primary cardiac tumor comprising 75% of the tumors of cardiac valves.[7] PFE is usually less than 1.5 cm, with stalk attaching to the leaflets and highly mobile. PFE may be associated to syncope and chest pain due to transient mechanical occlusion of left main coronary artery, or systemic embolism due to embolization of a portion of the tumor[8] (▶ Fig. 14.9).

Bicuspid Aortic Valve

Congenital malformations of aortic valve include unicuspid (rare), bicuspid (common), and quadricuspid (rare) aortic valve. Bicuspid aortic valve (BAV) is the most common of all congenital defects of the heart with a prevalence up to 2% of general population.[9] This anomaly is consequence of lack of septation of two

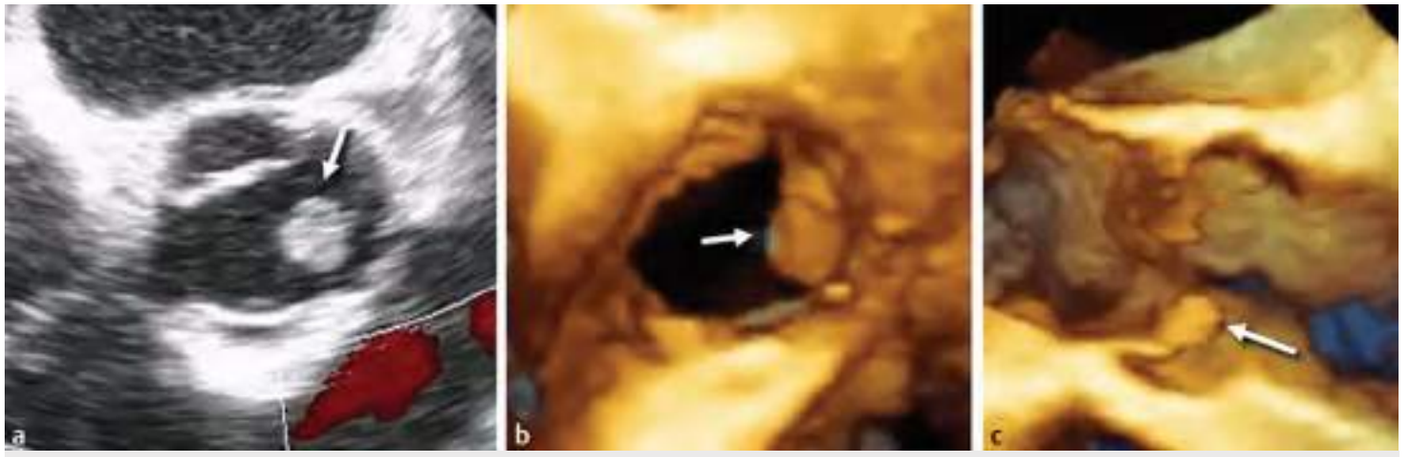

Fig. 14.9 **(a)** 2D transesophageal echo (TEE) image of a short-axis view of the aorta showing a papillary fibroelastoma attached at left coronary leaflet (*arrow*). **(b, c)** The same case in 3D TEE short- and long-axis perspective, respectively.

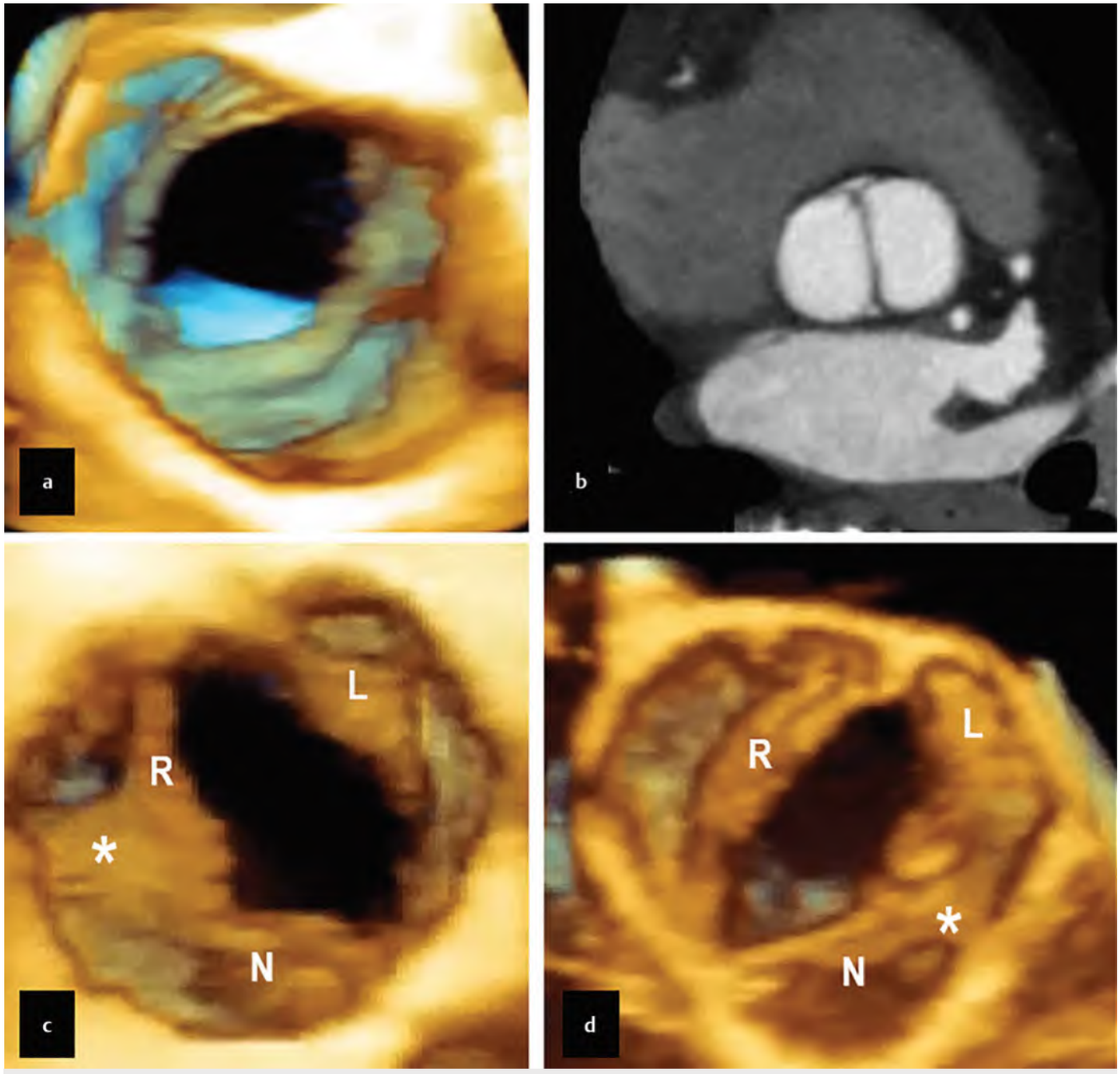

Fig. 14.10 3D transesophageal echo (TEE) images of different types of bicuspid aortic valve (BAV). **(a, b)** "Pure" BAV. **(c, d)** Variations of morphology according to the position of the raphe (*asterisks* [*]) and the line of coaptation of leaflets. L, left coronary sinus; N, noncoronary sinus; R, right coronary sinus.

adjacent leaflets during valvulogenesis. In absence of a raphe (i.e., a thick connective or calcified protuberance that marks the line of fusion between conjoined cusps), the two leaflets are symmetric and the valve presents two commissures and two sinuses (the so-called "pure" BAV). In presence of raphe (the most common form), the cusp with a raphe is usually larger than the other (▶ Fig. 14.10). Aortic stenosis is a common complication accounting for 85% of all BAV, followed by aortic insufficiency (15%).[10,11] Aortic stenosis in patients with BAV occurs early in life and usually in patients younger than 65 years (▶ Fig. 14.11). Aortic regurgitation in a patient with BAV is usually functional and secondary to dilation of the sinotubular junction that impedes an effective cusp coaptation.[12]

Aortic Stenosis

Calcific (degenerative) aortic stenosis (AS) is common in elderly patients and its prevalence increases with age (up to 10% in ≥ 80 years of age).[13,14] Calcifications are common and extend from the free margins toward the base of the leaflets causing leaflet rigidity, and flow obstruction.[15,16] Characteristically, calcific AS does not present fusion of commissures, and the morphological aspect is that of a three slit-like opening in systole (▶ Fig. 14.12). Aortic stenosis causes a chronic pressure overload leading to left ventricular hypertrophy. In presence of symptoms (i.e., angina, syncope, and heart failure), surgical or percutaneous aortic valve replacement is mandatory.

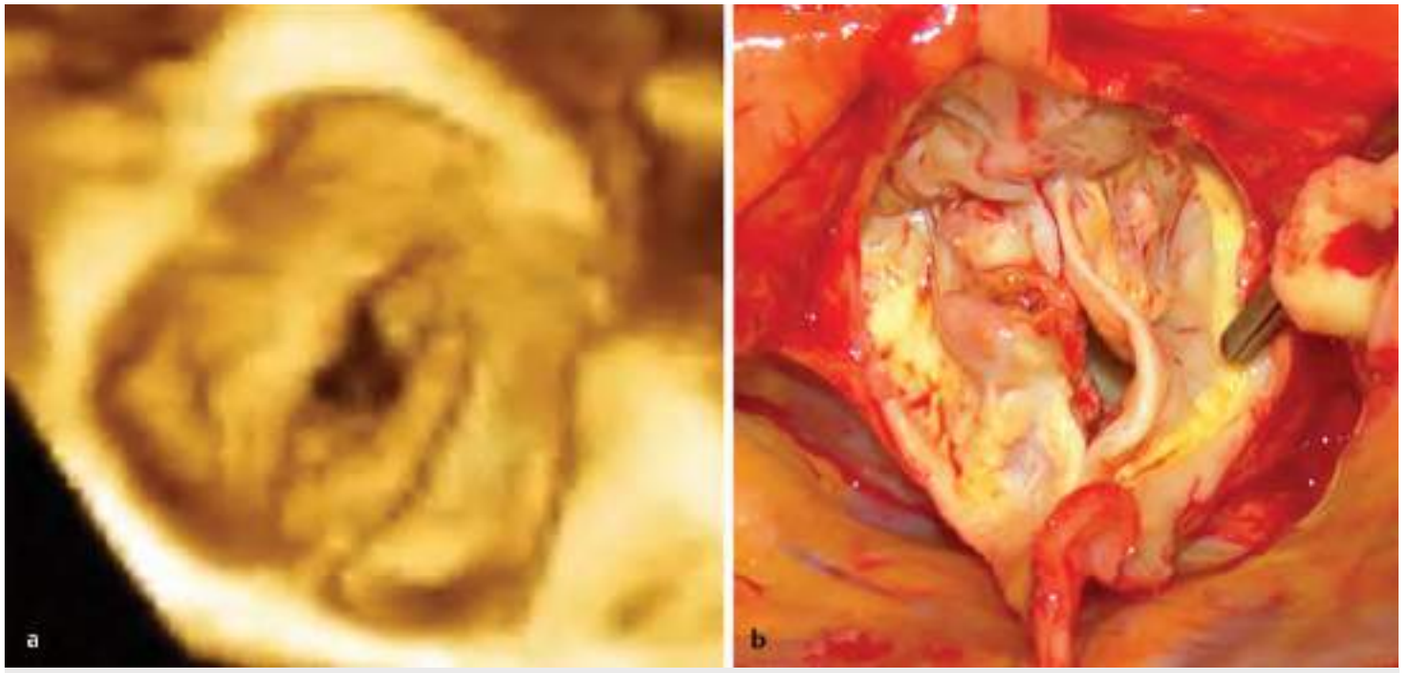

Fig. 14.11 Severe stenosis in bicuspid aortic valve. **(a)** 3D transesophageal echo (TEE) image and **(b)** surgical aspect of the same valve in patients aged 64 years.

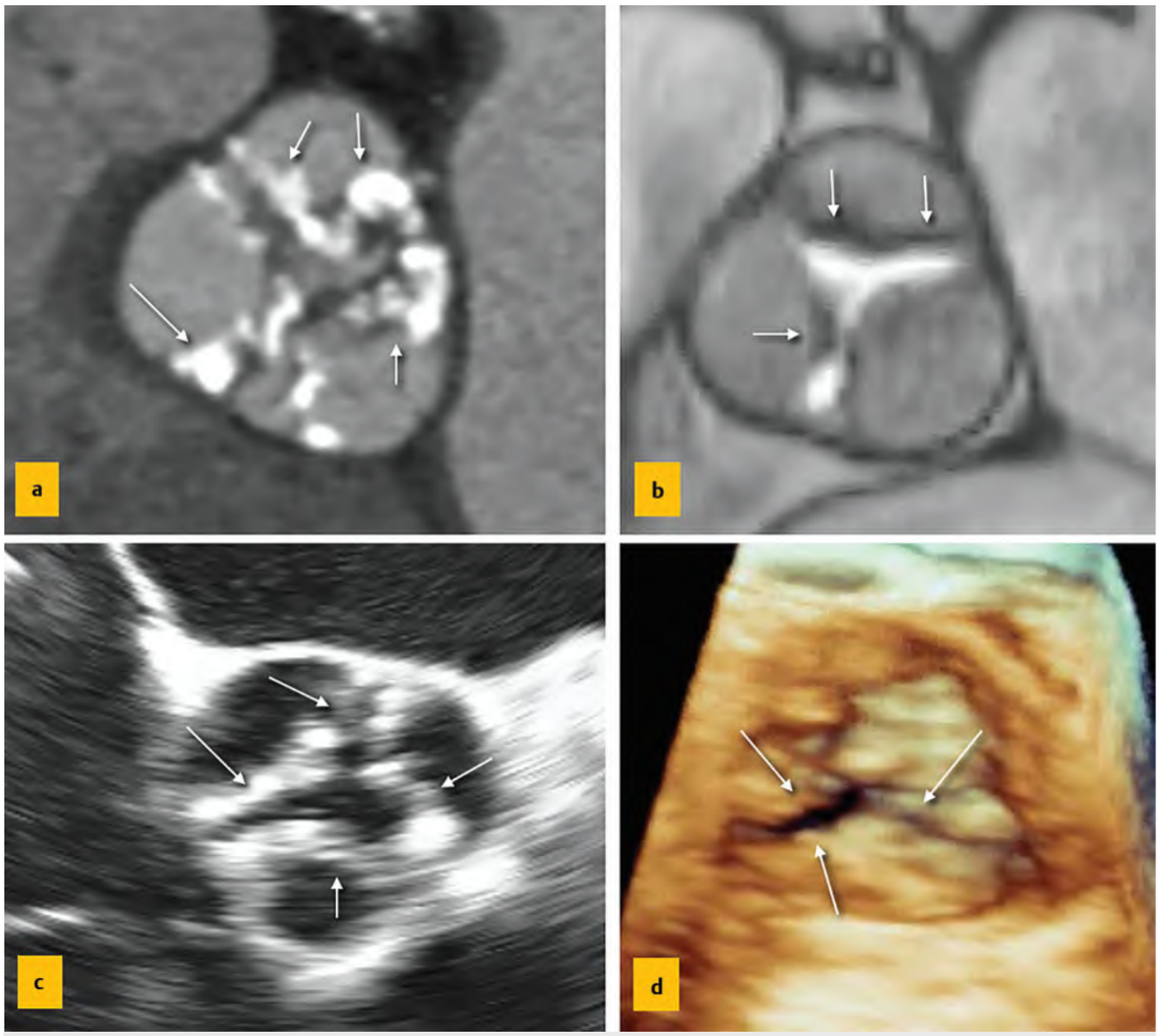

Fig. 14.12 **(a)** CT scan in cross-section short-axis view showing diffuse calcifications affecting the three leaflets. The absence of commissural fusion is characteristic of this form of aortic stenosis. Calcifications are bright white masses along the rim of leaflets (*arrows*). **(b)** Same image obtained with cardiac magnetic resonance showing a well-visible three-radiate orifice. Calcifications may be seen as a dark rim near the free margins of leaflets. **(c)** 2D and **(d)** 3D transesophageal echo (TEE) showing the same triradiate pattern (*arrows*).

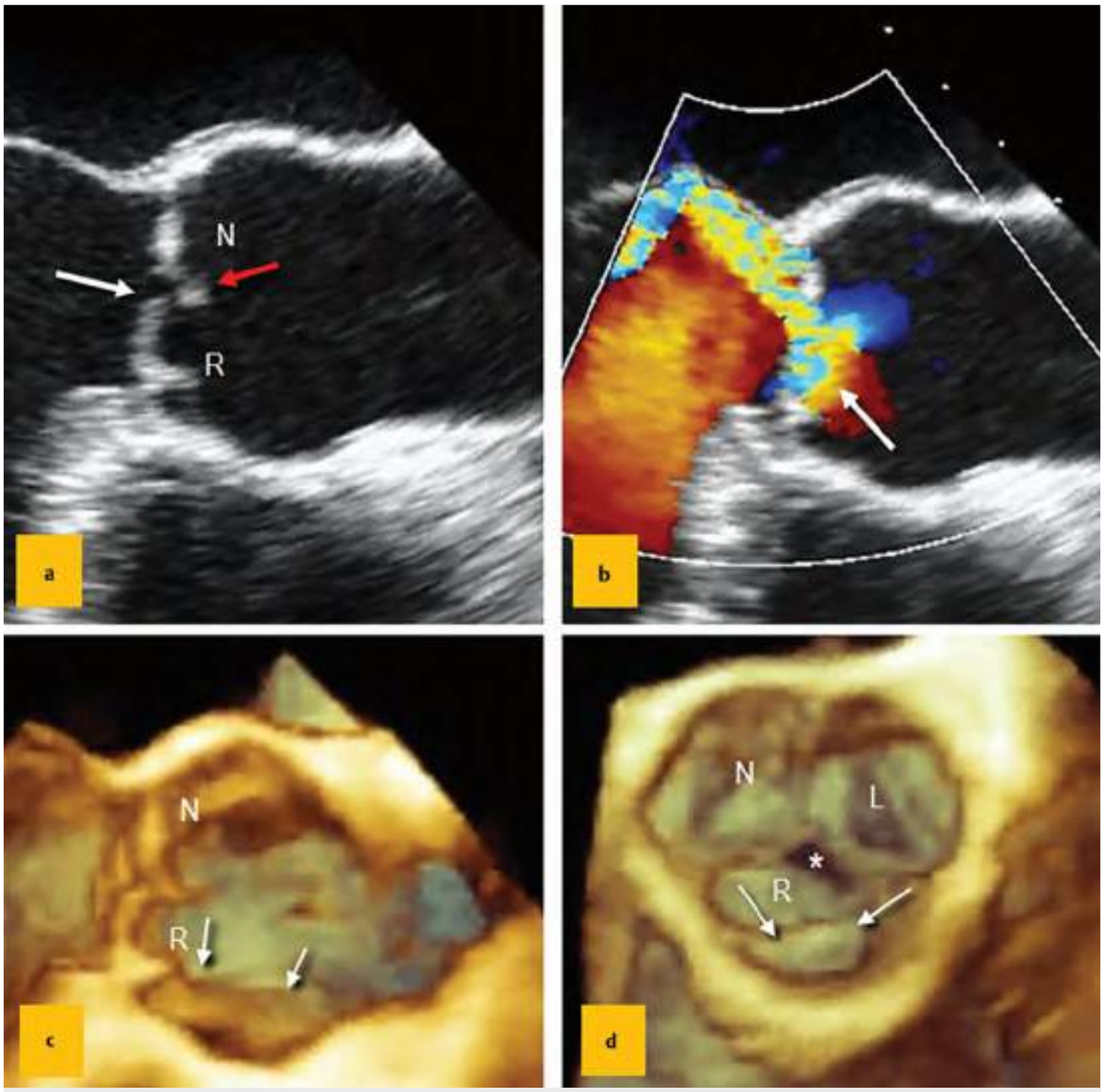

Fig. 14.13 **(a)** 2D transesophageal echo (TEE) image in long-axis cross-section showing the free margin of right coronary leaflet (R) prolapsing below the virtual annular plane (*white arrow*). The red arrow points at the free margin of noncoronary leaflet (N). **(b)** The regurgitant jet is directed toward the opposite direction of the prolapsing leaflet (*arrow*). **(c)** 3D TEE with the same orientation of the figure in **(a)**. This image shows a small enfolding (*arrows*) in the body of the prolapsing leaflet near the insertion. This bend is actually the hinge line where the distal part of prolapsing leaflet swings. **(d)** 3D TEE image from an aortic perspective. The arrows point the bending. The asterisk points the regurgitant orifice caused by the prolapsing leaflet. L, left coronary leaflet; L, left coronary sinus; N, noncoronary sinus; R, right coronary sinus.

Aortic Leaflet Prolapse

Aortic leaflet prolapse (ALP) is a leaflet dysfunction in which the margin of one leaflet remains in diastole below the "virtual plane" of the aortic annulus failing the coaptation with other two leaflets.[17] In general, ALP is due to a relative excess in the length of free margins the involved leaflet. The lack of leaflet apposition produces a regurgitant jet that is direct toward the contralateral leaflet (▶ Fig. 14.13). Although ALP may exist in isolation (in that case, prolapse of right and noncoronary are more frequent than that of left coronary leaflet), it is often associated with bicuspid valve of aortic root dilation.

Aortic Endocarditis

The aortic valve is the most common site of infective endocarditis. Vegetations are located on the ventricular aspect of one or more leaflet causing valve regurgitation by perforation of one or

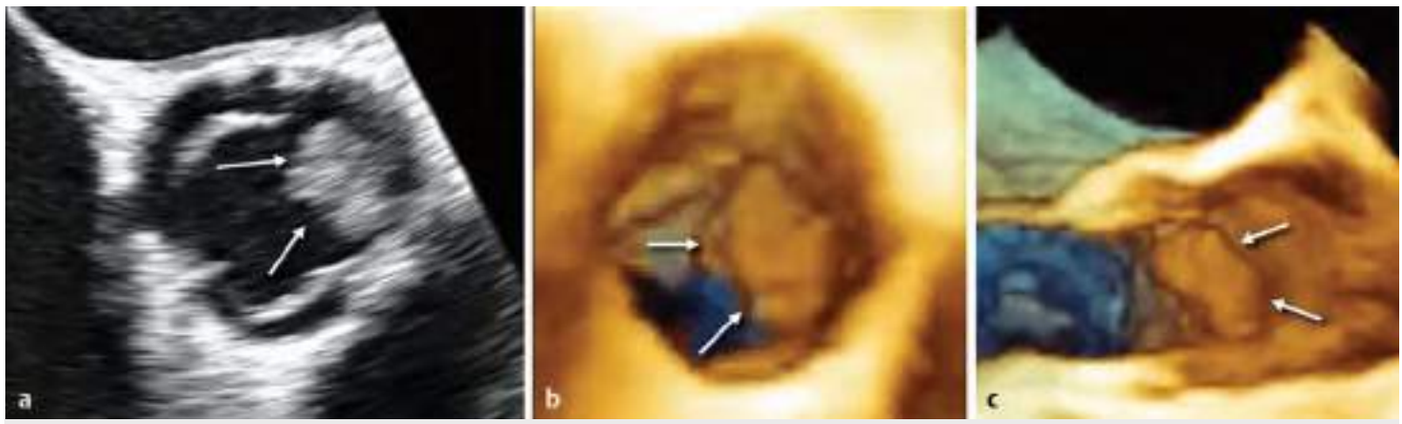

Fig. 14.14 Bacterial infective endocarditis of the aortic valve. **(a)** 2D transesophageal echo (TEE) showing a large mass attached to the left coronary leaflet (*arrows*). **(b)** Same case visualized in 3D TEE using a similar perspective; arrows delimit the internal border of the mass. **(c)** 3D TEE image of the same case in a longitudinal perspective. The arrows delimit the superior border.

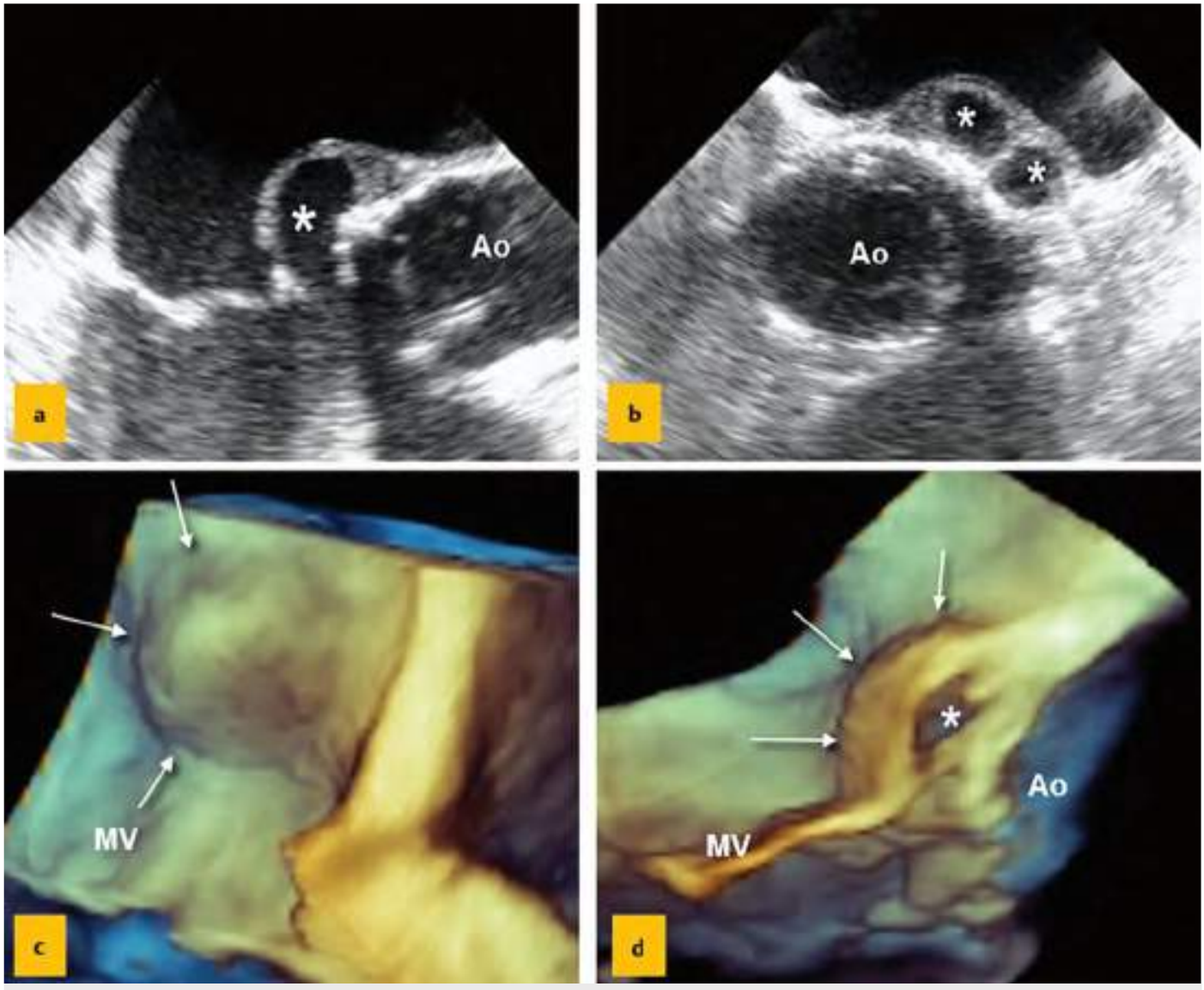

Fig. 14.15 **(a)** 2D transesophageal echo (TEE) image primary aortic vegetation (*white arrow*) and secondary larger mitral vegetation (*red arrow*) attached on the ventricular side of the anterior mitral leaflet (AML). **(b)** 3D TEE in a similar longitudinal perspective. **(c)** 3D TEE of the same case in a different longitudinal perspective. **(d)** 3D TEE of the same case from a ventricular perspective. Ao, aorta; LA, left atrium; LV, left ventricle.

more leaflets, indentations or tearing or simply by the fact that the vegetation prevents a normal coaptation[18] (▶ Fig. 14.14). Particularly interesting is the "kissing lesion" which is secondary involvement of the anterior mitral leaflet in primary aortic valve endocarditis (▶ Fig. 14.15).

Dilation of the Aortic Root (Aortic Aneurysm)

Isolated dilation of the aortic root or aortic root aneurysm (called also annuloaortic ectasia) is not very common. In general, most aortic root aneurysms are associated with dilation of ascending aorta[19] (▶ Fig. 14.16). Symptoms typically occur in the setting of either a complication of the disease (i.e., rupture or dissection) or when these complications are imminent. Aortic root is almost invariably associated with aortic aneurysm due to dilation of crow-shaped aortic annulus, which tethers leaflets preventing a complete closure and leaving a central regurgitant orifice (▶ Fig. 14.17).

Genetic connective disorders such as Marfan's syndrome and bicuspid aortic valve are often associated with aortic aneurysm. Once discovered, the aneurysm should be followed with serial imaging examinations. Indeed, aortic diameter is of paramount importance for determining risk for complications: the median aortic diameter at the time of rupture for the ascending or arch aorta is 6 cm.[20] Thus, the recommendation to intervene has been set at 5.5 cm or greater than 4.25 cm/m^2 for ascending aortic aneurysms.

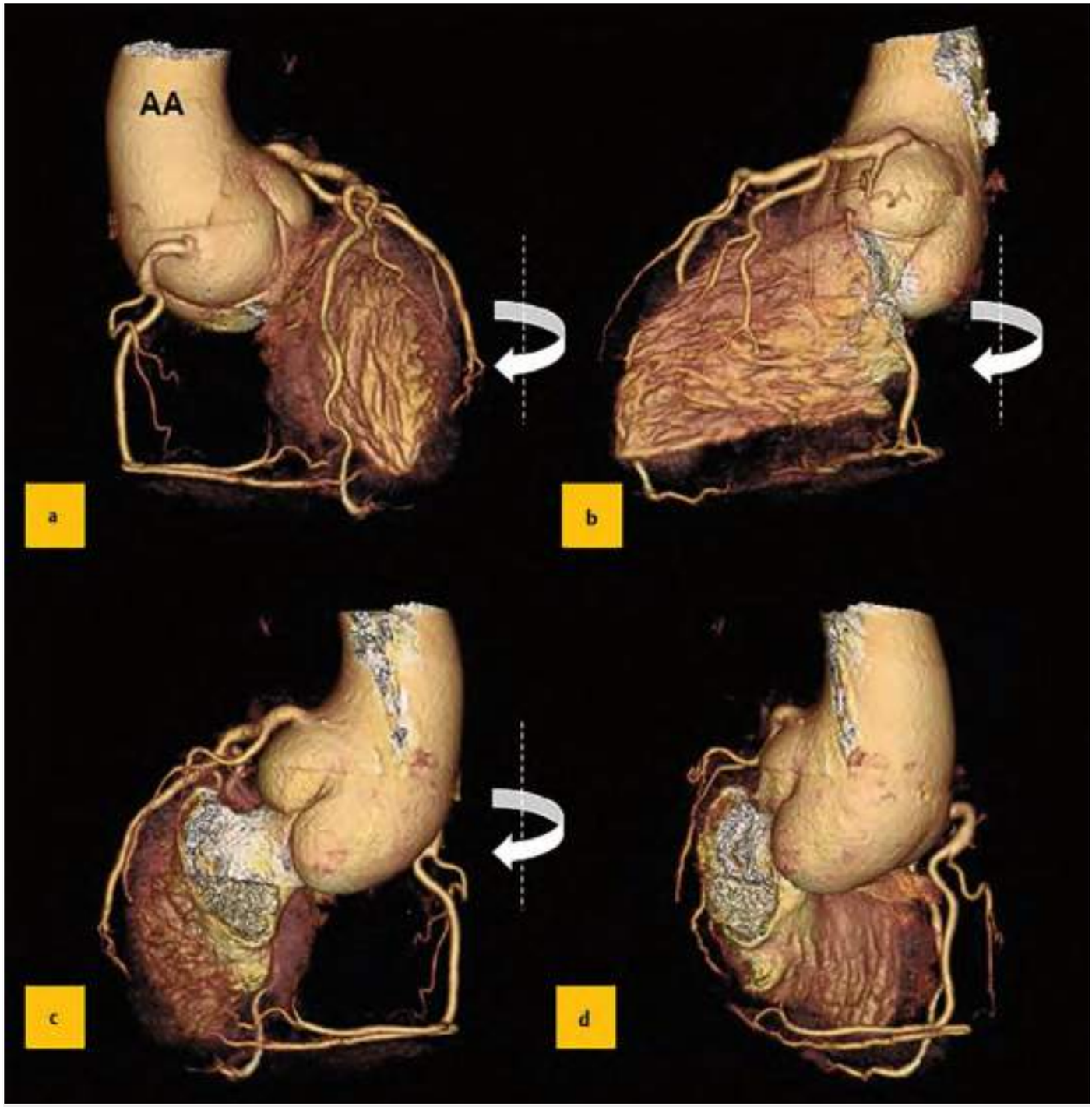

Fig. 14.16 (a–d) Classic aneurysm of the aortic root is shown in different perspective obtained by rotating the volumetric data set from right to left around the Z-axis (*curved arrow*). The size of ascending aorta (AA) is within limits.

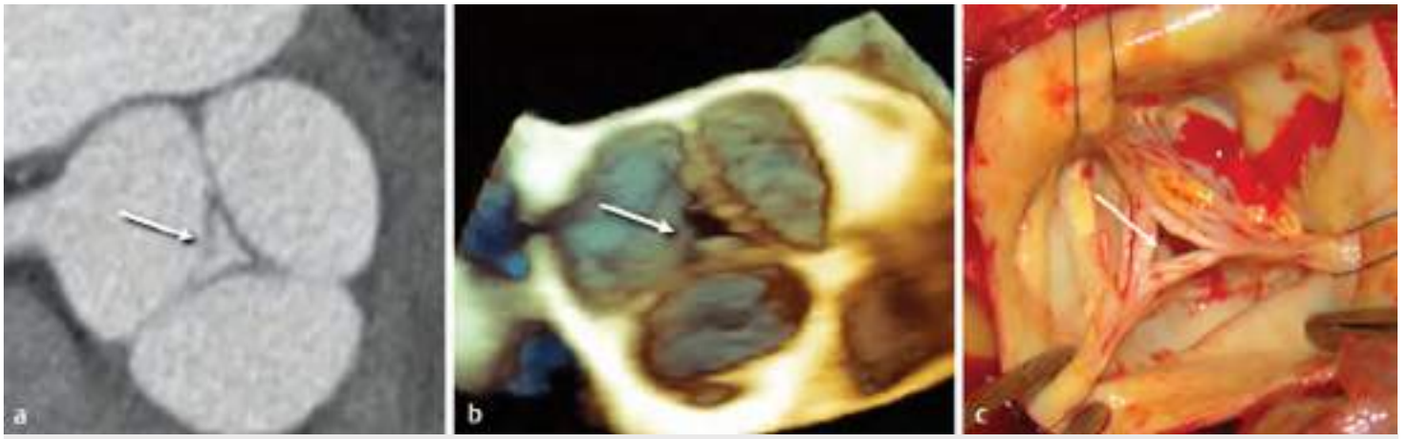

Fig. 14.17 Central aortic regurgitant orifice in a patient with dilation of the aortic root seen in **(a)** multiplanar CT scan, **(b)** 3D transesophageal echo (TEE), and **(c)** during the surgical repair.

References

[1] Anderson RH. Clinical anatomy of the aortic root. Heart.; 84(6):670–673

[2] Piazza N, de Jaegere P, Schultz C, Becker AE, Serruys PW, Anderson RH. Anatomy of the aortic valvar complex and its implications for transcatheter implantation of the aortic valve. Circ Cardiovasc Interv.; 1(1):74–81

[3] Anderson RH, Devine WA, Ho SY, Smith A, McKay R. The myth of the aortic annulus: the anatomy of the subaortic outflow tract. Ann Thorac Surg.; 52 (3):640–646

[4] Sutton JP, III, Ho SY, Anderson RH. The forgotten interleaflet triangles: a review of the surgical anatomy of the aortic valve. Ann Thorac Surg.; 59 (2):419–427

[5] Pisani G, Scaffa R, Ieropoli O, et al. Role of the sinuses of Valsalva on the opening of the aortic valve. J Thorac Cardiovasc Surg.; 145(4):999–1003

[6] Nighoghossian N, Trouillas P, Perinetti M, Barthelet M, Ninet J, Loire R. [Lambl's excrescence: an uncommon cause of cerebral embolism]. Rev Neurol (Paris).; 151(10):583–585

[7] Grinda JM, Couetil JP, Chauvaud S, et al. Cardiac valve papillary fibroelastoma: surgical excision for revealed or potential embolization. J Thorac Cardiovasc Surg.; 117(1):106–110

[8] Ngaage DL, Mullany CJ, Daly RC, et al. Surgical treatment of cardiac papillary fibroelastoma: a single center experience with eighty-eight patients. Ann Thorac Surg.; 80(5):1712–1718

[9] Michelena HI, Desjardins VA, Avierinos JF, et al. Natural history of asymptomatic patients with normally functioning or minimally dysfunctional bicuspid aortic valve in the community. Circulation.; 117(21):2776–2784

[10] Tzemos N, Therrien J, Yip J, et al. Outcomes in adults with bicuspid aortic valves. JAMA.; 300(11):1317–1325

[11] Fedak PW, Verma S, David TE, Leask RL, Weisel RD, Butany J. Clinical and pathophysiological implications of a bicuspid aortic valve. Circulation.; 106 (8):900–904

[12] Nkomo VT, Enriquez-Sarano M, Ammash NM, et al. Bicuspid aortic valve associated with aortic dilatation: a community-based study. Arterioscler Thromb Vasc Biol.; 23(2):351–356

[13] Carabello BA. Clinical practice. Aortic stenosis. N Engl J Med.; 346(9):677–682

[14] Carabello BA, Paulus WJ. Aortic stenosis. Lancet.; 373(9667):956–966

[15] Rajamannan NM, Evans FJ, Aikawa E, et al. Calcific aortic valve disease: not simply a degenerative process: a review and agenda for research from the National Heart and Lung and Blood Institute Aortic Stenosis Working Group. Executive summary: Calcific aortic valve disease—2011 update. Circulation.; 124(16):1783–1791

[16] Akat K, Borggrefe M, Kaden JJ. Aortic valve calcification: basic science to clinical practice. Heart.; 95(8):616–623

[17] Shapiro LM, Thwaites B, Westgate C, Donaldson R. Prevalence and clinical significance of aortic valve prolapse. Br Heart J.; 54(2):179–183

[18] Baddour LM, Wilson WR, Bayer AS, et al. Committee on Rheumatic Fever, Endocarditis, and Kawasaki Disease, Council on Cardiovascular Disease in the Young, Councils on Clinical Cardiology, Stroke, and Cardiovascular Surgery and Anesthesia, American Heart Association, Infectious Diseases Society of America. Infective endocarditis: diagnosis, antimicrobial therapy, and management of complications: a statement for healthcare professionals from the Committee on Rheumatic Fever, Endocarditis, and Kawasaki Disease, Council on Cardiovascular Disease in the Young, and the Councils on Clinical Cardiology, Stroke, and Cardiovascular Surgery and Anesthesia, American Heart Association: endorsed by the Infectious Diseases Society of America. Circulation.; 111(23):e394–e434

[19] Patel HJ, Deeb GM. Ascending and arch aorta: pathology, natural history, and treatment. Circulation.; 118(2):188–195

[20] Davies RR, Gallo A, Coady MA, et al. Novel measurement of relative aortic size predicts rupture of thoracic aortic aneurysms. Ann Thorac Surg.; 81(1):169–177

15 Pulmonary Valve

Farhood Saremi

◆ Introduction

Knowledge of pulmonary valve and root anatomy is useful in understanding the spectrum of complicated conotruncal anomalies that arise from abnormal formation of the major vessels in this region. Despite the frequency of pulmonary valve diseases including congenital malformations, the pulmonary valve is the least studied valve by imaging. Along with the evolution of surgical techniques and introduction of new percutaneous procedures in recent years, imaging assessment of the pulmonary root and related pathologies has attracted more attention than before.

Pulmonary valve assessment is primarily dependent on echocardiography. However, because of their retrosternal location, the pulmonary valve and right ventricular outflow tract (RVOT) can be difficult to assess with transthoracic echocardiography especially in adolescents and adults. Furthermore, since the RVOT and pulmonary valve are anterior structures, transesophageal echocardiography is not the best tool for assessment of the pathology. With rapid advancement in imaging technology, cardiac computed tomography (CT) and magnetic resonance imaging (MRI) are being used increasingly for anatomical evaluation, functional assessment, and pathological diagnosis of the pulmonary valve. Postoperative evaluation of the pulmonary valve and outflow tract is among common MR referrals. MR is especially helpful in postoperative follow-up of artificial pulmonary valve function. Anatomical detail of the pulmonary valve and perivalvular structures can be optimally studied with CT scan.

The goal of this review is to offer a general perspective on the development of right outflow tract (OFT) and associated structures with a focus on the morphology and function of the pulmonary valve. Pathologies including congenital heart disease (CHD) are briefly discussed.

◆ Embryology

The two fields of cardiac progenitors are now recognized as the primary, and secondary, or anterior, heart fields.[1,2] In mouse, there is firm evidence that the primary heart field gives rise to the left ventricle, with the secondary field forming both the right ventricle (RV) and the OFT.[1] Development of the semilunar valves occurs simultaneously with completion of the secondary (anterior) heart field.

The primordial outflow tract extends proximally from the distal ventricular groove to the pericardial reflections and demonstrates a characteristic dog-leg which divides it into two myocardial subsegments, a proximal subsegment or the conus (infundibulum) and a distal subsegment or the truncus.[1,3] The truncus arteriosus is a short segment interposed between the conus and the aortic sac (▶ Fig. 15.1). With further development, the aortic sac transforms into the extrapericardial ascending aorta and pulmonary trunks, and the truncus is remodeled into the intrapericardial portions of the aorta and pulmonary trunk. The boundary between the two parts of the primordial OFT becomes the sinotubular junctions. The primordial OFT is mainly myocardial. Gradual disappearance of the myocardium by apoptosis, transdifferentiation initially involves the truncus wall and the tissue surrounding the developing arterial sinuses. Later, further absorption of the left conus myocardium produces fibrous continuity between the leaflets of the aortic and mitral valves. On the right, conus myocardium remains as subpulmonary infundibulum. With extension of the developing fibroadipose tissue plane that already separates the aortic and pulmonary trunks, the muscularized partition becomes converted into the free-standing infundibulum of the pulmonary valve, and the supraventricular crest of the RV. As development proceeds, the single OFT undergoes remodeling into separate pulmonary and aortic arteries (▶ Fig. 15.1). This process involves interactions between diverse cell types, including myocardium, endocardium, and neural crest cells. Endocardial cells respond to signals from the overlying myocardium and undergo an epithelial-to-mesenchymal transformation to form the conotruncal cushions. Neural crest cells invade the extracellular matrix of the cushions and participate in aorticopulmonary septation.[4] OFT undergoes rotation during its remodeling. Rotation of the myocardium at the base of the OFT is probably essential to achieve normal positioning of the great arteries with respect to each other at the ventriculoarterial junction (VAJ).[5,6]

The valves and their supporting sinuses are believed to develop from the conotruncal endocardial cushions around the distal part of the conus.[3] Valves are formed by the formation of cavities within the cushions. The central parts of the cushions form the leaflets and the peripheral parts arterialize to form the sinus walls. The improper fusion or dedifferentiation of the endocardial cushions is thought to be responsible for congenitally abnormal semilunar valves. The aorticopulmonary septation by the endocardial cushions is a complex process and involves interaction between diverse cell types, including myocardium, endocardium, and neural crest cells.[3,4] In addition to abnormal OFT septation caused by neural crest cell defects, a spectrum of conotruncal anomalies with abnormally positioned great arteries may arise from a perturbation of myocardial rotation including tetralogy of Fallot (TOF), persistent truncus arteriosus, double outlet right ventricle (DORV), and transposition of great arteries (TGA).[5,6]

◆ Anatomy

The pulmonary root is the part of the RVOT that supports the leaflets of the pulmonary valve.[7,8] It consists of three sinuses of Valsalva confined proximally by the semilunar attachments of the valvular leaflets and distally by the sinotubular junction. This relationship can change in CHD. Different nomenclature has been used to define the anatomical location of the pulmonary valve sinuses based on their spatial location in relation to the thorax or the heart itself[7] (▶ Fig. 15.2, ▶ Fig. 15.3). The pulmonary valve is in the left anterior of the aorta and forms an angle of approximately 30 degrees with the aortic trunk. In normal individuals, this angle is related to the length of the ascending aorta. In

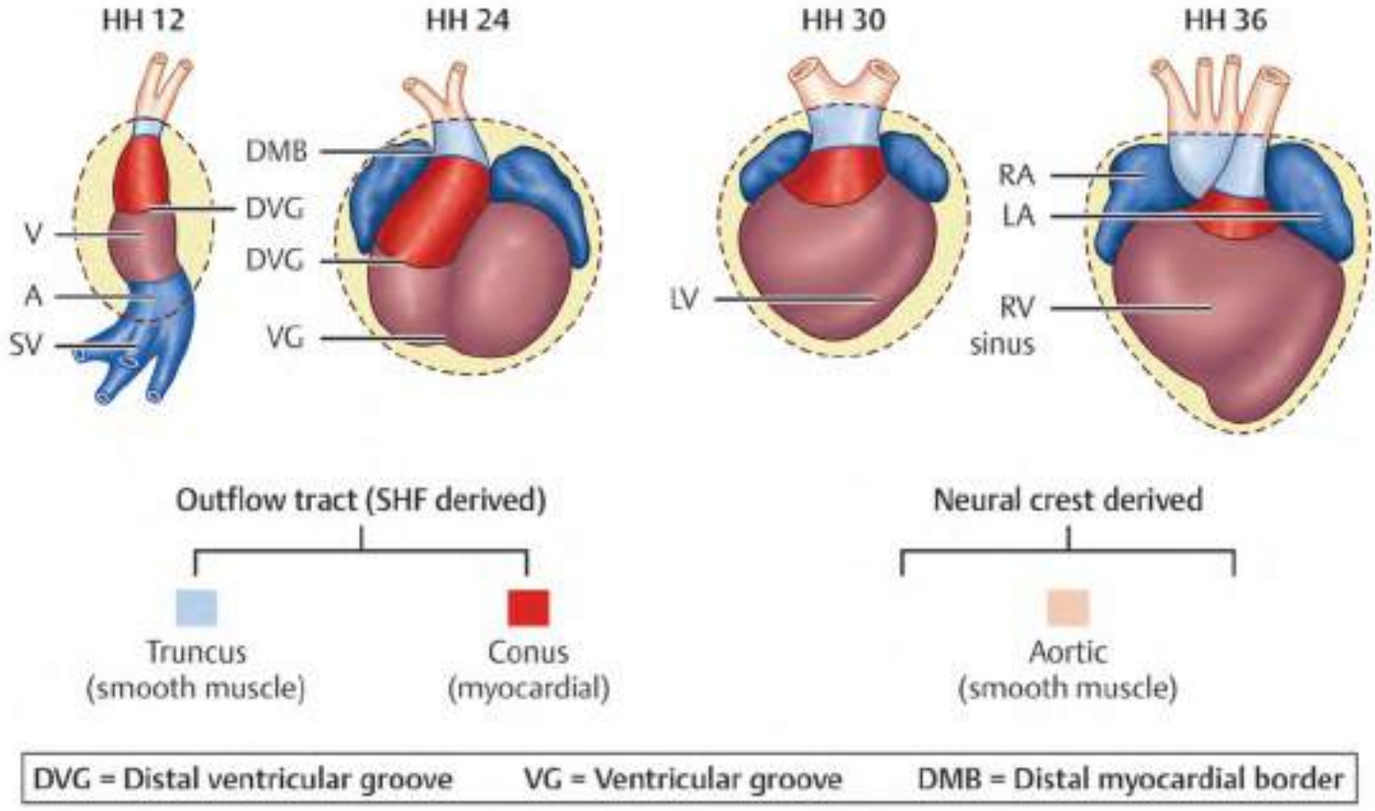

Fig. 15.1 The developing outflow tract in embryonic chicken hearts at stages 12, 24, 30, and 36 H/H. The area of the outflow tract (OFT) extends between the distal ventricular groove of the right ventricle and the junction with the aortic sac at the pericardial reflections and is divided into the conus (proximal OFT shown in red) and the truncus (distal OFT in light blue). In experiments in which myocardialization of the proximal OFT was compared with that of the distal OFT, the OFT was separated into two parts, the conus and the truncus and the junction between the two will be the distal myocardial border (DMB). These images show that the OFT is initially mainly myocardial (red part) in its entirety and increases in length up to HH24. The OFT myocardium, subsequently, shortens as a result of ventricularization, contributing to the trabeculated free wall, as well as the infundibulum, of the right ventricle (RV). Note the absolute reduction in the length of the OFT between 30 and 36 H/H stages, as well as the relative reduction in relation to the ventricles, which have increased in size by cardiomyocyte proliferation. The OFT has also been divided by septation into pulmonic and systemic outflows, and the aortic root has rotated to a posterior position, where it connects with the left ventricle (LV). The dotted line around the heart indicates the pericardium. DVG, distal ventricular groove; V, primitive ventricle; SV, sinus venosus; A, primitive atrium; RA, right atrium; LA, left atrium; VG, ventricular groove.

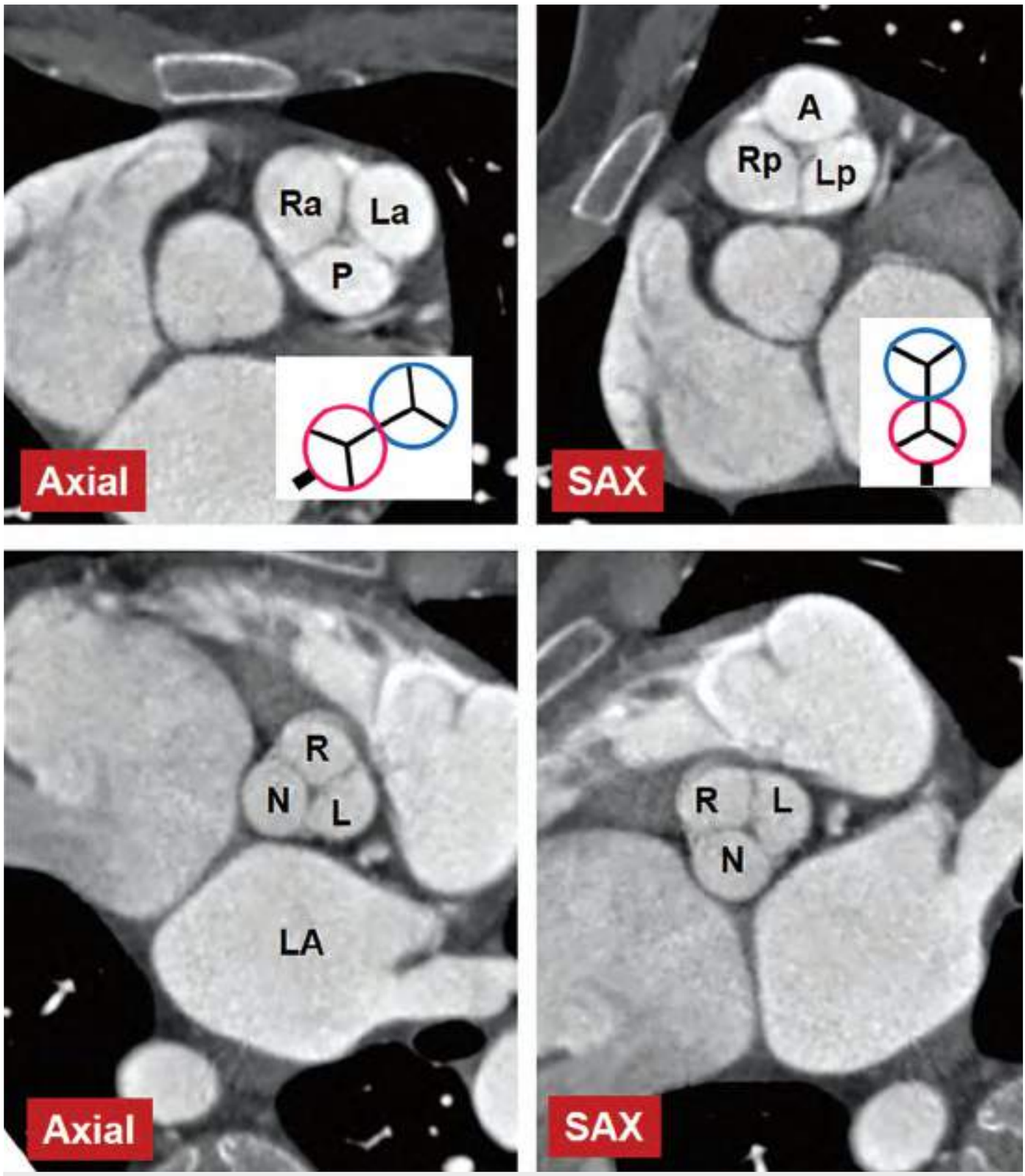

Fig. 15.2 Upper row: pulmonary valve sinuses. When heart is viewed in attitudinal anatomical position as sitting in the thorax (i.e., axial views), the pulmonary leaflets and sinuses are viewed as posterior (P), right anterolateral (Ra), and left anterolateral (La). However, in relation to the heart (i.e., short-axis views), the pulmonary sinuses can be named anterior (A), left posterior (Lp), and right posterior (Rp). Lower row: same rule can be applied to the aortic valve as seen in the above examples. N, noncoronary sinus. The relationship of the pulmonary and aortic valve (*blue and red circles*) as well as their orientation in relation to the body (axial) and the heart (SAX) are drawn; the black line shows the location of the interatrial septum. LA, left atrium, SAX, short axis; R, right coronary sinus; L, left coronary sinus.

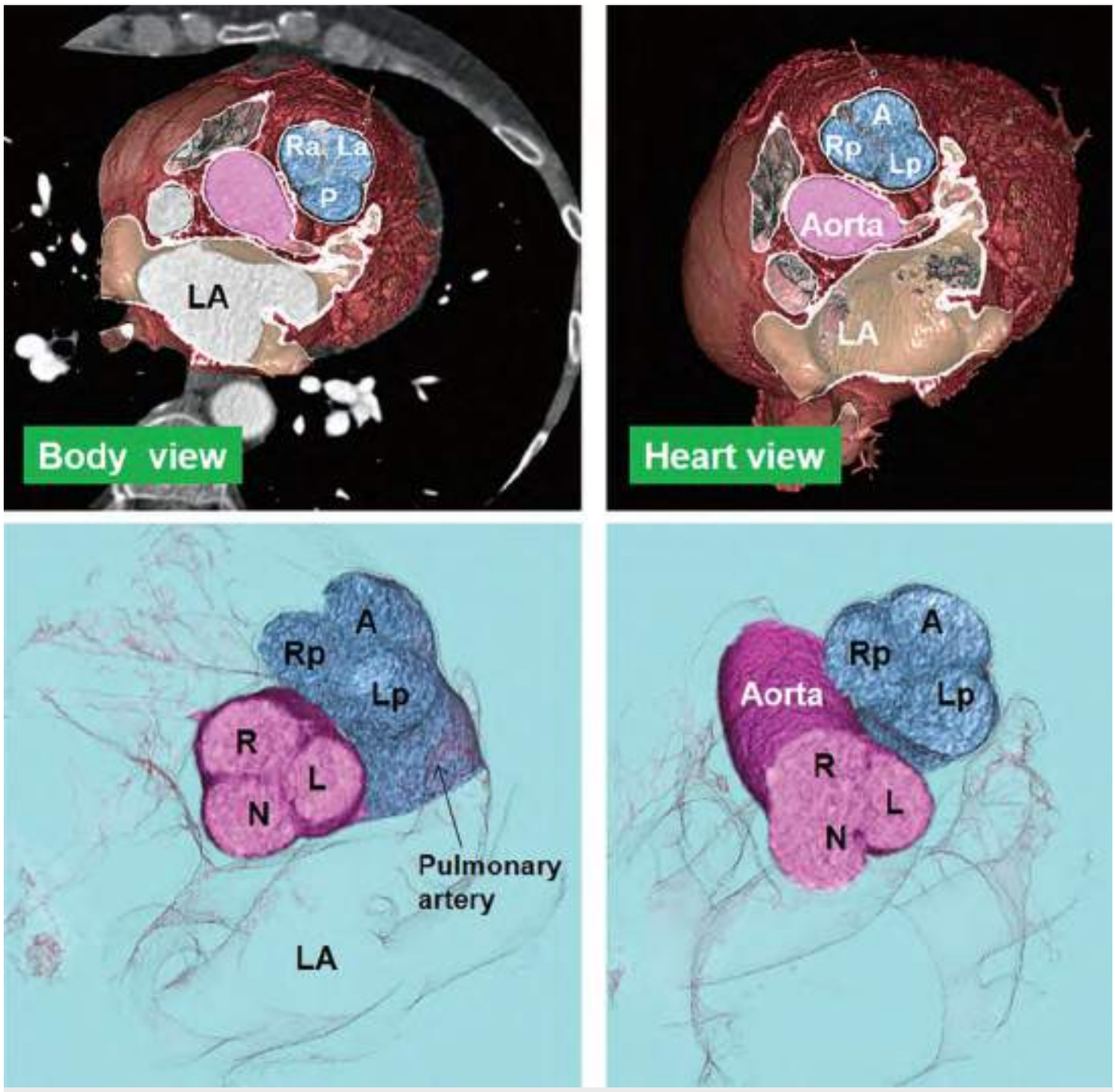

Fig. 15.3 Upper row showing the position of the pulmonary valve sinuses and relative nomenclature based on their relative location in the body or in relation to heart. Relative position in the body (thorax) are posterior (P), right anterolateral (Ra), and left anterolateral (La). Relative positions in the heart are anterior (A), left posterior (Lp), and right posterior (Rp). Lower row images showing the relative spatial position of the pulmonary valve to the aortic valve. The pulmonary valve is in the left anterior of the aorta. This relationship can change in congenital heart disease. LA, left atrium; R, right; L, left; N, noncoronary aortic sinuses.

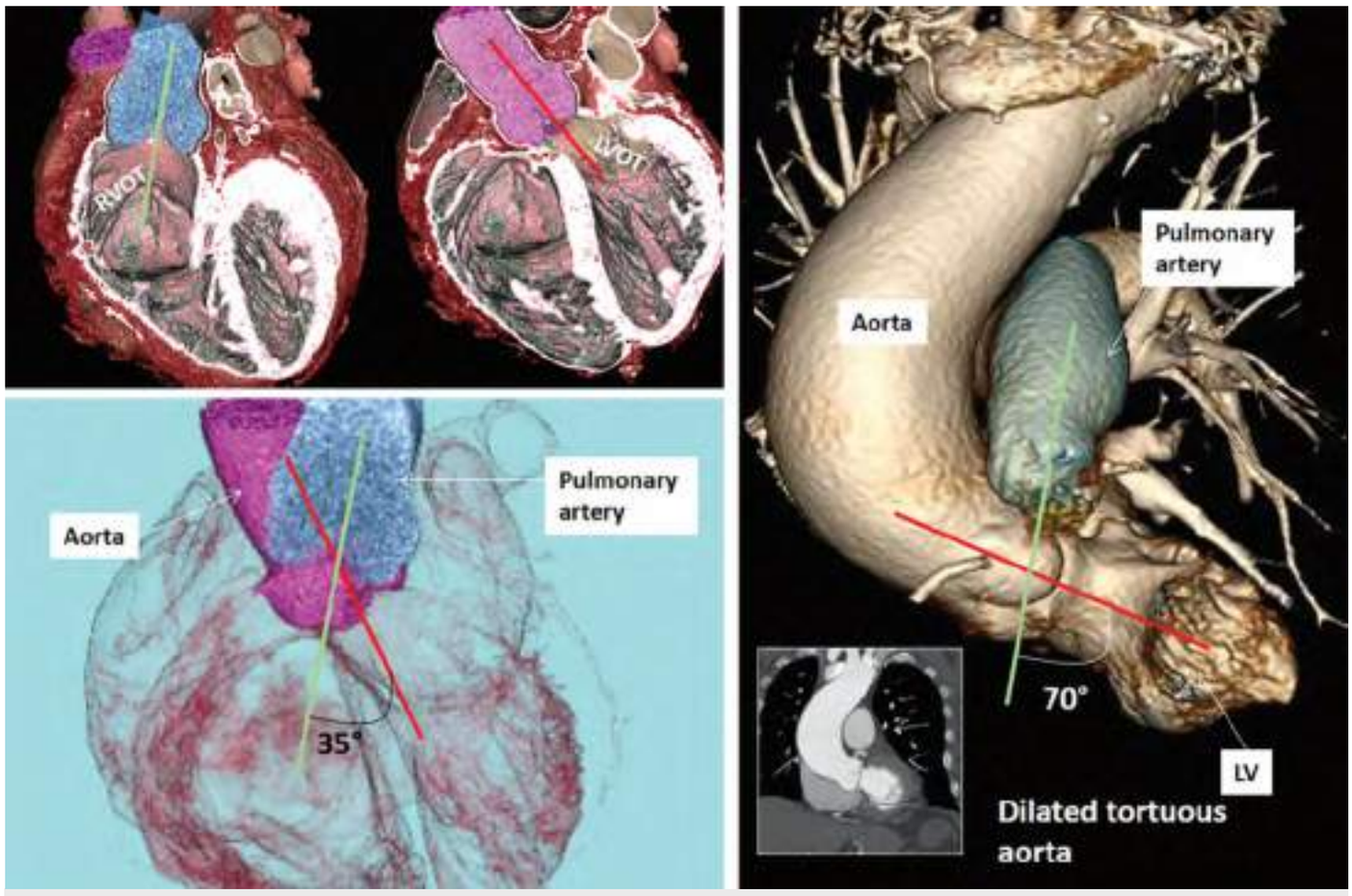

Fig. 15.4 Relative positions of the pulmonary trunk and the aortic root. The pulmonary trunk is located anterior to the aorta and forms an angle of approximately 30 degrees with the aortic trunk. In normal individuals, this angle is related to the length of the ascending aorta. In elongated tortuous ascending aorta, the inclination angle of the aortic root will be increased (inlay coronal CT) and the angle between the aorta and pulmonary artery will be increased. LVOT, left ventricular outflow tract; RVOT, right ventricular outflow tract.

elongated tortuous ascending aorta, the angle between the two arteries will be increased (▶ Fig. 15.4). Because of the semilunar shape of the pulmonary leaflets (similar to the aortic valve) this valve does not have a ring-like annulus. The sinotubular junction separates the pulmonary valvular sinuses from the tubular component of the pulmonary trunk and demarcates the level of the zones of apposition (commissures) between the annuli (▶ Fig. 15.5, ▶ Fig. 15.6). Compared to the aortic root, the pulmonary sinotubular junction is less obvious on CT images. A second junction exists at the VAJ between the infundibular muscle and the fibroelastic arterial wall. The anatomical VAJ forms the annulus. The semilunar attachment of the valvular leaflets, which forms the hemodynamic VAJ, crosses the anatomic VAJ. The leaflets are thickened along their semilunar line of attachment. The fibrous interleaflet triangles are the areas of arterial wall proximal to the semilunar attachments of the leaflets, and therefore are incorporated within the ventricular cavity. The fibrous triangle tips point toward the commissures (▶ Fig. 15.6). The pulmonary valve is surrounded by the ventricular muscle. The musculature of the subpulmonary infundibulum raises the pulmonary valve above the ventricular septum to position the pulmonary valve as the most superiorly situated of the cardiac valves (▶ Fig. 15.7, ▶ Fig. 15.8). This anatomical feature makes possible the safe resection of the pulmonary valve, including its basal attachments within the infundibulum from the rest of the RVOT.[8] The length of the free-standing infundibulum varies and some cases may be too short to resect (▶ Fig. 15.7**d**).

Arterial Supply

The conotruncal structures including the pulmonary valve are normally vascularized by anterior and posterior arterial branches from the right and left coronary arteries[9] (▶ Fig. 15.9). On the right side, the branches arise from the conal branch of the right coronary artery (RCA) or directly from the aorta. On the left side, they arise from the left anterior descending artery (LAD), the left main, or directly from the aorta. The right anterior conal branch is the most constant and conspicuous branch participating in the preconal circulation, also known as Vieussens' arterial ring.[9] This collateral intercoronary connection extends between the conus artery and first right ventricular branch (left anterior conus branch) of the LAD artery. The Vieussens' arterial ring will become dilated when there is proximal LAD artery occlusion or, less frequently, RCA occlusion[10] (▶ Fig. 15.10). Generally, three major collateral pathways at the conotruncal level provide circulation between the right and left coronary system in all congenital or acquired forms of one-sided coronary occlusion and are used as the basis for different classifications[10] (▶ Fig. 15.9). These

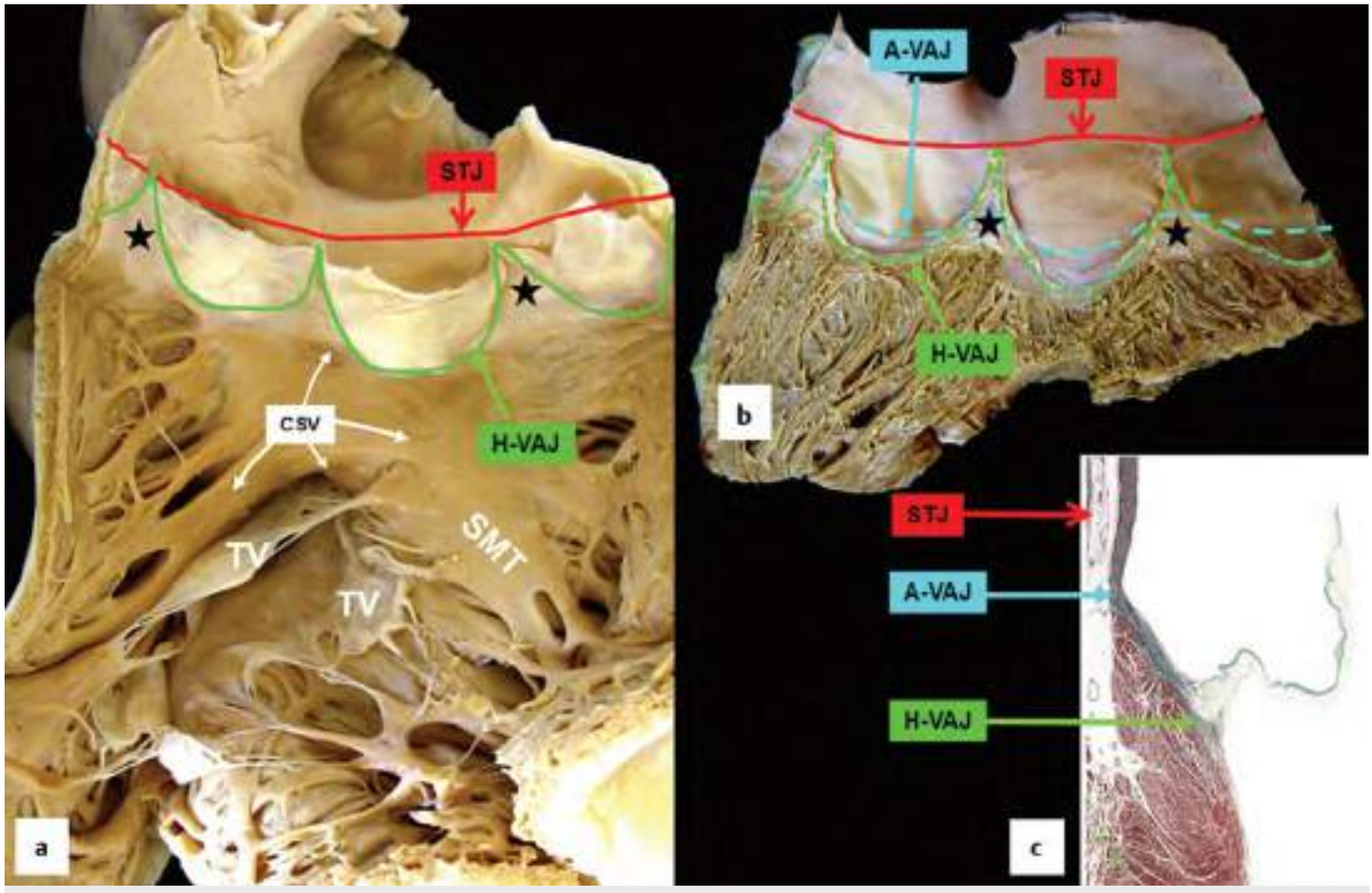

Fig. 15.5 Opened pulmonary root before **(a)** and after removal of valvular leaflets and endocardial dissection **(b)**. The red line shows the sinotubular junction (STJ). The blue line demarcates the anatomical ventriculoarterial junction (A-VAJ) which is the border between the muscular infundibulum and the arterial wall of pulmonary trunk. The semilunar attachments of the three arterial valvular leaflets are marked by the green lines, corresponding to the hemodynamic VAJ (H-VAJ). There is no "annulus" supporting the attachments of the leaflets. **(c)** Histological section of the pulmonary valve showing the different colored lines in **(a)** and **(b)**. Stars, intervalvular trigones; CSV, crista supraventricularis; SMT, septomarginal trabeculations; TV, tricuspid valve.

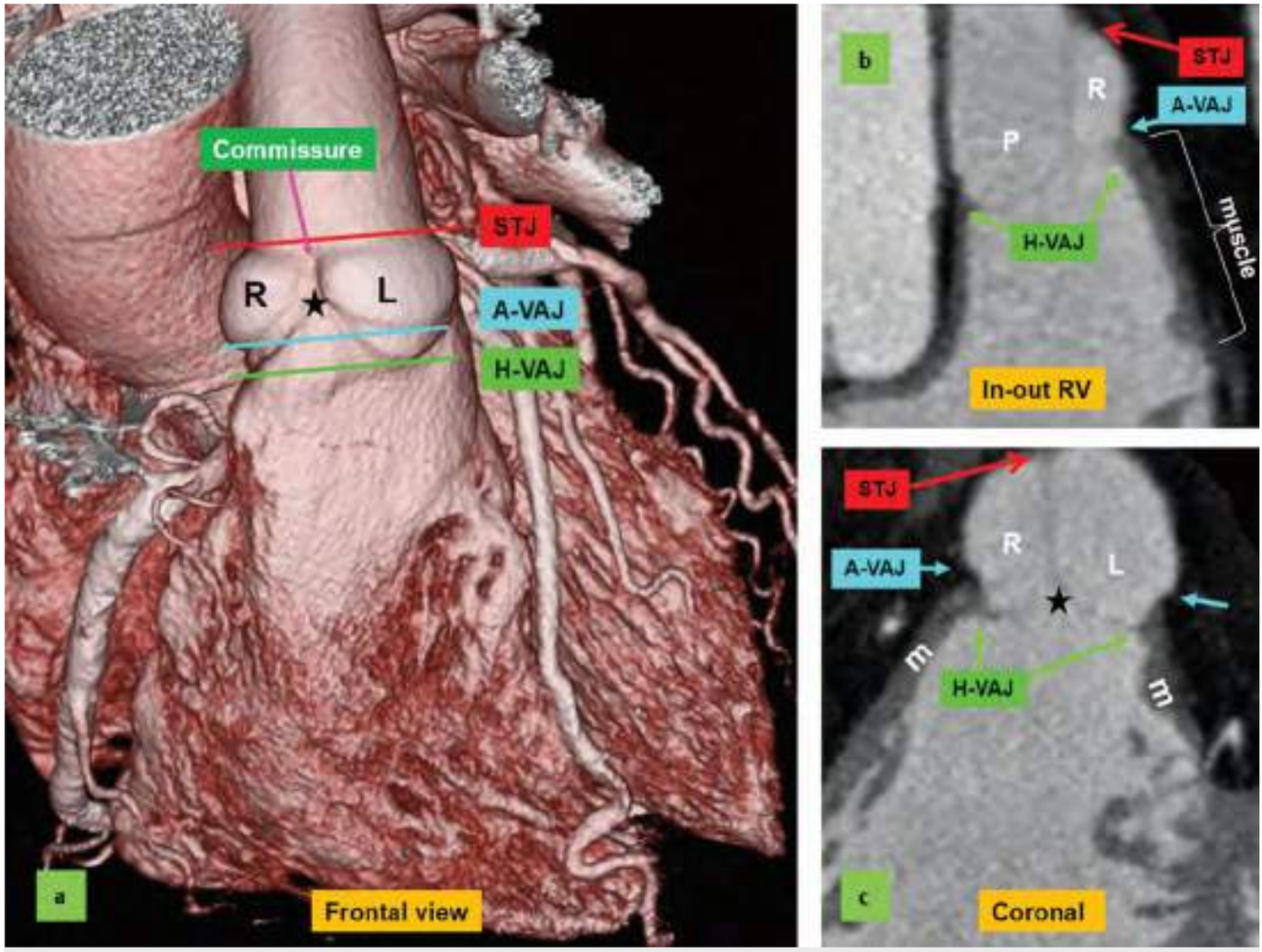

Fig. 15.6 Pulmonary valve (PV) anatomy shown by CT. **(a)** Anterior view of volume rendered, (**b**) inlet–outlet (in–out) of the right ventricle (RV), and **(c)** coronal views of the heart magnified at the right ventricular outflow tract. The anatomical ventriculoarterial junction (A-VAJ) which is demarcated by the blue line in **(a)** and arrows in **(b)** and **(c)** are the anatomical junction between the muscular infundibulum (m) and the elastic arterial wall. The green line in **(a)** and arrows in **(b)** and **(c)** mark the hemodynamic VAJ (H-VAJ), corresponding to the semilunar fibrous attachments of the leaflets to the wall or the "pulmonary annuli" which is much less sturdy than the aortic annuli. It is usually difficult to separate A-VAJ from H-VAJ on three-dimensional volume-rendering images. The yellow line connecting the commissures marks the sinotubular junction (STJ). Interannular fibrous trigone is shown by black star. The commissures between the annuli form peripheral apposition of the leaflets. The pulmonary sinuses including the right anterior (R) and left anterior (L) annuli are seen. The pulmonary valve sits above the ventricular septum and is the most superiorly situated of the cardiac valves. This anatomical feature makes safe resection of the pulmonary valve possible. M, muscle; P, posterior pulmonary valve sinus; RV, right ventricle.

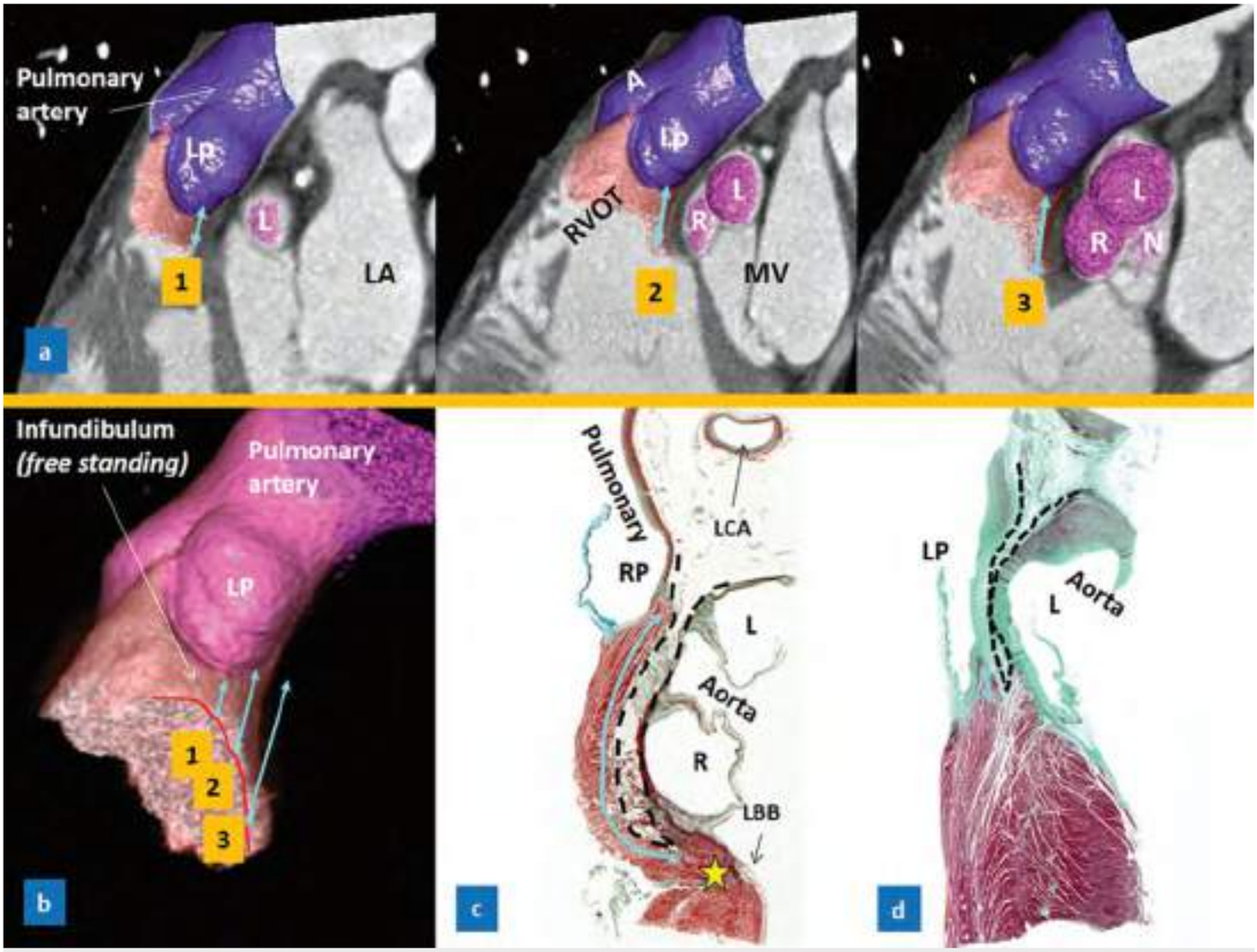

Fig. 15.7 The length of free-standing infundibulum. **(a)** Sagittal CT images through the right ventricular outflow tract (RVOT). **(b)** Three-dimensional view of the RVOT. Sections are obtained at three levels (1 through 3) from left to right. Images showing gradual increase in length of the free-standing muscle of the infundibulum with shortest on the left side. **(c, d)** Sagittal histological sections of the right ventricular infundibulum, pulmonary valve root, left ventricular outflow tract, and aortic root. Note the differences in length of the free-standing right ventricular outflow infundibulum and in the contact area between the right and left outflow tracts (*black dotted lines*) depending on the level of the section: at the right posterior pulmonary cusp **(c)** or left posterior pulmonary cusp **(d)**. The subendocardial fibers in the infundibulum run longitudinally. At subendocardial levels of the left ventricular outflow tract, the orientation is mainly spiral and circumferential. Note that there are connections (*star*) between myocytes in the contact area between both outflow tracts. Blue arrows show the length of free muscle of the infundibulum. R, right; L, left; N, noncoronary aortic sinuses; Lp, left posterior; Rp, right posterior pulmonary sinuses; LA, left atrium; LBB, left bundle branch; LCA, left coronary artery; MV, mitral valve.

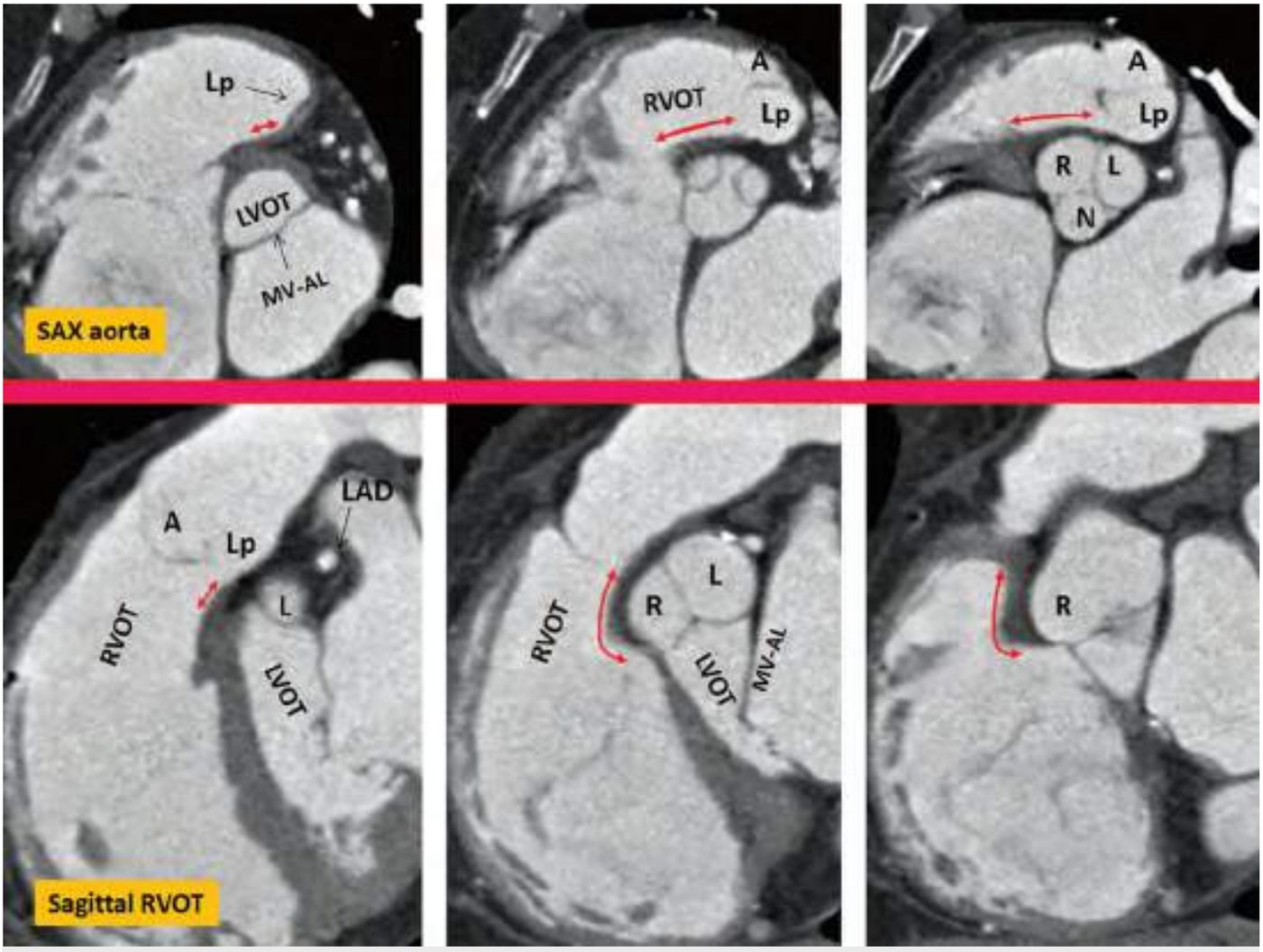

Fig. 15.8 The length of free-standing infundibulum. Upper row: Short-axis (SAX) CT views of the aortic valve from inferior to superior. Lower row: Sagittal CT images through the right ventricular outflow tract (RVOT) at three levels from left to right. Images showing gradual increase in length of the free-standing muscle of the infundibulum with shortest on the left side. Red arrows show the length of free muscle of the infundibulum. R, right; L, left; N, noncoronary aortic sinuses; Lp, left posterior; A, anterior pulmonary sinuses; LAD, left anterior descending artery; LVOT, left ventricular outflow tract; MV-AL, mitral valve anterior (aortic) leaflet.

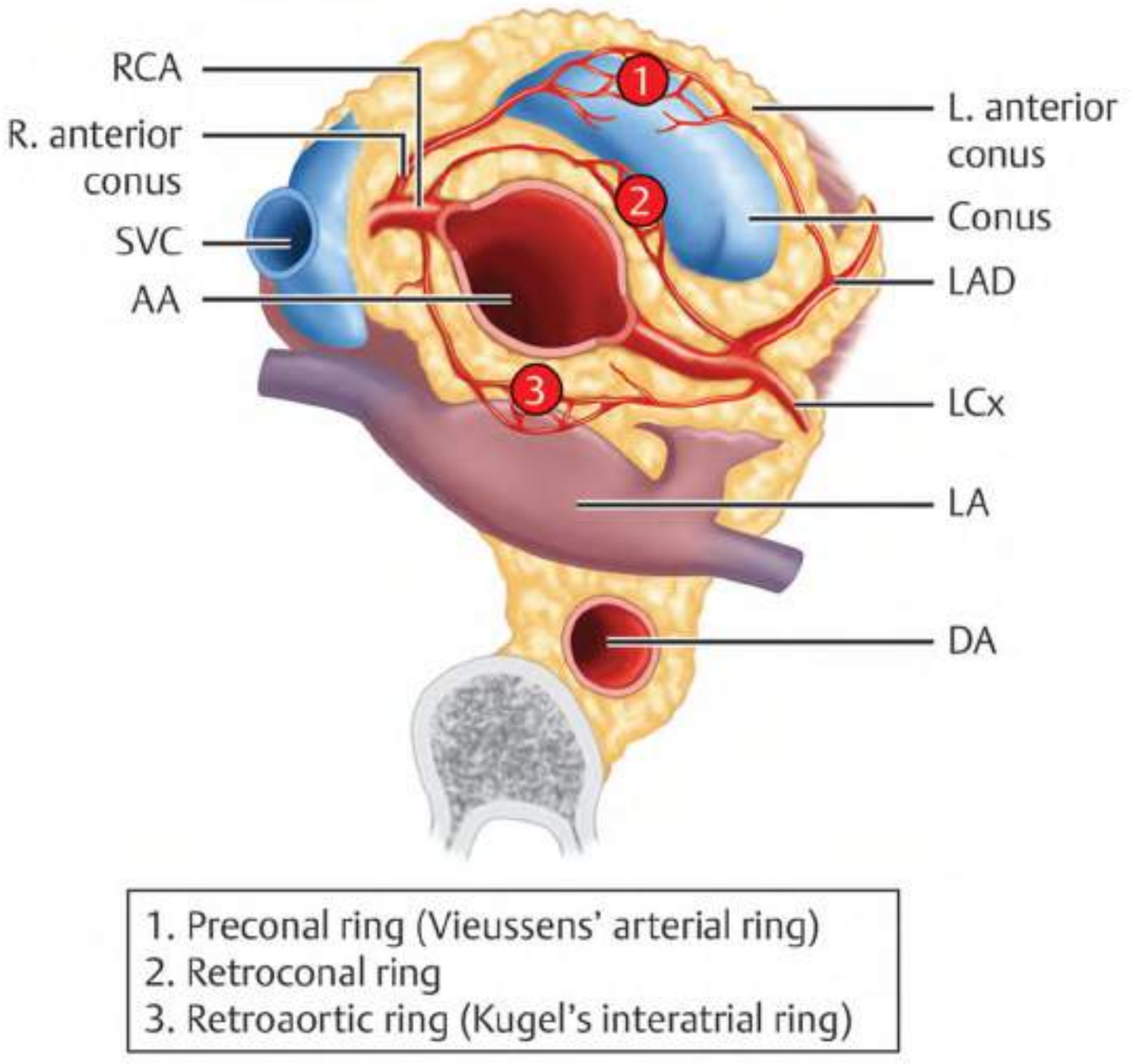

Fig. 15.9 Aortopulmonary trunk arterial anastomotic circulation is provided by three arterial anastomotic rings between the proximal right and left coronary arterial systems. The right pulmonary conal branches arise from the RCA or the aorta and the left conal branches from the left main or proximal LAD arteries. The right anterior conal branch exists in almost all individuals and in 50% it may arise from the right aortic sinus. The left anterior conal artery exists in 85%, the right posterior in 15%, and the left posterior in 15%. The retroaortic anastomotic ring is mainly related to the Kugel atrial anastomotic network which connects the proximal right and left coronary systems (as shown in this images) or on one side may communicate with the distal coronary system through the interatrial septum (not shown). AA, ascending aorta; LA, left atrium; DA, descending aorta; LAD, left anterior descending artery; LCx, left circumflex artery; RCA, right coronary artery; SVC, superior vena cava.

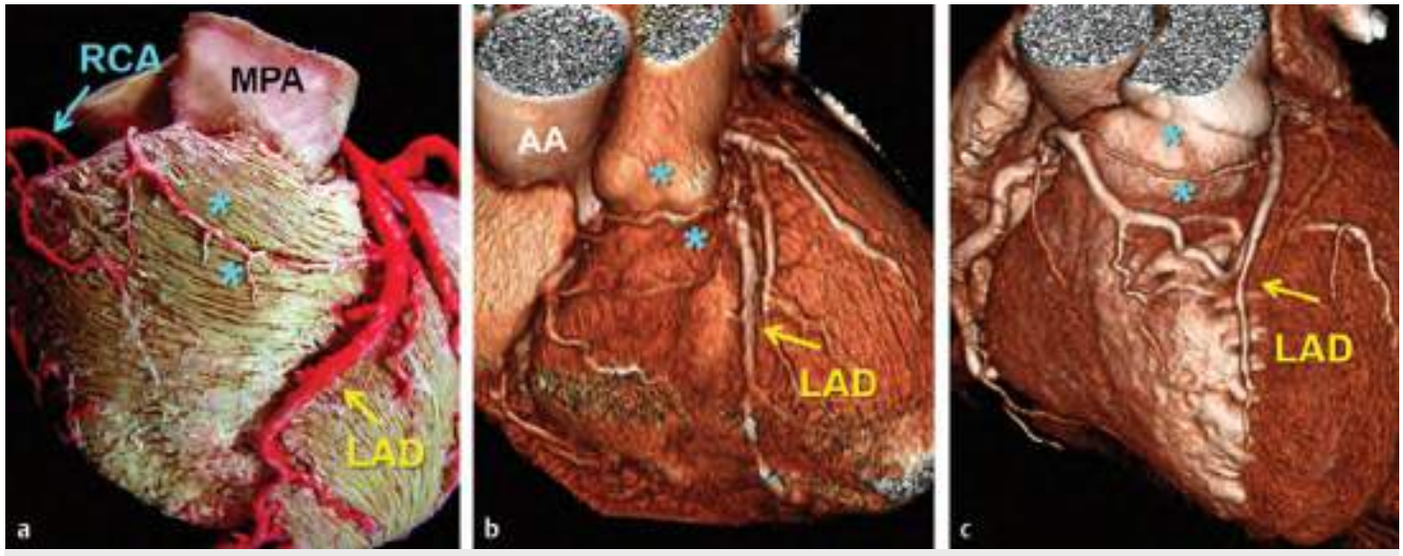

Fig. 15.10 Vieussens' arterial ring. Anterior arterial anastomotic rings (*asterisks* [*]) between pulmonary conus branches arising from the RCA and the LAD artery are shown **(a)** participating in vascular supply to the infundibulum as well as the proximal right ventricle. These collaterals may be enlarged in acquired **(b)** or congenital **(c)** obstructive coronary disease. AA, Ascending aorta; MPA, main pulmonary artery; RCA, right coronary artery; LAD, left anterior descending artery.

three collateral circulation pathways include preconal (precardiac), retroconal (interarterial), and retroaortic.

◆ Imaging Techniques

MR, CT, and echocardiography all provide valuable information on valve anatomy and mobility, RV size and function, the presence of poststenotic dilation, locating a pulmonary subvalvular stenosis, and associated pathologies of the pulmonary arteries. High spatial resolution and the availability of isotropic multiplanar data reconstruction make cardiac CT angiography (CTA) the preferred technique for detailed anatomical study of the pulmonary root and RVOT. Using current CT scanners, complete heart acquisition can be performed in a short breath-hold with the isotropic spatial resolution of 0.5 mm. Anatomical analysis of the RV and pulmonary valve can be performed with a dedicated ECG-gated right heart study or with some modification of contrast injection protocol as part of routine CT coronary angiography.[11,12] Evaluation of both native and prosthetic pulmonary valves with cardiac-gated CTA is now possible. Similar to its use for the aortic valve, CT of the pulmonary valve provides valuable information before percutaneous valve implantation. CT pulmonary angiogram is the examination of choice for assessment of the proximal and distal pulmonary arteries, also assessment of the proximity of the coronary artery origin and course relative to the area where the valve to be implanted. In patients with a pacemaker, CT may be a better choice for evaluation of the pulmonary valve.

Cardiac MRI is an excellent noninvasive imaging modality for pulmonary valve function analysis, especially when serial monitoring is necessary (i.e., progression of pulmonary regurgitation [PR]). Anatomy and function of the RVOT and pulmonary valve can optimally be obtained using balanced steady-state free precision (SSFP) cine images given its high blood–myocardial interface contrast. With the addition of gadolinium contrast, MRA can delineate the valve and pulmonary arteries. A comprehensive functional assessment of the pulmonary valve apparatus may necessitate through plane phase contrast MR flow quantification at, above, and below the level of the valve. Systolic forward flow and diastolic flow reversal can then be computed by integration of areas. Generally, peak velocities can be best encoded at the level of luminal narrowing for stenosis assessment and just proximal to the pulmonary valve for regurgitation evaluation (▶ Fig. 15.11). With new MR phase contrast techniques, volumetric evaluation of hemodynamics is possible.[12]

◆ Pathologies

Pulmonary Valve Stenosis

Isolated pulmonary stenosis (PS) is almost always congenital and can often be asymptomatic when first diagnosed. It is not unusual to suspect PS in a young patient on routine chest X-ray or CT by noticing enlarged main and left pulmonary arteries (▶ Fig. 15.12). With severe PS, symptoms of dyspnea, fatigue, chest pain, palpitations, and decreased exercise tolerance may occur. Symptoms occur at a variable valve gradient, but patients with peak gradients less than 25 mm Hg are usually asymptomatic. Three morphological groups are described.[13] The most common type of congenital PS (40–60%) is a dome-shaped pulmonary valve, which is characterized by a mobile valve with two to four raphes and incomplete separation of valve cusps due to commissural fusion resulting in a funnel shape with a small circular orifice. Bicuspid or multicuspid valve is rare[14,15] (▶ Fig. 15.11). Bicuspid pulmonary valves are seen in 0.1%, and quadricuspid pulmonary valves are seen in 0.2% of hearts, compared with the 0.7% incidence of bicuspid aortic valve.[16] Acquired causes of stenosis are significantly less common than acquired causes of stenosis in other cardiac valves.[17]

Chronic PS results in RV hypertrophy, especially at the RVOT. A hypertrophied RV can maintain its function for years, even when RV pressures are near systemic. When prominent, RVOT hypertrophy can lead to secondary dynamic subvalvar stenosis.

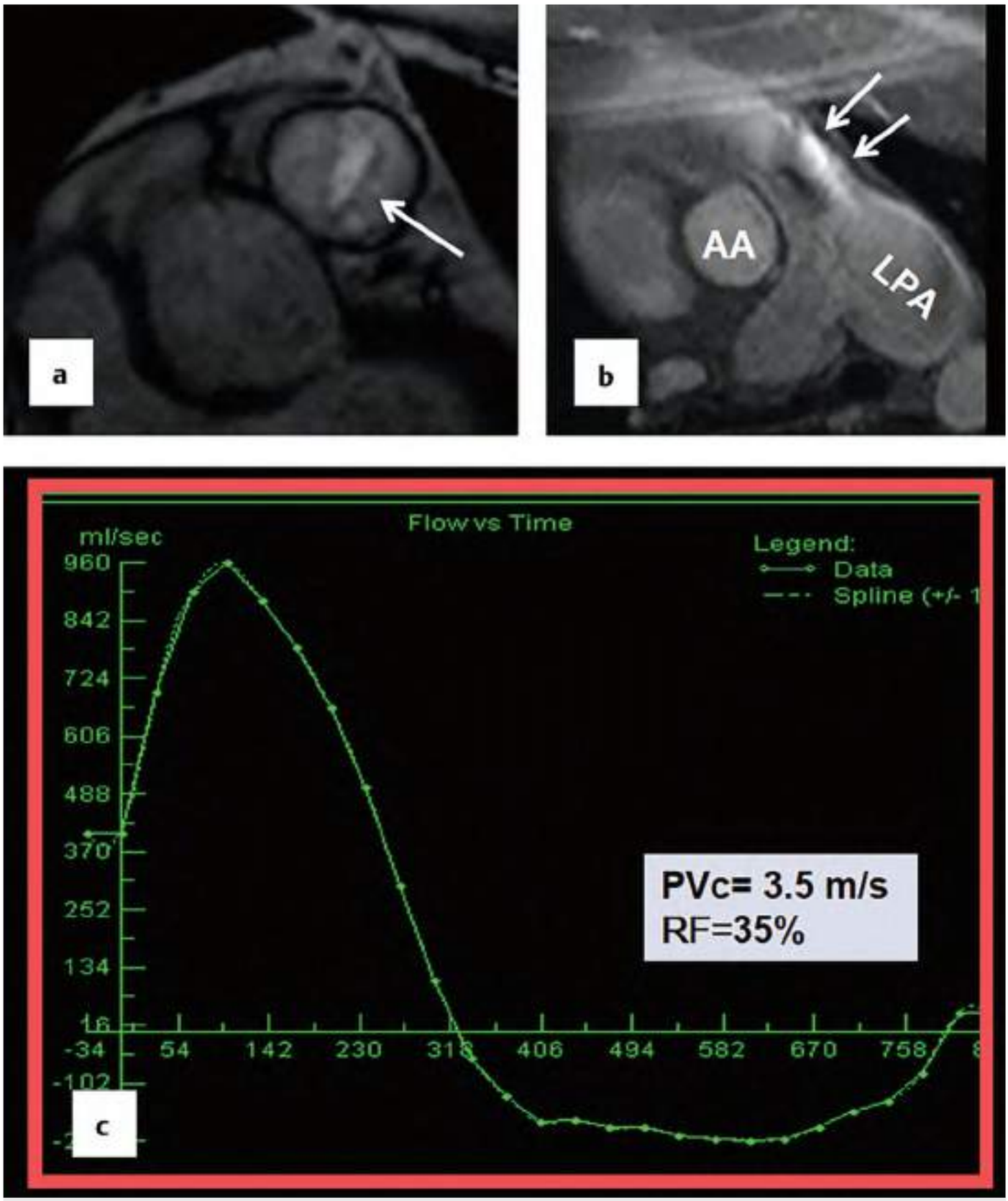

Fig. 15.11 **(a)** Transaxial and **(b)** long axis MRI of a stenotic bicuspid pulmonary valve (PV) (*arrow*) with jet of flow (*double arrows*) and poststenotic dilation of the left pulmonary artery (LPA) are shown in upper row. Systolic flow turbulence and increased peak velocity (PVc) of 3.5 m/s by phase velocity mapping were seen consistent with stenosis. **(c)** Flow profile, mL/s versus time (ms). There was moderate (free) pulmonary valve insufficiency with regurgitant fraction (RF) 35%. AA, ascending aorta.

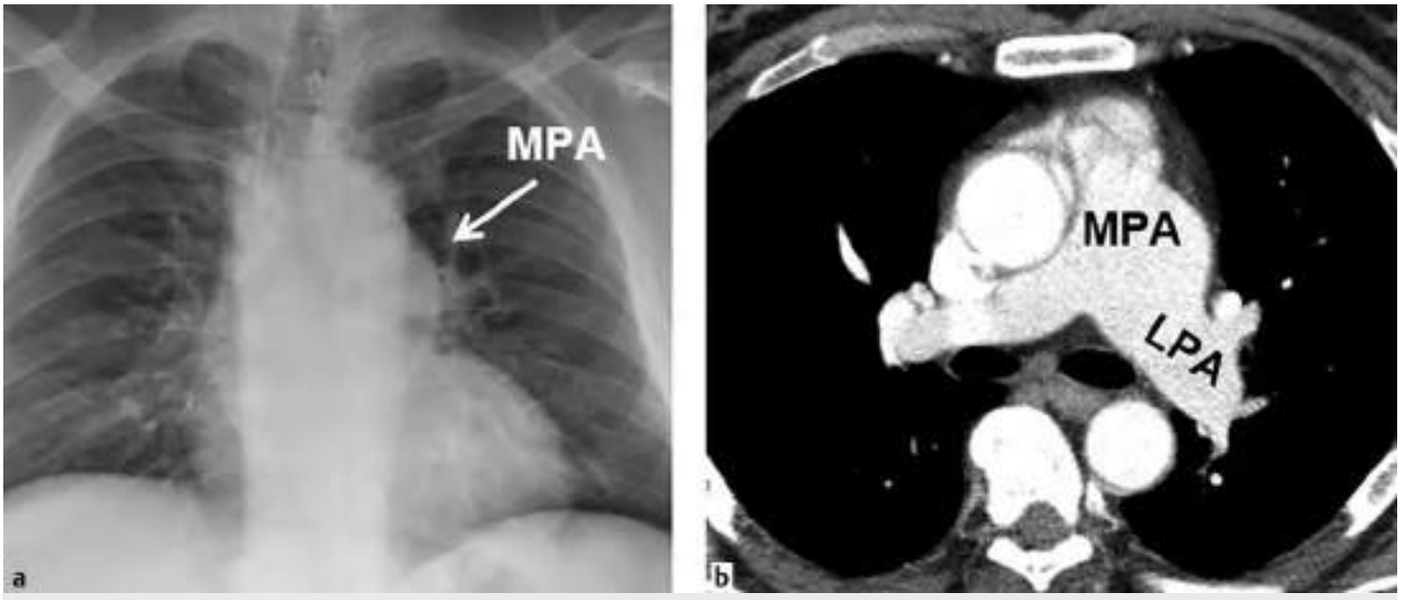

Fig. 15.12 Typical findings of pulmonary stenosis in a 51-year-old man found in **(a)** plain X-ray and **(b)** routine contrast-enhanced chest studies, showing enlarged main and left pulmonary arteries (MPA, LPA).

Table 15.1 Pulmonary valve pathology

Pathology	Normal	Congenital	Postoperative	Acquired
Pulmonary valve stenosis	None	Dome-shaped Dysplastic Other variants: *mixed, hourglass, unicuspid, bicuspid, quadricuspid*	Native valve Prosthetic valve Valve conduit	Bacterial endocarditis Carcinoid rheumatic heart disease Masses extrinsic: *aneurysm, hematoma*
Pulmonary valve regurgitation	Trivial or mild	Bicuspid or quadricuspid valve Absent pulmonary valve syndrome	Transannular RVOT patching The Ross operation Postpercutaneous relief of pulmonary stenosis	Bacterial endocarditis Carcinoid heart disease Rheumatic heart disease Behçet's disease Pulmonary hypertension Pulmonary artery aneurysm Systemic lupus erythematosus Syphilis

Abbreviation: RVOT, right ventricular outflow tract.

Echocardiography is the best modality for diagnosis and grading of stenosis. MR and CT can also provide valuable information on valve morphology and mobility, presence of poststenotic dilation, grading of stenosis, and locating a supravalvular or subvalvular stenosis (▶ Fig. 15.11). Stenotic pulmonary valve is commonly associated with poststenotic pulmonary arterial dilation and aneurysm formation due to separated poststenotic flow and increased wall shear stress which can be shown by four-dimensional phase contrast MR.[18]

Pulmonary Regurgitation

Trivial or mild PR is common in normal subjects (~30%), but rarely of importance.[19] A Regurgitant pulmonary valve is a common complication after surgical or percutaneous relief of PS and following repair of TOF. Carcinoid heart disease, rheumatic heart disease, infective endocarditis are uncommon causes of pulmonary valve stenosis or regurgitation[17] (▶ Table 15.1). In severe pulmonary hypertension, pulmonary and tricuspid regurgitation are common.

PR is generally better tolerated than aortic regurgitation. In PR, forward blood flow can be maintained directly by contractions of the right atrium and indirectly by the left heart pumping systemic venous return. Low resistance of the pulmonary vascular bed also helps systolic flow pass through the capillary bed. Moderate-to-severe chronic PR produces RV volume overload and increased end diastolic volumes followed by an increase of end-systolic volumes, and progressive deterioration of myocardial function.[20]

Echocardiography grading of PR is less robust than for aortic regurgitation due to technical difficulty. Cardiac MR is the gold standard for investigation and follow-up of such patients, as it accurately assesses two important parameters: the quantity of PR and the RV volumes/function[21] (▶ Fig. 15.11). A regurgitant fraction^{3}40% and flow reversal in pulmonary artery branches indicate severe PR.[22] The duration of regurgitant flow with respect to total diastole is shorter in the patient with severe PR.[21]

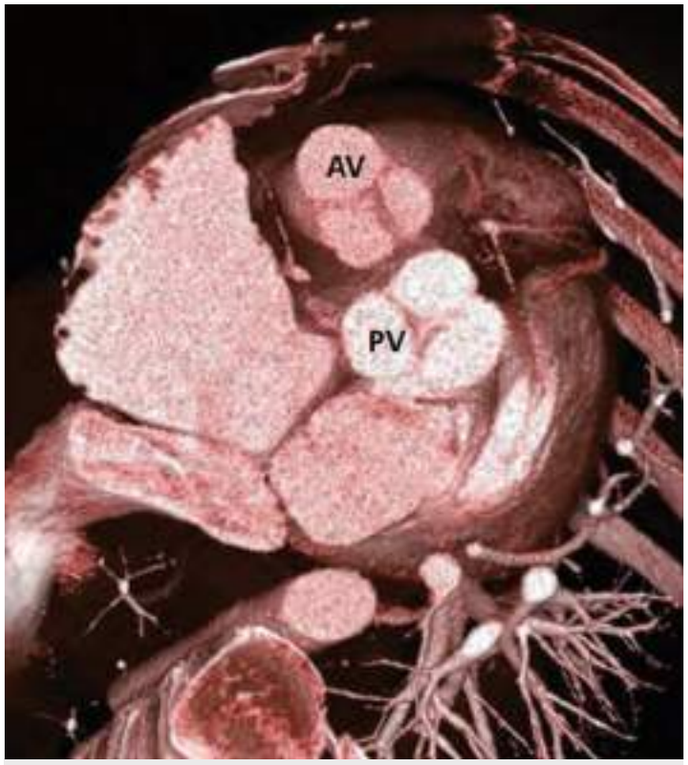

Fig. 15.13 Truncal arteries valvar arrangement. Short-axis CT angiography shows the relationships between aortic valve (AV) and pulmonary valve (PV) in transposition of the great arteries (TGA). In TGA, the AV is located anterior to the PV. Compare it with the normal arrangement in ▶ Fig. 15.3.

Congenital Heart Disease and the Pulmonary Root

Tetralogy of Fallot results from anterosuperior deviation of the outlet septum during embryonic development causing overriding of the aorta, RVOT obstruction, ventricular septal defect (VSD), and consequent RV hypertrophy. In the majority of TOF patients, RVOT stenosis is subpulmonary due to anterosuperior malalignment of the muscular outlet septum coupled with thickened septoparietal trabeculations.[23]

Pulmonary atresia is very rare, generally diagnosed and repaired in early childhood. Pulmonary atresia and VSD fall in the spectrum of TOF. In pulmonary atresia, blood supply to the right and left pulmonary arteries will be provided by a large patent ductus arteriosus.

Truncal arterial relationship varies in different CHDs. Knowing their arrangement may be important for diagnosis and classification of some congenital malformations. In TGA, the aorta and associated coronary arteries arise anteriorly from the RV, and the pulmonary artery arises posteriorly from the left ventricle (▶ Fig. 15.13). The great arteries are parallel rather than crossing as they do in the normal heart.

In congenitally corrected TGA, the morphological left ventricle sits between the right atrium and the pulmonary trunk and the morphological RV connects the left atrium to the aorta.[24] The two arterial trunks are parallel rather than crossing as they do with TGA, but the aorta is usually located to the left of the pulmonary trunk. DORV is a type of abnormal ventriculoarterial connection in which both great vessels arise entirely or predominantly (> 50% circumference) from the RV.[23] The arterial trunks may vary in location, with the aorta generally to the right of the pulmonary trunk. Truncus arteriosus consists of a single arterial trunk giving origin to the pulmonary arteries, coronary arteries, and the systemic circulation.[25]

Valve Replacement

Pulmonary valve replacement is one of the most common procedures performed in adults with CHD. Reoperation is a common pathway for all these different pathologies and it is not uncommon for many to require multiple valve replacement during their lifetime. A complete assessment of the pulmonary arterial system with CT or MR may be necessary before valve reoperation to find associated complications.[26] Recently, transcatheter valve replacement has been deployed successfully in RV outflow conduits, bioprosthetic valves, and has now been extended to include patients with native pulmonary valve stenosis.[27]

References

[1] Waldo KL, Hutson MR, Ward CC, et al. Secondary heart field contributes myocardium and smooth muscle to the arterial pole of the developing heart. Dev Biol.; 281(1):78–90
[2] Webb S, Qayyum SR, Anderson RH, Lamers WH, Richardson MK. Septation and separation within the outflow tract of the developing heart. J Anat.; 202 (4):327–342
[3] Anderson RH, Webb S, Brown NA, Lamers W, Moorman A. Development of the heart: (3) formation of the ventricular outflow tracts, arterial valves, and intrapericardial arterial trunks. Heart.; 89(9):1110–1118
[4] Waldo KL, Hutson MR, Stadt HA, Zdanowicz M, Zdanowicz J, Kirby ML. Cardiac neural crest is necessary for normal addition of the myocardium to the arterial pole from the secondary heart field. Dev Biol.; 281(1):66–77
[5] Restivo A, Piacentini G, Placidi S, Saffirio C, Marino B. Cardiac outflow tract: a review of some embryogenetic aspects of the conotruncal region of the heart. Anat Rec A Discov Mol Cell Evol Biol.; 288(9):936–943
[6] Bajolle F, Zaffran S, Kelly RG, et al. Rotation of the myocardial wall of the outflow tract is implicated in the normal positioning of the great arteries. Circ Res.; 98(3):421–428
[7] Stamm C, Anderson RH, Ho SY. Clinical anatomy of the normal pulmonary root compared with that in isolated pulmonary valvular stenosis. J Am Coll Cardiol.; 31(6):1420–1425
[8] Anderson RH, Razavi R, Taylor AM. Cardiac anatomy revisited. J Anat.; 205 (3):159–177
[9] Saremi F, Goodman G, Wilcox A, Salibian R, Vorobiof G. Coronary artery ostial atresia: diagnosis of conotruncal anastomotic collateral rings using CT angiography. JACC Cardiovasc Imaging.; 4(12):1320–1323
[10] Levin DC. Pathways and functional significance of the coronary collateral circulation. Circulation.; 50(4):831–837
[11] Revel MP, Faivre JB, Remy-Jardin M, Delannoy-Deken V, Duhamel A, Remy J. Pulmonary hypertension: ECG-gated 64-section CT angiographic evaluation of new functional parameters as diagnostic criteria. Radiology.; 250(2):558–566
[12] Saremi F, Gera A, Ho SY, Hijazi ZM, Sánchez-Quintana D. CT and MR imaging of the pulmonary valve. Radiographics.; 34(1):51–71
[13] Bashore TM. Adult congenital heart disease: right ventricular outflow tract lesions. Circulation.; 115(14):1933–1947
[14] Vedanthan R, Sanz J, Halperin J. Bicuspid pulmonic valve. J Am Coll Cardiol.; 54(8):e5
[15] Berdajs D, Lajos P, Zünd G, Turina M. The quadricuspid pulmonary valve: its importance in the Ross procedure. J Thorac Cardiovasc Surg.; 125(1):198–199
[16] Jashari R, Van Hoeck B, Goffin Y, Vanderkelen A. The incidence of congenital bicuspid or bileaflet and quadricuspid or quadrileaflet arterial valves in 3,861

donor hearts in the European Homograft Bank. J Heart Valve Dis.; 18(3):337–344
[17] Waller BF, Howard J, Fess S. Pathology of pulmonic valve stenosis and pure regurgitation. Clin Cardiol.; 18(1):45–50
[18] Fenster BE, Schroeder JD, Hertzberg JR, Chung JH. 4-Dimensional cardiac magnetic resonance in a patient with bicuspid pulmonic valve: characterization of post-stenotic flow. J Am Coll Cardiol.; 59(25):e49
[19] Klein AL, Burstow DJ, Tajik AJ, et al. Age-related prevalence of valvular regurgitation in normal subjects: a comprehensive color flow examination of 118 volunteers. J Am Soc Echocardiogr.; 3(1):54–63
[20] van Straten A, Vliegen HW, Hazekamp MG, et al. Right ventricular function after pulmonary valve replacement in patients with tetralogy of Fallot. Radiology.; 233(3):824–829
[21] Li W, Davlouros PA, Kilner PJ, et al. Doppler-echocardiographic assessment of pulmonary regurgitation in adults with repaired tetralogy of Fallot: comparison with cardiovascular magnetic resonance imaging. Am Heart J.; 147 (1):165–172
[22] Bouzas B, Kilner PJ, Gatzoulis MA. Pulmonary regurgitation: not a benign lesion. Eur Heart J.; 26(5):433–439
[23] Anderson RH, Jacobs ML. The anatomy of tetralogy of Fallot with pulmonary stenosis. Cardiol Young.; 18 Suppl 3:12–21
[24] Warnes CA. Transposition of the great arteries. Circulation.; 114(24):2699–2709
[25] Van Praagh R. Truncus arteriosus: what is it really and how should it be classified? Eur J Cardiothorac Surg.; 1(2):65–70
[26] Oosterhof T, van Straten A, Vliegen HW, et al. Preoperative thresholds for pulmonary valve replacement in patients with corrected tetralogy of Fallot using cardiovascular magnetic resonance. Circulation.; 116(5):545–551
[27] Lurz P, Coats L, Khambadkone S, et al. Percutaneous pulmonary valve implantation: impact of evolving technology and learning curve on clinical outcome. Circulation.; 117(15):1964–1972

16 The Mitral Valve

Francesco F. Faletra, Horia Muresian, Damián Sánchez-Quintana, and Farhood Saremi

◆ Introduction

Over the last two decades, echocardiography (two- and three-dimensional [2D and 3D] transthoracic [TTE] and transesophageal [TEE]), computed tomography (CT), and cardiac magnetic resonance (CMR), have become crucial in the modern diagnostic workflow and management of patients with cardiovascular disease. Each of these techniques has advantages and limitations. CT has been commonly used for evaluation of the integrity of the epicardial coronary arteries and CMR is primarily used to address the pathologies of the myocardium. Echocardiography has been the first-line imaging technique for evaluating morphology, size, and function of heart valves. However, CT and CMR can also provide added information in regard to the morphology and function of the cardiac valves. Furthermore, each of these studies can also explore surrounding structures not affected by the disease with an unprecedented quality and detail. In this chapter, we describe and illustrate the anatomy and variants of the mitral valve (MV) apparatus *"revisited"* by these techniques. To illustrate various anatomical aspects of MV, we use the imaging technique that best fits the described component/s. For instance, all three imaging techniques may visualize papillary muscles (PMs) but CT is the technique which best shows the anatomical details of the PMs. We also briefly describe common mitral pathologies.

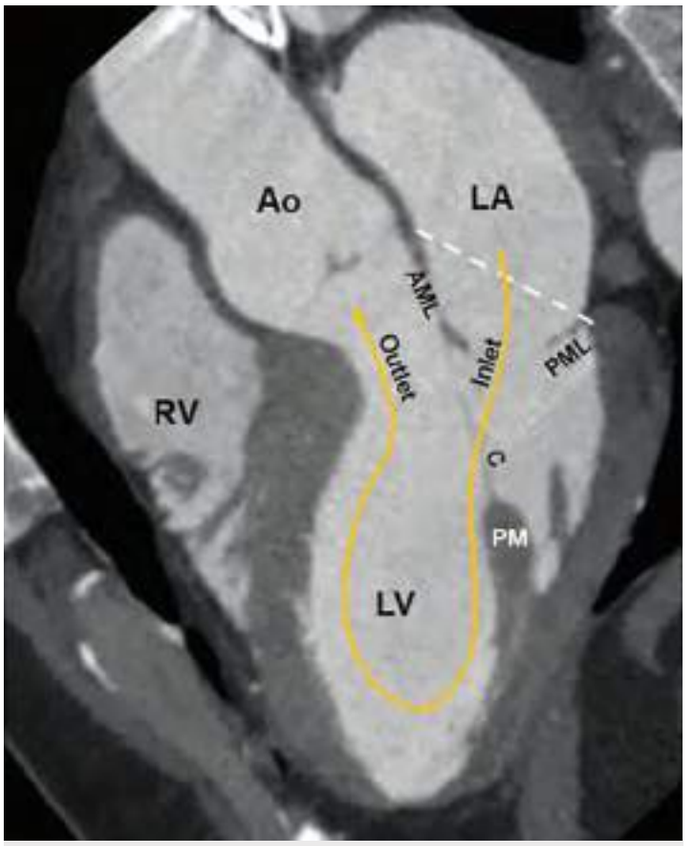

Fig. 16.1 Three-chamber CT view of the heart showing components of the mitral valve apparatus. To maintain the functional integrity of the apparatus and the effective competence, fine spatial and temporal coordination and perfect anatomical integrity of all the components are required. The dotted line marks the virtual plane of the mitral annulus. Blood flow direction from inlet to outlet is shown by curved arrow. AML, anterior (aortic) mitral leaflets; LA, left atrium; LV, left ventricle; PML, posterior (mural) mitral leaflet; C, chorda tendineae; PM, papillary muscle; RV, right ventricle.

◆ Mitral Valve Apparatus

In 1972, Perloff and Roberts[1] first described the MV as a complex apparatus, which requires for maintaining a perfect competence, morphological integrity combined with a precise spatial and temporal coordination of the annulus, leaflets, chordae tendineae, and PMs (▶ Fig. 16.1). Any anatomical change or disruption of one or more of these components inevitably leads to mitral regurgitation.

Mitral Annulus

Anatomical books describe the MV annulus as an interrupted fibrous ring, divided into anterior and posterior segments, which encircles the atrioventricular junction and support the mitral leaflets. Later Angelini et al[2] demonstrated that a continuous fibrous ring separating the atrial and ventricular myocardium is rather rare. Instead, the posterior segment of the annulus is often seen as a discontinuous fibrous arc interrupted by variable amount of atrial and ventricular myocardial fibers while the anterior segment is in fact a sheet-like structure made of dense connective tissue that connects the anterior mitral leaflet with the aortic interleaflet triangle. This area is called mitral–aortic fibrous continuity, also known as mitral–aortic curtain or intervalvular fibrosa (▶ Fig. 16.2).

Two nodules of dense fibrous tissue namely the "right and left fibrous trigons" near the commissures exist to reinforce the base of anterior leaflet. Finally, from a surgical point of view, the MV annulus is defined as the hinge line of attachment of mitral leaflets on the atrial and ventricular myocardium.

The MV annulus has a 3D saddle-shaped configuration with the highest points corresponding to the midpoints of aortic attachment of the mitral–aortic curtain and the lowest at the fibrous trigones.[3] This configuration concentrates the peak stress on the two fibrous trigons.[4,5]

Absence of a rigid fibrous ring makes the mitral annulus a deformable structure that changes in dimension and shape during the cardiac cycle. During early systole, the normal annulus contracts and its saddle-shaped configuration becomes more pronounced. These systolic changes are mainly due to the anteroposterior shortening while the bicommissural diameter remains unchanged (▶ Fig. 16.3).

Longitudinal shortening of the left ventricle with each contraction drags the MV annulus toward the apex. The resulting increase in the left atrial diameters facilitates its filling by

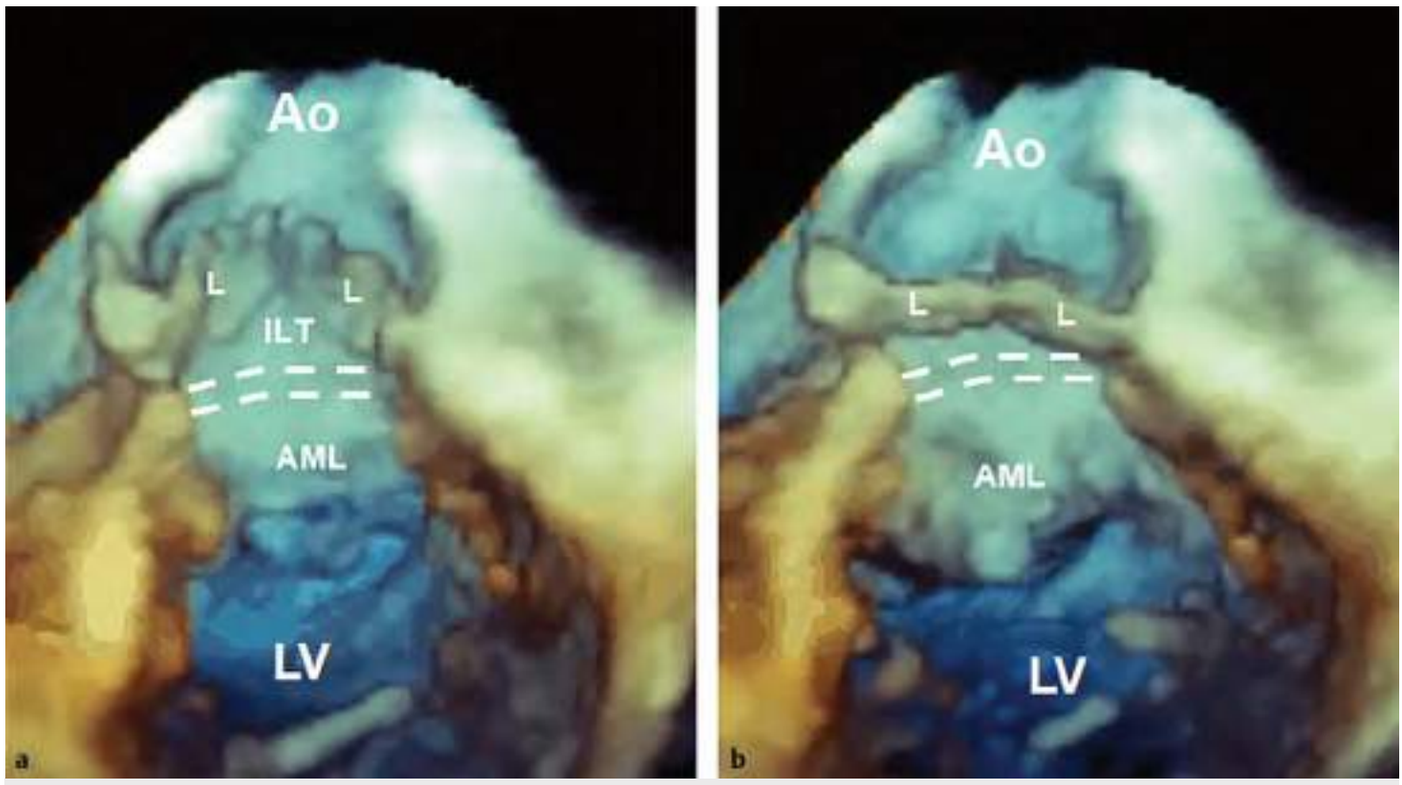

Fig. 16.2 Images obtained with three-dimensional transesophageal echocardiography in **(a)** systole and **(b)** diastole. A longitudinal cut of the aortic root (Ao) and left ventricle (LV) showing the ventricular site of the anterior mitral leaflet (AML) and the interleaflet triangle (ILT) between the aortic leaflets (L). The two dotted lines delimit a sheet-like connection between the AML and the ILT. This area is known with different names such as mitral–aortic fibrous continuity, mitral–aortic curtain, or intervalvular fibrosa.

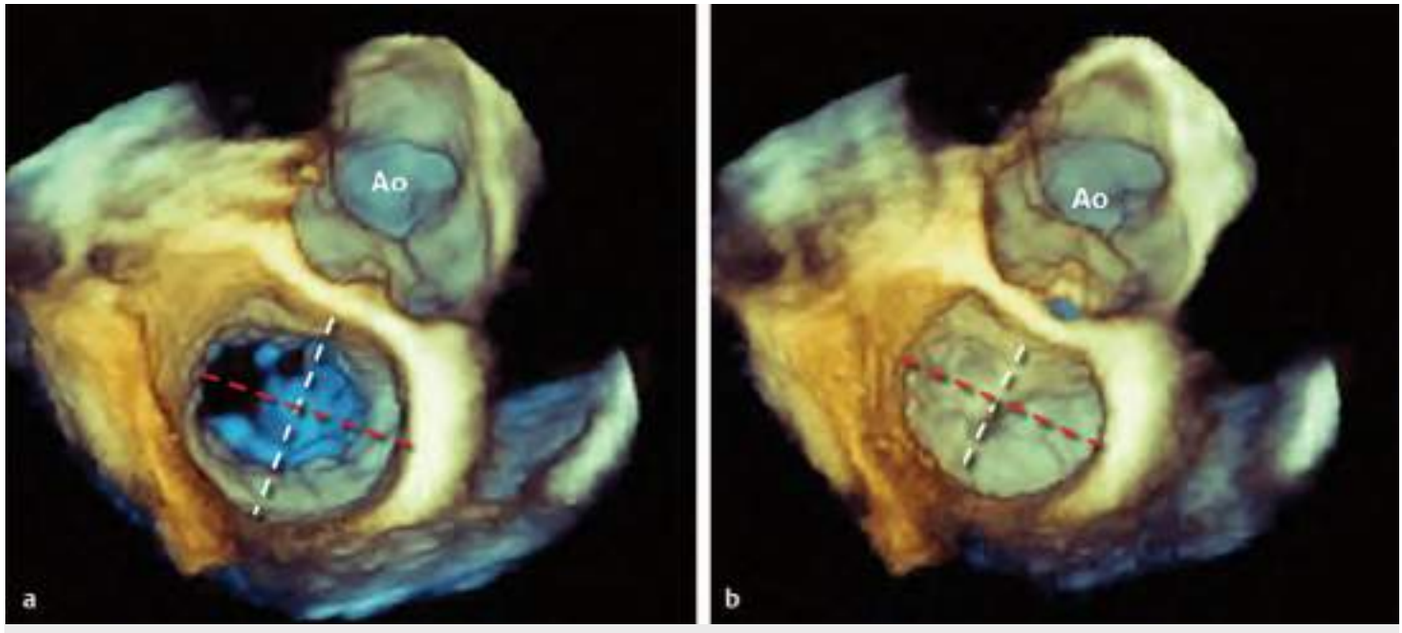

Fig. 16.3 Three-dimensional transesophageal echocardiography showing the mitral valve and annulus from an atrial perspective in **(a)** diastole and in **(b)** systole. Images show that the annulus as a very dynamic and deformable structure, being nearly circular in diastole **(a)** and elliptical in systole **(b)**. The change is primarily due to anteroposterior shortening (*white line*) while bicommissural diameter (*red line*) remains unchanged. Ao, aorta.

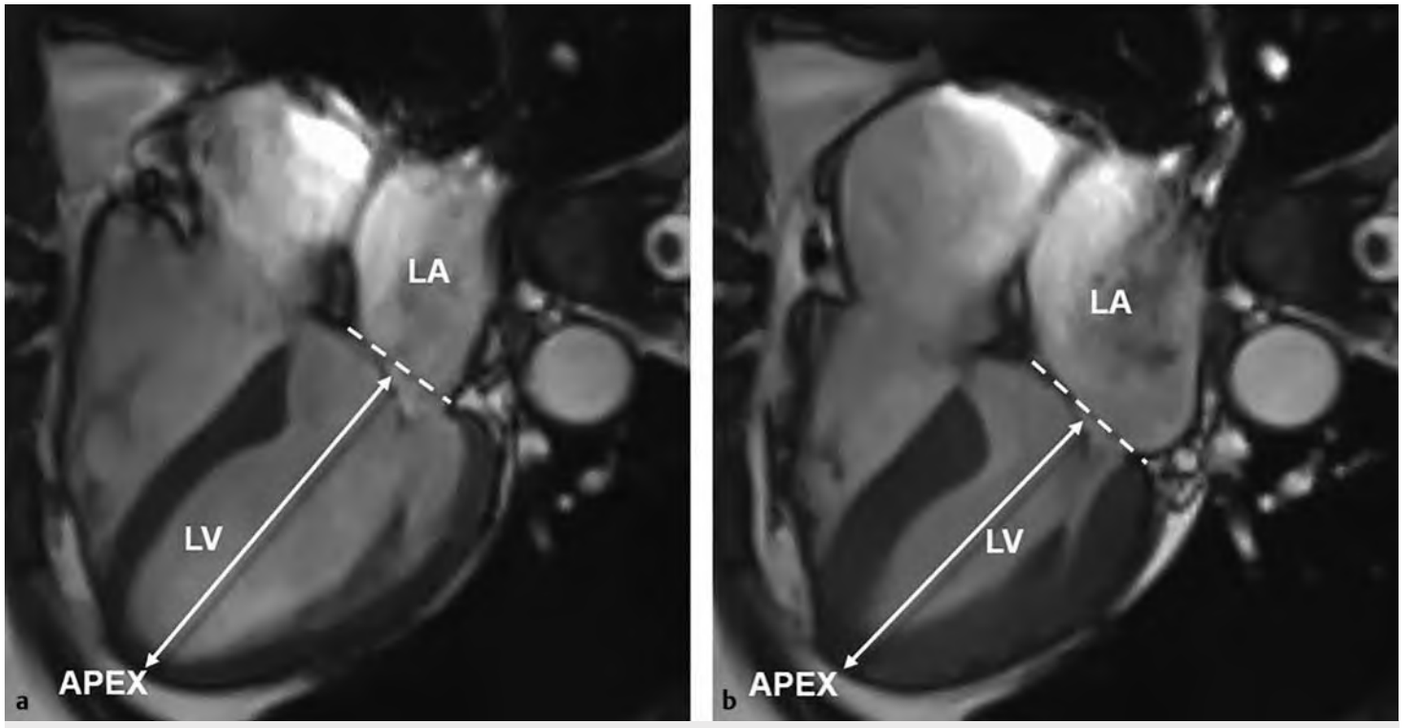

Fig. 16.4 Cardiac MR image in **(a)** diastole and in **(b)** systole showing longitudinal motion of the mitral annulus (*dotted line*) toward the apex due to longitudinal contraction of the left ventricle (LV). The resulting increase of the left atrium (LA) volume facilitates forward pulmonary venous flow.

increased systolic forward flow from the pulmonary veins. The opposite changes occur in diastole (▶ Fig. 16.4).

Finally, the posterior mitral annulus is close to important structures, including the left circumflex artery, the right coronary artery, the coronary sinus, and the bundle of His (posteromedially near the right fibrous trigone). The anatomical relationship of these structures with the hinge line of posterior annulus is important since the surgical suture during MV replacement occurs along the posterior hinge line and these vessels may be damaged (▶ Fig. 16.5).

Mitral Leaflets

Two deep incisures called commissures are seen between the anterior and posterior leaflets.[6] The anterior leaflet has a triangular shape and covers approximately one-third of the entire annular circumference while the posterior leaflet has quadrangular shape and covers the remaining two-thirds. In most normal MVs, two additional incisures divide the posterior leaflet into three small segments or scallops (▶ Fig. 16.6, ▶ Fig. 16.7). To facilitate valve analysis (i.e., in the presence of mitral prolapse/flail) cardiac surgeons name the lateral scallop P1, the central scallop P2, and the medial scallop P3. Usually, the central scallop is the largest. Even though the free edge of the anterior leaflet has no identifiable incisures, the free margin of the anterior leaflet across the P1, P2, and P3 segments are named A1, A2, and A3, respectively. Occasionally, additional scallops occupy the commissural areas. These small scallops are called *commissural scallops*[7] (▶ Fig. 16.7).

From a ventricular perspective, both leaflets present two distinct zones: the *rough zone* and the *clear zone* (▶ Fig. 16.8). The rough zone covers the distal surface of both leaflets and receives the insertions of chordae tendineae assuming a corrugate surface. The clear zone covers the remaining ventricular surface and has a smooth appearance. From an atrial perspective, the rough zones correspond to the so-called *coaptation surface*, the area where leaflets juxtapose each other during systole. The width of this coaptation surface measures 8 to 10 mm. The redundancy of the coaptation surface provides a comfortable "valvular reserve" that assures an effective coaptation in presence of a certain degree of annulus dilation or leaflet tethering. Moreover, as the ventricular pressure rises, the leaflets mutually support each other along this zone. Since the vast majority of chordae insert within the coaptation surface, they may share the mechanical stress upon the leaflets (▶ Fig. 16.9).

Chordae Tendineae

The chordae tendineae (tendinous chords) connect the PMs and the ventricular wall to MV leaflets. They arise from the tip of PMs or the ventricular wall and split in numerous branches interconnected to each other in a complex mesh that ensures balanced distribution of mechanical forces.[6] The chordae inserting on the lateral half of both leaflets arise from the anterolateral PM, while the chordae inserting on the medial half originate from the posteromedial PM. One classification divides the chordae into *first, second, and third order* based on their insertion point on the leaflets. The *first-order* chordae or *marginal chordae* are stiff and less extensible cord inserting on the free edges of leaflets (▶ Fig. 16.10, ▶ Fig. 16.11, ▶ Fig. 16.12). Commissural chordae and cleft chordae are subcategories of first-order chordae. Rupture of these chordae almost always causes leaflet prolapse and mitral regurgitation. The second-order chordate are larger, elastic, and fewer in number that insert on the ventricular surface of the anterior leaflet at the confine between the rough and clear zones

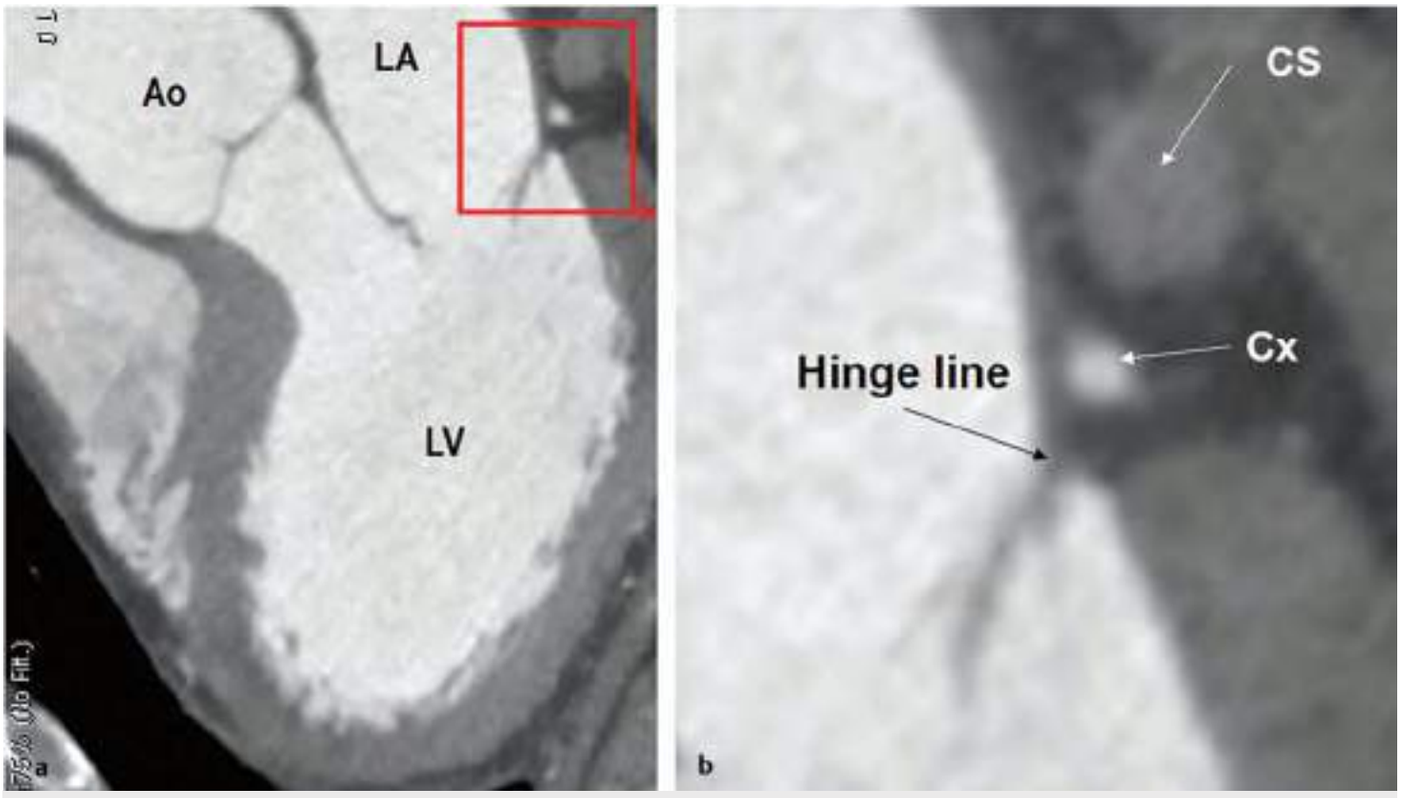

Fig. 16.5 **(a)** CT images in long-axis view. The red square delimits the area of the posterior annulus hinge line, which is magnified in **(b)**. The hinge line of the posterior leaflet is close to the posterior atrioventricular groove where the circumflex coronary artery (Cx) and the coronary sinus (CS) are located. Because of their proximity with the posterior annulus, the sutures may damage these vessels during mitral valve replacement. Ao, aorta; LV, left ventricle; LA, left atrium.

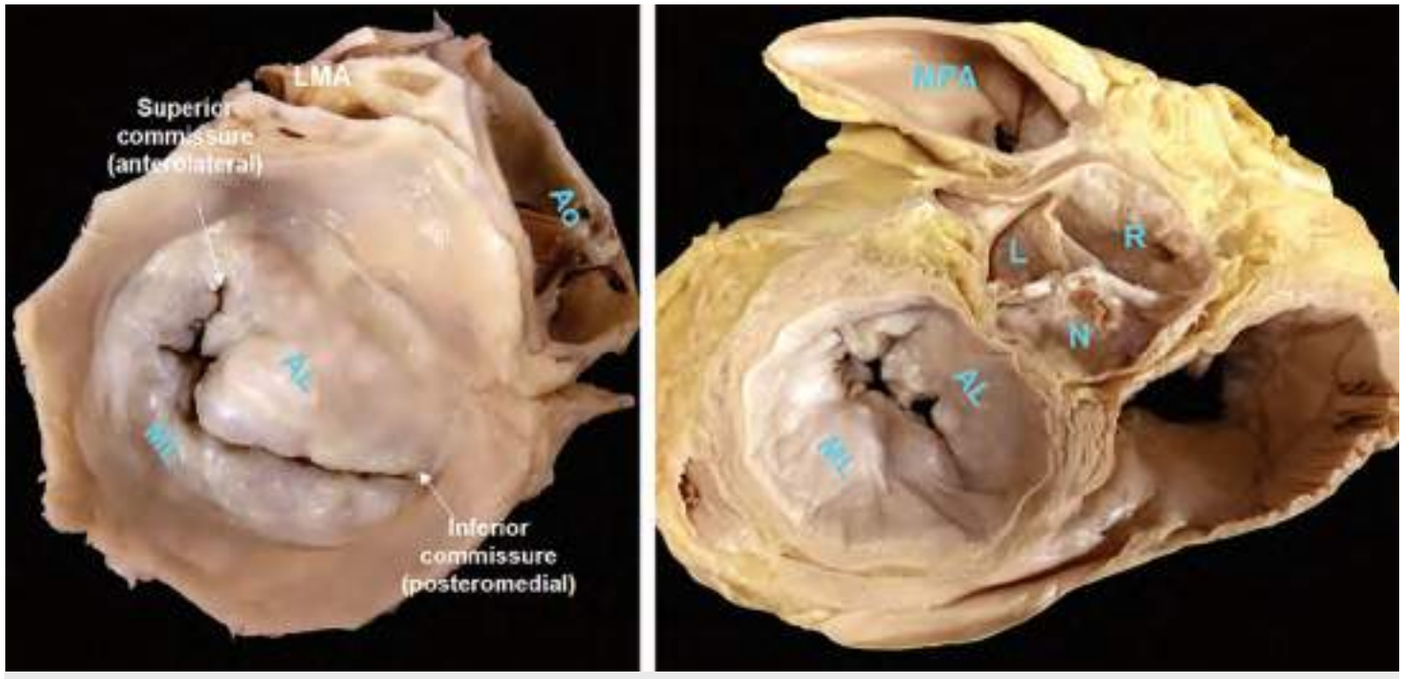

Fig. 16.6 Atrial (superior) views of the mitral valve in closed position showing the leaflets of the mitral valve and relation to the aortic valve. Ao, aorta; AL, aortic (anterior) leaflet; ML, mural (posterior) leaflet; L, left coronary sinus; N, nonfacing coronary sinus; LMA, left main artery; MPA, main pulmonary artery; R, right coronary sinus.

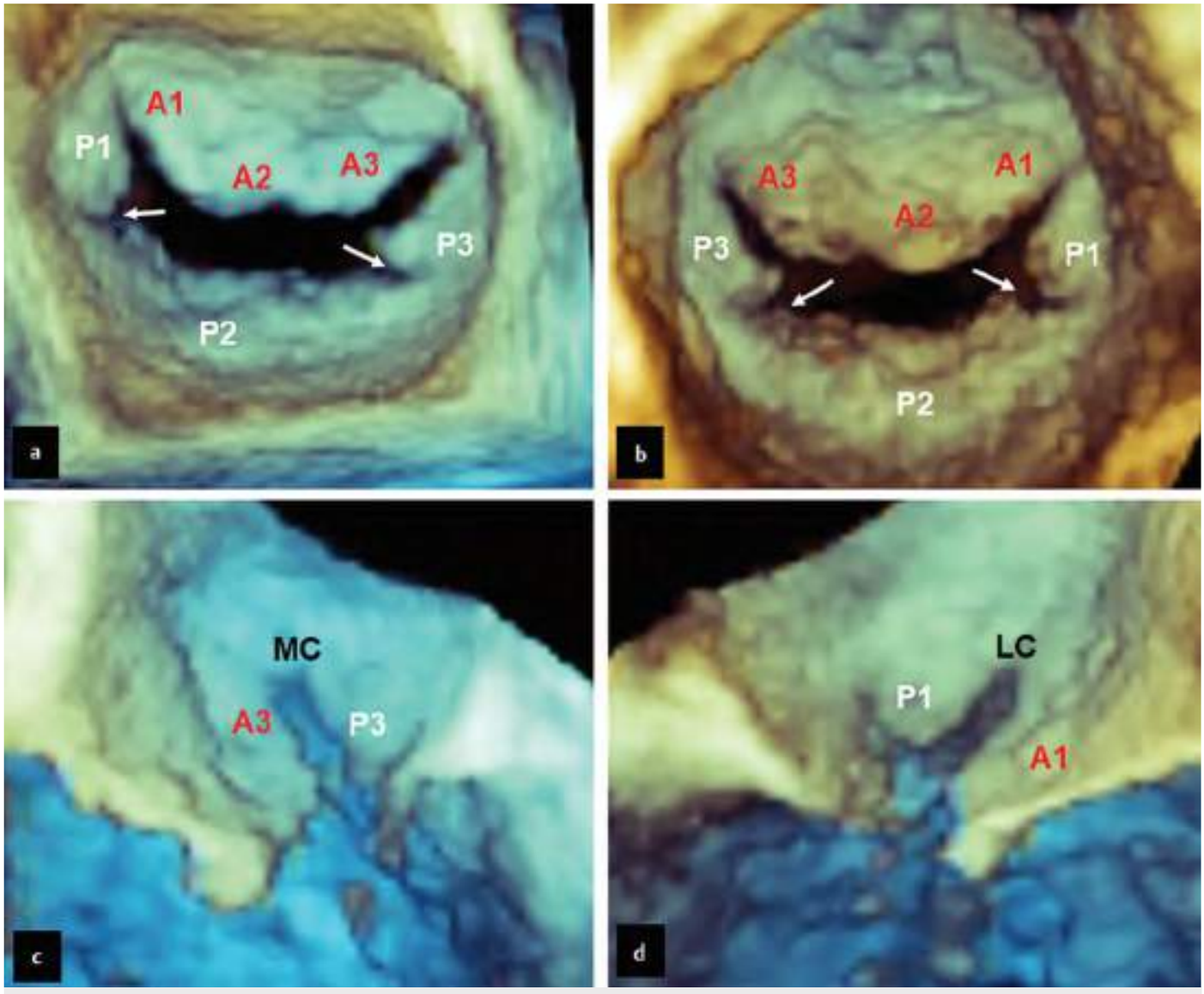

Fig. 16.7 Three-dimensional images of mitral valve from **(a)** atrial and **(b)** ventricular perspective. Two incisures (*arrows*) divide the posterior leaflet into P1, P2, and P3 scallops. The anterior leaflet has no incisure but the segments apposed P1, P2, and P3 take the name of A1, A2, and A3, respectively. Magnified image from a **(c)** medial and **(d)** lateral perspective showing the medial (MC) and lateral (LC) commissures.

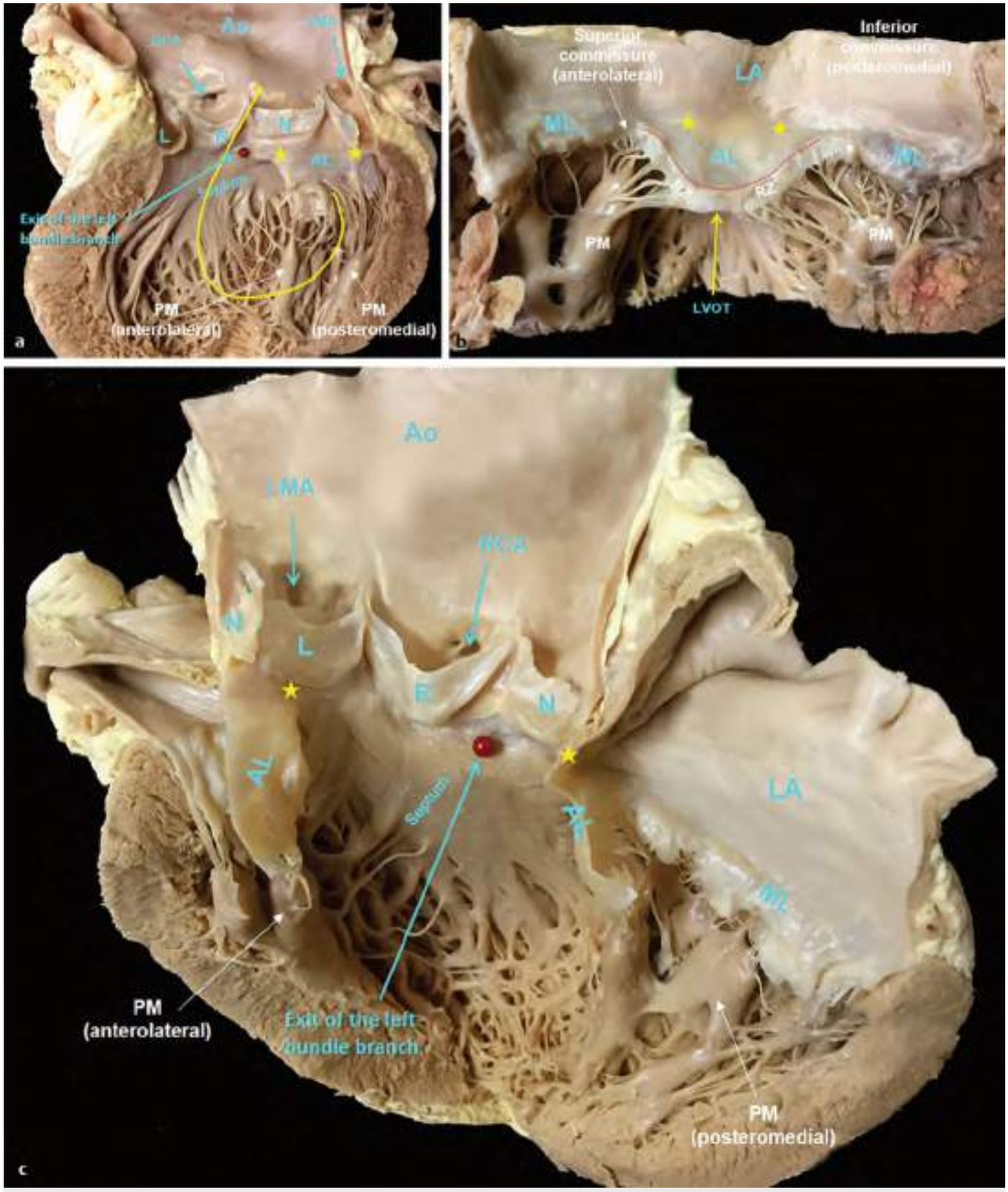

Fig. 16.8 **(a)** Opened view of the left ventricular outflow tract (LVOT) showing the ventricular surface of the aortic leaflet (AL). **(b)** Opened view of the left ventricular inflow tract (LVIT) showing the atrial surface of the mitral valve. The aortic leaflet (AL) forms the posterior wall of the LVOT. The chordae arising from each papillary muscles (PM) insert on both the mural and aortic leaflets of the mitral valve. The boundary of the rough zone (RZ) is shown by dotted red line. Direction of blood flow is shown by yellow arrows. Yellow stars show approximate location of the fibrous trigones. **(c)** Inlet/outlet view of the left heart. The aortic leaflet of the mitral valve is dissected longitudinally and continued along the noncoronary sinus into the aorta. Ao, aorta; AL, aortic (anterior) leaflet; ML, mural (posterior) leaflet; L, left coronary sinus; N, nonfacing coronary sinus; LMA, left main artery; MPA, main pulmonary artery; PM, papillary muscle; R, right coronary sinus; RCA, right coronary sinus.

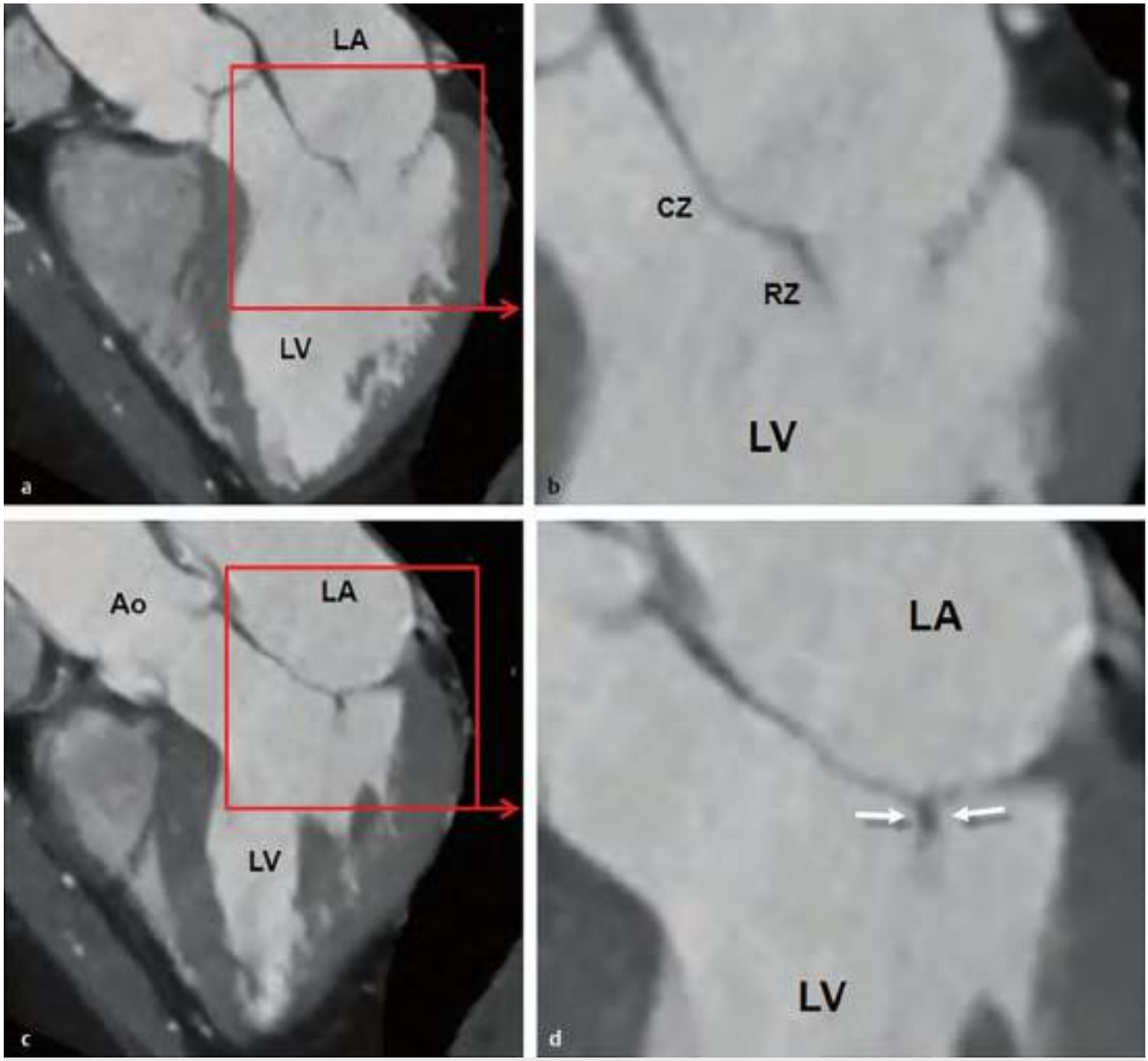

Fig. 16.9 CT image in long-axis view with focal magnification during **(a, b)** diastole and **(c, d)** systole. The anterior leaflet is divided into the rough (RZ) and clear (CZ) zones. The rough zone covers the distal surface of both leaflets and receives the insertions of chordae tendineae. The coaptation surface (*arrows*) in **(d)** is the area where leaflets juxtapose each other during systole. Ao, aorta; LV, left ventricle; LA, left atrium.

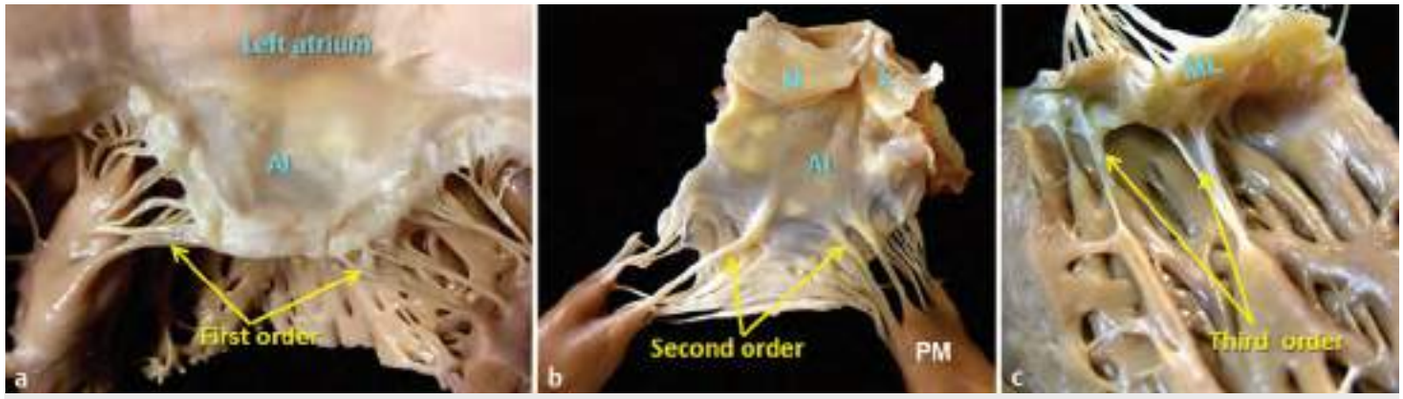

Fig. 16.10 Classification of the chordae tendineae. **(a)** Aerial surface of the AL. First-order (marginal) cords are essential for leaflet coaptation. **(b)** Aortic (ventricular) surface of the AL showing the second-order cords inserting on the body of anterior leaflet at the border between the rough and clear zones. Second-order cords of the rough zone cords are essential for maintaining leaflet geometry. Also shown in this view is the aortomitral fibrous curtain. **(c)** Third-order cords originate from the ventricular trabeculae and insert only on the mural leaflet. AL, aortic (anterior) leaflet; ML, mural (posterior) leaflet; L, left coronary sinus; N, nonfacing coronary sinus; PM, papillary muscle.

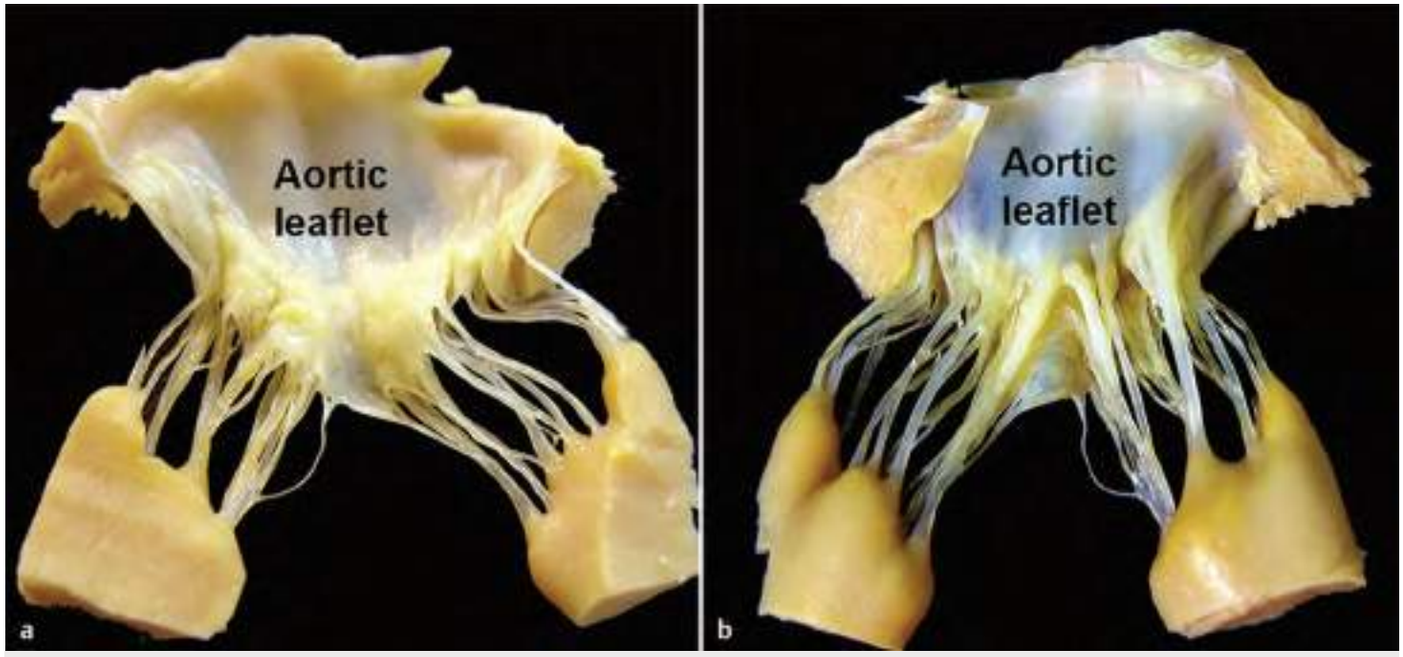

Fig. 16.11 Close-up views of the **(a)** atrial and **(b)** ventricular surfaces of the aortic leaflet of the mitral valve with detail of the chordae tendineae.

and often include two "*strut chordate*." Their function is to prevent the leaflets from eversion. Furthermore, with reducing the motion at the peripheral part of anterior leaflet, the strut cords help the central part of the anterior leaflet to remain mobile. Thus, in systole the anterior leaflet takes a concave shape toward the outflow tract, while in diastole it bulges toward the inflow tract. This configuration facilitates blood outflow into the aorta during systole or blood inflow into left ventricle during diastole. Moreover, strut cords provide a fibrous continuity between the leaflet and the ventricular wall, supporting the contraction of longitudinal fibers of left ventricle and maintain left ventricular geometry.[8] Second-order chordal transposition has been used to correct anterior MV leaflet prolapse.[9] *The third-order chordae* or *basal chordae* originate directly from the ventricular wall and insert only on the posterior leaflet. These chordae limit the motion of the posterior leaflet (▶ Fig. 16.10).

Papillary Muscles

The PMs originate, as a single entity or a group of two to three "papillae," from the distal third of the ventricular wall in the posterior medial and anterior lateral positions. The function of PMs is to provide support to mitral leaflets during the cardiac contractions. Indeed, in the body of PMs, the muscular fibers are organized in a longitudinal fashion resulting in a prevalent shortening of the long axis of PMs during the ventricular ejection. Because the length of chordae tendineae remains unchanged during the cardiac cycle, without normal contraction of PMs, the longitudinal shortening of the left ventricle would result in a prolapse of the leaflets (which actually occurs in the so-called PM dysfunction). It is important to know that the PMs do not attach directly on the compact myocardium. Instead a network of muscular trabeculae is located between the base of the PMs and the

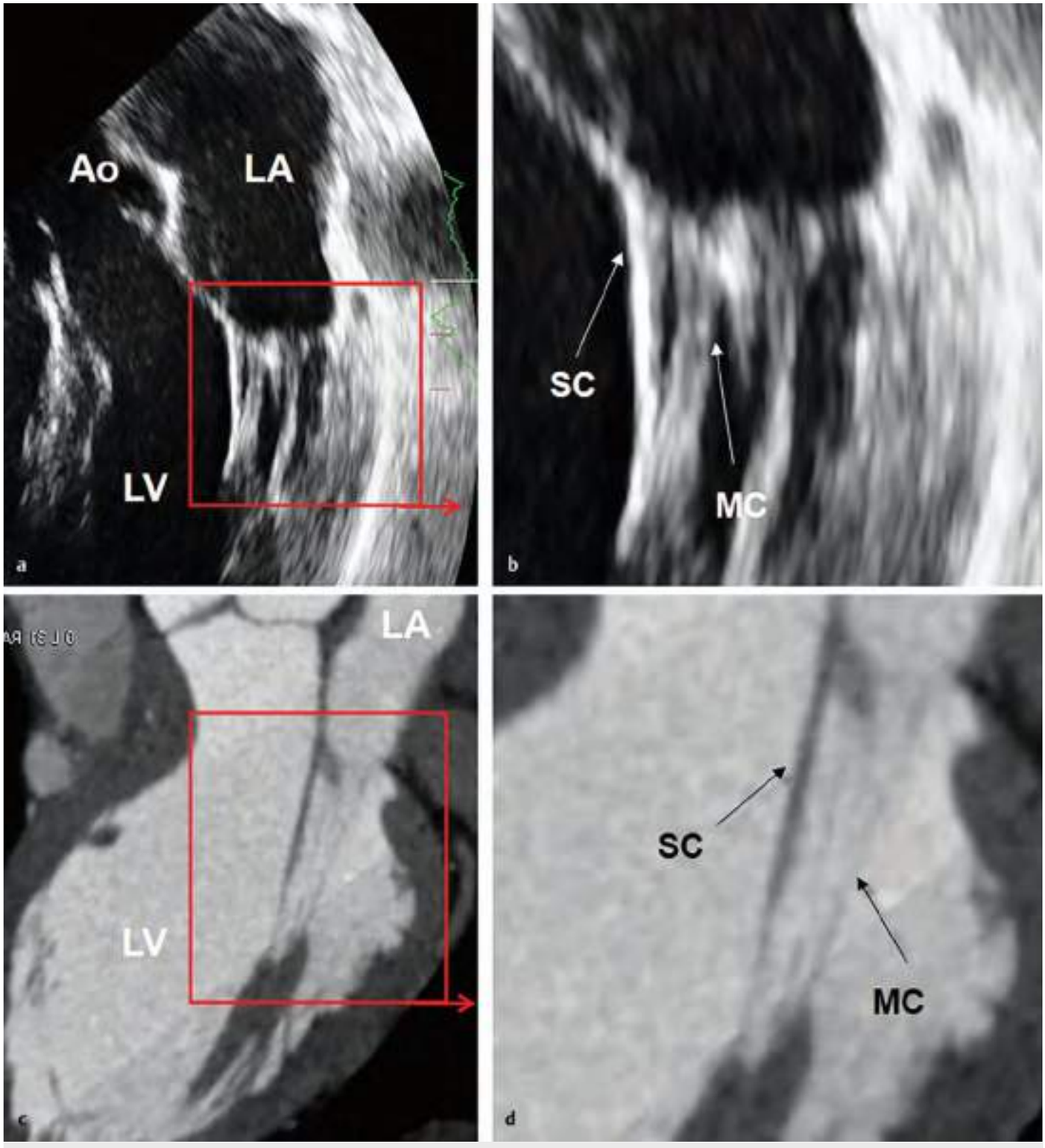

Fig. 16.12 (a, b) 2D transthoracic echocardiographic and **(c, d)** CT images in long-axis view with focal magnification. Arrows point at the strut chordae (SCs) and the marginal chordae (MC). The SCs are particularly thick and insert on the body of anterior leaflet at the border between the rough and clear zones. Ao, aorta; LV, left ventricle; LA, left atrium.

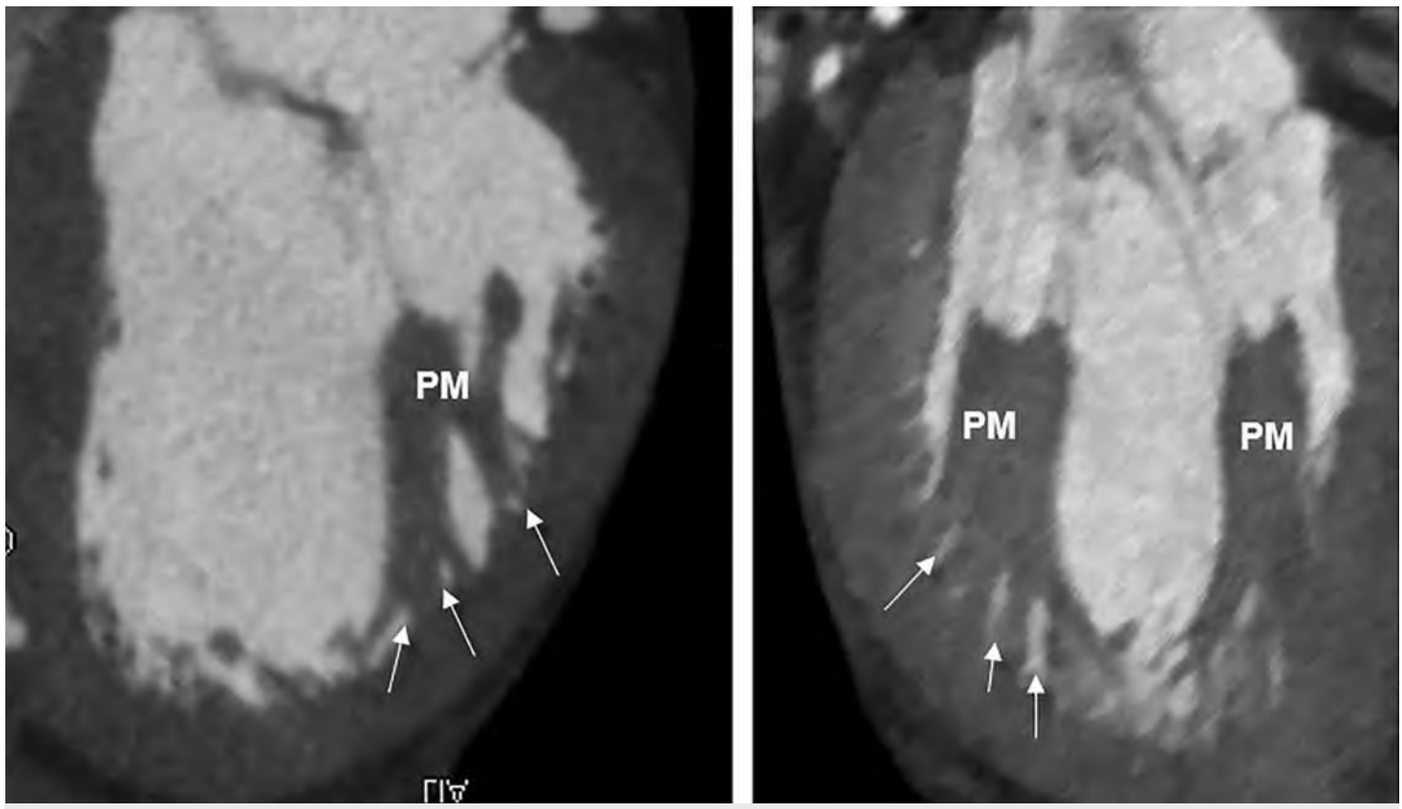

Fig. 16.13 CT images showing papillary muscles (PMs) taking origin from a trabecular muscle network intervened between the PMs and the compact myocardium. The advantages of such architecture are a more homogeneous distribution of the mechanical stress.

ventricular wall. With this anatomical arrangement, described for the first time by Axel,[10] the mechanical stress distributes more homogeneously on the trabecular network rather being concentrated on a single area of the left ventricle (▶ Fig. 16.13).

◆ Anatomical Variant

The posterior leaflet of MV may demonstrate variable morphologies. A common variant is the number of scallops. It is not yet clear how deep the incisures on posterior leaflet should be to call the valve tissue between the two incisures a scallop. Surgeons call it "scallop" when the incisures on posterior leaflet are deeper than one-half of the distance between the free margin and the insertion of the leaflet on the annulus. The significance of a scallop also is not clear. It is not rare to find a perfectly functioning MV with no evidence incisures or a perfectly competent valve with more than three scallops on the posterior leaflet. The free margin of the anterior leaflet is usually devoid of incisures, although in some cases it is not uncommon to observe irregularity or even small incisures (▶ Fig. 16.14).

◆ Common Pathologies

Mitral Valve Regurgitation

In the MV regurgitation, a variable amount of blood reflows from left ventricle to left atrium in systole. The causes of MV regurgitation are divided into two main categories: organic (OMR) and functional mitral regurgitation (FMR). In the OMR insufficiency, causes of regurgitation are a morphological change of one or more component of MV apparatus. Myxomatous or fibroelastic degeneration (FED) of leaflet tissue, calcification of mitral annulus (CMA), rheumatic disease, and bacterial endocarditis are the most common causes for OMR. FMR is described in a morphologically normal valve (even though this is not completely true) with the insufficiency due to a geometrical distortion of the left ventricle with which the valve is intimately connected. Echocardiography is the first-line diagnostic technique before MV surgery. In select cases, both magnetic resonance imaging (MRI) and CT may help in defining valve morphology.

Organic Mitral Insufficiency

In western countries, degenerative changes of mitral leaflets are the most common cause of OMR. Three types of degenerative changes may cause valve regurgitation: calcification of the annulus, myxomatous valve (or Barlow's disease), and FED.[11]

Calcification of Mitral Annulus

CMA affects elderly people (particularly women)[12] (▶ Fig. 16.15). The etiology is not clear. Since it occurs in older age, it is likely that a phenomenon connected with hydraulic stress may have a role. Hypertension, renal insufficiency, and diabetes may accelerate the process. Calcification often affects the posterior part of the annulus and only in advance cases it extends on the anterior part. When limited to the outline of the annulus, CMA is a benign condition, causing mild regurgitation due to the lack of sphincter

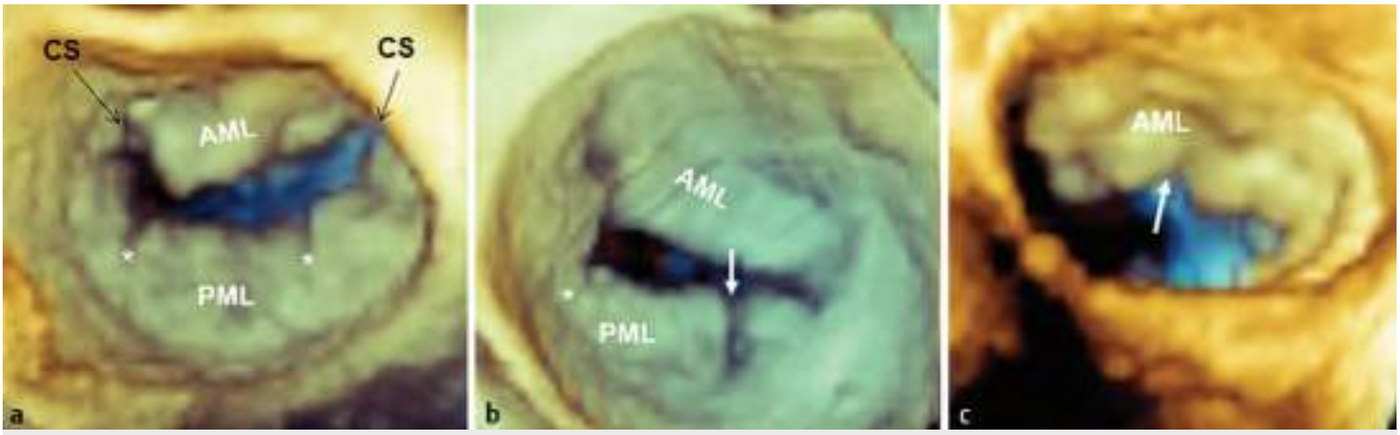

Fig. 16.14 Three-dimensional transesophageal echocardiographic images of mitral valve seen from overhead in three different cases. **(a)** The posterior mitral leaflet (PML) has two small incisures extending less than half of the distance between the free margin and the hinge line. Additionally, two small scallops are seen near the commissures (CS). **(b)** This mitral valve presents a posterior leaflet with a small incisure (*asterisk*) laterally and a deep cleft (*arrow*) medially. **(c)** This valve presents a small incisure in the middle of the anterior mitral leaflet (AML).

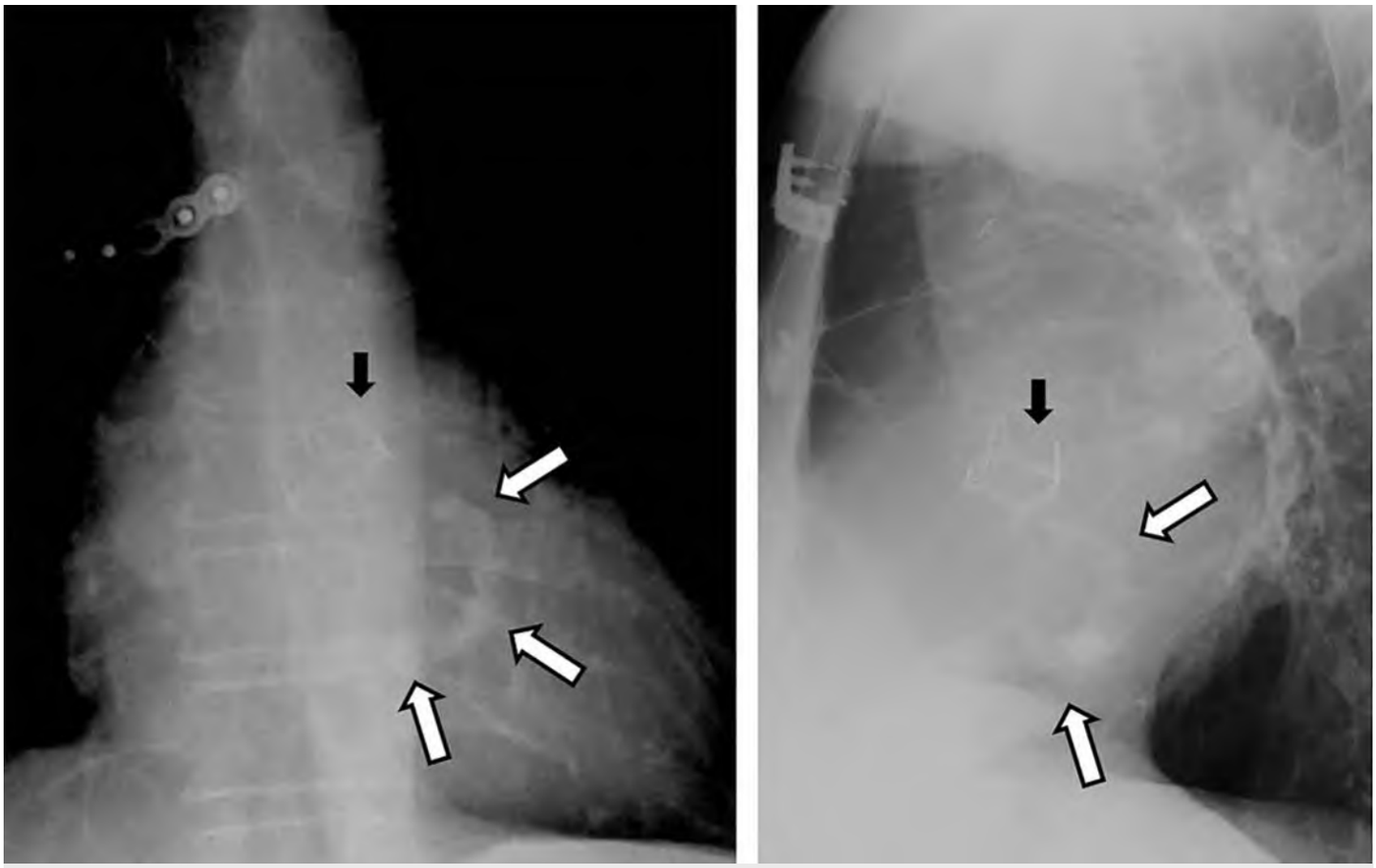

Fig. 16.15 Posteroanterior and lateral chest X-rays showing a calcified mitral ring involving the posterolateral margin (*white arrows*) of the annulus. The anterior margin facing aortomitral fibrous continuity is not calcified and any observed calcification in this area is in the leaflet not the annulus. Status postaortic valve replacement (*black arrows*).

action of the normal annulus. However, when calcifications extend on the body of the leaflets, significant mitral regurgitation, stenosis, or both conditions may occur. In these cases, calcifications may also infiltrate the ventricular myocardium (▶ Fig. 16.16). Large calcified masses may have a central "liquefaction." This variant is known as "caseous calcification" because the central part has a "toothpaste" consistency[13]

Myxomatous Degeneration

Myxomatous degeneration of MV may present with a spectrum of morphological changes ranging from a simple prolapse or flail of a single segment (FED) in an otherwise normal-sized valve to a multi-scallop prolapse (myxomatous valve or Barlow's disease) (▶ Fig. 16.17, ▶ Fig. 16.18).

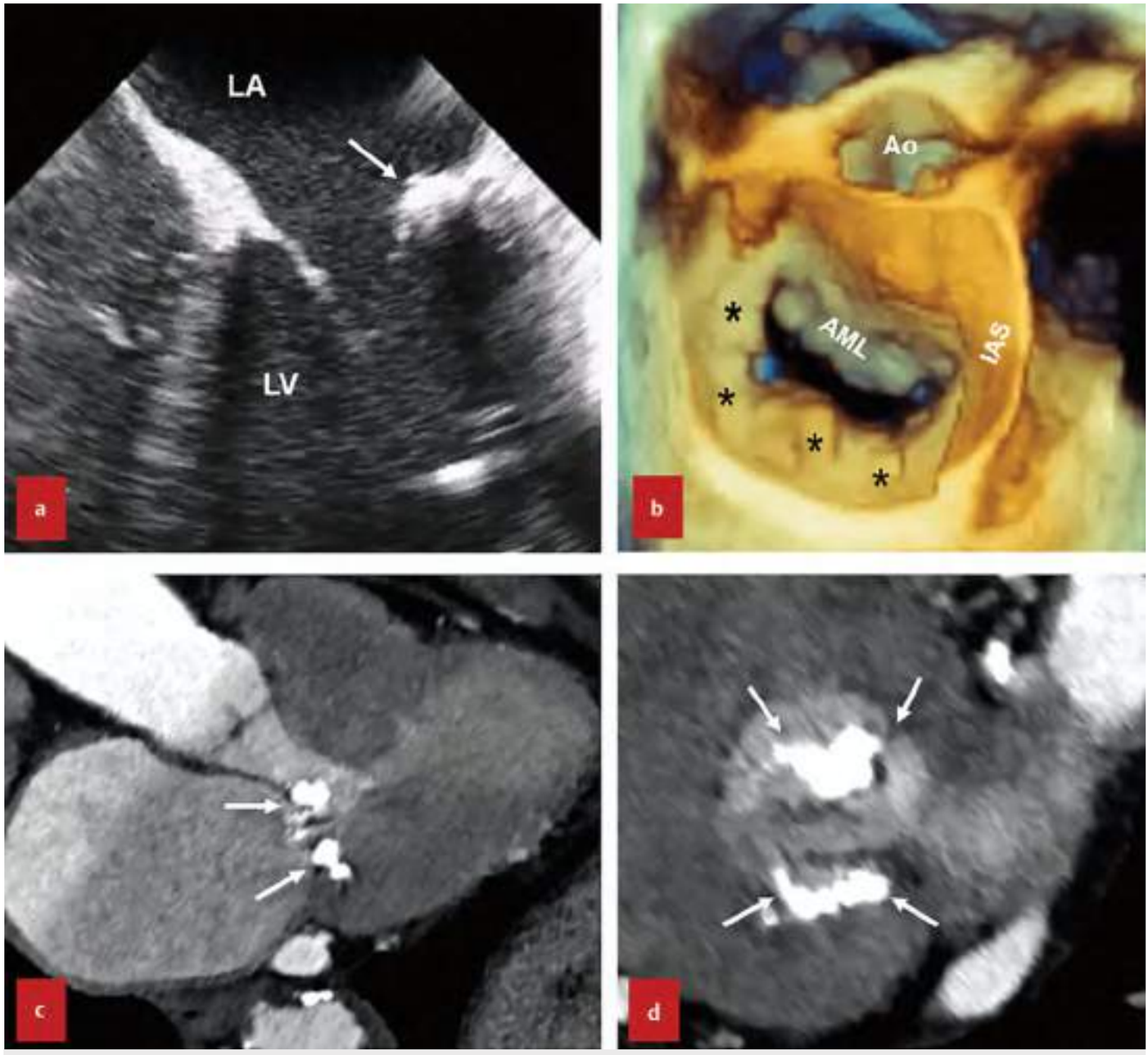

Fig. 16.16 (a, b) Extensive calcifications of mitral posterior annulus visualized in 2D transesophageal echocardiography (2D TEE; *arrow*) and 3D transesophageal echocardiography (3D TEE; *asterisks*). This latter modality allows a better perception of the extension of calcifications. Note as in 2D TEE calcifications assume a brighter aspect in comparison with surrounding structures, allows a kind of tissue characterization while in 3D TEE different shades of color are used to define the depth of the structure rather than its tissue characterization. Thus, different structures such as calcium and soft tissue have the same shades of color if sited at the same depth in respect to the transducer. **(c)** Two-chamber CT view of the left heart and **(d)** short-axis CT view of the mitral valve showing extensive calcifications (*arrows*) involving both the posterior mitral annulus and the anterior leaflet. Ao, aorta; AML, anterior mitral leaflet; IAS, interatrial septum; LA, left atrium; LV, left ventricle.

The macroscopic aspect of a *Barlow's disease* is that of a valve with large and thickened leaflets, annular dilation, and thickening and lengthening chordae tendineae[11] (▶ Fig. 16.17).

The *FED* has gross and microscopic features opposite to that of myxomatous degeneration. In this condition, the leaflets become thinner than the normal with a translucent appearance and the chordae become fragile. FED predisposes the valve to chordal rupture and insufficiency.[11]

Bacterial Endocarditis

Bacterial endocarditis remains one of the most "malign" MV disease even in the era of sophisticated antibiotics. Usually, the infection strikes an area of already damaged endocardium (thus the term "endocarditis") for previous rheumatic disease or a congenital lesion.[14]

The classic finding of bacterial endocarditis is the "*vegetation*," an inflammatory mass of variable size protruding from the atrial

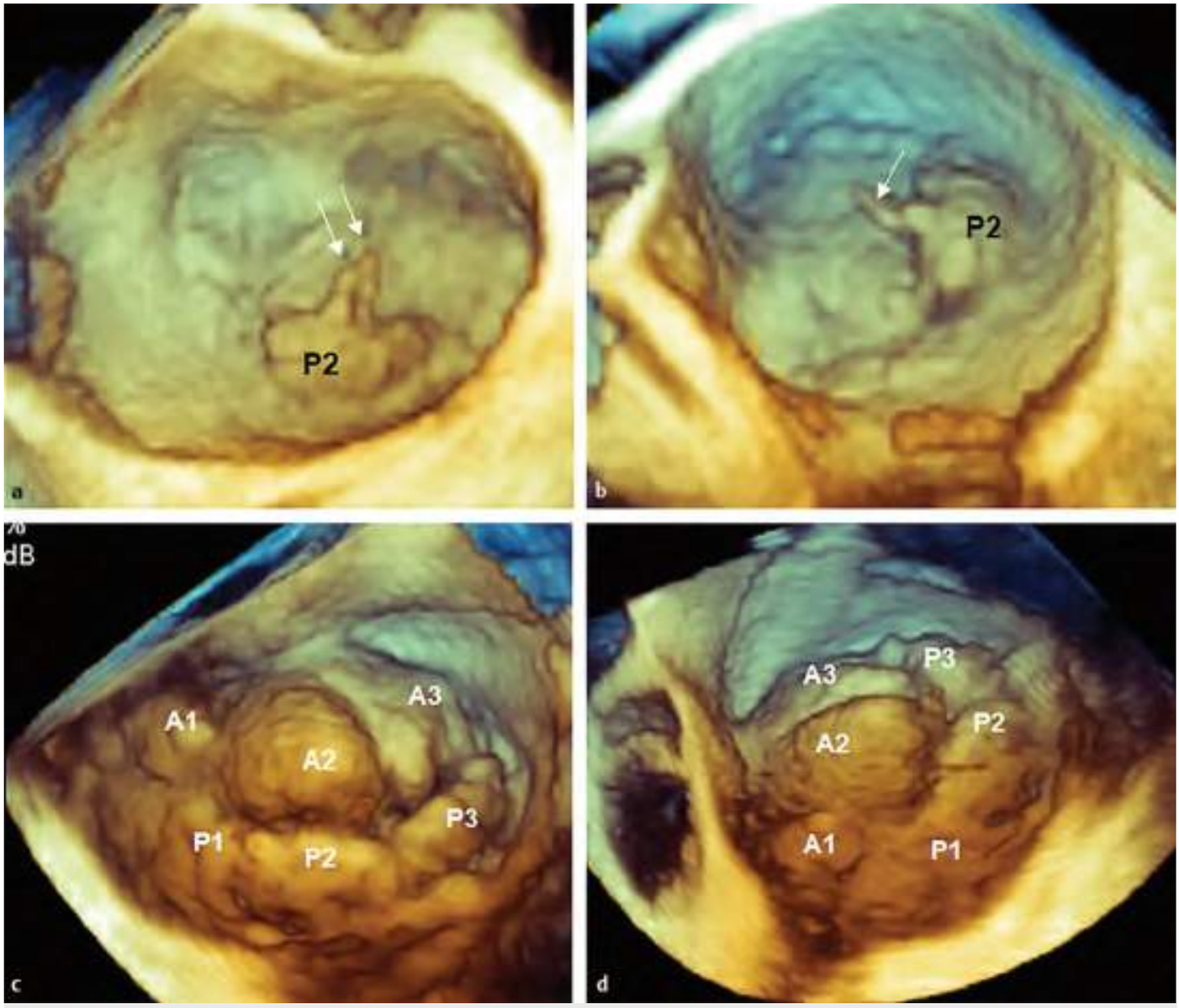

Fig. 16.17 Mitral prolapse. 3D TEE images of flail of a single P2 scallop of posterior leaflet with two ruptured chordae (*arrows*) in **(a)** overhead or surgical and in **(b)** lateral perspective in a valve with fibroelastic deficiency. **(c, d)** 3D TEE image of a Barlow's disease in **(c)** overhead or surgical and in **(b)** lateral perspective showing the multiscallop prolapse of the valve due to myxomatous degeneration.

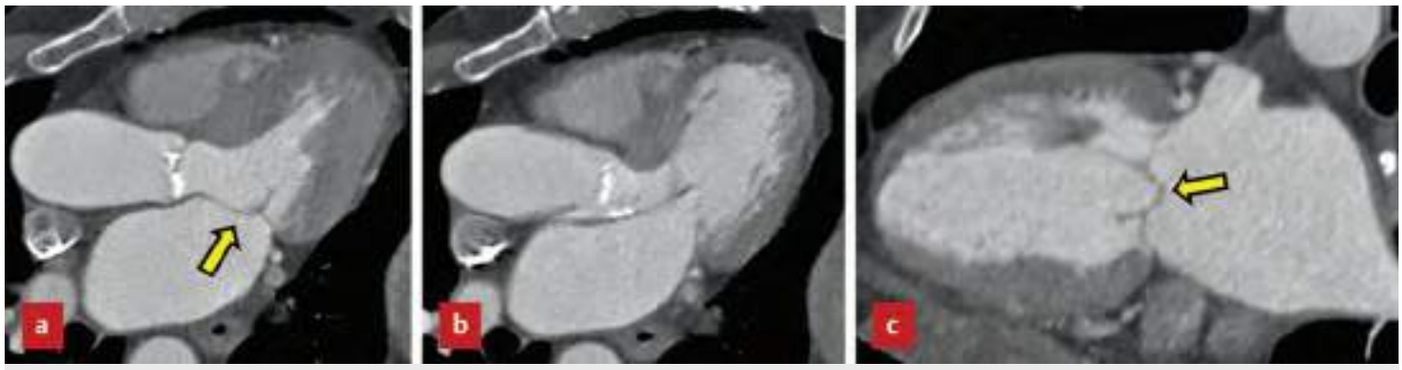

Fig. 16.18 CT of the heart showing prolapse of the midsegment of the anterior mitral leaflet. **(a)** Three-chamber views in systole. **(b)** Three-chamber views in diastole. **(c)** Two chambers of the left heart. The aortic valve leaflets are moderately calcified.

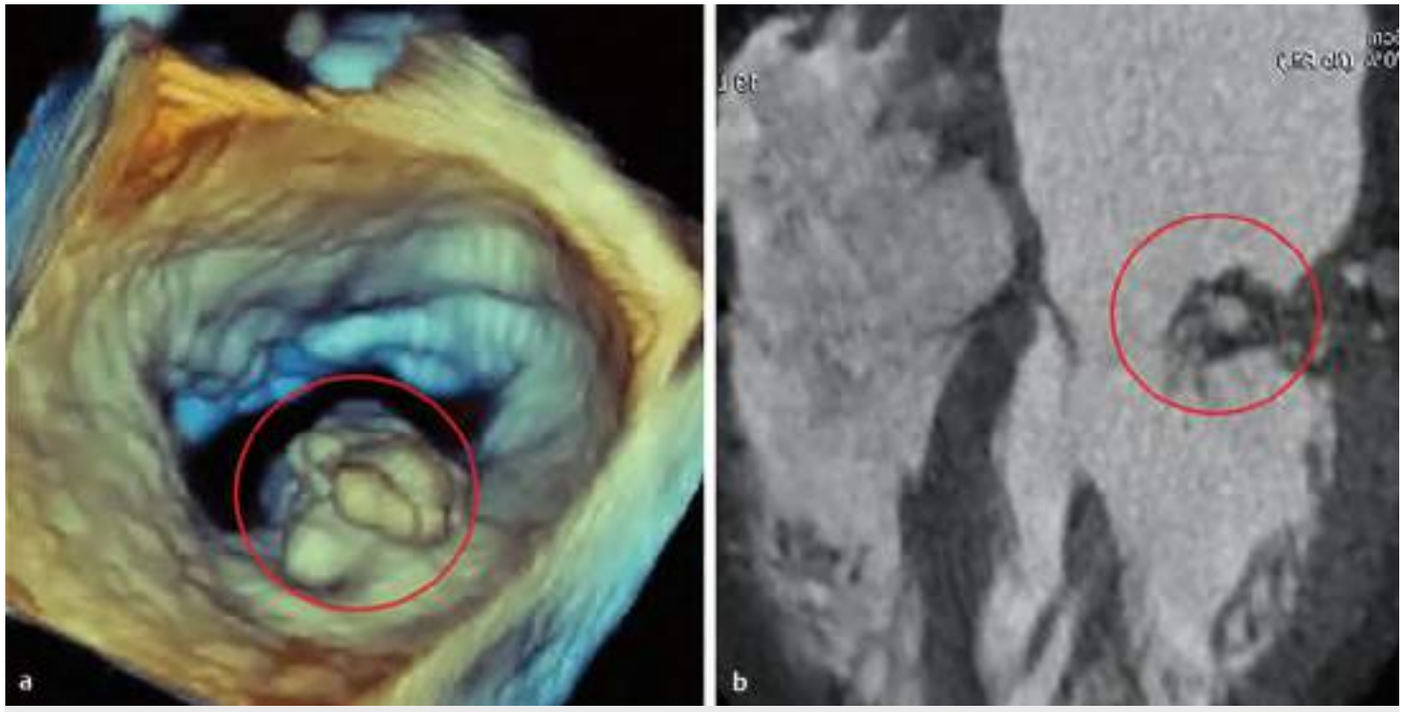

Fig. 16.19 Large vegetation (*within circles*) involving the posterior mitral leaflet shown in **(a)**. 3D TEE and **(b)** four-chamber CT angiography. A diagnosis of endocarditis was made by clinical and laboratory criteria.

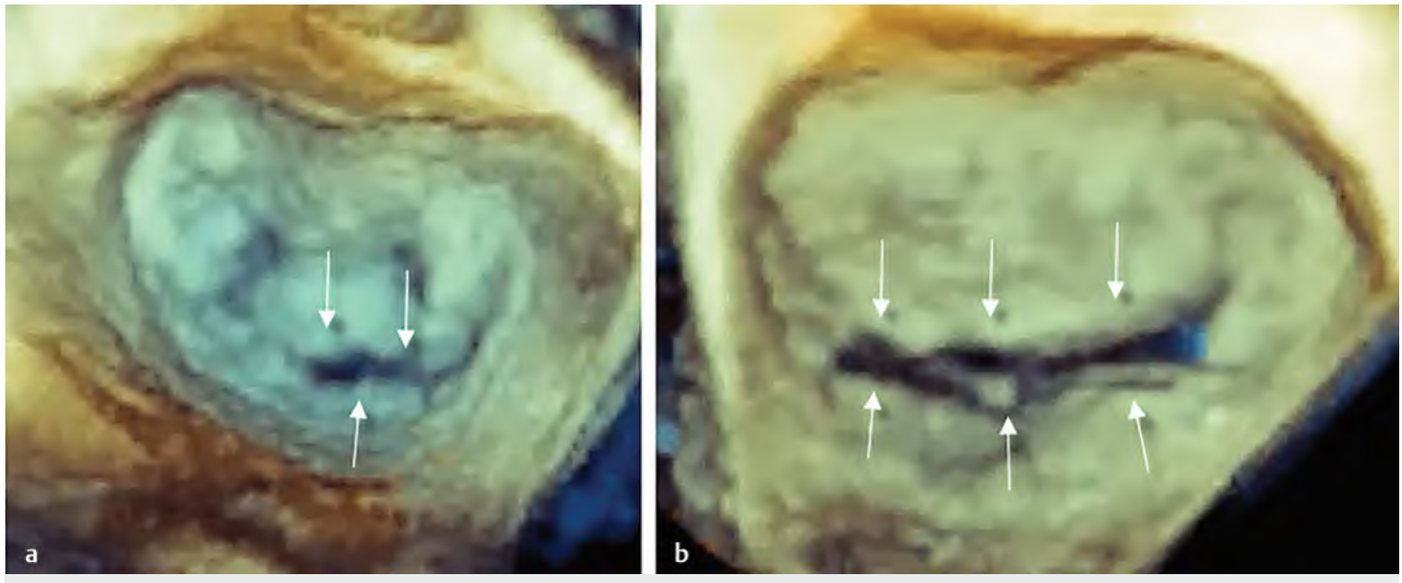

Fig. 16.20 Functional mitral regurgitation. **(a)** 3D TEE image of the mitral showing "asymmetrical" tethering due to inferior–posterior myocardial infarction. Tethering of medial half of the mitral leaflets due to systolic outward motion of the posterior left ventricular wall results in a rather asymmetric regurgitant orifice (*arrows*). **(b)** 3D TEE image showing "symmetrical" tethering due to a global left ventricular dilation. In this case the tether affects the entire line of leaflet coaptation (*arrows*), causing a more "symmetric" linear regurgitant orifice. The valves are seen from an overhead perspective in systole.

surface of the mitral leaflet. Valve insufficiency may originate by rupture of chordae, leaflet perforation or erosion of free margins, or by the presence of vegetation itself, which disrupt the normal coaptation (▶ Fig. 16.19).

Functional Mitral Regurgitation

FMR is secondary to either regional myocardial dysfunction (mainly in posterolateral infarction of the left ventricle) or global left ventricular enlargement. In posterolateral infarction, FMR is due to "asymmetrical" traction of the medial half of anterior and posterior leaflets due to dysfunction of the posterior medial PMs and myocardial wall. As a result, the regurgitant jet is usually directed posteriorly. In global dilation of the left ventricle enlargement of the mitral annulus along with displacement of both PMs result in tethering of both leaflets and entire mitral orifice becomes regurgitant (▶ Fig. 16.20).

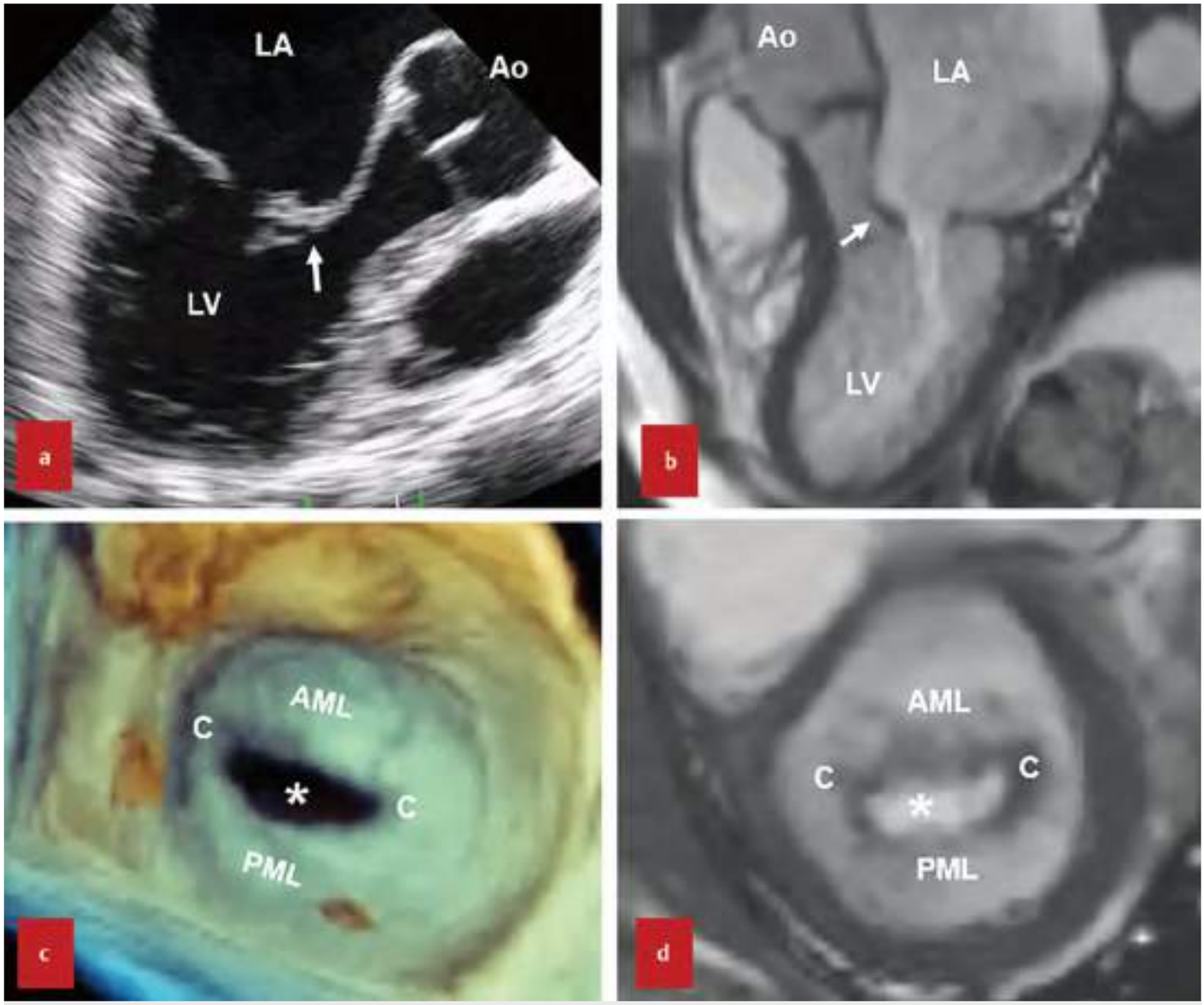

Fig. 16.21 Mitral stenosis. **(a)** 2D TEE imaging and **(b)** cardiac MR in long-axis view of the left heart in a patient with mitral stenosis showing doming of anterior leaflet (*arrows*). **(c)** 3D TEE and **(d)** cardiac MR short-axis views of mitral stenosis showing residual valve area (*asterisk*) and fused commissures **(c)**. Ao, aorta; AML, anterior mitral leaflet; LA, left atrium; LV, left ventricle; PML, posterior mitral leaflet.

Mitral Valve Stenosis

Rheumatic MV stenosis is a late complication of rheumatic fever.[15] The fundamental pathophysiological derangement in mitral stenosis (MS) is incomplete left ventricular filling due to commissural fusion, rigidity, and calcification of leaflets combined with fusion and shortening of chordae tendineae and PMs. Imaging is performed to assess the severity of MS and to show morphological changes such as doming (hockey stick appearance) of the anterior mitral leaflet and commissural fusion (symmetric or asymmetric) (▶ Fig. 16.21). Prognostic parameters including residual valve area, mean diastolic gradient between left ventricle and left atrium, and pulmonary pressure will be measured.

References

[1] Perloff JK, Roberts WC. The mitral apparatus. Functional anatomy of mitral regurgitation. Circulation.; 46(2):227–239

[2] Angelini A, Ho SY, Anderson RH, Davies MJ, Becker AE. A histological study of the atrioventricular junction in hearts with normal and prolapsed leaflets of the mitral valve. Br Heart J.; 59(6):712–716

[3] Levine RA, Triulzi MO, Harrigan P, Weyman AE. The relationship of mitral annular shape to the diagnosis of mitral valve prolapse. Circulation.; 75 (4):756–767

[4] Salgo IS, Gorman JH, III, Gorman RC, et al. Effect of annular shape on leaflet curvature in reducing mitral leaflet stress. Circulation.; 106(6):711–717

[5] Padala M, Hutchison RA, Croft LR, et al. Saddle shape of the mitral annulus reduces systolic strains on the P2 segment of the posterior mitral leaflet. Ann Thorac Surg.; 88(5):1499–1504

[6] Ho SY. Anatomy of the mitral valve. Heart.; 88 Suppl 4:iv5–iv10

[7] Carpentier A. Cardiac valve surgery—the "French correction". J Thorac Cardiovasc Surg.; 86(3):323–337

[8] Nielsen SL, Timek TA, Green GR, et al. Influence of anterior mitral leaflet second-order chordae tendineae on left ventricular systolic function. Circulation.; 108(4):486–491

[9] Sousa Uva M, Grare P, Jebara V, et al. Transposition of chordae in mitral valve repair. Mid-term results. Circulation.; 88(5 Pt 2) suppl II:II35–II38

[10] Axel L. Papillary muscles do not attach directly to the solid heart wall. Circulation.; 109(25):3145–3148

[11] Adams DH, Rosenhek R, Falk V. Degenerative mitral valve regurgitation: best practice revolution. Eur Heart J.; 31(16):1958–1966

[12] Fulkerson PK, Beaver BM, Auseon JC, Graber HL. Calcification of the mitral annulus: etiology, clinical associations, complications and therapy. Am J Med.; 66(6):967–977

[13] Gramenzi S, Mazzola AA, Tagliaferri B, et al. Caseous calcification of the mitral annulus: unusual case of spontaneous resolution. Echocardiography.; 22 (6):510–513

[14] Cabell CH, Abrutyn E, Karchmer AW. Cardiology patient page. Bacterial endocarditis: the disease, treatment, and prevention. Circulation.; 107(20):e185–e187

[15] Carabello BA. Modern management of mitral stenosis. Circulation.; 112 (3):432–437

17 The Tricuspid Valve Apparatus

Farhood Saremi

◆ Introduction

The tricuspid valve (TV) plays an important role in many pathological states and its abnormality may directly or indirectly influence the morbidity and mortality in many clinical scenarios involving the right and left heart diseases. Knowing the normal morphology of the TV apparatus is important to understand and explain the underlying pathophysiological mechanisms of the TV disorders. As an example of imaging demonstration, the three-dimensional (3D) geometry of the TV annulus in normal circumstances has helped define the mechanisms for the development of functional tricuspid regurgitation (TR), a common associated condition with mitral regurgitation, and has paved ways to improve therapy.[1]

In this chapter, imaging evaluation of the anatomy and function of the tricuspid apparatus with be reviewed. The embryology and cadaveric anatomy of the valve along with common pathological processes of the valve will be briefly discussed.

◆ Formation of the Tricuspid Valve

The formation of the valvular apparatus at the atrioventricular (AV) junction is a complex process, involving the endocardial cushions, subepicardial mesenchyme, and the myocardium, but the exact contribution of the different cell types remains controversial[1,2,3] (▶ Fig. 17.1). The septal leaflet of the TV, the aortic leaflet of the mitral valve, and the aortomitral fibrous continuity develop from the mesenchyme of the inferior and superior AV endocardial cushions.[3] The tricuspid septal leaflet then delaminates from the muscular ventricular septum late in development. The mural leaflets including the anterior and posterior leaflets of the TV and the posterior leaflet of the mitral valve primarily originate from the mesenchymal cushions that arise laterally in the AV canal after cushion fusion. The subepicardial mesenchyme and the myocardium of the AV groove also contribute to the

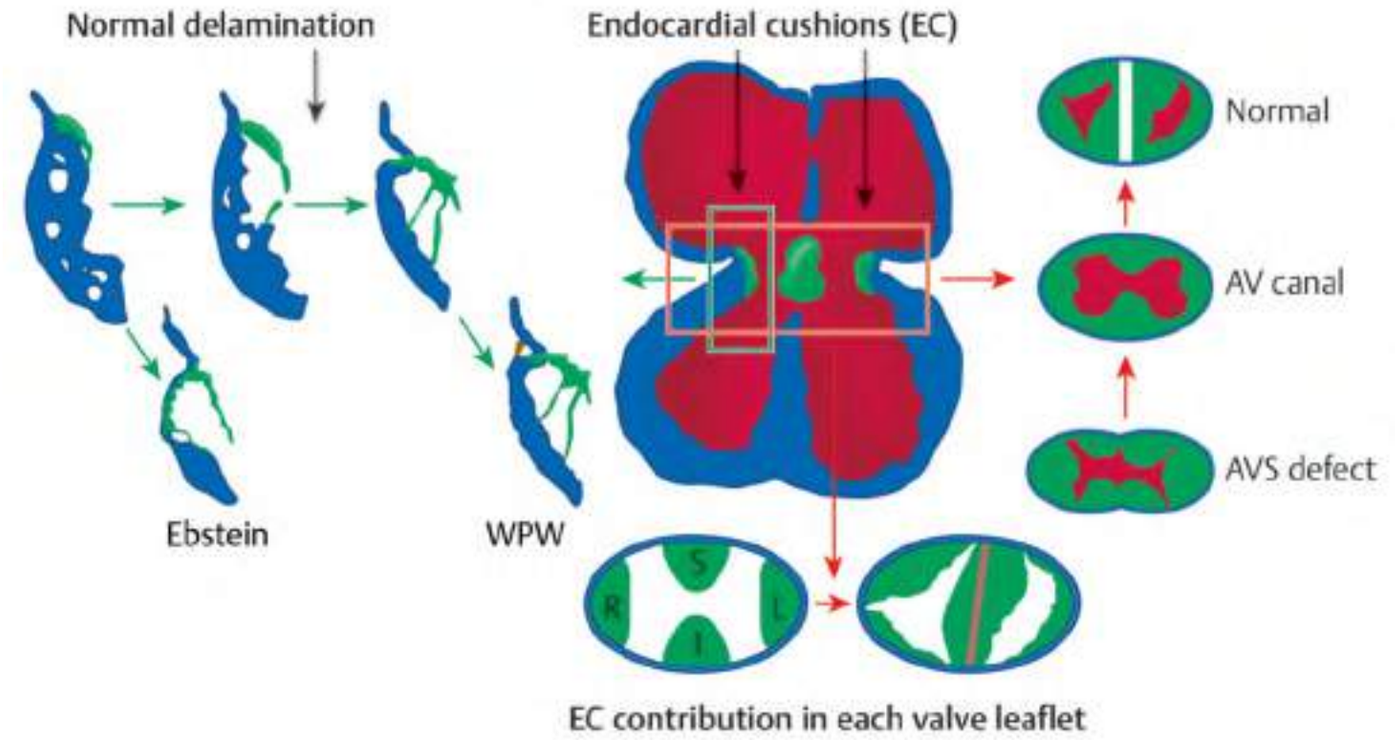

Fig. 17.1 Development of the atrioventricular (AV) valves. At 4 weeks of gestation, an endocardial cushion (EC) is formed by accumulation of the extracellular matrix (cardiac jelly) in between the endocardium and the myocardium. The ECs are subsequently cellularized by mesenchymal cells that migrate from the endocardium overlying the cushions. The septal leaflets of AV valves are derived from the fused inferior (I) and superior (S) ECs that also form the membranous septum. The septal leaflets are then delaminating from the myocardium. Failure of the superior and inferior ECs to fuse causes a "cleft" mitral valve, AV septal (AVS) defect, and ventricular septal defect. Failure of delamination can cause Ebstein's anomaly. The mural leaflets of the AV valves are derived from the right (R) and left (L) lateral ECs, subepicardial mesenchyme, and myocardium of the AV groove. The myocardial layer of the AV groove is then removed by the process of apoptosis. By the 12th week of development, the separation between the atrial and ventricular free wall myocardium is established by fusion of the AV groove tissue on the epicardial side and cushion tissue on the endocardial side. Failure of myocardial desorption in the AV groove can cause the Wolff–Parkinson–White syndrome.

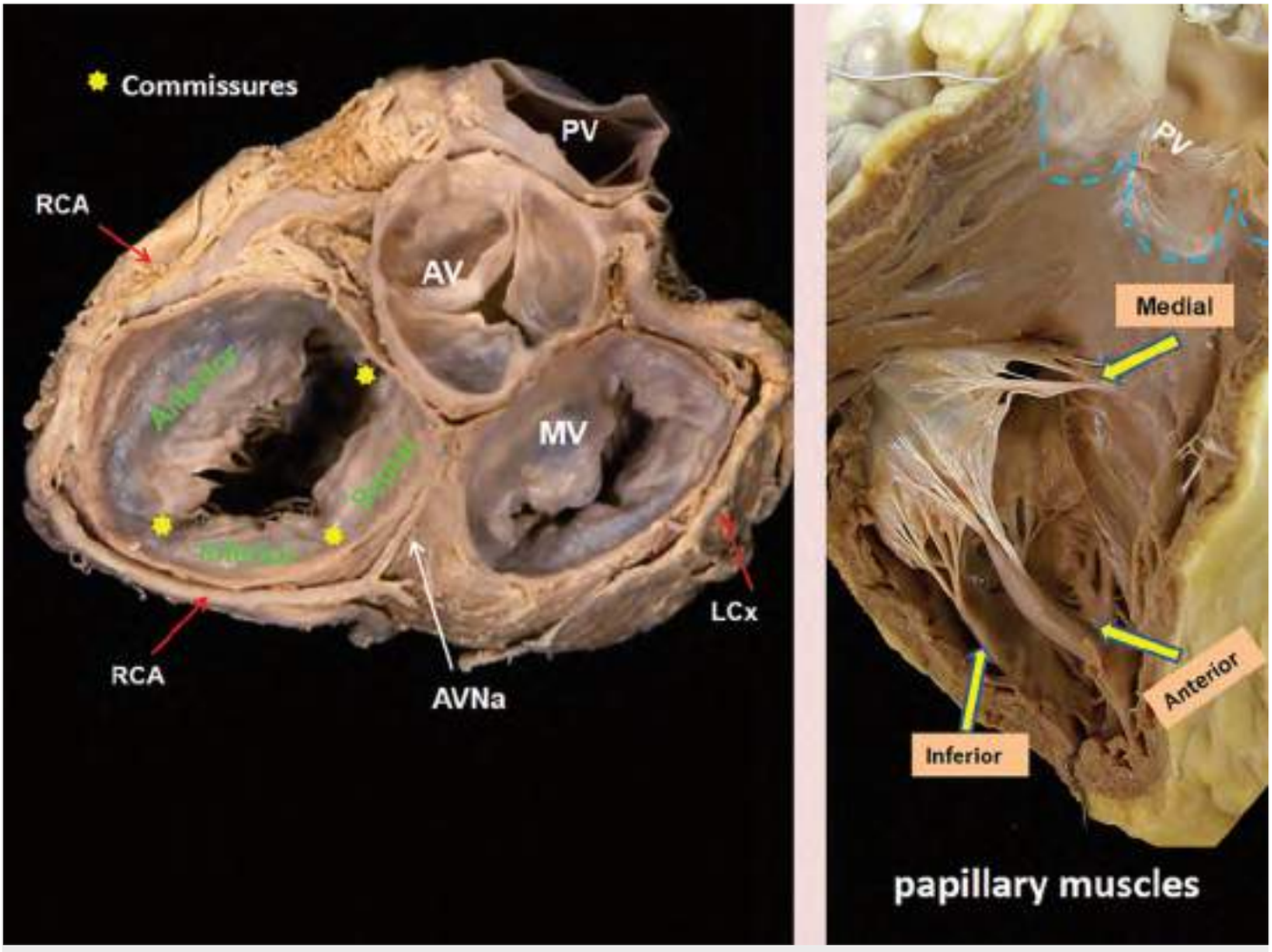

Fig. 17.2 Tricuspid valve (TV) apparatus. The TV has the largest orifice among the four cardiac valves. The anterior (mural) leaflet is the largest. The septal leaflet base inserts obliquely across the membranous interventricular septum where the anteroseptal commissure is located (*yellow asterisk*). The inferior (posterior) leaflet has more scallops and is relatively difficult to see with echo compared with CT and MR. The TV papillary muscles are smaller than the mitral apparatus, often multiple, and widely separated. AV, aortic valve; AVNa, atrioventricular nodal artery; LCx, left circumflex artery; MV, mitral valve; PV, pulmonary valve; RCA, right coronary artery.

development of the mural leaflets. The myocardial portion is subsequently removed by apoptosis.[3] The process of myocardial cell death forms the final appearance of the leaflets and tendon apparatus. This process is called "undermining," which delaminates the inner layers of the ventricular inlet and frees the fibrous leaflets and appears to differ somewhat for individual valve leaflets. Removal of the AV groove myocardium forms the fibrous annulus of the valve, which provides insulation between the myocardium of the atrium and that of the ventricle.[2,4] The epicardium will be contiguous with the insulating fibrous tissue of the fibrous annulus. This process will be completed around the 12th week of development.

A complete failure of development of the AV cushions results in AV canal defect with variable degree of insufficiency, primum type of atrial septal defect, and perimembranous ventricular septal defect (VSD). Incomplete resorption of the myocardial tissue on the septal leaflet of the TV can result in congenital heart defects such as Ebstein's malformation or accessory conduction pathways.[5] In Ebstein's malformation, the attached margin of the septal leaflet and occasionally the inferior leaflet of the TV are displaced apically and "plastered" onto the right ventricular wall.[2] Myocardial AV continuities between the atrial and ventricular sides can occur. These abnormal muscular connections are known as accessory conduction pathways classically causing the arrhythmias seen in Wolff–Parkinson–White (WPW) syndrome.

◆ Normal Tricuspid Valve

The TV apparatus consists of the three valve leaflets, the fibrous annulus, the supporting tension apparatus, which consists of the chordae tendineae (tendinous chords), and papillary muscles (PMs; ▶ Fig. 17.2). The leaflets include anterior (superior), septal, and posterior (inferior).[6] The PMs include anterior, posterior, and sometimes a medial (septal) PM (▶ Fig. 17.2, ▶ Fig. 17.3, ▶ Fig. 17.4). Some believe that the TV is bicuspid in original design.[7] Embryologically, the TV has a septal leaflet and a free-wall (mural) leaflet. With each cardiac contraction, the mural leaflet tends to deform and change its shape. Therefore, to strengthen its durability, the mural leaflet has adopted to develop extra hinge point by forming a cleft within the mural

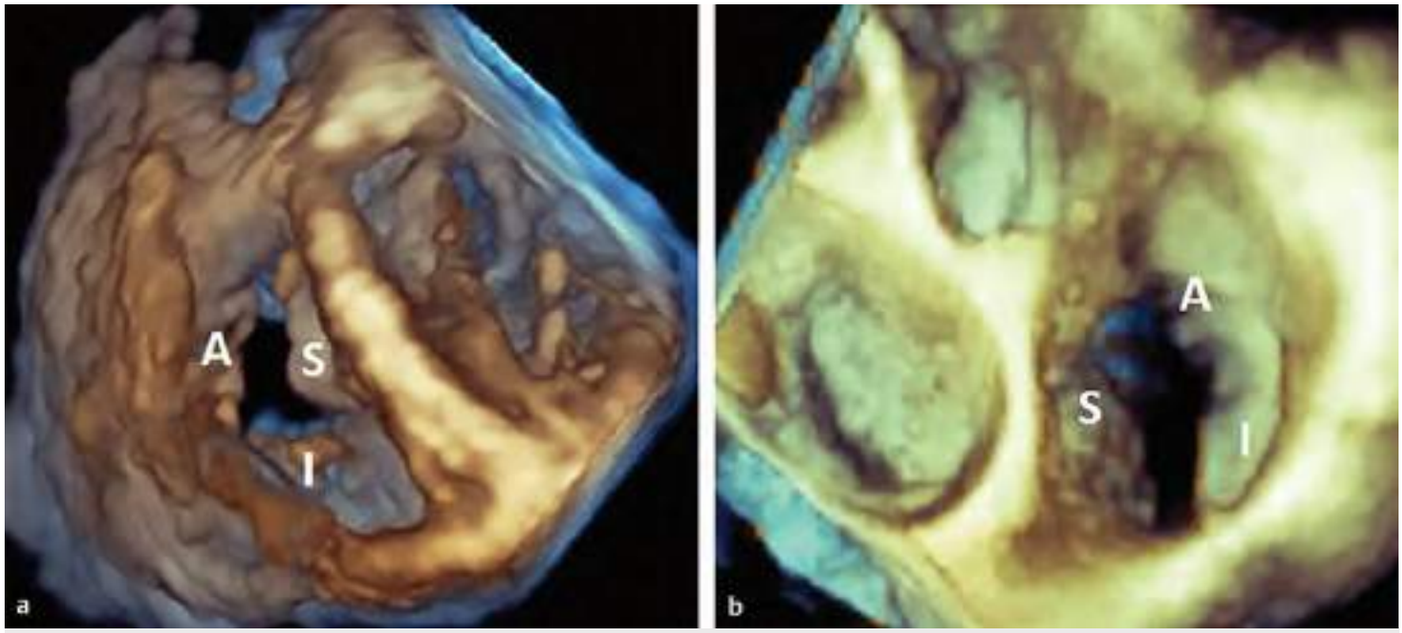

Fig. 17.3 3D transesophageal echocardiography showing the tricuspid valve from a ventricular perspective (**a**) and an overhead perspective (**b**). The three leaflets are clearly visible. S, septal; A, anterior; I, inferior. (These images are provided courtesy of Professor Francesco Faletra, MD, Italy.)

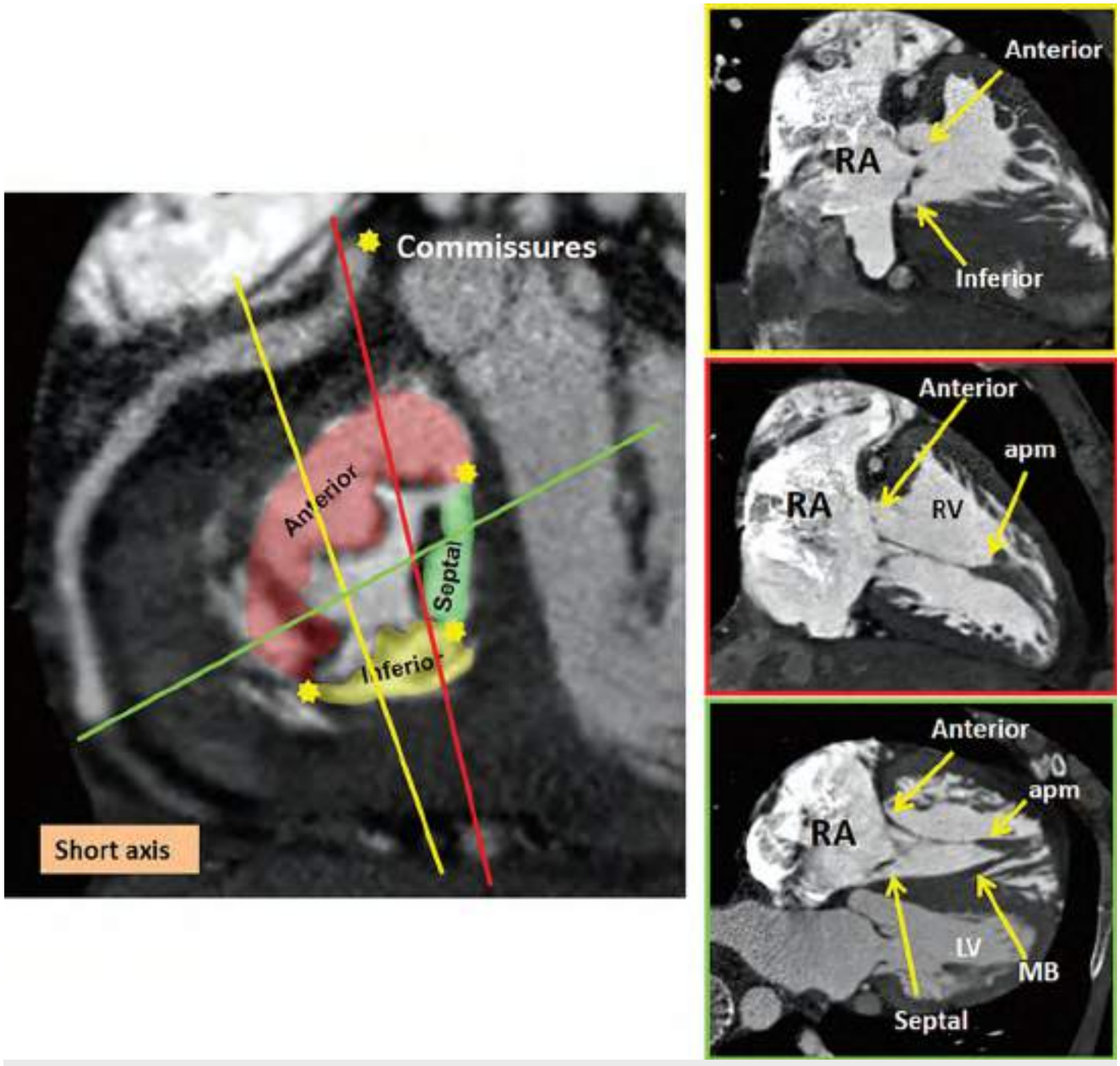

Fig. 17.4 The three leaflets of the tricuspid valve are shown in a short-axis view and three long-axis views. The anterior papillary muscle (apm) is seen arising from the moderator band (MB). Note the chordae extending between the apm and the leaflets. LV, left ventricle; RA, right atrium; RV, right ventricle.

leaflet that has divided it into two components, namely, the anterior and posterior (inferior) leaflets.[7] Depending on the location of the cleft (the anteroinferior commissure), the inferior leaflet can be very small. The inferior leaflet appears to be of less functional significance since it may be removed without impairment of the valve function. The septal leaflet is smaller than the anterior leaflet and arises medially directly from the tricuspid annulus above the interventricular (IV) septum. The commissure between the septal and anterior leaflets (anteroseptal commissure) is located over the membranous septum and divides it into the AV and IV components[8] (▶ Fig. 17.5, ▶ Fig. 17.6). The two leaflets may be fused at the anteroseptal commissure, but, in normal individuals, it is not uncommon to find a gap between the two leaflets at this level, in which case the gap is covered by the membranous septum.[8] In contrast to the mitral valve, the anatomical subdivision of the TV leaflets by imaging techniques appears to be less relevant since primary surgical reconstruction techniques for the TV are limited.[9] Each leaflet has an atrial and a ventricular surface. On the surface of each cord, two zones can be distinguished: a clear zone that is devoid of cordal attachments and a rough irregular zone extending between the free margin of the leaflet and the line of closure of the valve, where the leaflets coapt (▶ Fig. 17.7). At the coaptation area of the valve, the width of the rough zone is 7 to 8 mm and tapers toward the commissures. Tendinous cords attach to the ventricular side of the rough zone.

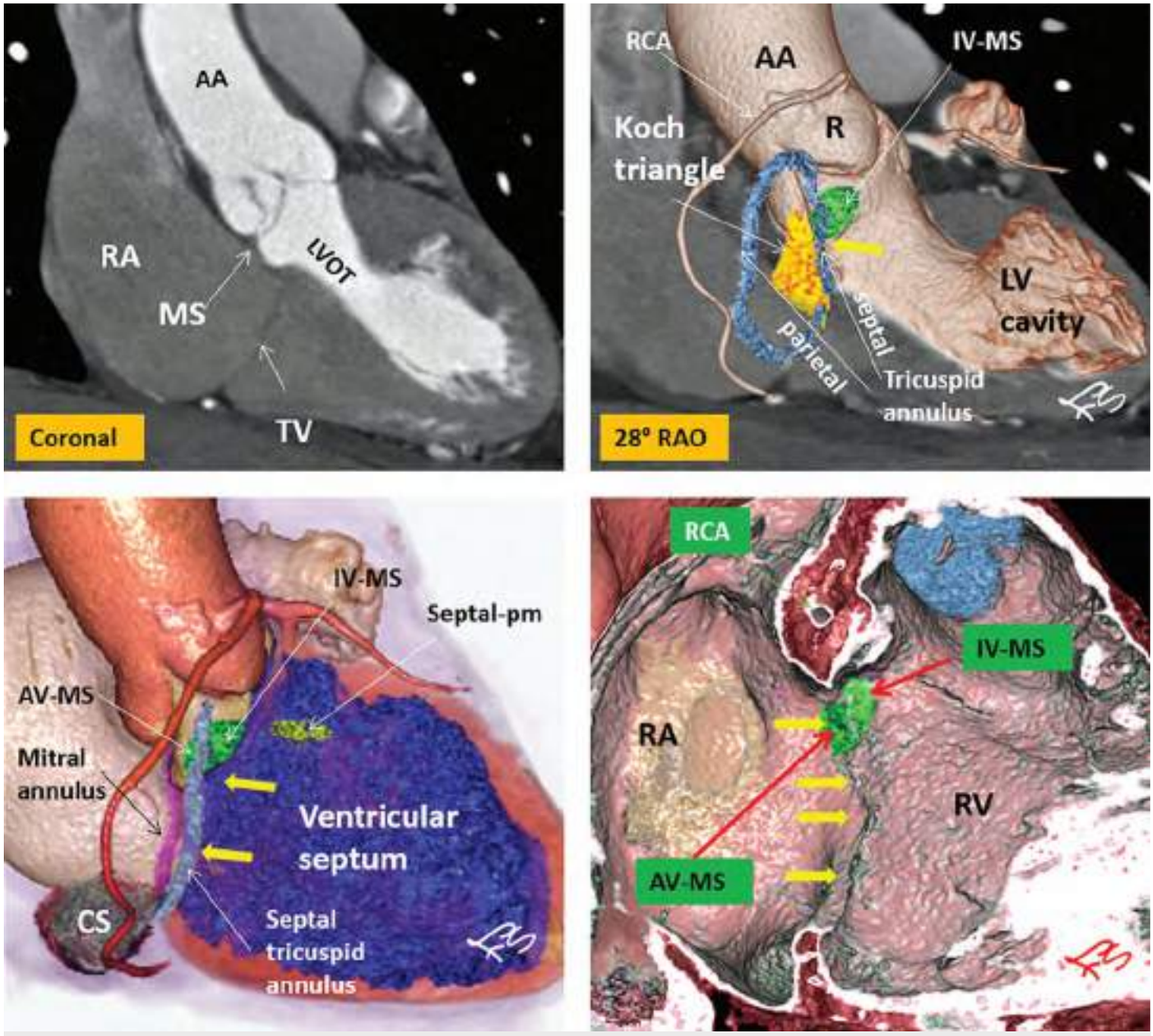

Fig. 17.5 Septal tricuspid leaflet (*yellow arrows*) and membranous septum. The commissure between the septal and the anterior leaflets of the TV is located over the membranous septum (MS) and divides it into the atrioventricular (AV-MS) and interventricular (IV-MS) components. Ventricular septum is shown in *navy blue* and the tricuspid annulus in *light blue*. AA, ascending aorta; CS, coronary sinus; LV, left ventricle; PM, papillary muscle; R, right coronary sinus; RA, right atrium; RCA, right coronary artery; RV, right ventricle; TV, tricuspid valve.

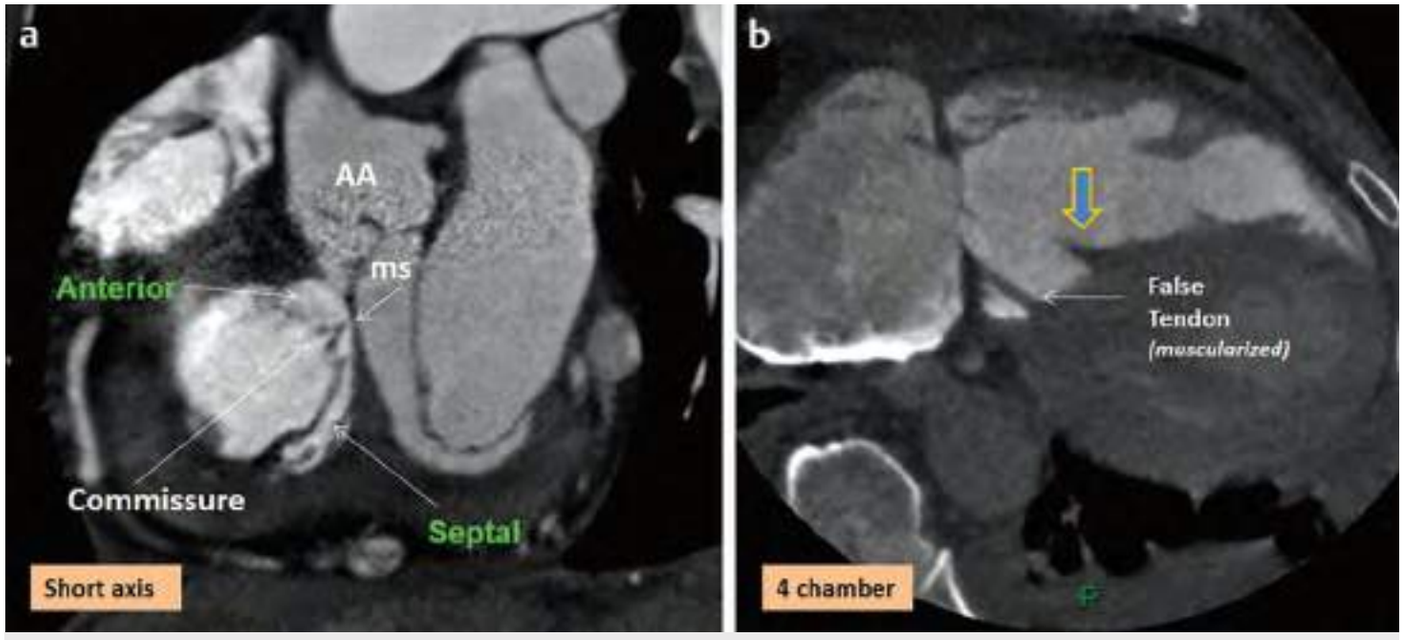

Fig. 17.6 **(a)** Short-axis CT at the level of the atrioventricular (AV) valves. The commissure between the septal and anterior leaflets (anteroseptal commissure) of the tricuspid valve is located over the membranous septum (ms) and divides it into the AV and interventricular (IV) components. **(b)** A four-chamber view CT showing a large medial (septal) papillary muscle (*arrow*).

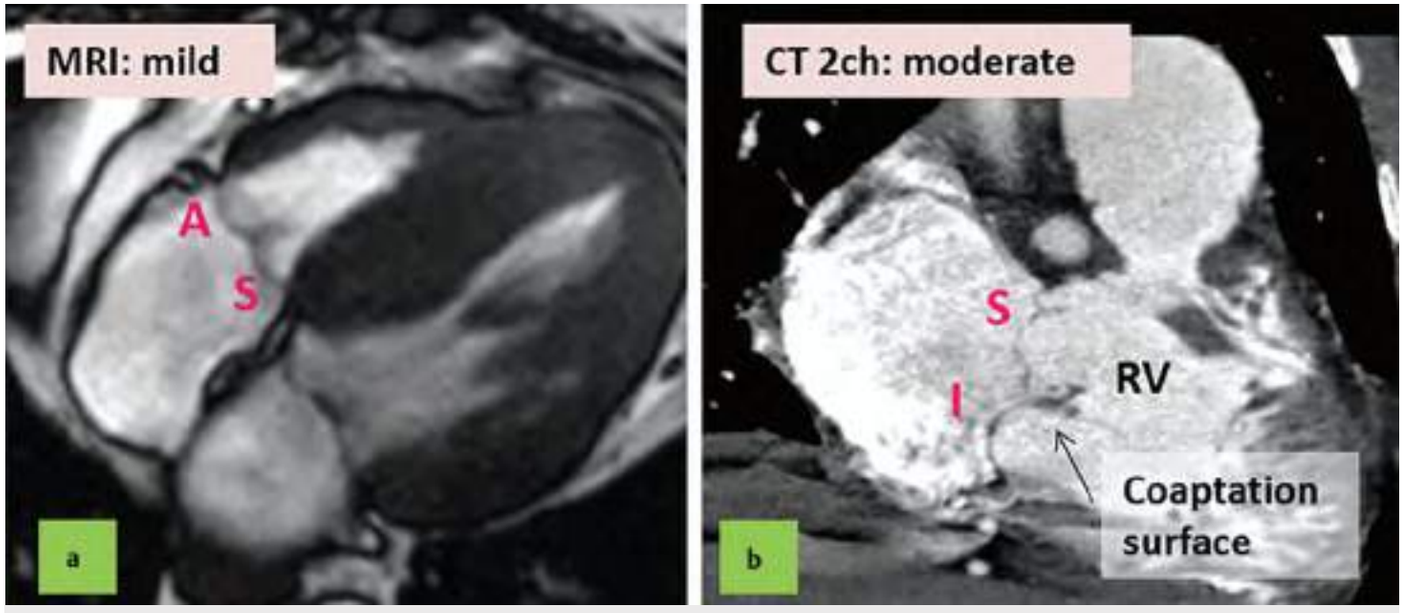

Fig. 17.7 Myxomatoses disease of the tricuspid valve. **(a)** A four-chamber MR showing mild disease. **(b)** Right ventricular two-chamber (2ch) CT showing moderate disease. Note the coaptation surface that is nicely preserved. Prolapse is diagnosed if one or more leaflets extend beyond tricuspid annulus in systole. It is seen in 20% of the myxomatous mitral valve disease and usually involves the anterior (A) and septal (S) leaflets. Determination of tricuspid prolapse may be difficult since the tricuspid ring is not easy to define. Confirmation in two perpendicular images improves diagnosis. I, inferior leaflet; RV, right ventricle.

The anterior PM provides chordae to the anterior and posterior leaflets, and the posterior PM provides chordae to the posterior and/or septal leaflets, but variation exists. The septal PM of the conus gives chordae to the anterior and septal leaflets. In addition, there may be accessory cordal attachments to the septum, right ventricular free wall, and the moderator band (▶ Fig. 17.4, ▶ Fig. 17.6, ▶ Fig. 17.8). The septal PM presents in 82% of the heart and can be large in some cases (▶ Fig. 17.6**b**). In the rest, it is replaced by tendinous chords.[10] It is a single papilla in 50% and double in 30%. The septal PM is located on the body of the septomarginal trabeculation inferior to the junction of the anterior and septal leaflets of the TV. It represents an important surgical landmark for the location of the right bundle branch (passing below the septal PM) to avoid its injury during surgical correction of certain types of VSDs.

The chordae tendineae (tendinous cords) are the thick, strong, tendinous connections between the AV valve leaflets and the PMs and help maintain the valve function (▶ Fig. 17.8). There are

Fig. 17.8 Subvalvular apparatus of the tricuspid valve. Tendinous cords are the thick, strong, tendinous connections between the rough zone of the valve leaflets and the tip of the papillary muscles (pm). Single straight, fan-shaped true cords and small false cords can be identified. Cordal elongation or rupture affects the valve function.

more chordae tendineae in the TV than in the mitral valve.[11] In order to perform their function efficiently, the chordae have to possess a high degree of elasticity, as well as considerable strength and endurance. The core of each cord is formed by collagen bundles covered by the endocardium composed of a superficial layer of squamous endothelial cells and an underlying dense layer of elastic fibers. Since both the valve leaflets and the chordae are composed of collagen, there is no distinguishable change in the tissue at the valvular attachment. There is variation in the origin, insertion, attachments, branching patterns, distribution, and the gross texture of the chordae (▶ Fig. 17.7). Commissural (marginal) cords arise as a single stem, but branch like the struts of a fan and allow the adjacent leaflets to coapt and to move apart. False chordae are seen in half of the cases, extend between PMs or a PM and the ventricle wall, and help in ventricular contraction. Rarely, cords retain their embryonic muscular structures (chordae muscularis).

Tricuspid Annulus

The normal tricuspid annulus has an elliptical shape and appears nonplanar, mimicking the saddle shape of the mitral valve annulus (▶ Fig. 17.9, ▶ Fig. 17.10). Common embryological origin of the two valves may explain this configuration. In an echocardiographic study by Fukuda et al[1] in healthy individuals, the tricuspid annulus was mapped throughout the cardiac cycle and reconstructed on a computer workstation. They showed a nonplanar, elliptical-shaped tricuspid annulus, with the posteroseptal portion being the "lowest" (toward the apex) and the anteroseptal portion being the "highest" (▶ Fig. 17.9). They suggested that future designs and techniques of TV annuloplasty should take into account not only the amount of annular dilation but also the nonplanar geometry of the TV annulus. Using, electrocardiographic (ECG) gated computed tomography angiography (CTA) images of the heart, this unique annulus morphology can be shown, provided that enough contrast exists in the right heart (▶ Fig. 17.9, ▶ Fig. 17.10). It is also possible to demonstrate the annulus changes in different phases of cardiac cycle if a retrospective data acquisition is obtained. An important consideration about the structure of the TV annulus that makes it different from the mitral annulus is the lack of extensive fibrous elements in the peripheral (mural) part of the valve in order to support its leaflets. Instead, the mural leaflets are hinged on the ventricular myocardium, with the fibrofatty tissue of the deep AV groove serving to prevent direct passage of electrical currents between the atrium and the ventricle.[8]

As mentioned earlier, the posteroseptal portion of the septal leaflet is the most apically displaced part. As a result of this inferior migration of the septal leaflet, the distance between the mitral valve and the TV is maximum where posterior cardiac crux is located[8] (▶ Fig. 17.9). In this region, also known as the muscular AV septum, the cavity of the right atrium is separated from that of the left ventricle by invagination of the AV junction myocardial walls, which is filled with epicardial fibrofatty tissue. Therefore, as emphasized by Restivo et al, this part does not appear to be a true muscular AV septum.[8] As a matter of fact, this fibrofatty space is where the AV nodal artery passes to supply the AV node. The septal leaflet of the TV also demarcates the anterior boundary of the triangle of Koch and the apex of the triangle is the membranous part of the AV septum where the bundle of His passes inferiorly. More laterally along the inferior AV groove, the septal and posterior leaflets separate the cavotricuspid isthmus part of the right atrial vestibule from the right ventricle (RV). This isthmus has an important role in the creation and maintenance of atrial flutter.

◆ Imaging of the TV Apparatus

Morphology

Echocardiography and MR are modalities of choice for evaluation of the tricuspid and mitral valve function. When it comes to demonstration of the anatomy and morphological changes of the AV junction, CT is probably the modality of choice. However, compared to the mitral valve, which can be optimally evaluated in most routine coronary CTAs, demonstration of the right AV junction in detail with routine gated cardiac CTA techniques can be

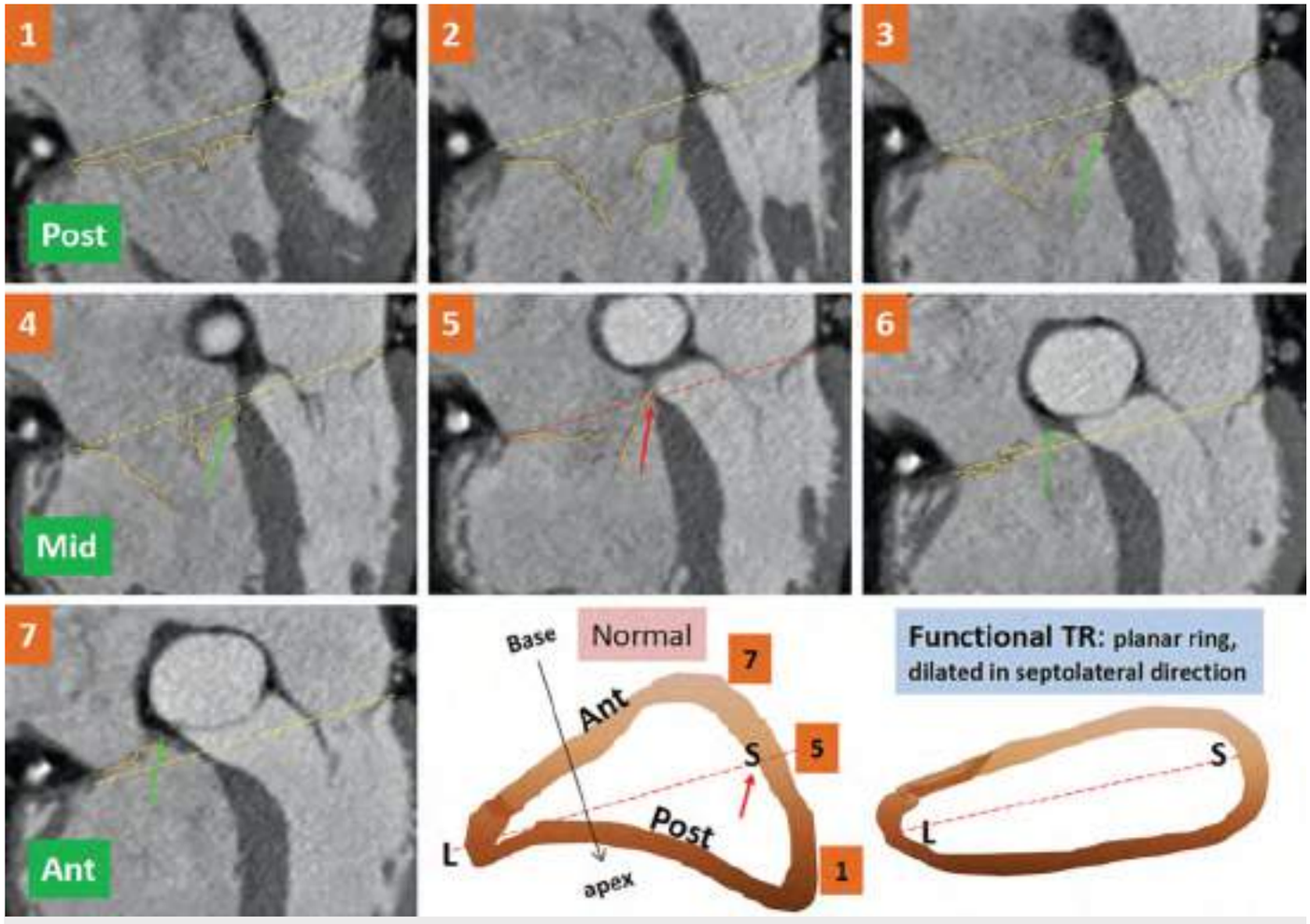

Fig. 17.9 Cross-sectional four-chamber CT images (1–7 from posterior to anterior of the heart) in a 38-year-old female patient with small atrial septal defect. The lower row includes schematic superior views of the attachment line of the tricuspid annulus in "normal" geometry and in patients with severe "functional TR." In moderate to severe functional TR, the annulus shape changes from a normal nonplanar, oval shape to a more planar rounded ring dilated in the septolateral direction (L-S). Note that in this patient despite mild annulus dilatation due to right heart enlargement, the normal tricuspid annulus geometry is maintained. TR, tricuspid regurgitation; L, lateral margin; S, septal annulus; Ant, anterior/superior annulus margin; Post, posterior/inferior annulus; Mid, middle.

very challenging. Clear depiction of this region requires homogenous enhancement of the structures around the TV annulus (▶ Fig. 17.4). Most ECG-gated/triggered cardiac CTA techniques modified for the right heart examination (i.e., 50% contrast/saline chase, in routine coronary CTA) can provide good-quality motion-free images along with optimum enhancement of intraventricular cavity to depict most parts of the RV outlet and trabeculated portions. However, the quality may not be enough to show the details of the RV inlet.[12] This is mainly due to inhomogeneous enhancement of the right atrium and the presence of steak artifacts arising from high-attenuation superior vena cava contrast when mixed with the noncontrast blood of the inferior vena cava. Right atrial artifacts may be decreased when injections are performed through the femoral vein. Best results, however, will be obtained with simultaneous injection of contrast in both femoral and antecubital veins.[13] At least two sets of images, one systole and one diastole, are required to see the valve in two different positions. Despite all these efforts, evaluation of small pathologies such as vegetation and leaflet deformities can be difficult and unreliable. These limitations also apply to most cardiac MR studies, and given its limited spatial and temporal resolution, demonstration of the detail of anatomy and pathology may not be feasible.

One advantage of CT is to show the extent of calcifications in this region. Degenerative calcium deposition in the TV annulus is relatively rare compared to the mitral annulus. This is likely due to incomplete fibrous ring on the right side. Reported calcifications are usually secondary diffuse cardiac calcinosis in chronic dialysis patients and inflammatory processes such rheumatoid heart disease.[14] In some cases, large calcium deposition in the mitral and aortic annuluses may grow into the right side and interfere with the normal function of the AV conduction axis and bundle branches.

MRI can be very useful to assess the TV annulus size and its morphological changes with cardiac cycle.[15,16] When measurements were compared between cardiac MRI and real-time 3D echocardiogram, there had been no significant difference in the measurements of tricuspid annular diameters, area, and its fractional shortening between the two modalities.[16] Therefore, MRI can also provide accurate measurements and can be useful in assessing the tricuspid annulus prior to TV surgery.

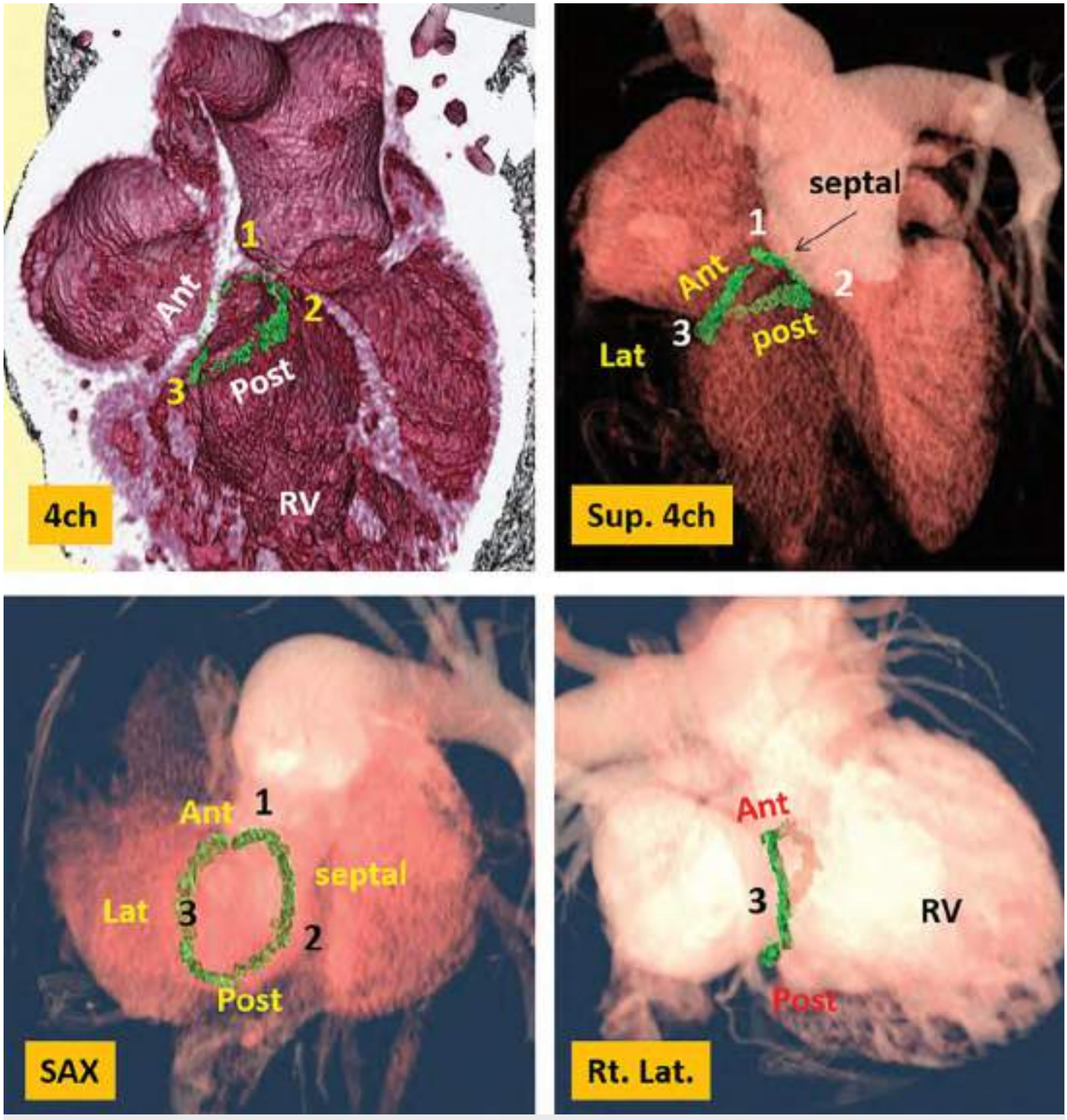

Fig. 17.10 Tricuspid valve (TV) annulus. Color-coded volume-rendered CT images in a 32-year-old female patient with transposition of the great arteries (TGA) status post Mustard operation. The tricuspid annulus in this patient with a systemic right ventricle (RV) is shown by the *green ring*. The normal nonplanar shape due to oblique attachment of the septal leaflet to the septum is well preserved. The TV annulus is generally weaker compared to mitral annulus and therefore dilates more easily with pressure or volume overload. 1–2, septal attachment, 3, lateral (lat.) wall; Post, posterior/inferior attachment; Ant, anterior/superior attachment; SAX, short axis; 4ch, four-chamber; Sup, superior; Rt. Lat., right lateral.

Due to nonplanar morphology of the TV, in contrast to the mitral or aortic valves, it would be difficult to show all three leaflets in one short-axis plane. Recently, 3D echocardiography has gained popularity and is able to show all leaflets through an endoscopic view from both the atrial and the ventricular sides[16] (▶ Fig. 17.3). However, deriving accurate and reliable quantitative data from these images would be difficult. Although endoscopic views of the RV including the TV annulus with CT are feasible, it would still be technically limited to show all TV leaflet positions at a specific time frame of the cardiac cycle.[12] The septal leaflet can be best assessed in four-chamber and short-axis views (▶ Fig. 17.4). Using these essential views, the AV and IV components of the membranous septum can be shown. In some cases, small defects of the membranous septum can only be seen in this

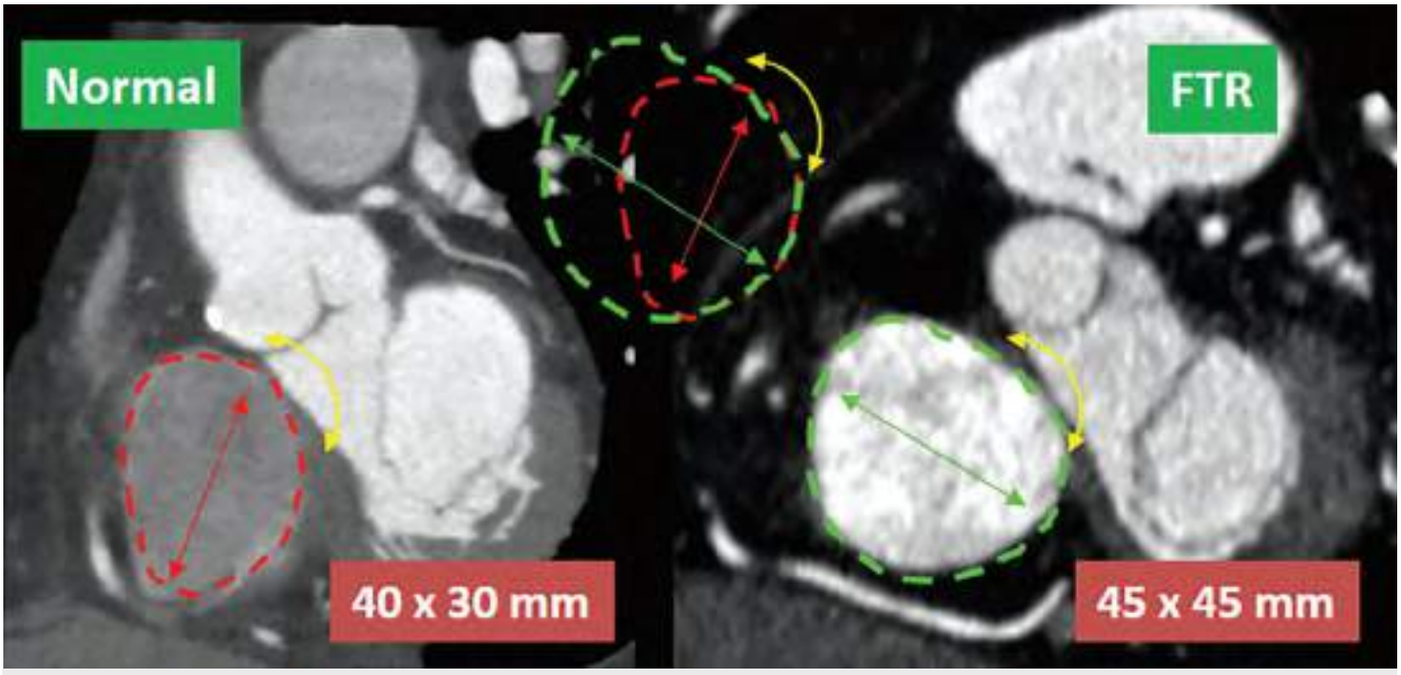

Fig. 17.11 The shape of the tricuspid annulus in a normal 34-year-old male and in functional tricuspid regurgitation (FTR) in a 32-year-old female with right heart enlargement. In FTR, dilatation occurs along the free wall in the mediolateral direction (*green arrow*). The septal wall (double-headed *yellow arrow*) remains intact. The septal portion of the tricuspid annulus is relatively fixed and its dilatation occurs in the free wall aspect. In normal condition, the annulus appears oval shaped and the ratio of the anteroposterior to mediolateral diameter is around 1.3. In FTR, the tricuspid annulus dilates in the lateral direction (> 35 mm) and tethering of the leaflets occurs. The tricuspid valve annulus is very dynamic and up to 30% reduction in the annular area in atrial systole can occur. Therefore, the degree of TR is variable and dependent on the right ventricle loading and function.

projection. In this regard, MRI not only provides data about the anatomy of this region but also is able to reveal the existence of any shunt by using cine or phase-contrast MR. Measurement of the septal isthmus width and demonstration of its relationship with the coronary sinus orifice and the AV node artery are generally simple in good-quality four-chamber cardiac CT images. Evaluation of the TV prolapse would also be easier on long-axis views (▶ Fig. 17.7). The two chambers of the right heart can provide additional information in regard to the relationship of the anterior and posterior leaflets (▶ Fig. 17.4, ▶ Fig. 17.7). It is the optimum view for measurements of the cavotricuspid isthmus of the right atrium, which is located superior to the hinge of posterior leaflet. Demonstration of the posterior TV leaflet is technically challenging in 2D transthoracic echocardiography. This leaflet is easy to show on cine views of MR.

In most congenital heart diseases, both MR and CT provide comprehensive data and demonstrate recurrent or neglected pathologies. The degree of tricuspid leaflet migration in Ebstein's anomaly will be shown by CT and MR. High spatial resolution of CT has the potential to show small bands of muscles between the right atrium and ventricle in patients with WPW. Cardiac CT and MRI provide excellent assessment of the RV size, dimensions, and volumes, as well as evaluation of the ventricular remodeling (i.e., dilatation and hypertrophy), which is common in chronic TR. Pulmonary arteries can be evaluated at the same time and some indirect information about pulmonary hypertension can be obtained.

Tricuspid Annulus Measurements

The average diameter of TV annulus is 4.0 ± 0.7 cm. In normal condition, the annulus is oval shaped with the mediolateral diameter larger than the anteroposterior diameter. With moderate or greater TR, the TV annulus becomes dilated, more planar with decreased high-low distance (< 4 mm), and more circular with decreased ratio of mediolateral to anteroposterior diameters compared with normal patients (1.1 vs. 1.3 mm, respectively; ▶ Fig. 17.11).

With echocardiography, the mean maximum tricuspid annular circumference and area in normal subjects are 12 ± 1 cm and 11 ± 1.8 cm^2, respectively.[17,18] The mean minimum annular sizes are much larger in TR (12.5 ± 0.6 cm and 13.0 ± 1.4 cm^2) than in normal subjects (9.6 ± 0.9 cm, 7.6 ± 1.4 cm^2). In autopsy, the mean TV annular circumference in the fresh state is 13.5 ± 0.8 cm, and the mean circumference index is 7.3 ± 0.9 cm/m^2. Tricuspid annulus area changes approximately 30% (~20% diameter) during the cardiac cycle.[18,19] In comparison, the area changes for the mitral annulus is around 25%. The anatomic structures surrounding the annulus may influence less reduction in the annular size in the mitral annulus compared with the TV. The mitral valve between the two fibrous trigons is not in contact with the myocardium. Therefore, the tricuspid annulus with only one fibrous attachment to the midline cardiac skeleton and more of its circumference in contact with the myocardium exhibits more systolic reduction.

Tricuspid dysfunction can result from alterations in any one or all the components of the TV apparatus. Although annulus dilatation may be an important mechanism of TR in secondary (functional) TV abnormality, it may not be the only mechanism. In turn, patients with functional TR may have a normal TV 3D geometry (▶ Fig. 17.10). In this case, as shown by a recent cardiac MR study, the longitudinal displacement of the TV annulus especially on the lateral margin of the annulus in patients with

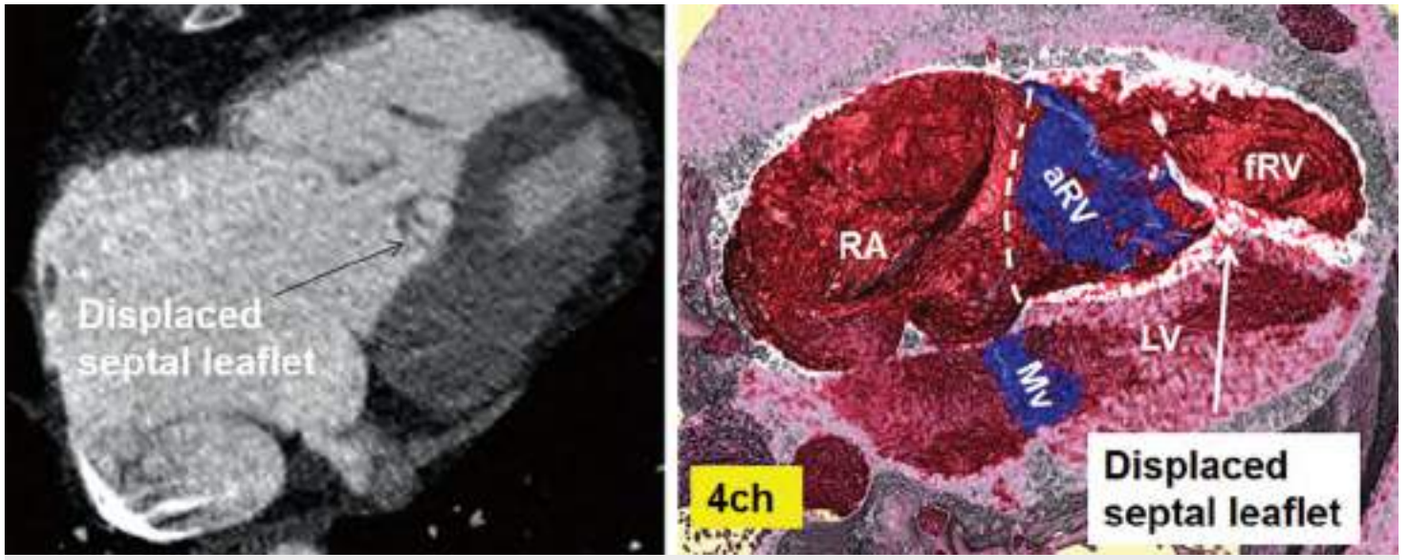

Fig. 17.12 A four-chamber (4ch) CT angiography of a 45-year-old female with Ebstein's anomaly showing apically displaced septal and inferior leaflets of the tricuspid valve resulting in an atrialized right ventricle (aRV) and a functional RV (fRV). The right atrioventricular groove is shown by the *dashed white line*. Of note, the anatomically normal tricuspid valve typically demonstrates less than 8 mm/m^2 apical displacement relative to the hinge point of the mitral valve (Mv). LV, left ventricle; RA, right atrium.

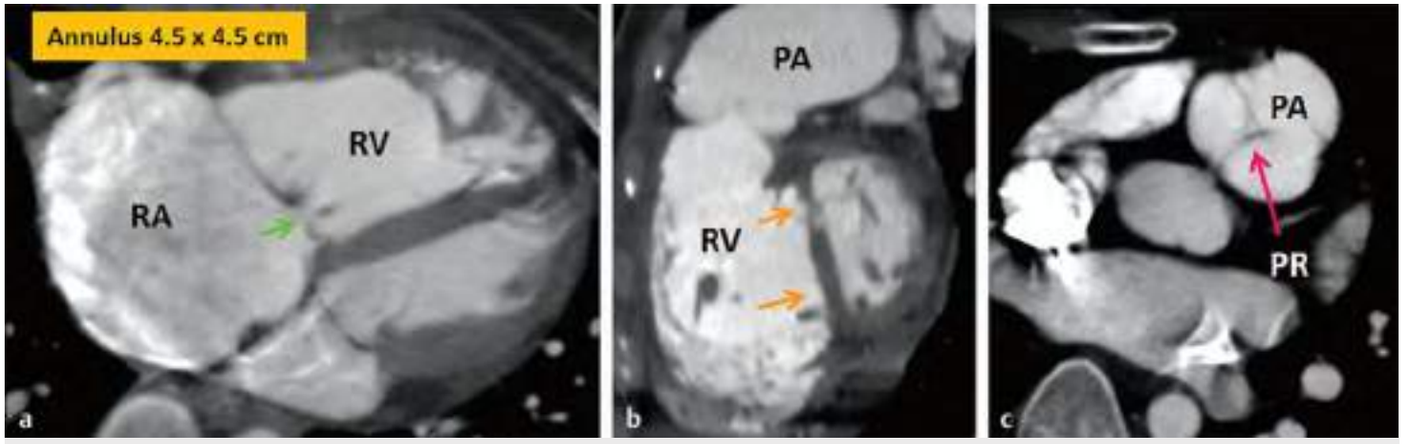

Fig. 17.13 Ancillary findings in severe tricuspid regurgitation due to pulmonary hypertension in a 39-year-old female patient with a history of atrial septal defect. **(a)** Four chambers and (**b**) short-axis CT images show specific signs of TR, lack of coaptation of leaflets (*green arrow*), and annulus diameter of greater than 40 mm. Nonspecific signs include straightening of septum (*arrows*) **(b)**, atrial septal leftward bulging **(a)**, and markedly dilated right atrium (RA). Enlarged pulmonary artery (PA) and mild pulmonary regurgitation (PR; **c**) are also related to pulmonary hypertension.

functional TR is smaller than that in normal individuals (12.3 mm ± 3.7 vs. 21.4 mm ± 3.7, respectively).[15]

◆ Morphological Abnormalities of Tricuspid

Primary malformations of the TV are rare with Ebstein's malformation being the most common anomaly. Ebstein's anomaly is due to failure of delamination of the valve tissue from the underlying myocardium.[20,21] The TV septal leaflet is displaced toward the apex, resulting in an "atrialized RV" and a "functional RV" (▶ Fig. 17.12). The anterior leaflet of the TV is rarely displaced but is often redundant, or "sail-like." The apical displacement of the septal leaflet may result in discontinuity of the central fibrous body and septal AV ring, creating a potential substrate for accessory pathway formation that increases the risk of sudden death.[22]

Among other rare anomalies of the TV leaflets are double-orifice TVs, leaflet clefts, and tricuspid atresia.[23,24]

Tricuspid Valve Dysfunction

The TV is the gateway to the RV and similar to the mitral valve, its major function is to prevent retrograde flow from the RV to the right atrium during systole. With initiation of systole, the TV closes. Incomplete closure causes TR, which is the most common abnormality of the TV. Tricuspid stenosis is rare.

The etiologies of TV malfunction are classified into two major groups of primary (intrinsic, organic, or structural) and secondary (functional or anatomically normal) diseases. Trivial to mild TR is very common (60–70%) and appears to be more common above age of 50 years.[25,26] The most common cause of TR is dilatation of the TV annulus caused by pulmonary hypertension either primary or secondary to the left heart failure[26]

(▶ Fig. 17.13). This condition is called functional TR and can be improved with the removal of the underlying cause. Annulus flattening in functional TR may cause the lowest point of the annulus to be displaced away from the PMs, resulting in increasing tethering of the tricuspid leaflets and regurgitation due to incomplete coaptation of the leaflets.[27,28] The critical diameter for the annulus to become dysfunctional TR is shown to be around 27 mm/m^2.[28] In an in vivo study of porcine TVs by Spinner et al, all valves lost competence at 40% dilatation.[29] Tricuspid annuloplasty is the most preferred technique for the treatment of functional TR. Structural causes of TR are multiple. In advanced countries, the prevalence of rheumatic heart disease as a common cause of regurgitation or stenosis in the past has declined considerably as a result of improvements in prevention and treatment.[30] Infection of the TV is seen in 5 to 10% of infective endocarditis.[31]

Prolapse of the tricuspid leaflets is not uncommon and may be a cause of TR. Myxomatous degeneration affecting the mitral valve and TV can lead to chordal elongation and prolapsing leaflets.[32] TV prolapse is seen in 20% of the myxomatous mitral valve disease and primarily involving the anterior and septal leaflets (▶ Fig. 17.7).

Functional study of the TV is performed by echocardiography or MRI. Normal tricuspid flow curve has two distinct diastolic peaks: an early prominent peak corresponding to ventricular passive filling and a late peak with smaller amplitude due to filling by atrial contraction. The normal flow curve pattern of the tricuspid will change in different diseases and is used for diagnosis of pathologies of the valve or RV. Echocardiography and CT are the best techniques to evaluate valve vegetation or perivalvular abscesses.

References

[1] Fukuda S, Saracino G, Matsumura Y, et al. Three-dimensional geometry of the tricuspid annulus in healthy subjects and in patients with functional tricuspid regurgitation: a real-time, 3-dimensional echocardiographic study. Circulation.; 114(1) Suppl:I492–I498

[2] Lamers WH, Virágh S, Wessels A, Moorman AF, Anderson RH. Formation of the tricuspid valve in the human heart. Circulation.; 91(1):111–121

[3] de Lange FJ, Moorman AF, Anderson RH, et al. Lineage and morphogenetic analysis of the cardiac valves. Circ Res.; 95(6):645–654

[4] de Vlaming A, Sauls K, Hajdu Z, et al. Atrioventricular valve development: new perspectives on an old theme. Differentiation.; 84(1):103–116

[5] Lin CJ, Lin CY, Chen CH, Zhou B, Chang CP. Partitioning the heart: mechanisms of cardiac septation and valve development. Development.; 139(18):3277–3299

[6] Virmani R. The tricuspid valve. Mayo Clin Proc.; 63(9):943–946

[7] Victor S, Nayak VM. The tricuspid valve is bicuspid. J Heart Valve Dis.; 3 (1):27–36

[8] Restivo A, Smith A, Wilkinson JL, Anderson RH. Normal variations in the relationship of the tricuspid valve to the membranous septum in the human heart. Anat Rec.; 226(2):258–263

[9] Shah PM, Raney AA. Tricuspid valve disease. Curr Probl Cardiol.; 33(2):47–84

[10] Loukas M, Tubbs RS, Louis RG, Jr, et al. An endoscopic and anatomical approach to the septal papillary muscle of the conus. Surg Radiol Anat.; 31 (9):701–706

[11] Hutchison J, Rea P. A comparative study of the morphology of mammalian chordae tendineae of the mitral and tricuspid valves. Vet Rec Open.; 2(2): e000150

[12] Saremi F, Ho SY, Cabrera JA, Sánchez-Quintana D. Right ventricular outflow tract imaging with CT and MRI: part 1, morphology. AJR Am J Roentgenol.; 200(1):W39–W50

[13] Saremi F, Kang J, Rahmanuddin S, Shavelle D. Assessment of post-atrial switch baffle integrity using a modified dual extremity injection cardiac computed tomography angiography technique. Int J Cardiol.; 162(2):e25–e27

[14] Gould L, Zahir M, DeMartino A, Gomprecht RF, Hayt D. Extensive calcification of the tricuspid valve in rheumatic heart disease. Angiology.; 22(9):529–532

[15] Maeba S, Taguchi T, Midorikawa H, Kanno M, Sueda T. Four-dimensional geometric assessment of tricuspid annulus movement in early functional tricuspid regurgitation patients indicates decreased longitudinal flexibility. Interact Cardiovasc Thorac Surg.; 16(6):743–749

[16] Anwar AM, Soliman OI, Nemes A, van Geuns RJ, Geleijnse ML, Ten Cate FJ. Value of assessment of tricuspid annulus: real-time three-dimensional echocardiography and magnetic resonance imaging. Int J Cardiovasc Imaging.; 23 (6):701–705

[17] Tei C, Shah PM, Cherian G, Trim PA, Wong M, Ormiston JA. Echocardiographic evaluation of normal and prolapsed tricuspid valve leaflets. Am J Cardiol.; 52 (7):796–800

[18] Tei C, Pilgrim JP, Shah PM, Ormiston JA, Wong M. The tricuspid valve annulus: study of size and motion in normal subjects and in patients with tricuspid regurgitation. Circulation.; 66(3):665–671

[19] Ton-Nu TT, Levine RA, Handschumacher MD, et al. Geometric determinants of functional tricuspid regurgitation: insights from 3-dimensional echocardiography. Circulation.; 114(2):143–149

[20] Attenhofer Jost CH, Connolly HM, Dearani JA, Edwards WD, Danielson GK. Ebstein's anomaly. Circulation.; 115(2):277–285

[21] Edwards WD. Embryology and pathologic features of Ebstein's anomaly. Prog Pediatr Cardiol.; 2:5–15

[22] Hebe J. Ebstein's anomaly in adults. Arrhythmias: diagnosis and therapeutic approach. Thorac Cardiovasc Surg.; 48(4):214–219

[23] Tutarel O, Westhoff-Bleck M. The double-orifice tricuspid valve: a review. J Heart Valve Dis.; 16(5):508–510

[24] Motoyoshi N, Tofukuji M, Sakurai M, Ohmi M, Tabayashi K. Cleft on tricuspid anterior leaflet. Ann Thorac Surg.; 71(4):1350–1351

[25] Singh JP, Evans JC, Levy D, et al. Prevalence and clinical determinants of mitral, tricuspid, and aortic regurgitation (the Framingham Heart Study). Am J Cardiol.; 83(6):897–902

[26] Hung J. The pathogenesis of functional tricuspid regurgitation. Semin Thorac Cardiovasc Surg.; 22(1):76–78

[27] Ubago JL, Figueroa A, Ochoteco A, Colman T, Duran RM, Duran CG. Analysis of the amount of tricuspid valve anular dilatation required to produce functional tricuspid regurgitation. Am J Cardiol.; 52(1):155–158

[28] Fukuda S, Song JM, Gillinov AM. Tricuspid valve tethering predicts residual TR after tricuspid annuloplasty. Circulation.; 111:975–979

[29] Spinner EM, Shannon P, Buice D, et al. In vitro characterization of the mechanisms responsible for functional tricuspid regurgitation. Circulation.; 124 (8):920–929

[30] Marcus RH, Sareli P, Pocock WA, Barlow JB. The spectrum of severe rheumatic mitral valve disease in a developing country. Correlations among clinical presentation, surgical pathologic findings, and hemodynamic sequelae. Ann Intern Med.; 120(3):177–183

[31] Akinosoglou K, Apostolakis E, Koutsogiannis N, Leivaditis V, Gogos CA. Right-sided infective endocarditis: surgical management. Eur J Cardiothorac Surg.; 42(3):470–479

[32] Weinreich DJ, Burke JF, Bharati S, Lev M. Isolated prolapse of the tricuspid valve. J Am Coll Cardiol.; 6(2):475–481

18 Coronary Arteries and Myocardial Perfusion

Farhood Saremi

◆ Introduction

Knowledge of gross anatomy and microcirculation of the coronary arterial system is important not only to address the spatial location of a lesion but also to understand the mechanisms that lead to myocardial dysfunction. The standard clinical tool to visualize the coronary artery has been invasive cardiac catheterization and coronary angiography. Catheter angiography images have higher spatial resolution compared to recently developed noninvasive coronary computed tomography angiography (CTA). The anatomy of the epicardial coronary arteries can be shown down to third-generation (medium- to small-sized) branches by catheter angiography and to second-generation (medium-sized) branches by CTA. As opposed to projectional views in catheter angiography, CT imaging has solved the problem of overlapping vessels by generating a volume of data consisting of 0.5 mm^3 voxels that can be reconstructed into 0.5-mm cuts in any desired direction. Although, the spatial and temporal resolutions of CT are lower than in invasive angiography, the noninvasive nature of the test has led to a rapidly increasing use in clinical practice. Using modern postprocessing workstations, maximum intensity projections or volume-rendered 3D images can be reconstructed. Vessel tracking, automated segmentation methods, and color-coding techniques have further improved the quality of postprocessing capabilities. In contrast to epicardial vessels, demonstration of microcirculation and tissue perfusion requires sophisticated imaging techniques such as micro-CT to show microcirculation and perfusion CT, magnetic resonance (MR) imaging, or echocardiography to evaluate tissue perfusion. This chapter will place special emphasis on typical epicardial coronary anatomy as seen in coronary CTA. Myocardial microcirculation will be discussed briefly.

◆ Epicardial Coronary Arteries

Embryology

It was suggested in earlier experiments that coronary vessels arise from the proepicardium, a transitory structure in the embryonic heart that forms epicardium and several internal tissues.[1] Recent histological analysis in mouse and cardiac organ culture has shown that coronary vessels arise from angiogenic sprouts of the sinus venosus, the major vein that returns circulating blood to the embryonic heart.[2] Some sprouting venous endothelial cells dedifferentiate into arteries and capillaries as they invade the myocardium and some remain on the surface and differentiate into veins.[2]

Gross Anatomy

Coronary arteries are variable in anatomic origin, course, and branching.[3] In general, coronary vessels are named for the structures that they supply rather than for their origin. This nomenclature is based on the embryologic development pattern that the coronary vessel sprouts arise on the surface of the heart and only later connect to the aorta. Thus, various perturbations in the connections of the coronary vessels to each other and to the aorta occur subsequent to the formation of the coronary vessels. In spite of variability in coronary artery origin, course, and branching, the vast majority of individuals have two coronary arteries: the right coronary artery (RCA) and the left coronary artery. The left main (LM) coronary artery branches into the left anterior descending (LAD) and left circumflex (LCx) arteries (▶ Fig. 18.1). These three major coronary vessels are considered arteries, while the secondary ramifications are generally termed coronary branches. In spite of this generalization, it is not uncommon to call some small branches "artery," that is, sinoatrial node (SAN) artery or posterior descending artery (PDA).

Instead of bifurcating into the LAD and LCx arteries, in 10 to 15% of patients, the LM trifurcates into the LAD, LCx, and ramus intermedius arteries[1,3] (▶ Fig. 18.2). The ramus may arise directly from the LM artery (trifurcation) or near the orifice of the LAD or the LCx. Therefore, the ramus may actually be considered the first branch of the LAD or the LCx when arising from these vessels.

The relationship between the coronary artery branches at the crux cordis is called coronary artery dominance and is determined by the artery giving rise to the posterior interventricular branch/artery (PDA)[1,3,4,5,6] (▶ Fig. 18.3). The PDA and posterolateral (PL) branches that supply the inferior ventricular septum and the inferior wall, respectively, can originate from only the RCA (right dominant, 65–90%), from only the LCx artery (left dominant), or from both arteries (codominant). In CT studies, a "codominant pattern" is commonly described when the RCA gives off to the PDA, but all PL branches of the left ventricle (LV) and sometimes a second PDA arise from the LCx artery. The left-dominant system is more common in bicuspid aortic valve particularly when fusion is between right and left leaflets and may reach up to 48%.[7] Another definition of coronary dominance involves the artery that gives rise to the atrioventricular nodal (AVN) artery. The AVN artery arises from the RCA in almost 85% of cases.

Segmental Classification

Coronary anatomy varies, and several nomenclatures have been proposed to describe the angiographic anatomy of the coronary arteries. Currently, the most commonly used classification is based on three major coronary arteries with right-dominant, balanced, or left-dominant circulations. The extent of disease is usually defined as one-vessel, two-vessel, three-vessel, or LM disease. Significant stenotic disease is the presence of a stenosis of greater than 70% diameter reduction.[8]

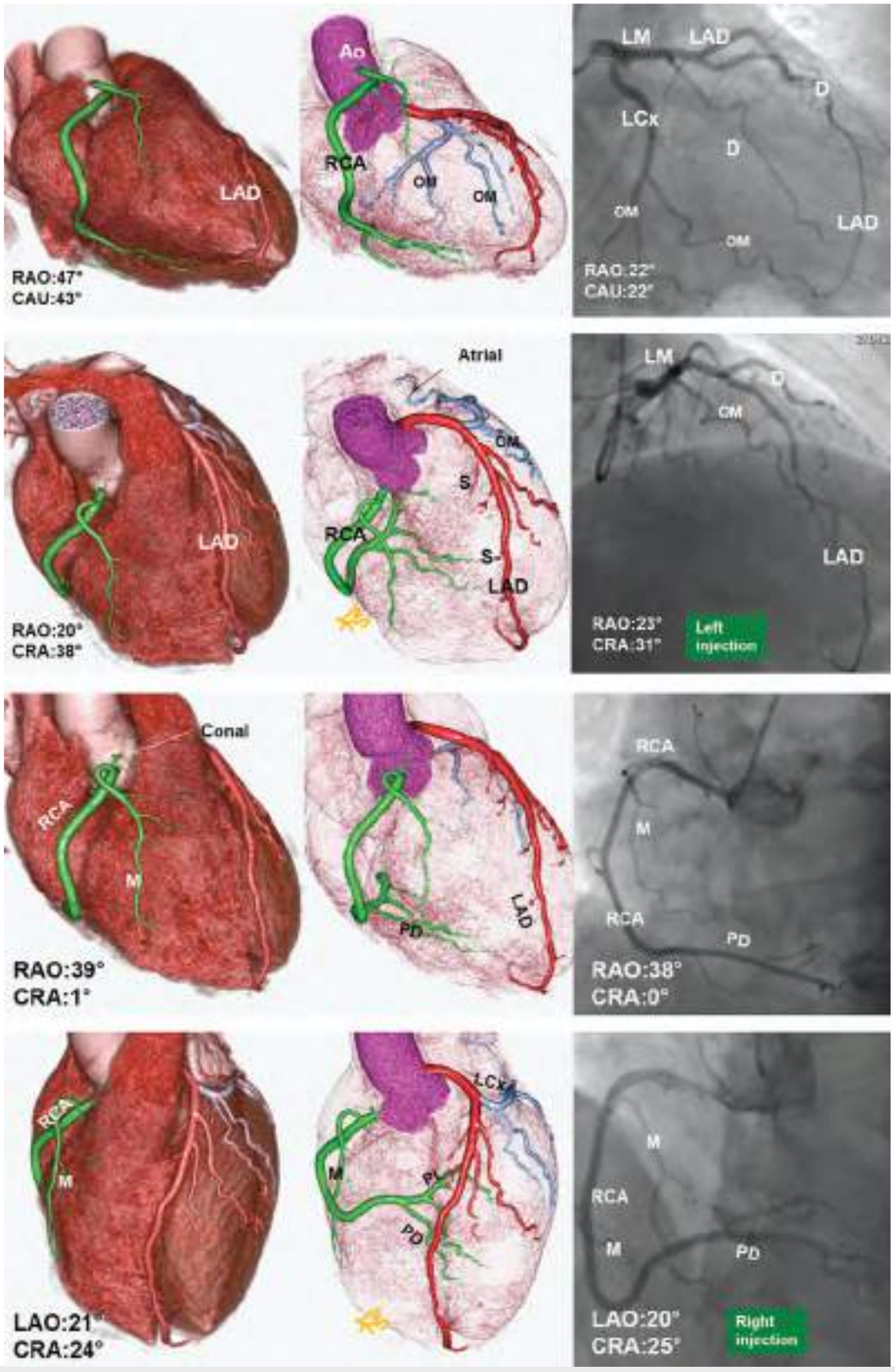

Fig. 18.1 Coronary artery system. Color-coded volume-rendered CT angiography and invasive angiography (left and right injections) images in standard projections demonstrate normal coronary artery anatomy. Right anterior oblique (RAO), left anterior oblique (LAO) projections with caudal (CAU), or cranial (CRA) tilts are shown. The left main (LM) coronary artery divides into the left anterior descending (LAD) and the left circumflex (LCx) arteries. The LAD descends in the anterior interventricular groove and gives off diagonal (D) and septal (S) branches. In some cases, the LAD wraps around the apex to the inferior wall (as shown in these examples). The LCX moves in the left atrioventricular groove and gives rise to the left lateral atrial branch and one or more obtuse marginal (OM) and left posterolateral (PL) branches. The OM branches may be large and supply part of the anterior wall and most of the lateral wall of the left ventricle. The right coronary artery (RCA) gives origin to the conus and sinoatrial node arteries and descends into the right atrioventricular groove. Several right ventricular branches can arise from the descending section of the RCA. At the crux, the RCA then gives rise to a small atrioventricular nodal branch and then continues in the inferior (posterior) interventricular groove to provide the posterior descending (PD) branch. In many cases, the RCA travels beyond the crux and gives off PL branches to the posterior wall of the left ventricle.

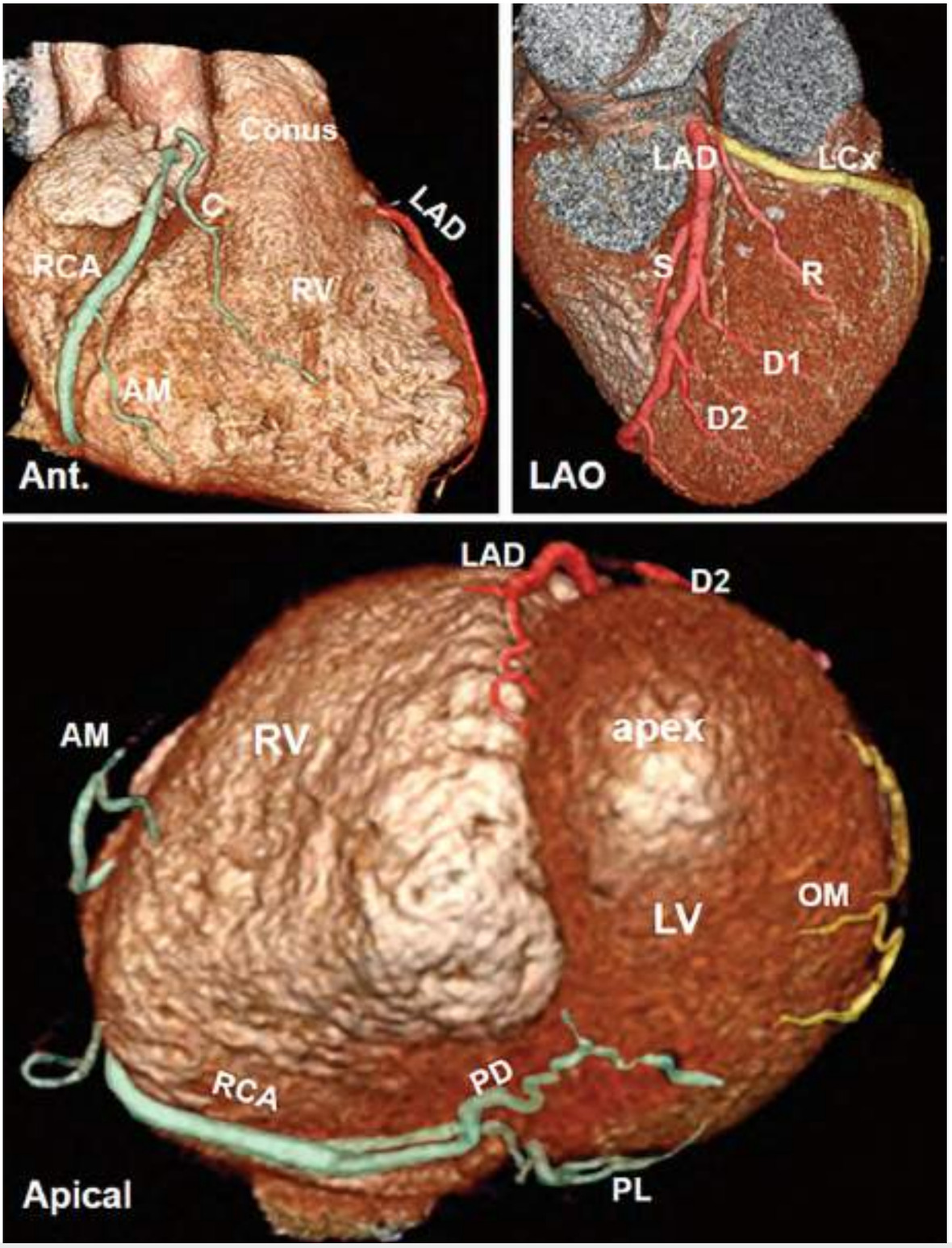

Fig. 18.2 Coronary anatomy. Volume rendered CT images in anterior (Ant.), left anterior oblique (LAO), and apical projections. The anterior view shows the right coronary artery (RCA) descending in the right atrioventricular groove. A large conus (C) branch is seen arising from the aorta near the RCA ostium and is directed toward the right ventricular (RV) free wall. Marginal and acute marginal (AM) branches are usually seen in this projection. The distal RCA usually descends into the inferior (posterior) interventricular groove to provide the posterior descending (PD) branch. The PD branch can reach the apex and provide posterior septal branches. If the RCA extends beyond the crux, the branches are called posterolateral (PL) branches. The LAO view shows trifurcation of the left main coronary artery into the left anterior descending (LAD), the left circumflex (LCx), and ramus intermedius arteries. The ramus intermedius, also known as the intermediate branch or ramus, varies in length and size. It typically supplies the lateral wall of the left ventricle (LV) in a territory similar to that supplied by the diagonal (D) or obtuse marginal (OM) branches. The LAD descends in the anterior interventricular groove to reach the apex. During its entire course, the LAD gives rise to septal branches that penetrate into the interventricular septum; the first septal branch (S) is often large. The diagonal (D) branches are variable in size and number. The LCX enters the left atrioventricular groove and usually gives rise to one or several OM branches and may continue to end in several left PL branches (LCx dominant or codominant).

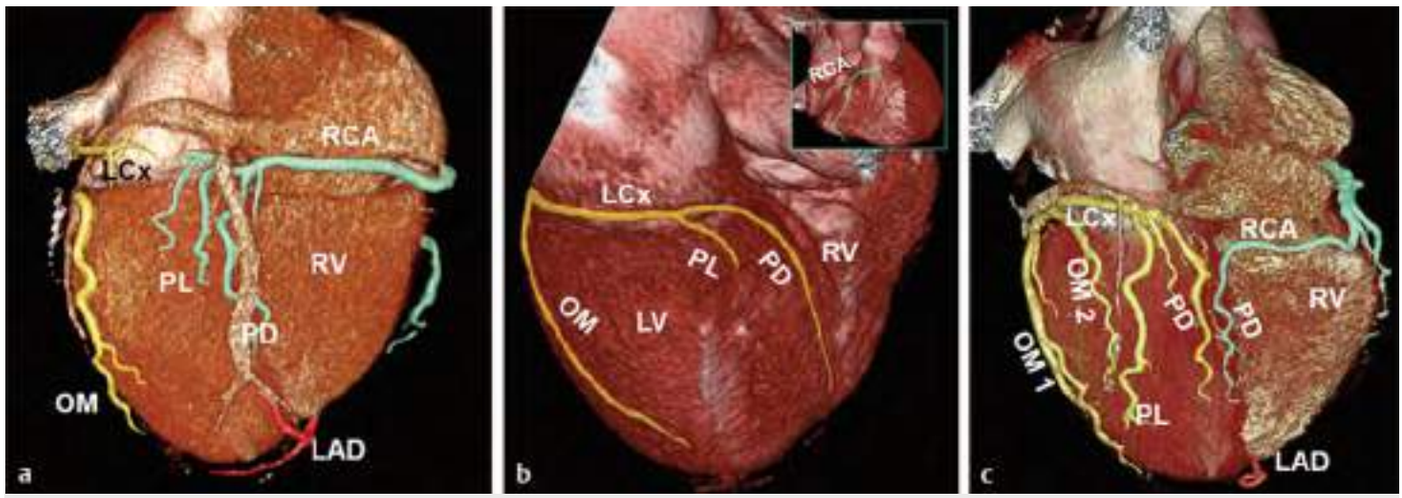

Fig. 18.3 Coronary dominance. Inferoposterior views of volume rendered CT angiographies. **(a)** In the right-dominant system, the right coronary artery (RCA) gives rise to the posterior descending (PD) branch and at least one posterolateral (PL) branch of the left ventricle. **(b)** In the left-dominant system, the left circumflex (LCx) artery is large and provides a PD branch. The RCA is small and does not extend beyond the acute margin of the heart (shown in inlay image). **(c)** In the codominant system, most of the PL branches are provided by the LCx and the PD branch by the RCA. LV, left ventricle; OM, obtuse marginal; RV, right ventricle.

Right Coronary Artery (RCA)		
1	Proximal	RCA from ostium to one-half the distance to the acute margin of the heart.
2	Mid	RCA from end of the above segment to acute margin of the heart.
3	Distal	RCA running along the posterior right atrioventricular groove from the acute margin of heart to the origin of the posterior descending branch (dominant RCA).
4	Posterior Descending	Posterior descending branch, when present
Left Main Coronary Artery (LCA)		
5	Left main	LCA extends from the ostium of LCA through bifurcation into LAD and LCx
Left Anterior Descending Artery (LAD)		
6	Proximal	To origin of first major septal perforator branch or first diagonal
7	Mid	LAD immediately distal to origin of first major septal perforator branch to the origin of second diagonal branch (D2) or at one-half the distance from the first major septal perforator branch to apex of heart.
8	Apical	Terminal portion of LAD running along interventricular sulcus
9	First Diagonal	First diagonal (D1): The largest, and usually the first. Occasionally, this can be a separate branch off main LCA (Ramus).
10	Second Diagonal	Second diagonal (D2): often has its origon at the "angle" of LAD in RAO projection.
Left Circumflex Coronary Artery (LCx)		
11	Proximal	From its origin to the origin of obtuse marginal branch
12	Obtuse Marginal (OM)	The largest branch of the circumflex running near obtuse margin of heart.
13	Distal	Distal to origin of obtuse marginal branch and running along the posterior left atrioventricular groove. Usually a small caliber vessel.
14	Posterolateral (PL)	Posterolateral surface of left ventricle. Usually a small vessel. May be absent or may be a division of obtuse marginal branch.
15	Posterior Descending (PD)	Posterior descending, when present as a branch of the circumflex.

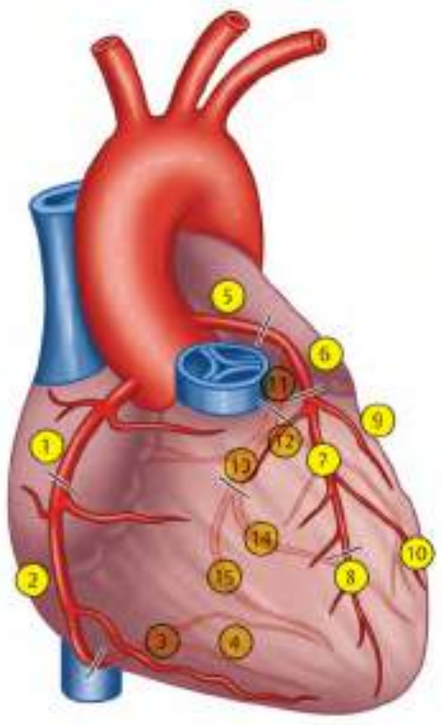

Fig. 18.4 Definition of coronary artery segments according to a report of the Ad Hoc Committee for Grading of Coronary Artery Disease, Council on Cardiovascular Surgery, American Heart Association. A simplified model is presented. (Used with permission from Austen et al.[9])

The American College of Cardiology and American Heart Association (AHA) Guidelines for invasive coronary angiography propose a topographic angiographic model that classifies the coronary arteries into 29 segments.[9] A more simplified classification based on an Ad Hoc Committee Report of the AHA is commonly used to interpret catheter and CT angiography studies[9] (▶ Fig. 18.4). Obviously, this model only shows a classic pattern of coronary vessel distribution and does not involve the variability that is frequently seen in the coronary artery branches.

Diagram of the topographic distribution of the coronary anatomy segments with description of the segments are shown in ▶ Fig. 18.4. This diagram has been modified to include the right PL branch and the ramus branches, which were not shown in the original version of this classification.

For cross-sectional imaging, the standard 17–myocardial segment model of LV is suggested by the AHA for all cardiac imaging modalities to facilitate a more detailed analysis of regional left ventricular function and perfusion[10] (▶ Fig. 18.5). However, the adopted model shows significant variability and overlap of these segments assigned to a specific territory that makes it difficult to compare the results between different studies (▶ Fig. 18.6).

The vascular supply to the inferior wall of the LV has a spectrum of variants. It is mainly supplied by the RCA and the LCx. The LAD artery that wraps around the apex can supply some of the apical inferior wall (▶ Fig. 18.3). The lateral wall territory is supplied by the LCx in a vast majority of individuals but can be shared by a large diagonal from the LAD or the ramus branch (▶ Fig. 18.6). Myocardial blood supply in the inferolateral region corresponds to LCx or RCA distribution, and the inferoseptal region can be supplied by the LAD or RCA.[15] In a correlative MR study, the presence of hyperenhancement in the basal and mid-anterior and anteroseptal or apical anterior wall has been 100% specific for LAD artery occlusion.[14] The LAD infarct frequently involves the mid-anterolateral, apical lateral, and apical inferior walls. No segment is 100% specific for the RCA occlusion. A combination of hyperenhancement in the anterolateral and inferolateral walls is 100% specific for an LCx occlusion, and, when extended to the inferior wall, is also 100% specific for a dominant or codominant LCx occlusion. Hybrid imaging combined with anatomic information of vascular distribution provided by CTA is useful to study myocardial tissue perfusion abnormalities and the coronary anatomy for more accurate assignment to culprit vessels and to improve monitoring of targeted therapy.[11] CT studies have shown common overlap between LAD and RCA perfusion territories at the inferoseptal region and between LAD and LCx territories at the anterolateral region. It is important to realize that the LAD territory can be larger than the AHA-proposed 17-segment model, due to the involvement of the anterolateral and all the apical segments of the LV.[15]

Common Variants

Left Coronary Artery

The LM coronary ostium is located in the midportion of the left sinus of Valsalva with a mean distance of 14 ± 3 mm from the annulus. It measures approximately 8 mm in diameter and travels for 5 to 15 mm before dividing into the LAD and LCx arteries. The mean bifurcation angle between the LAD and LCx is 80±23 degrees[12]

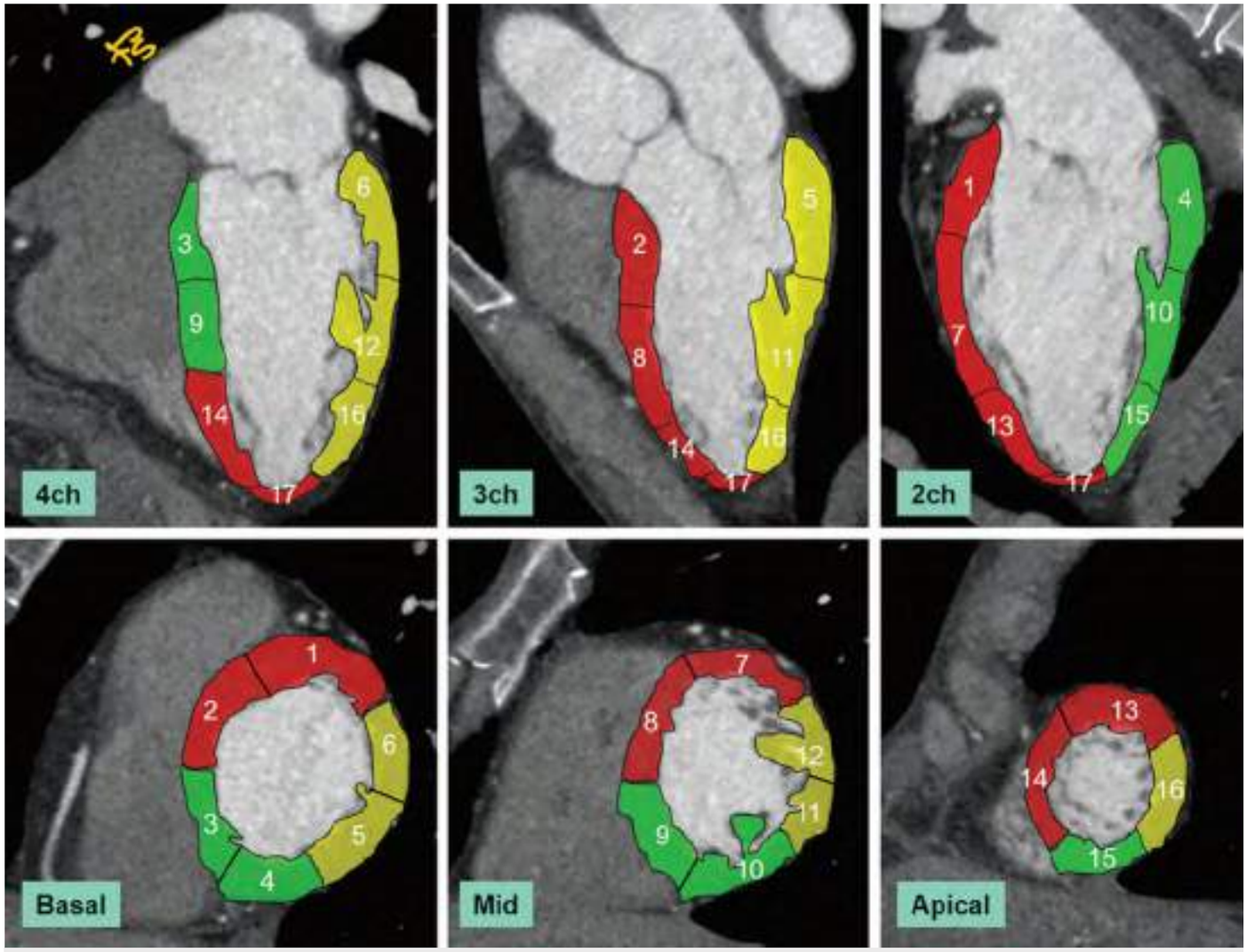

Fig. 18.5 Long- and short-axis CT angiography images show the distribution of the left ventricular 17 myocardial segments based on the American Heart Association (AHA) model: basal anterior,[1] basal anteroseptal,[2] mid-anterior,[7] mid-anteroseptal,[8] apical anterior,[11] apical septal,[12] and apex[13] segments corresponded to LAD (*red*). Basal anterolateral,[6] basal inferolateral,[5] mid-anterolateral,[14] mid-inferolateral,[15] and apical lateral[16] segments correspond to LCX (*yellow*). Basal inferoseptal,[3] basal inferior,[4] mid-inferoseptal,[9] mid-inferior,[10] and apical inferior[17] segments correspond to RCA (*green*) distribution. ch, chamber; LAD, left anterior descending; LCx, left circumflex artery; RCA, right coronary artery. Used with permission from Scanlon et al.[8]

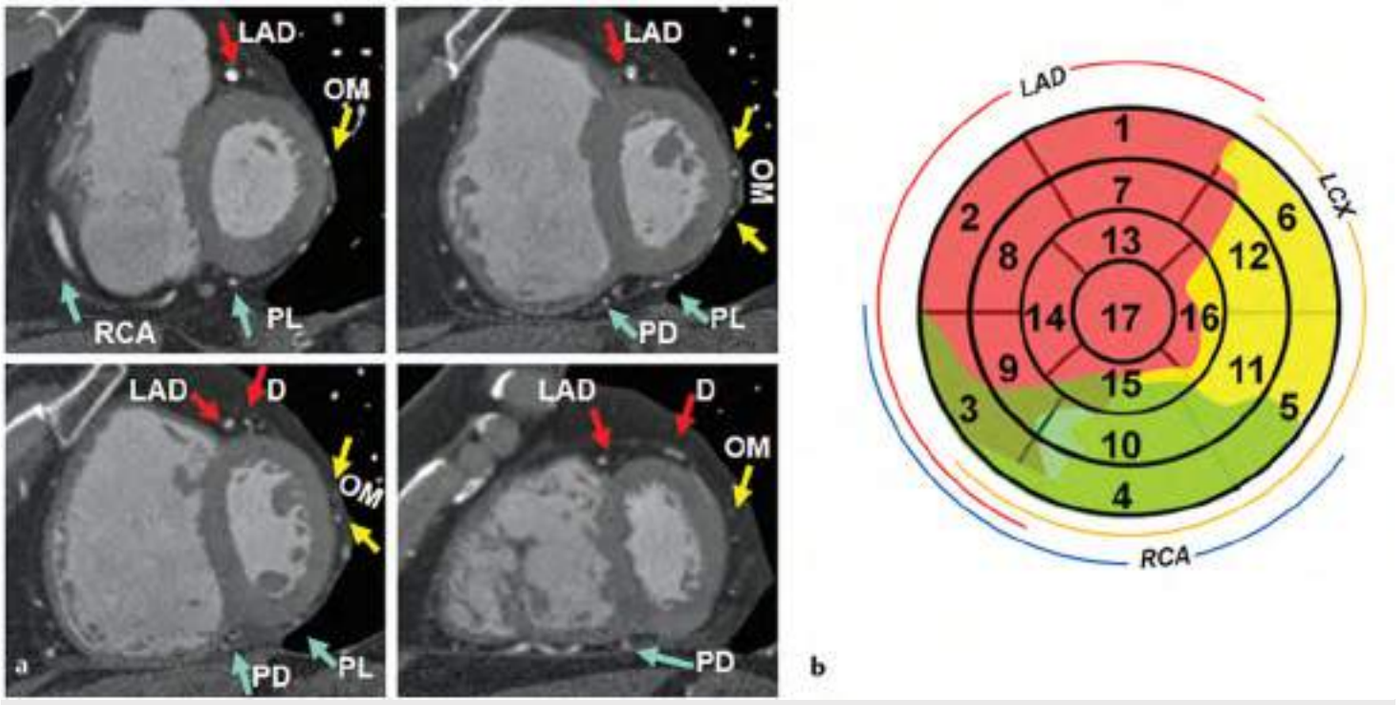

Fig. 18.6 **(a)** Short-axis CT angiography images show anatomical distribution of the coronary arteries in relation to the left ventricular segments. *Arrows* show territories of the LAD (*red*), RCA (*blue*), and LCx (*yellow*). **(b)** Maximal extent of myocardium perfusion for LAD (*red*), RCA (*green and blue*), and LCX (*yellow*) and overlapped regions in the polar map of 17 segments. D, diagonal branch; LAD, left anterior descending; OM, obtuse marginal branch of left circumflex artery (LCx); PD, posterior descending branch; PL, posterolateral; RCA, right coronary artery.[14]

(▶ Fig. 18.7, ▶ Fig. 18.8, ▶ Fig. 18.9). Knowing the angle of bifurcation may be important for optimal stent deployment.

Anatomical variants of the LM are common. The ostium of the LM artery may arise at or above the sinotubular junction. When it arises at the sinotubular, the ostium may be small. A high origin the LM may be prone to accidental cross clamping or transection during aortotomy (▶ Fig. 18.10). A very low position ostium may become obstructive after percutaneous aortic valve implantation. A very short LM artery can cause technical problem during stenting of the LAD stenosis at its takeoff. Separate origins of the LAD and LCx in left sinus of Valsalva are another relatively common variants (▶ Fig. 18.11). The incidence is more common in bicuspid aortic valve, especially with left–right fusion and may reach up to 28%.[7]

The LAD passes behind the main pulmonary artery to enter the anterior (superior) interventricular groove (sulcus) where it travels to reach the apex (▶ Fig. 18.7, ▶ Fig. 18.9). It gives rise to the perforating septal and one to three diagonal branches with viable sizes to supply the anterior two-thirds of the septum and the anterolateral wall of the LV including the superolateral papillary muscle, respectively (▶ Fig. 18.9). Small branches to the anterior wall of the right ventricle (RV) or the RV infundibulum may arise from the LAD. The distal segment of the LAD usually ends up near the apex, but it may wrap around it and travel further in the inferior interventricular groove. In rare cases, it may reach the cardiac crux (▶ Fig. 18.3**a**).

A confusing variant of the LAD is called dual LAD. Type I dual LAD is worth mentioning because it is relatively common and may have clinical implications. In this variant, the LAD trunk is bifurcated (split LAD) into a short and a long branch to give off septal perforators. The short LAD stays in the proximal anterior interventricular groove branching into several septal perforators (usually 3–4; ▶ Fig. 18.12).[17] This artery should not be confused with a large first perforating septal branch during catheter angiographies, which may need to be embolized for treatment of obstructive hypertrophic cardiomyopathy.

The LCx or circumflex artery arises from the LM coronary artery. It then passes under the left atrial appendage, to reach the left AV groove (▶ Fig. 18.7, ▶ Fig. 18.9). At this level, small atrial branches including a left SAN artery may arise from the LCx (▶ Fig. 18.13). The position of the LCx in relation to the AV groove is variable. The LCx gives off one or more obtuse marginal (left marginal) branches to supply the lateral and posteroinferior walls of the LV. It is not uncommon to see a small LCx to continue in the AV groove after giving off to a large obtuse marginal branch. The distal LCx can travel in the AV groove to reach cardiac crux. At the AV groove, it could be damaged during mitral valve surgical or percutaneous interventions. When dominant, the LCx gives rise to the posterior interventricular artery (▶ Fig. 18.3).

Myocardial bridging can be found in any epicardial artery, but greater than 60% occurs in the proximal LAD artery or one of diagonal branches (▶ Fig. 18.14). It refers to the intramyocardial course of a portion of a normally positioned epicardial coronary artery. The degree in which the coronary artery travels into the myocardium is variable in depth and length. The bridged segment is usually protected from atherosclerotic diseases and calcifications, but plaques can form proximal to it.[16] The significance of transient systolic narrowing (milking effect) of the bridged segment is not clear since most coronary blood flow occurs in diastole. The hemodynamic impact of myocardial bridging depends on the thickness and length of the bridge and rarely

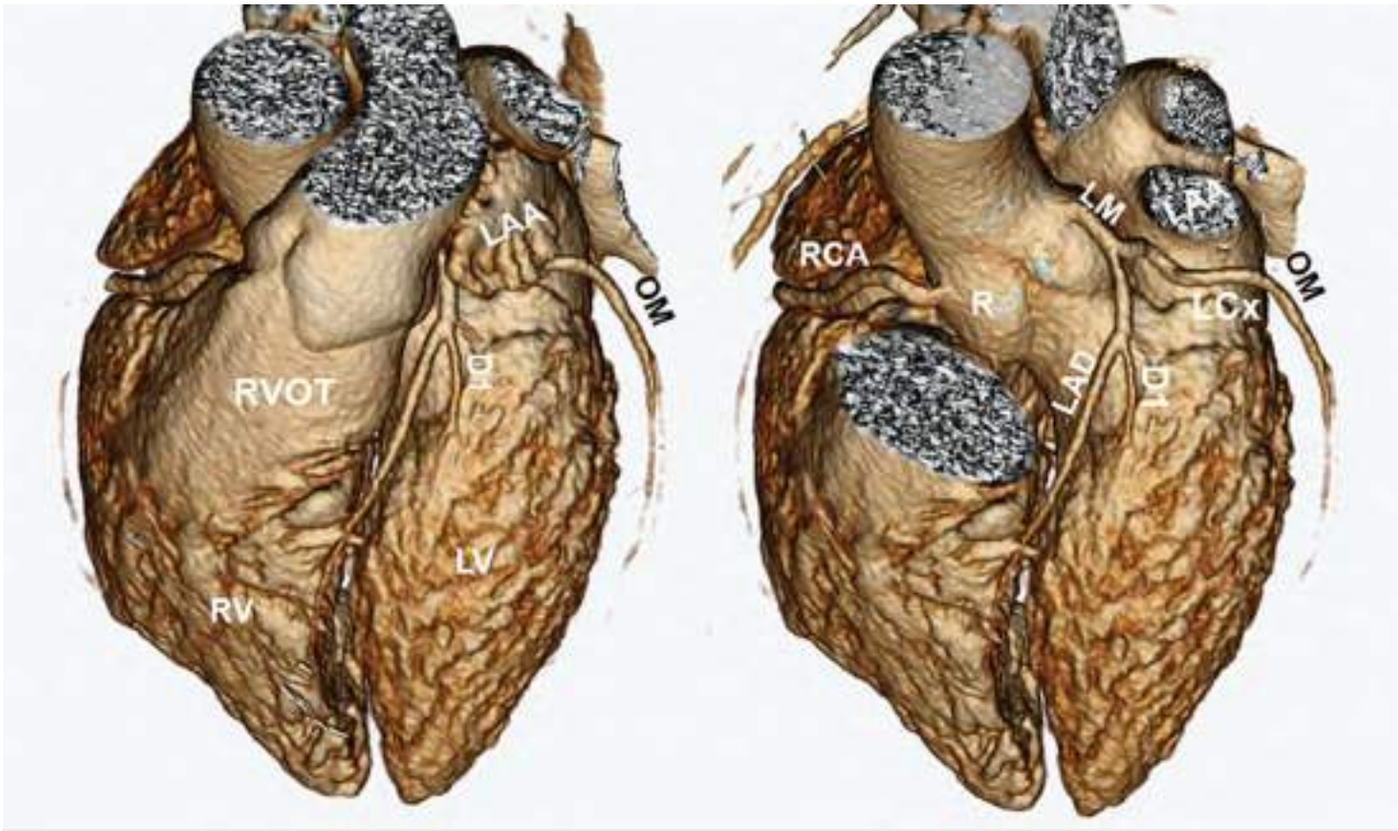

Fig. 18.7 Left coronary artery. Volume rendered CT images at 37-degree left anterior descending with 45-degree cranial tilt showing proximal coronary arteries before and after removal of the right ventricular outflow tract (RVOT) and the left atrial appendage (LAA). The left main (LM) is shown only after removal of the LAA. It measured 12 mm and the angle of bifurcation was 85 degrees. The LM and right coronary artery (RCA) ostia are located in mid to upper portion of the sinuses of Valsalva. D, diagonal; LAD, left anterior descending; LCx, left circumflex; LV, left ventricle; OM, obtuse marginal; R, right coronary sinus; RV, right ventricle.

Fig. 18.8 Early takeoff of the first diagonal (D1) branch. The location for ostial origin of the septal arteries is shown by *red dots*. The proximal segment of the LAD is defined from the origin to the takeoff of the first septal branch.

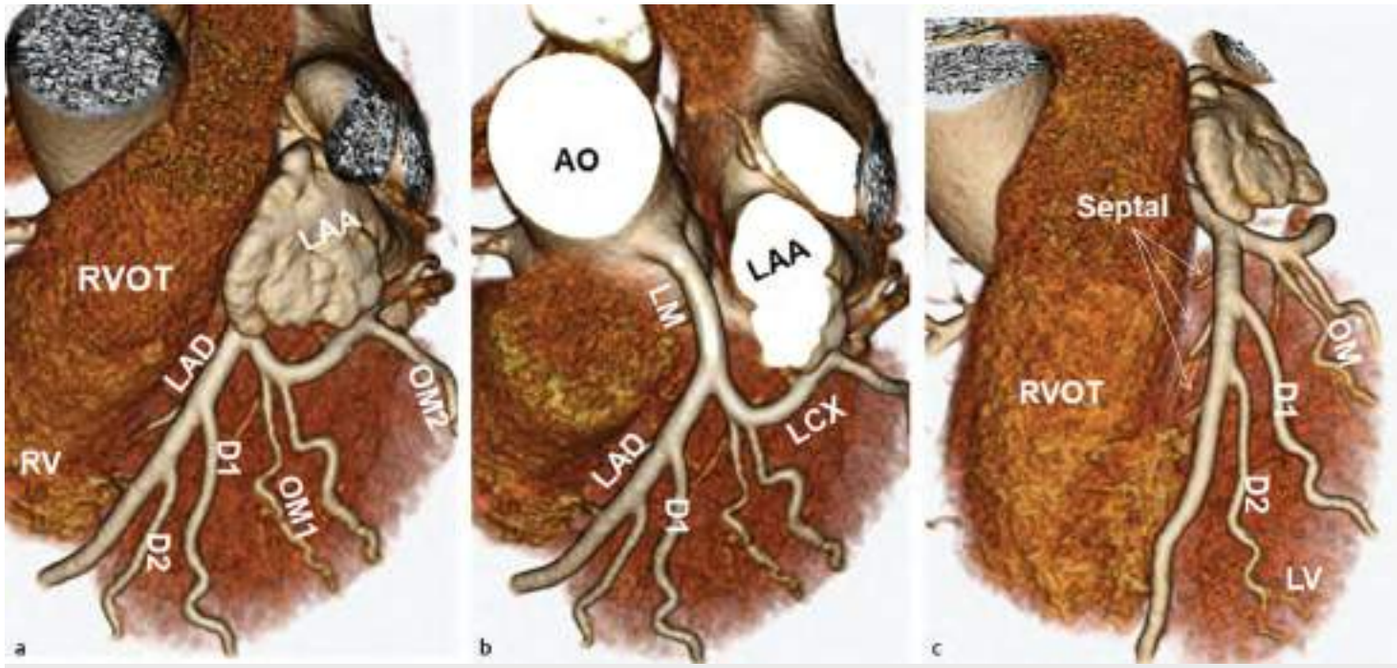

Fig. 18.9 Left coronary artery. Volume rendered CT images at 46-degree left anterior oblique with 53-degree cranial tilt showing proximal coronary arteries before **(a**, **c)** and after **(b)** removal of the right ventricular outflow tract (RVOT) and the left atrial appendage (LAA). The left main (LM) is shown after removal of the LAA and RVOT. It measured 21 mm. Ao, aorta; D, diagonal; LAD, left anterior descending; LCx, left circumflex; LV, left ventricle; OM, obtuse marginal; RV, right ventricle.

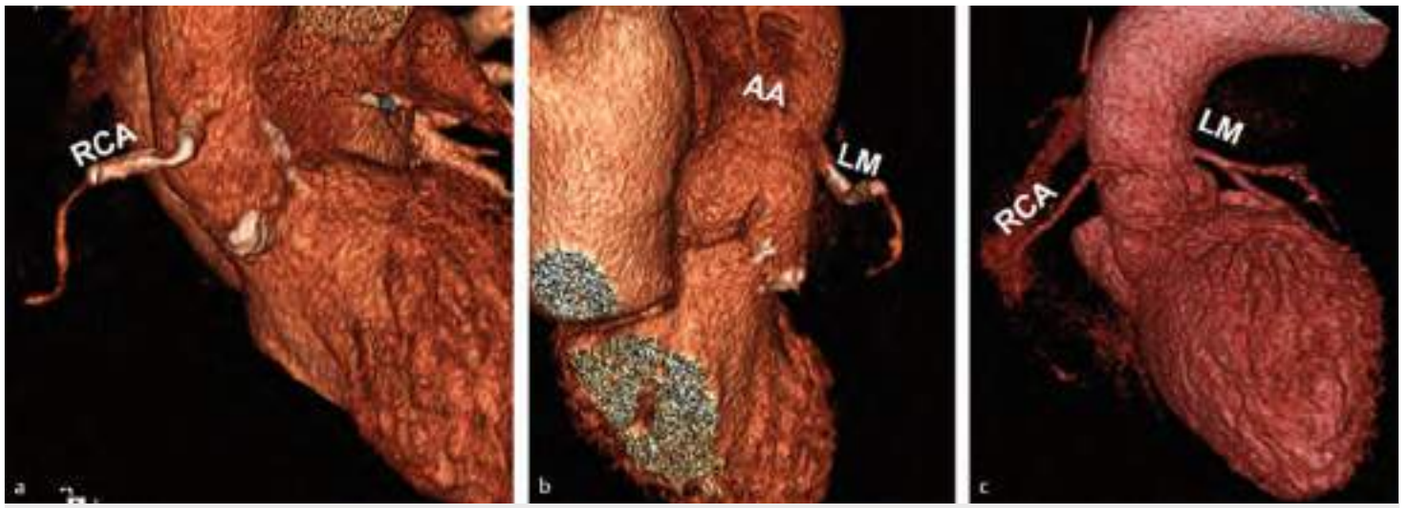

Fig. 18.10 High-riding right coronary artery (RCA) and left main (LM) artery. **(a**, **b)** Origin from the ascending aorta (AA). **(c)** Origin from the sinotubular junction.

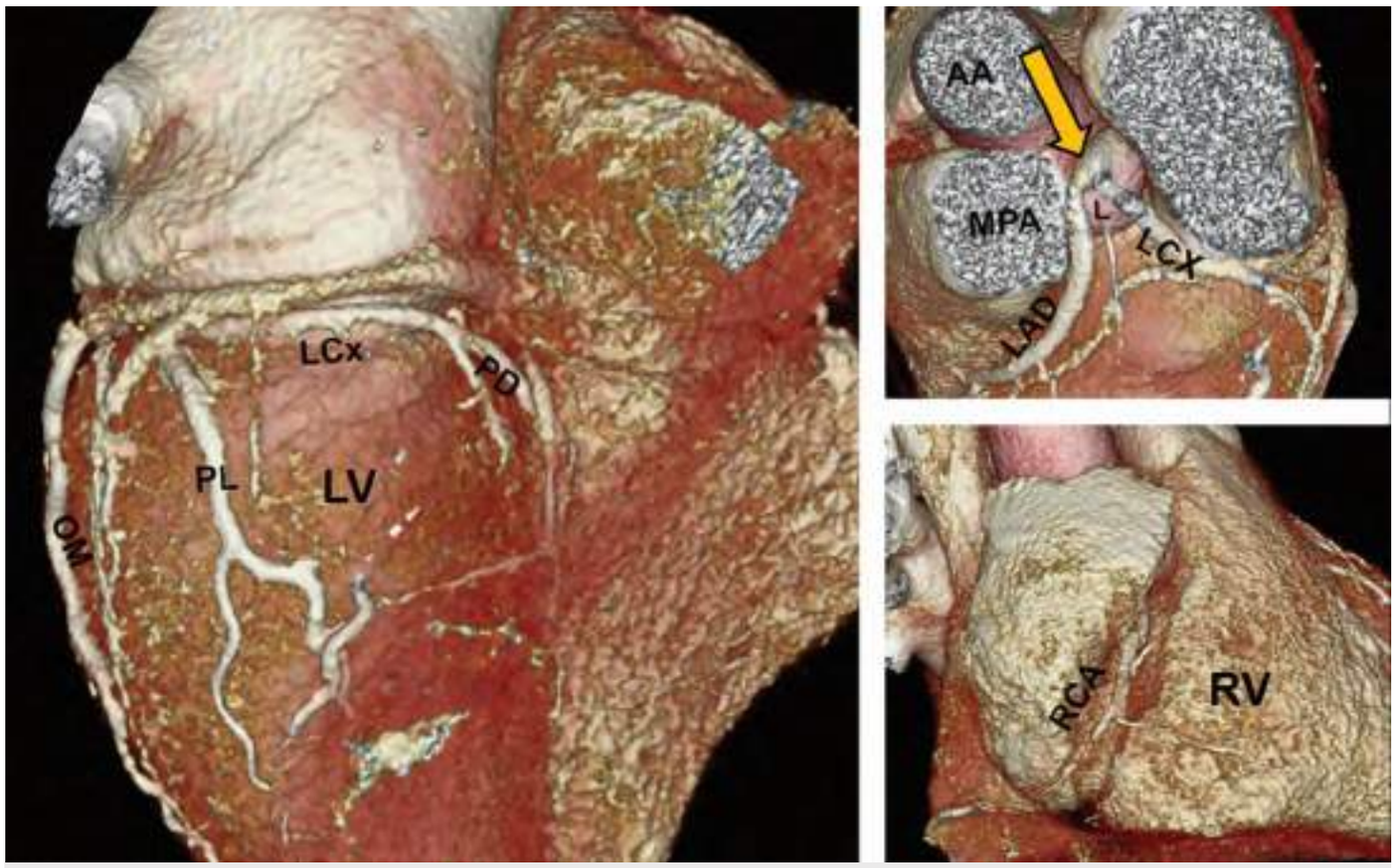

Fig. 18.11 Combination of separate origin (*arrow*) of the left anterior descending (LAD) and left circumflex (LCx) arteries and a left-dominant coronary system. This combination is common in the bicuspid valve of the aorta. The right coronary artery (RCA) is small and nondominant. AA, ascending aorta; L, left coronary aortic sinus; LV, left ventricle; MPA, main pulmonary artery; OM, obtuse marginal; PL, posterolateral; RD, posterior descending; RV, right ventricle.

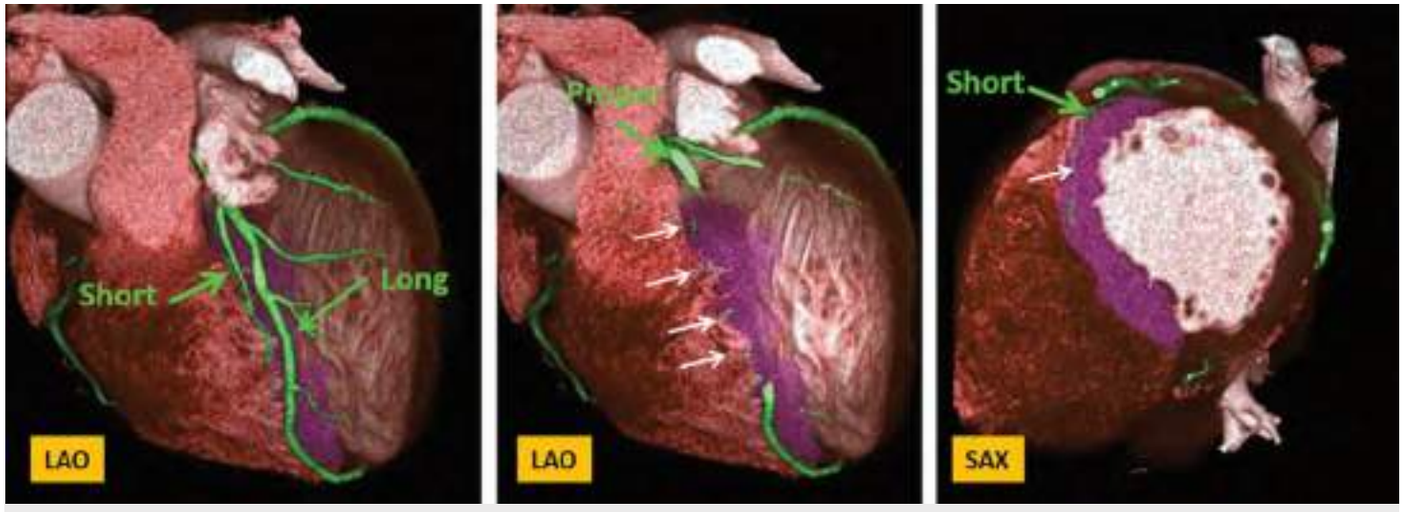

Fig. 18.12 Type 1 dual LAD. The dual LAD is defined and as an early bifurcation of the proximal LAD (the LAD proper) into a short and a long LAD. The short LAD stays in the proximal anterior interventricular groove (AIVG) and gives off most of the septal branches (*white arrows*). The long LAD travels to the apex, first along but outside the AIVG and gives off diagonal branches, then entering the AVIG to nourish the distal ventricular septum. LAO, left anterior descending; SAX, short axis.

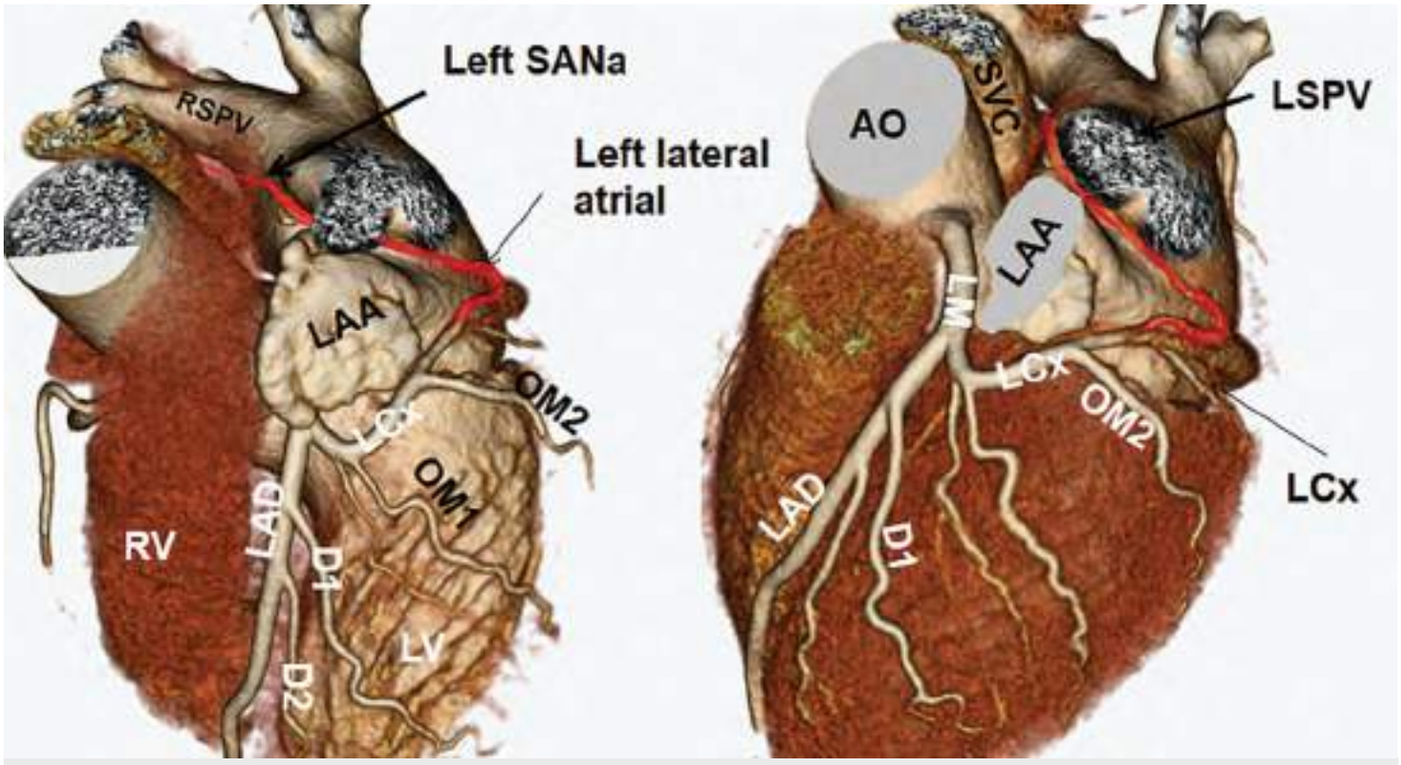

Fig. 18.13 Left lateral atrial branch of the left circumflex (LCx) artery giving rise to the left sinoatrial node (SAN) artery. This artery is also called an S-shaped SAN artery because of its long tortuous anatomic course toward the superior vena cava (SVC) where the SAN is located. The artery passes between the left atrial appendage (LAA) and the left superior pulmonary vein (LSPV). Ao, aorta; D, diagonal; LAD, left anterior descending; LM, left main; LV, left ventricle; OM, obtuse marginal; RSPV, right superior pulmonary vein; RV, right ventricle.

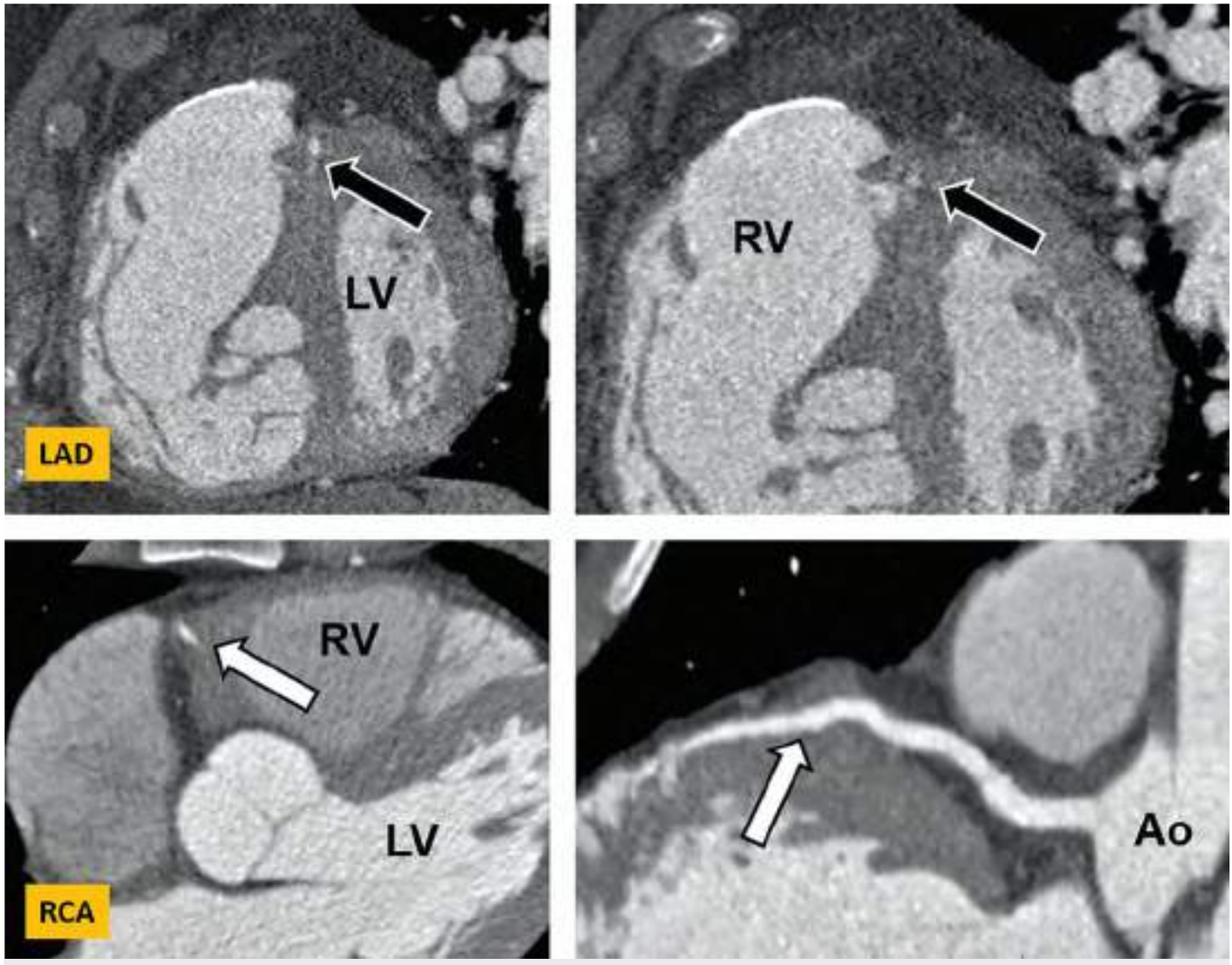

Fig. 18.14 Myocardial bridging (*arrows*). Upper row: Myocardial bridging can be found in any epicardial artery but greater than 60% occurs in the proximal LAD artery. It may travel deep in the muscle and even reach the right ventricular (RV) cavity. Lower row: Myocardial bridge of the right coronary artery (RCA) next to the right ventricle (RV). Ao, aorta; LV, left ventricle.

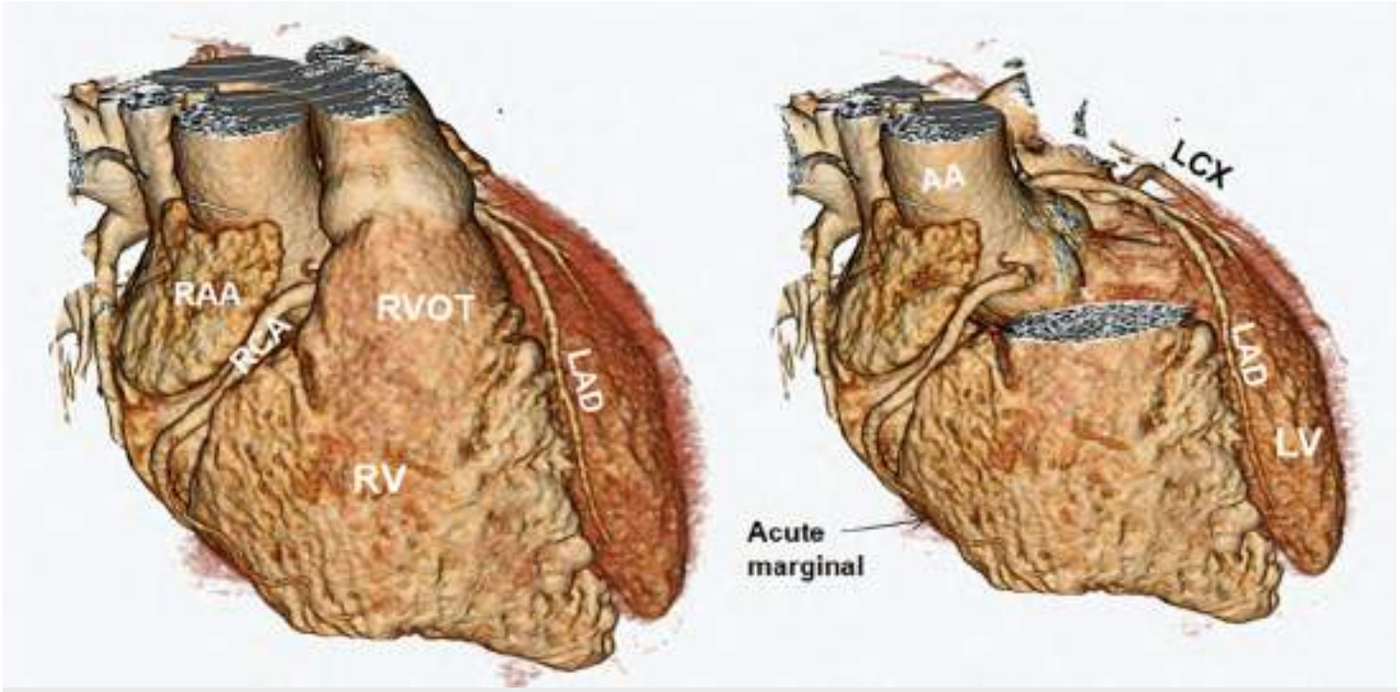

Fig. 18.15 Proximal right coronary artery (RCA). The RCA arises from the right coronary sinus behind the right ventricular outflow tract (RVOT) and enters the right atrioventricular groove and travels in it toward the posterior part of the interventricular groove. AA, ascending aorta; LCx, left circumflex artery; LV, left ventricle; RAA, right atrial appendage; RV, right ventricle.

may be associated with exertional angina and acute coronary syndromes.

Right Coronary Artery

The RCA arises from the right coronary sinus (▶ Fig. 18.15). Mean distance between the aortic annulus and the ostium of the RCA is 17 ± 3 mm.[13] There is remarkable variability in the branches of the proximal RCA or of the right aortic sinus close to the coronary ostium. The five arteries that may arise from the first 2 cm of the RCA include an anterior conal artery, a right SAN artery, an adventitial artery (vas vasorum) of the aortic root, a preventricular artery, and occasionally a right superior septal artery (right Kugel's; ▶ Fig. 18.16, ▶ Fig. 18.17). The conus, SAN, and superior septal arteries can arise with a separate ostium directly from the right coronary sinus, with the right conus artery being the most common variant. In its proximal course, the RCA enters the right AV groove and travels in it toward the posterior part of the interventricular groove to reach the crux of the heart. At this point or some time earlier, the RCA bifurcates into two branches: the posterior-descending branch and the PL branch(s) (▶ Fig. 18.3).

The PDA travels in the inferior (posterior) interventricular groove toward the apex of the heart. The right PL branch/branches supply the PL wall of the LV. These branches are usually small but can be large when the RCA is super-dominant and the LCx is diminutive (▶ Fig. 18.18). One or two marginal (acute marginal) branches arise from the mid-portion of the RCA to supply the RV free wall.

Variation in the course of middle and distal segments of the RCA is uncommon. A segment of the RCA may move outside the atrioventricular groove, dive into the myocardium (bridging; ▶ Fig. 18.14), or enter the cavity of the right atrium (intracameral).[18]

Posterior Descending Artery

Evaluation of the anatomical origin and course of the PDA is important in angiographic studies of the coronary arterial system. The PDA determines the coronary dominance. In most patients, the PDA arises from the distal portion of the coronary artery, but in some cases an early takeoff of the PDA from the RCA is seen, which then courses toward the apex along the diaphragmatic surface of the RV. This common variant is referred to as "split RCA"[17,19] (▶ Fig. 18.19). The splitting is usually proximal and leads to one branch with normal anatomical course in the right AV groove, giving rise to a PDA that supplies the proximal (basal) portion of the inferior interventricular groove, and a second branch that courses over the right ventricular free wall (acute marginal), and terminates in the distal part of the inferior interventricular groove as the distal PDA.[17] Other unusual variants include duplicated PDA or a single PDA that immediately bifurcates in two equal-sized branches (split PDA) running along the sides of the inferior interventricular groove (▶ Fig. 18.20). Split-RCA and dual-PDA cases appear to be benign and do not warrant a special management, except in the presence of atherosclerotic stenoses, which can make cannulation challenging during percutaneous coronary intervention.[20]

In the codominant (balanced) coronary system, branches from both the LCx and RCA share vascular supply to the inferior interventricular septum.[5,6] In other words, a "dual perfusion" exists that provides blood flow to both sides of the septum (▶ Fig. 18.3, ▶ Fig. 18.21). Therefore, using the perfusion concept, several vessel arrangements exist that can fit in the definition of a

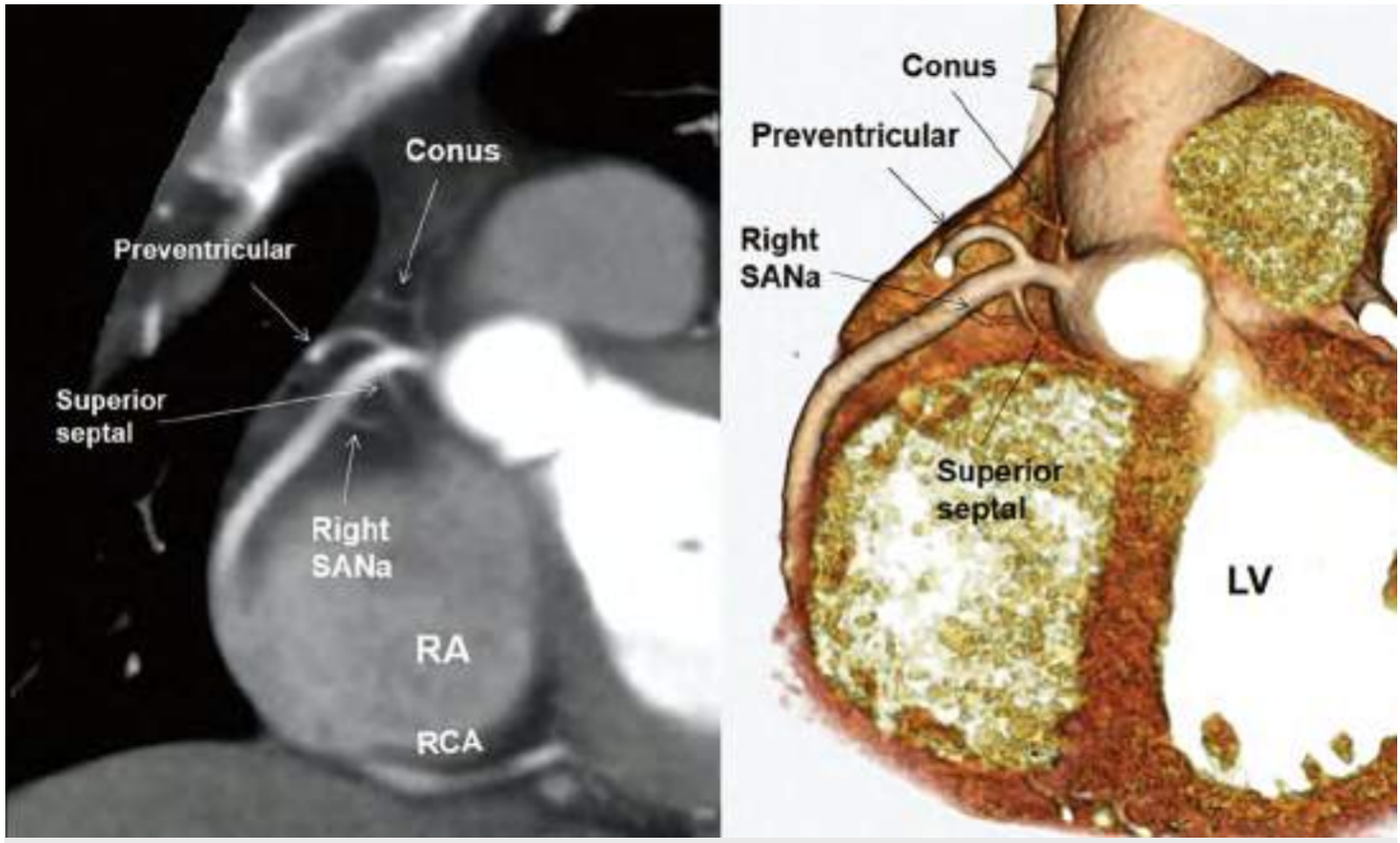

Fig. 18.16 Proximal right coronary artery (RCA) branches. Five arteries that may arise from first 2 cm (ostial segment) of the RCA including an anterior conal artery, a right sinoatrial node (SNA) artery, an adventitial artery (vasorum) of the aortic root, a preventricular (marginal) artery, and occasionally a right superior septal artery (right Kugel's). The right superior septal artery in this example is supplying the base of the ventricular septum. LV, left ventricle; RA, right atrium.

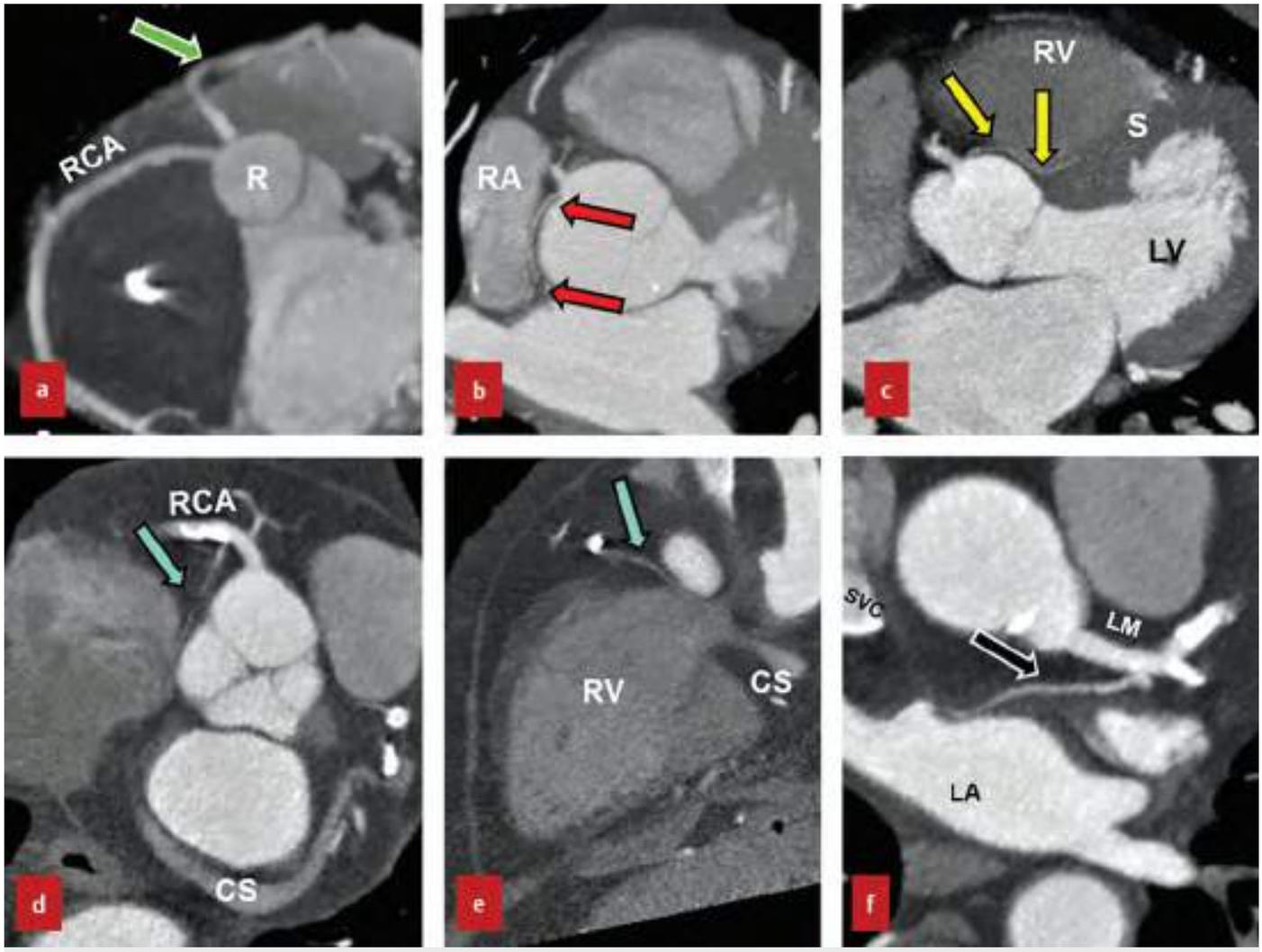

Fig. 18.17 Right coronary system branches. Most of these branches arise from ostial segment of the right coronary artery (RCA) or directly from the right coronary aortic sinus and may participate in conotruncal collateral circulation when a major artery is occluded. **(a)** Right anterior conus (direct origin from the aorta). It is the most common blood supply to the conal region. **(b)** Right sinoatrial node (SAN) artery (direct origin from the aorta) may provide branches to the atria and retroaortic circulation. Direct origin of the SAN artery (*red arrows*) can be seen in 1% of CT coronary studies. **(c)** Right superior septal artery (*arrow*) with direct origin from the aorta. This artery supplies the infundibular part of the basal ventricular septum and can participate in retroconal and retroaortic collateral circulations or connect with the first septal artery. It is seen in 3% of angiographic studies and 27% of heart dissections. **(d, e)** Right Kugel's artery. Oblique short-axis and right ventricle (RV) long-axis views at the level of the central fibrous body showing extension of the right Kugel from the RCA along the right side of the aortic root to the interatrial septum. The right Kugel artery is probably a variant of the right superior septal artery, which courses toward the atrium and the atrioventricular nodal region rather than the base of ventricular septum. **(f)** Left atrial branch extending from the left main (LM) artery to the interatrial septum. This artery can extend to the SAN or participate in the retroaortic collaterals. LV, left ventricle; CS, coronary sinus; IVC, inferior vena cava; R, right coronary sinus; RV, right ventricle; RVOT, right ventricle outflow tract; S, septum; SVC, superior vena cava.

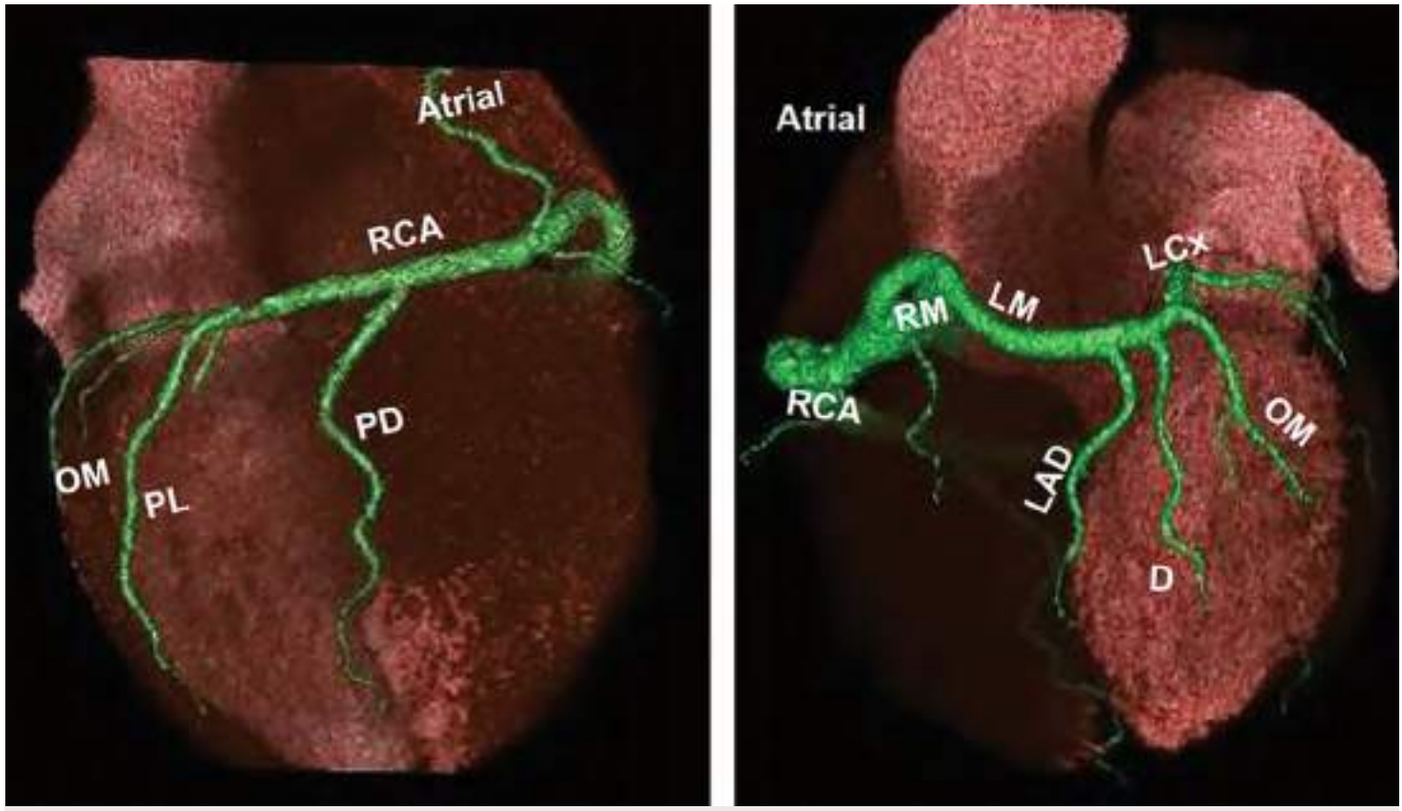

Fig. 18.18 Super-dominant right coronary artery (RCA) in a patient with single right main (RM) artery. The left main artery arises from the RM to supply the left anterior descending (LAD), left circumflex (LCx), diagonal (D), and obtuse marginal (OM) branches. Super-dominant RCA circles all the way to the left atrioventricular groove giving rise to the posterior descending (PD), posterolateral (PL), and OM branches.

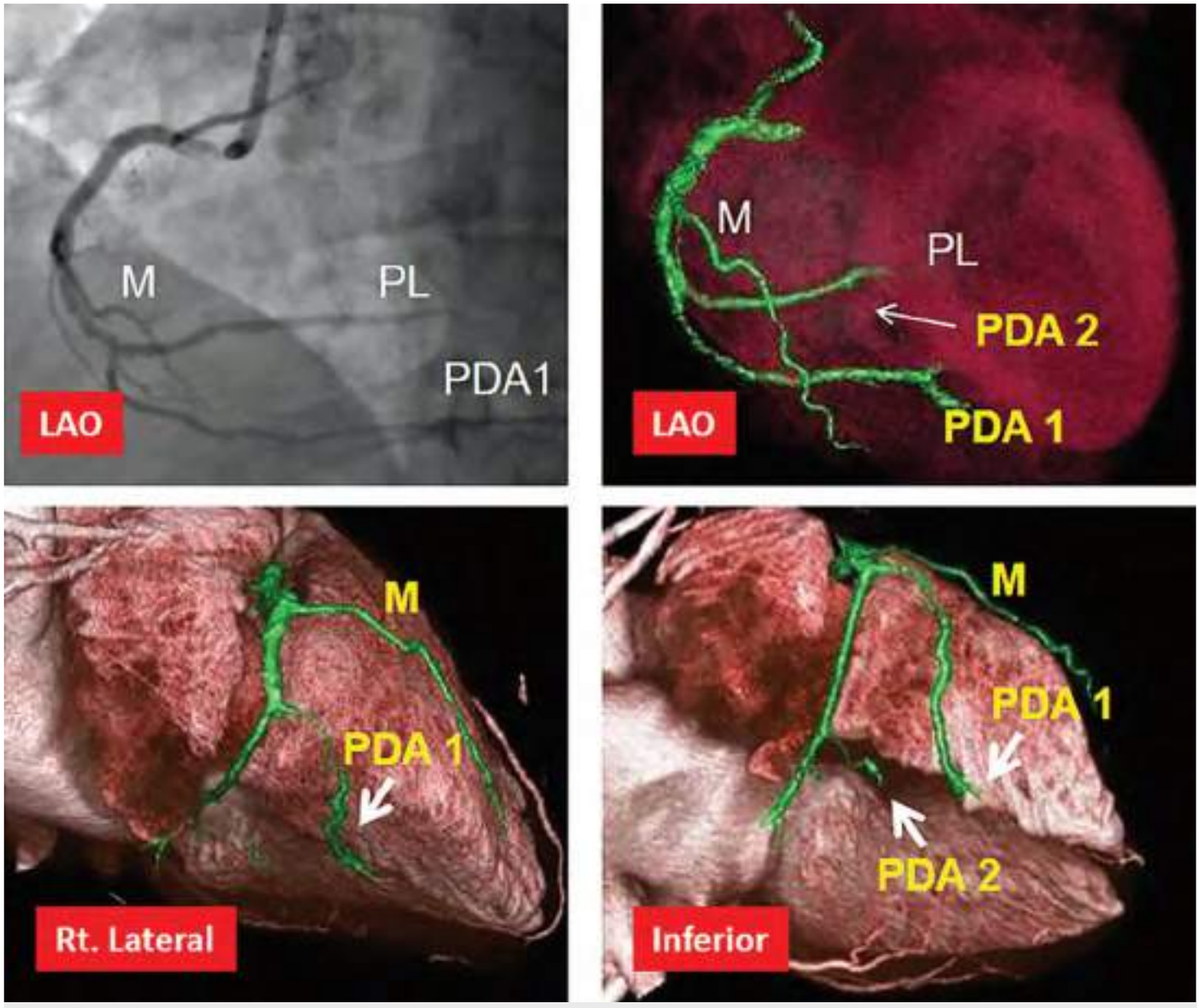

Fig. 18.19 Split RCA or dual PDA. Upper row: Catheter and CT angiograms of the right coronary artery (RCA) in LAO projection (80 degrees with 15-degree cranial tilt). Lower row: Volume rendered views of the right lateral and inferior surface of the heart. Since most posterior septal perforators are supplied by the posterior descending artery (PDA), it has been described that in the presence of a dual PDA, the RCA may be called "dual" (similar to dual LAD variant). In this example, the short PDA (PDA2) ends quickly in the proximal inferior interventricular groove, while the long PDA (PDA2) travels over the right ventricle free wall to supply distal inferior septum. LAO, left anterior oblique; M, marginal; PL, posterolateral.

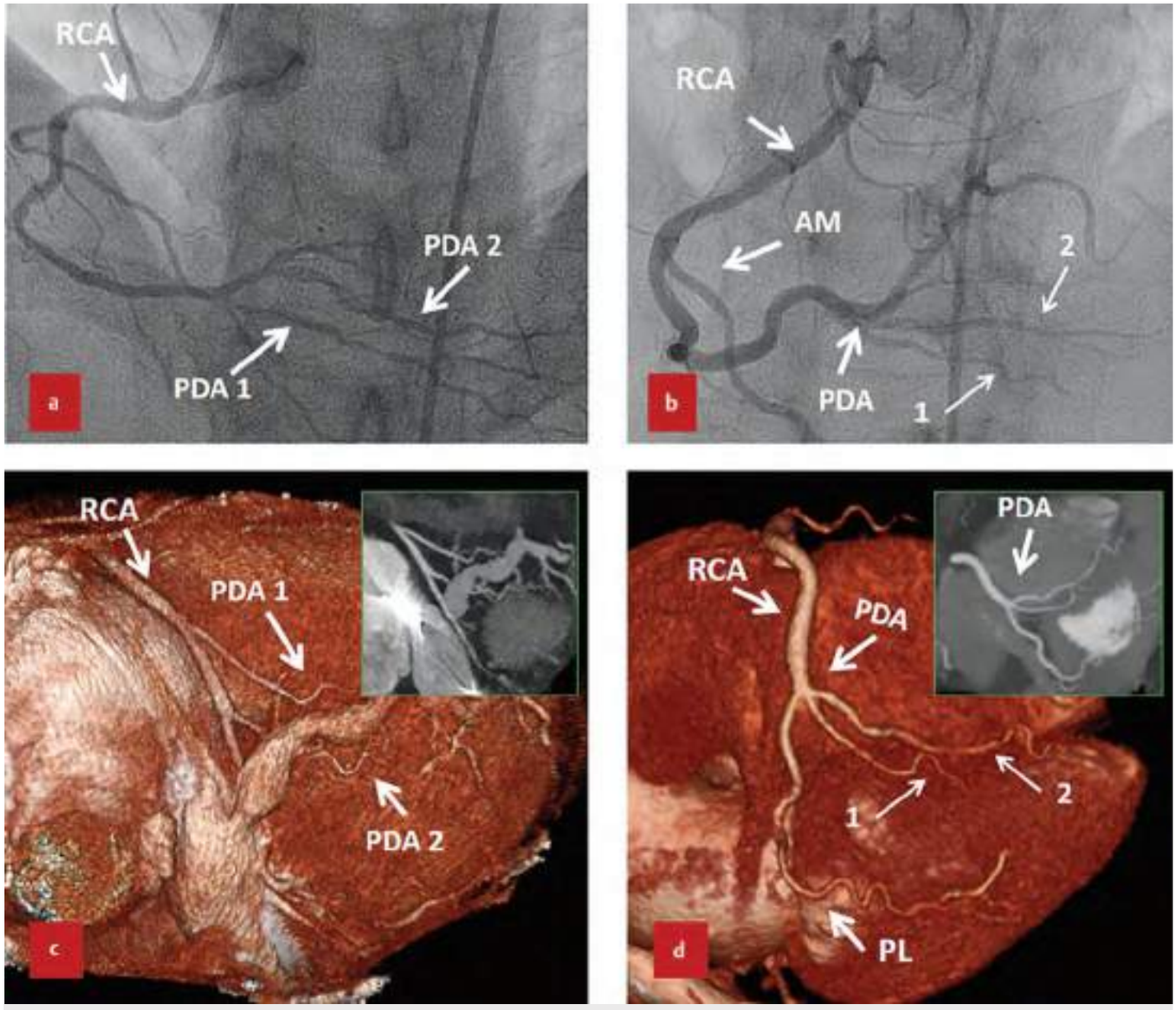

Fig. 18.20 Variants of the posterior descending artery (PDA). Left anterior oblique views of coronary angiograms in a patient with dual PDA **(a)** and one with a split PDA **(b)**. Volume rendered views of the inferior surface of the heart showing dual **(c)** versus split (bifurcated) PDA **(d)** variants. In these examples, both PDA branches are equal in caliber and length running along sides of the inferior interventricular groove. AM, acute marginal branch; PDA, posterior descending artery; PL, posterolateral; RCA, right coronary artery.

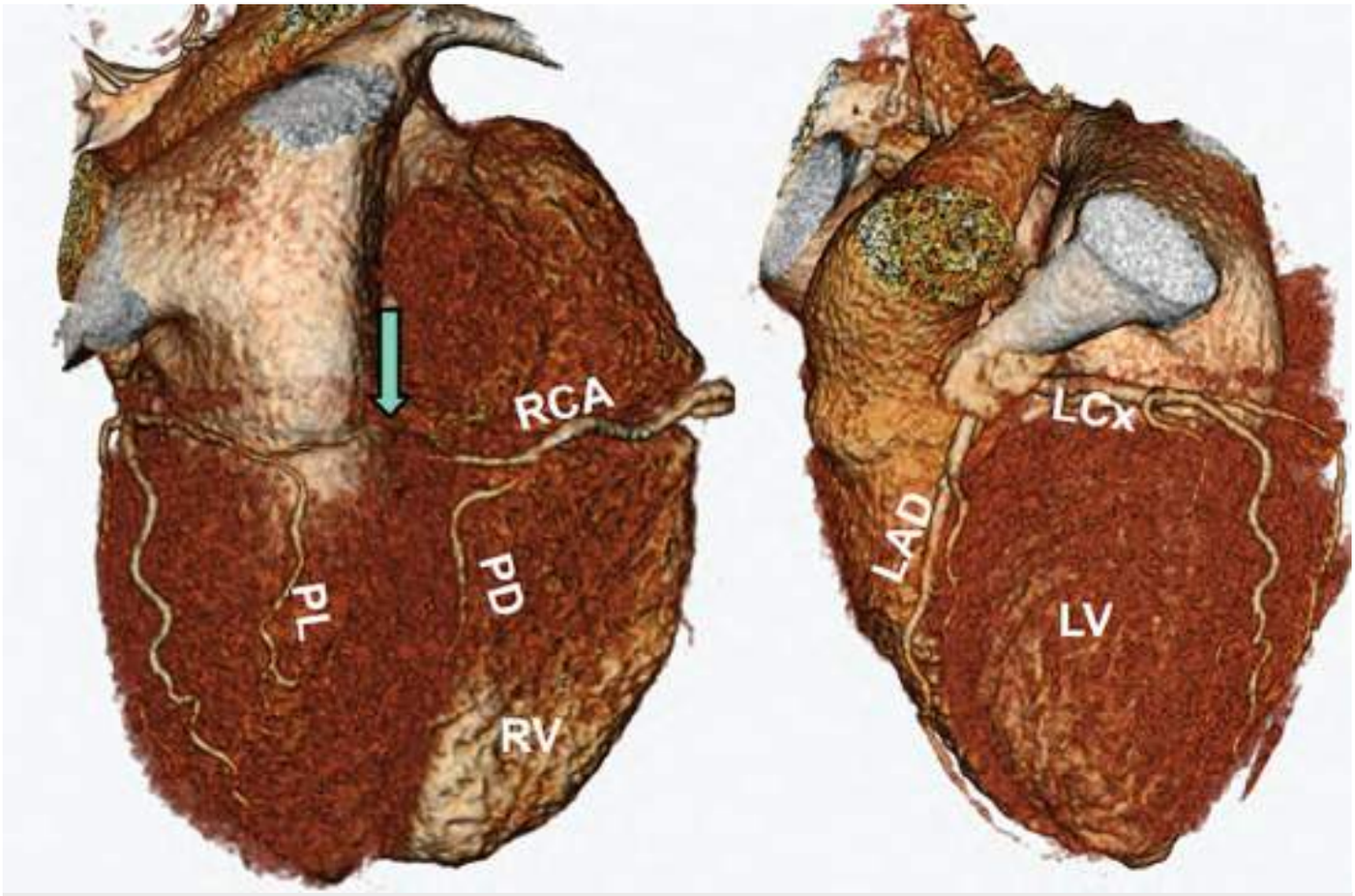

Fig. 18.21 Codominant coronary system. Inferior and left lateral views of the heart. Using perfusion concept, several vessel arrangements exist that can fit in the definition of a codominant coronary system. In this example, the posterior descending (PD) artery has originated from the right coronary artery (RCA) and the posterolateral (PL) branch from the left circumflex (LCx). Both the RCA and the LCx reach the crux (*arrow*) of the heart. LV, left ventricle; RV, right ventricle.

codominant coronary system. In patients presenting with an acute coronary syndrome, left coronary dominance appears to be associated with increased long-term mortality, especially with involvement of the inferior wall of the heart.[21] In most individuals with left coronary dominance, the RCA is usually a small and unreliable source of left myocardial perfusion.

◆ Participants of Intercoronary Connections

Collaterals are interarterial connections that provide blood flow to a vascular territory whose original supply vessel is obstructed (acquired or congenital). The interarterial collateral connections are small with a wide range, between 40 and 200 µm, which may reach up to 1 mm.[22] The size of the majority of these connections is below the 0.2-mm spatial resolution of most angiographic imaging equipment. The spatial resolution of most current CT scanners is above 0.4 mm. In case a major artery becomes occluded (> 90% stenosis), because of increased pressure through these small anastomotic vessels, they dilate and become visible by imaging methods.

Common sources for inter- and intracoronary collaterals include (1) peripheral branches of the right and left coronary arteries, (2) transseptal anterior and posterior septal perforators, (3) conotruncal anastomotic pathways, (5) distal LAD with PDA, (6) interatrial anastomotic pathways, and (7) intramyocardial pathways (▶ Fig. 18.22, ▶ Fig. 18.23).

The most common types of extracardiac aortocoronary collaterals are those between bronchial and coronary arteries and between the internal thoracic and coronary arteries[23,24] (▶ Fig. 18.24). The connections are through the sites of pericardial reflections, which allow the collaterals to enter the subepicardial layer. Extracardiac collaterals are occasionally seen between the SAN artery and the mediastinal or bronchial arteries in chronic pulmonary and bronchial diseases (▶ Fig. 18.23).

Collateral flow may protect myocardium from transmural infarction and preserve wall function when a vessel is totally occluded. This can occur in congenital absence or acquired obstructions (▶ Fig. 18.23). Collateral after infarction usually occurs within weeks after occlusion or severe stenosis with a great inter-individual variability in the potential to recruit collateral vessels.[22] Collaterals will regress once the ischemic territory is revascularized.[25]

◆ Interventricular Septum

Two groups of arteries are responsible for blood supply to the interventricular septum. These perforating septal branches are

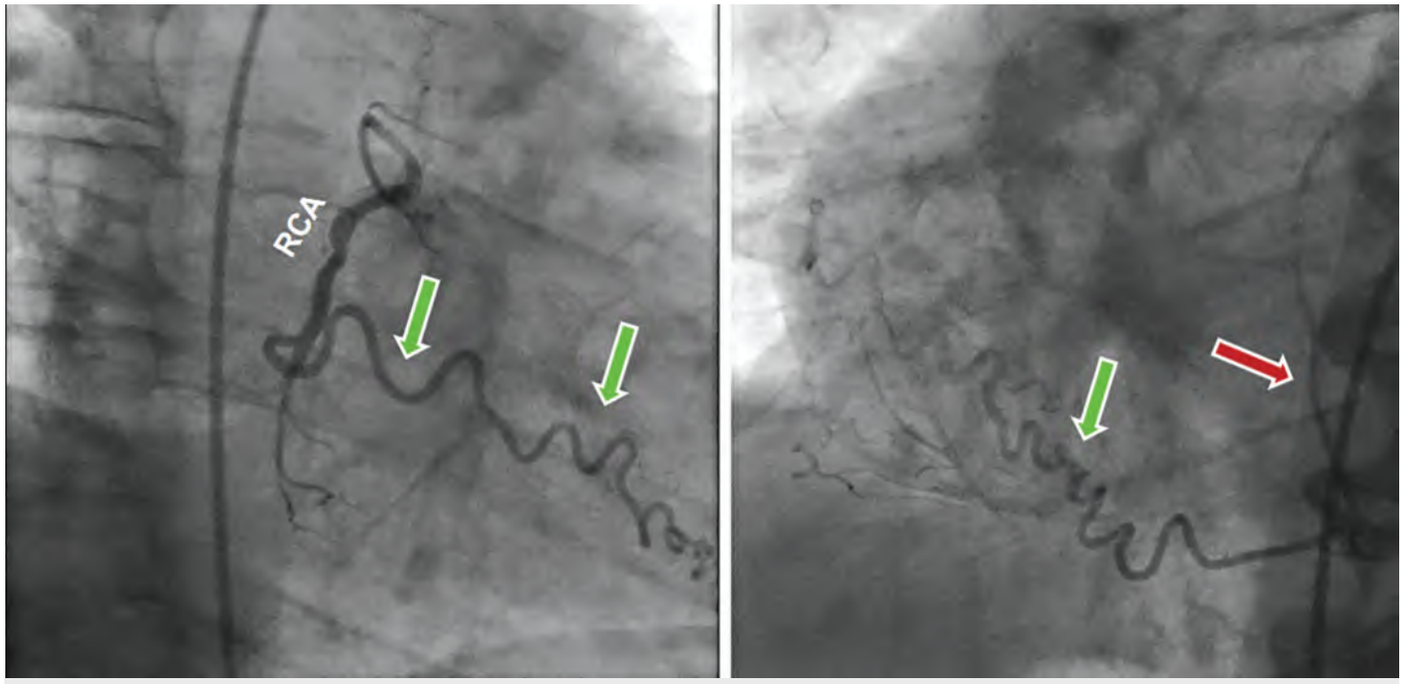

Fig. 18.22 Intercoronary collaterals. Right marginal collateral (*green arrows*) connecting the right coronary artery (RCA) with the left coronary system (*red arrow*).

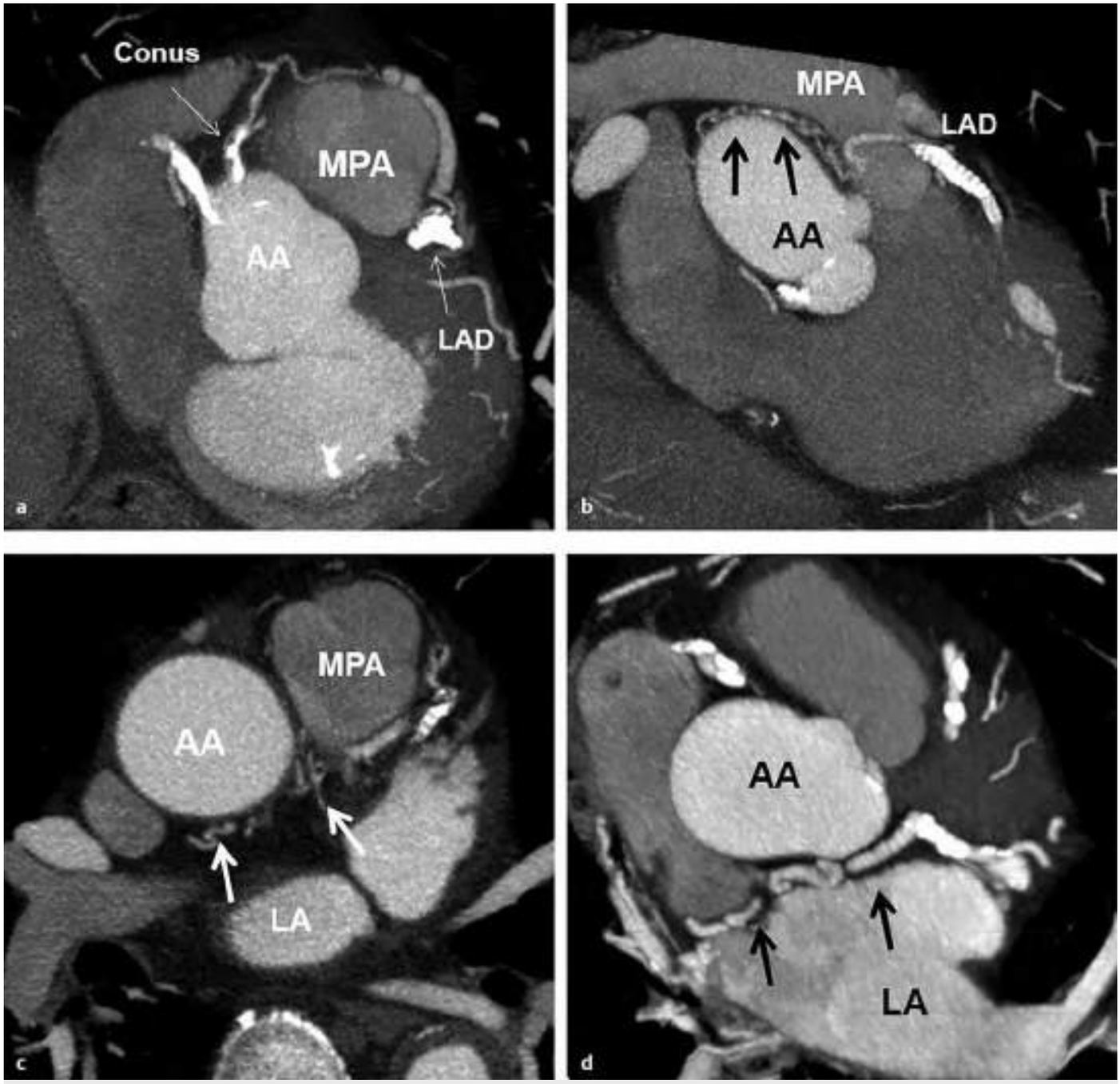

Fig. 18.23 Acquired conotruncal collaterals in chronic coronary artery disease. **(a–c)** Axial images in a patient with severe coronary artery disease. Extensive anastomotic collaterals are formed between the right and left coronary systems. **(a)** Preconal collateral between the conus artery and the left anterior descending (LAD). **(b)** Retroconal collaterals. **(c, d)** Retroaortic collaterals. **(d)** A different patient showing retroaortic collaterals through an enlarged left sinoatrial node (*black arrows*) artery supplying a diseased right upper lobe (chronic tuberculosis). AA, Ascending aorta; LA, left atrium; LAD, left anterior descending artery; MPA, main pulmonary artery; RCA, right coronary artery.

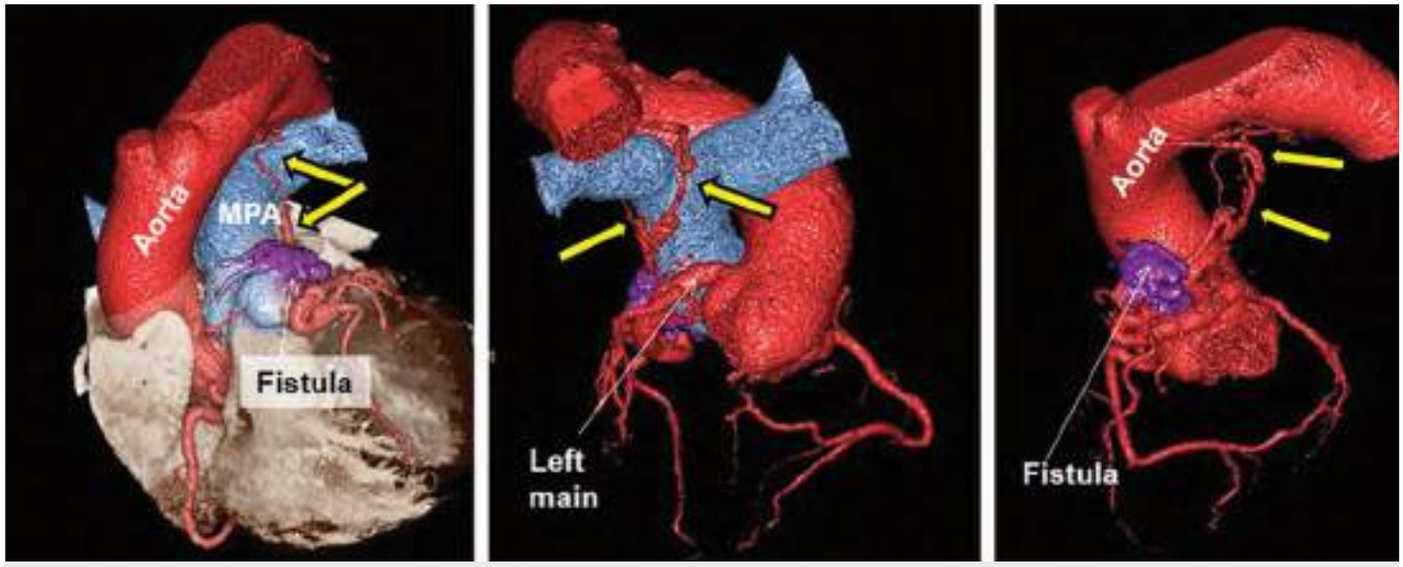

Fig. 18.24 Color-coded volume-rendered CT images showing extracardiac aortocoronary collaterals (*arrows*) between the aortic arch and left coronary system supplying a prepulmonary fistula (*purple*) between the left coronary arteries and the main pulmonary artery (MPA).

divided into the anterior and posterior septals. This nomenclature to define the anatomical position of these vessels is based on their relation within the heart. Within the thorax, however, the positions can more accurately be described as superior and inferior.[26]

The anterior septal branches arise from the LAD and the posterior septal branches arise from the PDA (▶ Fig. 18.9, ▶ Fig. 18.12). They travel within the septum close to the right ventricular endocardium (▶ Fig. 18.12). The anterior perforating septal arteries are significantly larger and more numerous than their inferior counterparts. The first branch is the largest in 80% of cases. The number of superior septal arteries ranges from 1 to 10, with an average of 4.2, and the inferior one's ranges from 0 to 7, with an average of 2.[26] The septal arteries are the basis of efficient intercoronary collateralization between the LAD and PDA and probably the most common type.[25]

The first septal perforating artery is a branch of LAD artery that originates between 13 and 37 mm from the LAD ostium and has a diameter of 1 mm (▶ Fig. 18.25). The artery branches into three smaller ones. The main branch passes toward the medial papillary muscle and the other two passes into the septomarginal trabeculation.[26] When the medial papillary muscle is present, the first septal artery tends to pass toward the base of the medial papillary muscle. The artery supplies the base of the ventricular septum and the right ventricular side of the septum including the moderator band with branches to the conduction system including the bundle of His and proximal bundle branches. In hypertrophic cardiomyopathy, the artery is enlarged. Embolization of this artery is commonly performed as a way to treat left ventricular outflow tract obstruction seen in some cases of hypertrophic cardiomyopathy.[27] The source of the moderator band artery is one of the first three anterior septal arteries, with the second septal being the most common. This artery can extend to the anterior papillary muscle where it may anastomose with the marginal branches of the RCA.[28]

The right superior descending (septal) artery is seen in 3 to 6% of angiography studies arising from the proximal RCA[29,30] (▶ Fig. 18.25). It could be a potential intercoronary collateral connecting the proximal RCA to the distal RCA, LCx, or LAD through the atrial anastomotic network, retroaortic anastomotic pathway or trans septal connections (▶ Fig. 18.26; see the following sections).

◆ Conotruncal Arterial Circulation

Three major collateral pathways at the conotruncal level provide circulation between the right and left coronary systems in all congenital or acquired forms of one-sided coronary artery occlusion and are used as the basis for different classifications.[31,32] These three collateral circulation pathways include preconal (precardiac), retroconal (interarterial), and retroaortic[32] (▶ Fig. 18.27). It is believed that most of these collaterals are a remnant of the embryonic conotruncal circle, which gives rise to the coronary ostia and makes a connection with the other two epicardial coronary circles (AV and interampullary).[33,34]

The pulmonary infundibulum is normally vascularized by anterior and posterior conal arterial branches from the right or left coronary arteries.[35] On the right side, the conal branches arise from the conus artery, the RCA, or directly from the aorta. On the left side, they arise from the LAD, the LM, or directly from the aorta. These four arteries form the preconal and retroconal anastomotic pathways (▶ Fig. 18.27). The right anterior branch is the most constant and conspicuous branch participating in the anterior collateral circulation, also known as Vieussens' arterial ring[33] (▶ Fig. 18.23, ▶ Fig. 18.28). This collateral intercoronary connection extends between the conus artery and the first right ventricular branch (left anterior conus branch) of the LAD artery (▶ Fig. 18.28). Although the conus artery is usually a branch of the proximal RCA, in many cases it may arise directly from the right aortic sinus, hence the name "third coronary artery" (▶ Fig. 18.17**a**). When there is proximal LAD artery occlusion or, less frequently, RCA occlusion, the Vieussens' arterial ring will become dilated[15] (▶ Fig. 18.23, ▶ Fig. 18.28).

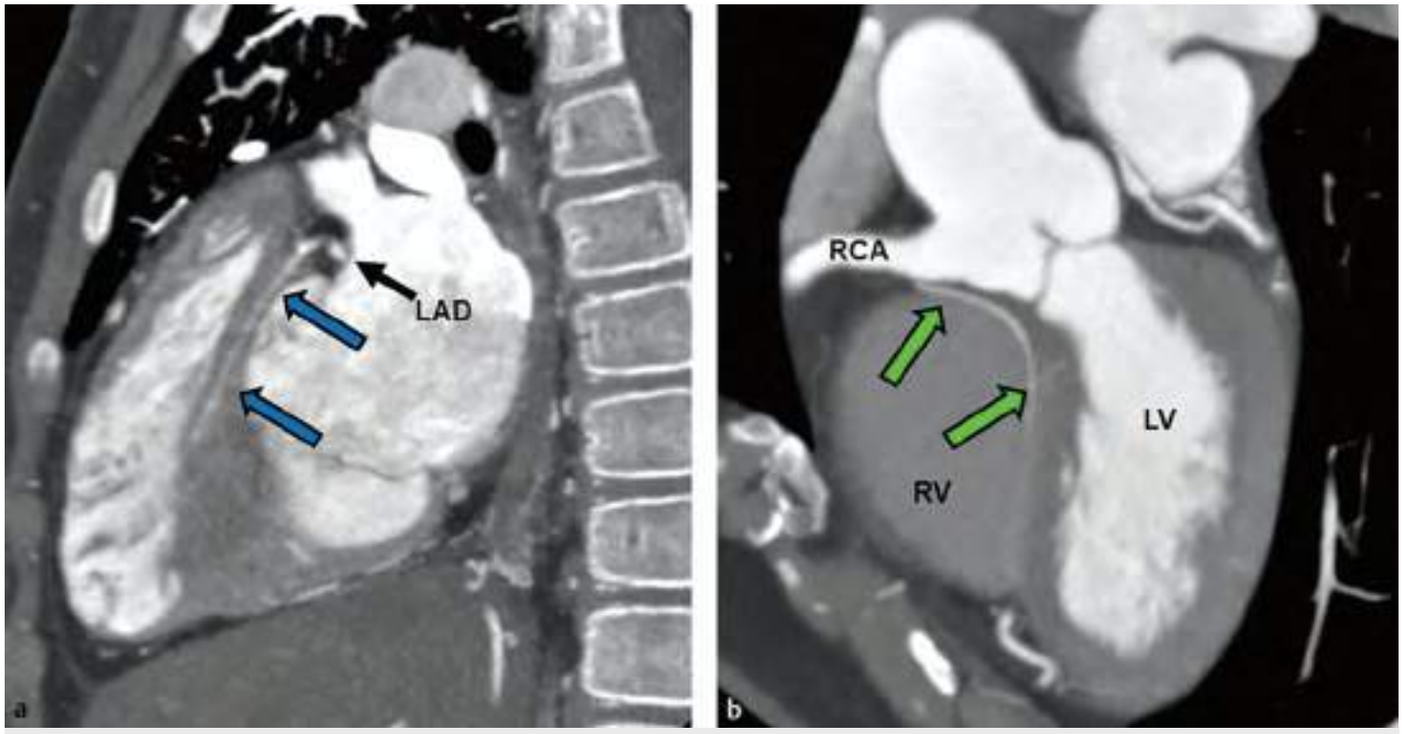

Fig. 18.25 **(a)** Sagittal CT showing the first septal perforating artery of the left anterior descending artery (LAD). The septal perforating arteries originate at a right angle from the LAD and travel on the right side of the interventricular septum. The first septal artery (*arrow*) is usually the largest and varies in length from 2 to 5 cm. The inferior branches of the first septal perforator are directed toward the moderator band and supply the anterior papillary muscle of the tricuspid valve. Its superior branches supply the right bundle branch and the bundle of His. **(b)** Oblique coronal view showing the right superior septal artery (*arrow*). This artery supplies the infundibular septum and can participate in the retroaortic intercoronary collateral circulation. LV, left ventricle; RCA, right coronary artery; RV, right ventricle.

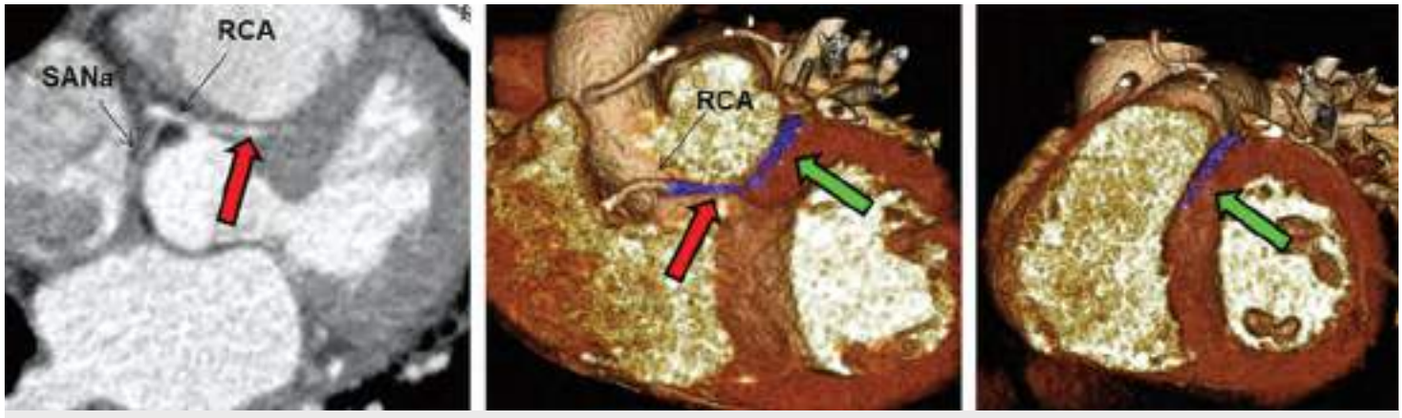

Fig. 18.26 Retroaortic intercoronary anastomotic pathway between the right superior septal artery (*red arrow*) and the left first septal artery (*green arrow*) in a patient with left main occlusion status post coronary artery bypass graft (CABG). RCA, right coronary artery; SANa, sinoatrial node artery.

The participants of the retroaortic anastomotic pathway usually are atrial branches such as the left SAN, the right superior septal, and Kugel's arteries (▶ Fig. 18.23, ▶ Fig. 18.28).[36] The retroaortic anastomotic pathway can connect the proximal left coronary arteries and RCA together behind the aorta or with the distal RCA at cardiac crux through the inferior pyramidal space. These arteries are described in detail in the following section.

◆ Arterial Supply of the Conduction System

The SAN artery provides vascular supply to the SAN. The arterial supply to the posterior base of the interventricular septum, interatrial septum (including the AV node), and penetrating His

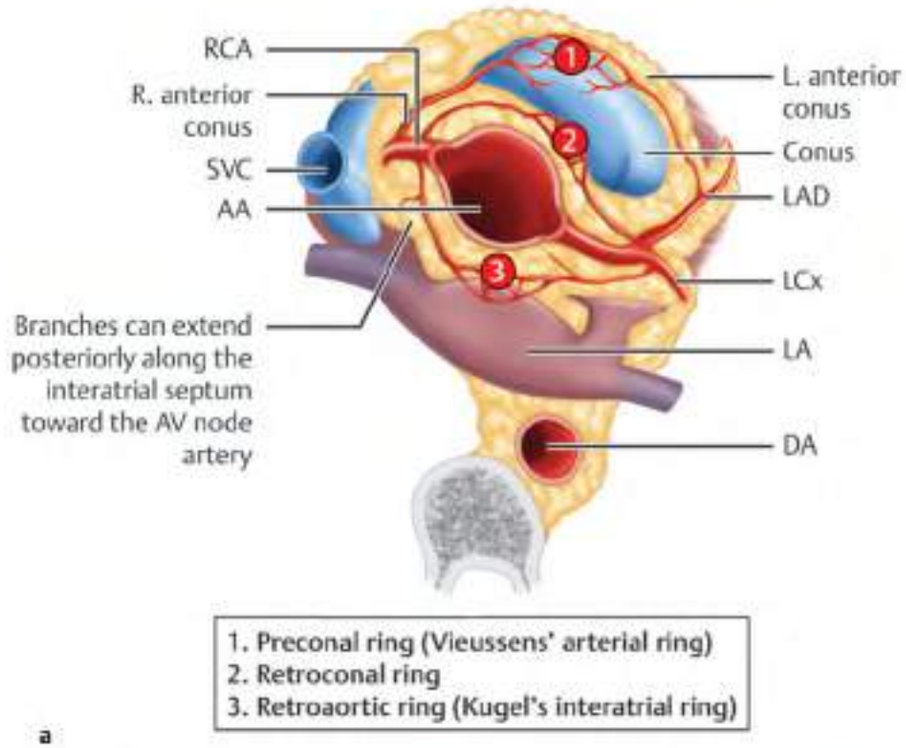

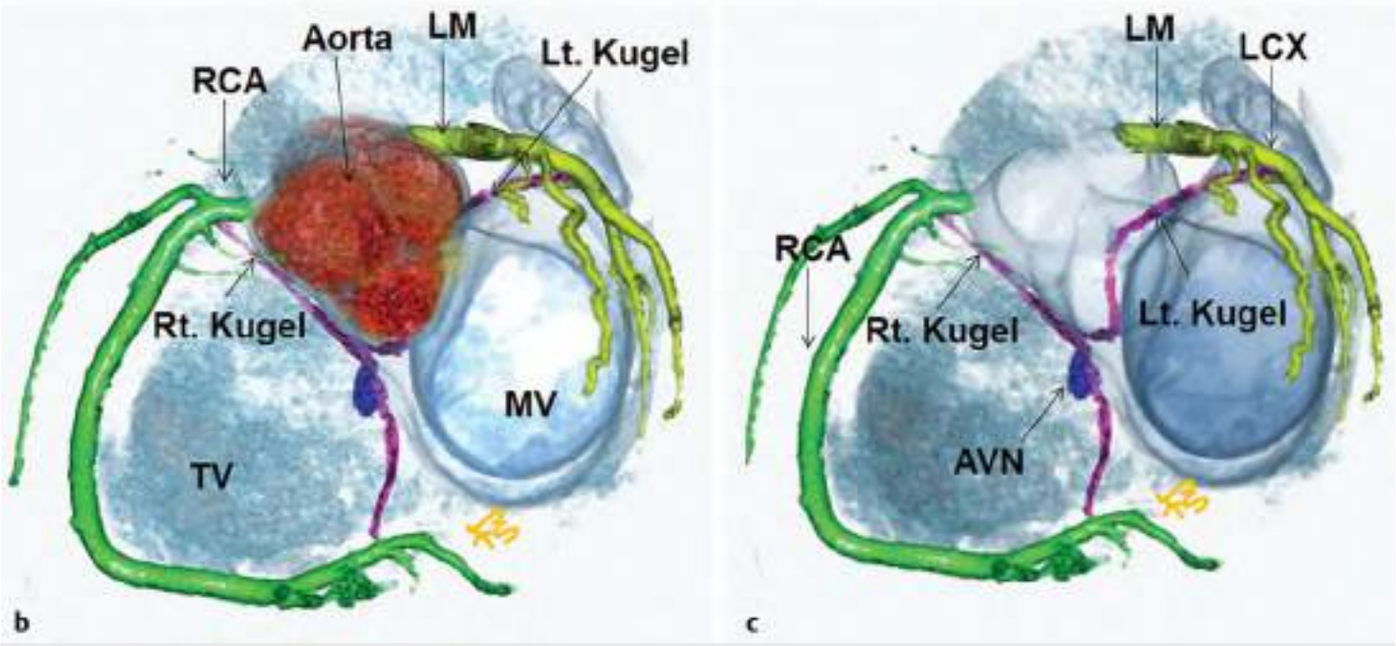

Fig. 18.27 **(a)** Conotruncal arterial anastomotic circulation. The schematic drawing demonstrates three arterial anastomotic rings participating in vascular supply to the aortopulmonary trunk as well as the collateral circulation between the proximal right and left coronary artery systems. The preconal ring (#1), also known as Vieussens' arterial ring, comprises right pulmonary conus branches arising from the RCA or the aorta and left conus branches arising from the left main or proximal LAD arteries. The right anterior conal branch exists in 100% of cases and in 50% it may arise from the right aortic sinus. The left anterior conus exists in 85%, right posterior in 15%, and left posterior in 15% of cases. The retroconal anastomotic ring (#2) forms connections from the right and left coronaries through collaterals, which traverse in the interarterial space behind the main pulmonary artery but anterior to the ascending aorta. The retroaortic anastomotic ring, otherwise known as the Kugel atrial anastomotic network, communicates the proximal right and left coronary systems together (#3) or individually with a distal coronary system through the interatrial septum (not shown). **(b)** The schematic view of the base of the heart after removal of the ventricles demonstrates atrial arterial supply to the atrioventricular node (AVN) region, including the right (Rt. Kugel) and left (Lt. Kugel) Kugel anastomotic arteries and the AVN artery (AVNa). AA, ascending aorta; AV, atrioventricular; DA, descending aorta; LA, left atrium; LAD, left anterior descending artery; LCx, left circumflex artery; RCA, right coronary artery; SVC, superior vena cava.

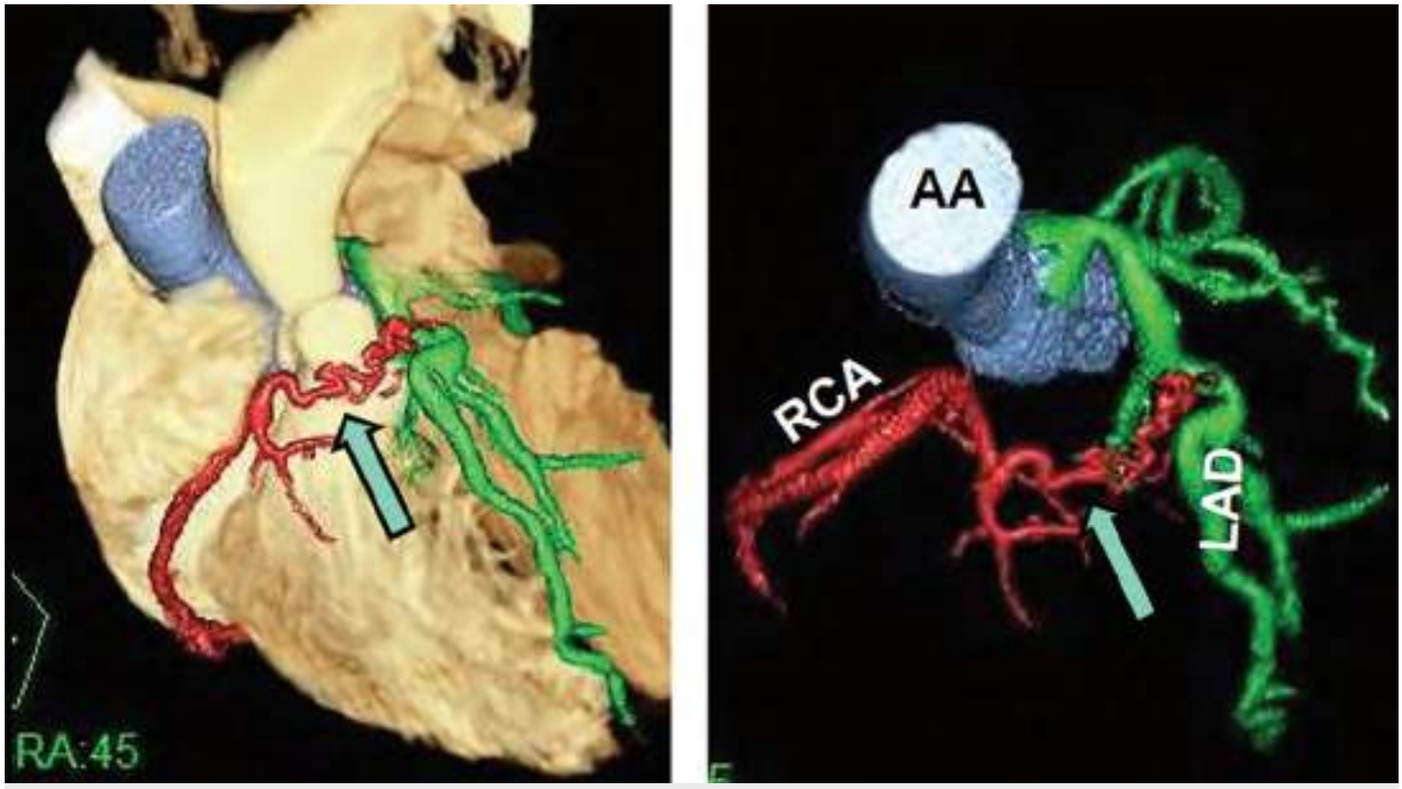

Fig. 18.28 Vieussens' arterial ring (*arrows*) in a patient with right coronary artery occlusion/atresia at its orifice. AA, ascending aorta; LAD, left anterior descending; RCA, Right coronary artery.

bundle is largely provided by the AV node artery[37,38,39,40,41,42] (see Chapter 12). The right superior septal artery and the left first septal artery may provide vascular supply to the right and left bundle branches.

Sinoatrial Nodal Artery

The SAN is supplied by a single branch from the proximal RCA in 60 to 70% of people. In the rest, it is a branch of the LCx artery.[30] Rarely, it arises from the distal RCA, or the aorta. The SAN artery is an atrial branch. That is why many small branches are seen arising from the vessel to supply atrial walls and the interatrial muscle bundles such as Bachmann's. The origin of the SAN artery is not related to coronary arterial dominance.[41] The right SAN artery arises from the first 3 cm of the RCA and dives down between the right atrial appendage and the aorta toward the superior cavoatrial junctions. Rarely, it arises directly from the aorta (▶ Fig. 18.17**b**). The left SAN artery arises from the very proximal part of the artery and runs anterior to the left atrial wall along the transverse sinus. At the cavoatrial junction, the SAN artery course becomes variable and may travel either anteriorly (precaval) or posteriorly (retrocaval), or uncommonly both anteriorly and posteriorly, around the cavoatrial junction (pericaval) to enter the node.[30,37] Patients who have undergone atrial surgery often exhibit postoperative disturbances in sinus node function, which may possibly be related to the SAN artery damage. However, this condition is usually transient and without clinically troublesome manifestations.[42] Potential sources of damage to the SAN artery are incisions near the superior cavoatrial junction, dome of the left atrium, or through the superior border of intra-atrial septum. The SAN artery rarely occludes by atherosclerotic occlusion of the parent coronary artery.

S-Shaped Posterior SAN Artery

A variant of the left SAN artery is called an S-shaped SAN artery (▶ Fig. 18.13). The S-shaped variant is seen in 14% of coronary CT angiographies. Thirty percent of the left SAN arteries show an S-shaped variant course.[43,44] This long artery arises from the proximal LCx artery and shows a predictable course to the right to reach the SAN. The artery starts its course behind the left atrial appendage and passes in the sulcus between the ostia of the left superior pulmonary vein and the left atrial appendage. The ligament or vein of Marshall and the left lateral atrial branch also may be seen in this sulcus (see Chapter 1). At this location, the artery is very close to the left atrial wall where it is susceptible to injury during catheter radiofrequency (RF) ablation of the left atrium or left atrial procedures such as a Maze procedure or left atrial appendage exclusion. The mid- and distal portions of the S-shaped SAN artery move in a path similar to the left SAN artery as they both travel anterior to the left atrium along the transverse sinus toward the superior vena cava.

Atrioventricular Nodal Artery

The AVN branch/artery is the first and longest inferior septal perforating branch arising from the apex of the U turn of the distal RCA at the cardiac crux, and penetrates the base of the posterior interatrial septum at the crux of the heart in 80 to 90% of patients[38,45] (▶ Fig. 18.29). In the remaining, it originates from

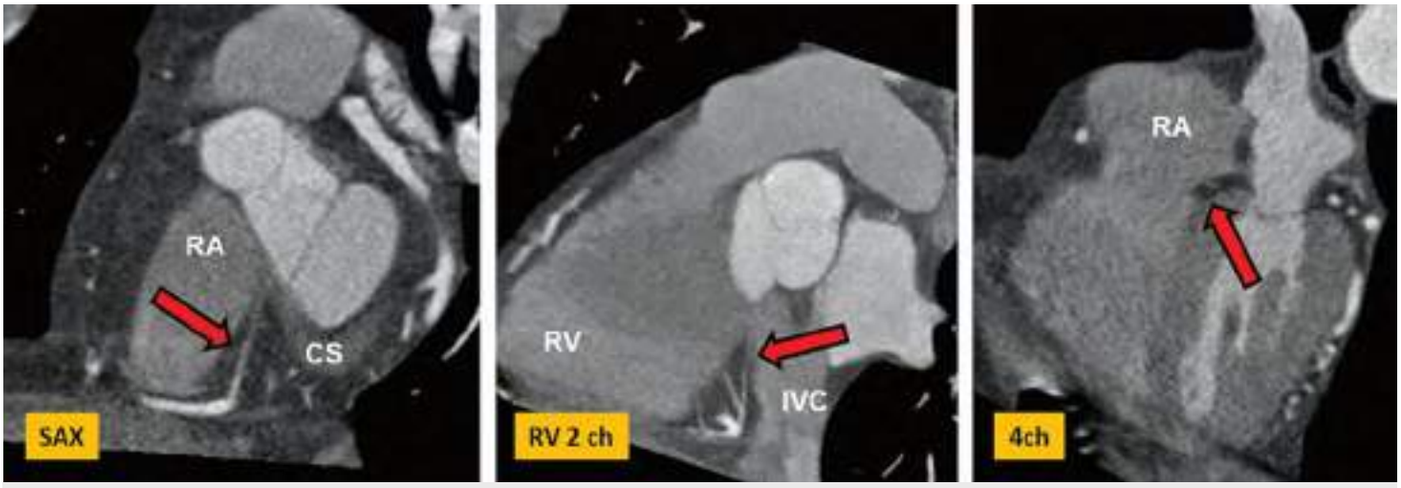

Fig. 18.29 The atrioventricular nodal (AVN) branch (*arrows*) is a small vessel that typically arises from the distal right coronary artery (RCA) in the area of the crux (atrioventricular septal junction). The AVN branch travels toward the AVN (apex of the Koch triangle) in the inferior pyramidal space filled with the epicardial fat. Typically, the dominant coronary artery gives rise to the AVN artery. ch, chamber; CS, coronary sinus; IVC, inferior vena cava; RA, right atrium; RV, right ventricle; SAX, short axis.

the terminal portion of the LCx artery (8–13%) or uncommonly from both RCA and LCx (2–10%).[30] Therefore, the origin of the AVN artery is dependent on coronary arterial dominance. The AVN artery is single but rarely can be double. The classic anatomic concept is that the AVN artery is the main vessel supplying the AVN. According to Anderson and Murphy,[45] the vessel supplies the AVN in 90% of hearts, but it terminates before reaching the node in 10%. Alternative sources of arterial supply to the AV conducting pathway include the first septal perforating, the descending septal artery, and Kugel's artery.[40,46] At the level of Koch's triangle, the AVN artery is very close to the ostium of the coronary sinus and septal isthmus (25% of cases; ▶ Fig. 18.29). This distance varies from1 to 6 mm.[30,47] In cardiac surgery or during arrhythmias ablation procedures, respect for the area of Koch's triangle and the base of the ventricular septum will reduce the risks of injury to the AVN artery.

◆ Atrial Branches

Atrial branches have a highly variable anatomic pattern and very little clinical significance with the exception of the AVN, SAN, and possible Kugel's arteries. Small atrial branches arising from the SAN arteries are seen in 50 to 60% of CT angiographies[30] supplying the anterior and superior atrial wall. The SAN artery may also supply the crista terminalis region.[48] Most of the right atrium and a part of the superior surface of the left atrium are supplied by the RCA. The right posterior atrial artery is seen in 35% of the time and may be prominent. The bulk of the LA may be supplied the LCx artery. A left lateral atrial artery may be seen in up to 60% of hearts (▶ Fig. 18.13). This artery may extend to the SAN to form the so-called S-shaped SAN artery. The atrial arteries may anastomose each other. The interatrial septum is supplied mainly by the SAN and AVN arteries. The atrial arterial branches participate in the intercoronary anastomosis. The clinical significance of these atrial collateral vessels is a matter of debate and their importance might primarily be their potential as a source of collateral circulation in the event of acquired obstruction in the vessel(s) with which they connect.

Kugel's Artery

Kugel's artery is a controversial artery first described by M.A. Kugel[49] as an unusually large atrial artery (*arteria anastomotica auricularis magna*). This artery is an uncommon (2–3%) but sometimes important collateral between the proximal LCx (left Kugel's) and the artery supplying the crux of the heart (the distal RCA or distal LCx).[30,50,51] In 60% of cases, the artery passes anterior to the mitral valve ring, coursing in the epicardial fat of the interatrial groove, to anastomose with the AVN artery.[51] In the remainder, the left kugel artery anastomoses with the proximal RCA behind the aortic root. Since the left SAN artery is an atrial artery, it may act as a retroaortic anastomotic Kugel arterial pathway between the right and left coronary arteries on its way to the SAN.[51] Nerantzis et al described a right Kugel artery arising from the proximal RCA to connect with the distal RCA at the crux through the base of the heart.[51] The right Kugel artery is probably a variant of the right superior septal artery (▶ Fig. 18.17). In CTA, the Kugel artery is seen in 2%.[30] Occasionally, the AVN artery arises from the proximal RCA, as a continuation of the right superior septal artery (right Kugel artery).[46,51] A rare variant of the latter is shown in ▶ Fig. 18.30.

Right Superior Descending (Septal) Artery

The right superior descending artery, also known as the right superior septal, descending septal artery, or right Kugel's artery, is also part of the atrial anastomotic network connecting the proximal RCA to the distal RCA or LCx[46,51] (▶ Fig. 18.5**b**). Narantzis[51] found this artery in 3% of the dissected hearts. The right superior descending artery is seen in 6% CT angiographies. Studies of human heart specimens have shown this artery in one-

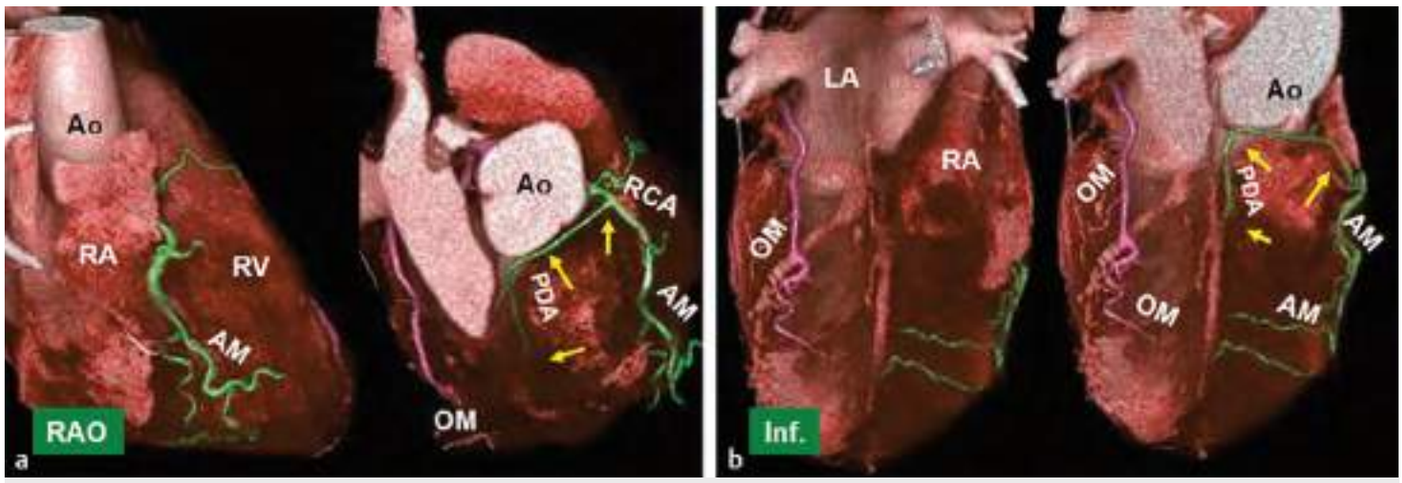

Fig. 18.30 An example of a split right coronary artery (RCA) with codominant coronary circulation. **(a)** 3D volume rendered right anterior oblique (RAO) and **(b)** inferior (inf.) views of coronary CT angiograms are shown before and after removal of the right atrium (RA). The RCA proper immediately bifurcates into a large acute marginal (AM) branch and a posterior descending artery (PDA). The AM supplies the entire lateral and inferior walls of the right ventricle (RV) and gives off small branches to the distal interventricular septum (IVS). The PDA on the other hand dives directly into the extracardiac epicardial space at the atrioventricular junction and exists the external cardiac crux (similar to a right Kugel artery) and finally runs in the inferior interventricular groove to supply the proximal third of the IVS. It is noteworthy that no RCA component runs in the atrioventricular groove. The obtuse marginal (OM) branches also participate in blood supply to the distal IVS. Ao, aortic root.

third of specimens, but in most examples the arteries are too small to be seen in clinical examples unless enlarged.

The right superior descending artery is a single vessel less than 2 cm in length originating from three different locations: (1) the proximal 15 mm of the RCA, (2) the right SAN artery, and (3) a conus artery or directly from the aortic sinus.[30,46] These arteries penetrate the epicardial fat in the AV groove and run along the side of the aortic root and behind it to meet the interatrial septum near its junction with the interventricular septum and penetrates into the base of the ventricular septum (▶ Fig. 18.25). If the artery ends in the AV nodal region, it would be considered a right Kugel artery (▶ Fig. 18.27, ▶ Fig. 18.30). The artery supplies the bundle of His and the AVN and may anastomose with the distal branches of the first septal artery, RCA, or LCx (▶ Fig. 18.26, ▶ Fig. 18.27).

◆ Coronary Microvasculature

In the past, most of the scientific work has been focused on diagnosis and treatment of the obstructive disease of the major epicardial coronary artery disease visible on conventional imaging. In recent years, attention has been shifted to the fact that the microvascular component of the coronary circulatory system may be the source of coronary dysfunction and increased vascular resistance. Microcirculation is responsible for the coronary flow reserve (CRF), which allows up to fourfold to fivefold increase in maximal flow rate. Endothelial dysfunction and loss of vasodilatory capacity of the microcirculation (microvascular dysfunction) are an early manifestation of vascular disease and play a role in the development of coronary artery disease.[52,53]

The coronary arterial system is composed of three compartments.[54] These three compartments include epicardial arteries, prearterioles, and arterioles, although the borders of each compartment cannot be clearly defined anatomically.

- Epicardial (conductant) coronary arteries are relatively large (> 500 µm) extramyocardial vessels that are visible by conventional imaging techniques such as coronary angiography and CT scan. They function as capacitance with little resistance to coronary blood flow.
- Prearterioles (100–500 µm) are also extramyocardial; therefore, they are not under direct vasomotor control by diffusible myocardial metabolites such as nitrogen oxide. Their specific function is to maintain pressure at the origin of arterioles within a narrow range when coronary perfusion flow or pressure changes. Proximal prearterioles are more responsive to changes in flow, whereas distal prearterioles are more responsive to changes in pressure.
- Arterioles (< 100 µm) are intramyocardial and their tone is influenced by myocardial metabolism. They are characterized by a considerable pressure drop along their length, and their specific function is to match the myocardial blood supply with the myocardial oxygen demand. Arterioles have a fundamental role in the metabolic regulation of coronary blood flow.

The microvascular compartment is the site of major resistance (~70% with normal vasomotor tone); pressure mainly drops in this compartment. About 30% of the pressure drops in prearterioles and 40% in arterioles.[52,55]

◆ Coronary Blood Flow and Myocardial Perfusion

At rest, approximately 4 to 5% of cardiac output is directed toward coronary circulation. The coronary circulation is distinguished from other vascular networks by its phasic flow pattern.[56] Most of the coronary arterial flow occurs in diastole, while during systole the arterial flow may slow down or even reverse and the venous flow may accelerate (▶ Fig. 18.31). Capillaries are relatively resistant to the systolic myocardial compression

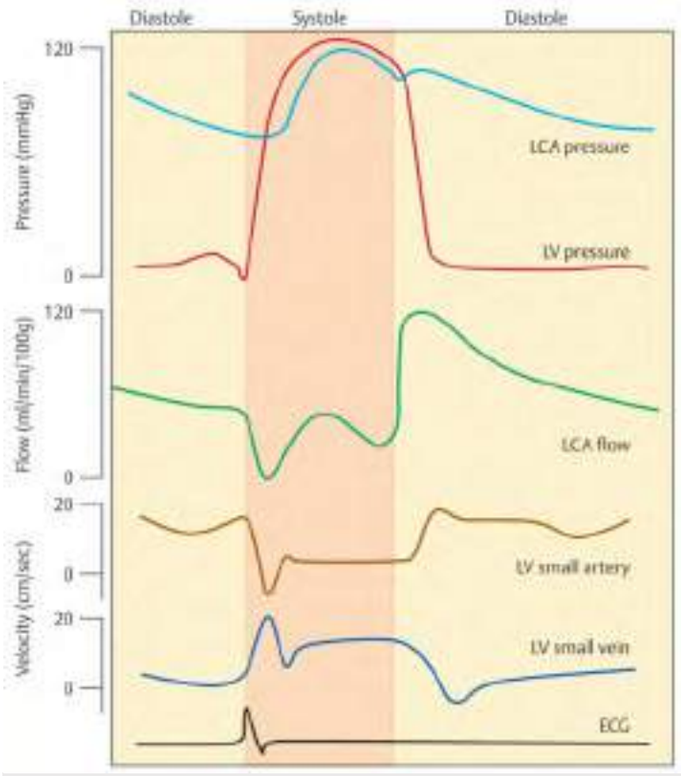

Fig. 18.31 Diagrams show pressure and flow in the left coronary artery (LCA), together with the left ventricular (LV) pressure. LCA flow is impeded during systolic phases due to contraction of the myocytes and the transmitted pressure from LV. The pressure in the LCA is maintained into diastole, where most arterial flow occurs, and depends primarily on the systemic afterload rather than LV pressure since the aortic valve is closed. Also shown are typical examples of the blood flow velocities in epicardial small arteries just before their entrance into myocardium and small veins just after their exit from myocardium. Note the phase difference between arterial inflow and venous outflow. A reverse flow is frequently recognized in artery in early systole, possibly due to abrupt increase in intramyocardial pressure and fiber deformation. A flow reversal is also observed in the vein in early diastole, which may be related to diastolic myocardial suction. (Used with permission from Kajiya et al[57] and Austin et al.[58])

compared with pre- and postcapillary microvessels.[57,58] Coronary perfusion is regulated in a number of ways. These can be divided into extrinsic, such as the humoral-nervous regulation, and intrinsic such as autoregulation. Autoregulation is the intrinsic tendency of the vascular system to maintain a constant flow in the setting of variation in perfusion pressure[59].

In the heart muscle, autoregulation is mainly due to a myogenic change in diameter of distal prearteriolar vessels in response to changes in perfusion pressure. The tone of the coronary resistive vessels (arterioles and prearterioles) is high at resting state. This intrinsically high resting tone allows the coronary circulation to increase flow by dilating small vessels when myocardial oxygen consumption increases.

Autoregulation is better maintained in the subepicardial myocardium compared with the subendocardium. When perfusion pressure at the origin of the arteriolar vessels, compared with that of the aorta, is reduced, perfusion becomes jeopardized earlier in the subendocardial than in the subepicardial layers of the LV. In addition, the subendocardium becomes even more susceptible to underperfusion if diastolic time is short and myocardial hypertrophy is present.[60]

◆ CT Imaging after Coronary Bypass Graft

Coronary artery bypass graft (CABG) surgery is one of the most commonly performed surgical procedures. Surgical indications for CABG include, but are not limited to, significant (50%) LM coronary artery stenosis, LM-equivalent diseases (critical stenoses of ostial LAD and ostial LCx coronary arteries), and severe three-vessel coronary artery diseases.[61,62,63] Coronary CTA has an important role in diagnostic imaging of CABG conduits both for postoperative graft surveillance and in preoperative planning for a redo surgery.[64,65]

There are two types of coronary bypass grafts: arterial and venous (▶ Fig. 18.32). As a rule, arterial grafts are smaller in caliber than venous grafts.[64,65] The most frequent arterial conduit is the left internal mammary artery. This conduit is used as a pedicled or rarely a free graft to bypass the LAD and/or a major diagonal branch of the LAD. The other arterial grafts are the right internal mammary artery, free radial artery, right gastroepiploic artery, and inferior epigastric artery. Reverse greater saphenous vein graft (SVG) is the most commonly used venous conduit that is primarily utilized for revascularization of non-LAD coronary artery territories. In general, during CT evaluation of bypass grafts, the proximal anastomosis is usually better visualized than the distal anastomosis. The proximal venous graft is anastomosed with an obtuse angle to the ascending aorta, few centimeters above the sinotubular junction. On occasions, a single great saphenous vein is utilized for distal anastomoses in a sequential fashion to two or more coronary targets. Typically, there are few surgical clips accompanying venous bypass grafts, lessening streak artifacts that may limit graft evaluation (▶ Fig. 18.32). Vein conduits are more prone to surgical trauma, both during harvest and during grafting procedures, and thus in general more prone to early graft closure. Also, early intimal hyperplasia at both proximal and distal anastomotic sites and poor distal coronary runoff can contribute to early vein graft failure.[66,67] The major cause of late vein or nonmammary arterial CABG conduit closure or stenosis is either development of occlusive atherosclerosis of the graft or progressive atherosclerosis of the native coronary runoff vasculature. Multidetector CT can produce excellent information regarding conduit patency and thus negate the need for repeat angiography in follow-up studies (▶ Fig. 18.29, ▶ Fig. 18.30).

CT is also used in preoperative evaluation of coronary patency in patients with prior CABG undergoing noncardiac or noncoronary valvular operations.[68,69] Furthermore, CT provides superior anatomic detail regarding the relationship of the live conduits with the inner table of the sternum, which may result in a major modification of the surgical approach and strategy during sternal reentry[70] (▶ Fig. 18.33).

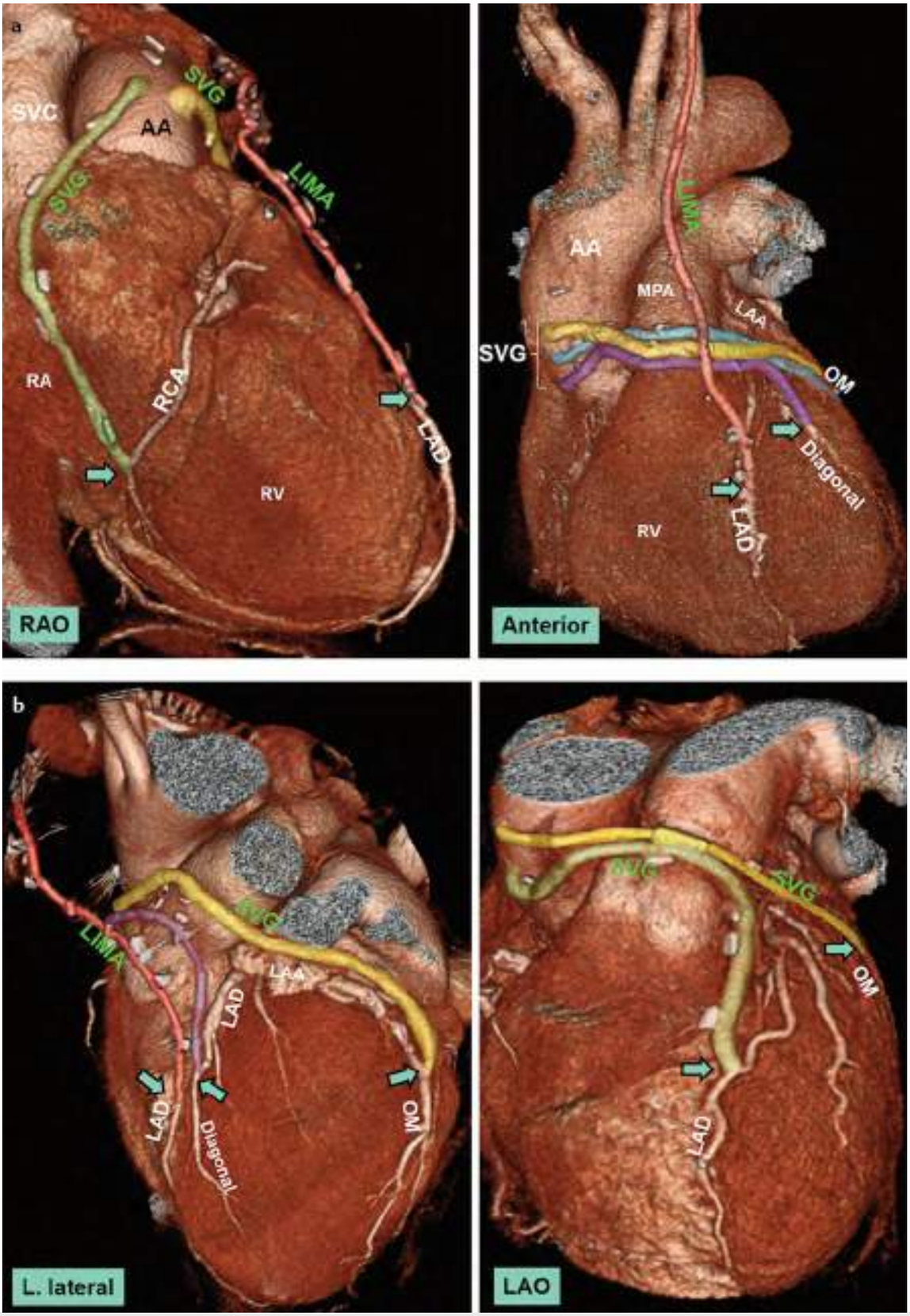

Fig. 18.32 **(a)** Various types of coronary graft. Anastomotic levels are shown by *arrows*. A right-sided saphenous vein graft (SVG) emerges from the obtuse angle of the right heart, overlying the free wall of right atrium (RA), passing anterior and medial to the cavoatrial junction to be attached to the greater curvature of the right aspect of the ascending aorta (AA). **(b)** A left-sided SVG will be connected to the left side of the AA, with the graft reaching the aorta draping over the main pulmonary artery (MPA) and left atrial appendage (LAA). An obtuse marginal (OM) graft typically attached to the AA in the most cephalad position and enters the oblique sinus of the pericardium before anastomosing to the OM. A diagonal vein graft courses over the MPA, passing underneath the left internal mammary artery (LIMA) graft, and is commonly attached to the AA proximal to the OM vein graft. Pedicle LIMA is left attached to the proximal subclavian artery after ligation of its segmental intercostal branches and is connected to the distal left anterior descending (LAD) artery of a diagonal. L, left; LAO, left anterior oblique; RAO, right anterior oblique; RV, right ventricle.

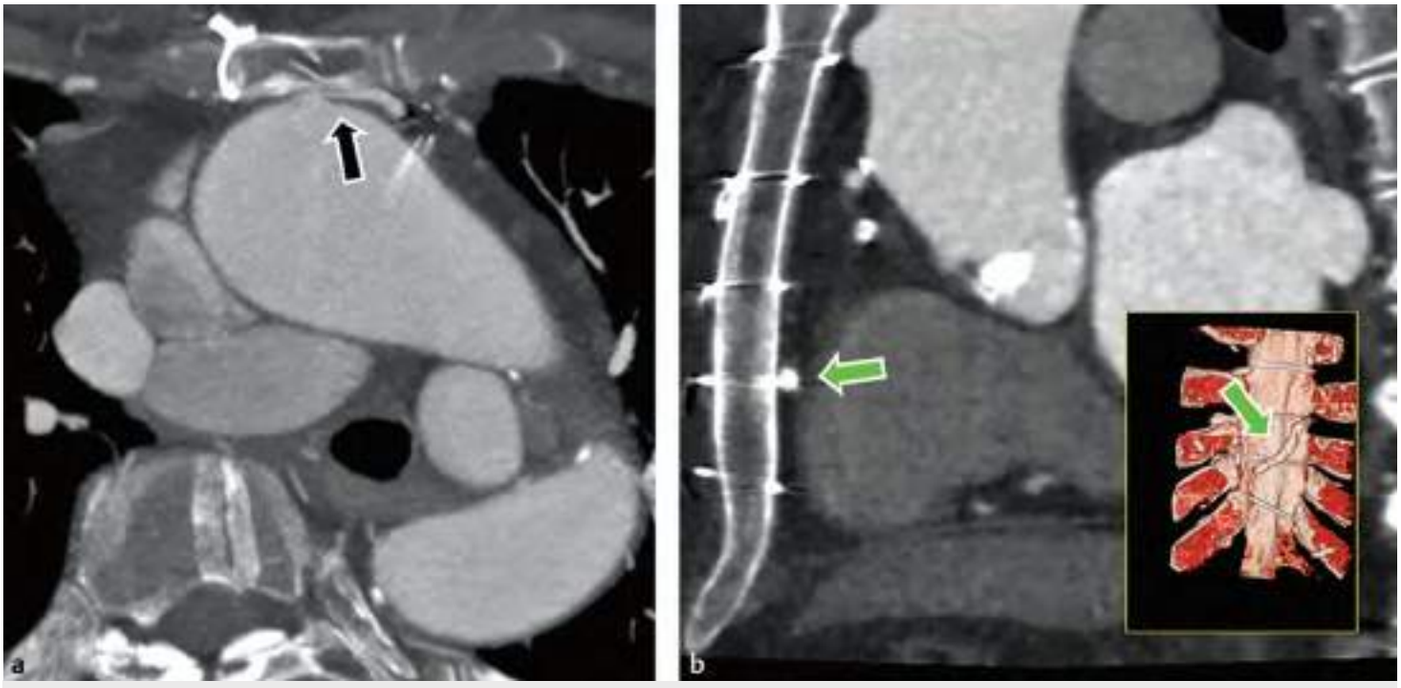

Fig. 18.33 (a) Axial CT showing close approximation of the saphenous vein graft (SVG; *arrow*) to the posterior wall of sternum. **(b)** Sagittal CT showing the left internal mammary artery (LIMA) graft passing close to the sternal wall (*arrow*). These variants may necessitate modification of the surgical approach during sternal reentry.

References

[1] Vasko JS, Gutelius J, Sabiston DC, Jr. A study of predominance of human coronary arteries determined by arteriographic and perfusion technics. Am J Cardiol.; 8:379–384

[2] Vrancken Peeters MP, Gittenberger-de Groot AC, Mentink MM, Hungerford JE, Little CD, Poelmann RE. Differences in development of coronary arteries and veins. Cardiovasc Res.; 36(1):101–110

[3] Schlessinger MJ. Significant variations in the anatomic pattern of coronary vessels. Blood Heart Circ..; 13:93–97

[4] Abuchaim DC, Spera CA, Faraco DL, Ribas Filho JM, Malafaia O. Coronary dominance patterns in the human heart investigated by corrosion casting. Rev Bras Cir Cardiovasc.; 24(4):514–518

[5] Ortale JR, Keiralla LC, Sacilotto L. The posterior ventricular branches of the coronary arteries in the human heart. Arq Bras Cardiol.; 82(5):468–472, 463–467

[6] Adams J, Treasure T. Variable anatomy of the right coronary artery supply to the left ventricle. Thorax.; 40(8):618–620

[7] Koenraadt WM, Tokmaji G, DeRuiter MC, et al. Coronary anatomy as related to bicuspid aortic valve morphology. Heart.; 102(12):943–949

[8] Scanlon PJ, Faxon DP, Audet AM, et al. ACC/AHA guidelines for coronary angiography: executive summary and recommendations. A report of the American College of Cardiology/American Heart Association Task Force on Practice Guidelines (Committee on Coronary Angiography) developed in collaboration with the Society for Cardiac Angiography and Interventions. Circulation.; 99 (17):2345–2357

[9] Austen WG, Edwards JE, Frye RL, et al. A reporting system on patients evaluated for coronary artery disease. Report of the Ad Hoc Committee for Grading of Coronary Artery Disease, Council on Cardiovascular Surgery, American Heart Association. Circulation.; 51(4) Suppl:5–40

[10] Cerqueira MD, Weissman NJ, Dilsizian V, et al. American Heart Association Writing Group on Myocardial Segmentation and Registration for Cardiac Imaging. Standardized myocardial segmentation and nomenclature for tomographic imaging of the heart. A statement for healthcare professionals from the Cardiac Imaging Committee of the Council on Clinical Cardiology of the American Heart Association. Circulation.; 105(4):539–542

[11] Jaadi MS, Lautamäki R, Merrill J, et al. Definition of vascular territories on myocardial perfusion images by integration with true coronary anatomy: a hybrid PET/CT analysis. J Nucl Med.; 51(2):198–203

[12] Temov K, Sun Z. Coronary computed tomography angiography investigation of the association between left main coronary artery bifurcation angle and risk factors of coronary artery disease. Int J Cardiovasc Imaging.; 32 Suppl 1:129–137

[13] Tops LF, Wood DA, Delgado V, et al. Noninvasive evaluation of the aortic root with multislice computed tomography implications for transcatheter aortic valve replacement. JACC Cardiovasc Imaging.; 1(3):321–330

[14] Ortiz-Pérez JT, Rodríguez J, Meyers SN, Lee DC, Davidson C, Wu E. Correspondence between the 17-segment model and coronary arterial anatomy using contrast-enhanced cardiac magnetic resonance imaging. JACC Cardiovasc Imaging.; 1(3):282–293

[15] Donato P, Coelho P, Santos C, Bernardes A, Caseiro-Alves F. Correspondence between left ventricular 17 myocardial segments and coronary anatomy obtained by multi-detector computed tomography: an ex vivo contribution. Surg Radiol Anat.; 34(9):805–810

[16] Corban MT, Hung OY, Eshtehardi P, et al. Myocardial bridging: contemporary understanding of pathophysiology with implications for diagnostic and therapeutic strategies. J Am Coll Cardiol.; 63(22):2346–2355

[17] Saremi F, Shavelle D. Dual origin, course and supply in coronary artery system. Int J Cardiol.; 168(5):4970–4974

[18] Rosamond T, Wetzel LH, Lakkireddy D, Ferrell R, Tadros P. IntraCameral right coronary artery: detection by 64 slice coronary computed tomographic angiography and implications for radiofrequency ablation of atrial dysrhythmias. Pacing Clin Electrophysiol.; 30(12):1571–1574

[19] Sawaya FJ, Sawaya JI, Angelini P. Split right coronary artery: its definition and its territory. Tex Heart Inst J.; 35(4):477–479

[20] Rohit M, Bagga S, Talwar KK. Double right coronary artery with acute inferior wall myocardial infarction. J Invasive Cardiol.; 20(2):E37–E40

[21] Khan AR, Khan Luni F, Bavishi C, Khan S, Eltahawy EA. Left dominant circulation increases mortality in acute coronary syndrome: A systematic review and meta-analysis of observational studies involving 2,55,718 patients. Catheter Cardiovasc Interv.

[22] Werner GS. The role of coronary collaterals in chronic total occlusions. Curr Cardiol Rev.; 10(1):57–64
[23] Björk L. Angiographic demonstration of extracardial anastomoses to the coronary arteries. Radiology.; 87(2):274–277
[24] Loukas M, Hanna M, Chen J, Tubbs RS, Anderson RH. Extracardiac coronary arterial anastomoses. Clin Anat.; 24(2):137–142
[25] McEntegart MB, Badar AA, Ahmad FA, et al. The collateral circulation of coronary chronic total occlusions. EuroIntervention.; 11(14):e1596–e1603
[26] Hosseinpour AR, Anderson RH, Ho SY. The anatomy of the septal perforating arteries in normal and congenitally malformed hearts. J Thorac Cardiovasc Surg.; 121(6):1046–1052
[27] Singh M, Edwards WD, Holmes DR, Jr, Tajil AJ, Nishimura RA. Anatomy of the first septal perforating artery: a study with implications for ablation therapy for hypertrophic cardiomyopathy. Mayo Clin Proc.; 76(8):799–802
[28] Reig J, Albertí N, Petit M. Arterial vascularization of the human moderator band: an analysis of this structure's role as a collateral circulation route. Clin Anat.; 13(4):244–250
[29] Bream PR, Souza AS, Jr, Elliott LP, Soto B, Curry GC. Right superior septal perforator artery: its angiographic description and clinical significance. AJR Am J Roentgenol.; 133(1):67–73
[30] Saremi F, Abolhoda A, Ashikyan O, et al. Arterial supply to sinuatrial and atrioventricular nodes: imaging with multidetector CT. Radiology.; 246(1):99–107, discussion 108–109
[31] Levin DC. Pathways and functional significance of the coronary collateral circulation. Circulation.; 50(4):831–837
[32] Saremi F, Goodman G, Wilcox A, Salibian R, Vorobiof G. Coronary artery ostial atresia: diagnosis of conotruncal anastomotic collateral rings using CT angiography. JACC Cardiovasc Imaging.; 4(12):1320–1323
[33] Hansen MW, Merchant N. Images in cardiovascular medicine. Vieussens' ring: combining computed tomography coronary angiography and magnetic resonance imaging in assessing collateral pathways. Circulation.; 114(16):e545–e546
[34] Corone P, Corone A, Dor X, Binet JP. [Coronary arteries and their variations. An embryological explanation]. C R Acad Sci III.; 299(11):451–458
[35] Muresian H. Clinical Anatomy of Coronary Arteries: An Anatomical Study on 100 Human Heart Specimens. Bucharest, Romania: Editura Enciclopedica; 2009:149–154
[36] Thompson AJ, Froelicher VF. Kugel's artery as a major collateral channel in severe coronary disease. Aerosp Med.; 45(11):1276–1280
[37] Anderson KR, Ho SY, Anderson RH. Location and vascular supply of sinus node in human heart. Br Heart J.; 41(1):28–32
[38] Sow ML, Ndoye JM, Lô EA. The artery of the atrioventricular node: an anatomic study based on 38 injection-dissections. Surg Radiol Anat.; 18(3):183–187
[39] Berdajs D, Künzli A, Shurr U, Zünd G, Turina MI, Genonni M. Clinical anatomy of the atrioventricular node artery. J Heart Valve Dis.; 15(2):225–229
[40] Abuin G, Nieponice A. New findings on the origin of the blood supply to the atrioventricular node. Clinical and surgical significance. Tex Heart Inst J.; 25 (2):113–117
[41] Pejković B, Krajnc I, Anderhuber F, Kosutić D. Anatomical aspects of the arterial blood supply to the sinoatrial and atrioventricular nodes of the human heart. J Int Med Res.; 36(4):691–698
[42] Takeshita M, Furuse A, Kotsuka Y, Kubota H. Sinus node function after mitral valve surgery via the transseptal superior approach. Eur J Cardiothorac Surg.; 12(3):341–344
[43] Saremi F, Channual S, Abolhoda A, Gurudevan SV, Narula J, Milliken JC. MDCT of the S-shaped sinoatrial node artery. AJR Am J Roentgenol.; 190(6):1569–1575
[44] Nerantzis C, Avgoustakis D. An S-shaped atrial artery supplying the sinus node area. An anatomical study. Chest.; 78(2):274–278
[45] Anderson KR, Murphy JG. The atrio-ventricular node artery in the human heart. Angiology.; 34(11):711–716
[46] von Lüdinghausen M, Ohmachi N. Right superior septal artery with "normal" right coronary and ectopic "early" aortic origin: a contribution to the vascular supply of the interventricular septum of the human heart. Clin Anat.; 14 (5):312–319
[47] Sánchez-Quintana D, Ho SY, Cabrera JA, Farré J, Anderson RH. Topographic anatomy of the inferior pyramidal space: relevance to radiofrequency catheter ablation. J Cardiovasc Electrophysiol.; 12(2):210–217
[48] Hutchinson MC. A study of the artrial arteries in man. J Anat.; 125(Pt 1):39–54
[49] Kugel MA. Anatomical studies on the coronary arteries and their branches. I. Arteria anastomotica auricularis magna. Am Heart J.; 3:260–270
[50] Smith C, Amplatz K. Angiographic demonstration of Kugel's artery (arteria anastomotica auricularis magna). Radiology.; 106(1):113–118
[51] Nerantzis CE, Marianou SK, Koulouris SN, Agapitos EB, Papaioannou JA, Vlahos LJ. Kugel's artery: an anatomical and angiographic study using a new technique. Tex Heart Inst J.; 31(3):267–270
[52] Camici PG, Crea F. Coronary microvascular dysfunction. N Engl J Med.; 356 (8):830–840
[53] Cecchi F, Olivotto I, Gistri R, Lorenzoni R, Chiriatti G, Camici PG. Coronary microvascular dysfunction and prognosis in hypertrophic cardiomyopathy. N Engl J Med.; 349(11):1027–1035
[54] Duncker DJ, Bache RJ. Regulation of coronary blood flow during exercise. Physiol Rev.; 88(3):1009–1086
[55] Kaufmann PA, Camici PG. Myocardial blood flow measurement by PET: technical aspects and clinical applications. J Nucl Med.; 46(1):75–88
[56] Lee J, Smith NP. The multi-scale modelling of coronary blood flow. Ann Biomed Eng.; 40(11):2399–2413
[57] Kajiya M, Hiramatsu O, Yada T, et al. Physiomic approach to biomechanics of coronary microcirculation. J Mech Med Biol.; 5:1–9
[58] Austin RE, Jr, Smedira NG, Squiers TM, Hoffman JI. Influence of cardiac contraction and coronary vasomotor tone on regional myocardial blood flow. Am J Physiol.; 266(6, Pt 2):H2542–H2553
[59] DeFily DV, Chilian WM. Coronary microcirculation: autoregulation and metabolic control. Basic Res Cardiol.; 90(2):112–118
[60] Fokkema DS, VanTeeffelen JW, Dekker S, Vergroesen I, Reitsma JB, Spaan JA. Diastolic time fraction as a determinant of subendocardial perfusion. Am J Physiol Heart Circ Physiol.; 288(5):H2450–H2456
[61] Campeau L, Lespérance J, Corbara F, Hermann J, Grondin CM, Bourassa MG. Aortocoronary saphenous vein bypass graft changes 5 to 7 years after surgery. Circulation.; 58(3, Pt 2):I170–I175
[62] Cameron A, Davis KB, Green G, Schaff HV. Coronary bypass surgery with internal-thoracic-artery grafts: effects on survival over a 15-year period. N Engl J Med.; 334(4):216–219
[63] Eagle KA, Guyton RA, Davidoff R, et al. American College of Cardiology, American Heart Association. ACC/AHA 2004 guideline update for coronary artery bypass graft surgery: a report of the American College of Cardiology/American Heart Association Task Force on Practice Guidelines (Committee to Update the 1999 Guidelines for Coronary Artery Bypass Graft Surgery). Circulation.; 110(14):e340–e437
[64] Meyer TS, Martinoff S, Hadamitzky M, et al. Improved noninvasive assessment of coronary artery bypass grafts with 64-slice computed tomographic angiography in an unselected patient population. J Am Coll Cardiol.; 49(9):946–950
[65] Frazier AA, Qureshi F, Read KM, Gilkeson RC, Poston RS, White CS. Coronary artery bypass grafts: assessment with multidetector CT in the early and late postoperative settings. Radiographics.; 25(4):881–896
[66] Cox JL, Chiasson DA, Gotlieb AI. Stranger in a strange land: the pathogenesis of saphenous vein graft stenosis with emphasis on structural and functional differences between veins and arteries. Prog Cardiovasc Dis.; 34(1):45–68
[67] Motwani JG, Topol EJ. Aortocoronary saphenous vein graft disease: pathogenesis, predisposition, and prevention. Circulation.; 97(9):916–931
[68] Cremer J, Teebken OE, Simon A, Hutzelmann A, Heller M, Haverich A. Thoracic computed tomography prior to redo coronary surgery. Eur J Cardiothorac Surg.; 13(6):650–654
[69] Kamdar AR, Meadows TA, Roselli EE, et al. Multidetector computed tomographic angiography in planning of reoperative cardiothoracic surgery. Ann Thorac Surg.; 85(4):1239–1245
[70] Follis FM, Pett SB, Jr, Miller KB, Wong RS, Temes RT, Wernly JA. Catastrophic hemorrhage on sternal reentry: still a dreaded complication? Ann Thorac Surg.; 68(6):2215–2219

19 The Coronary Veins

Farhood Saremi and Damián Sánchez-Quintana

◆ Introduction

The literature for coronary veins, in contrast to that for coronary arteries, is scarce. Moreover, a complete, highly efficient and clinically useful classification of the coronary venous system (CVS) is not as straightforward as in the case of the coronary arteries. Recent developments in cardiac pacing and transvenous ablations ask for a thorough and a more detailed knowledge of the cardiac venous anatomy and function, concomitantly demonstrating the increasing value of CVS imaging. This holds true especially in the case of cardiac computed tomography (CT) venous mapping and justifies the content of this chapter. Imaging information about the CVS in this chapter is useful for better understanding of the spatial orientation of the CVS and helps in the proper use of the correct nomenclature for this important system. The variations, anomalies, and modifications encountered in congenital heart disease are subsequently presented. We also describe clinical applications of this system in cardiac resynchronization therapy (CRT) and other interventions such as percutaneous mitral annuloplasty (PMA) and retrograde cardioplegia perfusion (RCP).

◆ Development of the Cardiac Veins

The right and left common cardinal veins (ducts of Cuvier) are formed by the confluence of the anterior and posterior cardinal veins.[1,2] The right horn of the sinus venosus and the right common cardinal vein will develop and eventually form the posterior wall of the right atrium (RA) and the superior vena cava (SVC), respectively. The left horn of the sinus venosus, in conjunction with the regressing left common cardinal vein, forms the coronary sinus (CS) and the ligament or vein of the left atrium (LA; Marshall; ▶ Fig. 19.1).[1,2] A vessel connecting the right and left superior cardinal veins enlarges and becomes the left brachiocephalic vein. The right sinus valve persists as the valve of the inferior vena cava (IVC; Eustachian valve) and the valve of the CS (Thebesian valve).[2]

It was suggested in earlier experiments that coronary vessels arise from the proepicardium, a transitory structure in the embryonic heart that forms epicardium and several internal tissues.[3] Recent histological analysis in mouse, and cardiac organ culture has shown that coronary vessels arise from angiogenic sprouts of the sinus venosus, the major vein that returns circulating blood to the embryonic heart.[4] Some sprouting venous endothelial cells dedifferentiate into arteries and capillaries as they invade the myocardium and some remain on the surface and differentiate into veins.[4]

◆ Classification of the Coronary Veins

The coronary veins depict a very different macroscopic disposition, as compared to the coronary arterial system, and show many more individual variations. Modern anatomical classification divides the cardiac veins into two major groups. These two groups include tributaries of the greater CVS and the smaller CVS, consisting of the Thebesian vessels.[5,6,7] For clarity, the greater CVS is divided into two groups: the CS and non-CS tributaries (▶ Fig. 19.2). Branches of the two systems can communicate. The term compound CVS has been used to describe structures in which venous drainage is performed equally by both systems (▶ Fig. 19.2).[6] In the ventricular myocardium, the external two-thirds are drained by the greater CVS and the internal third is mainly drained by tributaries of the smaller CVS.[6]

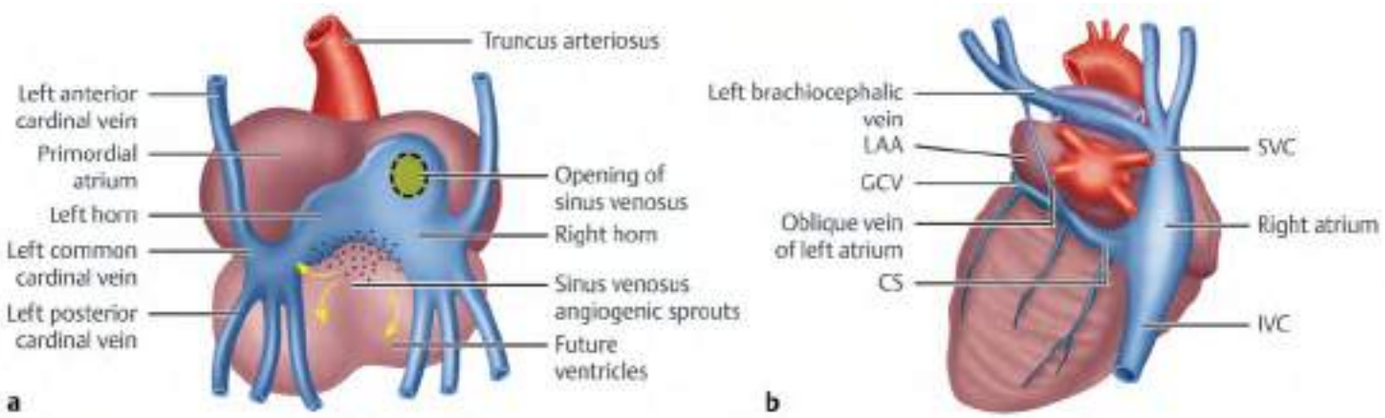

Fig. 19.1 Development of cardiac veins. Posterior drawings of the embryonic heart at 4 weeks **(a)** and well-developed heart **(b)** at 8 weeks. The right and left anterior cardinal veins connect through small anastomotic veins, which form the left brachiocephalic vein. The right horn of the sinus venosus and the cardinal veins eventually form the posterior wall of the right atrium and the vena cava, respectively. The left sinus horn regresses and loses its connection with the left anterior cardinal vein and becomes the coronary sinus (CS) and the oblique vein of left atrium (Marshall). Angiogenic sprouts (*small asterisks* in **a**) of the sinus venosus covering the epicardial surfaces (shown by *yellow curved arrows*) turn into the coronary vessels including veins. GCV, great cardiac vein; IVC, inferior vena cava; LAA, left atrial appendage; SVC, superior vena cava.

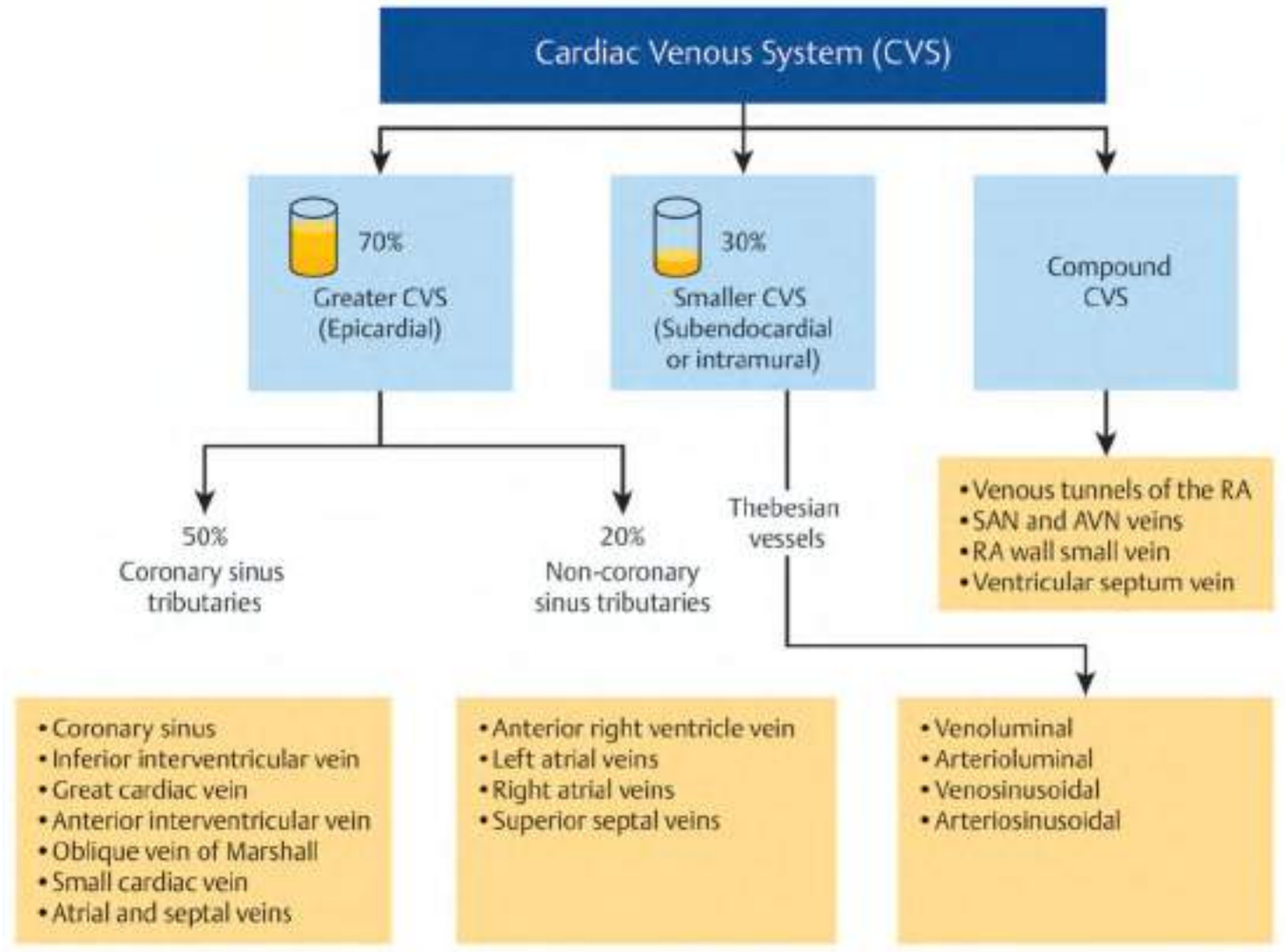

Fig. 19.2 Classification of the cardiac venous system.

The left ventricle (LV) and part of the right ventricle (RV) and the LA are drained by the CS tributaries and the majority of the RV and both atria are drained by the non-CS tributaries. Almost all veins of the greater CVS are finally drained into the right atrium. In the right atrium, the wall of sinus venosus is drained by tributaries of the greater CVS and the right atrial appendage is mainly drained by the smaller CVS.[8]

◆ Smaller Cardiovascular System (Thebesian Vessels)

Consisting of sinusoids, channels, and lacunae with variable sizes, this subendocardial and intramyocardial bidirectional communicating network runs in every direction conducting blood from epicardial coronaries into the cardiac chambers and provides myocardial nourishment (▶ Fig. 19.3**a**).

The vessels of the smaller CVS are collectively called *Thebesian veins*. However, in view of their arterial component, the term *Thebesian vessels* is preferred.[6] Four distinct parts are described (▶ Fig. 19.3**b**). Their orifices are found in cardiac chambers (mostly RA and RV) and the bases of the papillary muscles[9,10] and usually are greater than 0.5 mm in diameter but can be much larger especially in congenital heart disease with abnormal drainage of the CS.[11]

In adults, venous drainage of the myocardial wall takes place during systole. Approximately 70 to 80% of the left coronary artery blood flow drains through the CS tributaries and the remainder is drained via the smaller CVS. The right heart chambers mainly drain thorough the smaller CVS.[6,8]

This network can provide reverse flow from ventricles into the epicardial coronary arteries when their flow is compromised. However, it may be difficult to fill sinusoids directly from the heart chambers due to the existence of the monocuspid valve or sphincter at the outlet of the Thebesian veins.[12] It is shown that the Thebesian veins are increased in area with chronic myocardial infarction. In patients with congestive heart failure, congestion predominantly involves the large veins not the Thebesian veins.[13]

Thebesian Sinusoids of Special Structures

Sinusoids are large capillaries with different morphologies. They are remnants of the primitive cardiac circulation[9] (▶ Fig. 19.4).

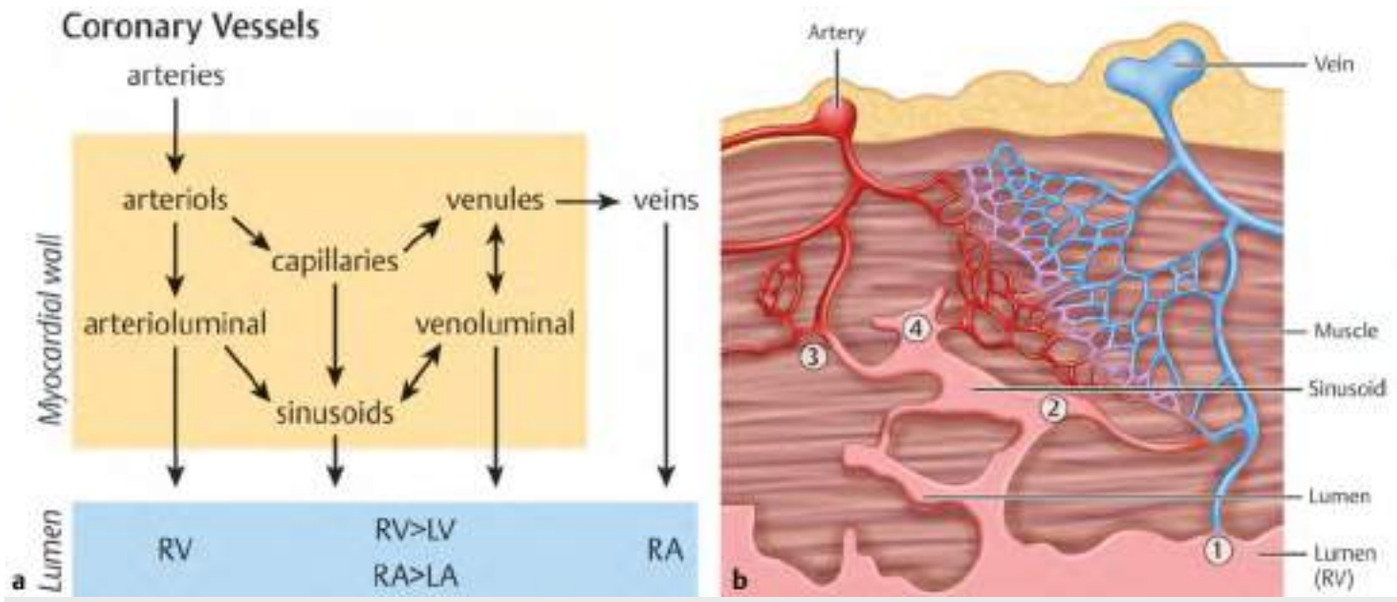

Fig. 19.3 **(a)** Schematic chart demonstrates extensive interconnection of the epicardial cardiac vessels through the intraluminal smaller cardiac venous system (CVS). **(b)** Tributaries of the smaller CVS (Thebesian vessels). (1) Venoluminal vessels: connect intramural venules with the lumen of cardiac chambers; (2) venosinusoidal vessels: connect intramural venules with subendocardial sinusoids and then the lumen; (3) arterioluminal vessels: connect arterioles with the atria or ventricles without traversing capillary beds; only exist in the right ventricle (RV); (4) arteriosinusoidal vessels: connect arterioles with sinusoidal spaces. RA, right atrium, LV, left ventricle, LA, left atrium.

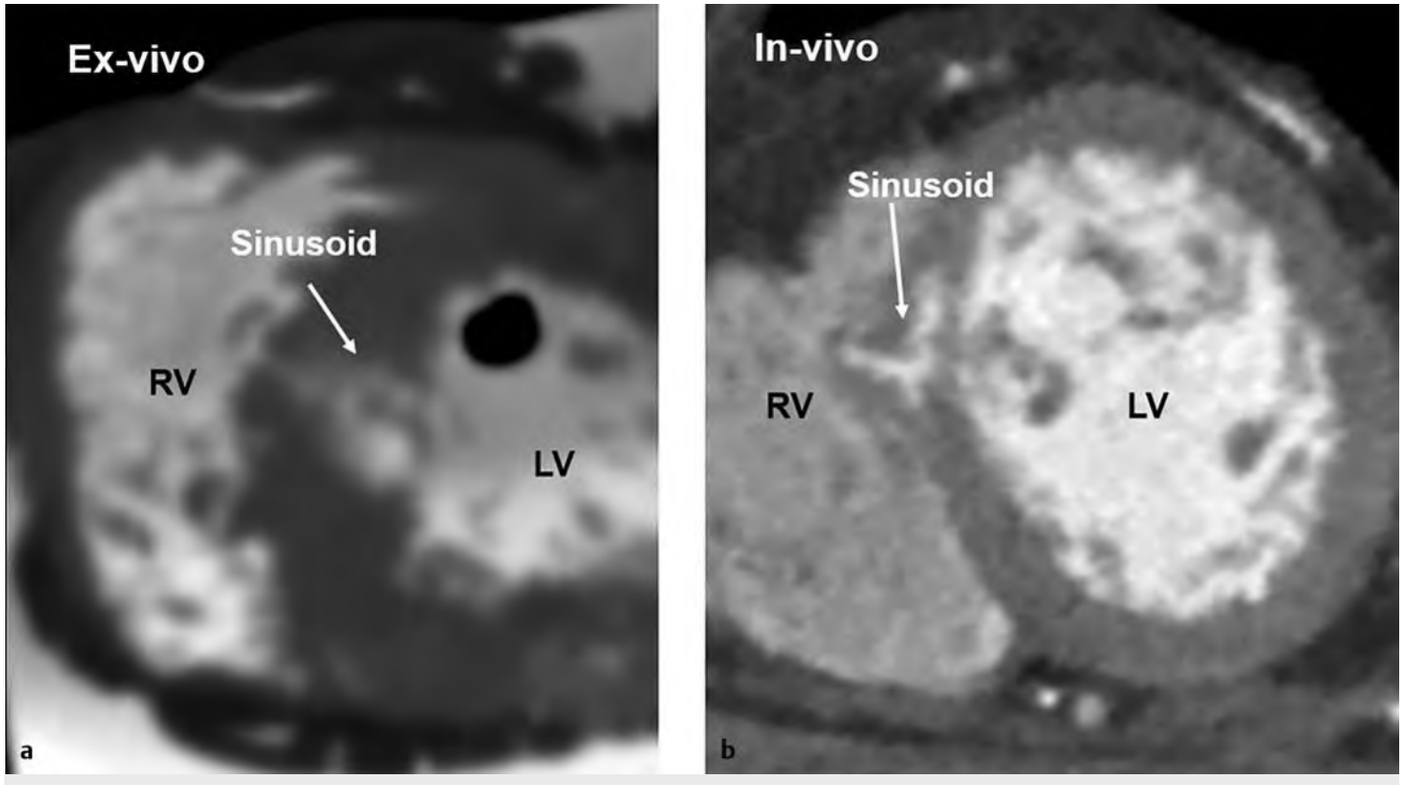

Fig. 19.4 **(a)** Ex vivo and **(b)** in vivo CT of the heart showing large sinusoids in the interventricular septum. In ex vivo examination, the heart specimen is immersed in 10% iodinated contrast and scanned with 0.6-mm slices. Coronary veins are filled slowly by retrograde injection of contrast into the coronary sinus.

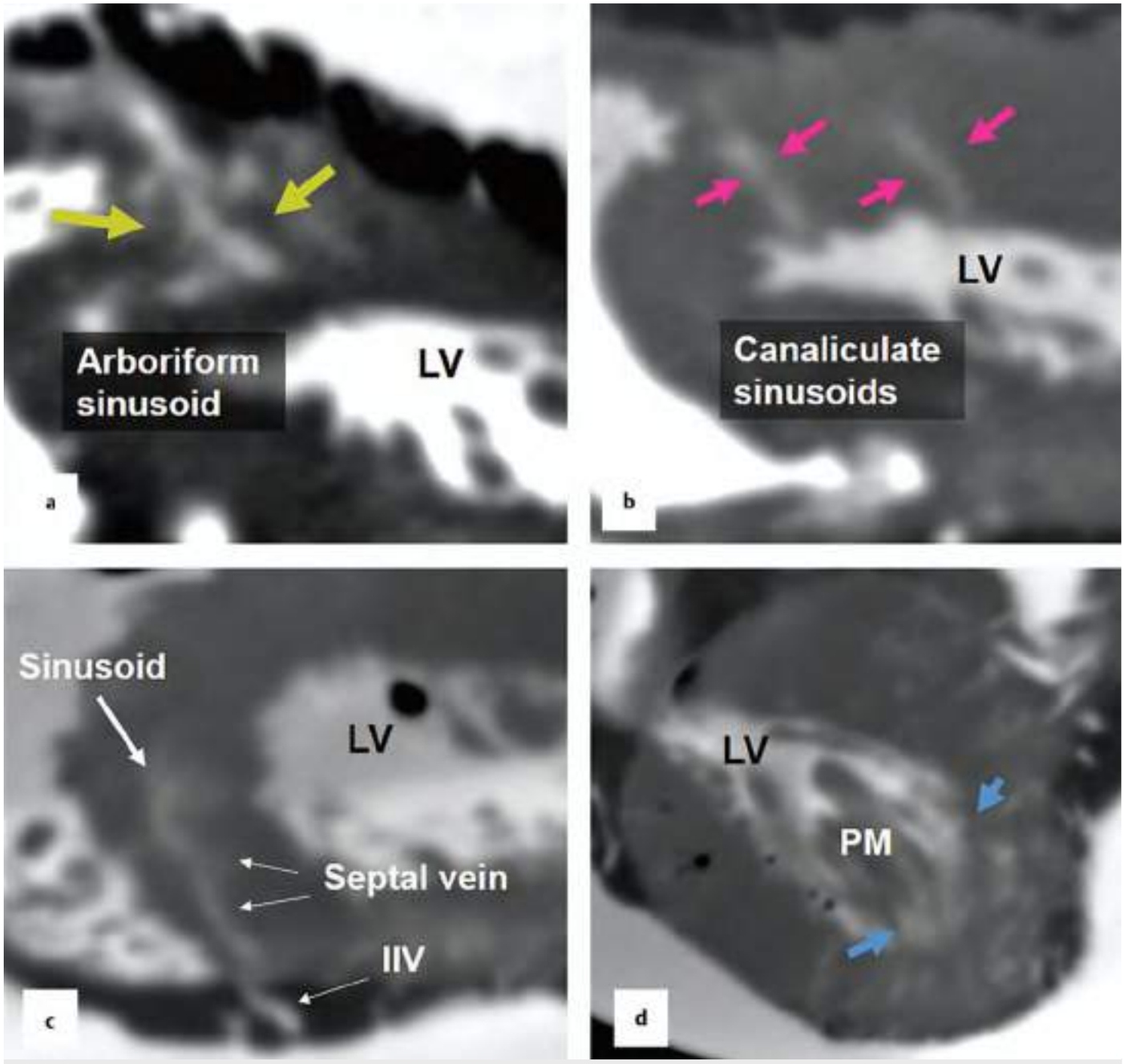

Fig. 19.5 Ex vivo CT of the heart in different specimens. The coronary veins are opacified with 10% iodinated contrast injected into the coronary sinus. Note numerous contrast-filled intramural Thebesian vessels including sinusoids (*thick arrows*), some opening into the ventricular lumen. Arboriform **(a)** and canaliculate **(b)** sinusoid morphologies are shown. **(c)** Venosinusoidal communication connecting the inferior interventricular vein (IIV) with a sinusoid through the septal vein. **(d)** Large sinusoids at the base of left ventricle (LV) papillary muscle (PM). Thebesian vessel foramina are common at the apex of the ventricles and at the base of the papillary muscles.

Conduction System

Both atrioventricular and sinoatrial nodal zones are sinusoid rich for retrograde blood flow to nodal conducting tissue[14] in case the arterial supply is compromised.

Papillary Muscles

The papillary muscles are mainly drained by the SVC in the RV and by the great cardiac vein (GCV) and SVC in the left.[6] Retrograde vascularization by sinusoids can supplement normal flow to papillary muscles and may prevent their rupture after ischemic damage.[15] Thebesian vessel foramina are common at the apex of the ventricles and at the base of the papillary muscles (▶ Fig. 19.5).

Left Ventricle Venoluminal Thebesian Vessels

A greater number of Thebesian veins are seen in the RV than in the LV.[10] Arterioluminal vessels are identified only in the RV, whereas venoluminal vessels are present in both ventricles.

Table 19.1 Venous drainage of the left and right atrial walls

Left atrium	Right atrium
1. Posterior and lateral walls (99%): Draining into the CS 2. Septal walls: Draining into the RA (92%) Anterosuperior (near SVC; 99%) Posteroinferior (near IVC; 35%) 3. Posterosuperior wall: Draining into the mediastinum (40%) Draining in the LA lumen (80%) Draining into the pulmonary veins (some)	1. Small intramural veins (73%): Draining into the RA,1-mm diameter 2. Venous tunnels of the RA (right atrial CS; 25–60%): 1–12 cm in length and 1–4 mm in diameter emptying into the RA or SCV. 3. SAN region: Small veins and sinusoids draining into the RA 4. AVN region: Small venous tunnels draining into the RA or CS

Abbreviations: AVN, atrioventricular node; CS, coronary sinus; IVC, inferior vena cava; LA, left atrium; RA, right atrium; SAN, sinoatrial node; SVC, superior vena cava.
Note: Incidence is shown in parentheses.

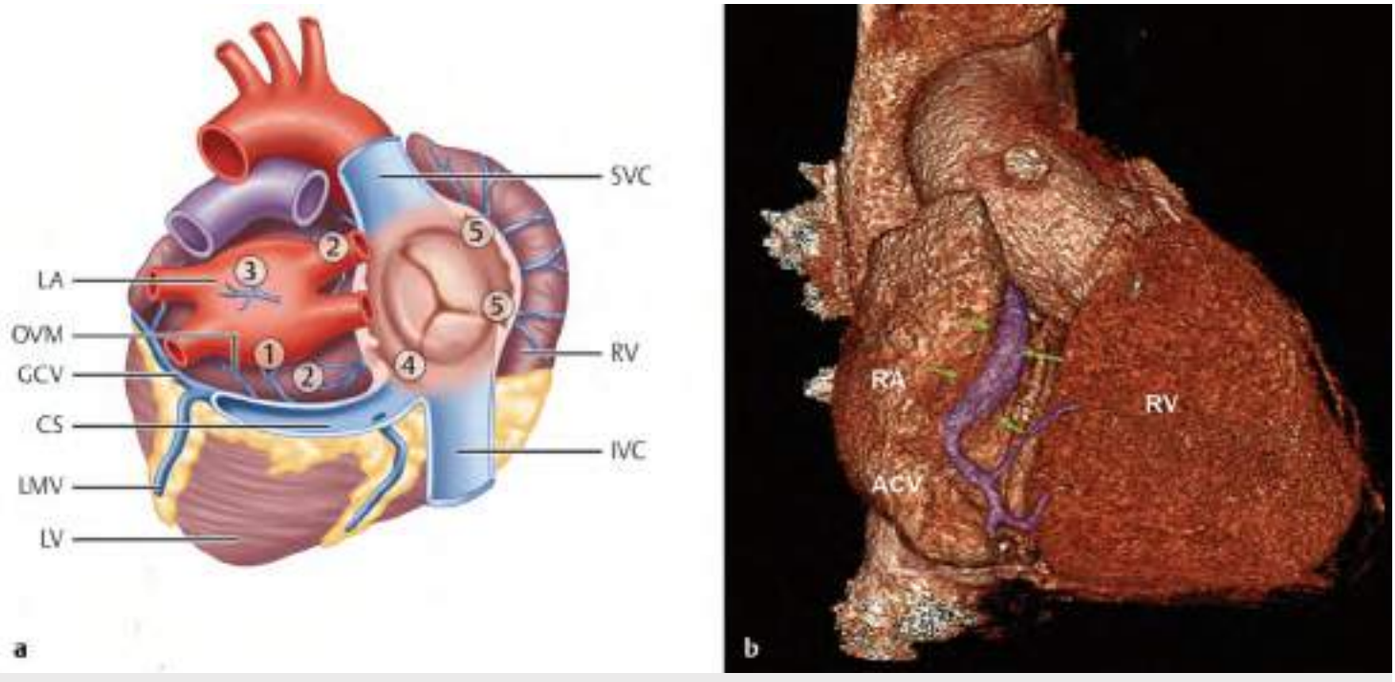

Fig. 19.6 **(a)** Atrial venous system. Posterosuperior view of the heart is depicted. The right atrium is removed. (1) Veins of the posterior and lateral walls of the left atrium (LA) empty into the coronary sinus (CS); (2) septal veins of the LA drain into the right atrium (RA); (3) posterosuperior wall of the LA drains into the LA lumen or the superior pulmonary veins; (4) atrioventricular node region contains small sinusoids draining into the RA near the CS ostium; (5) anterior cardiac veins may drain directly into the RA, small cardiac vein, or into a venous tunnel in the RA wall. **(b)** Right lateral view showing drainage of the anterior cardiac vein (ACV) into the venous tunnel running (*green arrows*) parallel to the atrioventricular groove. GCV, great cardiac vein; IVC, inferior vena cava; LMV, left marginal vein; LV, left ventricle; OVM, oblique vein of Marshall; RV, right ventricle; SVC, superior vena cava.

◆ Atrial Venous System

Imaging of these veins is difficult because of the small size of the vessels. However, careful evaluation of cardiac CT images can show these structures in many studies. Different classifications have been introduced.[6,8,16,17] The easiest classification is introduced by von Lüdinghausen[8] (▶ Table 19.1).

Veins of the Left Atrial Wall

The majority of the left atrial (LA) veins are tributaries of the greater CVS. Three groups are described[6,8]:

- Veins of the posterior and lateral walls of the LA empty into the CS and GCV (▶ Fig. 19.6).
- Septal veins of the LA drain into the RA through the interatrial septum. These veins are commonly seen with CT angiography (CTA). Veins anterosuperior to the fossa ovalis pass through the interatrial groove and empty into the right atrium near the superior cavoatrial junction (▶ Fig. 19.7). Some (12%) may pass through the superior interatrial muscle connections where Bachmann's bundle is located[18] (▶ Fig. 19.8). Veins inferoposterior to fossa ovalis are less common (▶ Fig. 19.7).
- The posterosuperior wall of the LA near the LA appendage drains into the LA and the superior pulmonary veins (▶ Fig. 19.7). They may connect mediastinal veins, azygos, or hemiazygos venous system, and the bronchial veins.[8] The mediastinal connections can be an important alternative route for venous return to the atria in case of occlusion of the pulmonary vein, brachiocephalic vein, or SVC (▶ Fig. 19.7, ▶ Fig. 19.9). In

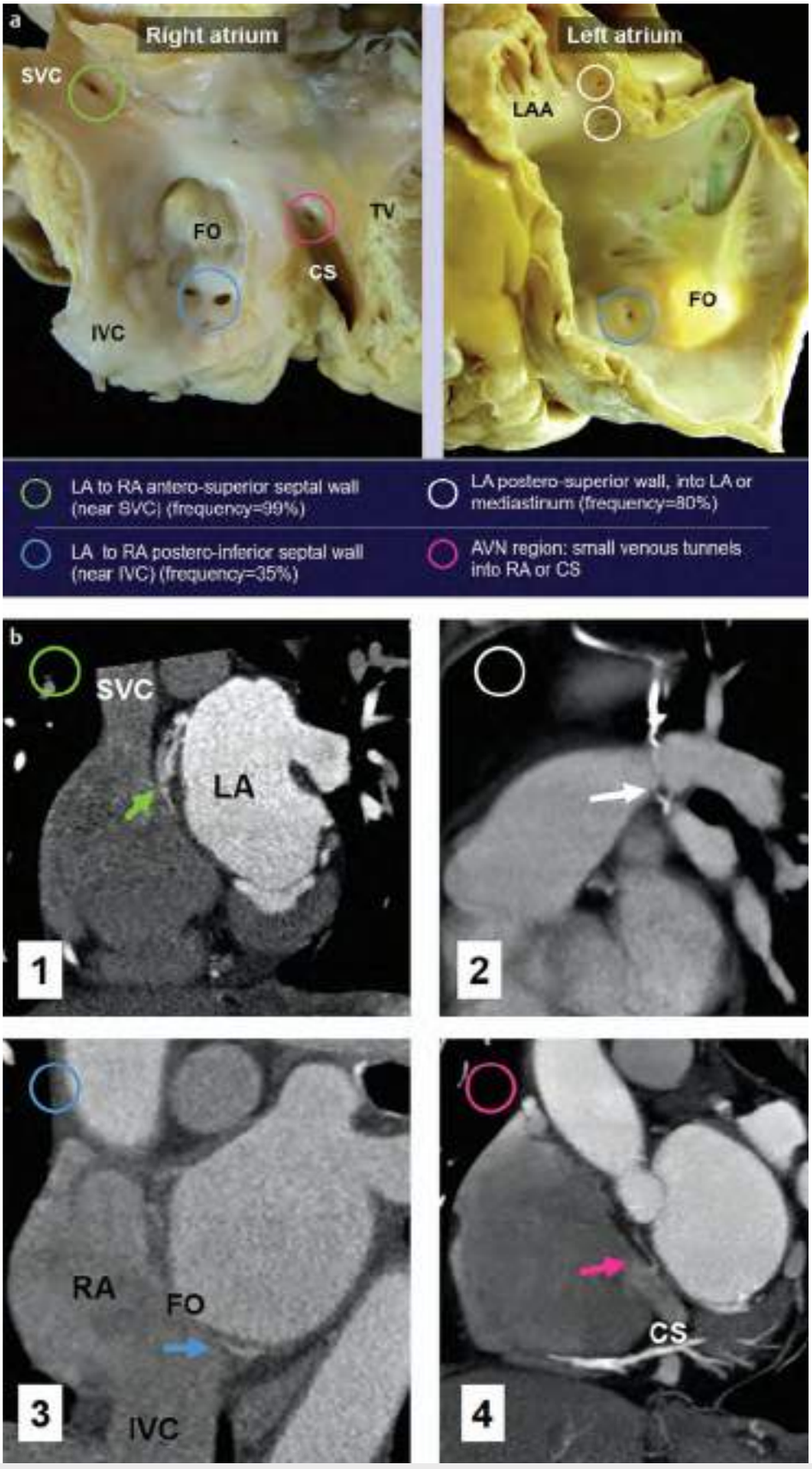

Fig. 19.7 **(a)** Septal views of the right atria (RA) and the left atria (LA) from two different cadaveric specimens are shown. Most of the septal venous drainage occurs from the LA into the RA. Venous drainage of the anterosuperior and posteroinferior of the interatrial septum and posterosuperior wall of LA and atrioventricular node (AVN) region are shown by *green*, *blue*, *white*, and *pink circles*, respectively. Most of the septal venous drainage occurs from the LA into the RA. The venous opening can be large enough to be detected by CT scan. **(b)** Short-axis CT images demonstrate the drainage pattern of atrial wall veins matching to the *colored circles* shown in **(a)**, including communication between the two atrial walls near the SVC (*green arrow* in b1) and IVC (*blue arrow* in b3), the superior wall of the LA near confluence with the left superior pulmonary vein (*white arrow* in b2), and the medial RA wall near the coronary sinus (CS) ostium (*pink arrow* in b4). Veins of the superior wall of LA may communicate with venous collaterals in the mediastinum (*white arrow* in b2). FO, fossa ovalis; IVC, inferior vena cava; LAA, left atrial appendage; SVC, superior vena cava; TV, tricuspid valve.

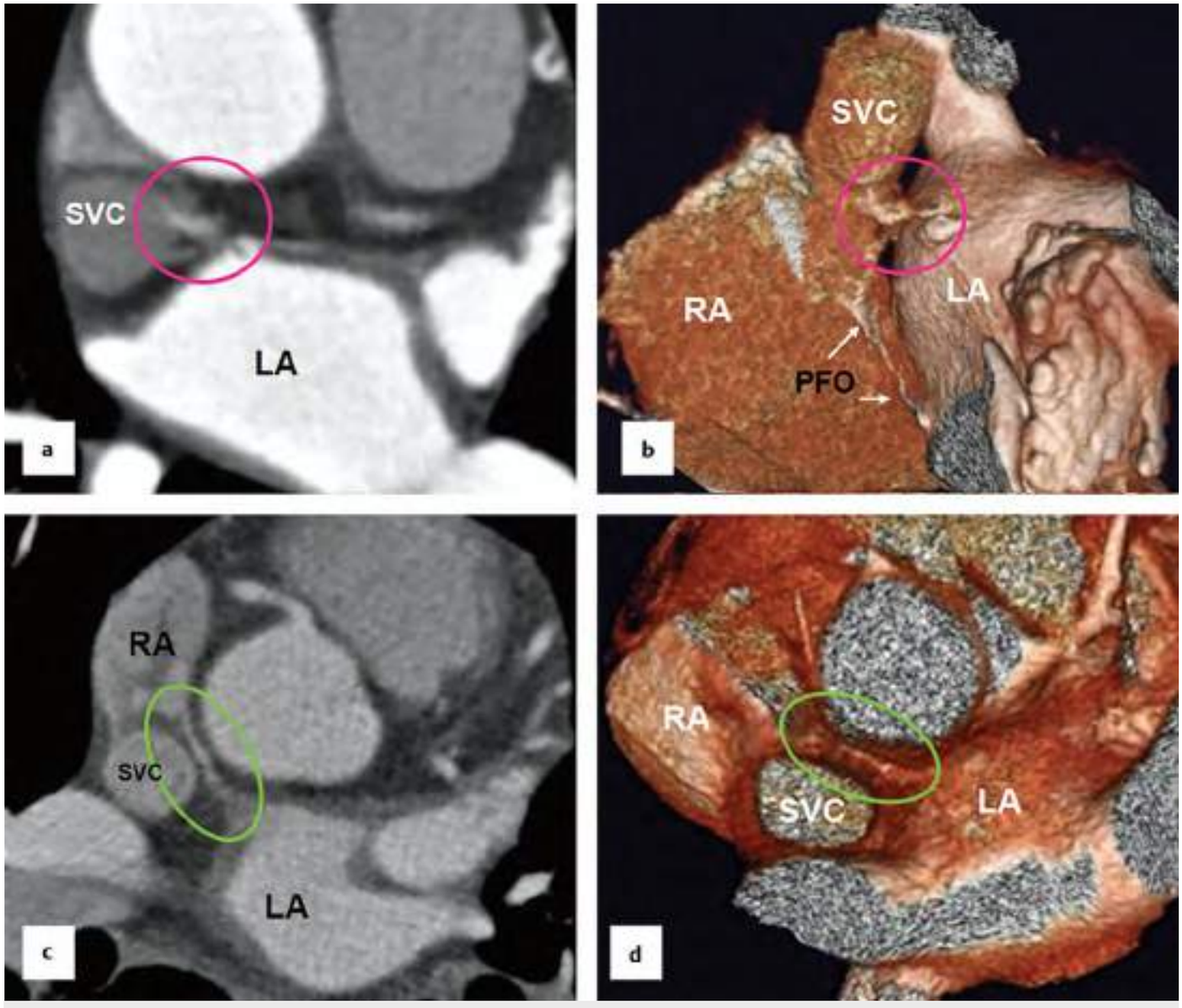

Fig. 19.8 Venous drainage of the anterosuperior septal wall of left atrium (LA) into the right atrium (RA) through the superior interatrial muscle connection where the Bachmann bundle resides. Communications found in two different patients are shown by *pink circles* **(a**, **b)** and *green circles* **(c**, **d)**. This communication is seen in 12% of CT angiographies. The lumen of a patent foramen ovalis (PFO) is incidentally seen (*white arrows*). SVC, superior vena cava.

congenital atresia of the CS, the myocardial venous drainage can be via ectatic atrial veins of the LA.[19]

Veins of the Right Atrial Wall

Majority of the right atrial wall veins are located intramurally and drain into the RA. The veins draining the wall of the right atrial appendage have no connection with the epicardial veins, and therefore are classified as smaller CVS. The RA veins are classified into four groups based on anatomical locations (▶ Table 19.1):

- Small intramural venous tunnels draining directly into the RA. They are a few millimeters in length and 1 mm in diameter.[6]
- Venous tunnels of the RA (the sinus coronaries atrii dextri or right atrial CS): Termination of the anterior cardiac veins of the RV is variable. They may drain directly into the RA, small cardiac vein, or in some into a venous tunnel.[6] When it exists, this venous tunnel runs parallel and 1 to 2 cm above the tricuspid orifice along the posterior or posterolateral wall of the RA[20] (▶ Fig. 19.6). In high-quality CTAs, these veins may be partially visible (▶ Fig. 19.6**b**).
- The sinoatrial node region has sinusoids draining into the RA.[14] This network of anastomosing blood vessels potentially can protect the node in case arterial supply is compromised. However, this phenomenon is rare given the common variants of dual or multiple arterial supplies to the node.
- Atrioventricular node region: Venous tunnels are seen at the base of the interatrial septum near the atrioventricular node and the bundle of His and usually open into the RA near the ostium of the CS or directly into the CS (▶ Fig. 19.6, ▶ Fig. 19.7). These tunnels can be seen in CTA and should not be confused with anomalous vessels or a patent foramen ovale.

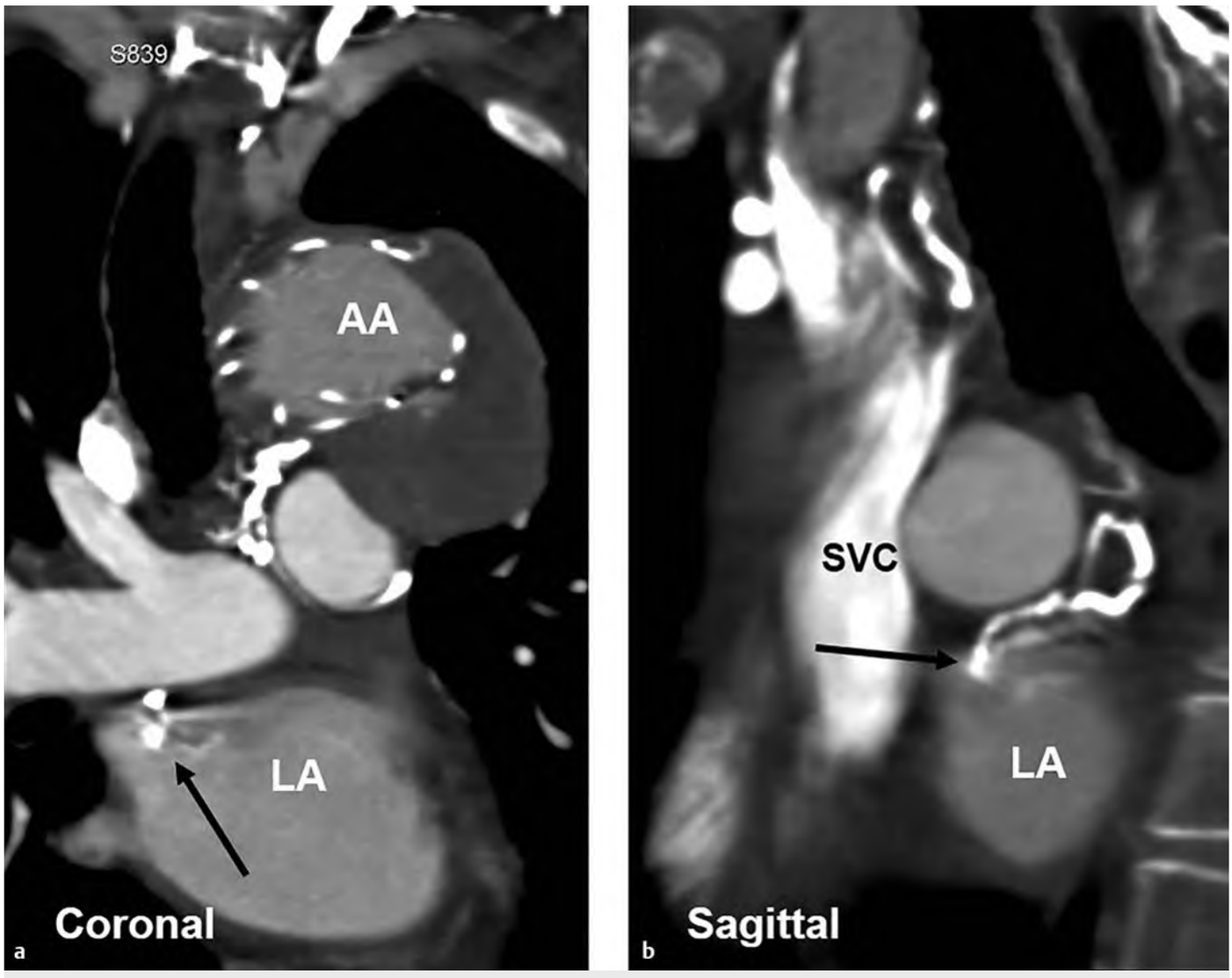

Fig. 19.9 **(a)** Coronal and **(b)** sagittal views demonstrate drainage of the collateral mediastinal veins (*arrows*) into the superior wall of the left atrium (LA) in a patient with chronic thrombosis of the left brachiocephalic vein. Note ascending aortic (AA) stent graft in the area of aneurysm. SVC, superior vena cava.

Table 19.2 Characteristics of the epicardial veins of coronary sinus and anterior right ventricle venous system

Veins	Origin	Territory	Ostial diameter (mm)	Frequency (%)	Drainage	Number	Variant	Ostial valve (%)
CS	GCV	Left atrioventricular groove	4–14[10]	99	RA	1, duplication is very rare	Absence (with left SVC), unroofed, atresia (1%), duplication	80
GCV/AIV	Apex	Anterior septum, anterior of both ventricles, parts of LA and apex	AIV = 0.9–4.4 (2.7), GCV = 1.2–6.3 (3.9)	100	CS (99%)	1 (98%)	Aberrant course to RA in 1%, aneurysm, myocardial bridge 2–8%, duplication 3%, myocardial belt (6%)	85
IIV	Apex	Posterior wall of the RV and LV, apex, posterior two-thirds of the interventricular septum	2–5.3 (3.6)	100	CS, rarely RA (2.5%)	1 (75%), 2 (24%)	Aneurysm (8%), varicoid, duplicated, myocardial cover (2.5%)	60
LPV	Posterior wall	Lateral and diaphragmatic walls of the LV	1–5.5 (2.4)	95	CS (37–77%), GCV (13%)	1 (63%), 2 (23%), multiple small (9%), non (5%)	Bulbar (5%), myocardial cover (2%)	30
LMV	Posterolateral wall of LV	Draining much of LV myocardium	1–3 (2.2)	70–85	GCV (80%), CS (20%)	1	Absence common	30
SCV	Right atrioventricular groove	Diaphragmatic surface of RV	<1	30–50	CS (85%); IIV (12%)	1	Can receive the right marginal vein in 10%	–
OVM	Junction of CS and GCV	Posterolateral LA, 2–3 cm in length	0.4–1.8	85–95	CS	1	Persistent SVC 0.5%	–
RMV	Apex	Anterior and posterior RV walls	0.5–3	13–80	SCV (30%), rest RA or tunnel of RA	1	Large draining into a vertical RA tunnel	–
ACV	Anterior RV	Anterior and anterolateral RV	0.5–1	90	RA (30%), venous tunnel of RA (66%), SCV	1 (24–57%), 2 (33–48%), 3 (9–28%), up to 15 tiny ones	Abnormal course of AIV into SVC, large conus vein	12

Abbreviations: ACV, anterior cardiac vein; AIV, anterior interventricular vein; AV, atrioventricular; CS, coronary sinus; GCV, great cardiac vein; IIV, inferior interventricular vein; IVC, inferior vena cava; LA, left atrium; LMV, left marginal vein; LPV, left posterior vein; LV, left ventricle; OVM, oblique vein of Marshall; RA, right atrium; RMV, right marginal vein; RV, right ventricle; SCV, small cardiac vein; SVC, superior vena cava.
Source: Data from von Lüdinghausen,[5,6,33] Pina,[21] Mierzwa and Kozielec,[22] Ortale et al,[30] Pejkovic and Bogdanovic,[32] Saremi et al,[35] and Cendrowska-Pinkosz.[41]

Anterior Right Ventricle Venous System

Including the anterior cardiac, right marginal, and conus veins are seen in 90% of cases[6,20,21] (▶ Table 19.2). The anterior cardiac veins drain two-thirds of the RV including the anterior and anterolateral walls of the RV. These veins are frequently seen in coronary CTAs (▶ Fig. 19.10). They are variable in sizes and numbers and usually drain into the RA above the atrioventricular groove.[6,16,21,22] In 5 to 27%, they merge to form a common trunk before entering the RA.[6,21] The right marginal vein originates near the right ventricular apex and receives branches from posterior and anterior surfaces of the RV (▶ Fig. 19.10). In one-third of cases, the vein continues as small cardiac vein into the CS.[6] In the remainder of cases, it drains into the RA or the venous tunnels of the RA.

The conus (infundibular) veins are usually small veins and drain into the RA. However, they can be large and varicoid (i.e., arteriovenous fistula) creating diagnostic problems (▶ Fig. 19.11) or causing excessive bleeding during surgery. Veins of Zuckerkandl and Cruveilhier are described in the anatomic literature for veins draining the anterior and posterior surfaces of the infundibulum, respectively[20,21] (▶ Fig. 19.11).

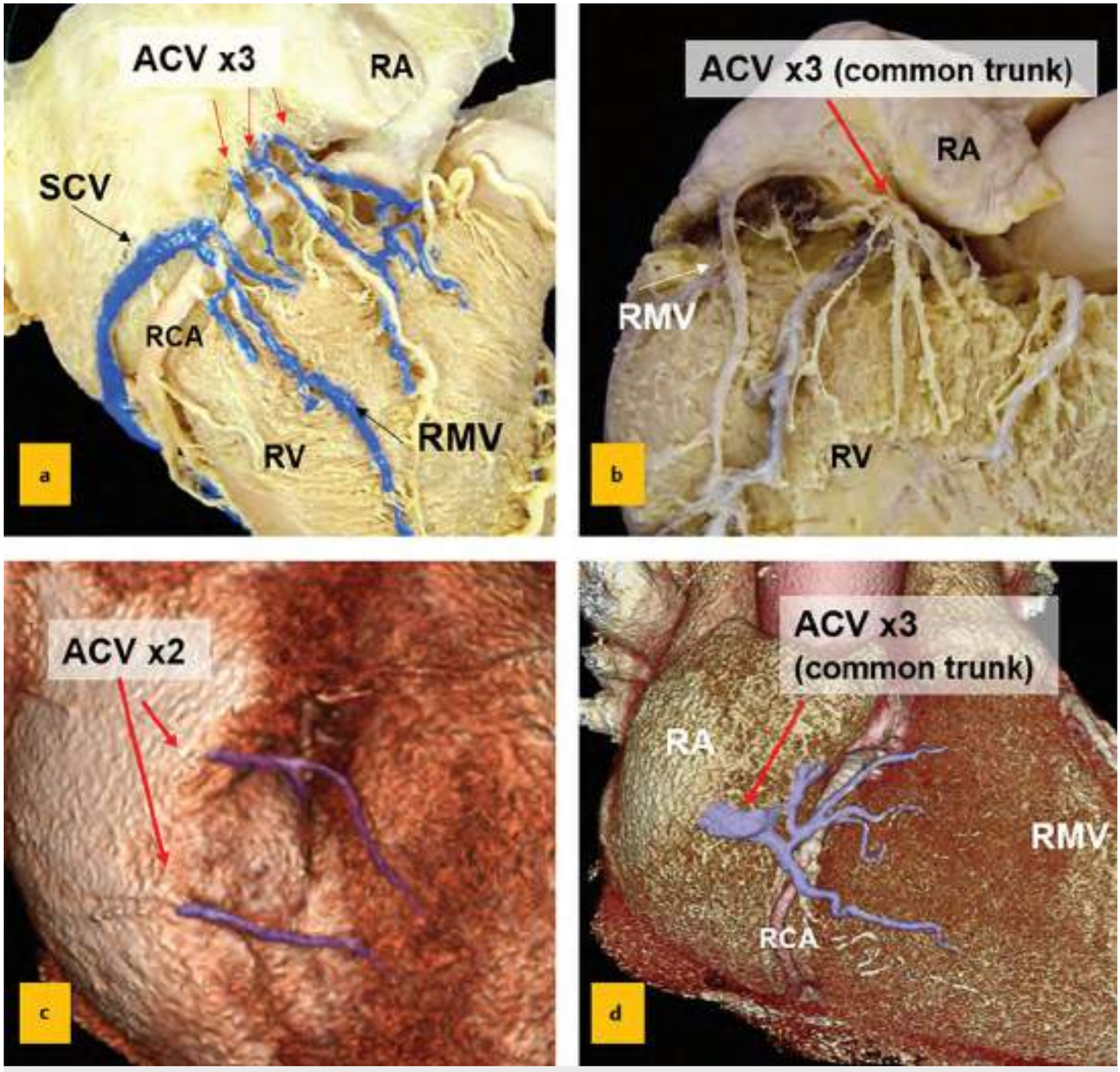

Fig. 19.10 Common variants of the right ventricle (RV) venous system are shown: cadaveric specimens **(a, b)** and CT angiograms **(c, d)**. Passing anterior to the right coronary artery (RCA), the anterior cardiac veins (ACV) commonly enter into right atrium (RA) as separate vessels or in some cases form a common trunk (5–27%). The right marginal vein (RMV) is seen in 80% of cases. It drains in to small cardiac vein (SCV) in 30% or drains directly into the RA in 70%.

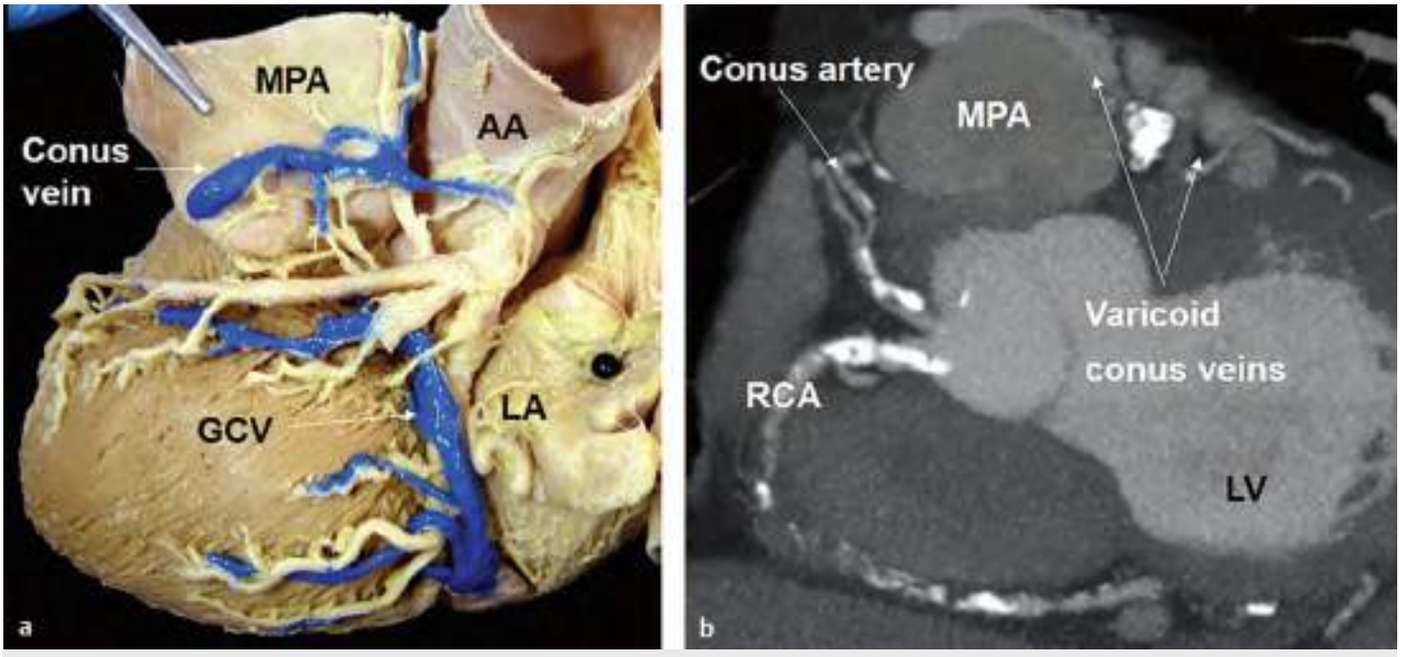

Fig. 19.11 Conus veins. **(a)** In this cadaveric specimen, the conus vein is the vein located between the main pulmonary artery (MPA) and the ascending aorta (AA). Large and varicoid conus veins are seen in coronary artery occlusions, myocardial bridging, and vascular malformations. **(b)** A dilated conus vein is shown in a patient with severe coronary artery disease and right coronary artery (RCA) occlusion. GCV, great cardiac vein; LA, left atrium; LV, left ventricle.

◆ Coronary Sinus Tributaries

The CS tributaries include the GCV, the left marginal vein, the posterolateral vein of the LV, and the inferior interventricular vein (IIV; ▶ Fig. 19.12). In 30% of cases, it receives the right marginal vein blood through the small cardiac vein[6] (▶ Table 19.2).

Imaging Methods

The CS is frequently used as a conduit for catheter treatment of arrhythmias as well as left ventricular pacing. These procedures are well known for their potential technical difficulties. As a result, different imaging methods are introduced for evaluation of this system. Each technique has its own advantages and limitations.[23,24,25,26,27,28,29]

Retrograde venography via the CS is currently the standard technique for defining the CS anatomy; however, it is invasive in nature and can be technically challenging. This technique is frequently used to show the anatomy of the CS and target veins for CRT. In this technique, using an occlusive balloon, contrast is injected into the CS and two orthogonal views including right anterior oblique 45 degrees and left anterior oblique 45 degrees are obtained.[23] High-speed rotational coronary venography uses rapid isocentric rotation over a 110-degree arc in 4 seconds, acquiring 120 frames per angiogram.[23] With this modification, vessel overlap and foreshortening will be reduced and target veins including second-degree tributaries can be better defined.

Levophase of coronary angiography is preferred by some investigators and claimed to better define the anterior (superior) interventricular vein (AIV) and IIV as well as the peripheral branches compared to retrograde venography.[24] The technique takes advantage of the coronary artery angiography procedure commonly indicated in the assessment of candidates for CRT.

Magnetic resonance imaging (MRI) and CT have been increasingly used to assess anatomy of the coronary vessels including coronary veins.[25,26,27,28,29] CT has the advantage of showing part of the CS and in some cases the origin of the IIV, which will be obscured with balloon in retrograde venography. With CT, there is no foreshortening or vessel overlap. CT also demonstrates many ancillary structures such as coronary arteries, old infarctions, interatrial septum anatomy, and variants of the normal anatomy. Higher radiation dose in CT is a limitation[26] that can be modified using dose reduction techniques. CT also may have difficulty showing second-order tributaries of the coronary veins in routine coronary CTAs. Demonstration of the oblique vein of LA is also more challenging with CT compared with retrograde venography. However, with some modification of the CT technique, most small branches can be nicely depicted.[18]

Great Cardiac Vein

The GCV is the longest and the most consistent vessels making up the cardiac venous system, almost always entering the CS.[30,31,32,33,34] This vein drains blood from the anterior interventricular septum, the anterior surfaces of both ventricles, part of the LA, and the apical region of the heart.[6] The AIV portion of the vein courses superiorly within the anterior (superior) interventricular groove (sulcus) and then enters the left atrioventricular groove where it is defined as the GCV. The GCV may originate at the apex or in the apical or middle third of the anterior interventricular groove with a highly variable position with respect to the left anterior descending (LAD) artery, which may render very difficult the localization of the latter especially in coronary artery bypass procedures.

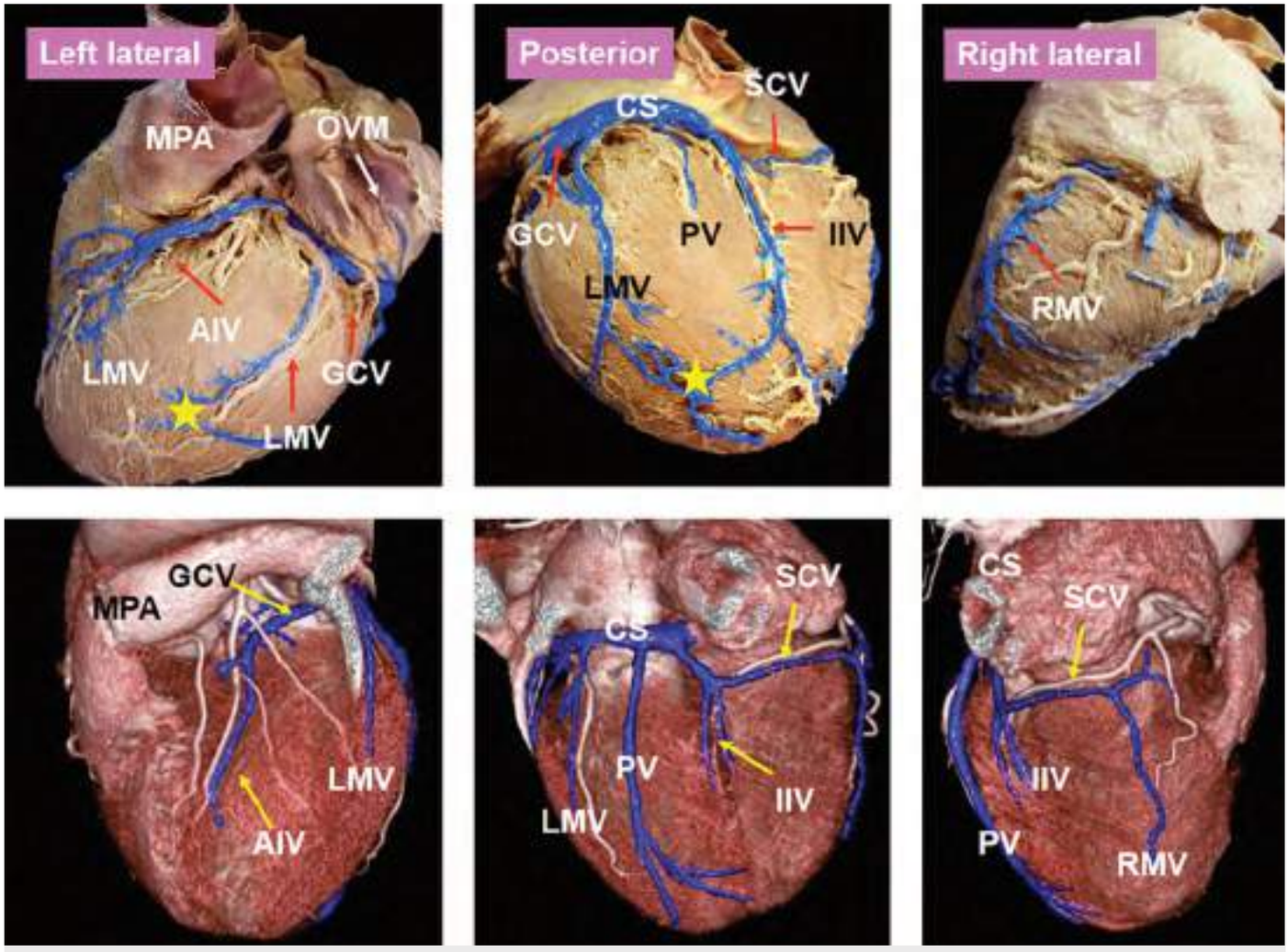

Fig. 19.12 Left lateral, posteroinferior, and right lateral views of the cadaveric heart (*upper row*) and CT angiographies of a patient with tetralogy of Fallot (*lower row*). Tributaries of the coronary sinus (CS) venous system are displayed in *blue*. The CS tributaries include the great cardiac vein (GCV), the anterior interventricular vein (AIV) portion of the GCV, the left marginal vein (LMV), the posterior vein (PV) of the left ventricle, the inferior interventricular vein (IIV), the oblique vein of Marshall (OVM), and the small cardiac vein (SCM). A very large PV and two small IIVs are shown in the CT image of a patient with tetralogy of Fallot. In the cadaveric heart, the right marginal vein (RMV) drains directly into the right atrium, while in tetralogy case it drains into the SCV. That is why SCV is large in this patient; it also drains into the IIV. MPV, main pulmonary artery.

The GCV crosses the branches of the left coronary artery system including the anterior descending and the circumflex branches forming a triangle[6,30] in which the vein is mainly superficial to arteries in 60 to 70%[31,32,33,34] of cases (▶ Fig. 19.13). Branches of the left coronary artery system traverse this triangle (i.e., the ramus intermedius). However, it is important to know that the relation of the vein and these arteries is highly variable and practically unpredictable in many cases.

Aberrant drainage of the GCV into the RA or SVC is described.[33] In this situation, the GCV runs in the transverse sinus and finally joins the azygos vein or the RA. Knowledge of this anatomy prior to surgery can be important for RCP.

Myocardial bridges are detected above the AIV or its tributaries in 8%.[30] Aneurysmal dilatation of the distal end of the GCV has been reported and may interfere with coronary artery bypass grafting (CABG).[34] It is the second most common location of coronary vein aneurysm seen in 1.5% of CT examinations[35] (▶ Fig. 19.14).

Inferior Interventricular Vein

The IIV, also known as middle cardiac vein or posterior interventricular, travels along the inferior aspect of the heart (attitudinal orientation) in the interventricular groove. The vein is a constant landmark and drains into the CS approximately 1 cm from the CS ostium. Extending from the apex to the CS, it drains the interior walls of the ventricles as well as the apical area and the posterior two-thirds of the septum[6] (▶ Fig. 19.15). The terminal portion of the vein measures 3 to 4 mm in diameter and appears angled in 35% or bulbous in 19% of population.[6] Fusiform aneurysmal dilatation (focal dilatation of twice the normal diameter; mean; 10.5 ± 1.4 mm) of the venous confluence is reported in CT studies in 8% (▶ Fig. 19.15). It is the most common location for bulbous enlargement of the coronary veins.[35] Aneurysms, especially the diverticular form, arising from the CS and the confluence of coronary veins with the CS, may be associated with cardiac arrhythmias such as ventricular preexcitation.[36,37]

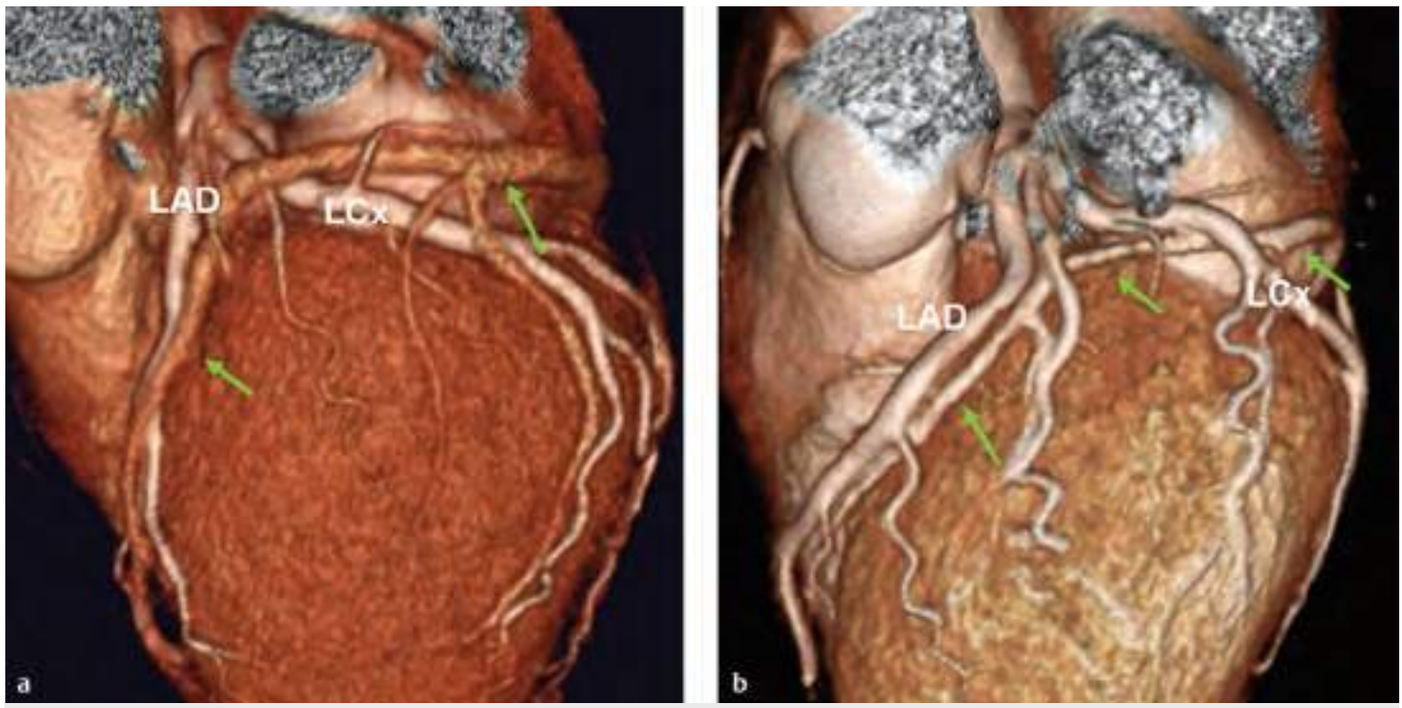

Fig. 19.13 The anterior interventricular vein (*green arrow*) portion of the great cardiac vein crosses the left anterior descending (LAD) and the left circumflex (LCx) arteries forming a triangle. **(a)** The vein runs superficial to arteries in 60 to 70% of population. The relations of the vein and these arteries are highly variable. (**b**) It passes under both arteries in 20% of population.

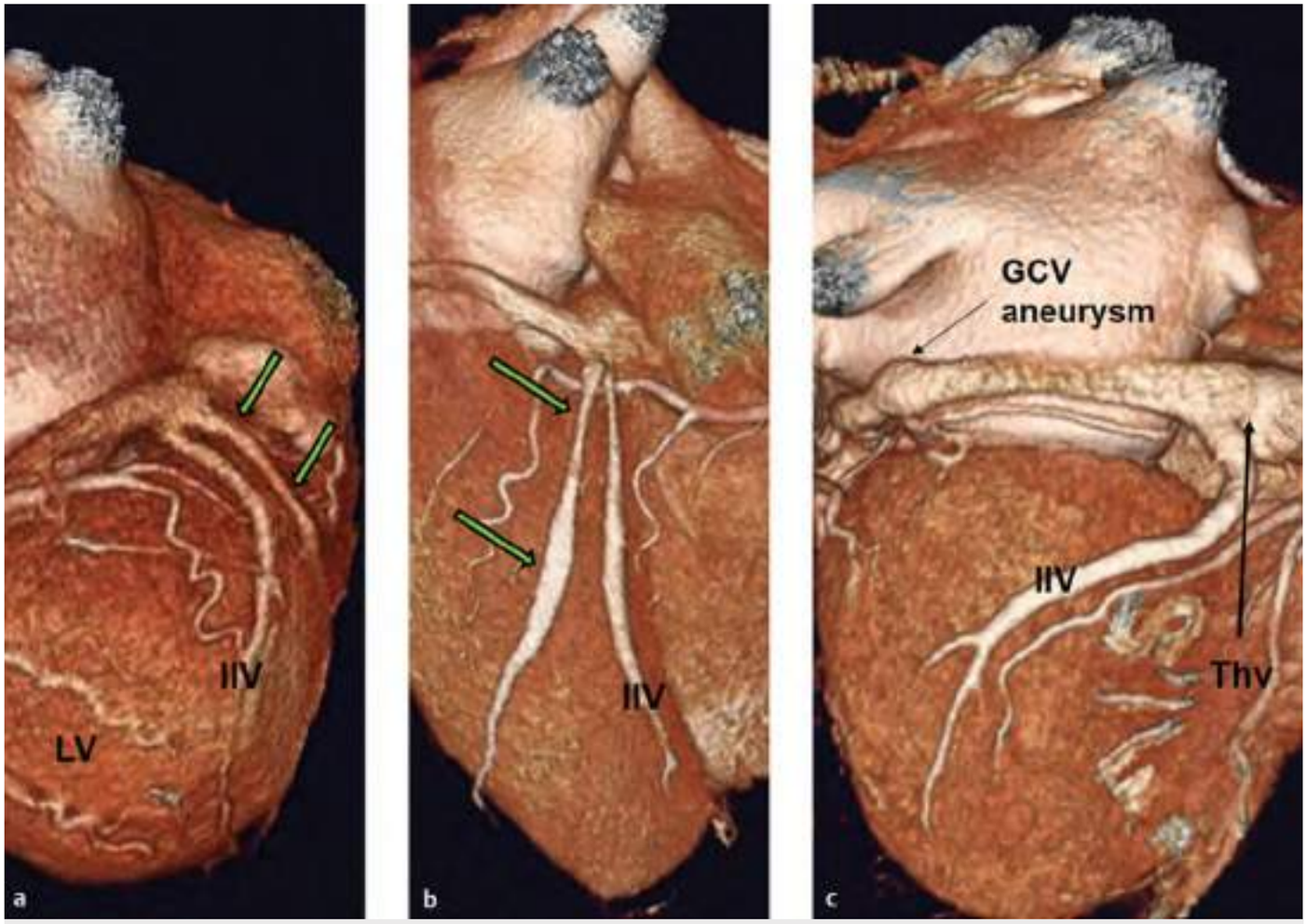

Fig. 19.14 Variants of the inferior interventricular vein (IIV). **(a)** Duplicated IIV with one posterior right ventricle (RV) vessel (*green arrows*). **(b)** Duplicated IIV with one vessel running along the posterior left ventricle (LV) wall (*green arrows*). Duplicated IIV can be seen in 3% of population. **(c)** Rare course of the IIV draining mainly the posterior LV wall. These variants are important as they may remain undetected as a result of their ostial occlusion with balloon at the time of retrograde venography for LV pacing. CT has the advantage of showing all these variants. Note aneurysm of the great cardiac vein (GCV), which is seen in 1.5% of coronary CT angiographies. Also note an outer ring marking the anatomic level of the Thebesian valve (Thv).

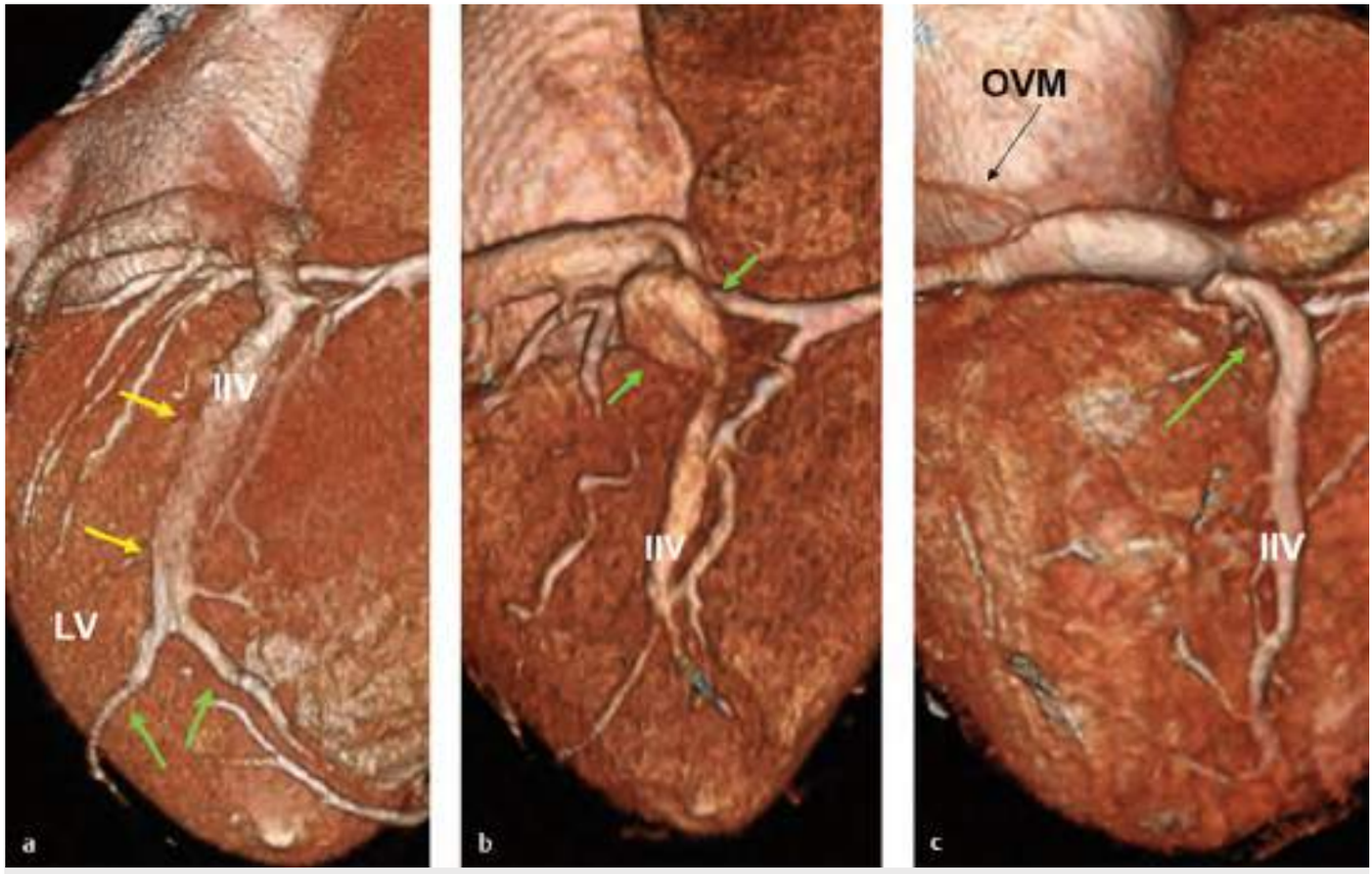

Fig. 19.15 Variants of the inferior interventricular vein (IIV) are common. **(a)** The IIV appears bifurcated near the LV apex in 45% (*green arrows*). This appearance is formed by the confluence of two tributaries with the same caliber. Uncommonly, the entire length may appear varicoid (*yellow arrows*). **(b)** Fusiform aneurysmal dilatation of the venous confluence is seen in 8% (*green arrows*). It is the most common location for bulbous enlargement of the coronary veins. **(c)** The terminal portion of the vein appears angled in 35% (*green arrow*). Note the confluence of the oblique vein of Marshall (OVM) with the coronary sinus. LV, left ventricle.

Left Posterior (Posterolateral) and Left Marginal Veins

Several venous branches drain the myocardial walls located between the IIV and the AIV.[30] Veins draining the posterior and lateral walls of the LV are of particular interest for the LV pacing in CRT[38] (▶ Fig. 19.16). Imaging techniques permit identification of potential anatomic factors that may pose difficulties to cannulate and advance the LV pacing lead including ostial valves, variceal veins, or absence of the posterior or lateral vein.

The left posterior (inferior) veins are one to three in numbers and measure 2.5 mm at ostium. While the distal myocardial origin of the left posterior vein is highly variable, it usually terminates in a uniform fashion in the CS (75%), although it can also drain into the GCV.[6,32,39] It is single in 60%. In the absence of the left posterior vein (5%), it is the left marginal vein that drains most of the left ventricular posterolateral wall.[5] Small diameter of the vein (< 2 mm) and acute angulation with the CS may complicate the insertion of the lead for CRT.[38]

The left marginal (obtuse marginal) vein is present in 70 to 95% of specimens, emptying into the GCV in 80% of cases and into the CS in the remaining.[30] The frequency of visualization is less with CT or MRI compared with retrograde venography.[25,26,27,28] It drains much of the LV myocardium, usually running superficial to the marginal branch of the circumflex artery.[32,40] Its diameter varies and, like other coronary veins, is enlarged in patients with cardiac failure.[40] Anastomosis of the epicardial veins in the periphery is common. This is especially common between the veins of the LV such as between the GCV and posterolateral vein or between the IIV and posterolateral or marginal veins (▶ Fig. 19.12).

Small Cardiac Vein

With a frequency of 30 to 50% and average diameter of 1 mm, the small cardiac vein (right coronary vein) drains the posterolateral wall of the RV into the CS (85%), the IIV (12%), or rarely the RA (1%)[16,30,41] (▶ Fig. 19.12). It is more common in women than in men.[41]

Oblique Vein of the Left Atrium (Marshall)

The oblique vein of Marshall (OVM), a remnant of the left SVC, descends along the lateral and inferior walls of the LA between the LA appendage and the left pulmonary veins and joins at the junction of the GCV and the CS approximately 3 cm from the CS ostium.[42,43] The vein is short (2–3 cm in length) and its superior

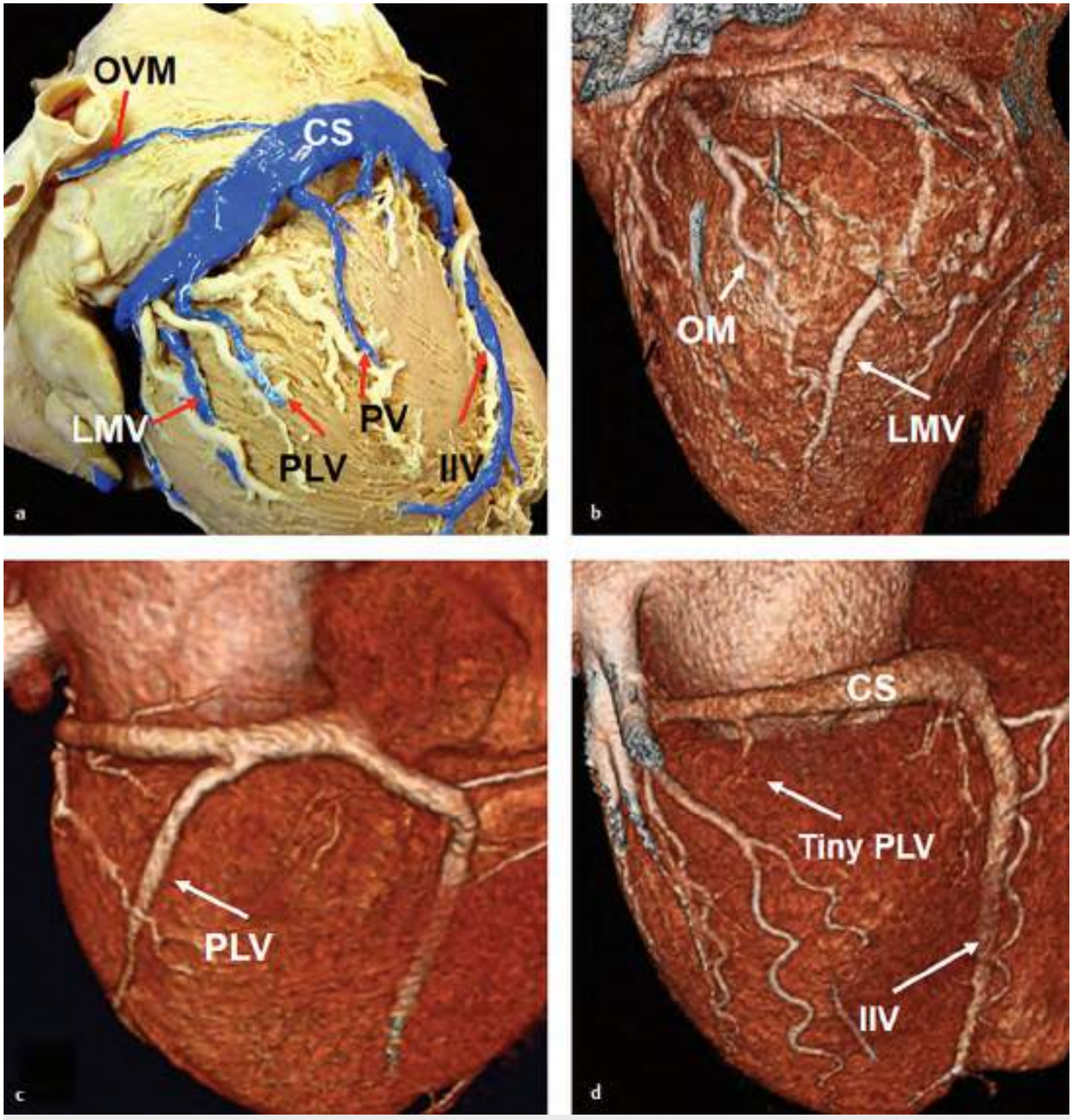

Fig. 19.16 Target veins used for CRT include the posterior, posterolateral, and marginal veins of the left ventricle. **(a)** Posterolateral view of a heart specimen. Veins are colored in *blue*. **(b)** Large left marginal vein (LMV) is shown crossing the obtuse marginal (OM) branch of the left circumflex artery near the apex. In absence of the left posterior vein (5%), it is the LMV that drains most of the left ventricular posterolateral wall. The LMV drains into the great cardiac vein in 80%. **(c)** Single but large posterolateral vein (PLV). In 75%, PLV drains into the CS. **(d)** Only a small PLV exists. PV, posterior vein.

part obliterated by fibrosis. Complete fibrosis or obliteration in the form of a cord is seen in 5 to 12%.[6] The average diameter is 1 mm (0.4–1.8) and the angle with the CS varies between 25 and 50 degrees. It is present in 85 to 95%[42] of cases (▶ Fig. 19.16). Balloon-occluded venography of the CS can visualize the OVM in 73% of the patients.[44] Demonstration of this vein with CT requires special attention to the detail and quality of the CTA. It is reported in 35 to 40% of cases[25,39] (▶ Fig. 19.15**c**, ▶ Fig. 19.16**a**). The best phase for visualization of the OVM is ventricular systole, likely due to coronary vein enlargement during this phase.[39]

The OVM is now implicated as a source of activation in atrial tachyarrhythmias.[45,46,47,48,49] This may originate from the muscle sleeve of the vein (Marshall's bundle).[50] This muscle sleeve is connected to the musculature surrounding the CS or the left

pulmonary veins[45,46,47] (also see section "Coronary Sinus Interatrial Muscle Connections"). The vein is of greater significance when it persists as a patent left SVC. It is seen in 0.5% of the normal population and up to 5% of congenitally malformed hearts[51] draining into the CS.

Ventricular Septal Veins

The right and left aspects of the septum are drained by 20 to 25 small parallel veins on each side. The anterior septal veins are drained into the AIV and the posterior septal veins into the IIV. The superior third of IV septum (ventricular outflow tracts) is drained by the left or right superior septal veins. The left superior septal vein, the longest and largest intramural venous channel, can reach 2 to 3 mm in diameter. It is found in 55% of the hearts and runs with the left superior septal artery.[6]

Valves of Coronary Veins

While retrograde coronary venous angiography and CTA reveal gross anatomical features of the CVS, venous valves are not easily viewed using these methods.

Venous valves are common in the human hearts. Knowledge of the venous valves' existence can be important before coronary vein catheterization, CRT, or retrograde cardioplegic administration.[42,52] Valves could hinder advancement of guide wires, catheters, or pacing leads.[53]

Venous valves are usually incomplete and unicuspid at ostium of the veins.[6] Larger veins including GCV, IIV, and posterior veins of the LV have an average of 2.5 to 3 valves per vein, while left marginal veins has an average of 0.8 valves per vein.[52]

Coronary Sinus Boundaries

The Thebesian valve demarcates the distal end of the CS. It can be seen in 80% of cadaveric heart specimens and is highly variable in size and morphology[20,54,55,56] (▶ Fig. 19.17). A complete circular valve is seen in 20 to 30% of the time and it is absent in 20%.[20,55] In most cases, a groove or depression is seen on the outer surface of the CS ostium,[56] which can localize the atrial end of CS in the absence of the CS valve (▶ Fig. 19.14**c**). Since the CS and IVC valves share the same embryologic origin, both can be affected in the congenital heart disease. For example, enlargement of these valves is seen in hypoplastic right heart.[57]

Variants of the CS morphology are shown in ▶ Fig. 19.18 and ▶ Fig. 19.19. The CS length is between 30 and 50 mm in 75% of the anatomic sections.[21,25] A short CS is defined as less than 2 cm in length[54] (▶ Fig. 19.19).

In order to identify the CS, it is important to localize its origin. Demonstration and localization of the OVM and the valve of GCV (Vieussens) is important for ablation approaches and cannulation of the CVS.[42,53] For example, the valve of Vieussens is a frequent cause of obstruction to passage of a catheter in postmortem and in vivo studies,[58,59] and cannulation of the OVM can be used to analyze the electrical activity for ablation of paroxysmal atrial fibrillation (AF).[50]

Three anatomic landmarks are recognized for localization of the CS–GCV junction including the orifice of the OVM, the valve of Vieussens, and the left margin of the CS myocardial sleeve with the OVM as the most constant landmark[6,30] (▶ Fig. 19.20). These anatomic landmarks are not at the same level and usually are located within a 10-mm interval.[30,42] Current resolution of clinical CT scanners does not permit directly localizing the CS muscle sleeve. The valve of Vieussens is present in 65 to 85% of cadaveric heart specimens as a unicuspid or incomplete valve adjacent or proximal to the OVM.[42,54,55,58,59] It is located at 32 ± 5 mm from the CS ostium.[46] Utilizing good-quality CT images, it is possible to demonstrate the valve of Vieussens in 50% coronary CTAs[39] (▶ Fig. 19.20). The level of valve of Vieussens at the CS–GCV junction can be localized by an annular narrowing on the external surface in 20% of cases[3,30,53] (▶ Fig. 19.20**a**; **b**). This is believed to be secondary to sphincterlike thickening of the CS myocardial sleeve.[3]

Variation of the Coronary Vein Sizes

Variation of the coronary vein sizes occurs during the cardiac cycle and in disease.[35,60,61] The diameter of the coronary veins is generally greater during late systole compared to mid-diastole. However, the difference between the two phases is not statistically significant.[35] The coronary veins are larger in heart failure and in patients with chronic AF.[60] The CS contracts normally during atrial systole[35] but not in patients with active AF. Windsock CS morphology is more common in patients with atrioventricular nodal reentrant tachycardia.[61]

Coronary Veins and Congenital Heart Disease

With improved treatment of the congenital heart disease and increasing longevity of these patients, long-term complications including arrhythmias and heart failure are arising as major management issues. These issues have led to increased interest in the roles of CRT and radiofrequency ablation in these patients.[11] CT can play an important role in assessment of cardiac morphology and coronary vessels in adult congenital heart disease (▶ Fig. 19.21, ▶ Fig. 19.22).

Device implantation is sometimes required in congenitally corrected transposition of the great arteries (ccTGA) because of morphologic RV dysfunction and complete heart block.[11,62] The CS develops with the morphologic atria and in the majority of patients with ccTGA, it drains into the RA. The venous branches, including the GCV and posterior branches, develop with the morphologic ventricles and can be affected in ccTGA (▶ Fig. 19.21). The location of the CS ostium may be difficult to find as a result of atresia or high ostial location, occurring in 15% of cases.[11] Abnormal arrangement of coronary venous return is common in hearts with isomeric atrial appendages (heterotaxy syndrome; ▶ Fig. 19.22).

A classification of CS anomalies was suggested by Mantini et al,[63] including (1) enlargement of the CS with/without a left-to-right shunt, (2) absent CS, (3) CS orifice atresia, and (4) hypoplasia of the CS (▶ Fig. 19.23, ▶ Fig. 19.24, ▶ Fig. 19.25). In CS atresia or hypoplasia, coronary veins are drained via multiple Thebesian veins into the atria. These enlarged Thebesian veins can be used to directly cannulate the ventricular veins for pacing (▶ Fig. 19.22**c, d**). The CS orifice atresia can be divided into cases

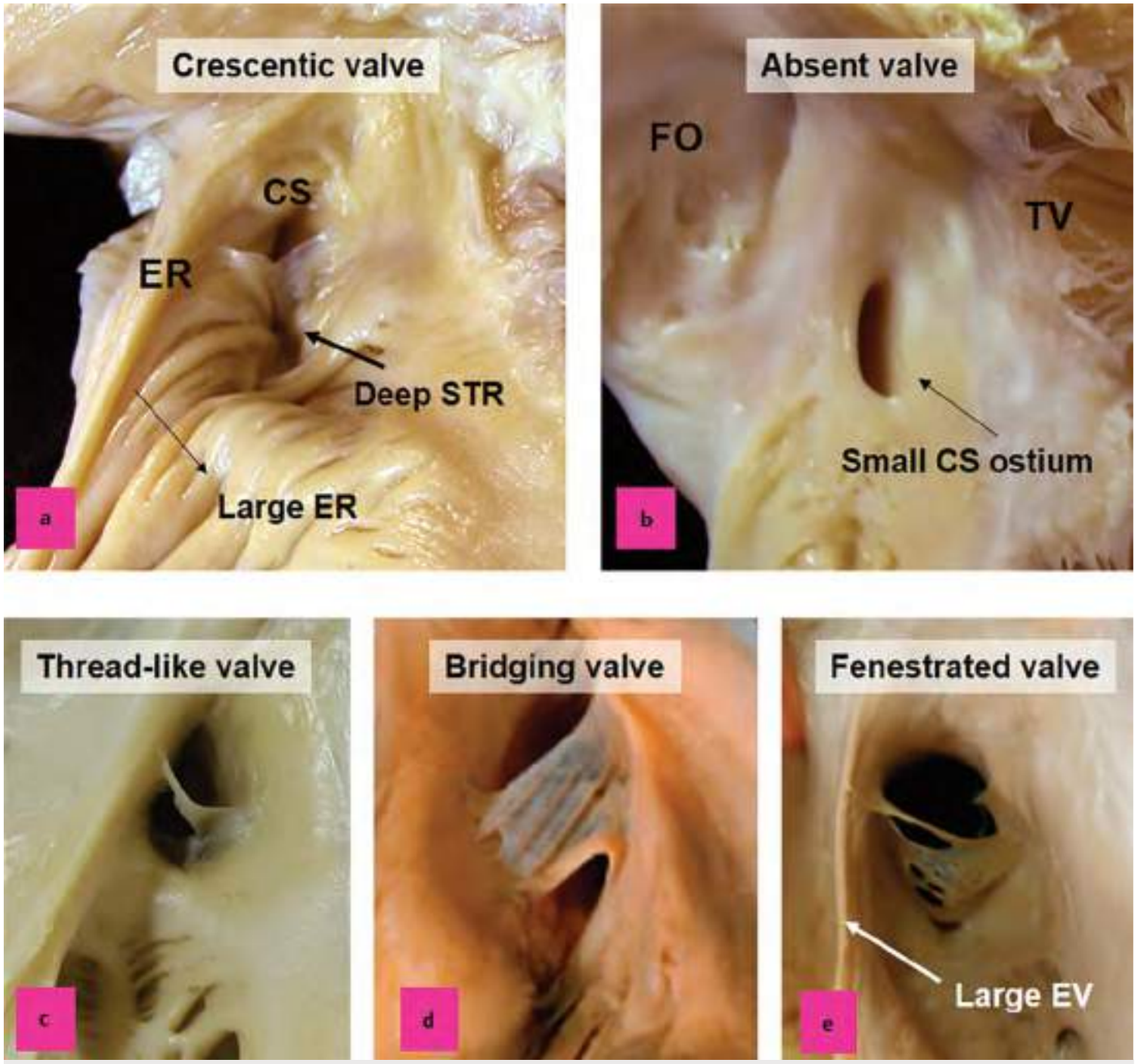

Fig. 19.17 Mechanical barriers to the coronary sinus (CS) ostium catheterization and anatomical variations. Mechanical barriers causing difficulty catheterization of the CS include large Eustachian valve/ridge (frequency = 25%), deep (> 5 mm) sub-Thebesian recess (STR) (frequency = 45%; **a**), hypoplastic CS ostium **(b)** and unusually large Thebesian valve. Anatomic variants of the Thebesian valve are common including circular in 30%, crescentic in 35%, absent in 20%, threadlike in 2% **(c)**, bridging **(d)**, and fenestrated **(e)** in 10% of population. ER, Eustachian ridge; EV, Eustachian valve; FO, fossa ovalis; STR, sub-Thebesian recess; TV, tricuspid valve.

with drainage to a persistent left SVC and those with drainage directly to the cardiac chambers (through fenestrations in the floor of the LA or by emptying of the CS tributaries to into the atria).[51,63,64,65]

Persistent left SVC draining into the CS causes an enlargement of this vessel, and this may interfere with the formation of the posterior wall of the LA causing either a CS–LA fenestration (unroofed CS) or an interatrial communication through the mouth of the CS (CS-type atrial septal defect).[51,63,66] The diagnosis of this CS anomaly is important to the prognosis of the patient because of potential consequences of brain abscess or cerebral emboli that may result from a right-to-left shunt (▶ Fig. 19.24, ▶ Fig. 19.25). Enlargement of the CS is also seen in coronary artery CS fistula (▶ Fig. 19.26).

◆ Cardiac Resynchronization Therapy

CRT has become an acceptable method of treatment in patients with depressed LV systolic function with advanced and symptomatic heart failure (New York Heart Association class III or IV).[67] Left ventricular lead placement in a suitable coronary vein branch along the dyssynchronous wall of the LV is an important

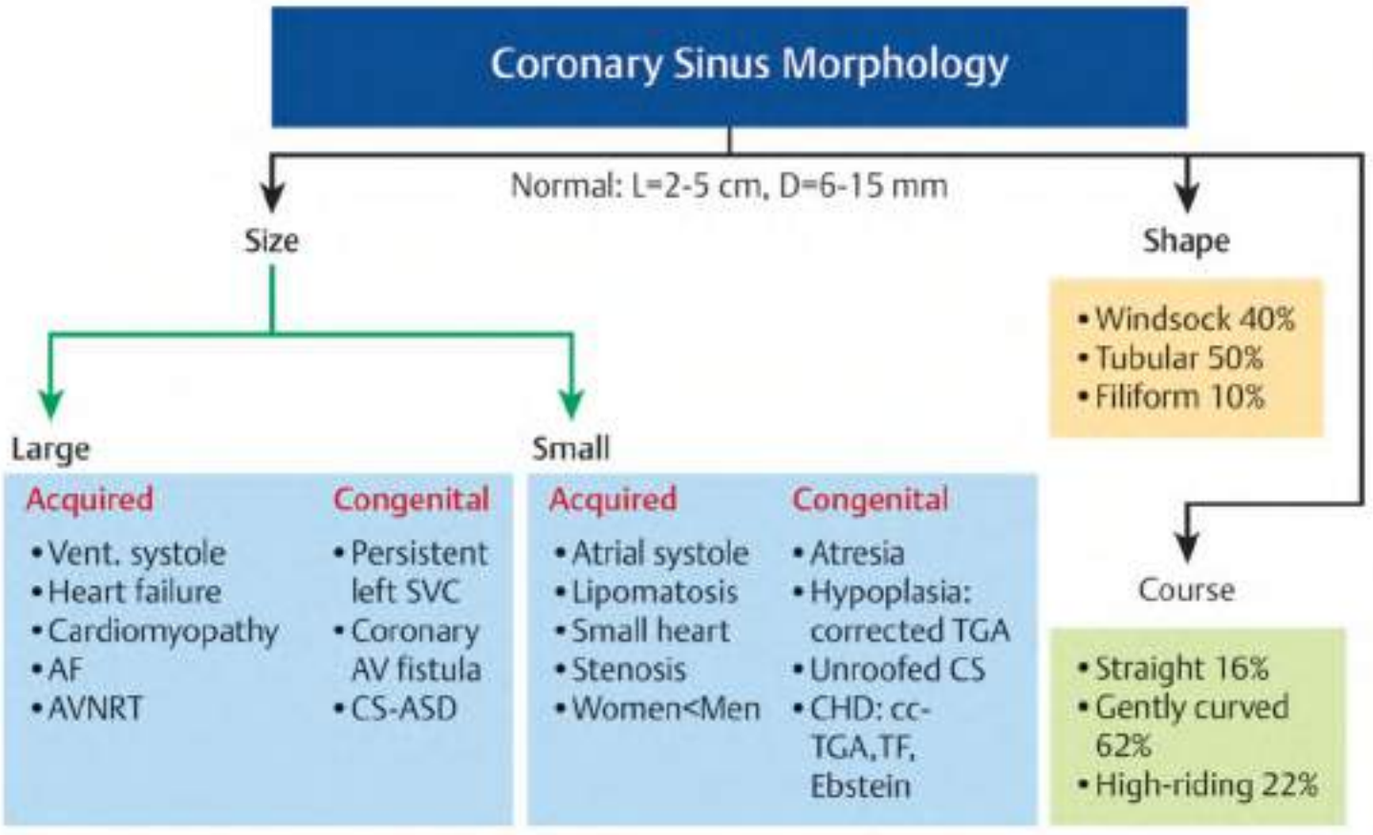

Fig. 19.18 Variants of the coronary sinus (CS) morphology. A normal CS is usually 2 to 5 cm in length (L) and 6 to 14 mm in diameter (D). The CS is normally larger during ventricular systole and contracts during atrial systole. It is usually tubular or windsock in shape and gently curved toward the left atrium. AF, atrial fibrillation; ASD, atrial septal defect; AV, arteriovenous; AVNRT, atrioventricular node reentrant tachycardia; ccTGA, congenitally corrected transposition of great vessels; CHD, congenital heart disease; SVC, superior vena cava, TF, tetralogy of Fallot.

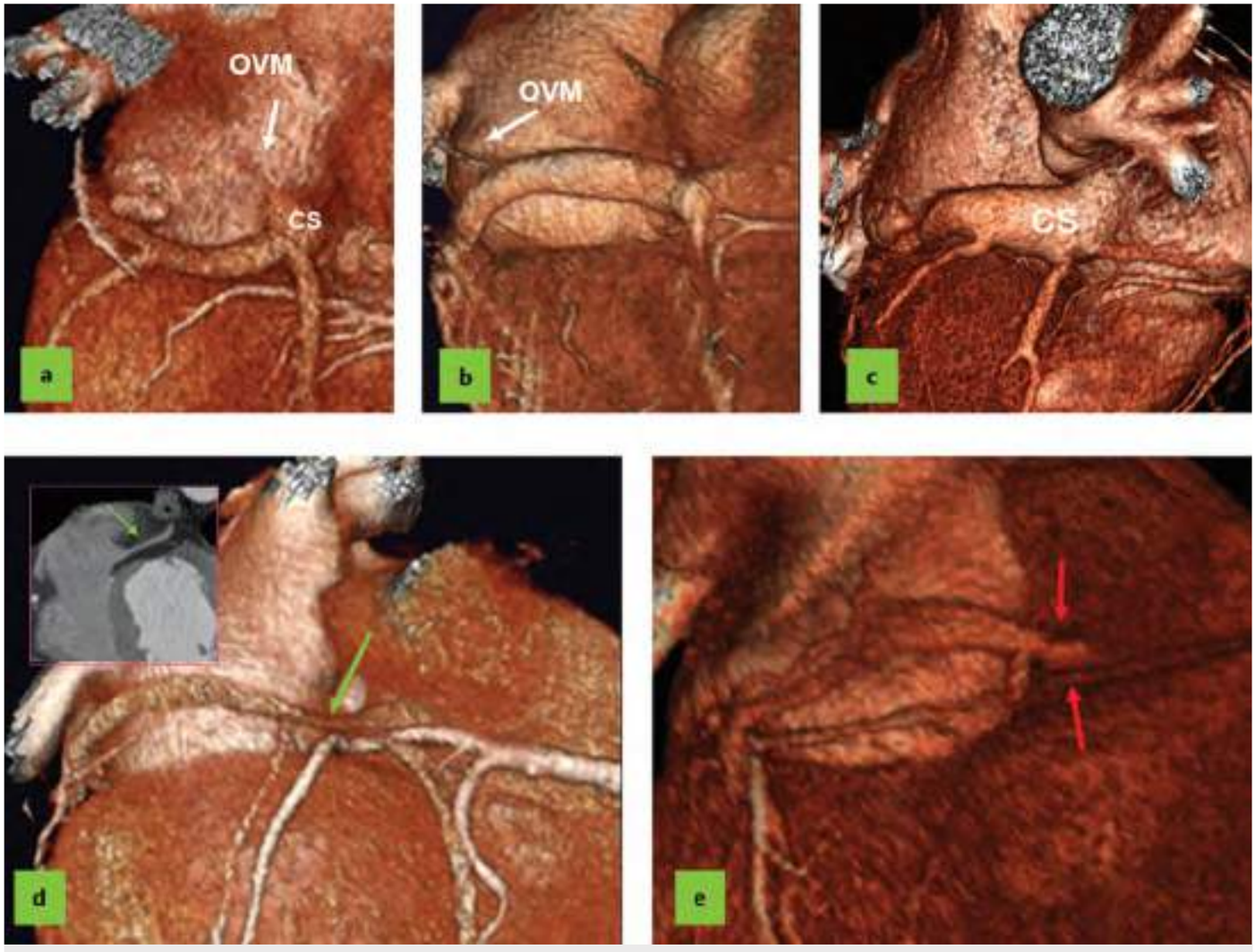

Fig. 19.19 Anatomic variants of the length and size of the coronary sinus. The oblique vein of Marshall (OVM) is the best landmark to localize the origin of the CS. The OVM is seen in 40% of CT studies. **(a)** Short CS (2 cm or shorter) is seen in 10% of population. **(b)** Long CS, defined as 5 cm or longer in length, is seen in 15% of population. In this example, the CS appears high riding and more atrialized. **(c)** A large windsock CS in a patient with persistent left SVC. **(d)** Narrowed (filiform) CS secondary to increased epicardial fat (*green arrows*). **(e)** Atretic CS/GCV (*red arrows*) is rare and is reported in less than 1%. GCV, great cardiac vein.

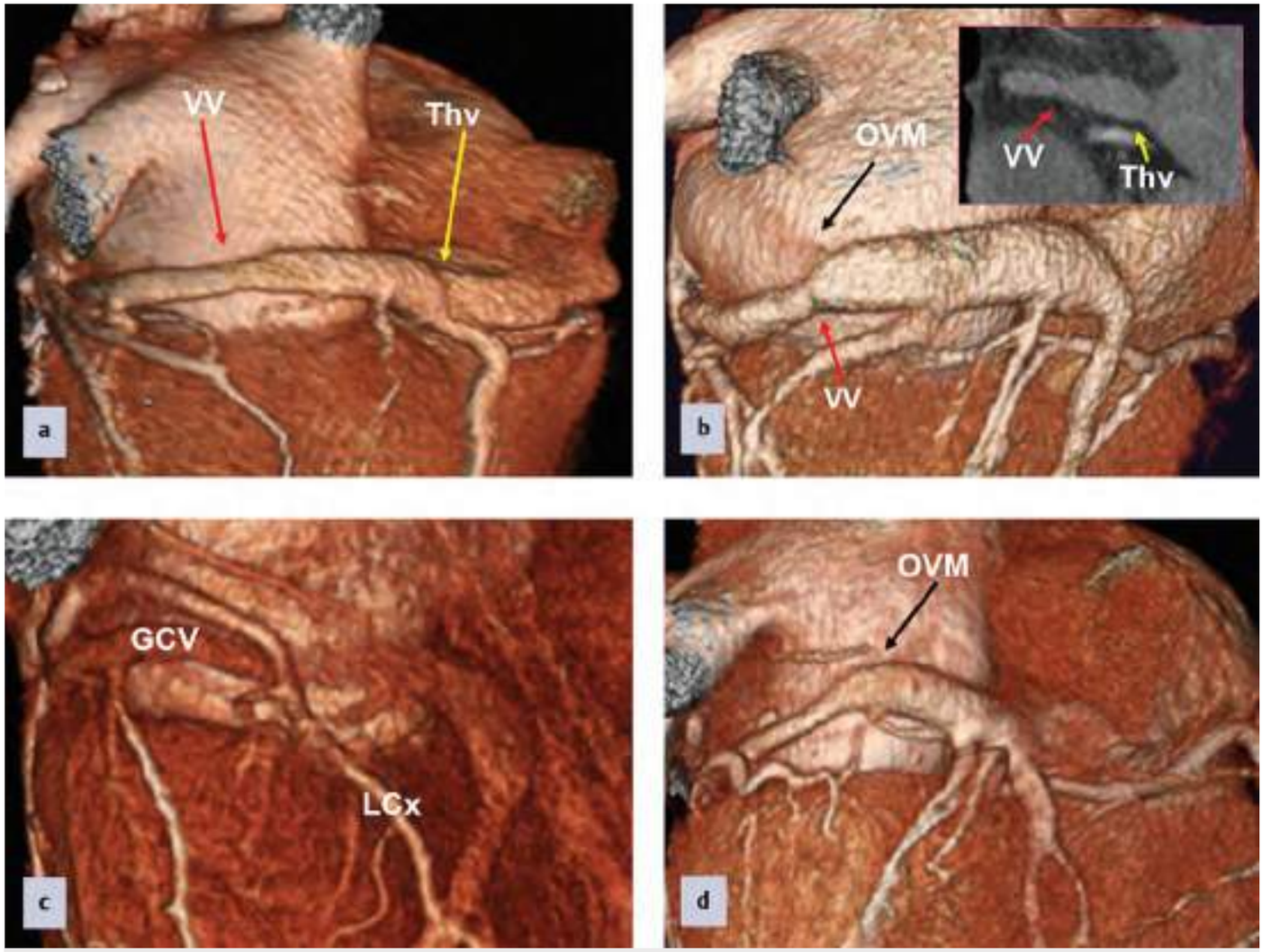

Fig. 19.20 Mechanical barriers for venous intervention: **(a**, **b)** valve of Vieussens (VV) and Thebesian valve (ThV). **(c)** Arterial compression by overlying left circumflex (LCx) artery. **(d)** Oblique vein of Marshall (OVM) and coronary sinus (CS) tortuosity. The VV exists in 80% and can be seen in 50% of high-quality CTA images. It is unicuspid (65%) or bicuspid. The OVM exists in 85%, and can be seen with CT in 35%. An acute angle with the CS, a small diameter, and a tortuous course are the anatomical characteristics that make cannulation of a vein difficult.

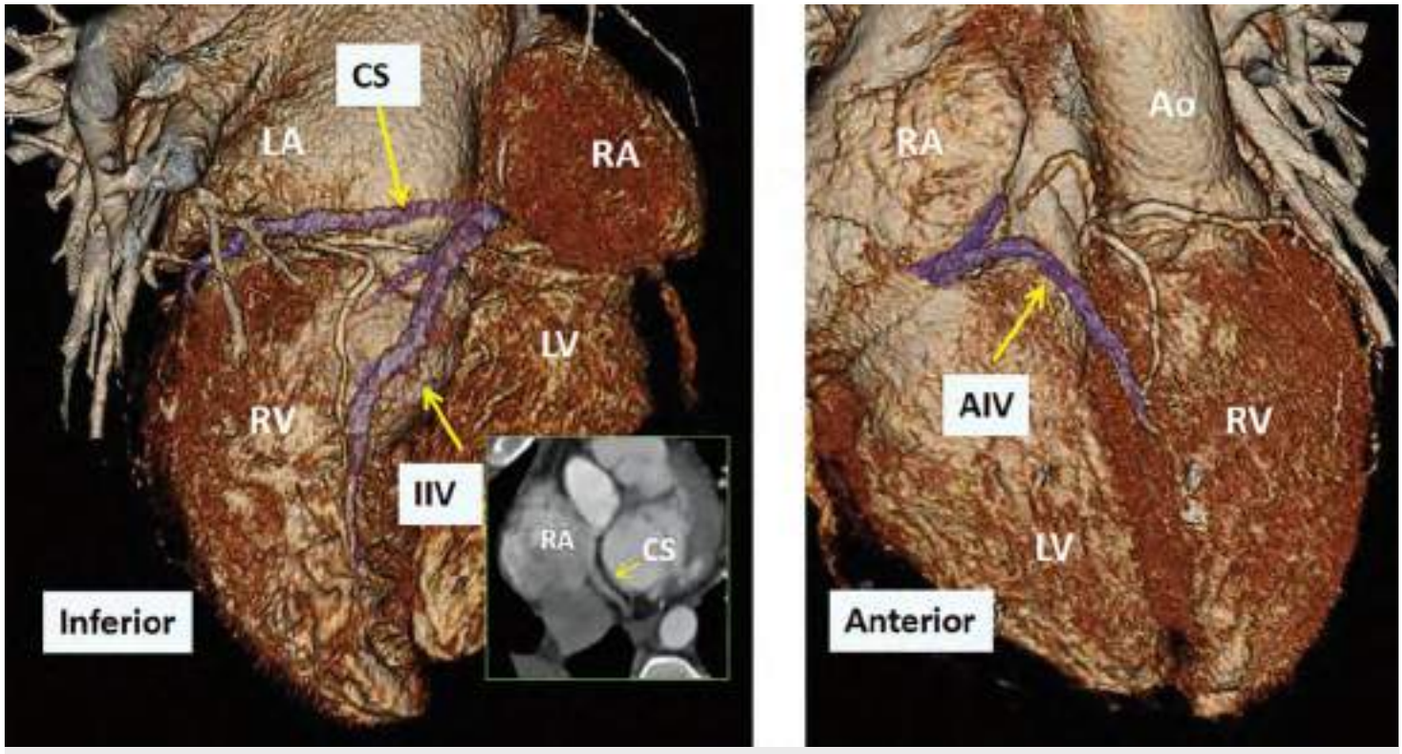

Fig. 19.21 Coronary venous system in congenitally corrected transposition of the great arteries. Posteroinferior view of the heart shows the coronary sinus (CS) and the inferior interventricular vein (IIV) draining into the right atrium (RA). Note that the CS appears hypoplastic and connecting high with the RA. High insertion of the CS ostium is not uncommon and may cause difficulty in CS catheterization. Anterior view of the heart shows the anterior interventricular vein (AIV) draining directly into the RA. Normally, it will continue as great cardiac vein. Ao, aorta, LV, morphologic left ventricle, RV, morphologic right ventricle.

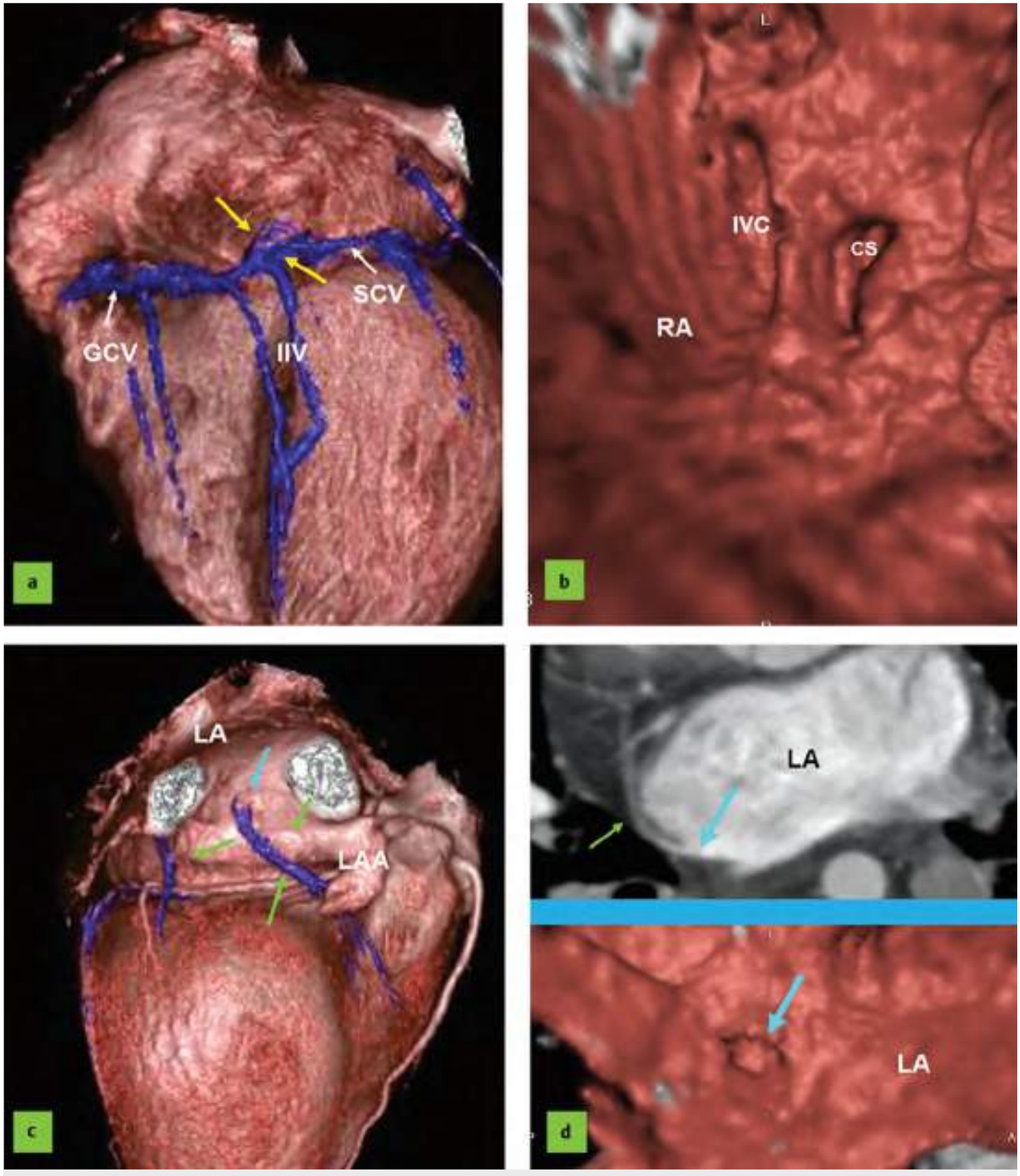

Fig. 19.22 Unusual coronary venous system in a patient with left atrial isomerism, dextrocardia, and azygos continuation of the inferior vena cava. **(a)** Posterior view of the heart shows a hypoplastic coronary sinus (*yellow arrows*) formed by equally sized inferior interventricular vein (IIV), great cardiac vein (GCV), and small cardiac vein (SCV). **(b)** Virtual endoscopy of the right atrium (RA) shows small coronary sinus (CS) ostium. **(c**, **d)** Direct drainage of multiple left ventricular veins (*green arrows*) into the left atrium (LA). Also shown is the orifice of large Thebesian veins (*blue arrows*) emptying into the LA best seen on endoscopic view **(d)**. IVC, inferior vena cava, LAA, left atrial appendage endoscopic view.

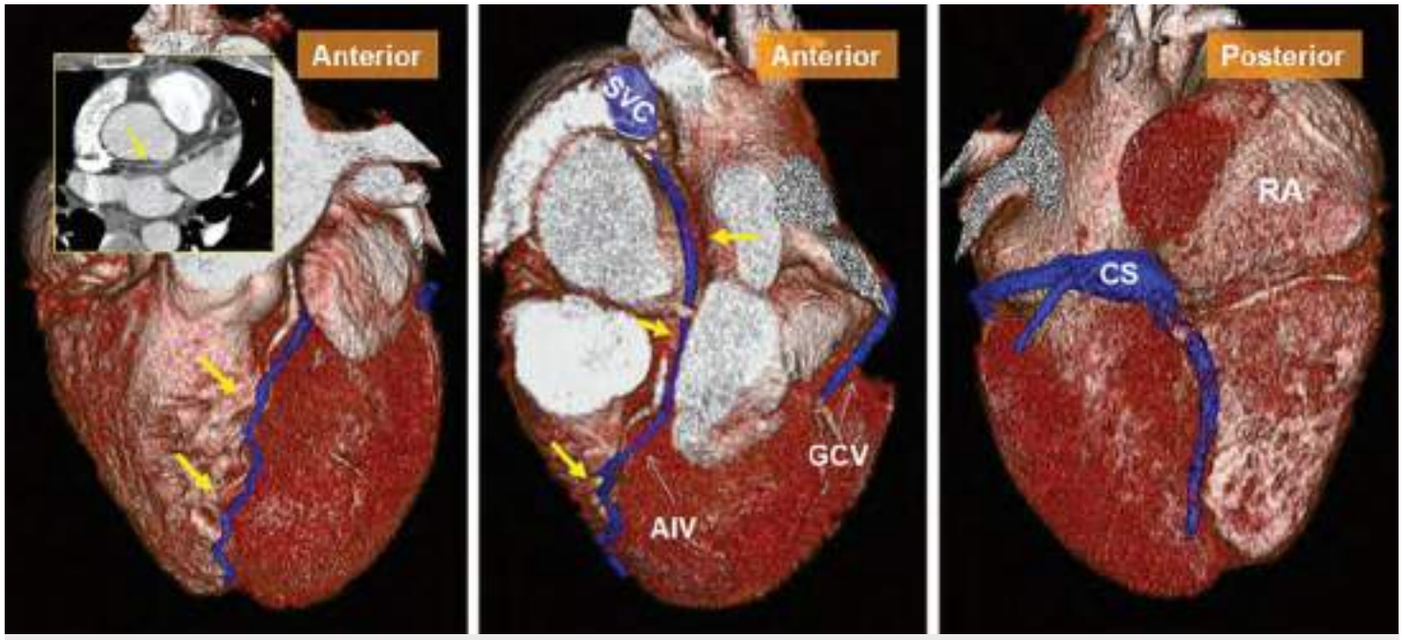

Fig. 19.23 Abnormal drainage of the anterior interventricular vein (AIV) into the superior vena cava (SVC; *yellow arrows*). In this patient, the coronary sinus (CS) is mainly formed by posterior and marginal veins of the left ventricle (not shown). The great cardiac vein (GCV) is not developed and appears short. Although this a rare anomaly, it may have clinical implications in regard to percutaneous mitral annuloplasty, retrograde cardioplegic perfusion, and myocardial gene transfer. RA, right atrium.

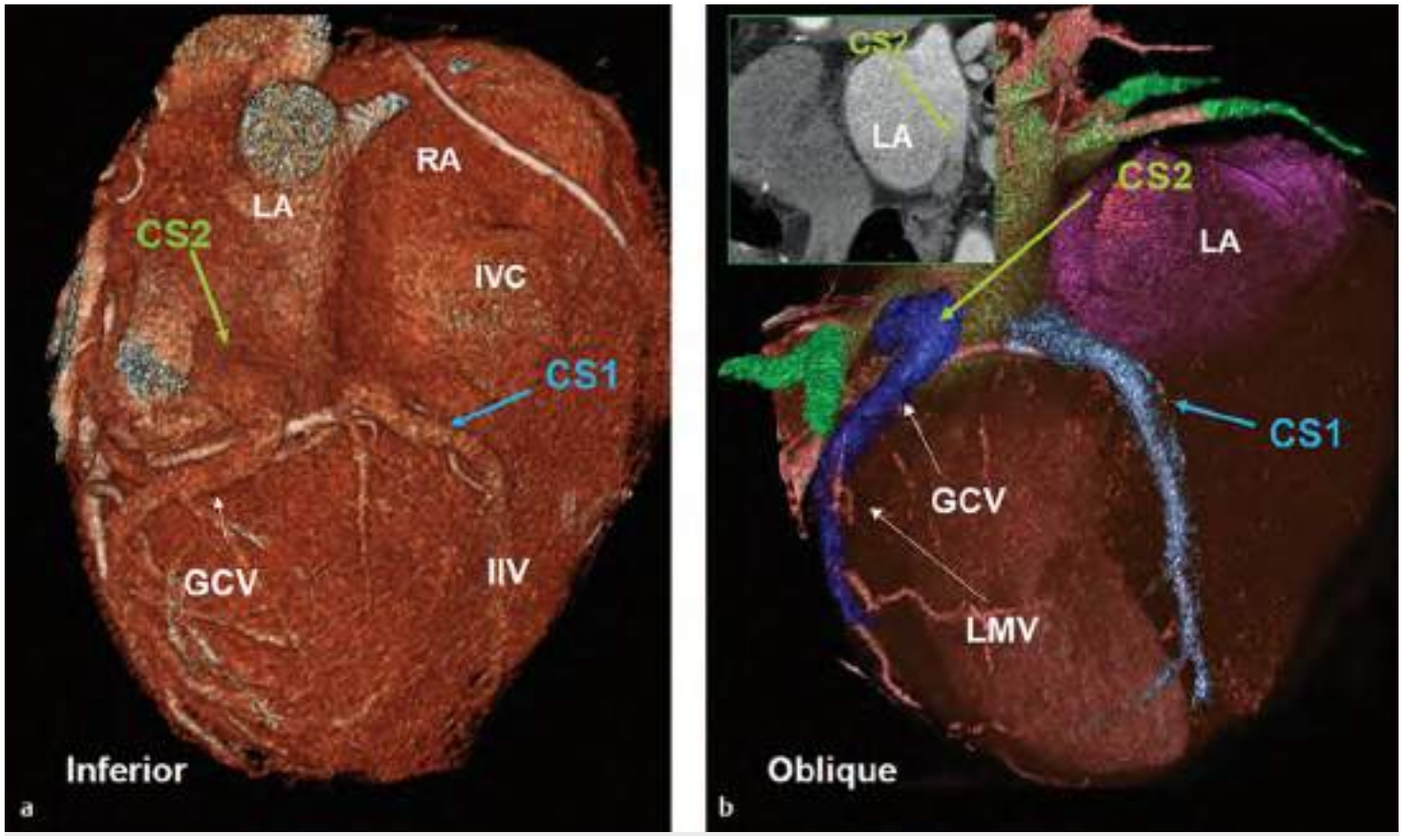

Fig. 19.24 Split coronary sinus (CS) in a patient with repaired tetralogy of Fallot. Status postsurgical correction of tetralogy and ligation of persistent left superior vena fistula to the left atrial roof. Inferior **(a)** and oblique inferior **(b)** views of the heart are shown. The inferior interventricular vein (IIV) and the posterior vein of left ventricle are drained by the CS1 (*blue arrow*) into the right atrium (RA) and the great cardiac vein (GCV) and the left marginal vein (LMV) are drained by the CS2 (*green arrows*) into the left atrium (LA). IVC, inferior vena cava.

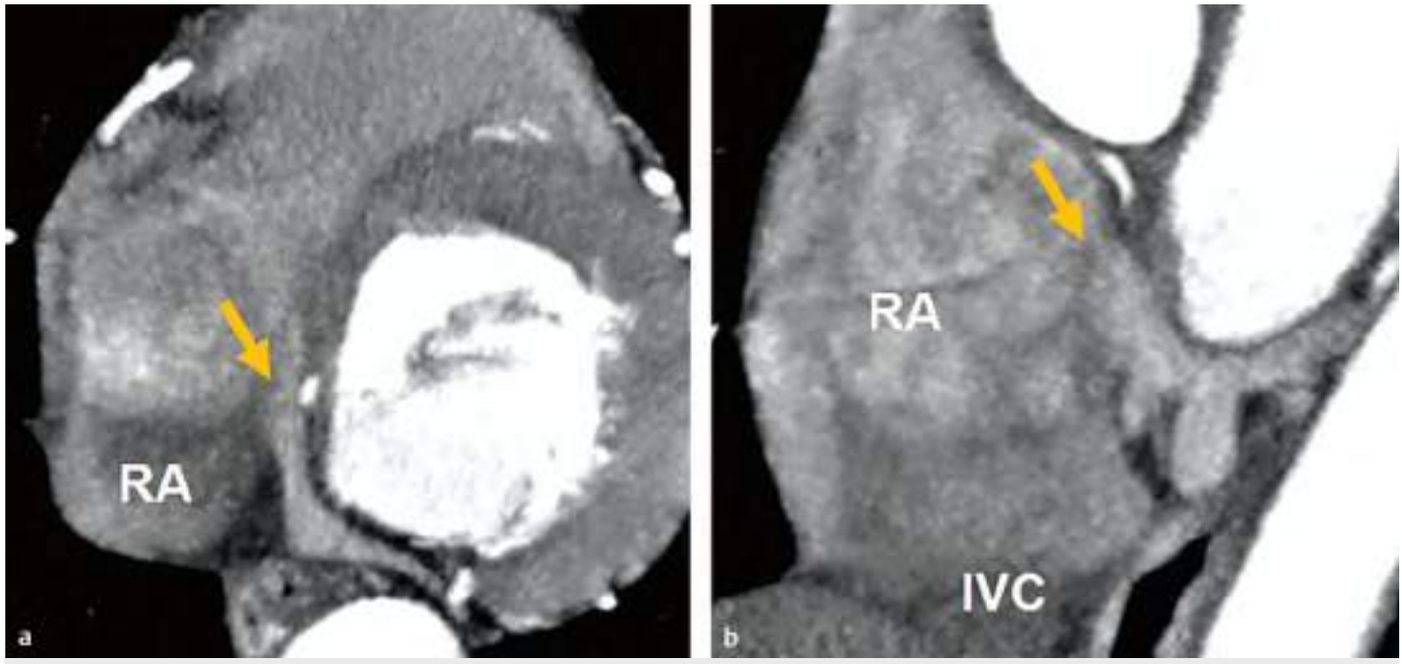

Fig. 19.25 (a, b) Posterior view of the heart from a volume-rendered CT angiography and a short axis at the level of the coronary sinus (CS) ostium. The ostium of the CS is atretic (*red arrows*). There is a large defect between the CS and the left atrium (LA) walls (*green arrows*). IVC, inferior vena cava; RA, right atrium.

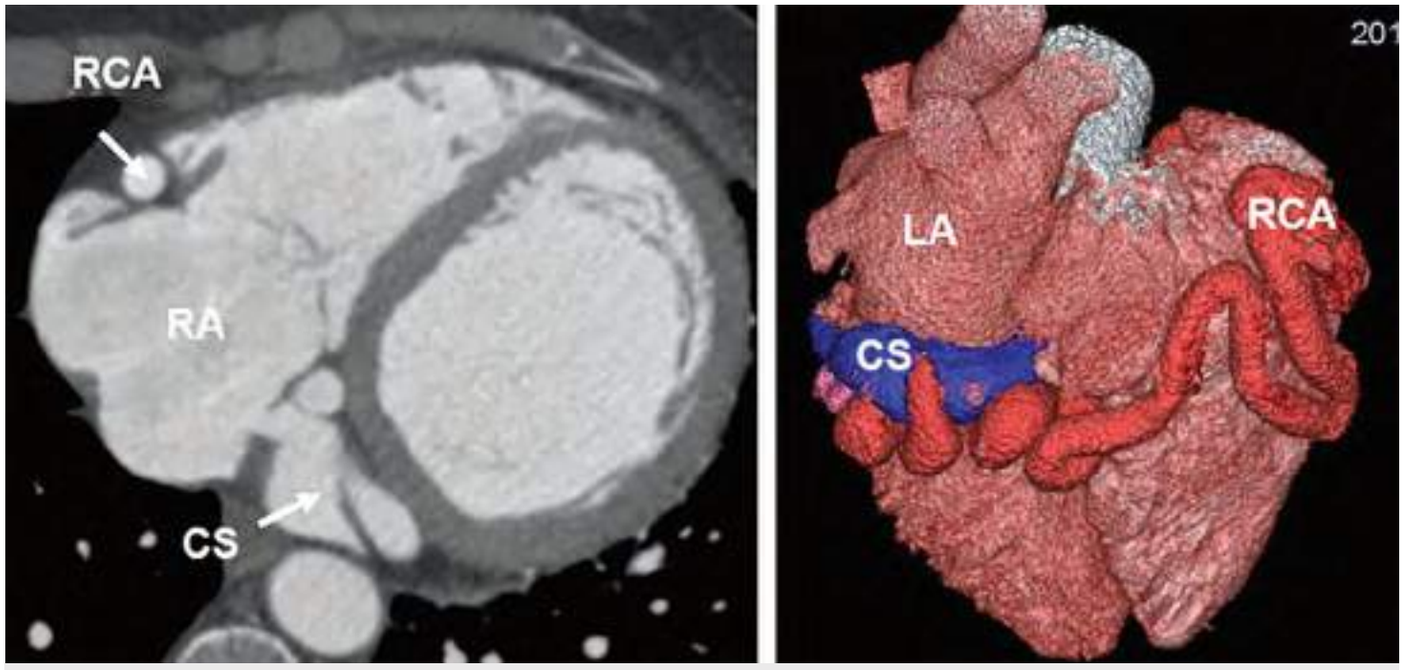

Fig. 19.26 Anomalous fistulous communications between the coronary sinus (CS; *blue colored*) with the right coronary artery (RCA; *red coded*). The RCA and the CS are markedly enlarged. LA, left atrium; RA, right atrium.

determinant of responsiveness to CRT.[38] Since most patients have cardiomegaly, generally the CS is larger and the anatomic location of a vein can be displaced.[23,26] Implanting the electrode in a coronary vein can be difficult in up to 20% of patients, a consequence of unfavorable anatomical factors (▶ Fig. 19.17, ▶ Fig. 19.20). In such groups, accurate anatomic depiction of the vessels can be crucial in the success of LV pacing.[23,68] Common target vein for placement of the lead is the LMV or posterior veins of the LV (▶ Fig. 19.16, ▶ Fig. 19.27**a**). In rare cases, the lead is placed in an anterolateral branch of the GCV (▶ Fig. 19.27**b**).

With the development of newer, smaller caliber pacing leads, an imaging modality to resolve and localize most first- or large second-order tributaries is necessary. Recently, a segmental classification of the venous tributaries is introduced using rotational venography.[68] Coronary CTA can easily be used to address the segmental location of the target vein and find anatomic

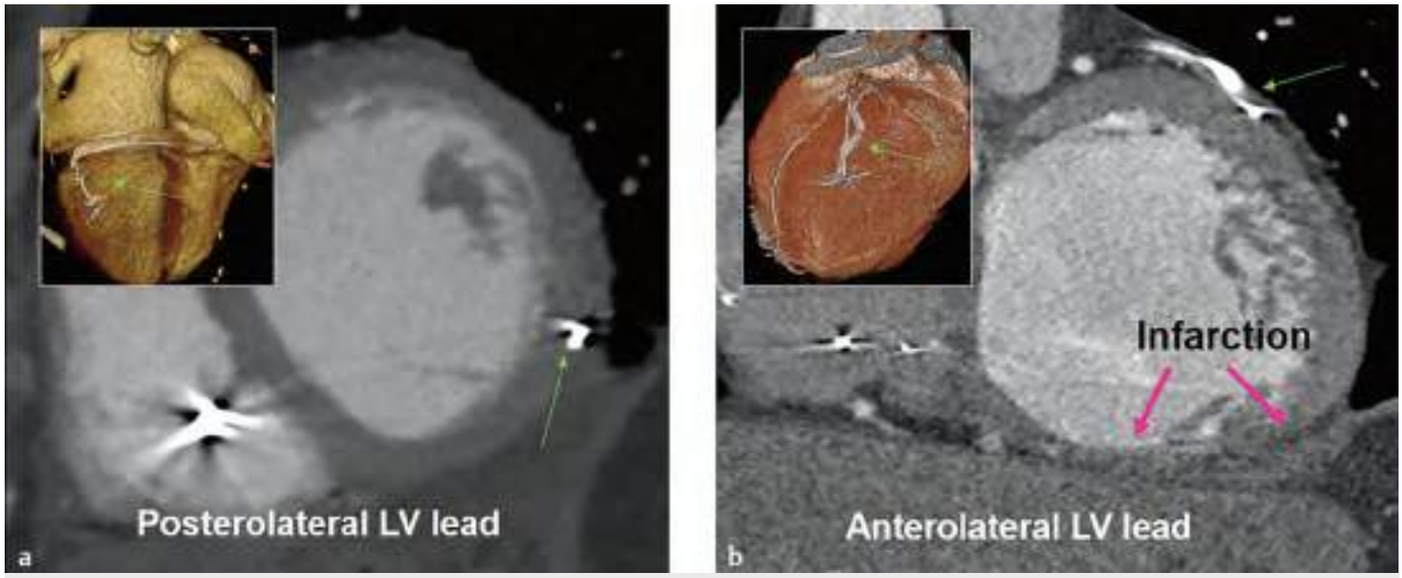

Fig. 19.27 Myocardial infarction and lead placement. CT can help localize the infarct zone. The LV lead should be placed in a region distant from the infarcted zone. **(a)** Common location of the lead along the lateral wall of the left ventricle (LV) in the left marginal vein (*green arrows*). **(b)** Unusual placement of the pacer lead in the anterolateral wall of the LV (*green arrows*) to avoid the posterior infarction (*red arrows*).

Table 19.3 CT angiography: what to look for before CRT

- Variants: hypoplasia, absence, duplication, diverticulum
- High insertion of the CS (▶ Fig. 19.23)
- Other anatomic barriers (▶ Fig. 19.15, ▶ Fig. 19.18)
- Sizes of the CS for balloon occlusion
- Distance of target vein from the Thebesian valve
- Tortuosity and acute angle of target vein confluence: the posterior and lateral veins have an acute takeoff in 30%
- First- or large second-order tributaries of the CS. Diameter > 1.5 mm (4 Fr, the current size of smallest LV pacing lead) allows a lead implant

Abbreviations: CRT, cardiac resynchronization therapy; CS, coronary sinus; LV, left ventricle.

barriers.[25,26,69,70] Information required in radiology report is included in ▶ Table 19.3.

The observation that patients with previous posterolateral LV infarction are frequently lacking the LMV (27% in infarcted vs. 70% in normal heart) has important implications for the selection of potential candidates for CRT.[27] The absence of CS tributaries may be related to thrombosis and scar formation secondary to previous myocardial infarction in the region drained by these specific veins[27,71] (▶ Fig. 19.28). It is important to avoid the infarcted tissue and place the lead over viable myocardium (▶ Fig. 19.27**b**).

◆ Other Topics

Coronary Sinus Interatrial Muscle Connections

The CS is surrounded by a myocardial sleeve along 25 to 50 mm of its length. The CS and the OVM are both remnants of the sinus venosus and their muscle sleeve can be an extension of the right atrial myocardium over the CS (CS–RA muscle continuity; ▶ Fig. 19.1, ▶ Fig. 19.29). Other fibers of varying thicknesses arise from this sleeve to the LA myocardium along the inferior mitral annulus providing the second largest electrical continuity between the two atria located posteroinferiorly (CS–LA muscle connections[46,72]; ▶ Fig. 19.19, ▶ Fig. 19.30). Along with Bachmann's bundle (anterosuperior interatrial muscle bridge), these striated muscle connections ensure rapid interatrial conduction leading to physiological biatrial contraction. The CS–LA muscle connections can be the source of recurrence of AF after ablation procedures.[73] In addition, abnormal CS muscle connections with the ventricular myocardium may form atrioventricular accessory connections, hence macro-reentrant atrial arrhythmias.[37] Most of the AFs originating from the CS are along the CS–LA interface. Electrical disconnection of the CS–LA connection can terminate AF persisting after PV isolation in 30 to 46%.[73] Detailed anatomical information provided by CT about the CS–LA myocardial connection may be useful in understanding AF recurrence in the subgroup requiring electrical disconnection of this region[39] (▶ Fig. 19.31).

Relationship of Coronary Veins and the Mitral Annulus

In patients in whom open heart surgery is contraindicated, PMA is performed as a palliative treatment for mitral regurgitation mainly in dilated ischemic or nonischemic cardiomyopathy with low left ventricular ejection fraction.[74,75] With this technique, a double-anchor PMA device is implanted in the CS/GCV at the level of the superior and inferior commissures of mitral valve (▶ Fig. 19.32). The anatomical course of the CS is important for a successful procedure. The CS courses around the posterior aspect of the "mitral annulus" but in a more atrial position (80–90%) and the success of PMA depends on close proximity of the CS to the mitral annulus.[76,77] With LA enlargement in mitral regurgitation, separation of CS and mitral annulus is increased in left free wall location.[78] Because of close proximity of the left circumflex artery or its branches and in some cases the distal right coronary artery branches to the CS/GCV, potential damage to the coronary vessels with resultant myocardial infarction exists. CTA of the

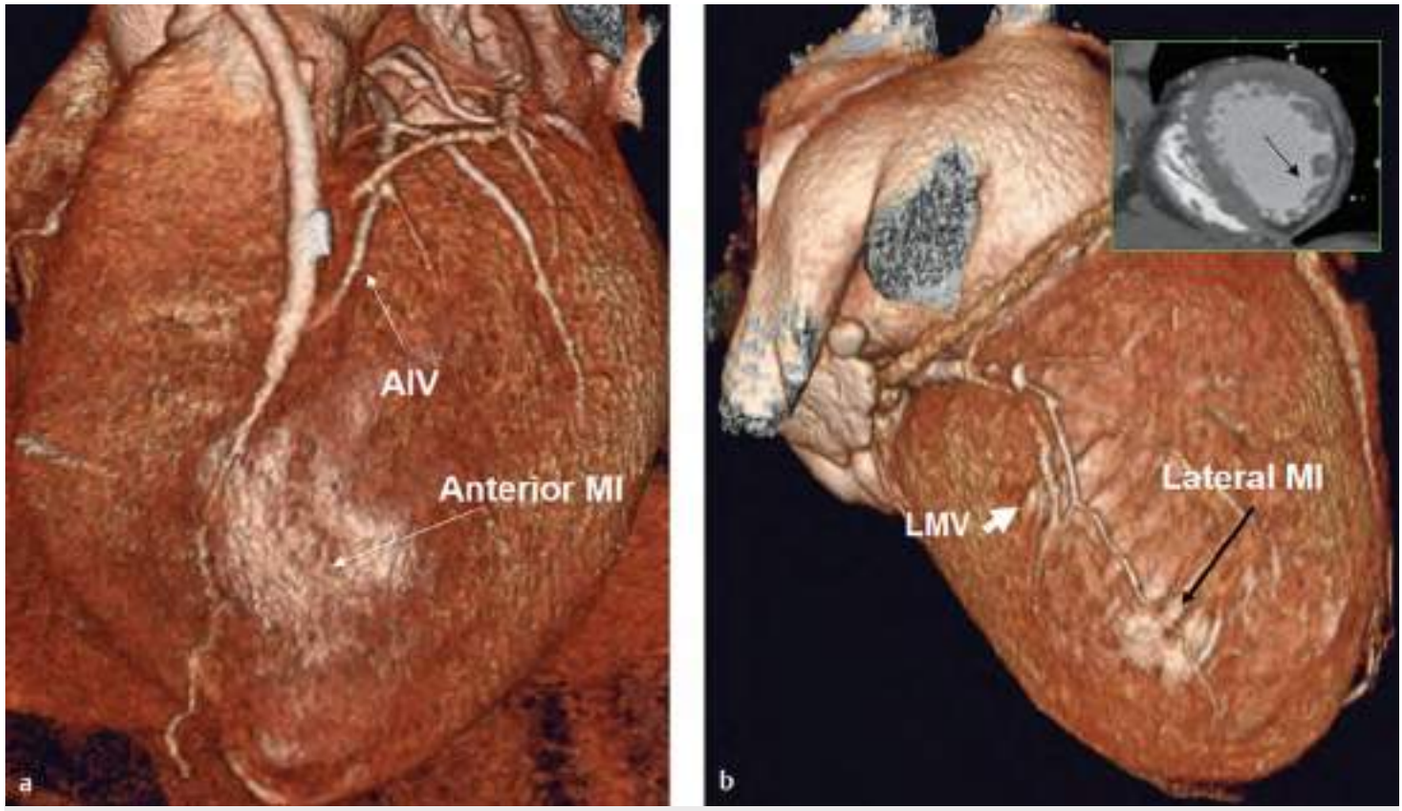

Fig. 19.28 Relation of the myocardial infarction (MI) and coronary vein visualization. The coronary vein can be thrombosed with MI. **(a)** Anterior view of the left ventricle demonstrates occluded anterior interventricular vein (AIV) in the area of anterior infarction. **(b)** The left lateral vein of the heart demonstrates attenuated left marginal vein (LMV; *white arrow*) in a patient with an old lateral infarction and left ventricular enlargement (*black arrows*).

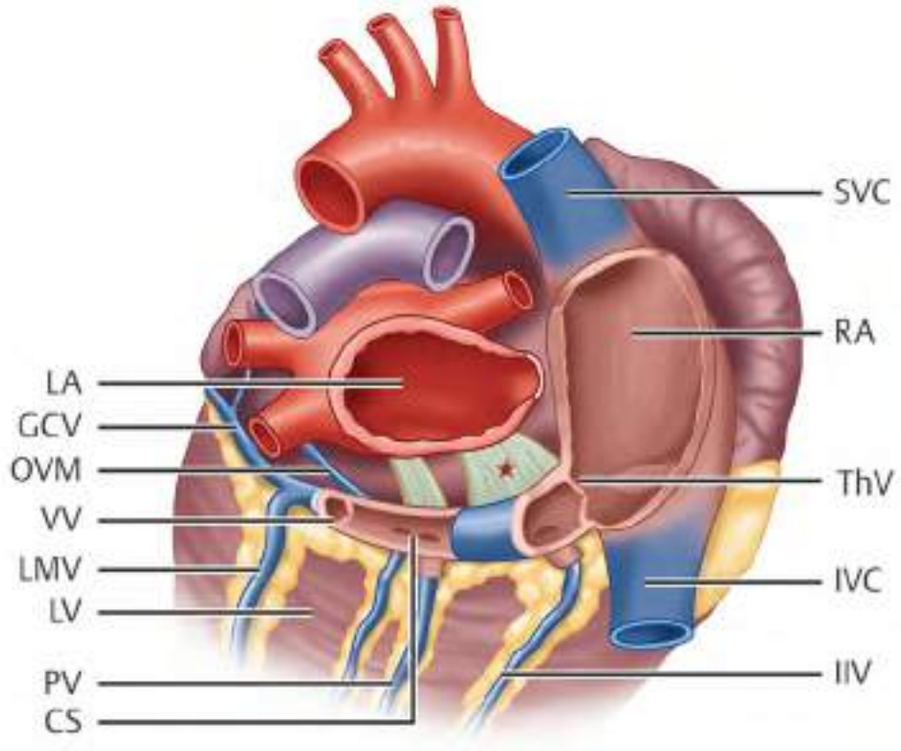

Fig. 19.29 Anatomy of the coronary sinus (CS) musculature is shown in this schematic posterior view of the heart. The beginning of the CS can be identified by the opening of the oblique vein of Marshall (OVM) externally or the valve of Vieussens internally. The CS is surrounded by a sleeve of myocardium, a remnant of the sinus venosus musculature, which is continuous with the muscle of the right atrium wall (CS–RA muscle continuity). This CS muscle sleeve normally stops abruptly at or shortly beyond the orifices of the entering coronary veins where it may thicken in a sphincterlike fashion. In normal hearts, bridging myocardial fibers exist between the CS and the left atrial walls (CS–LA connection; *red star*). These CS–LA muscle connections can be the source of atrial fibrillation recurrence after pulmonary vein isolation. GCV, great cardiac vein; IIV, inferior interventricular vein; IVC, inferior vena cava; LA, left atrium; PLV, posterolateral vein; PV, posterior vein; RA, right atrium; SVC, superior vena cava; ThV, Thebesian valve; VV, valve of Vieussens.

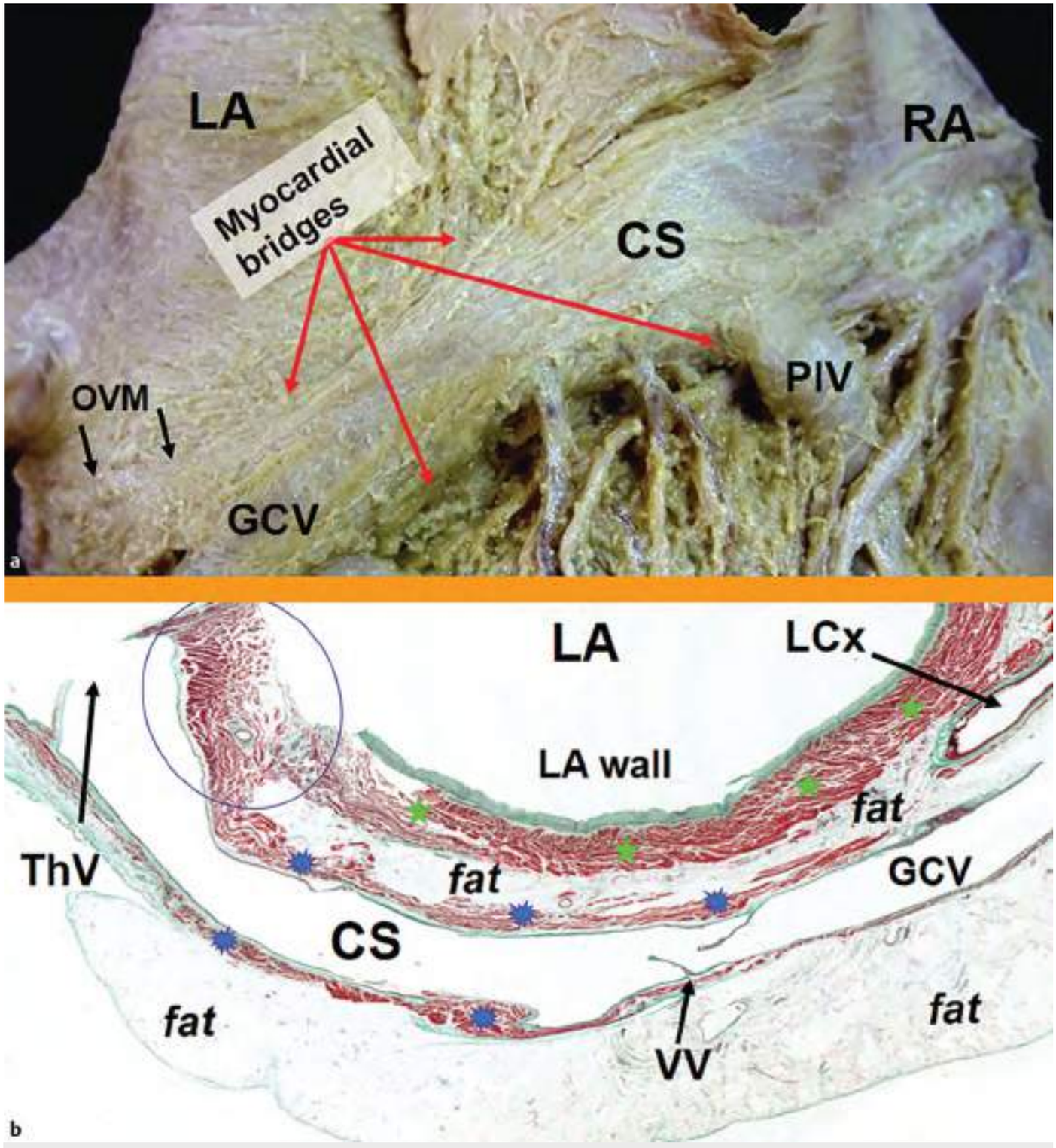

Fig. 19.30 **(a)** Posterior view of a myocardial dissection around the coronary sinus (CS) is shown. Myocardial bridges extending between the left atrial (LA) wall and the CS myocardial sleeve form the posterior interatrial muscle connections (CS–LA muscle connections). The CS myocardial bridges may also extend over the confluence of inferior interventricular vein (IIV) and great cardiac vein (GCV). **(b)** Histological section stained with Masson's trichrome through the coronary sinus demonstrates the CS–LA muscle connection (*within blue circle*) at the distal end of the CS. The rest of CS myocardial sleeve (*blue asterisks*) is separated from the LA wall by the epicardial fat. Green stars, LA myocardium; LCx, left circumflex artery; OVM, oblique vein of Marshall; RA, right atrium; VV, valve of Vieussens; ThV, Thebesian valve.

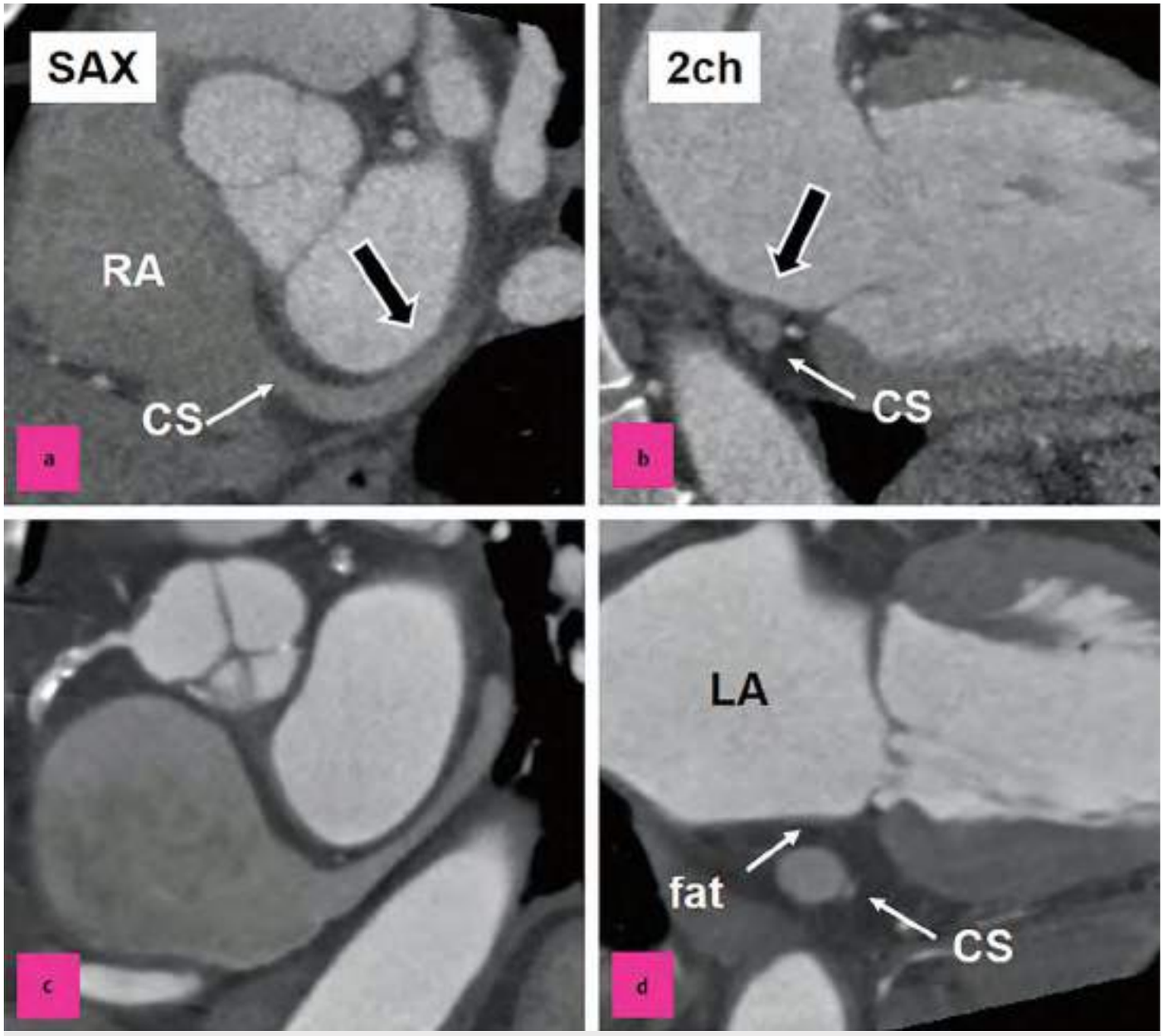

Fig. 19.31 Variants of coronary sinus–left atrial (CS-LA) muscle connections from two different patients. **(a**, **c)** The short-axis (SAX) view and **(b**, **d)** the left heart two-chamber (2ch) views. In the first patient **(a**, **b)**, a CS–LA muscle connection is shown, which usually is a single connection (*black arrows*) ending at some distance from the CS ostium. In patient 2 **(c**, **d)**, no CS–LA attachment exists. Instead, the CS and the LA walls are separated by the epidural fat.

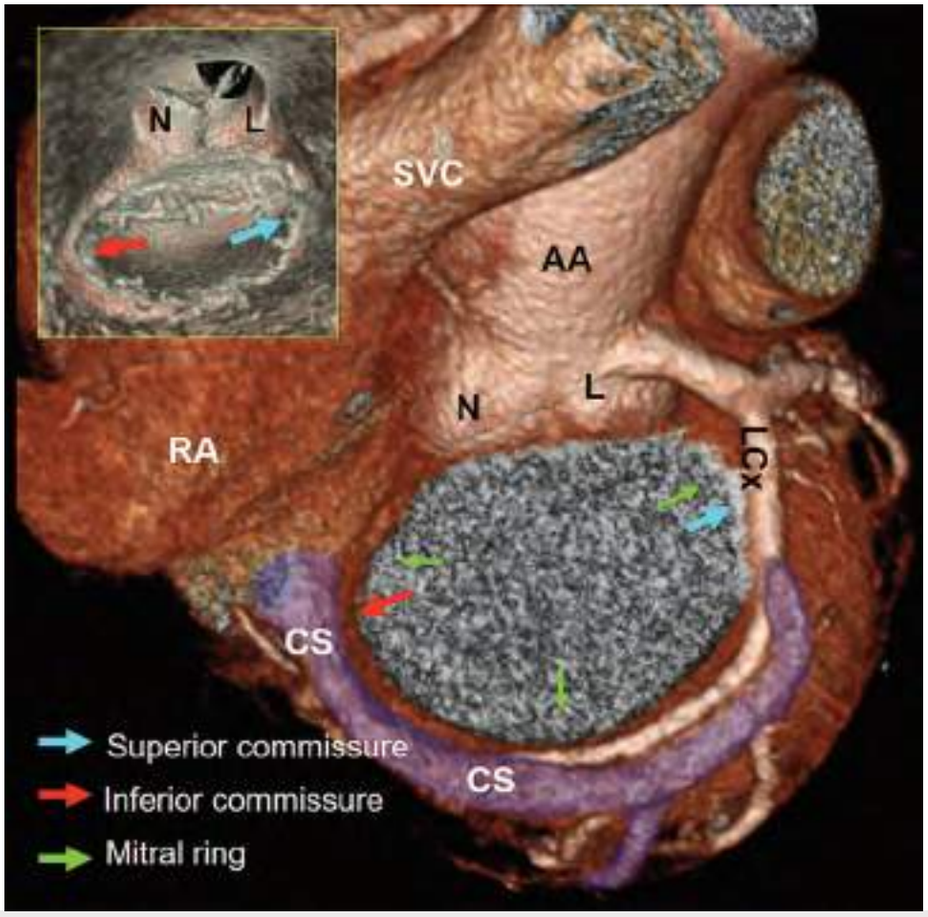

Fig. 19.32 The relationship of the posterior mitral ring and the coronary sinus (CS). The left circumflex artery (LCx) runs adjacent to the superior commissure, whereas the CS is adjacent to the inferior margin of the mitral ring. These structures can be damaged during surgical or percutaneous mitral valve interventions. When the circumflex artery is dominant, the entire attachment of the posterior leaflet may be closely related to this artery. AA, ascending aorta; L, left coronary sinus; N, noncoronary sinus; RA, right atrium; SVC, superior vena cava.

heart can provide accurate noninvasive information about mitral annulus, CS anatomy, and their relationship with the coronary arteries (▶ Fig. 19.33). In patients with severe calcifications of the mitral valve annulus, a surgical approach may be preferred over a percutaneous approach.

Coronary Sinus Retrograde Cardioplegia Perfusion Delivery

RCP is widely used as a method of myocardial protection especially in cases with severe coronary artery disease that can alter the distribution of antegrade cardioplegia.[79] The CS venous system is not affected by extensive coronary artery disease and a more uniform venous network remains in the subendocardial zone of both ventricles. RCP is also used in valve procedures, with normal coronary arteries, as this method allows the surgeon to deliver the maintenance doses only from the CS—facilitating the operation and shortening the aortic cross-clamping times. Knowledge of the anatomic variants of the CS and its tributaries is important as the efficiency and distribution of an RCP may be affected, which leads to partial or poor myocardial protection. It would be difficult to perform RCP in patients with an ostial atresia/stenosis of the CS, large Chiari network, and in congenital heart disease with venous drainage anomalies (▶ Fig. 19.22, ▶ Fig. 19.23). With regard to selective retroinfusion of cardiac veins, the GCV/AIV and IIV have highly consistent anatomic course (▶ Fig. 19.34). The distribution of RCP should be assessed by examining the posterior and anterior cardiac veins during perfusion because RCP may not perfuse all of the right ventricular free wall and septum. Distribution of RCP to the free wall of the RV is often poor because there is no direct communication between the CS and anterior cardiac veins. This may cause a problem in some patients especially in hypertrophied hearts in which delivery from the epicardial veins toward the subendocardial plexus is highly impeded.

◆ Conclusion

A complete and highly efficient and clinically useful classification of the CVS is not as straightforward as in the case of the coronary arteries. This chapter describes the role of coronary CTA in anatomic classification, assessment of anatomic variants, and pathologic changes of the CVS. It also emphasized on the role of CT in transvenous ablation procedures, left ventricular pacing for CRT, and PMA. Detailed information about the CVS in this review can be useful in better understanding of the clinical implications of the imaging techniques, among which coronary CT venography has major advantages.

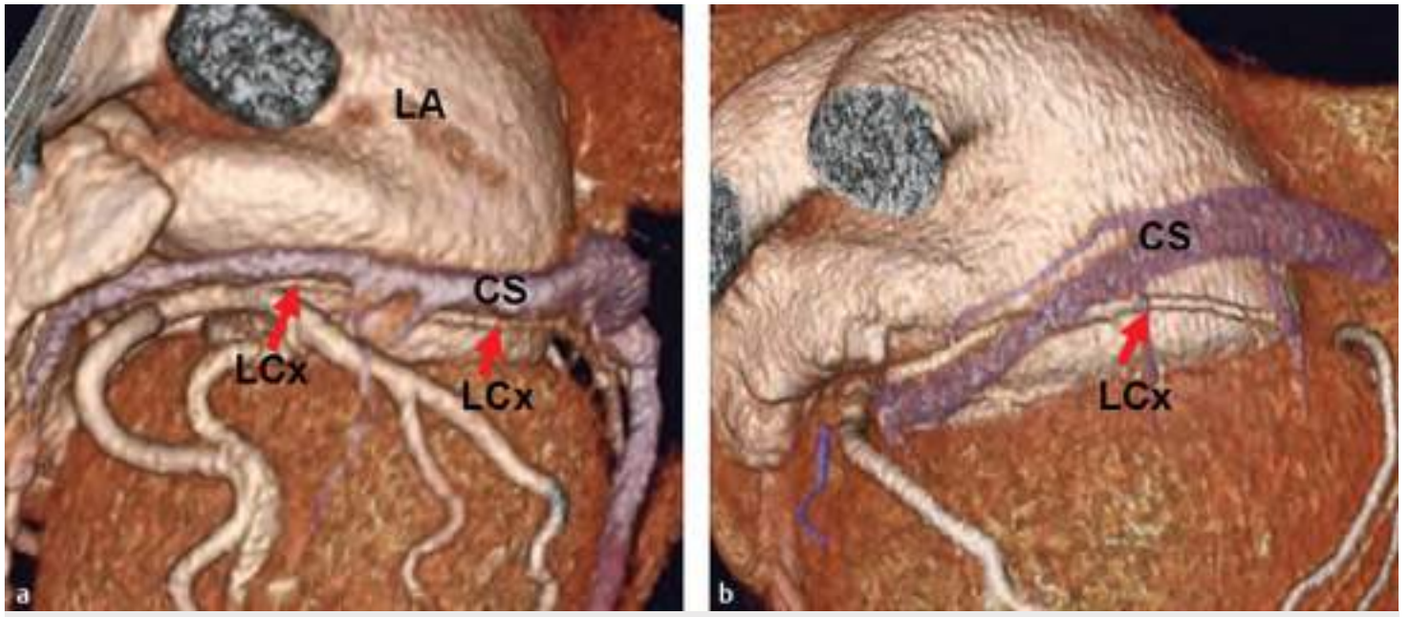

Fig. 19.33 Spatial relationship of the coronary sinus (CS), mitral annulus, and left circumflex (LCx) artery (*red arrows*). The LCx courses between the CS and the mitral annulus in 60 to 80% but with a significant variability in the location. It may cross the CS. **(a)** This close relationship between the CS and the LCx may limit the use of percutaneous mitral annuloplasty, particularly when the LCx courses underneath of the CS over a long distance **(b)**. LA, left atrium.

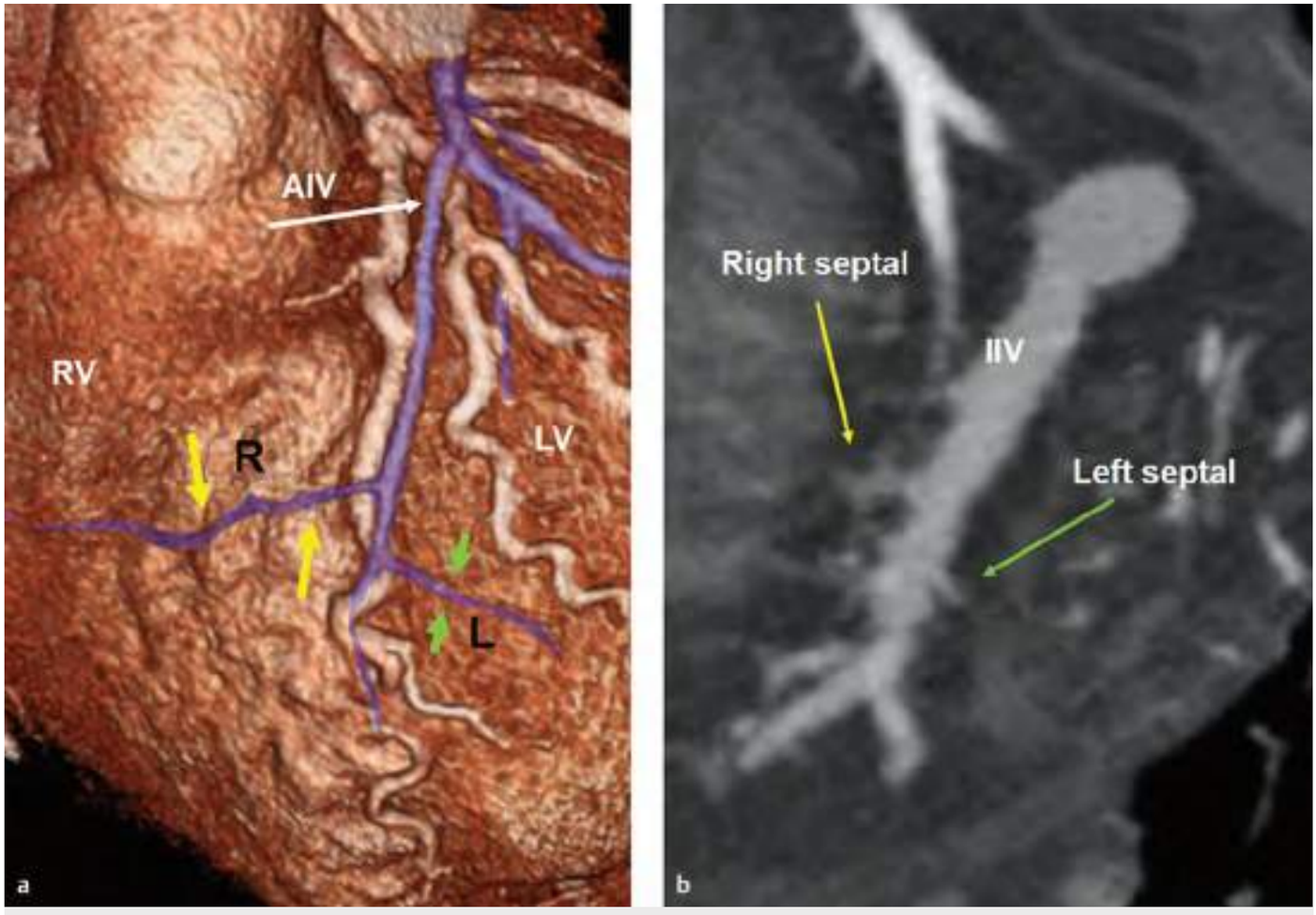

Fig. 19.34 **(a)** Tributaries from both ventricles join the anterior interventricular (AIV) portion of the great cardiac vein. **(b)** Inferior interventricular vein (IIV) draining the right (R) and left (L) (posterior) septal veins. The AIV and IIV are highly consistent veins. The right ventricle (RV) branches can drain into these veins. This helps provide distribution of cardioplegic solution in the RV with retrograde CS perfusion. LV, left ventricle.

References

[1] Anderson RH, Brown NA, Moorman AFM. Development and structures of the venous pole of the heart. Dev Dyn.; 235(1):2–9

[2] Steding G, Xu JW, Seidl W, Männer J, Xia H. Developmental aspects of the sinus valves and the sinus venosus septum of the right atrium in human embryos. Anat Embryol (Berl).; 181(5):469–475

[3] Red-Horse K, Ueno H, Weissman IL, Krasnow MA. Coronary arteries form by developmental reprogramming of venous cells. Nature.; 464(7288):549–553

[4] Vrancken Peeters MP, Gittenberger-de Groot AC, Mentink MM, Hungerford JE, Little CD, Poelmann RE. Differences in development of coronary arteries and veins. Cardiovasc Res.; 36(1):101–110

[5] von Lüdinghausen M. Clinical anatomy of cardiac veins, Vv. cardiacae. Surg Radiol Anat.; 9(2):159–168

[6] von Lüdinghausen M. The venous drainage of the human myocardium. Adv Anat Embryol Cell Biol.; 168:I–VIII, 1–104

[7] Ho SY, Sánchez-Quintana D, Becker AE. A review of the coronary venous system: a road less travelled. Heart Rhythm.; 1(1):107–112

[8] von Lüdinghausen M, Ohmachi N, Besch S, Mettenleiter A. Atrial veins of the human heart. Clin Anat.; 8(3):169–189

[9] Ratajczyk-Pakalska E. Variation of the smallest cardiac veins. Folia Morphol (Warsz).; 37(4):415–418

[10] Ansari A. Anatomy and clinical significance of ventricular Thebesian veins. Clin Anat.; 14(2):102–110

[11] Bottega NA, Kapa S, Edwards WD, et al. The cardiac veins in congenitally corrected transposition of the great arteries: delivery options for cardiac devices. Heart Rhythm.; 6(10):1450–1456

[12] Ratajczyk-Pakalska E, Fortak W, Gołab B. Sphincters and valves in the walls of the smallest cardiac veins. Folia Morphol (Warsz).; 43(2):121–127

[13] Ratajczyk-Pakalska E, Bloch P, Kulig A. Angioarchitectonics of the venous vessels and morphological changes in coronary heart disease. Basic Res Cardiol.; 86(6):554–560

[14] Taylor JR, Taylor AJ. The Thebesian circulation to developing conducting tissue: a nutrient-nodal hypothesis of cardiogenesis. Can J Cardiol.; 15(8):859–866

[15] Taylor JR, Taylor AJ. Thebesian sinusoids: forgotten collaterals to papillary muscles. Can J Cardiol.; 16(11):1391–1397

[16] Parsonnet V. The anatomy of the veins of the human heart with special reference to normal anastomotic channels. J Med Soc N J.; 50(10):446–452

[17] Huu N, Doutriaux M, Leroy JP, Thuan RH. [Small veins of the heart auricle]. Bull Assoc Anat (Nancy).; 59(167):955–967

[18] Saremi F, Channual S, Krishnan S, Gurudevan SV, Narula J, Abolhoda A. Bachmann Bundle and its arterial supply: imaging with multidetector CT: implications for interatrial conduction abnormalities and arrhythmias. Radiology.; 248(2):447–457

[19] von Lüdinghausen M, Lechleuthner A. Atresia of the right atrial ostium of the coronary sinus. Acta Anat (Basel).; 131(1):81–83

[20] Ortale JR, Marquez CQ. Anatomy of the intramural venous sinuses of the right atrium and their tributaries. Surg Radiol Anat.; 20(1):23–29

[21] Pina JA. Morphological study on the human anterior cardiac veins, venae cordis anteriores. Acta Anat (Basel).; 92(1):145–159

[22] Mierzwa J, Kozielec T. Variation of the anterior cardiac veins and their orifices in the right atrium in man. Folia Morphol (Warsz).; 34(2):125–133

[23] Blendea D, Shah RV, Auricchio A, et al. Variability of coronary venous anatomy in patients undergoing cardiac resynchronization therapy: a high-speed rotational venography study. Heart Rhythm.; 4(9):1155–1162

[24] Arbelo E, García-Quintana A, Caballero E, et al. Usefulness of hyperemic venous return angiography for studying coronary venous anatomy prior to cardiac resynchronization device implantation. Rev Esp Cardiol.; 61(9):936–944

[25] Jongbloed MR, Lamb HJ, Bax JJ, et al. Noninvasive visualization of the cardiac venous system using multislice computed tomography. J Am Coll Cardiol.; 45 (5):749–753

[26] Knackstedt C, Mühlenbruch G, Mischke K, et al. Imaging of the coronary venous system in patients with congestive heart failure: comparison of 16 slice MSCT and retrograde coronary sinus venography: comparative imaging of coronary venous system. Int J Cardiovasc Imaging.; 24(8):783–791

[27] Van de Veire NR, Schuijf JD, De Sutter J, et al. Non-invasive visualization of the cardiac venous system in coronary artery disease patients using 64-slice computed tomography. J Am Coll Cardiol.; 48(9):1832–1838

[28] Younger JF, Plein S, Crean A, Ball SG, Greenwood JP. Visualization of coronary venous anatomy by cardiovascular magnetic resonance. J Cardiovasc Magn Reson.; 11:26

[29] Chiribiri A, Kelle S, Götze S, et al. Visualization of the cardiac venous system using cardiac magnetic resonance. Am J Cardiol.; 101(3):407–412

[30] Ortale JR, Gabriel EA, Iost C, Márquez CQ. The anatomy of the coronary sinus and its tributaries. Surg Radiol Anat.; 23(1):15–21

[31] Bales GS. Great cardiac vein variations. Clin Anat.; 17(5):436–443

[32] Pejkovic B, Bogdanovic D. The great cardiac vein. Surg Radiol Anat.; 14(1):23–28

[33] von Lüdinghausen M. Aberrant course of the anterior interventricular part of the great cardiac vein in the human heart. Gegenbaurs Morphol Jahrb.; 135 (3):475–478

[34] Loukas M, Tubbs RS, Jordan R. Aneurysm of the great cardiac vein. Surg Radiol Anat.; 29(2):169–172

[35] Saremi F, Channual S, Sarlaty T, Tafti MA, Milliken JC, Narula J. Coronary venous aneurysm in patients without cardiac arrhythmia as detected by MDCT: an anatomic variant or a pathologic entity. JACC Cardiovasc Imaging.; 3(3):257–265

[36] Ho SY, Russell G, Rowland E. Coronary venous aneurysms and accessory atrioventricular connections. Br Heart J.; 60(4):348–351

[37] Sun Y, Arruda M, Otomo K, et al. Coronary sinus-ventricular accessory connections producing posteroseptal and left posterior accessory pathways: incidence and electrophysiological identification. Circulation.; 106(11):1362–1367

[38] Morgan JM, Delgado V. Lead positioning for cardiac resynchronization therapy: techniques and priorities. Europace.; 11 Suppl 5:v22–v28

[39] Saremi F, Thonar B, Sarlaty T, et al. Posterior interatrial muscular connection between the coronary sinus and left atrium: anatomic and functional study of the coronary sinus with multidetector CT. Radiology.; 260:671–679

[40] Loukas M, Bilinsky S, Bilinsky E, el-Sedfy A, Anderson RH. Cardiac veins: a review of the literature. Clin Anat.; 22(1):129–145

[41] Cendrowska-Pinkosz M. The variability of the small cardiac vein in the adult human heart. Folia Morphol (Warsz).; 63(2):159–162

[42] de Oliveira IM, Scanavacca MI, Correia AT, Sosa EA, Aiello VD. Anatomic relations of the Marshall vein: importance for catheterization of the coronary sinus in ablation procedures. Europace.; 9(10):915–919

[43] Kim DT, Lai AC, Hwang C, et al. The ligament of Marshall: a structural analysis in human hearts with implications for atrial arrhythmias. J Am Coll Cardiol.; 36(4):1324–1327

[44] Kurotobi T, Ito H, Inoue K, et al. Marshall vein as arrhythmogenic source in patients with atrial fibrillation: correlation between its anatomy and electrophysiological findings. J Cardiovasc Electrophysiol.; 17(10):1062–1067

[45] Shah D, Haissaguerre M, Jais P, Hocini M. Nonpulmonary vein foci: do they exist? Pacing Clin Electrophysiol.; 26(7, Pt 2):1631–1635

[46] Chauvin M, Shah DC, Haïssaguerre M, Marcellin L, Brechenmacher C. The anatomic basis of connections between the coronary sinus musculature and the left atrium in humans. Circulation.; 101(6):647–652

[47] Cabrera JA, Ho SY, Climent V, Sánchez-Quintana D. The architecture of the left lateral atrial wall: a particular anatomic region with implications for ablation of atrial fibrillation. Eur Heart J.; 29:356–362

[48] Tan AY, Chou CC, Zhou S, et al. Electrical connections between left superior pulmonary vein, left atrium, and ligament of Marshall: implications for mechanisms of atrial fibrillation. Am J Physiol Heart Circ Physiol.; 290(1):H312–H322

[49] Hsu LF, Jaïs P, Keane D, et al. Atrial fibrillation originating from persistent left superior vena cava. Circulation.; 109(7):828–832

[50] Hwang C, Wu TJ, Doshi RN, Peter CT, Chen PS. Vein of marshall cannulation for the analysis of electrical activity in patients with focal atrial fibrillation. Circulation.; 101(13):1503–1505

[51] Miraldi F, di Gioia CR, Proietti P, De Santis M, d'Amati G, Gallo P. Cardinal vein isomerism: an embryological hypothesis to explain a persistent left superior vena cava draining into the roof of the left atrium in the absence of coronary sinus and atrial septal defect. Cardiovasc Pathol.; 11(3):149–152

[52] Anderson SE, Quill JL, Iaizzo PA. Venous valves within left ventricular coronary veins. J Interv Card Electrophysiol.; 23(2):95–99

[53] Corcoran SJ, Lawrence C, McGuire MA. The valve of Vieussens: an important cause of difficulty in advancing catheters into the cardiac veins. J Cardiovasc Electrophysiol.; 10(6):804–808

[54] Maros TN, Rácz L, Plugor S, Maros TG. Contributions to the morphology of the human coronary sinus. Anat Anz.; 154(2):133–144
[55] Silver MA, Rowley NE. The functional anatomy of the human coronary sinus. Am Heart J.; 115(5):1080–1084
[56] Roberts JT.
[57] Schutte DA, Rowland DG, Allen HD, Bharati S. Prominent venous valves in hypoplastic right hearts. Am Heart J.; 134(3):527–531
[58] Duda B, Grzybiak M. About variability of Vieussen valve in the adult human heart. Folia Morphol (Warsz).; 59(1):43–45
[59] Karaca M, Bilge O, Dinckal MH, Ucerler H. The anatomic barriers in the coronary sinus: implications for clinical procedures. J Interv Card Electrophysiol.; 14(2):89–94
[60] D'Cruz IA, Johns C, Shala MB. Dynamic cyclic changes in coronary sinus caliber in patients with and without congestive heart failure. Am J Cardiol.; 83 (2):275–277, A6
[61] Ong MG, Lee PC, Tai CT, et al. Coronary sinus morphology in different types of supraventricular tachycardias. J Interv Card Electrophysiol.; 15(1):21–26
[62] Uemura H, Ho SY, Anderson RH, et al. Surgical anatomy of the coronary circulation in hearts with discordant atrioventricular connections. Eur J Cardiothorac Surg.; 10(3):194–200
[63] Mantini E, Grondin CM, Lillehei CW, Edwards JE. Congenital anomalies involving the coronary sinus. Circulation.; 33:317–327
[64] Rumisek JD, Pigott JD, Weinberg PM, Norwood WI. Coronary sinus septal defect associated with tricuspid atresia. J Thorac Cardiovasc Surg.; 92(1):142–145
[65] Gerlis LM, Gibbs JL, Williams GJ, Thomas GDH. Coronary sinus orifice atresia and persistent left superior vena cava. A report of two cases, one associated with atypical coronary artery thrombosis. Br Heart J.; 52(6):648–653
[66] Hahm JK, Park YW, Lee JK, et al. Magnetic resonance imaging of unroofed coronary sinus: three cases. Pediatr Cardiol.; 21(4):382–387
[67] Kautzner J, Riedlbauchová L, Cihák R, Bytesník J, Vancura V. Technical aspects of implantation of LV lead for cardiac resynchronization therapy in chronic heart failure. Pacing Clin Electrophysiol.; 27(6, Pt 1):783–790
[68] Singh JP, Houser S, Heist EK, Ruskin JN. The coronary venous anatomy: a segmental approach to aid cardiac resynchronization therapy. J Am Coll Cardiol.; 46(1):68–74
[69] Saremi F, Pourzand L, Krishnan S, et al. Right atrial cavotricuspid isthmus: anatomic characterization with multi-detector row CT. Radiology.; 247 (3):658–668
[70] Cabrera JA, Sánchez-Quintana D, Ho SY, et al. Angiographic anatomy of the inferior right atrial isthmus in patients with and without history of common atrial flutter. Circulation.; 99(23):3017–3023
[71] Hansen BF. Thrombosis of epicardial coronary veins in acute myocardial infarction. Am Heart J.; 97(6):696–700
[72] von Ludinghausen M, Ohmachi N, Boot C. Myocardial coverage of the coronary sinus and related veins. Clin Anat.; 5:1–15
[73] Haïssaguerre M, Hocini M, Takahashi Y, et al. Impact of catheter ablation of the coronary sinus on paroxysmal or persistent atrial fibrillation. J Cardiovasc Electrophysiol.; 18(4):378–386
[74] Webb JG, Harnek J, Munt BI, et al. Percutaneous transvenous mitral annuloplasty: initial human experience with device implantation in the coronary sinus. Circulation.; 113(6):851–855
[75] Schofer J, Siminiak T, Haude M, et al. Percutaneous mitral annuloplasty for functional mitral regurgitation: results of the CARILLON Mitral Annuloplasty Device European Union Study. Circulation.; 120(4):326–333
[76] Maselli D, Guarracino F, Chiaramonti F, Mangia F, Borelli G, Minzioni G. Percutaneous mitral annuloplasty: an anatomic study of human coronary sinus and its relation with mitral valve annulus and coronary arteries. Circulation.; 114 (5):377–380
[77] Choure AJ, Garcia MJ, Hesse B, et al. In vivo analysis of the anatomical relationship of coronary sinus to mitral annulus and left circumflex coronary artery using cardiac multidetector computed tomography: implications for percutaneous coronary sinus mitral annuloplasty. J Am Coll Cardiol.; 48(10):1938–1945
[78] Tops LF, Van de Veire NR, Schuijf JD, et al. Noninvasive evaluation of coronary sinus anatomy and its relation to the mitral valve annulus: implications for percutaneous mitral annuloplasty. Circulation.; 115(11):1426–1432
[79] Ruengsakulrach P, Buxton BF. Anatomic and hemodynamic considerations influencing the efficiency of retrograde cardioplegia. Ann Thorac Surg.; 71 (4):1389–1395

20 The Pericardium

Farhood Saremi

◆ Introduction

The lungs and the heart reside in separate compartments within the thoracic cavity. The lobes of the lung are located in two pleural cavities and the heart is located within the pericardial cavity, which occupies most of the lower mediastinum. The pleura and pericardium are potential fluid-filled spaces within the pleural and pericardial cavities (spaces) that are lined by thin mesothelial linings. The pericardium is composed of outer fibrous and two inner serous layers and contains a small amount of fluid. The pericardial cavity is involved in many inflammatory and malignant diseases. Along with the development of novel techniques for percutaneous access to the pericardial, increased interest in the detailed anatomy of the pericardial space and its recesses has developed. This chapter discusses the embryology and anatomy of the pericardial cavity. Common pathologies are briefly described. The epicardial and mediastinal fats are included in the discussion.

◆ Embryology

The pleural, pericardial, and peritoneal cavities originate from a single large intraembryonic coelom (cavity). The intraembryonic coelom is lined by the visceral and parietal layers of the lateral plate mesoderm, the splanchnopleura and the somatopleura, respectively. In early embryonic stage (i.e., week 4 of embryo), the intraembryonic coelom at the cranial level consists of a middle pericardial cavity and two pericardioperitoneal canals posterolaterally (▶ Fig. 20.1, ▶ Fig. 20.2). Within a few days, the lung buds start to grow from the primitive mediastinal mesoderm in midline out into the pericardioperitoneal canals. At the same time, the septum transversum, from which the anterior part of the diaphragm will derive, grows to divide the pericardioperitoneal canals into the peritoneal cavity and the thoracic cavity. In the human embryo, it is suggested that initially two folds grow out of the body wall: the ventral one is called the pleuropericardial membrane (fold) and the dorsal one is called the pleuroperitoneal membrane (fold). With rapid outgrowth of the lung buds from the foregut, the pericardioperitoneal canals expand into the future pleural cavity and the primitive mesenchyme splits into two layers that form the fibrous pericardium medially and the chest wall laterally.[1,2] Within the fibrous pericardium remains the phrenic neurovascular bundles.

The pleuropericardial membrane on each side grows inward toward the lung hilum. By week 7, the pleuropericardial membranes fuse with the dorsal mesocardium (primitive mediastinum) to obliterate the remaining communication between the two pericardioperitoneal canals (pleural cavities) and separate them from the pericardial cavity. At the caudal end of the pericardioperitoneal canals and during week 6, the pleuroperitoneal membranes, which are attached dorsolaterally to the body wall, grow to separate the pleural cavity from the peritoneal cavity. The pleuroperitoneal membranes fuse with the dorsal mesentery of the esophagus and the septum transversum to form the posterior part of the diaphragm.

Complete separation of the pleural, pericardial, and peritoneal cavities requires an active role of the pleuropericardial and pleuroperitoneal membranes. The mechanisms that drive this process have remained obscure. It is important to know that pleuropericardial membranes contain the common cardinal veins (ductus cuvieri[1,2]; ▶ Fig. 20.2). The common cardinal veins drain the primitive venous system into the sinus horns of the primitive heart.

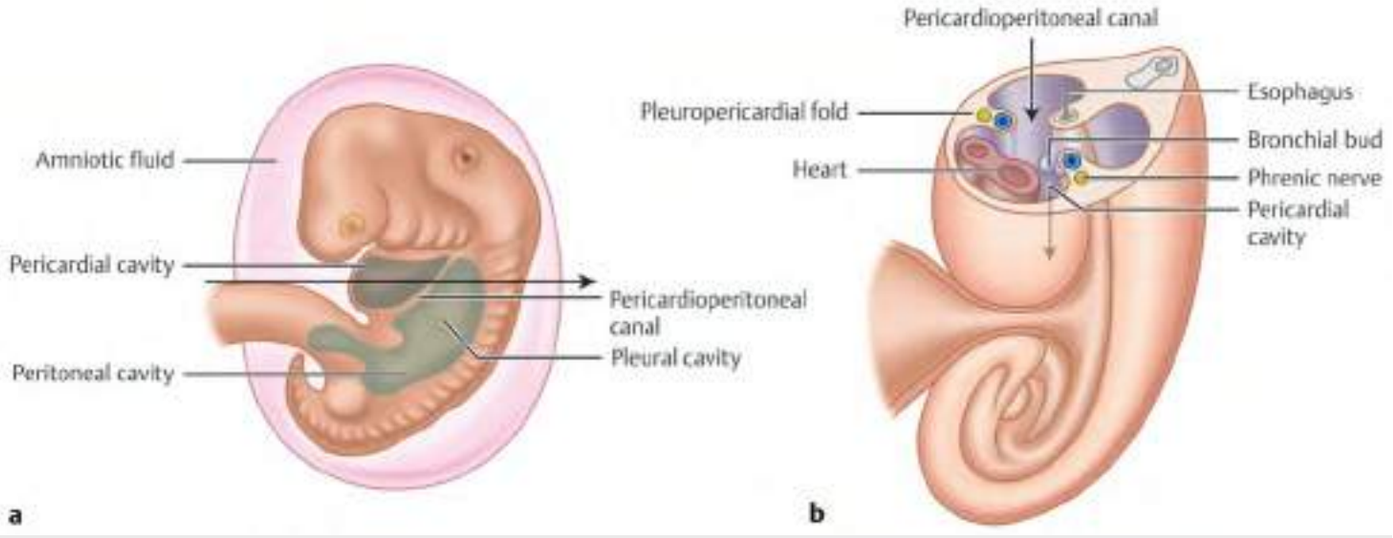

Fig. 20.1 **(a)** Lateral view of the fetus at 6 weeks. The extent of the pericardioperitoneal canal in the body and the anterior position of the pericardial cavity around the heart are shown in *green*. **(b)** Cross-section of the fetus at the level of the lower thorax showing the two pericardioperitoneal canals posterolaterally. The pleuropericardial membranes (folds) are seen separating the pericardial cavity from the pericardioperitoneal canals (future pleural cavity).

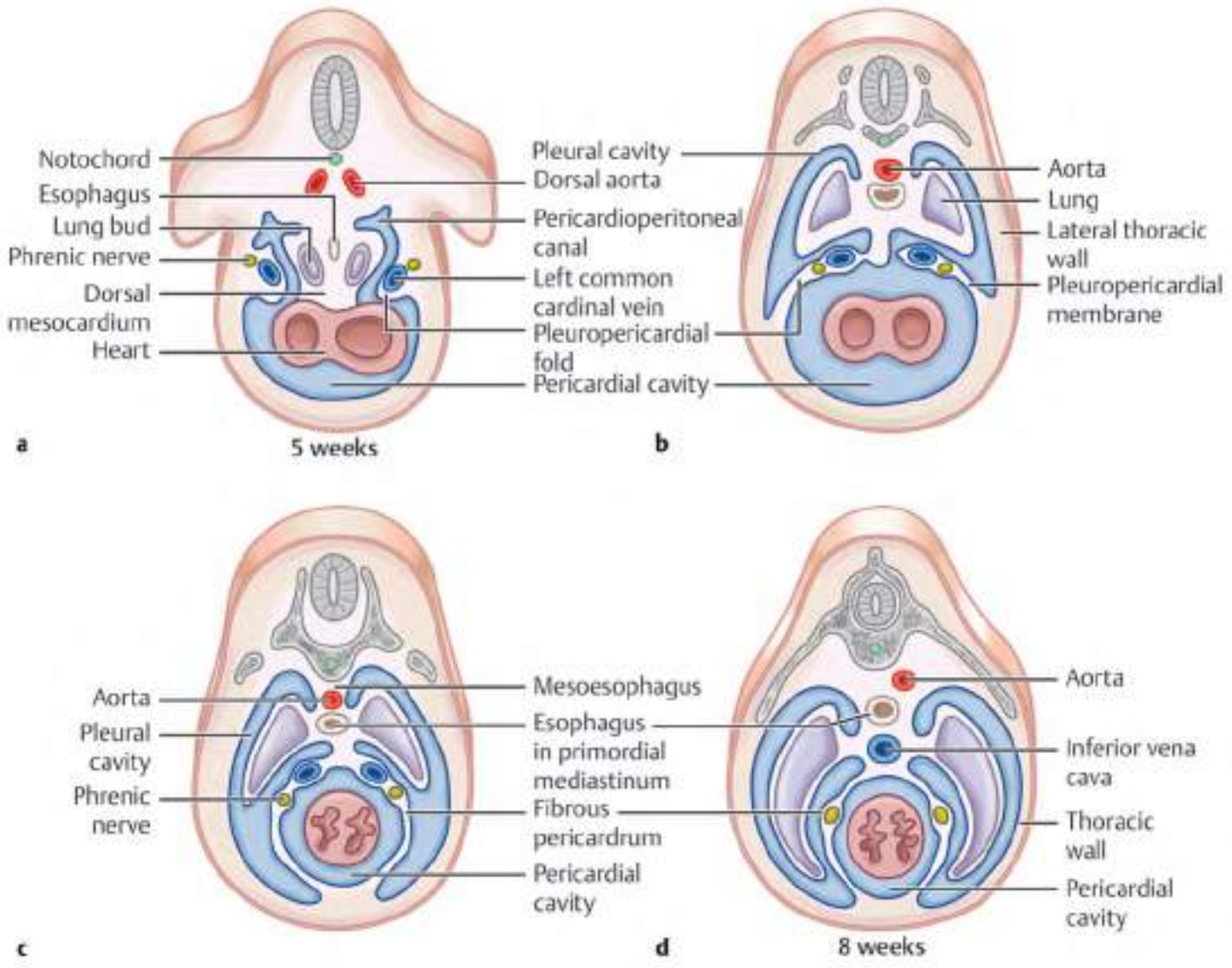

Fig. 20.2 (a–d) At 5 weeks, the pleuropericardial folds appear and by 6 weeks reach midline and later fuse with the splanchnic mesoderm (primitive mediastinum) at the lung hila to separate the pleural spaces from the pericardial cavity. The dorsal mesocardium connects the heart to the splanchnic mesoderm that overlies the embryonic pharynx/esophagus. This mesocardium is the site through which vessels or additional tissue can dorsally enter the heart. The lung buds develop from the foregut and grow into the pericardioperitoneal canals to form the pleural cavities. The cardinal veins are located in these folds and later transform into the sinus venosus of the heart. Along with growth of the pleural cavities, the mediastinal mesenchyma will be pushed against the pleural cavity to form the fibrous pericardium with the phrenic neurovascular bundle embedded in it.

Therefore, development of the pericardium and sinus horn formation are coupled, and sinus horn defects are tightly associated with pleuropericardial abnormalities including the pericardium. As a reminder, the sinus horns develop from pericardial precursors that differentiate into the sinus venosus myocardium around the systemic venous connections to the atrium. They form only after the outflow tract, the left and right ventricles, and common atrium have already been established. In adults, most of the right sinus horn myocardium is incorporated into the right atrium to form the sinus venarum. In humans, the left sinus horn will lose its connection to the body and forms the coronary sinus.

◆ Pericardium

The pericardium surrounds the heart and extends out to cover part of the superior vena cava (SVC), ascending aorta, main pulmonary artery, ostial pulmonary veins, and inferior vena cava (▶ Fig. 20.3, ▶ Fig. 20.4, ▶ Fig. 20.5, ▶ Fig. 20.6). The pericardium is a flask-shaped sac consisting of an outer fibrous component and an inner double-layered serous sac that surrounds the heart.[3,4,5] The outer serous layer, which is closely attached to the fibrous layer is the parietal pericardium. The visceral serous pericardium, or epicardium, adheres to the heart and great vessels and forms recesses and sinuses. While the parietal layer of the pleura is largely attached to the body wall, the serous parietal pericardium is largely aligned with the free aspect of the parietal pleura (mediastinal pleura) to form a double-layered wall that is further stiffened by deposition of fibrous material between them. This fibrous material is the fibrous pericardium that is the remnant of the pleuropericardial membranes that anchors the heart in the mediastinum and separates the pericardial from the pleural cavities.[1,2]

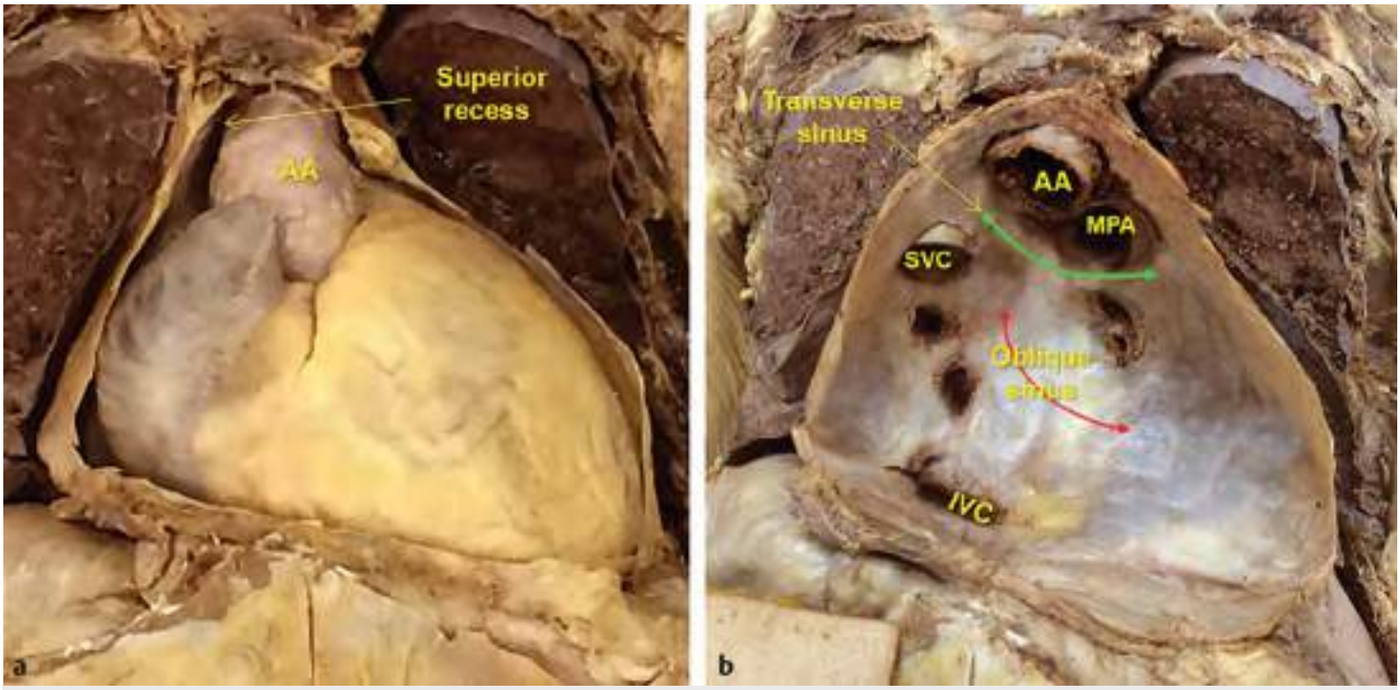

Fig. 20.3 **(a)** Anterior view of the pericardium after removal of the anterior fibrous pericardium. **(b)** View of the posterior pericardial sac after removal of the heart. AA, ascending aorta; IVC, inferior vena cava; MPA, main pulmonary artery; SVC, superior vena cava. (These images are provided courtesy of Professor Damián Sánchez-Quintana, MD, PhD.)

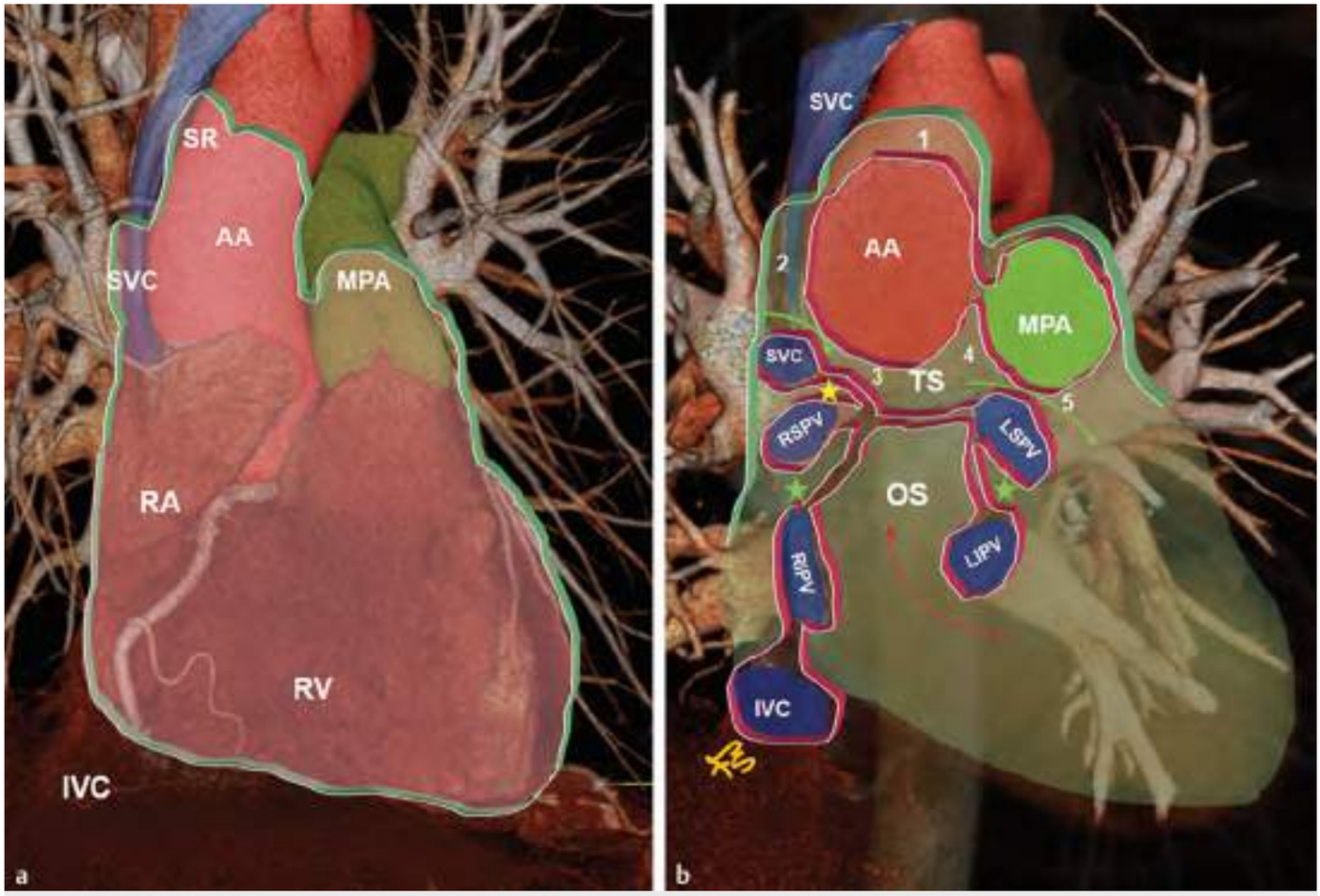

Fig. 20.4 Pericardial sac. **(a)** Anterior view of the heart and great vessels after removal of the parietal pericardium (*green band*). The visceral pericardium (*pink*) covers the heart and part of major vessels. **(b)** Posterior view of the pericardium after removal of the heart. The visceral pericardial sac reflections around the large vessels at their cardiac origin are shown by the *pink bands*. The *green band* shows the margin of the fibrous pericardium and the parietal pericardium is shown in *green*. The ascending aorta (AA) and main pulmonary artery (MPA) are enclosed in one tube. The superior vena cava (SVC), inferior vena cava (IVC), and pulmonary veins (PV) are enclosed in another tube. The transverse sinus (TS) is a complex interconnecting passage between these two tubes (*green arrows*). Note two layers of the serous pericardium separate the transverse sinus from the oblique sinus (OS). Components of the aortic recess of the transverse sinus including anterior/superior,[1] lateral,[2] and inferior/posterior[3] are shown. The right pulmonic[4] and the left pulmonic[5] recesses of the transverse sinus are also shown. The OS is located behind the left atrium (*red arrow*). The retrocaval recess (*yellow star*) is located between the SVC and the right superior PV (RSPV). The left and right lateral recesses (*green stars*) are formed between superior and inferior PVs. LIPV, left inferior pulmonary vein; LSPV, left superior pulmonary vein; RA, right atrium; RIPV, right inferior pulmonary vein; RSPV, right superior pulmonary vein; RV, right ventricle; SR, superior aortic recess.

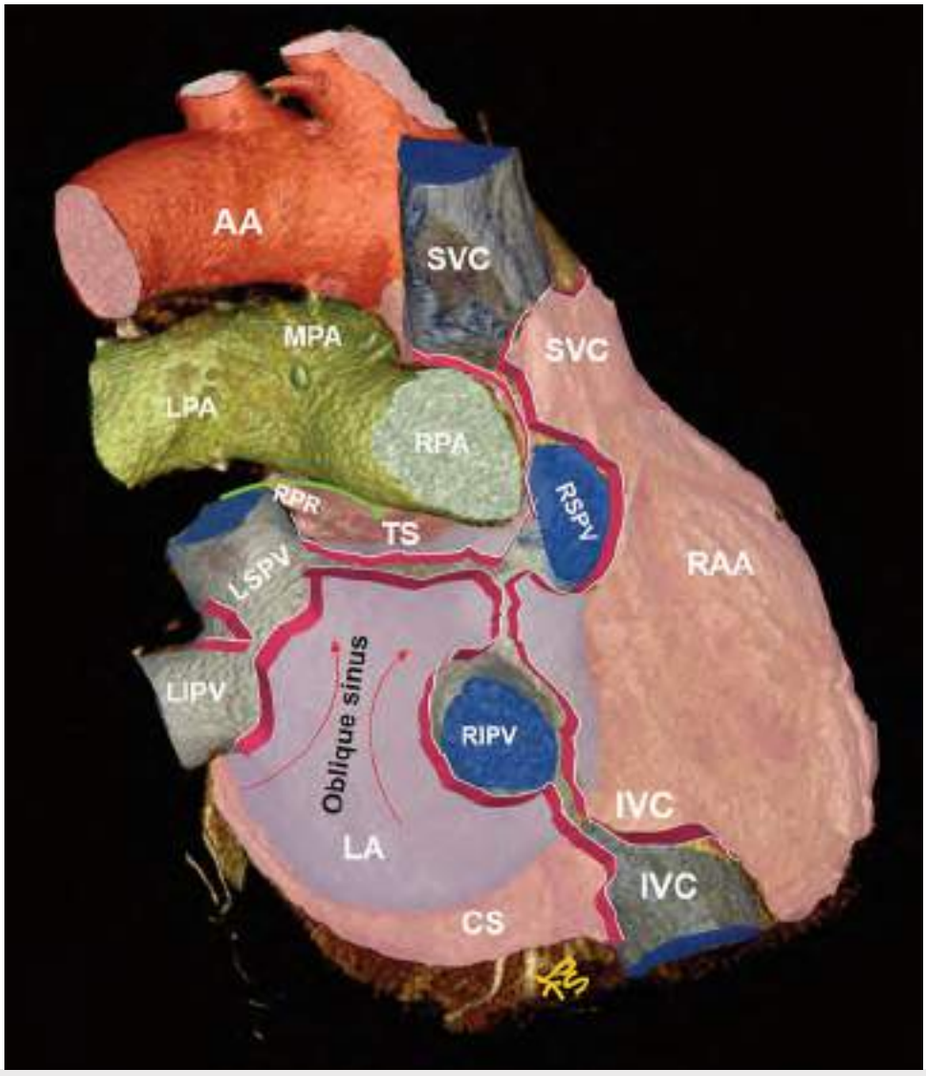

Fig. 20.5 Right posterolateral view of the heart demonstrates the venous pericardial reflections (*red band*) and the visceral pericardium (*pink lining*). The oblique sinus (*red arrows*) separated from the transverse sinus (TS; *green arrow*) by two layers of pericardial reflections that run between the left and right superior pulmonary veins. The right pulmonary artery (RPA) exits the transverse sinus immediately after its takeoff from the main pulmonary artery (MPA). The right pulmonic recess (RPS) is located below the RPA at its junction with the main pulmonary artery. AA, ascending aorta; CS, coronary sinus; IVC, inferior vena cava; LA, left atrium; LIPV, left inferior pulmonary vein; LPA, left pulmonary artery; LSPV, left superior pulmonary vein; RAA, right atrial appendage; RIPV, right inferior pulmonary vein; RPA, right pulmonary artery; RSPV, right superior pulmonary vein; SVC, superior vena cava.

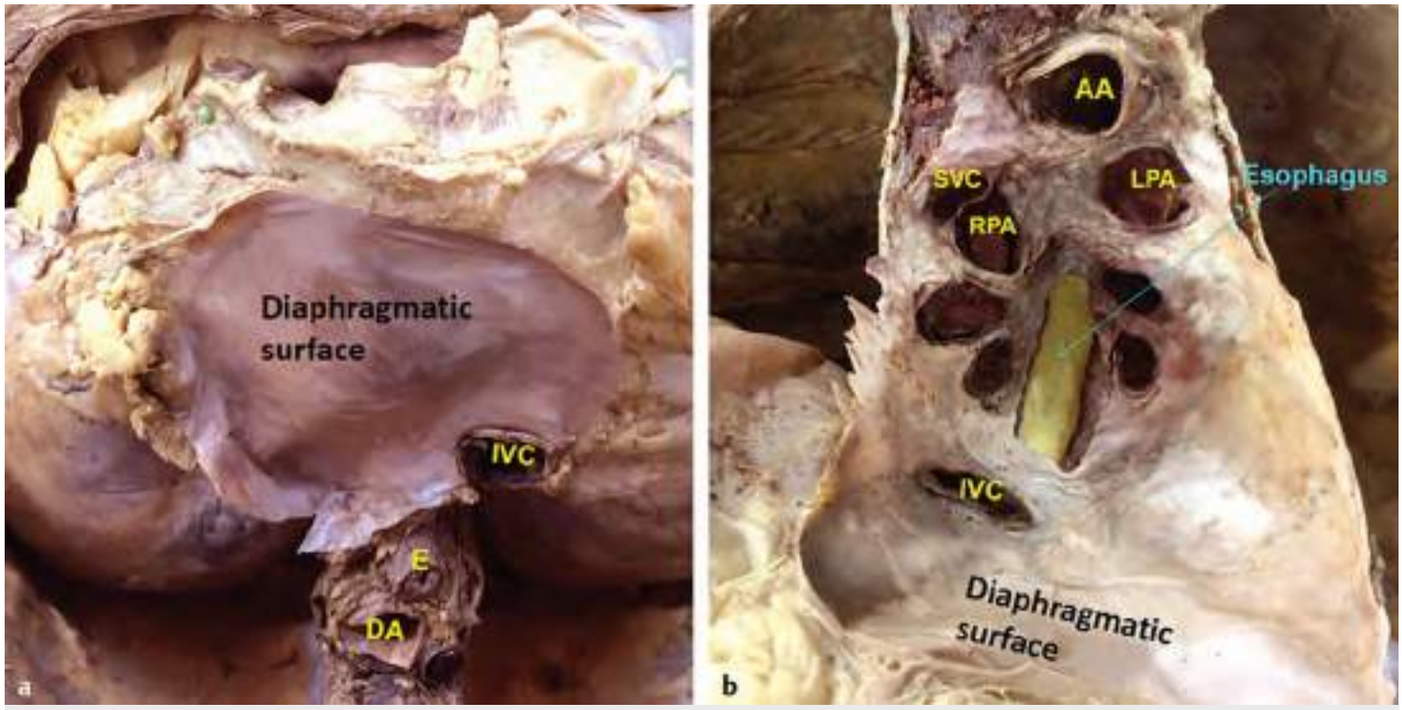

Fig. 20.6 **(a)** Diaphragmatic surface of the pericardium. **(b)** Posterior view of the pericardial sac after removal of the heart. A window is opened in the posterior pericardium showing the relationship of the esophagus and descending aorta to the pulmonary veins. AA, ascending aorta; DA, descending aorta; E, esophagus; IVC, inferior vena cava; LPA, left pulmonary artery; RPA, right pulmonary artery; SVC, superior vena cava. (These images are provided courtesy of Professor Damián Sánchez-Quintana, MD, PhD.)

Normally, the pericardial sac contains 15 to 25 mL of fluid, allowing visualization of the pericardial recesses on computed tomography (CT) or magnetic resonance imaging (MRI) studies.[3,4,5] The fibrous pericardium is fused with the central tendon of the diaphragm inferiorly and with the tunica adventitia of the great vessels superiorly (▶ Fig. 20.6). Anteriorly, it is attached to the sternum by superior and inferior sternopericardial ligaments (▶ Fig. 20.7; see Chapter 3). The serosal pericardium is avascular, but the fibrous pericardium is supplied by pericardial branches of the internal thoracic artery anteriorly and the mediastinal and bronchial branches posteriorly. The phrenic nerves descend in the fibrous pericardium between it and the mediastinal pleura and send branches to the pericardium, which contain vasomotor and sensory fibers.

Pericardial Reflection

The reflections of the serosal layers are arranged around two complex tubes. One tube encloses the aorta and pulmonary trunk. The second tube encloses the SVC, the inferior vena cava, and the four pulmonary veins[5,6] (▶ Fig. 20.4). The length and pattern of coverage of the major vessels are variable. CT is the best imaging modality to show the extent of the pericardium over the vessels.[7] Pericardial reflection over the ascending aorta and the main pulmonary artery is at the junction of vessels originated from the truncus part of the embryonic outflow tract proximally and the rest of vessels distally which are derived from the neural crest. The SVC is covered by the pericardium over its distal part at the cavoatrial junction. The intrapericardial portion of the SVC is 2 cm laterally and 3 cm medially.[8] Pericardial reflections over the pulmonary veins are very variable[9] (▶ Fig. 20.8).

Transverse Sinus

The transverse sinus is the passage between these two pericardial tubes (▶ Fig. 20.4**b**). The transverse sinus is located inferior and posterior to the aorta and the pulmonary trunk, and above and anterior the left atrium. It is possible to pass a finger through the transverse sinus.[10] Its posteroinferior boundary is formed by a pericardial reflection extending transversely between the right and left superior pulmonary veins at their junctions with the left atrium. The right pulmonary artery exits the transverse sinus soon after its takeoff from the main pulmonary artery (▶ Fig. 20.5). The transverse sinus is subdivided into the superior and inferior aortic recesses and the right and left pulmonic recesses[3,4,5,6] (▶ Fig. 20.4, ▶ Fig. 20.9). Some authors further subdivide the aortic recess, based on its relationship to the aorta, into posterior (inferior), lateral, anterior, and superior portions (▶ Fig. 20.4, ▶ Fig. 20.9). The superior extent of the transverse sinus along the aortocaval space forms the superior aortic recess.[3,4,5,6] Cephalad extension of this recess into the superior right paratracheal region (high-riding recess) can be mistaken for pathologies such as a bronchogenic cyst[11,12] (▶ Fig. 20.10).

The anterior extension of the superior aortic forms a characteristic crescent in front of the aorta and main pulmonary artery (▶ Fig. 20.9). On the right side, the sinus is continuous with the recess around the SVC (aortocaval recess; ▶ Fig. 20.10). Inferior extension of the transverse sinus along the posterior wall of the aorta and above the left atrium is called the inferior aortic recess. Lateral extent of the transverse sinus forms the left and right pulmonic recesses on each side between the pulmonary artery and the left atrium[13] (▶ Fig. 20.4, ▶ Fig. 20.5). The left pulmonic recess is bounded medially by the fold of ligament of Marshall

Fig. 20.7 Attachments of fibrous pericardium (P) to the sternum by superior and inferior sternopericardial ligaments (SPL and IPL) and to the central tendon of the diaphragm (D) are shown.

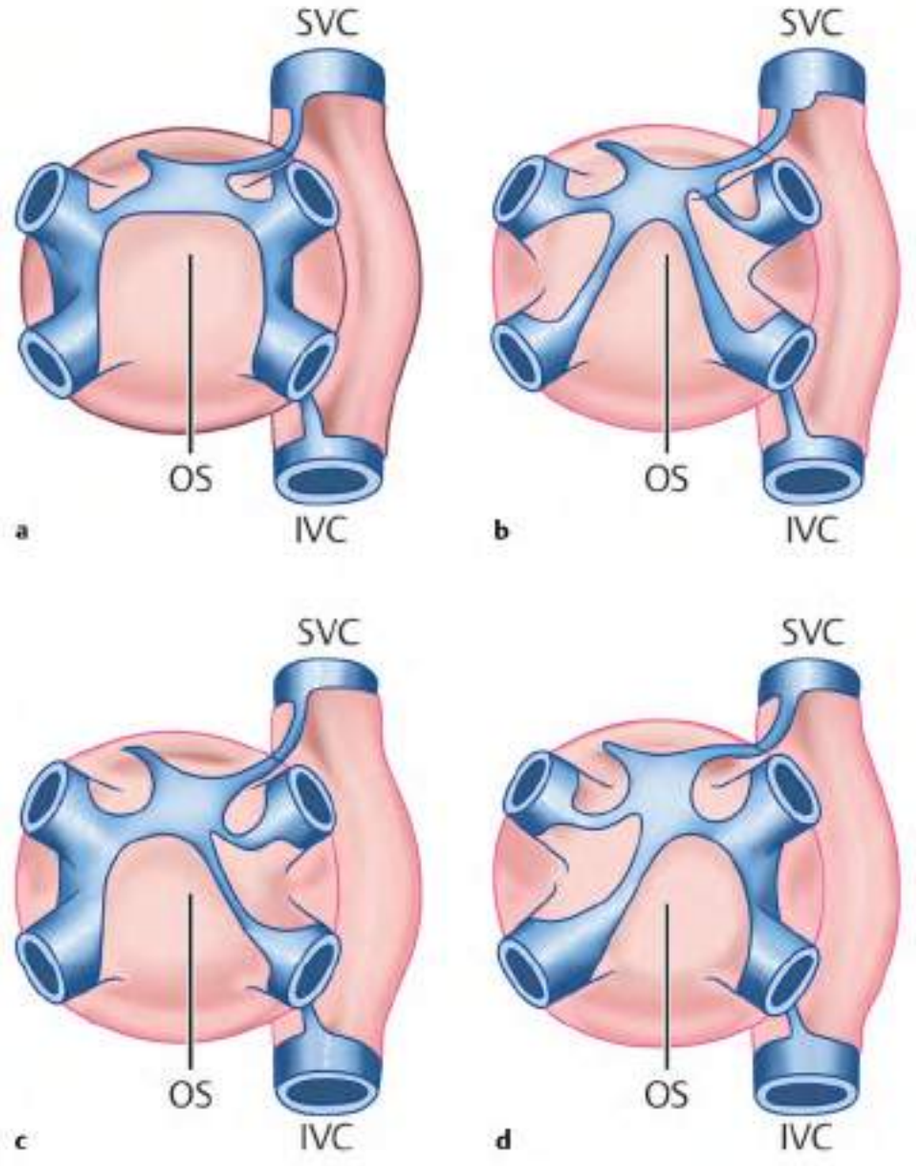

Fig. 20.8 (a–d) Posterior views of the left atrium showing variations of the pulmonary venous pericardial reflections. *White areas* indicate the uncovered areas between reflections of the serous pericardium. The most common anatomic variant is the presence of both the right and left pulmonary venous pericardial recesses **(b)**; this was seen in more than half of the patients studied. IVC, inferior vena cava; OS, oblique sinus; SVC, superior vena cava. (Adapted from Chaffanjon et al.[9])

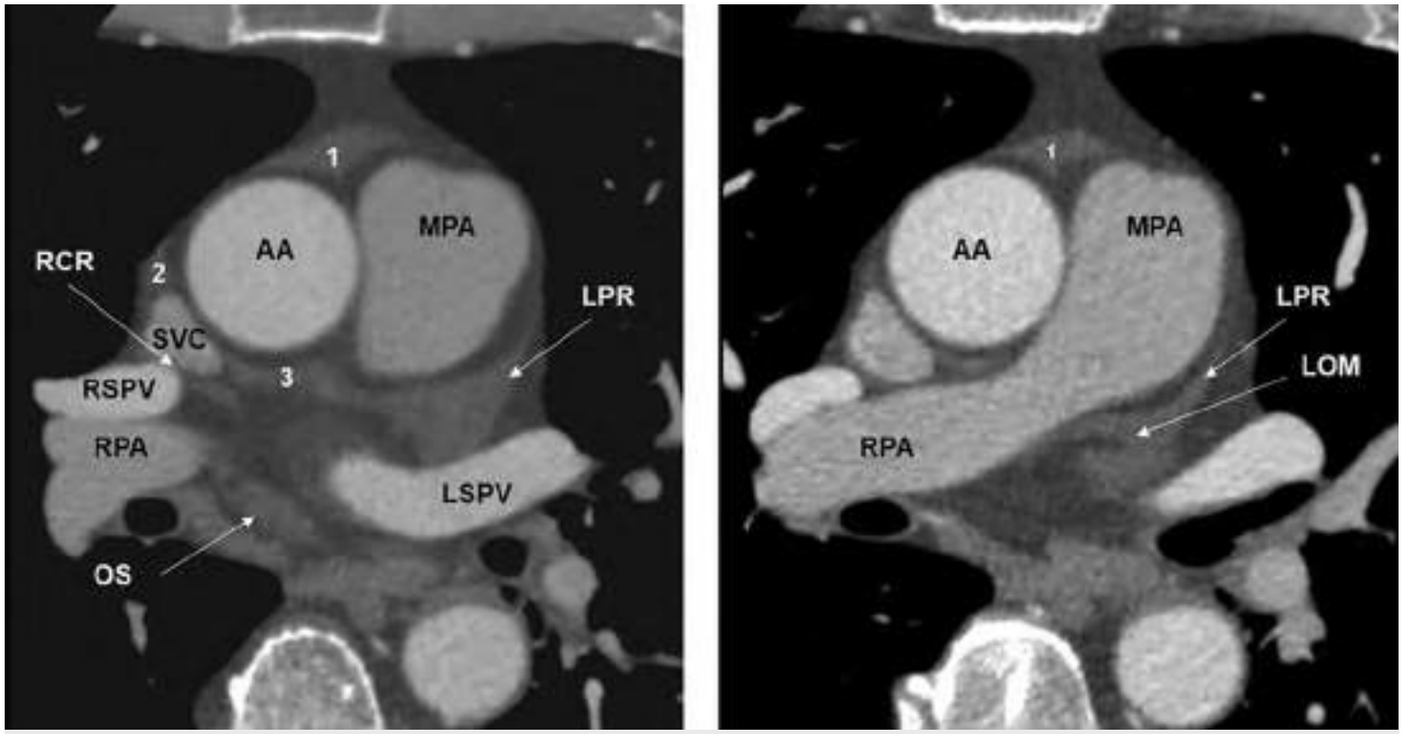

Fig. 20.9 Axial images of the heart at the level of the transverse sinus are shown. Components of the aortic recess of the transverse sinus including anterior/superior,[1] lateral,[2] and inferior/posterior[3] are shown. The left pulmonic recess (LPR) of the transverse sinus in seen anterior to the left superior pulmonary vein (LSPV). Fold of the ligament of Marshall (LOM) is seen deep in the LPR. A small retrocaval recess (RCR) and superior extension of the oblique sinus (OS) behind the right pulmonary artery (RPA), also known as "posterior pericardial recess," are also seen. AA, ascending aorta; LSPV, left superior pulmonary vein; MPA, main pulmonary artery; RSPV, right superior pulmonary vein; SVC, superior vena cava.

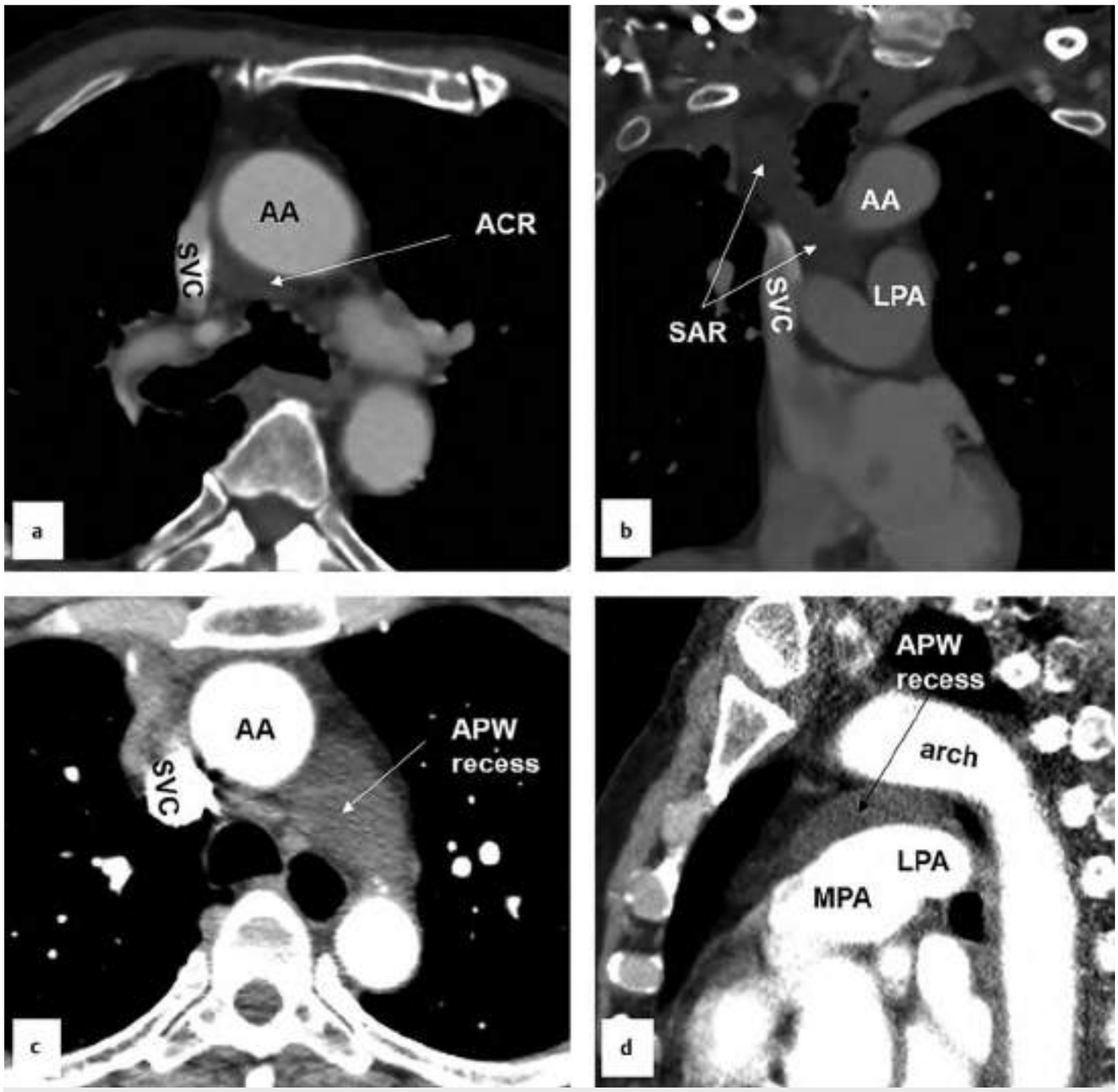

Fig. 20.10 Variants of the pericardial recess. **(a, b)** Axial and coronal CT images showing a high riding aortocaval recess (ACR) with its superior margin rising to the level of the thoracic inlet. **(c, d)** Axial and coronal CT images showing a large aortopulmonary window (APW) recess. Note the posterior margin of the pericardial sac extending to the left pulmonary artery (LPA) orifice. AA, ascending aorta; LPA, left pulmonary artery; MPA, main pulmonary artery; SAR, superior aortic recess; SVC, superior vena cava.

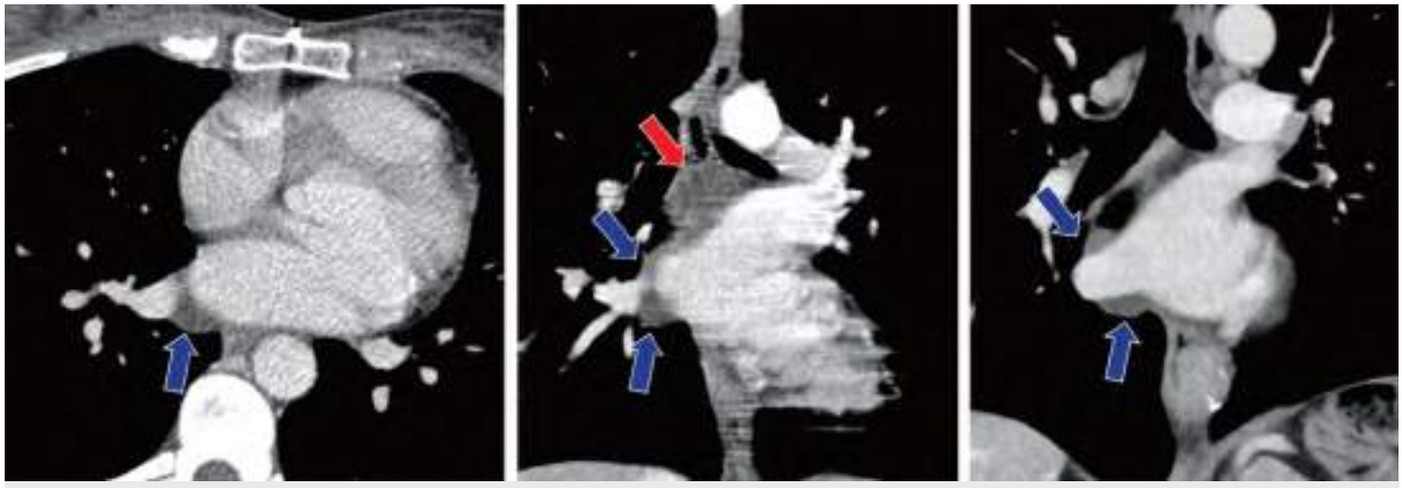

Fig. 20.11 Axial and coronal CT images. Right pulmonary vein recess (*blue arrows*) surrounding the right inferior pulmonary vein ostium. Coronal CT in the middle also shows a large superior extent of the oblique recess up to the subcarinal level (*red arrow*).

(▶ Fig. 20.9). Of relevance to interventional electrophysiology, the inferior aortic recess allows access to the epicardial aspect of the noncoronary and left coronary aortic sinuses.[14]

Oblique Sinus

The oblique sinus is located behind the left atrium, in the region between the four pulmonary veins and commonly contains a small amount of fluid, which makes it visible in 80 to 90% of CT scans[10] (▶ Fig. 20.4, ▶ Fig. 20.5). Posteriorly, it is bounded by the pericardial reflection on the ostial region of the pulmonary veins and the inferior vena cava where it forms small recesses. Superiorly, the oblique sinus is separated from the transverse sinus by a double reflection of serous pericardium extending between the left and right superior pulmonary veins[14] (▶ Fig. 20.4, ▶ Fig. 20.5). The size and shape of the oblique sinus is variable (▶ Fig. 20.8). The average width of the oblique sinus opening is 41 ± 7 mm and its depth is 31 ± 6.3 mm.[9] The depth of the pulmonary vein recesses is also variable and may be confused with pathologies such as enlarged lymph nodes (▶ Fig. 20.11). The left pulmonary vein recess is depicted at CT more often (60%) than the right pulmonary vein recess (30%).[10] Immediately behind the oblique sinus, the esophagus and the plexal branches of the vagus nerve pass (▶ Fig. 20.6). This anatomical relationship varies and its clinical relevance is related to cases admitted for radiofrequency ablation of the posterior wall of the left atrium with the potential injury of the passing esophagus and vagal nerves. The fold of Marshall is located in the left superior aspect of the sinus containing ligament or vein of Marshall, which is located between the left atrial appendage and the left superior pulmonary vein.[14,15]

◆ Imaging of the Pericardium

Transthoracic echocardiography is commonly used for evaluation of the pericardial fluid. CT and MRI are equally considered the preferred imaging methods for morphological assessment of the pericardial sac and the pericardium. Higher spatial resolution of the CT scan allows improved visualization of the normal pericardium. The normal pericardium can be identified at CT images as a thin (< 2 mm) smooth line of soft-tissue attenuation (isodense to the normal myocardium) outlined by low-attenuation mediastinal and epicardial fat (▶ Fig. 20.12). On MRI, the fibrous pericardium appears low in signal intensity on most sequences and is surrounded by high-intensity mediastinal and epicardial fat (▶ Fig. 20.12**b**). The pericardium is best visualized along the right atrium and ventricle (▶ Fig. 20.12). Physiologic amount of pericardial fluid allows imaging visualization of the pericardial recesses and parietal/fibrous pericardium. Generally, a pericardium thicker than 3 mm is considered abnormal. Although evaluation of pericardium and pericardial fluid is possible on nongated CT scans, electrocardiographic (ECG) gated methods are usually preferred particularly when detailed evaluation of the pathologies is required. For example, pericardial cysts or effusions can be characterized in most nongated CT scans of the heart, whereas detection of partial absence of pericardium can be optimally performed using a gated CT.

Percutaneous Approach to Pericardial Cavity

The pericardial space can be entered through a subxiphoid puncture technique using a spinal needle under CT or fluoroscopic guidance. The safest entry point is 2 to 3 cm below a line that joins the xiphoid process and the costal margin, left of the midline[14] (▶ Fig. 20.7**b**). Using CT guidance, the pericardial sac can also be approached anteriorly through the chest wall. The later technique is only used to drain pericardial fluid when the amount of fluid is large enough and the risk of myocardial injury is minimal.

The pericardial sac has also been used for placement of the epicardial leads, to exclude left atrial appendage, to treat cardiac arrhythmias, and for cardiac resynchronization therapy.[14,15]

Catheter exploration of the transverse sinus allows access to the anterior portion of the left atrium, the area of Bachman's bundle, and the noncoronary cusp. The oblique sinus provides access to the retroatrial ganglionated plexuses around the posterior and lateral aspects of the left atrium. The fold of Marshall can

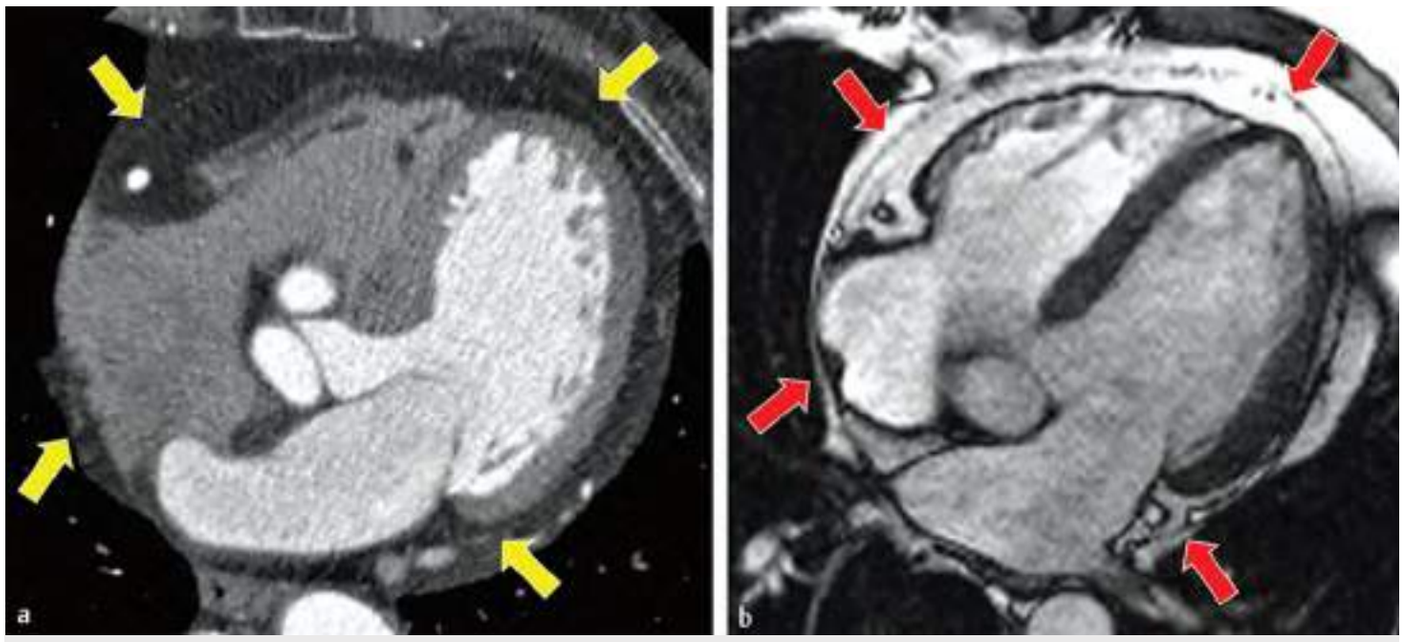

Fig. 20.12 Normal pericardium on CT **(a)** and MR **(b)** images. Images of the heart show the epicardial (inside) fat, the mediastinal (outside) fat, and the thin line of the pericardial sac (*arrows*) between the two adipose tissue compartments. On MRI, the fibrous pericardium appears low in signal intensity; the coronary vessels and coronary sinus are embedded in the epicardial fat.

be accessed through the oblique sinus for percutaneous ablation of certain ventricular arrhythmias.[15,16,17]

◆ Common Pathologies

Pericardial fluid accumulation (effusion) may occur in patients with heart failure, renal and liver insufficiency, inflammation, infection, neoplastic disease, trauma, and myocardial infarction[18] (▶ Fig. 20.13, ▶ Fig. 20.14). Imaging is often necessary to confirm the presence, severity, and extent of fluid. Fluid, whether blood, pus, or transudation, can be characterized by imaging. The pericardial sac has a limited capacity for stretching. Therefore, fast accumulation of a moderate amount of fluid can cause a substantial elevation in pericardial pressures and cardiac tamponade. However, slow accumulation of fluid (up to 2 L or more) can cause a large effusion. Typical findings of cardiac tamponade include compression of the right atrial or RV wall and distention of the caval veins (▶ Fig. 20.14).

Acute pericarditis is an important differential diagnosis of acute chest pain and is observed in about 5% of patients admitted to the emergency department.[18] In constrictive pericarditis, the compliance of the pericardium is decreased due to extensive calcifications or thickening (> 4 mm) of the parietal pericardium, which may result in impaired ventricular filling, severe diastolic dysfunction, and right heart failure (▶ Fig. 20.13**b**).

Pneumopericardium is a common finding after mediastinal surgery and pericardiectomy (▶ Fig. 20.15). Secondary involvement of the pericardium by a malignant process is common. Primary pericardial tumors are extremely rare. Malignant mesothelioma is the most common primary lesion.

Among congenital pericardial diseases, pericardial cyst is a common incidental finding in imaging studies of the thorax. Pericardial cyst is a congenital encapsulated cyst lined by mesothelium and filled with clear fluid. It is proposed that pericardial cyst derives from abnormal closure of the ventral recess of the pericardial coelom.[19] Pericardial cyst typically occurs at the cardiophrenic angle (90%) and in 20% may communicate with the pericardium (this variant is called diverticulum; ▶ Fig. 20.16).[20]

Partial pericardial defect especially on the right side is a common finding after cardiomediastinal surgery and most are related to pericardiectomy. On the other hand, congenital absence of the pericardium is a very rare condition and usually involves the left pericardium.[21,22] As mentioned earlier, the development of the pericardial and pleural cavities and the diaphragm is closely linked. Major part of the pericardium is derived from the parietal mesoderm of the pericardioperitoneal canals. The dorsal and inferior portions are probably derived from the mesoderm at the root of the dorsal mesocardium and the septum transversum (a derivative of the visceral layer). Premature atrophy of the left common cardinal vein may play a role in the abnormal development of the left pericardium.[1,2] The diagnosis usually needs confirmation by CT or MR as they more clearly delineate the anatomical relationships with adjacent structures than other modalities.[20] Despite high resolution and contrast in CT and MR, it is not always possible to trace the exact margins of the pericardial defect.

◆ Extracardiac Fat

The extracardiac or pericardial fat composes of the epicardial fat and the paracardial fat[23,24,25,26] (▶ Fig. 20.17, ▶ Fig. 20.18). The paracardial (mediastinal) fat is situated on the external surface of the parietal pericardium within the mediastinum. The epicardial (subepicardial) fat is located between the visceral layer of the pericardium and the myocardium. The epicardial adipose tissue is supplied by branches of the coronary arteries, whereas the mediastinal fat is supplied from different sources including the superior

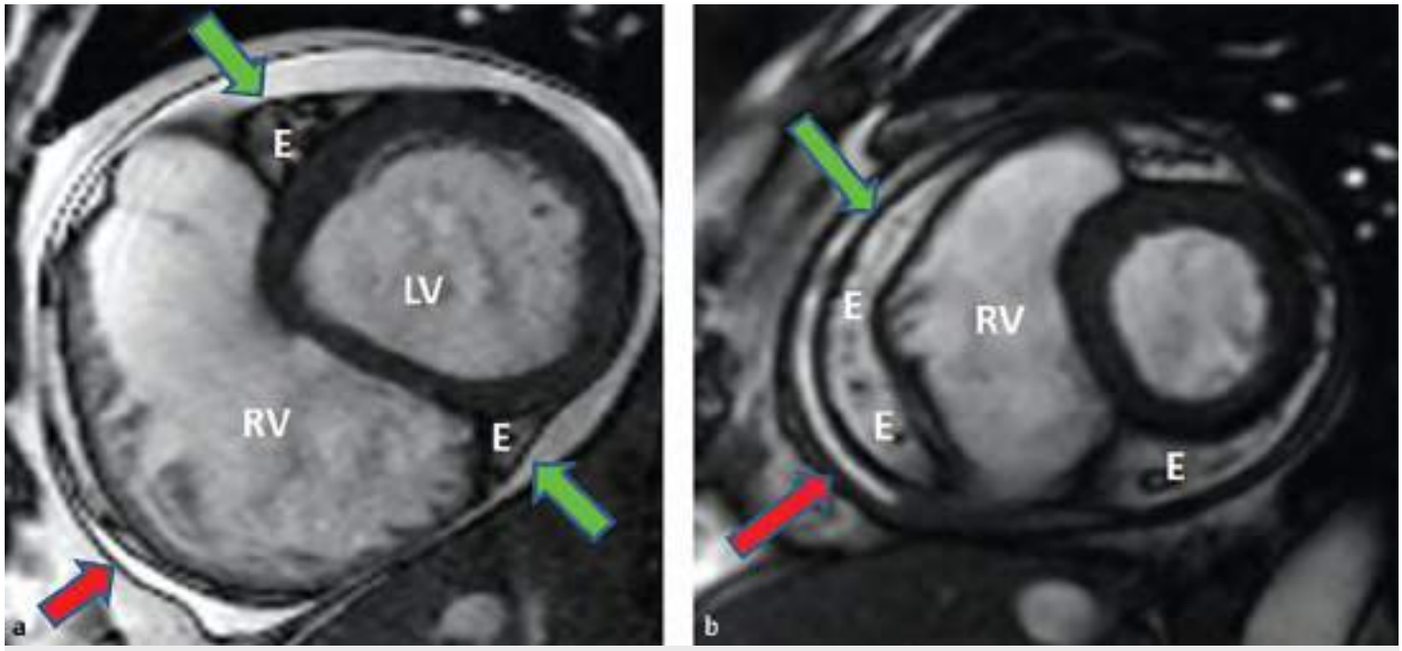

Fig. 20.13 Short-axis cine MR views in a patient with serous pericardial effusion **(a)** and another patient with constrictive pericarditis **(b)**. Both visceral (*green arrows*) and parietal (*red arrow*) pericardia appear thin and smooth in pericardial effusion case but show diffuse thickening in constrictive pericarditis. E, epicardial fat; LV, left ventricle; RV, right ventricle.

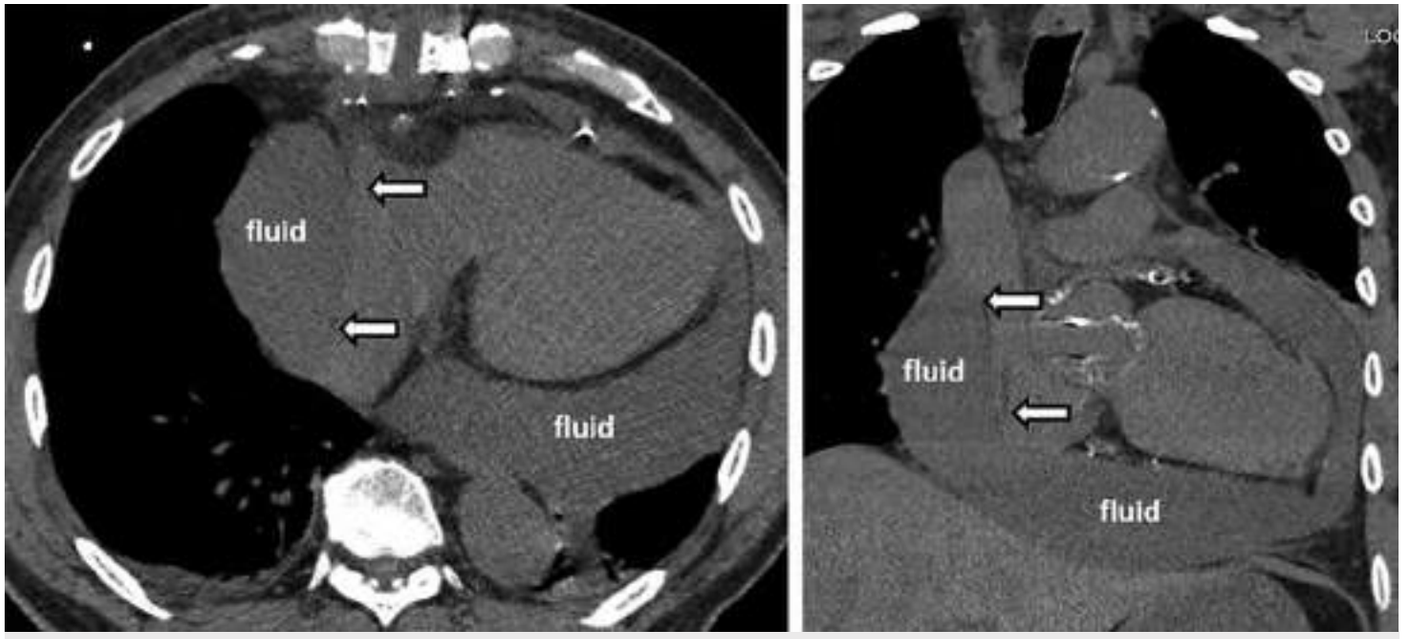

Fig. 20.14 Axial and coronal noncontrast CT images showing a large pericardial effusion in a patient with recent coronary artery bypass surgery. This form of reactive pericardial effusion is called postpericardiotomy syndrome. Note compression deformity of the lateral wall of the right atrium (*arrows*). Postpericardiotomy syndrome is a frequent complication of cardiac operations in 20 to 40% of patients usually appearing within a couple of months of the initial operation.

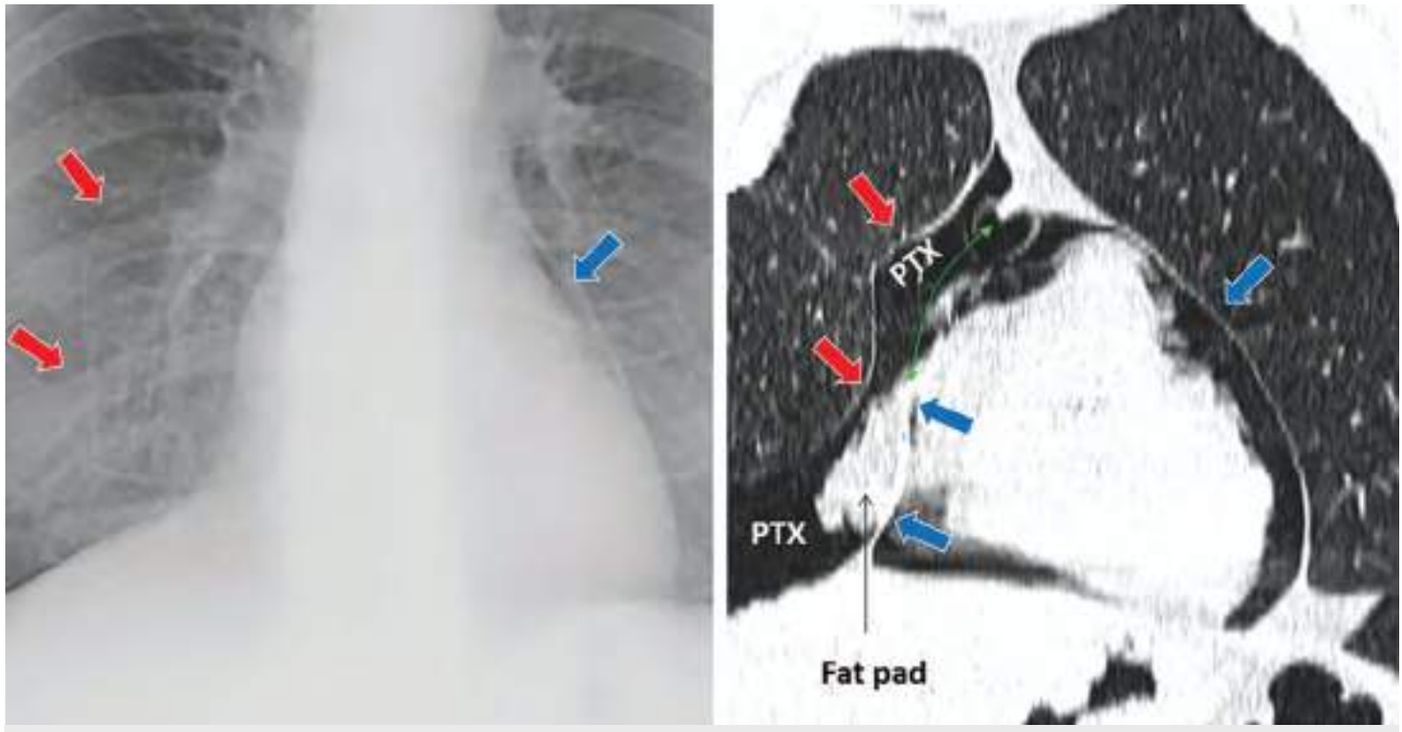

Fig. 20.15 Chest X-ray and coronal CT show a medium-sized right pneumothorax (PTX) with pleural air entering into the pericardial sac through a large right superior pericardial defect (*double-headed green arrow*) after pericardiectomy. The pericardial margin is shown by *blue arrows* and the mediastinal pleural margin by *red arrows*.

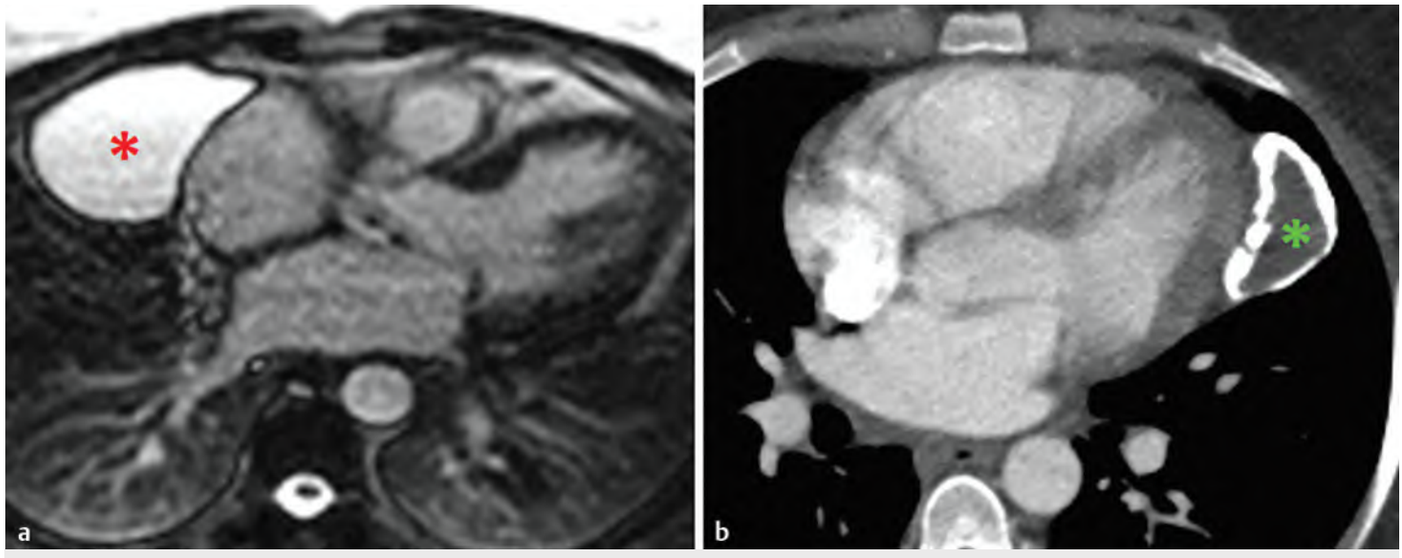

Fig. 20.16 Pericardial cysts. **(a)** Axial T2-weighted MR shows a high signal (*star*) cyst in typical location at the right anterior cardiophrenic angle. **(b)** Axial CT shows a calcified pericardial cyst (*star*) adjacent to the lateral wall of the left ventricle.

pericardial, middle pericardial, and pericardiophrenic arteries, branches of the internal mammary artery.[27]

The epicardial, mesenteric, and omental fats all share the same origin from the splanchnopleuric mesoderm associated with the gut. The epicardium forms from mesothelial cells associated with the septum transversum and is referred to as the proepicardium organ.[23,24]

The epicardial fat covers 80% of the heart's surface and is largely concentrated around the anatomic course of the coronary vessels in the atrioventricular or interventricular grooves.[25,26] There is threefold to fourfold more epicardial fat associated with the right than the left ventricle. Only a small amount of fat is present posteriorly. The epicardial fat can extend between the myocardial muscle bundles often following the adventitia of the penetrating coronary artery branches. Islands of mature adipocytes are more frequent within the subepicardial myocardium of the right ventricle than the left ventricle.[28,29] This finding is a relatively common finding in cardiac CT studies (▶ Fig. 20.17, ▶ Fig. 20.18).

The epicardial fat is not limited to the surface of the heart but can penetrate deep in the interatrial groove and septal atrioventricular junction. Because the subepicardial fat is covered by the pericardium, it cannot escape beyond the boundaries of the

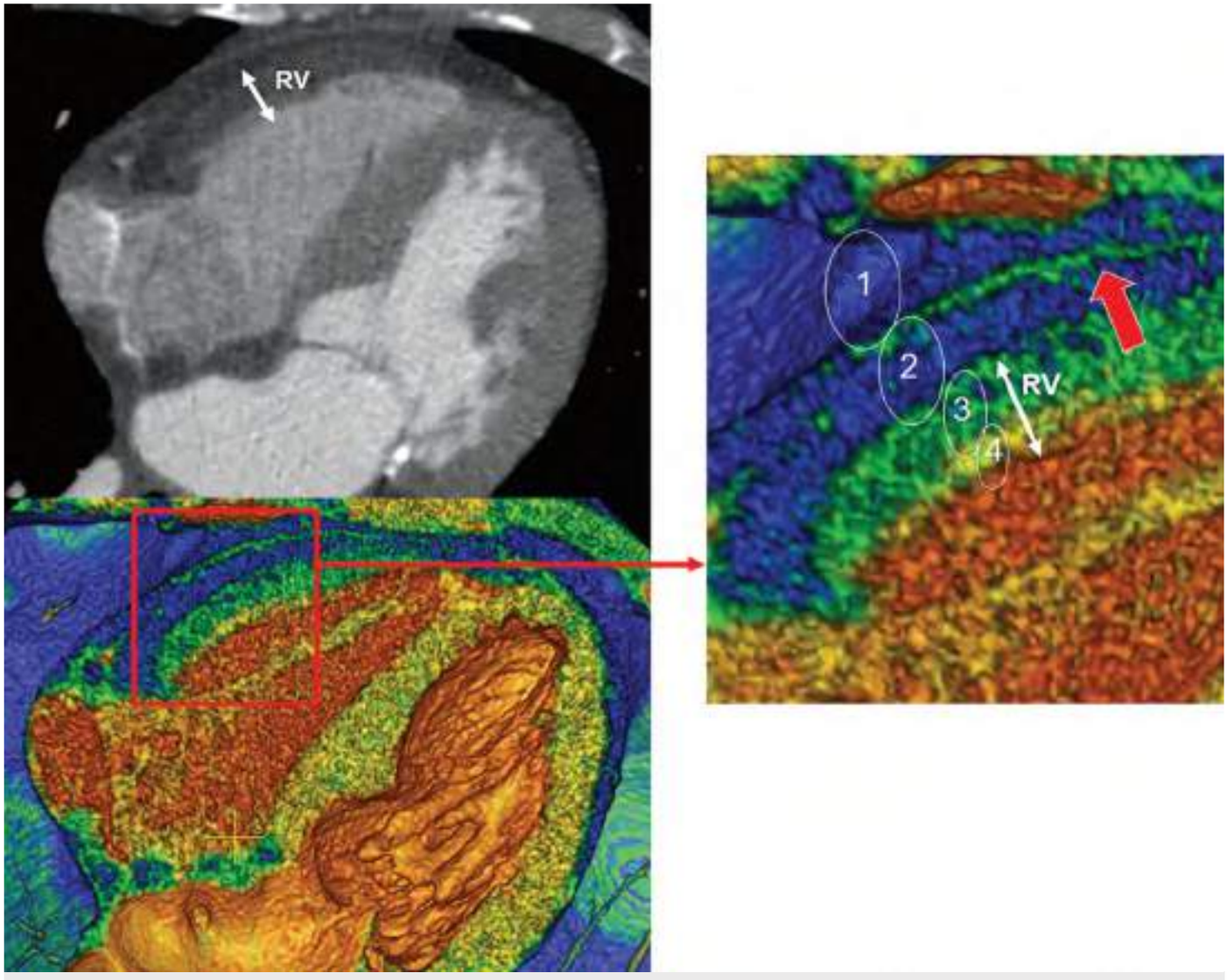

Fig. 20.17 Anatomy of the extracardiac fat. Axial CT image of the heart and color-coded version show compartments of the pericardial fat. The mediastinal (#1) and epicardial (#2) fat are seen as *blue*. The pericardial sac is shown as a thin line between the two compartments (*red arrow*). Fatty infiltration of the free wall of the right ventricle (RV) is shown changing the yellow color of the normal right myocardium (#4) to bluish green (#3) and also causing thickening of the myocardial wall (*double-headed arrow*). The endocardial RV surface is intact. Fatty infiltration of the free wall of the RV is common in elderly and large-weight patients.

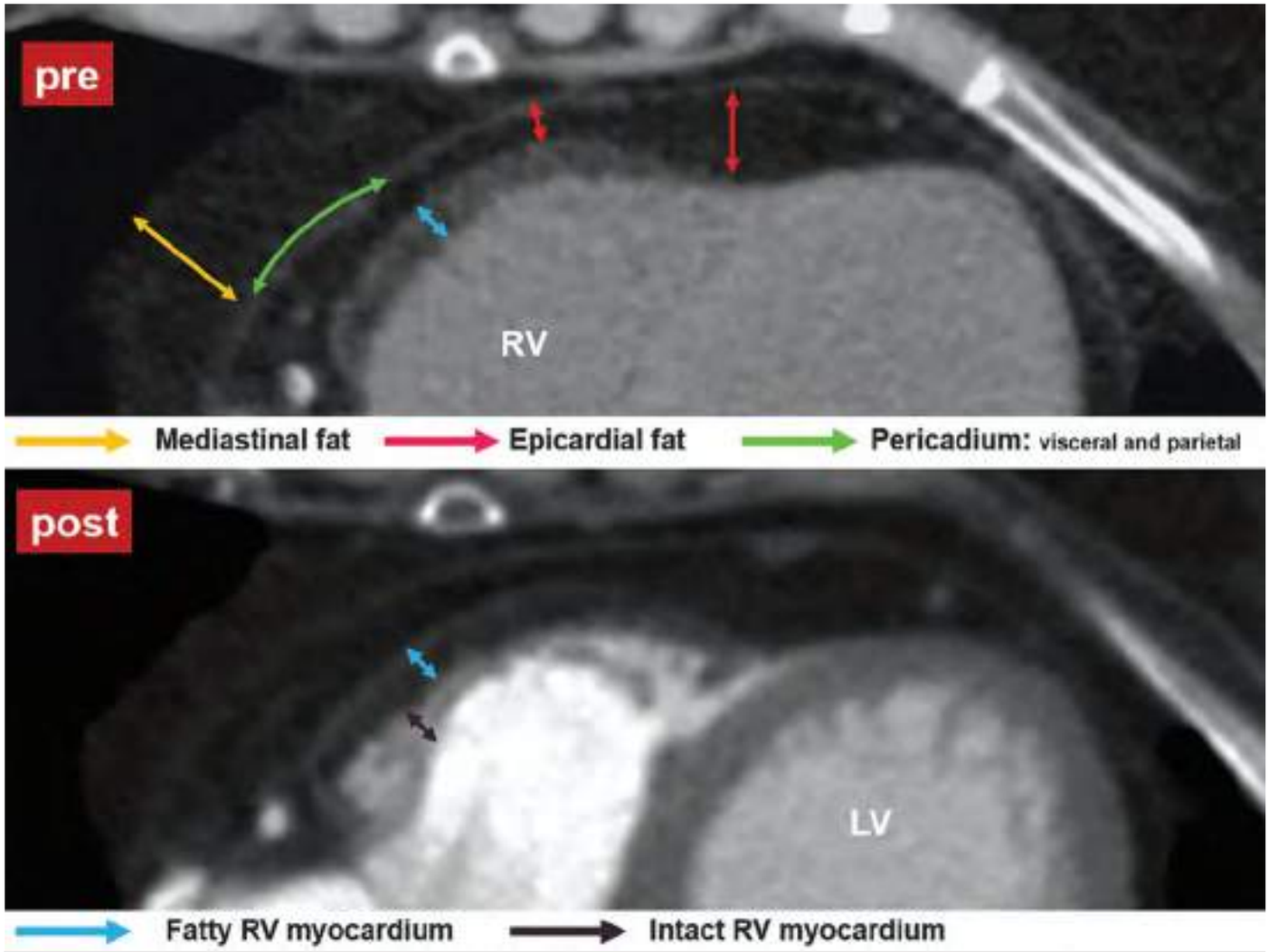

Fig. 20.18 Anatomy of the extracardiac fat and pericardium. Axial CT images are shown. Cardiac fat resides in three locations: epicardial, mediastinal (pericardial), and right intramyocardial. Adipose and muscular components of the heart share the same coronary blood supply, and no fascia separates the adipose and myocardial layers. LV, left ventricle; RV, right ventricle.

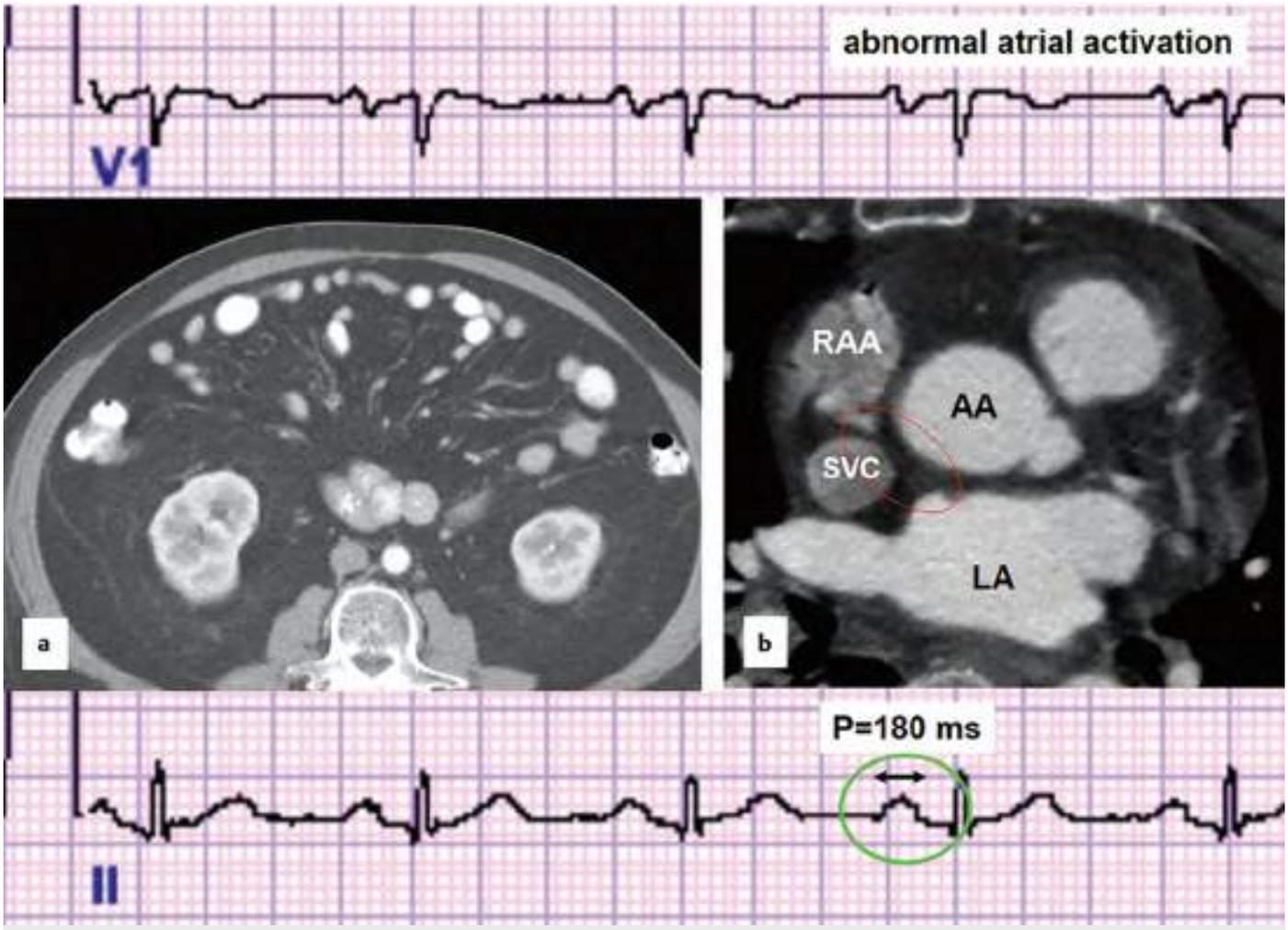

Fig. 20.19 Interatrial block (p > 120 ms) secondary and fatty replacement of Bachmann's bundle. **(a)** Axial CT of the abdomen showing large visceral fat compared to the subcutaneous fat. **(b)** Axial cardiac CT shows large amount of epicardial fat infiltrating and replacing normal myocardial band in the region of Bachmann's bundle (*red circle*). ECG shows P-wave duration of greater than 120 ms (identified as interatrial conduction block) representing delayed left atrial activation due to abnormalities in Bachmann's bundle. The interatrial conduction block is important because it is associated with abnormal atrial activation with increasing risk of atrial fibrillation. AA, ascending aorta; LA, left atrium; RAA, right atrial appendage; SVC, superior vena cava.

pericardium. Excess subepicardial fat will deposit around the caval vessels, and coronary sinus, or within the Bachmann bundle, crista terminalis, Eustachian ridge, and myocardium, and may interfere with the normal conduction function and provoke automaticity[30] (▶ Fig. 20.19). Excess accumulation of fat within the interatrial groove, which surrounds the interatrial septum, is known as lipomatous hypertrophy of the septum. At the base of the heart, the epicardial fat is continuous with the mediastinal fat. As a result, inflammatory and malignant pathologies of the mediastinum may penetrate inside along the epicardial fat planes to involve heart chambers.

Increased epicardial fat is directly related to the amount of visceral fat, age, weight, and key components of the metabolic syndrome[31,32] (▶ Fig. 20.19**a**). It is an important factor responsible for cardiovascular disease in obesity.[33] Excess epicardial fat reduces cardiac contractility, especially in the right ventricle.[34]

References

[1] Norden J, Grieskamp T, Christoffels VM, Moorman AF, Kispert A. Partial absence of pleuropericardial membranes in Tbx18- and Wt1-deficient mice. PLoS One.; 7(9):e45100

[2] Norden J, Grieskamp T, Lausch E, et al. Wt1 and retinoic acid signaling in the subcoelomic mesenchyme control the development of the pleuropericardial membranes and the sinus horns. Circ Res.; 106(7):1212–1220

[3] Choe YH, Im JG, Park JH, Han MC, Kim CW. The anatomy of the pericardial space: a study in cadavers and patients. AJR Am J Roentgenol.; 149(4):693–697

[4] Vesely TM, Cahill DR. Cross-sectional anatomy of the pericardial sinuses, recesses, and adjacent structures. Surg Radiol Anat.; 8(4):221–227

[5] Levy-Ravetch M, Auh YH, Rubenstein WA, Whalen JP, Kazam E. CT of the pericardial recesses. AJR Am J Roentgenol.; 144(4):707–714

[6] Kodama F, Fultz PJ, Wandtke JC. Comparing thin-section and thick-section CT of pericardial sinuses and recesses. AJR Am J Roentgenol.; 181(4):1101–1108

[7] de Schlichting E, Robert Y, Selek L, Palombi O, Chaffanjon P. A three-dimensional (3D) representation of pericardial cavity based on computed tomography (CT). Surg Radiol Anat.; 37(2):199–204
[8] Bayer O, Schummer C, Richter K, Fröber R, Schummer W. Implication of the anatomy of the pericardial reflection on positioning of central venous catheters. J Cardiothorac Vasc Anesth.; 20(6):777–780
[9] Chaffanjon P, Brichon PY, Faure C, Favre JJ. Pericardial reflection around the venous aspect of the heart. Surg Radiol Anat.; 19(1):17–21
[10] Groell R, Schaffler GJ, Rienmueller R. Pericardial sinuses and recesses: findings at electrocardiographically triggered electron-beam CT. Radiology.; 212 (1):69–73
[11] Choi YW, McAdams HP, Jeon SC, Seo HS, Hahm CK. The "High-Riding" superior pericardial recess: CT findings. AJR Am J Roentgenol.; 175(4):1025–1028
[12] Winer-Muram HT, Gold RE. Effusion in the superior pericardial recess simulating a mediastinal mass. AJR Am J Roentgenol.; 154(1):69–71
[13] Protopapas Z, Westcott JL. Left pulmonic recess of the pericardium: findings at CT and MR imaging. Radiology.; 196(1):85–88
[14] D'Avila A, Scanavacca M, Sosa E, Ruskin JN, Reddy VY. Pericardial anatomy for the interventional electrophysiologist. J Cardiovasc Electrophysiol.; 14 (4):422–430
[15] Lachman N, Syed FF, Habib A, et al. Correlative anatomy for the electrophysiologist, part I: the pericardial space, oblique sinus, transverse sinus. J Cardiovasc Electrophysiol.; 21(12):1421–1426
[16] d'Avila A, Koruth JS, Dukkipati S, Reddy VY. Epicardial access for the treatment of cardiac arrhythmias. Europace.; 14 Suppl 2:ii13–ii18
[17] Sosa E, Scanavacca M, d'Avila A, Oliveira F, Ramires JAF. Nonsurgical transthoracic epicardial catheter ablation to treat recurrent ventricular tachycardia occurring late after myocardial infarction. J Am Coll Cardiol.; 35(6):1442–1449
[18] Bogaert J, Francone M. Pericardial disease: value of CT and MR imaging. Radiology.; 267(2):340–356
[19] Lillie WI, McDONALD JR, Clagett OT. Pericardial celomic cysts and pericardial diverticula; a concept of etiology and report of cases. J Thorac Surg.; 20 (3):494–504
[20] Patel J, Park C, Michaels J, Rosen S, Kort S. Pericardial cyst: case reports and a literature review. Echocardiography.; 21(3):269–272
[21] Nasser WK, Helmen C, Tavel ME, Feigenbaum H, Fisch C. Congenital absence of the left pericardium. Clinical, electrocardiographic, radiographic, hemodynamic, and angiographic findings in six cases. Circulation.; 41(3):469–478
[22] Faridah Y, Julsrud PR. Congenital absence of pericardium revisited. Int J Cardiovasc Imaging.; 18(1):67–73
[23] Nesbitt T, Lemley A, Davis J, Yost MJ, Goodwin RL, Potts JD. Epicardial development in the rat: a new perspective. Microsc Microanal.; 12(5):390–398
[24] Ho E, Shimada Y. Formation of the epicardium studied with the scanning electron microscope. Dev Biol.; 66(2):579–585
[25] Marchington JM, Mattacks CA, Pond CM. Adipose tissue in the mammalian heart and pericardium: structure, foetal development and biochemical properties. Comp Biochem Physiol B.; 94(2):225–232
[26] Shirani J, Berezowski K, Roberts WC. Quantitative measurement of normal and excessive (cor adiposum) subepicardial adipose tissue, its clinical significance, and its effect on electrocardiographic QRS voltage. Am J Cardiol.; 76 (5):414–418
[27] Anderson TM, Miller JI, Jr. Surgical technique and application of pericardial fat pad and pericardiophrenic grafts. Ann Thorac Surg.; 59(6):1590–1591
[28] Tansey DK, Aly Z, Sheppard MN. Fat in the right ventricle of the normal heart. Histopathology.; 46(1):98–104
[29] Iacobellis G, Corradi D, Sharma AM. Epicardial adipose tissue: anatomic, biomolecular and clinical relationships with the heart. Nat Clin Pract Cardiovasc Med.; 2(10):536–543
[30] Bharati S, Lev M. Cardiac conduction system involvement in sudden death of obese young people. Am Heart J.; 129(2):273–281
[31] Wheeler GL, Shi R, Beck SR, et al. Pericardial and visceral adipose tissues measured volumetrically with computed tomography are highly associated in type 2 diabetic families. Invest Radiol.; 40(2):97–101
[32] Iacobellis G, Ribaudo MC, Assael F, et al. Echocardiographic epicardial adipose tissue is related to anthropometric and clinical parameters of metabolic syndrome: a new indicator of cardiovascular risk. J Clin Endocrinol Metab.; 88 (11):5163–5168
[33] Mazurek T, Zhang L, Zalewski A, et al. Human epicardial adipose tissue is a source of inflammatory mediators. Circulation.; 108(20):2460–2466
[34] House AA, Walley VM. Right heart failure due to ventricular adiposity: "adipositas cordis"—an old diagnosis revisited. Can J Cardiol.; 12(5):485–489

21 Appendix

◆ Catheter, Support Devices and Drains on Plain X-rays

- Biventricular ICD/pacer, is pacemaker or implantable cardioverter-defibrillator (ICD) with three leads, one is placed in the right atrium, the second lead in the right ventricle and the third lead in the coronary sinus. It is used for cardiac resynchronization therapy in heart failure patients.
- CardioMEMS, is a wireless pulmonary artery pressure monitor. It is used to monitor pulmonary artery pressure in patients with congestive heart failure.
- Dual chamber pacemaker, is a pacer or ICD with two leads, one is placed in the right atrium and second in the right ventricle. Its generator is implanted under the skin of chest wall. It is used to treat bradycardia and atrial fibrillation associated with bradycardia.
- DL-CVC=Double lumen central venous catheter, is most often used when an immediate need for hemodialysis arises
- Impella, is an intraventricular pump that provides left-sided or right-sided temporary cardiac support.
- IPMD= intrapulmonary pressure monitoring device
- IABP= intra-aortic balloon pump, is a catheter that is placed in the descending aorta with a distal marker that should be advanced to the distal aortic arch, approximately 2-cm from the origin of the left subclavian artery. It consists of a balloon which deflates in systole and inflates in diastole via counter pulsation. The device increases myocardial oxygen perfusion and increases cardiac output through afterload reduction.
- LVAD=left ventricular assist device, an electromechanical heart pump for assisting the function of a failing heart.
- LAA= Left atrial appendage occlusion device, is a clamp placed surgically over the neck of the LAA to reduce the risk of blood clot formation in the LAA, thereby preventing the risk of stroke in patients with non-valvular atrial fibrillation.
- MitraClip, is a device for percutaneous clipping of the mitral leaflets to reduce symptomatic mitral regurgitation
- Port-a-cath; an intravenous access catheter that is placed under the skin in the right side of the chest. The catheter is usually inserted in the internal jugular vein and the tip is advanced into the superior vena cava (SVC).
- PICC=peripherally inserted central catheter, an intravenous access catheter that is used for a prolonged administration of antibiotics or chemotherapy. The catheter is usually inserted in an antebrachial vein and the tip is advanced into the superior vena cava (SVC).
- SCV-CAC= subclavian vein central access catheter
- Swan-Ganz pulmonary artery catheter, a flow directed monitoring catheter that is usually inserted in the internal jugular vein and the tip is advanced into the pulmonary arteries. The catheter monitors the right atrial pressure, pulmonary artery pressure, pulmonary artery occlusion (wedge) pressure, and enables mixed venous blood sampling or infusing solutions.
- TAVI= transcatheter aortic valve implantation, is used to treat aortic stenosis. Common devices used include Medtronic's CoreValve and Edwards' Sapien aortic valve.
- Wireless (leadless) pacemaker or implantable cardioverter-defibrillator (ICD), is a device that is placed subcutaneously or in the apical right ventricle and has no leads.

Fig. 21.1

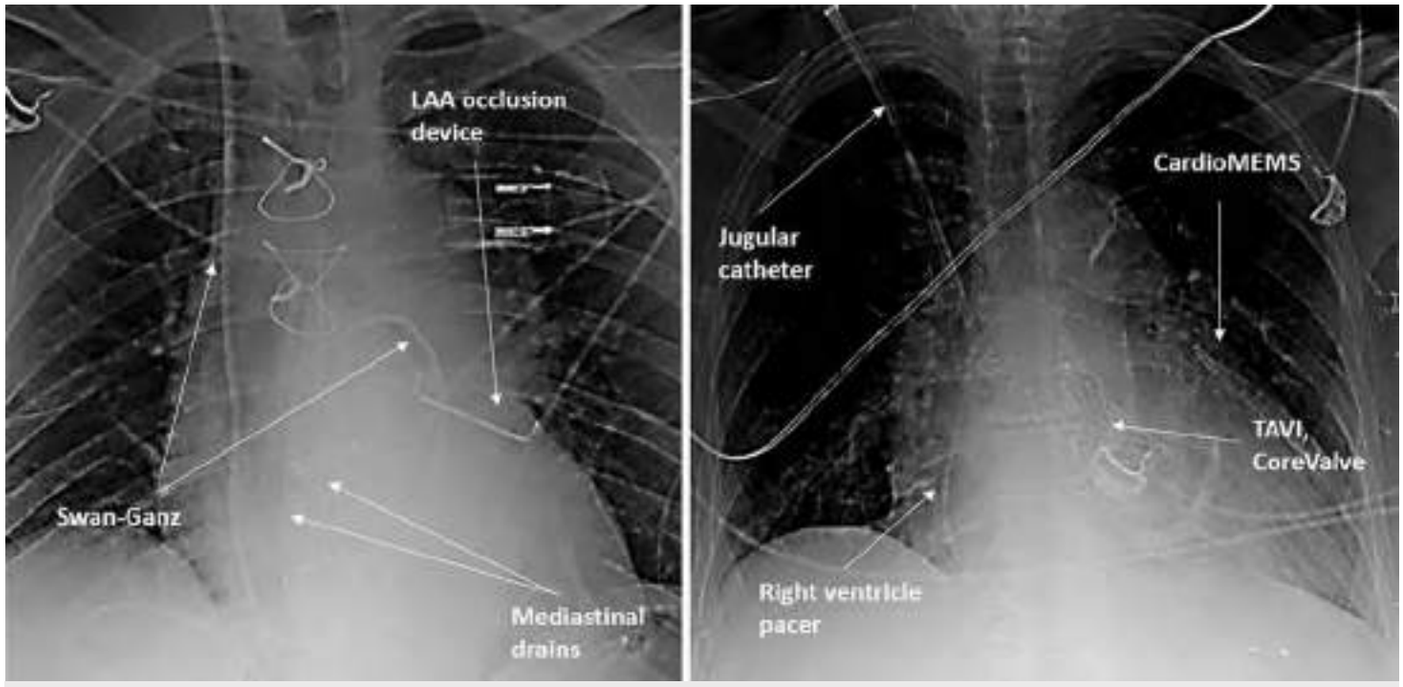

Fig. 21.2

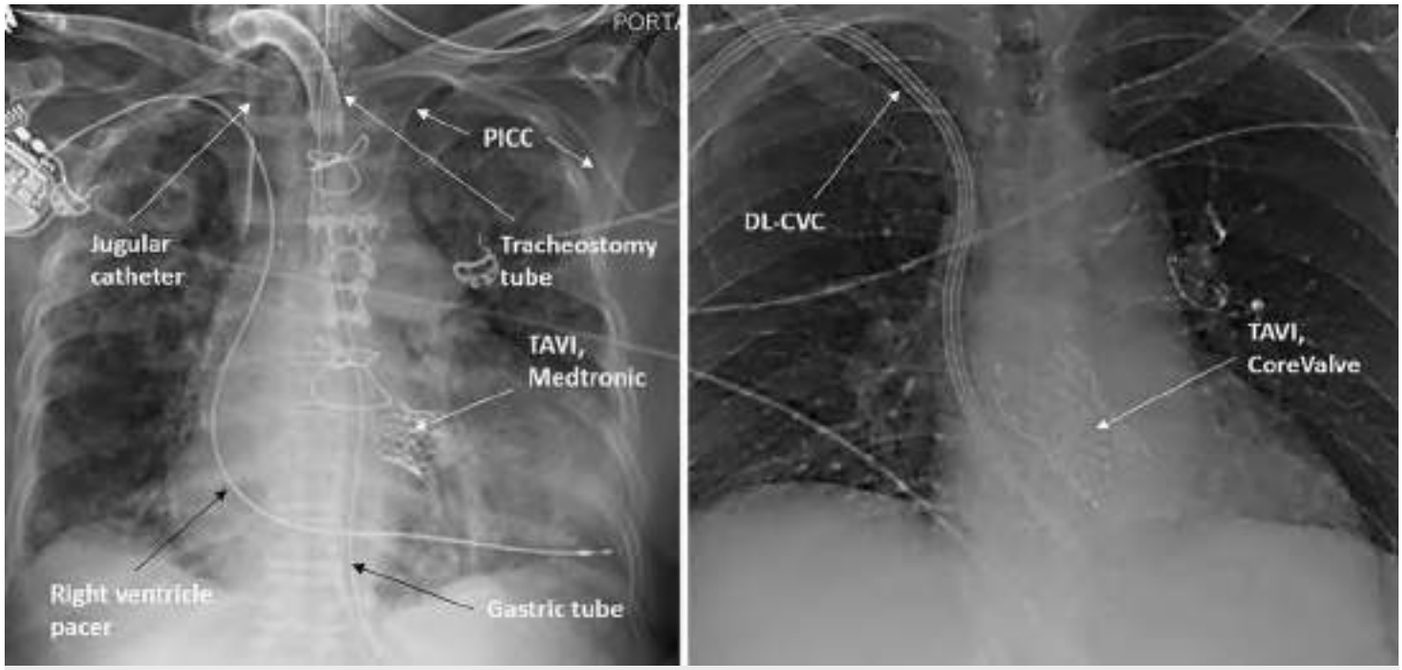

Fig. 21.3

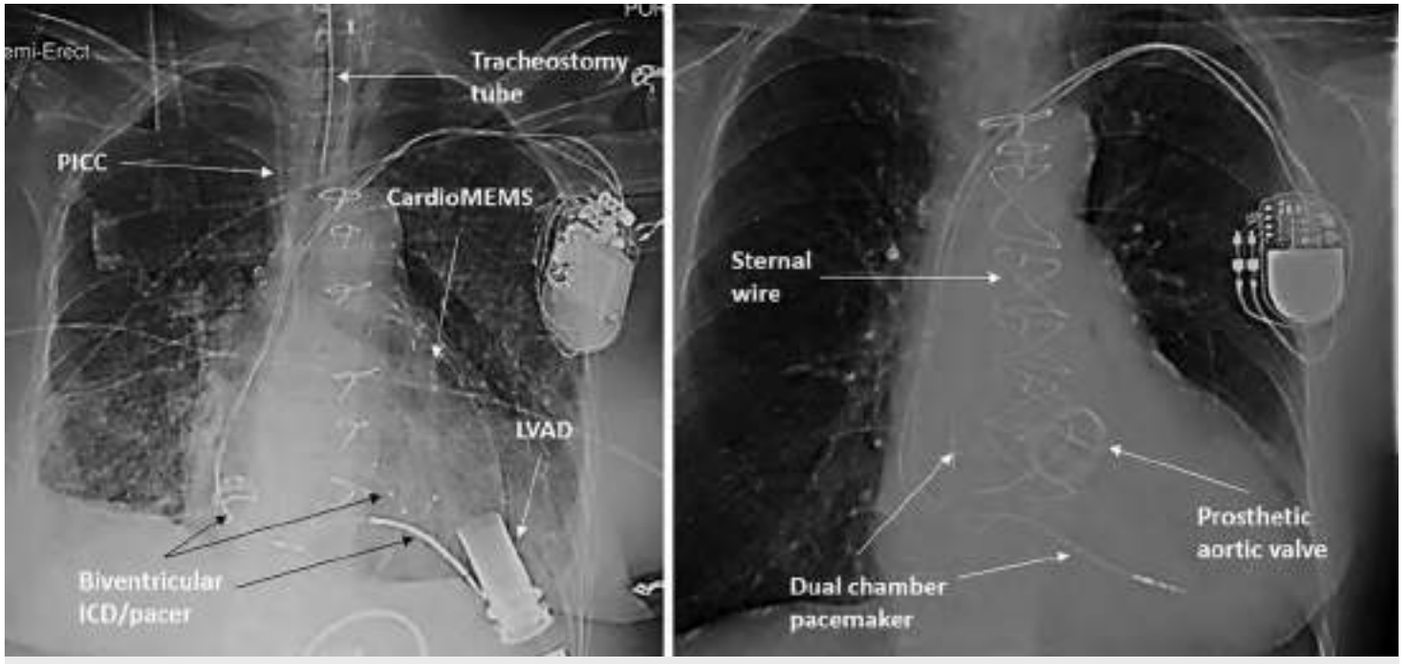

Fig. 21.4

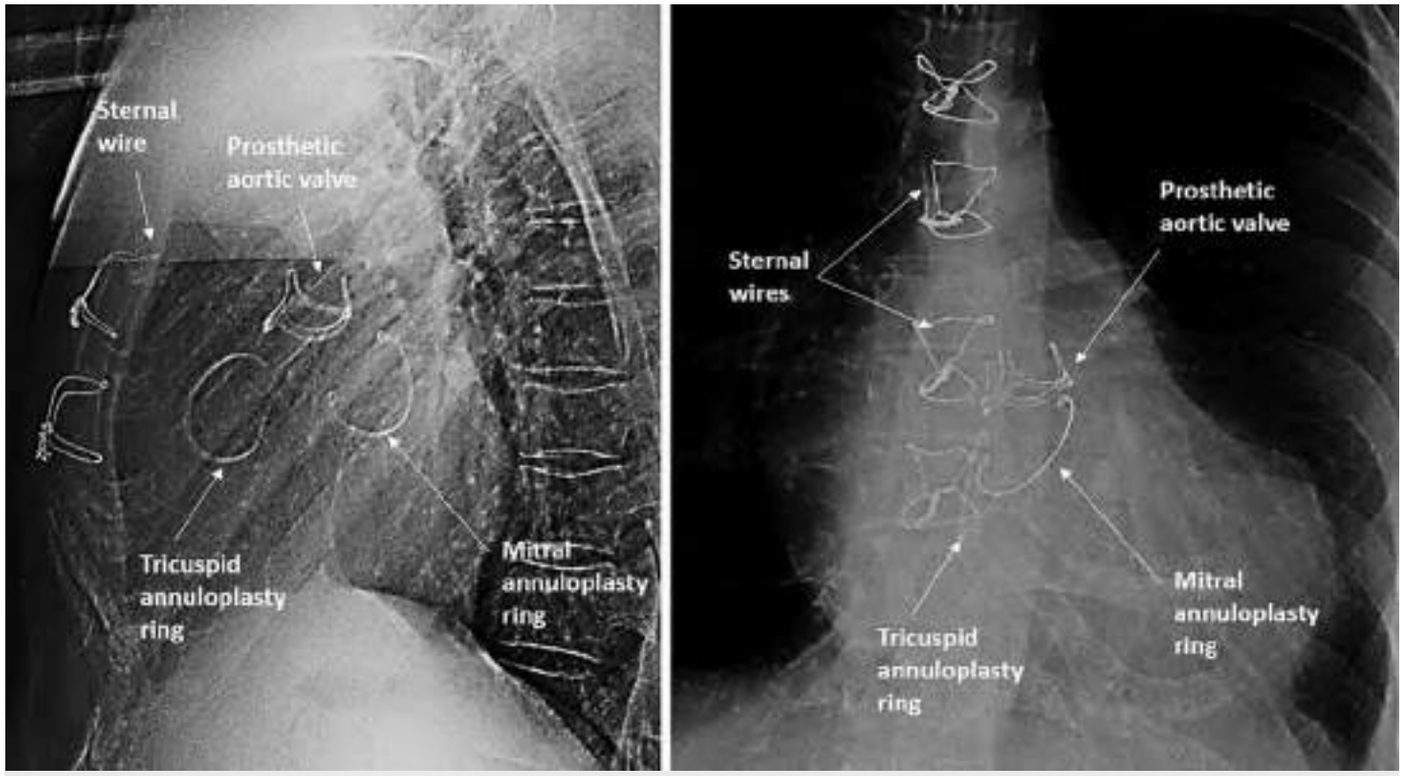

Fig. 21.5

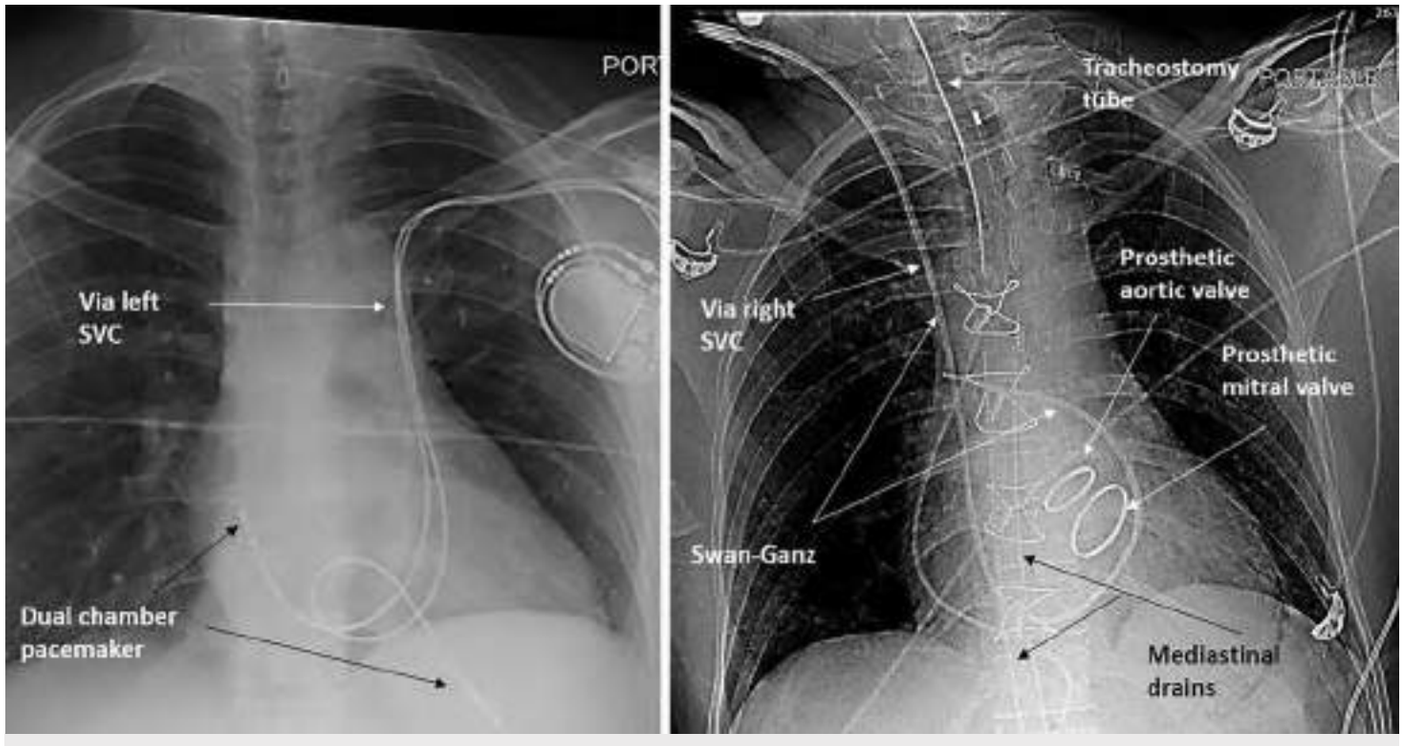

Fig. 21.6

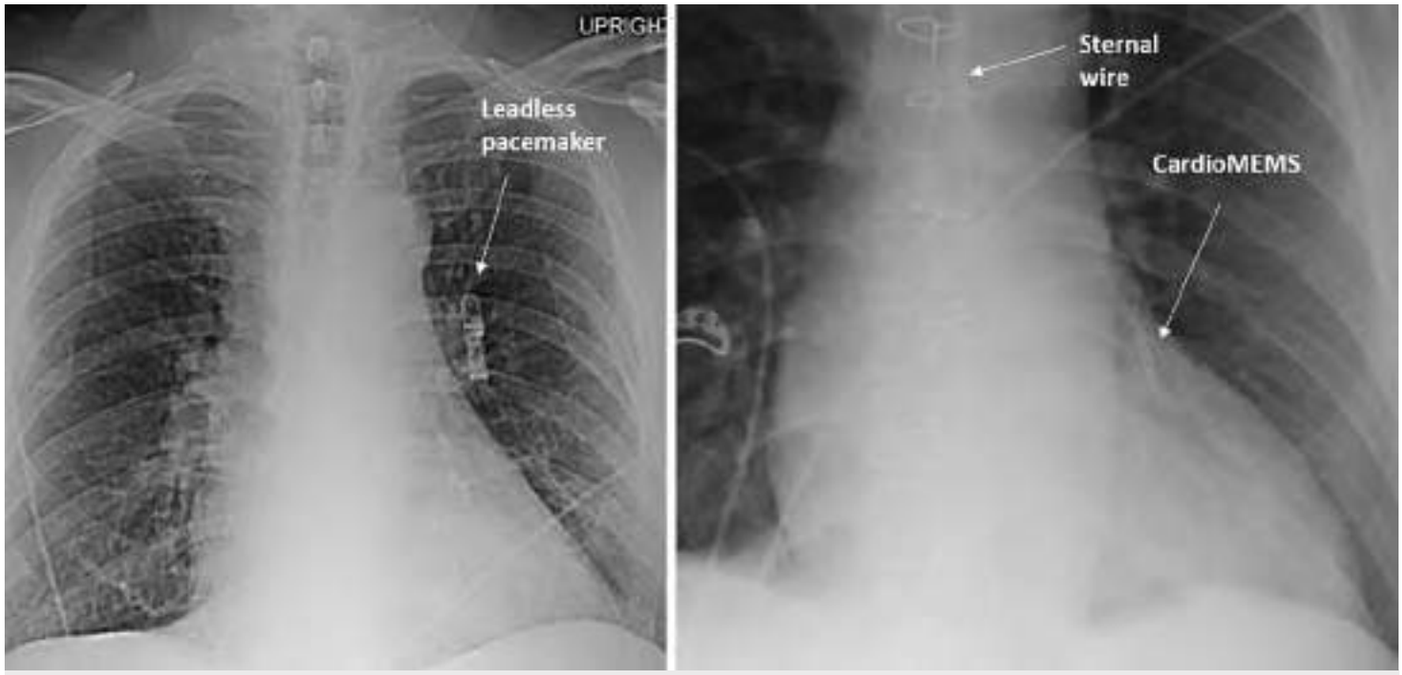

Fig. 21.7

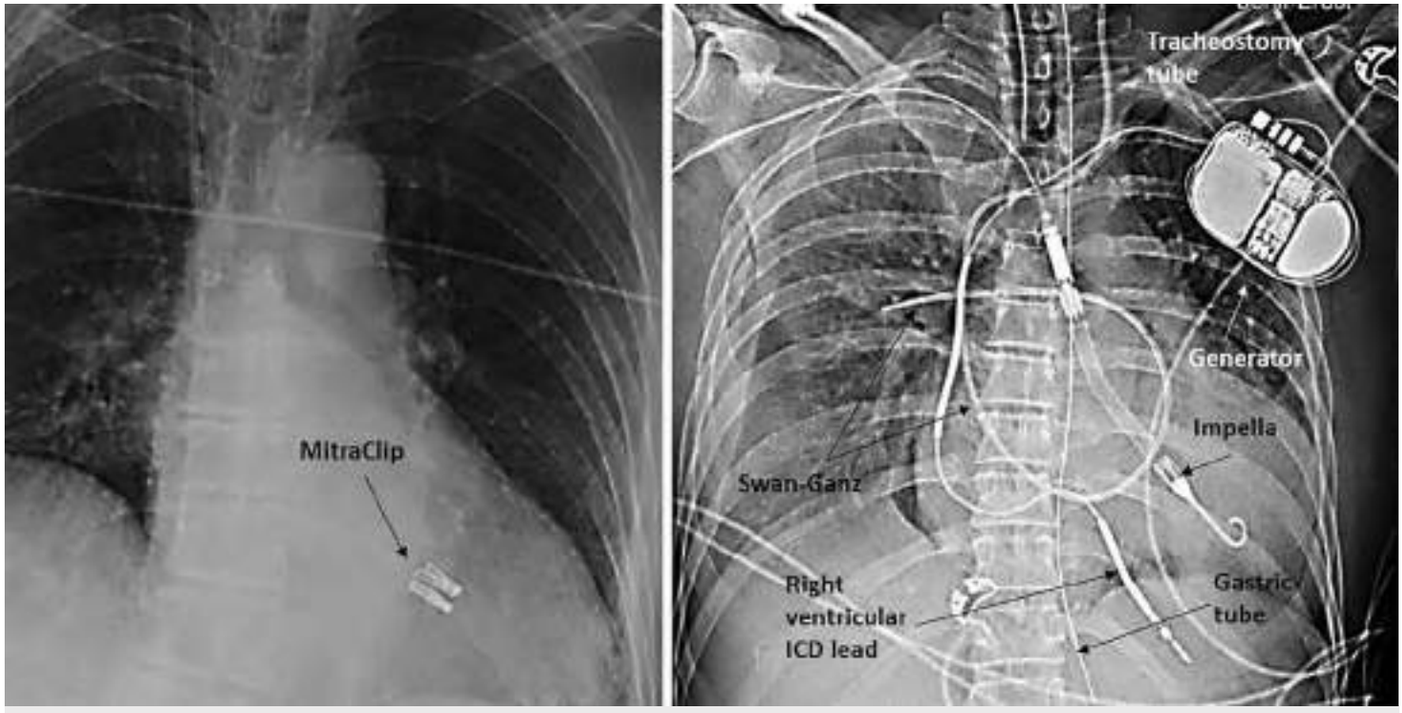

Fig. 21.8

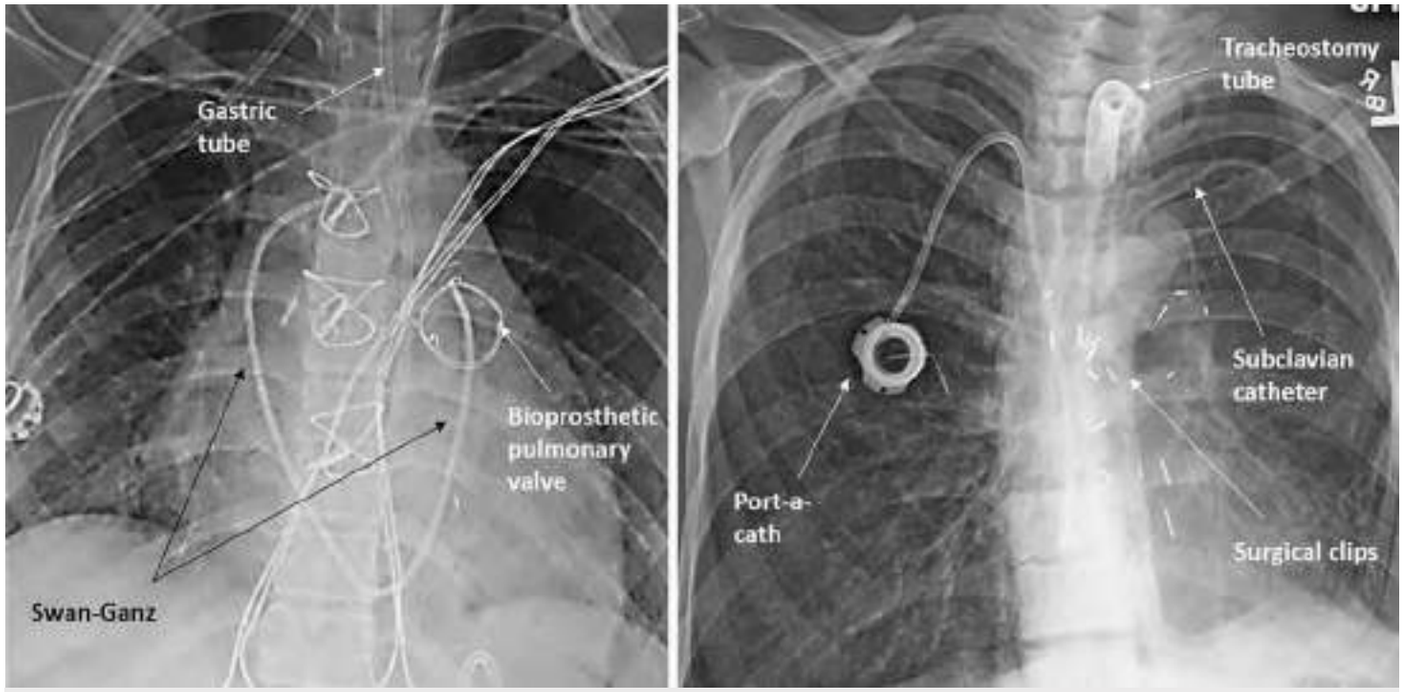

Fig. 21.9

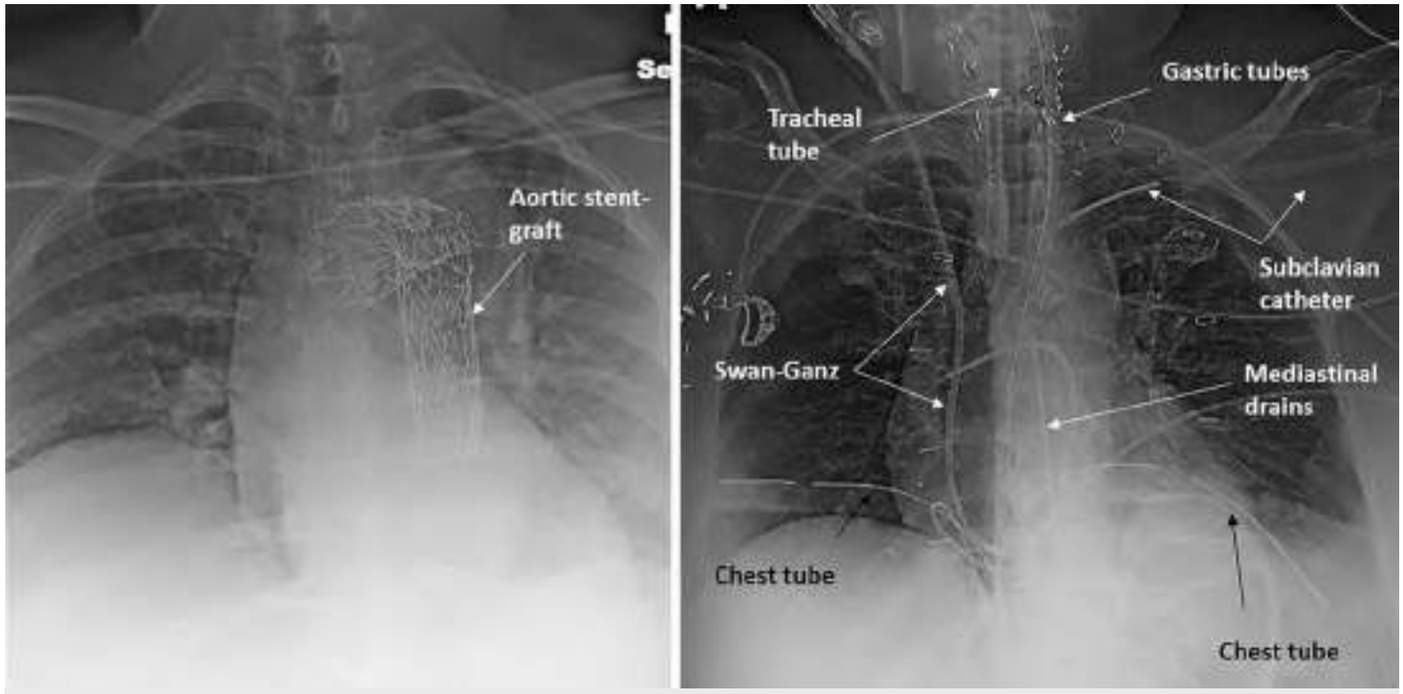

Fig. 21.10

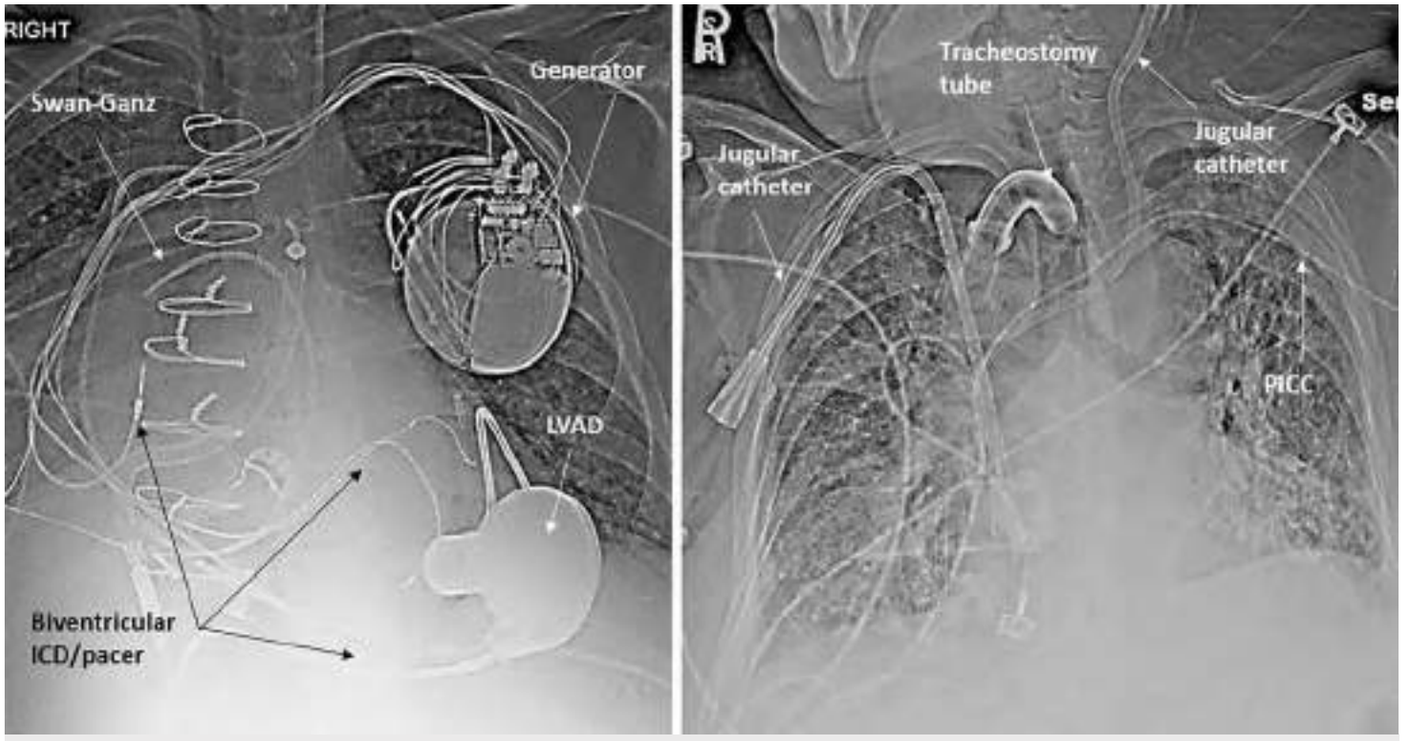

Fig. 21.11

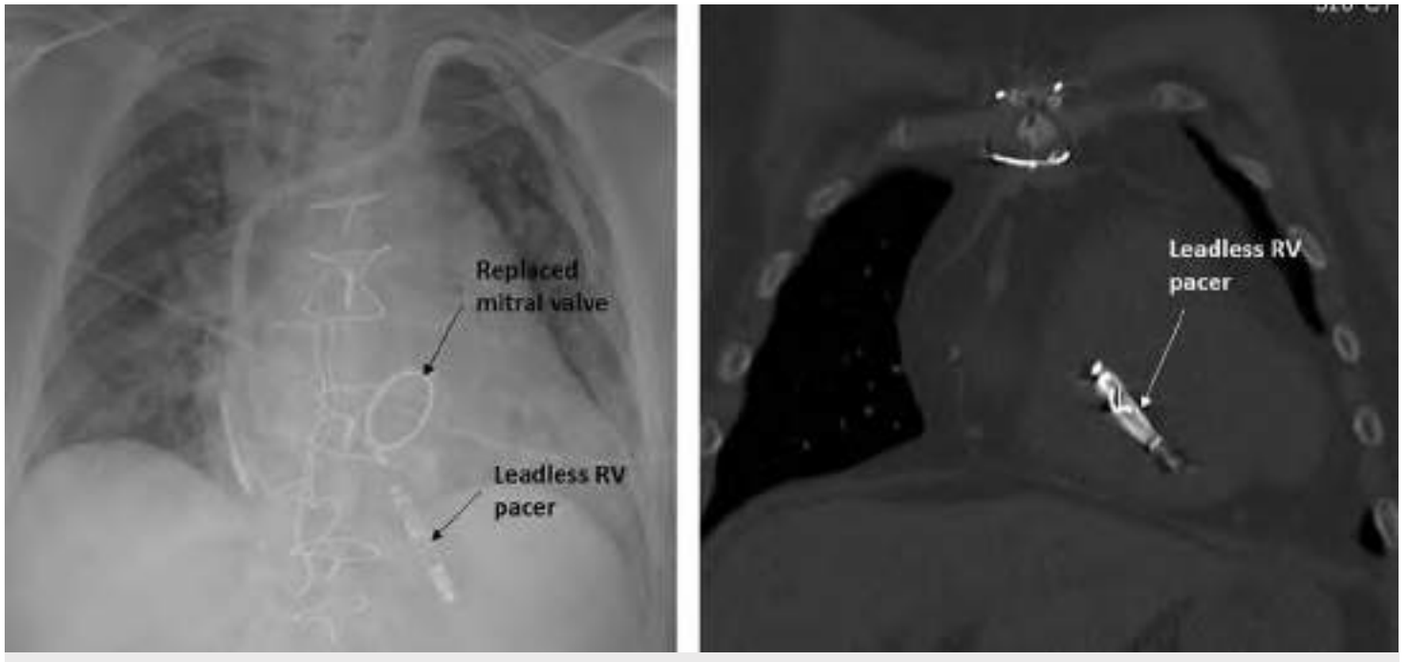

Fig. 21.12

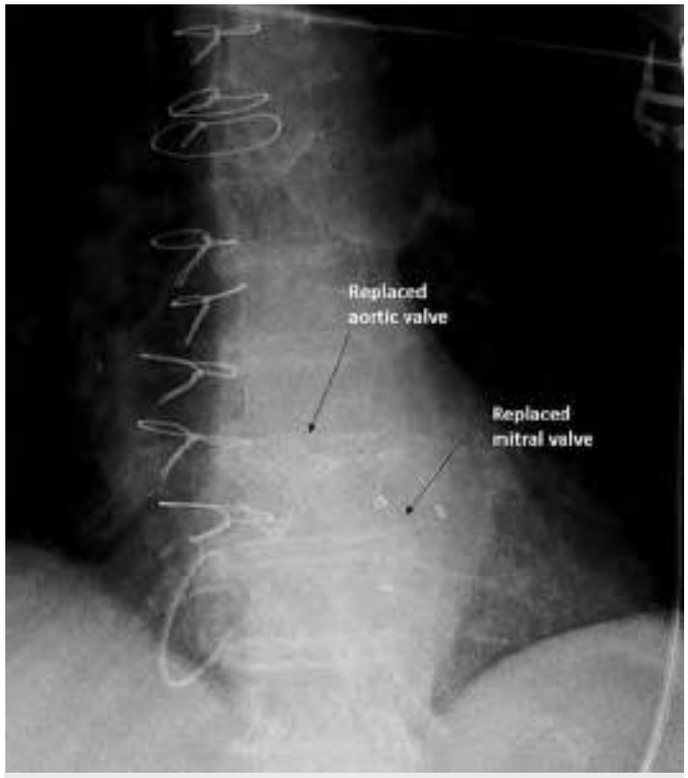

Fig. 21.13

Index

Note: Page numbers set **bold** or *italic* indicate headings or figures, respectively.

A

abdominal adenopathy *277*, 279
aberrant left pulmonary artery **191**, *194–195*
accessory cardiac bronchus 92, *93*
accessory fissures of pleura **157**, *162–163*
accessory nerve 26
acute coronary syndrome 501
adenocarcinoma 142, 161
airway classification *79*, 80
aneurysms
– aortic root **443**, *444–445*
– atrial septal *366*, **366**, *367*
– bronchial artery *239*
– coronary veins 531, *533*
– fusiform aneurysmal dilatation *534*
– patent ductus arteriosus **246**, *247*
– sinus of Valsalva 224
anomalous bronchi 90, *91–92*
anomalous pulmonary venous return **193**, *197*, 213
anterior cardiac vein 528
anterior circumflex humeral vein 52, *52–53*
anterior interventricular vein 528, 530, *531–532*
anterior spinal artery *237*
anterior thoracic chain 266
aorta
– anatomy *224*, **224**
– aortic arch 39, *224*, **227**, *228*
– aortic hiatus **282**
– ascending aorta **224**, *225–227*, *317*, *557*
– coarctation of *48*, 49, *248*, **248**
– descending thoracic *224*, **235**, **239**
– double aortic arch **243**, *246*
– embryology **239**, *240–242*
– endocarditis **441**, *442–443*
– leaflet prolapse *441*, **441**
– pseudocoarctation of **248**, *249*
– recess *557*, 559, *561–562*
– right aortic arch *243*, **243**, *244–245*
– root *409*, 410, *411*, *415*, *424*, 425, *427–428*
– root aneurysms **443**, *444–445*
– stenosis **438**, *440*
– stent graft *576*
aortic valve
– anatomy *346*, *371*, **392**, *394–397*
– aortic annulus 392, 394, **430**, *433*
– aortic endocarditis **441**, *442–443*
– aortic leaflet prolapse *441*, **441**
– aortic leaflets *390*, *396*, 425, 430, **430**, *431–432*
– aortic root aneurysms **443**, *444–445*
– aortic stenosis **438**, *440*
– bicuspid aortic valve **436**, *438–439*, 443
– interleaflet triangles (ILTs) *434*, **434**, *435*
– Lambl's excrescences *436*, **436**
– nodule of Arantius 430, *431*
– papillary fibroelastoma **436**, *437*
– prosthetic *573–574*
– replacement surgery *390*, 392
– sinotubular junction *376*, 382, 392, *431*, **434**
– sinuses of Valsalva 224, 392, *398*, *423*, **434**, *435*
– ventriculoarterial junction *376*, 382, *395*, *398*, 407, *407*, *423*, *427*, **430**, *431*
aortopulmonary ligament (ligamentum arteriosus) 227
aortopulmonary trunk *455*
arcuate ligaments *276*, 279, *280*
arterial thoracic outlet syndrome **58**, *59–60*
artery of Adamkiewicz 235, *237*
asbestos inhalation 161, *169*
ascending cervical artery 231, *234*
asplenia syndrome 87
asthma 95
atelectasis 139, *141*, 142, *143*
atria
– appendage 325, *329*
– esophageal fistula 354
– septal aneurysm *366*, **366**, *367*
– septal defect 213
– septation 359, *362–364*
– septum *408*, **412**, *416*
– tachyarrhythmias 334, 535
– venous system 524, *524*, **524**, *525–526*, **526**, *527*, 528, **528**, *529–530*
atrial fibrillation
– anatomy 214
– cardiac autonomic nervous system and **217**
– catheter ablation **217**, *218*
atrioventricular nodal (AVN) artery **513**, *514*
atrioventricular vein 528
AV bundle of His *399*, 401, *402*, 416, *417*, 511
AV conduction axis *329*, *331*, *346*, **401**, *402*, 408, *410*, *412–413*, **416**
AV node 345, *346*
AV node artery 345, *347*
AV node reentrant tachycardia (AVNRT) 345
AV valves, ventricular mass *422*
axillary artery 19, *40*, 41, *42*
axillary region muscles *20*
axillary vein 52
axillary vessels 19
azygoesophageal recess 155, *158–159*
azygos lobe 161, *163*
azygos vein *199*, *204*, 213, *358*
azygos/hemiazygos system 76, 84, *200*, **205**, *206–208*, **209**

B

Bachmann's bundle *333*, 334, *339*, 348, 545
bacterial endocarditis **472**, *474*
Barlow's disease 471, *473*
basilic vein 52
benign dynamic airway collapse *76*, 92
benign secretory calcifications *303*
bicuspid aortic valve **436**, *438–439*, 443
bifid rib 11, *12*
bioprosthetic pulmonary valve *575*
biventricular ICD/pacer 571, *573*, *576*
Bochdalek's foramen *276*, **282**, *284*
Bochdalek's hernia **286**, *287*
body of sternum 5, *5*
bovine arch 231, *231*
Boyden's classification 80
brachial artery *40*, 41
brachial vein 52
brachiocephalic artery *228–230*, **230**, 235, *239*
brachiocephalic vein 46, *126*, *199*, *201*, **202**, *204*
breasts
– acines/ductules 298, *301–302*
– alveolar buds 298, *301*
– arterial system **311**, *313*
– athelia 296
– axilla **308**
– axillary nodal evaluation 311, *312*
– chest wall **307**
– chest wall, breast cancer and 307, *308*
– ducts/lobules **298**, *300–302*
– embryology *296*, **296**, *297–298*
– hypoplasia 296
– in pregnancy 298, *301*, 311
– lactiferous ducts *300*
– lymphatics **308**, *310–311*
– malignant diseases of 301, *302–304*
– menopause/aging 301
– menstruation and 311
– milk lines 296, *297*
– Montgomery glands *300*, 305
– Morgagni tubercles *300*, 305
– neuromuscular anatomy *307*, **307**, *309*
– nipple retraction/inversion 305, *306*
– nipple–areolar complex 296, 298, *300*, *305*, **305**
– parenchyma **298**, *299*
– polythelia/polymastia 296, *297–298*
– puberty 297
– retromammary bursa/space 298, *299*
– sensory innervation 308
– terminal ductal–lobular unit (TDLU) 298, *300*, *302*
– truncated ducts 305, *305*
– varix 313
– vascular anatomy **311**
– venous system *313*, **313**
bridging bronchus 92, *93*
bronchiectasis 41, *239*
bronchii
– anatomy *71–72*, *74–75*, **77**, *78–79*
– anomalous *91*
– arterial aneurysm *239*
– arteries 76, *77*, 84–85, *85*, 86, *86–87*, *224*, **235**, *238–239*
– diverticula 90, *91*
– tree branching pattern classification *84*
– vascular anatomy **84**, *85–87*
– veins 84
bronchitis/bronchiolitis 92, *97*
bronchoconstriction/bronchodilation 77
bronchogenic carcinoma 267
bronchogenic cyst 559, *562*
bronchopneumonia 142, *146*

C

cardiac MRI 456, *457*
cardiac resynchronization therapy *535*, *537*, **537**, *540*, 545, *545–546*
CardioMEMS 571, *572–574*
carina/bronchial anatomy *71–72*, *74–75*, **77**, *78–79*
cavotricuspid isthmus 340, *341–342*
celiac trunk *288*
centrilobular emphysema 146, *147*
centrilobular nodules 146, *147*
cephalic vein 52
cervical rib 11, *12*
Chiari network 340, *344*, 420
chordae tendineae
– heart 387, **463**, *468–469*
– mitral valve 387, **463**, *468–469*
– third-order chordae (basal) chordae 463, *468*
– tricuspid valve 482, *482–483*
chronic heart disease 446
chronic obstructive pulmonary disease (COPD) 41, 73, 92, 95, 193
circulus venosus of Haller 313
circumflex scapular artery 47, *47*
cisterna chyli 121, *125*
cleft (bifid) sternum 14
clinical TNM (cTNM) staging system 115
clot formation risk factors 345
collateral ventilation **139**, *140–141*, **142**
common cardinal veins 200, *200*, 205, 213
compliance 139
congenital heart disease *459*, **459**, **536**, *541–542*
congenitally corrected transposition of the great arteries (ccTGA) 536
congestive heart failure 313

conus elasticus anatomy *71*
cor triatriatum sinister 354
coronary arteries
– anatomy 235, *239*, *322–323*, 392, *393*, **489**, *490–492*
– arterioles 515
– atrial branches *499*, **514**
– blood flow/myocardial perfusion **515**, *516*
– codominance *492*, 501, *507*
– conduction system **511**
– conotruncal circulation *503*, *509*, **510**, *512–513*
– CS fistula 537, *544*
– dominance 489, *492*
– dual perfusion 501
– embryology **489**
– epicardial **489**, 515
– fistulas 227
– imaging *492*, 493
– imaging, post-CABG *514–515*, **516**, *517–518*
– infundibulum 510, *512–513*
– intercoronary collaterals **507**, *508–510*
– interventricular septum *497–498*, **507**, *511*
– Kugel's artery 501, *503*, *509*, 511, *513*, 514, **514**
– left, aorta relationship *224*, **227**, *228*
– left, variants **493**, *496–498*
– microvasculature **515**
– myocardial bridging 495, *500*
– posterior descending artery *492*, **501**, *505–507*
– prearterioles 515
– right 450, *455–456*, 489, 493, *501*, **501**, *502–504*
– right superior descending artery *494*, *511–512*, **514**, *515*
– right, aorta relationship *225–227*, **227**
– segmental classification **489**, *492–495*
– septals *497–498*, **507**, *511*
coronary artery bypass surgery (CABG) 46, *514–515*, **516**, *517–518*, 531
coronary ligament 279, *280*
coronary sinus 528
coronary veins
– anatomic landmarks 536, *540*
– aneurysm 531, *533*
– anomalies, classification of 536, *542–544*
– atrial venous system 524, *524*, **524**, *525–526*, **526**, *527*, 528, **528**, *529–530*
– bulbous enlargement of *534*
– classification of **520**, *521*
– conduction system **523**
– congenital heart disease **536**, *541–542*
– coronary sinus tributaries **530**, *531*
– CS musculature *520*, *539*, **545**, *547–549*
– development of *520*, **520**
– great cardiac vein 528, **530**, *531–533*, *543*
– imaging **530**, *540*
– inferior interventricular vein 528, 530, *531*, **531**, *533–534*
– left marginal vein 528, *531*, **534**, *535*
– left posterior vein 528, *531*, **534**, *535*
– mitral annulus relationship **545**, *550–551*
– oblique vein of Marshall 528, *531*, *534*, **534**, *535*, 536
– papillary muscles *523*, **523**
– sinus boundaries *533*, **536**, *537–540*
– size variations **536**
– small cardiac vein 528, *531*, **534**
– Thebesian sinusoids **521**, *522–523*
– Thebesian vessels (smaller CVS) **521**, *522–523*
– valves of **536**
– venoluminal vessels **523**
– ventricular septal veins **536**
costal cartilages
– abscess *260*
– anatomy *5*, 7
– injury 14
costocervical trunk *229–230*, *232*, **232**, *235–236*
costoclavicular space *39*, *57–58*
costomediastinal recesses 155, *159*
crista supraventricularis *370–371*, 375, *375*, 395
crista terminalis 325, 329, *329*, *333*, 334, *337*
CS orifice atresia 536, *544*
CT applications 267, 530
cystic fibrosis 85, *86*, *91*, 95, *97*
cysts
– benign simple 301, *304*
– bronchogenic 559, *562*
– duplication 292
– pericardial 564, *566*
– thymic *114*, 115

D

deltoid muscle *20*, *26*
dermatomes, of thorax 252
diaphragm
– anatomy 121, 131, **272**, *273–276*
– anterior/sternal muscle attachments **272**, *275–278*
– aortic hiatus **282**
– arterial supply **287**, *288*
– central tendon **272**, *274*
– chest radiograph evaluation **291**
– crura *276*, **279**, *281*
– dysfunction of **290**
– embryology *271*, **271**
– esophageal hiatus **282**
– eventration *292*, **292**, *293*
– fenestrations **282**
– fluoroscopic evaluation **292**
– heart relationship to 316, *320*, 325, *325*
– hernias **282**, *285–286*, **286**, *287*
– hiatuses *274*, *276*, **282**
– innervation **287**
– ligaments *275–276*, *279*, **279**, *280*
– lumbocostal triangle *276*, **282**, *284*
– lymphatics **259**, *260*, *262*, **289**, *290–291*
– masses 292, *294*
– motor innervation **257**, *258*
– muscle bundles morphology **272**, *277–278*
– perforation/rupture 292, *293–294*
– physiology **289**
– posterior/lumbar muscle attachments **272**
– retrocrural space **281**, *283*
– sternocostal triangles *276*, **282**
– ultrasound **292**
– vena caval hiatus **282**, *284*
– venous supply **288**, *289*
diaphragmatic paralysis 254
diverticulum 564
DL-CVC 571, *573*
dorsal (descending) scapular artery 23
dorsal scapular artery 39, 42, *43*, *45*, *224*, *230*, *233*, **235**
double outlet right ventricle (DORV) 446, 459
dual chamber pacemaker 571, *572–574*
dual LAD 495, *498*
dual PDA 501, *505–506*
ductal carcinoma in situ (DCIS) 301, *302*
duplication cysts 292

E

Ebstein's anomaly 486–487, *487*
elastofibroma 22, *24*
empyema 161
enlargement of CS 536–537, *543–544*
eosinophilic pneumonia 142
erector spinae muscle *25*, *27–28*, **29**
esophagus
– anatomy 121
– esophageal hiatus **282**
– innervation *256–257*, **257**
– lymphatics **264**
– plexus *252*, *256–257*, 258
Eustachian ridge 325, 340, *345*
Eustachian valve *200*, 201, 340, *340–341*, 416, *419*
excessive dynamic airway collapse 92, *95*
expiratory tracheal narrowing 92, *95*
external oblique muscle 17, *18–19*, *25*
extracardiac fat **564**, *567–569*

F

falciform ligament *275*, 279, *280*
fiberoptic bronchoscopy/CT
– complementary roles of *82*, **92**, *94*
– dynamic airway evaluation *76*, **92**, *95*
– pathology *91*, **92**
fibroadenoma, benign 301, *304*
fibrotic interstitial lung disease 142
fibrous dysplasia 15, *16*
first rib *4*, 5, *8*
flail of single segment (FED) 471–472, *473*
floating ribs 1–2, 5, *6*
focal stenosis 92, *96*
fold of Marshall 563
foramen of Morgagni 131, *132*
fossa ovalis *340*, 359, *361*, 412
functional mitral regurgitation *474*, **474**
functional residual capacity (FRC) 139
fusiform aneurysmal dilatation *534*

G

gastric arteries *288*
gastric cancer, metastatic 263, 282, 289
gastric tubes *573*, *575–576*
gastric vein 288
gastrophrenic ligament *275*, 279, *280*
generator *575–576*
Gerota's pathway 311
great cardiac vein 528, **530**, *531–533*, *543*
great vein of Keynes 115
great vessels transposition 243
ground-glass opacity 142

H

heart
– ablation 340, 345, 350
– anterior wall/left atrium 348
– aortic valve *346*, *371*, **392**, *394–397*
– aortic valve replacement surgery *390*, 392
– aortoventricular membrane *385*, 389
– atrial appendage 325, *329*
– atrial septal aneurysm *366*, **366**, *367*
– atrial septation 359, *362–364*
– AV bundle of His *399*, 401, *402*, 416, *417*, 511
– AV conduction axis *329*, *331*, *346*, **401**, *402*, 408, *410*, *412–413*, **416**, *417*
– AV node 345, *346*
– AV node artery 345, *347*
– AV valves *422*
– Bachmann's bundle *333*, 334, *339*, 348, 545
– borders in thorax *315*, **315**, *316*
– cardiac bronchus 92, *93*, 348, *348–349*
– cardiac valvar attachments *407*, **408**, *409*, *411*
– cavotricuspid isthmus 340, *341–342*
– central fibrous body *396*, 401
– Chiari network 340, *344*, 420
– chordae tendineae (tendinous chords) 387, **463**, *468–469*
– coronary sinus 340, *345*
– crista supraventricularis *370–371*, 375, *375*, 395
– crista terminalis 325, 329, *329*, *333*, 334, *337*
– esophageal arteries 354, *358*
– esophageal plexuses 354
– Eustachian ridge 325, 340, *345*
– Eustachian valve *200*, 201, 340, *340–341*, 416, *419*
– fossa ovalis *340*, 359, *361*, 412
– helical loop model 400, *400*, 401
– infundibulum *372–373*, 375, 378, *378*
– innervation **258–259**
– interatrial groove 359
– interatrial septum **359**, *361*
– LAA/LA diverticula 354, *357*

– landmarks
–– anterolateral right atrium *333*, **334**, *337*, *339*
–– inferior right atrium *340*, **340**
–– medial right atrium *345*, **345**, *346*
–– superior right atrium *328*, **329**, *333–334*
– LCx artery 346, *347*, 350, 354, 392, *393*
– left atrial (mitral) isthmus 350, *351*, *357*
– left atrial appendage **354**, *355–356*
– left atrium *327*, *333*, **346**, *348*
– left atrium components *348*, **349**, *350*
– left atrium enlargement 348, *349*
– left tenia terminalis 354, *356*
– left ventricle **382**, *383–388*
– left ventricle function *377*, **398**, *399–400*
– left ventricle vascular supply 493
– LV ostium 382, *384–385*
– LVOT 375, *376*, *385*, **389**
– lymphatics **267**
– margins *318–319*, *326*
– membranes near pulmonary veins 354
– membranous septum *345–346*, **395**, *397–399*, *409*, **412**, *414–415*, 416, *418*
– mitral isthmus *357*
– mitral valvar hinges 408, 410, *411*
– mitral valvar leaflet 420, *421*
– mitral valve annulus *391*, 392, *393*
– moderator band 374, *374*
– muscular rim (limbus) 359, *361*
– myocardial sleeves 350
– origin of great vessels *317*, *320*
– papillary muscles *373–374*, 378, *380*, 387, *388*
– patent foramen ovale *340–341*, **359**, *365*
– periatrial structures **354**, *358*
– phrenic nerves 359, *360*
– planes of 316, *321–323*
– primary atrial foramen 359
– projections of 316, *322–323*
– pulmonary arteries *333*, 347
– pulmonary plexuses 354
– pulmonary veins 325, *328–329*, 347, 350, *352–353*, 354, *356*
– RA vestibule 325, *332–333*
– right atrium **325**, *326–333*
– right ventricle *317*, *322*, **366**, *368–372*
– right ventricle function *377*, **377**, *378*
– right ventricle size *373*, **375**
– RVOT *370*, *373–374*, **374**, *375*, 446, *453*, 456
– SA node 334, *335*
– SA node artery 334, *336*, 347, 354, *356*
– septal isthmus *328*, 345, *345–346*, *418*
– septoparietal trabeculations *373*, 378
– septum secundum 359
– sinotubular junction *376*, 382
– structures, anatomical positions **316**, *317–323*
– sub-Eustachian sinus of Keith 340, *342–343*
– superior cavoatrial junction *328*, 329
– surfaces/angles **316**, *317*, *320*, *325–326*
– tendon of Todaro *342*, 345, *345*, *410*, 416
– Thebesian valve *200*, 201, 325, 340, *344*, 416, *419*
– third-order chordae (basal) chordae *468*
– thoracic cage *322–323*
– tomographic imaging 382
– triangle of Koch 345, *345–346*, 359, *410*, 416, *418*
– vagus nerve 354, *358*
– ventricular septum **401**
– vestibular spine 359, *362*
helical loop model 400, *400*, 401
hemiazygos vein/accessory HAZ 205, *206*
hemorrhage 146, *147*
hepatocardiac channel *200*, 201
hiatal hernias **282**, *285–286*
high-speed rotational coronary venography 530
hilar anatomy **79**, *80–81*
Horner's syndrome 128
hyperplastic thymus *114*, 115
hypoplasia of CS 536

I

IABP 571
ICD lead *575*
iliocostalis muscle 29
imaging
– coronary arteries *492*, 493
– coronary arteries, post-CABG *514–515*, **516**, *517–518*
– coronary veins **530**, *540*
– CT applications 267, 530
– heart 382
– lungs, function **142**, *144–146*
– MRI 530
– pericardium **563**, *564*
– pulmonary valve **456**, *457*
– tricuspid valve *479–480*, *482*, **483**
Impella 571, *575*
implantable cardioverter-defibrillator (ICD) 571, *575*
infective chondritis *260*
inferior cava vena *557*
inferior interventricular vein 528, 530, *531*, **531**, *533–534*
inferior phrenic arteries 287, *288*
inferior phrenic veins 288, *289*
inferior pulmonary ligament (IPL) **106**, *107–108*, 122, 152, *153*, 279, *279*
inferior pyramidal space 407, *407–408*, *410–412*, **412**, *413*
inferior thyroid artery 231, *234*
inferior vena cava *200*, **205**, *206–208*, 528
inflammatory diseases, rib/sternal involvement 15, *16–17*
infraspinatus muscle *20*, *25–26*
infundibulum
– coronary arteries 510, *512–513*
– heart *372–373*, 375, 378, *378*
– pulmonary valve 450, *453–454*, *456*
– veins 528, *530*
innominate vein 52, *52–53*
inspiration/expiration 73, *76*, 142, *143*
intercostal arteries 32, **235**, *237*
intercostal muscles *13*, *29*, **29**, *30–33*, *62*, *64–65*
intercostal nerves 32, 155, 251
intercostal neurovascular bundle **47**, *48–51*
interlobar fissures *151*, 155, *156–157*
intermediate bronchus 82
internal mammary artery *87*
internal mammary vein *207*
internal thoracic arteries *37*, *41*, **42**, *46*, *228–230*, **231**, *233*
internal thoracic veins 46, *46*
interpleural triangles 155, *159*
interscalene triangle 56, *57–58*
intrathoracic rib 11, *12*
invasive ductal carcinoma *303*
involuntary respiration 289
IPMD 571
isovolumic diastolic relaxation 400

J

Jackson–Huber classification *79*, 80, *98–101*
jugular catheter *572*, *576*

K

Klippel–Feil anomaly 11
Kommerell's diverticulum 243, *245*
Kugel's artery 501, *503*, *509*, 511, *513*, 514, **514**

L

LAA occlusion device 571, *572*
Lambl's excrescences *436*, **436**
Larrey's space *276*, **282**
laryngotracheal junction *71*
late systolic contraction 400
lateral thoracic artery 19, 21, **46**, *47*, 311
latissimus dorsi muscle *18–20*, **23**, *24–26*, *307*
left anterior descending artery (LAD) *224*, 227, *228*, 450, *456*, 489, *490*, 493, 495, *496–498*, *503*, 510, *532*
left atrial (mitral) isthmus 350, *351*, *357*
left atrial appendage **354**, *355–356*
left circumflex (LCx) artery *224*, 227, *228*, 346, *347*, 350, 354, 392, *393*, 489, *490*, *492*, 493, 495, *496–498*, 501, *532*, *550*
left common carotid artery *231*, **231**
left eparterial bronchus *92*
left gastric vein 288
left lower paratracheal lymph nodes 122
left marginal vein 528, *531*, **534**, *535*
left oblique fissure *151–152*, 155, *156*
left phrenic nerve *253*, *255*, **256**
left posterior vein 528, *531*, **534**, *535*
left recurrent laryngeal nerve 227, 257
left subclavian artery 39, *40*
left superior intercostal vein **202**, *204–205*
left tenia terminalis 354, *356*
left tracheal bronchus *92*
left upper lobe bronchus 92, *93*
left upper paratracheal lymph nodes 122
left vagus nerve *254*, **254**
left ventricular outflow tract (LVOT) 375, *376*, *385*, **389**
left vertebral artery/aortic arch origin **246**, *248*
levatores costarum muscles 29, *33*
levophase of coronary angiography 530
ligament of Marshall *561*, 563
ligaments, rib 2, *6*
ligamentum arteriosum **106**, *109*
lipoma
– diaphragm 292, *294*
– left chest wall *17*
– pleural 161, *168*
liver cirrhosis 272, *278*
lobular carcinoma 301
lobular consolidation 142
long thoracic nerve of Bell 21, *23–24*
longissimus muscle 5, *8*, 29, *62*, *64–65*
lumbar rib 11
lungs
– aging effects on 142, *144–146*
– arterial microcirculation *138*, **141**
– bronchial circulation **142**
– bronchopulmonary arterial collateral flow **142**
– cancer staging 92, *94*, 115
– cancer, vascular supply 140
– circulation **140**
– embryology *135*, **135**
– function imaging **142**, *144–146*
– interalveolar air drift **139**, *140–141*
– lobes/segmental anatomy **135**, *136–137*
– lymphatics **261**, *262*
– perfusion measurement 140
– pulmonary acinus **137**, *138*
– pulmonary function **139**
– radiological diagnosis **142**, *146–147*
– secondary pulmonary lobule (SPL) **137**, *138*
– transplantation pathologies 92, *96*, 217, *219*
– ventilation **139**
– ventilation to perfusion matching **142**, *143–146*
LVAD 571, *573*, *576*
lymphangitic carcinomatosis *262*
lymphatics
– anatomy **121**, **259**, *262*
– breasts **308**, *310–311*
– cardiac/pericardial **267**
– diaphragm **259**, *260*, *262*, **289**, *290–291*
– drainage patterns 115, 121, *123*, **259**, *260*, *262*
– embryology 259
– esophageal **264**

– IASLC nomenclature 115, *118–121*, *123*
– lungs **261**, *262*
– lymph node chains 264
– mediastinal **115**
– mediastinal stations 122
– mediastinum **264**, *266–269*
– pleura **157**
– pleura/pleural spaces **261**
– thoracic duct **121**, *125*
– thymus **264**
– tracheobronchial 261, *262*
lymphoma 161, 259, 289

M

MAC infection 146, *147*
manubrium 5, *5*, 7, *10*
Marfan's syndrome 14, 443
Marshall's bundle 535
medial pectoral nerve 19
median arcuate ligament 279, *280*
median visceral chain 266
mediastinal drains *572*, *574*, *576*
mediastinal lipomatosis 115
mediastinum
– anatomy **103**
– inferior pulmonary ligament (IPL) **106**, *107–108*, 122, 152, *153*, 279, *279*
– ITMIG classification *103*, **103**, 104, *105–106*
– ligaments **106**
– ligamentum arteriosum **106**, *109*
– lymphatics **264**, *266–269*
– mediastinal (pericardial) fat **115**, *117*
– neck/abdomen communication **131**, *132*
– nerves **124**
– pericardiophrenic ligament **110**, *111*
– sternopericardial ligaments *110*, **110**
– superior pulmonary sulcus **128**, *129–131*
– sympathetic chains **124**, *129*
– thyrothymic ligament **110**, *112*, 115
Meigs syndrome 282
membranous septum
– of heart *345–346*, **395**, *397–399*
– ventricular mass *409*, **412**, *414–415*, 416, *418*
mesothelioma 161, *167*
MitraClip 571, *575*
mitral valve
– anatomical variants **470**, *471*
– anatomy **389**, *390–393*, 461, *461*
– anatomy, atrial view *390*
– anatomy, LA relationship *331*, 348, 350, *350*, *356*
– anatomy, RA relationship *330*
– annulus *391*, 392, *393*, **461**, *462–464*
– annulus calcification **470**, *471–472*
– annulus, coronary veins relationship **545**, *550–551*
– bacterial endocarditis **472**, *474*
– chordae tendineae (tendinous chords) 387, **463**, *468–469*
– coaptation surface 463, *467*
– functional mitral regurgitation *474*, **474**
– hinges 408, 410, *411*
– leaflets *385*, *421*, **463**, *464–466*, 470, *471*
– myxomatous degeneration **471**, *473*
– organic mitral insufficiency **470**
– papillary muscles 387, **468**, *470*
– prolapse/FED 471–472, *473*
– prosthetic *573–574*
– regurgitation **470**
– stenosis *475*, **475**
– strut chordae 463
– third-order chordae (basal) chordae 463
Mondor's disease 313
Morgagni's foramen *276*, **282**
Morgagni's hernia *286*, **286**
Morquio syndrome 14
mucous production 77
muscle attachments, rib 5, *8*
muscle slip 23
musculophrenic artery 42
myocardial gene transfer *544*
myocardial infarction/lead placement 537, *545–546*
myoepithelial cells 298, *302*
myofascial pain syndrome 26
myxomatous degeneration
– mitral valve **471**, *473*
– tricuspid valve *482*

N

neck of rib 2, *6–7*
neurogenic thoracic outlet syndrome **58**
nodal biopsy 92, *94*
nodule of Arantius 430, *431*
nondisplaced rib, post-CPR *16*
Noonan's syndrome 14

O

oblique sinus *557–560*, **563**
oblique vein of Marshall 528, *531*, *534*, **534**, *535*, 536
occipital artery 232, *232*
organic mitral insufficiency **470**
organizing pneumonia 142
osteoarthritis, manubriosternal synchondrosis *16*
osteomyelitis, rib/sternal 15, *16*
ostial pulmonary vein **214–215**
ostium secundum defect 359, *419*
ovarian fibroma 282
oxytocin 298

P

Pancoast's tumor 128, *129*
papillary fibroelastoma **436**, *437*
papillary muscles
– coronary veins *523*, **523**
– heart *373–374*, 378, *380*, 387, *388*
– mitral valve 387, **468**, *470*
– tricuspid valve 387, *388*, *480*, 482, *482–483*
– ventricular mass *420*, **420**, *421*
papillomas 301
para-aortic lymph nodes 122
paradoxical embolism 359
paraesophageal lymph nodes 122
paramediastinal recesses **155**, *158–160*
parasternal intercostals 29, *31–32*
parasympathetic innervation, cardiac **258**
paraumbilical vein *289*
paravertebral compartment of mediastinum *103*, 104, *105*, 106, *106*
partial anomalous pulmonary venous return (PAPVR) 193, *197*, 213, 219, *220–221*
partial pericardial defect 564
patent ductus arteriosus/aneurysm **246**, *247*
patent foramen ovale *340–341*, **359**, *365*
pectoral nerves 19
pectoralis major muscle **17**, *18–21*, 307, *307*
pectoralis minimus muscle 19
pectoralis minor muscle *18*, **19**, *20–21*, 307, *307*
pectus carinatum *14*, **14**, *15*
pectus excavatum *11*, **14**, *15*
percutaneous mitral annuloplasty (PMA) *544*, 545, *550–551*
pericardiacophrenic vessels 42, *46*, 256, *288*
pericardial cyst 564, *566*
pericardial effusion 564, *565*
pericardial lymphatics **267**
pericardiophrenic bundle **124**, *127–128*
pericardiophrenic ligament **110**, *111*
pericardiophrenic vein *289*
pericarditis, acute 564, *565*
pericardium
– aortic recess *557*, 559, *561–562*
– characterization **555**, *556–560*
– embryology *554*, **554**, *555*
– extracardiac fat **564**, *567–569*
– imaging **563**, *564*
– oblique sinus *557–560*, **563**
– parietal pericardium 555, *557*
– pathologies **564**
– percutaneous approach *560*, **563**
– pericardial sac *557*, 559, *560*
– pulmonary artery/vein *557*, 559, *561*, 563
– reflection **559**
– serous pericardium 555, *557*
– transverse sinus *557–558*, **559**, *561*
persistent truncus arteriosus **191**, *193*, 243
phrenic arteries 287, *288*
phrenic nerves
– accessory 287
– anatomy **124**, *126–127*, 155, **254**
– diaphragmatic 287
– heart 359, *360*
– injury to **290**
– left *253*, *255*, **256**
– right *256*, **256**, 257, *258*, 287
phrenic veins 288, *289*
phrenicocolic ligament *275*, 279
phrenicoesophageal ligaments 281
PICC 571, *573*, *576*
pleura
– accessory fissures **157**, *162–163*
– anatomy **149**, *150–154*, *156–157*
– blood supply *153*, **155**
– boundaries/pleural recesses **155**, *158–160*
– effusion **161**, *164–166*
– embryology *149*, **149**
– histology **155**
– innervation **155**
– lymphatic drainage **157**
– lymphatics **261**
– masses **161**, *166–168*
– pathologies **161**
– thickening 13, *13*
pneumomediastinum 131, *133*
pneumopericardium 564, *566*
pneumothorax 13, *13*, **161**, *167*
Poland's anomaly 14
Poland's syndrome 19, *22*
polysplenia syndrome 87, *90*
porous diaphragm syndrome 282
Port-a-cath 571, *575*
portal hypertension *207*
posteparterial bronchus *92*
posterior axillary fold 23
posterior descending artery *492*, **501**, *505–507*
posterior parietal chain 266
posterior scalene muscle 5, *8*
posthyparterial bronchus *92*
preeparterial bronchus *92*
preganglionic sympathetic fibers 257
prehyparterial bronchus *92*
prevascular compartment of mediastinum 103, *103*, 104, *105–106*
prevascular lymph nodes 122
prolactin 298
prosthetic aortic valve *573–574*
prosthetic mitral valve *573–574*
pseudotumor, pleural 161, *166*
psoas major muscle 29
pulmonary acinus **137**, *138*
pulmonary artery sling **191**, *194–195*
pulmonary artery/vein
– aberrant left pulmonary artery **191**, *194–195*
– anomalous pulmonary venous return **193**, *197*, 213
– artery
–– anatomy 170, *171–177*
–– diameters in pathology **193**
–– embryology **189**, *190*
–– segmental/subsegmental arteries 170, 178
– atresia *87*, 191
– AVMs **191**, *196*
– carina/bronchial anatomy 77
– embryology **189**, *190*, *192*, **209**, *213–214*
– heart 325, *328–329*, *333*, 347, 350, *352–353*, 354, *356*
– ostial pulmonary vein **214–215**
– pericardium *557*, 559, *561*, 563
– persistent truncus arteriosus **191**, *193*
– phrenic nerve relationship *126*
– systemic arterial supply to lung **191**, *195*
– vein

–– anatomical variants *215*
–– anatomy **170**, *171–174*, *179–184*, *188–189*, *209*, **209**, *210–212*
–– anomalies **219**, *220–221*
–– embryology **191**, *192*, **209**, *213–214*
–– ostia 214, *215*, **215**, *216–217*
–– pathology *215*, **217**, *218–219*
–– right inferior pulmonary vein 187
–– segmental variations 187, *188–189*
–– semicentral vein type *186*, 187
–– subsegmental veins 177, 185
pulmonary atresia 459
pulmonary edema 146, *147*, 217
pulmonary embolism *340–341*, 366
pulmonary hypertension 193
pulmonary infection 41
pulmonary innervation **257**
pulmonary thromboembolism 41
pulmonary tuberculosis 41
pulmonary valve
– anatomy *375–376*, *382*, **382**, **446**, *448–450*, *453–454*
– aortic root *450*
– arterial supply **450**, *455–456*
– bicuspid 456
– congenital heart disease *459*, **459**
– embryology **446**, *447*
– imaging **456**, *457*
– infundibulum 450, *453–454*, *456*
– pathology 458
– pulmonary leaflets 446
– pulmonary trunk *450*
– regurgitation *457*, 458, **458**
– replacement **459**
– sinotubular junction 446
– sinuses *448–449*
– stenosis **456**, 458, *458*

Q

quadratus lumborum muscle 29

R

rectus abdominal muscle 17, *19*
recurrent laryngeal nerves *254*, **254**, 257
regurgitation
– functional mitral *474*, **474**
– mitral valve **470**
– pulmonary valve *457*, 458, **458**
– tricuspid valve 487, *487*
relapsing polychondritis 92
respiration 289–290
retrograde cardioplegic perfusion *542–544*, **550**, *551*
retrograde venography 530
retrotracheal lymph nodes 122
rheumatic MV stenosis *475*, **475**
rhomboid minor/major muscles **23**, *25–26*, *62*, *64–65*
rib displacement 32
right common carotid artery *228–230*, **230**
right lower paratracheal lymph nodes 122
right marginal vein 528, *531*
right middle lobe syndrome 92
right minor fissure 155, *156–157*
right phrenic nerve *256*, **256**
right recurrent laryngeal nerve 227
right subcardinal vein 205
right subclavian artery 39, *40–41*
right superior descending artery *494*, *511–512*, **514**, *515*
right tracheal bronchus *92*
right upper lobe bronchus 92, *93*
right upper paratracheal lymph nodes 122
right vagus nerve **254**
right ventricular outflow tract (RVOT) *370*, *373–374*, **374**, *375*, 446, *453*, 456
right vitelline vein 201

S

SA node 334, *335*
SA node artery 334, *336*, 347, 354, *356*
saber-sheath trachea 73, *76*, 92
scalene muscles *8*, *36*, **36**, *37*
scalenus minimus (Sibson's muscle) 36, *38*
scapular circulatory anastomosis 41, *43*
Scimitar syndrome 219, *220*
scoliosis 14
SCV-CAC 571
secondary pulmonary lobule (SPL) **137**, *138*
segmental bronchial anatomy *79*, **80**, *82*, 83, 87, 90, *98–101*
sentinel lymph node identification 311, *312*
septal isthmus *328*, 345, *345–346*, *418*
septal thickening 142, *147*
septal tricuspid leaflet 345, *345*, 408, 410, *411*, 412, 416
serratus anterior muscle 5, *8*, 17, *18–19*, **21**, *23*, *62*, *64–65*, 307, *307*
serratus posterior inferior muscle **26**, *27–28*, *62*, *64–65*
serratus posterior superior muscle 5, *8*, **26**, *27–28*, *62*, *64–65*
sinoatrial nodal (SAN) artery 495, *503*, 511, **513**
sinoatrial nodal (SAN) artery, S-shaped *499*, **513**, 514
sinoatrial node (SNA) artery 199, *502*
sinotubular junction of aortic valve *376*, 382, 392, *431*, **434**
sinus of Valsalva aneurysm 224
sinus venosus/systemic venous sinus 200
sinuses of Valsalva 224, 392, *398*, *423*, **434**, *435*
situs inversus 87, *89*
situs solitus 87, *89*
small airway characteristics **83**, *84*
small airways disease 146, *147*
small cardiac vein 528, *531*, **534**
smaller CVS **521**, *522–523*
space of Retzius 131, *132*
splanchnic venous plexus 213
split CS *543*
squamous cell carcinoma 92
sternal angle of Louis *5*, 7, *11*
sternal fractures 14, *16*
sternal wire *573–574*
sternalis muscle **19**, *22*, 307, *309*
sternoclavicular joints 5, *9*
sternocleidomastoid muscles 5, *9*, *18*, 26, *35–36*, **36**
sternohyoid muscle 7, *9*
sternopericardial ligaments 7, *10*, *110*, **110**
sternothyroid muscle 7, *9*
sub-Eustachian sinus of Keith 340, *342–343*
sub-Thebesian sinus/recess 340, *342–343*
subaortic (AP windows) lymph nodes 122
subcarinal lymph nodes 122
subclavian arteries
– anatomy 19, 39, *40*, 41, *41*, 56
– branches of *40*, 41, *42*, **231**
– left 39, **231**, 243
– right 39, *41*, *228–230*, **230**, *246*, **246**
subclavian catheter *575–576*
subclavian veins 39, *40*, 52, *52*
subclavius muscle **37**, *39*
subcostal arteries **235**, *237*
subglottic region anatomy *71*
subscapular artery 21, *45*, *47*, **47**, 313
subsuperior bronchus 90
superior (supreme) thoracic artery *40*
superior cavoatrial junction of heart *328*, 329
superior epigastric artery *41*, 42, *46*
superior intercostal vein (SICV) *200*, 201
superior phrenic arteries 287, *288*
superior pulmonary sulcus **128**, *129–131*
superior vena cava *126*, 528, *557*
– anatomy *199*, **199**
– embryology *200*, **200**
– obstruction 313
– pathologies *201*, **201**, *202–203*
suprascapular artery 42, *45*, 231, *234*
suprasternal notch *5*, 7
suprasuperior bronchus 90
surgical clips *575*
Swan-Ganz pulmonary artery catheter 571, *572*, *574–576*
sympathetic innervation, cardiac **259**
sympathetic nerves **124**, *129*, *256*, **256**, *257–258*
systemic arterial supply to lung **191**, *195*

T

TAVI 571, *573*
tendon of Todaro *342*, 345, *345*, *410*, 416
teres major muscle *19–20*, 23, *25–26*
teres minor muscle *25–26*
tetralogy of Fallot 86, *87*, 459, *531*, *543*
Thebesian sinusoids **521**, *522–523*
Thebesian valve *200*, 201, 325, 340, *344*, 416, *419*
Thebesian vessels **521**, *522–523*
thoracic duct **121**, *125*, *256–257*, **261**, *262*
thoracic inlet **36**, 128, *130*
thoracic outlet *4*, *56*, **56**, *57–58*
thoracic outlet syndrome 36, **52**, *55*, **58**, *59–61*, **61**
thoracic sympathetic chain 77
thoracic wall
– anterior, muscles of **17**, *18–19*, *62*, *64–65*
– bones, anatomical variations *11*, **11**
– bony thorax **1**, *3–5*
– embryology **1**, *3–4*
– innervation *251*, **251**
– muscles of **17**, *18–19*
– pathologies **14**, *16–17*
– posterior, muscles of **23**, *25–26*
– rib cage morphology, age/gender effects *3–4*, 5
– ribs **1**, *6–7*
– ribs, developmental abnormalities 11, *12*, 13, *13*, 14
– sternum *5*, **5**, *9*
– sternum, anatomical variation *3*, 14
– vascular supply **39**, *40–44*
– veins *52*, **52**, *53–54*
thoracoacromial artery 19, 37, **46**, *62*, *64–65*, 313
thoracodorsal artery 21, 23, 47, *47*, 313
thoracolumbar fascia *28*, **29**, *62*, *64–65*
thymic cyst *114*, 115
thymoma *114*, 115
thymus **110**, *112–114*, *116*, **264**
thyrocervical trunk 26, *37*, *41–42*, **42**, *45*, *228–230*, **231**, *234*
thyroid cartilage anatomy *72*
thyroid gland *72*, *112*
thyrothymic ligament **110**, *112*, 115
tilted sternum *11*
total anomalous pulmonary venous return (TAPVR) 193, *197*, 213, *220*
tracheal arteries 76, *77*
tracheal bifurcation 77
tracheal bronchus 90, *91*
tracheal tubes *576*
tracheobronchial senile calcification 73, *75*
tracheobronchial system
– anatomical variations, malformation **87**, 88, *89–91*, *93*
– bronchial vascular anatomy **84**, *85–87*
– carina/bronchial anatomy *71–72*, *74–75*, **77**, *78–79*
– embryology **70**
– hilar anatomy **79**, *80–81*
– segmental bronchial anatomy *79*, **80**, *82*, 83, 87, 90, *98–101*
– small airway characteristics **83**, *84*
– tracheal anatomy **70**, *71–72*
– vascular/nerve supply **76**, *77*
tracheobronchomalacia 92, *95*
tracheoesophageal artery 76, *77*
tracheomalacia 92, *95*
tracheostomy tubes *573*, *575–576*
transposition of great arteries (TGA) 446, 459, *459*
transverse cervical artery 26, 42, 231, *234*
transverse sinus *557–558*, **559**, *561*
trapezius muscle **24**, *25*, 26, *26*
tree-in-bud sign 146, *147*

triangle of Koch 345, *345–346*, 359, *410*, 416, *418*, 483
triangular ligament 279, *280*
triceps muscle *20*, *26*
tricuspid valve
– anatomy **378**, *379–381*
– anatomy, RA relationship 325, *327–329*
– annulus **483**, 484, *484–485*
– annulus measurements *485–486*, **486**
– anteroseptal commissure 478, *482*
– AV valves/AV canal defect *477*, 478
– calcifications 484
– chordae tendineae (tendinous cords) 482, *482–483*
– dysfunction *487*, **487**
– Ebstein's anomaly 486–487, *487*
– formation of *477*, **477**
– functional study of 488
– imaging *479–480*, *482*, **483**
– membranous septum 486
– muscular AV septum 483
– myxomatoses disease *482*
– normal *478*, **478**, *479–482*
– papillary muscles 387, *388*, *480*, 482, *482–483*
– prolapse *482*, 486, 488
– regurgitation 487, *487*
– septal attachment *345*, 398, *399*
– septal leaflet 345, *345*, 408, *409*, 410, *411*, 412, 416, 420, *421*, *477*, 478, *478–482*, 483, *484*
– triangle of Koch 483
– ventricular septal defect (VSD) 478
tuberculosis 85
Turner's syndrome 14

U

umbilicovitelline system 213

V

vagus nerves
– anatomy **124**, *126–127*, *252*, **252**, *253–254*
– heart 354, *358*
– inferior ganglion 77
– left **254**
– right **254**
valve of Vieussens 536, *540*
vein of Marshall 200, *200*
vena caval hiatus 131, **282**, *284*
venolobar syndrome 219, *220*
venous thoracic outlet syndrome *60–61*, **61**
ventilation to perfusion matching **142**, *143–146*
ventricular mass
– anatomy 325, *326*
– aortic root *409*, 410, *411*, *415*, *424*, 425, *427–428*
– aortic valvar coronet 408
– aortoseptal angle 410
– arterial roots *407*, *409*, *411*, *422*, **422**, *423–426*
– arterial valve 407, *407*
– atrial septum *408*, **412**, *416*
– atrioventricular junction 407, *407*
– atrioventricular valve 407, *407*
– AV conduction axis *410*, *412–413*, **416**, *417*
– AV valves **420**, *422*
– base, anatomy *407*, **407**, *408–410*
– cardiac skeleton *407*, 408, *409*, **410**
– cardiac valvar attachments *407*, **408**, *409*, *411*
– central fibrous body 408, *409*
– inferior paraseptal area 416, *418*
– inferior pyramidal space 407, *407–408*, *410–412*, **412**, *413*
– membranous septum *409*, **412**, *414–415*, 416, *418*
– mitral valvar hinges 408, 410, *411*
– mitral valvar leaflet 420, *421*
– muscular ventricular septum 408, *408*
– papillary muscles *420*, **420**, *421*
– paraseptal areas, right-sided **416**, *418–419*
– pulmonary valvar coronet 408, *411*
– radiolucent band 415, *416*
– right coronary aortic sinus 425
– right fibrous trigone 408, *409*
– secondary septum 412
– septal isthmus *418*
– septal tricuspid leaflet 408, 410, *411*, 412, 420, *421*
– septomarginal trabeculation *421*
– sinus septum 416, *419*
– subaortic outflow tract *409*, *411*, *423*, 425, *427–428*
– superior paraseptal area *418*
– superior septal area *418*
– supraventricular crest *421*, 425
– tendon of Todaro *410*, 416
– triangle of Koch *410*, 416, *418*
– ventricular septum 425, *426*
– ventriculoarterial junction 407, *407*
– zone of fibrous continuity 420, *421*
ventriculoarterial junction of aortic valve *376*, 382, *395*, *398*, 407, *407*, *423*, *427*, **430**, *431*
vertebral artery *231*, **231**, 232, *232*
vestibular defect 359
Vieussens' arterial ring 450, *456*, *513*
Virchow's nodes 263
visceral afferents, cardiac **259**
visceral compartment of mediastinum *103*, 104, *105*, 106, *106*
visceral pleura receptors 157
vocal fold anatomy *72*
voluntary respiration 289

W

wireless (leadless) pacemaker 571, *574*
Wolff–Parkinson–White variants 416, 420

X

xiphoid process 5, *5*, 7, *10*
xiphoid process injury 14

Y

Yamashita Japanese classification 80